Handbook on the Physics and Chemistry of Rare Earths volume 7

Elsevier, 1984

CONTENTS

CONTENTS OF VOLUMES 1–6

VOLUME 4: NON-METALLIC COMPOUNDS – II

VOLUME 5

VOLUME 6

Chapter 51

PHASE EQUILIBRIA IN TERNARY AND HIGHER ORDER SYSTEMS WITH RARE EARTH ELEMENTS AND SILICON

Peter ROGL

Institut für Physikalische Chemie, Universität Wien, Währingerstrasse 42, A-1090 Vienna, Austria

Contents

Symbols and abbreviations

a,b,c	unit cell dimensions in Å (for rhombohedral symmetry denoted as a_R, α; for the equivalent triple-primitive hexagonal cell indicated as a_H, c_H)
a/o	composition in atomic percent
arc(Zr)	arc melting under Zr-gettered argon atmosphere
CP	powder mixtures were cold pressed
HT(Ar)	heat treatment under argon atmosphere
HV	high vacuum, $\approx 10^{-4}$ Pa
ME	metallographic analysis
mol%	composition in molar percent
PXD	powder X-ray diffraction analysis
QE	samples radiation quenched
Qu(Mo)	samples wrapped in Mo foil and sealed in evacuated silica (quartz) tubes for heat treatment
R	reliability factor of crystal structure determination defined as $\Sigma|\Delta F|/\Sigma|F_{obs}|$
T_c	superconducting transition temperature, in K
T_m	magnetic ordering temperature, in K
T_N	Néel temperature, in K
T_n	sample remained normal (with respect to superconductivity) down to T, in K
w/o	composition in weight percent
α,β,γ	unit cell angles in degrees (for rhombohedral symmetry denoted as a_R, α)
ρ_E	measured density (kg/dm³)
ρ_x	calculated density (kg/dm³); theoretical density, corresponding to the composition and parameters obtained from X-ray data, atomic weight based on ^{12}C, $N = 6.022 \times 10^{23}$ atoms/gmol

1. Introduction

The present status of information about phase equilibria and formation of ternary metal silicides with R elements (R = Sc, Y, and the lanthanides) is summarized in fig. 1. Phase equilibria have been investigated for only a small number of the possible ternary combinations R–M–Si, and for a larger number of ternary systems only a few compounds have been identified to date. Little information is available involving main group elements.

It is already some time ago that the comprehensive reviews on transition metal silicides were published by Parthé (1970) and Nowotny (1972). Since then the production and technical application of the so-called rare earth elements has drastically increased, hand in hand with an increased scientific metallurgical interest in the R–metal systems.

Most of the ternary phase diagram studies (isothermal sections) have been carried out by Gladyshevskij and coworkers at Lvov University, USSR. Only recently has the interesting interplay of superconducting and magnetic properties—first discovered by Matthias and coworkers in certain R–platinum metal borides (Bell Laboratory and University of California, San Diego)—stimulated new activity in low-temperature investigations of ternary R silicides in combination with metals from the iron group. A rather comprehensive review on the electrical and magnetic properties of these materials can be found in a recent article written by Johnston and Braun (1982).

As far as the present compilation of phase diagram data of R–M–Si systems is concerned, no efforts have been made to recompile data on the binary systems involved—and thus for details on binary systems the reader is referred to the well-known handbooks on binary phase diagrams by Hansen and Anderko (1958), Ageev (1959), Elliott (1965), Shunk (1969), Gschneidner and Verkade (1974),

Si	Ti	Zr	Hf	V	Nb	Ta	Cr	Mo	W	Mn	Tc	Re	Fe	Co	Ni	Ru	Rh	Pd	Os	Ir	Pt	Cu	Ag	Au	Zn	Cd	Hg	B	Al	Ga	In	Tl	C	Ge	Sn	Pb
Sc							1			■4		■3	■14	12	■16	2	◢9	1	1	4	1	5												0		
Y					■1			■1		■3		2	■7	6	◢17	3	6	3	2	2	3	4		1				■0	■5					■0		
La	◢0									2		5	■5	6	◢12	2	6	1	1	4	2	3	1	1				■0	1					◢0		
Ce							◢2					5	■4	■7	22	2	1	2	1	1	2	■6	1	1				■0	◢1					■0		
Pr										2		2	3	4	14	2	1	2	1		1	3	1	1												
Nd										2		2	3	6	11	2	5	2	1	2	2	3	3	1												
Pm																																				
Sm										2		2	4	6	8	2	4	2	1		2	3	1	1												
Eu												1	3	8	2	1	1			1	2	2	2												
Gd						1		2		2		■8	5	9	2	6	2	1	1	3	3	3	1	1					◢2						■0	
Tb								2		1		5	4	8	1	5	2	1		2	4		1													
Dy								2		1		5	4	9	2	5	3	1	1	3	4	1	1													
Ho								2		1		5	3	7	2	5	3	1	1	2	4		1													
Er								2		1		4	2	9	2	5	3	1	2	3	5	1	1							2						
Tm								3		1		3	1	6	2		2	1	1	3	4															
Yb								1				5	1	6	2	1	1		1	3	1	1														
Lu								2				3	1	5	2	1	1	2	1	3	3															

Fig. 1. Formation of ternary silicides and phase equilibria within ternary silicide systems: R–M–Si; filled squares: complete isothermal section established; filled triangles: partial isothermal section established. Numbers in each square correspond to the numbers of ternary silicide compounds characterized.

Eremenko et al. (1975) and Moffatt (1976). Binary phase diagrams are therefore rather briefly discussed, but it was the general intention to incorporate the most recent results and to point out those problems where further investigations will have to clarify points still in question. Critical assessments for binary R–Si or R–Ge systems unfortunately are available for only a few systems and many points of uncertainty still exist. This is particularly true for the complicated polymorphic transitions of the stoichiometric and nonstoichiometric disilicides and digermanides. The situation becomes even less transparent when one looks at the ternary solid solutions. In most cases a careful reinvestigation of the ternary phase regions containing ~ 60 to 70 a/o Si(Ge) over a larger temperature interval is still necessary in order to obtain more reliable phase diagram data.

Furthermore very few reliable data exist on the ternary solubility limits as a function of temperature. The same holds for the homogeneity ranges of the ternary compounds, which have been determined with a high degree of precision in only a few cases. Therefore the small solubilities of binary and ternary compounds indicated (~ 0.5 a/o) are schematic in all cases not especially specified and should serve as a guideline only.

From the various influences of the factors responsible for the stability of a crystal structure of a given composition (geometrical, electrochemical, and energy band factors), complete or extended solid solutions can be expected to form between isotypic binary silicides of the same or neighboring group numbers (see e.g. Ce–Y–Si or Ce–Th–Si). R–silicon germanides generally form extended solid solutions. The similarity in the chemical alloying behavior of the large as well as the small R members is well known. Thus in all those cases, where exact phase equilibria have not yet been derived, the known phase equilibria of one of the neighboring R elements may serve as a first order approximation. However, exchange of the second metal constituent by one of its homologous elements or even changing to a neighboring group number in general causes a considerable change in the resulting phase equilibria (compare e.g. Y–Cr–Si, Y–Mo–Si, Y–Mn–Si, Y–Re–Si).

All data used in this compilation were obtained from a manual collection of the author during the past 15 years as well as from a computerized literature search consulting CAS, and METADEX service up to December 31, 1983.

No attempt, however, has been made to include papers concerning the numerous technical alloys (e.g., much has been said about the production of nodular iron parts using Fe–Si–R alloys), unless they revealed valuable information on phase equilibria, solid solubilities, lattice parameters or crystal-structure data.

The "short" Hermann–Mauguin symbol (according to the International Tables for X-ray Crystallography, 1974) has been used to characterize the crystal structure of each ternary compound in combination with its formula and name of the structure type (representative substance). Whenever information on atomic parameters or metal ordering—deviating from the general description of the structure type concerned—was available, it has been included; however, for a more detailed description of the crystallographic structure types, the reader is referred to the contribution by Parthé and Chabot (1984) in vol. 6 of this Handbook, ch. 48.

Rare-earth–metal–silicon ternary phase diagrams are listed in alphabetical order

of the chemical symbol of the rare earth element (Ce, Dr, Er, ..., Yb). Under each rare earth the systems are listed alphabetically by the chemical symbol of the non-rare-earth element. After the ternary systems, higher order systems are presented following the same scheme.

References

Ageev, N.V., 1959, Phase Diagrams of Metallic Systems (Viniti Press, Acad. Sci. USSR, Moscow) (in Russian); regularly updated.

Elliott, R.P., 1965, Constitution of Binary Alloys, First Supplement (McGraw-Hill, New York).

Eremenko, V.N., Yu.I. Buyanov and V.G. Batalin, 1975, Phase Diagrams of Binary Systems of Germanium with Rare Earth Metals, in: Fiz.Khim.Kondensiv.Faz. Sverkhverd.Materialov i ikh Granits Razdela (Nauka Dumka, Kiev) pp. 191–201.

Gschneidner Jr., K.A. and M.E. Verkade, 1974, Selected Cerium Phase Diagrams, Document IS-RIC-7, Rare Earth Information Center, Iowa State Univ., Ames, IA, USA.

Hansen, M. and K. Anderko, 1958, Constitution of Binary Alloys, 2nd Ed. (McGraw-Hill, New York).

Johnston, D.C. and H.F. Braun, 1982, in: Superconductivity in Ternary Compounds, eds. O. Fischer and M.B. Maple (Springer, Heidelberg).

Moffatt, W.G., 1976, The Handbook of Binary Phase Diagrams (General Electric Comp., Schenectady, NY), updating service.

Nowotny, H., 1972, in: MTP, International Review of Science, vol. 10, Inorg. Chem. Series, ed. L.E.J. Roberts (Butterworths, New York, London).

Parthé, E., 1970, Coll. Int. CNRS **180**, 61.

Parthé, E. and B. Chabot, 1984, Crystal Structures and Crystal Chemistry of Ternary Rare Earth–Transition Metal Borides, Silicides and Homologues, in: Handbook on the Physics and Chemistry of Rare Earths, Vol. 6, eds. K.A. Gschneidner, Jr. and L. Eyring (North-Holland, Amsterdam) p. 113.

Shunk, F.A., 1969, Constitution of Binary Alloys, Second Supplement (McGraw-Hill, New York).

2. Ternary phase diagrams: rare-earth–metal–silicon

Ce–Ag–Si

From X-ray powder analysis Mayer et al. (1972) reported $CeAg_2Si_2$ to crystallize with the ordered $ThCr_2Si_2$-type of structure [space group I4/mmm; $a = 4.247(5)$, $c = 10.64(5)$]. For sample preparation, see $LaAg_2Si_2$; the alloys also contained some excess Ag as well as small amounts of $CeSi_2$ phases (tetragonal and/or orthorhombic modification?). For ^{29}Si NMR and susceptibility measurements, see Sampathkumaran et al. (1979). A ferri- or ferromagnetic ground state was suggested for $CeAg_2Si_2$ by Murgai et al. (1983); $T_m = 8$–10 K.

References

Mayer, I. and J. Cohen, 1972, J. Less-Common Metals **29**, 221.

Mayer, I., J. Cohen and I. Felner, 1973, J. Less-Common Metals **30**, 181.

Murgai, V., S. Raaen, L.C. Gupta and R.D. Parks, 1982, in: Valence Instabilities, eds. P. Wachter and H. Boppart (North-Holland, Amsterdam) p. 537.

Sampathkumaran, E.V., L.C. Gupta and R. Vijayaraghavan, 1979, Phys. Lett. **70A**(4), 356.

Ce–Al–Si

No complete phase diagram has been established, despite considerable interest has been devoted to the ternary system Ce–Al–Si.

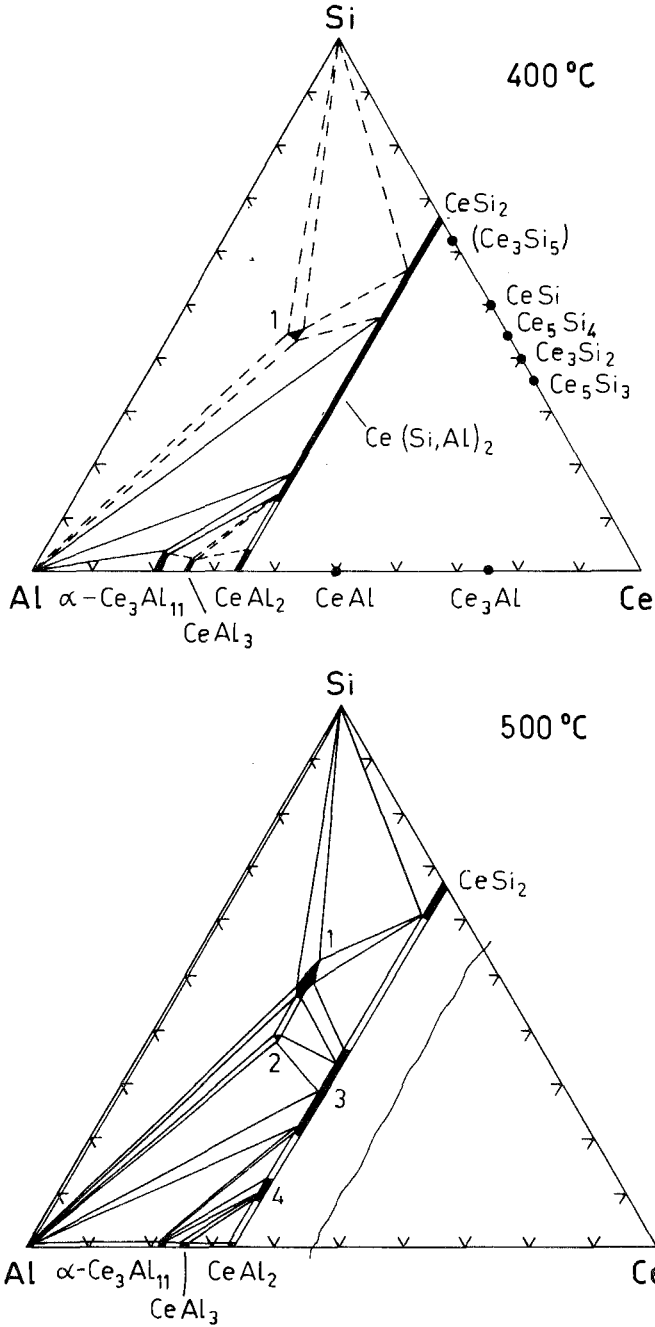Fig. 2. (a) Ce–Al–Si, partial isothermal section at 400 °C for 0–33 a/o Ce (after Altunina et al., 1963). 1: "$Ce_{20}Al_{35}Si_{45}$". (b) Ce–Al–Si, partial isothermal section at 500 °C for 0–33 a/o Ce (after Muravyova, 1972). 1: $CeAl_{1.25-1.75}Si_{2.75-2.25}$ (earlier "$Ce_{20}Al_{35}Si_{45}$" or "$Ce_2Al_3Si_2$"), 2: $CeAl_2Si_2$, 3: $CeAl_{1.4-0.9}Si_{0.6-1.1}$, 4: $CeAl_{1.64-1.55}Si_{0.36-0.45}$.

From a rather preliminary study of the phase equilibria at 400°C (the Al-rich region was studied at 500°C) Zarechnyuk (1963) and Altunina et al. (1963) attempted to construct an isothermal section (see fig. 2a). Samples were prepared from 99.99% pure Al and 99.567% pure Ce by melting in an Al_2O_3 crucible under a protective layer of a mixture of KCl + LiCl. The alloys were annealed for 50–100 h at 400°C, and 25 samples in the Al-rich region at 500°C. Phase composition was checked in some cases by chemical analysis. Phase equilibria were determined as based upon X-ray powder and metallographic analyses. Etching was possible in mixtures of HNO_3, HF and glycerin. Microhardness values were obtained at a load of 100 g.

A wide homogeneous region was found for mixed crystals $CeSi_{2-x}Al_x$ (α-$ThSi_2$-type) extending up to 55–60 a/o Al at 400°C (Si/Al substitution), and lattice parameters were claimed to change linearly from $a = 4.158$, $c = 13.898$ ($CeSi_2$) to $a = 4.239$, $c = 15.231$ at 60 a/o Al (data converted from kX units). Microhardness values were $H = 610$ (± 10) kg/mm^2 (at 2 w/o Al), and $H = 460$ (± 10) kg/mm^2 at 20 w/o Al.

The solid solubility of Ce and Si in Al has been studied at 500°C and the variations of the lattice parameters were recorded along two concentration lines at 95 w/o Al and at 98 a/o Al, respectively.

At a composition (in a/o) $Ce_{20}Al_{35}Si_{45}$ a ternary compound was observed, which tentatively was indexed hexagonal with $c/a \approx 1.17$; $H = 290$ (± 10) kg/mm^2. The ternary phase was suspected to correspond to the compound "$Ce_2Al_3Si_2$" mentioned by Brauer and Haag (1952), who obtained this phase in an unsuccessful attempt to prepare $CeSi_2$ by reaction of a $CeAl_{\sim 9}$ melt with excess Si at 900°C in an Al_2O_3 crucible under a protective layer of NaCl. After 1 h at 900°C and subsequent cooling to 600°C in 2.5 h the obtained alloy was boiled in 2n-NaOH. The remainder was of metallic luster and well crystallized. Indexing was possible on the basis of a hexagonal cell $a = 6.242$, $c = 7.304$ (converted from kX units).

At variance with the results of Altunina et al. (1963) concerning the wide homogeneous range of $CeSi_{2-x}Al_x$, Raman (1967) and Raman and Steinfink (1967) reported the existence of a ternary AlB_2-type of structure in a ternary alloy $CeAl_{1.625}Si_{0.375}$ annealed at 1000°C [P6/mmm, $a = 4.315(5)$ and $c = 4.298(5)$].

Muravyova et al. (1972) prepared and characterized the compound $CeAl_2Si_2$, which was found to crystallize with the La_2O_2S-type of structure with the space group $P\bar{3}m1$ and lattice parameters $a = 4.21$ and $c = 6.94$; powder intensities were calculated on the basis of the atom parameters as derived for the isotypic $CaAl_2Si_2$ (for details, see Sm–Al–Si), and correspondance to the observed intensity data was said to be satisfactory.

Muravyova (1972) reinvestigated the phase equilibria for the 0–33 a/o Ce section (see fig. 2b) of the Ce–Al–Si system by means of X-ray powder and metallographic analysis of 65 alloys which were arc-melted and subsequently annealed for 150–750 h at 500°C in evacuated silica tubes. The starting materials were 99.0% Ce and 99.90% Al, Si.

From a recent compilation of Ce phase diagram data, the binary Ce–Al system at 400–500°C comprises five intermetallic phases: β-Ce_3Al, CeAl, $CeAl_2$, $CeAl_3$, and

α-Ce$_3$Al$_{11}$ (Gschneidner and Verkade, 1974). Only two Ce aluminides were shown by Altunina et al. (1963): CeAl$_2$(MgCu$_2$-type) and "CeAl$_4$" (now α-Ce$_3$Al$_{11}$ with a BaAl$_4$-derivative type). Similarly only CeSi$_2$ (α-ThSi$_2$-type) was reported for the Ce–Si binary. The solid solubility of Si in α-Ce$_3$Al$_{11}$ (given as "CeAl$_4$"), in CeAl$_3$ and in CeAl$_2$ was observed to be rather small ($\sim$ 1 a/o Ce). Raman and Steinfink (1967) observed an alloy CeAl$_{1.94}$Si$_{0.06}$ annealed at 1000°C to be single phase MgCu$_2$-type with $a = 8.040(5)$ suggesting a solid solubility of $\sim$ 2 a/o Si in CeAl$_2$ (MgCu$_2$-type) at 1000°C. The solid solubility of Al in CeSi$_2$ was given by Muravyova (1972) to be $\sim$ 5 at% Al at 500°C, but according to the powder X-ray data of Raman and Steinfink (1967) the solubility of Al in CeSi$_2$ with α-ThSi$_2$ type at 1000°C at least was found to extend to CeAl$_{1.5}$Si$_{0.5}$ [$a = 4.280(5)$, $c = 14.90(1)$]; for details of sample preparation, see Nd–Al–Si.

Four ternary compounds were observed confirming the earlier findings concerning the compounds CeAl$_{1.25-1.75}$Si$_{2.75-2.25}$ (earlier "Ce$_{20}$Al$_{35}$Si$_{45}$", Zarechnyuk, 1963; Altunina et al., 1963; and "Ce$_2$Al$_3$Si$_2$", Brauer and Haag, 1952) and CeAl$_2$Si$_2$, Muravyova et al. (1972). The compound Ce$_{1.64-1.55}$Si$_{0.36-0.45}$ with the AlB$_2$-type and a considerable homogeneity region ranging from $a = 4.35$, $c = 4.30$ to $a = 4.32$, $c = 4.43$ reveals slightly larger unit cell dimensions than those obtained by Raman (1967) for CeAl$_{1.625}$Si$_{0.375}$ at 1000°C.

CeAl$_{1.4-0.9}$Si$_{0.6-1.1}$ was said to crystallize with the α-ThSi$_2$ type (I4$_1$/amd, $a = 4.25-4.27$, $c = 14.54-14.92$); the atom parameters were 4 Ce in (4a) 0, 0, 0 and a statistical occupation of 4 Al + 4 Si in (8e) 0, 0, 0.417. Around the composition CeAlSi ordering among Al and Si atoms in terms of a LaPtSi-type (α-ThSi$_2$-derivative type) seems likely.

No complete structure determination has been carried out for CeAl$_{1.25-1.75}$Si$_{2.75-2.25}$, but from a preliminary analysis of single crystal X-ray photographs, Muravyova (1972) was able to propose a trigonal symmetry corresponding to the possible space groups R$\bar{3}$m, R32 or R3m; lattice parameters for an alloy CeAl$_{1.25}$Si$_{2.75}$ were $a = 3.85$, $c = 9.47$.

References
Altunina, L.N., E.I. Gladyshevskij, O.S. Zarechnyuk and I.F. Kolobnev, 1963, Zh. Neorg. Khim. **8**(7), 1673.
Brauer, G. and H. Haag, 1952, Z. Anorg. Allg. Chem. **267**, 198.
Gschneidner Jr., K.A. and M.E. Verkade, 1974, Selected Cerium Phase Diagrams, Document IS-RIC-7, Iowa State Univ., Ames, IA, USA, p. 36.
Muravyova, A.A., 1972, Autoreferat Dis. Kand. Khim. (abstract of thesis, Russian) (Nauk, Lvov) 18 p.
Muravyova, A.A., O.S. Zarechnyuk and E.I. Gladyshevskij, 1972, Visn. L'vivsk. Univ., Ser. Khim. **13**, 14.
Raman, A., 1967, Z. Metallkde **58**(3), 179.
Raman, A. and H. Steinfink, 1967, Inorg. Chem. **6**(10), 1789.
Zarechnyuk, O.S., 1963, Zb. Robit Aspirantiv, L'vivsk. Univ., Prirodn. (Nauk, Lvov) pp. 15–20.

Ce–Au–Si

From X-ray powder analysis Mayer et al. (1973) reported CeAu$_2$Si$_2$ to crystallize with the ordered ThCr$_2$Si$_2$-type of structure: I4/mmm, $a = 4.326(5)$, $c = 10.24(5)$. For sample preparation, see LaAu$_2$Si$_2$. Antiferromagnetic ordering was observed by

Felner (1975) at $T_N = 6.6$ K and by Murgai et al. (1983) at $T_N = 8$–10 K (magnetic susceptibility and electrical resistivity measurements in the temperature range $1.5 < T < 300$ K and high field magnetization studies at 4.2 K up to 21 T). The paramagnetic behavior is characterized by $\mu_{eff}^{para} = 2.3\ \mu_B$ and $\theta_p = -2.8$ K (Felner, 1975). For ^{29}Si NMR and susceptibility measurements, see Sampathkumaran et al. (1979).

References

Felner, I., 1975, J. Phys. Chem. Sol. **36**, 1063.
Mayer, I., J. Cohen and I. Felner, 1973, J. Less-Common Metals **30**, 181.
Murgai, V., S. Raaen, L.C. Gupta and R.D. Parks, 1983, private communication.
Sampathkumaran, E.V., L.C. Gupta and R. Vijayaraghavan, 1979, Phys. Lett. **70A**(4), 356.

Ce–Co–Si

By means of X-ray powder and metallographic analysis of 160 arc-melted alloys Bodak and Gladyshevskij (1970) established two partial isothermal sections of the system Ce–Co–Si at 800 °C (region 0–33 a/o Ce) and at 400 °C for the region 33–100 a/o Ce. The alloy buttons were heat-treated for 250 h at 800 °C, and 500 h at 400 °C, respectively. Starting materials were powders of Ce 99.56%, Co 99.87% and Si 99.99%. Etching was possible in aqueous solutions of HF, HNO$_3$ and glycerin. Microhardness values were determined at a load of 50–100 g.
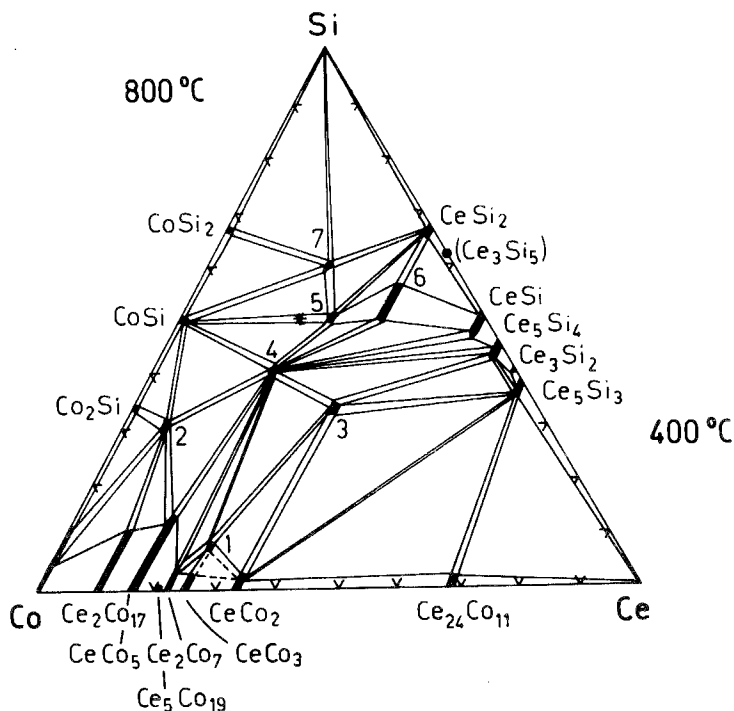
Fig. 3. Ce–Co–Si, partial isothermal sections at 800 °C (0–33 a/o Ce) and at 400 °C (33–100 a/o Ce). 1: Ce$_3$Co$_8$Si, ·2: CeCo$_{8.8-8.4}$Si$_{4.2-4.6}$, 3: CeCoSi, 4: CeCo$_2$Si$_2$, 5: CeCoSi$_2$, 6: CeCo$_{0.5-0.3}$Si$_{1.5-1.7}$, 7: CeCoSi$_3$; the location of a high-temperature phase (?) Ce$_2$Co$_3$Si$_5$ is marked by an asterisk.

The solid solubility of Si in Co ($\sim$ 13 a/o at 800°C) as well as the binary cobalt silicides are in agreement with the data in handbooks of binary phase diagrams [Co_2Si (Co_2Si-type), $CoSi$ (FeSi-type), $CoSi_2$ (CaF_2-type)]. For Ce silicides, see the Ce–Ni–Si system. The compound Ce_3Si_5 was not observed by Bodak and Gladyshevskij (1970); its position, however, is marked in fig. 3 by a black circle. The binary system Ce–Co basically agrees with a recent compilation of phase diagram data by Gschneidner and Verkade (1974) and Iandelli and Palenzona (1979). Ce_5Co_{19} with a new structure type will have to be included. Due to its reduced stability with respect to its neighboring phases $CeCo_5$ and Ce_2Co_7, a rather limited solid solubility of Si in Ce_5Co_{19} is likely, which in turn would result in the formation of a three-phase equilibrium: $Ce_5(Co,Si)_{19}$ + $Ce(Co,Si)_5$ + $Ce_2(Co,Si)_{17}$. Mutual solid solubilities of the binary compounds were observed to be small; Co silicides do not dissolve Ce, whereas Ce_2Co_{17} dissolves up to 10 a/o Si and $CeCo_5$ dissolves up to 14 a/o Si. Lattice parameters, as read from a small diagram, change from $a = 8.38$, $c = 8.13$ (Ce_2Co_{17}) to $a = 8.32$, $c = 8.15$ for $Ce_2(Co,Si)_{17}$, and from $a = 4.90$, $c = 4.035$ ($CeCo_5$) to $a = 4.835$, $c = 4.050$ for $Ce(Co,Si)_5$. Seven ternary compounds were observed, which all had variable Co,Si content at a fixed Ce concentration.

In an early study of phase equilibria within the Ce-poor region, Bodak and Gladyshevskij (1969) observed a ternary compound $CeCo_{8.8-8.4}Si_{4.2-4.6}$ with a tetragonal $NaZn_{13}$-derivative type [lattice parameters first were given as $a_0 = 11.01(1)$ and $c_0 = 11.53(1)$]. A more correct crystallographic description of this phase as an isotypic representative of the structure type of $Ce_2Ni_{17}Si_9$ was later given by Bodak and Gladyshevskij (1970): $a = 7.79$ ($a = a_0/\sqrt{2}$), $c = 11.53$ and the space group I4/mcm. The microhardness at a load of 50 or 100 g was reported to be $H = 681$ (± 50) kg/mm^2.

An extended homogeneity range was observed by Bodak and Gladyshevskij (1970) for the AlB_2-type phase $CeCo_{0.5-0.3}Si_{1.5-1.7}$ with space group P6/mmm. Lattice parameters range from $a = 4.044$, $c = 4.194$ at 50 a/o Si (microhardness 613 ± 50 kg/mm^2) to $a = 4.025$ and $c = 4.29$ at 54 a/o Si. Gladyskevsij and Bodak (1965) gave slightly different parameters for $Ce(Co,Si)_2$: $a = 4.051$, $c = 4.187$ (arc melted, 800°C, 100 h). In agreement with this Mayer and Tassa (1969) reported, from a phase equilibria study of the section $CeCo_xSi_{2-x}$ at 700–800°C, the existence of an AlB_2-type structure at the composition $CeCo_{0.4}Si_{1.6}$ (P6/mmm, $a = 4.046$, $c = 4.266$). In similarity to the X-ray powder data of $NdFe_{0.4}Si_{1.6}$ a statistical distribution of Si,Co atoms in the 2d sites was assumed. For $x < 0.4$ the $ThSi_2$-type was said to be stable, and for $x > 0.4$ X-ray powder patterns were claimed to be "complicated". For sample preparation, see $GdCo_{0.4}Si_{1.6}$. From susceptibility measurements of $CeCo_{0.4}Si_{1.6}$ (4.2 to 300 K), Felner and Schieber (1973) derived $\mu_{eff}^{para} = 4.9$ μ_B and $\theta_p = -9$ K.

CeCoSi is tetragonal with the PbFCl-type of structure: $a = 4.066(3)$, $c = 6.965(5)$, P4/nmm (X-ray powder analysis; Bodak et al., 1970). for atom parameters and sample preparation, see CeFeSi. Bodak and Gladyshevskij (1970) reported $a = 4.040$ and $c = 6.979$; the microhardness was $H = 166$ (± 50) kg/mm^2.

$CeCo_2Si_2$ crystallizes with the ordered $ThCr_2Si_2$-type of structure: space group I4/mmm, $a = 3.962(6)$, $c = 9.795(10)$, $\rho_x = 6.78$ kg/dm^3 (Rieger and Parthé, 1969;

X-ray powder analysis). Samples were arc-melted and heat-treated in evacuated silica tubes at 900 °C for 100 h. Ban and Sikirica (1965) reported $a = 3.957(10)$ and $c = 9.783(10)$ from X-ray powder analysis of arc-melted samples (Ce 99.56%, Co 99.8%, Si 99.99%). Bodak and Glayshevskij (1970) confirmed the structure ($a = 3.962$, $c = 9.809$) and measured the microhardness $H = 824$ (± 50) kg/mm^2.

CeCoSi$_3$ was first claimed by Bodak and Gladyshevskij (1970) to crystallize in a new superstructure of the BaAl$_4$-type with a crystal symmetry I4/mmm and lattice parameters $a = 4.14$, $c = 9.50$. The microhardness was given as 498 (± 50) kg/mm^2. More recently Chabot (1983) established, from X-ray powder data, the correct symmetry and atom order to be isostructural with the BaNiSn$_3$-type, I4mm, $a = 4.1344(8)$ and $c = 9.561(3)$.

CeCoSi$_2$ is isotypic with the crystal structure of CeNiSi$_2$: Cmcm, $a = 4.093(2)$, $b = 16.397(8)$, $c = 4.036(2)$; $\rho_{exp} = 6.15$, $\rho_{theor} = 6.219$ kg/dm^3; microhardness $H = 311$ (± 50) kg/mm^2 (Bodak and Gladyshevskij, 1970). Atom parameters were refined by Lukasziewicz and Bodak (1969) from single crystal X-ray photographs: all atoms were found to occupy the 4c sites (0, y,0) of Cmcm: Ce, $y = 0.1074(4)$; Co, $y = 0.3180(11)$; Si, $y = 0.4588(15)$ and Si, $y = 0.7482(21)$; $R = 0.171$. Single crystals were directly obtained from an arc-melted alloy of composition CeCoSi$_2$, by slowly cooling the melt. Pelizzone et al. (1982) confirmed the structure type and gave $a = 4.094(2)$, $b = 16.440(7)$, $c = 4.043(2)$. For magnetic data, see below.

Ce$_3$Co$_8$Si crystallizes with the ordered CeNi$_3$ (super-)structure: P6$_3$/mmc, $a = 4.960(1)$, $c = 16.450(10)$, $\rho_{exp} = 8.45$, $\rho_x = 8.65$ kg/dm^3. The atom order was determined by Bodak (1971) by X-ray powder methods: Ce in 2c) and 4f); Co in 12k), 2b), 2d), and Si in 2a); the reliability factor was $R = 0.144$. Bodak and Gladyshevskij (1970) reported a microhardness of 613 (± 50) kg/mm^2, but slightly different lattice parameters $a = 4.95$ and $c = 16.25$.

Chabot and Parthé (1984) observed the existence of a compound Ce$_2$Co$_3$Si$_5$ in arc-melted alloys which subsequently were sealed in quartz tubes and heat-treated at 1100 °C for 24 h and additionally at 1000 °C for 150 h. Ce$_2$Co$_3$Si$_5$ adopts the U$_2$Co$_3$Si$_5$-type of structure with space group Ibam and lattice parameters as follows: $a = 9.623(3)$, $b = 11.306(3)$ and $c = 5.652(2)$.

Magnetic susceptibility data obtained from a temperature range of 77–300 K were presented by Bodak et al. (1977) for CeCo$_{0.5}$Si$_{1.5}$ (AlB$_2$-type, $\mu_{eff}^{para} = 3.3$ μ_B, $\theta_p = -400$ K); CeCoSi (PbFCl-type, $\mu_{eff}^{para} = 3.6$ μ_B, $\theta_p = -110$ K); CeCoSi$_3$ (BaAl$_4$-derivative type, $\chi_g = 5.14 \times 10^{-6}$ cm^3 g^{-1}) and CeCo$_2$Si$_2$ (ThCr$_2$Si$_2$-type, $\mu_{eff}^{para} = 3.16$ μ_B, $\theta_p = -190$ K). For band-structure calculations and physical properties of CeCo$_2$Si$_2$, see Koterlin (1981), Koterlin et al. (1981), Levin (1979) and Levin et al. (1981). The magnetic data for CeCoSi$_2$ (CeNiSi$_2$-type, $\mu_{eff}^{para} = 1.6 \mu_B$, $\theta_p = -240$ K) as presented by Bodak et al. (1977) do not, however, correspond to the values recently published by Pelizzone et al. (1982), who observed at $T > 70$ K a temperature-independent paramagnetism, suggesting Ce in a tetravalent state according to its smaller lattice parameters as compared with the isotypic RCoSi$_2$ series of compounds.

References

Ban, Z. and M. Sikirica, 1965, Acta Crystallogr. 18, 594.

Bodak, O.I., 1971, Visn. L'vivsk. Derzh. Univ., Ser. Khim. **12**, 22.

Bodak, O.I. and E.I. Gladyshevskij, 1969, Dopov. Akad. Nauk. Ukr. RSR, Ser. A **12**, 1125.

Bodak, O.I. and E.I. Gladyshevskij, 1970, Izv. Akad. Nauk SSSR, Neorg. Mater. **6**(6), 1186.

Bodak, O.I., E.I. Gladyshevskij and P.I. Kripyakevich, 1970, Zh. Strukt. Khim. **11**(2), 305.

Bodak, O.I., E.I. Gladyshevskij, E.M. Levin and R.V. Lutsiv, 1977, Dopov. Akad. Nauk Ukr. RSR., Ser. A **12**, 1129.

Chabot, B., 1983, unpublished results.

Chabot, B. and E. Parthé, 1984, J. Less-Common Metals **97**, 285.

Felner, I. and M. Schieber, 1973, Solid State Commun. **13**, 457.

Gladyshevskij, E.I. and O.I. Bodak, 1965, Dopov. Akad. Nauk Ukr. RSR., Ser. A **5**, 601.

Gschneidner Jr., K.A. and M.E. Verkade, 1974, Selected Cerium Phase Diagrams Document IS-RIC-7, Iowa State Univ., Ames, IA, USA, p. 14.

Iandelli, A. and A. Palenzona, 1979, Crystal Chemistry of Intermetallic Compounds, in: Handbook on the Physics and Chemistry of Rare Earths, Vol. 2, eds. K.A. Gschneidner, Jr. and L. Eyring (North-Holland, Amsterdam) p. 1.

Koterlin, M.P., 1981, Dopov. Akad. Nauk Ukr. RSR., Ser. A **5**, 71.

Koterlin, M.P., E.M. Levin and R.I. Yasnitskii, 1981, Ukr. Fiz. Zh. **26**(11), 1917.

Levin, E.M., 1979, Ukr. Fiz. Zh. **24**(9), 1386.

Levin, E.M., R.V. Lutsiv, L.D. Finkelstein, N.D. Samsonova and R.I. Yasnitskii, 1981, Fiz. Tverd. Tela **23**(8), 2401.

Lukaszewicz, K. and O. Bodak, 1969, Bull. Acad. Polon. Sci., Ser. Sci. Chim. **XVII**(2), 63.

Mayer, I. and M. Tassa, 1969, J. Less-Common Metals **19**, 173.

Pelizzone, M., H.F. Braun and J. Müller, 1982, J. Magn. Magn. Mater. **30**, 33.

Rieger, W. and E. Parthé, 1969, Monatsh. Chem. **100**, 444.

Ce–Cu–Si

Bodak et al. (1974) investigated the phase equilibria of the system Ce–Cu–Si and produced two partial isothermal sections, at 600°C (region 0–33 a/o Ce) and at 400°C (33–100 a/o Ce). The phase equilibria were determined by means of metallographic and X-ray analysis of 160 alloys, prepared by arc melting under argon from 99.4% pure Ce, 99.93% pure Cu and 99.99% pure Si. No details were reported concerning the circumstances of the annealing technique (150 h at 600°C; 250 h at 400°C). Chemical analysis—performed in some cases—confirmed the correspondence between nominal and actual composition within 1%. Etching was possible by a mixture of HF, HNO_3 and glycerin; microhardness was measured at a load of 100 g, and pycnometric densities were measured in kerosene.

The Ce–Cu binary system corresponds to a recent critical assessment of phase diagram data by Gschneidner and Verkade (1974) [$CeCu_6$ ($CeCu_6$-type), $CeCu_5$ ($CaCu_5$-type), $CeCu_4$ ($CeCu_4$-type ?), $CeCu_2$ ($CeCu_2$-type) and CeCu (CsCl-type)]. The copper silicides, as recorded in fig. 4, were identified according to the system adopted by Hansen and Anderko (1958) [α is the solid solubility of Si in Cu (~ 10 a/o at 600°C); K (Mg-type), γ (β-Mn-type), ϵ ($Cu_{15}Si_4$-type), η, η' are crystallographic modifications of Ca_3Si]. The binary Ce silicides have been discussed in combination with the system Ce–Ni–Si. "Ce_3Si_5" (its location in fig. 4 is marked by a black circle) was not observed by Bodak et al. (1974). The two disilicide modifications with l-$GdSi_2$ and h-$ThSi_2$-type were both reported at the ideal concentration of $CeSi_2$, with a solid state transformation at 1000°C. Solid solubility
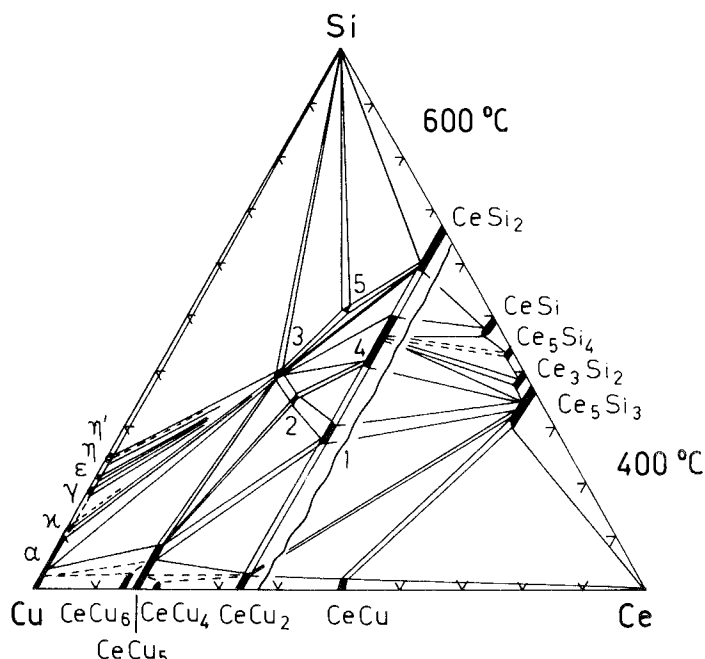
Fig. 4. Ce–Cu–Si, partial isothermal sections at 600 °C (0–33 a/o Ce) and at 400 °C (33–100 a/o Ce). 1: $CeCu_{1.19-1.10}Si_{0.81-0.90}$, 2: $CeCu_{1.6}Si_{1.4}$, 3: $CeCu_2Si_2$, 4: $CeCu_{0.76-0.44}Si_{1.24-1.56}$, 5: $CeCuSi_2$.

of Ce in copper silicides was said to be negligible (no details given) and mutual solid solubilities of binary Ce–Cu and Ce–Si compounds as well as the ternary homogeneous regions were found to extend at a fixed Ce concentration with Cu/Si substitution. Solubilities in general are less than 5 a/o Cu(Si). 7 a/o Cu was observed to dissolve in $CeSi_2$ (see also fig. 5 for the volume change), and ~ 9 a/o Cu dissolved in Ce_5Si_3. Similarly ~ 9 a/o Cu can be replaced by Si in $CeCu_5$.

Five ternary compounds were identified confirming earlier results about the existence of $CeCu_2Si_2$ (Bodak et al., 1966; Rieger and Parthé, 1969b), and the existence of phases with AlB_2-type (Gladyshevskij and Bodak, 1965; Raman, 1967; Rieger and Parthé, 1969a).

$CeCu_2Si_2$ crystallizes with the $ThCr_2Si_2$-type of structure: I4/mmm, $a = 4.103(10)$, $c = 9.986(10)$ (powder X-ray data, Bodak et al., 1966). Rieger and Parthé (1969b) reported smaller unit cell dimensions from an alloy annealed at 900°C $[a = 4.105(6), c = 9.933(10)]$ eventually indicating a wider homogeneous range at higher temperatures? For sample preparation, see $(Y,La)Cu_2Si_2$. Electric conductivity was measured by Bodak and Gladyshevskij (1970) ($\sigma = 7800$ Ω^{-1} cm^{-1}), and microhardness was $H = 394(50)$ kg/mm^3 (Bodak et al., 1974). $CeCu_2Si_2$ is paramagnetic above 4.2 K. Among the mixed valence compounds $CeCu_2Si_2$ so far is the only case for the possible existence of superconductivity (see Steglich et al., 1979 and Aliev et al., 1982, 1983). For a comprehensive review on the physical properties, see the papers of Sales and Viswanathan (1976), Sampathkumaran et al., (1979), Levin et al. (1981), Stewart et al. (1983) and Padalia et al. (1983); the anomalous

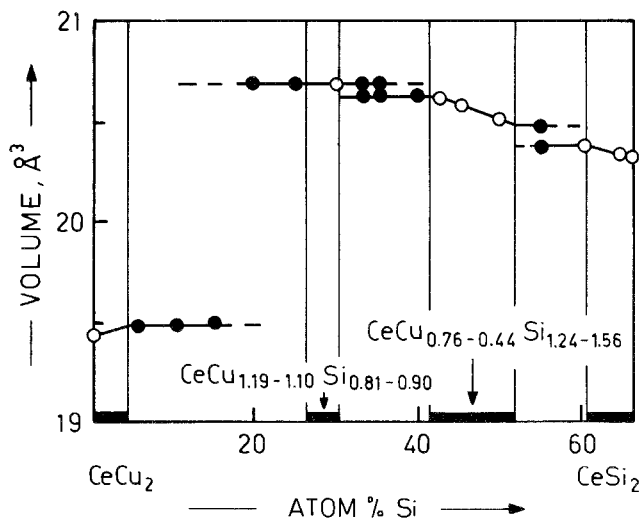Fig. 5. Ce–Cu–Si; section $CeCu_2$–$CeSi_2$: volume versus concentration. After Bodak et al. (1974). Single-phased regions are indicated by a black bar (see also fig. 4). With respect to recent data by Iandelli (1983) the unit cell parameters for the phase $CeCu_{1.19-1.10}Si_{0.81-0.90}$ might in fact be subcell parameters according to the relation: $a(Ni_2In) = a(AlB_2)$; $c(Ni_2In) = 2c(AlB_2)$.

low-temperature behavior (superconductivity at $T_c = 0.55(15)$ K) is reviewed by Lieke et al. (1982) and by Bredl et al. (1983) (gap-less superconductivity). For ^{29}Si NMR resonance and relaxation studies, see Aarts et al. (1983). Ishikawa et al. (1983) investigated the effect of composition on the superconductivity of $CeCu_2Si_2$. Their lattice parameters and superconducting transition temperatures are listed in table 1. Furthermore, from DTA experiments $CeCu_2Si_2$ was reported by Ishikawa et al. (1983) to form peritectically at $1540 \pm 15\,°C$ (liquid at $1550\,°C$).

For transport properties of $CeCu_2Si_2$ between 1.5 and 300 K (electrical resistivity, thermal conductivity and thermoelectric power) see Franz et al. (1978) and Gschneidner et al. (1983). Structural properties and band strucure are discussed by Jarlborg et al. (1983); details of crystal growth are given by Kletowski (1983).

The two ternary phases $CeCu_{1.6}Si_{1.4}$ and $CeCuSi_2$ were observed to crystallize in the same space group Cmcm with occupation of the same crystallographic sites. However, according to the phase equilibria at $600\,°C$ in fig. 4, these compounds are separated by a two-phase field $CeCu_2Si_2 + CeCu_{0.5}Si_{1.5}$. $CeCuSi_2$ was said to be isotypic with the crystal structure of $CeNiSi_2$ (Cmcm, $a = 4.12$, $b = 16.48$, $c = 4.16$, $H = 613(50)$ kg/mm^2). At variance with $CeCuSi_2$ with an ordered atomic arrangement, the compound $CeCu_{1.6}Si_{1.4}$ reveals a statistical occupation of Cu and Si atoms in equipoints 4c) of Cmcm ($a = 4.16$, $b = 17.21$, $c = 4.17$, X-ray powder and single-crystal data; $H = 464(50)$ kg/mm^2); Ce in 4c) $0, y = 0.109, \frac{1}{4}$; Cu in 4c) $y = 0.748$ and Cu + Si in 4c) $y = 0.462$; Si in 4c) $y = 0.322$; $\rho_{exp} = 6.41$, $\rho_x = 6.47$ kg/dm^3; $R = 0.177$ (Bodak et al., 1971).

A similar situation was met for the two phases with compositions $CeCu_{1.19-1.10}Si_{0.81-0.90}$ ($a = 4.231-4.238$, $c = 3.989-4.030$; $H = 446(50)$ kg/mm^2) and

TABLE 1

Superconducting transition temperatures T_c (midpoint; 10% and 90% of the transition in parentheses) and lattice parameters.

Nominal composition	T_c (K) 50% (90% ~ 10%)	Lattice parameters	
		a (Å)	c (Å)
$Ce_{18.7}Cu_{44}Si_{37.3}$	0.63 (0.65 ~ 0.58)	4.1034(4)	9.925(1)
$Ce_{19.3}Cu_{42}Si_{38.7}$	0.67 (0.68 ~ 0.60)	4.1012(3)	9.925(1)
$Ce_{19.7}Cu_{41}Si_{39.3}$	0.67 (0.68 ~ 0.60)	4.1003(3)	9.920(1)
$Ce_{20}Cu_{40}Si_{40}$	0.54 (0.58 ~ 0.44)	4.1004(7)	9.925(3)
$Ce_{20.3}Cu_{39}Si_{40.7}$	< 0.07	4.1014(5)	9.923(1)
$Ce_{20.7}Cu_{38}Si_{41.3}$	< 0.07	4.1026(8)	9.923(3)
$Ce_{20}Cu_{38.5}Si_{41.5}$	< 0.07	4.1053(8)	9.934(3)
$Ce_{20}Cu_{39.25}Si_{40.75}$	0.22 (0.325 ~ 0.1)	4.1016(6)	9.924(2)
$Ce_{20}Cu_{39.75}Si_{40.25}$	0.25 (0.325 ~ 0.1)	4.1010(4)	9.924(2)
$Ce_{20}Cu_{40.25}Si_{39.75}$	0.66 (0.675 ~ 0.58)	4.1017(8)	9.923(3)
$Ce_{20}Cu_{40.75}Si_{39.25}$	0.64 (0.675 ~ 0.58)	4.1010(6)	9.918(2)
$Ce_{20}Cu_{42.5}Si_{37.5}$	0.23 (0.33 ~ 0.14)	4.1106(5)	9.895(2)
$Ce_{20.7}Cu_{41.3}Si_{38}$	0.24 (0.39 ~ 0.1)	4.1132(4)	9.891(2)
$Ce_{19.3}Cu_{38.7}Si_{42}$	0.29 (0.37–0.1)	4.1013(4)	9.923(2)
$Ce_{18}Cu_{41}SI_{41}$	0.13 (0.22 ~ 0.07)	4.1026(4)	9.924(2)
$Ce_{22.8}Cu_{38.6}Si_{38.6}$	0.45 (0.5 ~ 0.39)	4.1062(4)	9.911(2)

$CeCu_{0.76-0.44}Si_{1.24-1.56}$ ($a = 4.103-4.070$, $c = 4.244-4.291$; $H = 634(50)$ kg/mm^2). Both phases were claimed to crystallize with the AlB_2-type and both compounds exhibit a homogeneous range, but according to fig. 4 they are separated by a common two-phase field. The existence of the wide-spread occurrence of AlB_2-type phases explains much of the discrepancies among the lattice parameters of earlier investigations. Thus Raman (1967), without giving further details, listed X-ray powder data for a "Cu-rich $CeCu_{0.5}Si_{1.5}$" [$a = 4.136(5)$, $c = 4.237(5)$], as well as a "Si-rich $CeCu_{0.5}Si_{1.5}$" [$a = 4.065(5)$, $c = 4.302(5)$]; lattice parameters were also given for a $CeCu_{1.5}Si_{0.5}$ with AlB_2-type [$a = 4.238(5)$, $c = 4.030(5)$; all samples were arc melted]. Similarly Gladyshevskij and Bodak (1965) reported $a = 4.077(2)$, $c = 4.314(3)$ for the alloy $CeCu_{0.5}Si_{1.5}$. Furthermore, Rieger and Parthé (1969a) measured $a = 4.075$, $c = 4.280$ for an alloy $CeCu_{0.67}Si_{1.33}$ and $a = 4.124$, $c = 4.214$ for CeCuSi (X-ray powder data of arc-melted alloys). Considering the data obtained by Raman (1967) and by Rieger and Parthé (1969a) a wider homogeneous region or even a closing of the miscibility gap at high temperatures seems conceivable. Magnetic susceptibility data as presented by Kido et al. (1983) for an alloy CeCuSi prepared by powder metallurgical reaction at 800–900 °C for 7 d in evacuated silica tubes revealed a Curie–Weiss behavior in good agreement with trivalent Ce ions (AlB_2-type, $\mu_{eff} = 3 \mu_B$, $\theta_p = -30$ K, temperature range 77–300 K, no magnetic moment was assumed on the Cu atoms).

Quite recently Iandelli (1983) observed the existence of a compound CeCuSi with the ordered Ni_2In-type [superstructure of the AlB_2-type, $P6_3/mmc$, $a = 4.239(2)$, $c = 7.980(4)$]. The superstructure reflections were said to be very faint and were observed in the X-ray patterns of arc-melted samples after annealing at 750 °C for

8–12 d. With respect to the data obtained by Rieger and Parthé (1969a), Gladyshevskij and Bodak (1965), and Raman (1967) on arc-melted alloys, the Ni_2In-type phase was concluded to be a low-temperature modification. No thermal analysis has been carried out yet; however, the corresponding c/a ratio obtained by Bodak et al. (1974) for the phase range $CeCu_{1.19-1.10}Si_{0.81-0.90}$ seems to be indicative for a Ni_2In-type lattice geometry.

From DTA measurements Ishikawa et al. (1983) reported a congruent melting behavior for the compound $CeCu_{0.5}Si_{1.5}$ with a melting temperature of $1785 \pm 15\,^\circ C$. $CeSi_{1.8}Cu_{0.2}$ (α-$ThSi_2$-type) orders ferromagnetically at $T_m = 6.5$ K (Ishikawa et al., 1983).

References

Aarts, J., F.R. de Boer and D.E. MacLaughlin, 1983, Physica **121B**, 162.
Aliev, F.G., N.B. Brandt, E.M. Levin, V.V. Moshchalkov, S.M. Chudinov and R.I. Yasnitskii, 1982, Sov. Phys. Solid State **24**(1), 164.
Aliev, F.G., N.B. Brandt, V.V. Moshchalkov and S.N. Chudinov, 1983, Solid State Commun. **45**(3), 215 and **47**(9), 693.
Bodak, O.I. and E.I. Gladyshevskij, 1970, Nekot. Vop. Khim. Fiz. Poluprop. Slozhn. Sostava, p. 105.
Bodak, O.I., E.I. Gladyshevskij and P.I. Kripyakevich, 1966, Izv. Akad. Nauk SSSR, Neorg. Mater. **2**, 2151.
Bodak, O.I., E.I. Gladyshevskij and Ya.M. Kalychak, 1971, Tesizy Dokl. Tret. Vses. Konf. Kristallokhim. Intermet. Soedin (Lvov) p. 40.
Bodak, O.I., Ya.M. Kalychak and E.I. Gladyshevskij, 1974, Izv. Akad. Nauk SSSR, Neorg. Mater. **10**(3), 450.
Bredl, C.D., H. Spille, U. Rauchschwalbe, W. Lieke, F. Steglich, G. Cordier, W. Assmus, M. Herrmann and J. Aarts, 1983, J. Magn. Magn. Mater. **31–34**, 373.
Franz, W., A. Griessel, F. Steglich and D. Wohlleben, 1978, Z. Phys. **B31**, 7.
Gladyshevskij, E.I. and O.I. Bodak, 1965, Dopov. Akad. Nauk Ukr. RSR, Ser. A **5**, 601.
Gschneidner Jr., K.A. and M.E. Verkade, 1974, Selected Cerium Phase Diagrams Document IS-RIC-7, Iowa State University, Ames, IA, USA, p. 18.
Hansen, M. and K. Anderko, 1958, Constitution of Binary Alloys (McGraw-Hill, New York) p. 629.
Iandelli, A., 1983, J. Less-Common Metals **90**, 121.
Ishikawa, M., H.F. Braun and J.L. Jorda, 1983, Phys. Rev. **B27**(5), 3092.
Jarlborg, T., H.F. Braun and M. Peter, 1983, Z. Phys. **B52**, 295.
Kido, H., T. Hoshikawa, M. Shimada and M. Koizumi, 1983, Phys. Stat. Sol. (a) **77**, K121.
Kletowski, Z., 1983, J. Less-Common Metals **95**, 127.
Levin, E.M., R.V. Lutsiv, L.D. Finkelstein, N.D. Samsonova and R.I. Yasnitskii, 1981, Fiz. Tverd. Tela **23**(8), 2401.
Lieke, W., U. Rauchschwalbe, C.D. Bredl, F. Steglich, J. Aarts and F.R. de Boer, 1982, J. Appl. Phys. **53**(3), 2111; see also 1984, Phys. Rev. Lett. **52**(6), 469.
Padalia, B.D., T.K. Hatwar and M.N. Ghatikar, 1983, J. Phys. **C16**, 1537.
Raman, A., 1967, Naturwiss. **54**, 560.
Rieger, W. and E. Parthé, 1969a, Monatsh. Chem. **100**, 439.
Rieger, W. and E. Parthé, 1969b, Monatsh. Chem. **100**, 444.
Sales, B.C. and R. Viswanathan, 1976, J. Low Temp. Phys. **23**(3,4), 449.
Sampathkumaran, E.V., L.C. Gupta and R. Vijayaraghavan, 1979, J. Phys. **C12**, 4323.
Schneider, H., Z. Kletowski, F. Oster and D. Wohlleben, 1983, Solid State Commun. **48**(12), 1093.
Steglich, F., J. Aarts, C.D. Bredl, W. Lieke, D. Meschede, W. Franz and H. Schäffer, 1979, Phys. Rev. Lett. **43**, 1892; see also 1981, Phys. Rev. **B23**, 3171.
Stewart, G.R., Z. Fisk and J.O. Willis, 1983, Phys. Rev. **B28**, 172.
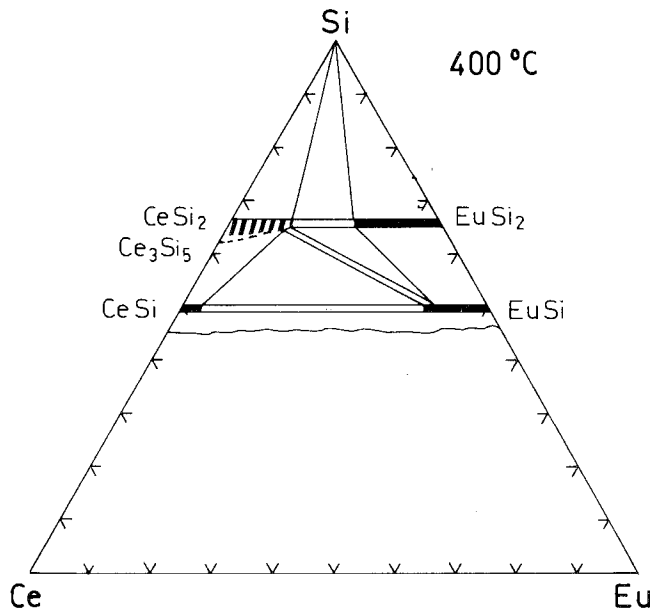
Fig. 6. Ce–Eu–Si, partial isothermal section at 400 °C (50–100 a/o Si).

Ce–Eu–Si

A partial isothermal section of the system Ce–Eu–Si at 400 °C has been derived by Mokra (1979) by means of X-ray powder analysis of 44 alloy specimens. Samples were prepared from 99.81% Eu, 99.56% Ce, and 99.99% Si by arc melting and were subsequently annealed at 400 °C for 350 h in evacuated silica tubes. No ternary compounds were formed. The mutual solid solubilities of mono- and disilicides were derived from the variation of the lattice parameters: only small amounts of EuSi were soluble in CeSi (FeB-type, Pnma, $a = 8.302$, $b = 3.962$, $c = 5.964$), whereas about 20 mole% of CeSi dissolved in EuSi (CrB-type, Cmcm, $a = 4.70$, $b = 11.15$, $c = 3.99$), linearly changing its unit cell dimensions to $a = 4.66$, $b = 11.10$, $c = 3.95$ at $Eu_{0.8}Ce_{0.2}Si$ (as read from a small diagram). In spite of the fact that both $CeSi_2$ ($a = 4.20$, $c = 13.90$) and $EuSi_2$ ($a = 4.31$, $c = 13.68$) crystallize with the $ThSi_2$-type ($I4_1/amd$), the $Ce_xEu_{1-x}Si_2$ solid solution exhibits a two-phase region (miscibility gap) extending at 400 °C from $Ce_{0.72}Eu_{0.28}Si_2$ ($a = 4.23$, $c = 13.81$) to $Ce_{0.4}Eu_{0.4}Si_2$ ($a = 4.30$, $c = 13.60$). The binary compound Ce_3Si_5 with $GdSi_2$-type (Imma) was included in the phase equilibria of the disilicide region by Mokra (1979) (fig. 6) and obviously a continuous transition was proposed from the orthorhombic α-$GdSi_2$-type solution $(Ce,Eu)_3Si_5$ to the tetragonal α-$ThSi_2$-type solution $(Ce,Eu)Si_2$ phase (no discontinuities of lattice parameters observed?). A more detailed reinvestigation of these complicated phase relations in fig. 6 will be necessary. The dashed area in fig. 6 represents the region of the α-$ThSi_2$-type.

Reference
Mokra, I.R., 1979, Vestn. Lvov Univ., Ser. Khim. **21**, 52.

TABLE 2

Formation and structural data of ternary compounds Ce–Fe–Si.

Compound	Structure type Space group	Lattice parameters Density	Preparation, Characterization	Refs.	Purity
CeFeSi [*]	PbFCl P4/nmm	$a = 4.062(3)$ $c = 6.752(5)$ $\rho_E = 6.54$ $\rho_x = 6.64$	arc, Qu, 800 °C, 250 h single crystal data $H = 256\ (\pm 50)\ kg/mm^2$	BoGK, 70b BoGKC, 70a	Ce 99.56 Fe 99.96 Si 99.99
			$T_M(\text{ferro}) \sim 470\ K$	BoGLL, 77	Ce 99.91 Fe 99.90 Si 99.99
CeFe$_2$Si$_2$	ThCr$_2$Si$_2$ I4/mmm	$a = 3.991(1)$ $c = 9.881(5)$	arc, Qu 800 °C, 250 h, PXD $H = 657\ (\pm 50)\ kg/mm^2$	BoGKC, 70a	Ce 99.56 Fe 99.96 Si 99.99
		$a = 3.986(10)$ $c = 9.871(10)$ $\rho_x = 6.52$	arc(Ar) PXD	BoGK, 66	Ce 99.56 Fe 99.9 Si 99.99
			$T_M (\text{ferro}) \sim 700\ K$	BoGLL, 77	Ce 99.91 Fe 99.90 Si 99.99
		$a = 3.995(6)$ $c = 9.876(10)$ $\rho_x = 6.49$	arc(Ar), Qu, 900 °C, 100 h, PXD	RiP, 69	high purity
CeFeSi$_2$	CeNiSi$_2$ Cmcm	$a = 4.094(3)$ $b = 16.854(10)$ $c = 4.031(3)$	arc, Qu 800 °C, 250 h, PXD $H = 707\ (\pm 50)\ kg/mm^2$	BoGKC, 70a	Ce 99.56 Fe 99.96 Si 99.99
			$\mu_{eff}^{para} = 2.94\ \mu_B;\ \theta_p = -110\ K$	BoGLL, 77	Ce 99.91 Fe 99.90 Si 99.99
Ce$_2$FeSi$_3$	AlB$_2$ P6/mmm	$a = 4.065(2)$ $c = 4.191(2)$	arc, Qu 800 °C, 250 h, PXD $H = 762\ (\pm 50)\ kg/mm^2$	BoGKC, 70a	Ce 99.56 Fe 99.96 Si 99.99
		$a = 4.068(2)$ $c = 4.140(5)$	arc, Qu PXD	GlB, 65	Ce 98.9 Fe 99.9 Si 99.9
			$\mu_{eff}^{para} = 3.2\ \mu_B;\ \theta_p = -315$	BoGLL, 77	Ce 99.91 Fe 99.90 Si 99.99
		$a = 4.058$ $c = 4.265$ for CeFe$_{0.4}$Si$_{1.6}$	induction melting Ar, Al$_2$O$_3$ crucible, 1500 °C, Qu, 700–800 °C 24–96 h, PXD	MaT, 69	Ce 99.9 Fe 99.95 Si 99.99

[*] The crystal structure of CeFeSi has been refined from X-ray single crystal photographs (Bodak et al., 1970b), $R = 0.135$. Atom parameters were Ce in 2c) 1/4, 1/4, 0.672(1); Si in 2c) $z = 0.175(2)$; Fe in 2a) 3/4, 1/4, 0. From unit cell dimensions Ce was indicated to be mainly tetravalent.

Ce–Fe–Si

Phase equilibria in the system Ce–Fe–Si were determined by Bodak et al. (1970a) in two partial isothermal sections, at 800°C for the region 0–33 a/o Ce, and at 400°C for the region 33–100 a/o Ce, by means of X-ray and metallographic analysis of 125 alloys. Samples were prepared by arc melting under argon and subsequent annealing in evacuated silica tubes (400°C, 500 h; 800°C, 250 h). Samples were also studied in as-cast condition, and those around the composition CeFe$_7$ were also annealed for 50 h at 1000°C; finally the allows were quenched in water. Etching was possible with aqueous solutions of HNO$_3$, HF and glycerin. Microhardness was determined at a load of 100 g. Starting materials were Ce 99.56%, Fe 99.96% and Si 99.99%.

The Ce–Fe binary system is in good agreement with a recent compilation of binary Ce systems by Gschneidner and Verkade (1974). Only two phases exist at 800°C: CeFe$_2$ with the MgCu$_2$-type and α-Ce$_2$Fe$_{17}$ at 84.5–88.5 a/o Fe with a defect Th$_2$Zn$_{17}$-type, corresponding to an approximate formula of CeFe$_7$. The binary Ce and Fe silicides were discussed in contect with the ternary systems Ce–Ni–Si and Y–Fe–Si, respectively. Four ternary compounds were found to exist; their crystallographic data are listed in table 2.

Solid solubilities were found to extend in the direction of a Fe/Si exchange at a fixed Ce concentration. Solubility limits were determined from the variation of unit cell dimensions. Data have been presented for the Fe solubility in CeSi$_2$ (ThSi$_2$-type,
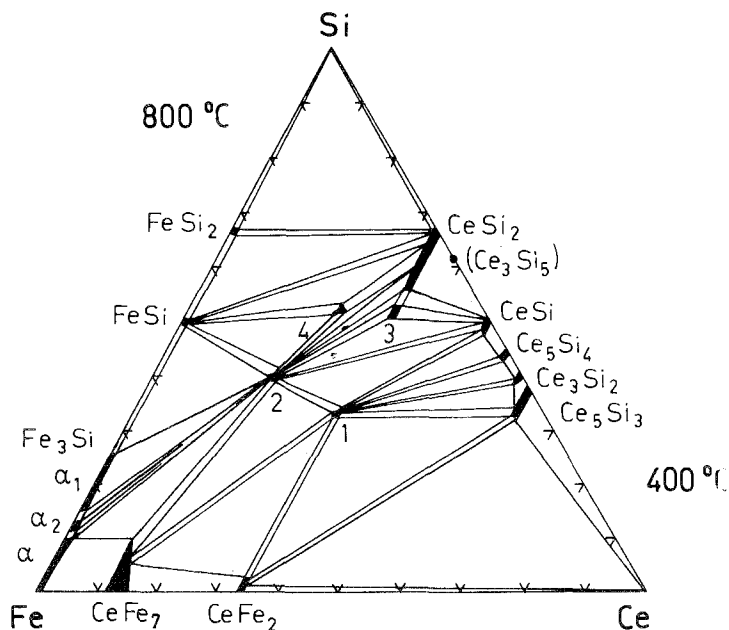

Fig. 7. Ce–Fe–Si, partial isothermal sections at 800°C (0–33 a/o Ce) and at 400°C (33–100 a/o Ce). 1: CeFeSi, 2: CeFe$_2$Si$_2$, 3: Ce(Fe$_{0.25}$Si$_{0.75}$)$_2$, 4: CeFeSi$_2$.

$a \sim 4.19$, $c \sim 13.83$, maximum solubility at 12 a/o Fe, $a \sim 4.12$, $c \sim 14.25$) and for the Si solubility in $CeFe_7$ (defect Th_2Zn_{17}-type $a \sim 8.48$, $c \sim 12.40$, maximum solubility at 10 a/o Si, $a \sim 8.45$, $c \sim 12.43$); values were read from a small diagram.

Mayer and Tassa (1969) investigated the concentration section $CeFe_xSi_{2-x}$ at 700–800 °C. For $x < 0.4$ the $ThSi_2$-type of structure was observed. $CeFe_{0.4}Si_{1.6}$ crystallizes with the AlB_2-type of structure in good agreement with the findings by Gladyshevskij and Bodak (1965). In analogy to the X-ray powder data obtained from $NdFe_{0.4}Si_{1.6}$ a statistical distribution of Fe, Si atoms in 2d was assumed. For lattice parameters and sample preparation see table 2.

Earlier structural information on $CeFe_2Si_2$ (Bodak et al., 1966) and $Ce(Fe,Si)_2$ (Gladyshevskij and Bodak, 1965) were confirmed, and are consistent with more recent findings by Rieger and Parthé (1969), Bodak et al. (1977) and Umarji et al. (1983) (see table 2). Physical properties have been reported by various authors, e.g. Levin et al. (1977) (Mössbauer data for CeFeSi and $CeFe_2Si_2$), Koterlin et al. (1980), Koterlin (1981) (band structure calculation for $CeFe_2Si_2$). More recent Mössbauer data by Umarji et al. (1983) confirmed only one type of Fe atoms in the structure, without magnetic moment. Furthermore the weak paramagnetic behavior indicates a tetravalent state of Ce (0.03 μ_B per $CeFe_2Si_2$ at 4.2 K and 18 kG).

Phase equilibria in fig. 7 are primarily based on the work of Bodak et al. (1970a). The Fe–Si-rich area was slightly modified in agreement with a recent critical assessment of the binary Fe–Si system by Schürmann and Hensgen (1980).

References

Bodak, O.I., E.I. Gladyshevskij and P.I. Kripyakevich, 1966, Izv. Akad. Nauk SSSR, Neorg. Mater. 2(12), 2151.

Bodak, O.I., E.I. Gladyshevskij, A.V. Kardash and E.E. Cherkashin, 1970a, Izv. Akad. Nauk SSSR, Neorg. Mater. 6(6), 1069.

Bodak, O.I., E.I. Gladyshevskij and P.I. Kripyakevich, 1970b, Zh. Strukt. Khimii 11(2), 305.

Bodak, O.I., E.I. Gladyshevskij, E.M. Levin and R.V. Lutsiv, 1977, Dopov. Akad. Nauk Ukr. RSR, Ser. A 12, 1129 and 1980, A2, 82.

Gladyshevskij, E.I. and O.I. Bodak, 1965, Dopov. Akad. Nauk Ukr, RSR, Ser. A 5, 601.

Gschneidner Jr., K.A. and M.E. Verkade, 1974, Selected Cerium Phase Diagrams, Document IS-RIC-7, Iowa State Univ., Ames, IA, USA, p. 20.

Koterlin, M.D., 1981, Dopov. Akad. Nauk Ukr. RSR, Ser. A 5, 71.

Koterlin, M.D., I.D. Shcherba, R.V. Lutsiv and R.I. Yasnitzkii, 1980, Ukr. Fiz. Zh. 25(2), 197.

Levin, E.M., R.V. Lutsiv, G.V. Popov and S.I. Yushchuk, 1977, Pisma Zh. Eksp. Teor. Fiz. 26(11), 740, and 1981, Fiz. Tverd. Tela 23(8), 2401.

Mayer, I. and M. Tassa, 1969, J. Less-Common Metals 19, 173.

Rieger, W. and E. Parthé, 1969, Monatsh. Chem. 100, 444.

Schürmann, E. and U. Hensgen, 1980, Archiv f. Eisenhüttenwesen 51(1), 1.

Umarji, A.M., D.R. Noakes, P.J. Viccaro, G.K. Shenoy, A.T. Aldred and D. Niarchos, 1983, J. Magn. Magn. Mater. 36, 61; see also 39, 309.

Ce–Ga–Si

No tertary phase diagram exists for the Ce–Ga–Si system. Some data concerning the mutual solid solubilities along the section $CeGa_2$–$CeSi_2$ were derived by Dzyana (1969) from an X-ray powder analysis of 19 samples annealed at 400 °C; the homogeneous regions obtained were as follows: $CeSi_{2-1.15}Ga_{0-0.85}$ (α-$ThSi_2$-type,

$a = 4.194\text{--}4.248$, $c = 13.90\text{--}14.49$) and $\text{CeGa}_{2-1.5}\text{Si}_{0-0.5}$ (AlB_2-type, $a = 4.314\text{--}4.224$, $c = 4.329\text{--}4.331$).

Reference

Dzyana, D.M., 1969, Autoreferat Dis. Kand. Khim. (abstract of thesis, Russian) (Nauk, Lvov) 16 p.

Ce–Gd–Si

The phase equilibria in the ternary system Ce–Gd–Si have been established by Mokra (1979) by means of X-ray and metallographic analysis of 105 alloys prepared by arc melting and subsequent annealing in evacuated silica capsules for 800 h at 600 °C. The samples were finally quenched in water. Starting materials were Ce 99.56%, Gd 99.85% and Si 99.99%.

The binary silicide systems Ce–Si and Gd–Si are discussed in context with the ternary systems Ce–Ni–Si and Gd–Fe–Si. Phase relations and solid solubility ranges in the Ce–Gd binary are in essential agreement with a recent critical assessment by Gschneidner and Calderwood (1982); Ce_3Gd_7 crystallizes with the Sm-type. The solubility of Si in the Ce–Gd intermetallic system was observed to be small (less than 1 a/o Si ?), whereas the mutual solid solubility of Ce and Gd silicides is rather large and a complete solid solution is observed for $\text{Ce}_{1-x}\text{Gd}_x\text{Si}$ with the FeB-type (Pnma). The solubility limits were reported to be the following: $\text{Ce}_{5-x}\text{Gd}_x\text{Si}_3$ (Cr_5B_3-type, $x \leqslant 1.76$), $\text{Ce}_x\text{Gd}_{5-x}\text{Si}_3$ (Mn_5Si_3-type, $x \leqslant 1.68$); $\text{Ce}_{3-x}\text{Gd}_x\text{Si}_2$ (U_3Si_2-type, $x \leqslant 0.9$); $\text{Ce}_{5-x}\text{Gd}_x\text{Si}_4$ (Zr_5Si_4-type, $x \leqslant 2.07$);
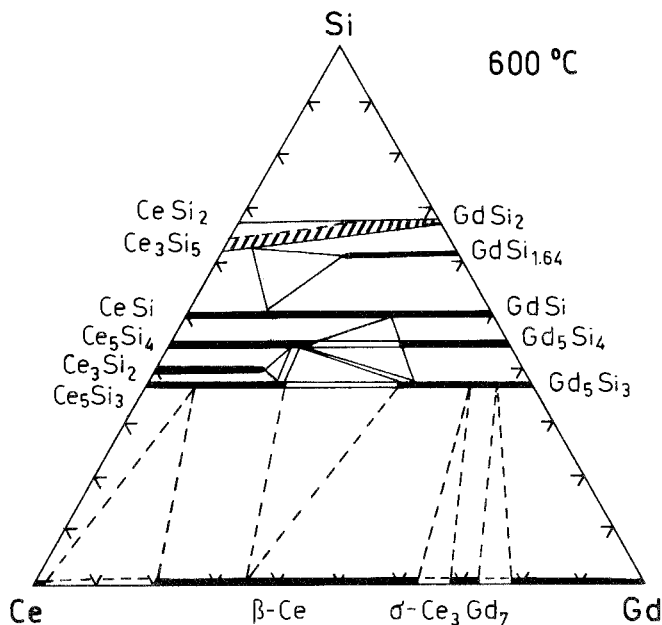

Fig. 8. Ce–Gd–Si, isothermal section at 600 °C; the dashed area represents the field of the α-GdSi_2-type structure.

$Ce_xGd_{5-x}Si_4$ (Gd_5Si_4-type, $x \leqslant 1.71$) and $Ce_xGd_{2-x}Si_3$ (defect AlB_2-type, $x \leqslant 0.9$). for the silicon-rich disilicide region $Ce_{1-x}Gd_xSi_2$ obviously a continuous transition from the tetragonal α-$ThSi_2$-type ($CeSi_2$) to the orthorhombic α-$GdSi_2$-type was claimed to be accompanied by the Ce/Gd substitution around $x \sim 0.5$. A similar situation is found between the silicon-rich α-$ThSi_2$-type and the cerium-rich α-$GdSi_2$-type solution. Consequently $Ce_{1-x}Gd_xSi_{2-y}$, appears to be a complete solid solution at the silicon-poor phase boundary with the α-$GdSi_2$-type. The α-$GdSi_2$-type region is represented by the dashed area in fig. 8.

References
Gschneidner Jr., K.A. and F.W. Calderwood, 1982, Bull. Alloy Phase Diagrams 3(2), 185.
Mokra, I.R., 1979, Autoreferat Dis. Kand. Khim. (abstract of thesis, Russian) (Nauk, Lvov) 22 p.

Ce–Ge–Si

Data on phase equilibria of the system Ce–Ge–Si have been collected by different authors in different regions of the ternary system. An isothermal section at $900\,°C$ was presented by Haschke et al. (1966). Samples were prepared by the powder-metallurgical method of reacting cold-pressed pellets in evacuated silica tubes for 50 to 100 h at $900\,°C$. Starting materials were filings of 99.5% pure Ce (containing 0.25% O), and Si 99.7%; Ge (pure, but no details). No reaction with the quartz walls was observed, but due to the low melting point of Ce ($795\,°C$), Ce-rich alloys with a Ce content higher than 65 a/o Ce were found to be molten.

Haschke et al. (1966) failed to observe $CeSi_{2-x}$ with the $GdSi_2$-type of structure at $900\,°C$. Phase equilibria were characterized by a series of extended solid solutions. Ce_5Si_3 (Cr_5B_3-type, $a = 7.89$, $c = 13.77$) was said to dissolve 60 mole% Ce_5Ge_3 with a linear change of lattice parameters to $a = 7.94$, $c = 13.83$, whereas about 27 mole% Ce_5Si_3 is soluble in Ce_5Ge_3 with the Mn_5Si_3-type ($a = 8.870$, $c = 6.588$), changing its parameter to $a = 8.85$, $c = 6.56$. Both phase solutions are separated by a narrow two-phase field. A rather limited solid solubility appears for the two cerium silicides Ce_3Si_2 (U_3Si_2-type, dissolving ~ 7 a/o Ge) and Ce_5Si_4 (Zr_5Si_4-type, dissolving ~ 10 a/o Ge). In a more recent compilation of rare-earth–germanium phase diagram data Eremenko et al. (1975) determined the stability range of Ce_4Ge_3 (Th_3P_4-type), Ce_5Ge_4 (Sm_5Ge_4-type) and "Ce_3Ge". At variance with Eremenko these new germanides were not observed by Haschke et al. (1966) and due to the lack in knowledge of the Si solubility in these compounds, they show as dots in the Ce–Ge binary and are not incorporated in the phase equilibria of fig. 9. $CeGe_{1-x}Si_x$ formed a continuous solid solution with the FeB-type structure. Lattice parameters were shown to vary monotonically from $a = 8.337$, $b = 4.061$, $c = 6.046$ (CeGe) to $a = 8.301$, $b = 3.957$, $c = 5.975$ for CeSi (recorded in a graph by Haschke et al., 1966).

Due to the polymorphic transformation of the α-$ThSi_2$- and $GdSi_2$-type as a function of temperature and concentration, the phase relations in the disilicide and digermanide region are rather complex. The diverging results obtained by Haschke et al. (1966), Mayer and Eshdat (1968), Muratova and Bodak (1974) and Bodak and Muratova (1979) are the expression of this complicated matter. Basic agreement however exists about the formation of a continuous solid solution $CeGe_{2-x}Si_x$. In
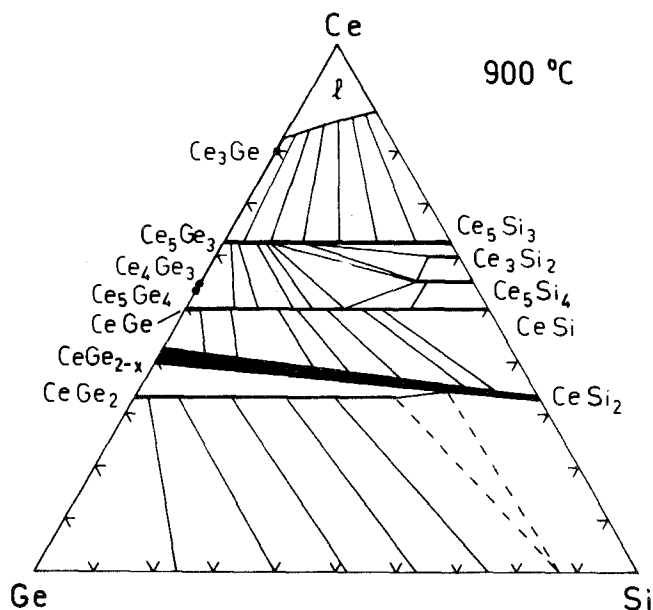
Fig. 9. Ce–Ge–Si, isothermal section at 900 °C; see text for discussion.

good agreement with the binary phase relations as shown by Eremenko et al. (1975), a ThSi$_2$-type of structure was reported by Haschke et al. (1966) for the solid solution CeGe$_{2-x}$ (or more recently called Ce$_3$Ge$_5$)–CeSi$_2$. Lattice parameters change practically linearly from Ce$_3$Ge$_5$ ($a = 4.205$, $c = 14.24$) to CeSi$_2$ ($a = 4.190$, $c = 13.930$).

Haschke et al. (1966) furthermore claimed the existence of a compound CeGe$_2$ at the stoichiometric composition and isostructural with the GdSi$_2$-type; CeGe$_2$ was said to be separated from nonstoichiometric CeGe$_{2-x}$ (α-Ce$_3$Ge$_5$) by a two-phase field. These findings are at variance with Eremenko et al. (1975) but correspond to Mayer and Eshdat (1968) (see below), despite the fact that smaller lattice parameters were reported by Mayer and Eshdat (1968) for CeGe$_2$. Furthermore an extended and stoichiometric solid solution CeGe$_{2-x}$Si$_x$ was claimed (Haschke) to proceed into the ternary up to a composition with $x \leqslant 1.30$, ending at the vertex of a narrow three-phase field: CeGe$_{2-x}$Si$_x$ + Ce(Ge,Si)$_{2-x}$ + (Ge,Si).

Mayer and Eshdat (1968) independently investigated the structural behavior in the pseudobinary system CeGe$_{2-x}$Si$_x$ by means of X-ray powder data. For sample preparation, see NdGe$_{2-x}$Si$_x$. Ge-rich alloys were said to adopt the GdSi$_2$-type (Imma) and furthermore a continuous transformation into the tetragonal ThSi$_2$-type of structure (I4$_1$/amd) was proposed for alloys richer in Si. The variation of the lattice parameters versus x is shown in fig. 10, the linear variation of the unit cell volume in fig. 11. Both functions are similar to those reported by Haschke, but no discontinuities were recorded and no three-phase or two-phase equilibria involving two separate phase solutions were observed. See also the discussion for NdGe$_{2-x}$Si$_x$.

The Ce-poor region from 0 to 42 a/o Ce was more recently also investigated at 600 °C by Bodak and Muratova (1979) on 92 melted and homogenized alloys
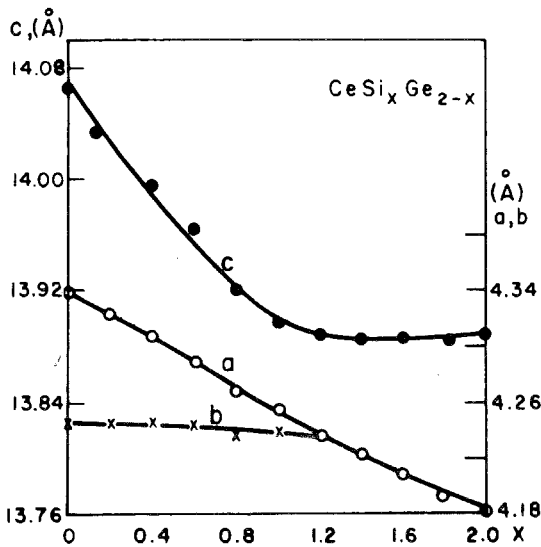
Fig. 10. Ce–Ge–Si, section $CeGe_{2-x}Si_x$, proposed lattice parameter variation versus concentration. After Mayer and Eshdat (1968).

(600 °C, 250 h) by means of X-ray and metallographic analysis. These is a basic agreement about the existence of a complete solid solution $Ce(Ge,Si)_{2-x}$ in the range of 35 to 39 a/o Ce. Samples with ~ 33 a/o Ce were two-phase: $Ce(Ge,Si)_{2-x}$ + (Ge,Si). At variance with Eremenko but in agreement with Haschke et al. (1966) (data at 900 °C) the two polymorphic forms of $CeGe_2$ were found to be separated by a narrow two-phase field whereas a continuous transition was concluded between $CeSi_2$(ThSi$_2$-type) and Ce_5Si_3 (defect GdSi$_2$-type). According to Bodak's results obtained at 600 °C, the ThSi$_2$-type solution along the section $CeGe_{2-x}$–$CeSi_2$ is
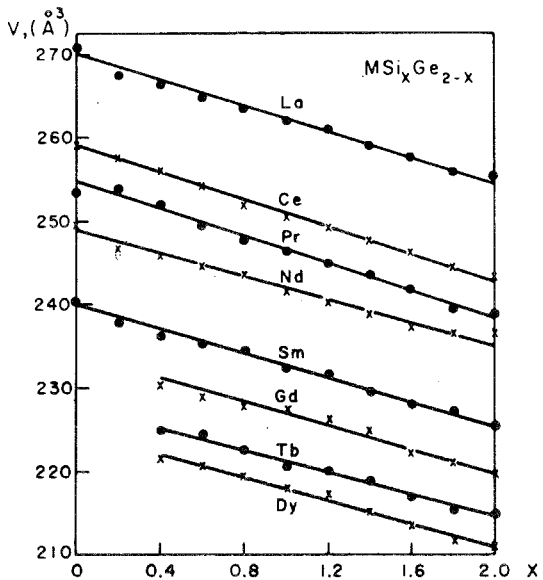
Fig. 11. R–Ge–Si, section $RGe_{2-x}Si_x$ variation of volume versus concentration; R = La,Ce,Pr,Nd,Sm,Gd,Tb,Dy. After Mayer and Eshdat (1968).

limited and a continuous transition from $CeGe_{2-x}$ ($ThSi_2$-type) to $CeSi_2$ ($ThSi_2$) was proposed via an intermediate range crystallizing with the $GdSi_2$-type of structure. In other words now at $600°C$ the solid solution along the section $CeGe_2-CeSi_{2-x}$ is proposed to be a complete one exhibiting the $GdSi_2$-type of structure with a gradual change in its amount of defects. The (Ge,Si)-rich boundary of the $ThSi_2$-type structure was claimed to be at a rather stoichiometric composition of ~ 35 a/o Ce. The maximum Si/Ge exchange in this solution was reported for 37 a/o Ge. The (Ge,Si)-poor boundary of the $Ce(Ge,Si)_{2-x}$ solid solution was shown at a Ce concentration of ~ 39 a/o Ce. Except for the immediate vicinity of the binary cerium digermanide no two-phase separation was expected to exist between the three different phase regions. The X-ray data from which the puzzling phase distribution was derived by Bodak were measured along sections at fixed Ge concentrations of 10, 20, 30, 40, 50 a/o Ge with a variable Ce content ranging from 33–42 a/o Ce; the resolution, however, is certainly not high enough to discriminate between a continuous or a discontinuous phase transformation, especially as the width of the phase fields is extremely narrow and discontinuities could not be observed.

References

Bodak, O.I. and L.A. Muratova, 1979, Vestn. Lvov Univ., Ser. Khim. **21**, 55.
Eremenko, V.N., Yu.I. Buyanov and V.G. Batalin, 1975, Sverkhtverd. Materilov i ikh Granits Razdela, in: Fiz. Khim. Kondensir. Faz. (Nauka Dumka, Kiev, USSR) p. 191.
Haschke, H., H. Nowotny and F. Benesovsky, 1966, Monatsh. Chem. **97**, 1452.
Mayer, I. and Y. Eshdat, 1968, Inorg. Chem. **9**, 1904.
Muratova, L.O. and O.I. Bodak, 1974, Tesizy Dokl. Tret. Vses. Konf. Kristallokhim. Intermet. Soedin, 2nd Ed., ed. R.M. Rykhal (Lvov Gos. Univ., Lvov, USSR) p.33.

Ce–Ir–Si

The crystal structure and magnetic behavior of $CeIr_2Si_2$ has been characterized by Hiebl et al. (1984). $CeIr_2Si_2$ is primitive tetragonal with a $BaAl_4$-derivative type similar to the $CaBe_2Ge_2$-type [$a = 4.1431(4)$ and $c = 9.8460(50)$; X-ray powder data of arc-melted alloys subsequently annealed at $1000°C$ for 48 h in evacuated silica tubes].

Reference

Hiebl, K., C. Horvath, P. Rogl and M.J. Sienko, 1984, J. Less-Common Metals, to be published.

Ce–La–Si

Magnetic susceptibilities and specific heat measurements on $CeSi_x$ ($1.55 \leqslant x \leqslant 2.00$) with the α-$ThSi_2$-type revealed the existence of a nonmagnetic–magnetic transition at $x = 1.83$. For $x \leqslant 1.80$ the system orders at $T_c \sim 10$ K and due to the large reduction of the magnetic moment of the Ce atom (0.3 μ_B) and from the magnetic entropy a ferromagnetic dense Kondo system was suggested. On Ce/La substitution in $Ce_yLa_{1-y}Si_{2.0}$ an increase was observed for both the ground state susceptibility and the coefficient of the T-linear term in the specific heat ($y = 0.2$, 0.4, 0.8 and 1.0, Yashima et al., 1983).

Reference

Yashima, H., H. Mori, N. Sato, T. Satoh and K. Kohn, 1983, J. Magn. Magn. Mater. **31–34**, 411.

Ce–Mg–Si

Zmii and Gladyshevskij (1974) presented a partial isothermal section of the system Ce–Mg–Si at 400°C. Phase equilibria as shown in fig. 12 were determined on the basis of X-ray powder and metallographic analysis of 70 alloys, which were prepared by arc melting, followed by a heat treatment in evacuated silica tubes for 100 h at 400°C. Purity of starting materials was as follows: Ce 99.99%, Mg 99.97%, Si 99.99%.

The binary compounds involved in the phase equilibria at 400°C are in agreement with a recent compilation about binary phase diagrams of Ce by Gschneidner and Verkade (1974): $CeMg_{12}$ ($CeMg_{12}$-type), Ce_5Mg_{41} ($CeMg_{8.4}$ in the original paper; Ce_5Mg_{41}-type), $CeMg_3$ (BiF_3-type); $CeSi_2$ ($ThSi_2$-type?) and Mg_2Si (CaF_2-type).

Mutual solid solubilities were observed to be small and practically no homogeneous range was observed for the three ternary compounds identified: $CeMg_2Si_2$, $CeMgSi$, $CeMg_3Si$.

$CeMgSi$ is tetragonal with space group $P4_2/nmm$ and lattice parameters $a = 7.589(5)$ and $c = 13.74(1)$. Experimental and theoretical densities compare as follows: $\rho_E = 5.43$, $\rho_x = 5.61$ kg/dm^3. The crystal structure was said to be related to α-$ThSi_2$.
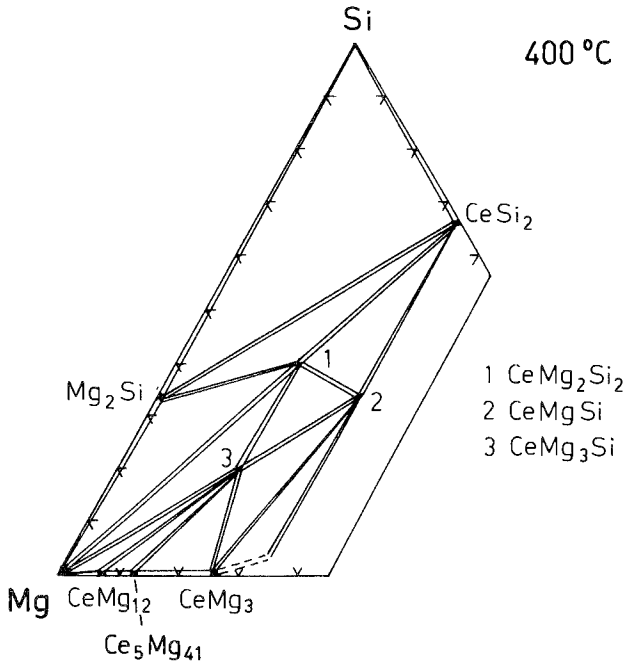

Fig. 12. Ce–Mg–Si, partial isothermal section at 400°C (0–33 a/o Ce).

Zmii and Gladyshevskij (1971) determined the crystal structure of $CeMg_2Si_2$ by means of single crystal X-ray photographs; the reliability values obtained were $R(F_{0kl}) = 0.119$ and $R(F_{1kl}) = 0.100$. A single crystal was prepared by melting a mixture (in a/o) of Ce(10)Mg(75)Si(15) in a quartz tube under Ar. The structure of $CeMg_2Si_2$ represents a new stacking variant of the $ThCr_2Si_2$-type and crystallizes in the tetragonal space group P4/mmm, a = 4.250(2), c = 5.765(2). Refinement of the X-ray powder data was as good as $R = 0.133$; accordingly the atomic parameters are Ce in 1a); Mg in 2e); Si and 2h) 1/2, 1/2, 0.223; $\rho_E = 3.83$, $\rho_x = 3.93$ kg/dm³.

The crystal structure of $CeMg_3Si$ has not yet been determined (tetragonal, $c/a = 1.8$).

References

Gschneidner Jr., K.A. and M.E. Verkade, 1974, Selected Cerium Phase Diagrams, Document IS-RIC-7, Iowa State Univ., Ames, IA, USA, p. 23.
Zmii, O.F. and E.I. Gladyshevskij, 1971, Sov. Phys. Crystallogr. 15(5), 817.
Zmii, O.F. and E.I. Gladyshevskij, 1974, Visn. L'vivsk. Univ., Ser. Khim. 15, 24.

Ce–Mn–Si

Phase equilibria in the ternary system Ce–Mn–Si at 600 °C have been determined by Knigenko et al. (1977) from alloys prepared by arc melting and subsequent annealing at 600 °C for 280 h in evacuated silica tubes (X-ray powder and metallographic analysis). Starting materials were Ce 99.9%, Mn 99.56% and Si 99.99%. In agreement with a recent critical assessment of Ce phase diagrams the solubility of Mn in Ce was observed to be ∼ 1 a/o Mn at 600 °C. Practically no Ce dissolves in Mn. The binary Mn–silicides and Ce–silicides have been discussed in connection with the Y–Mn–Si and Ce–Ni–Si systems. The solid solubility of Ce in manganese silicides was small; the solubility of Mn in Ce-rich silicides was less then 5 a/o Mn at a constant Ce content (Mn/Si substitution). Ternary phase equilibria concerning the extremely wide phase region for $Ce(Mn_xSi_{1-x})_{2-y}$ are rather tentative, and a more detailed investigation will be necessary to reveal the certainly complicated phase relations involving the different disilicide and defect types with respect to the Si/Mn substitution. Two ternary compounds, $CeMn_2Si_2$ and CeMnSi, were observed with small homogeneity ranges (∼ 5 at%) in the direction of Mn/Si exchange; however, no exact determination of the homogeneity regions (lattice parameter data etc.) was presented (fig. 13).

Bodak et al. (1966) prepared $CeMn_2Si_2$ with the $ThCr_2Si_2$-type of structure (I4/mmm, $a = 3.982$, $c = 10.430$, $\rho_x = 6.15$ kg/dm³) by means of arc melting (99.56% Ce, 99.8% Mn, 99.99% Si). Siek et al. (1978) studied the crystallographic and magnetic properties of $CeMn_2Si_2$ by means of powder X-ray neutron diffraction as well as magnetometric measurements. A sample was prepared by melting in an induction furnace and subsequently annealed in an evacuated silica tube at 950 °C for 100 h and then cooled to room temperature (Ce, Mn 99.99%, Si 99.999%). Complete ordering with Mn in the 4d and Si in the 4e sites [$z = 0.372(1)$ at 78–373 K] was observed. Lattice parameters were: $a = 3.986(5)$, $c = 10.491(5)$ at 78 K; $a = 4.026(5)$, $c = 10.568(5)$ at 293 K, and $a = 4.054(5)$, $c = 10.611(5)$ at 373 K;
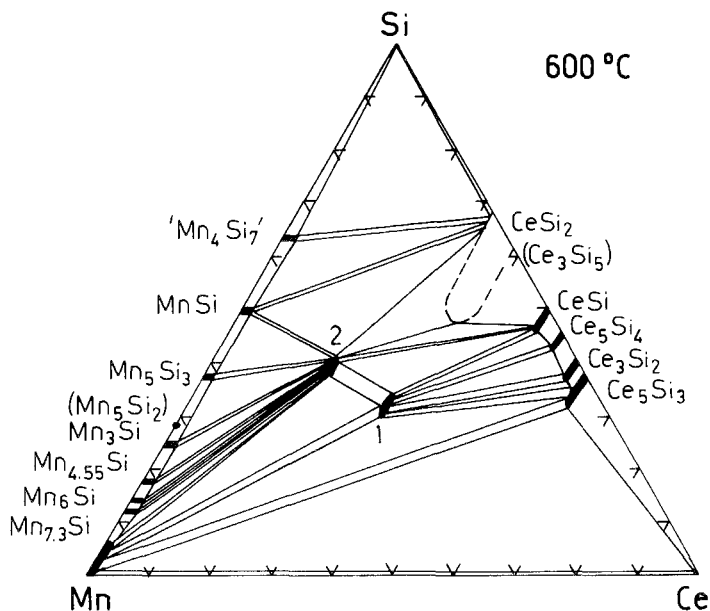
Fig. 13. Ce–Mn–Si, isothermal section at 600 ° C. 1: CeMnSi, 2: CeMn$_2$Si$_2$.

$R \sim 0.06$. At low temperatures CeMn$_2$Si$_2$ exhibits antiferromagnetic ordering with $T_N = 379(2)$ K. CeMn$_2$Si$_2$ is a collinear antiferromagnet with a $+ - + -$ sequence of ferromagnetic Mn-layers; the paramagnetic behavior is characterized by $\theta_p = 330(5)$ K and $\mu_{eff}^{para} = 3.0(1)$ μ_B mole^{-1}: the Ce ions were concluded to be tetravalent with a zero magnetic moment. Narasimhan et al. (1976) reported similar lattice parameters $a = 4.010(5)$, $c = 10.523(5)$, and confirmed the paramagnetic behavior; $T_m = 316$ K; for sample preparation, see Y–Mn–Si. Koterlin (1981) presented X-ray spectra (SiK$_\beta$, SiL$_{2,3}$) and band structure calculations.

According to X-ray powder data by Knigenko et al. (1977) the compound CeMnSi crystallizes with the PbFCl-type of structure with space group P4/nmm and lattice parameters $a = 4.130$, $c = 7.279$; for sample preparation, see YMnSi.

References

Bodak, O.I., E.I. Gladyshevskij and P.I. Krypiakevich, 1966, Izv. Akad. Nauk SSSR, Neorg. Mater. 2, 2151.
Knigenko, L.D., I.R. Mokra and O.I. Bodak, 1977, Vestn. Lvov Univ., Ser. Khim. 19, 68.
Koterlin, M.P., 1981, Dopov. Akad. Nauk Ukr. RSR, Ser. A 5, 71.
Narasimhan, K.S.V.L., V.U.S. Rao and W.E. Wallace, 1976, AIP Conf. Proc. 29, 594 and J. Appl. Phys. 46, 4957 (1975).
Siek, S., A. Szytula and J. Leciejewicz, 1978, Phys. Stat. Sol. (a) 46, K101.

Ce–Nd–Si

Phase equilibria in the ternary system Ce–Nd–Si have been determined at 600 ° C by Mokra et al. (1978) by means of powder X-ray and metallographic analysis. 115
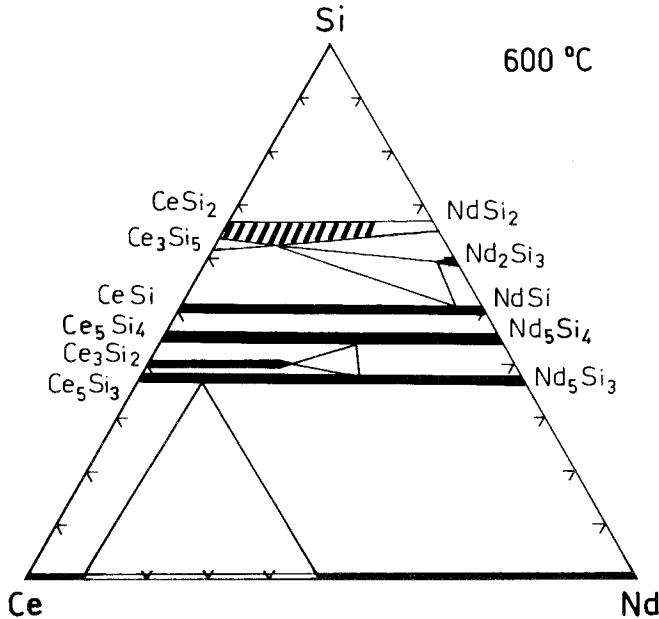
Fig. 14. Ce–Nd–Si, isothermal section at 600 °C.

alloys were prepared by arc melting compacts of 99.56% pure Ce, 99.44% Nd and 99.99% pure Si; weight losses were checked to be less than 0.5 wt%. The alloy buttons were sealed in evacuated silica tubes and heat-treated for 300 h at 600 °C. Solubilities of Si in binary Ce–Nd alloys are small, but no details were presented.

The phase equilibria in fig. 14 are characterized by a two-phase region in the Ce–Nd binary system ranging from $x_{Nd} = 0.1$ to $x_{Nd} = 0.47$ at 600 °C, and by the formation of extended solid solutions with Ce/Nd substitution: $Ce_{5-x}Nd_xSi_3$ (Cr_5B_3-type, $0 \leqslant x \leqslant 1$), $Ce_{5-x}Nd_xSi_4$ (Zr_5Si_4-type, $0 \leqslant x \leqslant 1$), $Ce_{1-x}Nd_xSi$ (FeB-type, $0 > x \leqslant 1$), $Ce_{3-x}Nd_xSi_2$ (U_3Si_2-type, $0 \leqslant x \leqslant 1.15$), $Nd_{2-x}Ce_xSi_3$ (defect AlB_2-type, $0 \leqslant x \leqslant 0.15$). For the silicon-rich disilicide region $Ce_{1-x}Nd_xSi_2$ a continuous transformation was claimed at $x \sim 0.7$ from the tetragonal α-$ThSi_2$ type ($CeSi_2$) to the orthorhombic $GdSi_2$-type ($NdSi_2$). Similarly Ce_3Si_5 with a defect $GdSi_2$-type structure was not observed as a seperate phase and again a continuous transformation was claimed between the α-$ThSi_2$ and the $GdSi_2$-type for the $CeSi_{2-x}$ binary, as well as for silicon-poor solutions $(Ce_{1-x}Nd_x)Si_{2-y}$. The region of the α-$ThSi_2$-type structure is indicated in fig. 14 by a dashed field.

Reference

Mokra, I.R., O.I. Bodak and E.I. Gladyshevskij, 1978, Dopov. Akad. Nauk Ukr. RSR, Ser. A, 1043.

Ce–Ni–Si

Phase equilibria in the system Ce–Ni–Si (fig. 15) have been studied by various authors. Bodak and Gladyshevskij (1969a,b) investigated the region 0–33 a/o Ce in

Fig. 15. Ce–Ni–Si, partial isothermal sections at 800 °C (0–33 a/o Ce) and at 400 °C (33–100 a/o Ce).
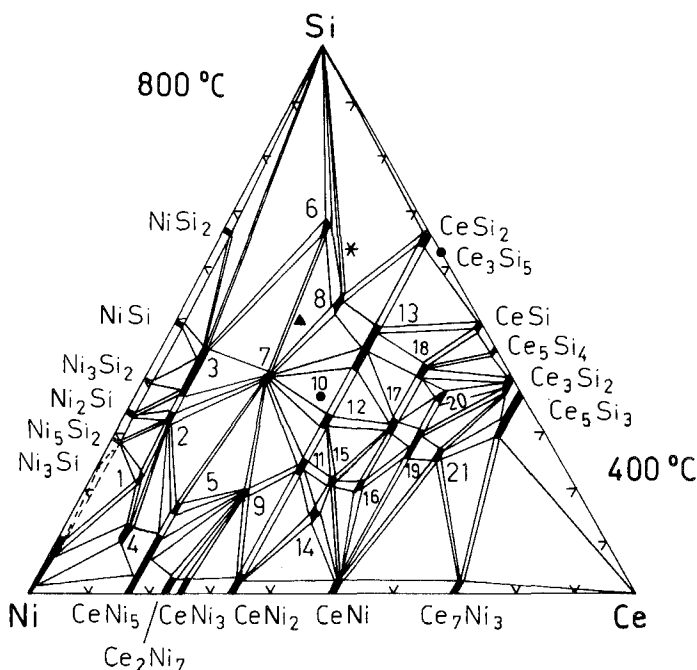1: $CeNi_{8.6}Si_{2.4}$, 2: $CeNi_{8.6-8.4}Si_{4.4-4.6}$, 3: $CeNi_{7.8-6.5}Si_{5.2-6.5}$, 4: $Ce_2Ni_{15.1-14.5}Si_{1.9-2.5}$, 5: "$CeNi_4Si$",
6: "$CeNiSi_4$" (according to a crystal structure determination a more precise formula should be
$Ce_3Ni_2Si_8$; the new location at $Ce_3Ni_2Si_8$ is marked by an asterisk), 7: $CeNi_2Si_2$, 8: $CeNiSi_2$, 9:
$Ce_3Ni_6Si_2$, 10: $Ce_6Ni_6Si_7$" (the location of this phase is uncertain, as it could not be obtained in
homogeneous form), 11: "$CeNi_{1.3}Si_{0.7}$", 12: $CeNiSi$, 13: $CeNi_{0.8-0.5}Si_{1.2-1.5}$, 14: "$Ce_4Ni_{4.5}Si_{1.5}$", 15:
"Ce_2Ni_2Si", 16: $Ce_{4.5}Ni_{3.5}Si_2$, 17: $Ce_{14}Ni_8Si_9$ (earlier "$Ce_{4.5}Ni_{2.5}Si_3$"), 18: $Ce_{15}Ni_4Si_{13}$ (earlier
"$Ce_{4.7}Ni_{1.2}Si_{4.1}$"), 19: $Ce_5Ni_2Si_3$ ("$Ce_2Ni_{0.8-1.2}Si_{1.2-0.8}$"), 20: $Ce_7Ni_2Si_5$ (earlier "$CeNi_{0.3}Si_{0.7}$"), 21:
$Ce_6Ni_2Si_3$. The location of the high-temperature phase (?) $Ce_2Ni_3Si_5$ is marked by a small filled triangle.

isothermal sections at 400 °C and 800 °C, whereas Bodak et al. (1973) and Mis'kiv
(1973) reported about the isothermal section at 400 °C in the region of 33–100 a/o
Ce. 350 alloys were prepared by arc melting under argon followed by heat treatment
at 400 °C for 240 h in evacuated silica tubes and quenching in cold water; all the
samples were investigated by means of X-ray and metallographic analysis. Alloys in
the region of 0–33 a/o Ce were first annealed at 800 °C for 250 h and after
examination reheated at 400 °C for 240 h. Weight losses during melting were less
than 0.5–1%. Starting materials were Ce 99.56%, Ni 99.91% and Si 99.99%. Etching
was possible in a mixture of aqueous solutions of HF and HNO_3 in glycerin, and
microhardness was determined at a load of 100 g. In many cases single crystals could
be isolated from the cavities of cast ingots (30–50 g). A total of 22 ternary silicides
have been characterized and are listed in table 3.

The Ce-rich part (0–12 a/o Ce) of the ternary system has been earlier investi-
gated by Bodak and Gladyshevskij (1969b) who studied the phase relationship
between the $NaZn_{13}$-type and $BaCd_{11}$-type structures (see also table 3). At variance

TABLE 3

Formation and structural data of ternary compounds Ce–Ni–Si.

Compound	Structure type Space group	Lattice parameters Density	Preparation, Characterization	Refs.	Purity
$Ce_2Ni_{15.1}Si_{1.9}-$ $Ce_2Ni_{14.5}Si_{2.5}$ [a]	$(Ce_2Co_{15}Al_2 ?)$ Th_2Ni_{17} $P6_3/mmc$	$a = 8.289(4)$ $c = 8.085(4)$ at 13 a/o Si	arc(Ar), Qu 800 °C, 250 h and 400 °, 240 h $H = 519(50)$ kg/mm^2 PXD	GlKB, 66a GlKB, 66b BoG, 69a BoMTKG, 73 GlKB, 67	Ce 99.56 Ni 99.91 Si 99.99
$Ce_4Ni_{4.5}Si_{1.5}$	orthorhombic unsolved Pbcm or Pca2$_1$ (Mi, 73)	$a = 7.50$ $b = 5.97$ $c = 29.20$	arc(Ar), Qu 400 °C, 240 h PXD $H = 420(50)$ kg/mm^2	BoMTKG, 73	Ce 99.56 Ni 99.91 Si 99.99
$CeNi_4Si$	unknown		arc(Ar), Qu 800 °C, 250 h and 400 °C, 240 h $H = 642(50)$ kg/mm^2	BoMTKG, 73	Ce 99.56 Ni 99.91 Si 99.99
$Ce_3Ni_6Si_2$ [b]	$Ce_3Ni_6Si_2$ ord. Ca_3Ag_8 Im3m	$a = 8.858(2)$ $\rho_x = 7.86$, $\rho_E = 7.82$	arc, Qu(Ni) 800 °C, 340 h 400 °C, 250 h PXD $H = 572(50)$ kg/mm^2	GlKB, 66b BoG, 69a BoMTKG, 73	Ce 99.57 Ni 99.99 Si 99.99
$CeNi_{8.6}Si_{2.4}$ [c]	$Ce_2Ni_{17}Si_5$ $BaCd_{11}$-deriv. $I4_1/amd$	$a = 9.799(5)$ $c = 6.249(10)$ $\rho_E = 7.86$, $\rho_x = 7.89$	arc, Qu 800 °C, 250 h and 400 °C, 240 h, single crystal data $H = 792(50)$ kg/mm^2 $\sigma = 60000\ \Omega^{-1}$ cm^{-1}	BoG, 69c BoG, 69a BoMTKG, 73 BoG, 70a	Ce 99.56 Ni 99.91 Si 99.99
Ce_2Ni_2Si	unknown		arc, Qu 400 °C, 240 h PXD	BoMTKG, 73	Ce 99.56 Ni 99.91 Si 99.99
$Ce_{4.5}Ni_{3.5}Si_2$ [d] $Ce_3(Ni_{0.615}$ $Si_{0.385})_4$	Ta_3B_4 Immm	$a = 4.30$ $b = 18.4$ $c = 4.10$ (Mi, 73)	arc, Qu 800 °C, 250 h and 400 °C, 250 h (PXD) $H = 383(50)$ kg/mm^2	BoMTKG, 73	Ce 99.56 Ni 99.91 Si 99.99
$CeNi_{1.3}Si_{0.7}$	unknown		arc, Qu 800 °C, 250 h and 400 °C, 240 h PXD $H = 383(50)$ kg/mm^2	BoG, 69a BoMTKG, 73	Ce 99.56 Ni 99.91 Si 99.99
$Ce_6Ni_2Si_3$	$Ce_6Ni_2Si_3$ filled Ho_4Co_3 $P6_3/m$	$a = 12.14$ $c = 4.328$	arc, Cu 400 °C, 240 h PXD $H = 420(50)$ kg/mm^2	BoMTKG-73	Ce 99.56 Ni 99.91 Si 99.99
[e]		$a = 12.112(5)$ $c = 4.323(2)$ $\rho_E = 6.23$, $\rho_x = 6.26$	arc single crystal study $R(F_{hk0}) = 0.115$	BoGK, 74	Ce 99.56 Ni 99.91 Si 99.99

TABLE 3 (continued)

Compound	Structure type Space group	Lattice parameters Density	Preparation, Characterization	Refs.	Purity
$Ce_{14}Ni_8Si_9$ "$Ce_{4.5}Ni_{2.5}Si_3$" [f]	$Ce_{14}Ni_8Si_9$ $P2_1/mm$	$a = 21.79$ $b = 16.43$ $c = 4.290$ $\gamma = 104.0$	arc, Qu 400 °C, 200–300 h single crystal data $H = 464(50)$ kg/mm^2	MiBG, 74 Mi, 73 BoMTKG, 73	Ce 99.71 Ni 99.99 Si 99.99
$Ce_5Ni_2Si_3$ "Ce_2NiSi" [g]	$Ce_5Ni_2Si_3$ filled $Rh_{20}Si_{13}$ $P6_3/m$	$a = 16.12(1)$ $c = 4.309(5)$ $\rho_E = 6.20,$ $\rho_x = 6.24$	arc, Qu 400 °C, 240 h single crystal data $R = 0.152$ $H = 514(50)$ kg/mm^2 $\sigma = 85000$ Ω^{-1} cm^{-1}	BoGM, 72 Mi, 73 BoMTKG, 73 BoG, 70a	Ce 99.56 Ni 99.99 Si 99.99
$CeNi_{8.6}Si_{4.4}-$ $CeNi_{8.4}Si_{4.6}$ 31–33 a/o Si	$Ce_2Ni_{17}Si_9$ $NaZn_{13}$-deriv. $I4/mcm$	$a = 7.84(1)$ $c = 11.49(1)$ at 32 a/o Si	arc(Ar), Qu 800 °C, 250 h 400 °C, 240 h PXD $H = 834(50)$ kg/mm^2	BoG, 69a BoG, 69b BoMTKG, 73	Ce 99.56 Ni 99.91 Si 99.99
[h]		$a = 7.857(4)$ $c = 11.503(5)$ ($CeNi_{8.5}Si_{4.5}$)	arc(Ar) single crystal data $R = 0.090$	Bo, 79	Ce 99.56 Ni 99.92 Si 99.99
$CeNi_{8.0}Si_{5.0}$ [i]	$NaZn_{13}$ $Fm3c$	$a = 11.15(1)$ at 37 a/o Si	arc(Ar), Qu 800 °C, 250 h 400 °C, 240 h PXD $H = 1080(50)$ kg/mm^2 $\sigma = 41000$ Ω^{-1} cm^{-1}	BoG, 69a BoG, 69b BoMTKG, 73 BoG, 70a	Ce 99.56 Ni 99.92 Si 99.99
$CeNiSi$	α-$ThSi_2$ (LaPtSi ?) $I4_1/amd$	$a = 4.055$ $c = 14.023$	arc(Ar) Qu 800 °C, 250 h 400 °C, 240 h PXD $H = 274(50)$ kg/mm^2	BoG, 69a BoMTKG, 73	Ce 99.56 Ni 99.92 Si 99.99
$Ce_7Ni_2Si_5$ "$CeNi_{0.3}Si_{0.7}$" [j]	$Ce_7Ni_2Si_5$ $Pnma$	$a = 23.31(3)$ $b = 4.299(5)$ $c = 13.90(3)$ $\rho_E = 6.01,$ $\rho_x = 6.04$	arc(Ar), Qu 600 °C, 300 h single crystal data 400 °C, 240 h PXD $H = 384(50)$ kg/mm^2	Mi, 73 Mi, 74 MiBG, 74a BoMTKG, 73	Ce 99.56 Ni 99.98 Si 99.99
$Ce_{\sim6}Ni_{\sim6}Si_{\sim7}$ [k]	($U_3Ni_4Si_4$?) $Immm$	$a = 4.092$ $b = 4.047$ $c = 23.61$	arc(Ar) Qu 800 °C, 250 h 400 °C, 240 h	BoG, 69a BoMTKG, 73	Ce 99.56 Ni 99.98 Si 99.99
$CeNi_2Si_2$	$ThCr_2Si_2$ $I4/mmm$	$a = 4.027$ $c = 9.557$	arc(Ar), Qu 800 °C, 250 h 400 °C, 240 h, PXD $H = 566(50)$ kg/mm^2 $\sigma = 3200$ Ω^{-1} cm^{-1}	BoGK, 66 BoG, 69a BoMTKG, 73 BoG, 70a	Ce 99.56 Ni 99.98 Si 99.99

TABLE 3 (continued)

Compound	Structure type Space group	Lattice parameters Density	Preparation, Characterization	Refs.	Purity
		$a = 4.036(6)$ $c = 9.608(10)$	arc(Ar), Qu 900 °C, 100 h PXD	RiP, 69	high purity
$Ce_{15}Ni_4Si_{13}$ "$Ce_{4.7}Ni_{1.2}Si_{4.1}$" [m]	$Ce_{15}Ni_4Si_{13}$ $P6_3/m$	$a = 20.27(1)$ $c = 4.306(5)$ $\rho_E = 5.89,$ $\rho_x = 5.90$	arc(Ar), Qu 400 °C, 240 h single crystal data $R \sim 0.17$ $H = 274(50)\ kg/mm^2$	MiBG, 74b Mi, 73 BoMTKG, 73	Ce 99.56 Ni 99.98 Si 99.99
$CeNi_{0.8}Si_{1.2}-$ $CeNi_{0.5}Si_{1.5}$ [n]	AlB_2 $P6/mmm$	$a = 4.039$ $c = 4.287$ at 49 a/o Si	arc(Ar), Qu 800 °C, 240 h 400 °C, 250 h PXD $H = 650(50)\ kg/mm^2$	BoG, 69a BoMTKG, 73	Ce 99.56 Ni 99.98 Si 99.99
		$a = 4.043(2)$ $c = 4.302(2)$ $CeNi_{0.5}Si_{1.5}$ $0.5Ni + 1.5Si$ in 2d	arc(Ar), Qu 800 °C, 100 h PXD $\sigma = 1600\ \Omega^{-1}\ cm^{-1}$	GlB, 65 BoG, 70a	Ce 98.90 Ni 99.8 Si 99.99
		$CeNi_{0.5}Si_{1.5}$ Ni-rich: $a = 4.061(5)$ $c = 4.149(5)$ Si-rich: $a = 4.071(5)$ $c = 4.202(5)$	no details	Ra, 67	
		$CeNi_{0.4}Si_{1.6}$ $a = 4.034$ $c = 4.294$ $Ni + Si$ in 2d	induction heating in Al_2O_3 (Ar), 1500°C Qu, 700–800 °C 24–96 h, PXD	MaT, 69	Ce 99.9 Ni 99.95 Si 99.99
$CeNiSi_2$ [o]	$CeNiSi_2$ $(BaCuSn_2)$ $Cmcm$	$a = 4.159$ $b = 16.465$ $c = 4.060$	arc(Ar), Qu 800 °C, 250 h 400 °C, 240 h PXD $H = 483(50)\ kg/mm^2$	BoG, 69a BoMTKG, 73	Ce 99.56 Ni 99.98 Si 99.99
		$a = 4.141(5)$ $b = 16.418(5)$ $c = 4.068(5)$ $\rho_E = 5.98,$ $\rho_x = 6.09$	arc(Ar) single crystal data	BoG, 70b	Ce 99.56 Ni 99.98 Si 99.99
$Ce_3Ni_2Si_8$	$Ce_3Ni_2Si_8$ $Cmmm$	$a = 4.08$ $b = 26.00$ $c = 4.22$	arc(Ar), Qu 800 °C, 250 h 400 °C, 240 h, PXD $H = 910(50)\ kg/mm^2$	BoG, 69a BoMTKG, 73	Ce 99.56 Ni 99.98 Si 99.99

TABLE 3 (continued)

Compound	Structure type Space group	Lattice parameters Density	Preparation, Characterization	Refs.	Purity
"CeNiSi$_4$"[p]		$a = 4.085(2)$ $b = 25.9558(8)$ $\rho_x = 5.714$ $c = 4.1786(9)$ $R = 0.103$	single crystal data	StLGB, 72	Ce 99.56 Ni 99.98 Si 99.99
Ce$_2$Ni$_3$Si$_5$[q]	U$_2$Co$_3$Si$_5$ Ibam	$a = 9.649(2)$ $b = 11.421(3)$ $c = 5.763(1)$	arc(Ar), Qu 1100 °C, 24 h 1000 °C, 150 h PXD	ChP, 84	Ce 99.99 Ni 99.99 Si 99.999

[a] Satisfactory agreement between observed and calculated X-ray powder intensities was claimed by Gladyshevskij et al. (1967) for Ce$_2$Ni$_{15}$Si$_2$ with the following atom positions and atomic order: Ce in 2b) and 2d); 30Ni + 4Si statistically in 4f) $z = 0.11$, 6g), 12j) 1/3, 0.962, 1/4 and 12k) 1/6, 1/3, 0; no R-value was given. (For different ordering variants of ternary Th$_2$Ni$_{17}$-derivative structures, see Parthé and Chabot (1984)).

[b] Satisfactory correspondence between observed and calculated X-ray powder intensities were obtained by Gladyshevskij et al. (1966b) with an ordered atomic arrangement as follows: Ce in 12e) $x = 0.280$; Ni in 24h) $x = 0.670$ and Si in 8c) (space group Im3m).

[c] The crystal structure of CeNi$_{8.6}$Si$_{2.4}$ has been refined by Bodak et al. (1969c) from single crystal photographs. $R(F_{0kl}) = 0.143$; $R(F_{hk0}) = 0.091$. Ce in 4a); 2.4Ni + 1.6Si in 4b); Si in 8d); Ni in 32i) 0.1234(2), 0.0494(2), 0.1778(10).

[d] For a discussion of the Ni/Si ordering, see the isotypic phase Y$_3$NiSi$_3$.

[e] Bodak et al. (1974) refined the crystal structure of Ce$_6$Ni$_2$Si$_3$ based on single crystal X-ray photographs. Single crystals were obtained from a melt (in a/o) Ce(60)Ni(20)Si(20). Atom parameters were as follows: Ce in 6h) 0.521(1), 0.379(2), 1/4; Ce in 6h) 0.236(1), 0.005(2), 1/4; 2Ni + 4Si in 6h) 0.165(3), 0.709(2), 1/4; Ni in 2b); Si in 2c).

[f] The crystal structure of Ce$_{14}$Ni$_8$Si$_9$ has been refined by Mis'kiv (1973) from single crystal photographs; all atoms were in 2e) of P2$_1$/m. Ce atoms were listed with $z = 1/4$: Ce ($x = 0.156$, $y = 0.074$); Ce (0.101, 0.283); Ce (0.071, 0.505); Ce (0.361, 0.074); Ce (0.288, 0.276); Ce (0.250, 0.499); Ce (0.219, 0.727); Ce (0.576, 0.711); Ce (0.428, 0.491); Ce (0.398, 0.719); Ce (0.557, 0.075); Ce (0.764, 0.069); Ce (0.923, 0.288); Ce (0.959, 0.072). Ni/Si atoms were listed with $z = 3/4$ (statistical distribution): Ni/Si (0.863, 0.137); Ni/Si (0, 0.0212); Ni/Si (0.076, 0.125); Ni/Si (0.012, 0.360); Ni/Si (0.270, 0.134); Ni/Si (0.183, 0.203); Ni/Si (0.222, 0.360); Ni/Si (0.139, 0.430); Ni/Si (0.170, 0.565); Ni/Si (0.477, 0.124); Ni/Si (0.508, 0.780); Ni/Si (0.470, 0.639); Ni/Si (0.823, 0.430); Ni/Si (0.362, 0.569); Ni/Si (0.278, 0.645); Ni/Si (0.316, 0.780); Ni/Si (0.675, 0.128). Ni/Si ordering has not been studied in detail. Hovestreydt and Parthé (1983) analyzed the crystal structure of a compound with the composition Ce$_{14}$Ni$_6$Si$_{11}$ and observed structural analogy with the ordered Pr$_{14}$Ni$_6$Si$_{11}$-type (space group C2/m).

[g] The crystal structure of Ce$_5$Ni$_2$Si$_3$ has been refined by Bodak et al. (1972) on the basis of X-ray single crystal photographs, $R(F_{hk0}) = 0.152$. Ce in 6h) 0.8322(5), 0.8205(5), 1/4; Ce in 6h) 0.6022(5), 0.8640(5); Ce in 6h) 0.3871(5), 0.9329(5); Ce in 2c); Ni in 2b); Si in 6h) 0.5472(16), 0.1672(16); 0.3Ni + 0.7Si in 6h) 0.7584(19), 0.0917(19); 0.7Ni + 0.3Si in 6h) 0.7166(16), 0.2187(16).

[h] Bodak (1979) determined the crystal structural of Ce$_2$Ni$_{17}$Si$_9$ from single crystal X-ray counter data, $R = 0.090$. Ce in 4a); Ni in 16l) 0.1294(6), 0.6294(6), 0.1832(4); Ni in 16k) 0.2024(6), 0.0691(6), 0; Ni + Si in 4d); Si in 16l) 0.3300(6), 0.8300(6), 0.1180(4).

[i] According to the investigation by Bodak et al. (1969a) a homogeneous range was observed: CeNi$_{7.8-6.5}$Si$_{5.2-6.5}$ (36–46 a/o Si). At low Si contents (~ 36 a/o) a cubic NaZn$_{13}$-type lattice occurs ($a = 11.15$), gradually deforming into a body-centered tetragonal lattice with increasing Si content. Lattice parameters change linearly to $a = 7.80$, $c = 11.22$ at 46 a/o Si. The precise space group and atom ordering have not been determined yet. See also CeNi$_{8.6}$Si$_{4.4}$.

[j] The crystal structure of Ce$_7$Ni$_2$Si$_5$ has been determined by Mis'kiv (1974) on the basis of single crystal

TABLE 3 (continued)

X-ray photographs; $R = 0.136$. All atoms are in 4c) x, $1/4$, z of Pnma: Ce ($x = 0.479$; $z = 0.614$); Ce (0.134, 0.028); Ce (0.116, 0.750); Ce (0.273, 0.899); Ce (0.433, 0.043); Ce (0.104, 0.313); Ce (0.266, 0.168); Ni (0.482, 0.248); Ni (0.270, 0.530); Si (0.001, 0.658); Si (0.431, 0.385); Si (0.313, 0.383); Si (0.166, 0.532); Si (0.341, 0.685).

[k] $Ce_{-6}Ni_{-6}Si_{-7}$ is the approximative composition, as this compound could not be obtained in homogeneous form. Preliminary structural results however indicate isotypism with the structure of $U_3Ni_4Si_4$ (Hovestreydt et al., 1982).

[l] Further physical properties are mentioned in the text.

[m] Mis'kiv et al. (1974) determined the crystal structure of $Ce_{15}Ni_4Si_{13}$ form single crystal X-ray photographs; $R \sim 0.170$. Ce in 6h) 0.144, 0.143, $1/4$; Ce in 6h) 0.112, 0.317; Ce in 6h) 0.074, 0.496; Ce in 6h) 0.030, 0.675; Ce in 6h) 0.290, 0.537; Ni in 2b); Si in 6h) 0.794, 0.715; Si in 6h) 0.860, 0.558; Si in 6h) 0.797, 0.408; Si in 2c); 0.5Ni + 0.5 Si in 6h) 0.897, 0.374; 0.5Ni + 0.5 Si in 6h) 0.828, 0.245.

[n] For a discussion of the lattice parameters, see text.

[o] The crystal structure of $CeNiSi_2$ was established by Bodak et al. (1970) by means of single crystal X-ray photographs; $R(F_{0kl}) = 0.133$, $R(F_{hk0}) = 0.158$. All atoms are in 4c) 0, y, $1/4$ of Cmcm: Ce (0.1070(2)); Ni (0.3158(8)); Si (0.4566(20)), Si (0.7492(4)).

[p] Stepien et al. (1972) determined the crystal structure of $Ce_3Ni_2Si_8$ based on single crystal X-ray counter data, $R = 0.103$. Ce in 2a); Ce in 4j) 0, 0.3162(5), 0; Ni in 4i) 0, 0.1335(1), 0; Si in 4i) 0.4077(3); Si in 4i) 0.2240(4); Si in 4j) 0, 0.941(2), 0; Si in 4j) 0, 0.4534(3), 0. In the original papers by Bodak et al. (1969a, 1973) the space group Cmcm was assumed and the original composition was given as $CeNiSi_4$ (see also text).

[q] $Ce_2Ni_3Si_5$ is likely to be a high-temperature compound.

with a statement by Kripyakevich et al. (1968) about the nonexistence of a $NaZn_{13}$-type phase in the Ce–Ni–Si system, the formation of the $NaZn_{13}$-type was observed at higher Si contents, i.e. $CeNi_{7.8-6.5}Si_{5.2-6.5}$; see table 3.

Phase equilibria along the concentration section $CeNi_xSi_{2-x}$ have been studied by several investigators. Mayer and Tassa (1969) studied it over the temperature region of 700–800 °C. In agreement with the work of Bodak and Gladyshevskij (1969a) and Bodak et al. (1973) the $ThSi_2$-type was observed to be stable for $x < 0.4$. $CeNi_{0.4}Si_{1.6}$ was observed to crystallize with the AlB_2-type of structure (see table 3) and satisfactory correspondence between observed and calculated X-ray powder intensities was obtained for a statistical distribution of Ni/Si atoms in the 2d site of P6/mmm. The unit cell dimensions are in agreement with the data obtained by Gladyshevskij and Bodak (1965, 1969a) and by Bodak et al. (1973). According to a more detailed study concerning the homogeneous range of $Ce(Ni,Si)_2$ by Bodak and Gladyshevskij (1969a), the lattice parameters of samples annealed at 800 °C and quenched were found to change linearly from $a \sim 4.06$, $c \sim 4.13$ at 40.5 a/o Si to $a \sim 4.03$, $c \sim 4.28$ at 49.5 a/o Si (as read from a small diagram). In this context the data reported by Raman (1967) about a "Ni-rich" and "Si-rich Ce_2NiSi_3" both seem to correspond to the Ni-rich side of the homogeneous range; the a-parameter however is considerably larger (see table 3); no details for preparation were presented by Raman (1967).

Ni silicides and Si solubility in Ni at 400 °C and 800 °C are in agreement with the literature data (see handbooks on phase diagrams). With respect to a crystal-structure determination by Frank and Schubert (1971) a more precise formula concerning

the phase "Ni_5Si_2" observed at $900\,^{\circ}C$ should be $Ni_{31}Si_{12}$. Alloys annealed at $500\,^{\circ}C$, 65 h or at $700\,^{\circ}C$, 40 h, however, revealed a similar X-ray subcell pattern, related to $Ni_{31}Si_{12}$ but of a slightly different type, and this was thus attributed to a new (low-temperature) phase with approximately the same composition as $Ni_{31}Si_{12}$. From DTA measurements a transition temperature of $T \sim 860\,^{\circ}C$ was derived by Frank and Schubert (1971). Oya and Suzuki (1983) confirmed the existence of this phase, but they failed to observe a DTA signal of a phase transition. A more detailed investigation of this region (~ 30 a/o Si) will be necessary to determine the phase equilibria at low temperatures beyond doubt. Binary Ce–Ni and Ce–Si compounds correspond to a recent phase diagram compilation by Gschneidner and Verkade (1974) [$CeNi_5$ ($CaCu_5$-type), Ce_2Ni_7 (Ce_2Ni_7-type), $CeNi_3$ ($CeNi_3$-type), $CeNi_2$ ($MgCu_2$-type), $CeNi$ (CrB-type), Ce_7Ni_3 (Th_7Fe_6-type); Ce_5Si_3 (Cr_5B_3-type), Ce_3Si_2 (U_3Si_2-type), Ce_5Si_4 (Zr_5Si_4-type), $CeSi$ (FeB-type), Ce_3Si_5 (defect $GdSi_2$-type) and $CeSi_2$ (α-$ThSi_2$-type)]. Actually, Ce_3Si_5 was not observed by Bodak et al. (1973) at $400\,^{\circ}C$ or $800\,^{\circ}C$ as a separate phase.

The solid solubility of Ce in Ni silicides in general was found to be small. Some Ni can be replaced by Si in Ce–Ni compounds and vice versa. Mutual solid solubilities are in the order of ~ 3 a/o Si(Ni) except for $CeNi_5$ which dissolves up to 10 a/o Si, and in the case of Ce_5Si_3 where ~ 9 a/o Si can be replaced by Ni, changing the lattice parameters from $a = 7.890$, $c = 13.85$ to $a = 7.850$, $c = 14.70$.

For most of the ternary compounds small homogeneity ranges were observed with a Ni/Si substitution of ~ 2–10 a/o at a fixed Ce concentration. Owing to the comparable size of Ni, Si atoms in some cases lattice dimensions do not change significantly (i.e. for $Ce_2Ni_{0.8-1.2}Si_{1.2-0.8}$ with the $Ce_5Ni_2Si_3$-type, see table 3). The color of the ternary Ce–Ni silicides was described as gray (metallic luster) with a yellow tint for the Ni-rich species and a violet tint in the case of Si-rich alloys. Ce-rich alloys had to be protected against oxidation and moisture by handling under inert oil. Brittleness and hardness increased with increasing Si content.

Various authors agreed on the existence of $CeNi_2Si_2$ with the $ThCr_2Si_2$-type (see also table 3); a series of physico-chemical properties have been studied, i.e. the valence of Ce (Levin et al., 1981), band structure (Koterlin et al., 1981; Koterlin, 1981), electrical and magnetic properties (Bodak et al., 1977; Levin et al., 1977; see also table 4).

Very recently Chabot and Parthé (1984) characterized the compound $Ce_2Ni_3Si_5$ with the $U_2Co_3Si_5$-type of structure. Due to the higher preparation and annealing temperatures (arc melted, $1100\,^{\circ}C$, 24 h and $1000\,^{\circ}C$, 150 h) $Ce_2Ni_3Si_5$ is likely to be a high-temperature phase.

Some discrepancy exists in connection with the compound "$CeNiSi_4$" first described by Bodak et al. 91969a, 1973). From a more recent structure refinement by Stepien et al. (1972) the composition was claimed to be $Ce_3Ni_2Si_8$. The new composition is marked by an asterisk in the isothermal section in fig. 15. If the phase equilibria involving "$CeNiSi_4$" were determined correctly by Bodak and Gladyshevskij (1969a) the composition of $Ce_3Ni_2Si_8$ would be located in the three-phase area of $CeSi_2 + CeNiSi_2 + Si$ and thus would have to enter two-phase equilibria different from those shown earlier for "$CeNiSi_4$". Considering the obvi-

TABLE 4

Magnetic properties of ternary Ce–Ni–Si compounds (after Bodak et al., 1977).

Compound	Structure type	$\chi \times 10^6$ (cm^{3}g^{-1})	θ_p (K)	μ_{eff} (μ_B)
Ce(Ni,Si)$_{13}$ 38% Si	NaZn$_{13}$-deriv.	4.89	−260	–
Ce(Ni,Si)$_{13}$ 41% Si	NaZn$_{13}$-deriv.	3.78	−50	–
CeNi$_4$Si	–	2.24	−280	2.0
CeNiSi$_4$	CeNiSi$_4$ (Ce$_3$Ni$_2$Si$_8$)	8.27	−65	2.64
CeNi$_2$Si$_2$	ThCr$_2$Si$_2$	4.28	−360	2.64
CeNiSi$_2$	CeNiSi$_2$	7.23	−150	2.60
Ce$_3$Ni$_6$Si$_2$	Ce$_3$Ni$_6$Si$_2$	3.41	−202	1.98
CeNi$_{1.3}$Si$_{0.7}$	–	7.47	−240	2.7
CeNiSi	α-ThSi$_2$	6.77	–	–
Ce(Ni,Si)$_2$ 43% Si	AlB$_2$	10.8	−85	2.6
Ce(Ni,Si)$_2$ 47% Si	AlB$_2$	12.93	−55	2.8
Ce(Ni,Si)$_2$ 50% Si	AlB$_2$	13.18	−25	2.7

ous scatter among the temperature factors of Ni,Si atoms in the structure refinement of Ce$_3$Ni$_2$Si$_8$ by Stepien et al. (1972) (negative B for two Si sites) the possibility of a small Ni/Si disorder in the direction of "Ce$_3$Ni$_3$Si$_7$" is conceivable. This would merely result in a shift of the original composition "CeNiSi$_4$" towards a lower Si content but conserve the original phase relations.

References

Bodak, O.I., 1979, Sov. Phys. Crystallogr. **24**, 732.
Bodak, O.I. and E.I. Gladyshevskij, 1969a, Izv. Akad. Nauk SSSR, Neorg. Mater. 5(12), 2060.
Bodak, O.I. and E.I. Gladyshevskij, 1969b, Dopov. Akad. Nauk Ukr. RSR, Ser. A **12**, 1125.
Bodak, O.I. and E.I. Gladyshevskij, 1969c, Dopov. Akad. Nauk Ukr. RSR, Ser. A **5**, 452.
Bodak, O.I. and E.I. Gladyshevskij, 1970a, Nekot. Vop. Khim. Fiz. Poluprop. Slozhn Sostava, 105.
Bodak, O.I. and E.I. Gladyshevskij, 1970b, Sov. Phys. Crystallogr. 14(6), 859.
Bodak, O.I., E.I. Gladyshevskij and P.I. Kripyakevich, 1966, Izv. Akad. Nauk SSSR, Neorg. Mater. 2(12), 2151.
Bodak, O.I., E.I. Gladyshevskij and M.G. Mis'kiv, 1972, Sov. Phys. Crystallogr. 17(3), 439.
Bodak, O.I., M.G. Mis'kiv, A.T. Tyvanchuk, O.I. Kharchenko and E.I. Gladyshevskij, 1973, Izv. Akad. Nauk SSSR, Neorg. Mater. 9(5), 864.
Bodak, O.I., E.I. Gladyshevskij and O.I. Kharchenko, 1974, Sov. Phys. Crystallogr. **19**, 45.
Bodak, O.I., E.I. Gladyshevskij, E.M. Levin and R.V. Lutsiv, 1977, Dopov. Akad. Nauk Ukr. RSR., Ser. A **12**, 1129.
Chabot, B. and E. Parthé, 1984, J. Less-Common Metals, **97**, 285.
Frank, K. and K. Schubert, 1971, Acta Crystallogr. **B27**, 916.
Gladyshevskij, E.I. and O.I. Bodak, 1965, Dopov. Akad. Ukr. RSR, Ser. A **5**, 601.
Gladyshevskij, E.I., P.I. Kripyakevich and O.I. Bodak, 1966a, Acta Crystallogr. **A21**, 80.
Gladyshevskij, E.I., P.I. Kripyakevich and O.I. Bodak, 1966b, Z. Anorg. Allg. Chem. **344**, 95.
Gladyshevskij, E.I., P.I. Kripyakevich and O.I. Bodak, 1967, Visn. L'vivsk. Derzh. Univ., Ser. Khim. 9, 34.
Gschneidner Jr., K.A. and M.E. Verkade, 1974, Selected Cerium Phase Diagrams, Document IS-RIC-7, Iowa State Univ., Ames, IA, USA, p. 28.
Hovestreydt, E. and E. Parthé, 1983, to be published.
Hovestreydt, E., K. Klepp and E. Parthé, 1982, Acta Crystallogr. **B38**, 1803.

Koterlin, M.D., 1981, Dopov. Akad. Nauk Ukr. RSR, Ser. A **5**, 71.

Koterlin, M.D., E.M. Levin and R.I. Yasnitskii, 1981, Ukr. Fiz. Zh. **26**(11), 1971.

Kripyakevich, P.I., O.S. Zarechnjuk, E.I. Gladyshevskij and O.I. Bodak, 1968, Z. Anorg. Allg. Chem., **358**, 90.

Levin, E.M., R.V. Lutsiv, E.I. Gladyshevskij and O.I. Bodak, 1977, Fiz. Elektron. Resp. Mezhved. Nauch-Tekhn. Sbor. **15**, 59.

Levin, E.M., R.V. Lutsiv, L.D. Finkelstein, N.D. Samsonova and R.I. Yasnitskii, 1981, Fiz. Tverd. Tela **23**(8), 2401.

Mayer, I. and M. Tassa, 1969, J. Less-Common Metals **19**, 173.

Mis'kiv, M.G., 1973, Thesis, Ivano Franko Univ., Lvov, USSR.

Mis'kiv, M.G., 1974, Visn. L'vivsk. Derzh. Univ., Ser. Khim. **15**, 17.

Mis'kiv, M.G., O.I. Bodak and E.I. Gladyshevskij, 1974a, Tesizy Dokl. Vses. Konf. Kristallokhim. Intermet. Soedin, 2nd Ed., ed. R.M. Rykhal (Lvov. Gos. Univ., Lvov, USSR) p. 31.

Mis'kiv, M.G., O.I. Bodak and E.I. Gladyshevskij, 1974b, Sov. Phys. Crystallogr. **18**(4), 450.

Oya, Y. and T. Suzuki, 1983, Z. Metallkde **74**, 21.

Parthé, E. and B. Chabot, 1984, Crystal Structures and Crystal Chemistry of Ternary Rare Earth–Transition Metal Borides, Silicides and Homologues, in: Handbook on the Physics and Chemistry of Rare Earths, Vol. 6, eds. K.A. Gschneidner, Jr. and L. Eyring (North-Holland, Amsterdam) p. 113.

Raman, A., 1967, Naturwiss. **54**, 560.

Rieger, W. and E. Parthé, 1969, Monatsh. Chem. **100**, 444.

Stepien, J.A., K. Lukaszewicz, E.I. Gladyshevskij and O.I. Bodak, 1972, Bull. Acad. Polon. Sci., Ser. Sci. Chim. **20**(11–12), 1029.

Ce–Os–Si

The crystal structure of $CeOs_2Si_2$ has been refined from single crystal counter data (Horvath and Rogl, 1983): $CeOs_2Si_2$ crystallizes with the $ThCr_2Si_2$-type of structure. According to the reliability value obtained ($R = 0.027$) the atom parameters derived were: Ce in 2a); Os in 4d) and Si in the 4e) site of space group I4/mmm with $z(Si) = 0.37128(71)$. Samples were prepared in an arc furnace under argon. For heat treatment the samples were carefully wrapped in Ta foil and sealed in evacuated silica tubes. No significant structural changes were observed from samples homogenized at 1000°C for 48 h and at 500°C for 600 h, respectively. The lattice parameters data were: $a = 4.1617(5)$, $c = 9.8481(28)$ for the as-cast alloy; $a = 4.1618(4)$, $c = 9.8502(44)$ (1000°C); and $a = 4.1609(9)$, $c = 9.8466(50)$ for an alloy quenched from 500°C. Hiebl et al. (1983) investigated the magnetochemical behavior in the temperature range of 1.5 K to 1100 K. The observed paramagnetic moment $\mu_{eff}^{para} = 0.98$ μ_B is compatible with a rather low concentration of Ce^{3+} (15%). θ_p was −5 K.

References
Hiebl, K., C. Horvath, P. Rogl and M.J. Sienko, 1983, Solid State Commun. **48**, 211.

Horvath, C. and P. Rogl, 1983, Mater. Res. Bull. **18**, 443.

Ce–Pd–Si

$CePd_2Si$ crystallizes with the ordered Fe_3C-type of structure: Pnma, $a = 7.609(2)$, $b = 6.877(1)$, $c = 5.695(1)$ (Moreau et al., 1982; X-ray powder analysis); for sample preparation, see YPd_2Si.

Ballestracci (1976) refined the crystal structure of $CePd_2Si_2$ from X-ray powder diffraction data; ordered $ThCr_2Si_2$-type, I4/mmm, $a = 4.212$, $c = 9.98$; Si in 4e) with $z = 0.375$; $R = 0.06$. Samples were prepared by melting under argon in an induction furnace. From X-ray powder diffraction Rossi et al. (1979) confirmed the $ThCr_2Si_2$-type of structure with $a = 4.232$, $c = 9.911$ and $\rho_x = 7.65$ kg/dm^3; in this case samples were prepared by melting in an induction furnace under argon (99.9% Ce and 99.9% Rh,Si), followed by a heat treatment for 1 week at 500°C. From the difference in unit cell parameters a homogeneous range and/or a change in the valency of Ce seems likely. Magnetic susceptibility measurements (1.5 to 300 K) and high-field magnetization studies at 4.2 K up to 21 T revealed an antiferromagnetic ordering at $T_N = 10$ K. The energy of the spin fluctuation was considered large compared to the ordering energy. Electrical resistivity measurements (1.5 to 300 K) show Kondo sideband effects indicating the importance of moment instabilities (Murgai et al., 1983). The crystal symmetry and atomic order, the unit cell parameters [$a = 4.2372(10)$, $c = 9.8893(26)$] and magnetic behavior ($T_N = 10$ K) were confirmed by Hiebl et al. (1984).

Malik et al. (1982) investigated the effect of Si addition on the valence state of Ce in $CePd_3Si_x$. From lattice parameters and susceptibilities (4.2 to 300 K) a change in the valency of Ce was observed from mixed valent in $CePd_3$ ($AuCu_3$ type) to nearly trivalent in $CePd_3Si_{0.3}$. Unit cell dimensions and paramagnetic data were given as follows: $CePd_3$ ($a = 4.129$); $CePd_3Si_{0.05}$ ($a = 4.158$, $\mu_{eff} = 2.24$ μ_B, $\theta_p = -50$ K); $CePd_3Si_{0.1}$ ($a = 4.186$, $\mu_{eff} = 2.40$ μ_B, $\theta_p = -21$ K); $CePd_3Si_{0.2}$ ($a = 4.219$, $\mu_{eff} = 2.66$ μ_B, $\theta_p = -11$ K); $CePd_3Si_{0.3}$ ($a = 4.244$, $\mu_{eff} = 2.66$ μ_B, $\theta_p = -15$ K). Alloys were prepared by rf induction melting in a water-cooled copper boat. Alloys with a composition $x > 0.3$ where multiphase.

References

Ballestracci, R., 1976, C.R. Acad. Sci. Paris, Ser. B **282**, 291.
Hiebl, K., C. Horvath, P. Rogl and M.J. Sienko, 1984, J. Less-Common Metals, to be published.
Malik, S.K., R. Vijayaraghavan, E.B. Boltich, R.S. Craig, W.E. Wallace and S.K. Dhar, 1982, Solid State
    Commun. **43**(4), 243.
Moreau. J., J. LeRoy and D. Paccard, 1982, Acta Crystallogr. **B38**, 2446.
Murgai, V., S. Raaen, L.C. Gupta and R.D. Parks, 1982, in: Valance Instabilities, eds. P. Wachter and H.
    Boppart (North-Holland, Amsterdam) p. 537.
Rossi, D., R. Marazza and R. Ferro, 1979, J. Less-Common Metals **66**, P17.

Ce–Pr–Si

No ternary phase diagram is available for the system Ce–Pr–Si.
The formation of an extended solid solution $(Ce_{1-x}Pr_x)_3Si_2$ crystallizing with the U_3Si_2-type of structure and with a Ce substitution up to 58 a/o Pr was reported by Mokra (1979). For details of sample preparation, see Ce–Y–Si.

Reference

Mokra, I.R., 1979, Autoreferat Dis. Kand. Khim. (abstract of thesis, Russian) (Nauk, Lvov) 22 p.

Ce–Pt–Si

So far only two ternary compounds have been observed in the Ce–Pt–Si system.

According to X-ray powder data by Klepp and Parthé (1982) the compound CePtSi crystallizes congruently from the melt and with the LaPtSi-type of structure [I4$_1$md, $a = 4.1982(7)$, $c = 14.488(3)$]. For sample preparation, see LaPtSi.

CePt$_2$Si$_2$ was claimed to be body-centered tetragonal with the ThCr$_2$Si$_2$-type ($a = 4.246$, $c = 9.837$, $\rho_x = 10.98$ kg/dm^3); from X-ray diffraction data Pt and Si atoms were said to be randomly distributed on the 4d and 4e sites of I4/mmm (Rossi et al., 1979); for sample preparation, see CePd$_2$Si$_2$. At variance with the above, Ballestracci and Astier (1978) observed CePt$_2$Si$_2$ with a primitive tetragonal symmetry, $a = 4.256$, $c = 9.77$; their data were based on a X-ray powder analysis of alloys melted in an induction furnace under argon. In agreement with the data by Ballestracci the primitive tetragonal symmetry reduction from the ThCr$_2$Si$_2$ parent lattice was confirmed from a recent determination of the crystal structure of CePt$_2$Si$_2$ by Horvath and Rogl (1984). The unit cell dimensions were given as $a = 4.2519(10)$ and $c = 9.7951(48)$.

References
Ballestracci, R. and G. Astier, 1978, C.R. Acad. Sci. Paris, Ser. B **286**, 109.
Horvath, C. and P. Rogl, 1984, Mater. Res. Bull., to be published.
Klepp, K. and E. Parthé, 1982, Acta Crystallogr. **B38**, 1105.
Rossi, D., R. Marazza and R. Ferro, 1979, J. Less-Common Metals **66**, P17.

Ce–Re–Si

The phase equilibria in the ternary system Ce–Re–Si have been investigated by Pecharskij (1979) by means of X-ray analysis of 129 ternary samples which were arc melted and subsequently annealed in evacuated quartz capsules for 400–600 h at 800°C and quenched in water. Starting materials were Ce 99.56%, Re 99.99% and Si 99.99%.

The binary systems Ce–Si and Re–Si have been discussed in context with the ternary systems Ce–Ni–Si and Y–Re–Si, respectively. The mutual solid solubilities of Ce and Re silicides at 800°C were found to be small and within 1–2 a/o of the third constituent.

The ternary phase equilibria (fig. 16, isothermal section at 800°C) are characterized by the existence of three ternary compounds: CeRe$_4$Si$_2$, Ce$_2$Re$_3$Si$_5$, and "Ce$_2$ReSi$_2$".

Bodak et al. (1977) refined the crystal structure of CeRe$_4$Si$_2$ from X-ray single crystal photographs. Single crystals were obtained from an arc-melted button after annealing for 340 h at 800°C in an evacuated quartz capsule. Starting materials were Ce 99.56%, Re 99.9% and Si 99.99%.

CeRe$_4$Si$_2$ crystallizes with a new structure type: CeRe$_4$Si$_2$-type, Cmmm, $a = 4.167(5)$, $b = 14.001(5)$, $c = 4.145(5)$, $\rho_{exp} = 12.87$, $\rho_x = 12.88$ kg/dm^3. The reliability values for this structure determination were $R(F_{hk0}) = 0.149$ and $R(F_{0kl}) = 0.110$ corresponding to the following atom parameters: Ce in 2a); Re in 4j) 0, 0.1855(5),
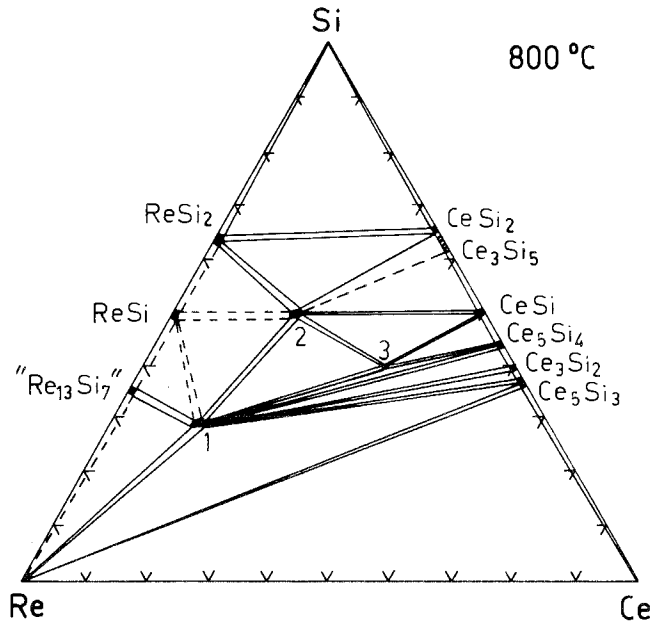
Fig. 16. Ce–Re–Si, isothermal section at 800 °C. 1: $CeRe_4Si_2$, 2: $Ce_2Re_3Si_5$, 3: "Ce_2ReSi_2".

1/2; Re in 4i) 0, 0.3058(7), 0; Si in 4j) 0, 0.405(1), 1/2.

From X-ray powder analysis of arc-melted alloys $Ce_2Re_3Si_5$ was observed to crystallize with the structure type of $Sc_2Fe_3Si_5$ (space group P4/mnc, lattice parameters: $a = 10.96(1)$, $c = 5.626(5)$, Bodak et al., 1978). No detailed conditions of heat treatment were given. From the smaller lattice parameters as compared to the isotypic compounds $R_2Re_3Si_5$, Ce was concluded to be partly in a tetravalent state. The structure type was confirmed by Segre (1981), who measured slightly larger lattice parameters: $a = 10.98(1)$, $c = 5.630(8)$; $T_n = 1$ K.

No detailed crystallographic data are available yet for the compound "Ce_2ReSi_2".

References

Bodak, O.I., E.I. Gladyshevskij and V.K. Pecharskij, 1977, Kristallograpfiya **22**(1), 178.
Bodak, O.I., V.K. Pecharskij and E.I. Gladyshevskij, 1978, Izv. Akad. Nauk SSSR, Neorg. Mater. **14**(2), 250.
Pecharskij, V.K., 1979, Autoreferat Dis. Kand. Khim. (abstract of thesis, Russian) (Nauk, Lvov) 23 p.
Segre, C.U., 1981, Thesis, Univ. of Calif., San Diego, USA.

Ce–Rh–Si

The crystal structure of $CeRh_2Si_2$ has been refined by Ballestracci (1976) by means of X-ray powder diffraction data. $CeRh_2Si_2$ adopts the ordered $ThCr_2Si_2$-type with lattice parameters $a = 4.086$ and $c = 10.17$. According to the refinement yielding a reliability value of $R = 0.057$, the silicon atoms were confirmed to occupy the 4e site of I4/mmm with $z_{Si} = 0.375$. For sample preparation, see YRh_2Si_2. Atomic

order and crystal symmetry was confirmed by a structural and magnetochemical investigation by Hiebl et al. (1983) in the temperature range 1.5 K $< T <$ 1100 K. The crystallographic and magnetic data obtained were: $a = 4.0894(3)$, $c = 10.1762(60)$, $\mu_{eff}^{para} = 2.33 \ \mu_B$ and $\theta_p = -26$ K. CeRh$_2$Si$_2$ orders antiferromagnetically at $T_N = 36$ K. Felner and Nowik (1983) reported considerably larger lattice parameters [I4/mmm, $a = 4.092(2)$, $c = 10.21(1)$] in combination with a larger paramagnetic moment $\mu_{eff}^{para} = 2.9(1) \ \mu_B$, $\theta_p = -81(3)$ K. An additional peak in the susceptibility curve at $T_m = 5(2)$ K was interpreted as itinerant electron ordering of the Rh sublattice.

The variation of lattice parameters versus temperature (X-ray powder data) as measured in the temperature range of 20 to 300 K by Godart et al. (1983) constantly decreases from 300 to 50 K ($\Delta a \sim 0.01$ Å, $\Delta c \sim 0.05$ Å) and reveal a rather small increase between 40 K and 12 K. Data at room temperature ($a = 4.093$, $c = 10.185$) agree with those by Ballestracci (1976) and by Hiebl et al. (1983). Furthermore the L_{III} absorption edge and the extended X-ray absorption fine structure spectra did not change between 20 and 300 K indicating no valence changes on the cerium site at $T_N = 37$ K. Godart et al. (1983) also confirmed the existence of a second peak in the susceptibility versus temperature (1.5–300 K) curve at 5.2 K (magnetism of the Rh 4d band ?). At variance with the data by Hiebl et al. (1984) a rather high paramagnetic effective moment was obtained from the restricted temperature range of 1.5–300 K (Godart et al., 1983): $\mu_{eff}^{para} = 2.9 \ \mu_B$, $\theta_p = -72$ K.

Slightly different values (2.56 μ_B, $\theta_p = -61$ K, $T_N = 36$ K) were reported by Quezel et al. (1984) from susceptibility data between 4.2 and 300 K. The antiferromagnetic order in CeRh$_2$Si$_2$ was studied by means of neutron diffraction and revealed a tetragonal magnetic unit cell of $a = a_0\sqrt{2} = 5.763$ and $c = 10.13$ and a simple antiferromagnetic ordering within the (001) planes and a $+ - + -$ stacking sequence in [110]; $R = 0.08$ and $m_0 = 1.50(15) \ \mu_B$ at $T = 10$ K (Quezel et al., 1984).

Ce$_2$RhSi$_3$ is isostructural with the structure type of Er$_2$RhSi$_3$ (Chevalier et al., 1984); crystal data as derived from X-ray powder diffraction of arc-melted samples annealed at 800°C, 4 d, were as follows: P$\bar{6}$2c, $a = 8.210(5)$, $c = 8.410(5)$. Ce$_2$RhSi$_3$ is antiferromagnetic below $T_N = 6$ K; paramagnetic susceptibilities (1.5–300 K) correspond to trivalent cerium: $\mu_{eff}^{para} = 2.40 \ \mu_B$, $\theta_p = -83$ K (Chevalier et al., 1984).

References

Ballestracci, R., 1976, C.R. Acad. Sci. Paris, Ser. B, **282**, 291.

Chevalier, B., P. Lejay, J. Etourneau and P. Hagenmuller, 1984, Solid State Commun. 49(9), 753.

Felner, I. and I. Nowik, 1983, Solid State Commun. 47, 831.

Godart, C., L.C. Gupta and M.F. Ravet-Krill, 1983, J. Less-Common Metals **94**, 187.

Hiebl, K., C. Horvath, P. Rogl and M.J. Sienko, 1984, J. Less-Common Metals, to be published.

Quezel, S., J. Rosset-Mignod, B. Chevalier, P. Lejay and J. Etourneau, 1984, Solid State Commun. 49(7), 685.

Ce–Ru–Si

Two ternary compounds have been characterized in the Ce–Ru–Si system.

The crystal structure of CeRu$_2$Si$_2$ has been refined by Ballestracci and Astier

(1978) by means of powder X-ray diffraction methods. $CeRu_2Si_2$ crystallizes with the $ThCr_2Si_2$-type of structure with the space group I4/mmm and lattice parameters $a = 4.192$ and $c = 9.78$. According to the obtained reliability value $R = 0.052$, the atomic parameters were as follows: Ce in 2a), Ru in 4d) and Si in 4e) with $z = 0.375$. Hiebl et al. (1983) confirmed the structure type but reported slightly different unit cell dimensions: $a = 4.1968(8)$ and $c = 9.7972(48)$. The magnetic behavior was studied by Hiebl et al. (1983) in the temperature range $1.5 < T < 1100$ K and is characterized by a Van Vleck paramagnetism of widely spaced multiplets: $\mu_{eff}^{para} = 2.12$ μ_B, $\theta_p = 0.5$ K. From detailed measurements of magnetic susceptibilities, ^{29}Si nuclear magnetic resonance and electrical resistivity in the temperature range of 1.5 to 300 K, a non-magnetic ground state was suggested (Gupta et al., 1983). The magnetic susceptibility at high temperatures (corrected for impurity contributions) was represented by $\mu_{eff}^{para} = 2.38$ μ_B and $\theta_p = -54$ K; the saturation of χ below 10 K was attributed to spin fluctuations due to Kondo and/or valence fluctuations. In contrast to mixed valent systems a linear dependence was obtained for the ^{29}Si NMR shift versus the corrected susceptibility. Samples were prepared by arc melting under argon starting from 99.99% pure Ce, 99.999% pure Si and 99.9% pure Ru. Lattice parameters from powder X-ray data were $a = 4.20$ and $c = 9.81$, $ThCr_2Si_2$-type.

The existence of a ternary compound with the $LaRu_3Si_2$-type of structure was reported by Barz (1980). Sample preparation and assumed phase equilibria (Ru + $CeRu_3Si_2$ and $CeRu_2Si_2 + CeRu_3Si_2$) were said to be the same as for $LaRu_3Si_2$. No lattice parameter data were given.

References

Ballestracci, R. and G. Astier, 1978, C.R. Acad. Sci. Paris, Ser. B **286**, 109.
Barz, H., 1980, Mater. Res. Bull. **15**, 1489.
Gupta, L.C., D.E. MacLaughlin, Cheng Tien, G. Godart, M.A. Edwards and R.D. Parks, 1983, Phys. Rev. **B28**, 3673.
Hiebl, K., C. Horvath, P. Rogl and M.J. Sienko, 1983, J. Magn. Magn. Mater. **37**, 287.

Ce–Sc–Si

The phase equilibria in the ternary system Ce–Sc–Si have been established by Mokra (1979) by means of X-ray and metallographic analysis of 128 alloys, prepared by arc melting and subsequent annealing in evacuated silica capsules for 800 h at 600°C. The samples were finally quenched in water. Starting materials were Ce 99.56%, Sc 99.92: and Si 99.99%.

Solid solubilities in the Ce–Sc binary system are in agreement with a recent critical assessment by Gschneidner and Calderwood (1982): γ-Ce (18 a/o Sc) and α-Sc (13 a/o Ce). The binary systems Ce–Si and Sc–Si are discussed ion context with the ternary systems Ce–Ni–Si and Sc–Co–Si, respectively. Sc_3Si_5 was not observed at 600°C; $CeSi_2$ at 600°C was found to crystallize with the α-$ThSi_2$ type in the range of 33.3–35 a/o Ce, but with the α-$GdSi_2$ type for 36–38 a/o Ce. The mutual solid solubilities of the binary silicides were observed to be small and were said to be ≤ 6 a/o of the third component. The ternary phase relations (fig. 17,
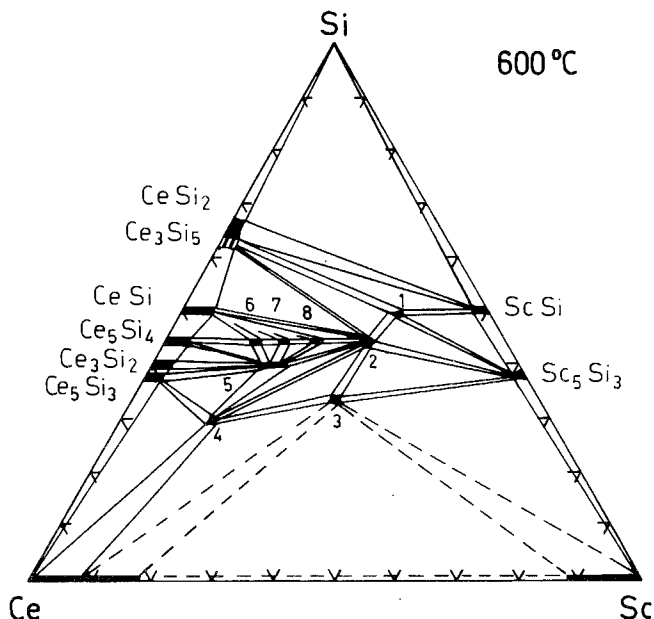
Fig. 17. Ce–Sc–Si, isothermal section at 600 °C. 1: "$Ce_3Sc_7Si_{10}$", 2: $Ce_2Sc_3Si_4$, 3: CeScSi, 4: "$Ce_{11}Sc_3Si_6$", 5: Ce_2ScSi_2, 6: "$Ce_8Sc_3Si_9$", 7: "$Ce_7Sc_4Si_9$", 8: "$Ce_6Sc_5Si_9$".

isothermal section at 600 °C) are characterized by the formation of eight ternary compounds: $Ce_2Sc_3Si_4$, CeScSi, Ce_2ScSi_2, "$Ce_3Sc_7Si_{10}$", "$Ce_{11}Sc_3Si_6$", "$Ce_8Sc_3Si_9$", "$Ce_7Sc_4Si_9$" and "$Ce_6Sc_5Si_9$"; the structure types of the latter five are uncertain.

Mokra and Bodak (1979) refined the crystal structure of CeScSi from single crystal X-ray photographs. Samples were prepared by arc melting and annealing at 600 °C. Starting materials were Ce 99.56%, Sc 99.90% and Si 99.99%. CeScSi is tetragonal [space group I4/mmm, $a = 4.300(5)$, $c = 15.80(2)$, $\rho_{exp} = 4.78$, $\rho_{theor} = 4.83$ kg/dm^3] with a superstructure of the Ca_2As- or Ti_2Bi-type of structure. The atom parameters derived were: Ce in 4e) 0, 0, 0.326(1); Sc in 4c) 0, 0.5, 0; Si in 4e) 0, 0, 0.124(5); the reliability value was $R = 0.108$.

The crystal structure of $Ce_2Sc_3Si_4$ was determined by Mokra et al. (1969) based on single crystal counter data; $Ce_2Sc_3Si_4$ crystallizes with the ordered Sm_5Ge_4-type of structure: space group Pnma, $a = 7.248(2)$, $b = 14.255(4)$, $c = 7.551(2)$. The atom parameters as corresponding to the final reliability value of $R = 0.045$ were: Sc in 4c) 0.3392(6), 1/4, $-0.0016(6)$; Sc in 8d) 0.1716(3), 0.1240(2), 0.3248(4); Ce in 8d) 0.0104(1), 0.0971(1), 0.8279(1); Si in 4c) 0.2123(9), 1/4, 0.6191(10); Si in 4c) 0.9673(9), 0.2500, 0.1241(9); Si in 8d) 0.1533(6), 0.9611(4), 0.5367(7). $Ce_2Sc_3Si_4$ exists both in as-cast alloys and in alloys annealed at 600 °C.

Bodak and Mokra (1978) reported the X-ray powder intensity refinement of the crystal structure of Ce_2ScSi_2; the reliabilility value obtained was $R = 0.051$. Ce_2ScSi_2 has the ordered U_3Si_2-type of structure [P4/mbm, $a = 7.61(1)$, $c = 4.402(3)$]. Atom

parameters were derived as follows: Ce in 4h) $x = 0.177(1)$, $y = 0.677(1)$; Sc in 2a) and Si in 4g) $x = 0.387(3)$, $y = 0.887(3)$. It is interesting to note, that the binary compound Ce_3Si_2 also crystallizes with the U_3Si_2-type of structure.

References

Bodak, O.I. and I.R. Mokra, 1978, Tesizy Dokl. Tret. Vses. Konf. Kristallokhim. Intermet. Soedin, 2nd Ed., ed. R.M. Rykhal (Lvov Gos. Univ., Lvov, USSR) p. 66.

Gschneidner Jr., K.A. and F.W. Calderwood, 1982, Bull. Alloy Phase Diagrams **3**(2), 189.

Mokra, I.R., 1979, Autoreferat Dis. Kand. Khim. (abstract of thesis, Russian) (Nauk, Lvov) 22 p.

Mokra, I.R. and O.I. Bodak, 1979, Dopov. Akad. Nauk Ukr. RSR, Ser. A, 312.

Mokra, I.R., O.I. Bodak and E.I. Gladyshevskij, 1969, Sov. Phys. Crystallogr. **24**(6), 729.

Ce–Sm–Si

No complete phase diagram has been established for the system Ce–Sm–Si, but the phase equilibria in the Si-rich part of 50–100 a/o Si have been investigated by Mokra (1979) by means of X-ray and metallographic analysis of 30 alloys, which were prepared by arc melting under argon. The samples were subsequently annealed at 600 °C for 800 h in evacuated silica tubes. Starting materials were Ce 99.56%, Sm 99.70% and Si 99.99%.

A complete solid solution $(Ce_{1-x}Sm_x)Si$ is formed crystallizing with the FeB-type of structure (Pnma). At 600 °C Sm_2Si_3 (defect AlB_2-type) dissolves up to 9 a/o Ce. For the disilicide region $Ce_{1-x}Sm_xSi_2$, a continuous transformation from the tetragonal α-$ThSi_2$-type $(CeSi_2)$ to the orthorhombic α-$GdSi_2$-type $(SmSi_2)$ was
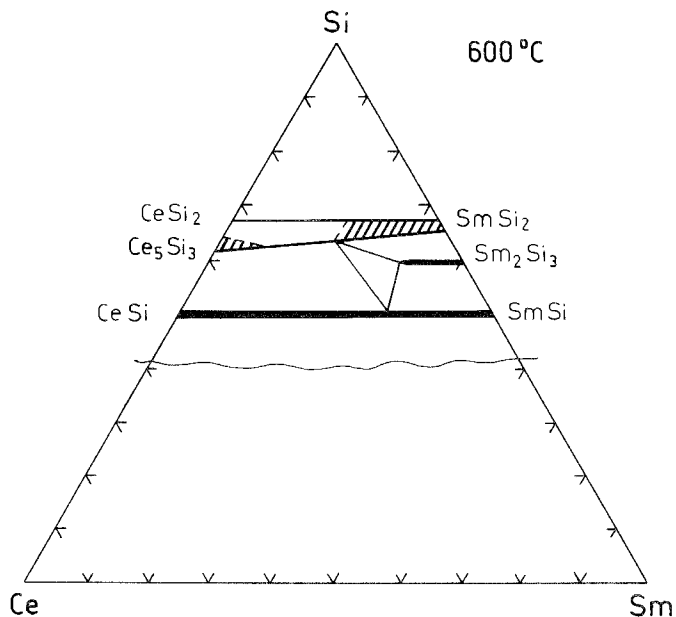

Fig. 18. Ce–Sm–Si, partial isothermal section at 600 °C (50–100 a/o Si); the dashed area represents the range of the α-$GdSi_2$-type.

claimed to be accompanied by the Ce/Sm substitution around $x \sim 0.5$. A similar situation is met between the α-ThSi$_2$-type and the silicon poor α-GdSi$_2$-type solution Ce$_{1-x}$Sm$_x$Si$_{2-y}$; the region of the α-GdSi$_2$-type structure is represented by the dashed area in fig. 18.

Reference
Mokra, I.R., 1979, Autoreferat Dis. Kand. Khim. (abstract of thesis, Russian) (Nauk, Lvov) 22 p.

Ce–Th–Si

Benesovsky et al. (1967) investigated the phase equilibria of the system Ce–Th–Si in an isothermal section at 1300 °C by means of X-ray powder and metallographic analysis; the metal-rich part was studied at 1100–1200 °C. Samples were prepared by arc melting as well as by direct heating of compacted powder mixtures of cerium hydride (0.5% O, 1.2% H), Th (0.4% O) and 99.7% Si at 1300 °C (1100–1200 °C for the metal-rich part) in vacuum for 10 to 20 h. According to the literature, Ce and Th are completely soluble, and four Th silicides have been observed: ThSi$_2$ (α-ThSi$_2$-type), Th$_3$Si$_5$ (defect AlB$_2$-type), ThSi (FeB-type), Th$_3$Si$_2$ (U$_3$Si$_2$-type). The Ce–Si binary system has been slightly modified according to a more recent compilation by Gschneidner and Verkade (1974) revealing six binary compounds: Ce$_5$Si$_3$ (Cr$_5$B$_3$-type, earlier Ce$_{\sim 2}$Si), Ce$_3$Si$_2$ (U$_3$Si$_2$-type), Ce$_5$Si$_4$ (Zr$_5$Si$_4$-type, earlier Ce$_{\sim 1.2}$Si), CeSi (FeB-type) and Ce$_3$Si$_5$ (GdSi$_{2-x}$-type) and CeSi$_2$ (α-ThSi$_2$-type).

Ternary phase equilibria at 1300 °C (fig. 19) are characterized by the formation of continuous solid solutions Ce$_{3-x}$Th$_x$Si$_2$ with the U$_3$Si$_2$-type, Ce$_{1-x}$Th$_x$Si with
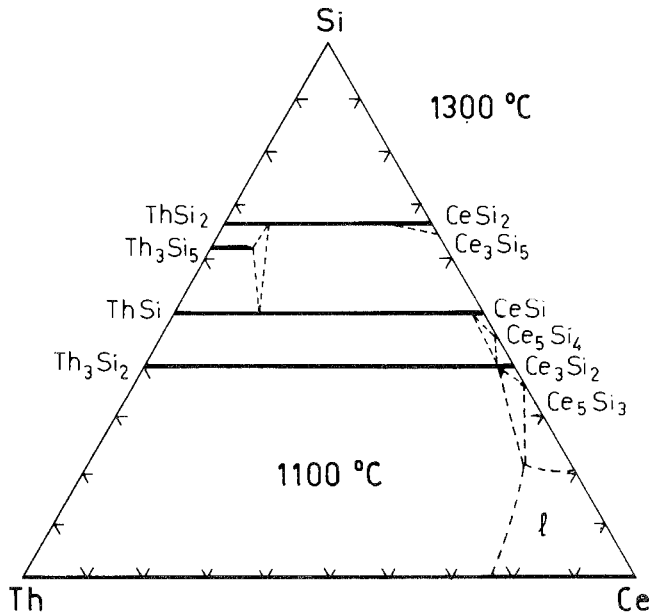

Fig. 19. Ce–Th–Si, partial isothermal sections at 1300 ° C (10–100 a/o Si) and at 1100 ° C (0–40 a/o Si).

FeB-type and $Ce_{1-x}Th_xSi_2$ with the α-$ThSi_2$-type of structure. Th was found to be practically insoluble in Ce_5Si_3 (Cr_5B_3-type) and Ce_5Si_4 (Zr_5Si_4-type), whereas approximately 25% of the Th atoms in Th_5Si_3 (defect AlB_2-type) can be replaced by Ce. Phase relations in the vicinity of the phase Ce_3Si_5 are complex and apparently a continuous transition from the $Ce_{1-x}Th_xSi_{2-y}$ phase ($GdSi_2$-type) to the α-$ThSi_2$-type solid solution was indicated. According to the low melting point of Ce at 795 °C the Ce-rich corner of the isothermal section at 1100 °C will be liquid.

References

Benesovsky, F., P. Stecher, H. Nowotny and W. Rieger, 1967, Coll. Intern. CNRS **157**, 419.
Gschneidner Jr., K.A. and M.E. Verkade, 1974, Selected Cerium Phase Diagrams, Document IS-RIC-7, Iowa State Univ., Ames, IA, USA, p. 36

Ce–Ti–Si

An alloy containing 0.4 w/o Ce, 0.48 w/o Si and 99.12 w/o Ti was reported to be heterogeneous, representing the three-phase equilibrium $Ce + Ti + Ti_5Si_3$ (Hiltz and Grant, 1957).

Reference

Hiltz Jr., R.H. and N.J. Grant, 1957, Amer. Soc. Testing Mater. Proc. **57**, 808.

Ce–U–Si

From a preliminary study of phase equilibria by means of X-ray and metallographic analysis very limited mutual solid solubilities of cerium and uranium silicides in general were reported by Benesovsky et al. (1967). For sample preparation, see the Ce–Th–Si system. A small solubility was determined for the disilicides of the α-$ThSi_2$-type with space group $I4_1/amd$; the lattice parameters of USi_2 ($a = 3.95$, $c = 13.69$) change to $a = 3.96$, $c = 13.70$ for $U_{0.85}Ce_{0.15}Si_2$, whereas the parameters of $CeSi_2$ ($a = 4.19$, $c = 13.93$) decrease on Ce/U substitution to $a = 4.165$ and $c = 13.85$ for $U_{0.33}Ce_{0.67}Si_2$.

Reference

Benesovsky, F., P. Stecher, H. Nowotny and W. Rieger, 1967, Coll. Intern. CNRS **157**, 419.

Ce–Y–Si

The phase equilibria in the ternary system Ce–Y–Si have been established by Mokra (1979) by means of X-ray and metallographic analysis of 128 alloys prepared by arc melting and subsequent annealing in evacuated silica capsules for 800 h at 600 °C. The samples were finally quenched in water. Starting materials were Ce 99.56%, Y 99.90% and Si 99.99%.

The binary silicide systems Ce–Si and Y–Si are discussed in context with the ternary systems Ce–Ni–Si and Y–Ni–Si; phase relations and solid solubilities in the Ce–Y binary are in agreement with a more recent critical assessment by Gschneidner

and Calderwood (1982); the phase CeY crystallizes with the Sm-type structure. The solubility of Si in the Ce–Y intermetallic system was observed to be small (less than 1 a/o Si ?).

No ternary compound is formed, but ternary phase equilibria at 600 °C are characterized by the formation of extended solid solutions $(Ce_{1-x}Y_x)Si_y$; the solubility limits at 600 °C were reported to be the following: $Ce_{5-x}Y_xSi_3$ (Cr_5B_3-type, $x \leqslant 0.24$), $Ce_xY_{5-x}Si_3$ (Mn_5Si_3-type, $x \leqslant 1.6$), $Ce_{3-x}Y_xSi_2$ (U_3Si_2-type, $x \leqslant 1.25$), $Ce_{5-x}Y_xSi_4$ (Zr_5Si_4-type, $x \leqslant 2.7$), $Ce_xY_{5-x}Si_4$ (Sm_5Si_4-type, $x \leqslant 0.63$), $Ce_{1-x}Y_xSi$ (FeB-type, $x \leqslant 0.7$), $Ce_xY_{1-x}Si$ (CrB-type, $x \leqslant 0.12$) and $Ce_xY_{2-x}Si_3$ (defect AlB_2-type, $x \leqslant 1.25$). At 600 °C, $CeSi_2$ was said to crystallize with the α-$ThSi_2$-type in the range from 33.3 to 35 a/o Ce but with the α-$GdSi_2$-type for 36–38 a/o Ce. For the disilicide region $Ce_{1-x}Y_xSi_2$ a continuous transformation from the tetragonal α-$ThSi_2$-type ($CeSi_2$) to the orthorhombic α-$GdSi_2$-type (YSi_2) was claimed to result from the Ce/Y substitution at $x = 0.44$ (600 °C). A similar situtation is met with the α-$ThSi_2$-type and the silicon-poor α-$GdSi_2$-type solution $Ce_{1-x}Y_xSi_{2-y}$; the region of the α-$GdSi_2$-type structure is represented by the dashed area in fig. 20. Solid solutions between CeSi (FeB-type) and YSi (CrB-type) are separated by a narrow two-phase field. A similar situation is found among the pair Y_5Si_4 (Sm_5Ge_4-type) and Ce_5Si_4 (Zr_5Si_4-type). The maximum solubility of Y in Ce_3Si_2 (U_3Si_2-type) was observed for 29 a/o Y at 600 °C. Bodak and Mokra (1978) reported a distinct metal atom ordering for Ce_2YSi_2 derived from X-ray powder diffraction data: Ce_2YSi_2 was found to crystallize with the ordered U_3Si_2-type [P4/mbm, $a = 7.65(1)$, $c = 4.410(3)$]. Ordering among metal atoms was similarly suspected by Bodak et al. (1974) for the composition $Ce_3Y_2Si_4$ of the $Ce_{5-x}Y_xSi_4$ solid solution.
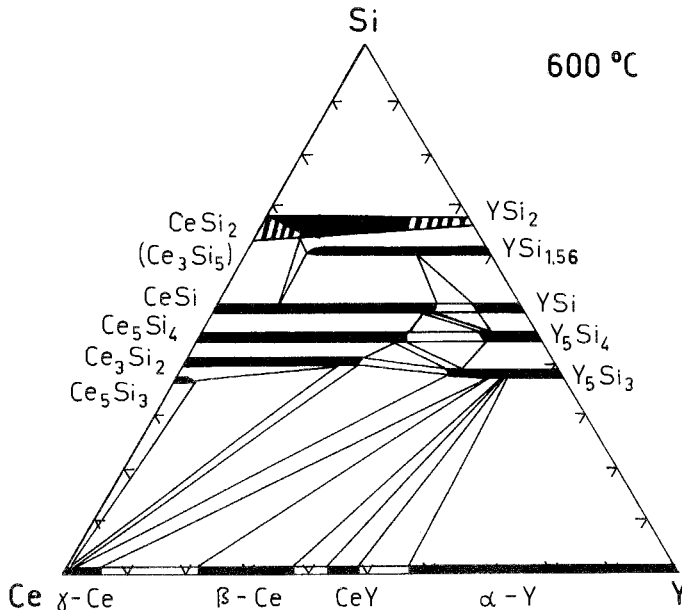

Fig. 20. Ce–Y–Si, isothermal section at 600 °C; the dashed area represents the range of the α-$GdSi_2$-type.

References

Bodak, O.I. and I.R. Mokra, 1978, Tesizy Dokl. Treat. Vses. Konf. Kristallokhim. Intermet. Soedin., 2nd
    Ed., ed. R.M. Rykhal (Lvov Gos. Univ., Lvov, USSR) p. 66.
Bodak, O.I., L.A. Muratova, N.P. Mokra, V.I. Yarovets, A.S. Sobolev and E.I. Gladyshevskij, 1974,
    Strukt. Faz. Fazov. Prevrash, Diagr. Sostoj. Met. Syst. (Nauka, Moscow) p. 182.
Gschneidner Jr., K.A. and F.W. Calderwood, 1982, Bull. Alloy Phase Diagrams 3(2), 192.
Mokra, I.R., 1979, Autoreferat Dis. Kand. Khim. (abstract of thesis, Russian) (Nauk, Lvov) 22 p.

$Dy-Ag-Si$

The AlB_2-type structure with space group P6/mmm was observed for the composition range $DyAg_{0.67}Si_{1.33}$ ($a = 4.133$, $c = 4.036$) to DyAgSi (Mayer and Felner, 1973a,b). For sample preparation, see $NdAg_xSi_{2-x}$.

References

Mayer, I. and I. Felner, 1973a, J. Solid State Chem. **7**, 292.
Mayer, I. and I. Felner, 1973b, J. Solid State Chem. **8**, 355.

$Dy-Al-Si$

No ternary phase diagram is available for the system Dy–Al–Si, but two ternary compounds have been observed: Dy_2Al_2Si and $DyAl_2Si_2$.

Yanson (1975) refined the crystal structure of Dy_2Al_2Si by means of single crystal photography; the space group was P4/mbm, lattice parameters were $a = 6.945(4)$, $c = 4.304(3)$, and $Z = 2$. The reliability values obtained from the refinement were $R_{hh0} = 0.134$ and $R_{hkl} = 0.139$, corresponding to the following atom coordinates: 4 Dy in site 4h) 0.1751(1), 0.6751, 0.5; 2 Al in 2a) 0,0,0; and a statistical distribution of 2 Al + 2 Si in site 4g) 0.3671(5), 0.8671, 0. The crystal structure of $Dy_2Al_2Si \equiv (Dy_2Al)(Al,Si)_2$ is an ordered variant of the U_3Si_2-type.

$DyAl_2Si_2$ adopts the La_2O_2S-type of structure: $P\bar{3}m1$, $a = 4.18$, $c = 6.56$ (Muravyova et al., 1972; X-ray powder diffraction data). For sample preparation and atom parameters, see Sm–Al–Si.

References

Muravyova, A.A., O.S. Zarechnyuk and E.I. Gladyshevskij, 1972, Visn. L'vivsk. Univ., Ser. Khim. **13**, 14.
Yanson, T.I., 1975, Autoreferat Dis. Kand. Khim. (abstract of thesis, Russian) (Nauk, Lvov) 22 p.

$Dy-Au-Si$

From X-ray powder diffraction data Mayer et al. (1973) reported $DyAu_2Si_2$ to crystallize with the ordered $ThCr_2Si_2$-type of structure (I4/mmm, $a = 4.218(5)$, $c = 10.15(5)$]. For sample preparation, see $LaAu_2Si_2$. Antiferromagnetic ordering occurs at $T_N = 7.5$ K (Felner, 1975); $\mu_{eff}^{para} = 10.6$ μ_B, $\theta_p = 3.6$ K.

References

Felner, I., 1975, J. Phys. Chem. Sol. **36**, 1063.
Mayer, I., J. Cohen and I. Felner, 1973, J. Less-Common Metals **30**, 181.

Dy–Co–Si

No ternary phase diagram is available for the system Dy–Co–Si, however at least five ternary compounds seem to exist.

$DyCo_2Si_2$ is tetragonal with the ordered $ThCr_2Si_2$-type of structure: I4/mmm, $a = 3.885$, $c = 9.748$, $\rho_x = 7.59$ kg/dm^3 (Rossi et al., 1978; X-ray powqder analysis). For sample preparation and etching conditions, see YCo_2Si_2. Yarovets (1978) from X-ray powder data confirmed the crystal data ($a = 3.891$, $c = 9.771$), and Yarovets et al. (1977) measured the magnetic behavior in the temperature range of 300–1200 K, $\mu_{eff}^{para} = 11.2$ μ_B and $\theta_p = -42$ K. Antiferromagnetic ordering an $T_N = 21$ K was observed by Yakinthos et al. (1980) from susceptibility measurements (4.2–200 K); the paramagnetic behavior corresponds to $\mu_{eff}^{para} = 13.2$ μ_B mole^{-1} and $\theta_p = -35$ K. Görlich et al. (1979) reported $T_N \sim 19$ K and measured [161]Dy resonance absorption spectra ($a = 3.89$, $c = 9.75$, X-ray powder data). From neutron diffraction data at 300 K Pinto et al. (1983) confirmed the crystal symmetry and atomic order consistent with the $ThCr_2Si_2$-type ($a = 3.885$, $c = 9.748$, $z(Si) = 0.380(4)$, $R = 0.091$). Neutron diffraction data at 4.2 K reveal a type-I antiferromagnetic ordering of the Dy sublattice: The magnetic moments of 9.5(5) μ_B are aligned along the c-axis ($R = 0.109$). Indexing of the 4.2 K neutron diffraction pattern was possible using the unit cell parameters $a = 3.872$ and $c = 9.669$; however, additional reflections were observed that were inconsistent with a body-centered symmetry. From the peak intensities versus temperature curve a transition temperature of $T_N = 21(2)$ K was derived. [161]Dy Mössbauer data revealed an effective magnetic hyperfinefield $H_{eff} \sim 600$ μ. A recent and independent neutron diffraction study by Leciejewicz et al. (1983) confirmed these results: $ThCr_2Si_2$-type, $a = 3.868(3)$, $c = 9.707(4)$, Si in 4e) with $z = 0.3717(7)$, $R_N = 0.084$ at 300 K; neutron data at 4.2 K reveal a primitive tetragonal magnetic unit cell, $a = 3.892(4)$, $c = 9.783(9)$, $z = 0.3934(8)$, $\mu_{eff} = 9.4(2)$ μ_B, $R_N = 0.094$; with $+ - + -$ collinear antiferromagnetic ordering at $T_N = 21(1)$ K.

Pellizzone et al. (1982) investigated the magnetic·and structural behavior of $DyCoSi_2$ with the $CeNiSi_2$-type [Cmcm, $a = 4.012(2)$, $b = 16.277(9)$, $c = 3.959(2)$]. For sample preparation, see $HoCoSi_2$. Magnetic susceptibilities (2–250 K) are characteristic for $\mu_{eff}^{para} = 10.7(2)$ μ_B and $\theta_p = 8$ K. $DyCoSi_2$ exhibits antiferromagnetic ordering at 10.5 K. Slightly different lattice parameters were measured by Yarovets (1978): $a = 3.989$, $b = 16.367$ and $c = 3.965$ (X-ray powder data).

The existence of a compound $Dy(Co,Si)_{11}$ with the $BaCd_{11}$-type of structure was first mentioned by Bodak and Gladyshevskij (1969). The atom order and crystal symmetry was confirmed by Yarovets (1978) from X-ray powder data obtained for $DyCo_{8.5}Si_{2.5}$ ($CeNi_{8.5}Si_{2.5}$-type, I4$_1$/amd, occupation variant of $BaCd_{11}$-type, $a = 9.679$ and $c = 6.300$). For sample preparation and atomic parameters, see Tb–Co–Si.

DyCoSi is orthorhombic with the TiNiSi-type of structure: Pnma, $a = 6.819$, $b = 4.172$ and $c = 7.174$ (X-ray powder data by Yarovets, 1978); for sample preparation and atomic parameters, see YNiSi.

Furthermore Gladyshevskij and Bodak (1973) mentioned, without details, the formation of a compound $DyCoSi_3$, probably isostructural with $CeCoSi_3$. Magnetic susceptibility data were recorded in the temperature range of 293–1150 K, $\mu_{eff}^{para} = 10.1(2)$ μ_B, $\theta_p = 12$ K (Yarovets, 1978).

References

Bodak, O.I. and E.I. Gladyshevskij, 1969, Dopov. Akad. Nauk Ukr. RSR, Ser. A **5**, 452.
Gladyshevskij, E.I. and O.I. Bodak, 1973, in: Khim. Met. Splavov, ed. N.M. Zhavoronkov (Nauka, Moscow) p. 46.
Görlich, E.A., A.Z. Hrynkiewicz, K. Latka, R. Kmiec, A. Szytula and K. Tomala, 1979, J. Physique Coll. **C2**, 656; 1982, J. Phys. **C15**, 6049.
Leciejewicz, J. and A. Szytula, 1983, Solid State Commun. **48**, 55.
Pellizzone, M., H.F. Braun and J. Müller, 1982, J. Magn. Magn. Mater. **30**, 33.
Pinto, H., M. Melamud, J. Gal, H. Shaked and G.M. Kalvius, 1983, Phys. Rev. **B27**(3), 1861.
Rossi, D., R. Marazza and R. Ferro, 1978, J. Less-Common Metals **58**, 203.
Yakinthos, J.K., Ch. Routsi and P.F. Ikonomou, 1980, J. Less-Common Metals **72**, 205.
Yarovets, V.I., 1978, Autoreferat Dis. Kand. Khim. (abstract of thesis, Russian) (Nauk, Lvov) 24 p.
Yarovets, V.I., Yu.K. Gorelenko and R.V. Skolozdra, 1977, Tesizy Dokl. IX. Ukr. Vses. Konf. Neorg. Khim., Lvov, p. 192.

Dy–Cu–Si

No ternary phase diagram of the system Dy–Cu–Si has been established yet, but at least four ternary compounds were found to exist,

The occurrence of AlB_2-type phases has been investigated by Rieger and Parthé (1969a) by means of X-ray powder diffraction of arc-melted alloys with the composition $DyCu_{0.67}Si_{1.33}$ ($a = 4.020$, $c = 3.971$) and DyCuSi ($a = 4.049$, $c = 3.913$). Cu and Si were said to statistically occupy the 2d site of P6/mmm (homogeneous range ?).

From arc-melted alloys annealed at $750°C$, Iandelli (1983) recorded the formation of DyCuSi with the ordered Ni_2In-type [superstructure of the AlB_2-type, $P6_3/mmc$, $a = 4.146(2)$, $c = 7.416(4)$]. The superstructure reflections were said to be very faint and with respect to the different results obtained by Rieger and Parthé (1969a) from arc-melted alloys the new phase was suspected to be a low-temperature modification. For sample preparation and purities of starting materials, see LaCuSi.

$Dy_3Cu_4Si_4$ crystallizes with the $Gd_3Cu_4Ge_4$-type of structure with the space group Immm and the lattice parameters $a = 13.69$, $b = 6.53$, $c = 4.13$ (Hanel and Nowotny, 1970; X-ray powder data). For sample preparation, see $Sc_3Cu_4Si_4$.

According to an X-ray powder diffraction analysis by Rieger and Parthé (1969b), $DyCu_2Si_2$ is tetragonal with the $ThCr_2Si_2$-type of structure [I4/mmm, $a = 3.964(6)$, $c = 9.982(1)$]. For sample preparation, see YCu_2Si_2. The differences in the unit cell dimensions ($a = 3.98$, $c = 10.10$) as presented by Görlich et al. (1979) might be indicative for the existence of an extended homogeneous range. Samples were arc melted and annealed at $800°C$ for 4 d. Mössbauer data were recorded on ^{161}Dy. Routsi and Yakinthos (1981) investigated the magnetic behavior of $DyCu_2Si_2$ ($ThCr_2Si_2$-type, no X-ray data were presented) within the temperature range of 4.2 K to 150 K and in magnetic fields of 1 to 18 kOe. Above 50 K a paramagnetic behavior was observed according to $\mu_{eff} = 10.5$ μ_B and $\theta_p = -4$ K. $DyCu_2Si_2$ orders antiferromagnetically below $T_N = 10$ K.

The crystal symmetry and atomic order were recently confirmed by Pinto et al. (1983) from neutron diffraction data at 300 K to be consistent with the $ThCr_2Si_2$-type ($a = 3.964$, $c = 9.982$, Si in the 4e sites with $z(Si) = 0.384(4)$, $R = 0.075$). Neutron

diffraction data obtained at 4.2 K, however, revealed the existence of superlattice lines according to an orthorhombic unit cell with $a = 2a_0$, $b = a_0$, $c = 2c_0$ ($a_0 = 3.95$ and $c_0 = 9.953$, $z_{Si} = 0.38(1)$; $R = 0.098$). The magnetic structure was said to consist of ferromagnetic (101) planes of Dy coupled antiferromagnetically with the Dy moments of 8.3(4) μ_B aligned along the b-axis. From the peak intensities versus temperature curve a transition temperature of $T_N = 11(1)$ K was derived. The effective magnetic hyperfine field corresponds to $H_{eff} \sim 600\ \mu$ (μ_B) (^{161}Dy Mössbauer data).

For X-ray absorption spectroscopy of $DyCu_2Si_2$, see Padalia et al. (1983).

References
Görlich, E.A., A.Z. Hrynkiewicz, K. Latka, R. Kmiec, A. Szytula and K. Tomala, 1979, J. Physique Coll. C2, 656.
Hanel, G. and H. Nowotny, 1970, Monatsh. Chem. **101**, 463.
Iandelli, A., 1983, J. Less-Common Metals **90**, 121.
Padalia, B.D., T.K. Hatwar and M.N. Ghatikar, 1983, J. Phys. **C16**, 1537.
Pinto, H., M. Melamud, J. Gal, H. Shaked and G.M. Kalvius, 1983, Phys. Rev. **B27**(3), 1861.
Rieger, W. and E. Parthé, 1969a, Monatsh. Chem. **100**, 439.
Rieger, W. and E. Parthé, 1969b, Monatsh. Chem. **100**, 444.
Routsi, Ch. and J.K. Yakinthos, 1981, Phys. Stat. Sol. (a) **68**, K153.

Dy–Fe–Si

No ternary phase diagram of the system Dy–Fe–Si exists; however, at least six ternary compounds have been characterized.

$Dy_2Fe_4Si_9$ is hexagonal with the $Y_2Fe_4Si_9$-type of structure: $P6_3/mmc$, $a = 3.930(5)$, $c = 15.45(1)$ (Gladyshevskij et al., 1978; X-ray powder analysis). For sample preparation, see $Y_2Fe_4Si_9$. Magnetic susceptibility data were obtained within the temperature range 300–1200 K and are characterized by $\mu_{eff}^{para} = 9.26\ \mu_B$ mole^{-1} and $\theta_p = 2$ K.

The crystal structure of $Dy_3Fe_2Si_7$ (earlier known as $DyFeSi_3$) was found to be isostructural with the $Ho_3Co_2Si_7$-type: $Amm2$, $a = 3.881$, $b = 24.660$ and $c = 3.913$ (X-ray powder data by Yarovets, 1978). From susceptibility data (300–1200 K) the effective moment μ_{eff}^{para} was found to be 9.72 μ_B mole^{-1} and $\theta_p = 82$ K (Gladyshevskij et al., 1978). For sample preparation, see $Y_2Fe_4Si_9$.

Mayer and Felner (1972) reported the existence of $DyFe_2Si_2$ with the $ThCr_2Si_2$-type of structure and space group $I4/mmm$. Samples were prepared by melting in an induction furnace in Al_2O_3 crucibles under helium. Thermal expansion coefficients were measured by means of high-temperature X-ray diffraction: $\alpha_a = 8.1 \times 10^{-6}$ deg^{-1}, $\alpha_c = 21.5 \times 10^{-6}$ deg^{-1}, $\bar{\alpha} = 12.6 \times 10^{-6}$ deg^{-1}; the volume expansion coefficient is $\gamma = 35.5 \times 10^{-6}$ deg^{-1}. Lattice parameters change as follows: at 25 °C, $a = 3.904(1)$, $c = 9.95$ (2); at 300 °C, $a = 3.914(1)$, $c = 9.99(2)$; at 500 °C, $a = 3.921(1)$, $c = 10.04(2)$; at 700 °C, $a = 3.928(1)$, $c = 10.08(2)$; at 910 °C, $a = 3.942(1)$, $c = 10.14(2)$. $DyFe_2Si_2$ was said to decompose at 700 °C; thermal expansion coefficients were also presented for Dy_5Si_3. The crystal structure of $DyFe_2Si_2$ was also confirmed by Felner et al. (1975) [$a = 3.896(5)$, $c = 9.890(5)$], and by Bauminger et al.

(1973), who in addition reported magnetic susceptibility data: weak ferromagnetic ordering was observed at $T_m = 753(5)$ K. From magnetization and Mössbauer-effect measurements most of the iron ($\sim 94\%$) was concluded to be diamagnetic. Electrical resistivity was 4.7 mΩ cm at 300 K (Felner and Mayer, 1973). At variance with Bauminger et al. (1973) and Felner et al. (1975), who claimed a $3d^{10}$ configuration for the Fe ions, Görlich et al. (1979), from ^{161}Dy Mössbauer spectra and Fe resonance absorption of $DyFe_2Si_2$, suggested a Fe^{2+} low-spin configuration ($a = 3.90$, $c = 9.97$). For sample preparation, see $DyNi_2Si_2$. Structural and magnetic data (80–1050 K) were also presented by Skolozdra et al. (1980): $a = 3.905(5)$, $c = 9.93$ (1); $\mu_{eff}^{para} = 12.4$ μ_B per formula unit yielding a moment of 4.5 μ_B per Fe atom; $\theta_p = -95$ K, $T_m = 310$ K. Slightly different values were reported by Yarovets (1978): $a = 3.912$, $c = 9.945$ and $\mu_{eff}^{para} = 12.6(2)$ μ_B, $\theta_p = -123$ K in the range 329–686 K, and $\mu_{eff}^{para} = 11.5(2)$ μ_B, $\theta_p = -53$ K for the temperature range 807–1112 K. At variance with these data, ^{57}Fe Mössbauer data at 4.2 K and 300 K prove the ordered atom arrangement with only a single nonmagnetic Fe site (Noakes et al., 1983); the magnetic ordering temperature as derived by ac susceptibility measurements was $T_N = 3.8$ K with a planar aabbaabb antiferromagnetic ordering similar to $NdFe_2Si_2$.

$DyFe_{4.48}Si_{1.52}$ was found to adopt the $ZrFe_4Si_2$-type of structure ($P4_2/mnm$, $a = 7.122$ and $c = 3.784$); atom parameters were refined from single crystal X-ray photographs and were derived as follows: Dy in 2b) 0,0,1/2; Fe in 8i) 0.0858(5), 0.3565(4), 0 and a statistical distribution of 3.04 Si + 0.48 Fe in 4g) 0.2121(8), 0.2121, 0; the reliability value obtained was $R = 0.102$ (Yarovets, 1978). Samples were prepared by arc melting powder compacts under argon, followed by a heat treatment in evacuated silica tubes at 800°C for 720 h. Starting materials were Dy 99.83%, Fe 99.98% and Si 99.99%.

DyFeSi crystallizes with the PbFCl-type of structure: $P4/nmm$ $a = 3.961(3)$, $c = 6.745(5)$ (Bodak et al., 1970; X-ray powder data). For sample preparation, see CeFeSi.

The crystal structure of $Dy_2Fe_3Si_5$ has been refined by Bodak et al. (1977) by means of single crystal X = ray photographs. $Dy_2Fe_3Si_5$ is isotypic with the structure of $Sc_2Fe_3Si_5$: $P4/mnc$, $a = 10.11(1)$, $c = 5.492(5)$, $\rho_{exp} = 6.81$, $\rho_x = 6.92$ kg/dm³; the reliability value is $R = 0.142$. Single crystals were obtained from arc-melted buttons. Starting materials were 99.92% Dy, 99.89% Fe and 99.99% Si. Atom parameters were presented as follows: Dy in 8h) 0.0703, 0.2385, 0; Fe in 8h) 0.3770, 0.3407, 0; Fe in 4d) 0, 0.5, 0.25; Si in 8g) 0.1840, 0.6840, 0.25; Si in 4e) 0, 0, 0.2706; Si in 8h) 0.1779, 0.4876, 0. In a later paper by Yarovets (1978) the unit cell dimensions of $Dy_2Fe_3Si_5$ were listed as $a = 10.465$ and $c = 5.272$. Braun (1980) confirmed the structure, but reported $a = 10.423(8)$ and $c = 5.465(8)$ (X-ray powder analysis). Samples were prepared by arc melting followed by a heat treatment in evacuated quartz tubes (backfilled with argon), 1 day at 1150°C, 14 days at 800°C. Starting materials were R99.9%, Fe 99.999% and Si 99.99999%. $Dy_2Fe_3Si_5$ orders antiferromagnetically at $T_N = 4.4$ K (Braun et al., 1981). From susceptibility measurements [$\mu_{eff}^{para} = 10.4(1)$ μ_B mole^{-1}, $\theta_{c,\parallel} = -11.4(4)$ K] as well as Mössbauer data no magnetic moment was observed at the iron site. See also Cashion et al. (1981). For low temperature heat capacity data see Vining and Shelton (1983); $T_N = 4.20$ K.

References

Bauminger, E.R., I. Felner, L. Froindlich, A. Grill, D. Lebenbaum, I. Mayer, I. Nowik, S. Ofer and M. Schieber, 1973, Proc. Intern. Conf. on Magnetism, Moscow.

Bodak, O.I., E.I. Gladyshevskij and P.I. Kripyakevich, 1970, Zh. Strukt. Khim. **11**(2), 305.

Bodak, O.I., Ya.B. Kotur, V.I. Yarovets and E.I. Gladyshevskij, 1977, Sov. Phys. Crystallogr. **22**(2), 217.

Braun, H.F., 1980, Phys. Lett. **75a**(5), 386.

Braun, H.F., C.U. Segre, F. Acker, M. Rosenberg, S. Dey and P. Deppe, 1981, J. Magn. Magn. Mater. **25**, 117.

Cashion, J.D., G.K. Shenoy, D. Niarchos, P.J. Viccaro, A.T. Aldred and C.M. Falco, 1981, J. Appl. Phys. **52**, 2180.

Felner, I. and I. Mayer, 1973, Mater. Res. Bull. **8**, 1317.

Felner, I., I. Mayer, A. Grill and M. Schieber, 1975, Solid State Commun. **16**, 1005.

Gladyshevskij, E.I., O.I. Bodak, V.I. Yarovets, Yu.K. Gorelenko and R.V. Skolozdra, 1978, Ukr. Fiz. Zh. **23**(1), 77.

Görlich, E.A., A.Z. Hrynkiewicz, K. Latka, R. Kmiec, A. Szytula and K. Tomala, 1979, J. Physique Coll. C2, 656.

Mayer, I. and I. Felner, 1972, J. Less-Common Metals **29**, 25.

Noakes, D.R., A.M. Umarji and G.K. Shenoy, 1983, J. Magn. Magn. Mater. **39**, 309.

Skolozdra, R.V., Yu.K. Gorelenko, O.I. Bodak and V.I. Yarovets, 1980, Ukr. Fiz. Zh. **25**(10), 1683.

Vining, C.B. and R.N. Shelton, 1983, Phys. Rev. **B28**(5), 2732.

Yarovets, V.I., 1978, Autoreferat Dis. Kand. Khim. (abstract of thesis, Russian) (Nauk, Lvov) 24 p.

Dy–Ge–Si

Structural behavior in the "pseudobinary" system $DyGe_{2-x}Si_x$ has been studied by Mayer and Eshdat (1968) by X-ray powder techniques. For sample preparation, see $NdGe_{2-x}Si_x$. Phase equilibria were interpreted in analogy to the system $NdGe_{2-x}Si_x$ (see there and figs. 11 and 21).

Reference
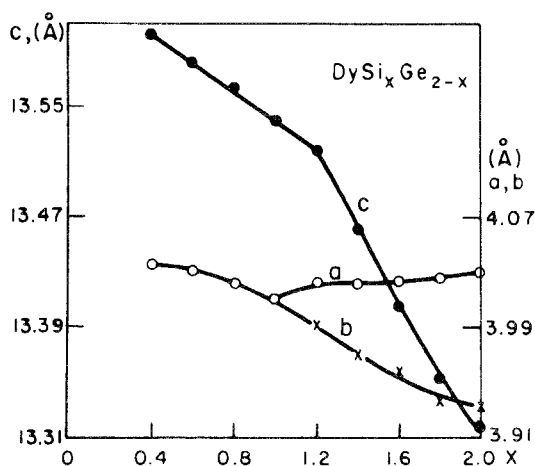
Mayer, I. and V. Eshdat, 1968, Inorg. Chem. **9**, 1904.

Fig. 21. Dy–Ge–Si, section $DyGe_{2-x}Si_x$, variation of lattice parameters versus concentration. After Mayer and Eshdat (1968).

Dy–Ir–Si

$Dy_5Ir_4Si_{10}$ crystallizes with the $Sc_5Co_4Si_{10}$-type of structure (P4/mbm, $a =$ 12.569(8), $c = 4.227(5)$; $T_m = 5.0$ K) (Braun and Segre, 1981; X-ray powder analysis). For sample preparation, see $Sc_5Ir_4Si_{10}$.

Reference

Braun, H.F. and C.U. Segre, 1981, Ternary Superconductors of $Sc_5Co_4Si_{10}$-type, in: Ternary Superconductors, Proc. Intern. Confer. on Ternary Superconductors, Lake Geneva, Wi, USA, eds. G.K. Shenoy. B.D. Dunlap and F.Y. Fradin (North-Holland, Amsterdam) pp. 239–246.

Dy–Mn–Si

Two ternary compounds exist in the Dy–Mn–Si system.

$DyMn_2Si_2$ crystallizes with the $ThCr_2Si_2$-type of structure: I4/mmm, $a = 3.915$, $c = 10.440$, $\rho_x = 6.82$ kg/dm^3 (Rossi et al., 1978; powder X-ray diffraction). For sample preparation, see $LaMn_2Si_2$. Szytula and Szott (1981) and Narasimhan et al. (1976) both confirmed the crystal symmetry and atomic order from X-ray powder diffraction data and investigated the magnetic behavior. According to Szytula antiferromagnetic ordering occurs at $T_N = 473$ K and an additional magnetic transition was observed at $T_m = 55$ K, $\mu_n = 6.5$ μ_B mole^{-1}. The paramagnetic data are characterized by $\mu_{eff}^{para} = 11.0$ μ_B mole^{-1}. Narasimhan et al. (1976) measured $a = 3.923(5)$ and $c = 10.453(5)$ and Knigenko et al. (1970) reported $a = 3.912$, $c = 10.400$ (X-ray powder data); for sample preparations, see the Y–Mn–Si system. Mössbauer data (at 1.85 K, ^{161}Dy) were recorded by Görlich et al. (1979) ($a = 3.93$, $c = 10.24$; samples were arc melted and annealed at 800°C for 4 d).

$Dy_2Mn_3Si_5$ is isotypic with the $Sc_2Fe_3Si_5$-type of structure: P4/mnc, $a = 10.62(1)$, $c = 5.454(8)$ (Segre, 1981; X-ray powder data of arc melted alloys); $T_n = 1$ K.

References

Görlich, E.A., A.Z. Hrynkiewicz, K. Latka, R. Kmiec, A. Szytula and K. Tomala, 1979, J. Physique Coll. C2, 656.
Knigenko, L.D., I.R. Mokra and O.I. Bodak, 1977, Vestn. Lvov Univ., Ser. Khim. 19, 68.
Narasimhan, K.S.V.L., V.U.S. Rao and W.E. Wallace, 1976, AIP Conf. Proc. 29, 594.
Rossi, D., R. Marazza, D. Mazzone and R. Ferro, 1978, J. Less-Common Metals 59, 79.
Segre, C.E., 1981, Thesis, Univ. of Calif., San Diego, USA.
Szytula, A. and I. Szott, 1981, Solid State Commun. 40, 199.

Dy–Nd–Si

The magnetic behavior of $Dy_{5-x}Nd_xSi_3$ alloys with the Mn_5Si_3-type (P6$_3$/mmc) was studied by Ganapathy et al. (1976) for different values of x and in the temperature range of $T \leqslant 600$ K and in fields up to 77 kOe (see table 5). Antiferromagnetic behavior is indicated but θ_p was always positive. A helical spin arrangement was suggested.

Single- phase samples were prepared by arc melting under argon. The alloy buttons were then sealed in a Ta tube (10^{-4} cm Ar) and annealed in an induction

Crystallographic and magnetic data for $Dy_{5-x}Nd_xSi_3$ alloys, after Ganapathy et al. (1976).

Alloy	a	c	θ (K)	Curie constant observed $(10^{-2}\,cm^3/g)$	Effective moment (paramagnetic), observed
Dy_5Si_3	8.405	6.302	90	7.59	10.47
Dy_4NdSi_3	8.432	6.316	53	6.51	–
$Dy_3Nd_2Si_3$	8.440	6.360	43	5.63	–
$Dy_2Nd_3Si_3$	8.525	6.366	21	4.03	–
$DyNd_4Si_3$	8.540	6.418	5	2.64	–
Nd_5Si_3	8.663	6.562	54	1.04	3.67

furnace as follows: heated to 1400 °C within 3 h, then 2 min at 1700–1750 °C, cooled to 1500 °C and annealed for 2 h and finally slowly cooled (8–10 h) to room temperature. Starting materials were of 99.9% min. purity.

Reference

Ganapathy, E.V., K. Kugimiya, H. Steinfink and D.I. Tchernev, 1976, J. Less-Common Metals **44**, 245.

Dy–Ni–Si

No ternary phase diagram of the system Dy–Ni–Si has yet been established, but at least ten ternary compounds have been identified (table 6).

Mayer and Felner (1973) investigated the phase equilibria within the concentration section $DyNi_xSi_{2-x}$ by means of X-ray powder analysis. for sample preparation, see $ErNi_xSi_{2-x}$. $DySi_2$ is orthorhombic with the $GdSi_2$-type: Imma, $a = 4.030(5)$, $b = 3.931(5)$, $c = 13.32(1)$. $DyNi_{0.25}Si_{1.75}$ crystallizes with the $ThSi_2$-type of structure ($I4_1/amd$, $a = 4.00(5)$, $c = 13.63(1)$, stabilization of a binary modification?). At higher Ni concentrations the AlB_2-type of structure was observed to be stable from $DyNi_{0.5}Si_{1.5}$ to $DyNi_{0.75}Si_{1.25}$ (see table 6). The alloy DyNiSi revealed the powder pattern of the $ThCr_2Si_2$-type with additional reflections of Dy_2O_3! (With respect to the results obtained by Dwight (1982) and Bodak et al. (1974)—concerning the existence of a TiNiSi-type phase—this alloy probably does not represent an equilibrium condition and might be the result of a reaction with the crucible material.) $DyNi_{1.25}Si_{0.75}$ [$a = 8.300(5)$, $c = 6.881(5)$] and $DyNi_{1.5}Si_{0.5}$ [$a = 8.290(5)$, $c = 6.895(5)$] were claimed to crystallize with an unknown hexagonal structure type. $DyNi_{1.75}Si_{0.25}$ is cubic with the $MgCu_2$-type ($a = 7.18$) and probably part of the solid solution originating at the binary $DyNi_2$ with $a = 7.16$.

References

Bodak, O.I. and E.I. Gladyshevskij, 1969, Kristallografiya **14**(6), 990.
Bodak, O.I., E.I. Gladyshevskij and P.I. Kripyakevich, 1966, Izv. Akad. Nauk SSSR, Neorg. Mater. **2**(12), 2151.
Bodak, O.I., V.I. Yarovets and E.I. Gladyshevskij, 1974, Tesizy Dokl. Tret. Vses. Konf. Kristallokhim. Intermet. Soedin, 2nd Ed., ed. R.M. Rykhal (Lvov Gos. Univ., Lvov, USSR) p. 32.
Chabot, B. and E. Parthé, 1984, J. Less-Common Metals **97**, 285.

TABLE 6

Formation and structural data of ternary compounds Dy–Ni—Si.

Compound	Structure type Space group	Lattice parameters Density	Preparation, Characterization	Refs.	Purity
$DyNi_{10}Si_2$	$YNi_{10}Si_2$ ord. $ThMn_{12}$ I4/mmm	$a = 8.204$ $c = 4.673$	$\mu_{\text{eff}}^{\text{para}} = 10.7\ \mu_B$, $\theta_p = 5$ K arc(Ar), Qu 800 °C, 720 h PXD	GlBYGS, 77 Ya, 78a	Dy 99.83 Ni 99.98 Si 99.9
$DyNi_{6.72}Si_{6.28}$	$Ce_2Ni_{17}Si_9$? ($NaZn_{13}$-deriv.) I4/mcm ?	$a = 10.961$ $c = 11.124$ [(**)]	arc(Ar), Qu 800 °C, 720 h PXD	Ya, 78b	Dy 99.83 Ni 99.98 Si 99.9
$Dy_3Ni_6Si_2$	$Ce_3Ni_6Si_2$ ord. Ca_3Ag_8) Im3m	$a = 8.763(2)$	arc, Qu(Ni) 800 °C, 2 weeks PXD	GlKB, 66	Dy 98.7 Ni 99.99 Si 99.99
Dy_3NiSi_2	Gd_3NiSi_2 filled Hf_3P_2 Pnma	$a = 11.248(2)$ $b = 4.119(1)$ $c = 11.156(3)$	arc(Ar), Qu(Ta) 800 °C, 2 weeks PXD	KlP, 82	Dy 99.9 Ni 99.99 Si 5N
DyNiSi	TiNiSi Pnma	$a = 6.859$ $b = 4.182$ $c = 7.161$	PXD $\mu_{\text{eff}}^{\text{para}} = 10.7\ \mu_B$, $\theta_p = -82$ K	BoYG, 74 GlBYGS, 77	Dy 99.83 Ni 99.98 Si 99.99
		$a = 6.86$ $b = 4.16$ $c = 7.15$	PXD	Dw, 82	
		$a = 6.880$ $b = 4.132$ $c = 7.214$	arc(Ar), Qu 800 °C, 720 h PXD	Ya, 78b	Dy 99.83 Ni 99.98 Si 99.9
$DyNi_2Si_2$	$ThCr_2Si_2$ I4/mmm	$a = 3.938(10)$ $c = 9.532(10)$	arc(Ar) PXD	BoGK, 66	Dy 98.7 Ni 99.8 Si 99.99
		$a = 3.938(5)$ $c = 9.532(5)$ [(*)] at compos. DyNiSi	induction melting ~ 1600 °C, Ar, in Al_2O_3 annealed for 30 min at 1600 °C, PXD	MaF, 73	99.9
		$a = 3.94$ $c = 9.53$	induction melting Ar, PXD $T_N = 7.0$ K, $\theta_p = -4$ K, $\mu_{\text{eff}}^{\text{para}} = 10.7\ \mu_B$	YaI, 80	
		$a = 3.95$ $c = 9.55$	arc(Ar) 800 °C, 4 d, in vacuum PXD; Mössbauer data, 2.1 K	GöHLKST, 79	
$DyNiSi_2$	$CeNiSi_2$ Cmcm	$a = 3.971(2)$ $b = 16.025(10)$ $c = 3.949(2)$	arc(Ar) PXD	BoG, 69	Dy 98.7 Ni 99.8 Si 99.99

TABLE 6 (continued)

Compound	Structure type Space group	Lattice parameters Density	Preparation, Characterization	Refs.	Purity
Dy(Ni,Si)$_2$	AlB$_2$ P6/mmm	$a = 3.970(5)$ $c = 4.013(5)$ for compos. DyNi$_{0.5}$Si$_{1.5}$	induction melting $\sim 1600\,^\circ$C, Ar, in Al$_2$O$_3$ annealed for 30 min at $\sim 1600\,^\circ$C	MaF, 73	99.9
		$a = 4.000(5)$ $c = 3.960(5)$ for compos. DyNi$_{0.75}$Si$_{1.25}$	PXD		
DyNiSi$_3$	ScNiSi$_3$ Amm2	$a = 3.973$ $b = 3.906$ $c = 21.121$	arc, Qu (10^{-2} Torr Ar) $800\,^\circ$C, 720 h $\mu_{\text{eff}}^{\text{para}} = 9.54\,\mu_B$, $q_p = -52$ k	GoBGY, 77 Ya, 78b	Dy 99.83 Ni 99.98 Si 99.99
Dy$_2$Ni$_3$Si$_5$	U$_2$Co$_3$Si$_5$ Ibam	$a = 9.544(3)$ $b = 11.116(4)$ $c = 5.633(2)$	arc, Qu(Ar) $1100\,^\circ$C, 24 h $1000\,^\circ$C, 150 h, PXD	ChP, 84	Dy 99.99 Ni 99.99 Si 99.999

$^{(*)}$ The sample contained also Dy$_2$O$_3$!

$^{(**)}$ For a correct setting of a bct-unit cell $a = a_0/\sqrt{2} = 7.750$.

Dwight, A.E., 1982, private communication.

Gladyshevskij, E.I., P.I. Kripyakevich and O.I. Bodak, 1966, Acta Crystallogr. **A21**, 80, and Z. Anorg. Allg. Chem. **344**, 95.

Gladyshevskij, E.I., O.I. Bodak, V.I. Yarovets, Yu.K. Gorelenko and R.V. Skolozdra, 1977, Fiz. Magnit. Plenok (Irkutsk) **10**, 182.

Gorelenko, Yu.K., O.I. Bodak, E.I. Gladyshevskij and V.I. Yarovets, 1977, Ukr. Fiz. Zh. **22**(6), 1020.

Görlich, E.A., A.Z. Hrnkiewicz, K. Latka, R. Kmiec, A. Szytula and K. Tomala, 1979, J. Physique Coll. **C2**, 656.

Klepp, K. and E. Parthé, 1982, J. Less-Common Metals **83**, L33.

Mayer, I. and I. Felner, 1973, J. Solid State Chem. **7**, 292.

Yakinthos, J.K. and P.F. Ikonomou, 1980, Solid State Commun. **34**, 777.

Yarovets, V.I., 1978a, Tesizy Dokl. Tret. Vses. Konf. Kristallokhim. Intermet. Soedin, 2nd Ed., ed. R.M. Rykhal (Lvov Gos. Univ., Lvov, USSR) p. 124.

Yarovets, V.I., 1978b, Autoreferat Dis. Kand. Khim. (abstract of thesis, Russian) (Nauk, Lvov) 24 p.

Dy–Os–Si

Hiebl et al. (1983) prepared the compound DyOs$_2$Si$_2$. According to their data DyOs$_2$Si$_2$ is tetragonal with the ThCr$_2$Si$_2$-type of structure [$a = 4.1316(3)$, $c = 9.6988(26)$]. For sample preparation, see YOs$_2$Si$_2$. The magnetic behavior in the range 300 K $< T <$ 1100 K is characterized by a typical Van Vleck paramagnetism with $\mu_{\text{eff}}^{\text{para}} = 10.35\,\mu_B$ and $\theta_p = 101$ K. Antiferromagnetic ordering was observed at 23 K with a field dependence of the susceptibility below 25 K, probably due to crystal field splitting.

Reference

Hiebl, K., C. Horvath, P. Rogl and M.J. Sienko, 1983, Solid State Commun. **48**, 211.

Dy–Pd–Si

Three ternary compounds have been characterized in the Dy–Pd–Si system.

$DyPd_2Si$ crystallizes with the ordered Fe_3C-type of structure with space group Pnma and lattice parameters $a = 7.299(1)$, $b = 6.923(2)$, $c = 5.501(1)$ (X-ray powder data, Moreau et al., 1982). For sample preparation, see YPd_2Si. The magnetic behavior of polycristalline $DyPd_2Si$ was studied by Gignoux et al. (1984) in the temperature range of 1.5 K to 300 K and in fields up to 77 kOe. The paramagnetic moment was $\mu_{eff}^{para} = 10.61$ μ_B, $\theta_p = 6$ K. $DyPd_2Si$ is ferromagnetic below $T_m = 9$ K; the saturation moment at 1.5 K and in 77 kOe was 7.68 μ_B.

$DyPd_2Si_2$ is tetragonal with the ordered $ThCr_2Si_2$-type of structure: $a = 4.113$, $c = 9.91$ (Ballestracci, 1976; X-ray powder diffraction). For sample preparation, see $CePd_2Si_2$. Slaski and Szytula (1982) confirmed both the atomic order and the crystal symmetry I4/mmm, but measured slightly smaller lattice patameters [$a = 4.106(1)$, $c = 9.881(4)$]. The magnetic behavior of $DyPd_2Si_2$ was investigated in the temperature range 100–600 K and paramagnetic behavior was characterized by $\mu_{eff}^{para} = 6.8$ μ_B and $\theta_p = -25$ K. Magnetic properties (4.2–300 K) were also studied by Yakinthos and Gamari-Seale (1982), who obtained quite different paramagnetic data ($\mu_{eff}^{para} = 10.8$ μ_B, $\theta_p = -4$ K) in good agreement with the moment of free Dy^{3+}. The susceptibility of $DyPd_2Si_2$ increases abruptly below 30 K but no clear ordering is observed (Yakinthos and Gamari-Seale, 1982).

According to X-ray powder data of Klepp et al. (1983) Dy_2Pd_2Si is isotypic with the crystal structure of Er_2Pd_2Si [Pnnm, $a = 7.419(2)$, $b = 13.857(4)$, $c = 4.305(1)$]. Samples were prepared by arc melting.

References
Ballestracci, R., 1976, C.R. Acad. Sci. Paris, Ser. B **282**, 291.
Gignoux, D., J.C. Gomez-Sal and D. Paccard, 1984, Solid State Commun. **49**(1), 75.
Klepp, K., E. Hovestreydt and E. Parthé, 1983, Acta Crystallogr. **C39**, 662.
Moreau, J.M., J. LeRoy and D. Paccard, 1982, Acta Crystallogr. **B38**, 2446.
Slaski, M. and A. Szytula, 1982, J. Less-Common Metals **87**, L1.
Yakinthos, J.K. and H. Gamari-Seale, 1982, Z. Phys. **B48**, 251.

Dy–Pt–Si

Three ternary compounds have been reported for the Dy–Pt–Si system.

$DyPt_2Si$ crystallizes with the ordered Fe_3C-type of structure: Pnma, $a = 7.288(2)$, $b = 6.909(2)$, $c = 5.469(2)$ (X-ray powder analysis by Moreau et al., 1982). For sample preparation, see YPd_2Si.

$DyPt_2Si_2$ was first claimed to be tetragonal with the $BaAl_4$-type ($a = 4.149$, $c = 9.790$) by Mayer and Yetor (1977) from X-ray powder data. in analogy to $ErPt_2Si_2$, Pt and Si atoms were said to be randomly distributed in the 4e and 4d sites of I4/mmm. For sample preparation, see $LaPt_2Si_2$. Rossi et al. (1979) confirmed the statistical Pt/Si distribution and gave $a = 4.152$, $c = 9.810$, $\rho_x = 11.95$ kg/dm^3; for sample preparation, see $CePd_2Si_2$. However, at variance with the findings of Mayer and Yetor (1977) and Rossi et al. (1979) a primitive tetragonal

lattice was reported by Ballestracci and Astier (1978) from X-ray powder analysis of alloys melted in an induction furnace under Ar: $a = 4.153$, $c = 9.80$. The lower crystal symmetry was confirmed by Rogl (1984) and an atomic arrangement similar to the $CaBe_2Ge_2$-type was derived from Guinier powder photographs of arc-melted samples; $a = 4.1556(7)$, $c = 9.8249(97)$, $CePt_2Si_2$-type.

DyPtSi is isotypic with the TiNiSi-type of structure: Pnma, $a = 6.962(1)$, $b = 4.2597(8)$, $c = 7.416(2)$ (X-ray powder data by Hovestreydt et al., 1982). For sample preparation, see ScPtSi.

References

Ballestracci, R. and G. Astier, 1978, C.R. acad. Sci. Paris, Ser. B **286**, 109.
Hovestreydt, E., N. Engel, K. Klepp, B. Chabot and E. Parthé, 1982, J. Less-Common Metals **86**, 247.
Mayer, I. and P.D. Yetor, 1977, J. Less-Common Metals **55**, 171.
Moreau, J.M., J. Leroy and D. Paccard, 1982, Acta Crystallogr. **B38**, 2446.
Rogl, P., 1984, Inorgan. Chem., to be published.
Rossi, D., R. Marazza and R. Ferro, 1979, J. Less-Common metals **66**, P17.

Dy–Re–Si

No phase diagram has been established for the Dy–Re–Si system; however, the existence of two ternary compounds has been reported.

From X-ray powder analysis of arc-melted alloys Bodak et al. (1978) observed the compound $Dy_2Re_3Si_5$ to be tetragonal with the $Sc_2Fe_3Si_4$-type: $P4/mnc$, $a = 10.87(1)$ and $c = 5.524(5)$. No detailed conditions for heat treatments were reported. Segre (1981) confirmed the space group, but reported different unit cell dimensions: $a = 10.92(1)$ and $c = 5.514(8)$; samples were arc melted; $T_n = 1$ K.

$DyRe_4Si_2$ was found to be isostructural with the $ZrFe_4Si_2$-type: $P4_2/mnm$, $a = 7.312(5)$, $c = 4.103(2)$ (Pecharskij, 1979; X-ray powder data of arc-melted alloys annealed at $800\,^\circ C$); for details of sample preparation, see Tb–Re–Si.

References

Bodak, O.I., V.K. Pecharskij and E.I. Gladyshevskij, 1978, Izv. Akad. Nauk SSSR, Neorg. Mater. **14**(2), 250.
Pecharskij, V.K., 1979, Autoreferat Dis. Kand. Khim. (abstract of thesis, Russian) (Nauk, Lvov) 23 p.
Segre, C.U., 1981, Thesis, Univ. of Calif., San Diego, USA.

Dy–Rh–Si

At least five ternary compounds exist in the Dy–Rh–Si system.

Chevalier et al. (1982a) reported DyRhSi to crystallize with the TiNiSi-type of structure (Pnma, $a = 6.835(1)$, $b = 4.1931(5)$ and $c = 7.338(1)$; X-ray powder diffraction). For sample preparation, see YRhSi. DyRhSi shows spontaneous magnetization below $T_m = 25$ K and a noncollinear arrangement of the moments was said to be likely; the paramagnetic behavior is characterized by $\mu_{eff}^{para} = 10.31\ \mu_B\ mol^{-1}$ and $\theta_p = 11.5$ K.

$DyRh_2Si_2$ adopts the ordered $ThCr_2Si_2$-type of structure: $I4/mmm$, $a = 4.026$ and $c = 9.92$ (Ballestracci, 1976; X-ray powder data). For sample preparation, see

YRh_2Si_2. Slaski and Szytula (1982) recently confirmed both the crystal symmetry and atomic order [$a = 4.019(3)$ and $c = 9.880(6)$] from an X-ray powder analysis of induction-melted alloys. The magnetic behavior studied in the temperature range of 100 to 600 K was paramagnetic with $\mu_{eff}^{para} = 6.8$ μ_B and $\theta_p = -50$ K. Felner and Nowik (1983) reported $a = 4.022(2)$, $c = 9.90(1)$ from X-ray powder data of induction-melted alloys. $DyRh_2Si_2$ orders antiferromagnetically at $T_N = 55(2)$ K; the second peak in the susceptibility curve at $T_m = 15(2)$ K was interpreted as intinerant electron ordering of the 4d sublattice. Furthermore at 4.1 K and 36 kOe a spin-flip transition was reported; the paramagnetic behavior at temperatures below 300 K was represented by $\mu_{eff}^{para} = 10.6(1)$ μ_B and $\theta_p = 7(3)$ K.

$DyRh_3Si_2$ is isotypic with the crystal structure of $CeCo_3B_2$: P6/mmm, $a = 5.486(6)$, $c = 3.541(4)$ (Chevalier et al., 1981; X-ray powder methods). For sample preparation, see $LaRh_3Si_2$. $DyRh_3Si_2$ orders ferromagnetically at $T_m = 29$ K; the paramagnetic data observed were: $\mu_{eff}^{para} = 10.81$ μ_B mole^{-1} and $\theta_p = 36$ K.

Chevalier et al. (1982b) investigated the structural and magnetic behavior (4.2 to 300 K) of the compound $Dy_2Rh_3Si_5$. The crystal symmetry has been derived from single crystal photographs and the atomic parameters were refined from X-ray powder diffraction data as follows: $U_2Co_3Si_5$-type, Ibam, $a = 9.80(1)$, $b = 11.68(1)$, $c = 5.686(5)$; $\rho_{exp} = 7.75$ kg/dm^3, $\rho_x = 7.90$ kg/dm^3; Dy in 8j) 0.267(1), 0.135(1), 0; Rh in 4a); Rh in 8j) 0.107(1), 0.358(1), 0; Si in 4b); Si in 8g) 0, 0.217(1), 1/4; Si in 8j) 0.340(1), 0.396(1), 0. The paramagnetic data obtained were: $\mu_{eff}^{para} = 11.0$ μ_B and $\theta_p = -1$ K. The formation of a compound Dy_2RhSi_3 with an AlB_2-derivative type has been reported by Chevalier et al. (1982b).

From X-ray powder data of arc-melted alloys annealed at 800°C for 4 d, Dy_2RhSi_3 was observed to be isostructural with Er_2RhSi_3: P$\bar{6}$2c, $a = 8.097(5)$, $c = 7.823(5)$ (Chevalier et al., 1984). No ordering was observed from magnetic susceptibility measurements (1.5 to 300 K); Dy_2RhSi_3 is paramagnetic with $\mu_{eff}^{para} = 10.67$ μ_B and $\theta_p = -7$ K.

References

Ballestracci, R., 1976, C.R. Acad. Sci. Paris, Ser. B **282**, 291.
Chevalier, B., A. Cole, P. Lejay and J. Etourneau, 1981, Mater. Res. Bull. **16**, 1067.
Chevalier, B., A. Cole, P. Lejay, M. Vlasse, J. Etourneau and P. Hagenmuller, 1982a, Mater. Res. Bull. **17**, 251.
Chevalier, B., P. Lejay, J. Etourneau, M. Vlasse and P. Hagenmuller, 1982b, Paper presented at the 7th Intern. Conf. on Solid Compounds of Transition Elements, Grenoble, France, Collected Abstracts, II B 16; and 1982, Mater. Res. Bull. **17**, 1211.
Chevalier, B., P. Lejay, J. Etourneau and P. Hagenmuller, 1984, Solid State Commun. **49**(8), 753.
Felner, I., and I. Nowik, 1983, Solid State Commun. **47**(10), 831.
Slaski, M. and A. Szytula, 1982, J. Less-Common Metals **87**, L1.

Dy–Ru–Si

Barz (1980) reported the existence of $DyRu_3Si_2$ with the $LaRu_3Si_2$-type of structure; no lattice parameters were given. For sample preparation and melting behavior (phase equilibria), see also $LaRu_3Si_2$; $T_m = 14.95$ K.

Ballestracci and Astier (1978) were first to report a tetragonal compound $DyRu_2Si_2$ with the $ThCr_2Si_2$-type of structure. The space group is $I4/mmm$ and the lattice parameters were given as $a = 4.145$ and $c = 9.51$ (X-ray powder data of induction-melted alloys). Hiebl et al (1983) confirmed the structure type and reported slightly different unit cell dimensions, $a = 4.1521(3)$, $c = 9.5363(59)$, obtained from X-ray powder diffraction. For sample preparation, see YOs_2Si_2. Magnetic susceptibilities were investigated in the temperature range from 1.5 K to 1100 K. The paramagnetic behavior is characterized by a typical Van Vleck type behavior with $\mu_{eff}^{para} = 10.59$ μ_B and $\theta_p = 100$ K. Due to antiferromagnetic ordering at lower temperatures ($T_N = 25$ K) the slopes of the reciprocal susceptibilities start to change at $T \sim 300$ K. Crystal and magnetic data were also reported by Slaski and Szytula (1982); however, discrepancies exist between their unit cell dimensions [$a = 4.137(1)$, $c = 9.483(3)$] and magnetic data from limited temperature section (100 K $< T < 600$ K, $\mu_{eff}^{para} = 6.3$ μ_B, $\theta_p = -18$ K) as compared with the data presented by Hiebl et al. (1983).

References

Ballestracci, R. and G. Astier, 1978, C.R. Acad. Sci. Paris, Ser. B **286**, 109.
Barz, H., 1980, Mater. Res. Bull. **15**, 1489.
Hiebl, K., C. Horvath, P. Rogl and M.J. Sienko, 1983, J. Magn. Magn. Mater. **37**, 287.
Slaski, M. and A. Szytula, 1982, J. Less-Common Metals **87**, L1.

Er–Ag–Si

The AlB_2-type structure with space group $P6/mmm$ was observed for the compositional range $ErAg_{0.67}Si_{1.33}$ ($a = 4.196$, $c = 4.095$) to $ErAgSi$ (Mayer and Felner, 1973a,b). For sample preparation, see $NdAg_xSi_{2-x}$.

References

Mayer, I. and I. Felner, 1973a, J. Solid State Chem. **7**, 292.
Mayer, I. and I. Felner, 1973b, J. Solid State Chem. **8**, 355.

Er–Al–Si

No complete phase diagram exists for the Er–Al–Si system, but limited information is available from the work of Raman (1968), Muravyova et al. (1972) and Yanson (1975).

Raman (1968) investigated the phase equilibria within the concentration section $ErAl_xSi_{1-x}$ by means of X-ray powder analysis of as-cast alloys (arc melted) as well as of alloys, annealed for 3 d at $100\,^\circ C$ in evacuated silica tubes (air cooled). Starting materials were Er 99.9%, Al 99.99% and Si 99.99%. $ErAl_{0.25}Si_{0.75}$ was observed to crystallize with the CsCl-type of structure with space group $Pm3m$ and a unit cell dimension of $a = 3.388(5)$. The alloys $ErAl_{0.5}Si_{0.5}$ [$a = 6.865(5)$, $b = 4.307(5)$, $c = 5.350(5)$, $\rho_{exp} = 7.98(1)$, $\rho_x = 8.179$ kg/dm^3] and $ErAl_{0.75}Si_{0.25}$ [$a = 6.910(5)$, $b = 4.223(5)$, $c = 5.395(5)$] were found to be homogeneous and isostructural with the FeB-type of structure (branch II, space group Pnma). Binary ErSi has either the

CrB-type [$a = 4.190(5)$, $b = 10.35(1)$, $c = 3.778(5)$, Cmcm] or the FeB-type, branch I [$a = 7.772(5)$, $b = 3.785(5)$, $c = 5.599(5)$]; ErAl is isostructural with the DyAl type [Pbcm, $a = 5.801(5)$, $b = 11.272(5)$, $c = 5.570(5)$]. The different branches of the FeB and CrB structure types were differentiated according to Hohnke and Parthé (1966) by their different prism ratios (ratio of height to edge of base of the typical triangular prismatic building element).

Er$_2$Al$_2$Si is a structural analogue of Dy$_2$Al$_2$Si, i.e., an ordered variant of the U$_3$Si$_2$-type of structure (space group P4/mbm); the lattice parameters were given as: $a = 6.890(4)$ and $c = 4.223(3)$ (Yanson, 1975).

ErAl$_2$Si$_2$ adopts the La$_2$O$_2$S-type of structure: P$\bar{3}$m1, $a = 4.17$, $c = 6.48$ (Muravyova et al., 1972; X-ray powder diffraction data); for details of sample preparation and atom parameters, see Sm–Al–Si.

References

Hohnke, D. and E. Parthé, 1966, Acta Crystallogr. **20**, 572.
Muravyova, A.A., O.S. Zarechnyuk and E.I. Gladyshevskij, 1972, Visc. L'vivsk. Univ., Ser. Khim. **13**, 14.
Raman, A., 1968, Inorg. Chem. 7(5), 973.
Yanson, T.I., 1975, Autoreferat Dis. Kand. Khim. (abstract of thesis, Russian) (Nauk, Lvov) 22 p.

Er–Au–Si

From an X-ray powder diffraction study Mayer et al. (1973) reported ErAu$_2$Si$_2$ to be tetragonal with the ordered ThCr$_2$Si$_2$-type [I4/mmm, $a = 4.244(5)$, $c = 10.17(5)$]. For sample preparation, see LaAu$_2$Si$_2$. Felner (1975) confirmed the ordered structure type, but gave considerably smaller unit cell dimensions, $a = 4.214$ and $c = 10.17$ (homogeneous range ?). Ferromagnetic ordering occurs at $T_m = 40.0$ K; $\mu_{eff}^{para} = 9.0\ \mu_B$, $\theta_p = 13$ K (Felner, 1975).

References

Felner, I., 1975, J. Phys. Chem. Sol. **36**, 1063.
Mayer, I., J. Cohen and I. Felner, 1973, J. Less-Common Metals **30**, 181.

Er–Co–Si

Four compounds have been characterized in the Er–Co–Si system.

ErCoSi is orthorhombic with the TiNiSi-type of structure: Pnma, $a = 6.768$, $b = 4.097$ and $c = 7.158$ (X-ray powder data by Yarovets, 1978). For sample preparation and atom parameters, see YNiSi.

Er$_3$Co$_2$Si$_7$ crystallizes with the Ho$_3$Co$_2$Si$_7$-type of structure: Amm2, $a = 3.850$, $b = 24.464$ and $c = 3.890$ (X-ray powder data by Yarovets, 1978). For sample preparation and atom parameters, see Ho$_3$Co$_2$Si$_7$. The magnetic behavior was studied in the temperature range of 293–1150 K, $\mu_{eff}^{para} = 9.3(1)\ \mu_B$, $\theta_p = -8$ K (Yarovets, 1978). Yakinthos et al. (1980) reported antiferromagnetic ordering below $T_N = 6$ K; the paramagnetic behavior (4.2–200 K) is characterized according to $\theta_p = -9$ K and $\mu_{eff}^{para} = 10.4\ \mu_B$ mole^{-1}. A magnetic transition at 4.2 K was observed between 6 and 12 kOe.

$ErCo_2Si_2$ is tetragonal with the ordered $ThCr_2Si_2$-type of structure: I4/mmm, $a = 3.867$, $c = 9.705$, $\rho_x = 7.81$ kg/dm^3 (Rossi et al., 1978; X-ray powder analysis). For sample preparation and etching conditions, see YCo_2Si_2. Yarovets (1978) reported slightly different unit cell dimensions, $a = 3.864$ and $c = 9.719$ (X-ray powder data), and Yarovets et al. (1977) measured magnetic susceptibilities (300–1200 K), $\mu_{eff}^{para} = 9.8$ μ_B, $\theta_p = -23$ K.

In a later study by Yakinthos et al. (1983) the antiferromagnetic ordering of $ErCo_2Si_2$ has been studied by means of neutron diffraction at 293 K and 4.2 K. The refinement of the nuclear intensities at 293 K yielded a reliability value of $R = 0.13$ for the following crystal data: $a = 3.8758(8)$, $c = 9.7275(28)$, Er in 2a), Co in 4d) and Si in 4e) of I4/mmm with $z(Si) = 0.37472(65)$. Attempts of refinement in lower crystal symmetries were said to be unsuccessful and the low reliability value was attributed to preferential orientation effects or overlapping impurity lines. The magnetic lattice of the 4.2 K neutron pattern, however, was tetragonal primitive. The following crystal data were given: $a = 3.8599(5)$, $c = 9.7097(24)$, $z(Si) = 0.3757(10)$; $R_n = 0.13$, $R_m = 0.06$. A collinear antiferromagnetic model assuming the Er atoms with opposite moments in the sites, 0, 0, 0 and 1/2, 1/2, 1/2 was satisfactory. The resulting magnetic moment of Er is 6.75 μ_B in an angle of 56.2° with the c-axis. The corresponding magnetic space group was derived as $P_{2s}\bar{1}(Sh_2^7)$. No magnetic moment was carried by the Co atoms. Slightly different parameters were obtained from an independent neutron diffraction study by Leciejewicz et al. (1983). At 300 K they reported $a = 3.883(1)$, $c = 9.761(3)$ and $z(Si$ in 4e$) = 0.3750(5)$, $R = 0.058$; the primitive tetragonal magnetic cell at 4.2 K was confirmed [$a = 3.892(1)$, $c = 9.779(6)$, $z = 0.3896(3)$, $R = 0.053$, $\mu = 8.7(2)$ μ_B]. At variance with the results obtained by Yakinthos et al. (1983) the Er moments, however, were claimed to be perpendicular to the c-axis, i.e., in the basal plane; $T_N = 11(1)$ K. Samples were prepared by induction melting and subsequent annealing in evacuated silica tubes at 800°C for 100 h and slowly cooled to room temperature; starting materials were 4N-R metal, 4N-Co and 5N-Si.

Pelizzone et al. (1982) investigated the structural and magnetochemical behavior of $ErCoSi_2$ with the $CeNiSi_2$-type [Cmcm, $a = 3.981(2)$, $b = 16.262(7)$, $c = 3.932(2)$]. For sample preparation, see $HoCoSi_2$. Paramagnetic behavior was characterized by $\theta_p = -17$ K and $\mu_{eff}^{para} = 9.6(1)$ μ_B. $ErCoSi_2$ orders antiferromagnetically below 4.5 K. The existence of $ErCoSi_2$ with the $CeNiSi_2$-type was earlier reported by Yarovets (1978) who gave slightly different lattice dimensions, $a = 3.990$, $b = 16.148$ and $c = 3.959$ (X-ray powder data).

References

Leciejewicz, J., M. Kolenda and A. Szytula, 1983, Solid State Commun. **45**, 145.

Pelizzone, M., H.F. Braun and J. Müller, 1982, J. Magn. Magn. Mater. **30**, 33.

Rossi, D., R. Marazza and R. Ferro, 1978, J. Less-Common metals **58**, 203.

Yakinthos, J.K., Ch. Routsi and P.F. Ikonomou, 1980, J. Less-Common Metals **72**, 205.

Yakinthos, J.K., Ch. Routsi and P. Schobinger-Papamantellos, 1983, J. Magn. Magn. Mater. **30**, 355.

Yarovets, V.I., 1978, Autoreferat Dis. Kand. Khim. (abstract of thesis, Russian) (Nauk, Lvov) 24 p.

Yarovets, V.I., Yu.K. Gorelenko and R.V. Skolozdra, 1977, Tesizy Dokl. IX. Ukr. Vses. Konf. Neorg. Khim., Lvov, p. 188.

Er–Cu–Si

At least five ternary phases have been characterized in the Er–Cu–Si system. Raman (1967) and Rieger and Parthé (1969a) investigated the occurrence of the AlB_2-type of structure by means of X-ray powder analysis of arc-melted alloys. The following data were presented by Rieger and Parthé (1969a) for $ErCu_{0.67}Si_{1.33}$ ($a = 3.988$, $c = 3.944$) and ErCuSi ($a = 4.114$, $c = 3.687$). Si and Cu atoms were said to be statistically distributed in the 2d sites of P6/mmm. Raman (1967) listed for a Cu-rich alloy "$ErCu_{1.5}Si_{0.5}$" $a = 4.139(5)$ and $c = 3.636(5)$ and for the Si-rich alloy "$ErCu_{1.5}Si_{0.5}$" $a = 4.115(5)$ and $c = 3.683(5)$. From the different compositions and unit cell dimensions an extended homogeneous range and/or eventually separated AlB_2-type phases with ordering among Cu, Si atoms are likely (see, e.g., phase equilibria in the Ce–Cu–Si system). At variance with the data by Rieger and Parthé (1969a) obtained from arc-melted samples, Iandelli (1983) obtained ErCuSi with the ordered Ni_2In-type of structure [superstructure of the AlB_2-type, $P6_3/mmc$, $a = 4.129(3)$, $c = 7.299(7)$]. The superstructure reflections were said to be very faint and were obtained from arc-melted samples after annealing at 750°C for 8–12 d. The Ni_2In-type phase was thus concluded to be a low-temperature modification.

$Er_3Cu_4Si_4$ crystallizes with the $Gd_3Cu_4Ge_4$-type of structure, Immm, $a = 13.60$, $b = 6.51$, $c = 4.10$; X-ray powder diffraction (Hanel and Nowotny, 1970). For sample preparation, see $Sc_3Cu_4Si_4$.

$ErCu_{0.5}Si_{1.5}$ was claimed by Raman (1967) to crystallize with the $GdSi_2$-type of structure: $a = 3.967(5)$, $b = 13.73(1)$, $c = 3.46(5)$.

$ErCu_2Si_2$ is isotypic with the $ThCr_2Si_2$-type of structure: I4/mmm, $a = 3.938(6)$, $c = 9.987(10)$ (Rieger and Parthé, 1969b; X-ray powder methods). For sample preparation, see the YCu_2Si_2 system. The magnetic behavior of $ErCu_2Si_2$ was studied by Routsi and Yakinthos (1981) in the temperature range of 4.2 K to 150 K and in magnetic fields of 1 to 18 kOe: $\mu_{eff}^{para} = 9.4$ μ_B and $\theta_p = -3$ K. From the field dependence and the negative Curie–Weiss temperature a ferrimagnetic behavior at low temperatures was concluded. NMR data were presented by Sampathkumaran et al. (1979); and for X-ray absorption spectroscopy, see Padalia et al. (1983).

References

Hanel, G. and H. Nowotny, 1970, Monatsh. Chem. **101**, 463.
Iandelli, A., 1983, J. Less-Common Metals **90**, 121.
Padalia, B.D., T.K. Hatwar and M.N. Ghatikar, 1983, J. Phys. C**16**, 1537.
Raman, A., 1967, Naturwiss. **54**, 560.
Rieger, W. and E. Parthé, 1969a, Monatsh. Chem. **100**, 439.
Rieger, W. and E. Parthé, 1969b, Monatsh. Chem. **100**, 444.
Routsi, Ch. and J.K. Yakinthos, 1981, Phys. Stat. Sol. (a) **68**, K153.
Sampathkumaran, E.V., L.C. Gupta and R. Vijayaraghavan, 1979, J. Phys. C**12**, 4323.

Er–Fe–Si

At least five ternary compounds exist in the Er–Fe–Si system.
$Er_2Fe_4Si_9$ crystallizes with the $Y_2Fe_4Si_9$-type of structure: $P6_3/mnc$, $a = 3.924(5)$,

$c = 15.42(1)$ (Gladyshevskij et al., 1978; X-ray powder analysis). Magnetic susceptibilities were measured within the temperature range of 300–1200 K and are characterized by $\mu_{eff}^{para} = 8.09$ μ_B mole^{-1} and $\theta_p = -31$ K. For sample preparation, see $Y_2Fe_4Si_9$.

The crystal structure of $Er_3Fe_2Si_7$ (earlier mentioned as $ErFeSi_3$) was observed to be isostructural with the $Ho_3Co_2Si_7$-type: Amm2, $a = 3.874$, $b = 24.481$ and $c = 3.984$ (Yarovets, 1978; X-ray powder data). From magnetic susceptibility data (300–1200 K) $\mu_{eff}^{para} = 9.10$ μ_B mole^{-1} and $\theta_p = 65$ K (Gladyshevskij et al., 1978).

$Er_2Fe_3Si_5$ is isotypic with the structure type of $Sc_2Fe_3Si_5$: P4/mnc, $a = 10.385(9)$, $c = 5.425(8)$ (X-ray powder diffraction data by Braun, 1980). For sample preparation, see $Dy_2Fe_3Si_5$. Antiferromagnetic ordering was observed at $T_N = 2.9$ K (Braun et al., 1981). Magnetic susceptibility data [$\mu_{eff}^{para} = 9.7(1)$ μ_B; $\theta_{c\parallel} = -8.0(3)$ K] as well as Mössbauer spectra proved the absence of a magnetic moment at the iron site. See also Cashion et al. (1981) and Noakes et al. (1983). Low temperature heat capacity data reveal multiple magnetic phase transitions at $T_m = 2.79$, 2.401, 2.381 and 2.352 K (Vining and Shelton, 1983). Yarovets (1978) reported different unit cell dimensions for $Er_2Fe_3Si_5$ with a much smaller c/a ratio: $a = 10.410$, $c = 5.282$ (X-ray powder data); for sample preparation, see Y–Fe–Si.

$ErFe_2Si_2$ belongs to the ordered $ThCr_2Si_2$-type of structure (I4/mmm, $a = 3.90$, $c = 9.92$) and according to magnetization and Mössbauer data by Umarji et al. (1983) there is no magnetic moment at 300 K on the Fe sites. $ErFe_2Si_2$ orders antiferromagnetically at $T_N = 2.6$ K and its magnetic structure as derived from a 1.3 K Mössbauer spectrum of ^{57}Fe appears to be an antiferromagnetic sequence aabbaabb.... Thus two magnetic sites exist for the Fe atoms without and with an internal field of 6 ± 1 kG. From X-ray powder diffraction small discrepancies were observed for calculated and observed (00l) intensities. It was said, that these discrepancies were not due to an Fe/Si exchange but could be attributed to orientation effects. Samples were prepared from high purity starting elements by arc melting under argon and subsequent annealing in evacuated quartz capsules at 900 °C for 8 d. Yarovets (1978) was first to prepare $ErFe_2Si_2$ with the $ThCr_2Si_2$-type and from powder data reported $a = 3.888$ and $c = 9.897$. Magnetic susceptibility data were measured in the temperature range 289–1211 K and effective paramagnetic moments were extrapolated for different temperature intervals as follows: $\mu_{eff} = 9.95(6)$ μ_B, $\theta_p = -114$ (289–496 K), $\mu_{eff} = 9.83(2)$ μ_B, $\theta_p = -21$ K (563–1000 K) and $\mu_{eff} = 9.52(8)$ μ_B, $\theta_p = 406$ (1000–1211 K).

$ErFe_{4.48}Si_{1.52}$ crystallizes with the $ZrFe_4Si_2$-type of structure: P4$_2$/mnm, $a = 7.107$ and $c = 3.793$ (Yarovets, 1978; X-ray powder data); for details of sample preparation and atom parameters, see Dy–Fe–Si.

References

Braun, H.F., 1980, Phys. Lett. **75A**(5), 386.
Braun, H.F., C.U. Segre, F. Acker, M. Rosenberg, S. Dey and P. Deppe, 1981, J. Magn. Magn. Mater. **25**, 117.
Cashion, J.D., G.K. Shenoy, D. Niarchos, P.J. Viccaro, A.T. Aldred and C.M. Falco, 1981, J. Appl. Phys. **52**, 2180.
Gladyshevskij, E.I., O.I. Bodak, V.I. Yarovets, Yu.K. Gorelenko and R.V. Skolozdra, 1978, Ukr. Zh. **23**(1), 77.

Noakes, D.R., G.K. Shenoy, D. Niarchos, A.M. Umarji and A.T. Aldred, 1983, Phys. Rev. **B27**(7), 4317.
Umarji, A.M., D.R. Noakes, P.J. Viccaro, G.K. Shenoy and A.T. Aldred, 1983, J. Magn. Magn. Mater.
    36, 61, see also **39**, 309.
Vining, C.B. and R.N. Shelton, 1983, Phys. Rev. **B28**(5), 2732.
Yarovets, V.I., 1978, Autoreferat Dis. Kand. Khim. (abstract of thesis, Russian) (Nauk, Lvov) 24 p.

Er–Ir–Si

ErIrSi is orthorhombic with the TiNiSi-type: Pnma, $a = 6.701(9)$, $b = 4.174(3)$ and $c = 7.467(5)$ (Hovestreydt et al., 1982; X-ray powder analysis). For sample preparation, see YPdSi; atomic parameters are as derived for ScPtSi.

According to X-ray powder data by Braun and Segre (1981) $Er_5Ir_4Si_{10}$ was observed to crystallize with the $Sc_5Co_4Si_{10}$-type of structure: P4/mbm, $a = 12.543(8)$, $c = 4.203(5)$. For sample preparation, see Sc_5Si_{10}. $Er_5Ir_4Si_{10}$ orders ferromagnetically at $T_m = 2.3$ K.

Slaski and Szytula (1982) investigated the structural and magnetochemical behavior of $ErIr_2Si_2$ in the temperature range from 100 to 600 K. $ErIr_2Si_2$ from X-ray powder photographs of induction-melted alloys was concluded to be isostructural with $ThCr_2Si_2$. The lattice parameters were $a = 4.028(2)$ and $c = 9.855(9)$. Magnetic behavior was characterized by $\mu_{eff}^{para} = 6.8$ μ_B and $\theta_p = -27$ K.

References
Braun, H.F. and C.U. Segre, 1981, Ternary Superconductors of the $Sc_5Co_4Si_{10}$-type, in: Ternary
    Superconductors, Proc. Intern. Conf. on Ternary Superconductors, Lake Geneva, WI, USA, eds. G.K.
    Shenoy, B.D. Dunlap and F.Y. Fradin (North-Holland, Amsterdam) pp. 239–246.
Hovestreydt, E., N. Engel, K. Klepp, B. Chabot and E. Parthé, 1982, J. Less-Common Metals **86**, 247.
Slaski, M. and A. Szytula, 1982, J. Less-Common Metals **87**, L1.

Er–Mn–Si

$ErMn_2Si_2$ is tetragonal with the $ThCr_2Si_2$-type of structure: $a = 3.895$, $c = 10.407$, $\rho_x = 7.01$ kg/dm^3 (Rossi et al., 1978; powder X-ray diffraction); for sample preparation see $LaMn_2Si_2$. Szytula and Szott (1981) confirmed the atomic order and crystal symmetry (I4/mmm) and characterized the magnetic behavior by antiferromagnetic ordering at $T_N = 508$ K, $\mu_n = 4.22$ μ_B mole^{-1}, $\mu_{eff}^{para} = 10.2$ μ_B mole^{-1}; an additional magnetic transition was observed at $T_m = 34$ K. Knigenko et al. (1977) reported considerably different lattice parameters $a = 3.889$, $c = 10.370$ (from X-ray powder data). For sample preparation, see the Y–Mn–Si system.

$Er_2Mn_3Si_5$ crystallizes with the $Sc_2Fe_3Si_5$-type of structure, P4/mnc, $a = 10.59(1)$, $c = 5.412(8)$ (Segre, 1981; X-ray powder analysis of arc-melted samples).

References
Knigenko, L.D., I.R. Mokra and O.I. Bodak, 1977, Vestn. Lvov Univ., Ser. Khim. **19**, 68.
Rossi, D., R. Marazza, D. Mazzone and R. Ferro, 1978, J. Less-Common Metals **59**, 79.
Segre, C.U., 1981, Thesis, Univ. of Calif., San Diego, USA.
Szytula, A. and I. Szott, 1981, Solid State Commun. **40**, 199.

Er–Ni–Si

No ternary phase diagram of the system Er–Ni–Si has been provided, but at least eleven ternary compounds exist (see table 7).

Mayer and Felner (1973) investigated the phase equilibria within the concentration section $ErNi_xSi_{2-x}$ by means of X-ray powder analysis. Samples were prepared by induction melting in an Al_2O_3 crucible at $\sim 1600\,°C$ under argon. For annealing the temperature was kept somewhat lower than the heating temperature for 30 min. $ErSi_2$ is hexagonal with the AlB_2-type (P6/mmm, $a = 3.80$, $c = 4.09$). $ErNi_{0.25}Si_{1.75}$ crystallizes with the $ThSi_2$-type of structure: $I4_1/amd$, $a = 4.002(5)$, $c = 13.59(1)$ (stabilization of a binary modification?). At higher Ni concentrations, from $ErNi_{0.5}Si_{1.5}$ to $ErNi_{0.75}Si_{1.25}$, the AlB_2-type was obtained (see table 7). Alloys

TABLE 7

Formation and structural data of ternary compounds Er–Ni–Si.

Compound	Structure type Space group	Lattice parameters Density	Preparation, Characterization	Refs.	Purity
$ErNi_{0.75}Si_{0.25}$ [*]	CrB Cmcm	$a = 3.735(5)$ $b = 10.20(1)$ $c = 4.082(5)$ $\rho_E = 9.15(1)$, $\rho_x = 9.325$	arc(Ar), Qu(Mo) 1000 °C, 3 d, QE(air) PXD	Ra, 68	Er 99.9 Ni 99.99 Si 99.99
$ErNi_{10}Si_2$	$YNi_{10}Si_2$ ord. $ThMn_{12}$ I4/mmm	$a = 8.193$ $c = 4.646$	$\mu_{eff}^{para} = 9.7\ \mu_B$, $\theta_p = 18$ K PXD arc(Ar), Qu, 800 °C, 720 h	Ya, 78a, b GlBYGS, 77	Er 99.83 Ni 99.98 Si 99.9
$Er_3Ni_6Si_2$	$Ce_3Ni_6Si_2$ (ord. Ca_3Ag_8) Im3m	$a = 8.725(2)$	arc, Qu(Ni) 800 °C, 2 weeks PXD	GlKB, 66	Er 99.7 Ni 99.99 Si 99.99
$ErNi_{6.72}Si_{6.28}$?	$Ce_2Ni_{17}Si_9$? ($NaZn_{13}$-deriv.) I4/mcm ?	$a = 10.996$ $c = 11.126$ [+]	arc(Ar), Qu 800 °C, 720 h PXD	Ya, 78b	Er 99.83 Ni 99.98 Si 99.9
$ErNi_{4.23}Si_{0.70}$	$ErNi_{4.23}Si_{0.70}$ ($EuMg_5$ or $Sc_3Ni_{11}Si_4$) $P6_3/mmc$	no details [●]	arc(Ar), Qu, 800 °C, 720 h PXD refinement, $R = 0.133$	Ya, 78b	Er 99.93 Ni 99.98 Si 99.9
ErNiSi	TiNiSi Pnma	$a = 6.857$ $b = 4.094$ $c = 7.200$	arc, Qu, 800 °C, 720 h PXD $\mu_{eff}^{para} = 9.7\ \mu_B$, $\theta_p = -133$ K	BoYG, 74 GlBYGS, 77	Er 99.83 Ni 99.98 Si 99.9
		$a = 6.772$ $b = 4.130$ $c = 7.140$	PXD	Dw, 82	
		$a = 6.774$ $b = 4.121$ $c = 7.144$	arc(Ar), Qu 800 °C, 720 h PXD	Ya, 78b	Er 99.93 Ni 99.98 Si 99.9

TABLE 7 (continued)

Compound	Structure type Space group	Lattice parameters Density	Preparation, Characterization	Refs.	Purity
$ErNi_5Si_3$	YNi_5Si_3 Pnma	$a = 18.762$ $b = 3.772$ $c = 6.558$	arc(Ar) 800 °C PXD	AkYBYG, 76	Ni 99.92 Si 99.99
		$a = 18.73$ $b = 3.780$ $c = 6.607$	arc(Ar), Qu 800 °C, 720 h PXD	Ya, 78b	Er 99.83 Ni 99.98 Si 99.9
$ErNi_2Si_2$	$ThCr_2Si_2$ I4/mmm	$a = 3.924(10)$ $c = 9.532(10)$	arc(Ar) PXD	BoGK, 66	Er 99.7 Ni 99.8 Si 99.99
		$a = 3.930(5)$ $c = 9.560(5)$ [○] at compos. ErNiSi	induction melting ~ 1600 °C, Ar in Al_2O_3 annealed for 30 min at ~ 1600 °C, PXD	MaF, 73	99.9
		$a = 3.929$ $c = 9.636$ [○] at compos. $ErNi_{1.25}Si_{0.75}$ and at $ErNi_{1.5}Si_{0.5}$			
		$a = 3.92$ $c = 9.53$	induction melting Ar, PXD $\theta_p = 1.4$ K, $\mu_{eff}^{para} = 9.4 \mu_B$	YaI, 80	
$ErNiSi_2$	$CeNiSi_2$ Cmcm	$a = 3.917(2)$ $b = 15.935(10)$ $c = 3.917(2)$	arc(Ar) PXD	BoG, 69	Er 99.7 Ni 99.8 Si 99.99
$Er(Ni,Si)_2$	AlB_2 P6/mmm	$a = 3.960(5)$ $c = 3.986(5)$ for compos. $ErNi_{0.5}Si_{1.5}$ $a = 3.980(5)$ $c = 3.900(5)$ for compos. $ErNi_{0.75}Si_{1.25}$	induction melting ~ 1600 °C, Ar in Al_2O_3 annealed for 30 min at ~ 1600 °C, PXD	MaF, 73	99.9
$ErNiSi_3$	$ScNiSi_3$ Amm2	$a = 3.965$ $b = 3.877$ $c = 21.108$	arc, Qu (10^{-2} Torr Ar) 800 °C, 720 h $\mu_{eff}^{para} = 7.98 \mu_B$, $\theta_p = 5$ K	GoBGY, 77 Ya, 78b	Er 99.83 Ni 99.98 Si 99.99

[*] Statistical occupation of Ni/Si atoms on the boron sites.

[○] Samples contained also Er_2O_3!

[+] For a correct setting of a bct unit cell $a = a_0/\sqrt{2} = 7.750$.

[•] Atom parameters were refined by Yarovets (1978) from X-ray powder data, $R = 0.133$: Er in 6h) 0.1963, $2x$; 1/4; Ni in 6h) $x = 0.5660$; 0.78 Ni+0.22 Si in 6g) 1/2, 0, 0; 0.9 Ni+0.10 Si in 12k) 0.8396, $2x$, 0.1030, 0.78; Si in 2a) 0,0,0; 0.97 Ni+0.03 Si in 4f) 1/3, 2/3, 0. The structure is closely related to the $EuMg_5$-type but structural analogy is suspected with the $Sc_3Ni_{11}Si_4$-type by Kotur et al. (1983).

ErNiSi, $ErNi_{1.25}Si_{0.75}$ and $ErNi_{1.5}Si_{0.5}$ revealed the powder pattern of the $ThCr_2Si_2$-type of structure but in addition contained small amounts of Er_2O_3! (table 7). For $ErNi_{1.75}Si_{0.25}$ the $MgCu_2$-type of structure was observed [$a = 7.220(5)$] as part of the solid solution originating from the binary $ErNi_2$ with $a = 7.118(2)$. Raman (1968) studied the phase equilibria within the concentration section $ErNi_xSi_{1-x}$ by means of X-ray powder analysis. For sample preparation, see the Er–Al–Si system. $ErNi_{0.75}Si_{0.25}$ was observed to crystallize with the CrB-type of structure [branch II; Cmcm, $a = 3.735(5)$, $b = 10.20(1)$ and $c = 4.082(5)$]. Binary ErNi has the FeB-type [Pnma; branch II, $a = 6.946(5)$, $b = 4.100(5)$ and $c = 5.368(5)$]. Interestingly ErSi was said to crystallize with the CrB-type of branch I [$a = 4.190(5)$, $b = 10.35(1)$, $c = 3.778(5)$]. According to a classification by Hohnke and Parthé (1966) the two branches were differentiated by their different prism ratios (ratio of height to edge of base of the typical prismatic building element).

References

Aksel'rud, L.G., V.I. Yarovets, O.I. Bodak, Ya.P. Yarmolyuk and E.I. Gladyshevskij, 1976, Sov. Phys. Crystallogr. **21**(2), 210.
Bodak, O.I. and E.I. Gladyshevskij, 1969, Kristallografiya **14**(6), 990.
Bodak, O.I., E.I. Gladyshevskij and P.I. Kripyakevich, 1966, Izv. Akad. Nauk SSSR, Neorg. Mater. **2**(12), 2151.
Bodak, O.I., V.I. Yarovets and E.I. Gladyshevskij, 1974, Tesizy Dokl. Tret. Vses. Konf. Kristallokhim. Intermet. Soedin, 2nd Ed., ed. R.M. Rykhal (Lvov Gos. Univ., Lvov, USSR) p. 32.
Dwight, A.E., 1982, private communication.
Gladyshevskij, E.I., P.I. Kripyakevich and O.I. Bodak, 1966, Acta Crystallogr. **A21**, 80; and Z. Anorg. Allg. Chem. **344**, 95.
Gladyshevskij, E.I., O.I. Bodak, V.I. Yarovets, Yu.K. Gorelenko and R.V. Skolozdra, 1977, Fiz. Magnit. Plenok (Irkutsk) **10**, 182.
Gorelenko, Yu.K., O.I. Bodak, E.I. Gladyshevskij and V.I. Yarovets, 1977, Ukr. Fiz. Zh. **22**(6), 1020.
Hohnke, D. and E. Parthé, 1966, Acta Crystallogr. **20**, 572.
Kotur, B.Ya., M. Sikiritza, O.I. Bodak and E.I. Gladyshevskij, 1983, Sov. Phys. Crystallogr. **28**, 387.
Mayer, I. and I. Felner, 1973, J. Solid State Chem. **7**, 292.
Raman, A., 1968, Inorg. Chem. **7**(5), 973.
Yakinthos, J.K. and P.F. Ikonomou, 1980, Solid State Commun. **34**, 777.
Yarovets, V.I., 1978a, Tesizy Dokl. Tret. Vses. Konf. Kristallochim. Intermet. Soedin, 2nd Ed., ed. R.M. Rykhal (Lvov Gos. Univ., Lvov, USSR) p. 124.
Yarovets, V.I., 1978b, Autoreferat dis. Kand. Khim. (abstract of thesis, Russian) (Nauk, Lvov) 24 p.

Er–Os–Si

$ErOs_2Si_2$ is tetragonal with space group I4/mmm and with the $ThCr_2Si_2$-type of structure (Hiebl et al., 1983; X-ray powder data). The unit cell dimensions were given as $a = 4.1253(4)$, $c = 9.6447(34)$. For sample preparation, see YOs_2Si_2. A typical Van Vleck paramagnetism was found for the temperature region 300 K < T < 1100 K with $\mu_{eff}^{para} = 9.70 \mu_B$ and $\theta_p = 30$ K. Ferromagnetic ordering occurs at 5.1 K.

Reference

Hiebl, K., C. Horvath, P. Rogl and M.J. Sienko, 1983, Solid State Commun. **48**, 211.

Er–Pd–Si

Three ternary compounds have been reported for the Er–Pd–Si system.

The crystal structure of Er_2Pd $(Pd_{0.575}Si_{0.425})_2$ has been refined from X-ray single crystal counter data (Er_2Pd_2Si-type, Pnnm, $a = 7.391(1)$, $b = 13.724(2)$, $c = 4.2807(8)$, $\rho_x = 8.92$ kg/dm^3; Klepp et al., 1983). The single crystal was obtained from an alloy with a nominal composition of $Er_{0.44}(Pd_{0.6}Si_{0.4})_{0.56}$. Atom ordering and atom parameters were derived as follows [all atoms in 4g) x, y, 0 of Pnnm, $R = 0.091$]: 0.58 Pd + 0.42 Si (0.164(2), 0.5325(7)); 0.57 Pd + 0.43 Si (0.167(2), 0.0168(7)); Pd (0.172(1), 0.2262(6)); Er (0.4590(5), 0.3723(4)); Er (0.5462(5), 0.1264(4)). A critical evaluation of powder X-ray data for stoichiometric Er_2Pd_2Si showed a remarkable tendency towards an ordered distribution of Pd/Si atoms: Pd prefers the 4g) site 0.164, 0.5325 and Si preferentially occupies the 4g) site 0.167, 0.0168. Samples were prepared by arc melting of master alloys of ErPd and ErSi under argon. Starting materials were Er 99.9%, Pd 99.99% and Si 99.999%.

ErPd$_2$Si has been characterized by Moreau et al. (1982) by means of X-ray powder data (ordered Fe$_3$C-type, Pnma, $a = 7.234(2)$, $b = 6.932(3)$, $c = 5.469(2)$]. For sample preparation, see YPd$_2$Si. The magnetic behavior of polycrystalline ErPd$_2$Si was studied by Gignoux et al. (1984) in the temperature range of 1.5 K to 300 K and in fields up to 77 kOe. The paramagnetic moment was $\mu_{eff}^{para} = 9.48$ μ_B, $\theta_p = 1$ K. ErPd$_2$Si orders ferromagnetically at $T_m = 2.8$ K; the saturation moment at 1.5 K and in 77 kOe was 6.62 μ_B.

Ballestracci (1976) was first to prepare the compound ErPd$_2$Si$_2$ crystallizing with the ordered ThCr$_2$Si$_2$-type of structure. Lattice parameters as derived from X-ray powder data were $a = 4.093$ and $c = 9.90$. For sample preparation, see CePd$_2$Si$_2$. Slaski and Szytula (1982) confirmed both the atomic order and the crystal symmetry I4/mmm. Unit cell dimensions as derived from X-ray powder data of induction-melted alloys [$a = 4.101(2)$, $c = 9.881(6)$] show poor agreement (homogeneous range ?). The magnetic behavior (100–600 K) was characterized by a paramagnetic moment $\mu_{eff}^{para} = 7.3$ μ_B and $\theta_p = -20$ K. Magnetic properties (4.2–300 K) were also studied by Yakinthos and Gamari-Seale (1982), who obtained quite different data ($\mu_{eff}^{para} = 9.5$ μ_B, $\theta_p = -3$ K) in good agreement with the ideal moment of a free Er^{3+} ion. The susceptibility increases abruptly below 30 K, but no clear ordering is observed.

Ottaviani et al. (1983) investigated the interaction of silicon with Pd–Er alloys at temperatures up to 650°C by means of in-situ resistivity measurements, MeV ^{4}He$^+$ backscattering, X-ray diffraction, barrier height measurements and Auger electron spectroscopy combined with Ar sputtering. Samples of three different compositions Pd$_{65}$Er$_{35}$, Pd$_{45}$Er$_{55}$ and Pd$_{15}$Er$_{85}$ have been prepared by electron beam coevaporation of 1000 Å thick amorphous films on both p- and n-type silicon wafers. Alloys and bilayers of Pd/Er were also deposited on a SiO$_2$ surface and annealed up to 650°C in purified He.

In the initial stage of the reaction at 350–400°C those Er–Pd intermetallic phases are formed which are closest to the starting composition; the excess metal forms a binary silicide (ErSi$_2$ or Pd$_2$Si); in the later stages of the reaction a ternary silicide is
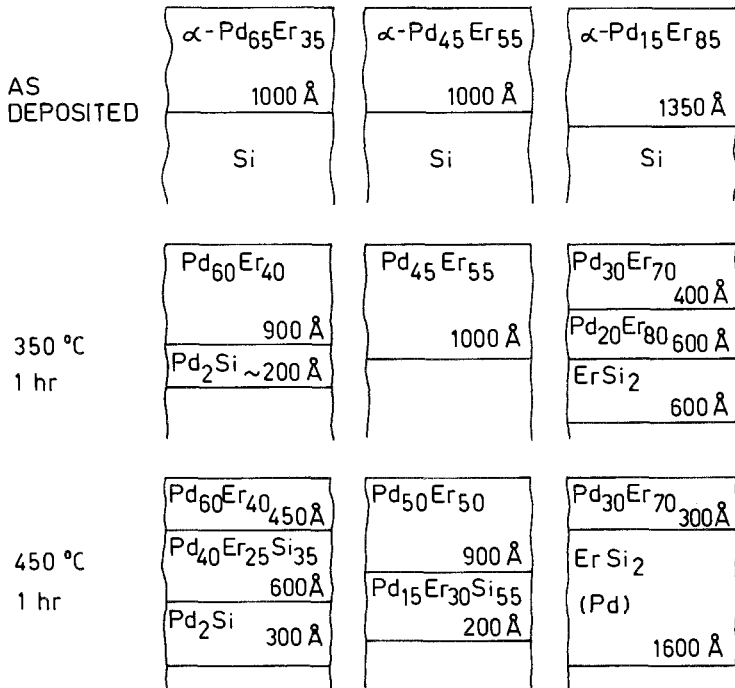
Fig. 22. Schematic diagram of the initial reaction between a silicon substrate and an amorphous deposited layer of an Er–Pd alloy (for three different alloy concentrations and after different annealing conditions); the layer thickness is indicated in Å; after Ottaviani et al. (1983).

observed. From powder X-ray diffraction analysis of the alloy film $Pd_{65}Er_{35}$ after annealing at $650\,°C$, the presence of ternary $ErPd_2Si_2$, $(ThCr_2Si_2$-type) was revealed. The $Pd_{45}Er_{55}$ alloy formed PdEr and due to the high stability of this intermetallic phase a slightly higher temperature was necessary to promote the reaction with silicon. The different stages of phase formatin are illustrated in fig. 22.

Reaction in the bilayers deposited on SiO_2 was found to start at $250\,°C$ with the formation of PdEr. Recristallization of the Pd- and Er-rich alloys on Si is faster than on the SiO_2 substrate, whereas the recrystallization of the $Pd_{45}Er_{55}$ alloys was independent of the substrate. From the observed data, the phase formation was suspected to be determined by reaction kinetics rather than by the free energies.

References

Ballestracci, R., 1976, C.R. Acad. Sci. Paris, Ser. B **282**, 291.
Gignoux, D., J.C. Gomez-Sal and D. Paccard, 1984, Solid State Commun. **49**(1), 75.
Klepp, K., E. Hovestreydt and E. Parthé, 1983, Acta Crystallogr. **C39**, 662.
Moreau, J.M., J. Le Roy and D. Paccard, 1982, Acta Crystallogr. **B38**, 2446.
Ottaviani, G., K.N. Tu, R.D. Thompson, J.W. Mayer and S.S. Lau, 1983, J. Appl. Phys. **54**(8), 4614.
Slaski, M. and A. Szytula, 1982, J. Less-Common Metals **87**, L1.
Yakinthos, J.K. and H. Gamari-Seale, 1982, Z. Phys. **B48**, 251.

Er–Pt–Si

Three ternary compounds have been characterized in the Er–Pt–Si system.

ErPt$_2$Si crystallizes with the ordered Fe$_3$C-type of structure: Pnma, $a = 7.234(2)$, $b = 6.909(2)$, $c = 5.431(2)$ (Moreau et al., 1982; X-ray powder analysis); for sample preparation, see YPd$_2$Si.

The crystal structure of ErPt$_2$Si$_2$ has been refined from X-ray powder diffraction data: BaAl$_4$-type of structure, I4/mmm, $a = 4.115$, $c = 9.822$ and $\rho_x = 12.25$ kg/dm^3. Pt and Si atoms were claimed to occupy the 4d and 4e sites in a random distribution, $R = 0.156$. The z-parameter has been evaluated as $z(4e) = 0.370$ (Mayer and Yetor, 1977). For sample preparation, see LaPt$_2$Si$_2$. At variance Ballestracci and Astier (1978) observed ErPt$_2$Si$_2$ with a primitive tetragonal unit cell and reported $a = 4.124$ and $c = 9.82$ (X-ray powder diffraction of alloys melted in an induction furnace under argon). The lower crystal symmetry with an atomic arrangement similar to the CaBe$_2$Ge$_2$-type was confirmed by Rogl (1984) from X-ray powder data of arc-melted alloys; $a = 4.1304(4)$, $c = 9.8633(42)$; CePt$_2$Si$_2$-type.

ErPtSi is orthorhombic with the TiNiSi-type of structure: Pnma, $a = 6.908(1)$, $b = 4.2444(7)$, $c = 7.401(1)$ (X-ray powder methods by Hovestreydt et al., 1982). For sample preparation, see ScPtSi.

References

Ballestracci, R. and G. Astier, 1978, C.R. Acad. Sci. Paris, Ser. B **286**, 109.
Hovestreydt, E., N. Engel, K. Klepp, B. Chabot and E. Parthé, 1982, J. Less-Common Metals **86**, 247.
Mayer, I. and P.D. Yetor, 1977, J. Less-Common Metals **55**, 171.
Moreau, J.M., J. Leroy and D. Paccard, 1982, Acta Crystallogr. **B38**, 2446.
Rogl, P., 1984, Inorg. chem., to be published.

Er–Re–Si

Two compounds have been characterized in the Er–Re–Si system.

According to X-ray powder data by Bodak et al. (1978) Er$_2$Re$_3$Si$_5$ is tetragonal with the Sc$_2$Fe$_3$Si$_5$-type of structure [P4/mnc, $a = 10.84(1)$, $c = 5.477(5)$]. The samples were arc melted but no conditions of heat treatment were given. Segre (1981) confirmed the space group, but observed considerably different lattice parameters: $a = 10.90(1)$, $c = 5.479(8)$. Samples were arc melted; $T_n = 1$ K.

Pecharsky (1979), from X-ray powder data of arc-melted alloys annealed at 800 °C, observed the formation of a compound ErRe$_4$Si$_2$ with the ZrFe$_4$Si$_2$-type of structure: P4$_2$/mnm, $a = 7.301(5)$ and $c = 4.103(2)$; for details of sample preparation, see Tb–Re–Si.

References

Bodak, O.I., V.K. Pecharskij and E.I. Gladyshevskij, 1978, Izv. Akad. Nauk SSSR, Neorg. Mater. **14**(2), 250.
Pecharskij, V.K., 1979, Autoreferat Dis. Kand. Khim. (abstract of thesis, Russian) (Nauk, Lvov) 23 p.
Segre, C.U., 1981, Thesis, Univ. of Calif., San Diego, USA.

Er–Rh–Si

ErRhSi is isotypic with the crystal structure of TiNiSi; the space group is Pnma and the lattice parameters were given as $a = 6.766(1)$, $b = 4.1695(5)$ and $c = 7.356(1)$ (Chevalier et al., 1982a; X-ray powder analysis). For sample preparation, see YRhSi. ErRhSi orders antiferromagnetically at $T_N = 7.5$ K. A metamagnetic or spin-flopping transition was reported to occur at 4.2 K for magnetic fields $\geqslant 12$ kOe; the paramagnetic behavior is characterized by $\mu_{eff}^{para} = 9.54$ μ_B mole^{-1} and $\theta_p = -3$ K. Hovestreydt et al. (1982) confirmed the structure type by means of X-ray powder analysis of arc-melted samples but reported slightly different unit cell dimensions $a = 6.787(4)$, $b = 4.201(3)$ and $c = 7.451(7)$.

ErRh$_2$Si$_2$ is tetragonal with the ordered ThCr$_2$Si$_2$-type of structure: I4/mmm, $a = 4.015$, $c = 9.88$ (Ballestracci, 1976; X-ray powder methods). For sample preparation, see YRh$_2$Si$_2$. Slaski and Szytula (1982) confirmed both atomic order and crystal symmetry. Their lattice parameter data obtained from X-ray powder diffraction are slightly different from those observed by Ballestracci (1976) [$a = 4.025(3)$ and $c = 9.888(9)$]. Samples were prepared by induction melting. Magnetic behavior as reported from the temperature range of 100 to 600 K was paramagnetic, characterized by $\mu_{eff}^{para} = 7.9$ μ_B and $\theta_p = -27$ K. Felner and Nowik (1983) reported $a = 4.012(2)$ and $c = 9.88(1)$ (X-ray powder diffraction data obtained from induction-melted alloys); ErRh$_2$Si$_2$ orders antiferromagnetically at $T_N = 103(2)$ K. There is also a second peak in the susceptibility versus temperature curve at $T_m = 13(2)$ K, which was interpreted as itinerant electron ordering of the 4d sublattice. The paramagnetic behavior [1.5–300 K; $\mu_{eff}^{para} = 7.6(1)$ μ_B, $\theta_p = 8(3)$ K] shows a remarkable deviation from the paramagnetism of the free R^{3+} ion.

ErRh$_3$Si$_2$ adopts the CeCo$_3$B$_2$-type of structure: P6/mmm, $a = 5.472(6)$, $c = 3.542(4)$ (Chevalier et al., 1981); X-ray powder methods). For sample preparation, see LaRh$_3$Si$_2$. ErRh$_3$Si$_2$ orders ferromagnetically at $T_m = 24$ K; the paramagnetic data were $\mu_{eff}^{para} = 9.20$ μ_B mole^{-1} and $\theta_p = 41$ K.

Chevalier et al. (1982b) investigated the structural and magnetic properties (4.2 to 300 K) of the compound Er$_2$Rh$_3$Si$_5$ crystallizing with the Sc$_2$Co$_3$Si$_5$-type of structure [Ibam, $a = 9.77(1)$, $b = 11.64(1)$, $c = 5.662(5)$]. The paramagnetic data obtained were: $\mu_{eff}^{para} = 9.72$ μ_B and $\theta_p = -3$ K. Er$_2$Rh$_3$Si$_5$ was said to order antiferromagnetically at very low temperatures.

Chevalier et al. (1982b) mentioned the existence of a compound Er$_2$RhSi$_3$ with a structure type closely related to AlB$_2$. The crystal strycture of Er$_2$RhSi$_3$ was refined from single crystal photographs and X-ray powder data and was found to be a superstructure of the AlB$_2$-type according to a unit cell $a = 2a_0$, $c = 2c_0$ and with an ordered arrangement of Rh and Si atoms on the B sites: Er$_2$RhSi$_3$-type, P$\bar{6}$2c, $a = 8.036(5)$, $c = 7.712(5)$, $\rho_{exp} = 7.97(8)$, $\rho_{theor} = 8.04$ kg/dm^3. The atom parameters were derived as follows: Er in 2b); Er in 6h) 0.481(1), 0.019(1), 1/4; Rh in 4f) 1/3, 2/3, 0.000(1); and Si in 12i) 0.167(1), 0.333(1), 0.000(1). Magnetic measurements in the temperature range of 1.5 to 300 K revealed a paramagnetic behavior according to $\mu_{eff}^{para} = 9.36$ μ_B and $\theta_p = 6$ K; no ordering was observed (Chevalier et al., 1984).

References

Ballestracci, R., 1976, C.R. Acad. Sci. Paris, Ser. B **282**, 291.
Chevalier, B., A. Cole, P. Lejay and J. Etourneau, 1981, Mater. Res. Bull. **16**, 1067.
Chevalier, B., A. Cole, P. Lejay, M. Vlasse, J. Etourneau and P. Hagenmuller, 1982a, Mater. Res. Bull. **17**, 251.
Chevalier, B., P. Lejay, J. Etourneau, M. Vlasse and P. Hagenmuller, 1982b, Paper presented at the 7th Intern. Conf. on Solid Compounds of Transition Elements, Grenoble, France, Collected Abstracts, II B 16, and 1982, Mater. Res. Bull. **17**, 1211.
Chevalier, B., P. Lejay, J. Etourneau and P. Hagenmuller, 1984, Solid State Commun. **49**(9), 753.
Felner, I. and I. Nowak, 1983, Solid State Commun. **47**, 831.
Hovestreydt, E., N. Engel, K. Klepp, B. Chabot and E. Parthé, 1982, J. Less-Common Metals **68**, 247.
Slaski, M. and A. Szytula, 1982, J. Less-Common Metals **87**, L1.

Er–Ru–Si

Barz (1980) reported the existence of a ternary compound $ErRu_3Si_2$ with the $LaRu_3Si_2$-type of structure. No crystal structure data were presented. For sample preparation and melting behavior (phase equilibria), see $LaRu_3Si_2$; $T_m = 16.19$ K.

From an X-ray powder analysis of induction-melted alloys Ballestracci and Astier (1978) were first to observe the compound $ErRu_2Si_2$ with the $ThCr_2Si_2$-type of structure. The lattice parameters were $a = 4.141$ and $c = 9.45$. Hiebl et al. (1983) confirmed the structure type and reported $a = 4.1442(3)$, $c = 9.4899(46)$ (X-ray powder data). For sample preparation, see YOs_2Si_2. The magnetic behavior was investigated in the temperature range 1.5 K $< T <$ 1100 K and at higher temperatures is characterized by a typical Van Vleck paramagnetism ($\mu_{eff}^{para} = 9.66$ μ_B, $\theta_p = 39.6$ K). Due to ferromagnetic ordering at 4.5 K the slopes of the reciprocal susceptibilities start to change at $T < 300$ K. Slaski and Szytula (1982) also reported crystallographic and magnetic data (100 $< T <$ 600 K) of $ErRu_2Si_2$. Their data ($a = 4.191(8)$, $c = 9.495(6)$ and $\mu_{eff}^{para} = 6.7$ μ_B, $\theta_p = -33$ K), however, show a remarkable deviation from the values reported by Ballestracci and Astier (1978) and by Hiebl et al. (1983).

References

Ballestracci, R. and G. Astier, 1978, C.R. Acad. Sci. Paris, Ser. B **286**, 109.
Barz, H., 1980, Mater. Res. Bull. **15**, 1489.
Hiebl, K., C. Horvath, P. Rogl and M.J. Sienko, 1983, J. Magn. Magn. Mater **37**, 287.
Slaski, M. and A. Szytula, 1982, J. Less-Common Metals **87**, L1.

Er–Y–Si

Raman (1968) observed a complete solid solution for the system $Er_{1-x}Y_xSi$ at 1000°C, crystallizing with the CrB-type of structure. For sample preparation and structural details (CrB-type, branch I, Cmcm), see $ErAl_xSi_{1-x}$. The following lattice parameters were reported: YSi: $a = 4.251(5)$, $b = 10.53(1)$, $c = 3.826(5)$; $Er_{0.5}Y_{0.5}Si$: $a = 4.233(5)$, $b = 10.44(1)$, $c = 3.804(5)$ and ErSi: $a = 4.190(5)$, $b = 10.35(1)$, $c = 3.778(5)$.

Reference

Raman, A., 1968, Inorg. Chem. **7**(5), 973.

Eu–Ag–Si

According to X-ray powder data by Mayer et al. (1973) and Mayer and Cohen (1972) $EuAg_2Si_2$ is tetragonal with the ordered $ThCr_2Si_2$-type [I4/mmm, $a = 4.309(5)$, $c = 10.49(5)$]; for sample preparation, see $LaAg_2Si_2$. From the large unit cell dimensions as well as from ^{151}Eu Mössbauer spectroscopy Mayer and Cohen (1972) concluded Eu to be divalent. The sample also contained the hexagonal AlB_2-type phase $EuAg_{0.67}Si_{1.33}$ with lattice parameters $a = 4.203$ and $c = 4.465$ and space group P6/mmm (see also Mayer and Felner, 1973). According to Felner and Schieber (1973), $EuAg_{0.67}Si_{1.33}$ orders ferromagnetically at $T_m = 34$ K but is paramagnetic (Eu^{2+}) at higher temperatures with $\mu_{eff}^{para} = 7.94$ μ_B and $\theta_p = 21$ K.

References

Felner, I. and M. Schieber, 1973, Solid State Commun. **13**, 457.
Mayer, I., J. Cohen and I. Felner, 1973, J. Less-Common Metals **30**, 181.
Mayer, I. and I. Felner, 1973, J. Solid State Chem. **8**, 355.
Mayer, I. and J. Cohen, 1972, J. Less-Common Metals **29**, 221.

Eu–Al–Si

No ternary phase diagram is established for the system Eu–Al–Si; the only data available were presented by Muravyova et al. (1972) and concern the existence of a ternary compound $EuAl_2Si_2$ with the La_2O_2S-type of structure (space group P$\bar{3}$m1); for sample preparation and atom parameters, see Sm–Al–Si. Lattice parameters were $a = 4.18$, $c = 7.25$ and suggest the presence of divalent Eu.

Reference

Muravyova, A.A., O.S. Zarechnyuk and E.I. Gladyshevskij, 1972, Visn. L'vivsk. Univ., Ser. Khim. **13**, 14.

Eu–Au–Si

$EuAu_2Si_2$ was reported with the ordered $ThCr_2Si_2$-type of structure, I4/mmm, $a = 4.352(5)$, $c = 10.11(5)$ (Mayer et al., 1973; X-ray powder analysis). For sample preparation, see $LaAu_2Si_2$. From susceptibility measurements ($\mu_{eff} = 6.7(1)$ μ_B, $\theta_p = -5.0$ K and ferromagnetic (?) ordering at $T_m = 15.5$ K) as well as from Mössbauer effect studies a divalent character of Eu was concluded (Felner, 1975).

According to an X-ray powder analysis by Mayer and Felner (1973) $EuAu_{0.5}Si_{1.5}$ crystallizes with the AlB_2-type of structure with space group P6/mmm and lattice parameters $a = 4.150$ and $c = 4.515$, for sample preparation, see $LaAu_2Si_2$.

References

Felner, I., 1975, J. Phys. Chem. Sol. **36**, 1063.
Mayer, I. and I. Felner, 1973, J. Solid State Chem. **8**, 355.
Mayer, I., J. Cohen and I. Felner, 1973, J. Less-Common Metals **30**, 181.

TABLE 8

Lattice parameters versus concentration for series of $M^1_{1-x}M^2_xSi_2$ alloys, after Evers et al. (1978)

Composition, x	Phase [*]	a-axis	c-axis
	$Eu_{1-x}Sr_xSi_2$		
0.00	NP	4.303(3)	13.65(1)
0.10	NP	4.314(6)	13.68(2)
0.25	NP	4.336(6)	13.69(2)
0.50	NP	4.365(10)	13.76(3)
0.75	NP	4.402(6)	13.80(2)
0.90	HP	4.419(6)	13.81(2)
1.00	HP	4.438(3)	13.83(1)
	$Ca_{1-x}Eu_xSi_2$		
0.00	HP	4.283(3)	13.52(1)
0.10	HP	4.285(3)	13.54(1)
0.25	NP	4.288(3)	13.58(1)
0.50	NP	4.295(3)	13.59(1)
0.75	NP	4.299(3)	13.63(1)
0.90	NP	4.301(3)	13.64(1)
1.00	NP	4.303(3)	13.65(1)

[*] HP = high pressure, NP = normal pressure.

Eu–Ca–Si

No ternary phase diagram exists for the Eu–Ca–Si system; the stability range of the α-ThSi$_2$-type structure was investigated along the concentration section $Ca_{1-x}Eu_xSi_2$ in the pressure range up to 40 kbar (quenched from 1000–1500 °C). For sample preparation, see Eu–Sr–Si.

A limited solid solution $Ca_{1-x}Eu_xSi_2$, $0.2 \leqslant x \leqslant 1$, was observed at normal pressures, whereas a complete homogeneous range exists at 40 kbar, with a linear variation of the unit cell dimensions versus concentration (see Table 8). A statistical distribution of Ca, Eu atoms was assumed (X-ray powder data).

Reference

Evers, J., G. Oehlinger and A. Weiss, 1978, J. Less-Common Metals **60**, 249.

Eu–Co–Si

Three ternary compounds have been characterized in the Eu–Co—Si system.

EuCo$_9$Si$_2$ is tetragonal with the BaCd$_{11}$-type of structure [I4$_1$/amd, $a = 9.798(5)$ and $c = 6.330(10)$]. Atomic ordering was reported by Bodak and Gladyshevskij (1969) to be similar to CeNi$_{8.6}$Si$_{2.4}$ (X-ray powder analysis of arc-melted alloys).

According to X-ray powder data by Mayer and Felner (1973) EuCo$_{0.5}$Si$_{1.5}$ was observed to crystallize with the AlB$_2$-type of structure (P6/mmm, $a = 4.046$, $c = 4.500$). Samples were prepared by melting in Al$_2$O$_3$ crucibles in an induction furnace under argon.

Mayer and Felner (1977) prepared $EuCo_2Si_2$ with the $ThCr_2Si_2$-type of structure ($I4/mmm$, $a = 3.921(5)$, $c = 9.850(5)$; X-ray powder analysis). For sample preparation, see $EuCu_2Si_2$. Starting materials were 99.9% pure. From Mössbauer effect measurements Eu was said to appear in two valence states. The thermoelectromotive force (80–1050 K) was investigated by Levin (1981).

References

Bodak, O.I. and E.I. Gladyshevskij, 1969, Dopov. Akad. Nauk Ukr. RSR, Ser. A **5**, 452.
Levin, E.M., 1981, Ukr. Fiz. Zh. **26**(3), 407.
Mayer, I. and I. Felner, 1973, J. Solid State Chem. **8**, 355.
Mayer, I. and I. Felner, 1977, J. Phys. Chem. Solids **38**, 1031.

Eu–Cu–Si

Mayer and Felner (1973) studied the valency of Eu in an $EuCu_{0.5}Si_{1.5}$ alloy with the AlB_2-type of structure ($P6/mmm$, $a = 4.080$, $c = 4.466$) by means of ^{151}Eu Mössbauer effect and X-ray powder diffraction measurements. Eu was found to be divalent. Samples were prepared by melting in an Al_2O_3 crucible under argon. The minimum purity of the starting elements was 99.9%.

$EuCu_2Si_2$ crystallizes with the $ThCr_2Si_2$-type of structure (Mayer and Felner, 1977; X-ray powder data). Lattice parameters were reported for an $EuCuSi_3$ alloy [$a = 4.118(5)$, $c = 9.990(5)$] containing a second phase $EuCu_{0.5}Si_{1.5}$ with the AlB_2-type. Unpublished research by Felner as quoted by Bauminger et al. (1973) showed that the Cu and Si atoms in $EuCu_2Si_2$ are distributed among the 4d and 4e sites of I4/mmm with the Cu atoms prefering the 4d sites. Mössbauer data reveal Eu in the divalent and trivalent state. Samples were prepared by melting in Al_2O_3 crucibles in an induction furnace at ~ 1600 °C under Ar and subsequent heating for ~ 30 min at somewhat lower temperature. Starting materials were 99.9% pure. From X-ray absorption spectroscopy measurements at 77 and 300 K on an arc-melted $EuCu_2Si_2$ sample, two absorption peaks were observed, corresponding to two different valence states of Eu. The population of Eu^{2+} decreases at lower temperatures (Hatwar et al., 1980) and was also monitored by the quadrupolar interaction of Cu as a function of temperature (Sampathkumaran et al., 1980). See also Bauminger et al. (1973), Buschow et al. (1977) and Scherzberg et al. (1984). For a comprehensive literature review on the physical properties of $EuCu_2Si_2$, see Gupta et al. (1981) and Sales and Viswanathan (1976). The thermoelectromotive force was measured by Levin (1981).

For X-ray absorption spectroscopy (L_3-absorption edge), see Padalia et al. (1983).

Bodak et al. (1971) mentioned the existence of a compound $EuCu_{1.6}Si_{1.4}$ with the $CeNiSi_2$-type.

References

Bauminger, E.R., D. Froindlich, I. Nowik, S. Ofer, I. Felner and I. Mayer, 1973, Phys. Rev. Lett. **30**(21), 1053.
Bodak, O.I., E.I. Gladyshevskij and Ya.M. Kalvijak, 1971, Tesizy Dokl. Vses. Konf. Kristallokhim. Intermet. Soedin, Lvov, p. 40.
Buschow, K.H.J., M. Campagna and G.K. Wertheim, 1977, Solid State Commun. **24**, 253.

Gupta, L.C., E.V. Sampathkumaran, R. Vijayaraghavan, P.D. Prabhawalkar and B.D. Padalia, 1981,
    Phys. Rev. **B23**(18), 4283; and 1981, in: Valence Fluctuations in Solids, eds. L.M. Falicov, W. Hanke
    and M.B. Maple (North-Holland, Amsterdam) pp. 241, 439.
Hatwar, T.K., R.M. Nayak, B.D. Padalia and M.N. Ghatikar, 1980, Solid State Commun. **34**, 617.
Levin, E.M., 1981, Ukr. Fiz. Zh. **26**(3), 407.
Mayer, I. and I. Felner, 1973, J. Solid State Chem. **8**, 355.
Mayer, I. and I. Felner, 1977, J. Phys. Chem. Sol. **38**, 1031.
Padalia, B.D., T.K. Hatwar, and M.N. Ghatikar, 1983, J. Phys. **C16**, 1537.
Sales, B.C. and R. Viswanathan, 1976, J. Low Temp. Phys. **23**(3,4), 449.
Sampathkumaran, E.V., L.C. Gupta and R. Vijayaraghavan, 1980, J. Magn. Magn. Mater. **15–18**, 977; see
    also 1979, Phys. Rev. Lett. **43**(16), 1189; 1979, J. Phys. **C12**, 4323.
Scherzberg, A., Ch. Sauer, U. Köbler, W. Zinn and J. Röhler, 1984, Solid State Commun. **49**(11), 1027.

Eu–Fe–Si

$EuFe_2Si_2$ crystallizes with the $ThCr_2Si_2$-type of structure: $I4/mmm$, $a = 3.970(5)$ and $c = 10.120(5)$ (Mayer and Felner, 1977; X-ray powder analysis). Samples were prepared by melting in an induction furnace at $\sim 1600\,°C$ in an Al_2O_3 crucible under argon. For annealing the samples were kept at a somewhat lower temperature than the heating temperature for 30 min. Mössbauer data were interpreted by the existence of "two well-defined valencies of Eu". The electrical resistivity was 9.5 mΩ cm at 300 K (Felner and Mayer, 1973). The thermoelectromotive force in the range between 90–1000 K was investigated by Levin (1981).

The AlB_2-type structure was not observed in the concentration section $EuFe_xSi_{2-x}$ (Mayer and Felner, 1973).

References
Felner, I. and I. Mayer, 1973, Mater. Res. Bull. **8**, 1317.
Levin, E.M., 1981, Ukr. Fiz. Zh. **26**(3), 407.
Mayer, I. and I. Felner, 1973, J. Solid State Chem. **8**, 355.
Mayer, I. and I. Felner, 1977, J. Phys. Chem. Sol. **38**, 1031.

Eu–Gd–Si

Mayer and Felner (1971) studied the concentration section $Gd_{5-x}Eu_xSi_3$ at various compositions $x = 0.25$, 0.5, 0.75 and 1.0, by means by X-ray powder analysis, and in the case of $^{155}Gd_5Si_3$ and Gd_4EuSi_3 by means of Mössbauer measurements. Mixtures of a total weight of 500–700 mg were prepared in a dry-box and induction-heated at $\sim 1600\,°C$ under argon.

All compounds were claimed to be homogeneous and to crystallize with the Mn_5Si_3-type of structure, $P6_3/mcm$. Lattice parameters were as follow: Gd_5Si_3: $a = 8.52$, $c = 6.39$; $Gd_{4.75}Eu_{0.25}Si_3$: $a = 8.50$, $c = 6.39$; $Gd_{4.5}Eu_{0.5}Si_3$: $a = 8.49$, $c = 6.38$; $Gd_{4.25}Eu_{0.75}Si_3$: $a = 8.49$, $c = 6.39$; $Gd_{4.0}Eu_{1.0}Si_3$: $a = 8.49$, $c = 6.37$; the composition was accurate to ± 0.5 a/o. Samples with a Eu concentration higher than 20 a/o were said to be multiphase with complex X-ray powder patterns. From the decreasing lattice parameter values as well as a smaller Gd isomer shift in Gd_4EuSi_3, Mayer and Felner (1971) concluded the formation of Gd vacancies, the Eu atoms being located interstitially (?) or in octahedral holes (Ti_5Ge_4-type ?).

Reference
Mayer, I. and I. Felner, 1971, J. Less-Common Metals **24**, 243.

Eu–Ge–Si

Mayer and Tendy (1970) mentioned unpublished results obtained by Mayer and Felner, concerning the concentration section $Eu_5Ge_xSi_{3-x}$ (Mn_5Si_3-type, $P6_3/mcm$).

Reference
Mayer, I. and S. Tendy, 1970, Israel J. Chem. **8**, 955.

Eu–Ni–Si

No ternary phase diagram of the system Eu–Ni–Si is available yet. At least eight ternary compounds were identified (see table 9).

Bodak et al. (1966) were first to report the existence of a compound $EuNiSi_3$ with the $BaAl_4$-type of structure (I4/mmm). Mayer and Felner (1977) confirmed the existence of $EuNiSi_3$, and in addition provided structural data for a composition $EuNi_2Si_2$. Refinement of X-ray powder diffraction data of $EuNi_2Si_2$ yielded the lowest R-value ($R = 0.218$) for the $ThCr_2Si_2$-type of arrangement with Eu atoms in 2a), Ni in 4d) and Si in 4e) with $z = 0.375(1)$. In the case of $EuNiSi_3$ a statistical occupation of $2Si + 2Ni$ in 4e) was obtained [Eu in 2a), Si in 4d)]. This type of atomic order with symmetry I4/mmm is consistent with the $PrNiGa_3$-type of structure ($BaAl_4$-type derivative). Mössbauer data at 300 K and 4.2 K indicated divalent Eu in $EuNiSi_3$, but two valencies for Eu in $EuNi_2Si_2$. The thermoelectromotive force in $EuNi_2Si_2$ (80–1050 K) has been measured by Levin (1981) and electrophysical properties (temperature dependence of electrical resistance, thermoelectrical coefficient and magnetic susceptibility) of $EuNi_2Si_2$ were reported by Levin et al. (1977).

References
Bodak, O.I. and E.I. Gladyshevskij, 1969a, Dopov. Akad. Nauk Ukr. RSR, Ser. A **5**, 452.
Bodak, O.I. and E.I. Gladyshevskij, 1969b, Dopov. Akad. Nauk Ukr. RSR, Ser A **12**, 1125.
Bodak, O.I. and E.I. Gladyshevskij, 1969c, Kristallografiya **14**(6), 990.
Bodak, O.I., E.I. Gladyshevskij and P.I. Kripyakevich, 1966, Ivz. Akad. Nauk SSSR, Neorg. Mater. **2**(12), 2151.
Gladyshevskij, E.I., P.I. Kripyakevich and O.I. Bodak, 1966, Acta Crystallogr. **A21**, 80; and Z. Anorg. Allg. Chem. **344**, 95.
Levin, E.M., 1981, Ukr. Fiz. Zh. **26**(3), 407.
Levin, E.M., R.V. Lutsiv, E.I. Gladyshevskij and O.I. Bodak, 1977, Fiz. Elektron. Resp. Mezhved. Nauch-tekhn. Sbor. **15**, 59.
Mayer, I. and I. Felner, 1973, J. Solid State Chem. **8**, 355.
Mayer, I. and I. Felner, 1977, J. Phys. Chem. Sol. **38**, 1031.

Eu–Pd–Si

According to X-ray powder diffraction data by Ballestracci (1976), $EuPd_2Si_2$ is body-centered tetragonal with the ordered $ThCr_2Si_2$-type, I4/mmm, $a = 4.190$ and

TABLE 9

Formation and structural data of ternary compounds Eu–Ni–Si.

Compound	Structure type Space group	Lattice parameters Density	Preparation, Characterization	Refs.	Purity
$Eu_3Ni_6Si_2$	$Ce_3Ni_6Si_2$ ord. Ca_3Ag_8 Im3m	$a = 8.913(2)$	arc, Qu(Ni) 800 °C, 2 weeks PXD	GlKB, 66	Eu 98.4 Ni 99.99 Si 99.99
$EuNi_{8.6}Si_{2.4}$	$Ce_2Ni_{17}Si_5$ $(BaCd_{11})$ $I4_1/amd$	$a = 9.801(5)$ $c = 6.216(10)$	arc(Ar), Qu 800 °C, 250 h, PXD atom order as for $CeNi_{8.6}Si_{2.4}$	BoG, 69a	Ni 99.91 Si 99.99
$EuNi_{8.6}Si_{4.4}$ ~ 30 a/o Si [*]	$Ce_2Ni_{17}Si_9$ $(NaZn_{13}$-deriv.) I4/mcm	$a = 11.04(1)$ [*] $c = 11.48(1)$	arc(Ar), Qu 800 °C, 100 h, PXD	BoG, 69b	Eu 99.2 Ni 99.99 Si 99.99
$Eu(Ni,Si)_{13}$ 37–45 a/o Si	$NaZn_{13}$ Fm3c	$a = 11.18$	arc(Ar), Qu 800 °C, 100 h, PXD	BoG, 69b	Eu 99.2 Ni 99.99 Si 99.99
"$EuNiSi_3$" [**]	$PrNiGa_3$ I4/mmm	$a = 4.143(10)$ $c = 9.625(10)$	arc(Ar) PXD	BoGK, 66	Eu 98.4 Ni 99.8 Si 99.99
		$a = 4.150(5)$ $c = 9.636(5)$	induction heating at 1600 °C (Ar) in Al_2O_3 30 min, PXD refinement	MaF, 77	99.9
$EuNi_2Si_2$ [**]	$ThCr_2Si_2$ I4/mmm	$a = 4.008(5)$ $c = 9.636(5)$	induction heating at 1600 °C (Ar) in Al_2O_3 30 min, PXD refinement	MaF, 77	99.9
$EuNiSi_2$	$CeNiSi_2$ Cmcm	$a = 4.137(2)$ $b = 16.562(10)$ $c = 4.002(2)$	arc(Ar) PXD	BoG, 69c	Eu 98.4 Ni 99.8 Si 99.99
$EuNi_{0.5}Si_{1.5}$	AlB_2 P6/mmm	$a = 4.034$ $c = 4.496$	induction melting in Al_2O_3 (Ar), 30 min, 1600 °C, PXD	MaF, 73	99.9

[*] For a correct setting of the bct unit cell $a = 7.808$ ($a = a_0/\sqrt{2}$).

[**] Physical properties as well as atom ordering are discussed in the text.

$c = 9.98$; for sample preparation, see $CePd_2Si_2$. The temperature variation of the lattice parameters, the magnetic susceptibility and ^{151}Eu Mössbauer measurements indicate a mixed valency system with a continuous valence transition near 140 K; see, e.g., Sampathkumaran et al. (1981) (fig. 23), Croft et al. (1982), Nagarajan et al. (1981) (XAS-data). From these investigations the average valence of Eu ions in $EuPd_2Si_2$ was derived to be ~ 2.3 at 300 K and ~ 2.7 at 120 K. A continuous valence transition with an increase of the average valency of Eu up to pressures of 48 kbar has also been found from measurements of electrical resistivity and thermoelectric power; the Eu valency remained constant in the pressure range of 48 to 70 kbar;
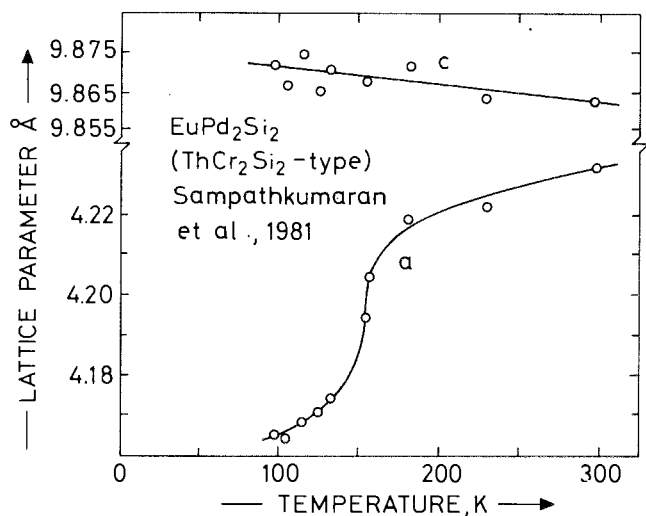
Fig. 23. Variation of lattice parameters versus temperature for $EuPd_2Si_2$, after Sampathkumaran et al. (1981).

no quantitative values were given (Vijayakumar et al., 1981). For sample preparation, see the Eu–Au–Pd–Si system.

The valence instability caused by Si additions in $EuPd_3Si_x$ $(0 \leqslant x < 0.25)$ has been investigated by Dhar et al. (1983). As compared to $LaPd_3Si_x$ the cell volume of $EuPd_3Si_x$ increases at a larger rate, indicating a valence change on the Eu. The samples were prepared by arc melting and studied by X-ray powder diffraction techniques. All compounds crystallize with the $AuCu_3$-type with the Si atoms likely to fill the center position. Magnetic susceptibility measurements on $EuPd_3$, $EuPd_3Si_{0.2}$ and $EuPd_3Si_{0.25}$ show an increase in the susceptibility in case of $EuPd_3Si_{0.25}$ in good agreement with the ^{151}Eu Mössbauer data revealing a valence fluctuation. Lattice parameters as read from a small diagram were: $EuPd_3$ $(a = 4.10)$, $EuPd_3Si_{0.1}$ $(a \sim 4.123)$, $EuPd_3Si_{0.2}$ $(a = 4.165)$ and $EuPd_3Si_{0.25}$ $(a = 4.18)$.

References

Ballestracci, R., 1976, C.R. Acad. Sci. Paris, Ser. B **282**, 291.

Croft, M., J.A. Hodges, E. Kemly, A. Krishnan, V. Murgai and L.C. Gupta, 1982, Phys. Rev. Lett. **48**(12), 826.

Dhar, S.K., R. Nagarajan, S.K. Malik, D. Rambabu and R. Vijayaraghavan, 1983, J. Magn. Magn. Mater. **31–34**, 393.

Nagarajan, R., E.V. Sampathkumaran, L.C. Gupta, R. Vijayaraghavan, Bhaktdarshan and B.D. Padalia, 1981, Phys. Lett. **81A**(7), 397.

Vijayakumar, V., S.N. Vaidya, E.V. Sampathkumaran, L.C. Gupta and R. Vijayaraghavan, 1981, Phys. Lett. **83A**(9), 469.

Sampathkumaran, E.V., L.C. Gupta, R. Vijayaraghavan, K.V. Gopalakrishnan, R.G. Pillay and H.G. Devare, 1981, J. Phys. **C14**, L237.

Eu–Pt–Si

EuPt$_2$Si$_2$ was claimed by Mayer and Yetor (1977) to be body-centered tetragonal (I4/mmm, BaAl$_4$-type, $a = 4.275$, $c = 9.810$, $\rho_x = 11.08$ kg/dm^3). In analogy to ErPt$_2$Si$_2$, Pt and Si atoms were said to statistically occupy the 4d and 4e sites of I4/mmm. From the variation of the unit cell parameters versus the R elements, Eu is indicated to be (partly?) divalent. For sample preparation, see LaPt$_2$Si$_2$.

Reference
Mayer, I. and P.D. Yetor, 1977, J. Less-Common Metals 55, 171.

Eu–Rh–Si

According to an X-ray powder analysis by Ballestracci (1976) EuRh$_2$Si$_2$ is tetragonal with the space group I4/mmm and the ordered ThCr$_2$Si$_2$-type of structure ($a = 4.087$, $c = 10.23$). For sample preparation, see YRh$_2$Si$_2$.

The crystal symmetry of EuRh$_2$Si$_2$ was confirmed by Felner and Nowik (1983) from X-ray powder diffraction analysis of induction-melted alloys [ThCr$_2$Si$_2$-type, $a = 4.107(2)$, $c = 10.25(1)$]. Antiferromagnetic ordering was observed below $T_N = 25$ K. The paramagnetic behavior (temperature range investigated was 1.5 to 300 K) corresponds to $\mu_{\text{eff}}^{\text{para}} = 7.2$ μ_B, $\theta_p = 22$ K and suggests Eu to be mainly divalent.

References
Ballestracci, R., 1976, C.R. Acad. Sci. Paris 282, 291.
Felner, I. and I. Nowik, 1983, Solid State Commun. 47, 831.

Eu–Ru–Si

Barz (1980) reported the existence of a compound EuRu$_3$Si$_2$ with the LaRu$_3$Si$_2$-type of structure (X-ray powder analysis). No lattice parameters were given. For sample preparation and melting behavior (phase equilibria), see also LaRu$_3$Si$_2$; $T_m > 25$ K.

Sampathkumaran et al. (1981) measured the magnetic susceptibility of EuRu$_2$Si$_2$ with the ThCr$_2$Si$_2$-type versus temperature ($80 < T < 400$ K). Eu was said to be trivalent, no crystallographic details were presented. Samples were prepared by arc melting and annealed at 800°C for 1 week.

References
Barz, H., 1980, Mater. Res. Bull. 15, 1489.
Sampathkumaran, E.V., L.C. Gupta, R. Vijayaraghavan, K.V. Gopalakrishnan, R.G. Pillay and H.G. Devare, 1981, J. Phys. C14, L237.

Eu–Sr–Si

No ternary phase diagram exists for the ternary system Eu–Sr–Si, but the stability range of the α-ThSi$_2$-type structure was investigated along the concentra-

tion section $Eu_{1-x}Sr_xSi_2$ in the pressure range up to 40 kbar (Evers et al., 1978). Samples were prepared from binary disilicide master alloys by melting in a copper boat under argon. Evaporation losses were less than 1 wt%. All samples were handled in a glove box. A limited solid solution $Eu_{1-x}Sr_xSi_2$, $0 \leqslant x < 0.8$ was observed at normal pressures (quenched from 100–1500°C), whereas a complete homogeneous range exists at 40 kbar, with a linear variation of the lattice parameters (see Table 8). X-ray powder patterns exhibit line broadening except for $x = 0$ and 1; statistical occupation of Eu, Sr atoms was assumed.

Reference
Evers, J., G. Oehlinger and A. Weiss, 1978, J. Less-Common Metals **60**, 249.

Gd–Ag–Si

Rossi et al. (1979) prepared $GdAg_2Si_2$ with the $ThCr_2Si_2$-type of structure (I4/mmm, $a = 4.151$, $c = 10.709$, $\rho_x = 7.72$ kg/dm³). A homogeneous range was reported to exist at lower temperatures from $GdAg_{1.8}Si_{2.2}$ ($a = 4.153$, $c = 10.693$) to $GdAg_{2.2}Si_{1.8}$ ($a = 4.152$, $c = 10.706$); larger variations of lattice parameters have been observed in quenched specimens: $a = 4.14$–4.15, $c = 10.69$–10.76. From metallographic analysis complex phase equilibria were reported at high temperatures. For sample preparation, see $CePd_2Si_2$.

Reference
Rossi, D., R. Marazza and R. Ferro, 1979, J. less-Common Metals **66**, P17.

Gd–Al–Si

Zarechnyuk et al. (1981) investigated the phase equilibria in an partial isothermal section of the system Gd–Al–Si (0–33 a/o Gd, fig. 24) by means of X-ray and metallographic analysis of 80 samples which were arc melted and subsequently heat treated at 500°C for 700 h in evacuated silica tubes. Starting materials were 99.85% Gd, 99.99% Al und 99.99% Si. Earlier data obtained by Raman and Steinfink (1967) for the section $Gd(Al_{1-x}Si_x)_2$ were confirmed.

Binary compounds are in agreement with a recent compilation of rare-earth–aluminum systems; the compounds involved are $GdAl_3$ (Ni_3Sn-type), $GdAl_2$ ($MgCu_2$-type) and $GdSi_2$ (α-$GdSi_2$-type). The mutual solid solubilities in general were observed to be small except in case of $GdSi_2$, which was found to dissolve up to 10 a/o Al at 600°C. The lattice parameters change from $a = 4.066$, $b = 3.999$, $c = 13.45$ at $GdSi_2$ to $a = 4.093$, $b = 4.032$, $c = 13.49$ for a composition $Gd_{33}Al_{10}Si_{57}$ (as read from a small graph).

Two ternary compounds have been observed, whereby earlier data by Muravyova et al. (1972) concerning the existence of the compound $GdAl_2Si_2$ with the La_2O_2S-type of structure have been confirmed (P3m1, $a = 4.20$, $c = 6.66$). X-ray powder intensity data were found to be satisfactory using the atom parameters as derived for the isostructural compound $CaAl_2Si_2$; for details, see Sm–Al–Si.
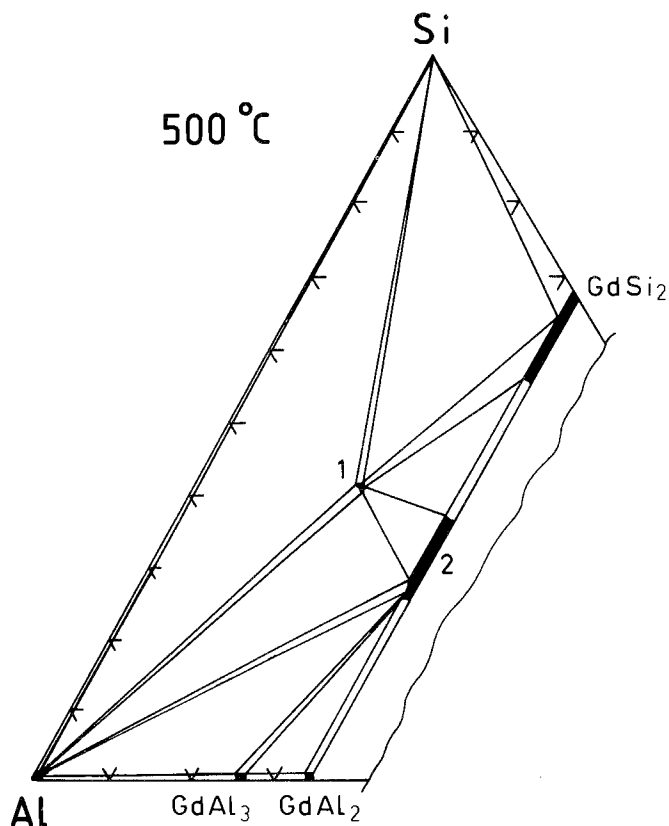
Fig. 24. Gd–Al–Si, partial isothermal section at 500 °C (0–33 a/o Gd), 1: GdAl$_2$Si$_2$, 2: GdAl$_{0.96-1.42}$Si$_{1.04-0.58}$.

GdAl$_{0.96-1.42}$Si$_{1.04-0.58}$ was reported to crystallize with the α-ThSi$_2$-type of structure. For a composition GdAlSi the following atom parameters have been refined from X-ray powder data with a corresponding reliability factor of $R = 0.07$: I4$_1$/amd, Gd in 4a) and 4Al + 4Si statistically in 8e) 0, 0, $z = 0.4165$. Lattice parameters were $a = 4.238$ and $c = 13.98$ for Gd$_{33}$Al$_{32}$Si$_{35}$, and $a = 4.180$, $c = 13.76$ for Gd$_{33}$Al$_{47}$Si$_{20}$. Slightly different unit cell dimensions were reported by Raman and Steinfink (1967) for the alloy GdAlSi annealed at 1000 °C [α-ThSi$_2$-type, $a = 4.131(5)$ and $c = 14.44(1)$]. Similarly the alloy GdAl$_{1.75}$Si$_{0.25}$ was claimed to be single phase MgCu$_2$-type with a 7.860(5), suggesting a much larger solubility of Si in GdAl$_2$ at 1000 °C; for sample preparation, see Nd–Al–Si.

Raman (1968) studied the phase equilibria within the concentrational section GdAl$_x$Si$_{1-x}$ by means of X-ray powder diffraction methods. GdAl$_{0.25}$Si$_{0.75}$ was observed to crystallize with the CrB-type of structure (branch I, Cmcm, $a = 4.322(5)$, $b = 10.66(1)$, $c = 3.866(5)$, $\rho_{exp} = 6.70(1)$, $\rho_x = 6.887$ kg/dm^3). Binary GdSi was FeB-type [branch I, Pnma, $a = 7.935(5)$, $b = 3.856(5)$, $c = 5.730(5)$], and GdAl has the

DyAl-type [Pbcm, $a = 5.888(5)$, $b = 11.527(10)$, $c = 5.656(5)$]. For sample preparation and structural details, see $ErAl_xSi_{1-x}$.

References
Muravyova, A.A., O.S. Zarechnyuk and E.I. Gladyshevskij, 1972, Vestn. Lvov Univ., Ser. Khim. **13**, 14.
Raman, A., 1968, Inorg. Chem. 7(5), 973.
Raman, A. and H. Steinfink, 1967, Inorg. Chem. 6(10), 1789.
Zarechnyuk, O.S., T.I. Yanson and A.A. Muravyova, 1981, Vestn. Lvov. Univ., Ser. Khim. **23**, 64.

Gd–Au–Si

Felner (1975) was first to observe the compound $GdAu_2Si_2$ with the ordered $ThCr_2Si_2$-type of structure (I4/mmm, $a = 4.236$, $c = 10.10$) and antiferromagnetic ordering at $T_N = 5.7$ K. For sample preparation, see $LaAu_2Si_2$. Rossi et al. (1979) confirmed the ordered structure type, but reported considerably larger unit cell dimensions: $a = 4.244$ and $c = 10.159$; $\rho_x = 11.02$ kg/dm^3 (X-ray powder analysis).

References
Felner, I., 1975, J. Phys. Chem. Sol. **36**, 1063.
Rossi, D., R. Marazza and R. Ferro, 1979, J. Less-Common Metals **66**, P17.

Gd–Co–Si

Six ternary compounds have been reported for the Gd–Co–Si system.

Mayer and Tassa (1969) investigated the phase equilibria within the silicon-rich region of the section $GdCo_xSi_{2-x}$. Samples were prepared by melting in alumina or magnesia crucibles in an induction furnace under argon ($\sim 1500\,°C$). The reguli were subsequently sealed in evacuated quartz capsules and heat-treated at 700–800 °C for 24–96 h. Starting materials were R 99.9%, Co 99.95%, Si 99.99%. From X-ray powder analysis the $ThSi_2$-type of structure was observed to be stable for $x < 0.4$. At the composition $GdCo_{0.4}Si_{1.6}$ the hexagonal AlB_2-type of structure was found to exist ($a = 3.989$, $c = 4.086$). Powder intensity calculations were in agreement with a statistical distribution of Co and Si atoms in the 2d sites of P6/mmm. $GdCo_{0.4}Si_{1.6}$ is paramagnetic with $\mu_{eff}^{para} = 8.94\ \mu_B$ and $\theta_p = 0$ K (Felner and Schieber, 1973).

GdCoSi was observed to crystallize with the TiNiSi-type of structure with the space group Pnma and lattice parameters $a = 6.868$, $b = 4.194$ and $c = 7.262$ (X-ray powder data; Yarovets, 1978); for sample preparation and atom parameters, see YNiSi.

$GdCo_2Si_2$ is tetragonal with the ordered $ThCr_2Si_2$-type of structure: I4/mmm, $a = 3.913(6)$, $c = 9.811(10)$, $\rho_x = 7.32$ kg/dm^3 (Rieger and Parthé, 1969; X-ray powder diffraction data). For sample preparation, see $CeCo_2Si_2$. Antiferromagnetic behavior ($T_N = 44$ K) was observed by Yakinthos et al. (1980) from susceptibility measurements (4.2–200 K); the paramagnetic behavior corresponds to $\mu_{eff}^{para} = 9.9\ \mu_B$ mole^{-1} and $\theta_p = -55$ K. Atom ordering and crystal data were confirmed by Latka et al. (1979) from X-ray powder data. Less correspondence, however, exists for the magnetic data derived from susceptibility measurements (1.8 to 290 K): $\mu_{eff}^{para} = 8.19$

μ_B, $\theta_p = -29$ K and $T_N = 45(4)$ K. From ^{155}Gd Mössbauer spectra the magnetic moments were concluded to be nearly perpendicular to the c-axis. The magnetic behavior at higher temperatures (300–1200 K) was recorded by Yarovets et al. (1977), $\mu_{eff}^{para} = 8.6$ μ_B and $\theta_p = -86$ K ($a = 3.912$, $c = 9.799$; Yarovets, 1978, from X-ray powder data).

The existence of a compound $GdCo_9Si_2$ with the $BaCd_{11}$-type of structure was first mentioned by Bodak and Gladyshevskij (1969) from X-ray powder analysis of arc-melted alloys [$I4_1/amd$, $a = 9.738(5)$, $c = 6.293(10)$]. The atom order and crystal symmetry was confirmed by Yarovets (1978) from X-ray powder data obtained for $GdCo_{8.5}Si_{2.5}$ [$Ce_2Ni_{17}Si_5$-type, occupation variant of $BaCd_{11}$, $a = 9.774$, $c = 6.327$)]; for sample preparation and atom parameters, see Tb–Co–Si.

Pelizzone et al. (1982) investigated the structural and magnetochemical behavior of $GdCoSi_2$ with the $CeNiSi_2$-type [$Cmcm$, $a = 4.067(1)$, $b = 16.304(5)$, $c = 3.995(1)$]. For sample preparation, see $HoCoSi_2$. $GdCoSi_2$ orders antiferromagnetically at 7.5 K. Magnetic susceptibilities at higher temperatures correspond to $\mu_{eff}^{para} = 7.5(1)$ μ_B and $\theta_p = -8$ K. Slightly different unit cell dimensions were reported by Yarovets (1978), $a = 4.043$, $b = 16.396$ and $c = 4.007$.

Without details, Gladyshevskij and Bodak (1973) mentioned the existence of the compound $GdCoSi_3$ probably isostructural with $CeCoSi_3$. Magnetic susceptibility were recorded in the temperature interval of 293–1150 K, $\mu_{eff}^{para} = 7.94(10)$ μ_B, $\theta_p = -89$ K (Yarovets, 1978).

References

Bodak, O.I. and E.I. Gladyshevskij, 1969, Dopov. Akad. Nauk Ukr. RSR, Ser. A **5**, 452.
Felner, I. and M. Schieber, 1973, Solid State Commun. **13**, 457.
Gladyshevskij, E.I. and O.I. Bodak, 1973, in: Khim. Met. Splavov, ed. N.M. Zhavoronkov (Nauka, Moscow, USSR) p. 46.
Latka, K., H. Schmidt, V. Oestreich, F. Götz and G. Czjzek, 1979, KFK Progress Report, KFK-2881, p. 79.
Mayer, I. and M. Tassa, 1969, J. Less-Common Metals **19**, 173.
Pelizzone, M., H.F. Braun and J. Müller, 1982, J. Magn. Magn. Mater. **30**, 33.
Rieger, W. and E. Parthé, 1969, Monatsh. Chem. **100**, 444.
Yakinthos, J.K., Ch. Routsi and P.F. Ikonomou, 1980, J. Less-Common Metals **72**, 205.
Yarovets, V.I., 1978, Autoreferat Dis. Kand. Khim. (abstract of thesis, Russian) (Nauk, Lvov) 24 p.
Yarovets, V.I., Yu.K. Gorelenko and R.V. Skolozdra, 1977, Tesizy Dokl. IX. Ukr. Vses. Konf. Neorg. Khim., Lvov, p. 188.

Gd–Cr–Si

According to X-ray powder data by Rieger and Parthé (1969), $GdCr_2Si_2$ crystallizes with the $ThCr_2Si_2$-type of structure [$I4/mmm$, $a = 3.944(6)$, $c = 10.672(10)$]. Samples were arc melted and subsequently annealed in evacuated silica tubes at 900°C for 100 h.

Reference

Rieger, W. and E. Parthé, 1969, Monatsh. Chem. **100**, 444.

Gd–Cu–Si

Raman (1967) and Rieger and Parthé (1969a) both investigated the occurrence of the AlB_2-type of structure, by means of X-ray analysis of arc-melted alloys. Rieger and Parthé (1969a) derived a statistical distribution of Si and Cu atoms in the 2d site of P6/mmm, observed on two alloys with the composition $GdCu_{0.67}Si_{1.33}$ ($a = 4.029$, $c = 4.057$) and GdCuSi ($a = 4.044$, $c = 4.027$). Raman (1967) measured $GdCu_{1.5}Si_{0.5}$ with the lattice parameters $a = 4.165(5)$ and $c = 3.771(5)$. For the different compositions an extended homogeneous region and/or eventually separated AlB_2-type phases with ordering among Cu, Si atoms are likely (see, e.g., phase equilibria in the Ce–Cu–Si system).

The magnetic properties of an alloy GdCuSi were first investigated by Oesterreicher (1976) (4.2 to 150 K and up to 50 kOe) and more recently by Kido et al. (1983) (77 to 300 K). The samples were annealed at 800 °C (Oesterreicher) and at 800–900 °C (Kido et al., 1983); from X-ray powder analysis an AlB_2-type of structure was reported. Essential agreement exists about the paramagnetic behavior: $\mu_{eff}^{para} = 8.32$ μ_B, $\theta_p = 58$ K (Oesterreicher), and $\mu_{eff}^{para} = 7.0$ μ_B, $\theta_p = 30$ K (Kido). GdCuSi orders ferromagnetically at $T_m = 49$ K; $\mu_S = 7.3$ μ_B. Highly anisotropic exchange interactions are indicated by the high fields needed for saturation. With respect to their low annealing temperatures, ordering among Cu, Si atoms is suspected especially in connection with the recent observation of an ordered compound GdCuSi by Iandelli (1983) (see below).

At variance with the data of Rieger and Parthé (1969a) obtained from arc-melted samples, Iandelli (1983) observed the formation of GdCuSi with the ordered Ni_2In-type of structure [superstructure of AlB_2-type, $P6_3/mmc$, $a = 4.168(1)$, $c = 7.573(4)$]. The superstructure reflections were said to be very faint and were obtained from arc-melted samples after annealing at 750 °C for 8–12 d. The Ni_2In phase was thus concluded to be a low-temperature modification. For details in sample preparation, see La–Cu–Si.

$GdCu_2Si_2$ is isotypic with the $ThCr_2Si_2$-type of structure, I4/mmm, $a = 4.003(6)$, $c = 9.947(10)$ (Rieger and Parthé, 1969b; X-ray powder data). For sample preparation, see YCu_2Si_2. The magnetic behavior was studied by Oesterreicher (1976) (4.2 to 150 K, and up to 50 kOe). $GdCu_2Si_2$ is paramagnetic with $\mu_{eff}^{para} = 7.28$ μ_B and $\theta_p = -10$ K; weak antiferromagnetic ordering was observed at $T_N = 10$ K and metamagnetism was suspected. For sample preparation, see below ($Gd_3Cu_4Si_4$).

Physical properties were reviewed by Sales and Viswanathan (1976); NMR data were presented by Sampathkumaran et al. (1979); for X-ray absorption spectroscopy (L_3-absorption edge), see Padalia et al. (1983).

$Gd_3Cu_4Si_4$ with the $Gd_3Cu_4Ge_4$-type was prepared by Oesterreicher (1976), who also studied the magnetic behavior from 4.2 K to 150 K in fields up to 50 kOe (Immm, $\mu_{eff}^{para} = 7.38$ μ_B, $\theta_p = -14$ K). A weak antiferromagnetic exchange interaction was observed at $T_N = 12$ K and metamagnetism was suspected. The compounds were prepared by induction melting in MgO crucibles under argon with subsequent heat treatment in vacuum (on MgO substrates) at 800 °C for 200 h; no lattice parameters were reported.

Bodak et al. (1971) reported the formation of $GdCu_{1.6}Si_{1.4}$ with the $CeNiSi_2$-type.

References

Bodak, O.I., E.I. Gladyshevskij and Ya.M. Kalvijak, 1971, Tesizy Dokl. Vses. Konf. Kristallokhim. Intermet. Soedin, Lvov, p. 40.

Iandelli, A., 1983, J. Less-Common Metals **90**, 121.

Kido, H., T. Hoshikawa, M. Shimada and M. Koizumi, 1983, Phys. Stat. Sol. (a) **77**, K121.

Oesterreicher, H., 1976, Phys. Stat. Sol. (a) **34**, 723.

Padalia, B.D., T.K. Hatwar and M.N. Ghatikar, 1983, J. Phys. **C16**, 1537.

Raman, A., 1967, Naturwiss. **54**, 560.

Rieger, W. and E. Parthé, 1969a, Monatsh. Chem. **100**, 439.

Rieger, W. and E. Parthé, 1969b, Monatsh. Chem. **100**, 444.

Sales, B.C. and R. Viswanathan, 1976, J. Low Temp. Phys. **23**(3,4), 449.

Sampathkumaran, E.V., L.C. Gupta and R. Vijayaraghavan, 1979, J. Phys. **C12**, 4323.

Gd–Fe–Si

Bodak et al. (1978) investigated the phase equilibria in the system Gd–Fe–Si at 800 °C by means by X-ray powder and metallographic analysis of 250 alloys which were prepared by arc melting and subsequent annealing in evacuated silica tubes (800 °C, 720 h).

Gd_6Fe_{23} was not observed among Gd–Fe phases stable at 800 °C (see e.g. Moffatt): Gd_2Fe_{17}, Gd_2Fe_{17-x} (Th_2Zn_{17}-, Th_2Ni_{17}-type), $GdFe_3$ ($PuNi_3$-type), $GdFe_2$-type ($MgCu_2$-type). The two phases Gd_2Fe_{17} and Gd_2Fe_{17-x}, separated by a narrow two-phase field, were both claimed to exist at the same temperature (800 °C).

Except for Gd_5Si_4, which obviously was not found at 800 °C, all binary Gd silicides have been confirmed: Gd_5Si_3 (Mn_5Si_3-type) GdSi (FeB-type), $GdSi_{1.64}$ (defect AlB_2-type) and $GdSi_2$. $GdSi_2$ at 800 °C supposedly was observed with the $ThSi_2$-type (see also Elliott). The binary iron silicides were discussed in context with the Y–Fe–Si system. Solid solubilities of binary compounds are extending in the direction of a Fe/Si exchange with fixed Gd concentration and in some cases the solid solubility limits have been determined from the variation of the unit cell dimensions; however, no further details were presented: Gd_2Fe_{17-x} dissolves up to 18 a/o Si, Gd_2Fe_{17} dissolves up to 16 a/o Si, and ~10 a/o Fe is dissolved in Gd_5Si_3.

No ternary AlB_2-type phase was observed, but an extended solid solution based on the binary AlB_2-type phase $GdSi_{1.64}$ was found (~8.9 a/o Fe in $GdSi_{1.64}$ at 800 °C). At variance with this, Mayer and Tassa (1969)—from a phase equilibria study of the system $GdFe_xSi_{2-x}$—claimed the existence of a ternary compound $GdFe_{0.4}Si_{1.6}$ with the AlB_2-type of structure ($a = 3.995$, $c = 4.075$). In analogy to X-ray intensity data of $NdFe_{0.4}Si_{1.6}$ a statistical distribution of Fe, Si atoms in the 2d sites of P6/mmm was assumed. Mayer and Tassa (1969) prepared their samples at considerably higher temperatures (see $GdCo_{0.4}Si_{1.6}$) than Bodak et al. (1978); thus it is conceivable that either $GdFe_{0.4}Si_{1.6}$ is a high-temperature phase or simply the Fe solubility in $GdSi_{1.65}$ increases considerably at elevated temperatures.

Eight ternary compounds were found to exist (Bodak et al., 1978); the crystal structures of several of them, however, have not yet been determined (see table 10).

TABLE 10

Formation and structural data of ternary compounds Gd–Fe ≠ Si.

Compound	Structure type Space group	Lattice parameters Density	Preparation, Characterization	Refs.	Purity
GdFe$_{1.13}$Si$_{0.87}$ [(+)]	PbFCl P4/nmm	$a = 4.004$ $c = 6.831$	arc, 800 °C, 720 h refinement of powder X-ray data	Ya, 78	Gd 99.7 Fe 99.96 Si 99.99
		$a = 4.001(3)$ $c = 6.798(5)$ at GdFeSi	arc, 800 °C, 720 h	BoGK, 70	Fe 99.96 Si 99.99
GdFe$_{0.65}$Si$_{1.05}$	unknown		arc, Qu, 800 °C, 720 h, PXD	BoGYDI, 78	Gd 99.85 Fe 99.98 Si 99.99
GdFe$_2$Si$_2$	ThCr$_2$Si$_2$ I4/mmm	$a = 3.90$ $c = 9.70$	arc, Qu, 800 °C, 720 h PXD	BoGYDI, 78	Gd 99.85 Fe 99.98 Si 99.99
		$a = 3.932$ $c = 9.971$	$\mu_{\text{eff}}^{\text{para}} = 8.6(1)\,\mu_{\text{B}}$, $\theta_{\text{p}} = 545$ K (292–719 K) $\mu_{\text{eff}}^{\text{para}} = 7.7(1)\,\mu_{\text{B}}$, $\theta_{\text{p}} = 390$ K (719–1095 K)	Ya, 78	
		$a = 3.940(6)$ $c = 9.974(10)$	arc, Qu 900 °C, 100 h PXD	RiP, 69	high
		$a = 3.940(5)$ $c = 9.974(5)$	HF melting (Ar) Al$_2$O$_3$ crucible 1500 °C, 30 min PXD $T_{\text{m}} = 738(5)$ K; $T_{\text{N}} = 7$ K	FeMGS, 75	99.9
Gd$_2$Fe$_3$Si$_5$	Sc$_2$Fe$_3$Si$_5$ P4/mnc	$a = 10.15$ $c = 5.55$	arc, Qu 800 °C, 720 h PXD	BoGYDI, 78	Gd 99.85 Fe 99.98 Si 99.99
		$a = 10.503$ $c = 5.342$		Ya, 78	
		$a = 10.47(1)$ $c = 5.513(8)$	arc, 1200 °C, 2 d 800 °C, 2 d, PXD $\mu_{\text{eff}} = 7.8(1)\,\mu_{\text{B}}$ $\theta_{\text{p}} = -15.4(6)$ K $T_{\text{N}} = 8.6$ K [(*)]	Br, 80 BrSARDD, 81	Gd 99.9 Fe 5N Si 7N
			arc, 1000 °C, 20 d $\mu_{\text{eff}}^{\text{para}} = 8.1(2)\,\mu_{\text{B}}$ $\theta_{\text{p}} = -23(1)$ K	NoSNUA, 83	
Gd$_2$Fe$_4$Si$_9$ [(**)]	Y$_2$Fe$_4$Si$_9$ P6$_3$/mmc	$a = 3.90$ $c = 15.66$	arc, Qu 800 °C, 720 h PXD	BoGYDI, 78	Gd 99.85 Fe 99.98 Si 99.99
		$a = 3.936(5)$ $c = 15.50(10)$	arc, Qu 800 °C, 720 h, PXD $\mu_{\text{eff}} = 7.25\,\mu_{\text{B}}$ mole^{-1} $\theta_{\text{p}} = 102$ K	GlBYGS, 78	Gd 99.85 Fe 99.98 Si 99.99

TABLE 10 (continued)

Compound	Structure type Space group	Lattice parameters Density	Preparation, Characterization	Refs.	Purity
$GdFe_{0.71}Si_{2.46}$	unknown		arc, Qu 800 °C, 720 h	BoGYDI, 78	Gd 99.85 Fe 99.98 Si 99.99
$GdFeSi_3$ ($Gd_3Fe_2Si_7$?)	$Ho_3Co_2Si_7$ (?) Amm2		arc, Qu 800 °, 720 h, PXD $\mu_{eff} = 7.79\ \mu_B\ mole^{-1}$ $\theta_p = 35$ K	Ya, 78	Gd 99.85 Fe 99.98 Si 99.99
$GdFe_{0.61}Si_{2.74}$	unknown		arc, Qu 800 °C, 720 h, PXD	BoGYDI, 78	Gd 99.85 Fe 99.98 Si 99.99

[+] First identified by Bodak et al. (1970) with a considerable homogeneous range from GdFeSi to $GdFe_{1.13}Si_{0.87}$. Atom parameters were refined for $GdFe_{1.13}Si_{0.87}$ from X-ray powder diffraction data by Yarovets (1978); the parameters obtained were: Gd in 2c) 1/4, 1/4, 0.6632(9), Fe in 2a) 0,0,0 and a statistical distribution of 0.87 Si + 0.13 Fe in 2c) 1/4, 1/4, 0.1862(9); $R = 0.153$.

[*] From Mössbauer spectra no magnetic moment was found on the iron site (Braun et al., 1981).

[**] First identified as $Gd_2Fe_5Si_8$ by Bodak et al. (1978) but later characterized with the $Y_2Fe_4Si_9$-type (Gladyshevskij et al., 1978).

Felner et al. (1975) confirmed the structure type of $GdFe_2Si_2$ [$ThCr_2Si_2$-type, $a = 3.940(5)$, $c = 9.974(5)$] and measured magnetic susceptibility data. Weak ferromagnetic ordering occurs at 738(5) K and the Gd sublattice was observed to order antiferromagnetically at $T_N = 7$ K. From magnetization and Mössbauer effect measurements most of the iron was concluded to be diamagnetic ($\sim 94\%$). More recent Mössbauer data (300 K, ^{57}Fe) by Umarij et al. (1983), however, proved the existence of only one type of Fe atom in the structure carrying no magnetic moment. According to earlier data by Felner et al. (1975) and Bauminger et al. (1973), Umarji et al. (1983) reported antiferromagnetic ordering below 10 K. The magnetic structure as derived from a 4.2 K Mössbauer spectrum appeared to be an antiferromagnetic sequence aabbaa.... Thus two magnetic sites exist for the Fe atoms without and with an internal field of 16(1) kG. Samples were prepared by arc melting under argon starting from high purity elements with subsequent annealing in evacuated quartz tubes at 900 °C for 4 days. From X-rays powder data the ordered $ThCr_2Si_2$-type was confirmed and lattice parameters were given as $a = 3.94$, $c = 10.03$. The small discrepancies observed for calculated and observed (00l) reflections were said to be due to preferred orientation effects. According to ^{155}Gd data by Bauminger et al. (1973) the Gd moments are aligned perpendicular to the c-axis.

From magnetization and ^{57}Fe and ^{155}Gd Mössbauer data of $Gd_2Fe_3Si_5$ ($Sc_2Fe_3Si_5$-type, see table 10) at 4.2 K (magnetically ordered) and at 10 K (paramagnetic), the absence of a magnetic moment on the Fe site was confirmed (the observed field at the iron nuclei corresponded to a moment of 0.03 μ_B or less).
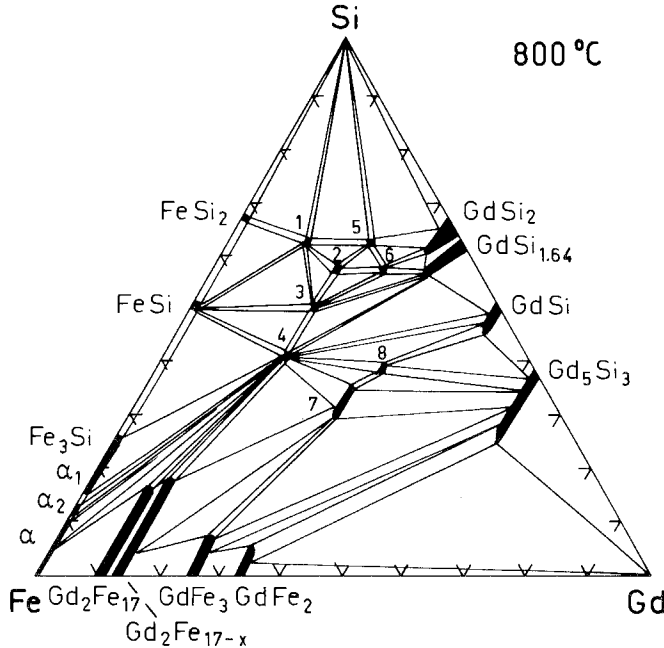
Fig. 25. Gd–Fe–Si, isothermal section at 800°C. 1: $Gd_2Fe_4Si_9$ ($Y_2Fe_4Si_9$-type, earlier obtained at $Gd_2Fe_2Si_8$), 2: $GdFeSi_3$, 3: $Gd_2Fe_3Si_5$, 4: $GdFe_2Si_2$, 5: "$GdFe_{0.61}Si_{2.74}$", 6: "$GdFe_{0.71}Si_{2.46}$", 7: $GdFeSi$, 8: "$GdFe_{0.65}Si_{1.05}$".

Values for crystalline electric field parameters were derived to predict magnetic anisotropy and spin orientation at low temperatures (Noakes et al., 1983).

For low temperature heat capacity data, see Vining and Shelton (1983), $T_N = 8.40$ K.

Phase equilibria as presented in fig. 25 are primarily based on the work of Bodak et al. (1978), Braun (1980) and Gladyshevskij et al. (1978) (see also table 10). The Fe–Si-rich region was slightly changed to agree with a recently published critical evaluation of the binary Fe–Si system by Schürmann and Hensgen (1980).

Stadnyk et al. (1979) investigated the resistivity as a function of temperature (300–1000 K) for all the Gd–Fe silicides listed in table 10.

References

Bauminger, E.R., I. Felner, D. Froindlich, A. Grill, D. Lebenbaum, I. Mayer, I. Nowik, S. Ofer and M. Schieber, 1973, Proc. Intern. Conf. on Magnetism, Moscow, p. 55.

Bodak, O.I., E.I. Gladyshevskij and P.I. Kripyakevich, 1970, Zh. Strukt. Khim. **11**(2), 305.

Bodak, O.I., E.I. Gladyshevskij, V.I. Yarovets, V.N. Davydov and T.V. Il'Chuk, 1978, Izv. Akad. Nauk SSSR, Neorg. Mater. **14**(3), 481.

Braun, H.F., 1980, Phys. Lett. **75A**(5), 386.

Braun, H.F., C.U. Segre, F. Acker, M. Rosenberg, S. Dey and P. Deppe, 1981, J. Magn. Magn. Mater. **25**, 117.

Felner, I., I. Mayer, A. Grill and M. Schieber, 1975, Solid State Commun. **16**, 1005.

Gladyshevskij, E.I., O.I. Bodak, V.I. Yarovets, Yu.K. Gorelenko and R.V. Skolozdra, 1978, Ukr. Fiz. Zh. **23**(1), 77.

Mayer, I. and M. Tassa, 1969, J. Less-Common Metals **19**, 173.

Noakes, D.R., G.K. Shenoy, D. Niarchos, A.M. Umarji and A.T. Aldred, 1983, Phys. Rev. **B27**(7) 4317.

Rieger, W. and E. Parthé, 1969, Monatsh. Chem. **100**, 444.

Schürmann, E. and U. Hensgen, 1980, Archiv f. Eisenhüttenwesen **51**(1), 1.

Stadnyk, Yu.V., Yu.K. Gorelenko, R.V. Skolozdra, V.I. Yarovets and O.I. Bodak, 1979, Splavy Redk. Tugoplavk. Met. Osob. Fiz. Svoistvami (Moscow) p. 124.

Umarji, A.M., D.R. Noakes, P.J. Viccaro, G.K. Shenoy, A.T. Aldred and D. Niarchos, 1983, J. Magn. Magn. Mater. **36**, 61.

Vining, C.B. and R.N. Shelton, 1983, Phys. Rev. **B28**(5), 2732.

Yarovets, V.I., 1978, Autoreferat Dis. Kand. Khim. (abstract of thesis, Russian) (Nauk, Lvov) 24 p.

Gd–Ge–Si

Muratova et al. (1975) determined the phase equilibria in an isothermal section of the system Gd–Ge–Si at 600 °C. 134 alloys, prepared by arc melting and annealed at 600 °C for 250 h in evacuated silica tubes, were analyzed by X-ray powder diffraction techniques and metallography (fig. 26). Starting materials were 99.98% pure Gd and 99.99% pure Ge,Si. Phase equilibria are characterized by the formation of three complete solid solutions: $Gd_5(Ge,Si)_3$ with the Mn_5Si_3-type ($P6_3/mcm$), $Gd_2(Ge,Si)_3$ with a defect AlB_2-derivative type, and $Gd(Ge,Si)_{2-x}$. Gd–Ge–Si alloys with a Gd content between 30 to 40 a/o Gd have been investigated earlier by Muratova and Bodak (1974).

Lattice parameters for $Gd_5Ge_{3-x}Si_x$ at 600 °C show a linear variation versus x, ranging between $a = 8.60$, $c = 6.43$ (for Gd_5Ge_3), and $a = 8.50$, $c = 6.35$ (for Gd_5Si_3); values were read from a small diagram given by Muratova et al. (1975).
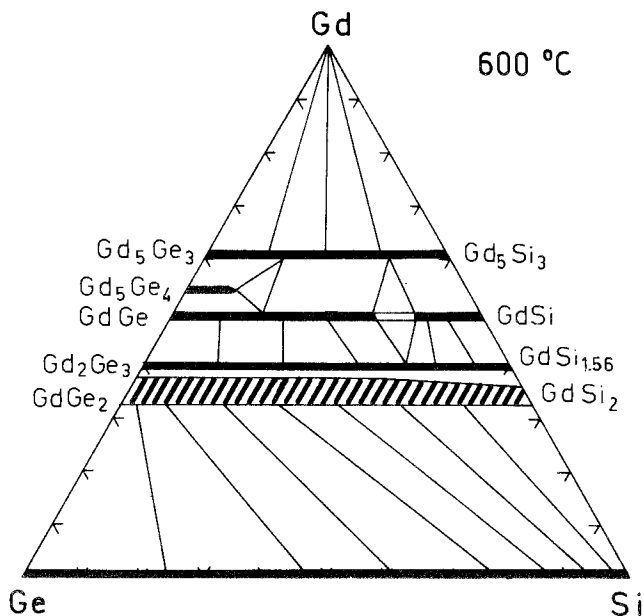
Fig. 26. Gd–Ge–Si, isothermal section at 600°C.

GdSi (FeB-type, Pnma, $a = 8.00$, $b = 3.84$, $c = 5.70$) and GdGe (CrB-type, $a = 4.32$, $b = 10.79$, $c = 3.98$) at 600 °C form an extended solid solution separated by a narrow two-phase field, Up to 10 a/o Ge dissolves in GdSi and lattice parameters change linearly from GdSi to $a = 8.02$, $b = 3.87$, $c = 5.75$. 33 a/o Si was found to substitute Ge in GdGe (lattice parameters vary linearly from GdGe to $a = 4.30$, $b = 10.56$, $c = 3.88$). All data were read from a small diagram presented by Muratova et al. (1975).

Gd$_5$Ge$_4$ (Sm$_5$Ge$_4$-type) was observed to form a rather limited solid solution up to 8 a/o Si (no details given). Holtzberg et al. (1967) studied the magnetic behavior of Gd$_5$Si$_{4-x}$Ge$_x$ alloys, which were prepared by arc melting from 99.9% pure Gd and 99.999% pure Si, Ge. Annealing at 1600 °C (in Ta crucibles, 5 h) under 5N(Ar) was necessary to dissolve small amounts of secondary phases, which occurred during the melting process of the peritectically formed compounds. In substituting Ge for Si the magnetic properties abruptly changed at $x \approx 2$, followed by an unidentified intermediate solid solution phase in the region from $x = 2$ to $x = 3$. For values $3 < x \leqslant 4$ the "Sm$_5$Ge$_3$-type pattern" reappeared with the c/a ratio different from the c/a for 5 : 4 silicides and characteristic for the germanide Sm$_5$Ge$_4$-type phases.

Gd$_5$Si$_4$ and similarly Gd$_{11}$Ge$_{10}$, GdGe$_{\sim 3}$ were not observed at 600 °C.

A rather wide and continuous homogeneous range (dashed area in fig. 26) was reported by Muratova and Bodak (1974) to extend from GdGe$_{1.67-2.00}$ to GdSi$_{1.78-1.94}$. At variance with Eremenko et al. (1980) (see below), the ThSi$_2$-type occurring at Ge-poor concentrations GdGe$_{1.76}$, was said to continuously transform into the α-GdSi$_2$-type at GdGe$_{2.00}$. GdSi$_{2-x}$ was found to adopt the GdSi$_2$-type at $T = 600$ °C. The structural behavior along the phase region GdGe$_{2-x}$Si$_x$ was also investigated by Mayer and Eshdat (1968) by means of X-ray powder analysis (for sample preparation, see NdGe$_{2-x}$Si$_x$). In this case a continuous transformation
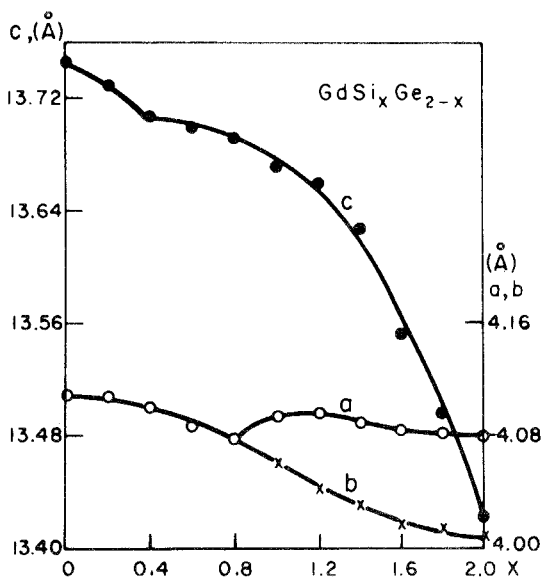
Fig. 27. Gd–Ge–Si, section GdGe$_{2-x}$Si$_x$, variation of lattice parameters versus concentration, after Mayer and Eshdat (1968).

from $GdGe_2$ ($ThSi_2$-type) to $GdSi_2$ ($GdSi_2$-type) was proposed (see figs. 11, 27). According to a most recent version of the Gd–Ge system by Eremenko et al. (1980), the composition of the α-$ThSi_2$-type germanide was fixed without a homogeneous range at $GdGe_{1.63}$. Furthermore, $GdGe_{1.63}$ was said to decompose peritectoidically at 808°C according to the reaction $GdGe_{1.63} \rightleftharpoons Gd_{1.04}Ge_{1.56}$ (AlB_2-derivative type) + Ge. Obviously no $GdSi_2$-type modification is present. A small homogeneous range, however, was shown for the phase at $Gd_{1.04}Ge_{1.56}$. Three modifications were reported ($T_1 = 833°C$, $T_2 = 1210$–1070 °C), which derive from the defect AlB_2-type of structure (the AlB_2-type, P6/mmm, was confirmed at 700°C, but its modifications have not been determined yet).

With respect to the existing disagreement concerning the complicated phase relations between the two closely related structural types $GdSi_2$, $ThSi_2$, a careful reinvestigation of the dashed area in fig. 26 seems to be necessary; this is also true for the defect AlB_2-type solution with respect to possible lattice distortions.

References

Eremenko, V.N., V.G. Batalin, Yu.I. Buyanov and I.M. Obushenko, 1980, Poroshk. Metall. **2**, 40.
Holtzberg, F., R.J. Gambino and T.R. McGuire, 1967, J. Phys. Chem. Sol. **28**, 2283.
Mayer, I. and Y. Eshdat, 1968, Inorg. Chem. **9**, 1904.
Muratova, L.O. and O.I. Bodak, 1974, Tesizy Dokl. Tret. Vses. Konf. Kristallokhim. Intermet. Soedin, 2nd Ed., ed. R.M. Rykhal (Lvov. Gos. Univ., Lvov, USSR) p. 33.
Muratova, L.O., O.I. Bodak and E.I. Gladyshevskij, 1975, Visn. L'vivsk Derzh. Univ., Ser. Khim. **17**, 30.

Gd–Ir–Si

Three ternary compounds have been reported for the Gd–Ir–Si system.

GdIrSi is isotypic with the structure type of TiNiSi, Pnma, $a = 6.913(6)$, $b = 4.235(4)$, $c = 7.434(7)$ (Hovestreydt et al., 1982; X-ray powder diffraction). For sample preparation, see YPdSi; atom parameters as derived for ScPtSi.

$GdIrSi_2$ was reported to be isotypic with the crystal structure of $CeNiSi_2$ (Chevalier et al., 1982).

Rossi et al. (1979) by means of X-ray powder diffraction concluded $GdIr_2Si_2$ to be isostructural with the $ThCr_2Si_2$-type of structure (space group I4/mmm, $a = 4.063$ and $c = 9.952$, $\rho_x = 12.08$ kg/dm³). For sample preparation, see $CePd_2Si_2$. Slaski and Szytula (1982) confirmed both the atomic order and crystal symmetry I4/mmm, but measured slightly different lattice parameters $a = 4.058(1)$ and $c = 9.963(3)$ (X-ray powder data of induction-melted alloys). Magnetic sysceptibilities as recorded in the temperature range of 100 to 600 K seem to be characterized by a paramagnetic behavior of $\mu_{eff}^{para} = 10.3$ μ_B and $\theta_p = 35$ K.

References

Chevalier, B., P. Lejay, J. Etourneau, M. Vlasse and P. Hagenmuller, 1982, Paper presented at the 7th Intern. Conf. on Solid Compounds of Transition Elements, Grenoble, France, Collected Abstracts, II B 16.
Hovestreydt, E., N. Engel, K. Klepp, B. Chabot and E. Parthé, 1982, J. Less-Common Metals **86**, 247.
Rossi, D., R. Marazza and R. Ferro, 1979, J. Less-Common Metals **66**, P17.
Slaski, M. and A. Szytula, 1982, J. Less-Common Metals **87**, L1.

Gd–La–Si

Raman (1968) observed a complete solid solution $Gd_{1-x}La_xSi$ at $1000\,°C$, crystallizing with the FeB-type of structure. For structural details (FeB-type, branch I, Pnma) and sample preparation, see $ErAl_xSi_{1-x}$. The following lattice parameters were reported: GdSi [$a = 7.935(5)$, $b = 3.856(5)$, $c = 5.730(5)$]; $Gd_{0.74}La_{0.26}Si$ [$a = 8.015(5)$, $b = 3.910(5)$, $c = 5.813(5)$], $Gd_{0.5}La_{0.5}Si$ [$a = 8.178(5)$, $b = 3.946(5)$, $c = 5.880(5)$], $Gd_{0.26}La_{0.74}Si$ [$a = 8.308(5)$, $b = 3.960(5)$, $c = 5.972(5)$] and LaSi [$a = 8.380(5)$, $b = 3.990(5)$, $c = 6.024(5)$].

Reference
Raman, A., 1968, Inorg. Chem. 7(5), 973.

Gd–Mn–Si

Only two ternary compounds have been characterized in the Gd–Mn–Si system. $GdMn_2Si_2$ adopts the $ThCr_2Si_2$-type of structure: I4/mmm, $a = 3.950$, $c = 10.478$, $\rho_x = 6.57$ kg/dm^3 (Rossi et al., 1978; X-ray powder diffraction). Samples were prepared as $LaMn_2Si_2$. Szytula et al. (1981), Latka et al. (1979) and Narasimhan et al. (1976) confirmed atom ordering and crystal symmetry from X-ray powder data and investigated the magnetic behavior. Antiferromagnetic ordering occurs at $T_N = 453$ K and an additional magnetic transition was observed at $T_m = 65$ K. The paramagnetic data were given as $\mu_{eff}^{para} = 8.4$ μ_B mole^{-1}, $\mu_n = 4.37$ μ_B mole^{-1}. Knigenko et al. (1977) measured a slightly larger cell volume $a = 3.950$, $c = 10.520$ (X-ray powder analysis). Narasimhan et al. (1975) reported $a = 3.951(5)$ and $c = 10.479(5)$; for sample preparation, see the Y–Mn–Si system; magnetic data were interpreted by antiparallel spin coupling of the rare earths and the Mn atoms.

GdMnSi crystallizes with the PbFCl-type of structure (P4/nmm, $a = 4.02$, $c = 7.16$) and orders ferromagnetically at $T_m = 295$ K (Johnson, 1974/76). For sample preparation see YMnSi. GdMnSi can also be obtained by solid state reactions from mixtures of GdSi and Mn within an Al_2O_3 crucible and sealed in silica tubes ($800\,°C$, 2 d).

References
Johnson, V., 1974/76, Du Pont de Nemours Co., US. Patent 396829.
Knigenko, L.D., I.R. Mokra and O.I. Bodak, 1977, Vestn. Lvov. Univ., Ser. Khim. **19**, 68.
Latka, K., H. Schmidt, V. Östreich, F. Götz and G. Czjzek, 1979, KFK Progress Report, KFK-2881.
Narasimhan, K.S.V.L., V.U.S. Rao and W.E. Wallace, 1975, AIP Conf. Proc. **29**, 594, see also 1976, J. Appl. Phys. **46**, 4957.
Rossi, D., R. Marazza, D. Mazzone and R. Ferro, 1978, J. Less-Common Metals **59**, 79.
Szytula, A. and I. Szott, 1981, Solid State Commun. **40**, 199.

Gd–Ni–Si

No ternary phase diagram of the system Gd–Ni–Si is available; however, twelve ternary compounds have been characterized (see table 11).

TABLE 11

Formation and structural data of ternary compounds Gd–Ni–Si.

Compound	Structure type Space group	Lattice parameters Density	Preparation, Characterization	Refs.	Purity
$GdNi_{10}Si_2$	$YNi_{10}Si_2$ ord. $ThMn_{12}$ I4/mmm	$a = 8.231$ $c = 4.699$	$\mu_{eff}^{para} = 7.8\ \mu_B,\ \theta_p = 35$ K PXD arc(Ar), Qu, 800 °C, 720 h	GlBYGS, 77 Ya, 78a	Gd 99.85 Ni 99.98 Si 99.9
$GdNi_{6.72}Si_{6.28}$	$Ce_2Ni_{17}Si_9$? ($NaZn_{13}$-deriv.) I4/mcm	$a = 11.010$ $c = 11.129$ [***]	arc(Ar), Qu 800 °C, 720 h PXD	Ya, 78b	Gd 99.85 Ni 99.92 Si 99.9
$Gd(Ni,Si)_{13}$ 37–45 a/o Si	$NaZn_{13}$ Fm3c	$a = 11.07(1)$	arc(Ar), Qu 800 °C, 100 h, PXD	BoG, 69a	Gd 99.2 Ni 99.99 Si 99.99
$GdNi_{4.23}Si_{0.70}$	$ErNi_{4.23}Si_{0.70}$ ($EuMg_5$ or $Sc_3Ni_4Si_4$) $P6_3/mmc$	$a = 8.15$ $c = 8.62$	arc(Ar), Qu 800 °C, 720 h PXD	Ya, 78b	Gd 99.85 Ni 99.92 Si 99.9
$GdNi_5Si_3$	YNi_5Si_3 Pnma	$a = 18.88(2)$ $b = 3.820(5)$ $c = 6.616(7)$	arc(Ar), Qu 800 °C, 720 h PXD	Ya, 78b	Gd 99.85 Ni 99.92 Si 99.9
$Gd_3Ni_6Si_2$	$Ce_3Ni_6Si_2$ ord. Ca_3Ag_8 Im3m	$a = 8.838(2)$	arc, Qu(Ni) 800 °C, 2 weeks PXD	GlKB, 66	Gd 99.5 Ni 99.99 Si 99.99
GdNiSi	TiNiSi Pnma	$a = 6.97$ $b = 4.19$ $c = 7.17$	PXD $\mu_{eff}^{para} = 7.8\ \mu_B,\ \theta_p = 5$ K	Dw, 82 GlBYGS, 77	
		$a = 6.993$ $b = 4.179$ $c = 7.224$	arc(Ar), Qu 800 °C, 720 h PXD	Ya, 78b	Gd 99.85 Ni 99.92 Si 99.9
Gd_3NiSi_2 [*]	Gd_3NiSi_2 filled Hf_3P_2 Pnma	$a = 11.398(4)$ $b = 4.155(1)$ $c = 11.310(1)$ $\rho_x = 7.27$	arc(Ar), Qu(Ta) 800 °C, 2 weeks single crystal data	KlP, 81	Gd 99.9 Ni 99.99 Si 99.999
$GdNi_2Si_2$	$ThCr_2Si_2$ I4/mmm	$a = 3.977(10)$ $c = 9.557(10)$	arc(Ar) PXD	BoGK, 66	Gd 99.5 Ni 99.8 Si 99.99
		$a = 3.98$ $c = 9.56$	induction melting Ar, PXD $T_N = 15.5$ K, $\theta_p = -6$ K $\mu_{eff}^{para} = 8.0\ \mu_B$	YaI, 80	
$GdNiSi_2$	$CeNiSi_2$ Cmcm	$a = 4.025(2)$ $b = 16.095(10)$ $c = 3.976(2)$	arc(Ar) PXD	BoG, 69b	Gd 99.5 Ni 99.8 Si 99.99

TABLE 11 (continued)

Compound	Structure type Space group	Lattice parameters Density	preparation, Characterization	Refs.	Purity
GdNi$_{0.4}$Si$_{1.6}$ (**)	AlB$_2$ P6/mmm	$a = 3.973$ $c = 4.100$	induction heating (Ar) in Al$_2$O$_3$, 1500 °C, Qu 700–900 °C, 24–96 h, PXD	MaT, 69	Gd 99.9 Ni 99.95 Si 99.99
GdNiSi$_3$	ScNiSi$_3$ Amm2	$a = 3.997$ $b = 3.915$ $c = 21.159$	arc, Qu (10^{-2} torr Ar) 800 °C, 720 h $\mu_{eff}^{para} = 6.87 \, \mu_B$; $\theta_p = 5$ K	GoBGY, 77 Ya, 78b	Gd 99.85 Ni 99.98 Si 99.99

(*) The crystal structure of Gd$_3$NiSi$_2$ has been refined by Klepp and Parthé (1981) by means of single crystal counter data; $R = 0.059$. Atom parameters were (all atoms in site 4c of Pnma): Gd, 0.3814(2), 1/4, 0.4403(2); Gd, 0.0576(2), 1/4, 0.3750(2); Gd, 0.2137(2), 1/4, 0.6976(2); Ni, 0.1285(5), 1/4, 0.1334(5); Si, 0.473(1), 1/4, 0.685(1); Si, 0.303(1), 1/4, 0.005(1).

(**) The compound of this type exists already in the binary system (see also text).

(***) For a correct setting of a bct-unit cell, $a = a_0/\sqrt{2} = 7.785$.

The phase equilibria within the concentrational section GdNi$_x$Si$_{2-x}$ were studied by Mayer and Tassa (1969) by means of X-ray powder analysis. For $x < 0.4$ the ThSi$_2$-type of structure was observed to be stable, whereas GdNi$_{0.4}$Si$_{1.6}$ crystallizes with the AlB$_2$-type of structure (Table 11). In analogy to the X-ray data of NdNi$_{0.4}$Si$_{1.6}$ a statistical distribution of Ni/Si atoms in the 2d site of P6/mmm was assumed.

Latka et al. (1979) and Yakinthos and Ikonomou (1980) studied the magnetic behavior of GdNi$_2$Si$_2$. Good agreement exists about the data obtained: $\mu_{eff}^{para} = 7.97$ μ_B, $\theta_p = 1$ K, $T_N = -15.0$ K (Latka) and $\mu_{eff}^{para} = 8.0 \, \mu_B$, $\theta_p = -6$ K, $T_N = -15.5$ K (Yakinthos). Mössbauer spectra of ^{61}Ni in GdNi$_2$Si$_2$ showed no hyperfine splitting down to 1.2 K, confirming the 3d moment to be zero. The magnetic structure was said to consist of ferromagnetic Gd planes nearly $\perp$ to the c-axis stacked in some sequence to give a net antiferromagnetic order. The angle between the Gd moments and the c-axis was approximately 30° (^{155}Gd Mössbauer data, Latka).

References

Bodak, O.I. and E.I. Gladyshevskij, 1969a, Dopov. Akad. Nauk Ukr. RSR, Ser. A 12, 1125.

Bodak, O.I. and E.I. Gladyshevskij, 1969b, Kristallografiya 14(6), 990.

Bodak, O.I., E.I. Gladyshevskij and P.I. Kripyakevich, 1966, Izv. Akad. Nauk SSSR, Neorg. Mater. 2(12), 2151.

Dwight, A.E., 1982, private communication.

Gladyshevskij, E.I., P.I. Kripyakevich and O.I. Bodak, 1966, Acta Crystallogr. A21, 80, and Z. Anorg. Allg. Chem. 344, 95.

Gladyshevskij, E.I., O.I. Bodak, V.I. Yarovets, Yu.K. Gorelenko and R.V. Skolozdra, 1977, Fiz. Magnit. Plenok (Irkutsk) 10, 182.

Gorelenko, Yu.K., O.I. Bodak, E.I. Gladyshevskij and V.I. Yarovets, 1977, Ukr. Fiz. Zh. 22(6), 1020.

Klepp, K. and E. Parthé, 1981, Acta Crystallogr. B37, 1500.

Latka, K., H. Schmidt, V. Oestreich, F. Götz and G. Czjzek, 1979, KFK Progress Report, KFK-2881, p. 79.

Mayer, I. and M. Tassa, 1969, J. Less-Common Metals **19**, 173.
Yakinthos, J.K. and P.F. Ikonomou, 1980, Solid State Commun. **34**, 777.
Yarovets, V.I., 1978a, Tesizy Dokl. Tret. Vses. Konf. Kristallokhim. Intermet. Soedin, 2nd Ed., ed. R.M.
    Rykhal (Lvov Gos. Univ., Lvov, USSR) p. 124.
Yarovets, V.I., 1978b, Autoreferat Dis. Kand. Khim. (abstract of thesis, Rissian) (Nauk, Lvov) 24 p.

Gd–Os–Si

GdOs$_2$Si$_2$ is isotypic with the crystal structure of ThCr$_2$Si$_2$ (Hiebl et al., 1983; X-ray powder analysis). Space group and unit cell dimensions are: I4/mmm, $a = 4.1403(5)$ and $c = 9.7656(39)$. For sample preparation, see YOs$_2$Si$_2$. From magnetic susceptibility measurements (1.5 K $<$ T $<$ 1100 K) GdOs$_2$Si$_2$ is paramagnetic at higher temperatures with $\mu_{\text{eff}}^{\text{para}} = 8.12$ μ_B and $\theta_p = 27$ K. Antiferromagnetic ordering occurs at 26 K.

Reference
Hiebl, K., C. Horvath, P. Rogl and M.J. Sienko, 1983, Solid State Commun. **48**, 211.

Gd–Pd–Si

Only two ternary compounds have been characterized in the Gd–Pd–Si system.

GdPd$_2$Si crystallizes with the ordered Fe$_3$C-type of structure with space group Pnma and lattice parameters $a = 7.364(2)$, $b = 6.920(2)$ and $c = 5.545(1)$ X-ray powder data by Moreau et al., 1982). For sample preparation, see YPd$_2$Si.

The magnetic behavior of polycrystalline GdPd$_2$Si was investigated by Gignoux et al. (1984) in the temperature range of 1.5 K to 300 K and in fields up to 77 kOe. The paramagnetic parameters obtained were: $\mu_{\text{eff}}^{\text{para}} = 8.06$ μ_B, $\theta_p = 14$ K. GdPd$_2$Si orders antiferromagnetically below $T_N = 13.5$ K. The saturation moment at 1.5 K and in 77 kOe was 6.98μ_B.

Ballestracci (1976) observed GdPd$_2$Si$_2$ with the ordered ThCr$_2$Si$_2$-type of structure with space group I4/mmm. From X-ray powder analysis the unit cell dimensions were given as $a = 4.138$, $c = 9.93$. For sample preparation, see CePd$_2$Si$_2$. From X-ray powder diffraction analysis Rossi et al. (1979) confirmed the ThCr$_2$Si$_2$-type of structure but reported considerably different values ($a = 4.153$, $c = 9.874$, $\rho_x = 8.31$ kg/dm^3). Samples were prepared by melting in an induction furnace under argon (starting from 99.9% Gd and 99.99% Rh,Si), followed by a heat treatment for 1 week at 500°C. From the different lattice parameters a homogeneous range is likely. Slaski and Szytula (1982) and Yakinthos and Gamari-Seale (1982) investigated the magnetic behavior of GdPd$_2$Si$_2$ in the temperature range of 4.2 to 300 K (Yakinthos) and from 100 to 600 K (Slaski) [$a = 4.149(1)$, $c = 9.894(4)$]. At higher temperatures paramagnetic behavior was confirmed. The magnetic data were $\mu_{\text{eff}}^{\text{para}} = 8.7$ μ_B and $\theta_p = -39$ K (Slaski) and $\mu_{\text{eff}}^{\text{para}} = 8.8$ μ_B, $\theta_p = 2$ K (Yakinthos). GdPd$_2$Si$_2$ orders antiferromagnetically at $T_N = 13$ K (Yakinthos).

References
Ballestracci, R., 1976, C.R. Acad. Sci. Paris, Ser. B **282**, 291.
Gignoux, D., J.C. Gomez-Sal and D. Paccard, 1984, Solid State Commun. **49**(1), 75.

Moreau, J.M.J. LeRoy and D. Paccard, 1982, Acta Crystallogr. **B38**, 2446.
Rossi, D., R. Marazza and R. Ferro, 1979, J. Less-Commun Metals **66**, P17.
Slaski, M. and A. Szytula, 1982, J. Less-Common Metals **87**, L1.
Yakinthos, J.K. and H. Gamari-Seale, 1982, Z. Phys. B. **48**, 251.

Gd–Pr–Si

Mayer and Tendy (1970) investigated the phase equilibria along the concentration section $Pr_{5-x}Gd_xSi_3$ by means of X-ray powder methods. For sample preparation, see $La_5Si_{3-x}Ge_x$. Among the two competing structure types the Mn_5Si_3-type of structure ($P6_3/mcm$) was claimed to be stable in the range $2 < x \leqslant 5$, whereas the Cr_5B_3-type with space group $I4/mcm$ occurred for $0 \leqslant x < 1.5$. For lattice parameters versus x, see fig. 28. The discontinuities of V and a, however, do not seem to coincide!

Reference
Mayer, I. and S. Tendy, 1970, Israel J. Chem. **8**, 955.

Gd–Pt–Si

$GdPt_2Si$ crystallizes with the ordered Fe_3C-type structure: Pnma, $a = 7.356(2)$, $b = 6.916(2)$, $c = 5.515(2)$ (X-ray powder data by Moreau et al., 1982). For sample preparation, see YPd_2Si.

Alloys of GdPtSi in as-cast condition (arc melted) were observed by Klepp and Parthé (1982) to crystallize with the LaPtSi-type of structure, $I4_1md$, $a = 4.0996(3)$,
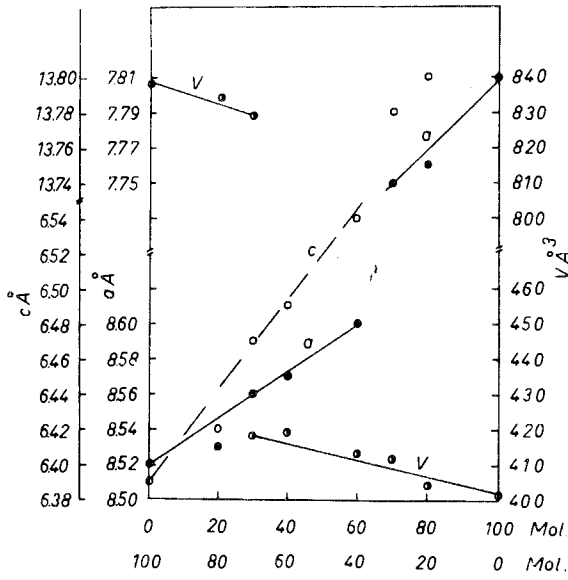
Fig. 28. Gd–Pr–Si, section $(Pr_{5-x}Gd_x)Si_3$, lattice parameters versus concentration, after Mayer and Tendy (1970).

$c = 14.329(2)$ (X-ray powder data). Annealing at $775\,^\circ$C for 2 weeks revealed a phase transition to an unknown low-temperature phase.

Mayer and Yetor (1977) claimed $GdPt_2Si_2$ to be tetragonal with the $BaAl_4$-type ($a = 4.175$, $c = 9.783$). In analogy to $ErPt_2Si_2$, Pt and Si atoms were said to statistically occupy the 4d and 4e sites of I4/mmm. For sample preparation, see $LaPt_2Si_2$. Rossi et al. (1979) confirmed the Pt/Si random distribution from a nearly single-phase sample ($a = 4.182$, $c = 9.808$, $\rho_x = 11.68$ kg/dm^3). For sample preparation, see $CePd_2Si_2$. At variance with this, Ballestracci and Astier (1978) reported $GdPt_2Si_2$ with a primitive tetragonal lattice and from X-ray powder analysis of alloys melted under argon in an induction furnace they found $a = 4.182$ and $c = 9.79$. More recent X-ray powder data of arc-melted alloys confirm the primitive tetragonal crystal symmetry with an atomic arrangement similar to the $CaBe_2Ge_2$-type (Rogl, 1984): $a = 4.1851(4)$, $c = 9.7875(44)$, $CePt_2Si_2$-type.

References
Ballestracci, R. and G. Astier, 1978, C.R. Acad. Sci. paris, Ser. B **286**, 109.
Klepp, K. and E. Parthé, 1982, Acta Crystallogr. **B38**, 1105.
Mayer, I. and P.D. Yetor, 1977, J. Less-Common Metals **55**, 171.
Moreau, J.M., J. Leroy and D. Paccard, 1982, Acta Crystallogr. **B38**, 2446.
Rogl, P., 1984, Inorgan. Chem., to be published.
Rossi, D., R. Marazza and R. Ferro, 1979, J. Less-Common Metals **66**, P17.

Gd–Re–Si

Only two ternary compounds have been characterized in the Gd–Re–Si system.

According to X-ray powder data by Bodak et al. (1978) $Gd_2Re_3Si_5$ crystallizes with the $Sc_2Fe_3Si_5$-type of structure [P4/mmc, $a = 10.91(1)$, $c = 5.571(5)$]. Samples were arc melted; however, no detailed conditions for heat treatment were given. Segre (1981) confirmed the structure type, but reported different lattice parameters $a = 10.93(1)$, $c = 5.550(8)$. Samples were arc melted; $T_n = 1.2$ K.

The crystal structure of $GdRe_4Si_2$ is isotypic with the structure type of $ZrFe_4Si_2$. The space group is P4$_2$/mnm, the lattice parameters are $a = 7.330(5)$ and $c = 4.112(1)$ (Bodak et al., 1978; X-ray powder analysis of arc-melted alloys).

References
Bodak, O.I., V.K. Pecharskij and E.I. Gladyshevskij, 1978, Izv. Akad. Nauk SSSR, Neorg. Mater. **14**(2), 250.
Segre, C.U., 1981, Thesis, Univ. of Calif., San Diego, USA.

Gd–Rh–Si

GdRhSi crystallizes with the TiNiSi type structure, the space group is Pnma and the lattice parameters were given as $a = 6.919(1)$, $b = 4.2257(5)$ and $c = 7.334(1)$ (powder X-ray analysis, Chevalier et al., 1982a). For sample preparation, see YRhSi. GdRhSi exhibits spontaneous magnetization below $T_m = 100$ K (a noncollinear arrangement of the moments was said to be likely); the paramagnetic behavior is characterized by $\theta_p = 94$ K and $\mu_{eff}^{para} = 7.95$ μ_B mole^{-1}.

According to an X-ray powder analysis by Ballestracci (1976) $GdRh_2Si_2$ is isotypic with the crystal structure of $ThCr_2Si_2$ (I4/mmm, $a = 4.040$, $c = 9.98$). For sample preparation, see YRh_2Si_2. Slasky and Szytula (1982) confirmed atomic order and crystal symmetry [$a = 4.045(1)$ and $c = 9.980(3)$] from X-ray powder data of induction-melted alloys. Magnetic behavior was investigated in the temperature range 100 to 600 K revealing an effective paramagnetic moment $\mu_{eff}^{para} = 6.9 \mu_B$ with $\theta_p = 31$ K. From X-ray powder data of induction-melted alloys Felner and Nowik (1983) reported slightly different unit cell dimensions $a = 4.037(2)$, $c = 9.99(1)$, and from magnetization and ^{155}Gd Mössbauer data they derived antiferromagnetic ordering at $T_N = 132(2)$ K. The second peak in the susceptibility curve at $T_m = 16(2)$ K was interpreted as itinerant electron ordering of the 4d sublattice. The observed paramagnetism in the temperature range $T < 300$ K was described by $\mu_{eff}^{para} = 5.6(1)$ μ_B and $\theta_p = 25(3)$ K. The Mössbauer data at 77 K revealed a magnetically ordered Gd sublattice whereas the identical spectra at 4.1 and 20 K showed that Gd atoms are not involved in the ordering at $T_m = 16$ K.

$GdRh_3Si_2$ adopts the $CeCo_3B_2$-type of structure [P6/mmm, $a = 5.505(6)$, $c = 3.549(4)$] as observed by Chevalier et al. (1981) from X-ray powder data. For sample preparation, see $LaRh_3Si_2$. Ferromagnetic ordering occurs at $T_m = 31$ K. At higher temperatures ($T \sim 300$ K) $GdRh_3Si_2$ behaves as a paramagnet with $\mu_{eff}^{para} = 7.91$ μ_B mole^{-1} and $\theta_p = 36$ K.

Chevalier et al. (1982b) investigated the structural and magnetic properties (4.2 to 300 K) of the compound $Gd_2Rh_3Si_5$ crystallizing with the $Sc_2Co_3Si_5$-type structure (Ibam, $a = 9.80(1)$, $b = 11.72(1)$ and $c = 5.748(5)$]. The paramagnetic data obtained were $\mu_{eff}^{para} = 8.18$ μ_B, $\theta_p = -26$ K. At low temperatures $Gd_2Rh_3Si_5$ is said to order antiferromagnetically.

The existence of further compounds such as $GdRhSi_2$ ($CeNiSi_2$-type) and Gd_2RhSi_3 with a structure type deriving from AlB_2 has been recently reported by Chevalier et al. (1982b).

According to X-ray powder data obtained from arc-melted alloys annealed at 800°C for 4 d, Gd_2RhSi_3 is isostructural with the Er_2RhSi_3-type. The crystal data are: P$\bar{6}$2c, $a = 8.112(5)$, $c = 7.976(5)$. Gd_2RhSi_3 orders antiferromagnetically at $T_N = 14$ K; the paramagnetic behavior in the temperature range below 300 K is represented by $\mu_{eff}^{para} = 7.61$ μ_B and $\theta_p = 2$ K (Chevalier et al., 1984).

References

Ballestracci, R., 1976, C.R. Acad. Sci. Paris, Ser. B **282**, 291.
Chevalier, B., A. Cole, P. Lejay and J. Etourneau, 1981, Mater. Res. Bull. **16**, 1067.
Chevalier, B., A. Cole, P. Lajay, M. Vlasse, J. Etourneau and P. Hagenmuller, 1982a, Mater. Res. Bull. **17**, 251.
Chevalier, B., P. Lejay, J. Etourneau, M. Vlasse and P. Hagenmuller, 1982b, Paper presented at the 7th Intern. Conf. on Solid Compounds of Transition Elements, Grenoble, France, Collected Abstracts, II B 16, and 1982, Mater. Res. Bull. **17**, 1211.
Chevalier, B., P. Lejay, J. Etourneau and P. Hagenmuller, 1984, Solid State Commun. **49**(8), 753.
Felner, I. and I. Nowik, 1983, Solid State Commun. **47**, 831.
Slaski, M. and A. Szytula, 1982, J. Less-Common Metals **87**, L1.

Gd–Ru–Si

Only two ternary compounds have been reported for the Gd–Ru–Si system.

Barz (1980) reported the existence of a ternary compound $GdRu_3Si_2$ with the $LaRu_3Si_2$-type of structure. No lattice parameters were given. For sample preparation and melting behavior (phase equilibria), see also $LaRu_3Si_2$; $T_m > 25$ K.

According to an X-ray powder diffraction study by Hiebl et al. (1983) $GdRuSi_2$ is isostructural with the $ThCr_2Si_2$-type of structure: I4/mmm, $a = 4.1634(4)$ and $c = 9.6102(49)$. For sample preparation, see YOs_2Si_2. Magnetic susceptibilities were investigated in the temperature range from 1.5 K to 1100 K; the paramagnetic behavior is characterized by an effective moment $\mu_{eff}^{para} = 8.02$ μ_B ($\theta_p = 54.7$ K). Due to antiferromagnetic ordering at lower temperature ($T_N = 31$ K) the slopes of the reciprocal susceptibilities start to change at $T < 300$ K. Crystal and magnetic data were also presented by Slaski and Szytula (1982) and fairly good agreement exists with respect to unit cell dimensions [$a = 4.163(1)$, $c = 9.605(2)$] and magnetic data ($\mu_{eff}^{para} = 7.9$ μ_B, $\theta_p = 12$ K).

References
Barz, H., 1980, Mater. Res. Bull. **15**, 1489.
Hiebl, K., C. Horvath, P. Rogl and M.J. Sienko, 1983, J. Magn. Magn. Mater. **37**, 287.
Slaski, M. and A. Szytula, 1982, J. Less-Common Metals **87**, L1.

Ho–Al–Si

No ternary phase diagram exists for the Ho–Al–Si system, but the formation of two ternary compounds has been observed: Ho_2Al_2Si and $HoAl_2Si_2$.

Yanson (1975) from powder X-ray diffraction data characterized the compound $Ho_2Al_2Si \equiv (Ho_2Al)(Al,Si)_2$ to be isostructural with Dy_2Al_2Si (see Dy–Al–Si), whose structure is an ordered variant of the U_3Si_2-type (space group P4/mbm). The lattice parameters were measured: $a = 6.910(4)$ and $c = 4.237(3)$.

From X-ray powder analysis, $HoAl_2Si_2$ was found to adopt the La_2O_2S-type of structure: P$\bar{3}$m1, $a = 4.19$ and $c = 6.49$ (Muravyova et al., 1972). For atom parameters and details of sample preparation, see Sm–Al–Si.

References
Muravyova, A.A., O.S. Zarechnyuk and E.I. Gladyshevskij, 1972, Visn. L'vivsk Univ., Ser. Khim. **13**, 14.
Yanson, T.I., 1975, Autoreferat Dis. Kand. Khim. (abstract of thesis, Russian) (Nauk, Lvov) 22 p.

Ho–Au–Si

From an X-ray powder diffraction analysis, Felner (1973) reported the existence of $HoAu_2Si_2$ with the ordered $ThCr_2Si_2$-type of structure (I4/mmm, $a = 4.224$, $c = 10.12$); sample preparation as for $LaAu_2Si_2$. Magnetic ordering (Ferromagnetic?) was observed at $T_m = 14.8$ K; the asymptotic Curie temperature was $\theta_p = -2.1$ K; $\mu_{eff}^{para} = 10.6$ μ_B.

Reference
Felner, I., 1973, J. Phys. Chem. Sol. **36**, 1063.

Ho–Co–Si

No ternary phase diagram has been established for the Ho–Co–Si system, but at least five ternary compounds have been characterized.

$HoCo_2Si_2$ crystallizes with the ordered $ThCr_2Si_2$-type of structure: I4/mmm, $a = 3.880$, $c = 9.740$, $\rho_x = 7.68$ kg/dm^3 (Rossi et al., 1978; X-ray powder diffraction data). For sample preparation and etching conditions, see YCo_2Si_2. Ferromagnetic ordering at $T_m = 15$ K was suspected by Yakinthos et al. (1980); the paramagnetic behavior is characterized by $\mu_{eff}^{para} = 10.7$ μ_B mole^{-1} (4.2–200 K) and $\theta_p = -8$ K. Structural and magnetic data were also derived by Skolozdra et al. (1980) and presented as follows (80–1150 K): $a = 3.878(5)$, $c = 9.73(1)$; $\mu_{eff}^{para} = 11.5$ μ_B per formula unit, and $\mu_{eff}^{para} = 3.2$ μ_B per Co atom; $\theta_p = -47$ K; magnetic ordering was observed at $T_m = 295$ K. Nguyen et al. (1983) confirmed the crystal symmetry and atomic order from neutron diffraction and magnetic measurements of samples melted in an induction furnace and annealed at 900 °C for 100 h in evacuated silica tubes. The starting materials were of 99.99% purity. A neutron diffraction study at room temperature confirmed the ordered $ThCr_2Si_2$-type with $a = 3.887(3)$, $c = 9.688(2)$ and $z(Si) = 0.371$.

Neutron diffraction data at 4.2 K and magnetic measurements (4.4–300 K) revealed a collinear antiferromagnetic order below $T_N = 13(1)$ K with the rare earth moment of 8.1(1) μ_B oriented along the c-axis. The magnetic structure consists of ferromagnetic layers perpendicular to the c-axis coupled antiferromagnetically in a sequence $+ - + -$. The fitting of the calculated and observed magnetic intensities led to reliability values of $R_N = 0.08$ and $R_m = 0.05$; the Co atoms did not participate in the magnetic ordering. The low-temperature data, however, are at variance with the observations of Yakinthos et al. (1980), who claimed a ferromagnetic type of order (see above). The paramagnetic behavior was characterized by $\mu_{eff}^{para} = 10.6$ μ_B and $\theta_p = 4$ K (Nguyen et al., 1983). An independent neutron diffraction study by Leciejewicz et al. (1983) confirmed the antiferromagnetic ordering at $T_N = 10(1)$ K; the data obtained were at 4.2 K: $a = 3.902(5)$, $c = 9.827(2)$, $z(Si$ in 4e$) = 0.3733(4)$, $\mu = 10.4(8)$ μ_B, $R = 0.036$, and at 300 K: $a = 3.884(1)$, $c = 9.748(5)$, $z = 0.3736(7)$, $R = 0.022$. For sample preparation, see Er–Co–Si. Yarovets (1978) from X-ray powder analysis reported slightly different unit cell dimensions, $a = 3.885$ and $c = 9.761$. The antiferromagnetic type of order was furthermore confirmed from a neutron diffraction study by Schobinger et al. (1983); the crystallographic data obtained at 300 K were: $a = 3.8799(9)$, $c = 9.735(2)$, $z(Si) = 0.3734(6)$, $R_N = 0.08$, and at 4.2 K: $a = 3.8717(3)$, $c = 9.731(1)$, $z(Si) = 0.3763(7)$, $R_N = 0.03$, $R_m = 0.04$; $\mu = 9.85$ μ_B. Magnetic susceptibilities were measured by Yarovets et al. (1977) in the temperature range of 300 to 1200 K, $\mu_{eff}^{para} = 10.3$ μ_B and $\theta_p = -12$ K.

Pelizzone et al. (1982) investigated the structural and magnetochemical behavior of $HoCoSi_2$ with the $CeNiSi_2$-type [Cmcm, $a = 3.996(2)$, $b = 16.268(6)$ and $c = 3.946(2)$]. Samples were prepared by arc melting and subsequent annealing in sealed quartz capsules (150 Torr argon) at 1000 °C for one week. Purity of starting materials was 99.9%. Magnetic susceptibilities were characterized by a paramagnetic

behavior according to $\mu_{eff}^{para} = 10.5(1)$, $\theta_p = -6$ K and antiferromagnetic ordering at 6.3 K. The resistivity versus temperature (300–1000 K) was reported by Stadnyk et al. (1979) (6.5–10^{-6} Ω m at 300 K).

The existence of a compound Ho(Co,Si)$_{11}$ with the BaCd$_{11}$-type structure was first mentioned by Bodak and Gladyshevskij (1969); the atom order and crystal symmetry was confirmed by Yarovets (1978) from X-ray powder data obtained for HoCo$_{8.5}$Si$_{2.5}$ (Ce$_2$Ni$_{17}$Si$_5$-type, I4$_1$/amd, occupation variant of BaCd$_{11}$, $a = 9.670$ and $c = 6.230$). For sample preparation and atom parameters, see Tb–Co–Si.

HoCoSi is orthorhombic with the TiNiSi-type of structure: Pnma, $a = 6.804$, $b = 4.112$ and $c = 7.131$ (X-ray powder data by Yarovets, 1978). For sample preparation and atom parameters, see YNiSi.

The crystal structure of Ho$_3$Co$_2$Si$_7$ was refined by Yarovets (1978) from single crystal X-ray photographs. The reliability factor obtained was $R = 0.212$; the crystallographic data derived are listed as follows: Ho$_3$Co$_2$Si$_7$-type, space group Amm2, $a = 3.854(5)$, $b = 24.468(10)$ and $c = 3.885(5)$; Ho in 2a) 0, 0, 0.0062(7), Ho in 2b) 1/2, 0, 0.3170(5); Ho in 2b) $z = 0.6822(4)$, Co in 2a) $z = 0.1321(5)$, Co in 2a) $z = 0.8673(7)$; Si in 2a) $z = 0.2200(7)$; Si in 2a) $z = 0.7762(8)$; Si in 2a) $z = 0.3934(7)$; Si in 2a) $z = 0.6123(9)$; Si in 2b) $z = 0.0992(3)$; Si in 2b) $z = 0.8917(10)$, and Si in 2b) $z = 0.5391(0)$. Samples were prepared by arc melting powder compacts under argon and subsequent annealing in evacuated silica tubes at 800°C for 720 h. Magnetic susceptibilities were measured within the temperature range of 327–1172 K, $\mu_{eff}^{para} = 10.20(30)$ μ_B, $\theta_p = 16$ K (Yarovets, 1978).

References

Bodak, O.I. and E.I. Gladyshevskij, 1969, Dopov. Akad. Nauk Ukr. RSR, Ser. A **5**, 452.
Leciejewicz, J., M. Kolenda and A. Szytula, 1983, Solid State Commun. **45**, 145.
Nguyen, V.N., F. Tcheou, J. Rossat-Mignod and R. Ballestracci, 1983, Solid State Commun. **45**(2), 209.
Pelizzone, M., H.F. Braun and J. Müller, 1982, J. Magn. Magn. Mater. **30**, 33.
Rossi, D., R. Marazza and R. Ferro, 1978, J. Less-Common Metals **58**, 203.
Schobinger-Papamantellos, P., Ch. Routsi and J.K. Yakinthos, 1983, J. Phys. Chem. Solids, **44**(9), 875.
Skolozdra, R.V., Yu.K. Gorelenko, O.I. Bodak and V.I. Yarovets, 1980, Ukr. Fiz. Zh. **25**(10), 1683.
Stadnyk, Yu.V., Yu.K. Gorelenko, R.V. Skolozdra, V.I. Yarovets and O.I. Bodak, 1979, Splavy Redk. Tugoplavk. Met. Osob. Fiz. Svoistvami (Moscow) p. 124–128.
Yakinthos, J.K., Ch. Routsi and P.F. Ikonomou, 1980, J. Less-Common Metals **72**, 205.
Yarovets, V.I., 1978, Autoreferat Dis. Kand. Khim. (abstract of thesis, Russian) (Nauk, Lvov) 24 p.
Yarovets, V.I., Yu.K. Gorelenko and R.V. Skolozdra, 1977, Tesizy Dokl. IX. Ukr. Vses. Konf. Neorg. Khim., Lvov, p. 188.

Ho–Cu–Si

Four ternary compounds have been reported for the Ho–Cu–Si system. The occurrence of the AlB$_2$-type of structure was investigated by Rieger and Parthé (1969a) by means of X-ray powder diffraction of an arc-melted alloy with the composition HoCu$_{0.67}$Si$_{1.33}$: Cu and Si atoms were concluded to statistically occupy the 2d sites of P6/mmm; $a = 3.988$, $c = 3.976$. The magnetic behavior of an alloy HoCuSi, prepared by heating a powder mixture in an evaluated silica capsule for 7 d at 800 to 900°C, was studied in the temperature range of 77–300 K by Kido et al. (1983). X-ray powder data were reported to reveal an AlB$_2$-type structure. HoCuSi

was observed to be paramagnetic with $\mu_{\text{eff}}^{\text{para}} = 10.2\ \mu_B$ and $\theta_p = 30$ K.

From arc-melted alloys annealed at $750\,^{\circ}$C, Iandelli (1983) observed the formation of a compound HoCuSi with the ordered Ni_2In-type of structure (superstructure of AlB_2-type): $P6_3/mmc$, $a = 4.137(2)$, $c = 7.355(6)$. The superstructure reflections were said to be very faint; with respect to the results obtained by Rieger and Parthé (1969a) from arc-melted samples (see above) of similar composition, HoCuSi was suspected to be the low-temperature modification. For details of sample preparation and purities of starting materials, see LaCuSi.

$Ho_3Cu_4Si_4$ crystallizes with the $Gd_3Cu_4Ge_4$-type of structure: $Immm$, $a = 13.63$, $b = 6.52$, $c = 4.11$ (X-ray powder analysis by Hanel and Nowotny, 1970). For sample preparation, see $Sc_3Cu_4Si_4$.

According to X-ray powder data by Rieger and Parthé (1969b) $HoCu_2Si_2$ is tetragonal with the $ThCr_2Si_2$-type of structure: $I4/mmm$, $a = 3.949(6)$, $c = 9.977(10)$. For sample preparation, see YCu_2Si_2.

Routsi and Yakinthos (1981) investigated the magnetic properties of $HoCu_2Si_2$ within the temperature range of 4.2 K to 150 K and up to 18 kOe ($ThCr_2Si_2$-type, but no X-ray data given). Above 50 K a paramagnetic behavior was observed corresponding to $\mu_{\text{eff}}^{\text{para}} = 10.3\ \mu_B$ and $\theta_p = -3$ K. $HoCu_2Si_2$ orders antiferromagnetically at $T_N = 8$ K; from the field dependence of the magnetization at 4.2 K metamagnetism was suggested.

For X-ray adsorption studies (L_3-absorption edge), see Padalia et al. (1983).

References

Hanel, G. and H. Nowotny, 1970, Monatsh. Chem. **101**, 463.

Iandelli, A., 1983, J. Less-Common Metals **90**, 121.

Kido, H., T. Hishikawa, M. Shimada and M. Koizumi, 1983, Phys. Stat. Sol. (a) **77**, K121.

Padalia, B.D., T.K. Hatwar and M.N. Ghatikar, 1983, J. Phys. **C16**, 1537.

Rieger, W. and E. Parthé, 1969a, Monatsh. Chem. **100**, 439.

Rieger, W. and E. Parthé, 1969b, Monatsh. chem. **100**, 444.

Routsi, C. and J.K. Yakinthos, 1981, Phys. Stat. Sol. (a) **68**, K153.

Ho–Fe–Si

Six ternary compounds have been characterized in the system Ho–Fe–Si.

$Ho_2Fe_3Si_5$ crystallizes with the $Sc_2Fe_3Si_5$-type of structure: $P4/mnc$, $a = 10.39(1)$, $c = 5.44(1)$ (X-ray powder analysis, Braun, 1980). $Ho_2Fe_3Si_5$ orders antiferromagnetically at $T_N = 2.9$ K. Magnetic susceptibility data [$\mu_{\text{eff}}^{\text{para}} = 10.4(1)\ \mu_B$ and $\theta_{c\parallel} = 0.3(7)$] as well as Mössbauer spectra indicate the absence of a magnetic moment at the iron site (Braun et al., 1981). For sample preparation, see $Dy_2Fe_3Si_5$. For low temperature heat capacity data, see Vining and Shelton (1983), $T_N = 2.82$ K. Yarovets (1978) reported different unit cell dimensions for $Ho_2Fe_3Si_5$ with a much smaller c/a-ratio: $a = 10.434$, $c = 5.285$ (X-ray powder data; for sample preparation, see Y–Fe–Si).

HoFeSi is tetragonal with the PbFCl-type of structure: $P4/nmm$, $a = 3.937(3)$, $c = 6.774(5)$ (Bodak et al., 1970; X-ray powder data). For sample preparation, see CeFeSi.

$Ho_2Fe_4Si_9$ crystallizes with the $Y_2Fe_4Si_9$-type of structure: $P6_3/mmc$, $a = 3.924(5)$,

$c = 15.43(1)$ (X-ray powder analysis by Gladyshevskij et al., 1978). Magnetic suscept-ibility data were measured within the temperature range of 300–1200 K and are characterized by $\mu_{eff}^{para} = 9.05 \ \mu_B$ mole^{-1} and $\theta_p = -41$ K. For sample preparation, see $Y_2Fe_4Si_9$.

The crystal structure of $Ho_3Fe_2Si_7$ (earlier denoted as $HoFeSi_3$) was found to be isostructural with the $Ho_3Co_2Si_7$-type: Amm2, $a = 3.863$, $b = 24.655$ and $c = 3.916$ (Yarovets, 1978; from X-ray powder data). From susceptibility measurements (300–1200 K) the effective moment μ_{eff}^{para} was obtained to be 10.18 μ_B mole^{-1} and $\theta_p = 49$ K (Gladyshevskij et al., 1978). For sample preparation, see $Y_2Fe_4Si_9$.

Structural and magnetic data for $HoFe_2Si_2$ (80–1050 K) have been presented by Skolozdra et al. (1980). Crystal symmetry and atomic order were confirmed from X-ray powder data [$ThCr_2Si_2$-type, I4/mmm, $a = 3.900(5)$, $c = 9.93(1)$]. The mag-netic parameters were as follows: $\mu_{eff}^{para} = 11.9 \ \mu_B$/formula unit and $\mu_{eff}^{para} = 3.8 \ \mu_B$ per Fe atom; $\theta_p = -100$ K, $T_m = 300$ K. Yarovets (1978) refined the crystal structure of $HoFe_2Si_2$ from single crystal X-ray photographs; according to the obtained reliability factor $R = 0.137$, the atom parameters were listed as follows: $ThCr_2Si_2$-type, I4/mmm, Ho atoms in 2a) 0,0,0, Fe in 4d) 0,1/2,1/4 and Si in 4e) 0,0,0.3762(8); $a = 3.904$, $c = 9.920$. Magnetic susceptibilities were measured in the temperature range of 623 K–1118 K and effective paramagnetic moments were extrapolated from two temperature intervals as follows: $\mu_{eff}^{para} = 16.4(1) \ \mu_B$, $\theta_p = 233$ K in the range 623–816 K and $\mu_{eff}^{para} = 10.3(1) \ \mu_B$, $\theta_p = 174$ K for the region 970–1118 K (Yarovets, 1978). ^{57}Fe Mössbauer data at 1.3 K prove the absence of a magnetic moment on the Fe site (Noakes et al., 1983); the magnetic ordering temperature as derived from ac susceptibility measurements was $T_N = 2.2$ K with a planar aabbaabb antiferromagnetic ordering similar to $NdFe_2Si_2$.

$HoFe_{4.48}Si_{1.52}$ crystallizes with the $ZrFe_4Si_2$-type of structure: P4$_2$/mnm, $a = 7.114$, $c = 3.791$ (Yarovets, 1978; from X-ray powder data). For sample preparation and atom parameters, see Dy–Fe–Si.

References

Bodak, O.I., E.I. Gladyshevskij and P.I. Kripyakevich, 1970, Zh. Strukt. Khim. 11(2), 305.
Braun, H.F., 1980, Phys. Lett. 75A(5), 386.
Braun, H.F., C.U. Segre, F. Acker, M. Rosenberg, S. Dey and P. Deppe, 1981, J. Magn. Magn. Mater. 25, 117.
Gladyshevskij, E.I., O.I. Bodak, V.I. Yarovets, Yu.K. Gorelenko and R.V. Skolozdra, 1978, Ukr. Fiz. Zh. 23(11), 77.
Noakes, D.R., A.M. Umarji and G.K. Shenoy, 1983, J. Magn. Magn. Mater. 39, 309.
Skolozdra, R.V., Yu.K. Gorelenko, O.I. Bodak and V.I. Yarovets, 1980, Ukr. Fiz. Zh. 25(10), 1683.
Vining, C.B. and R.N. Shelton, 1983, Phys. Rev. B28(5), 2732.
Yarovets, V.I., 1978, Autoreferat Dis. Kand. Khim. (abstract of thesis, Russian) (Nauk, Lvov) 24 p.

Ho–Ir–Si

$Ho_5Ir_4Si_{10}$ is isotypic with the structure type of $Sc_5Co_4Si_{10}$: P4/mbm, $a = 12.554(8)$, $c = 4.215(5)$ (Braun and Segre, 1981; X-ray powder diffraction). For sample preparation, see $Sc_5Ir_4Si_{10}$. Ferromagnetic ordering occurs at $T_m = 1.5$ K.

Reference

Braun, H.F. and C.U. Segre, 1981, Ternary Superconductors of $Sc_5Co_4Si_{10}$-type, in: Ternary Supercon-
ductors, Proc. Intern. Conf. on Ternary Superconductors, eds. G.K. Shenoy, B.D. Dunlap and F.Y.
Fradin (North-Holland, Amsterdam) pp. 239–246.

Ho–Mn–Si

Only two ternary compounds have been observed in the Ho–Mn–Si system.

$HoMn_2Si_2$ is tetragonal with the $ThCr_2Si_2$-type of structure: I4/mmm, $a = 3.913$, $c = 10.476$, $\rho_x = 6.85$ kg/dm^3 (Rossi et al., 1978; X-ray powder analysis). For sample preparation, see $LaMn_2Si_2$. Szytula and Szott (1981) and Narasimhan et al. (1976) confirmed the crystal symmetry and atomic order from X-ray powder data and investigated the magnetic behavior. Antiferromagnetic ordering occurs at $T_N = 453$ K; the paramagnetic moment at high temperatures was $\mu_{eff}^{para} = 10.5$ μ_B mole^{-1} whereas at low temperatures $\mu_n = 6.65$ μ_B mole^{-1}. Narasimhan et al. (1976) measured: $a = 3.909(5)$ and $c = 10.424(5)$ and Knigenko et al. (1977) reported: $a = 3.900$ and $c = 10.400$ (X-ray powder analysis). For sample preparation, see the Y–Mn–Si system.

$Ho_2Mn_3Si_5$ crystallizes with the $Sc_2Fe_3Si_5$ type of structure: P4/mnc, $a = 10.61(1)$, $c = 5.429(8)$ (Segre, 1981; X-ray powder data or arc-melted alloys); $T_n = 1.2$ K.

References

Knigenko, L.D., I.R. Mokra and O.I. Bodak, 1977, Vestn. Lvov. Univ., Ser. Khim. **19**, 68.
Narasimhan, K.S.V.L., V.U.S. Rao and W.E. Wallace, 1976, AIP Conf. Proc. **29**, 594.
Rossi, D., R. Marazza, D. Mazzone and R. Ferro, 1978, J. Less-Common Metals **59**, 79.
Segre, C.U., 1981, Thesis, Univ. of Calif., San Diego, USA.
Szytula, A. and I. Szott, 1981, Solid State Commun. **40**, 199.

Ho–Ni–Si

No ternary phase diagram of the Ho–Ni–Si system has been established, but nine ternary compounds were observed. Their crystallographic data are listed in table 12.

TABLE 12

Formation and structural data of ternary compounds Ho–Ni–Si.

Compound	Structure type Space group	Lattice parameters Density	Preparation, Characterization	Refs.	Purity
$HoNi_{10}Si_2$	$YNi_{10}Si_2$		$\mu_{eff}^{para} = 10.7$ μ_B, $\theta_p = -35$ K	GlBYGS, 77	Ho 99.83 Ni 99.98
	ord. $ThMn_{12}$ I4/mmm	$a = 8.189$ $c = 4.663$	PXD arc(Ar), Qu 800 °C, 720 h	Ya, 78a	Si 99.9
$HoNi_{6.72}Si_{6.28}$	$Ce_2Ni_{17}Si_9$? ($NaZn_{13}$-deriv.) I4/mcm ?	$a = 10.906$ $c = 11.112$ [*]	arc(Ar), Qu 800 °C, 720 h PXD	Ya, 78b	Ho 99.83 Ni 99.98 Si 99.9

TABLE 12 (continued)

Compound	Structure type Space group	Lattice parameters Density	Preparation, Characterization	Refs.	Purity
$Ho_3Ni_6Si_2$	$Ce_3Ni_6Si_3$ ord. Ca_2Ag_8 Im3m	$a = 8.742(2)$	arc, Qu(Ni) 800 °C, 2 weeks PXD	GiKB, 66	Ho 97.4 Ni 99.99 Si 99.99
HoNiSi	TiNiSi Pnma	$a = 6.863$ $b = 4.143$ $c = 7.195$	PXD $\mu_{eff}^{para} = 10.4\,\mu_B$, $\theta_p = -18$ K	BoYG, 74 GlBYGS, 77	Ho 99.83 Ni 99.98 Si 99.9
		$a = 6.817$ $b = 4.139$ $c = 7.161$	PXD	Dw, 82	
		$a = 6.811$ $b = 4.120$ $c = 7.170$	arc(Ar), Qu 800 °C, 720 h PXD	Ya, 78b	Ho 99.83 Ni 99.98 Si 99.9
$HoNi_5Si_3$	YNi_5Si_3 Pnma	$a = 18.785$ $b = 3.787$ $c = 6.584$	arc(Ar) 800 °C PXD	AkYBYG, 76	Ni 99.92 Si 99.99
		$a = 18.77$ $b = 3.780$ $c = 6.612$	arc(Ar), Qu 800 °C, 720 h PXD	Ya, 78b	Ho 99.83 Ni 99.98 Si 99.9
$HoNi_{4.23}Si_{0.70}$	$ErNi_{4.23}Si_{0.70}$ ($EuMg_5$ or $Sc_3Ni_{11}Si_4$) $P6_3/mmc$	$a = 8.15$ $c = 8.63$	arc(Ar), Qu 800 °C, 720 h PXD	Ya, 78b	Ho 99.83 Ni 99.98 Si 99.9
$HoNi_2Si_2$	$ThCr_2Si_2$ I4/mmm	$a = 3.938(10)$ $c = 9.527(10)$	arc(Ar) PXD	BoGK, 66	Ho 97.4 Ni 99.8 Si 99.99
		$a = 3.94$ $c = 9.53$	induction melting, Ar, PXD $\theta_p = -6$ K, $\mu_{eff}^{para} = 10.9\,\mu_B$	YaI, 80	
$HoNiSi_2$	$CeNiSi_2$ Cmcm	$a = 3.943(2)$ $b = 15.995(10)$ $c = 3.933(2)$	arc(Ar) PXD	BoG, 69	Ho 97.4 Ni 99.8 Si 99.99
$HoNiSi_3$	$YNiSi_3$ Amm2	$a = 3.969$ $b = 3.898$ $c = 21.116$	arc, Qu (10^{-2} Torr Ar) 800 °C, 720 h $\mu_{eff}^{para} = 9.03\,\mu_B$, $\theta_p = 58$ K	GoBGY, 77 Ya, 78b	Ho 99,83 Ni 99.98 Si 99.99

(*) For a correct setting of a bct unit cell, $a = a_0/\sqrt{2} = 7.712$.

References

Aksel'rud, L.G., V.I. Yarovets, O.I. Bodak, Ya.P. Yarmolyuk and E.I. Gladyshevskij, 1976, Sov. Phys. Crystallogr. **21**(2), 210.

Bodak, O.I. and E.I. Gladyshevskij, 1969, Kristallografiya **14**(6), 990.

Bodak, O.I., E.I. Gladyshevskij and P.I. Kripyakevich, 1966, Izv. Akad. Nauk SSSR, Neorg. Mater. **2**(12), 2151.

Bodak, O.I., V.I. Yarovets and E.I. Gladyshevskij, 1974, Tesizy Dokl. Tret. Vses. Konf. Kristallokhim. Intermet. Soedin, 2nd Ed., ed. R.M. Rykhal (Lvov. Gos. Univ., Lvov, USSR) p. 32.

Dwight, A.E., 1982, private communication.

Gladyshevskij, E.I., P.I. Kripyakevich and O.I. Bodak, 1966, Acta Crystallogr. A**21**, 80, and Z. Anorg. Allg. Chem. **344**, 95.

Gladyshevskij, E.I., O.I. Bodak, V.I. Yarovets, Yu.K. Gorelenko and R.V. Skolozdra, 1977, Fiz. Magnit. Plenok (Irkutsk) **10**, 182.

Gorelenko, Yu.K., O.I. Bodak, E.I. Gladyshevskij and V.I. Yarovets, 1977, Ukr. Fiz. Zh. **22**(6), 1020.

Yakinthos, J.K. and P.F. Ikonomou, 1980, Solid State Commun. **34**, 777.

Yarovets, V.I., 1978a, Tret. Tesizy Dokl. Vses. Konf. Kristallokhim. Intermet. Soedin, 2nd Ed., ed. R.M. Rykhal (Lvov Gos. Univ., Lvov, USSR) p. 124.

Yarovets, V.I., 1978b, Autoreterat Dis. Kand. Khim. (abstract of thesis, Russian) (Nauk, Lvov) 24 p.

Ho–Os–Si

$HoOs_2Si_2$ crystallizes with the $ThCr_2Si_2$-type of structure (Hiebl et al., 1983). The crystallographic data, derived from X-ray powder diffraction analysis, were: I4/mmm, $a = 4.1251(4)$ and $c = 9.6679(45)$. For sample preparation, see YOs_2Si_2. Above $T = 300$ K $HoOs_2Si_2$ is paramagnetic with $\mu_{eff}^{para} = 10.61$ K and $\theta_p = 30$ K. Ferromagnetic ordering occurs at 8.5 K.

Reference

Hiebl, K., C. Horvath, P. Rogl and M.J. Sienko, 1983, Solid State Commun. **48**, 211.

Ho–Pd–Si

Only three ternary compounds have been observed in the Ho–Pd–Si system.

$HoPd_2Si$ crystallizes with the ordered Fe_3C-type structure with space group Pnma and lattice parameters $a = 7.265(2)$, $b = 6.923(2)$ and $c = 5.484(2)$ (X-ray powder data by Moreau et al., 1982). For sample preparation, see YPd_2Si.

The magnetic properties of polycrystalline $HoPd_2Si$ have been studied by Gignoux et al. (1984) in the temperature range of 1.5–300 K and in fields up to 77 kOe. The paramagnetic moment was $\mu_{eff}^{para} = 10.53$ μ_B, $\theta_p = 2$ K; $HoPd_2Si$ is ferromagnetic below $T_m = 3.5$ K. The saturation moment at 1.5 K and in 77 kOe was 7.68 μ_B.

According to X-ray powder diffraction data by Ballestracci (1976) $HoPd_2Si_2$ is tetragonal with the ordered $ThCr_2Si_2$-type and lattice parameters, $a = 4.102$ and $c = 9.90$. For sample preparation, see $CePd_2Si_2$. Slaski and Szytula (1982) confirmed both the atomic order and crystal symmetry I4/mmm, but reported slightly different lattice parameters ($a = 4.108(1)$, $c = 9.864(2)$, X-ray powder data of induction-melted alloys). Magnetic susceptibilities were investigated by Slaski and Szytula (1982) in the range from 100 to 600 K and by Yakinthos and Gamari-Seale (1982) in the range of 4.2 to 300 K. A paramagnetic behavior was observed with $\mu_{eff}^{para} = 10.0$ μ_B,

$\theta_p = 0$ K (Slaski) and $\mu_{eff}^{para} = 10.5$ μ_B, $\theta_p = -5$ K (Yakinthos). The susceptibility was said to increase abruptly below 30 K, but no clear ordering was observed (Yakinthos).

Ho$_2$Pd$_2$Si is isotypic with the crystal structure of Er$_2$Pd$_2$Si: Pnnm, $a = 7.403(2)$, $b = 13.793(3)$ and $c = 4.2910(9)$ (X-ray powder data of arc-melted samples; Klepp et al., 1983).

References

Ballestracci, R., 1976, C.R. Acad. Sci. Paris, Ser. B **282**m 291.
Gignoux, D., J.C. Gomez-Sal and D. Paccard, 1984, Solid State Commun. **49**(1), 75.
Klepp, K., E. Hovestreydt and E. Parthé, 1983, Acta Crystallogr. **C39**, 662.
Moreau, J.M., J. LeRoy and D. Paccard, 1982, Acta Crystallogr. **B38**, 2446.
Slaski, M. and A. Szytula, 1982, J. Less-Common Metals **87**, L1.
Yakinthos, J.K. and H. Gamari-Seale, 1982, Z. Phys. **B48**, 251.

Ho–Pt–Si

HoPt$_2$Si crystallizes with the ordered Fe$_3$C-type of structure: Pnma, $a = 7.269(2)$, $b = 6.909(2)$, $c = 5.449(2)$ (Moreau et al., 1982; X-ray powder analysis). For sample preparation, see YPd$_2$Si.

HoPtSi is isostructural with the TiNiSi-type, Pnma, $a = 6.931(1)$, $b = 4.2527(8)$ and $c = 7.409(1)$ (X-ray powder analysis by Hovestreydt et al., 1982). For sample preparation, see ScPtSi.

HoPt$_2$Si$_2$ crystallizes with the primitive tetragonal CePt$_2$Si$_2$-type, $a = 4.1455(4)$, $c = 9.8270(62)$ (Rogl, 1984).

References

Hovestreydt, E., N. Engel, K. Klepp, B. Chabot and E. Parthé, 1982, J. Less-Common Metals **86**, 247.
Moreau, J.M., J. LeRoy and D. Paccard, 1982, Acta Crystallogr. **B38**, 2446.
Rogl, P., 1984, Inorg. Chem., to be published.

Ho–Re–Si

Two compounds have been characterized in the Ho–Re–Si system.

According to an X-ray powder diffraction investigation of arc-melted alloys by Bodak et al. (1978) Ho$_2$Re$_3$Si$_5$ is isotypic with the crystal structure of Sc$_2$Fe$_3$Si$_5$ [P4/mnc, $a = 10.85(1)$, $c = 5.506(5)$]. No detailed conditions of heat treatment were given. Segre (1981) confirmed the space group, but measured slightly different lattice parameters: $a = 10.93(1)$, $c = 5.491(8)$ (samples were arc melted); $T_n = 1.2$ K.

Pecharskij (1979) reported about the existence of the compound HoRe$_4$Si$_2$ with the ZrFe$_4$Si$_2$-type (P4$_2$/mnm, $a = 7.304(5)$ and $c = 4.103(2)$, X-ray powder data). Samples were prepared by arc melting and subsequent annealing at 800°C for 400 + 600°C in evacuated silica tubes.

References

Bodak, O.I., V.K. Pecharskij and E.I. Gladyshevskij, 1978, Izv. Akad. Nauk SSSR, Neorg. Mater. **14**(2), 250.
Pechardskij, V.K., 1979, Autoreferat Dis. Kand. Khim. (abstract of thesis, Russian) (Nauk, Lvov) 23 p.
Segre, C.U., 1981, Thesis, Univ. of Calif., San Diego, USA.

Ho–Rh–Si

Five ternary compounds were reported for the Ho–Rh–Si system.

HoRhSi is isotypic with the crystal structure of TiNiSi; the space group is Pnma and the lattice parameters were given as $a = 6.799(1)$, $b = 4.1857(5)$ and $c = 7.348(1)$ (Chevalier et al., 1982a; X-ray powder methods). For sample preparation, see YRhSi. HoRhSi orders antiferromagnetically at $T_N = 8$ K. A metamagnetic transition was reported at 4.2 K and for magnetic fields $\geqslant 6$ kOe; the paramagnetic behavior is characterized by $\theta_p = 10.5$ K and $\mu_{eff}^{para} = 10.71$ μ_B mole^{-1}.

Ballestracci (1976) was the first to report the existence of HoRh$_2$Si$_2$ crystallizing with the ordered ThCr$_2$Si$_2$-type of structure (I4/mmm, $a = 4.018$, $c = 9.89$; X-ray powder methods). For sample preparation, see YRh$_2$Si$_2$. Slaski and Szytula (1982) confirmed atomic order and crystal symmetry [$a = 4.024(3)$, $c = 9.891(6)$] from X-ray powder data of induction-melted alloys. Magnetic behavior was studied in the temperature range of 100 to 600 K revealing paramagnetism with $\mu_{eff}^{para} = 9.7$ μ_B and $\theta_p = -10$ K. From X-ray powder analysis of induction-melted alloys Felner and Nowik (1983) reported $a = 4.015(2)$ and $c = 9.89(1)$; HoRh$_2$Si$_2$ orders antiferromagnetically at $T_N = 27(2)$ K; the second peak in the susceptibility at $T_m = 14(2)$ K was interpreted as itinerant electron ordering of the 4d sublattice; the paramagnetic behavior (1.5–300 K) corresponds to $\mu_{eff}^{para} = 9.3(1)$ μ_B, $\theta_p = 3$ K. The atomic order and crystal symmetry (ThCr$_2$Si$_2$-type, I4/mmm) was confirmed from a room temperature neutron diffraction study on polycrystalline material: $a = 4.084(3)$, $c = 10.009(9)$, z(Si in 4e) $= 0.3765(13)$, $R_N = 0.054$ (Slaski et al., 1983). From neutron diffraction data at 4.2 K Slaski et al. (1983) confirmed the antiferromagnetic order at $T_N = 27(1)$ K and determined the type of order to be of a simple collinear $+ - + -$ type with the magnetic moments (Ho^{3+}) under an angle $\phi = 28(3)°$ with the c-axis [$a = 4.086(6)$, $c = 10.094(9)$, z(Si) $= 0.3773(5)$, $R_N = 0.027$. data at 4.2 K].

According to X-ray powder-diffraction data by Chevalier et al. (1981) HoRh$_3$Si$_2$ adopts the CeCo$_3$B$_2$-type of structure [P6/mmm, $a = 5.475(6)$, $c = 3.544(4)$]. For sample preparation, see LaRh$_3$Si$_2$. HoRh$_3$Si$_2$ orders ferromagnetically at $T_m = 10$ K; the paramagnetic data are as follows: $\mu_{eff}^{para} = 10.61$ μ_B mole^{-1} and $\theta_p = 18$ K.

Chevalier et al. (1982b) characterized the structural and magnetic properties (4.2 to 300 K) of the compound Ho$_2$Rh$_3$Si$_5$ crystallizing with the Sc$_2$Co$_3$Si$_5$-type of structure [Ibam, $a = 9.78(1)$, $b = 11.67(1)$ and $c = 5.685(5)$]. The paramagnetic data obtained were: $\mu_{eff}^{para} = 10.61$ μ_B and $\theta_p = -1$ K. Ho$_2$Rh$_3$Si$_5$ was said to order antiferromagnetically at very low temperatures.

The existence of a compound Ho$_2$RhSi$_3$ with a structure type deriving from AlB$_2$ has been reported by Chevalier et al. (1982b). X-ray powder data obtained from arc-melted alloys, annealed at 800 °C for 4 days, proved that Ho$_2$RhSi$_3$ adopted the Er$_2$RhSi$_3$-type structure: P$\bar{6}$2c, $a = 8.072(5)$, $c = 7.771(5)$ (Chevalier et al., 1984). Er$_2$RhSi$_3$ is paramagnetic with $\mu_{eff}^{para} = 10.66$ μ_B, $\theta_p = 1$ K; no ordering was observed in the temperature range of 1.5 K to 300 K.

References

Ballestracci, R., 1976, C.R. Acad. Sci. Paris, Ser. B **282**, 291.

Chevalier, B., A. Cole, P. Lejay and J. Etourneau, 1981, Mater. Res. Bull. **16**, 1067.

Chevalier, B., A. Cole, P. Lejay, M. Vlasse, J. Etourneau and P. Hagenmuller, 1982a, Mater. Res. Bull. **17**, 251.

Chevalier, B., P. Lejay, J. Etourneau, M. Vlasse and P. Hagenmuller, 1982b, Paper presented at the 7th Intern. Conf. on Solid Compounds of Transition Elements, Grenoble, France, Collected Abstracts, II B 16, and 1982, Mater. Res. Bull. **17**, 1211.

Chevalier, B., P. Lejay, J. Etourneau and P. Hagenmuller, 1984, Solid State Commun. **49**(8), 753.

Felner, I. and I. Nowik, 1983, Solid State Commun. **47**, 831.

Slaski, M. and A. Szytula, 1982, J. Less-Common Metals **87**, L1.

Slaski, M., J. Leciejewicz and A. Szytula, 1983, J. Magn. Magn. Mater. **39**, 268.

Ho–Ru–Si

The existence of a compound $HoRu_3Si_2$ with the $LaRu_3Si_2$-type of structure was reported by Barz (1980). No lattice parameters were given. For sample preparation and melting behavior (phase equilibria), see $LaRu_3Si_2$. A probably ferromagnetic transition was said to occur at $T_m = 14.17$ K.

According to a crystal and magnetochemical investigation by Hiebl et al. (1983) the compound $HoRu_2Si_2$ crystallizes with the $ThCr_2Si_2$-type of structure with the space group I4/mmm and lattice parameters $a = 4.1482(3)$, $c = 9.5158(30)$ (X-ray powder data of arc-melted alloys). Magnetic susceptibilities were recorded in the temperature range from 1.5 K to 1100 K; and paramagnetic behavior is characterized by an effective moment $\mu_{eff}^{para} = 10.6$ μ_B ($\theta_p = 47.0$ K). Due to ferromagnetic ordering at $T_m = 6.4$ K the slopes of the reciprocal susceptibilities start to change at $T \sim 300$ K. Slaski and Szytula (1982) also presented crystallographic and magnetic data for $HoRu_2Si_2$. Their samples were prepared by melting in an induction furnace with subsequent annealing in an argon-filled quartz tube at 800°C for 100 h. Purities of starting materials were Ho 99.99%, Ru 99.9% and Si 99.999%. Small discrepancies exist between their unit cell parameters [$a = 4.124(2)$, $c = 9.506(4)$] and magnetic data from a limited temperature section 100 K $< T <$ 600 K ($\mu_{eff}^{para} = 9.9$ μ_B, $\theta_p = -12$ K) as compared to the data presented by Hiebl et al. (1983).

In a later paper Slaski et al. (1983) confirmed the atom order and crystal symmetry I4/mmm from a room temperature neutron diffraction analysis: $a = 4.170(4)$, $c = 9.579(9)$, z(Si in 4e) $= 0.360(2)$, $R_N = 0.088$. Low temperature neutron patterns of $HoRu_2Si_2$, however, were said to represent a helicoidal magnetic structure with the magnetic spin alignment of a linear transverse wave mode below the $T_N = 19$ K; according to Slaski et al. (1983) the static moment wave is polarized in the c-axis and propagates along b with $k = (0,0.2,0)$ [data at 4.2 K are $a = 4.206(4)$, $c = 9.563(9)$, z(Si) $= 0.360(2)$; $R_N = 0.091$].

References

Barz, H., 1980, Mater. Res. Bull. **15**, 1489.

Hiebl, K., C. Horvath, P. Rogl and M.J. Sienko, 1983, J. Magn. Magn. Mater. **37**, 287.

Slaski, M. and A. Szytula, 1982, J. Less-Common metals **87**, L1.

Slaski, M., J. Leciejewicz and A. Szytula, 1983, J. Magn. Magn. Mater. **39**, 268.

La–Ag–Si

The crystal structure of $LaAg_2Si_2$ has been refined by Mayer and Cohen (1972) and Mayer et al. (1973) from X-ray powder diffraction data [ordered $ThCr_2Si_2$-type, I4/mmm, a = 4.295(5), c = 10.64(5)]. Ag atoms were in 4d), and Si atoms in 4e) with z = 0.378; any random distribution of Ag and Si atoms was excluded; the reliability value thus obtained was given as R = 0.036. Samples were prepared by melting in alumina crucibles in an induction furnace at 1600–1800°C under Ar, and subsequently annealed for 48–60 h at 800°C in an electric furnace. Starting materials were 99.9% pure.

Reference
Mayer, I. and J. Cohen, 1972, J. Less-Common Metals **29**, 221.
Mayer, I., J. Cohen and I. Felner, 1973, J. Less-Common Metals **30**, 181.

La–Al–Si

Phase equilibria in the La-poor region (0–33 a/o La) of the ternary system La–Al–Si are presented in fig. 29 in form of a partial isothermal section at 500°C and are mainly based on the work by Muravyova (1972) and Raman and Steinfink (1967).

Raman (1967) and Raman and Steinfink (1967) investigated the phase relations
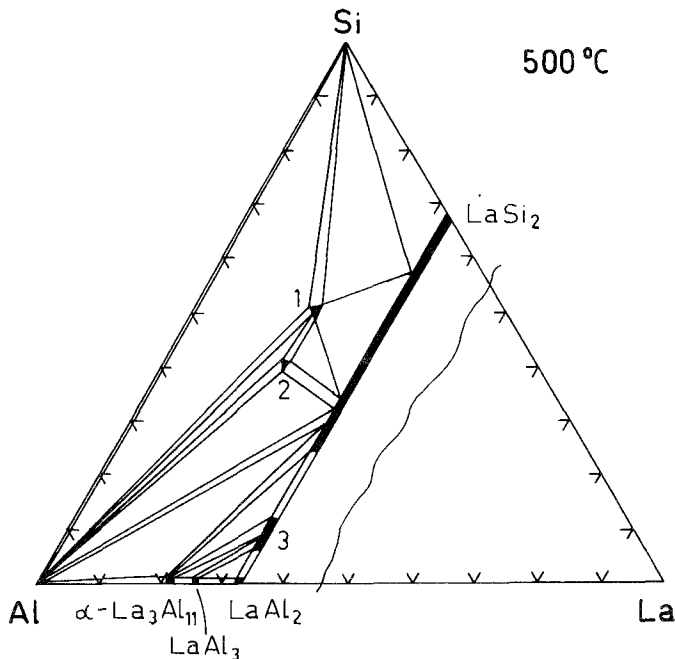
Fig. 29. La–Al–Si, partial isothermal section at 500°C (0–33 a/o La). 1: $LaAlSi_2$, 2: $LaAl_2Si_2$, 3: $LaAl_{1.64-1.85}Si_{0.36-0.15}$.

within the concentrational section $La(Al_{1-x}Si_x)_2$ by means of powder X-ray diffraction analysis of alloys which were arc melted and subsequently wrapped in Mo foils, sealed in evacuated quartz capsules and annealed at $1000°C$ for 4 d. Starting materials were 99.9% La, 99.999% Al and 99.99% Si. Samples with composition and lattice parameters as listed below were said to be single phase with the α-$ThSi_2$-type of structure and suggest an extended solubility of Al in binary $LaSi_2$ [α-$ThSi_2$-type, $a = 4.305(5)$, $c = 13.84(1)$], $LaAl_{0.5}Si_{1.5}$ [$a = 4.303(5)$, $c = 14.21(1)$], LaAlSi [$a = 4.284(5)$, $c = 14.56(1)$] and $LaAl_{1.25}Si_{0.75}$ [$a = 4.334(5)$, $c = 14.88(1)$]. The variation of the unit cell dimensions and the mean atomic volume versus concentration shows a rather linear dependence but with a significant dip around the composition LaAlSi, which in the present view might give an indication for an ordered atomic arrangement in terms of a LaPtSi-type of structure (α-$ThSi_2$-derivative type). The alloys $LaAl_{1.80}Si_{0.20}$ [$a = 4.387(5)$, $c = 4.387(5)$] and $LaAl_{1.75}Si_{0.25}$ [$a = 4.302(5)$, $c = 4.397(5)$] were found to crystallize with the AlB_2-type, whereas $LaAl_{1.94}Si_{0.06}$ [$a = 8.130(5)$] was single-phase and isotypic with the cubic $MgCu_2$-type, revealing a limited solid solubility of Si in $LaAl_2$ [$MgCu_2$-type, $a = 8.145(5)$].

Muravyova et al. (1972) prepared the compound $LaAl_2Si_2$ with the La_2O_2S-type of structure ($P\bar{3}m1$, $a = 4.23$, $c = 7.01$; from X-ray powder diffraction). Agreement between observed and calculated powder intensities was said to be satisfactory using the atom parameters as derived for the isotypic $CaAl_2Si_2$; for details, see Sm–Al–Si.

Confirming the earlier data by Raman (1967), Raman and Steinfink (1967) and by Muravyova et al. (1972), Muravyova (1972) investigated the phase relations in a partial isothermal section at $500°C$ for 0–33 a/o La. 54 alloys were prepared by arc melting powder compacts under argon, followed by a heat treatment at $500°C$ for 150–750 h in evacuated silica tubes. The starting materials were 98.5% La and 99.90% Al,Si.

The La–Al binary system with the compounds $La_3Al(Ni_3Sn$-type), $LaAl(CeAl$-type), $LaAl_2(MgCu_2$-type), $LaAl_3(Ni_3Sn$-type) and α-La_3Al_{11}, has been revised according to a recent critical assessment by Elliott and Shunk (1981).

Besides the extended α-$ThSi_2$-type solid solution of $LaAl_xSi_{2-x}$ with lattice parameters ranging from $a = 4.32$, $c = 13.86$ to $a = 4.35$, $c = 14.73$ [$I4_1/amd$, La in 4a) 0,0,0 and a statistical distribution of 8(Al + Si) 0,0,0.417], the phase equilibria are characterized by the formation of three ternary compounds $LaAl_2Si_2$ (La_2O_2S-type), $LaAl_{1.64-1.85}Si_{0.36-0.15}$ (AlB_2-type, $P6/mmm$, $a = 4.30–4.38$, $c = 4.41–4.40$) and $LaAlSi_{-2}$, whose structure type is unknown, but is likely to correspond to the analogous cerium compound ($Ce_{20}Al_{35}Si_{45}$).

References

Elliott, R.P. and F.A. Shunk, 1981, Bull. of Alloy Phase Diagrams 2(2), 219.
Muravyova, A.A., O.S. Zarechnyuk and E.I. Gladyshevskij, 1972, Visn. L'vivsk. Univ., Ser. Khim. 13, 14.
Muravyova, A.A., 1972, Autoreferat Dis. Kand. Khim. (abstract of thesis, Russian) (Nauk, Lvov) 22 p.
Raman, A., 1967, Metallkde 58(3), 179.
Raman, A. and H. Steinfink, 1967, Inorg. Chem. 6(10), 1789.

La–Au–Si

$LaAu_2Si_2$ crystallizes with the ordered $ThCr_2Si_2$-type of structure: I4/mmm, $a = 4.337(5)$, $c = 10.18(5)$ (Mayer et al., 1973; powder X-ray analysis). Samples were

prepared by melting in Al_2O_3 crucibles in an induction furnace at 1600–1800 °C under Ar, and subsequently annealed by keeping them for 30–60 min slightly below the heating temperature. Starting materials were 99.9% pure.

Reference

Mayer, I., J. Cohen and I. Felner, 1973, J. Less-Common Metals **30**, 181.

La–Co–Si

Bodak and Gladyshevskij (1969) studied the La-poor region of the La–Co–Si system by means of X-ray powder and metallographic analysis of arc-melted alloys, which subsequently were heat-treated at 800 °C for 100 h in evacuated silica tubes. An extended solid solubility of Si was observed in $LaCo_{13-11.1}Si_{0-1.9}$ with the $NaZn_{13}$-type, $a = 11.33–11.29(1)$. For ~ 30–33 a/o Si a tetragonal $NaZn_{13}$ derivative structure [$a = 11.06(9)$, $c = 11.53(1)$] was first reported by Bodak and Gladyshevskij (1969); in a later study by Bodak (1979) isotypic behavior was claimed with the structure type of $Ce_2Ni_{17}Si_9$ (I4/mcm, $a_0/\sqrt{2}$, c_0). No further details were given. More recently Palstra et al. (1983) studied the critical behavior of magnetization (4.2 to 300 K) in ferromagnetic $LaCo_{13-x}Si_x$ alloys ($x = 0$, 1.5, 2 and 2.5, see also table 13). Samples were prepared from 99.9% pure elements by arc melting and subsequent annealing at 900 °C for 10 days. Alloys with $x \leqslant 2.47$ were found to be homogeneous and isotypism was claimed with the cubic $NaZn_{13}$ structure type (X-ray powder data, but no lattice parameters were given). In comparison to the solubility data obtained at 800 °C by Bodak and Gladyshevskij (1969) ($x \leqslant 1.9$) the homogeneous range is now slightly increased at 900 °C. Mössbauer spectroscopy was performed on a ^{57}Fe-doped $LaCo_{11}Si_2$ alloy at 4.2 K and revealed an effective hyperfine field $H_{eff} \approx 25.5$ T.

TABLE 13

Magnetic properties of various $LaT_{13-x}Si_x$ compounds with the cubic $NaZn_{13}$ structure (T = Fe, Co, Ni) (after Palstra et al., 1983)

$LaT_{13-x}Si_x$	T_{Curie} (K)	μ_s (μ_B/T)
$LaFe_{11.5}Si_{1.5}$	198	2.08
$LaFe_{11.2}Si_{1.8}$	211	–
$LaFe_{11.1}Si_{1.9}$	219	–
$LaFe_{11.0}Si_{2.0}$	230	1.95
$LaFe_{10.9}Si_{2.1}$	234	–
$LaFe_{10.8}Si_{2.2}$	245	–
$LaFe_{10.5}Si_{2.5}$	262	1.85
$LaCo_{13}$	1 290	1.58
$LaCo_{11.5}Si_{1.5}$	–	1.29
$LaCo_{11}Si_2$	–	1.14
$LaCo_{10.5}Si_{2.5}$	–	0.88
$LaNi_{11}Si_2$	$\chi = 2.5 \times 10^{-7}$ m^{3}kg^{-1}	

Mayer and Tassa (1969) investigated the phase equilibria of the section $LaCo_xSi_{2-x}$ at 700–800 °C. For $x < 0.4$ a $ThSi_2$-type of structure was observed to be stable. $LaCo_{0.4}Si_{1.6}$ crystallizes with the AlB_2-type of structure ($a = 4.075$, $c = 4.386$). In analogy to the X-ray data obtained from $NdFe_{0.4}Si_{1.6}$ a statistical distribution of Co and Si atoms was assumed in the 2d sites of $P6/mmm$. X-ray powder patterns of alloys with $x > 0.4$ were said to be complex.

LaCoSi crystallizes with the PbFCl-type of structure: $P4/nmm$, $a = 4.089(3)$, $c = 7.140(5)$ (Bodak et al., 1970). For sample preparation and atom parameters, see CeFeSi.

$LaCo_2Si_2$ is tetragonal with the ordered $ThCr_2Si_2$-type of structure: $I4/mmm$, $a = 4.018$, $c = 10.080$, $\rho_x = 6.38$ kg/dm^3 (Rossi et al., 1978; X-ray powder diffraction). For sample preparation and etching conditions, see YCo_2Si_2. The thermoelectromotive force (80–1050 K) was measured by Levin (1981).

In a review article Gladyshevskij and Bodak (1973) mentioned the existence of a compound $LaCoSi_3$ with a $BaAl_4$-derivative type ($a = 4.147$, $c = 9.569$); more recently $LaCoSi_3$ was characterized by Chabot (1983), by means of X-ray powder techniques, to crystallize with the $BaNiSn_3$-type [$I4mm$, $a = 4.1868(8)$, $c = 9.654(2)$]. Samples were arc melted and subsequently annealed in quartz tubes backfilled with argon (900 °C, 1 d and 800 °C, 7 d).

Furthermore the formation of the compounds $LaCoSi_2$ with the $CeNiSi_2$-type, $La_{15}Co_4Si_{13}$ with the $Ce_{15}Ni_4Si_{13}$-type and of a compound $LaCo_{1.85}Si_{0.15}$ whose structure is unknown, was reported by Gladyshevskij and Bodak (1982).

References

Bodak, O.I., 1979, Sov. Phys. Crystallogr. **24**(6), 732.
Bodak, O.I. and E.I. Gladyshevskij, 1969, Dopov. Akad. Nauk Ukr. RSR, Ser A, **12**, 1125.
Bodak, O.I., E.I. Gladyshevskij and P.I. Kripyakevich, 1970, Zh. Strukt. Khim. **11**(2), 305.
Chabot, B., 1983, unpublished results.
Gladyshevskij, E.I. and O.I. Bodak, 1973, in: Khim. Met. Splavov, ed. N.M. Zhavornonkov (Nauka, Moscow, USSR) p. 46.
Gladyshevskij, E.I. and O.I. Bodak, 1982, Kristallokhim. Intermet. Soedin, Redkozemel, Metallov, Lvov, Vysha Schola.
Levin, E.M., 1981, Ukr. Fiz. Zh. **25**(3), 407.
Mayer, I. and M. Tassa, 1969, J. Less-Common Metals **19**, 173.
Palstra, T.T.M., J.A. Mydosh, G.J. Nieuwenhuys, A.M. van der Kraan and K.H.J. Buschow, 1983, J. Magn. Magn. Mater. **36**, 290.
Rossi, D., R. Marazza and R. Ferro, 1978, J. Less-Common Metals **58**, 203.

La–Cu–Si

Raman (1967) and Rieger and Parthé (1969a) investigated the occurrence of the AlB_2-type structure by means of X-ray powder analysis of arc-melted samples with composition as follows: $LaCu_{0.67}Si_{1.33}$ ($a = 4.107$, $c = 4.345$) and $LaCuSi$ ($a = 4.142$, $c = 4.299$) (Rieger and Parthé, 1969a) and $LaCu_{0.5}Si_{1.5}$, Cu-rich: $a = 4.144(5)$, $c = 4.286(5)$; Si-rich: $a = 4.071(5)$, $c = 4.383(5)$ (Raman, 1967). Cu and Si atoms were said to statistically occupy the 2d sites of $P6/mmm$ (Rieger and Parthé, 1969a). Thus extended homogeneous regions but eventually separated AlB_2-type phases with

ordering among Si and Cu atoms are conceivable (see e.g. the Ce–Cu–Si system). Iandelli (1983) confirmed the AlB_2-type structure of an arc-melted alloy $LaCu_{0.67}Si_{1.33}$ and gave $a = 4.129(1)$, $c = 4.324(2)$. [The AlB_2-type was also confirmed for this alloy after annealing at 750°C (identical lattice parameters).] Annealing of LaCuSi at 750°C for 8–12 d in evacuated silica tubes yielded a homogeneous alloy with the Ni_2In-type (superstructure of the AlB_2-type) with space group $P6_3/mmc$ and lattice parameters $a = 4.265(1)$ and $c = 8.154(5)$. Atomic parameters were rare earth in 2a, Cu in 2c and Si in the 2d sites of $P6_3/mmc$. The superstructure reflections were said to be faint, but the atomic order was confirmed by neutron diffraction; $R = 0.061$ (Mugnoli et al., 1984). The Ni_2In-type phase was concluded to be a low-temperature modification. Thermal analysis up to 1400°C revealed thermal effects at 830°C and 1090°C; however, no further explanation was given. Starting materials were 99.8–99.9% La, 99.999% Cu and 99.9999% Si.

$LaCu_2Si_2$ crystallizes with the $ThCr_2Si_2$-type of structure: I4/mmm, $a = 4.153(6)$ and $c = 9.918(10)$ (Rieger and Parthé, 1969b; X-ray powder data). For sample preparation, see YCu_2Si_2. Bodak et al. (1966) reported $a = 4.143(10)$, $c = 9.914(10)$ (X-ray powder analysis of arc-melted samples, 98.48% La, 99.9% Cu and 99.99% Si). The magnetic behavior was investigated by Routsi and Yakinthos (1981); the temperature range was 4.2 to 150 K and fields were up to 18 kOe. Susceptibility values were said to be small (no details given).

The thermoelectromotive force (80–1050 K) has been measured by Levin (1981). For physical properties, see also Sampathkumaran et al. (1979); for X-ray absorption studies (L_3-edge), see Padalia et al. (1983); for transport properties of $LaCu_2Si_2$ between 1.5 and 300 K (electrical resistivity, thermal conductivity and thermoelectric power), see Franz et al. (1978).

The existence of a compound $LaCu_{1.6}Si_{1.4}$ with the $CeNiSi_2$-type was reported by Bodak et al. (1971).

References

Bodak, O.I., E.I. Gladyshevskij and P.I. Kripyakevich, 1966, Izv. Akad. Nauk SSSR, Neorg. Mater. **2**, 2151.
Bodak, O.I., E.I. Gladyshevskij and Ya.M. Kalvijak, 1971, Tesizy Dokl. Vses. Konf. Kristallokhim. Intermet. Soedin., Lvov, p. 40.
Franz, W., A. Griessel, F. Steglich and D. Wohlleben, 1978, Z. Phys. **B31**, 7.
Iandelli, A., 1983, J. Less-Common Metals **90**, 121.
Levin, E.M., 1981, Ukr. Fiz. Zh. **26**(3), 407.
Mugnoli, A., A. Albinati and A.W. Hewat, 1984, J. Less-Common Metals **97**, L1.
Padalia, B.D., T.K. Hatwar and M.N. Ghatikar, 1983, J. Phys. **C16**, 1537.
Raman, A., 1967, Naturwiss. **54**, 560.
Rieger, W. and E. Parthé, 1969a, Monatsh. Chem. **100**, 439.
Rieger, W. and E. Parthé, 1969b, Monatsh. Chem. **100**, 444.
Routsi, C. and J.K. Yakinthos, 1981, Phys. Stat. Sol. (a) **68**, K153.
Sampathkumaran, E.V., L.C. Gupta and R. Vijayaraghavan, 1979, J. Phys. **C12**, 4323.

La–Fe–Si

Bodak and Gladyshevskij (1972) investigated the phase equilibria at 600°C by means of X-ray and metallographic analysis of 120 alloys. Samples were prepared by

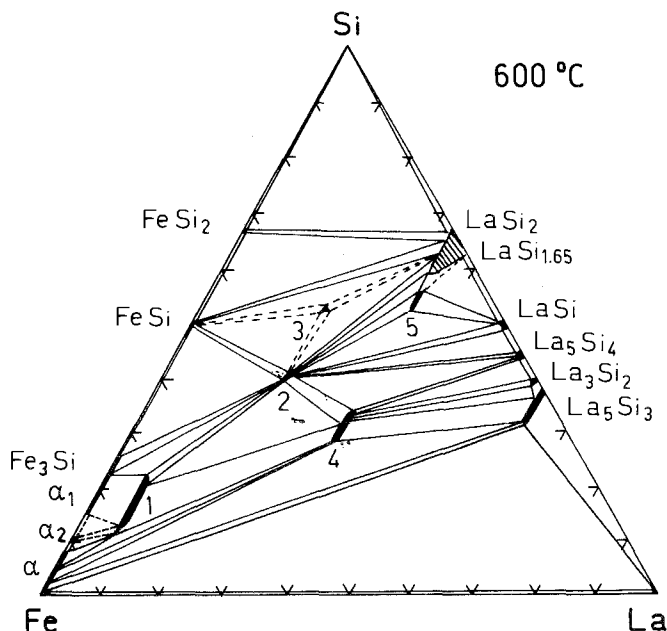Fig. 30. La–Fe–Si, isothermal section at 600°C. 1: $LaFe_{11.3-9.8}Si_{1.7-3.2}$, 2: $LaFe_2Si_2$, 3: "$LaFe_{1.3}Si_{2.7}$", 4: LaFeSi, 5: $LaFe_{0.3-0.5}Si_{1.7-1.5}$.

arc melting and annealing in evacuated silica tubes (100 h at 800°C and 150 h at 600°C for the region 0–33 a/o La; 150 h at 600°C for the region 33–100 a/o La). Starting materials were La 99.48%, Fe 99.96% and Si 99.99%.

Binary La silicides are basically in agreement with a recent compilation by Iandelli and Palenzona (1979): $LaSi_2$ ($ThSi_2$-type, $a = 4.322$, $c = 13.86$; $GdSi_2$-type at the composition $LaSi_{1.65}$, $a = 4.270$, $b = 4.170$, $c = 14.05$), LaSi (FeB-type, $a = 8.48$, $b = 4.02$, $c = 6.04$), La_5Si_4 (Zr_5Si_4-type, $a = 8.04$, $c = 15.43$), La_3Si_2 (U_3Si_2-type, $a = 7.87$, $c = 4.50$), and La_5Si_3 (Cr_5B_3-type, $a = 7.95$, $c = 14.04$). However, no detailed investigation of the La disilicide region (dashed area in fig. 30) has been carried out.

The La–Fe system was confirmed; no intermediate phases form and La and Fe are practically immiscible. The binary Fe silicides were discussed with the Y–Fe–Si system.

Solid solubilities are extending in the direction of Fe/Si exchange at a fixed La concentration: $LaSi_2$ dissolves up to 7 a/o Fe, La_5Si_3 up to ~5 a/o Fe; no variations of the unit cell dimensions have been given.

Earlier data on LaFeSi (Bodak et al., 1970), $La(Fe,Si)_2$ (Raman, 1967), and $La(Fe,Si)_{13}$ (Bodak and Gladyshevskij, 1969) were confirmed and a total of five ternary compounds were identified. The data presented in fig. 30 are consistent with more recent findings (see table 14) concerning the existence of $LaFe_{0.4}Si_{1.6}$ with the AlB_2-type structure ($a = 4.092$, $c = 4.370$), reported by Mayer and Tassa (1969). In analogy to $NdFe_{0.4}Si_{1.4}$ a statistical distribution of Fe,Si atoms in the 2d sites of

P6/mmm was assumed. Mössbauer data also indicate a partial ordering. For sample preparation, see $GdCo_{0.4}Si_{1.6}$.

Felner et al. (1975) confirmed the existence of $LaFe_2Si_2$ [$a = 4.061(5)$, $c = 10.16(5)$]

TABLE 14

Formation and structural data of ternary compounds La–Fe–Si.

Compound	Structural type Space group	Lattice parameters Density	Preparation, Characterization	Refs.	Purity
$LaFe_{11.3}Si_{1.7}-$ $LaFe_{9.8}Si_{3.2}$	$NaZn_{13}$-deriv. Fm3c, transformed into tetragonal	$a = 11.45–11.34(1)$ $c = 11.45–11.61(1)$ [*]	arc, Qu, 800 °C, 100 h 600 °C, 150 h PXD	BoG, 69 BoG, 72	La 99.48 Fe 99.96 Si 99.99
LaFeSi	PbFCl P4/nmm	$a = 4.062(3)$ $c = 7.179(5)$	arc, Qu, 800 °C, 100 h 600 °C, 150 h PXD	BoGK, 70 BoG, 72	La 99.48 Fe 99.96 Si 99.99
$LaFe_2Si_2$	$ThCr_2Si_2$ I4/mmm	$a = 4.042(5)$ $c = 10.14(1)$	arc, Qu, 800 °C, 100 h 600 °C, 150 h PXD	BoG, 72	La 99.48 Fe 99.96 Si 99.99
		$a = 4.061(5)$ $c = 10.16(5)$	HF melting (Ar) Al_2O_3 crucible 1500 °C, 30 min, PXD $T_m = 668(5)$ K	FeMGS, 75	99.9
		$a = 4.053$ $c = 10.153$ $\rho_x = 6.11$	induction melting Ar, 500 °C, 1 week PXD	RoMF, 78	La 99.9 Fe 99.99 Si 99.99
$LaFe_{0.3}Si_{1.7}-$ $LaFe_{0.5}Si_{1.5}$	AlB_2 P6/mmm	$a = 4.066–4.102(3)$ $c = 4.378–4.324(3)$	arc, Qu 600 °C, 150 h PXD	BoG, 72	La 99.48 Fe 99.96 Si 99.99
		$a = 4.092$ $c = 4.370$ for $LaFe_{0.4}Si_{1.6}$	induction melting Ar, Al_2O_3 crucible 1500 °C, 30 min, Qu 700–800 °C, 24–96 h, PXD	MaT, 69	La 99.9 Fe 99.95 Si 99.99
		Fe-rich $a = 4.069$ $c = 4.101$ for $LaFe_{0.5}Si_{1.5}$		Ra, 67	
		Si rich $a = 4.097$ $c = 4.331$			
$LaFe_{1.3}Si_{2.7}$	unknown			BoG, 72	La 99.48 Fe 99.96 Si 99.99

[*] Within the homogeneous range of this phase ($LaFe_{13.3–9.8}Si_{1.7–3.2}$) a transformation from cubic ($LaFe_{11.3}Si_{1.7}$) to tetragonal symmetry takes place; for a correct setting of the bct unit cell, $a = a_0/\sqrt{2}$ ($a = 8.096–8.019$), I4/mcm – $Ce_2Ni_{17}Si_9$-type?.

P6/mmm was assumed. Mössbauer data also indicate a partial ordering. For sample preparation, see $GdCo_{0.4}Si_{1.6}$.

Felner et al. (1975) confirmed the existence of $LaFe_2Si_2$ [$a = 4.061(5)$, $c = 10.16(5)$] with the $ThCr_2Si_2$-type of structure and also reported magnetic susceptibility data $\mu_{eff} = 0.29$ μ_B at 4.2 K and a weak ferromagnetic ordering at $T_m = 668(5)$ K. From magnetization and Mössbauer effect studies most of the iron (94%) was concluded to be diamagnetic. From more recent Mössbauer data (300 K, ^{57}Fe) Umarji et al. (1983) observed only one type of Fe atoms in the structure without a magnetic moment (the largest measurable moment was 0.03 μ_B at 4.2 K and 18 kG). The lattice parameters were $a = 4.06$, $c = 10.15$. The magnetic data are in contradiction to the data reported by Felner et al. (1975), which thus were suspected to be due to impurity phases. The thermoelectromotive force was measured by Levin (1981) (80–1050 K).

Palstra et al. (1983) studied the anomalous critical behavior of magnetization (4.2 to 300 K and up to 1.8 T) and of electric resistivity in ferromagnetic $LaFe_{13-x}Si_x$ alloys ($x = 1.5$, 1.8, 1.9, 2.0, 2.1, 2.2 and 2.5, see table 13). Samples were prepared from 99.9% pure elements by arc melting and subsequent annealing in vacuum at 900°C for 10 d. Alloys with the concentration $1.56 \leqslant x \leqslant 2.47$ were found to be homogeneous (at 900°C) and isotypic with the cubic $NaZn_{13}$ structure type (X-ray powder data; no lattice parameters were presented). The alloys are ferromagnetic (table 13) and their susceptibility $\chi_o(T > T_c) = \text{const} \times (T - T_c)^{-1.38}$ corresponds to an isotropic Heisenberg ferromagnet. The anomalous critical behavior of the resistivity was explained in terms of lattice softening (Invar-type alloys). Mössbauer data for $LaFe_{11}Si_2$ at 4.2 K revealed an effective hyperfine field $H_{eff} \approx 28$ T.

Phase equilibria in fig. 30 are primarily based on the work of Bodak and Gladyshevskij (1972) but were slightly modified with respect to a recent critical evaluation of the binary Fe–Si system (Schürmann and Hensgen, 1980).

References

Bodak, O.I. and E.I. Gladyshevskij, 1969, Dopov. Akad. Nauk Ukr. RSR, Ser. A 12, 1125.
Bodak, O.I. and E.I. Gladyshevskij, 1972, Vestn. Lvov Derzh. Univ., Ser. Khim. **14**, 29.
Bodak, O.I., E.I. Gladyshevskij, P.I. Kripyakevich, 1970, Zh. Strukt. Khim. **11**(2), 305.
Felner, I., I. Mayer, A. Grill and M. Schieber, 1975, Solid State Commun. **16**, 1005.
Iandelli, A. and A. Palenzona, 1979, Crystal Chemistry of Intermetallic Compounds, in: Handbook on the Physics and Chemistry of the Rare Earths, vol. 2, eds. K.A. Gschneidner, Jr. and L. Eyring (North-Holland, Amsterdam) p. 1.
Levin, E.M., 1981, Ukr. Fiz. Zh. **26**(3), 407.
Mayer, I. and M. Tassa, 1969, J. Less-Common Metals **19**, 173.
Palstra, T.T.M., J.A. Mydosh, G.J. Nieuwenhuys, A.M. van der Kraan and K.H.J. Buschow, 1983, J. Magn. Magn. Mater. **36**, 290.
Raman, A., 1967, Naturwiss. **54**, 560.
Rossi, D., R. Marazza and R. Ferro, 1978, J. Less-Common Metals **58**, 203.
Schürmann, E. and U. Hensgen, 1980, Archiv f. Eisenhüttenwesen **51**(1), 1.
Umarji, A.M., D.R. Noakes, P.J. Viccaro, G.K. Shenoy, A.T. Aldred and D. Niarchos, 1983, J. Magn. Magn. Mater. **36**, 61.

La–Ga–Si

No ternary phase diagram exists for the La–Ga–Si system. Some data regarding the mutual solid solubility within the concentration section $LaGa_2$–$LaSi_2$ were

derived by Dzyana (1969). The homogeneous regions obtained by powder X-ray analysis of 17 samples heat treated at $400\,^\circ$C were the following: $LaGa_{2-1.5}Si_{0-0.5}$ (AlB_2-type, $a = 4.321-4.239$, $c = 4.408-4.419$) and $LaSi_{2-1.14}Ga_{0-0.86}$ (α-$ThSi_2$-type, $a = 4.310-4.301$, $c = 13.83-14.25$).

Reference

Dzyana, D.M., 1969, Autoreferat Dis. Kand. Khim. (abstract of thesis, Russian) (Nauk, Lvov) 16 p.

La–Ge–Si

The La–Ge–Si system has been investigated by various authors; no ternary compounds are formed and phase equilibria as presented in an isothermal section at $600\,^\circ$C in fig. 31 are mainly characterized by extended solid solutions.

Mayer and Eshdat (1968) investigated the structural behavior in the pseudobinary system $LaSi_xGe_{2-x}$ by means of X-ray powder diffraction methods. For sample preparation, see $NdSi_xGe_{2-x}$. Ge-rich alloys were said to crystallize with the orthorhombic $GdSi_2$-type of structure with the space group Imma. For alloys richer in Si a continuous transformation into the tetragonal $ThSi_2$-type was proposed. The variation of lattice parameters versus x is given in fig. 32 and a linear variation of the unit cell volume was observed (see fig. 11). The structural change has been related to the different modes of distributing the Si/Ge atoms in the nonmetal chain of the two structure types. With respect to later data by Muratova and Bodak (1974), the data of Mayer and Eshdat (1968) represent the La-poor phase boundary of the disilicide–digermanides region.
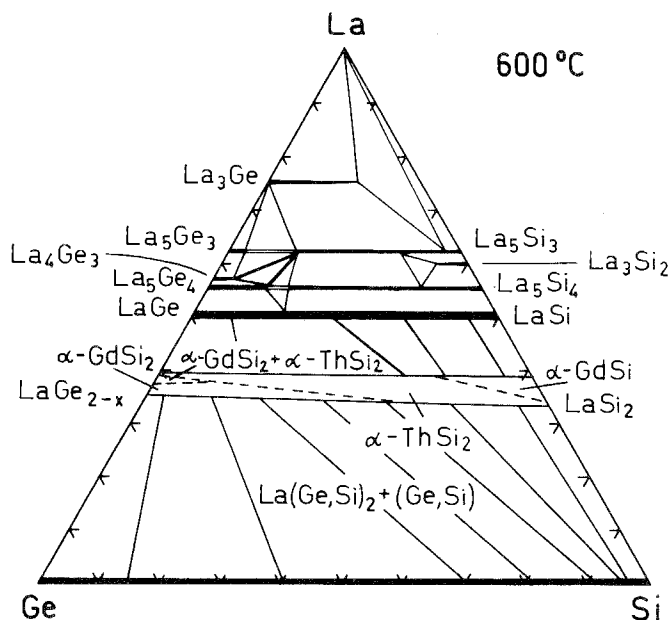
Fig. 31. La–Ge–Si, isothermal section at 600°C.
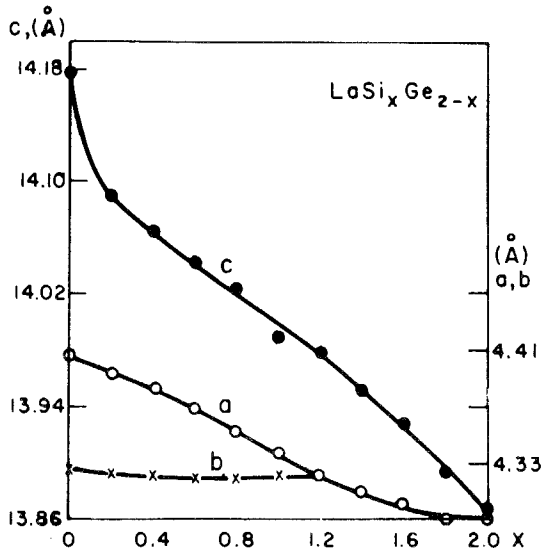
Fig. 32. La–Ge–Si, section $LaGe_{2-x}Si_x$, proposed lattice parameter variation versus concentration, after Mayer and Eshdat (1968).

Mayer and Tendy (1970) studied the phase equilibria within the concentration section $La_5Si_{3-x}Ge_x$ (X-ray powder data). Samples were prepared by heating the compacted powder mixtures of 99.9% purity in an induction furnace under argon (no further details given). In many cases the obtained specimens were annealed in evacuated vycor tubes at $800\,°C$ for 24–48 h. The Mn_5Si_3-type of structure with space group $P6_3/mcm$ was observed to be stable for compositions $2.5 < x \leqslant 3$ and the tetragonal Cr_5B_3-type with space group $I4/mcm$ for $0 \leqslant x < 2$; for compositions with $2 < x < 2.5$ two-phase mixtures of Mn_5Si_3-type and Cr_5B_3-type were reported.
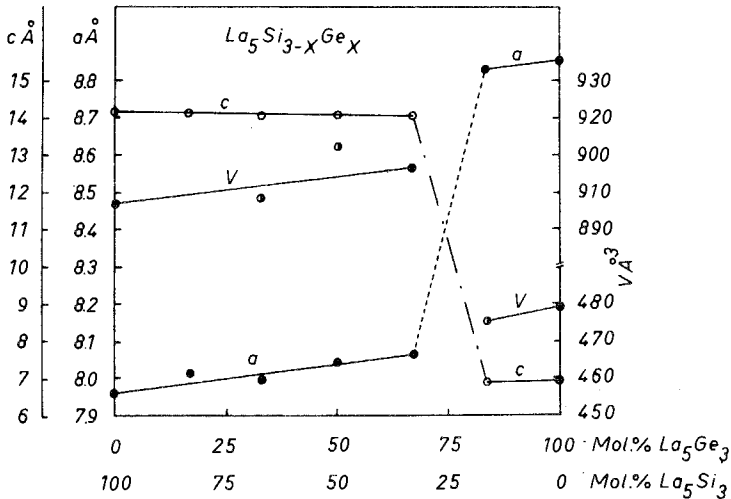
Fig. 33. La–Ge–Si, section $La_5Ge_{3-x}Si_x$, lattice parameters versus composition, after Mayer and Tendy (1970).

The variation of the lattice parameters versus x is presented in fig. 33. Complete solid solutions $LaGe_{2-x}Si_x$ and $LaGe_{1-x}Si_x$ were also reported by Muratova and Bodak (1974).

Bodak and Muratova (1981) investigated the phase equilibria in the La-rich part (50–100 a/o La) of an isothermal region at 600 °C. 120 samples were prepared by arc melting and subsequent annealing at 600 °C for 250 h in evacuated silica tubes. Starting materials were 98.86% La, 99.99% Ge,Si.

The binary compounds are in agreement with recent phase diagram data: LaSi and LaGe both crystallize with the FeB-type and form a continuous solid solution at 600 °C. The solid solubilities have been determined by X-ray analysis but no crystal data were presented: La_3Ge (unsolved structure type) dissolves 15 a/o Si; La_5Ge_3 (Mn_5Si_3-type) dissolves 2 a/o Si, La_4Ge_3(Th_3P_4-type) dissolves 3 a/o Si. La_5Ge_4(Sm_5Ge_4-type) and La_5Si_4 with the Zr_5Si_4-type form a small two-phase equilibrium, whereby La_5Si_4 dissolves up to 29.5 a/o Ge but only 10 a/o Si is soluble in La_5Ge_4. A limited solid solution was observed from La_3Si_2 with U_3Si_2-type (5 a/o Ge), whereas in La_5Si_3 up to 27.5 a/o Si is substituted by Ge (Cr_5B_3-type).

References
Bodak, O.I. and L.A. Muratova, 1981, Vestn. Lvov Univ., Ser. Khim. **23**, 69.

Mayer, I. and Y. Eshdat, 1968, Inorg. Chem. **9**, 1904.

Mayer, I. and S. Tendy, 1970, Israel. J. Chem. **8**, 955.

Muratova, L.O. and O.I. Bodak, 1974, Tesizy Dokl. Tret. Vses. Konf. Kristallokhim. Intermet. Soedin, 2nd Ed., ed. R.M. Rykhal (Lvov Gos. Univ., Lvov, USSR) p. 33.

La–Ir–Si

At least four ternary compounds have been observed in the La–Ir–Si system.

The crystal structure of LaIrSi has been independently refined by Chevalier et al. (1982a) and by Klepp and Parthé (1982) by means of single crystal X-ray counter data. LaIrSi crystallizes with the ZrOS-type of structure: $P2_13$, $a = 6.337(2)$, $\rho_x = 9.378$, $\rho_E = 9.18(9)$ kg/dm^3; La in 4a) $x = 0.635(1)$; Ir in 4a) $x = 0.923(1)$; Si in 4a) $x = 0.326(2)$; $R = 0.12$, $T_c = 2.3$ K. Samples were prepared by arc melting under argon, and annealed at 800 °C for 4 d (Chevalier et al., 1982a). Klepp and Parthé (1982) gave $a = 6.363(3)$, $\rho_x = 9.26$ kg/dm^3 and a reliability value of $R = 0.056$; LaIrSi was also described as a derivative structure of the $SrSi_2$-type, and comparison was made to the closely related tetragonal LaPtSi-type; samples were arc melted under argon (La,Ir 99.9% and Si 99.999%).

According to Engel et al. (1983) $LaIrSi_3$ was found to be tetragonal with the $BaNiSn_3$-type of structure: I4mm, $a = 4.282(1)$, $c = 9.838(2)$, $\rho_x = 7.64$ kg/dm^3. A single crystal was prepared by arc melting a $LaIrSi_{3.5}$ alloy under argon. Atom parameters were refined from single crystal counter data: La in 2a) $z = 0.3455(2)$; Ir in 2a) fixed arbitrarily at $z = 0$; Si in 2a) $z_1 = 0.7599$ and Si in 4b) 0,1/2,0.1088(9); $R = 0.031$. Atomic order and atom parameters in $LaIrSi_3$ were recently refined from single crystal counter data by Lejay et al. (1984): $BaNiSn_3$-type, $a = 4.278(5)$, $c = 9.83(1)$; La in 2a) $z = 0$; Ir in 2a) $z = 0.6553$; Si in 2a) $z = 0.4112$ and Si in 4b)

$z = 0.2615$. Superconductivity was observed between 1.9 and 2.7 K strongly depending on stoichiometry and annealing conditions.

LaIrSi$_2$ was reported to crystallize with the CeNiSi$_2$-type of structure (Chevalier et al., 1982b).

Polymorphism and superconductivity of LaIr$_2$Si$_2$ has been studied recently by Braun et al. (1983). Samples were prepared by arc melting under argon starting from 99.99% La, 99.9% Ir and 99.999% Si. The alloy buttons were annealed using an rf furnace for temperatures above 1000°C, whereas for heat treatment below 1000°C they were sealed in quartz capsules under argon. The melting temperature of LaIr$_2$Si$_2$ was determined at 1890(10)°C by DTA using W crucibles. Similarly the solid state transition H-LaIr$_2$Si$_2$ ⇌ L-LaIr$_2$Si$_2$ was determined at 1720(10)°C. There was no other transition down to 700°C. From nonstoichiometric samples a slight dependency of the transformation temperature on composition was indicated. Transformation of an Ar-jet quenched sample of H-LaIr$_2$Si$_2$ to L-LaIr$_2$Si$_2$ was complete after annealing at 1000°C for 6 d. The crystal structures of the two polymorphic forms of LaIr$_2$Si$_2$ have been derived from single crystal counter data. The low temperature form of L-LaIr$_2$Si$_2$ has the ordered body-centered ThCr$_2$Si$_2$ type: I4/mmm, $a = 4.109(1)$, $c = 10.299(3)$, La in 2a), Ir in 4d) and Si in 4e) with $z(\mathrm{Si}) = 0.3733(7)$; $R = 0.061$. The presence of up to 4% Si or vacancies on the 4d sites cannot be ruled out. The high-temperature form crystallizes with the tetragonal primitive CaBe$_2$Ge$_2$-type: P4/nmm, $a = 4.191(1)$, $c = 9.944(4)$; La in 2c) with $z(\mathrm{La}) = 0.7447(1)$; Ir in 2c) $z = 0.3745(1)$; Ir in 2a); Si in 2c) $z = 0.1262(7)$ and Si in 2b); $R = 0.049$. There was no indication for either vacancy formation nor a statistical occupation on the Ir,Si sites. H-LaIr$_2$Si$_2$ is superconducting at 1.58 K whereas L-LaIr$_2$Si$_2$ does not show superconductivity down to $T_n = 1$ K.

References

Braun, H.F., N. Engel and E. Parthé, 1983, Phys. Rev. B27(9).
Chevalier, B., P. Lejay, A. Cole, M. Vlasse and J. Etourneau, 1982a, Solid State Commun. 41(11), 801.
Chevalier, B., P. Lejay, J. Etourneau, M. Vlasse and P. Hagenmuller, 1982b, Paper presented at the 7th Intern. Conf. on Solid Compounds of Transition Elements, Grenoble, France, Collected Abstracts, II B 16.
Engel, N., H.F. Braun and E. Parthé, 1983, J. Less-Common Metals 95, 309.
Klepp, K. and E. Parthé, 1982, Acta Crystallogr. B38, 1544.
Lejay, P., I. Higashi, B. Chevalier, J. Etourneau and P. Hagenmuller, 1984, Mater. Res. Bull. 19, 115.

La–Mn–Si

Two ternary compounds of the system La–Mn–Si have been characterized so far.

LaMn$_2$Si$_2$ crystallizes with the ThCr$_2$Si$_2$-type of structure: I4/mmm, $a = 4.105$, $c = 10.642$ (Bodak et al., 1966; X-ray powder analysis of arc-melted samples, 98.48% La, 99.8% Mn, 99.99% Si). In good agreement with this Knigenko et al. (1977) measured $a = 4.103$ and $c = 10.650$; for sample preparation, see the Y–Mn–Si system; $T_m = 303$ K. Rossi et al. (1978) reported $a = 4.108$, $c = 10.685$ and $\rho_x = 5.62$ kg/dm^3 (X-ray powder diffraction of samples melted in an induction furnace under

Ar and subsequently annealed at $500\,^\circ$C for 1 week; starting materials were 99.9% La and 99.99% Mn,Si). Szytula and Szott (1981) confirmed the ferromagnetic ordering at $T_m = 303$ K; the magnetic behavior was characterized by $\mu_{eff}^{para} = 4.8\ \mu_B$ mole^{-1} and a magnetic moment of $\mu_n = 3.08\ \mu_B$ at 4.2 K; samples were prepared by a combination of induction melting and a solid state diffusion technique, annealed at $800\,^\circ$C for 100 h and cooled to room temperature. Narasimhan et al. (1967) using X-ray powder analysis reported slightly different lattice parameters $a = 4.114(5)$, $c = 10.611(5)$; $T_m = 300$ K and $\mu_{eff}^{para} = 3.08\ \mu_B$ per formula unit; for sample preparation see the Y–Mn–Si system.

From a detailed study of the magnetic properties in the concentration section $La_{1-x}Y_xMn_2Si_2$ Sampathkumaran et al. (1983) reported slightly higher lattice parameters for the as-cast alloys prepared by induction melting in a water cooled copper boat: $ThCr_2Si_2$ type with $a = 4.113$ and $c = 10.620$. Magnetization measurements in the temperature range of 77 to 575 K and in fields up to 10 kOe confirmed ferromagnetic ordering at $T_m = 310$ K; $\mu_{eff}^{para} = 4.3\ \mu_B$ and θ_p was 310 K. From nuclear magnetic resonance measurements a high degree of crystallographic order was suggested (Sampathkumaran et al., 1982).

LaMnSi is tetragonal with the PbFCl-type: P4/nmm, $a = 4.177$, $c = 7.372$ (Knigenko et al., 1977; X-ray powder analysis). For sample preparation, see Y–Mn–Si. Johnson (1974/76) confirmed the structure ($a = 4.185$, $c = 7.433$) and the ferromagnetic ordering temperature of $T_m = 305$ K. Sample preparation as for YMnSi. LaMnSi can also be obtained by solid state reactions from LaSi and Mn in sealed silica tubes lined with graphite ($800\,^\circ$C, 3d).

References

Bodak, O.I., E.I. Gladyshevskij, P.I. Krypjakevich, 1966, Izv. Akad. Nauk SSSR, Neorg. Mater. 2, 2157.
Johnson, V., 1974/76, Du Pont de Nemours Co., US Patent 3963.829.
Knigenko, L.D., I.R. Mokra and O.I. Bodak, 1977, Vestn. Lvov Univ., Ser. Khim. 19, 68.
Narasimhan, K.S.V.L., V.U.S. Rao and W.E. Wallace, 1976, AIP Conf. Proc. 29, 584; and 1975, J. Appl. Phys. 46, 4957.
Rossi, D., R. Marazza, D. Mazzone and R. Ferro, 1978, J. Less-Common Metals 59, 79.
Sampathkumaran, E.V., L.C. Gupta, R. Vijayaraghavan, Le Dang Khoi and P. Veillet, 1982, J. Phys. F12, 1039.
Sampathkumaran, E.V., R.S. Chaughule, K.V. Gopalakrishnan, S.K. Malik and R. Vijayaraghavan, 1983, J. Less-Common Metals 92, 35.
Szytula, A. and I. Szott, 1981, Solid State Commun. 40, 199.

La–Ni–Si

No complete phase diagram study has been reported for the La–Ni–Si system, but at least twelve ternary compounds were observed to exist (see table 15).

Bodak and Gladyshevskij (1969b) studied the phase equilibria in the La-poor region (up to 10 a/o La) at $800\,^\circ$C by means of X-ray powder analysis. Samples were prepared by arc melting and subsequent annealing in evacuated silica tubes for 100 h at $800\,^\circ$C. The solid solubility of La in the Ni silicides generally was less than 2 a/o La. Phase equilibria in the La-poor region are dominated by the formation of three compounds with extended homogeneous regions (Ni/Si exchange). The crystal

TABLE 15

Formation and structural data of ternary compounds La–Ni–Si.

Compound	Structure type Space group	lattice parameters Density	Preparation, Characterization	Refs.	Purity
$LaNi_9Si_2$	$Ce_2Ni_{17}Si_5$ $(BaCd_{11})$ $I4_1/amd$	$a = 9.899(5)$ $c = 6.265(10)$	arc(Ar), Qu 800 °C, 250 h, PXD atom order similar to $CeNi_{8.6}Si_{2.4}$	BoG, 69a	La 99.7 Ni 99.91 Si 99.99
$LaNi_{7.8-6.5}-$ $Si_{5.2-6.5}$ (37–46 a/o Si)	? $(NaZn_{13}\text{-deriv.})$ $I4/mcm$	$a = 11.20–11.05(1)$ $c = 11.20–11.22(1)^{(*)}$	arc(Ar), Qu 800 °C, 100 h PXD	BoG, 69b	La 99.2 Ni 99.99 Si 99.99
$LaNi_{8.8-8.4}-$ $Si_{4.2-4.6}^{(*)}$ (30–33 a/o Si)	$Ce_2Ni_{17}Si_9$ $I4/mcm$	$a = 7.85(1)$ $c = 11.51(11)$ at 30 a/o Si	arc(Ar), Qu 800 °C, 100 h PXD	BoG, 69b	La 99.2 Ni 99.99 Si 99.99
$LaNi_{11.6-9.5}-$ $Si_{1.4-3.5}^{(**)}$ (10–25 a/o Si) transformed into tetragonal	$(NaZn_{13}\text{-deriv.})$ cubic (10–18 a/o Si)	$a = 11.26–11.20(1)$ (10–18 a/o Si, cubic) $a = 11.20–11.27(1)$ $c = 11.20–11.14(1)$ (18–25 a/o Si) tetragonal$^{(**)}$	arc(Ar), Qu 800 °C, 100 h	BoG, 69b	La 99.2 Ni 99.99 Si 99.99
$La_5Ni_2Si_3$ ("La_2NiSi")	$Ce_5Ni_2Si_3$ filled $Rh_{20}Si_{13}$ $P6_3/m$	$a = 16.34(1)$ $c = 4.322(5)$	arc(Ar) PXD	BoG, 72	Ni 99.98 Si 99.99
$La_6Ni_2Si_3$	$Ce_6Ni_2Si_3$ filled Ho_4Co_3 $P6_3/m$	$a = 12.200(5)$ $c = 4.350(2)$	no details PXD	BoGK, 74	
$La_{14}Ni_8Si_9$	$Ce_{14}Ni_8Si_9$ $P2_1/m$	$a = 22.03$ $b = 16.61$ $c = 4.302$ $\gamma = 104.20°$	arc(Ar) PXD	MiBG, 74	
$La_7Ni_2Si_5$	$Ce_7Ni_2Si_5$ Pnma	$a = 23.63$ $b = 4.312$ $c = 14.09$	arc(Ar) PXD	MiBG, 74	
$LaNi_2Si_2$	$ThCr_2Si_2$ $I4/mmm$	$a = 4.103(10)$ $c = 9.698(10$	arc(Ar) PXD	BoGK, 66	La 99.48 Ni 99.8 Si 99.99
$La_{15}Ni_4Si_{13}$	$Ce_{15}Ni_4Si_{13}$ $P6_3/m$	$a = 20.44$ $c = 4.336$	arc(Ar) PXD	Mi, 73	Ni 99.5 Si 99.99
$LaNiSi_2$	$CeNiSi_2$ Cmcm	$a = 4.193(2)$ $b = 16.581(10)$ $c = 4.073(2)$	arc(Ar) PXD	BoG, 69c	La 98.48 Ni 99.8 Si 99.99
$La(Ni,Si)_2$	AlB_2 $P6/mmm$	$a = 4.077(5)$ $c = 4.367(5)$	arc(Ar) PXD	GlB, 65	Ni 99.8 Si 99.99

TABLE 15 (continued)

Compound	Structure type Space group	lattice parameters Density	Preparation, Characterization	Refs.	Purity
Ni-rich		"La(Ni, Si)$_2$ $a = 4.077(5)$ $c = 4.300(5)$ Si-rich $a = 4.057(5)$ $c = 4.388(5)$	no details PXD	Ra, 67	
		LaNi$_{0.4}$Si$_{1.6}$ $a = 4.063$ $c = 4.400$	induction heating Ar, in Al$_2$O$_3$ or MgO$_2$ 1500 °C, Qu, 700–900°C 24–96 h, PXD	MaT, 69	La 99.9 Ni 99.95 Si 99.99
		alloy LaNi$_{0.5}$Si$_{1.5}$ at 25 ° C $a = 4.045(1)$ $c = 4.381(1)$ at 500 ° C $a = 4.050(1)$ $c = 4.392(1)$ at 800 ° C $a = 4.062(1)$ $c = 4.395(1)$ decomposes at 800 ° C	induction melting Ar, in Al$_2$O$_3$, Qu 700 ° C, 2 d, PXD $\alpha_a = 5.4 \times 10^{-6}$ deg^{-1} $\alpha_c = 7.1 \text{–} 10^{-6}$ deg^{-1} $\alpha = 6.0 \times 10^{-6}$ deg^{-1} $\gamma = 23.0 \times 10^{-6}$ deg^{-1}	MaF, 72	99.9

(*) For a correct setting of the bct unit cell, $a = 7.920 \text{–} 7.814$ ($a = a_0 / \sqrt{2}$).

(**) Within the homogeneous range of this phase (LaNi$_{11.6-9.5}$Si$_{1.4-3.5}$) a transformation from cubic to tetragonal takes place at 18 a/o Si; for a correct setting of the bct unit cell, $a = 7.920 \text{–} 7.970$ ($a = a_0 / \sqrt{2}$).

structure of all three compounds is closely related to the NaZn$_{13}$-type of structure with a body-centered tetragonal distortion in certain regions (see table 15 and fig. 34).

Palstra et al. (1983) investigated the magnetic behavior of the compound LaNi$_{11}$Si$_2$ which was claimed to crystallize with a cubic NaZn$_{13}$-type structure; X-ray powder data were obtained from an arc-melted specimen after annealing at 900 ° C for 10 d.
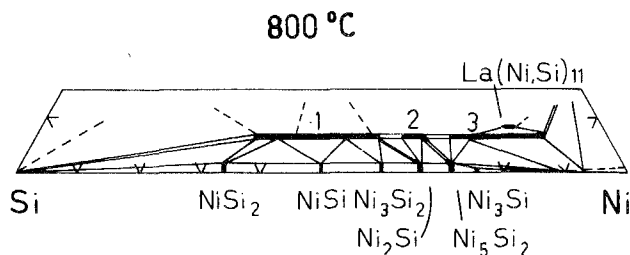
Fig. 34. La–Ni–Si, partial isothermal section at 800°C (0–15 a/o La). 1: LaNi$_{7.8-6.5}$Si$_{5.2-6.5}$, 2: LaNi$_{8.8-8.4}$Si$_{4.2-4.6}$, 3: LaNi$_{11.6-9.6}$Si$_{1.4-3.5}$.

$LaNi_{11}Si_2$ is a Pauli paramagnet with $\chi = 2.5 \times 10^{-7}$ m³ kg⁻¹ (see also table 13).

Mayer and Tassa (1969) and Mayer and Felner (1973) investigated the concentration section $LaNi_xSi_{2-x}$ by means of X-ray powder diffraction methods. For $x < 0.4$ the $ThSi_2$-type structure was claimed to be stable. $LaNi_{0.4}Si_{1.6}$ crystallizes with the AlB_2-type structure. In analogy to the X-ray data of the isotypic $NdNi_{0.4}Si_{1.6}$ a statistical distribution of Ni,Si atoms at the 2d site of $P6/mmm$ was assumed.

The thermoelectromotive force (80–1050 K) has been measured by Levin (1981) and electrophysical properties of $LaNi_2Si_2$ (temperature dependence of electrical resistance, thermoelectrical coefficient, magnetic susceptibility as well as the preparation of stoichiometric thin films) were reported by Levin et al. (1977).

References

Bodak, O.I. and E.I. Gladyshevskij, 1969a, Dopov. Akad. Nauk Ukr. RSR, Ser. A 5, 452.
Bodak, O.I. and E.I. Gladyshevskij, 1969b, Dopov. Akad. Nauk Ukr. RSR, Ser. A 12, 1125.
Bodak, O.I. and E.I. Gladyshevskij, 1969c, Kristallografiya, 14(6), 990.
Bodak, O.I. and E.I. Gladyshevskij, 1972, Sov. Phys. Crystallogr. 17(3), 439.
Bodak, O.I., E.I. Gladyshevskij and P.I. Kripyakevich, 1966, Izv. Akad. Nauk SSSR, Neorg. Mater. 2(12), 2151.
Bodak, O.I., E.I. Gladyshevskij and O.I. Kharchenko, 1974, Sov. Phys. Crystallogr. 19(1), 45.
Gladyshevskij, E.I. and O.I. Bodak, 1965, Dopov. Akad. Nauk Ukr. RSR, Ser. A 5, 601.
Levin, E.M., 1981, Ukr. Fiz. Zh. 26(3), 407.
Levin, E.M., R.V. Lutsiv, E.I. Gladyshevskij and O.I. Bodak, 1977, Fiz. Elektron. Resp. Mezhved. Nauch-tekhn. Sbor. 15, 59.
Mayer, I. and I. Felner, 1972, J. Less-Common Metals 29, 25.
Mayer, I. and M. Tassa, 1969, J. Less-Common Metals 19, 173.
Mis'kiv, M.G., 1973, Thesis, Lvov Univ., USSR.
Mis'kiv, M.G., O.I. Bodak and E.I. Gladyshevskij, 1974, Tezisy Dokl. Tret. Vses. Konf. Kristallokhim. Intermet. Soedin, 2nd Ed., ed. R.M. Rykhal (Lvov Gos. Univ., Lvov, USSR) p. 31.
Palstra, T.T.M., J.A. Mydosh, G.J. Nieuwenhuys, A.M. van der Kraan and K.H.J. Buschow, 1983, J. Magn. Magn. Mater. 36, 290.
Raman, A., 1967, Naturwiss. 54, 560.

La–Os–Si

According to Hiebl et al. (1983) $LaOs_2Si_2$ crystallizes with the $ThCr_2Si_2$-type of structure. X-ray powder data were: space group I4/mmm and lattice parameters $a = 4.1995(3)$ and $c = 10.0609(43)$. For sample preparation, see YOs_2Si_2. $LaOs_2Si_2$ is temperature independent paramagnetic (temperature range 1.5 K $< T <$ 1100 K) with a characteristic value $\chi_m(300 \text{ K}) = 0.00008$ cm³ per mole.

Reference

Hiebl, K., C. Horvath, P. Rogl and M.J. Sienko, 1983, Solid State Commun. 48, 211.

La–Pd–Si

$LaPd_2Si_2$ crystallizes with the ordered $ThCr_2Si_2$-type of structure: I4/mmm, $a = 4.223$, $c = 9.99$ (Ballestracci, 1976; X-ray powder diffraction data). For sample preparation, see YPd_2Si_2.

Silicon was observed to stabilize the Cu_3Au-type structure when added to $LaPd_3$ (Dhar et al., 1983). The Si atoms are likely to occupy the octahedral voids, slightly increasing the unit cell dimensions of $LaPd_3Si_x$ ($0 \leqslant x < 0.25$). Lattice parameters as read from a graph were: $LaPd_3$ ($a = 4.23$), $LaPd_3Si_{0.1}$ ($a \sim 4.227$), $LaPd_3Si_{0.2}$ ($a \sim 4.275$) and $LaPd_3Si_{0.3}$ ($a = 4.285$). Samples were arc melted.

References

Ballestracci, R., 1976, C.R. Acad. Sci. Paris, Ser B **282**, 291.
Dhar, S.K., R. Nagarayan, S.K. Malik, D. Rambabu and R. Vijayaraghavan, 1983, J. Magn. Magn. Mater. **31–34**, 393.

La–Pt–Si

The crystal structure of LaPtSi has been refined by Klepp and Parthé (1982) by means of X-ray single crystal counter data: LaPtSi-type (derivative of $ThSi_2$-type), $I4_1md$, $a = 4.2490(3)$, $c = 14.539(2)$, $\rho_x = 9.16$ kg/dm³, La in 4a) 0, 0, 0.0; Pt in 4a) 0, 0, 0.5850(4); Si in 4a) 0, 0, 0.419(2); $R = 0.052$. Samples were prepared by arc melting under argon; alloys were also annealed at 775 °C for two weeks indicating congruent melting behavior.

$LaPt_2Si_2$ was claimed to be body-centered tetragonal with the $BaAl_4$-type, $a = 4.277$, $c = 9.822$ (Mayer and Yetor, 1977). In analogy to $ErPt_2Si_2$, Pt and Si atoms were said to occupy the 4d and 4e sites of $I4/mmm$ in random distribution (X-ray powder diffraction data). Samples were melted in Al_2O_3 crucibles (HF furnace, under He; min. purity 99.9%). The random distribution and symmetry were confirmed by Rossi et al. (1979); lattice parameters, however, were slightly different: $a = 4.281$, $c = 9.862$, $\rho_x = 10.75$. For sample preparation, see $CePd_2Si_2$. X-ray powder photographs of arc-melted alloys, however, are not compatible with a body-centered symmetry and do reveal a primitive tetragonal lattice with an atomic arrangement similar to the $CaBe_2Ge_2$-type (Rogl, 1984): $a = 4.2871(5)$, $c = 9.8282(25)$, $CePt_2Si_2$-type.

References

Klepp, K. and E. Parthé, 1982, Acta Crystallogr. **B38**, 1105.
Mayer, I. and P.D. Yetor, 1977, J. Less-Common Metals **55**, 171.
Rogl, P., 1984, Inorg. Chem., to be published.
Rossi, D., R. Marazza and R. Ferro, 1979, J. Less-Common Metals **66**, P17.

La–Re–Si

The phase equilibria in the ternary system La–Re–Si have been investigated by Pecharskij (1979) by means of X-ray and metallographic analysis of 71 ternary samples which were arc melted and subsequently annealed in evacuated silica tubes for 400 + 600 h at 800 °C and quenched in water. Starting materials were La 98.70%, Re 99.99% and Si 99.99%.

The binary systems La–Si and Re–Si have been discussed in context with the ternary systems La–Fe–Si and Y–Re–Si, respectively. The mutual solid solubilities
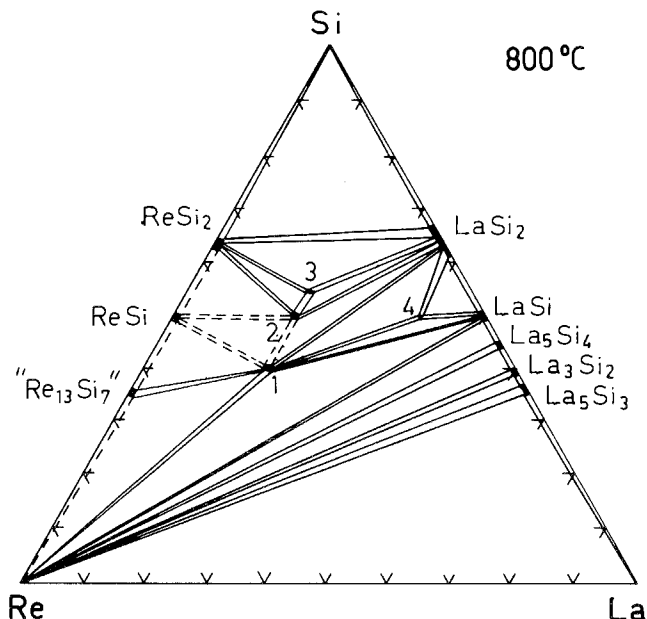
Fig. 35. La–Re–Si, isothermal section at 800°C. 1: LaRe$_2$Si$_2$, 2: La$_2$Re$_3$Si$_5$, 3: "La$_4$Re$_5$Si$_{11}$", 4: "La$_4$ReSi$_5$".

of La and Re silicides were found to be small and within 1–2 a/o of the third constituent.

The ternary phase equilibria (fig. 35, isothermal section at 800 °C) are characterized by the existence of four ternary compounds: LaRe$_2$Si$_2$, La$_2$Re$_3$Si$_5$, "La$_4$Re$_5$Si$_{11}$" and "La$_4$ReSi$_5$".

The crystal structure of LaRe$_2$Si$_2$ was refined by Pecharskij et al. (1977) from single crystal X-ray photographs. Single crystals were obtained from arc-melted buttons. Starting materials were 99.8% Re, 99.5% La and 99.99% Si. LaRe$_2$Si$_2$ crystallizes with a new structure type: LaRe$_2$Si$_2$-type, Imma, $a = 4.206(5)$, $b = 4.116(5)$, $c = 20.89(1)$; $R = 0.10$; La in 4e) 0, 1/4, 0.915(1); Re in 4e) 0, 1/4, 0.2119(1); Re in 4e) 0, 1/4, 0.7129(1); Si in 4e) 0, 1/4, 0.356(3); Si in 4e) 0, 1/4, 0.466(1).

La$_2$Re$_3$Si$_5$ is isotypic with the crystal structure of Sc$_2$Fe$_3$Si$_5$, P4/mnc, $a = 11.02(1)$, $c = 5.821(8)$ (Segre, 1981; X-ray powder analysis of arc-melted alloys); $T_n = 1.2$ K. Pecharskij (1979) reported $a = 11.02(1)$ and $c = 5.814(5)$.

No crystallographic data are available on the compounds "LaReSi$_2$" (or "La$_4$Re$_5$Si$_{11}$") and "La$_4$ReSi$_5$".

References

Pecharskij, V.K., 1979, Autoreferat Dis. Kand. Khim. (abstract of thesis, Russian) (Nauk, Lvov) 23 p.
Pecharskij, V.K., O.I. Bodak and E.I. Gladyshevskij, 1977, Sov. Phys. Crystallogr. **22**(3), 359.
Segre, C.U., 1981, Thesis, Univ. of Calif., San Diego, USA.

La–Rh–Si

Seven ternary compounds have been characterized in the ternary La–Rh–Si system (see table 16).

TABLE 16
Formation and structural data of ternary compounds La–Rh–Si.

Compound	Structure type Space group	Lattice parameters Density	Preparation, Characterization	Refs.	Purity
LaRhSi	ZrOS $P2_13$	$a = 6.296(2)$ $\rho_E = 7.11(7)$ $\rho_x = 7.185$	arc(Ar), 800 °C, 4d $T_c = 4.35$ K PXD	ChLCVE, 82b	high purity
$LaRh_2Si_2$	$ThCr_2Si_2$ I4/mmm	$a = 4.092$ $c = 10.20$	melted, HF(Ar) PXD $T_c = 3.90$ K	Ba, 76 ChLVEH, 82a	high purity
		$a = 4.114(2)$ $c = 10.31(1)$	induction melting PXD; traces of RhSi $T_c = 3.8(2)$ K, type II $\theta_p = -41(3)$ K, $\mu_{eff}^{para} = 2.0(1)\,\mu_B$ $T_m = 7(2)$ K	FeN, 83	99.9%
$LaRh_3Si_2$	$CeCo_3B_2$ P6/mmm	$a = 5.603(6)$ $c = 3.567(4)$	arc(Ar), Qu, 800 °C, several days or 950 °C, 4 d, PXD $T_n = 50$ mK $\chi_m = -49876 \times 10^{-9}$ emu/mole at 300 K	ChCLE, 81	La 99.9 Rh 99.9 Si 99.999
$La_2Rh_3Si_5$	$Sc_2Co_3Si_5$ Ibam	$a = 9.90(1)$ $b = 11.84(1)$ $c = 5.828(5)$	arc(Ar), Qu, 800 °C several days, PXD $T_c = 4.45(1)$ K $\chi_m = 3.88 \times 10^{-4}$ emu/mole at 300 K	ChLVEH, 82a	La 99.9 Rh 99.9 Si 99.999
$LaRhSi_2$	$CeNiSi_2$		PXD $T_c = 3.42$ K	ChLVEH, 82a	
La_2RhSi_3	Er_2RhSi_3 (AlB_2-deriv.) P6̄2c	$a = 8.233(5)$ $c = 8.594(5)$	arc(Ar), Qu, 800 °C 4 d, PXD $T_n = 1.6$ K $\chi_m = $ temperature independent	ChLEH, 84	La 99.9 Rh 99.9 Si 99.999
$LaRhSi_3$	$BaNiSn_3$ I4mm	$a = 4.272$ $c = 9.83$	arc(Ar), Qu, 900°C, 10d $T_c = 1.9–2.7$ K	LeHCEH, 84	high purity

Agreement exists about the crystal symmetry in $LaRh_2Si_2$ ($ThCr_2Si_2$-type) as well as about the superconducting transition at $T_c = 3.9$ K (Ballestracci, 1976; Chevalier et al., 1982a; Felner and Nowik, 1983). Detailed measurements of magnetization, ac-susceptibility, electric resistivity and specific heat seem to indicate a magnetic ordering at $T_m = 7$ K interpreted as itinerant electron long-range order (Felner and Nowik, 1983).

References

Ballestracci, R., 1976, C.R. Acad. Sci. Paris, Ser. B **282**, 291.
Chevalier, B., A. Cole, P. Lejay and J. Etourneau, 1981, Mater. Res. Bull. **16**, 1067.
Chevalier, B., P. Lejay, M. Vlasse, J. Etourneau and P. Hagenmuller, 1982a, paper presented at the 2nd Conf. on Solid State Chemistry, Veldhoven, The Netherlands; 1982, Mater. Res. Bull. **17**, 1211; 1983, Mater. Res. Bull. **18**, 315.
Chevalier, B., P. Lejay, A. Cole, M. Vlasse and J. Etourneau, 1982b, Solid State Commun. **41**, 801.
Chevalier, B., P. Lejay, J. Etourneau and P. Hagenmuller, 1984, Solid State Commun., to be published.
Felner, I. and I. Nowik, 1983, Solid State Commun. **47**(10), 831.
Lejay, P., I. Higashi, B. Chevalier, J. Etourneau and P. Hagenmuller, 1984, Mater. Res. Bull. **19**, 115.

La–Ru–Si

Only two ternary compounds have been characterized in the La–Ru–Si system.

The crystal structure of $LaRu_3Si_2$ has been refined by Vandenberg and Barz (1980), from X-ray powder diffraction data. $LaRu_3Si_2$ crystallizes with a new structure type (superstructure of $CeCo_3B_2$-type according to $a = a_o$, $c = 2c_o$). The following crystallographic data were presented: $a = 5.676(1)$, $c = 7.120(1)$, $\rho_x = 7.5$ kg/dm³. Atomic positions were La in 0, 0, 0 and 0, 0, 1/2; Ru in 6h) 0.480, −0.01, 1/4 and Si in the 4f) sites 1/3, 2/3, 0 of a tentatively assigned space group $P6_3/m$. Arc-melted alloys of composition $LaRu_3Si_2$ were two-phase, containing also $LaRu_2Si_2$. Annealing at 1000°C did not increase the amount of the $LaRu_2Si_2$ phase and alloys richer in Ru showed the presence of free Ru according to two-phase equilibria such as $LaRu_3Si_2 + Ru$ and $LaRu_3Si_2 + LaRu_2Si_2$. A peritectic melting behavior of $LaRu_3Si_2$ is suggested. Good powder patterns of $LaRu_3Si_2$ were obtained from an arc-melted alloy $LaRu_4Si_2$ (with some extra Ru). $LaRu_3Si_2$ is a superconductor with a critical temperature $T_c = 7.60$–7.02 K (Barz, 1980).

$LaRu_2Si_2$ was reported to be isotypic with the crystal structure of $ThCr_2Si_2$ (Ballestracci and Astier, 1978; X-ray powder analysis of alloys melted in an induction furnace under Ar). The crystallographic data were: I4/mmm, $a = 4.215$, $c = 9.93$, Hiebl et al. (1983) confirmed the structure type with slightly different lattice parameters: $a = 4.2196(3)$, $c = 9.9506(45)$. For sample preparation, see YOs_2Si_2. From magnetic susceptibility measurements (1.5–1100 K) $LaRu_2Si_2$ is temperature independent paramagnetic with a characteristic value of $\chi_m(300$ K$) = 0.00020$ cm³ per mole (Hiebl et al., 1983).

References

Ballestracci, R. and G. Astier, 1978, C.R. Acad. Sci. Paris, Ser. B **286**, 109.
Barz, H., 1980, Mater. Res. Bull. **15**, 1489.
Hiebl, K., C. Horvath, P. Rogl and M.J. Sienko, 1983, J. Magn. Magn. Mater. **37**, 287.
Vandenberg, J.M. and H. Barz, 1980, Mater. Res. Bull. **15**, 1493.

La–Sc–Si

From X-ray powder data Mokra and Bodak (1979) reported LaScSi to be isotypic with the crystal structure of CeScSi; the space group is I4/mmm and lattice parameters are $a = 4.344(5)$ and $c = 15.98(2)$. For sample preparation, see CeScSi.

Reference
Mokra, I.P. and O.I. Bodak, 1979, Dopov. Akad. Nauk. Ukr. RSR, Ser. A, 312.

La–Y–Si

No ternary phase diagram has been established for the system La–Y–Si.

Mokra (1979) mentioned the existence of a compound La_2YSi_2 with the U_3Si_2-type structure and with an ordered arrangement of the R atoms: P4/mbm, $a = 7.736(8)$, $c = 4.448(4)$; La in 4h), Y in 2a) and 4 Si atoms in 4g). For details of sample preparation, see Ce–Y–Si.

Reference
Mokra, I.R., 1979, Autoreferat Dis. Kand. Khim. (abstract of thesis, Russian) (Nauk, Lvov) 22 p.

La–Zr–Si

Raman (1968) investigated the section $La_{1-x}Zr_xSi$ by means of X-ray powder analysis of arc-melted alloys which subsequently were wrapped in Mo foil, sealed in evacuated quartz tubes, and annealed for 3 d at 1000°C. Minimum purities of starting materials were Zr 99.99%, La 99.9%, Si 99.99%. A restricted mutual solid solubility of the binary monosilicides was observed. Samples at the compositions $x = 0.25$, 0.5 and 0.75 were two-phase. The following lattice parameter values were obtained for the endpoints of the solid solutions: La(Zr)Si [FeB-type, Pnma, $a = 8.380(5)$, $b = 3.990(5)$, $c = 6.025(5)$] and Zr(La)Si [CrB-type, Cmcm, $a = 3.738(5)$, $b = 9.875(5)$, $c = 3.738(5)$]. Lattice parameters of the binary compounds were: LaSi [$a = 8.380(5)$, $b = 3.990(5)$, $c = 6.024(5)$] and ZrSi [$a = 3.780(5)$, $b = 10.05(1)$, $c = 3.780(5)$]. Thus practically no Zr dissolved in LaSi, but approximately 5 a/o La was estimated to dissolve in ZrSi.

Reference
Raman, A., 1968, Inorg. Chem. 7(5), 973.

Lu–Co–Si

No ternary phase diagram exists but the formation of five ternary compounds was reported.

$Lu_5Co_4Si_{10}$ with the $Sc_5Co_4Si_{10}$-type structure and space group P4/mbm has been observed by Pelizzone et al. (1982).

LuCoSi is orthorhombic with the TiNiSi-type structure: Pnma, $a = 6.656$, $b = 4.075$

and $c = 7.094$; X-ray powder data by Yarovets (1978). For sample preparation and atom parameters, see YNiSi.

The compound $Lu_3Co_2Si_7$ has been characterized by Yarovets (1978) from X-ray powder data to be isostructural with the $Ho_3Co_2Si_7$-type (Amm2, $a = 3.826$, $b = 24.315$ and $c = 3.872$).

$LuCoSi_2$ crystallizes with the $CeNiSi_2$-type structure (Cmcm, $a = 3.951$, $b = 16.067$ and $c = 3.915$); Yarovets (1978) from X-ray powder data of arc-melted alloys annealed at $800\,^\circ C$ for 720 h in evacuated silica tubes.

$LuCo_2Si_2$ is tetragonal, $ThCr_2Si_2$-type with space group I4/mmm and lattice parameters $a = 3.841$ and $c = 9.664$ (Yarovets, 1978; from X-ray powder data).

References

Pelizzone, M., H.F. Braun and J. Müller, 1982, to be published.
Yarovets, V.I., 1978, Autoreferat Dis. Kand. Khim. (abstract of thesis, Russian) (Nauk, Lvov) 24 p.

Lu–Cu–Si

At least three ternary compounds exist in the Lu–Cu–Si system.

$Lu_3Cu_4Si_4$ crystallizes with the $Gd_3Cu_4Ge_4$-type of structure: Immm, $a = 13.45$, $b = 6.47$, $c = 4.05$ (X-ray powder diffraction analysis by Hanel and Nowotny, 1970). For sample preparation, see $Sc_3Cu_4Si_4$.

$LuCu_2Si_2$ is tetragonal with the $ThCr_2Si_2$-type: $a = 3.907(6)$, $c = 10.004(10)$, I4/mmm (X-ray powder diffraction by Rieger and Parthé, 1969). For sample preparation, see YCu_2Si_2.

From an X-ray powder analysis of arc-melted alloys annealed at $750\,^\circ C$, Iandelli (1983) reported the appearance of a compound LuCuSi with the ordered Ni_2In-type (superstructure of AlB_2-type, $P6_3/mmc$, $a = 4.130(2)$, $c = 7.040(5)$]. For details of sample preparation and purity of the starting materials, see LaCuSi.

References

Hanel, G. and H. Nowotny, 1970, Monatsh. Chem. **101**, 463.
Iandelli, A., 1983, J. Less-Common Metals **90**, 121.
Rieger, W. and E. Parthé, 1969, Monatsh. Chem. **100**, 444.

Lu–Fe–Si

Five ternary compounds have been reported for the Lu–Fe–Si system.

According to X-ray powder data by Gladyshevskij et al. (1978) $Lu_2Fe_4Si_9$ crystallizes with the $Y_2Fe_4Si_9$-type of structure [$P6_3/mmc$, $a = 3.910(5)$, $c = 15.39(1)$]; the magnetic susceptibility was given as 0.77×10^{-6} emu/mole. For sample preparation, see $Y_2Fe_4Si_9$.

$Lu_2Fe_3Si_5$ is isotypic with the crystal structure of $Sc_2Fe_3Si_5$: P4/mnc, $a = 10.34(1)$, $c = 5.375(8)$ (Braun, 1980; X-ray powder diffraction data). For sample preparation, see $Dy_2Fe_3Si_5$. Mössbauer data confirm the absence of a magnetic moment on the iron site (Braun et al., 1981). $Lu_2Fe_3Si_5$ is superconducting below $T_c = 6.1$–5.8 K. The pressure dependence was measured by Segre (1981) as dT_c/dp

$= -7.3 \times 10^{-5}$ K bar^{-1}. The low-temperature powder X-ray diffraction proved the absence of a structure transition down to 30 K. An anomalously large T^5 contribution to the normal state heat capacity was observed by Vining et al. (1983). Yarovets (1978), from X-ray powder data, confirmed the crystal symmetry but reported different unit cell dimensions for $Lu_2Fe_3Si_5$ with a much smaller c/a ratio: $a = 10.391$ and $c = 5.255$.

The crystal structure of $Lu_3Fe_2Si_7$ (earlier mentioned as "LuFeSi$_3$" by Gladyshevskij et al., 1978) was reported to be isostructural with the $Ho_3Co_2Si_7$-type: Amm2, $a = 3.847$, $b = 24.400$ and $c = 3.884$ (Yarovets, 1978; X-ray powder data).

$LuFe_2Si_2$ crystallizes with the $ThCr_2Si_2$-type structure with the space group I4/mmm and lattice parameters as follows: $a = 3.794$ and $c = 9.956$ (Yarovets, 1978; powder X-ray diffraction analysis). Magnetic susceptibilities were recorded for the temperature range 293–1157 K. ^{57}Fe (14.4 keV) Mössbauer measurements at 4.2 K prove the absence of a magnetic moment on the Fe site (Noakes et al., 1983).

$LuFe_{4.48}Si_{1.52}$ crystallizes with the $ZrFe_4Si_2$-type of structure: P4$_2$/mnm, $a = 7.060$ and $c = 3.778$ (Yarovets, 1978; powder X-ray analysis). For sample preparation and atom parameters, see Dy–Fe–Si.

References

Braun, H.F., 1980, Phys. Lett. **75A**(5), 386.
Braun, H.F., C.U. Segre, F. Acker, M. Rosenberg, S. Dey and P. Deppe, 1981, J. Magn. Magn. Mater. **25**, 117.
Gladyshevskij, E.I., O.I. Bodak, V.I. Yarovets, Yu.K. Gorelenko and R.V. Skolozdra, 1978, Ukr.Fiz.Zh. **23**(1), 77.
Noakes, D.R., A.M. Umarji and G.K. Shenoy, 1983, J. Magn. Magn. Mater. **39**, 309.
Segre, C.U., 1981, Thesis, Univ. of California, San Diego, USA.
Vining, C.B., R.N. Shelton, H.F. Braun and M. Pelizzone, 1983, Phys. Rev. **B27**(5), 2800.
Yarovets, V.I., 1978, Autoreferat Dis. Kand. Khim. (abstract of thesis, Russian) (Nauk, Lvov) 24 p.

Lu–Ir–Si

$Lu_5Ir_4Si_{10}$ is tetragonal with the space group P4/mbm and the $Sc_5Co_4Si_{10}$-type of structure: $a = 12.475(8)$, $c = 4.171(4)$ (X-ray powder analysis by Braun and Segre, 1981). For sample preparation, see $Sc_5Ir_4Si_{10}$. A superconducting transition exists at $T_c = 3.76–3.72$ K.

Reference

Braun, H.F. and C.U. Segre, 1981, Ternary Superconductors of the $Sc_5Co_4Si_{10}$-type, in: Ternary Superconductors, Proc. Intern. Conf. on Ternary Superconductors, Lake Geneva, WI, USA, eds. G.K. Shenoy, B.D. Dunlap and F.Y. Fradin (North-Holland, Amsterdam) pp. 239–246.

Lu–Mn–Si

According to X-ray powder data by Segre (1981) on arc-melted alloys $Lu_2Mn_3Si_5$ crystallizes with the $Sc_2Fe_2Si_5$-type of structure [P4/mnc, $a = 10.54(1)$, $c = 5.370(8)$]; $T_n = 1.2$ K.

Antiferromagnetic ordering at $T_N = 464$ K has been reported by Szytula and

Szott (1981) for a compound $LuMn_2Si_2$ with the $ThCr_2Si_2$-type of structure (no crystallographic data given). The paramagnetic effective moment was recorded as $\mu_{eff}^{para} = 4.2\ \mu_B$.

TABLE 17

Formation and structural data of ternary compounds Lu–Ni–Si.

Compound	Structure type Space group	Lattice parameters Density	Preparation, Characterization	Refs.	Purity
$LuNi_{10}Si_2$ [*]	ord. $ThMn_{12}$ $YNi_{10}Si_2$ I4/mmm	arc(Ar), Qu, 800°C, 720 h $a = 8.164$ $c = 4.650$	Pauli paramagn. PXD refinement	GlBYGS, 77 Ya, 78a,b	Lu 99.83 Ni 99.98 Si 99.9
$LuNi_{6.72}Si_{6.28}$ [○]	$Ce_2Ni_{17}Si_9$? (NaZn$_{13}$-deriv.) I4/mcm ?	$a = 10.949$ $c = 11.107$	arc(Ar), Qu 800 °C, 720 h PXD	Ya, 78b	Lu 99.93 Ni 99.98 Si 99.9
$Lu_3Ni_6Si_2$	$Ce_3Ni_6Si_2$ (ord. Ca_3Ag_8) Im3m	$a = 8.659(2)$	arc, Qu(Ni) 800 °C, 2 weeks PXD	GlKB, 66	Lu 95.7 Ni 99.99 Si 99.99
LuNiSi	TiNiSi Pnma	$a = 6.675$ $b = 4.093$ $c = 7.117$	PXD	Dw, 82	
		$a = 6.667$ $b = 4.092$ $c = 7.225$	arc(Ar), Qu 800 °C, 720 h PXD	Ya, 78b	Lu 99.83 Ni 99.98 Si 99.9
$LuNi_2Si_2$	$ThCr_2Si_2$ I4/mmm	$a = 3.905$ $c = 9.495$	arc(Ar) PXD	BoGK, 66	Lu 95.7 Ni 99.8 Si 99.99
$LuNiSi_2$	$CeNiSi_2$ Cmcm	$a = 3.851(2)$ $b = 15.810(10)$ [+] $c = 3.851(2)$	arc(Ar) PXD	BoG, 69	
$LuNiSi_3$	$ScNiSi_3$ Amm2	$a = 3.891(1)$ $b = 3.889(1)$ $c = 20.834(6)$	arc, Qu (10^{-2} Torr Ar) 800 °C, 720 h $\mu_{eff}^{para} = 0.1\ \mu_B$, $\theta_p = -30$ K	Ch, 83 GoBGY, 77 GlBYGS, 77	Lu 99.83 Ni 99.98 Si 99.9
		$a = 3.963$ $b = 3.887$ $c = 21.037$	arc(Ar), Qu 800 °C, 720 h PXD	Ya, 78b	Lu 99.83 Ni 99.98 Si 99.9

[*] Atom parameters were derived by Yarovets (1978): Lu in 2a) 0, 0, 0; Ni in 8f) 1/4, 1/4, 1/4; Ni in 8j) 0.2871(7), 1/2, 0; Ni+Si in 8i) 0.3631(10), 0, 0.

[+] Pseudotetragonal.

[○] For a correct setting of a bct unit cell $a = a_0/\sqrt{2} = 7.742$.

References
Segre, C.U., 1981, Thesis, Univ. of Calif., San Diego, USA.
Szytula, A. and I. Szott, 1981, Solid State Commun. **40**, 199.

Lu–Ni–Si

No phase diagram of the system Lu–Ni–Si has been established. At least seven ternary compounds have been characterized (see table 17).

References
Bodak, O.I. and E.I. Gladyshevskij, 1969, Kristallografiya **14**(6), 990.
Bodak, O.I., E.I. Gladyshevskij and P.I. Kripyakevich, 1966, Izv. Akad. Nauk SSSR, Neorg. Mater. **2**(12), 2151.
Chabot, B., 1983, unpublished results.
Dwight, A.E., 1982, private communication.
Gladyshevskij, E.I., P.I. Kripyakevich and O.I. Bodak, 1966, Acta Crystallogr. **A21**, 80, and Z. Anorg. Allg. Chem. **344**, 95.
Gladyshevskij, E.I., O.I. Bodak, V.I. Yarovets, Yu.K. Gorelenko and R.V. Skolozdra, 1977, Fiz. Magnit. Plenok (Irkutsk) **10**, 182.
Gorelenko, Yu.K., O.I. Bodak, E.I. Gladyshevskij and V.I. Yarovets, 1977, Ukr. Fiz. Zh. **22**(6), 1020.
Yarovets, V.I., 1978a, Tesizy Dokl. Tret. Vses. Konf. Kristallokhim. Intermet. Soedin, 2nd Ed., ed. R.M. Rykhal (Lvov Gos. Univ., Lvov, USSR) p. 124.
Yarovets, V.I., 1978b, Autoreferat Dis. Kand. Khim. (abstract of thesis, Russian) (Nauk, Lvov) 24 p.

Lu–Os–Si

According to an X-ray powder analysis of arc-melted alloys, annealed at 1150 °C for 7 d, Segre (1981) observed the compound $Lu_2Os_3Si_5$ to crystallize with the $Sc_2Fe_3Si_5$ type structure: P4/mnc, $a = 10.62(1)$, $c = 5.588(8)$. The electrical resistivity was measured in the temperature range $1 < T < 300$ K; no superconductivity was observed above $T_n = 1$ K.

$LuOs_2Si_2$ has the $ThCr_2Si_2$-type of structure: I4/mmm, $a = 4.1197(5)$ and $c = 9.5734(34)$ (Hiebl et al., 1983; X-ray powder data). For sample preparation, see YOs_2Si_2. From magnetic susceptibility measurements (temperature range $1.5 < T < 1100$ K) $LuOs_2Si_2$ is temperature independent paramagnetic with a characteristic value of $\chi_m(300$ K$) = 0.00012$ cm^3 per mole.

References
Hiebl, K., C. Horvath, P. Rogl and M.J. Sienko, 1983, Solid State Commun. **48**, 211.
Segre, C.U., 1981, Thesis, Univ. of Calif., San Diego, USA.

Lu–Pd–Si

According to X-ray powder data by Moreau et al. (1982) $LuPd_2Si$ crystallizes with the ordered Fe_3C-type of structure [Pnma, $a = 7.151(2)$, $b = 6.924(3)$, $c = 5.438(2)$]. For sample preparation, see YPd_2Si.

Reference
Moreau, J., J. Leroy and D. Paccard, 1982, Acta Crystallogr. **B38**, 2446.

Lu–Pt–Si

LuPt$_2$Si crystallizes with the ordered Fe$_3$C-type of structure: Pnma, $a = 7.170(2)$, $b = 6.917(3)$, $c = 5.398(2)$ (X-ray powder analysis by Moreau et al., 1982). For sample preparation, see YPd$_2$Si.

LuPtSi is TiNiSi-type, Pnma, $a = 6.810(1)$, $b = 4.2125(6)$, $c = 7.369(1)$ (X-ray powder methods by Hovestreydt et al., 1982). For sample preparation, see ScPtSi.

LuPt$_2$Si$_2$ was claimed to be body-centered tetragonal with the BaAl$_4$-type ($a = 4.075$, $c = 9.952$, $\rho_x = 12.48$ kg/dm^3). In analogy to ErPt$_2$Si$_2$, Pt and Si atoms were said to statistically occupy the 4d and 4e sites of I4/mmm. For sample preparation, see LaPt$_2$Si$_2$ (Mayer and Yetor, 1977). X-ray powder photographs of arc-melted alloys, however, are not compatible with a body-centered crystal symmetry and reveal a primitive tetragonal lattice with an atomic arrangement similar to the CaBe$_2$Ge$_2$-type (Rogl, 1984): $a = 4.0952(6)$, $c = 9.9387(59)$, CePt$_2$Si$_2$-type.

References
Hovestreydt, E., N. Engel, K. Klepp, B. Chabot and E. Parthé, 1982, J. Less-Common Metals **86**, 247.
Mayer, I. and P.D. Yetor, 1977, J. Less-Common Metals **55**, 171.
Moreau, J.M., J. Leroy and D. Paccard, 1982, Acta Crystallogr. **B38**, 2446.
Rogl, P., 1984, Inorg. Chem., to be published.

Lu–Re–Si

According to X-ray powder data by Pecharskij (1979), LuRe$_4$Si$_2$ is tetragonal with the ZrFe$_4$Si$_2$-type structure [P4$_2$/mnm, $a = 7.286(5)$ and $c = 4.103(2)$]. The samples were arc melted and annealed at 800 °C; for details see, Tb–Re–Si.

Reference
Pecharskij, V.K., 1979, Autoreferat Dis. Kand. Khim. (abstract of thesis, Russian) (Nauk, Lvov) 23 p.

Lu–Rh–Si

Lu$_5$Rh$_4$Si$_{10}$ with the Sc$_5$Co$_4$Si$_{10}$-type structure and space group P4/mbm has been observed in the Lu–Rh–Si system by Pellizone et al. (1983).

Felner and Nowik (1983) observed the formation of LuRh$_2$Si$_2$ with the ordered ThCr$_2$Si$_2$-type structure: I4/mmm, $a = 4.000(2)$, c = 9.87(1) (X-ray powder data of induction-melted alloys). LuRh$_2$Si$_2$ is not superconducting down to $T_n = 1.4$ K, however, from susceptibility measurements (1.5 to 300 K) magnetic ordering was found at $T_m = 17(2)$ K, which was attributed to an itinerant electron ordering of the Rh sublattice. Furthermore a paramagnetic moment was claimed $\mu_{eff}^{para} = 0.7$ μ_B and $\theta_p = -28$ K.

References
Felner, I. and I. Nowik, 1983, Solid State Commun. **47**, 831.
Pellizone, M., H.F. Braun and J. Müller, 1983, to be published.

Lu–Ru–Si

According to X-ray powder data by Segre (1981) the compound $Lu_2Ru_3Si_5$ crystallizes with the $Sc_2Fe_3Si_5$-type of structure: space group P4/mnc and lattice parameters $a = 10.62(1)$, $c = 5.541(8)$. For sample preparation, see $Lu_2Os_3Si_5$. Resistivity was measured in the temperature range $1 < T < 300$ K; no superconductivity was observed above $T_n = 1$ K.

$LuRu_2Si_2$ has the $ThCr_2Si_2$-type of structure: I4/mmm, $a = 4.1357(4)$, $c = 9.4169(31)$ (Hiebl et al., 1983; X-ray powder analysis of arc-melted alloys). From magnetic susceptibility measurements (1.5–1100 K) $LuRu_2Si_2$ is temperature-independent paramagnetic with a characteristic value of $\chi_m(300$ K$) = 0.00008$ cm^3 per mole.

References

Hiebl, K., C. Horvath, P. Rogl and M.J. Sienko, 1983, J. Magn. Magn. Mater. 37, 287.
Segre, C.U., 1981, Thesis, Univ. of Calif., San Diego, USA.

Nd–Ag–Si

$NdAg_2Si_2$ adopts the ordered $ThCr_2Si_2$-type structure: I4/mmm, $a = 4.212(5)$, $c = 10.69(5)$ (Mayer et al., 1973, Mayer and Cohen, 1972, and Mayer and Felner, 1973; X-ray powder analysis). For sample preparation, see $LaAg_2Si_2$.

The stability ranges of the three competing structure types of the $GdSi_2$-type, the $ThSi_2$-type and the AlB_2-type have been investigated by Mayer and Felner (1973) for the concentration section $NdAg_xSi_{2-x}$ and for concentrations with $x \leqslant 1.25$ (see table 18). The AlB_2-type structure (space group P6/mmm) was observed only at compositions of $1 \leqslant x \leqslant 1.25$. From magnetic susceptibility measurements on a NdAgSi alloy in the temperature range of 4.2 to 300 K and in fields up to 15 kOe ferromagnetic ordering was observed at $T_m = 20$ K. The paramagnetic behavior is characterized by $\mu_{eff} = 3.62$ μ_B and $\theta_p = 17$ K (Felner and Schieber, 1973). Samples were prepared by melting at $\sim 1600\,^\circ$C in alumina crucibles in an induction furnace under Ar, and for annealing samples were kept for ~ 30 min somewhat lower than the melting temperature. Starting materials were of 99.9% purity.

TABLE 18

Crystal data for the System $NdAg_xSi_{2-x}$ (after Mayer and Felner, 1973).

x	Structure type	a (Å)	b (Å)	c (Å)
0.00	$GdSi_2$	4.18	4.15	13.56
0.20	$ThSi_2$	4.166		14.10
0.33	$ThSi_2$	4.172		14.22
0.50	$ThSi_2$	4.175		14.31
0.66	$ThSi_2$	4.184		14.50
0.75	$ThSi_2$	4.188		14.70
1.00	AlB_2	4.244		4.138
1.25	AlB_2	4.295		4.135

References

Felner, I. and M. Schieber, 1973, Solid State Commun. **13**, 457.
Mayer, I. and I. Felner, 1973, J. Solid State Chem. **7**, 292.
Mayer, I. and J. Cohen, 1972, J. Less-Common Metals **29**, 221.
Mayer, I., J. Cohen and I. Felner, J. Less-Common Metals **30**, 181.

Nd–Al–Si

No ternary phase diagram has been established for the system Nd–Al–Si; limited information on the phase equilibria, however, is available from the work of Raman and Steinfink (1967), Muravyova et al. (1972) and Yanson (1975).

Raman and Steinfink (1967) studied the phase equilibria within the concentration section $Nd(Al_xSi_{1-x})_2$ by means of X-ray powder diffraction analysis of alloys which were arc melted under argon and subsequently wrapped in Mo foil and annealed for 4 d at 1000 °C in evacuated quartz capsules. Starting materials were 99.9% Gd, 99.999% Al and 99.99% Si. Whereas the stoichiometric disilicide $NdSi_2$ is α-ThSi$_2$-type [$a = 4.162(5)$, $c = 13.58(1)$], the AlB$_2$-type is observed for the Si-defect compound $NdSi_{1.5}$ [$a = 3.940(5)$, $c = 4.258(5)$]. The alloy $NdAl_{1.25}Si_{0.75}$ was AlB$_2$-type [$a = 4.276(5)$, $c = 4.204(5)$] and thus probably part of an extended solid solution which starts from the binary defect $NdSi_{1.5}$ with Al atoms first filling the voids, rather than replacing the Si atoms in terms of a statistical substitution. Accordingly, Yanson (1975) reported the alloy $NdAl_{1.5}Si_{0.5}$ to be AlB$_2$-type with even larger unit cell dimensions ($a = 4.283$, $c = 4.226$). The alloys $NdAl_{1.75}Si_{0.25}$ [$a = 7.986(5)$] and $NdAl_2$ [$a = 8.000(5)$] were found to be single-phase and MgCu$_2$-type (Raman and Steinfink, 1967).

$NdAl_2Si_2$ was observed to adopt the La$_2$O$_2$S-type of structure with space group P3̄m1 and lattice parameters as follows: $a = 4.23$, $c = 6.71$ (Muravyova et al., 1972; from X-ray powder data). For details concerning the sample preparation and the atom parameters, see Sm–Al–Si.

References

Muravyova, A.A., O.S. Zarechnyuk and E.I. Gladyshevskij, 1972, Visn. L'vivsk. Univ., Ser. Khim. **13**, 14.
Raman, A. and H. Steinfink, 1967, Inorg. Chem. **6**(10), 1789.
Yanson, T.I., 1975, Autoreferat Dis. Kand. Khim. (abstract of thesis, Russian) (Nauk, Lvov) 22 p.

Nd–Au–Si

According to an X-ray powder diffraction analysis Mayer et al. (1973) reported the compound $NdAu_2Si_2$ to adopt the ordered ThCr$_2$Si$_2$-type of structure [I4/mmm, $a = 4.280$, $c = 10.17(5)$]. For sample preparation, see LaAu$_2$Si$_2$. Felner (1975) gave slightly different parameters: $a = 4.276$ and $c = 10.19$; paramagnetic behavior was observed within the temperature range of 4.2 to 300 K. The resultant paramagnetic data were given as $\mu_{eff}^{para} = 3.6$ μ_B, $\theta_p = -6.1$ K. NdAu$_2$Si$_2$ has a spontaneous moment of 0.035 μ_B at 4.2 K, which disappears at 5.5 K.

References

Felner, I., 1975, J. Phys. Chem. Sol. **36**, 1063.
Mayer, I., J. Cohen and I. Felner, 1973, J. Less-Common Metals **30**, 181.

Nd–Co–Si

No phase diagram of the Nd–Co–Si system is available yet; six ternary compounds have been characterized.

Phase equilibria within the section $NdCo_xSi_{2-x}$ have been studied by various authors. Mayer and Tassa (1969) reported the $ThSi_2$-type of structure to be stable for $x < 0.4$. $NdCo_{0.4}Si_{1.6}$ was found to crystallize with the AlB_2-type ($a = 4.029$, $c = 4.211$). In similarity to the powder X-ray data of $NdFe_{0.4}Si_{1.6}$ a statistical distribution of Si and Co atoms in the 2d sites of $P6/mmm$ was assumed; however, Mössbauer effect measurements on the isotypic $LaFe_{0.4}Si_{1.6}$ indicate a possible ordering among Co and Si atoms. For sample preparation, see $GdCo_{0.4}Si_{1.6}$. Mayer and Felner (1972) determined the thermal expansion coefficient of $NdCo_{0.4}Si_{1.6}$ by means of high-temperature X-ray diffraction. Samples were placed within a Ta sample holder and temperatures were accurate within $\pm 10 °C$: $\alpha_a = 7.1 \times 10^{-6}$ deg^{-1}, $\alpha_c = 9.4 \times 10^{-6}$ deg^{-1}, $\bar{\alpha} = 8.2 \times 10^{-6}$ deg^{-1}, the volume expansion coefficient is: $\gamma = 32 \times 10^{-6}$ $deg^{-1} \cdot NdCo_{0.4}Si_{1.6}$ decomposes above $1200 °C$. The variation of lattice parameters was as follows: at $25 °C$, $a = 4.034(1)$, $c = 4.218(1)$; at $110 °C$, $a = 4.045(1)$, $c = 4.232(1)$; at $340 °C$, $a = 4.052(1)$, $c = 4.232(1)$; at $610 °C$, $a = 4.059(1)$, $c = 4.237(1)$; at $730 °C$, $a = 4.063(1)$, $c = 4.244(1)$; at $910 °C$, $a = 4.076(1)$, $c = 4.252(1)$. Thermal expansion coefficients were also presented for Nd_5Si_3. Samples were prepared by melting in an induction furnace at $\sim 1600 °C$ in alumina crucibles under argon. For homogenization the molten samples were kept for 30 min somewhat lower than the heating temperature. Mayer and Felner (1973) reported phase equilibria and crystal data as follows: The alloy with the composition $NdCo_{0.25}Si_{1.75}$ was two-phase: $ThSi_2$-type ($a = 4.168$, $c = 13.74$) + AlB_2-type. $NdCo_{0.4}Si_{1.6}$ crystallized with the AlB_2-type ($a = 4.029$, $c = 4.211$). $NdCo_{0.67}Si_{1.33}$ was two-phase: AlB_2 ($a = 4.039$, $c = 4.199$) + $ThCr_2Si_2$-type. Similarly $NdCo_{0.75}Si_{1.25}$ was two-phase: AlB_2-type ($a = 4.054$, $c = 4.169$) + $ThCr_2Si_2$-type. NdCoSi crystallized with the PbFCl-type ($a = 4.035$, $c = 6.895$). At this composition also a $ThCr_2Si_2$-phase was observed ($a = 3.954$, $c = 9.911$); $NdCo_{1.75}Si_{0.25}$ was single-phase with the $MgCu_2$-type ($a = 7.428$) and can be regarded as a solid solution of Si in binary $NdCo_2$ ($a = 7.283$).

NdCoSi with the PbFCl-type of structure [$P4/nmm$, $a = 4.032(3)$, $c = 6.872(5)$] was confirmed by Bodak et al. (1970) from X-ray powder analysis. for atom parameters and sample preparation, see CeFeSi.

$NdCo_2Si_2$ is tetragonal with the ordered $ThCr_2Si_2$-type of structure: $I4/mmm$, $a = 3.960$, $c = 9.910$, $\rho_x = 6.80$ kg/dm^3 (Rossi et al., 1978; X-ray powder methods). For sample preparation and etching conditions, see YCo_2Si_2. Crystal symmetry and atomic order was confirmed by Leciejewicz et al. (1983) from neutron diffraction data of samples melted in an induction furnace and annealed at $800 °C$ in evacuated quartz capsules for 100 h. The samples were then slowly cooled to room temperature; starting materials were 4N-R–metal, 4N-Co and 5N-Si. Neutron data at 300 K were compatible with the ordered $ThCr_2Si_2$-type ($I4/mmm$, $a = 4.007(2)$, $c = 10.002(5)$, z(Si in 4e) = 0.3742(7); $R = 0.069$). The neutron diffraction pattern at 4.2 K revealed a collinear antiferromagnetic order with the Nd moments of 3.39(5) μ_B

oriented along the c-axis. The primitive tetragonal magnetic structure consists of ferromagnetic layers perpendicular to the c-axis coupled antiferromagnetically in a $+ - + -$ sequence: $a = 3.982(4)$, $c = 9.968(9)$, $z(Si) = 0.3805(10)$, $R = 0.099$. The magnetic moments are on the Nd atoms only, $T_N = 26(2)$ K and from the temperature dependence of the $M(100)$ intensity a magnetic phase transition was suggested at $T_m \sim 10$ K.

Bodak and Gladyshevskij (1969) prepared $NdCo_9Si_2$ with the $BaCd_{11}$-type of structure: $I4_1/amd$, $a = 9.794(5)$, $c = 6.328(10)$ (X-ray powder diffraction analysis of arc-melted alloys). Atomic ordering is similar to $CeNi_{8.6}Si_{2.4}$ ($Ce_2Ni_{17}Si_5$-type).

Pelizzone et al. (1982) investigated the structural and magnetochemical behavior of $NdCoSi_2$ with the $CeNiSi_2$-type [Cmcm, $a = 4.142(2)$, $b = 16.395(6)$ and $c = 4.045(2)$]. Samples were prepared by arc melting and subsequent annealing in sealed quartz capsules (150 Torr argon) at $1000\,^\circ$C for one week. Magnetic susceptibilities (2–250 K) are characterized by a paramagnetic behavior with $\mu_{eff}^{para} = 3.0(2)$ μ_B, $\theta_p = -28$ K and the onset of magnetic ordering below 2.5 K.

The existence of a compound $NdCo_{\sim 10.5}Si_{\sim 2.5}$ with the $NaZn_{13}$-type (Fm3c, $a = 11.24$) was reported by Kripyakevich et al. (1968) from X-ray powder diffraction data of arc-melted alloys.

Without further details Gladyshevskij and Bodak (1973) mentioned the existence of a compound $NdCoSi_3$ probably analogous to $CeCoSi_3$: $a = 4.123$, $c = 9.570$, $BaAl_4$-derivative type; as cited by Bodak and Gladyshevskij (1982).

References

Bodak, O.I. and E.I. Gladyshevskij, 1969, Dopov. Akad. Nauk Ukr. RSR, Ser. A **5**, 452.
Bodak, O.I. and E.I. Gladyshevskij, 1982, Kristallokhim. Intermet. Soedin, Redkozemel, Metallov, Lvov, Vysha Schola.
Bodak, O.I., E.I. Gladyshevskij and P.I. Kripyakevich, 1970, Zh. Strukt. Khim. **11**(2), 305.
Gladyshevskij, E.I. and O.I. Bodak, 1973, in: Khim. Met. Splavov, ed. N.M. Zhavoronkov (Nauka, Moscow, USSR) p. 46.
Kripyakevich, P.I., O.S. Zarechnjuk, E.I. Gladyshevskij and O.I. Bodak, 1968, Z. Anorg. Allgem. Chem. **358**, 90.
Leciejewicz, J., M. Kolenda and A. Szytula, 1983, Solid State Commun. **45**, 145.
Mayer, I. and M. Tassa, 1969, J. Less-Common Metals **19**, 173.
Mayer, I. and I. Felner, 1972, J. Less-Common Metals **29**, 25.
Mayer, I. and I. Felner, 1973, J. Solid State Chem. **7**, 292.
Pelizzone, M., H.F. Braun and J. Müller, 1982, J. Magn. Magn. Mater. **30**, 33.
Rossi, D., R. Marazza and R. Ferro, 1978, J. Less-Common Metals **58**, 203.

Nd–Cu–Si

Raman (1967), and Rieger and Parthé (1969a) investigated the occurrence of the AlB_2-type structure by means of X-ray powder diffraction of arc-melted alloys. The data presented by Rieger and Parthé (1969a) were $NdCu_{0.67}Si_{1.33}$: $a = 4.048$, $c = 4.214$; NdCuSi: $a = 4.115$, $c = 4.108$, Cu and Si atoms were said to statistically occupy the 2d sites of P6/mmm. $NdCu_{1.5}Si_{0.5}$: $a = 4.210(5)$, $c = 3.914(5)$ (Raman, 1967). Thus extended homogeneous regions and eventually separated AlB_2-type phases with ordering among Si and Cu atoms are likely (see e.g. phase equilibria in

the system Ce–Cu–Si). At variance with the data by Rieger and Parthé (1969a) obtained from arc-melted alloys, Iandelli (1983) observed NdCuSi with the ordered Ni_2In-type [superstructure of the AlB_2-type, $P6_3/mmc$, $a = 4.210(1)$ and $c = 7.822(4)$]. The superstructure reflections were said to be faint and were found from alloys annealed at 750 °C for 8–12 d. The Ni_2In-type phase was thus concluded to be a low-temperature modification. For detailed sample preparation and purities of starting materials, see LaCuSi.

Kido et al. (1983) studied the magnetic properties of NdCuSi alloys (77–300 K). Samples were prepared by powder metallurgical reaction in evacuated silica tubes at 800–900 °C for 7 d. From X-ray powder analysis an AlB_2-type was claimed; magnetic data were $\mu_{eff}^{para} = 4.2 \mu_B$, $\theta_p = -45$ K.

$NdCu_2Si_2$ crystallizes with the $ThCr_2Si_2$-type of structure with the space group $I4/mmm$ and lattice parameters $a = 4.064(6)$ and $c = 9.926(10)$ (Rieger and Parthé, 1969b; X-ray powder data). For sample preparation, see YCu_2Si_2.

Routsi and Yakinthos (1981) investigated the magnetic behavior of $NdCu_2Si_2$ alloys prepared by induction melting under argon (~ 1500 °C); the temperature range was 4.2 to 300 K and fields were up to 18 kOe. $NdCu_2Si_2$ is paramagnetic with $\mu_{eff}^{para} = 3.7 \mu_B$, $\theta_p = -7$ K; and no ordering was observed at $T \geqslant 4.2$ K; from the field dependence of the magnetization at 4.2 K ferrimagnetism was suggested. For X-ray absorption spectroscopy, see Padalia et al. (1983).

Bodak et al. (1971) mentioned the existence of $NdCu_{1.6}Si_{1.4}$ with the $CeNiSi_2$-type.

References
Bodak, O.I., E.I. Gladyshevskij and Ya.M. Kalvijak, 1971, Tesizy Dokl. Vses. Konf. Kristallokhim. Intermet. Soedin, Lvov, p. 40.
Iandelli, A., 1983, J. Less-Common Metals **90**, 121.
Kido, H., T. Hoshikawa, M. Shimada and M. Koizumi, 1983, Phys. Stat. Sol. (a) **77**, K121.
Padalia, B.D., T.K. Hatwar and M.N. Ghatikar, 1983, J. Phys. C16, 1537.
Raman, A., 1967, Naturwiss. **54**, 560.
Rieger, W. and E. Parthé, 1969a, Monatsh. Chem. **100**, 439.
Rieger, W. and E. Parthé, 1969b, Monatsh. Chem. **100**, 444.
Routsi, C. and J.K. Yakinthos, 1981, Phys. Stat. Sol. (a) **68**, K153.

Nd–Fe–Si

No ternary phase diagram of the system Nd–Fe–Si exists, but phase equilibria along the concentration section $NdFe_xSi_{2-x}$ have been investigated by various authors. The $ThSi_2$-type structure was reported by Mayer and Tassa (1969) to be stable for compositions $x < 0.4$ at 700–800 °C. $NdFe_{0.4}Si_{1.6}$ crystallizes with the AlB_2-type of structure ($a = 4.031$, $c = 4.192$). For a statistical distribution of Fe and Si atoms in the 2d sites of $P6/mmm$ the calculated and observed X-ray powder intensity data were said to be in good agreement. For sample preparation, see $GdCo_{0.4}Si_{1.6}$. Mayer and Felner (1972) determined the thermal expansion coefficient of $NdFe_{0.4}Si_{1.6}$ by means of high-temperature X-ray diffraction. Samples were held in Ta crucibles and the temperature was accurate within ± 10 °C: $\alpha_a = 10.5 \times 10^{-6}$ deg^{-1}, $\alpha_c = 15.00 \times 10^{-6}$ deg^{-1} and $\bar{\alpha} = 12.0 \times 10^{-6}$ deg^{-1}; the volume expansion

coefficient was $\gamma = 35.0 \times 10^{-6} \text{ deg}^{-1}$. The variation of lattice parameters was given as follows: at $25\,°C$, $a = 4.046(1)$, $c = 4.217(1)$; at $330\,°C$, $a = 4.051(1)$, $c = 4.225(1)$; at $500\,°C$, $a = 4.059(1)$, $c = 4.237(1)$; at $620\,°C$, $a = 4.065(1)$, $c = 4.253(1)$; at $820\,°C$, $a = 4.072(1)$, $c = 4.261(1)$.

$NdFe_{0.67}Si_{1.33}$ was said to transform above $950\,°C$: the d values of the new phase were reported as 2.61 (90), 2.53 (100), 2.06 (70) and 1.62 (50), with relative intensities in brackets. Thermal expansion coefficients were also presented for Nd_5Si_3. Some alloys within the section $NdFe_xSi_{2-x}$ have been reinvestigated by Mayer and Felner (1973). In this case samples were prepared by heating proper mixtures in an induction furnace at $\sim 1600\,°C$ in Al_2O_3 crucibles under argon. For homogenization, the samples were kept for 30 min somewhat lower than the heating temperature. According to the earlier data by Mayer and Tassa (1969) the alloy with the composition $NdFe_{0.25}Si_{1.75}$ crystallized with the $ThSi_2$-type ($a = 4.115$, $c = 13.90$) and $NdFe_{0.4}Si_{1.6}$ was single phase AlB_2-type ($a = 4.031$, $c = 4.192$).

NdFeSi was claimed to be single-phase with an orthorhombic "TiNiSi-type" of structure. The lattice parameters ($a = 11.18$, $b = 6.89$ and $c = 5.32$), however, do not correspond to a TiNiSi-type unit cell. The existence of a compound NdFeSi was confirmed by Bodak et al. (1970) but at variance with Mayer and Felner (1973) a PbFCl-type of structure [P4/nmm, $a = 4.057(3)$, $c = 6.893(5)$] was obtained from arc-melted alloys heat treated at $800\,°C$ for 3 months (low-temperature phase?). Due to the high temperature of preparation and homogenization the "TiNiSi-type" phase as reported by Mayer and Felner (1973) is likely to represent a high-temperature modification.

$NdFe_2Si_2$ is tetragonal with the ordered $ThCr_2Si_2$-type of structure: I4/mmm, $a = 3.992$, $c = 10.070$, $\rho_x = 6.46 \text{ kg/dm}^3$ (Rossi et al., 1978; X-ray powder diffraction). For sample preparation and etching conditions, see YCo_2Si_2. In a neutron powder diffraction study of $NdFe_2Si_2$ by Pinto and Shaked (1973) five superlattice reflections were observed at 4.2 K. These lines were found to be consistent with a doubling of the c-axis according to a new unit cell $a' = 3.980$ and $c' = 19.90$ with the magnetic space group $P_{2c}4/nm'm'$. The Nd sublattice with Nd atoms in the "2a sites" [3.01(3) μ_B per Nd atom] orders antiferromagnetically. A collinear magnetic structure with tetragonal symmetry of the Fe sublattice could be excluded. The Néel temperature at $T_N = 15.6$ K was determined from the intensity–temperature curve of the strongest superlattice reflections. The magnetic structure consists of ferromagnetic sheets perpendicular to the c-axis (magnetic axis along c) and with a stacking sequence $+ + - -$. The neutron powder diffraction pattern at room temperature (I4/mmm, $a = 3.983$, $c = 10.03$) was refined to $R = 0.083$ and yielded a small statistical distribution of Fe/Si atoms according to: Nd in 2a), 0.902 Fe + 0.098 Si in 4d), and 0.098 Fe + 0.902 Si in the 4e sites with $z_{Si} = 0.372$. The structure type at room temperature was confirmed [a = 3.995(5), c = 10.07(5)] by Felner et al. (1975), who also reported magnetic susceptibility data with a weak ferromagnetic ordering at 713(5) K; the rare earth sublattice orders antiferromagnetically at $T_N = 11$ K, and from magnetization measurements a spin-flop transition is observed for a field of 11 kOe below the Néel temperature. Mössbauer effect and magnetization measurements reveal most of the iron to be diamagnetic (94%). More recent magnetization and

Mössbauer data by Umarji et al. (1983) (^{57}Fe, 297 K, 4.2 K) prove the absence of a magnetic moment at the Fe site and the spectra at 4.2 K were interpreted by the presence of an internal magnetic field at the Fe nucleus, due to the antiferromagnetic ordering of the R atom. Thus two magnetic sites were concluded for the Fe atoms without and with an internal field of 22(1) kG. Lattice parameters were given as $a = 4.00$, $c = 10.04$ (ordered ThCr$_2$Si$_2$-type). The thermal expansion coefficients of NdFe$_2$Si$_2$ have been determined by Mayer and Felner (1972) by means of high temperature diffractometry (see also NdFe$_{0.4}$Si$_{1.6}$): $\alpha_a = 5.5 \times 10^{-6}$ deg^{-1}; $\alpha_c = 11.1 \times 10^{-6}$ deg^{-1}; $\bar{\alpha} = 7.4 \times 10^{-6}$ deg^{-1}. The volume expansion coefficient was $\gamma = 22.6 \times 10^{-6}$ deg^{-1}. Lattice parameters change as follows: at 25 °C, $a = 3.981(1)$, $c = 10.02(3)$; at 220 °C, $a = 3.986(1)$, $c = 10.08(2)$; at 400 °C, $a = 3.992(1)$, $c = 10.11(2)$; at 780 °C, $a = 3.998(1)$, $c = 10.15(2)$; at 950 °C, $a = 4.002(1)$, $c = 10.17(2)$; at 1150 °C, $a = 4.007(1)$, $c = 10.26(2)$. Heating of NdFe$_2$Si$_2$ above 700 °C resulted in a mixture of Nd$_5$Si$_4$ and Fe$_3$Si. The electrical resistivity of NdFe$_2$Si$_2$ was 9.7 mΩ cm at 300 K (Felner and Mayer, 1973). For a calculation of the electronic state of the Fe atoms in NdFe$_2$Si$_2$, see Koterlin and Lutsiv (1978).

References
Bodak, O.I., E.I. Gladyshevskij and P.I. Kripyakevich, 1970, Zh. Strukt. Khim. **11**(2), 305.
Felner, I. and I. Mayer, 1973, Mater. Res. Bull. **8**, 1317.
Felner, I., I. Mayer, A. Grill and M. Schieber, 1975, Solid State Commun. **16**, 1005.
Koterlin, M.D. and R.V. Lutsiv, 1978, Fiz. Elektron. **17**, 18.
Mayer, I. and M. Tassa, 1969, J. Less-Common Metals **19**, 173.
Mayer, I. and I. Felner, 1972, J. Less-Common Metals **29**, 25.
Mayer, I. and I. Felner, 1973, J. Solid State Chem. **7**, 292.
Pinto, H. and H. Shaked, 1973, Phys. Rev. **B7**(7), 3261.
Rossi, R., R. Marazza and R. Ferro, 1978, J. Less-Common Metals **58**, 203.
Umarji, A.M., D.R. Noakes, P.J. Viccaro, G.K. Shenoy, A.T. Aldred and D. Niarchos, 1983, J. Magn. Magn. Mater. **36**, 61.

Nd–Ge–Si

Mayer and Eshdat (1968) studied the structural variation of the concentration section NdSi$_x$Ge$_{2-x}$, by means of X-ray powder diffraction methods. Samples were prepared by direct reaction at 1500–1700 °C in a Ta boat under argon. The compacted mixture of 99.9% purity was heated for a few minutes in an induction furnace slightly above the melting point.

For the Ge-rich region the tetragonal ThSi$_2$-type of structure (I4/mmm) was observed. With increasing Ge/Si exchange the tetragonal set of lattice parameters successively is found to become orthorhombic. No two-phase field was observed and a continuous transition into the orthorhombic GdSi$_2$-type with space group Imma was proposed. The variation of the lattice parameters versus x is shown in fig. 36. In addition, a rather linear variation of the unit cell volume was observed as shown in fig. 11. The structural change was related to the different modes of distributing Si/Ge atoms in the nonmetal chains of the two structure types.

According to Mayer and Eshdat (1968) their results are representative for the Ge,Si-rich phase boundary. Alloy composition, however, was not monitored by chemical analysis and no detailed investigation was carried out in the immediate region of the phase transition to definitely prove the absence of a two-phase region.
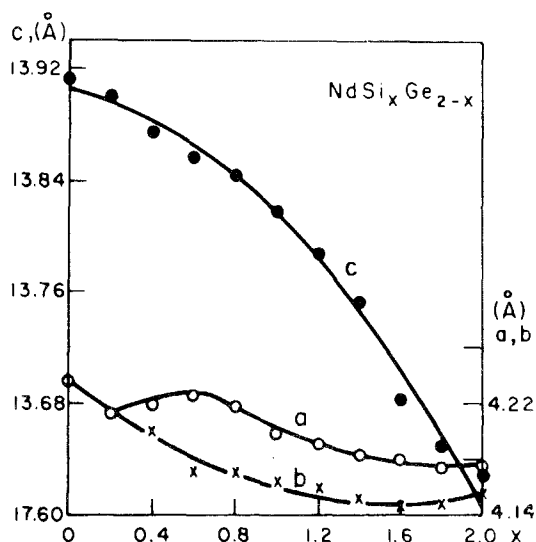
Fig. 36. Nd–Ge–Si, section $NdGe_{2-x}Si_x$; proposed lattice parameter variation versus concentration, after Mayer and Eshdat (1968).

Reference
Mayer, I. and Y. Eshdat, 1968, Inorg. Chem. **9**, 1904.

Nd–Ir–Si

NdIrSi has been found by Chevalier et al. (1982a) from X-ray powder diffraction to be isostructural with LaIrSi with the ZrOS-type of structure: $P2_13$, $a = 6.185(2)$, $\rho_x = 10.237$, $\rho_E = 10.16(10)$ kg/dm^3. For sample preparation, see LaIrSi. Magnetic susceptibility data (4.2–300 K) were characterized by $\mu_{eff} = 3.62 \ \mu_B$, $\theta_p \sim 12$ K and with a noncollinear magnetic ordering suspected below $T_m = 10$ K. A hysteresis loop was obtained at 4.2 K with a coercive field of 0.5 kOe.

NdIrSi$_2$ was reported to crystallize with the CeNiSi$_2$-type of structure (Chevalier et al., 1982b).

References
Chevalier, B., P. Lejay, A. Cole, M. Vlasse and J. Etourneau, 1982a, Solid State Commun. **41**(11), 801.
Chevalier, B., P. Lejay, J. Etourneau, M. Vlasse and P. Hagenmuller, 1982b, Paper presented at the 7th Intern. Conf. on Solid Compounds of Transition Elements, Grenoble, France, Collected Abstracts, II B 16.

Nd–Li–Si

Nd$_2$LiSi$_2$ was found to be isostructural with the ordered U$_3$Si$_2$-type. The space group is P4/mbm and lattice parameters are $a = 7.370$, $c = 4.242$; the densities compare as $\rho_{exp} = 5.02$, $\rho_x = 5.067$ kg/dm^3 (Steinberg and Schuster, 1979; X-ray powder diffraction data). Samples were prepared by heating elemental mixtures of a nominal composition NdLi$_2$Si in Ta crucibles under argon (5 min at 1030 °C). The

resultant heterogeneous powdery specimens were ground and reheated at $670\,^\circ$C for 24 h. The excess Li was dissolved in i-C_3H_7OH plus water. Thus a shiny crystallized powder of light-grey color was obtained. Nd_2LiSi_2 proved to be stable in air and water, but was completely decomposed by dilute acids into a mixture of Si and silicic acid. The composition has been checked by chemical analysis [atom absorption (Li), complexometric (Nd), classic (Si)]. See also Y_2LiSi_2.

Reference
Steinberg, G. and H.U. Schuster, 1979, Z. Naturforsch. **34B**, 1237.

Nd–Mn–Si

Two ternary compounds were observed within the system Nd–Mn–Si.

$NdMn_2Si_2$ crystallizes with the $ThCr_2Si_2$-type of structure: I4/mmm, $a = 4.011$, $c = 10.552$, $\rho_x = 6.07$ kg/dm^3 (Rossi et al., 1978; X-ray powder diffraction. For sample preparation, see $LaMn_2Si_2$. Knigenko et al. (1977) confirmed the existence and structure of this compound and reported similar lattice parameters: $a = 3.997$, $c = 10.470$ (X-ray powder data). For sample preparation, see YMn_2Si_2.

Crystallographic and magnetic properties of $NdMn_2Si_2$ have been investigated by means of powder X-ray, neutron diffraction and magnetometric measurements by Siek et al. (1981) and by Narasimhan et al. (1976). For sample preparation, see YMn_2Si_2. Ordering of Mn· and Si atoms in the 4d and 4e sites of I4/mmm, respectively, was found to be complete. Structural and magnetic data are listed in

TABLE 19

Structural and magnetic parameters in $NdMn_2Si_2$ and $PrMn_2Si_2$ (after Siek et al., 1981).

$T(K) =$	1.8	9.2	90	293
		$PrMn_2Si_2$		
a (Å)	4.024(9)	4.020(11)	4.024(4)	4.030(3)
c (Å)	10.552(33)	10.555(40)	10.566(11)	10.559(10)
c/a	2.622	2.626	2.626	2.670
V (Å^3)	170.86(1.28)	170.55(1.52)	171.15(46)	171.49(44)
z	0.381(4)	0.382(6)	0.383(2)	0.375(2)
R_N (%)	6.9	6.1	5.6	8.3
μ (μ_B)	2.48(12)	2.45(16)	1.96(10)	0.85(23)
R_m (%)	12.9	13.1	12.5	15.7
		$NdMn_2Si_2$	$T = 150$ K	
a (Å)	4.043(7)	4.054(9)	4.061(7)	4.063(4)
c (Å)	10.478(34)	10.509(27)	10.500(25)	10.522(16)
c/a	2.592	2.592	2.586	2.590
V (Å^3)	171.27(1.04)	172.71(1.04)	173.16(99)	173.73(59)
z	0.369(1)	0.365(1)	0.365(3)	0.358(2)
R_N (%)	6.0	4.6	6.2	6.5
μ (μ_B)	2.57(18)	2.57(18)	2.46(14)	1.32(20)
R_m (%)	7.8	9.5	10.2	16.5

table 19. Antiferromagnetic ordering of Mn ions in zero magnetic field was concluded, but it seemed likely that already a low external field induces a metamagnetic transition at 32 K (i.e. magnetic ordering within the Nd sublattice occurs below 36 K and a ferromagnetic coupling with the Mn sublattice). The characteristic magnetic data were $T_N = 365$ K, $\mu_{eff}^{para} = 5.1$ μ_B mole^{-1} and $\theta_p = 290$ K. Narasimhan et al. (1977) reported $a = 4.015(5)$, $c = 10.542(5)$, from X-ray powder analysis. For sample preparation, see Y–Mn–Si.

NdMnSi is tetragonal with the PbFCl-type of structure P4/nmm, $a = 4.099$, $c = 7.236$ (Knigenko et al., 1977; X-ray powder data). For sample preparation, see Y–Mn–Si.

References

Knigenko, L.D., I.R. Mokra and O.I. Bodak, 1977, Vestn. L'vov Univ., Ser. Khim. **19**, 68.
Narasimhan, K.S.V.L., V.U.S. Rao and W.E. Wallace, 1976, AIP Conf. Proc. **29**, 594.
Rossi, D., R. Marazza, D. Mazzone and R. Ferro, 1978, J. Less-Common Metals **59**, 79.
Siek, S., A. Szytula and J. Leciejewicz, 1981, Solid State Commun. **39**, 863; see also Szytula, A. and I. Szott, 1981, Solid State Commun. **40**, 199.

Nd–Ni–Si

No ternary phase diagram of the system Nd–Ni–Si is available yet. At least eleven ternary compounds have been identified (see table 20).

Mayer and Tassa (1969), Mayer and Felner (1972, 1973) and Felner and Schieber (1973) investigated the phase equilibria within the concentration section NdNi$_x$Si$_{2-x}$ by means of X-ray powder analysis. For sample preparation, see ErNi$_x$Si$_{2-x}$. NdSi$_2$ is orthorhombic with the GdSi$_2$-type (Imma, $a = 4.18$, $b = 4.15$, $c = 13.56$). NdNi$_{0.25}$Si$_{1.75}$ crystallizes with the ThSi$_2$-type structure (I4$_1$/amd, $a = 4.103(5)$, $c = 13.85(5)$; stabilization of a binary modification?). At higher Ni concentrations the AlB$_2$-type was observed to be stable for $0.4 < x < 0.75$ (see table 20). A refinement of powder X-ray diffraction data of NdNi$_{0.4}$Si$_{1.6}$ suggested a statistical distribution of Ni/Si atoms in the 2d site. Ni/Si atom ordering, however, seems to be likely (see also Mössbauer data of isotypic LaFe$_{0.4}$Si$_{1.6}$ (25–800 °C) by Mayer and Tassa, 1969). NdNiSi was claimed to be isotypic with the α-ThSi$_2$-type structure, but more likely crystallizes with the LaPtSi-type structure. An unknown tetragonal structural ($a = 7.243$, $c = 8.763$) was observed for the allow NdNi$_{1.5}$Si$_{0.5}$. NdNi$_{1.75}$Si$_{0.25}$ was cubic with the MgCu$_2$-type ($a = 7.284$) and probably represents the end member (?) of a solid solution originating at the binary NdNi$_2$ with $a = 7.270$.

The electrophysical properties of NdNi$_2$Si$_2$ were reported by Levin et al. (1977) including the temperature dependence of the electrical resistance, the thermoelectrical coefficient, magnetic susceptibilities as well as the preparation of stoichiometric thin films.

References

Bodak, O.I. and E.I. Gladyshevskij, 1969a, Dopov. Akad. Nauk Ukr. RSR, Ser. A **5**, 452.
Bodak, O.I. and E.I. Gladyshevskij, 1969b, Dopov. Akad. Nauk Ukr. RSR, Ser A **12**, 1125.

TABLE 20

Formation and structural data of ternary compounds Nd–Ni–Si

Compound	Structure type Space group	Lattice parameters Density	Preparation, Characterization	Refs.	Purity
$Nd_2(Ni,Si)_{17}$ $(Nd_2Ni_{15}Si_2)$	Th_2Ni_{17} $P6_3/mmc$	$a = 8.390(4)$ $c = 8.066(4)$	arc, PXD see $Ce_2Ni_{15}Si_2$	GlKB, 66 GlKB, 67	Nd 97.07 Ni 99.99 Si 99.99
$Nd_3Ni_6Si_2$	$Ce_3Ni_6Si_2$ (ord. Ca_2Ag_8) $Im3m$	$a = 8.907(2)$	arc, Qu(Ni) 800 °C, 2 weeks PXD	GlKB, 66	Nd 97.07 Ni 99.99 Si 99.99
$NdNi_{8.6}Si_{2.4}$	$Ce_2Ni_{17}Si_5$ $(BaCd_{11})$ $I4_1/amd$	$a = 9.788(5)$ $c = 6.246(10)$	arc(Ar), Qu 800 °C, PXD atom order as for $CeNi_{8.6}Si_{2.4}$	BoG, 69a	Nd 99.7 Ni 99.91 Si 99.99
$Nd_6Ni_2Si_3$	$Ce_6Ni_2Si_3$ filled Ho_4Co_3 $P6_3/m$	$a = 11.905(5)$ $c = 4.275(2)$	no details PXD	BoGK, 74	
$NdNi_{8.6}Si_{4.4}$ [*] 30 a/o Si	$Ce_2Ni_{17}Si_9$ ($NaZn_{13}$-deriv.) $I4/mcm$	$a = 11.06(1)$ [*] $c = 11.16(1)$	arc(Ar), Qu 800 °C, 100 h PXD	BoG, 69b	Nd 99.2 Ni 99.99 Si 99.99
$Nd(Ni,Si)_{13}$ 37–45 a/o Si	$NaZn_{13}$ $Fm3c$	$a = 11.16(1)$	arc(Ar), Qu 800 °C, 100 h PXD	BoG, 69b	Nd 99.2 Ni 99.99 Si 99.99
NdNiSi [**]	$(ThSi_2)$ [**]	$a = 4.081(5)$ $c = 13.990(5)$	induction melting at 1600 °C (Ar) in Al_2O_3 30 min, PXD	MaF, 73	99.9
$NdNi_2Si_2$	$ThCr_2Si_2$ $I4/mmm$	$a = 4.022(10)$ $c = 9.598(10)$	arc(Ar) PXD	BoGK, 66	Nd 97.07 Ni 99.8 Si 99.99
$NdNiSi_2$	$CeNiSi_2$ $Cmcm$	$a = 4.105(2)$ $b = 16.450(10)$ $c = 4.012(2)$	arc(Ar) PXD	BoG, 69c	Nd 97.07 Ni 99.8 Si 99.99
$Nd(Ni,Si)_2$ [+]	AlB_2 $P6/mmm$	$a = 4.020(5)$ $c = 4.207(5)$ at composition $NdNi_{0.5}Si_{1.5}$	induction melting ~ 1600 °C, in Al_2O_3 annealed for 30 min at ~ 1600 °C,	MaF, 73	99.9
		$a = 4.036(5)$ $c = 4.156(5)$ at composition $NdNi_{0.75}Si_{1.25}$	PXD		
		$a = 4.044$ $c = 4.168$ at composition $NdNi_{0.67}Si_{1.33}$	induction heating (Ar) PXD $\mu_{eff}^{para} = 3.68\ \mu_B$, $\theta_p = 12$ K $T_m = 23$ K	FeS, 73	

TABLE 20 (continued)

Compound	Structure type Space group	Lattice parameters Density	Preparation, Characterization	Refs.	Purity
AlB$_2$ (cont'd)	Nd(Ni, Si)$_2$	$a = 4.014$ $c = 4.231$ at composition NdNi$_{0.4}$Si$_{1.4}$	induction heating (Ar) in Al$_2$O$_3$ or MgO$_2$ 1500 °C, Qu, 700–900 °C, 24–96 hrs PXD-refinement	MaT, 69	Nd 99.9 Ni 99.95 Si 99.99
			$\mu_{\mathrm{eff}}^{\mathrm{para}} = 4.48\,\mu_{\mathrm{B}}$, $\theta_{\mathrm{p}} = 0$ K	FeS, 73	
		alloy NdNi$_{0.4}$Si$_{1.6}$:	induction melting (Ar) in Al$_2$O$_3$, Qu 700 °C, 2 d, PXD	MaF, 72	99.9
		$a = 4.013(1)$ $c = 4.202(1)$ at 25°C	$\alpha_{\mathrm{a}} = 11.3 \times 10^{-6}\ \mathrm{deg}^{-1}$ $\alpha_{\mathrm{c}} = 8.9 \times 10^{-6}\ \mathrm{deg}^{-1}$		
		$a = 4.038(1)$ $c = 4.221(1)$ at 480°C	$\alpha = 10.2 \times 10^{-6}\ \mathrm{deg}^{-1}$		
		$a = 4.046(1)$ $c = 4.231(1)$ at 800°C	$\gamma = 30.8 \times 10^{-6}\ \mathrm{deg}^{-1}$		
		$a = 4.042(5)$ $c = 4.163(5)$	arc (Ar) Qu, 800 °C, 100 h PXD	GIB, 65	Ni 99.8 Si 99.99

[*] For a correct setting of the bct-unit cell $a = 7.821$ ($a = a_0/\sqrt{2}$).

[**] A ThSi$_2$-type of structure (I4$_1$/amd) was claimed by Mayer and Felner (1973); however, as no detailed investigation of the Ni/Si atom order has been carried out, the actual structure type might be better represented by the LaPtSi-type of structure (ThSi$_2$-derivative structure, I4$_1$md; see LaPtSi).

[+] For NdNi$_{0.4}$Si$_{1.6}$ a transition to a second phase was observed by Mayer and Felner (1972) for $T \geqslant 800$ °C. Characteristic reflections (and their intensities) were $d = 2.86(3)$, 2.22(100), 1.65(30), 1.58(20) and 1.38(5). The reflections were tentatively indexed on the basis of a hexagonal cell: $a = 6.62$, $c = 6.07$.

Bodak, O.I. and E.I. Gladyshevskij, 1969c, Kristallografiya, 14(6), 990.

Bodak, O.I., E.I. Gladyshevskij and P.O. Kripyakevich, 1966, Izv. Akad. Nauk SSSR, Neorg. Mater. 2(12), 2151.

Bodak, O.I., E.I. Gladyshevskij and O.Kharchenko, 1974, Sov. Phys. Crystallogr. 19(1), 45.

Felner, I. and M. Schieber, 1973, Solid State Commun. 13, 457.

Gladyshevskij, E.I. and O.I. Bodak, 1965, Dopov. Akad. Nauk Ukr. RSR, Ser. A 5, 601.

Gladyshevskij, E.I., P.I. Kripyakevich and O.I. Bodak, 1966, Acta Crystallogr. A21, 80, and Z. Anorg. Allg. Chem. 344, 95.

Gladyshevskij, E.I., P.I. Kripyakevich and O.I. Bodak, 1967, Visn. L'vivsk. Derzh. Univ., Ser. Khim. 9, 34.

Levin, E.M., R.V. Lutsiv, E.I. Gladyshevskij and O.I. Bodak, 1977, Fiz. Elektron. Resp. Mezhved. Nauch-tekhn. Sbor. **15**, 59.

Mayer, I. and I. Felner, 1972, J. Less-Common Metals **29**, 25.

Mayer, I. and I. Felner, 1973, J. Solid State Chem. **7**, 292.

Mayer, I. and M. Tassa, 1969, J. Less-Common Metals **19**, 173.

Nd–Os–Si

From X-ray powder analysis Hiebl et al. (1983) reported $NdOs_2Si_2$ to crystallize with the $ThCr_2Si_2$-type structure. The crystallographic data were: I4/mmm, $a = 4.1635(4)$ and $c = 9.8784(21)$. For sample preparation, see YOs_2Si_2. Above $T = 300$ K $NdOs_2Si_2$ is paramagnetic with $\mu_{eff}^{para} = 3.56$ μ_B and $\theta_p = 19$ K. $NdOs_2Si_2$ orders ferromagnetically at 2.9 K.

Reference

Hiebl, K., C. Horvath, P. Rogl and M.J. Sienko, 1983, Solid State Commun. **48**, 211.

Nd–Pd–Si

The formation of two ternary neodymium palladium silicides has been reported. $NdPd_2Si$ crystallizes with the ordered Fe_3C-type structure, Pnma, $a = 7.513(2)$, $b = 6.892(2)$, $c = 5.638(1)$ (X-ray powder diffraction). For sample preparation, see YPd_2Si (Moreau et al., 1982).

According to an X-ray powder analysis by Ballestracci (1976) $NdPd_2Si_2$ is tetragonal with the ordered $ThCr_2Si_2$-type: I4/mmm, $a = 4.187$ and $c = 9.96$. For sample preparation, see $CePd_2Si_2$.

References

Ballestracci, R., 1976, C.R. Acad. Sci. Paris, Ser. B **282**, 291.

Moreau, J., J. Leroy and D. Paccard, 1982, Acta Crystallogr. **B38**, 2446.

Nd–Pt–Si

Only two ternary compounds have been characterized in the Nd–Pt–Si system.

NdPtSi crystallizes with the LaPtSi-type structure, I4$_1$md, $a = 4.1630(8)$, $c = 14.415(4)$ (Klepp and Parthé, 1982; X-ray powder diffraction). For sample preparation, see LaPtSi; congruent melting behavior is indicated.

$NdPt_2Si_2$ was claimed to be body-centered tetragonal with the $BaAl_4$-type, $a = 4.218$, $c = 9.790$ (Mayer and Yetor, 1977). In analogy to $ErPt_2Si_2$, Pt and Si atoms were said to be randomly distributed in the 4d and 4e sites of I4/mmm. For sample preparation, see $LaPt_2Si_2$. Rossi et al. (1979) confirmed the atomic arrangement ($a = 4.226$, $c = 9.816$, $\rho_x = 11.19$ kg/dm^3). For sample preparation, see $CePd_2Si_2$. However, Ballestracci and Astier (1978) reported $CePt_2Si_2$ to crystallize with a primitive tetragonal unit cell, $a = 4.232$, $c = 9.77$ (powder X-ray analysis of alloys melted in an induction furnace under argon). According to recent X-ray powder photographs of arc-melted alloys the crystal symmetry is primitive and not

compatible with a body-centered Bravais lattice; the atomic arrangement is similar to the $CaBe_2Ge_2$-type (Rogl, 1984): $a = 4.2330(9)$, $c = 9.7807(52)$, $CePt_2Si_2$-type.

References

Ballestracci, R. and G. Astier, 1978, C.R. Acad. Sci. Paris, Ser. B **286**, 109.
Klepp, K. and E. Parthé, 1982, Acta Crystallogr. **B38**, 1105.
Mayer, I. and P.D. Yetor, 1977, J. Less-Common Metals **55**, 171.
Rogl, P., 1984, Inorg. Chem., to be published.
Rossi, D., R. Marazza and R. Ferro, 1979, J. Less-Common Metals **66**, P17.

Nd–Re–Si

The phase equilibria in the Si,Re-rich part of the Nd–Re–Si system have been investigated by Pecharskij (1979) by means of X-ray and metallographic analysis of 42 ternary alloys, which were arc melted and subsequently annealed in evacuated silica tubes for 400 + 600 h at 800°C and finally quenched in water. Starting materials were Nd 99.07%, Re 99.99% and Si 99.99%.

$NdRe_2$ crystallizes with the $MgZn_2$-type; the phase relations in the binary systems Nd–Si and Re–Si are discussed in context with the ternary systems Ce–Nd–Si and Y–Re–Si. The mutual solid solubilities of Nd and Re silicides as well as of $NdRe_2$ at 800°C were found to be small and within 1–2 a/o of the third constituent.

The ternary phase equilibria (fig. 37, partial isothermal section for 0–33 a/o Nd, at 800°C) are characterized by the existence of three ternary compounds: $NdRe_4Si_2$,
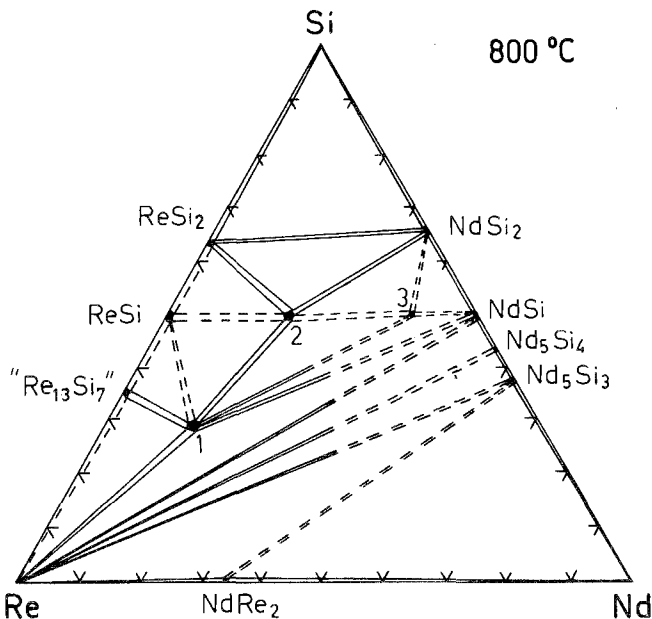
Fig. 37. Nd–Re–Si, partial isothermal section at 800°C (0–33 a/o Nd). 1: $NdRe_4Si_2$, 2: $Nd_2Re_3Si_5$, 3: "Nd_4ReSi_5".

$Nd_2Re_3Si_5$ and "Nd_4ReSi_5"; the crystal structure of the latter compound has not been solved.

Bodak et al. (1978) refined the crystal structure of $Nd_2Re_3Si_5$ from X-ray single crystal photographs. $Nd_2Re_3Si_5$ is tetragonal (P4/mnc) with the $Sc_2Fe_3Si_5$-type; lattice parameters are $a = 10.99(1)$ and $c = 5.652(5)$. With a reliability value of $R = 0.120$ the atomic parameters are: Nd in 8h) 0.0757(2), 0.2408(2), 0; Re in 8h) 0.3764(1), 0.3512(1), 0; Re in 4d) 0, 1/2, 1/4; Si in 8h) 0.184(1), 0.489(1), 0; Si in 8g) 0.177(2), 0.677(2), 1/4; Si in 4e) 0, 0, 0.260(2). Segre (1981) confirmed the structure type from arc-melted samples [$a = 10.97(1)$, $c = 5.643(8)$]; $T_n = 1.2$ K.

The crystal structure of $NdRe_4Si_2$ was refined by Pecharskij et al. (1978) from single crystal X-ray photographs. Single crystals were obtained from an arc-melted sample of composition (in a/o) $Nd_{14}Re_{56}Si_{30}$. Starting materials were 99.6% Nd, 99.8% Re and 99.99% pure Si. NRe_4Si_2 crystallizes with a new structure type: $NdRe_4Si_2$-type with space group Pnnm and lattice parameters $a = 7.368(5)$, $b = 15.38(1)$ and $c = 4.089(2)$. Atom parameters were Nd in 4g) 0.5745(4), 0.1203(4), 0; Re in 4g) 0.1400(1), 0.0519(2), 0; Re in 4g) 0.7350(1), 0.3212(3), 0; Re in 4g) 0.4294(2), 0.4193(2), 0; Re in 4g) 0.9864(2), 0.2041(3), 0; Si in 4g) 0.828(1), 0.475(1), 0; Si in 4g) 0.281(1), 0.273(1), 0; $R_{hk0} = 0.114$, $R_{hk1} = 0.112$ and $R_{hk2} = 0.113$.

References

Bodak, O.I., V.K. Pecharskij and E.I. Gladyshevskij, 1978, Izv. Akad. Nauk SSSR, Neorg. Mater. **14**(2), 250.

Pecharskij, V.K., 1979, Autoreferat Dis. Kand. Khim. (abstract of thesis, Russian) (Nauk, Lvov) 23 p.

Pecharskij, V.K., O.I. Bodak and E.I. Gladyshevskij, 1978, Sov. Phys. Crystallogr. **23**(1), 22.

Segre, C.U., 1981, Thesis, Univ. of Calif., San Diego, USA.

Nd–Rh–Si

Five ternary compounds have been reported for the Nd–Rh–Si system.

$NdRh_2Si_2$ is tetragonal (I4/mmm) with the ordered $ThCr_2Si_2$-type. The following lattice parameters were given by Ballestracci (1976) resulting from an X-ray powder analysis: $a = 4.069$ and $c = 10.11$. For sample preparation, see YRh_2Si_2. The crystal symmetry of $NdRh_2Si_2$ was recently confirmed by Felner and Nowik (1983) from X-ray powder diffraction of induction-melted alloys [I4/mmm, $a = 4.069(2)$, $c = 10.11(1)$]. $NdRh_2Si_2$ was said to order antiferromagnetically at $T_N = 56$ K with a second peak in the susceptibility versus T curve at $T_m = -8(2)$ K, which was interpreted as itinerant electron ordering of the Rh sublattice. The paramagnetic behavior corresponds to $\mu_{eff}^{para} = 4.7(1)$ μ_B, $\theta_p = -4(3)$ K (the investigated temperature range was 1.5 to 300 K).

$NdRh_3Si_2$ is isotypic with the crystal structure of $CeCo_3B_2$: P6/mmm, $a = 5.545(6)$, $c = 3.557(4)$ (Chevalier et al., 1981; X-ray powder analysis). For sample preparation, see $LaRh_3Si_2$. The magnetic behavior was studied in the temperature range of 4.2 to 300 K and was found to be characterized by a Van Vleck type paramagnetism ($\mu_{eff}^{para} = 3.92$ μ_B, $\theta_p = 2$ K).

Chevalier et al. (1982) reported structure and magnetochemical properties of the compound $Nd_2Rh_3Si_5$ crystallizing with the $Sc_2Co_3Si_5$-type of structure. The space

group is Ibam and lattice parameters were reported as $a = 9.82(1)$, $b = 11.77(1)$, $c = 5.802(5)$. Magnetic susceptibilities in the temperature range from 4.2 K to 300 K were characterized by a Van Vleck type paramagnetism with $\mu_{eff}^{para} = 3.85$ μ_B and $\theta_p = -3$ K and an antiferromagnetic ordering at very low temperatures.

The existence of other compounds was reported by Chevalier et al. (1982), who found NdRhSi$_2$ (CeNiSi$_2$-type) and Nd$_2$RhSi$_3$ with an ordered derivative of the AlB$_2$-type. According to X-ray powder data obtained from arc-melted alloys annealed at 800°C for 4 d, Nd$_2$RhSi$_3$ crystallizes with the Er$_2$RhSi$_3$-type [P$\bar{6}$2c, $a = 8.186(5)$, $c = 8.272(5)$]; Nd$_2$RhSi$_3$ is ferromagnetic below $T_c = 15$ K; the paramagnetic data were $\mu_{eff}^{para} = 3.76$ μ_B and $\theta_p = 7$ K (temperature range 1.5 to 300 K) (Chevalier et al., 1984).

References

Ballestracci, R., 1976, C.R., Acad. Sci. Paris., Ser. B **282**, 291.

Chevalier, B., A. Cole, P. Lejay and J. Etourneau, 1981, Mater. Res. Bull. **16**, 1067.

Chevalier, B., P. Lejay, J. Etourneau, M. Vlasse and P. Hagenmuller, 1982, Paper presented at the 7th Intern. Conf. on Solid Compounds of Transition Elements, Grenoble, France, Collected Abstracts II B 16, and 1982, Mater. Res. Bull. **17**, 1211.

Chevalier, B., P. Lejay, J. Etourneau and P. Hagenmuller, 1984, Solid State Commun. **49**(8), 753.

Felner, I. and I. Nowik, 1983, Solid State Commun. **47**, 831.

Nd–Ru–Si

Barz (1980) reported the existence of a compound NdRu$_3$Si$_2$ with the LaRu$_3$Si$_2$-type of structure. No lattice parameters were given. For sample preparation and melting behavior (phase equilibria), see also LaRu$_3$Si$_2$. Magnetic ordering was said to occur at $T_m = 17.95$ K.

NdRu$_2$Si$_2$ is isotypic with the crystal structure of ThCr$_2$Si$_2$ with the space group I4/mmm and lattice parameters $a = 4.186$ and $c = 9.75$ (Ballestracci and Astier, 1978; X-ray powder analysis). Samples were prepared by induction melting under argon. Hiebl et al. (1983) confirmed the structure type ($a = 4.1859(6)$, $c = 9.7342(51)$, X-ray powder data) and in addition studied the magnetic behavior for the temperature range 1.5 K $< T <$ 1100 K: $\mu_{eff}^{para} = 3.54$ μ_B, $\theta_p = 29.9$ K; ferromagnetic ordering was observed at $T_m = 17.4$ K.

References

Ballestracci, R. and G. Astier, 1978, C.R. Acad. Sci. Paris, Ser. B **286**, 109.

Barz, H., 1980, Mater. Res. Bull. **15**, 1489.

Hiebl, K., C. Horvath, P. Rogl and M.J. Sienko, 1983, J. Magn. Magn. Mater. **37**, 287.

Nd–Sc–Si

Based on X-ray powder data, Mokra and Bodak (1979) reported the compound NdScSi to be tetragonal with the CeScSi-type structure [ordered Ca$_2$As-type, space group I4/mmm, $a = 4.284(5)$, $c = 15.73(2)$]. For sample preparation, see CeScSi.

Reference

Mokra, I.P. and O.I. Bodak, 1979, Dopov. Akad. Nauk Ukr. RSR., Ser. A, 312.

Pr–Ag–Si

PrAg$_2$Si$_2$ was reported to crystallize with the ordered ThCr$_2$Si$_2$-type structure: space group I4/mmm and lattice parameters $a = 4.235(5)$ and $c = 10.68(5)$ (Mayer et al., 1973; Mayer and Cohen, 1972; X-ray powder analysis). For sample preparation, see LaAg$_2$Si$_2$.

Reference
Mayer, I. and J. Cohen, J. Less-Common Metals **29**, 221.
Mayer, I., J. Cohen and I. Felner, 1973, J. Less-Common Metals **30**, 181.

Pr–Al–Si

No ternary phase diagram exists for the Pr–Al–Si system; however, the formation of two compounds PrAl$_2$Si$_2$ and Pr(Al$_{0.75}$Si$_{0.25}$)$_2$ was reported by Muravyova et al. (1972) and by Yanson (1975), respectively.

PrAl$_2$Si$_2$ crystallizes with the La$_2$O$_2$S-type: P$\bar{3}$m1, $a = 4.21$, $c = 6.81$ (Muravyova et al., 1972; powder X-ray diffraction data). For details of sample preparation and atom parameters, see Sm–Al–Si.

Yanson (1975), from X-ray powder diffraction data, characterized the compound Pr(Al$_{0.75}$Si$_{0.25}$)$_2$ to be isostructural with the AlB$_2$-type (P6/mmm, $a = 4.635$ and $c = 4.261$).

References
Muravyova, A.A., O.S. Zarechnyuk and E.I. Gladyshevskij, 1972, Visn. L' vivsk. Univ., Ser. Khim. **13**, 14.
Yanson, T.I., 1975, Autoreferat Dis. Kand. Khim. (abstract of thesis, Russian) (Nauk, Lvov) 22 p.

Pr–Au–Si

PrAu$_2$Si$_2$ is isostructural with the ordered ThCr$_2$Si$_2$-type structure: space group I4/mmm; $a = 4.303(5)$, $c = 10.19(5)$ (Mayer et al., 1973; X-ray powder diffraction). For sample preparation, see LaAu$_2$Si$_2$. Paramagnetic behavior was reported by Felner (1975) from susceptibility measurements in the temperature range of 4.2 K to 300 K ($\mu_{eff}^{para} = 3.3\ \mu_B$, $\theta_p = -9.2$ K).

References
Felner, I., 1975, J. Phys. Chem. Sol. **36**, 1063.
Mayer, I., J. Cohen and I. Felner, 1973, J. Less-Common Metals **30**, 181.

Pr–Co–Si

Mayer and Tassa (1969) investigated the phase equilibria at 700–800 °C in the section PrCo$_x$Si$_{2-x}$. For $x < 0.4$ the ThSi$_2$-type structure was found to be stable. PrCo$_{0.4}$Si$_{1.6}$ was observed to crystallize with the AlB$_2$-type structure ($a = 4.038$, $c = 4.247$). In similarity to the X-ray data of NdFe$_{0.4}$Si$_{1.6}$ a statistical distribution of Co and Si atoms was assumed in the 2d sites of P6/mmm. For sample preparation, see GdCo$_{0.4}$Si$_{1.6}$. Powder patterns of samples with $x > 0.4$ were said to be complex.

PrCoSi is isostructural with the PbFCl-type structure: P4/nmm, $a = 4.035(3)$, $c = 6.934(5)$ (X-ray powder analysis by Bodak et al., 1970). For sample preparation and atom parameters, see CeFeSi.

$PrCo_2Si_2$ crystallizes with the ordered $ThCr_2Si_2$-type structure: I4/mmm, $a = 3.970$, $c = 9.920$, $\rho_x = 6.69$ kg/dm^3 (Rossi et al., 1978; X-ray powder diffraction). For sample preparation and etching conditions, see YCo_2Si_2. A neutron powder diffraction analysis confirmed crystal symmetry and atomic order (Leciejewicz et al., 1983). For sample preparation, see the Er–Co–Si system. Neutron data at 300 K were: $ThCr_2Si_2$-type, I4/mmm, $a = 3.969(1)$, $c = 9.925(4)$, z(Si in 4e) = 0.3719(4), $R = 0.099$. The neutron data obtained at 4.2 K revealed a collinear antiferromagnetic order with a $+ - + -$ sequence along [001] and the Pr moments of 3.19(6) μ_B oriented parallel to c: $a = 3.972(5)$, $c = 9.949(9)$, $z = 0.3759(1)$, $R = 0.058$. Only the Pr atoms carry a magnetic moment; $T_N = 49(19)$ K.

The existence of a compound $PrCo_{\sim 10.5}Si_{\sim 2.5}$ with the $NaZn_{13}$-type (Fm3c, $a = 11.28$) was reported by Kripyakevich et al. (1968) from X-ray powder analysis of arc-melted alloys.

Without further details Gladyshevskij and Bodak (1973) mentioned the existence of a compound $PrCoSi_3$ probably isostructural with $CeCoSi_3$: $a = 4.123$, $c = 9.585$; $BaAl_4$-derivative type, as cited by Bodak and Gladyshevskij (1982).

References

Bodak, O.I., and E.I. Gladyshevskij, 1982, Kristallokhim. Intermet. Soedin, Redkozemel. Metallov, Lvov, Vysha Schola.
Bodak, O.I., E.I. Gladyshevskij and P.I. Kripyakevich, 1970, Zh. Strukt. Khim. 11(2), 305.
Gladyshevskij, E.I. and O.I. Bodak, 1973, in: Khim. Met. Splavov, ed. N.M. Zhavoronkov (Nauka, Moscow, USSR) p. 46.
Kripyakevich, P.I., O.S. Zarechnjuk, E.I. Gladyshevskij and O.I. Bodak, 1968, Z. Anorg. Allgem. Chem. **358**, 90.
Leciejewicz, J., M. Kolenda and A. Szytula, 1983, Solid State Commun. **45**, 145.
Mayer, I. and M. Tassa, 1969, J. Less-Common metals **19**, 173.
Rossi, D., R. Marazza and R. Ferro, 1978, J. Less-Common Metals **58**, 203.

Pr–Cu–Si

Rieger and Parthé (1969a) investigated the occurrence of the AlB_2-type structure by means of X-ray powder analysis of arc-melted alloys of composition $PrCu_{0.67}Si_{1.33}$ ($a = 4.053$, $c = 4.251$) and PrCuSi ($a = 4.123$, $c = 4.162$). Cu and Si atoms were said to statistically occupy the 2d site of space group P6/mmm. From arc-melted alloys annealed at 750°C, Iandelli (1983) recorded the formation of PrCuSi with the ordered Ni_2In-type [superstructure of the AlB_2-type with P6$_3$/mmc, $a = 4.222(2)$, $c = 7.908(5)$]; the superstructure reflections are faint and with respect to the results obtained by Rieger and Parthé (1969a), the Ni_2In phase was concluded to be the low-temperature modification. A thermal analysis up to 1400°C revealed two thermal arrests at 980 and 1230°C. For details in sample preparation and purities of the starting materials, see LaCuSi.

$PrCu_2Si_2$ crystallizes with the $ThCr_2Si_2$-type structure: I4/mmm, $a = 4.086(6)$, $c = 9.929(10)$ (Rieger and Parthé, 1969b; X-ray powder data). For sample prepara-

tion, see YCu_2Si_2. NMR data were presented by Sampathkumaran et al. (1979). For X-ray absorption spectroscopy, see Padalia et al. (1983).

Oesterreicher (1976) prepared and characterized (powder X-ray analysis) the compound $Pr_3Cu_4Si_4$ with the $Gd_3Cu_4Ge_4$-type (Immm) by induction melting under argon in MgO crucibles; the alloys were subsequently annealed in vacuum on a MgO substrate for 200 h at $800\,°C$; no structural details were given.

Magnetism of $Pr_3Cu_4Si_4$, PrCuSi (AlB_2-type) and $PrCu_2Si_2$ ($ThCr_2Si_2$-type) was studied in the temperature range of 4.2 to 150 K and in fields up to 50 kOe (Oesterreicher, 1976). PrCuSi orders ferromagnetically at $T_m = 14$ K, $\mu_S = 2.02$ μ_B; $\mu_{eff}^{para} = 3.39$ μ_B and $\theta_p = 8$ K. For $Pr_3Cu_4Si_4$ ($\mu_{eff}^{para} = 3.45$ μ_B, $\theta_p = -3$ K, $\mu_S = 0.85$ μ_B) and $PrCu_2Si_2$ ($\mu_{eff}^{para} = 3.41$ μ_B, $\theta_p = -2$ K, $\mu_S = 0.53$ μ_B) antiferromagnetic interaction was suspected from the negative Curie–Weiss constants; however, magnetization was practically constant at 4.2 K and both compounds are probably metamagnets.

Atomic order and crystal symmetry of $PrCu_2Si_2$ was confirmed by Szytula et al. (1983) from a room temperature neutron diffraction study on a polycrystalline sample [$ThCr_2Si_2$-type, $a = 4.086(2)$, $c = 9.929(5)$, $z(Si$ in 4e) $= 0.3790(9)$, $R_N = 0.055$]. Values at 80 K were as follows: $a = 4.076(3)$, $c = 9.949(9)$, $z(Si) = 0.3790(9)$, $R_N = 0.056$. The antiferromagnetic type of magnetic order at 4.2 K was revealed from a neutron experiment to be of a simple $+ - + -$ sequence of ferromagnetic (001) planes along [001] [$a = 4.064(1)$, $c = 9.885(6)$, $z(Si) = 0.3808(5)$, $\mu = 2.51(4)$ μ_B, $R_N = 0.043$); $T_N = 19(1)$ K].

Bodak et al. (1971) reported the existence of $PrCu_{1.6}Si_{1.4}$ with the $CeNiSi_2$-type.

References

Bodak, O.I., E.I. Gladyshevskij and Ya.M. Kalvijak, 1971, Tesizy Dokl. Vses. Konf. Kristallokhim. Intermet. Soedin., Lvov, p. 40.
Iandelli, A., 1983, J. Less-Common Metals **90**, 121.
Oesterreicher, H., 1976, Phys. Stat. Sol. (a) **34**, 723.
Padalia, B.D., T.K. Hatwar and M.N. Ghatikar, 1983, J. Phys. **C16**, 1537.
Rieger, W. and E. Parthé, 1969a, Monatsh. Chem. **100**, 439.
Rieger, W. and E. Parthé, 1969b, Monatsh. Chem. **100**, 444.
Sampathkumaran, E.V., L.C. Gupta and R. Vijayaraghavan, 1979, J. Phys. **C12**, 4323.
Szytula, A., W. Bazela and J. Leciejewicz, 1983, Solid State Commun. **48**(12), 1053.

Pr–Fe–Si

At least three ternary compounds have been reported for the Pr–Fe–Si system.

Mayer and Tassa (1969) investigated the phase equilibria at 700–$800\,°C$ along the concentration section $PrFe_xSi_{2-x}$. For $x < 0.4$ the $ThSi_2$-type structure was observed. $PrFe_{0.4}Si_{1.6}$ crystallizes with the AlB_2-type structure ($a = 4.041$, $c = 4.222$). In analogy to the X-ray powder data obtained from $NdFe_{0.4}Si_{1.6}$ a statistical distribution of Fe,Si atoms in the 2d sites of P6/mmm was assumed. For sample preparation, see $GdCo_{0.4}Si_{1.6}$.

According to an X-ray powder analysis by Bodak et al. (1970) PrFeSi was observed to crystallize with the PbFCl-type of structure [P4/nmm, $a = 4.072(3)$ and

$c = 6.927(5)$]. For sample preparation, see CeFeSi. At variance with this, Mayer and Felner (1973) obtained a compound PrFeSi, and from X-ray powder photographs assigned the orthorhombic "TiNiSi-type of structure". Their lattice parameters ($a = 11.13$, $b = 7.04$, $c = 5.30$), however, do not correspond to a TiNiSi-type unit cell. Samples were heated in an induction furnace at $\sim 1600\,°C$ in Al_2O_3 crucibles under argon. Thus the "TiNiSi-type" (?) phase very likely represents a high-temperature modification.

$PrFe_2Si_2$ is tetragonal with the ordered $ThCr_2Si_2$-type of structure: I4/mmm, $a = 4.005$, $c = 10.099$, $\rho_x = 6.33$ kg/dm^3 (Rossi et al., 1978; X-ray powder analysis). For sample preparation and etching conditions, see YCo_2Si_2. Felner et al. (1975) confirmed the structure type [$a = 4.018(5)$, $c = 10.06(5)$] and reported a weak ferromagnetic ordering at $T_m = 693(5)$ K from magnetic susceptibility data. From magnetization and Mössbauer effect measurements most of the iron was concluded to be diamagnetic ($\sim 94\%$).

References

Bodak, O.I., E.I. Gladyshevskij and P.I. Kripyakevich, 1970, Zh. Strukt. Khim. **11**(2), 305.
Felner, I., I. Mayer, A. Grill and M. Schieber, 1975, Solid State Commun. **16**, 1005.
Mayer, I. and I. Felner, 1973, J. Solid State Chem. **7**, 292.
Mayer, I. and M. Tassa, 1969, J. Less-Common Metals **19**, 173.
Rossi, R., R. Marazza and R. Ferro, 1978, J. Less-Common Metals **58**, 203.

Pr–Ge–Si

Structural behavior in the concentration section $PrGe_{2-x}Si_x$ has been investigated by Mayer and Eshdat (1968) on the basis of X-ray powder data. For sample preparation, see $NdGe_{2-x}Si_x$. Alloys with intermediate values of x were orthorhombic ($GdSi_2$-type, Imma), whereas $PrGe_2$ and the alloys at the Si-rich end
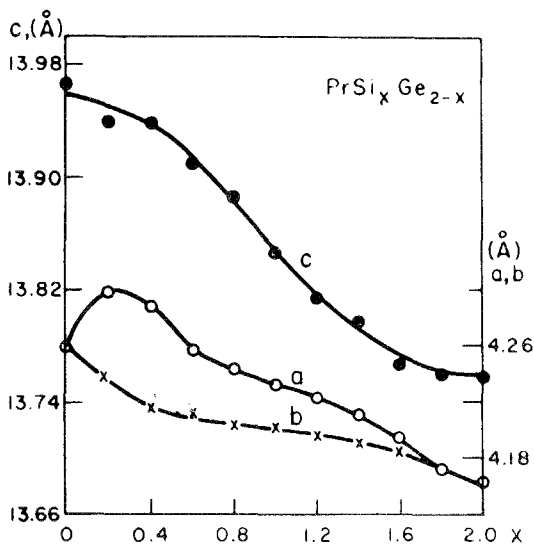
Fig. 38. Pr–Ge–Si, section $PrGe_{2-x}Si_x$, proposed lattice parameter variation versus concentration, after Mayer and Eshdat (1968).
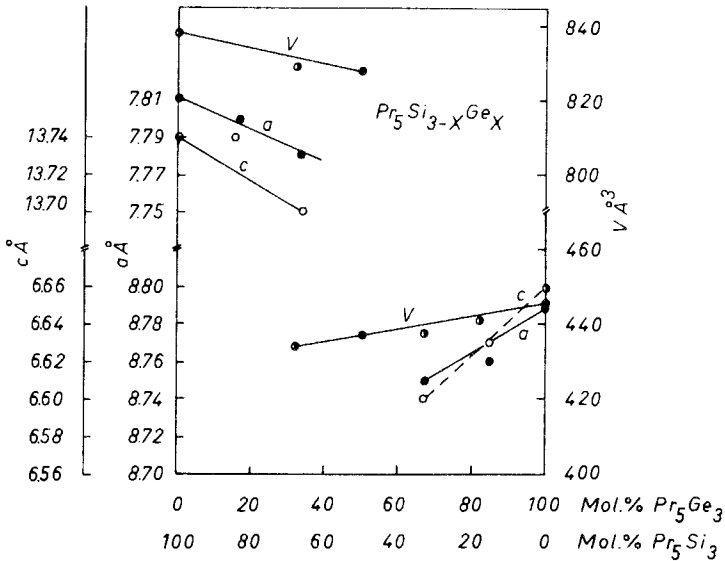
Fig. 39. Pr–Ge–Si, section $Pr_5Ge_{3-x}Si_x$, lattice parameters versus concentration, after Mayer and Tendy (1970).

crystallized with the $ThSi_2$-type ($I4_1/amd$). No discontinuity was observed for the variation of the lattice parameters versus x (fig. 38), and the unit cell volume was shown to change linearly with x (fig. 11). See also Muratova and Bodak (1974).

Mayer and Tendy (1970) studied the phase equilibria within the concentration section $Pr_5Si_{3-x}Ge_x$ (X-ray powder data). For sample preparation, see $La_5Si_{3-x}Ge_x$. The Mn_5Si_3-type of structure ($P6_3/mcm$) was observed to be stable in the range $2 < x \leqslant 3$, whereas the Cr_5B_3-type ($I4/mcm$) was stable for $0 \leqslant x < 1$. Alloys with intermediate values of x were said to be two-phase. Lattice parameters versus x are presented in fig. 39.

References

Mayer, I. and Y. Eshdat, 1968, Inorg. Chem. 9, 1904.
Mayer, I. and S. Tendy, 1970, Israel. J. Chem. 8, 955.
Muratova, L.O. and O.I. Bodak, 1974, Tesizy Dokl. Tret. Vses. Konf. Kristallokhim. Intermet. Soedin, 2nd Ed., ed. R.M. Rykhal (Lvov Gos. Univ., Lvov, USSR) p. 33.

Pr–Mn–Si

So far only two ternary compounds have been characterized in the system Pr–Mn–Si.

$PrMn_2Si_2$ crystallizes with the $ThCr_2Si_2$-type structure: $I4/mmm$, $a = 4.025$, $c = 10.555$; $\rho_x = 5.96$ kg/dm³ (Rossi et al., 1978; X-ray powder analysis). For sample preparation, see $LaMn_2Si_2$. From X-ray powder diffraction Knigenko et al. (1977) reported similar values: $a = 4.022$ and $c = 10.530$. For sample preparation, see Y–Mn–Si.

Siek et al. (1981) and Narasimhan et al. (1976) studied the crystallographic and magnetic properties of $PrMn_2Si_2$ by means of powder X-ray, neutron diffraction and magnetometric measurements. For sample preparation, see YMn_2Si_2. From X-ray and neutron data complete ordering was observed for Mn in the 4d and Si in 4e the sites of I4/mmm. Structural and magnetic parameters are listed in table 16. No magnetic ordering on the Pr sublattice was observed at low temperatures. The magnetic behavior is characterized by $T_N = 348$ K, $\mu_{eff} = 5.1$ μ_B mole^{-1} and $\theta_p = 290$ K. From X-ray powder data Narasimhan et al. (1976) reported $a = 4.031(5)$ and $c = 10.559(5)$. For sample preparation, see Y–Mn–Si.

PrMnSi is tetragonal with the PbFCl-type structure P4/nmm, $a = 4.097$, $c = 7.256$ (Knigenko et al., 1977; X-ray powder methods). For sample preparation, see Y–Mn–Si.

References

Knigenko, L.D., I.R. Mokra and O.I. Bodak, 1977, Vestn. Lvov Univ., Ser. Khim. **19**, 68.
Narasimhan., K.S.V.L., V.U.S. Rao and W.E. Wallace, 1976, AIP Conf. Proc. **29**, 594.
Rossi, D., R. Marazza, D. Mazzone and R. Ferro, 1978, J. Less-Common Metals **59**, 79.
Siek, S., A. Szytula and J. Leciejewicz, 1981, Solid State Commun **39**, 863; see also Szytula, A. and I. Szott, 1981, Solid State Commun. **40**, 199.

Pr–Ni–Si

At least fourteen ternary compounds have been identified in the system Pr–Ni–Si (see table 21), but no ternary phase diagram exists.

TABLE 21
Formation and structural data of ternary compounds Pr–Ni–Si.

Compound	Structure type Space group	Lattice parameters Density	Preparation, Characterization	Refs.	Purity
$Pr_2(Ni,Si)_{17}$ $(Pr_2Ni_{15}Si_2)$	Th_2Ni_{17} $P6_3/mmc$	$a = 8.399(4)$ $c = 8.089(4)$	arc, PXD see $Ce_2Ni_{15}Si_2$	GIKB, 66 GIKB, 67	Pr 98.0 Ni 99.99 Si 99.99
$Pr_3Ni_6Si_2$	$Ce_3Ni_6Si_2$ (ord. Ca_3Ag_8) Im3m	$a = 8.976(2)$	arc, Qu(Ni) 800 °C, 2 weeks PXD	GIKB, 66	Pr 98.0 Ni 99.99 Si 99.99
$PrNi_{8.6}Si_{2.4}$	$Ce_2Ni_{17}Si_5$ $(BaCd_{11})$ $I4_1/amd$	$a = 9.817(5)$ $c = 6.249(10)$	arc(Ar), Qu 800 °C, 250 h, PXD atom order as for $CeNi_{8.6}Si_{2.4}$	BoG, 69a	Pr 99.7 Ni 99.91 Si 99.99
$Pr_5Ni_2Si_3$ (quoted as Pr_2NiSi)	$Ce_5Ni_2Si_3$ filled $Rh_{20}Si_{13}$ $P6_3/m$	$a = 16.05(1)$ $c = 4.302(5)$	arc(Ar) PXD	BoGM, 72	Ni 99.98 Si 99.99
$Pr_6Ni_2Si_3$	$Ce_6Ni_2Si_3$ filled Ho_4Co_3 $P6_3/m$	$a = 12.005(5)$ $c = 4.273(2)$	no details PXD	BoGK, 74	

TABLE 21 (continued)

Compound	Structure type Space group	Lattice parameters Density	Preparation, Characterization	Refs.	Purity
PrNi$_{8.6}$Si$_{4.4}$ [*] 30 a/o Si	Ce$_2$Ni$_{17}$Si$_9$ (NaZn$_{13}$-deriv.) I4/mcm	$a = 11.09(1)$ [*] $c = 11.43(1)$	arc(Ar), Qu 800 °C, 100 h PXD	BoG, 69b	Pr 99.2 Ni 99.99 Si 99.99
Pr(Ni,Si)$_{13}$ 37–45 a/o Si	NaZn$_{13}$ Fm3c	$a = 11.19(1)$	arc(Ar), Qu 800 °C, 100 h PXD	BoG, 69b	Pr 99.2 Ni 99.99 Si 99.99
PrNiSi [**]	(ThSi$_2$) [**]	$a = 4.109(5)$ $c = 13.970(5)$	induction melting at ~1600 °C (Ar) in Al$_2$O$_3$ 30 min, 1600 °C, PXD, refinement: $R = 0.29$	MaF, 73	99.9
Pr$_{14}$Ni$_6$Si$_{11}$	Pr$_{14}$Ni$_6$Si$_{11}$ C2/m	$a = 33.991(3)$ $b = 4.2328(4)$ $c = 21.330(3)$ $\beta = 113.72(1)°$ $\rho_x = 6.226$	arc(Ar), Qu(Ta) 800 °C, 2 weeks single crystal study $R = 0.072$	HoKP, 83	Pr 99.9 Ni 99.99 Si 5N
Pr$_7$Ni$_2$Si$_5$	Ce$_7$Ni$_2$Si$_5$ Pnma	$a = 23.32$ $b = 4.302$ $c = 13.84$	arc(Ar) PXD	MiBG, 74	
PrNi$_2$Si$_2$	ThCr$_2$Si$_2$ I4/mmm	$a = 4.043(10)$ $c = 9.619(10)$	arc(Ar) PXD	BoGK, 66	Pr 98.08 Ni 99.8 Si 99.99
Pr$_{15}$Ni$_4$Si$_{13}$	Ce$_{15}$Ni$_4$Si$_{13}$ P6$_3$/m	$a = 20.19$ $c = 4.297$	arc(Ar) PXD	Mi, 73	Ni 99.5 Si 99.99
PrNiSi$_2$	CeNiSi$_2$ Cmcm	$a = 4.126(2)$ $b = 16.470(10)$ $c = 4.032(2)$	arc(Ar) PXD	BoG, 69c	Pr 98.08 Ni 99.8 Si 99.99
Pr(Ni,Si)$_2$	AlB$_2$ P6/mmm	$a = 4.021(5)$ $c = 4.025(5)$ at compos. PrNi$_{0.5}$Si$_{1.5}$	induction melting ~1600 °C, Ar, in Al$_2$O$_3$, annealed for 30 min at ~1600 °C PXD	MaT, 69	Pr 99.9 Ni 99.95 Si 99.99
		$a = 4.050(5)$ $c = 4.181(5)$ at compos. PrNi$_{0.75}$Si$_{1.25}$		MaF, 73	99.9
		$a = 4.045(5)$ $c = 4.226(5)$	arc(Ar) Qu, 800 °C, 100 h PXD	GlB, 65	Ni 99.8 Si 99.99

[*] For a correct setting of the bct-unit cell, $a = 7.842$ ($a = a_0/\sqrt{2}$).

[**] A ThSi$_2$-type of structure (I4$_1$/amd) was claimed by Mayer and Felner (1973) from a refinement of X-ray powder data. The reliability value $R = 0.29$ was in favor of an ordered Ni/Si distribution; however, agreement was rather poor, thus the actual structure type might be better represented by the LaPtSi-type (ThSi$_2$-derivative structure, I4$_1$md; see LaPtSi).

Mayer and Tassa (1969) and Mayer and Felner (1973) studied the phase equilibria within the concentration section $PrNi_xSi_{2-x}$, by means of X-ray powder diffraction methods. For sample preparation, see $ErNi_xSi_{2-x}$. $PrSi_2$ [$a = 4.290(5)$, $c = 13.760(6)$] and $PrNi_{0.25}Si_{1.75}$ [$a = 4.187(5)$, $c = 13.846(5)$] were claimed to be tetragonal with the $ThSi_2$-type of structure and space group $I4_1/amd$. At higher Ni concentrations ($0.5 \leqslant x \leqslant 0.75$) the AlB_2-type was found to be stable (see table 21). PrNiSi was claimed to be isotypic with the α-$ThSi_2$-type, but more likely crystallizes with the LaPtSi-type of structure. The alloy $PrNi_{1.25}Si_{0.75}$ was two-phase, containing an unknown tetragonal second phase ($a = 7.18$, $c = 8.71$). $PrNi_{1.75}Si_{0.25}$ was hexagonal with the $MnZn_2$-type [$a = 5.227(5)$, $c = 7.709(5)$], probably stabilized from the Pr–Ni binary by additions of Si. $PrNi_2$ is cubic with the $MgCu_2$-type ($a = 7.284$).

The electrophysical properties of $PrNi_2Si_2$ were reported by Levin et al. (1977), including the temperature dependence of the electrical resistance, the thermoelectrical coefficient, magnetic susceptibilities as well as the preparation of stoichiometric thin films.

References
Bodak, O.I. and E.I. Gladyshevskij, 1969a, Dopov. Akad. Nauk Ukr. RSR, Ser. A 5, 452.
Bodak, O.I. and E.I. Gladyshevskij, 1969b, Dopov. Akad. Nauk Ukr. RSR, Ser. A 12, 1125.
Bodak, O.I. and E.I. Gladyshevskij, 1969c, Kristallographiya 14(6), 990.
Bodak, O.I., E.I. Gladyshevskij and M.G. Miskiv, 1972, Sov. Phys. Crystallogr. 17(3), 439.
Bodak, O.I., E.I. Gladyshevskij and P.I. Kripyakevich, 1966, Izv. Akad. Nauk SSSR, Neorg. Mater. 2(12), 2151.
Bodak, O.I., E.I. Gladyshevskij and O.I. Kharchenko, 1974, Sov. Phys. Crystallogr. 19(1), 45.
Gladyshevskij, E.I. and O.I. Bodak, 1965, Dopov. Akad. Nauk RSR, Ser. A, 601.
Gladyshevskij, E.O., P.I. Kripyakevich and O.I. Bodak, 1966, Acta Crystallogr. A21, 80, and Z. Anorg. Allg. Chem. 344, 95.
Gladyshevskij, E.I., P.I. Kripyakevich and O.I. Bodak, 1967, Visn. L'vivsk. Derzh. Univ., Ser. Khim. 9, 34.
Hovestreydt, E., K. Klepp and E. Parthé, 1983, Acta Crystallogr. B 39, 422.
Levin, E.M., R.V. Lutsiv, E.I. Gladyshevskij and O.I. Bodak, 1977, Fiz. Elektron. Resp. Mezhved. Nauch-tekhn. Sbor. 15, 59.
Mayer, I. and I. Felner, 1973, J. Solid State Chem. 7, 292.
Mayer, I. and M. Tassa, 1969, J. Less-Common Metals 19, 173.
Mis'kiv, M.G., 1973, Thesis, Lvov, USSR.
Mis'kiv, M.G., O.I. Bodak and E.I. Gladyshevskij, 1974, Tesizy Dokl. Tret. Vses. Konf. Kristallokhim. Intermet. Soedin, 2nd Ed., ed. R.M. Rykhal (Lvov Gos. Univ., Lvov, USSR) p. 32.

Pr–Os–Si

$PrOs_2Si_2$ is tetragonal with space group $I4/mmm$ and the $ThCr_2Si_2$-type of structure (Hiebl et al., 1983; X-ray powder analysis). The lattice parameters were $a = 4.1711(4)$ and $c = 9.9151(26)$. For sample preparation, see YOs_2Si_2. $PrOs_2Si_2$ is paramagnetic above $T = 300$ K with $\mu_{eff}^{para} = 3.53$ μ_B and $\theta_p = 53$ K. Ferromagnetic order exists below 12.6 K.

Reference
Hiebl, K., C. Horvath, P. Rogl and M.J. Sienko, 1983, Solid State Commun. 48, 211.

Pr–Pd–Si

PrPd$_2$Si adopts the ordered Fe$_3$C-type: Pnma, $a = 7.561(3)$, $b = 6.885(2)$ and $c = 5.672(3)$ (X-ray powder analysis). For sample preparation, see YPd$_2$Si (Moreau et al., 1982).

PrPd$_2$Si$_2$ crystallizes with the ordered ThCr$_2$Si$_2$-type structure: I4/mmm, $a = 4.198$, $c = 9.97$ (Ballestracci, 1976; X-ray powder diffraction). For sample preparation, see CePd$_2$Si$_2$.

References
Ballestracci, R., 1976, C.R. Ac. Sci. Paris, Ser. B **282**, 291.
Moreau, J., J. Leroy and D. Paccard, 1982, Acta Crystallogr. **B38**, 2446.

Pr–Pt–Si

According to X-ray powder diffraction data by Klepp and Parthé (1982) PrPtSi crystallizes with the LaPtSi-type structure with space group I4$_1$md and lattice parameters $a = 4.1797(7)$ and $c = 14.458(3)$. For sample preparation, see LaPtSi; congruent melting behavior is indicated.

PrPt$_2$Si$_2$ crystallizes with the primitive tetragonal CePt$_2$Si$_2$-type, $a = 4.2453(12)$, $c = 9.7866(34)$ (Rogl, 1984).

Reference
Klepp, K. and E. Parthé, 1982, Acta Crystallogr. **B38**, 1105.
Rogl, P., 1984, Inorg. Chem., to be published.

Pr–Re–Si

According to X-ray powder diffraction data by Bodak et al. (1978) Pr$_2$Re$_3$Si$_5$ adopts the Sc$_2$Fe$_3$Si$_5$-type structure with the space group P4/mnc and lattice patameters $a = 11.00(1)$ and $c = 5.684(5)$. The alloys were arc melted but no detailed conditions of heat treatment were given; Segre (1981) confirmed the structure type, but measured considerably different lattice parameters: $a = 10.98(1)$ and $c = 5.675(8)$. Samples were in as-cast condition; $T_n = 1.2$ K.

PrRe$_4$Si$_2$ is isostructural with the CeRe$_4$Si$_2$-type structure: Cmmm, $a = 4.28(1)$, $b = 13.62(1)$ and $c = 4.09(1)$ (Bodak et al., 1977; X-ray powder analysis of arc-melted samples).

References
Bodak, O.I., E.I. Gladyshevskij and V.K. Pecharskij, 1977, Kristallografiya **22**(1), 178.
Bodak, O.I., V.K. Pecharskij and E.I. Gladyshevskij, 1978, Izv. Akad. Nauk SSSR, Neorg. Mater. **14**(2), 250.
Segre, C.U., 1981, Thesis, Univ. of Calif., San Diego, USA.

Pr–Rh–Si

PrRh$_2$Si$_2$ is isotypic with the crystal structure of ThCr$_2$Si$_2$ (space group I4/mmm). The unit cell parameters as reported from an X-ray powder analysis by Ballestracci (1976) were: $a = 4.081$, $c = 10.15$. For sample preparation, see YRh$_2$Si$_2$.

Reference
Ballestracci, R., 1976, C.R. Acad. Sci. Paris, Ser. B **282**, 291.

Pr–Ru–Si

The existence of a phase $PrRu_3Si_2$ with the $LaRu_3Si_2$-type structure was reported by Barz (1980). No crystal data have been presented. For sample preparation and melting behavior (phase equilibria), see also $LaRu_3Si_2$.

According to an X-ray powder diffraction analysis of arc-melted and heat-treated alloys by Hiebl et al. (1983) $PrRu_2Si_2$ crystallizes with the $ThCr_2Si_2$-type structure. The space group is I4/mmm and the lattice parameters are: $a = 4.1945(4)$ and $c = 9.7779(37)$. For sample preparation, see YOs_2Si_2. The magnetic behavior has been investigated for the temperature region 1.5 K $< T < 1100$ K and is characterized by the following data: $\mu_{\text{eff}}^{\text{para}} = 3.49$ μ_B, $\theta_p = 46.8$ K and ferromagnetic ordering at 17.8 K.

References
Barz, H., 1980, Mater. Res. Bull. **15**, 1489.
Hiebl, K., C. Horvath, P. Rogl and M.J. Sienko, 1983, J. Magn. Magn. Mater. **37**, 287.

Pr–Sc–Si

PrScSi is isotypic with the structure type CeScSi. The crystallographic data as presented by Mokra and Bodak (1979) were derived by means of X-ray powder diffraction: ordered Ca_2As-type, I4/mmm, $a = 4.292(5)$, $c = 15.78(2)$. For sample preparation, see CeScSi.

Reference
Mokra, I.P. and O.I. Bodak, 1979, Dopov. Akad. Nauk Ukr. RSR, Ser. A, 312.

Sc–Co–Si

A partial isothermal section of the Sc-poor region (0–67 a/o Sc) has been investigated by Kotur et al. (1977) by means of X-ray powder and metallographic analysis of arc-melted samples, which were then annealed at 800°C and some of them at 700°C. Starting materials were 99.9% pure.

So far three binary Sc silicides have been widely accepted in the literature: Sc_5Si_3 with the Mn_5Si_3-type, ScSi with CrB-type and Sc_3Si_5 or Sc_2Si_3 with a defect AlB_2-type of structure (high temperature form ?). Sc_3Si_5 was not observed at 800°C by Kotur et al. (1977). The binary Sc cobalt compounds were confirmed [$ScCo_2$(MgCu$_2$-type), ScCo(CsCl-type) and Sc_2Co(CuAl$_2$-type, Imcm, $a = 6.370(4)$, $c = 5.618(4)$]. The Sc_2Co modification with the Ti_2Ni-type of structure probably is metastable in the Sc–Co binary system, but is easily stabilized by small amounts of Si (see also table 22). The binary cobalt silicides are discussed in context with the system Ce–Co–Si.

TABLE 22

Formation and structural data or ternary compounds Sc–Co–Si.

Compound	Structure type Space group	Lattice parameters Density	Preparation, Characterization	Refs.	Purity
$ScCo_{0.25}Si_{1.75}$ [*]	$ZrSi_2$ Cmcm	$a = 3.856(3)$ $b = 14.54(1)$ $c = 3.744(3)$	arc(Ar), 800 °C $H = 884 \ (\pm 50) \ kg/mm^2$ single crystal data	KoBG, 77 KoB, 77 KoB, 80	99.9
$Sc_5Co_4Si_{10}$ [**]	$Sc_5Co_4Si_{10}$ P4/mbm	$a = 12.01(1)$ $c = 3.936(5)$ $\rho_E = 4.33(1)$ $\rho_x = 4.34(1)$	arc(Ar); slowly cooled from 1700 to 1100 K (6 K h^{-1}) $T_c = 5.0–4.8$ K Co atoms carry no magnetic moment	BrYB, 80 BrS, 80 BrS, 81	99.9
		$a = 11.846$ $c = 3.949$ (for compos. $Sc_3Co_2Si_5$)	arc(Ar), 800 °C, PXD $H = 1061 \ (\pm 50) \ kg/mm^2$	KoBG, 77 KoB, 80	99.9
$Sc_2Co_3Si_5$	$U_2Co_3Si_5$ Ibam	$a = 9.206$ $b = 11.26$ $c = 5.320$	arc(Ar), 800 °C $H = 1122 \ (\pm 50) \ kg/mm^2$ PXD	KoBG, 77	99.9
		$a = 9.206$ $b = 11.30$ $c = 5.348$		KoB, 80	
Sc_2CoSi_2	Sc_2CoSi_2 C2/m	$a = 9.74(1)$ $b = 3.954(3)$ $c = 9.82(1)$ $\beta = 122.6°$ $\rho_E = 4.15$	arc(Ar), 800 °C refined from single crystal photographs, $R = 0.098$ $H = 962 \ (\pm 50) \ kg/mm^2$	GlK, 78 KoB, 80 KoBG, 77	Sc 99.9 Co 99.92 Si 99.99
$ScCo_2Si_2$	$ThCr_2Si_2$ I4/mmm	$a = 3.72$ $c = 9.51$	arc(Ar), 800 °C, PXD $H = 1237 \ (\pm 50) \ kg/mm^2$	KoBG, 77 KoB, 80	99.9
$Sc_3Co_2Si_3$	$Sc_3Co_2Si_3$ Cmcm	$a = 3.996(3)$ $b = 9.815(10)$ $c = 12.670(10)$ $\rho_E = 4.40$	arc(Ar), 800 °C refined from single crystal photographs $R = 0.104$ $H = 1130 \ (\pm 50) \ kg/mm^2$	GlK, 78 KoB, 80 KoBG, 77	Sc 99.9 Co 99.92 Si 99.99 99.9
$Sc_4Co_{14}Si_9$	Hexagonal	$a = 10.16$ $c = 3.614$	arc(Ar), 800 °C, PXD $H = 1616 \ (\pm 50) \ kg/mm^2$	KoBG, 77 KoB, 80	99.9
$ScCo_7Si_4$	$P\bar{6}$	$a = 14.62$ $c = 3.610$	arc(Ar), 800 °C, PXD $H = 1446 \ (\pm 50) \ kg/mm^2$	KoBG, 77 KoB, 80	99.9
ScCoSi	TiNiSi Pnma	$a = 6.419(5)$ $b = 3.953(3)$ $c = 6.896(5)$	arc(Ar), 800 °C, PXD $H = 761 \ (\pm 50) \ kg/mm^2$	KoB, 77 KoBG, 77 KoB, 80	99.9
$Sc_6Co_{16}Si_7$	$Mg_6Cu_{16}Si_7$ Fm3m	$a = 11.438$	arc(Ar), 800 °C, PXD $H = 1114 \ (\pm 50) \ kg/mm^2$ arc(Ar), 900 °C, PXD	KoBG, 77 KoB, 80 DwCD, 63	99.9

<div align="center">TABLE 22 (continued)</div>

Compound	Structure type Space group	Lattice parameters Density	Preparation, Characterization	Refs.	Purity
Sc_2Co_3Si [+]	Mg_2Cu_3Si ($MgZn_2$) $P6_3/mmc$	$a = 4.947$ $c = 7.892$	arc(Ar), 800 °C, PXD $H = 1324$ (± 50) kg/mm^2 PXD	KoBG, 77 KoB, 80 Ko, 77	
$Sc_2Co_{0.85}Si_{0.15}$	Ti_2Ni $Fd3m$	$a = 12.099$	arc(Ar), 800 °C, PXD $H = 705$ (± 50) kg/mm^2	KoBG, 77	99.9

[*] The crystal structure of $ScCo_{0.25}Si_{1.75}$ (ZrSi$_2$-type) has been refined from X-ray single crystal photographs; $R = 0.138$. The single crystal specimen was obtained from an arc-melted alloy of composition (in a/o) $Sc_{33}Co_8Si_{59}$. Atom ordering and parameters were Sc in 4c) 0, 0.104, 1/4; Co + 3 Si in 4c) $y = 0.445$; Si in 4c) $y = 0.745$ (Kotur and Bodak, 1977).

[**] The crystal structure of $Sc_5Co_4Si_{10}$ has been refined from X-ray single crystal counter data, $R = 0.04$. From space group as well as lattice parameters $Sc_5Co_4Si_{10}$ seems to be identical with the compound observed at the composition $Sc_3Co_2Si_5$ by Kotur et al. (1977).

[+] The crystal structure of Sc_2Co_3Si has been refined from X-ray powder diffraction data: Sc in 4f; Co in 6h; Si in 2a. Lattice parameters within the homogeneity range at 800 °C (350 h) were found to vary from $a = 4.935$, $c = 7.915$ for 16.2 a/o Si to $a = 4.972$, $c = 7.83$ at 18 a/o Si (as read from a graph) (Kotur, 1977).
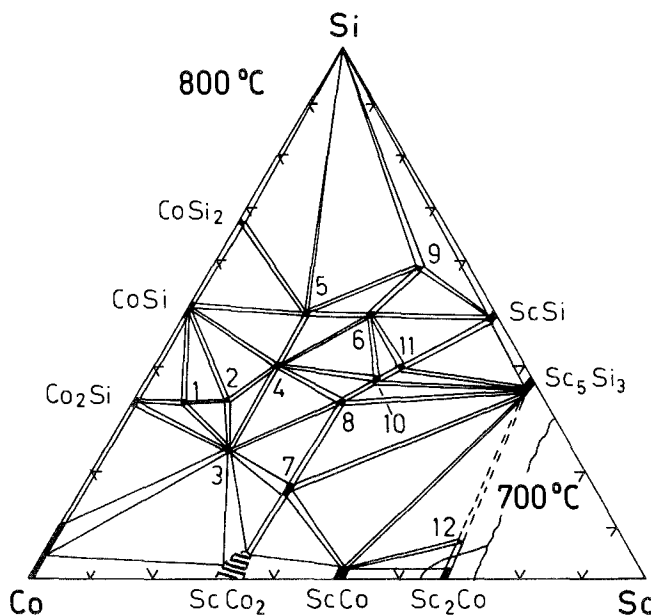
Fig. 40. Sc–Co–Si, partial isothermal sections at 800°C (0–60 a/o Sc) and at 700°C (60–70 a/o Sc). 1: $ScCo_7Si_4$, 2: $Sc_4Co_{14}Si_9$, 3: $Sc_6Co_{16}Si_7$, 4: $ScCo_2Si_2$, 5: $Sc_2Co_3Si_5$, 6: "$Sc_3Co_2Si_5$" (probably identical with the later independently derived $Sc_5Co_4Si_{10}$-type), 7: Sc_2Co_3Si, 8: ScCoSi, 9: $ScCo_{0.25}Si_{1.75}$, 10: $Sc_3Co_2Si_3$, 11: Sc_2CoSi_2, 12: $Sc_2Co_{0.85}Si_{0.15}$.

A small ternary homogeneous range was observed for $ScCo_2$ with the $MgCu_2$-type, which dissolves up to 6 a/o Si, and similarly ~ 3.5 a/o Co is dissolved in Sc_5Si_3. Twelve ternary compounds were found to exist (see table 22). For a listing of Sc–Co silicides, see also Kotur and Bodak (1980). Phase equilibria as shown in fig. 40, are mainly based upon the work of Kotur et al. (1977), Braun et al. (1980) and Braun and Segre (1980).

References

Braun, H.F. and C.U. Segre, 1980, Solid State Commun. **35**, 735.

Braun, H.F. and C.U. Segre, 1981, in: Ternary Superconductors, Proc. Conf. on Ternary Superconductors, Lake Geneva, WI, USA, eds. G.K. Shenoy, B.D. Dunlap and F.Y. Fradin (North-Holland, Amsterdam) p. 239.

Braun, H.F., K. Yvon and R.M. Braun, 1980, Acta Crystallogr. **B36**, 2397.

Dwight, A.E., R.A. Conner, Jr. and J.W. Downey, 1963, Nature **9**, 587.

Gladyshevskij, E.I. and B.Ya. Kotur, 1978, Sov. Phys. Crystallogr. **23**, 533.

Kotur, B.Ya., 1977, Dopov. Akad. Nauk Ukr. RSR, Ser. A, 164.

Kotur, B.Ya. and O.I. Bodak, 1977, Sov. Phys. Crystallogr. **22**(6), 687.

Kotur, B.Ya. and O.I. Bodak, 1980, Izv. Akad. Nauk SSSR, Neorg. Mater. **16**(3), 459.

Kotur, B.Ya., O.I. Bodak and E.I. Gladyshevskij, 1977, Dopov. Akad. Nauk Ukr. RSR., Ser. A, 664.

Sc–Cr–Si

$Sc_2Cr_4Si_5$ crystallizes with the $Nb_2Cr_4Si_5$-type structure [ordered V_6Si_5-type, Ibam, $a = 7.585(3)$, $b = 16.138(5)$, $c = 4.932(2)$]. The crystal structure has been refined from single crystal counter data, $R = 0.060$. Atomic parameters were: Sc in 8j) 0.1181(5), 0.1421(2), 0; Cr in 8j) 0.2460(5), 0.4380(2), 0; Cr in 8g) 0, 0.3093(2), 1/4; Si in 8j) 0.2947(8), 0.2888(4), 0; Si in 8j) 0.4223(8), 0.0638(4), 0; Si in 4a) 0, 0, 1/4. Practically no homogeneous region (at 800°C) was observed from X-ray powder diffraction and metallographic analysis (Kotur and Sikirica, 1982).

Reference

Kotur, B.Ya. and M. Sikirica, 1982, J. Less-Common Metals **83**, L29.

Sc–Cu–Si

At least five ternary compounds have been reported in the Sc–Cu–Si system. Alloys with Si and Cu contents in the range of 20–35 a/o have been investigated by Kotur et al. (1981). Samples were prepared by arc melting under argon and subsequent homogenizing at 800°C for 750 h in evacuated silica tubes. Starting materials were Sc 99.92: and Si, Cu 99.99%. Two structure types, ZrNiAl and TiNiSi, were observed from X-ray powder analysis; the compositions of both phases, coexisting at 800°C, were found to be close to 1:1:1. No phase transition with temperature was observed. ScCuSi with the ZrNiAl-type of structure [ordered Fe_2P-type, P$\bar{6}$2m, $a = 6.426(1)$, c = 3.922(1)] was obtained after heat treatment only (low-temperature phase?) and from alloys with up to 33 a/o Si in equilibrium with $ScCu_2$. Atomic positions and atom ordering were refined from X-ray powder diffraction data: Sc in 3g) 0.574, 0, 1/2; Cu in 3f) 0.241, 0, 0; Si in 1b) and 2c); the

reliability value obtained was $R = 0.149$. From arc-melted alloys homogenized at 900°C in evacuated silica tubes Dwight et al. (1973) reported $a = 6.44$, $c = 3.92$; Kotur and Bodak (1980) listed $a = 6.418$ and $c = 3.929$. ScCuSi with the TiNiSi-type of structure [Pnma, $a = 6.566(3)$, $b = 3.976(2)$, $c = 7.224(2)$] was obtained by Kotur et al. (1981) in as-cast and heat-treated alloys with 35 a/o Si. The crystal structure has been refined from single crystal counter data; all atoms were found in the 4c sites of Pnma: Sc, 0.5089(4), 1/4, 0.3046(5); Cu, 0.1576(3), 1/4, 0.5665(3) and Si, 0.7702(6), 1/4, 0.6097(7); $R = 0.059$.

Without detailed information a compound $Sc_2(Cu,Si)$ with the Ti_2Ni-type structure (Fd3m, $a = 12.32$) was listed by Kotur and Bodak (1980).

$Sc_3Cu_4Si_4$ crystallizes with the $Gd_3Cu_4Ge_4$-type structure: Immm, $a = 13.09$, $b = 6.42$ and $c = 3.94$ (Hanel and Nowotny, 1970; powder X-ray analysis of samples, arc melted under argon and heat-treated in evacuated silica tubes at 1200°C for 70 h or at 950°C for 250 h). From microprobe analysis a small Cu/Si exchange was indicated (~ 3 a/o Cu replaced by Si). In good agreement Kotur and Bodak (1980) measured $a = 13.096$, $b = 6.411$ and $c = 3.945$.

$ScCu_2Si_2$ is tetragonal with the $ThCr_2Si_2$-type: I4/mmm, $a = 3.815$ and $c = 10.09$. The composition was determined from microprobe analysis (Hanel, 1970).

References

Dwight, A.E., W.C. Harper and C.W. Kimball, 1973, J. Less-Common Metals **30**, 1.
Hanel, G., 1970, Thesis, Univ. of Vienna, Austria.
Hanel, G. and H. Nowotny, 1970, Monatsh. Chem. **101**, 463.
Kotur, B.Ya. and O.I. Bodak, 1980, Izv. Akad. Nauk Ukr. SSR, Neorg. Mater. **16**, 459.
Kotur, B.Ya., E.I. Gladyshevskij and M. Sikirica, 1981, J. Less-Common Metals **81**, 71.

Sc–Fe–Si

Gladyshevskij et al. (1977) attempted to investigate the phase equilibria in the system Sc–Fe–Si within an isothermal section at 800°C by means of X-ray and metallographic analysis of 256 alloys. Samples were prepared by arc melting and subsequent annealing in evacuated silica tubes (750 h at 800°C). Starting materials were Sc 99.96%, Fe 99.96% and Si 99.99%. The existence of Sc_3Fe at 800°C was not confirmed and mutal solid solubilities were observed to be rather small. Gladyshevskij et al. (1977) identified 14 ternary compounds within the section at 800°C, but with more recent data by Chabot (1982) and Chabot et al. (1984), the number of ternary compounds is certainly higher (see table 23). As for the different conditions of preparation, some of the newly discovered phases, e.g. $Sc_4Fe_4Si_7$, probably exist as high-temperature phases only. "$Sc_3Fe_3Si_4$" (unknown structure type, Gladyshevskij et al., 1977) is possibly identical with either ScFeSi (TiNiSi-type, Chabot et al., 1984) or, less likely, with $Sc_4Fe_4Si_7$ ($Zr_4Co_4Si_7$-type; Chabot, 1982). Structural data of some of the Sc–Fe silicides were also listed by Kotur and Bodak (1980).

Small amounts of Sc (~ 3 a/o Sc) stabilize the binary Fe_5Si_3 phase with Mn_5Si_3-type at 800°C, and similarly the high-temperature cubic Laves phase $ScFe_2$ with $MgCu_2$-type was found to be stabilized by small amounts of Si at a composition (in a/o) $Sc_{35}Fe_{63}Si_2$, corresponding to the formula $Sc(Sc_{0.026}Fe_{0.945}Si_{0.029})_2$ (Gladyshevskij et al., 1977).

TABLE 23

Formation and structural data of ternary compounds Sc–Fe–Si

Compound	Structure type Space group	Lattice parameters Density	Preparation, Characterization	Refs.	Purity
$Sc(Sc_{0.03}$ $Fe_{0.786}$ $Si_{0.184})_{12}$ [+]	$ThMn_{12}$ I4/mmm	$a = 8.304(4)$ $c = 4.716(2)$ $\rho_E = 6.38,$ $\rho_x = 6.39$	arc, Qu, 800 °C 750 h, single crystal data $H = 1237\ (\pm 50)\ kg/mm^2$	Ko, 77a GlKBS, 77	Sc 99.9 Fe 99.96 Si 99.99
$Sc(Sc,Fe,Si)_2$	$MgCu_2$ Fd3m	$a = 7.038$	arc, Qu, 800 °C, 750 h, PXD $H = 1071\ (\pm 50)\ kg/mm^2$	GlKBS, 77	Sc 99.96 Fe 99.96 Si 99.99
Sc_2Fe_3Si small homo- geneous range 16.5–19.2 a/o Si	Mg_2Cu_3Si $P6_3/mmc$	$a \sim 4.972$ $c \sim 8.060$ at 19.2 a/o Si	arc, Qu, 800 °C 350 h, PXD	Ko, 77b	99.92
		$a \sim 4.962$ $c \sim 8.079$ at 16.5 a/o Si	$H = 1389\ (\pm 50)\ kg/mm^2$	GlKBS, 77	Sc 99.96 Fe 99.96 Si 99.99
$ScFe_4Si_2$	$ZrFe_4Si_2$ $P4_2/mnm$	$a = 6.947$ $c = 3.796$	arc, Qu, 800 °C 750 h, PXD, $R = 0.089$ $H = 962\ (\pm 50)\ kg/mm^2$	GlKBS, 77	Sc 99.96 Fe 99.96 Si 99.99
ScFeSi	TiNiSi Pnma	$a = 6.519(2)$ $b = 3.846(2)$ $c = 7.298(2)$ $\rho_x = 4.679$	arc, and 800 °C, 7 d single crystal data $R = 0.062, T_n = 1\ k$	ChEP, 84	Sc 99.999 Fe 99.999 Si 99.999
$ScFe_5Si_3$	unknown		arc, Qu, 800 °C 750 h, PXD $H = 833\ (\pm 50)\ kg/mm^2$	GlKBS, 77	Sc 99.96 Fe 99.96 Si 99.99
$(Sc_{0.07}$ $Fe_{0.93})_5Si_3$	Mn_5Si_3 $P6_3/mcm$	$a = 6.763$ $c = 4.718$	arc, Qu, 800 °C 750 h, PXD $H = 978\ (\pm 50)\ kg/mm^2$	GlKBS, 77	Sc 99.96 Fe 99.96 Si 99.99
$Sc_3Fe_2Si_3$ (high-temp. phase ?)	$Hf_3Ni_2Si_3$ (Cmcm)	$a = 3.966(1)$ $b = 9.971(2)$ $c = 12.947(5)$ $\rho_x = 4.292$	arc, and 800 °C, 7 d single crystal data $R = 0.047$	ChEP, 84	Sc 99.999 Fe 99.999 Si 99.999
Sc_2FeSi_2	Sc_2CoSi_2 C2/m	$a = 9.916(2)$ $b = 3.9912(7)$ $c = 9.414(3)$ $\beta = 118.15(2)°$ $\rho_x = 4.085$	arc, Qu, 1150 °C, 1 d, 1000 °C, 15 d single crystal study $R = 0.054$ $T_n = 1\ K$	ChEP, 84	Sc 99.999 Fe 99.999 Si 99.999
		$a = 9.938(3)$ $b = 3.984(1)$ $c = 9.409(3)$ $\beta = 118.46(3)°$	arc, Qu, 800 °C, 750 h, single crystal $H = 682\ (\pm 50)\ kg/mm^2$	GlKBS, 77 KoS, 83	Sc 99.96 Fe 99.96 Si 99.99
$ScFe_2Si_2$ [+]	$HfFe_2Si_2$ Pbcm	$a = 7.263$ $b = 7.076$ $c = 5.009$	arc, Qu, 800 °C 750 h single crystal data $H = 1032\ (\pm 50)\ kg/mm^2$	GlKBS, 77	Sc 99.96 Fe 99.96 Si 99.99

TABLE 23 (continued)

Compound	Structure type Space group	Lattice parameters Density	Preparation, Characterization	Refs.	Purity
$Sc_3Fe_3Si_4$ [*]	unknown		arc, Qu, 800 °C 750 h, PXD $H = 968\ (\pm 50)\ kg/mm^2$	GIKBS, 77	Sc 99.96 Fe 99.96 Si 99.99
$Sc_4Fe_4Si_7$	$Zr_4Co_4Ge_7$ I4/mmm	$a = 13.099(4)$ $c = 5.075(3)$	arc	Ch, 82	99.9
$Sc_2Fe_3Si_5$ [+]	$Sc_2Fe_3Si_5$ P4/mnc	$a = 10.05(1)$ $c = 5.313(5)$ $\rho_E = 4.82,$ $\rho_x = 4.89$	arc, Qu, 800 °C 750 h, single crystal data $H = 1123\ (\pm 50)\ kg/mm^2$	BoKYG, 77 GIKBS, 77	Sc 99.96 Fe 99.9 Si 99.99
		$a = 10.225(5)$ $c = 5.275(5)$ $\rho_x = 4.790(1)$	arc, Qu(Ar), 1150 °C, 1 d, 800 °C, 14 d PXD $T_c = 4.52\text{–}4.25$ K	Br, 81	Sc 3N Fe 5N Si 7N
$ScFeSi_2$	$TiFeSi_2$ Pbam	$a = 9.739$ $b = 8.984$ $c = 7.795$	arc, Qu, 800 °C 750 h, PXD $H = 1200\ (\pm 50)\ kg/mm^2$	GIKBS, 77	Sc 99.96 Fe 99.96 Si 99.99
"$Sc_3Fe_2Si_6$" [+]	$ZrFeSi_2$ Cmca	$a = 5.115(2)$ $b = 18.929(7)$ $c = 14.298(5)$	single crystal from a melt $Sc_{27}Fe_{18}Si_{55}$	YaKG, 80	Sc 99.96 Fe 99.96 Si 99.99
		$a = 5.094$ $b = 18.73$ $c = 14.12$	arc, Qu, 800 °C, 750 h PXD $H = 1090\ (\pm 50)\ kg/mm^2$	GIKBS, 77	Sc 99.96 Fe 99.96 Si 99.99
"$ScFe_3Si_6$"	$Zr_{0.2}Fe_{0.8}Si_{2-n}$ (?) $P6_3/mmc$	$a = 3.893$ $c = 15.16$	arc, Qu, 800 °C, 750 h PXD $H = 1114\ (\pm 50)\ kg/mm^2$	GIKBS, 77	Sc 99.96 Fe 99.96 Si 99.99
$ScFe_{0.25}Si_{1.75}$	$ZrSi_2$ Cmcm	$a = 3.861(3)$ $b = 14.48(1)$ $c = 3.762(3)$	arc, Qu, 800 °C, 750 h PXD $H = 828\ (\pm 50)\ kg/mm^2$	KoB, 77 GIKBS, 77	Sc 99.96 Fe 99.96 Si 99.9

[*] $Sc_{\sim 3}Fe_{\sim 3}Si_{\sim 4}$ very probably is identical with either ScFeSi (TiNiSi-type, Chabot et al., 1983) or $Sc_4Fe_4Si_7$ ($Zr_4Co_4Ge_7$-type, Chabot, 1982). in both cases no detauled data concerning the stability with respect to temperature are available.

[+] For details on physical properties and crystal structure determination(s), see text.

The crystal structure of $Sc(Sc_{0.03}Fe_{0.786}Si_{0.184})_{12}$ has been refined by Kotur (1977a) by means of X-ray powder diffraction data (ThMn$_{12}$-type of structure, see table 23). The atomic order was derived to be as follows: Sc in 2a); 0.73 Sc + 5.89 Fe + 1.38 Si statistically in 8i) 0.361, 0, 0; 12.96 Fe + 3.04 Si statistically in 8f) 1/4, 1/4, 1/4 and 8j 0.277, 1/2, 0; $R = 0.129$. Homogenous samples were obtained at a composition (in a/o) $Sc_{11}Fe_{72}Si_{17}$.

Gladyshevskij et al. (1977) first claimed the existence of an orthorhombic com-

pound with the composition "$Sc_3Fe_2Si_6$". Consequently, a single crystal was obtained from a melt (in a/o) of $Sc_{27}Fe_{18}Si_{55}$. Yarmolyuk et al. (1980) refined the crystal structure by means of single crystal X-ray counter data ($R = 0.060$). Atomic parameters derived were as follows: Sc in 8f) 0, 0.2958(4), 0.3198(4); Sc in 8f) 0, 0.0323(4), 0.3223(4); Sc in 8f) 0, 0.3769(4), 0.0848(4); Fe in 8e) 1/4, 0.1617(2), 1/4; Fe in 8f) 0, 0.4589(3), 0.3770(3); Fe in 8c) 1/4, 1/4, 0; Si in 8f) 0, 0, 0.1662(6), 0.4002(6); Si in 8f) 0, 0.0873(5), 0.1432(6); Si in 8d) 0.2563(23), 0, 0; Si in 8f) 0, 0.2365(4), 0.1433(6); Si in 8f) 0, 0.1397(5), 0.9932(6); Si in 8e) 1/4, 0.4134(5), 1/4. From this a formula of $ScFeSi_2$ was concluded ($ZrFeSi_2$-type of structure). However, no detailed data concerning the occupation factors were given and considerably smaller unit cell dimensions were reported from alloys annealed at 800 °C (Gladyshevskij et al., 1977; see table 23). Thus the occurrence of Fe defects according to a formula $ScFe_{0.67}Si_2$ ("$Sc_3Fe_2Si_6$") at 800 °C cannot be ruled out completely, the more so since "$Sc_3Fe_2Si_6$" at the same temperature was claimed to be in equilibrium with stoichiometric $ScFeSi_2$ with the $TiFeSi_2$-type.

$ScFe_2Si_2$ with the $HfFe_2Si_2$-type has been characterized from single crystal X-ray photographs (Gladyshevskij et al., 1977). Atom parameters were as follows: Sc in 4d) 0.2482, 0.0981, 1/4; Fe in 4d) 0.1176, 0.4895, 1/4; Fe in 4c) 0.6173, 1/4, 0; Si in 4d) 0.4170, 0.4490, 1/4; Si in 4c) 0.9493, 1/4, 0; Pbcm; $R = 0.087$.

Bodak et al. (1977) analyzed the crystal structure of $Sc_2Fe_3Si_5$ ($Sc_2Fe_3Si_5$-type, P4/mnc) by means of X-ray single crystal photographs ($R = 0.104$): Sc in 8h) 0.0701, 0.25, 0; Fe in 8h) 0.3790, 0.3601, 0; Fe in 4d) 0, 1/2, 1/4; Si in 8g) 0.1779, 0.6779, 1/4; Si in 4e) 0, 0, 0.2528; Si in 8h) 0.1799, 0.4761, 0. Braun (1980, 1981) confirmed the structure type, but reported considerably different lattice parameters (see table 24). Mössbauer effect studies revealed that the magnetic moment on both iron sites is less than 0.03 μ_B (Braun et al., 1981 and Cashion et al., 1980). A small variation of lattice parameters was found from a comprehensive study of the homogeneous range and the dependence of superconductivity on composition. T_c was highest on the Fe-deficient side and drops sharply for Fe-rich alloys (see table 24). Under hydrostatic pressure $dT_c/dp = -7.1 \times 10^{-5}$ K bar^{-1} was negative (Segre, 1981). The low-temperature heat capacity has been measured by Vining et al. (1983).

The crystal structures of $ScFeSi$ ($TiNiSi$-type), $Sc_3Fe_2Si_3$ ($Hf_3Ni_2Si_3$-type) and Sc_2FeSi_2 (Sc_2CoSi_2-type) have been refined by Chabot et al. (1984) by means of single crystal counter data. Samples were prepared by arc melting under argon

TABLE 24

Lattice parameters and T_c for $Sc_2Fe_3Si_5$ alloys (Braun, 1980).

Composition	a (Å)	c (Å)	T_c (K)
$Sc_{19.5}Fe_{31.0}Si_{49.5}$	10.222(8)	5.270(5)	3.9–2.8
$Sc_{21.9}Fe_{30.1}Si_{48.0}$	10.222(8)	5.272(5)	3.0–2.6
$Sc_{18.7}Fe_{29.7}Si_{51.6}$	10.222(8)	5.274(5)	3.9–3.5
$Sc_{20.2}Fe_{29.2}Si_{50.7}$	10.221(8)	5.269(5)	4.5–3.7
$Sc_{20.9}Fe_{28.9}Si_{50.2}$	10.224(8)	5.274(5)	4.5–3.6
$Sc_{21.5}Fe_{29.6}Si_{48.9}$	10.220(8)	5.273(5)	4.0–3.6
$Sc_2Fe_3Si_5$	10.225(5)	5.275(5)	4.52–4.25

starting from 99.95% Sc, 99.999% Fe and 99.999% Si. Single crystals were obtained from as-cast alloys except in the case of an Sc_2FeSi_2 alloy which had to be annealed for 1 d at 1100°C and then for 7 d at 1000°C. The crystallographic data were as follows:

ScFeSi, TiNiSi-type, Pnma, $a = 6.519(2)$, $b = 3.846(2)$, $c = 7.298(2)$ and $\rho_x = 4.679$ kg/dm³ for an as-cast alloy, and $a = 6.512(2)$, $b = 3.8391(1)$, $c = 7.298(2)$ in annealed condition. All atoms are in the 4c sites $(x, 1/4, z)$: Sc 0.0133(4), 0.6829(3), Fe 0.1481(3), 0.0588(3), Si 0.2853(6), 0.3803(5); $R = 0.062$,

$Sc_3Fe_2Si_3$, $Hf_3Ni_2Si_3$-type, Cmcm, $a = 3.959(1)$, $b = 9.960(2)$, $c = 12.941(1)$, $\rho_x = 4.292$ kg/dm³ for an annealed alloy, and $a = 3.966(1)$, $b = 9.971(2)$, $c = 12.947(5)$ in as-cast condition. Atom parameters were as follows: Sc in 8f) 0, 0.0789(2), 0.1131(2); Fe in 8f) 0, 0.2141(1), 0.5835(1); Si in 8f) 0, 0.3858(3), 0.0401(2); Sc in 4c) 0, 0.3595(3), 1/4; Si in 4c) 0, 0.6667(4), 1/4; $R = 0.047$.

Sc_2FeSi_2, Sc_2CoSi_2-type, C2/m, $a = 9.916(2)$, $b = 3.9912(7)$, $c = 9.414(3)$, $\beta = 118.15(2)°$, $\rho_x = 4.085$ kg/dm³, for an annealed alloy. All atoms are in the 4i sites $(x,0,z)$: Sc 0.9998(2), 0.3269(3); Sc 0.1856(2), 0.1077(3); Fe 0.2720(2), 0.6305(2); Si 0.3567(4), 0.4348(4) and Si 0.4891(4), 0.1234(4); $R = 0.054$. The crystal structure of Sc_2FeSi_2 has been also and independently refined and confirmed by Kotur and Sikiritsa (1983) from single crystal counter data, $R = 0.032$.
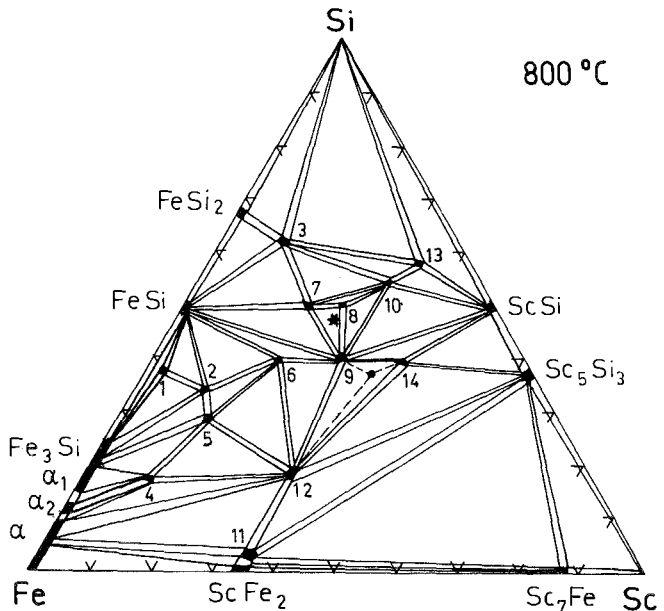
Fig. 41. Sc–Fe–Si, isothermal section at 800°C as presented by Gladyshevskij et al. (1977). 1: $(Sc_{0.07}Fe_{0.93})_5Si_3$, 2: "$ScFe_5Si_3$", 3: $ScFe_3Si_6$ ($Zr_{0.2}Fe_{0.8}Si_{2-n}$-type?), 4: Sc $(Sc_{0.03}Fe_{0.786}Si_{0.184})_{12}$, 5: $ScFe_4Si_2$, 6: $ScFe_2Si_2$, 7: $Sc_2Fe_3Si_5$, 8: $ScFeSi_2$, 9: "$Sc_3Fe_3Si_4$" (TiNiSi?), 10: $Sc_2Fe_2Si_6$ ($ZrFeSi_2$-type), 11: $Sc(Sc_{0.026}Fe_{0.945}Si_{0.029})_2$, 12: Sc_2Fe_3Si, 13: $ScFe_{0.25}Si_{1.75}$, 14: Sc_2FeSi_2. For the existence of the high-temperature phases (?) $Sc_3Fe_2Si_3$, $Sc_4Fe_4Si_7$ and ScFeSi, see text. ScFeSi might in fact be identical with the "$Sc_3Fe_3Si_4$" phase, earlier observed at 800°C. The location of the phase $Sc_3Fe_2Si_3$ is marked by a filled circle, the location of $Sc_4Fe_4Si_7$ by an asterisk.

Stadnyk et al. (1981) investigated the magnetic susceptibilities of $ScFe_2$, $Sc(Sc_{0.026}Fe_{0.945}Si_{0.029})_2$ with the $MgCu_2$-type, Sc_2Fe_3Si as well as the specific resistance of Sc_2Fe_3Si.

The phase equilibria as shown in fig. 41 are based on the work of Gladyshevskij et al. (1977). Only the Fe–Si-rich area was slightly modified with respect to a recent critical evaluation of the binary Fe–Si system (Schürmann and Hensgen, 1980). Phase equilibria in the region $1:1:1$, however, are still dubious and cannot be solved with respect to the new findings by Chabot (1982) and Chabot et al. (1984); a revision of this portion of the isothermal section is necessary.

References
Bodak, O.I., B.Ya. Kotur, V.I. Yarovets and E.I. Gladyshevskij, 1977, Sov. Phys. Crystallogr. **22**(2), 217.
Braun, H.F., 1980, Phys. Lett. **75A**(5), 386.
Braun, H.F., 1981, in: Ternary Superconductors, Proc. Intern. Conf. on ternary Superconductors, Lake Geneva, WI, USA, eds. G.K. Shenoy, B.D. Dunlap and F.Y. Fradin (North-Holland, Amsterdam) p. 225.Braun, H.F., C.U. Segre, F. Acker, M. Rosenberg, S. Dey and P. Deppe, 1981, J. Magn. Magn. Mater. **25**, 117.
Cashion, J.D., G.K. Shenoy, D. Niarchos, P.J. Viccaro and C.M. Falco, 1980, Phys. Lett. **79A**(5,6), 454.
Chabot, B., 1982, unpublished results.
Chabot, B., N. Engel and E. Parthé, 1984, J. Less-Common Metals **96**, 331.
Gladyshevskij, E.I., B.Ya. Kotur, O.I. Bodak and U.R. Svorchuk, 1977, Dokl. Akad. Nauk Ukr. SSR, Ser. A, 751.
Kotur, B.Ya., 1977a, Visn. L'vivsk. Derzh Univ., Ser. Khim. **19**, 42.
Kotur, B.Ya., 1977b, Dopov. Akad. Nauk Ukr. RSR, Ser. A **2**, 164.
Kotur, B.Ya. and O.I. Bodak, 1977, Sov. Phys. Crystallogr. **22**(6), 687.
Kotur, B.Ya. and O.I. Bodak, 1980, Izv. Akad. Nauk SSSR, Neorg. Mater. **16**(3), 459.
Kotur, B.Ya. and M. Sikiritsa, 1983, Sov. Phys. Crystallogr. **28**(4), 472.
Schürman, E. and U. Hensgen, 1980, Archiv. f. Eisenhüttenwesen **51**(1), 1.
Segre, C.U., 1981, Thesis, Univ. of Calif., San Diego, USA.
Stadnyk, Yu.V., B.Ya. Kotur, Yu.K. Gorelenko and R.V. Skolozdra, 1981, Vestn. Lvov Univ., Ser. Khim. **23**, 71.
Vining, C.B., R.N. Shelton, H.F. Braun and M. Pelizzone, 1983, Phys. Rev. **B27**(5), 2800.
Yarmolyuk, Ya.P., B.Ya. Kotur and Yu.N. Grin, 1980, Dopov. Akad. Nauk Ukr. RSR, Ser. B **11**, 68.

Sc–Ge–Si

In the course of a phase diagram study at 600°C, Muratova (1978) reported the existence of two continuous solid solutions: $ScGe_{1-x}Si_x$ with the CrB-type of structure, and $Sc_5Ge_{3-x}Si_x$ with the Mn_5Si_3-type of structure. $ScGe_2$ with the $ZrSi_2$-type was observed at 35 a/o Si. No further details concerning lattice parameters have been presented.

Reference
Muratova, L.A., 1978, Tesizy Dokl. Tret. Vses. Konf. Kristallokhim. Intermet. Soedin, 2nd Ed., ed. R.M. Rykhal (Lvov Gos. Univ., Lvov, USSR) p. 98.

Sc–Ir–Si

ScIrSi crystallizes with the TiNiSi-type of structure: Pnma, $a = 6.418(1)$, $b = 4.036(1)$, $c = 7.299(2)$ (Hovestreydt et al., 1982; X-ray powder analysis). For sample

preparation, see ScPdSi. Atomic parameters are as derived for ScPtSi.

$Sc_4Ir_7Si_6$ with the $U_4Re_7Si_6$-type of structure (closely related to the Cu_3Au-type) has been characterized by Engel et al. (1984) by means of X-ray powder data of arc-melted alloys. Starting materials were Sc 99.95, Ir 99.98 and Si 99.998. The following crystallographic data were obtained: space group $Im\overline{3}m$ and $a = 8.003(1)$.

$Sc_5Ir_4Si_{10}$ has the $Sc_5Co_4Si_{10}$-type of structure: P4/mbm, $a = 12.316(5)$, $c = 4.076(3)$, $\rho_x = 6.84(2)$, $\rho_E = 6.81(7)$ kg/dm^3. The Laue symmetry 4/mmm has been derived from single crystal Weissenberg and precession photographs (Braun et al. 1980). A superconducting transition at $T_c = 8.46$–8.38 K was measured by Braun and Segre (1980). Samples were prepared by arc melting under Zr-gettered argon. Subsequently the alloy buttons were wrapped in Ta foil, sealed in quartz capsules under 150 Torr argon and heat treated at 1000°C for 48 h and finally quenched in water. Starting materials were of 99.9% min purity.

The crystal structure of $ScIr_3Si_7$ has been refined from single crystal counter data: $ScRh_3Si_7$-type, $R\overline{3}c$, $a = 7.5010(2)$, $c = 19.909(1)$, $\rho_x = 8.403$ kg/dm^3; Sc in 6b); Ir in 18e) 0.3234(3), 0, 1/4; Si in 36f) 0.539(1), 0.680(1), 0.029(1); Si in 6a); $R = 0.072$ (Chabot et al., 1981). Samples were prepared by arc melting under Ar (Sc 99.95%, Ir 99.9% and Si 99.999%). Single crystals were obtained from a melt with composition $ScIr_3Si_6$ (congruent melting?). Magnetic susceptibility and electric resistance data were reported by Braun and Segre (1981) (metallic behavior, resistivity ~ 10 $\mu\Omega$). A small effective magnetic moment (~ 0.06 μ_B) was obtained, probably due to R-impurities or impurity phases.

References

Braun, H.F. and C.U. Segre, 1980, Solid State Commun. **35**, 735.
Braun, H.F. and C.U. Segre, 1981, Ternary Superconductors of the $Sc_5Co_4Si_{10}$-type, in: Ternary Superconductors, Proc. Intern. Conf. on Ternary Superconductors, Lake Geneva, WI, USA, eds. G.K. Shenoy, B.D. Dunlap and F.Y. Fradin (North-Holland, Amsterdam) p. 239.
Braun, H.F., K. Yvon and R.M. Braun, 1980, Acta Crystallogr. **B36**, 2397.
Chabot, B., N. Engel and E. Parthé, 1981, Acta Crystallogr. **B37**, 671.
Engel, N., B. Chabot and E. Parthé, 1984, J. Less-Common Metals **96**, 291.
Hovestreydt, E., N. Engel, K. Klepp, B. Chabot and E. Parthé, 1982, J. Less-Common Metals **86**, 247.

Sc–Mn–Si

Kotur et al. (1980) investigated the phase equilibria of the system Sc–Mn–Si at 800°C (isothermal section in the range of 0–67 a/o Sc), by means of X-ray powder and metallographic analysis of 92 ternary alloys. Samples were prepared by arc melting under argon followed by a heat treatment at 800°C for 750 h in evacuated silica tubes. Starting materials were Sc 99.9%, Mn 99.91% and Si 99.99%. Etching was possible with an aqueous mixture of HF and HNO_3 or with a 3% solution of HNO_3 in alcohol. Microhardness values were determined at a load of 100 g.

The binary systems have been reinvestigated and $ScMn_2$ ($MgZn_2$-type), Sc_5Si_3 (Mn_5Si_3-type) and ScSi (CrB-type) were confirmed, but Sc_3Si_5 with the defect AlB_2-type could not be obtained at 800°C. Similarly, one of the so-called Nowotny chimney ladder structures of the general formula Mn_nSi_{2n-m} was confirmed
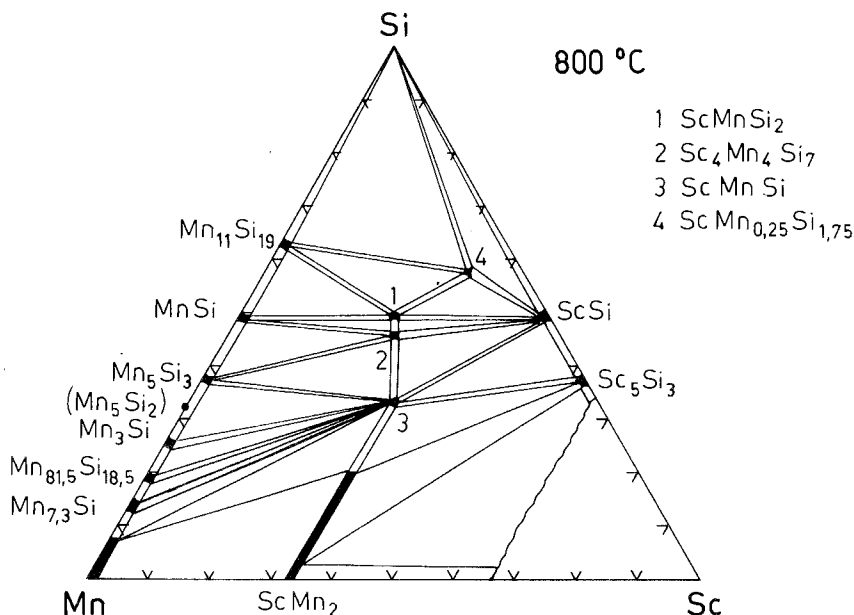
Fig. 42. Sc–Mn–Si, partial isothermal section at 800°C (0–67 a/o Sc).

($Mn_{11}Si_{19}$, see also the Gmelin Handbook of Inorganic Chemistry, Vol. C8, 1982). MnSi (FeSi-type), Mn_5Si_3 (Mn_5Si_3-type), Mn_3Si (W-type), $Mn_{81.5}Si_{18.5}$ (so-called N-phase) and $Mn_{7.3}Si$ (R-phase) are in agreement with a recent review of Mn silicides (Gmelin Handbook, Vol. C8, 1982). According to Kotur et al. (1980) the D-phase Mn_5Si_2 could not be obtained at 800°C; the location of this phase, however, is marked by a filled circle in fig. 42.

Mutual solid solubilities of manganese and scandium silicides were observed to be rather small, whereas up to 20 a/o Si are dissolved in $ScMn_2$ along with a fixed Sc content of 33.3 a/o Sc (Mn/Si substitution). The lattice parameters change linearly from $a = 5.04$, $c = 8.268$ for $ScMn_2$ to $a = 5.022$ and $c = 8.18$ for $ScMn_{1.4}Si_{0.6}$ (as read from a small diagram).

Four ternary compounds were identified: $ScMn_{0.25}Si_{1.75}$, ScMnSi, $Sc_4Mn_4Si_7$ and $ScMnSi_2$. A listing of structural data was also presented by Kotur and Bodak (1980).

$ScMnSi_2$ crystallizes with the $TiFeSi_2$-type of structure (Pbam, $a = 9.854(8)$, $b = 9.077(8)$, $c = 7.928(6)$; X-ray powder data). The microhardness was $H = 859(50)$ kg/mm^2.

The crystal structure of ScMnSi has been refined on the basis of X-ray single crystal photographs. ScMnSi is isotypic with the ZrNiAl-type (ordered Fe_2P-type), $a = 6.551(5)$, $c = 3.861(3)$, P$\bar{6}$2m. According to the reliability factor $R = 0.105$ the following atom distribution and parameters were obtained: Sc in 3g) 0.586, 0, 0.5; Mn in 3f) 0.234, 0, 0; Si in 2c) 1/3, 2/3, 0 and Si in 1b) 0, 0, 1/2. The microhardness was $H = 978(50)$ kg/mm^2.

$Sc_4Mn_4Si_7$ is isotypic with the crystal structure of $Zr_4Co_4Ge_7$ [I4/mmm, $a =$ 13.063(10), $c = 5.227(4)$]. The crystal structure has been confirmed from a refinement of X-ray single crystal photographs, $R = 0.142$. Sc in 8h) 0.137, 0.137, 0; Sc in 8j) 0.694, 0.5, 0; Mn in 16k 0.150, 0.650, 0.25; Si in 8j) 0.908, 0.5, 0; Si in 8j) 0.215, 0.5, 0; Si in 8h) 0.296, 0.296, 0; Si in 4e) 0, 0, 0.25. The microhardness was $H = 1046(5)$ kg/mm^2.

Kotur and Bodak (1977) determined the crystalstructure of $ScMn_{0.25}Si_{1.75}$ from X-ray powder diffraction data. $ScMn_{0.25}Si_{1.75}$ adopts the $ZrSi_2$-type [Cmcm, $a =$ 3.878(3), $b = 14.46(1)$, $c = 3.776(3)$]. A microhardness of $H = 761(50)$ kg/mm^2 was measured by Kotur et al. (1980).

References

Kotur, B.Ya, and O.I. Bodak, 1977, Sov. Phys. Crystallogr. **22(6)**, 687.
Kotur, B.Ya. and O.I. Bodak, 1980, Izv. Akad. Nauk SSSR, Neorg. Mater. **16(3)**, 459.
Kotur, B.Ya., O.I. Bodak and O.Ya. Kotur, 1980, Dopov. Akad. Nauk Ukr. RSR., Ser. A, 82.

Sc–Ni–Si

Phase equilibria within an isothermal section of the system Sc–Ni–Si at 800°C (region 0–67 a/o Sc) have been derived by Bodak et al. (1976) by means of X-ray and metallographic analysis of 376 alloys (fig. 43). Samples were prepared by arc
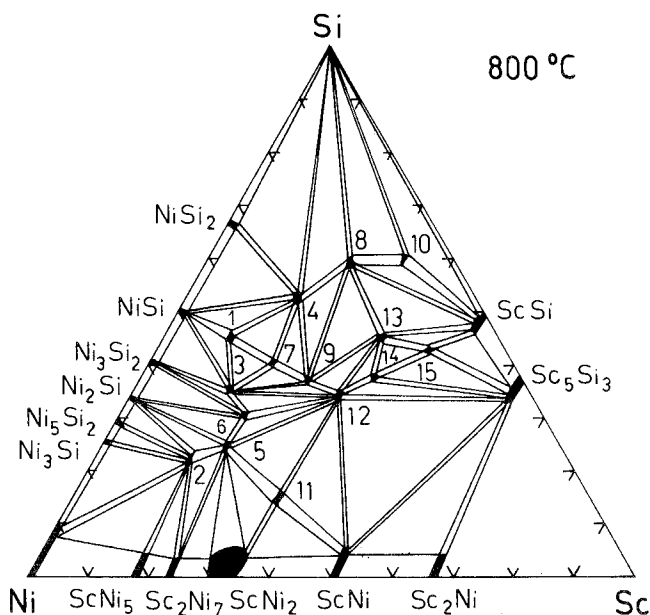
Fig. 43. Sc–Ni–Si, isothermal section at 800°C. 1: "$Sc_2Ni_9Si_9$", 2: "$Sc_3Ni_{11}Si_4$", 3: "$Sc_3Ni_{10}Si_7$", 4: $ScNi_2Si_3$ (probably corresponds to the phase observed at (in a/o) $Sc_{17.5}Ni_{30}Si_{52.5}$), 5: $Sc_6Ni_{16}Si_7$, 6: "$Sc_2Ni_5Si_3$", 7: $ScNi_2Si_2$, 8: $ScNiSi_3$, 9: $Sc_3Ni_4Si_4$, 10: $ScNi_{0.25}Si_{1.75}$, 11: Sc_2Ni_3Si (probably corresponds to the phase observed at (in a/o) $Sc_{33.3}Ni_{51.7}Si_{15}$), 12: $ScNiSi$, 13: "$Sc_4Ni_2Si_5$" (observed at $Sc_{35}Ni_{20}Si_{45}$), 14: "Sc_2NiSi_2", 15: Sc_3NiSi_3.

melting and subsequent annealing at 800°C for 350 h in evacuated silica tubes. Starting materials were Sc 99.9%, Ni 99.92% and Si 99.99%. Etching was possible in aqueous solutions of HNO_3 and HF with glycerin. Microhardness values were determined at a load of 100 g. Binary nickel silicides (see also Ce–Ni–Si) and Sc silicides are in agreement with literature data: Sc_5Si_3 (Mn_5Si_3-type), ScSi (CrB-type). Sc_3Si_5 with a defect AlB_2-type of structure was not observed at $T = 800°C$. Sc–Ni compounds [Sc_2Ni (Ti_2Ni-type), ScNi (CsCl-type), $ScNi_2$ ($MgCu_2$-type), Sc_2Ni_7 (Ce_2Ni_7-type) and $ScNi_5$ ($CaCu_5$-type)] are in agreement with a recent compilation by Iandelli and Palenzona (1979). Solubility of Sc in nickel silicides was found to be small; ternary solid solubilities of Sc–Ni and Sc–Si compounds generally were less than 5 a/o in the direction of Ni/Si exchange.

Earlier data concerning the compounds $ScNi_2Si_2$ and $Sc_6Ni_{16}Si_7$ have been confirmed and a total of 15 ternary compounds identified (see table 25). Crystal structure data were also listed by Kotur and Bodak (1980); the crystal structures of several compounds, however, are still unknown.

Stadnyk et al. (1981) investigated the magnetic properties and specific resistance of the compounds $ScNi_2Si_2$, $ScNi_2Si_3$, $ScNiSi_3$, $ScNi_{0.25}Si_{1.75}$ and $Sc_6Ni_{16}Si_7$ in the range from 293 to 1200 K.

References

Bodak, O.I., B.Ya. Kotur and E.I. Gladyshevskij, 1976, Dopov. Akad. Nauk Ukr. RSR, Ser. A 7, 655.
Dwight, A.E., 1982, private communication.
Dwight, A.E., R.A. Conner, Jr. and J.W. Downey, 1963, Nature 9, 587.
Gladyshevskij, E.I., V.Ya. Markiv and Yu.B. Kuz'ma, 1962, Dopov. Akad. Nauk Ukr. RSR, Ser. A, 481.
Iandelli, A. and A. Palenzona, 1979, Crystal Chemistry of Intermetallic Compounds, Handbook on the Physics and Chemistry of Rare Earths, Vol. 2, eds. K.A. Gschneidner, Jr. and L. Eyring (North-Holland, Amsterdam) p. 1.
Kotur, B.Ya., 1977, Dopov. Akad. Nauk Ukr. RSR, Ser. A, 164.
Kotur, B.Ya. and O.I. Bodak, 1977, Kristallografiya 22, 1209.
Kotur, B.Ya. and O.I. Bodak, 1980, Izv. Akad. Nauk SSSR, Neorg. Mater. 16(3), 459.
Kotur, B.Ya. and E.I. Gladyshevskij, 1983, Sov. Phys. Crystallogr. 28(3), 271.

TABLE 25

Formation and structural data of ternary compounds Sc–Ni–Si

Compound (nom.comp.a/o)	Structure type Space group	Lattice parameters Density	Preparation, Characterization	Refs.	Purity
Sc_2Ni_3Si 33.3–51.7–15 [*]	Mg_2Cu_3Si $P6_3/mmc$	$a = 4.998(2)$ $c = 7.722(4)$ at 17 a/o Si	arc(Ar), Qu 800 °C, 350 h PXD	Ko, 77	Sc 99.9 Ni 99.92 Si 99.99
		$a \sim 4.99$ $c \sim 7.73$ at 16 a/o Si	$H = 1310 (\pm 50)$ kg/mm^2	BoKG, 76	
$Sc_3Ni_{11}Si_4$ 15–62.5–22.5	$Sc_3Ni_{11}Si_4$ $P6_3/mmc$ (○○)	$a = 8.024(5)$ $c = 8.429(3)$	arc(Ar), Qu, 800 °C, 350 h, PXD $H = 956 (\pm 50)$ kg/mm^2	BoKG, 76 KoSBG, 83	Sc 99.9 Ni 99.92 Si 99.99

TABLE 25 (continued)

Compound (nom.comp.a/o)	Structure type Space group	Lattice parameters Density	Preparation, Characterization	Refs.	Purity
$Sc_6Ni_{16}Si_7$	$Mg_6Cu_{16}Si_7$ Fm3m	$a = 11.45$	arc(Ar), Qu 800 °C, 350 h, PXD	GlMK, 62	Sc 99.9 Ni 99.92
		$a = 11.75(?)$ $a = 11.429$	$H = 824 \, (\pm 50) \, kg/mm^2$ arc(Ar), 900 °C	BoKG, 76 DwCD, 63	Si 99.99
$Sc_2Ni_5Si_3$ 20–50–30	unknown		arc(Ar), Qu 800 °C, 350 h, PXD $H = 856 \, (\pm 50) \, kg/mm^2$	BoKG, 76	Sc 99.9 Ni 99.92 Si 99.99
ScNiSi	TiNiSi Pnma	$a = 6.38$ $b = 4.02$ $c = 6.93$	arc(Ar), Qu 800 °C, 350 h, PXD $H = 792 \, (\pm 50) \, kg/mm^2$	BoKG, 76	Sc 99.9 Ni 99.92 Si 99.99
(**)		$a = 6.383(5)$ $b = 4.011(3)$ $c = 6.868(5)$ $\rho_E = 4.92$ $\rho_x = 4.97$	arc(Ar) single crystal study $R = 0.113$	KoB, 77	99.9
		$a = 6.406$ $b = 4.006$ $c = 6.976$	arc(Ar), PXD	Dw, 82	
$Sc_3Ni_{10}Si_7$ 15–50–35	unknown Immm	$a = 17.78$ $b = 12.26$ $c = 8.08$	arc(Ar), Qu 800 °C, 350 h, PXD $H = 1117 \, (\pm 50) \, kg/mm^2$	BoKG, 76	Sc 99.9 Ni 99.92 Si 99.99
$Sc_3Ni_4Si_4$	$Gd_3Cu_4Ge_4$ Immm	$a = 12.68$ $b = 6.38$ $c = 3.89$	arc(Ar), Qu 800 °C, 350 h, PXD $H = 1184 \, (\pm 50) \, kg/mm^2$	BoKG, 76	Sc 99.9 Ni 99.92 Si 99.99
		$a = 12.77 \, (?)$ $b = 6.382$ $c = 3.886$		KoB, 80	
$ScNi_2Si_2$	$ThCr_2Si_2$ I4/mmm	$a = 3.72$ $c = 9.50$	arc(Ar), Qu 800 °C, 350 h, PXD $H = 894 \, (\pm 50) \, kg/mm^2$	BoKG, 76	Sc 99.9 Ni 99.92 Si 99.99
		$a = 3.806$ $c = 9.579$	arc(Ar), Qu 900 °C, 100 h, PXD	RiP, 69	high purity
Sc_2NiSi_2 37.5–25–37.5	unknown		arc(Ar), Qu 800 °C, 350 h, PXD $H = 936 \, (\pm 50) \, kg/mm^2$	BoKG, 76	Sc 99.9 Ni 99.92 Si 99.99
Sc_3NiSi_3 44–12–44	Sc_3NiSi_3 C2/m	$a = 9.801(3),$ $\beta = 114.16°$ $b = 3.974(2)$ $c = 13.193(4)$	arc (Ar), Qu 800 °C, 350 h, PXD $H = 1095 \, (\pm 50) \, kg/mm^2$ single crystal data [○]	BoKG, 76 KoG, 83	Sc 99.9 Ni 99.92 Si 99.99

TABLE 25 (continued)

Compound (nom.comp.a/o)	Structure type Space group	Lattice parameters Density	Preparation, Characterization	Refs.	Purity
$Sc_2Ni_9Si_9$ 10–45–45	unknown		arc(Ar), Qu 800 °C, 350 h, PXD $H = 1110$ (± 50) kg/mm^2	BoKG, 76	Sc 99.9 Ni 99.92 Si 99.99
$Sc_4Ni_2Si_5$ 35–20–45	unknown		arc(Ar), Qu 800 °C, 350 h, PXD $H = 1017$ (± 50) kg/mm^2	BoKG, 76	Sc 99.9 Ni 99.92 Si 99.99
$ScNi_2Si_3$ [+] 17.5–30–52.5	$ScNi_2Si_3$ I4/mmm	$a = 3.830(3)$ $c = 23.500(10)$	arc(Ar) single crystal study 800 °C, 350 h $H = 634$ (± 50) kg/mm^2	KoBG, 78 BoKG, 76	99.9 Sc 99.9 Ni 99.92 Si 99.99
$ScNi_{0.25}Si_{1.75}$ 32–8–60	$ZrSi_2$ Cmcm	$a = 3.843(3)$ $b = 14.68(1)$ $c = 3.727(3)$	arc(Ar) 800 °C, 350 h PXD $H = 669$ (± 50) kg/mm^2	KoB, 77 BoKG, 76	Sc 99.9 Ni 99.92 Si 99.99
$ScNiSi_3$ [++] 20–20–60	$ScNiSi_3$ Amm2	$a = 3.815(3)$ $b = 3.825(3)$ $c = 20.62(1)$ $\rho_E = 4.09$ $\rho_x = 4.12$	arc(Ar) single crystal study	KoBMG,77	Sc 99.9 Ni 99.92 Si 99.99

[*] With a nominal composition (in a/o) $Sc_{33.3}Ni_{51.7}Si_{15}$ Bodak et al. (1976) reported a compound with unknown structure, which very likely corresponds to Sc_2Ni_3Si. The homogeneity range of Sc_2Ni_3Si has been determined by Kotur (1977) (linear variation of lattice parameters between 16 a/o Si and 17 a/o Si). From X-ray powder data the ordered Mg_2Cu_3Si-type was assumed.

[**] The crystal structure of ScNiSi has been refined from X-ray single crystal photographs (Kotur and Bodak, 1977); $R = 0.113$. Atomic parameters were: Sc in 4c) 0.498, 0.25, 0.300; Ni in 4c) 0.177, 0.25, 0.576; Si in 4c) 0.793, 0.25, 0.594.

[+] The crystal structure of $ScNi_2Si_3$ was refined from X-ray single crystal photographs (Kotur et al., 1978); $R = 0.079$. Atom parameters were: Sc in 4e) 0, 0, 0.1488; Ni in 4d) 0, 0.5, 0.25; Ni in 4e) 0, 0, 0.4017; Si in 4c) 0, 0, 03065; Si in 8g) 0, 0.5, 0.0488.

[++] The crystal structure of $ScNiSi_3$ was refined from X-ray single crystal counter data as well as from photographs (Kotur et al., 1977); $R = 0.118$. Atom parameters were (as derived from counter data): Sc in 2a) 0, 0, 0.1630; Sc in 2a) $z = 0.8251$; Ni in 2b) 0.5, 0, 0.3878; Ni in 2b) $z = 0.6107$; 4×2 Si in 2b) $z_1 = 0.2779$, $z_2 = 0.7135$, $z_3 = 0.0518$, $z_4 = 0.9380$; 2×2 Si in 2a) $z_1 = 0.5524$, $z_2 = 0.4364$.

[○] The crystal structure of Sc_3NiSi_3 was refined from X-ray single crystal counter data (Kotur and Gladyshevskij, 1983); $R = 0.049$. All atoms are in the 4i-sites of C2/m $(x,0,z)$: Sc $[x_1 = 0.1474(2)$, $z_1 = 0.6212(2)]$, Sc $[x_2 = 0.4832$, $z_2 = 0.2260(2)]$, Sc $[x_3 = 0.3193(2)$, $z_3 = 0.9215(2)]$, Ni $[x = 0.1582(2)$, $z = 0.4024]$; Si $[x_1 = 0.4116(3)$, $z_1 = 0.5449(3)]$, Si $[x_2 = 0.0419(3)$, $z_3 = 0.9249(3)]$, Si $[x_3 = 0.1988$, $z_3 = 0.235(3)]$.

[○○] Kotur et al. (1983) refined the crystal structure of $Sc_3Ni_{11}Si_4$ from single crystal X-ray counter data, $R = 0.079$: Sc in 6h) 0.1920(13), $2x$, 1/4; Ni in 12k) 0.1614(7), $2x$, 0.5857(5); Ni in 6h) 0.5618(8), $2x$, 1/4, Ni in 4f) 1/3, 2/3, 0.0086(9); Si in 6g) 1/2, 0, 0 and Si in 2b) 0, 0, 1/4. The crystal structure is closely related to the $EuMg_5$-type. Single crystals were obtained from an arc-melted alloy, annealed at 800 °C for 700 h.

Kotur, B.Ya., O.I. Bodak, M.G. Mys'kiv and E.I. Gladyshevskij, 1977, Sov. Phys. Crystallogr. **22(2)**, 151.
Kotur, B.Ya., O.I. Bodak and E.I. Gladyshevskij, 1978, Sov. Phys. Crystallogr. **23(1)**, 101.
Kotur, B.Ya., M. Sikiritsa, O.I. Bodak and E.I. Gladyshevskij, 1983, Sov. Phys. Crystallogr. **28(4)**, 387.
Rieger, W. and E. Parthé, 1969, Monatsh. Chem. **100**, 444.
Stadnyk, Yu.V., B.Ya. Kotur, Yu.K. Gorelenko and R.V. Skolozdra, 1981, Vestn. Lvov Univ., Ser. Khim.
    23, 71.

Sc–Os–Si

Braun and Segre (1980) reported the existence of a compound $Sc_3Os_2Si_6$. Samples were arc melted and subsequently wrapped in Ta foil, sealed in quartz capsules under 150 Torr of argon, annealed for 48 h at 1000°C and finally quenched in water. The purity of the starting materials was 99.9%. The X-ray powder patterns of $Sc_3Os_2Si_6$ revealed a striking similarity to those of $Sc_5Ir_4Si_{10}$ and were tentatively indexed on the basis of an orthorhombic unit cell [$a = 8.963(5)$, $b = 9.044(5)$, $c = 4.195(4)$, $\rho_x = 6.68(2)$, $\rho_{exp} = 6.63(2)$ kg/dm^3]. A simple relation between the unit cells of $Sc_3Os_2Si_6$ and $Sc_5Ir_4Si_{10}$ was pointed out: $a \approx b(Sc_3Os_2Si_6) \approx (\sqrt{2}/2)a(Sc_5Ir_4Si_{10})$, and $c(Sc_3Os_2Si_6) \approx c(Sc_5Ir_4Si_{10})$. No superconductivity was observed above $T_n = 1.2$ K.

Reference
Braun, H.F. and C.U. Segre, 1980, Solid State Commun. **35**, 735.

Sc–Pd–Si

From X-ray powder analysis of arc-melted (Ar) samples Hovestreydt et al. (1982) characterized the compound ScPdSi with the TiNiSi-type of structure [Pnma, $a = 6.543(1)$, $b = 4.069(1)$, $c = 7.396(1)$]. A binary ScSi alloy was used as master alloy; heat treatment was at 1000°C for 1–2 weeks. Starting materials were Sc 99.9%, Pd 99.99% and Si 99.999%.

Reference
Hovestreydt, E., N. Engel, K. Klepp, B. Chabot and E. Parthé, 1982, J. Less-Common Metals **86**, 247.

Sc–Pt–Si

Hovestreydt et al. (1982) refined the crystal structure of ScPtSi from single crystal counter data [TiNiSi-type of structure, Pnma, $a = 6.566(2)$, $b = 4.130(1)$, $c = 7.275(8)$]. With respect to the reliability value obtained, $R = 0.046$, the atomic parameters were derived as follows: Sc in 4c) 0.000(1), 1/4, 0.700(1); Pt in 4c) 0.1998(3), 1/4, 0.0835(2); Si in 4c) 0.305(2); 1/4; 0.407(1). Samples were prepared by arc melting using a binary ScSi alloy as master alloy. Starting materials were Sc 99.9%, Pt 99.99% and Si 99.999%.

Reference
Hovestreydt, E., N. Engel, K. Klepp, B. Chabot and E. Parthé, 1982, J. Less-Common Metals **86**, 247.

Sc–Re–Si

The phase equilibria in the ternary system Sc–Re–Si have been investigated by Pecharskij (1979) by means of X-ray analysis of 129 ternary samples which were arc melted as well as subsequently annealed in evacuated silica capsules for 400 + 600 h at 800°C and quenched in water. Starting materials were Sc 99.92%, Re 99.99% and Si 99.99%.

$ScRe_2$ with $MgZn_2$-type and Sc_5Re_{24} with the α-Mn-type structure were confirmed. For scandium silicides, see Sc–Co–Si, and the binary rhenium silicides have been discussed in context with the ternary system Y–Re–Si. The mutual solid solubilities of Sc and Re silicides as well as of the Sc–Re intermetallics were generally found to be small (< 2 a/o); $ScRe_2$ shows a considerably wide Re/Si substitution up to 21 a/o Si.

The ternary phase relations are characterized by the formation of five ternary compounds: $Sc_2Re_3Si_4$, $Sc_3Re_2Si_3$, $ScRe_2Si_3$, "$ScReSi_2$" and "$Sc_8Re_3Si_9$" (fig. 44, isothermal section at 800°C).

The crystal structure of $Sc_2Re_3Si_4$ has been refined by Pecharskij et al. (1978) by means of X-ray single crystal photographs. $Sc_2Re_3Si_4$ adopts the ordered Zr_5Si_4-type of structure with the space group $P4_12_12$ and lattice parameters $a = 6.619(2)$ and $c = 12.36(1)$. According to the reliability value $R = 0.078$ the atomic parameters were as follows: Sc in 8b) 0.3504(98), 0.9967(82), 0.4730(44); Re in 8b) 0.1863(19), 0.9805(19), 0.8649(9); Re in 4a) 0.3324(31), 0.3324, 0; Si in 8b) 0.2117(98), 0.1710(97), 0.6988(66); Si in 8b) 0.2899(97), 0.9920(94), 0.0513(54).
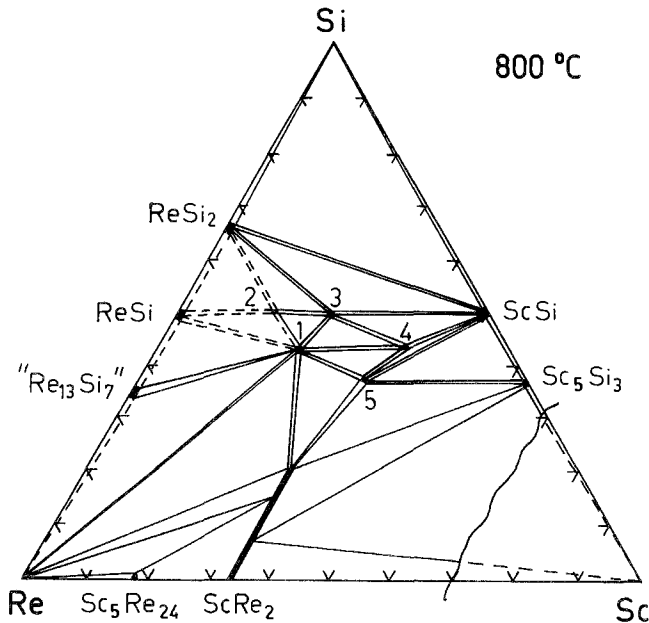
Fig. 44. Sc–Re–Si, isothermal section at 800°C. 1: $Sc_2Re_3Si_4$, 2: $ScRe_2Si_3$, 3: "$ScReSi_2$", 4: "$Sc_8Re_3Si_9$", 5: $Sc_3Re_2Si_3$.

TABLE 26a

Atomic coordinates and individual thermal parameters B for the $ScRe_2Si_3$ structure, after Pecharskij et al. (1979).

Atoms, site	x	y	z	B
Sc 8f)	0.1706(12) [*]	0.1312(8)	0.4880(29)	0.90(10)
Sc 8f)	0.3241(14)	0.1425(8)	0.9970(27)	0.90(10)
Re 8f)	0.3877(3)	0.2049(1)	0.4858(12)	0.17(4)
Re 8f)	0.1221(4)	0.2008(1)	0.9922(14)	0.85(6)
Re 4d)	0	0.0848(1)	0.2534(13)	0.34(2)
Re 4e)	1/2	0.1044(2)	0.7444(12)	0.48(3)
Re 4c)	0.2653(2)	0	0.2110(12)	−0.27(9)
Re 4c)	0.2165(3)	0	0.7175(13)	0.39(4)
Si 8f)	0.3733(12)	0.0752(10)	0.5003(31)	1.10(12)
Si 8f)	0.1568(12)	0.0874(11)	−0.0036(37)	1.02(8)
Si 8f)	0.2688(17)	0.2570(11)	0.2365(36)	1.20(14)
Si 4d)	0	0.3544(9)	0.2169(34)	1.01(12)
Si 4e)	1/2	0.1309(12)	0.2901(33)	1.00(11)
Si 4d)	0	0.2057(12)	0.3649(29)	1.90(19)
Si 4e)	1/2	0.2791(11)	0.3342(32)	1.21(12)
Si 4c)	0.1116(13)	0	0.3386(33)	1.19(13)
Si 4c)	0.3896(16)	0	0.9115(31)	1.14(11)

$Sc_3Re_2Si_3$ crystallizes with the $Sc_3Re_2Si_3$-type of structure with the space group B2 and lattice parameters: $a = 19.604(6)$, $b = 13.741(5)$, $c = 5.339(1)$ and $\gamma = 125.92(2)°$. The crystal structure has been refined by means of X-ray single crystal

TABLE 26b

Atomic coordinates and individual thermal parameters B for the $Sc_3Re_2Si_3$ structure, after Pecharskij et al. (1979).

Atoms, site	x	y	z	B
Sc 4c)	0.1219(9) [*]	0.2092(14)	0.2333(31)	0.88(9)
Sc 4c)	0.3812(8)	0.3113(12)	0.4794(28)	0.94(7)
Sc 4c)	0.3413(9)	0.398(13)	−0.0395(32)	0.80(6)
Sc 4c)	0.0807(7)	0.3987(11)	−0.0020(27)	0.76(9)
Sc 4c)	0.1705(8)	0.1255(12)	0.7158(31)	0.72(8)
Sc 4c)	0.4215(8)	0.0916(13)	0.7369(30)	0.66(7)
Re 4c)	0.0238(1)	0.1654(2)	0.7284(12)	0.22(2)
Re 4c)	0.0257(1)	0.6752(3)	0.4954(14)	0.28(4)
Re 4c)	0.2634(2)	0.0320(2)	0.5023(11)	0.21(3)
Re 4c)	0.2631(1)	0.5322(2)	0.6854(14)	0.02(4)
Si 4c)	0.1190(14)	0.3737(17)	0.4922(41)	1.06(12)
Si 4c)	0.2676(16)	0.3473(18)	0.4612(39)	1.21(9)
Si 4c)	0.3963(11)	0.1352(14)	0.2370(36)	0.97(14)
Si 4c)	0.2248(10)	0.1307(12)	0.2128(42)	1.18(7)
Si 2a)	0	0	−0.0361(48)	1.16(12)
Si 2a)	0	0	0.5036(49)	1.28(10)
Si 2b)	0	1/2	0.2452(43)	1.56(14)
Si 2a)	0	1/2	0.7439(46)	1.29(16)

[*] The figures in brackets are the standard deviations.

counter data to a reliability value of $R = 0.092$ (Pecharskij et al., 1979). Single crystals were obtained from an arc-melted specimen with composition (in a/o) $Sc_{37.5}Re_{25}Si_{37.5}$. This compound was claimed to exist at 800°C. The atom parameters are listed in table 26a.

$ScRe_2Si_3$ crystallizes with the $ScRe_2Si_3$-type of structure: Amm2, $a = 14.486(3)$, $b = 5.2397(13)$. Pecharskij et al. (1979) refined the crystal structure by means of single crystal counter data; the obtained reliability value was $R = 0.102$. Single crystals were obtained from an arc-melted alloy with composition (in a/o) $Sc_{16.6}Re_{33.3}Si_{50}$. This compound was claimed to exist at 800°C. The atomic parameters are listed in table 26b.

The structure types of "$ScReSi_2$" and "$Sc_8Re_3Si_9$" have not been evaluated yet.

References

Pecharskij, V.K., 1979, Autoreferat Dis. Kand. Khim. (abstract of thesis, Russian) (Nauk, Lvov) 23 p.
Pecharskij, V.K., O.I. Bodak and E.I. Gladyshevskij, 1978, Dopov. Akad. Nauk Ukr. RSR, Ser. A, 755.
Pecharskij, V.K., O.I. Bodak and E.I. Gladyshevskij, 1979, Kristallografiya 24, 757.

Sc–Rh–Si

A partial isothermal section (40–100 a/o Si, fig. 45) of the Sc–Rh–Si phase diagram at 1000°C has been derived by Braun et al. (1979) by means of X-ray and metallographic analysis of arc-melted samples, which subsequently were wrapped in Ta foil and heat treated for 7 d and up to 8 weeks at 1000°C in evacuated silica tubes (backfilled with a partial pressure of UHP Ar) and finally quenched in water. Starting materials were Sc 99.9%, Rh 99.9% and Si 99.99999%. Ten of the annealed
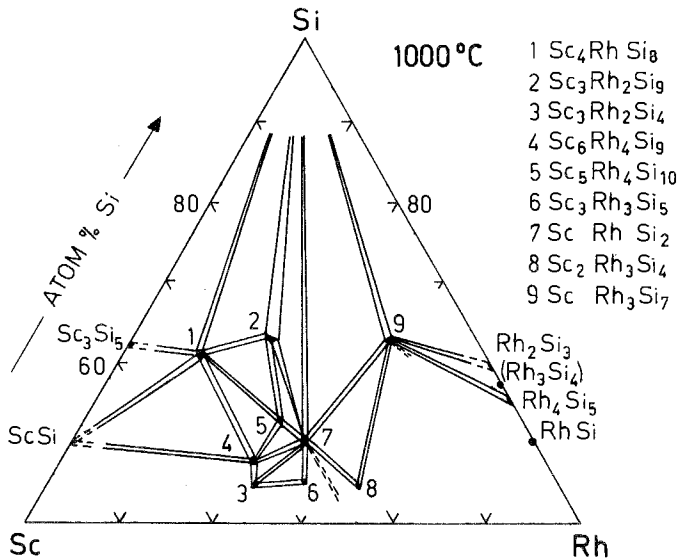
Fig. 45. Sc–Rh–Si, partial isothermal section at 1000°C (50–100 a/o Si). The compound $ScRh_3Si_7$ (no. 9), obtained at (in a/o) $Sc_{9.2}Rh_{28.0}Si_{62.9}$, was earlier called "$ScRh_3Si_6$".

alloys were investigated by electron microprobe analysis (10 kV; Sc-, SiKα, Rh-Lα) using the composition "$Sc_3Rh_2Si_4$" (unknown structure type) as an internal standard. Some of the annealed samples were said to be in the non-equilibrium condition containing about 5 vol% of a fourth phase.

The existence of Sc_3Si_5 (defect AlB_2-type) and ScSi (CrB-type), of RhSi (MnP-type) and Rh_4Si_5 (Rh_4Si_5-type) has been confirmed as well as the crystal structure of Rh_3Si_4, which was observed close to the composition of Rh_2Si_3. Nine ternary phases have been established for Si contents higher than 40 a/o Si.

An additional compound was furthermore observed by Hovestreydt et al. (1982) from arc-melted alloys (see below). The crystal structures of $Sc_3Rh_2Si_9$ [ρ_{exp} = 4.3(1) kg/dm^3], $Sc_3Rh_2Si_4$ [ρ_{exp} = 5.19(6)], "$Sc_6Rh_4Si_9$" [ρ_{exp} = 4.96(6)], $Sc_3Rh_3Si_5$ [ρ_{exp} = 5.50(9)] and $Sc_2Rh_3Si_4$ [ρ_{exp} = 6.2(1)] have not yet been characterized. The actual composition of "$Sc_6Rh_4Si_9$" as derived by microprobe was $Sc_{31.5}Rh_{20.6}Si_{47.9}$ and thus with equal likelihood might be represented by a formula such as "$Sc_3Rh_2Si_5$". The X-ray powder diagrams of "$Sc_3Rh_2Si_4$" and "$Sc_6Rh_4Si_9$" were claimed to reveal striking similarities in d values and intensities. Microprobe measurements indicate a small homogeneous range (14.0–15.5 a/o Rh) for "$Sc_3Rh_2Si_9$".

In a later paper by Braun and Segre (1980) the crystal structure of "Sc_4RhSi_8" was suspected to be isotypic with the crystal structure of $ScCo_{0.25}Si_{1.75}$ with the $ZrSi_2$-type. Furthermore "Sc_4RhSi_8" is superconducting below T_c = 1.8 K.

Braun et al. (1980) characterized the crystal structure of $Sc_5Rh_4Si_{10}$ from X-ray powder diffractometer data: $Sc_5Co_4Si_{10}$-type of structure, P4/mbm, a = 12.325(6), c = 4.032(3), ρ_x = 4.97(2), ρ_{exp} = 4.90(6). $Sc_5Rh_4Si_{10}$ is superconducting at T_c = 8.5 K (Braun and Segre, 1980). The investigation of phase equilibria involving $Sc_5Rh_4Si_{10}$ at 1150°C (samples annealed for 2–7 d) and at 800°C (samples annealed for 7 d), revealed that $Sc_5Rh_4Si_{10}$ is a high-temperature compound absent at 800°C but stable at temperatures higher than 800°C. Thus "Sc_4RhSi_8" and $ScRhSi_2$ were observed to form a two-phase equilibrium at 800°C, whereas phase equilibria at 1150°C are consistent with those at 1000°C.

$ScRhSi_2$ is a derivative structure of Re_3B and crystallizes with the ordered YZn_3-type of structure [Pnma, a = 6.292(4), b = 4.025(4), c = 9.517(5), ρ_x = 5.62(1), ρ_{exp} = 5.36(7) kg/dm^3]. The crystal structure has been refined by Chabot et al. (1981a) from single crystal counter data with a reliability value as low as R = 0.052. Accordingly the atom parameters were: Sc in 4c) 0.2385(4), 1/4, 0.3181(3); Rh in 4c) 0.5832(2), 1/4, 0.9008(1); Si in 4c) 0.9573(6), 1/4, 0.8413(4); Si in 4c) 0.2318(7), 1/4, 0.0282(4). No superconductivity was observed for temperatures above T_n = 1 K.

Chabot et al. (1981b) refined the crystal structure of $ScRh_3Si_7$ with the $ScRh_3Si_7$-type by means of single crystal counter data; the space group is R$\bar{3}$c with hexagonal cell units a_H = 7.5056(6) and c_H = 19.691(4), ρ_x = 5.706, ρ_{exp} = 5.81(7). The reliability value obtained was R = 0.037. In the earlier paper by Braun et al. (1979) this compound was denoted as "$ScRh_3Si_6$". No superconductivity was reported.

Hovestreydt et al. (1982) characterized the crystal structure of ScRhSi from single crystal counter data: TiNiSi-type of structure, Pnma, a = 6.4736(7), b = 4.0500(3)

and $c = 7.2483(9)$. Atom parameters according to $R = 0.052$ were as follows: Sc in 4c) 0.0094(6), 1/4, 0.6893(5); Rh in 4c) 0.1568(2), 1/4, 0.0620(2) and Si in 4c) 0.2857(8), 1/4, 0.3851(7). Samples were obtained by arc melting under argon.

References

Braun, H.F. and C.U. Segre, 1980, Solid State Commun. **35**, 735.
Braun, H.F., G. Burri and L. Rinderer, 1979, J. Less-Common Metals **68**, P1.
Braun, H.F., K. Yvon and R.M. Braun, 1980, Acta Crystallogr. **B36**, 2397.
Chabot, B., H.F. Braun, K. Yvon and E. Parthé, 1981a, Acta Crystallogr. **B37**, 668.
Chabot, B., N. Engel and E. Parthé, 1981b, Acta Crystallogr, **B37**, 671.
Hovestreydt, E., N. Engel, K. Klepp, B. Chabot and E. Parthé, 1982, J. Less-Common Metals **86**, 247.

Sc–Ru–Si

Braun and Segre (1980) reported the existence of a compound $Sc_3Ru_2Si_6$. For sample preparation, see $Sc_3Os_2Si_6$. X-ray powder diffraction patterns were tentatively indexed on the basis of an orthorhombic unit cell [$a = 8.939(8)$, $b = 9.061(8)$, $c = 4.175(7)$, $\rho_x = 4.96(2)$] with a close resemblance to the unit cell of $Sc_5Ir_4Si_{10}$: $a \approx b(Sc_3Ru_2Si_6) \approx (\sqrt{2}/2)a(Sc_5Ir_4Si_{10})$ and $c(Sc_3Ru_2Si_6) \approx c(Sc_5Ir_4Si_{10})$; $T_n = 1.2$ K.

According to X-ray powder diffraction data of Hovestreydt et al. (1982) ScRuSi has the ZrNiAl-type of structure (ordered Fe_2P-type) with space group $P\bar{6}2m$ and lattice parameters $a = 6.851(3)$, $c = 3.423(2)$. Alloys were prepared by arc melting under argon and subsequent annealing at 1000°C for 1–2 weeks. Starting materials were Sc 99.9%, Ru 99.99%, Si 99.999%.

References

Braun, H.F. and C.U. Segre, 1980, Solid State Commun. **35**, 735.
Hovestreydt, E., N. Engel, K. Klepp, B. Chabot and E. Parthé, 1982, J. Less-Common Metals **86**, 247.

Sc–Sm–Si

According to X-ray powder data by Mokra and Bodak (1979) SmScSi is tetragonal with the CeScSi-type of structure (ordered Ca_2As-type, I4/mmm) and lattice parameters $a = 4.255(5)$ and $c = 15.56(2)$. For sample preparation, see CeScSi.

Reference

Mokra, I.P. and O.I. Bodak, 1979, Dopov. Akad. Nauk Ukr. RSR, Ser. A, 312.

Sm–Ag–Si

According to an X-ray powder analysis by Mayer et al. (1972) the compound $SmAg_2Si_2$ crystallizes with the ordered $ThCr_2Si_2$-type of structure [I4/mmm, $a = 4.169(5)$ and $c = 10.69(5)$]. For sample preparation, see $LaAg_2Si_2$. Alloys were multiphase also containing some excess Ag as well as small amounts of $SmSi_2$ phases (tetragonal and/or orthorhombic modification?).

Reference

Mayer, I., J. Cohen and I. Felner, 1972, J. Less-Common Metals **29**, 221 and 1973, J. Less-Common Metals **30**, 181.

Sm–Al–Si

No ternary diagram is available for the system Sm–Al–Si; the formation of a compound $SmAl_2Si_2$, however, was reported by Muravyova et al. (1972). From powder X-ray diffraction studies $SmAl_2Si_2$ was found to adopt the La_2O_2S-type of structure with the space group $P\bar{3}m1$ and $z = 1$. The atomic order and parameters as derived for the isostructural compound $CaAl_2Si_2$ were found to be appropriate for the powder intensity calculation: 1 R(Sm) in 1a) 0,0,0; 2 Al in 2d) $1/2$, $2/3$, $z = 0.63$ and 2 Si in 2d) $z = 0.27$. The lattice parameters were $a = 4.19$ and $c = 6.62$ Å. Samples were prepared by arc melting the powder compacts under argon, followed by a heat treatment in evacuated silica tubes for 150–750 h at 500°C. Starting materials were Sm 98.5%, Al 99.98% and Si 99.99%.

Reference

Muravyova, A.A., O.S. Zarechnyuk and E.I. Gladyshevskij, 1972, Visn. L'vivsk. Univ. Ser. Khim. **13**, 14.

Sm–Au–Si

The crystal structure of $SmAu_2Si_2$ has been refined by Mayer et al. (1973) from X-ray powder diffraction data. $SmAu_2Si_2$ adopts the ordered $ThCr_2Si_2$-type of structure with space group $I4/mmm$ and lattice parameters: $a = 4.260(5)$ and $c = 10.17(5)$. Random distribution of Au and Si atoms was excluded and atom parameters with respect to the obtained reliability value $R = 0.044$ were given as follows: Au in 4d) and Si in 4e) $z = 0.390$. For sample preparation, see $LaAu_2Si_2$. From susceptibility measurements in the range of 4.2 K to 300 K Felner (1975) observed antiferromagnetic ordering at $T_N = 15.9$ K. Paramagnetic data were $\mu_{eff}^{para} = 0.63$ μ_B and $\theta_p = 2.5$ K.

References

Felner, I., 1975, J. Phys. Chem. Sol. **36**, 1063.
Mayer, I., J. Cohen and I. Felner, 1973, J. Less-Common Metals **30**, 181.

Sm–Co–Si

At least six ternary phases have been characterized in the Sm–Co–Si system. Mayer and Tassa (1969) investigated the phase equilibria at 700–800°C in the $SmCo_xSi_{2-x}$ system. For $x < 0.4$ the $ThSi_2$-type of structure was observed, and for $x > 0.4$ the X-ray powder patterns were said to be complex. At a composition $SmCo_{0.4}Si_{1.6}$ the hexagonal AlB_2-type of structure was found to be stable ($a = 4.017$, $c = 4.180$). In similarity to the X-ray diffraction data of $NdFe_{0.4}Si_{1.6}$ a statistical distribution of Co and Si atoms in the sites of $P6/mmm$ was assumed. For sample preparation, see $GdCo_{0.4}Si_{1.6}$.

SmCoSi is isostructural with the PbFCl-type of structure: P4/nmm, $a = 4.010(3)$, $c = 6.776(5)$ (Bodak et al., 1970; X-ray powder analysis). For atom parameters and sample preparation, see CeFeSi.

SmCo$_2$Si$_2$ crystallizes with the ordered ThCr$_2$Si$_2$-type of structure: I4/mmm, $a = 3.934$, $c = 9.845$, $\rho_x = 7.07$ kg/dm^3 (Rossi et al., 1978; X-ray powder analysis). For sample preparation and etching conditions, see YCo$_2$Si$_2$.

Bodak and Gladyshevskij (1969) reported SmCo$_9$Si$_2$ to crystallize with the BaCd$_{11}$-type of structure: I4$_1$/amd, $a = 9.775(5)$, $c = 6.306(10)$ (X-ray powder analysis of arc-melted alloys). Atomic ordering is quite similar to CeNi$_{8.6}$Si$_{2.4}$.

Pelizzone et al. (1982) investigated the structural and magnetochemical behavior of SmCoSi$_2$ with the CeNiSi$_2$-type [Cmcm, $a = 4.097(2)$, $b = 16.358(7)$ and $c = 4.010(2)$]. Samples were prepared by arc melting and subsequent annealing in sealed quartz capsules at 1000°C for one week. The magnetic susceptibilities are characterized by a typical Van Vleck paramagnetism of closely spaced multiplets; magnetic ordering occurs at 4.0 K.

Without any further details, Gladyshevskij and Bodak (1973) reported the existence of a compound SmCoSi$_3$ probably isotypic with CeCoSi$_3$ ($a = 4.085$, $c = 9.536$, BaAl$_4$-derivative; as cited by Gladyshevskij and Bodak, 1982).

References

Bodak, O.I. and E.I. Gladyshevskij, 1969, Dopov. Akad. Nauk Ukr. RSR, Ser. A **5**, 452.

Bodak, O.I., E.I. Gladyshevskij and P.I. Kripyakevich, 1970, Zh. Strukt. Khim. **11**(2), 305.

Gladyshevskij, E.I. and O.I. Bodak, 1973, in: Khim. Met. Splavov, N.M. Zhavoronkov ed. (Nauka, Moscow, USSR) p. 46.

Gladyshevskij, E.I. and O.I. Bodak, 1982, Kristallokhim. Intermet. Soedin, Redkozemel, Metallov, Lvov, Vysha Schola.

Mayer I. and M. Tassa, 1969, J. Less-Common Metals **19**, 173.

Pelizzone, M., H.F. Braun and J. Müller, 1982, J. Magn. Magn. Mater. **30**, 33.

Rossi, D., R. Marazza and R. Ferro, 1978, J. Less-Common Metals **58**, 203.

Sm–Cu–Si

Rieger and Parthé (1969a) investigated the occurrence of the AlB$_2$-type structure in arc-melted alloys with composition SmCu$_{0.67}$Si$_{1.33}$ ($a = 4.044$, $c = 4.117$) and SmCuSi ($a = 4.082$, $c = 4.075$). In accordance with the X-ray powder intensities Si and Cu atoms were reported to statistically occupy the 2d site of space group P6/mmm. From arc-melted alloys annealed at 750°C, Iandelli (1983) recorded the formation of SmCuSi with the ordered Ni$_2$In-type [superstructure of the AlB$_2$-type, P6$_3$/mmc, $a = 4.185(1)$, $c = 7.669(4)$]. The superstructure reflections were said to be faint. Iandelli (1983) obtained different results than Rieger and Parthé (1969a), in that the new phase was suspected to be the low-temperature modification and accordingly a thermal analysis up to 1400°C revealed a thermal arrest at 1210°C. For details in sample preparation and purities of the starting materials, see YbCuSi.

The compound SmCu$_2$Si$_2$ crystallizes with the ThCr$_2$Si$_2$-type of structure. X-ray powder data given by Rieger and Parthé (1969b) were as follows: $a = 4.025(6)$, $c = 9.928(10)$ and I4/mmm. For sample preparation, see YCu$_2$Si$_2$. No temperature

dependence was observed for the magnetic susceptibility of $SmCu_2Si_2$ (77–300 K, Kido et al., 1983). NMR data have been presented by Sampathkumaran et al. (1979). For X-ray absorption measurements, see Padalia et al. (1983). Without details Bodak et al. (1971) mentioned the existence of a compound $SmCu_{1.6}Si_{1.4}$ with the $CeNiSi_2$-type.

References

Bodak, O.I., E.I. Gladyshevskij and Ya.M. Kalvijak, 1971, Tesizy. Dokl. Vses. Konf. Kristallokhim. Intermet. Soedin, Lvov, p. 40.
Iandelli, A., 1983, J. Less-Common Metals **90**, 121.
Kido, H., T. Hoshikawa, M. Shimada and M. Koizumi, 1983. Phys. Stat. Sol. (a) 77, K121.
Padalia, B.D., T.K. Hatwar and M.N. Ghatikar, 1983, J. Phys. **C16**, 1537.
Rieger, W. and E. Parthé, 1969a, Monatsh. Chem. **100**, 439.
Rieger, W. and E. Parthé, 1969b, Monatsh. Chem. **100**, 444.
Sampathkumaran, E.V., L.C. Gupta and R. Vijayaraghavan, 1979, J. Phys. **C12**, 4323.

Sm–Fe–Si

At least four ternary compounds exist in the Sm–Fe–Si system.

Mayer and Tassa (1969) investigated the phase equilibria within the section $SmFe_xSi_{2-x}$ at 700–800°C. For $x < 0.4$ the $ThSi_2$-type structure was said to be stable. $SmFe_{0.4}Si_{1.6}$ crystallizes with the AlB_2-type of structure ($a = 4.020$, $c = 4.165$). In analogy to the X-ray powder intensity data of $NdFe_{0.4}Si_{1.6}$ a statistical distribution of Fe, Si atoms in the 2d site of P6/mmm was assumed. Both sublattices in $SmFe_{0.4}Si_{1.6}$ are paramagnetic above 4.2 K (high-spin state); the high value for its molar Curie constant of 4.10 emu was claimed to be due to iron impurities. For sample preparation, see $GdCo_{0.4}Si_{1.6}$, Felner and Schieber (1973).

The thermal expansion coefficients have been determined by Mayer and Felner (1972), by means of high-temperature X-ray diffractometry: $\alpha_a = 8.9 \times 10^{-6}$ deg^{-1}, $\alpha_c = 18.6 \times 10^{-6}$ deg^{-1}, $\bar{\alpha} = 12.1 \times 10^{-6}$ deg^{-1}, $\gamma = 34.5 \times 10^{-6}$ deg^{-1} (volume expansion coefficient). Lattice parameters change as follows: at 25°C, $a = 4.076(1)$, $c = 4.263(1)$; at 430°C, $a = 4.089(1)$, $c = 4.283(1)$; at 600°C, $a = 4.096(1)$, $c = 4.310(1)$; at 800°C, $a = 4.104(1)$, $c = 4.323(1)$; at 940°C, $a = 4.112(1)$, $c = 4.347(1)$. $SmFe_{0.4}Si_{1.6}$ was said to decompose at 1100°C.

$SmFe_2Si_2$ was reported by Felner et al. (1975) to crystallize with the ordered $ThCr_2Si_2$-type of structure: I4/mmm, $a = 3.952(5)$, $c = 9.985(5)$ (X-ray powder analysis of alloys melted in a high-frequency furnace). Weak ferromagnetic ordering occurs at $T_m = 723(5)$ K. From magnetization and Mössbauer effect studies most of the iron was concluded to be diamagnetic ($\sim 94\%$).

SmFeSi crystallizes with the PbFCl-type of structure: P4/nmm, $a = 4.031(3)$, $c = 6.829(5)$ (Bodak et al., 1970; X-ray powder diffraction). For sample preparation, see CeFeSi.

$Sm_2Fe_3Si_5$ is isotypic with the structure type of $Sc_2Fe_3Si_5$: P4/mnc, $a = 10.47(1)$, $c = 5.55(1)$ (X-ray powder diffraction data by Braun, 1980). For sample preparation, see $Dy_2Fe_3Si_5$. Mössbauer data indicate the absence of a magnetic moment at the iron site (Braun et al., 1981). No superconductivity was observed above $T_n = 1$ K.

Low temperature heat capacity data reveal multiple antiferromagnetic transitions at $T_m = 8.96$, 7.35, 6.19 and 5.05 K (Vining and Shelton, 1983).

References
Bodak, O.I., E.I. Gladyshevskij and P.I. Kripyakevich, 1970, Zh. Strukt. Khim. **11**(2), 305.
Braun, H.F., 1980, Phys. Lett. **75A**(5), 386.
Braun, H.F., C.U. Segre, F. Acker, M. Rosenberg, S. Dey and P. Deppe, 1981, J. Magn. Magn. Mater, **25**, 117.
Mayer, I. and I. Felner, 1972, J. Less-Common Metals **29**, 25.
Mayer, I. and M. Tassa, 1969, J. Less-Common Metals **19**, 173.
Felner, I. and M. Schieber, 1973, Solid State Commun. **13**, 457.
Felner, I., I. Mayer, A. Grill and M. Schieber, 1975, Solid State Commun. **16**, 1005.
Vining, C.B. and R.N. Shelton, 1983, Phys. Rev. **B28**(5), 2732.

Sm–Ge–Si

Mayer and Eshdat (1968) investigated the concentration sections $SmGe_{2-x}Si_x$ and $SmGe_{1.6-x}Si_x$ by means of X-ray powder diffraction methods. For sample preparation, see $NdGe_{2-x}Si_x$. Ge-rich alloys of the series $SmGe_{2-x}Si_x$ were said to adopt the $ThSi_2$-type of structure ($I4_1/amd$). Alloys richer in Si crystallized with the orthorhombic $GdSi_2$-type (Imma). The variation of lattice parameters versus x is shown in fig. 46a; the unit cell volume changes linearly with x as presented in fig. 11. All the alloys of the $SmGe_{1.6-x}Si_x$ series had the tetragonal $ThSi_2$-type of structure, which was tentatively related to a uniform distribution of Ge and Si atoms and random vacancy formation on the non-metal sites (fig. 46b). See also $NdGe_{2-x}Si_x$.

Reference
Mayer, I. and Y. Eshdat, 1968, Inorg. Chem. **9**, 1904.
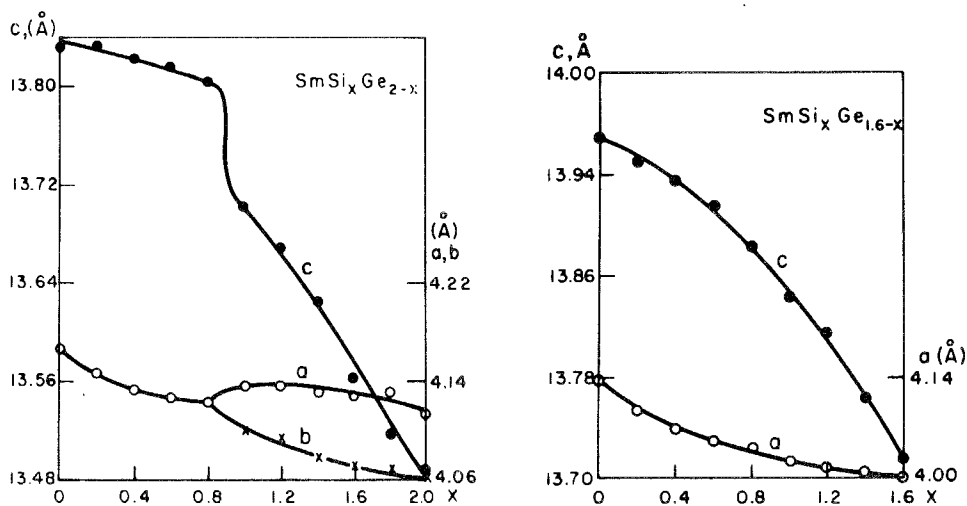
Fig. 46. Sm–Ge–Si, (a) section $SmGe_{2-x}Si_x$ and (b) section $SmGe_{1.6-x}Si_x$, lattice parameter variation versus concentration, after Mayer and Eshdat (1968).

Sm–Mn–Si

SmMn$_2$Si$_2$ crystallizes with the ThCr$_2$Si$_2$-type of structure: I4/mmm, $a = 3.975$, $c = 10.520$, $\rho_x = 6.32$ kg/dm^3 (Rossi et al., 1978; X-ray powder diffraction). For sample preparation, see LaMn$_2$Si$_2$. Knigenko et al. (1977) measured $a = 3.964$ and $c = 10.500$ (X-ray powder data). For sample preparation, see Y–Mn–Si. Szytula and Szott (1981) characterized the magnetic behavior by antiferromagnetic ordering at $T_N = 398$ K and $\mu_{eff}^{para} = 3.3$ μ_B mole^{-1}.

SmMnSi is tetragonal with the PbFCl-type of structure: P4/nmm, $a = 4.060$, $c = 7.215$ (Knigenko et al., 1977; X-ray powder data). For sample preparation, see Y–Mn–Si.

References

Knigenko, L.D., I.R. Mokra and O.I. Bodak, 1977, Vestn. Lvov Univ., Ser. Khim. **19**, 68.
Rossi, D., R. Marazza, D. Mazzone and R. Ferro, 1978, J. Less-Common Metals **59**, 79.
Szytula, A. and I. Szott, 1981, Solid State Commun. **40**, 199.

Sm–Ni–Si

No phase diagram has been published. At least eight ternary compounds exist (see table 27).

Mayer and Tassa (1969) investigated the phase equilibria within the concentration section SmNi$_x$Si$_{2-x}$ by means of X-ray powder analysis. For $x < 0.4$ the ThSi$_2$-type of structure was found to be stable. SmNi$_{0.4}$Si$_{1.6}$ crystallizes with the AlB$_2$-type of structure (see table 27). In analogy to the X-ray powder data of NdNi$_{0.4}$Si$_{1.6}$ a statistical distribution of Ni/Si atoms in the 2d site of P6/mmm was assumed. Ni/Si atom ordering, however, seems to be likely (see also Mössbauer data of isotypic LaFe$_{0.4}$Si$_{1.6}$).

Levin et al. (1977) reported electrophysical properties of SmNi$_2$Si$_2$ (temperature dependence of electrical resistance, thermoelectric coefficient, magnetic susceptibility as well as the preparation of stoichiometric thin films).

References

Bodak, O.I. and E.I. Gladyshevskij, 1969a, Dopov. Akad. Nauk Ukr. RSR, Ser. A **5**, 452.
Bodak, O.I. and E.I. Gladyshevskij, 1969b, Dopov. Akad. Nauk Ukr. RSR, Ser. A **12**, 1125.
Bodak, O.I. and E.I. Gladyshevskij, 1969c, Kristallografiya **14** (6), 990.
Bodak, O.I., E.I. Gladyshevskij and P.I. Kripyakevich, 1966, Izv. Akad. Nauk SSSR, Neorg. Mater. **2**(12), 2151.
Gladyshevskij, E.I. and O.I. Bodak, 1965, Dopov. Akad. Nauk Ukr. RSR, Ser. A **5**, 601.
Gladyshevskij, E.I., P.I. Kripyakevich and O.I. Bodak, 1966, Acta Crystallogr. **A21**, 80; Z. Anorg. Allg. Chem. **344**, 95.
Klepp, K. and E. Parthé, 1982, J. Less-Common Metals **83**, L33.
Levin, E.M., R.V. Lutsiv, E.I. Gladyshevskij and O.I. Bodak, 1977, Fiz. Elektron. Resp. Liezhved. Nauch-tekn. Sbor. **15**, 59.
Mayer, I. and M. Tassa, 1969, J. Less-Common Metals **19**, 173.

TABLE 27

Formation and structural data of ternary compounds Sm–Ni–Si.

Compound	Structure type Space group	Lattice parameters Density	Preparation, Characterization	Refs.	Purity
$Sm_3Ni_6Si_2$	$Ce_3Ni_6Si_2$ ord. Ca_3Ag_8 Im3m	$a = 8.850(2)$	arc, Qu(Ni) 800 °C, 2 weeks PXD	GlKB, 66	Sm 97.7 Ni 99.99 Si 99.99
$SmNi_{8.6}Si_{2.4}$	$Ce_2Ni_{17}Si_5$ $(BaCd_{11})$ $I4_1/amd$	$a = 9.779(5)$ $c = 6.206(10)$	arc(Ar), Qu 800 °C, 250 h, PXD atom order as for $CeNi_{8.6}Si_{2.4}$	BoG, 69a	Ni 99.91 Si 99.99
$SmNi_{8.6}Si_{4.4}$ [*] ~ 30 a/o Si	$Ce_2Ni_{17}Si_9$ $(NaZn_{13}$-deriv.) I4/mcm	$a = 11.02(1)$ [*] $c = 11.40(1)$	arc(Ar), Qu 800 °C, 100 h, PXD	BoG, 69b	Sm 99.2 Bi 99.99 Si 99.99
$Sm(Ni,Si)_{13}$ ~ 37–45 a/o Si	$NaZn_{13}$ Fm3c	$a = 11.12(1)$	arc(Ar), Qu 800 °C, 100 h, PXD	BoG, 69b	Sm 99.2 Ni 99.99 Si 99.99
Sm_3NiSi_2 [**]	Gd_3NiSi_2 filled Hf_3P_2 Pnma	$a = 11.505(3)$ $b = 4.189(3)$ $c = 11.388(3)$	arc(Ar), Qu(Ta) 800 °C, 4 weeks single crystal study	KlP, 82	Sm 99.9 Ni 99.99 Si 5N
$SmNi_2Si_2$	$ThCr_2Si_2$ I4/mmm	$a = 3.997(10)$ $c = 9.577(10)$	arc(Ar) PXD	BoGK, 66	Sm 97.7 Ni 99.8 Si 99.99
$SmNiSi_2$	$CeNiSi_2$ Cmcm	$a = 4.073(2)$ $b = 16.423(10)$ $c = 4.002(2)$	arc(Ar) PXD	BoG, 69c	Sm 97.7 Ni 99.8 Si 99.99
$SmNi_{0.4}Si_{1.6}$	AlB_2 P6/mmm	$a = 3.997$ $c = 4.175$	HT in Al_2O_3 or MgO_2 induction heating 1500 °C, Ar, Qu 700–800 °C, 24–96 h, PXD	MaT, 69	Sm 99.9 Ni 99.95 Si 99.99
		$a = 4.002(2)$ $c = 4.160(5)$	arc(Ar) PXD	GlB, 65	Ni 99.8 Si 99.99

[*] For a correct setting of the bct unit cell $a = 7.793$ ($a = a_0/\sqrt{2}$).

[**] The crystal structure of Sm_3NiSi_2 (filled-up Hf_3P_2-type) has been refined from X-ray single crystal counter data (Klepp et al., 1982): $R = 0.023$. Atom parameters were (all atoms in site 4c of Pnma): Sm, 0.05775(6), 1/4, 0.37559(6); Sm, 0.21373(7), 1/4, 0.69768(6); Sm, 0.38207(7), 1/4, 0.44029(6); Ni, 0.1286(2), 1/4, 0.1332(1); Si, 0.3013(3), 1/4, 0.0061(3); Si, 0.4726(4), 1/4, 0.6866(3).

Sm–Os–Si

$SmOs_2Si_2$ is tetragonal with the space group I4/mmm and with the $ThCr_2Si_2$-type of structure (Hiebl et al., 1983; X-ray powder analysis). The lattice parameters were

$a = 4.1490(5)$ and $c = 9.8122(50)$. For sample preparation, see YOs_2Si_2. For temperatures above 25 K, the magnetic susceptibility corresponds to a Van Vleck behavior of closely spaced multiplets with $\mu_{eff}^{para} = 0.47$ μ_B and $\theta_p = 12$ K. Antiferromagnetic order was observed at 5 K.

Reference
Hiebl, K., C. Horvath, P. Rogl and M.J. Sienko, 1983, Solid State Commun. **48**, 211.

Sm–Pd–Si

$SmPd_2Si$ is orthorhombic with the ordered Fe_3C-type: Pnma, $a = 7.445(3)$, $b = 6.905(2)$ and $c = 5.584(2)$ (X-ray powder data by Moreau et al., 1982). For sample preparation, see YPd_2Si.

According to an X-ray powder diffraction investigation by Ballestracci (1976) $SmPd_2Si_2$ was observed to crystallize with the ordered $ThCr_2Si_2$-type of structure: I4/mmm, $a = 4.160$, $c = 9.96$. For sample preparation, see $CePd_2Si_2$.

References
Ballestracci, R., 1976, C.R. Acad. Sci. Paris, Ser. B **282**, 291.
Moreau, J., J. Leroy and D. Paccard, 1982, Acta Crystallogr. **B38**, 2446.

Sm–Pt–Si

SmPtSi crystallizes with the LaPtSi-type of structure: $I4_1md$, $a = 4.1300(9)$, $c = 14.376(4)$ (Klepp and Parthé, 1982; X-ray powder analysis). For sample preparation, see LaPtSi. Congruent melting behavior is indicated.

$SmPt_2Si_2$ was reported by Ballestracci and Astier (1978) to crystallize in a primitive tetragonal symmetry, $a = 4.205$, $c = 9.78$ (X-ray diffraction of alloys melted in an induction furnace under argon). The primitive tetragonal crystal symmetry with an atomic arrangement similar to the $CaBe_2Ge_2$-type was recently confirmed from X-ray powder data of arc-melted alloys (Rogl, 1984): $a = 4.2040(7)$, $c = 9.7751(57)$, $CePt_2Si_2$-type.

References
Ballestracci, R. and G. Astier, 1978, C.R. Acad. Sci. Paris, Ser. B **286**, 109.
Klepp, K. and E. Parthé, 1982, Acta Crystallogr. **B38**, 1105.
Rogl, P., 1984, Inorg. Chem., to be published.

Sm–Re–Si

The phase equilibria in the ternary system Sm–Re–Si have been investigated by Pecharskij (1979), by means of X-ray analysis of 36 ternary alloys which were arc melted and subsequently annealed in evacuated quartz capsules for 400 + 600 h at 800°C and finally quenched in water. Starting materials were Sm 97.7%, Re 99.99% and Si 99.99%.

$SmRe_2$ crystallizes with the $MgZn_2$-type; the phase relations in the binary systems
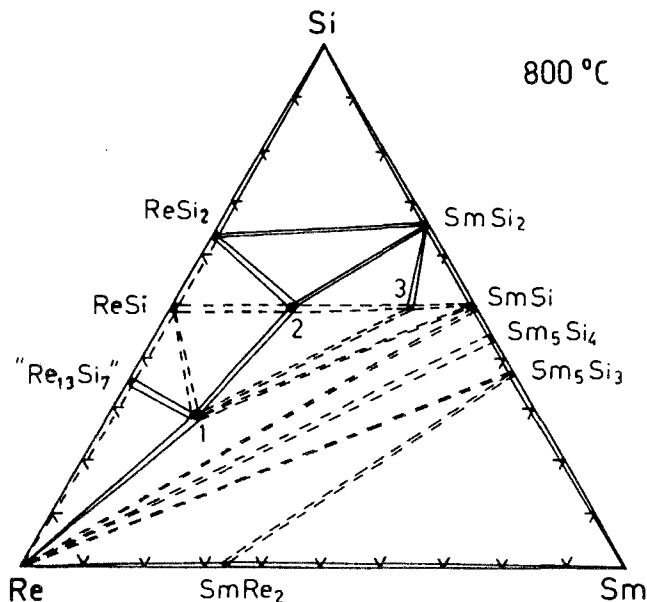
Fig. 47. Sm–Re–Si, partial isothermal section at 800°C (0–33 a/o Sm). 1: $SmRe_4Si_2$, 2: $Sm_2Re_3Si_5$, 3: "Sm_4ReSi_5".

Sm–Si and Re–Si are discussed in context with the ternary systems Ce–Sm–Si and Y–Re–Si, respectively. The mutual solid solubilities of Sm and Re silicides as well as of $SmRe_2$ at 800°C were found to be small and within 1–2 a/o of the third constituent.

The ternary phase equilibria (fig. 47, partial isothermal section for 0–33 a/o Sm at 800°C) are characterized by the existence of three ternary compounds: $SmRe_4Si_2$, $Sm_2Re_3Si_5$ and "Sm_4ReSi_5"; the crystal structure of the latter is uncertain.

$Sm_2Re_3Si_5$ is isotypic with the $Sc_2Fe_3Si_5$-type of structure, P4/mnc, $a = 10.95(1)$, $c = 5.599(5)$ (Bodak et al., 1978; X-ray powder diffraction of arc melted alloys; no detailed conditions for heat treatment were presented). Segre (1981) confirmed the structure type, but observed slightly different lattice parameters: $a = 10.97(1)$ and $c = 5.604(8)$. Samples were arc melted; $T_n = 1.2$ K.

$SmRe_4Si_2$ crystallizes with the $ZrFe_4Si_2$-type of structure: $P4_2/mnm$, $a = 7.332(5)$ and $c = 4.112(1)$ (Bodak et al., 1978; X-ray powder diffraction of arc-melted alloys).

References
Bodak, O.I., V.K. Pecharskij and E.I. Gladyshevskij, 1978, Izv. Akad. Nauk SSSR, Neorg. Mater. **14**(2), 250.
Pecharskij, V.K., 1979, Autoreferat Dis. Kand. Khim. (abstract of thesis, Russian) (Nauk, Lvov) 23 p.
Segre, C.U., 1981, Thesis, Univ. of Calif., San Diego, USA.

Sm–Rh–Si

Four ternary silicides have been reported for the Sm–Rh–Si system.
According to X-ray powder data by Ballestracci (1976), the compound $SmRh_2Si_2$

crystallizes with the ordered $ThCr_2Si_2$-type of structure: I4/mmm, $a = 4.053$ and $c = 10.03$. For sample preparation, see YRh_2Si_2. In good agreement with this, Felner and Nowik (1983) reported $a = 4.054(2)$ and $c = 10.03(1)$ (X-ray powder analysis of induction melted alloys); $SmRh_2Si_2$ is antiferromagnetic below $T_N = 46$ K. The existence of a second peak in the susceptibility curve versus temperature at $T_m = 8(2)$ K was interpreted as itinerant electron ordering of the Rh sublattice.

$SmRh_3Si_2$ is isotypic with the crystal structure of $CeCo_3B_2$: P6/mmm, $a = 5.510(6)$, $c = 3.552(4)$ (Chevalier et al., 1981; X-ray powder analysis). For sample preparation, see $LaRh_3Si_2$. $SmRh_3Si_2$ orders ferromagnetically at $T_m = 34$ K. At 300 K the effective paramagnetic moment was $\mu_{eff}^{para} = 1.63\ \mu_B$ mole^{-1}. The coercive force at 4.2 K is $H_c = 14$ kOe and the saturation magnetization is 0.15 μ_B.

Chevalier et al. (1982) reported structure and magnetochemical properties of the compound $Sm_2Rh_3Si_5$ crystallizing with the $Sc_2Co_3Si_5$-type of structure. The space group is Ibam and lattice parameters were given as $a = 9.83(1)$, $b = 11.75(1)$ and $c = 5.772(5)$. Magnetic susceptibilities in the temperature range from 4.2 K to 300 K were characterized by a Van Vleck paramagnetism of closely spaced multiplets. No superconductivity has been found above 2 K.

The existence of Sm_2RhSi_3 with an AlB_2-derivative type of structure has been reported by Chevalier et al. (1982).

References

Ballestracci, R., 1976, C.R. Acad. Sci. Paris, Ser. B **282**, 291.
Chevalier, B., A. Cole, P. Lejay and J. Etourneau, 1981, Mater. Res. Bull. **16**, 1067.
Chevalier, B., P. Lejay, J. Etourneau, M. Vlasse and P. Hagenmuller, 1982, Paper presented at the 7th Intern. Conf. on Solid Compounds of Transition Elements, Grenoble, France, Collected Abstracts, II B 16, and 1982, Mater. Res. Bull. **17**, 1211.
Felner, I. and I. Nowik, 1983, Solid State Commun. **47**, 831.

Sm–Ru–Si

The existence of a compound $SmRu_3Si_2$ with the $LaRu_3Si_2$-type of structure was reported by Barz (1980) from X-ray powder analysis. No lattice parameter data were given. For sample preparation and melting behavior (phase equilibria), see $LaRu_3Si_2$. Magnetic ordering was reported at $T_m > 25$ K.

From X-ray powder data Ballestracci and Astier (1978) reported the compound $SmRu_2Si_2$ to crystallize with the $ThCr_2Si_2$-type of structure: I4/mmm, $a = 4.178$ and $c = 9.71$. Samples were prepared by induction melting under argon. Hiebl et al. (1983) confirmed the structure type, but from X-ray powder data reported slightly different unit cell dimensions: $a = 4.1710(5)$ and $c = 9.6601(59)$. For sample preparation, see YOs_2Si_2. The magnetic behavior of $SmRu_2Si_2$—investigated in the temperature range of 1.5 K to 1100 K—is characterized by $\mu_{eff}^{para} = 0.54\ \mu_B$, $\theta_p = 14.4$ K and antiferromagnetic ordering at 7 K (Hiebl et al., 1983).

References

Ballestracci, R. and G. Astier, 1978, C.R. Acad. Sci. Paris, Ser. B **286**, 109.
Barz, H., 1980, Mater. Res. Bull. **15**, 1489.
Hiebl, K., C. Horvath, P. Rogl and M.J. Sienko, 1983, J. Magn. Magn. Mater. **37**, 287.

Tb–Al–Si

No ternary phase diagram exists for the system Tb–Al–Si. Muravyova et al. (1972) and Yanson (1975), however, reported the formation of two ternary compounds.

$TbAl_2Si_2$ adopts the structure type La_2O_2S [space group $P\bar{3}m1$; Muravyova et al. (1972), from X-ray powder diffraction analysis]. For sample preparation and atom parameters, see Sm–Al–Si. The lattice parameters measured were $a = 4.18$ and $c = 6.60$ Å.

Yanson (1975) from powder X-ray diffraction analysis, characterized the compound $TbAl_{2.8}Si_{0.2}$ as isostructural with the Ni_3Sn-type ($P6_3/mmc$, $a = 6.242$, $c = 4.593$). For atom parameters, see Y–Al–Si.

References
Muravyova, A.A., O.S. Zarechnyuk and E.I. Gladyshevskij, 1972, Visn. L'vivsk. Univ. Ser. Khim. **13**, 14.
Yanson, T.I., 1975, Autoreferat Dis. Kand. Khim. (abstract of thesis, Russian) (Nauk, Lvov) 22 p.

Tb–Au–Si

Felner (1975) reported the existence of $TbAu_2Si_2$ with the ordered $ThCr_2Si_2$-type of structure; the crystal data as derived from an X-ray powder analysis were: I4/mmm, $a = 4.230$ and $c = 10.16$; sample preparation as for $LaAu_2Si_2$. $TbAu_2Si_2$ orders anti-ferromagnetically below $T_N = 14.8$ K; the paramagnetic data were $\mu_{eff}^{para} = 8.0 \mu_B$ and $\theta_p = -14.8$ K.

Reference
Felner, I., 1975, J. Phys. Chem. Sol. **36**, 1063.

Tb–Co–Si

No ternary phase diagram is available for the Tb–Co–Si system; so far five ternary compounds have been characterized.

By means of X-ray powder analysis of arc-melted alloys Bodak and Gladyshevskij (1969) alloys characterized the compound $TbCo_9Si_2$ with the $BaCd_{11}$-type structure: $I4_1/amd$, $a = 9.702(5)$, $c = 6.268(10)$; atom ordering was similar to $CeNi_{8.6}Si_{2.4}$. The crystal structure of $TbCo_{8.5}Si_{2.5}$ has been more recently refined from X-ray powder data to be isostructural with the $CeNi_{8.6}Si_{2.4}$-type (occupation variant of the $BaCd_{11}$-type, $I4_1/amd$, $a = 9.689$ and $c = 6.293$; Yarovets, 1978. No reliability factor was reported but the atomic parameters as refined are listed below: Tb in 4a) 0, 3/4, 1/8; Co in 32i) 0.1261(10), 0.0492(9), 0.1779(8); Si in 8d) 0, 0, 1/2 and a statistical occupation of 2.4 Co + 1.6 Si in 4b) 0, 1/4, 3/8. Samples were prepared by arc melting under argon and subsequent annealing in evacuated silica tubes at 800°C for 720 h.

TbCoSi was observed to adopt the TiNiSi-type structure: Pnma, $a = 6.812$, $b = 4.178$ and $c = 7.216$ (X-ray powder data by Yarovets, 1978). For sample preparation and atom parameters, see YNiSi.

$TbCo_2Si_2$ is tetragonal with the ordered $ThCr_2Si_2$-type structure: $I4/mmm$, $a = 3.896$, $c = 9.766$, $\rho_x = 7.46$ kg/dm^3 (Rossi et al., 1978; X-ray powder diffraction). For sample preparation and etching conditions, see YCo_2Si_2. Yarovets (1978), from X-ray powder data, confirmed the crystal data ($a = 3.894$ and $c = 9.782$), and Yarovets et al. (1977) investigated the paramagnetism in the temperature range 300 to 1200 K, $\mu_{eff}^{para} = 9.9$ μ_B, $\theta_p = -35$ K. From susceptibility measurements (4.2–200 K) a ferromagnetic ordering at $T_m = 8$ K was suspected by Yakinthos et al. (1980), whereas the paramagnetic behavior was characterized by $\mu_{eff}^{para} = 9.4$ μ_B mole^{-1} and $\theta_p = -18$ K.

Nguyen et al. (1983) confirmed the crystal symmetry and atomic order from neutron diffraction studies and magnetic measurements of samples melted in an induction furnace and annealed at 900°C for 100 h in evacuated silica tubes; starting materials were 99.99% pure. A neutron diffraction study at room temperature confirmed the ordered $ThCr_2Si_2$-type, with $a = 3.885(3)$, $c = 9.743(2)$ and $z(Si) = 0.370$. Neutron diffraction data at 4.2 K and magnetic measurements (4.4–300 K) revealed a collinear antiferromagnetic order below $T_N = 30(2)$ K with the Tb moments of 8.8(2) μ_B oriented along the c-axis. The magnetic structure consists of ferromagnetic layers perpendicular to the c-axis coupled antiferromagnetically in a sequence $+ - + -$. The fitting of the calculated and observed magnetic intensities led to reliability values of $R_n = 0.075$ and $R_m = 0.05$; the Co atoms did not participate in the magnetic ordering. The low temperature data, however, are at variance with the observations of Yakinthos et al. (1980) who claimed a ferromagnetic type of order (see above). The paramagnetic behavior was characterized by $\mu_{eff}^{para} = 10.2$ μ_B and $\theta_p = 20(2)$ K (Nguyen et al., 1983). Good agreement is found from an independent neutron diffraction investigation by Leciejewicz et al. (1983); data obtained at 4.2 K were: $a = 3.857(4)$, $c = 9.665(9)$, $z(Si\ in\ 4e) = 0.3844(3)$, $\mu = 8.9(2)$ μ_B, $R = 0.108$; and at 300 K $a = 3.901(2)$, $c = 9.781(6)$, $z = 0.3715(6)$, $R = 0.063$; $T_N = 45(1)$. For sample preparation, see Er–Co–Si.

The magnetic (2–250 K) and structural behavior of $TbCoSi_2$ with the $CeNiSi_2$-type [Cmcm, $a = 4.037(1)$, $b = 16.276(4)$, $c = 3.974(1)$] has been investigated by Pelizzone et al. (1982). For sample preparation, see $HoCoSi_2$. $TbCoSi_2$ orders antiferromagnetically at $T_N = 18.5$ K. The paramagnetic behavior at higher temperatures corresponds to $\mu_{eff}^{para} = 9.8(1)$ μ_B and $\theta_p = -18$ K. Yarovets (1978) presented slightly different lattice parameters: $a = 4.002$, $b = 16.409$ and $c = 3.974$ (X-ray powder data).

Gladyshevskij and Bodak (1973) first mentioned the existence of a compound $TbCoSi_3$, isostructural with $CeCoSi_3$. The crystal structure of $TbCoSi_3$ was recently refined from single crystal X-ray photographs by Yarovets (1978). According to the reliability factor of $R = 0.161$ the crystal symmetry was found to be $I4/mmm$, and the atom parameters were: Tb in 2a) 0, 0, 0; Si in 4d) 0, 1/2, 1/4 and a statistical distribution of 2 Co + 2 Si in 4c) 0, 0, 0.3681(6). Interestingly the crystal structure of $CeCoSi_3$, however, was found to crystallize with the $BaNiSn_3$ type and space group $I4mm$ (see Ce–Co–Si). Magnetic susceptibilities were measured within the temperature range of 293–1150 K, $\mu_{eff}^{para} = 9.3(1)$ μ_B, $\theta_p = -22$ K (Yarovets, 1978).

References

Bodak, O.I. and E.I. Gladyshevskij, 1969, Dopov. Akad. Nauk Ukr. RSR, Ser. A **5**, 452.

Gladyshevskij, E.I. and O.I. Bodak, 1973, in: Khim. Met. Splavov, ed. N.M. Zhavoronkov (Nauka, Moscow, USSR) p. 46.

Leciejewicz, J., M. Kolenda and A. Szytula, 1983, Solid State Commun. **45**, 145.

Nguyen, V.N., F. Tcheou, J. Rossat-Mignod and R. Ballestracci, 1983, Solid State Commun. **45**(2), 209.

Pelizzone, M., H.F. Braun and J. Müller, 1982, J. Magn. Magn. Mater. **30**, 33.

Rossi, D., R. Marazza and R. Ferro, 1978, J. Less-Common Metals **58**, 203.

Yakinthos, J.K., Ch. Routsi and P.F. Ikonomou, 1980, J. Less-Common Metals **72**, 205.

Yarovets, V.I., Yu.K. Gorelenko and R.V. Skolozdra, 1977, Tesizy Dokl. IX. Ukr. Vses. Konf. Neorgan. Khim, Lvov, p. 188.

Yarovets, V.I., 1978, Autoreferat Dis. Kand. Khim. (abstract of thesis, Russian) (Nauk, Lvov) 24 pp.

$Tb-Cu-Si$

Rieger and Parthé (1969a) investigated the existence of AlB_2-type phases in arc-melted alloys with the compositions $TbCu_{0.67}Si_{1.33}$ ($a = 4.010$, $c = 4.028$) and $TbCuSi$ ($a = 4.060$, $c = 3.949$). From X-ray powder analysis of arc-melted alloys, Cu and Si atoms were said to statistically occupy the 2d sites of P6/mmm. At variance with the data by Rieger and Parthé (1969a) obtained from arc-melted alloys, Iandelli (1983) observed the formation of $TbCuSi$ with the ordered Ni_2In-type (superstructure of AlB_2, $P6_3/mmc$, $a = 4.156(1)$ and $c = 7.476(2)$]. The superstructure reflections were said to be faint and were obtained on arc-melted samples after annealing at 750°C for 8–12 days. Thus the Ni_2In-type phase was concluded to be a low-temperature modification. For details of sample preparation and purities of starting materials, see LaCuSi.

$Tb_3Cu_4Si_4$ crystallizes with the $Gd_3Cu_4Ge_4$-type of structure: Immm, $a = 13.71$, $b = 6.54$ and $c = 4.14$ (Hanel and Nowotny, 1970; X-ray powder data). For sample preparation, see $Sc_3Cu_4Si_4$.

According to an X-ray powder analysis by Rieger and Parthé (1969b) $TbCu_2Si_2$ is isotypic with the $ThCr_2Si_2$-type of structure [$a = 3.980(6)$, $c = 9.966(10)$]. For sample preparation, see YCu_2Si_2. For X-ray absorption measurements, see Padalia et al. (1983).

Oesterreicher (1976) investigated the magnetic behavior of $TbCuSi$, $Tb_3Cu_4Si_4$ and $TbCu_2Si_2$ alloys in the temperature range of 4.2 to 150 K and in fields up to 50 kOe. Samples were prepared by induction melting in MgO crucibles and subsequent annealing in vacuum at 800°C for 200 h on a MgO substrate. $TbCuSi$ (AlB_2-type?) orders ferromagnetically below $T_m = 47$ K, $\mu_S = 7.3$ μ_B; paramagnetic data are $\mu_{eff}^{para} = 9.62$ μ_B, $\theta_p = 52$ K. $Tb_3Cu_4Si_4$ shows a linear dependence of the magnetization on the field and weak antiferromagnetic interaction at $T_N = 14$ K; the paramagnetic behavior corresponds to $\mu_{eff}^{para} = 9.54$ μ_B, $\theta_p = -13$ K. $TbCu_2Si_2$ is metamagnetic with antiferromagnetic ordering at $T_N = 12$ K; $\mu_{eff}^{para} = 9.33$ μ_B, $\theta_p = -12$ K.

References

Hanel, G. and H. Nowotny, 1970, Monatsh. Chem. **101**, 463.

Iandelli, A., 1983, J. Less-Common Metals **90**, 121.

Oesterreicher, H., 1976, Phys. Stat. Sol. (a) **34**, 723.
Padalia, B.D., T.K. Hatwar and M.N. Ghatikar, 1983, J. Phys. **C16**, 1537.
Rieger, W. and E. Parthé, 1969a, Monatsh. Chem. **100**, 439.
Rieger, W. and E. Parthé, 1969b, Monatsh. Chem. **100**, 444.

Tb–Fe–Si

Five ternary compounds have been reported for the Tb–Fe–Si system.

$Tb_2Fe_3Si_5$ is isotypic with the structure type of $Sc_2Fe_3Si_5$: P4/mnc, $a = 10.43(1)$, $c = 5.48(1)$ (Braun, 1980; X-ray powder analysis). Antiferromagnetic ordering was observed at $T_N = 10.3$ K. Magnetic susceptibility data [$\mu_{eff}^{para} = 9.6(2)\,\mu_B$; $\theta_{c\|} = 1.8(3.5)$ K] as well as Mössbauer data indicate the absence of a magnetic moment on the iron site (Braun et al., 1981). Samples were prepared by arc melting and subsequently annealed in sealed quartz capsules backfilled with argon at 1200°C, 2 d and at 800°C, 2d. Starting materials were Tb-3N, Fe-5N and Si-7N. Neutron diffraction showed the appearance of a noncommensurate magnetic phase at T_N, which gradually is replaced at ~ 7 K by commensurate ordering (Moodenbaugh et al., 1981). For low temperature heat capacity data, see Vining and Shelton (1983). Yarovets (1978), from X-ray powder data, confirmed the crystal symmetry of $Tb_2Fe_3Si_5$, but reported different unit cell dimensions with a much smaller c/a ratio; $a = 10.479$ and $c = 5.310$.

TbFeSi crystallizes with the PbFCl-type of structure: P4/nmm, $a = 3.984(3)$, $c = 6.751(5)$ (Bodak et al., 1970; X-ray powder data). For sample preparation, see CeFeSi.

$Tb_2Fe_4Si_9$ is hexagonal with the $Y_2Fe_4Si_9$-type of structure: P6_3/mmc, $a = 3.943(5)$, $c = 15.48(1)$ (Gladyshevskij et al., 1978; X-ray powder data). For sample preparation, see $Y_2Fe_4Si_9$. Magnetic susceptibility was measured within the temperature range 300–1200 K; $\mu_{eff}^{para} = 7.91\,\mu_B$ mole^{-1} and $\theta_p = 167$ K.

The crystal structure $Tb_3Fe_2Si_7$ (earlier known as $TbFeSi_3$) was reported to be isostructural with the $Ho_3Co_2Si_7$-type: Amm2, $a = 3.903$, $b = 24.760$, $c = 3.918$ (Yarovets, 1978; X-ray powder data). Magnetic susceptibilities were measured within the temperature range 300–1200 K: $\mu_{eff}^{para} = 9.36\,\mu_B$ mole^{-1}, $\theta_p = 47$ K (Gladyshevskij et al., 1978). For sample preparation, see $Y_2Fe_4Si_9$.

Yarovets and Gorelenko (1981) refined the crystal structure of $TbFeSi_2$ by means of single-crystal X-ray photographs. $TbFeSi_2$ crystallizes with a new ordering variant of the $CeNiSi_2$-type: Cmcm, $a = 4.017(2)$, $b = 16.308(12)$, $c = 3.933(2)$, $\rho_{exp} = 6.95$ kg/dm³. Atom parameters and ordering derived were as follows: Fe in 4c) 0, 0.7480, 1/4; Si in 4c) 0, 0.4541, 1/4; Si in 4c) 0, 0.3128, 1/4; Tb in 4c) 0, 0.1045, 1/4; $R = 0.135$. Single crystals were obtained from a melt of composition (in a/o) $Tb_{20}Fe_{20}Si_{60}$. Starting materials were Tb 99.83%, Fe 99.98% and Si 99.99%.

$TbFe_2Si_2$ with the $ThCr_2Si_2$-type of structure (I4/mmm, $a = 3.925$, $c = 9.964$) was characterized by Yarovets (1978) from powder diffraction data. For sample preparation, see Y–Fe–Si. Magnetic susceptibilities were measured in the temperature range of 288 K to 1208 K and effective moments were extrapolated as follows: $\mu_{eff}^{para} = 11.69\,\mu_B$, $\theta_p = 593$ K in the range 288–669 K, and $\mu_{eff}^{para} = 9.33\,\mu_B$, $\theta_p = 301$ K for the range 800–1208 K.

The lattice generated electric field gradient at the rare earth site was deduced by Noakes et al. (1983) from ^{155}Gd (86.5 keV) Mössbauer data; ^{57}Fe (14.4 keV) Mössbauer measurements 4.2 K prove the absence of a magnetic moment on the Fe site; the magnetic ordering temperature as derived from ac susceptibility data was $T_N = 6$ K with a planar aabbaabb antiferromagnetic ordering similar as observed in $NdFe_2Si_2$.

References

Bodak, O.I., E.I. Gladyshevskij and P.I. Kripyakevich, 1970, Zh. Strukt. Khim. **11**(2), 305.

Braun, H.F., 1980, Phys. Lett. **75A**(5), 386.

Braun, H.F., C.U. Segre, F. Acker, M. Rosenberg, S. Dey and P. Deppe, 1981, J. Magn. Magn. Mater. **25**, 117.

Gladyshevskij, E.I., O.I. Bodak, V.I. Yarovets, Yu.K. Gorelenko and R.V. Skolozdra, 1978, Ukr. Fiz. Zh. **23**(1), 77.

Moodenbaugh, A.R., D.E. Cox and H.F. Braun, 1981, Bull. Am. Phys. Soc. **26**, 468.

Noakes, D.R., A.M. Umarji and G.K. Shenoy, 1983, J. Magn. Magn. Mater. **39**, 309.

Vining, C.B. and R.N. Shelton, 1983, Phys. Rev. **B28**(5), 2732.

Yarovets, V.I., 1978, Autoreferat Dis. Kand. Khim. (abstract of thesis, Russian) (Nauk, Lvov) 22 p.

Yarovets, V.I. and Y.K. Gorelenko, 1981, Vestn. Lvov Univ. Ser. Khim. **23**, 20.

Tb–Ge–Si

Mayer and Eshdat (1968) investigated the structural behavior in the concentrational section $TbGe_{2-x}Si_x$ by means of X-ray powder diffraction. For sample preparation, see $NdGe_{2-x}Si_x$. Phase equilibria were interpreted in analogy to the system $NdGe_{2-x}Si_x$ (see there and figs. 48, 11).

Reference

Mayer, I. and Y. Eshdat, 1968, Inorg. Chem. **9**, 1904.
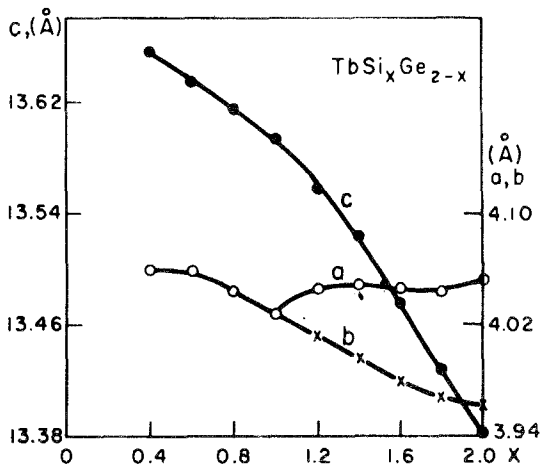
Fig. 48. Tb–Ge–Si, section $TbGe_{2-x}Si_x$, lattice parameters versus concentration, after Mayer and Eshdat (1968).

Tb–Ir–Si

TbIr$_2$Si$_2$ was reported to crystallize with the ThCr$_2$Si$_2$-type structure (I4/mmm); the atom order and crystal symmetry was derived from neutron diffraction data (4.2 and 300 K) on polycrystalline material (Slaski et al., 1983): $a = 4.143(5)$, $c = 10.155(9)$, z(Si in 4e) $= 0.372(2)$, $R_N = 0.088$ at 300 K. TbIr$_2$Si$_2$ orders antiferromagnetically below $T_N = 72(3)$ K with a primitive magnetic cell corresponding to a simple collinear antiferromagnet with $a + - + -$ stacking of ferromagnetic (001) sheets in [001] [$a = 4.158(7)$, $c = 10.203(16)$, z(Si) $= 0.369(3)$, $R_N = 0.092$ at 4.2 K].

Reference
Slaski, M., J. Leciejewicz and A. Szytula, 1983, J. Magn. Magn. Mater. **39**, 268.

Tb–Mn–Si

TbMn$_2$Si$_2$ has been characterized by Rossi et al. (1978) by means of X-ray powder analysis: ThCr$_2$Si$_2$-type of structure, I4/mmm, $a = 3.931$, $c = 10.456$, $\rho_x = 6.68$ kg/dm^3; for sample preparation, see LaMn$_2$Si$_2$. Antiferromagnetic ordering at $T_N = 501$ K was reported by Szytula and Szott (1981) and no magnetic ordering of the Tb sublattice was observed at 80 K from their neutron diffraction experiments. The magnetic behavior is further characterized by an effective paramagnetic moment of $\mu_{eff}^{para} = 9.3$ μ_B; the magnetic moment at low temperatures was given as $\mu_n = 5.6$ μ_B. Data by Knigenko et al. (1977) were $a = 3.924$ and $c = 10.460$ (X-ray powder technique); for sample preparation, see Y–Mn–Si. In agreement with this Narasimhan et al. (1975) reported $a = 3.930(5)$, $c = 10.468(5)$ (X-ray powder data); for sample preparation, see Y–Mn–Si.

From an X-ray powder diffraction analysis of arc-melted samples Segre (1981) characterized the compound Tb$_2$Mn$_3$Si$_5$ to crystallize with the Sc$_2$Fe$_3$Si$_5$-type of structure: P4/mnc, $a = 10.66(1)$, $c = 5.466(8)$; $T_n = 1.2$ K.

References
Knigenko, L.D., I.R. Mokra and O.I. Bodak, 1977, Vestn. Lvov Univ., Ser. Khim. **19**, 68.
Narasimhan, K.S.V.L., V.U.S. Rao and W.E. Wallace, 1976, AIP Conf. Proc. **29**, 594; see also 1976, J. Appl. Phys. **46**, 4957.
Rossi, D., R. Marazza, D. Mazzone and R. Ferro, 1978, J. Less-Common Metals **59**, 79.
Segre, C.U., 1981, Thesis, Univ. of Calif., San Diego, USA.
Szytula, A. and I. Szott, 1981, Solid State Commun. **40**, 199.

Tb–Ni–Si

No phase diagram has been established, but nine ternary compounds have been identified (see table 28).

The ordered ThCr$_2$Si$_2$-type of structure was recently confirmed by Nguyen et al. (1983) for the compound TbNi$_2$Si$_2$ (from neutron diffraction data at room temperature $a = 3.952(3)$, $c = 9.542(2)$, z(Si) $= 0.372$). Samples were prepared from 4N materials by melting in an induction furnace followed by a heat treatment at 900°C

TABLE 28
Formation and structural data of ternary compounds Tb–Ni–Si.

Compound	Structure type Space group	Lattice parameters Density	Preparation, Characterization	Refs.	Purity
TbNi$_{10}$Si$_2$	ord. ThMn$_{12}$ I4/mmm	$a = 8.207$ $c = 4.679$	$\mu_{\text{eff}}^{\text{para}} = 9.7\ \mu_{\text{B}}$, $\theta_{\text{p}} = 60$ K PXD arc(Ar), Qu, 800 °C, 720 h	GlBYGS, 77 Ya, 78a	Tb 99.83 Ni 99.98 Si 99.9
TbNi$_{6.72}$Si$_{6.28}$ [(**)]	Ce$_2$Ni$_{17}$Si$_9$? (NaZn$_{13}$-deriv. I4/mcm ?	$a = 10.960$ $c = 11.124$	arc(Ar), Qu 800 °C, 720 h PXD	Ya, 78b	Tb 99.83 Ni 99.98 Si 99.9
Tb$_3$Ni$_6$Si$_2$	Ce$_3$Ni$_6$Si$_2$ ord. Ca$_3$Ag$_8$ Im3m	$a = 8.801(2)$	arc, Qu(Ni) 800 °C, 2 weeks PXD	GlKB, 66	Tb 99.15 Ni 99.99 Si 99.99
Tb$_3$NiSi$_2$	Gd$_3$NiSi$_2$ filled Hf$_3$P$_2$ Pnma	$a = 11.306(2)$ $b = 4.132(1)$ $c = 11.212(3)$	arc(Ar), Qu(Ta) 800 °C, 4 weeks PXD	KlP, 82	Tb 99.9 Ni 99.99 Si 5N
TbNiSi	TiNiSi Pnma	$a = 6.932$ $b = 4.142$ $c = 7.119$	PXD $\mu_{\text{eff}}^{\text{para}} = 9.7\ \mu_{\text{B}}$, $\theta_{\text{p}} = -61$ K	BoYG, 74 GlBYGS, 77	Tb 99.83 Ni 99.98 Si 99.9
		$a = 6.91$ $b = 4.17$ $c = 7.17$	PXD	Dw, 82	
		$a = 6.890$ $b = 4.120$ $c = 7.229$	arc(Ar), Qu 800 °C, 720 h PXD	Ya, 78b	Tb 99.83 Ni 99.98 Si 99.9
TbNi$_5$Si$_3$	YNi$_5$Si$_3$ Pnma	$a = 18.730$ $b = 3.860$ $c = 6.623$	arc(Ar) 800 °C PXD	AkYBYG, 76	Ni 99.92 Si 99.99
		$a = 18.87$ $b = 3.809$ $c = 6.610$	arc(Ar), Qu 800 °C, 720 h PXD	Ya, 78b	Tb 99.83 Ni 99.98 Si 99.9
TbNi$_2$Si$_2$	ThCr$_2$Si$_2$ I4/mmm	$a = 3.952(10)$ $c = 9.542(10)$	arc(Ar) PXD	BoGK, 66	Tb 99.15 Ni 99.8 Si 99.99
		$a = 3.95$ $c = 9.54$	induction melting Ar, PXD $T_{\text{N}} = 14.0$ K, $\theta_{\text{p}} = 9$ K [(*)] $\mu_{\text{eff}}^{\text{para}} = 10.2\ \mu_{\text{B}}$	YaI, 80	
TbNiSi$_2$	CeNiSi$_2$ Cmcm	$a = 3.982(2)$ $a = 16.030(10)$ $c = 3.952(2)$	arc(Ar) PXD	BoG, 69	Tb 99.15 Ni 99.8 Si 99.99
TbNiSi$_3$	ScNiSi$_3$ Amm2	$a = 3.994$ $b = 3.912$ $c = 21.136$	arc, Qu (10^{-2} Torr Ar) 800 °C, 720 h $\mu_{\text{eff}}^{\text{para}} = 7.92\ \mu_{\text{B}}$, $\theta_{\text{p}} = -27$ K	GoBGY, 77 Ya, 78b	Tb 99.83 Ni 99.98 Si 99.99

[(*)] Magnetic susceptibility of TbNi$_2$Si$_2$ exhibits anomalous behavior in the temperature range 40–80 K, probably due to a phase transition.

[(**)] For a correct setting of a bct-unit cell, $a = a_0/\sqrt{2} = 7.750$.

for 100 h in silica tubes. Neutron diffraction studies at 4.2 K and magnetic measurements (4.4–300 K) revealed a collinear antiferromagnetic order below $T_N = 10(1)$ K with the rare earths moments of 8.8 μ_B aligned along the c-axis. The ordering within the (001) plane is antiferromagnetic and the planes are decoupled. The Ni atoms were assumed to carry no magnetic moment. The fitting of the calculated and observed magnetic intensities led to reliability values of $R_n = 0.07$ and $R_m = 0.08$. At higher temperatures a paramagnetic behavior was observed with $\mu_{eff}^{para} = 10.1$ μ_B and $\theta_p = -5$ K. The low-temperature data are in agreement with the observations of an antiferromagnetic ordering by Yakinthos and Ikonomou (1980); see also table 25.

References

Aksel'rud, L.G., V.I. Yarovets, O.I. Bodak, Ya.P. Yarmolyuk and E.I. Gladysheveskij, 1976, Sov. Phys. Crystallogr. **21**(2), 210.

Bodak, O.I. and E.I. Gladyshevskij, 1969, Kristallografiya **14**(6), 990.

Bodak, O.I., E.I. Gladyshevskij and P.I. Kripyakevich, 1966, Izv. Akad. Nauk SSSR, Neorg. Mater. **2**(12), 2151.

Bodak, O.I., V.I. Yarovets and E.I. Gladyshevskij, 1974, Tesizy Dokl. Tret. Vses. Konf. Kristallokhim. Intermet. Soedin, 2nd Ed. ed. R.M. Rykhal (Lvov Gos. Univ., Lvov, USSR) p. 32.

Dwight, A.E., 1982, private communication.

Gladyshevskij, E.I., P.I. Kripyakevich and O.I. Bodak, 1966, Acta Crystallogr. **A21**, 80, and Z. Anorg. Allg. Chem. **344**, 95.

Gladyshevskij, E.I., O.I. Bodak, V.I. Yarovets, Yu.K. Gorelenko and R.V. Skolozdra, 1977, Fiz. Magnit. Plenok (Irkutsk) **10**, 182.

Gorelenko, Yu.K., O.I. Bodak, E.I. Gladyshevskij and V.I. Yarovets, 1977, Ukr. Fiz. Zh. **22**(6), 1020.

Klepp, K. and E. Parthé, 1982, J. Less-Common Metals **83**, L33.

Nguyen, V.N., F. Tcheou, J. Rossat-Mignod and R. Ballestracci, 1983, Solid State Commun. **45**(2), 209.

Yakinthos, J.K. and P.F. Ikonomou, 1980, Solid State Commun. **34**, 777.

Yarovets, V.I., 1978a, Tesizy Dokl. Tret. Vses. Konf. Kristallokhim. Intermet. Soedin, 2nd Ed., ed. R.M. Rykhal (Lvov Gos. Univ., Lvov, USSR) p. 124.

Yarovets, V.I., 1978b, Autoreferat Dis. Kand. Khim. (abstract of thesis, Russian) (Nauk, Lvov) 24 p.

Tb–Os–Si

According to X-ray powder diffraction data by Hiebl et al. (1983) $TbOs_2Si_2$ is tetragonal with the space group I4/mmm and the $ThCr_2Si_2$-type of structure: the lattice parameters were $a = 4.1340(4)$ and $c = 9.7248(40)$. For sample preparation, see YOs_2Si_2. Paramagnetic behavior was observed above 250 K with $\mu_{eff}^{para} = 9.64$ μ_B and $\theta_p = 100$ K; antiferromagnetic ordering occurs at 42 K.

Reference

Hiebl, K., C. Horvath, P. Rogl and M.J. Sienko, 1983, Solid State Commun. **48**, 211.

Tb–Pd–Si

$TbPd_2Si$ adopts the ordered Fe_3C-type of structure with space group Pnma and lattice parameters $a = 7.323(2)$, $b = 6.906(2)$ and $c = 5.513(1)$ (X-ray powder data by Moreau et al.; 1982). For sample preparation, see YPd_2Si.

The magnetic behavior of polycrystalline $TbPd_2Si$ was investigated by Gignoux et al. (1984) in the temperature range of 1.5–300 K and in fields up to 77 kOe. The paramagnetic parameters obtained were $\mu_{eff}^{para} = 9.90 \; \mu_B$, $\theta_p = 16$ K. The low temperature susceptibilities exhibit two maxima, which were attributed to an antiferromagnetic ordering temperature at $T_N = 21$ K and to a transition between two distinct antiferromagnetic structures at $T = 8.5$ K. This interpretation is confirmed from preliminary neutron diffraction data. The saturation moment at 1.5 K and in 77 kOe is 5.64 μ_B.

According to X-ray powder data by Ballestracci (1976) $TbPd_2Si_2$ crystallizes with the ordered $ThCr_2Si_2$-type of structure and lattice parameters $a = 4.125$ and $c = 9.91$; for sample preparation, see $CePd_2Si_2$. Yakinthos and Gamari-Seale (1982) confirmed the data reported by Ballestracci (1976); however, in the X-ray data of their samples prepared by induction melting they observed a few more lines of low intensity which could not be indexed (superstructure lines?). Magnetic susceptibilities (4.2 to 300 K) are characterized by paramagnetic behavior ($\mu_{eff}^{para} = 9.8 \; \mu_B$, $\theta_p = -1$ K) and the onset of antiferromagnetic ordering at $T_N = 20$ K with some anomalous behavior below $T = 15$ K, probably due to magnetocrystalline anisotropy.

References

Ballestracci, R., 1976, C.R. Acad. Sci. Paris, Ser. B **282**, 291.
Gignoux, D., J.C. Gomez-Sal and D. Paccard, 1984, Solid State Commun. **49**(1), 75.
Moreau, J.M. J. LeRoy and D. Paccard, 1982, Acta Crystallogr. **B38**, 2446.
Yakinthos, J.K. and H. Gamari-Seale, Z. Phys. **B48**, 251.

Tb–Pt–Si

$TbPt_2Si$ crystallizes with the ordered Fe_3C-type of structure, Pnma, $a = 7.325(2)$, $b = 6.913(2)$, $c = 5.486(2)$ (Moreau et al., 1982; X-ray powder diffraction). For sample preparation, see YPd_2Si.

TbPtSi adopts the TiNiSi-type of structure: Pnma, $a = 7.0045(9)$, $b = 4.2743(6)$, $c = 7.426(1)$ (X-ray powder analysis by Hovestreydt et al., 1982). For sample preparation, see ScPtSi.

$TbPt_2Si_2$ crystallizes with a primitive tetragonal symmetry and the atom order is similar to that of the $CaBe_2Ge_2$-type (Rogl, 1984; X-ray powder data of arc-melted samples): $a = 4.1686(6)$, $c = 9.7986(57)$, $CePt_2Si_2$-type.

References

Hovestreydt, E., N. Engel, K. Klepp, B. Chabot and E. Parthé, 1982, J. Less-Common Metals **86**, 247.
Moreau, J.M., J. LeRoy and D. Paccard, 1982, Acta Crystallogr. **B38**, 2446.
Rogl, P., 1984, Inorg. Chem., to be published.

Tb–Re–Si

No phase diagram is available for the system Tb–Re–Si; the formation of two ternary compounds $Tb_2Re_3Si_5$ and $TbRe_4Si_2$ has been observed.

From X-ray powder diffraction analysis Bodak et al. (1978) reported $Tb_2Re_3Si_5$

to be tetragonal with the $Sc_2Fe_3Si_5$-type: P4/mnc, $a = 10.88(1)$ and $c = 5.535(5)$. Samples were arc melted but no conditions for heat treatment were given. Segre (1981) confirmed the structure type, but reported different lattice parameters $a = 10.94(1)$ and $c = 5.530(8)$. Samples were arc melted; $T_n = 1.2$ K.

TbRe$_4$Si$_2$ with the ZrFe$_4$Si$_2$-type structure was synthesized and characterized by Pecharskij (1979) by means of X-ray powder and metallographic techniques [P4$_2$/mnm, $a = 7.325(5)$ and $c = 4.106(2)$]. Samples were prepared by arc melting powder compacts under argon, followed by an annealing procedure in evacuated silica tubes at 800°C for 400 + 600 h. Starting materials were 98.4% Tb, 99.99% Si and 99.99% Re.

References

Bodak, O.I. and V.K. Pecharskij and E.I. Gladyshevskij, 1978, Izv. Akad. Nauk SSSR, Neorg. Mater. **14**(2), 250.
Pecharskij, V.K., 1979, Autoreferat Dis. Kand. Khim. (abstract of thesis, Russian) (Nauk, Lvov) 23 p.
Segre, C.U., 1981, Thesis, Univ. of Calif., San Diego, USA.

Tb–Rh–Si

TbRhSi crystallizes with the TiNiSi-type structure with space group Pnma and lattice parameters $a = 6.879(1)$, $b = 4.2091(5)$ and $c = 7.345(1)$ (Chevalier et al., 1982a; X-ray powder analysis). For sample preparation, see YRhSi. TbRhSi shows spontaneous magnetization below $T_m = 55$ K (a noncolinear arrangement of their moments was said to be likely); $\theta_p = 48$ K, $\mu_{eff}^{para} = 9.92$ μ_B mole^{-1}.

According to X-ray powder diffraction data by Ballestracci (1976) TbRh$_2$Si$_2$ has the ordered ThCr$_2$Si$_2$-type structure: I4/mmm, $a = 4.031$, $c = 9.95$. For sample preparation, see YRh$_2$Si$_2$. Data by Felner and Nowik (1983) were $a = 4.037(2)$, $c = 9.95(1)$ (X-ray powder analysis of induction-melted alloys); $\mu_{eff}^{para} = 8.4(1)$ μ_B, $\theta_p = -26(3)$ K and $T_N = 92(2)$ K. A second peak occurs in the susceptibility curve at $T_m = 12(2)$ K and was interpreted as itinerant electron ordering of the Rh sublattice. Slightly different magnetic parameters ($a = 4.031$, $c = 9.96$, $\mu_{eff}^{para} = 10.0$ μ_b, $\theta_p = -43$ K and $T_N = 94$ K) were reported by Quezel et al. (1984) from susceptibility data between 4.2 and 300 K. Atom order and crystal symmetry (ThCr$_2$Si$_2$-type, I4/mmm) was confirmed from a room temperature neutron diffraction study on polycrystalline TbRh$_2$Si$_2$ [$a = 4.034(3)$, $c = 9.919(10)$, z(Si in 4e) = 0.3770(4), $R_N = 0.047$ at 300 K, Slaski et al., 1983]. The type of antiferromagnetic order was independently derived by Slaski et al. (1983) and Quezel et al. (1984) with a primitive tetragonal magnetic unit cell; in agreement the values obtained were as follows: $a = 3.983(4)$, $c = 9.842(8)$, z(Si in 4e) = 0.3718(19), $T_N = 98(2)$ K, $R_N = 0.089$ at 4.2 K (Slaski et al., 1983) and $a = 4.027$, $c = 9.952$, z(Si) = 0.375, $R_N = 0.027$; $R = 0.067$, $T_N = 92$ K, $m_0 = 8.5 \pm 0.3$ μ_B at 15 K (Quezel et al., 1984). In both investigations a stacking of ferromagnetic (001) planes with a $+ - + -$ sequence in [001] was derived. Tb moments are parallel to the c-axis. No evidence was found for a magnetic moment on the rhodium atoms.

According to recent X-ray powder data by Chevalier et al. (1981) TbRh$_3$Si$_2$ is isotypic with the crystal structure of CeCo$_3$B$_2$ [P6/mmm, $a = 5.488(6)$, $c = 3.544(4)$].

For sample preparation, see $LaRh_3Si_2$. The magnetic behavior (4.2 to 300 K) is characterized by the onset of ferromagnetic ordering at $T_m = 37$ K; and by a Van Vleck type paramagnetism at higher temperatures ($\mu_{eff}^{para} = 9.82$ μ_B mole^{-1}, $\theta_p = 55$ K).

Chevalier et al. (1982b) reported magneto- and structure chemical properties of $Tb_2Rh_3Si_5$. This compound crystallizes with the $Sc_2Co_3Si_5$-type structure with space group Ibam and lattice parameters $a = 9.82(1)$, $b = 11.71(1)$, $c = 5.698(5)$. Magnetic susceptibilities in the temperature range from 4.2 K to 300 K are characterized by a paramagnetic behavior according to $\mu_{eff}^{para} = 10.04$ μ_B and $\theta_p = -8$ K. $Tb_2Rh_3Si_5$ orders antiferromagnetically at $T_N = 8.5$ K.

The formation of a further compound with formula Tb_2RhSi_3 and a structure type deriving from AlB_2 has been mentioned by Chevalier et al. (1982b). According to X-ray powder data obtained from arc-melted alloys annealed at 800°C for 4 d, Tb_2RhSi_3 crystallizes with the Er_2RhSi_3-type structure: $P\bar{6}2c$, $a = 8.110(5)$, $c = 7.860(5)$; Chevalier et al. (1984). Tb_2RhSi_3 is antiferromagnetic below $T_N = 11$ K, the paramagnetic behavior in the temperature range below 300 K is represented by $\mu_{eff}^{para} = 9.61$ μ_B and $\theta_p = 6$ K.

References

Ballestracci, R., 1976, C.R. Acad. Sci. Paris, Ser. B **282**, 291.

Chevalier, B., A. Cole, P. Lejay and J. Etourneau, 1981, Mater. Res. Bull. **16**, 1067.

Chevalier, B., A. Cole, P. Lejay, M. Vlasse, J. Etourneau and P. Hagenmuller, 1982a, Mater. Res. Bull. **17**, 251.

Chevalier, B., P. Lejay, J. Etourneau, M. Vlasse and P. Hagenmuller, 1982b, Paper presented at the 7th Intern. Conf. on Solid Compounds of Transition Elements, Grenoble, June 21, France, Collected Abstracts, II B16, and 1982, Mater. Res. Bull. **17**, 1211.

Chevalier, B., P. Lejay, J. Etourneau and P. Hagenmuller, 1984, Solid State Commun. **49**(8), 753.

Felner, I. and I. Nowik, 1983, Solid State Commun. **47**, 831.

Quezel, S., J. Rossat-Mignod, B. Chevalier, P. Lejay and J. Etourneau, 1984, Solid State Commun. **49**(7), 685.

Slaski, M., J. Leciejewicz and A. Szytula, 1983, J. Magn. Magn. Mater. **39**, 268.

Tb–Ru–Si

Ballestracci and Astier (1978) were first to report a compound $TbRu_2Si_2$ crystallizing with the $ThCr_2Si_2$-type of structure: I4/mmm, $a = 4.150$ and $c = 9.54$ (X-ray powder analysis of induction-melted alloys). Hiebl et al. (1983) confirmed the structure type and reported $a = 4.1560(4)$, $c = 9.5726(22)$ (X-ray powder data of arc-melted alloys). For sample preparation, see YOs_2Si_2. The magnetic behavior was investigated in the temperature range of 1.5 K to 1100 K and was characterized by $\mu_{eff}^{para} = 9.65$ μ_B, $\theta_p = 100$ K and antiferromagnetic ordering at $T_N = 55$ K (Hiebl et al., 1983).

References

Ballestracci, R. and G. Astier, 1978, C.R. Acad. Sci. Paris, Ser. B **286**, 109.

Hiebl, K., C. Horvath, P. Rogl and M.J. Sienko, 1983, J. Magn. Magn. Mater. **37**, 287.

Tm–Al–Si

No ternary phase diagram has been established for the system Tm–Al–Si, but the formation of one ternary compound Tm_2Al_2Si has been reported by Yanson (1975). From X-ray powder diffraction data Tm_2Al_2Si was found to be isostructural with Dy_2Al_2Si, whose atomic arrangement constitutes an ordered variant of the U_3Si_2-type. The space group was given as P4/mbm and lattice parameters were measured to be $a = 6.810(4)$ and $c = 4.223(3)$.

Reference

Yanson, T.I., 1975, Autoreferat Dis. Kand. Khim. (abstract of thesis, Russian) (Nauk, Lvov) 22 p.

Tm–Co–Si

No ternary phase diagram has been established for the Tm–Co–Si system, but four ternary compounds have been observed. Structural and magnetic behavior (2–250 K) of $TmCoSi_2$ with the $CeNiSi_2$-type [Cmcm, $a = 3.956(2)$, $b = 16.244(8)$ and $c = 3.912(2)$] has been investigated by Pelizzone et al. (1982). Antiferromagnetic ordering occurs at $T_N = 2.5$ K. The paramagnetic behavior is characterized by $\mu_{eff}^{para} = 7.8(2)$ μ_B and $\theta_p = -76$ K. $TmCoSi_2$ with the $CeNiSi_2$-type was earlier reported by Yarovets (1978), who measured slightly different unit cell dimensions: $a = 3.981$, $b = 16.073$ and $c = 3.931$ (X-ray powder data).

From neutron diffraction data of the compound $TmCo_2Si_2$ with the $ThCr_2Si_2$-type (I4/mmm) Leciejewicz and Szytula (1983) reported a collinear antiferromagnetic ordering ($+ - + -$) below $T_N = 3.0(5)$ K, with the magnetic moments (no magnetic moment exists on the Co atoms) coupled ferromagnetically within the basal plane and normal to the tetragonal axis. The magnetic moment at 2 K was 6.2(1) μ_B. Samples were prepared by melting and annealing at 800°C for 100 h and subsequent slow cooling to room temperature. The structural data obtained from neutron diffraction at 300 K were: $a = 3.854(2)$, $c = 9.672(5)$, and z(Si in 4e) = 0.3761(6), $R = 0.077$; and at 4.2 K: $a = 3.880(3)$, $c = 9.753(7)$, z(Si) = 0.3769(6), $R = 0.064$. The magnetic unit cell obtained at 2 K is of primitive tetragonal symmetry but of the same size as the crystallographic cell. Yarovets (1978) from X-ray powder data measured slightly different unit cell dimensions, $a = 3.856$, $c = 9.707$. Magnetic susceptibility data were recorded by Yarovets et al. (1977) in the temperature range 300–1200 K, $\mu_{eff}^{para} = 7.8$ μ_B and $\theta_p = -37$ K.

TmCoSi was observed to crystallize with the TiNiSi-type structure: Pnma, $a = 6.726$, $b = 4.076$ and $c = 7.128$; X-ray powder data by Yarovets (1978). For sample preparation and atom parameters, see YNiSi.

$Tm_3Co_2Si_7$ is isotypic with the crystal structure of $Ho_3Co_2Si_7$: Amm2, $a = 3.841$, $b = 24.394$ and $c = 3.885$ (X-ray powder data by Yarovets, 1978). For sample preparation and atom parameters see $Ho_3Co_2Si_7$. Magnetic susceptibilities were measured in the temperature range of 286–1150 K, $\mu_{eff}^{para} = 7.20(1)$ μ_B, $\theta_p = 19$ K (Yarovets, 1978).

References

Leciejewicz, J. and A. Szytula, 1983, Solid State Commun. **48**, 55.

Pelizzone, M., H.F. Braun and J. Müller, 1982, J. Magn. Magn. Mater. **30**, 33.

Yarovets, V.I., 1978, Autoreferat Dis. Kand. Khim. (abstract of thesis, Russian) (Nauk, Lvov) 24 p.

Yarovets, V.I., Yu.K. Gorelenko and R.V. Skolozdra, 1977, Tesizy Dokl. IX. Ukr. Vses. Konf. Neorg. Khim., Lvov, p. 188.

Tm–Cu–Si

Four ternary compounds have been identified in the Tm–Cu–Si system.

Rieger and Parthé (1969a) investigated the occurrence of the AlB_2-type of structure by means of X-ray powder diffraction of an arc-melted alloy with composition $TmCu_{0.67}Si_{1.33}$. Cu and Si atoms were concluded to statistically occupy the 2d sites of P6/mmm; $a = 3.977$, $c = 3.929$.

From arc-melted samples annealed at 750°C, Iandelli (1983) observed the formation of a compound TmCuSi with the ordered Ni_2In-type of structure [$P6_3/mmc$, $a = 4.134(2)$ and $c = 7.172(4)$]. As was pointed out by Iandelli (1983) the Ni_2In-type arrangement is considered as a superstructure of the AlB_2-type ($a = a_0$, $c = 2c_0$) with rather faint superstructure reflections. With respect to the results by Rieger and Parthé (1969a) from arc-melted samples of similar composition (see above) the Ni_2In-type phase was suspected to be a low-temperature phase.

$Tm_3Cu_4Si_4$ is orthorhombic with the $Gd_3Cu_4Ge_4$-type of structure: Immm, $a = 13.53$, $b = 6.50$ and $c = 4.08$ (X-ray powder diffraction data by Hanel and Nowotny, 1970). For sample preparation, see $Sc_3Cu_4Si_4$.

$TmCu_2Si_2$ crystallizes with the $ThCr_2Si_2$-type of structure: I4/mmm, $a = 3.928(6)$, $c = 9.997(10)$ (X-ray powder diffraction data by Rieger and Parthé, 1969b). For sample preparation, see YCu_2Si_2. NMR data were presented by Sampathkumaran et al. (1979). For X-ray absorption measurements, see Padalia et al. (1983).

Routsi and Yakinthos (1981) investigated the magnetic properties of $TmCu_2Si_2$ in the temperature range of 4.2 to 150 K and in magnetic fields up to 18 kOe. Samples were prepared by induction melting under argon at ~ 1500°C. A ferromagnetic or ferrimagnetic ordering was indicated at low temperatures despite the fact that saturation was not reached at 18 kOe. At higher temperatures $TmCu_2Si_2$ is paramagnetic with $\mu_{eff}^{para} = 7.4\ \mu_B$ and $\theta_p = -2$ K.

References

Hanel, G. and H. Nowotny, 1970, Monatsh. Chem. **101**, 463.

Iandelli, A., 1983, J. Less-Common Metals **90**, 121.

Padalia, B.D., T.K. Hatwar and M.N. Ghatikar, 1983, J. Phys. **C16**, 1537.

Routsi, Ch. and J.K. Yakinthos, 1981, Phys. Stat. Sol. (a) **68**, K153.

Rieger, W. and E. Parthé, 1969a, Monatsh. Chem. **100**, 439.

Rieger, W. and E. Parthé, 1969b, Monatsh. Chem. **100**, 444.

Sampathkumaran, E.V., L.C. Gupta and R. Vijayaraghavan, 1979, J. Phys. **C12**, 4323.

Tm–Fe–Si

At least five ternary compounds exist in the Tm–Fe–Si system.

$Tm_2Fe_4Si_9$ crystallizes with the $Y_2Fe_4Si_9$-type of structure: $P6_3/mnc$, $a = 3.923(5)$,

$c = 15.40(1)$ (Gladyshevskij et al., 1978; X-ray powder diffraction data). Magnetic susceptibilities were measured within the temperature range of 300–1200 K and are characterized by $\mu_{eff}^{para} = 6.55\ \mu_B$ mole^{-1} and $\theta_p = -47$ K. For sample preparation, see $Y_2Fe_4Si_9$.

The crystal structure of $Tm_3Fe_2Si_7$ (earlier mentioned as "$TmFeSi_3$") was reported to be isostructural with the $Ho_3Co_2Si_7$-type: Amm2, $a = 3.855$, $b = 24.385$ and $c = 3.900$ (Yarovets, 1978; X-ray powder data). From magnetic susceptibility data (300–1200 K) μ_{eff}^{para} was 7.25 μ_B mole^{-1} and $\theta_p = 74$ K (Gladyshevskij et al., 1978). For sample preparation, see $Y_2Fe_4Si_9$.

$Tm_2Fe_3Si_5$ is isostructural with the structure type of $Sc_2Fe_3Si_5$: P4/mnc, $a = 10.37(1)$, $c = 5.400(9)$ (X-ray powder diffraction data by Braun, 1980). For sample preparation, see $Dy_2Fe_3Si_5$. $Tm_2Fe_3Si_5$ is superconducting at $T_c = 1.3$ K, but reenters to the normal state at $T_N = 1.13$ K (Segre and Braun, 1981; Braun et al., 1981). Yarovets (1978), from X-ray powder diffraction data, confirmed the crystal symmetry of $Tm_2Fe_3Si_5$ but reported different unit cell dimensions with a much smaller c/a ratio: $a = 10.423$ and $c = 5.265$. For low temperature heat capacity data, see Vining and Shelton (1983); $T_N = 1.06$ K.

$TmFe_{4.48}Si_{1.52}$ crystallizes with the $ZrFe_4Si_2$ type structure: $P4_2/mnm$, $a = 7.065$ and $c = 3.777$ (Yarovets, 1978; X-ray powder diffraction data). For sample preparation and atom parameters, see Dy–Fe–Si.

$TmFe_2Si_2$ adopts the $ThCr_2Si_2$-type structure with the space group I4/mmm and lattice parameters as follows: $a = 3.882$ and $c = 9.889$ (X-ray powder data; Yarovets, 1978). ^{57}Fe Mössbauer data at 4.2 K prove the absence of a magnetic moment on the Fe site (Noakes et al., 1983). No magnetic ordering was observed from ac susceptibility measurements as low as 1.4 K.

References

Braun, H.F., 1980, Phys. Lett. **75A**(5), 386.
Braun, H.F., C.U. Segre, F. Acker, M. Rosenberg, S. Dey and P. Deppe, 1981, J. Magn. Magn. Mater. **25**, 117.
Gladyshevskij, E.I., O.I. Bodak, V.I. Yarovets, Yu.K. Gorelenko and R.V. Skolozdra, 1978, Ukr. Fiz. Zh., **23**(11), 77.
Noakes, D.R., A.M. Umarji and G.K. Shenoy, 1983, J. Magn. Magn. Mater. **39**, 309.
Segre, C.U. and H.F. Braun, 1981, Phys. Lett. **85A**(6,7), 372.
Vining, C.B. and R.N. Shelton, 1983, Phys. Rev. **B28**(5), 2732.
Yarovets, V.I., 1978, Autoreferat Dis. Kand. Khim. (abstract of thesis, Russian) (Nauk, Lvov) 24 p.

Tm–Ir–Si

$Tm_5Ir_4Si_{10}$ was reported by Braun and Segre (1981) with the $Sc_5Co_4Si_{10}$-type of structure with space group P4/mbm and lattice parameters $a = 12.520(8)$ and $c = 4.195(5)$ (X-ray powder diffraction); for sample preparation, see $Sc_5Ir_4Si_{10}$. $Tm_5Ir_4Si_{10}$ orders magnetically at 1.0 K.

References

Braun, H.F. and C.U. Segre, 1981, Ternary Superconductors of the $Sc_5Co_4Si_{10}$-type, in: Ternary Superconductors, Proc. Intern. Conf. on Ternary Superconductors, Lake Geneva, WI, USA, eds. G.K. Shenoy, B.D. Dunlap and F.Y. Fradin (North-Holland, Amsterdam) pp. 239–246.

Tm–Mn–Si

Three ternary compounds have been reported for the ternary Tm–Mn–Si system. An antiferromagnetic transition at $T_N = 498$ K ($\mu_{eff}^{para} = 3.7$ μ_B mole^{-1}) has been reported by Szytula and Szott (1981) for $TmMn_2Si_2$ with the $ThCr_2Si_2$-type of structure (I4/mmm).

TABLE 29

Formation and structural data of ternary compounds Tm–Ni–Si.

Compound	Structure type Space group	Lattice parameters Density	Preparation, Characterization	Refs.	Purity
$TmNi_{10}Si_2$	$YNi_{10}Si_2$ ord. $ThMn_{12}$ I4/mmm	$a = 8.172$ $c = 4.652$	$\mu_{eff}^{para} = 8.2$ μ_B, $\theta_p = -65$ K arc(Ar), Qu, 800 °C, 720 h	GlBYGS, 77 Ya, 78a	Tm 99.82 Ni 99.98 Si 99.9
$TmNi_{6.72}Si_{6.28}$	$Ce_2Ni_{17}Si_9$? ($NaZn_{13}$-deriv.) I4/mcm ?	$a = 10.943$ $c = 11.103$ (*)	arc(Ar), Qu 800 °C, 720 h PXD	Ya, 78b	Tm 99.82 Ni 99.98 Si 99.9
$TmNi_{4.23}Si_{0.70}$	$ErNi_{4.23}Si_{0.70}$ ($EuMg_5$ or $Sc_3Ni_{11}Si_4$) $P6_3/mmc$	$a = 8.14$ $c = 8.60$	arc(Ar), Qu 800 °C, 720 h PXD	Ya, 78b	Tm 99.82 Ni 99.98 Si 99.9
$TmNi_5Si_3$	YNi_5Si_3 Pnma	$a = 18.71$ $b = 3.770$ $c = 6.602$	arc(Ar), Qu 800 °C, 720 h PXD	Ya, 78b	Tm 99.82 Ni 99.98 Si 99.9
$Tm_3Ni_6Si_2$	$Ce_3Ni_6Si_2$ (ord. Ca_3Ag_8) Im3m	$a = 8.696(2)$	arc, Qu(Ni) 800 °C, 2 weeks PXD	GlKB, 66	Tm 99.65 Ni 99.99 Si 99.99
$TmNi_2Si_2$	$ThCr_2Si_2$ I4/mmm	$a = 3.914(10)$ $c = 9.516(10)$	arc(Ar) PXD	BoGK, 66	Tm 99.65 Ni 99.8 Si 99.99
		$a = 3.91$ $c = 9.52$	induction melting, Ar, PXD $\theta_p = 8$ K, $\mu_{eff}^{para} = 7.6$ μ_B	Yal, 80	
$TmNiSi_2$	$CeNiSi_2$ Cmcm	$a = 3.898(2)$ $b = 15.905(10)$ $c = 3.898(2)$ (+)	arc(Ar) PXD	BoG, 69	Tm 99.65 Ni 99.8 Si 99.99
$TmNiSi_3$	$ScNiSi_3$ Amm2	$a = 3.962$ $b = 3.876$ $c = 21.103$	arc, Qu (10^{-2} Torr, Ar) 800 °C, 720 h $\mu_{eff}^{para} = 6.70$ μ_B, $\theta_p = -10$ K	GoBGY, 77 Ya, 78b	Tm 99.82 Ni 99.98 Si 99.99
$TmNiSi$	$TiNiSi$ Pnma	$a = 6.717$ $b = 4.107$ $c = 7.118$	arc, Qu, 800 °C, 720 h $\mu_{eff}^{para} = 7.1$ μ_B, $\theta_p = 24$ K	GlBYGS, 77 Ya, 78b	Tm 99.82 Ni 99.98 Si 99.9

(*) For a correct setting of a bct-unit cell, $a = a_0/\sqrt{2} = 7.738$ Å.

(+) Pseudo-tetragonal.

According to X-ray powder data by Knigenko et al. (1977) TmMnSi crystallizes with the TiNiSi-type of structure: Pnma, $a = 6.845$ and $c = 4.002$; for sample preparation, see Y–Mn–Si.

$Tm_2Mn_3Si_5$ was characterized by Segre (1981) as tetragonal $Sc_2Fe_3Si_5$-type, P4/mnc, $a = 10.57(1)$ and $c = 5.392(8)$ (X-ray powder data of arc-melted alloys); $T_n = 1.2$ K.

References

Knigenko, L.D., I.R. Mokra and O.I. Bodak, 1977, Vestn. Lvov Univ., Ser. Khim. **19**, 68.
Segre, C.U., 1981, Thesis, Univ. of Calif., San Diego, USA.
Szytula, A. and I. Szott, 1981, Solid State Commun. **40**, 199.

Tm–Ni–Si

No phase diagram has been established yet. At least nine ternary compounds exist (see table 29).

References

Bodak, O.I. and E.I. Gladyshevskij, 1969, Kristallografiya **14**(6), 990.
Bodak, O.I., E.I. Gladyshevskij, P.I. Kripyakevich, 1966, Izv. Akad. Nauk SSSR, Neorg. Mater. **2**(12), 2151.
Gladyshevskij, E.I., P.I. Kripyakevich and O.I. Bodak, 1966, Acta Crystallogr. **A21**, 80; and Z. Anorg. Allg. Chem. **344**, 95.
Gladyshevskij, E.I., O.I. Bodak, V.I. Yarovets, Yu.K. Gorelenko and R.V. Skolozdra, 1977, Fiz. Magnit. Plenok (Irkutsk) **10**, 182.
Gorelenko, Yu.K., O.I. Bodak, E.I. Gladyshevskij and V.I. Yarovets, 1977, Ukr. Fiz. Zh. **22**(6), 1020.
Yakinthos, J.K. and P.F. Ikonomou, 1980, Solid State Commun. **34**, 777.
Yarovets, V.I., 1978a, Tesizy Dokl. Tret. Vses. Konf. Kristallochim. Intermet. Soedin, 2nd Ed., ed. R.M. Rykhal (Lvov Gos. Univ., Lvov, USSR) p. 124.
Yarovets, V.I., 1978b, Autoreferat Dis. Kand. Khim. (abstract of thesis, Russian) (Nauk, Lvov) 24 p.

Tm–Os–Si

Hiebl et al. (1983) investigated the structural and magnetochemical properties of $TmOs_2Si_2$ in the temperature range 1.5 K $< T <$ 1100 K. $TmOs_2Si_2$ is isotypic with the crystal structure of $ThCr_2Si_2$: I4/mmm, $a = 4.1240(3)$, $c = 9.6211(48)$ (X-ray powder data). The magnetic data are characterized by $\mu_{eff}^{para} = 7.34$ μ_B, $\theta_p = 64$ K and ferromagnetic order below 1 K. For sample preparation, see YOs_2Si_2.

Reference

Hiebl, K., C. Horvath, P. Rogl and M.J. Sienko, 1983, Solid State Commun. **48**, 211.

Tm–Pd–Si

Two ternary thulium palladium silicides have been characterized. $TmPd_2Si$ has the ordered Fe_3C-type of structure with space group Pnma and lattice parameters $a = 7.201(2)$, $b = 6.927(2)$ and $c = 5.452(2)$ (Moreau et al., 1982; X-ray powder data). For sample preparation, see YPd_2Si.

Tm$_2$Pd$_2$Si crystallizes with the Er$_2$Pd$_2$Si-type structure: Pnnm, $a = 7.380(2)$, $b = 13.658(4)$, $c = 4.269(2)$ (X-ray powder data by Klepp et al., 1983). Samples were arc melted.

References

Klepp, K., E. Hovestreydt and E. Parthé, 1983, Acta Crystallogr. **C39**, 662.
Moreau, J.M., J. Leroy and D. Paccard, 1982, Acta Crystallogr. **B38**, 2446.

Tm–Pt–Si

TmPt$_2$Si crystallizes with the ordered Fe$_3$C-type of structure: Pnma, $a = 7.212(3)$, $b = 6.916(3)$, $c = 5.422(2)$ (X-ray powder data by Moreau et al., 1982). For sample preparation, see YPd$_2$Si.

TmPtSi is orthorhombic, Pnma, TiNiSi-type of structure, $a = 6.860(1)$, $b = 4.2315(8)$, $c = 7.383(1)$ (X-ray powder data by Hovestreydt et al., 1982). For sample preparation, see ScPtSi.

TmPt$_2$Si$_2$ was claimed to be tetragonal with the BaAl$_4$-type ($a = 4.113$, $c = 9.838$, $\rho_x = 12.27$ kg/dm^3). In analogy to ErPt$_2$Si$_2$, Pt and Si atoms were said to occupy the 4d and 4e sites of I4/mmm in a statistical distribution; for sample preparation, see LaPt$_2$Si$_2$ (Mayer and Yetor, 1977). According to more recent X-ray powder data of arc-melted alloys the crystal symmetry is primitive tetragonal with an ordered atomic arrangement similar to the CaBe$_2$Ge$_2$-type (Rogl, 1984): $a = 4.1195(4)$, $c = 9.8591(35)$, CePt$_2$Si$_2$-type.

References

Hovestreydt, E., N. Engel, K. Klepp, B. Chabot and E. Parthé, 1982, J. Less-Common Metals **86**, 247.
Mayer, I. and P.D. Yetor, 1977, J. Less-Common Metals **55**, 171.
Moreau, J.M., J. Leroy and D. Paccard, 1982, Acta Crystallogr. **B38**, 2446.
Rogl, P., 1984, Inorg. Chem., to be published.

Tm–Re–Si

Two compounds have been characterized in the Tm–Re–Si system.

By X-ray powder methods Bodak et al. (1978) observed the compound Tm$_2$Re$_3$Si$_5$ to crystallize with the Sc$_2$Fe$_3$Si$_5$-type of structure [P4/mnc, $a = 10.83(1)$, $c = 5.474(5)$]. Samples were arc melted, but no detailed conditions of heat treatment were reported. Segre (1981) confirmed the structure type but measured different lattice parameters: $a = 10.89(1)$ and $c = 5.456(8)$. Samples were arc melted; $T_n = 1.2$ K.

TmRe$_4$Si$_2$ was found to be isostructural with the ZrFe$_4$Si$_2$-type: P4$_2$/mnm, $a = 7.302(5)$ and $c = 4.103(2)$ (Pecharsky, 1979); X-ray powder data of arc-melted alloys annealed at 800°C). For details of sample preparation, see Tb–Re–Si.

References

Bodak, O.I., V.K. Pecharskij and E.I. Gladyshevskij, 1978, Izv. Akad. Nauk SSSR, Neorg. Mater. **14**(2), 250.
Pecharskij, V.K., 1979, Autoreferat Dis. Kand. Khim. (abstract of thesis, Russian) (Nauk, Lvov) 23 p.
Segre, C.U., 1981, Thesis, Univ. of Calif., San Diego, USA.

Tm–Ru–Si

Barz (1980) reported the existence of a ternary compound $TmRu_3Si_2$ with the $LaRu_3Si_2$-type of structure. No lattice parameters were presented. For sample preparation, melting behavior and phase equilibria, see $LaRu_3Si_2$. Magnetic ordering was observed at $T_m = 7.50$ K.

$TmRu_2Si_2$ crystallizes with the $ThCr_2Si_2$-type of structure: I4/mmm, $a = 4.1427(4)$, $c = 9.4692(49)$ (Hiebl et al., 1983; X-ray powder analysis of arc melted samples). The magnetic behavior of $TmRu_2Si_2$ was investigated in the temperature region 1.5 K to 1100 K. The magnetic data were: $\mu_{eff}^{para} = 7.38$ μ_B, $\theta_p = 65.7$ K; ferromagnetic ordering exists at ~ 1 K.

References
Barz, H., 1980, Mater. Res. Bull. **15**, 1489.
Hiebl, K., C. Horvath, P. Rogl and M.J. Sienko, 1983, J. Magn. Magn. Mater. **37**, 287.

Y–Al–Si

Muravyova et al. (1971) and Muravyova (1972) investigated the phase relations near the Y–Si binary (isothermal section at 500°C for 0–33 a/o Y). Alloys were prepared by arc melting under argon, followed by heat treatment for 750 h at 500°C. 96 samples were analyzed by X-ray powder diffraction methods. Starting materials were Y 99.6%, Al 99.98% and Si 99.98%.

The binary systems were partly reinvestigated and were found to be in agreement with recent phase diagram data (Al–Si is a simple eutectic; the binary Y silicides are discussed in context with the system Y–Ni–Si). YAl_2 with the $MgCu_2$-type was confirmed; however, at variance with earlier data on the polymorphism of YAl_3(Ni_3Sn- or/and $BaPb_3$-type), Muravyova et al. (1971) could not confirm a polymorphic transition and the $BaPb_3$-type structure was the only modification reported. These findings are in good agreement with an investigation by Zalitskii et al. (1966), who observed the $BaPb_3$-type in the complete temperature interval of $100°C < T < 1000°C$ [$a = 6.196(1)$, $c = 21.14(1)$]. It was concluded that small amounts of impurities such as Si easily stabilize the Ni_3Sn-type.

Ternary phase equilibria in fig. 49a show the existence of 5 ternary silicides; the crystal structures of YAl_2Si and $Y_{33.3}Al_{46.7}Si_{20}$ have been solved by Yanson (1975) from single crystal photographs.

A monoclinic unit cell was proposed for YAl_2Si with space group C2/m and the lattice parameters $a = 10.42$, $b = 4.070$, $c = 6.741$ and $\beta = 101°$. Atom parameters were reported as follows: 4 Y in site 4i) 0.12, 0, 0.17, and a statistical distribution of Al, Si atoms in each of the three following sites 4i): $x_1 = 0.33$, 0, $z_1 = 0.11$; $x_2 = 0.46$, 0, $z_2 = 0.34$; $x_3 = 0.73$, 0, $z_3 = 0.34$.

$Y_{33.3}Al_{46.7}Si_{20}$ (or $YAl_{1.4}Si_{0.6}$) represents a new structure type, with space group Immm and the lattice parameters $a = 4.072$, $b = 5.812$ and $c = 8.823$; according to Yanson (1975) the atom parameters were Y in 2a) 0, 0, 0; in 2c) 1/2, 1/2, 0, and a statistical occupation of 5.6 Al + 2.4 Si in the 8ℓ site 0, 0.2901, 0.2812, the
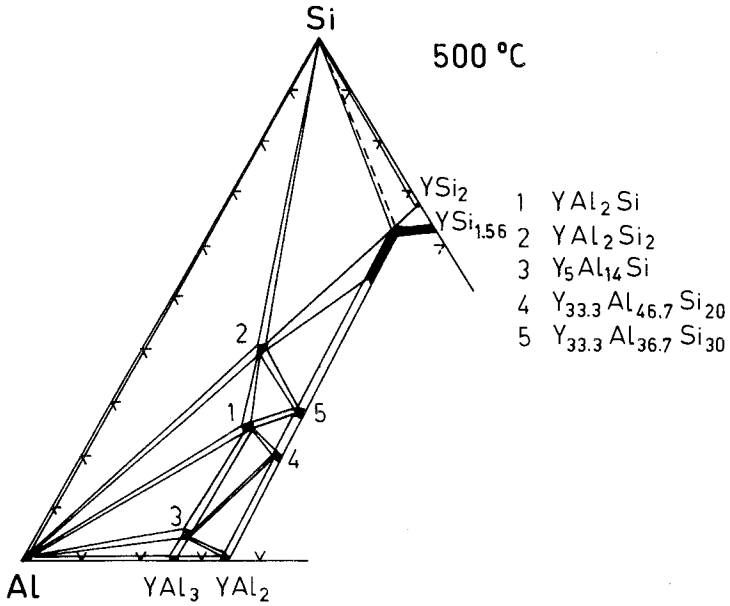
Fig. 49a. Y–Al–Si, partial isothermal section at 500°C. 1: YAl_2Si, 2: YAl_2Si_2, 3: $Y_5Al_{14}Si \equiv Y(Al, Si)_3$, 4: $Y_{33.3}Al_{46.7}Si_{20}$ ($YAl_{1.4}Si_{0.6}$), 5: $Y_{33.3}Al_{36.7}Si_{30}$ (crystal structure unsolved).

corresponding reliability factors of the refinement were $R(F_{0kl}) = 0.154$ and $R(F_{1kl}) = 0.153$.

YAl_2Si_2 crystallizes with the La_2O_2S-type of structure: $P\bar{3}m1$, $a = 4.181$, $c = 6.559$; X-ray powder intensity data were found to be satisfactory using the atom
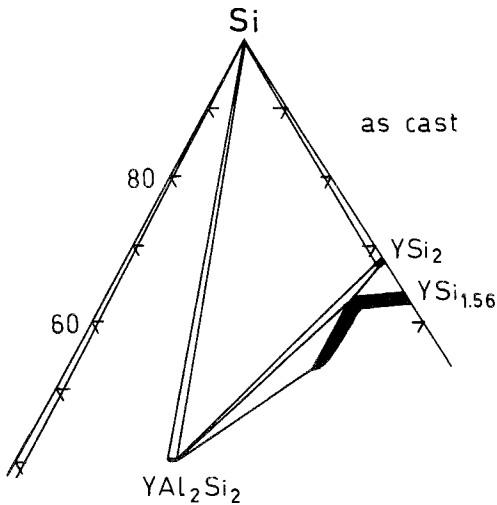
Fig. 49b. Phase distribution in as-cast alloys.
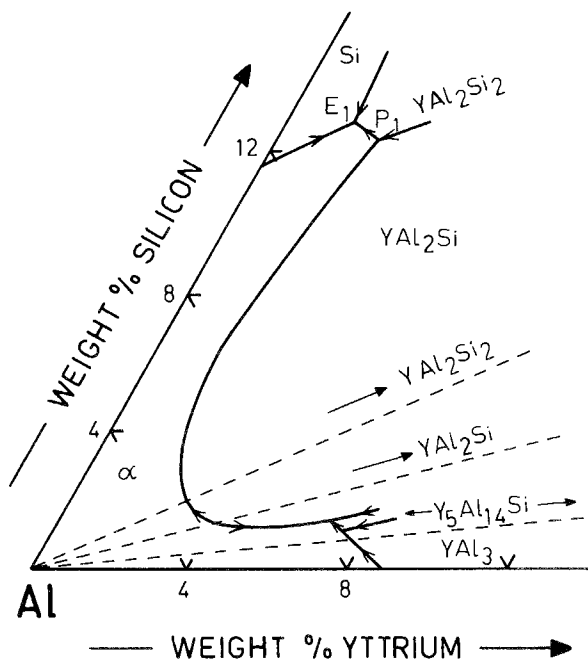
Fig. 50. Y–Al–Si, liquidus projection in the Al-rich corner; the dashed lines indicate low-temperature solid state two-phase equilibria.

parameters derived for the isostructural compound $CaAl_2Si_2$ (Muravyova et al., 1972; for details, see Sm–Al–Si).

$Y_5Al_{14}Si$ was successfully indexed on the basis of a hexagonal unit cell ($P6_3/mmc$, $a = 6.247$, $c = 4.590$); calculated X-ray powder intensities were in agreement with a Ni_3Sn-type of structure (see also YAl_3, above), assuming 2Y in the 2c site 1/3, 2/3, 1/4 and a statistical distribution of Si, Al atoms in 6h) 0.860, 0.720, 1/4 (Muravyova, 1972).

Ternary alloys in the vicinity of Y disilicides revealed different phase equilibria depending on the heat treatment: the phase distribution as derived from alloys in as-cast condition is shown in fig. 49b. The solubility of Al in $YSi_{1.56}$ (AlB_2-defect type) in both cases of as-cast and annealed alloys was claimed to proceed along an unusual path similar to the solution of Ni in $YSi_{1.56}$ (see Y–Ni–Si); the maximum solubility of Al at 500°C was shown to be at ∼ 15 a/o Al (Muravyova et al., 1971).

More recently Drits et al. (1980) investigated the melting behavior in the Al rich corner and established the liquidus projection (fig. 50) as well as the phase equilibria within three isopleths at a constant concentration of 92% Al (fig. 51a), 1% Si (fig. 51b) and at 3% Y (fig. 51c). The following reaction isotherms have been observed:
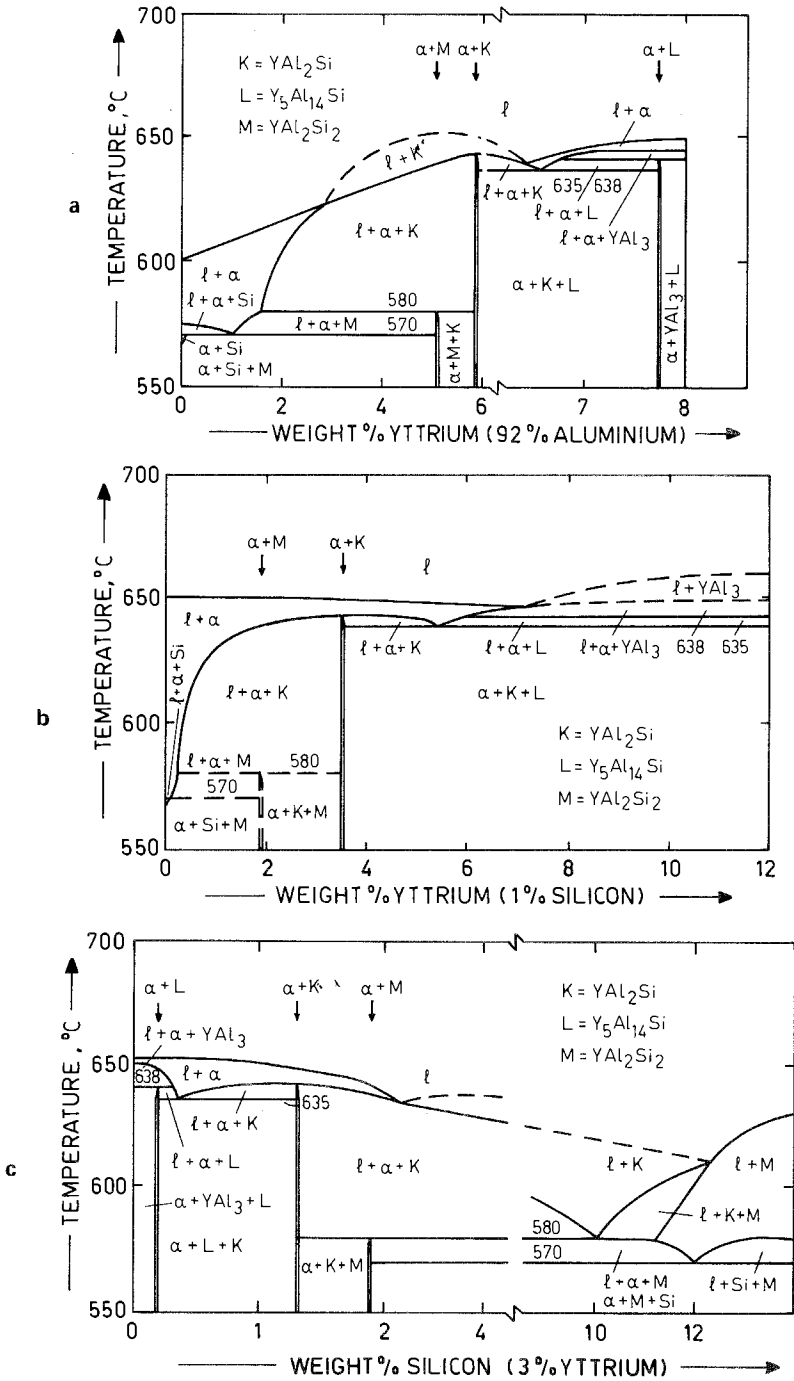
Fig. 51. Y–Al–Si. (a) Isopleth at a constant concentration of 92% Al, Al-rich corner. (b) Isopleth at a constant concentration of 1% Si, Al-rich corner. (c) Isopleth at a constant concentration of 3% Y.

Temperature	Reaction	Composition at invariant point (w/o)
570°C	$\ell \rightleftharpoons \alpha + Si + YAl_2Si_2(M)$	13 Si, 2 Y, 85 Al
635°C	$\ell \rightleftharpoons \alpha + YAl_2Si(K) + Y_5Al_{14}Si(L)$	1.5 Si, 7 Y, 91.5 Al
580°C	$\ell + YAl_2Si(K) \rightleftharpoons \alpha + YAl_2Si_2(M)$	12.5 Si, 2.5 Y, 85 Al
638°C	$\ell + YAl_3 \rightleftharpoons \alpha + Y_5Al_{14}Si(L)$	1 Si, 7.3 Y, 91.7 Al

References

Drits, M.E., V.I. Kuzmina and N.I. Tyrkina, 1980, Metally **3**, 212.
Muravyova, A.A., 1972, Autoreferat Dis. Kand. Khim. (abstract of thesis, Russian) (Nauk, Lvov) 22 p.
Muravyova, A.A., O.S. Zarechnyuk and E.I. Gladyshevskij, 1971, Izv. Akad. Nauk SSSR, Neorg. Mater. **7**(1), 38.
Muravyova, A.A., O.S. Zarechnyuk and E.I. Gladyshevskij, 1972, Visn. L'vivsk. Univ. Ser. Khim. **13**, 14.
Yanson, T.I., 1975, Autoreferat Dis. Kand. Khim. (abstract of thesis, Russian) (Nauk, Lvov) 22 p.
Zalitskii, I.I., P.I. Kripyakevich, V.R. Ryasov and K.V. Rysas, 1966, Dokl. Akad. Nauk Ukr. SSR **10**, 1287.

Y–Au–Si

Felner (1975) reported the existence of YAu_2Si_2 with the ordered $ThCr_2Si_2$-type of structure (X-ray powder analysis); sample preparation as for $LaAu_2Si_2$. The crystallographic data were given as I4/mmm, $a = 4.230$ and $c = 10.18$. From susceptibility measurements diamagnetic behavior was observed for a temperature range of 4.2 K to 300 K.

Reference

Felner, I., 1975, J. Phys. Chem. Sol. **36**, 1063.

Y–Co–Si

Phase equilibria within isothermal sections at 800°C (region 0–33 a/o Y) and at 600°C (33–100 a/o Y), have been published by Bodak et al. (1974) without details.

The yttrium–cobalt binary system was modified with respect to a recent review on binary rare-earth–cobalt systems by Ray (1974) and a reinvestigation by Grover et al. (1982). According to this new data the compound Y_3Co_2 characterized by Moreau et al. (1975) is a metastable phase, and the compound Y_4Co_3 earlier characterized by a Ho_4Co_3-type in fact was shown to be a superstructure, better represented by the formula Y_9Co_7. Thus at 600–800°C the Y–Co system comprises the following phases: Y_2Co_{17} (Th_2Zn_{17}-type), YCo_5 ($CaCu_5$-type), Y_2Co_7 (Gd_2Co_7-type), YCo_3 ($PuNi_3$-type), YCo_2 ($MgCu_2$-type), Y_2Co_3 (Gd_2Co_3-type), YCo, Y_9Co_7 (Y_9Co_7-type), Y_8Co_5 (Y_8Co_5-type) and Y_3Co (Fe_3C-type). The crystal structure of Y_8Co_5 was recently derived by Moreau et al. (1976); however, the existence of "YCo" and "Y_2Co_3" needs further confirmation.

The binary cobalt and yttrium silicides are in good agreement with more recent data and are discussed in combination with the systems Ce–Co–Si and Y–Ni–Si, respectively. Mutual solid solubilities of binary compounds have been found to be
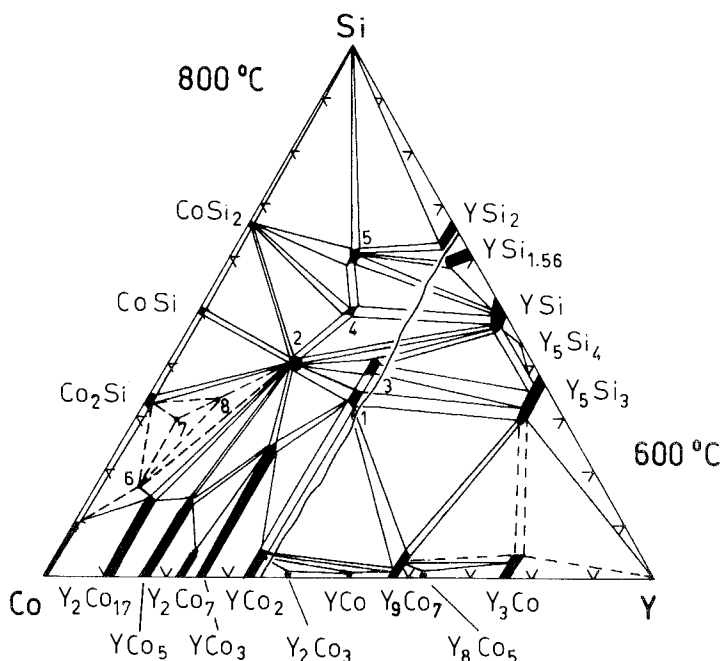
Fig. 52. Y–Co–Si, partial isothermal sections at 800°C (0–33 a/o Y) and at 600°C (33–100 a/o Y). 1: $YCoSi$, 2: YCo_2Si_2, 3: $Y(Co, Si)_2$, 4: $YCoSi_2$, 5: $YCoSi_3$, 6: $YCo_{8.6}Si_{2.4}$, 7: YCo_9Si_4, 8: YCo_5Si_3.

considerably large with extended Co/Si exchange at a fixed Y concentration (see fig. 52). YCo_3 dissolves up to 25 a/o Si; Y_2Co_{17} and YCo_5 dissolve up to 15 a/o Si; and Y_2Co_7, YCo_2, Y_9Co_7, Y_3Co dissolve ~ 5 a/o Si; Y_5Si_3 dissolves up to 7 a/o Co; YSi_2, $YSi_{1.56}$ and YSi dissolve ~ 5 a/o Co. Nothing is known at present about the Si solubility in Y–Co compounds such as YCo, Y_2Co_3 and Y_8Co_5. Due to a probably peritectoid reaction at 725°C the formation of binary Y_9Co_7 is extremely sluggish and Y_9Co_7 is only obtained after long annealing times (arc-melted samples, annealed at 680°C up to 1000 h in quartz capsules). From micrograph analysis the stabilizing influence of small amounts of silicon (Co/Si substitution) was suspected to change the type of reaction into peritectic (Yvon et al., 1983); a solid solubility of ~ 8 a/o Si was derived from X-ray powder data of alloys quenched from 680°C and is in good agreement with the data by Bodak et al. (1978) from 600°C alloys.

Eight ternary compounds were reported; the crystal structures of three of them, $YCoSi_3$ (tetragonal, $a = 4.066$, $c = 9.577$), YCo_5Si_3 and YCo_9Si_4 have not been characterized. Furthermore, from X-ray powder analysis of arc-melted alloys Bodak and Gladyshevskij (1969) reported the existence of a compound $YCo_{8.6}Si_{2.4}$ with the $BaCd_{11}$-type structure [$I4_1/amd$, $a = 9.714(5)$, $c = 6.266(10)$]; the atomic order and crystal symmetry was confirmed to be isostructural with the $Ce_2Ni_{17}Si_5$ type by Yarovets (1978), from X-ray powder data obtained for $YCo_{8.5}Si_{2.5}$ [$a = 9.706(9)$, $c = 6.300(5)$]. For sample preparation and atom parameters, see Tb–Co–Si.

The crystal structure of YCo_2Si_2 has been confirmed and refined by Rossi et al. (1978) by means of X-ray powder diffraction data. YCo_2Si_2 crystallizes with the ordered $ThCr_2Si_2$-type structure: I4/mmm, $a = 3.892$, $c = 9.759$, $\rho_x = 5.91$ kg/dm^3; Y in 2a); Co in 4d); Si in 4e) with $z = 0.375$. Samples were prepared by melting in an induction furnace under argon, followed by heat treatment for 1 week at 500°C. Etching is possible with dilute solutions of HNO_3^- or $HNO_3 + HCl$ or $HNO_3 + HF$. Starting material were of 99.9% minimum purity. Bodak et al. (1974) reported $a = 3.96$, $c = 9.78$. The magnetic susceptibility (4.2–200 K) was studied by Yakinthos et al. (1980). Slightly different lattice parameters were reported by Yarovets (1978) from X-ray powder data ($a = 3.887$ and $b = 9.734$).

YCoSi was observed to adopt the TiNiSi-type structure with the space group Pnma and lattice parameters $a = 6.854$, $b = 4.156$ and $c = 7.215$ (X-ray powder data; Yarovets, 1978). For sample preparation and atom parameters, see YNiSi.

$YCoSi_2$ was said to crystallize with the $CeNiSi_2$-type of structure: Cmcm, $a = 4.043(5)$, $b = 16.579(8)$, $c = 3.969(5)$ (Bodak et al., 1974; Yarovets, 1978). Pelizzone et al. (1982) confirmed the crystal symmetry from X-ray powder data and recorded $a = 4.025(2)$, $b = 16.280(7)$, $c = 3.963(3)$. For sample preparation, see $HoCoSi_2$. Magnetic susceptibilities were studied in the range 2–250 K and were found to be a constant value of 22×10^{-6} emu/g. From this rather low value the paramagnetism was suggested to be due to the conduction electrons and no magnetic moment is carried by the Co atoms. An onset to superconductivity was recorded at 1.2 K.

A rather small homogeneous region was reported by Bodak et al. (1974) for the ternary compound $YCo_{0.8}Si_{1.2}$ with the AlB_2-type of structure ($a = 3.99$, $c = 4.21$). Phase equilibria in fig. 52 are mainly based on the work of Bodak and Gladyshevskij (1969) and Bodak et al. (1974).

References

Bodak, O.I. and Gladyshevskij, 1969, Dopov. Akad. Nauk Ukr. RSR, Ser. A 5, 452.
Bodak, O.I., P.A. Muratova, I.P. Mokra, V.I. Yarovets, A.S. Sobolev and E.I. Gladyshevskij, 1974, Strukt. Faz. Fazov. Prevrash. Diagr. Sostojan. Met. Sist. (Nauka, Moscow, USSR) p. 182.
Grover, A.K., B.R. Coles, B.V.B. Sarkissian and H.E.N. Stone, 1982, J. Less-Common Metals **86**, 29.
Moreau, J.M., E. Parthé and D. Paccard, 1975, Acta Crystallogr. **B31**, 747.
Moreau, J.M., D. Paccard and E. Parthé, 1976, Acta Crystallogr. **B32**, 496.
Pelizzone, M., H.F. Braun and J. Müller, 1982, J. Magn. Magn. Mater. **30**, 33.
Ray, A.E., 1974, Cobalt **1**, 13.
Rossi, D., R. Marazza and R. Ferro, 1978, J. Less-Common Metals **58**, 203.
Yakinthos, J.K., Ch. Routsi and P.F. Ikonomou, 1980, J. Less-Common Metals **58**, 203.
Yarovets, V.I., 1978, Autoreferat Dis. Kand. Khim. (abstract of thesis, Russian) (Nauk, Lvov) 24 p.
Yvon, K., H.F. Braun and E. Gratz, 1983, J. Phys. F. **13**, L131.

Y–Cr–Si

Sobolev et al. (1971) determined the phase equilibria within an isothermal section of the system Y–Cr–Si at 800°C based on metallographic and X-ray powder analysis of 80 alloy specimens. Samples were prepared by arc melting and subsequent annealing for 500 h at 800°C, and finally quenched in cold water. Starting
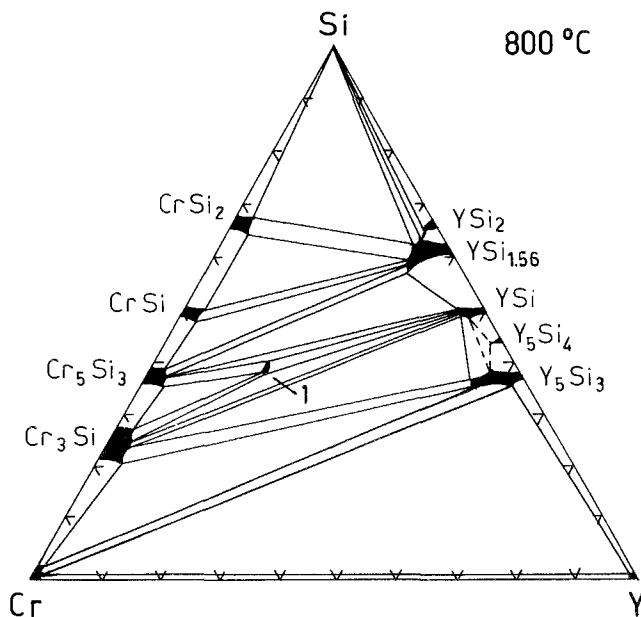
Fig. 53. Y–Cr–Si, isothermal section at 800°C.

materials were Y 99.3%, Cr 99.7% and Si 99.9%. Etching was possible with a mixture of HNO_3 and HF in glycerin.

In agreement with phase diagram data, the existence of the four binary Cr silicides was confirmed. Cr_3Si (Cr_3Si-type), Cr_5Si_3 (W_5Si_3-type), CrSi (FeSi-type) and $CrSi_2$ ($CrSi_2$-type). Extensive homogeneous regions(?) were shown by Sobolev et al. (1971) for Cr_3Si, Cr_5Si_3, and $CrSi_2$; no detailed data, however, were presented (see fig. 53). The binary yttrium silicides have been discussed in connection with the system Y–Ni–Si. Practically no solid solubility exists for the pair Y, Cr.

Mutual solid solubilities of Y and Cr silicides were derived from the variation of the lattice parameters and generally were found to be less than 5% (see fig. 53). $YSi_{1.56}$ (AlB_2-type, $a = 3.83$, $c = 4.14$) dissolves up to ~ 8 a/o Cr; Y_5Si_3 (Mn_5Si_3-type, $a = 8.418$, $c = 6.337$) dissolves up to ~ 5 a/o Cr, whereas Y_5Si_4 (Sm_5Ge_4-type, $a = 7.39$, $b = 14.52$, $c = 7.64$) and YSi (CrB-type, $a = 4.254$, $b = 10.526$, $c = 7.64$) dissolve less than 5 a/o Cr. YSi_2-type ($a = 4.04$, $b = 3.93$, $c = 13.36$) was studied in the temperature range 20–600°C; however, no indication of a phase transformation was observed!

Ternary phase equilibria at 800°C are characterized by the formation of one ternary compound YCr_2Si_2 with the $ThCr_2Si_2$-type of structure, $a = 3.916(2)$, $c = 10.631(10)$; Y in 2a), Cr in 4d), and Si in 4e) of I4/mmm with $z = 0.375$. The microhardness, measured at a load of 100 g, was $H = 858(40)$ kg/mm^2.

Reference

Sobolev, A.S., O.I. Bodak and E.I. Gladyshevskij, 1971, Izv. Akad. Nauk SSSR, Neorg. Mater. 7(1), 41.

Y–Cu–Si

Raman (1967) and Rieger and Parthé (1969a) studied the occurrence of the AlB_2-type structure in correlation with the valence electron concentration by means of X-ray powder analysis of arc-melted alloys. Rieger and Parthé (1969a) investigated the alloys with concentrations $YCu_{0.67}Si_{1.33}$ ($a = 4.000$, $c = 4.023$) and $YCuSi$ ($a = 4.046$, $c = 3.951$). Cu and Si atoms were said to statistically occupy the 2d site of P6/mmm. Raman (1967) reported unit cell dimensions for a Cu-rich "$YCu_{1.5}Si_{0.5}$" [$a = 4.144(5)$ and $c = 3.727(5)$] and for a Si-rich "$YCu_{1.5}Si_{0.5}$" [$a = 4.146(5)$ and $c = 3.757(5)$]. Thus extended homogeneous regions and/or separated AlB_2-type phases with ordering among Cu,Si atoms seem to be conceivable (see e.g. phase equilibria in the system Ce–Cu–Si).

At variance with the crystal data obtained by Rieger and Parthé (1969a) from arc-melted samples, Iandelli (1983) reported the existence of a compound YCuSi with the ordered Ni_2In-type [superstructure of the AlB_2-type; $P6_3/mmc$, $a = 4.147(1)$, $c = 7.448(5)$]. The superstructure reflections were said to be faint and were observed from arc-melted samples annealed at 750°C for 8–12 d. The Ni_2In phase thus was concluded to be a low temperature modification. For detailed sample preparation and purity of starting materials, see LaCuSi.

Kido et al. (1983) investigated the magnetic behavior of YCuSi alloys prepared by powder metallurgical sintering at 800–900°C for 7 d in evacuated silica tubes. From X-ray powder analysis an AlB_2-type was claimed and magnetic data were obtained in the temperature range of 77 to 300 K. No temperature dependence of the susceptibility was observed.

$Y_3Cu_4Si_4$ crystallizes with the $Gd_3Cu_4Ge_4$-type of structure: Immm, $a = 13.71$, $b = 6.55$, $c = 4.13$ (Hanel and Nowotny, 1970; X-ray powder diffraction). For sample preparation, see $Sc_3Cu_4Si_4$. From microprobe analysis a small exchange Cu/Si was indicated (~ 4 a/o Cu replaced by Si).

The crystal structure of YCu_2Si_2 has been refined by Rieger and Parthé (1969b) by means of powder diffraction data of arc-melted samples, which subsequently were annealed in evacuated silica tubes at 900°C for 100 h. Complete metal ordering has been derived from powder intensities: $ThCr_2Si_2$-type of structure, $a = 3.967(6)$, $c = 9.959(10)$; Y in 2a); Cu in 4d) and Si in 4e) of I4/mmm with $z = 0.375(5)$. NMR data were presented by Sampathkumaran et al. (1979).

Magnetic properties of YCu_2Si_2 were reported by Routsi and Yakinthos (1981) in the temperature region of 4.2 to 150 K and in fields up to 15 kOe. Susceptibilities were found to be insignificant.

References

Hanel, G. and H. Nowotny, 1970, Monatsh. Chem. **101**, 463.
Iandelli, A., 1983, J. Less-Common Metals **90**, 121.
Kido, H., T. Hoshikawa, M. Shimada and M. Koizumi, 1983, Phys. Stat. Sol. (a) **77**, K121.
Raman, A., 1967, Naturwiss. **54**, 560.
Rieger, W. and E. Parthé, 1969a, Monatsh. Chem. **100**, 439.
Rieger, W. and E. Parthé, 1969b, Monatsh. Chem. **100**, 444.
Routsi, C. and J.K. Yakinthos, 1981, Phys. Stat. Sol. (a) **68**, K 153.
Sampathkumaran, E.V., L.C. Gupta and R. Vijayaraghavan, 1979, J. Phys. C12, 4323.

Y–Fe–Si

Bodak et al. (1978) investigated the phase equilibria in the system Y–Fe–Si at 800°C by means of X-ray powder and metallographic analysis of 200 alloys. Samples were arc melted and annealed in evacuated quartz tubes for 720 h at 800°C. Starting materials were Y 99.83%, Fe 99.98% and Si 99.99%.

Y–Fe compounds observed at 800°C are in agreement with the compilation by Iandelli and Palenzona (1979): Y_2Fe_{17}, Y_2Fe_{17-x} (Th_2Zn_{17}, Th_2Ni_{17}-types), Y_6Fe_{23} (Th_6Fe_{23}-type), YFe_3 (PuNi$_3$-type), YFe_2 (MgCu$_2$-type). The two phases Y_2Fe_{17} and Y_2Fe_{17-x}—separated by an extremely small two-phase field—were both claimed to exist at the same temperature (800°C).

Three iron silicides were confirmed at 800°C: Fe_3Si (BiF$_3$-type, α_1), FeSi (FeSi-type) and $FeSi_2$ (ℓ-FeSi$_2$-type). Despite the extensive investigations by different research groups, some controversies still exist in the region up to 25 a/o Si, particularly regarding the phase boundaries of the solid solutions α(Fe,Si), α_1, α_2. According to Schlatte and Pitsch (1976) continuous phase transitions higher than first order were proposed, whereas an eutectoid decomposition of the CsCl-type α_2-phase was accepted by Schürmann and Hensgen (1980) at $T_{ED} = 540°C$ ($\alpha_2 \rightleftharpoons \alpha + \alpha_1$). For a more recent critical review, see e.g. Rivlin and Raynor (1981). The phase equilibria in fig. 54 are thus to be understood subject to this controversy. The binary Y silicides have been discussed with the system Y–Ni–Si.

Solid solubilities of binary compounds in most cases extend in the direction of a Fe/Si exchange at a fixed Y concentration. In some cases solubility limits were
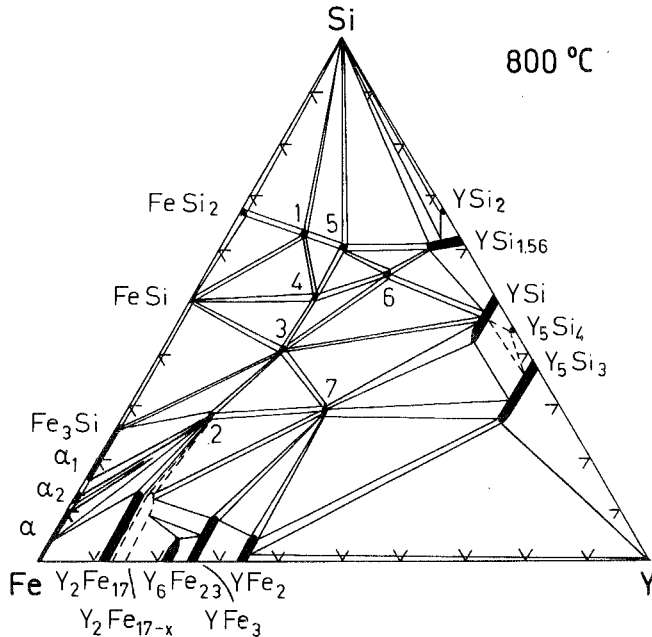
Fig. 54. Y–Fe–Si, isothermal section at 800°C. 1: $Y_2Fe_4Si_9$ (earlier obtained at $Y_2Fe_5Si_8$), 2: $YFe_{4.48}Si_{1.52}$, 3: YFe_2Si_2, 4: $Y_2Fe_3Si_5$, 5: $Y_3Fe_2Si_7$ (earlier YFeSi$_3$), 6: "$YFe_{0.5}Si_{1.83}$", 7: $YFe_{1.16}Si_{0.84}$.

TABLE 30
Formation and structural data of ternary compounds Y–Fe–Si.

Compound	Structure type Space group	Lattice parameters Density	Preparation, Characterization	Refs.	Purity
$YFe_{1.16}Si_{0.84}$ [○]	PbFCl P4/nmm	$a = 3.970(5)$ $c = 6.800(7)$	arc, Qu, 800 °C 720 h, PXD refinement of X-ray powder data	Ya, 78	Y 99.83 Fe 99.98 Si 99.99
YFe_2Si_2	$ThCr_2Si_2$ I4/mmm	$a = 3.91$ $c = 9.89$	arc, Qu, 800 °C 720 h, PXD $\mu_{eff}^{para} = 2.35(5)\,\mu_B$; $\theta_p = 648$ K (817–1152 K)	BoGYDI, 78 Ya, 78	Y 99.83 Fe 99.98 Si 99.99
		$a = 3.920$ $c = 9.920$ $\rho_x = 5.59$	induction melting (Ar), 500 °C, 1 week PXD	RoMF, 78	Y 99.9 Fe 99.99 Si 99.99
		$a = 3.914(5)$ $c = 9.93(1)$	arc, PXD (80–1050 K) $T_m = 275$ K $\mu_{eff}^{para} = 0.6\,\mu_B/Fe$, $\theta_p = 100$ K	SkGBY, 80	
$Y_2Fe_3Si_5$	$Sc_2Fe_3Si_5$ P4/mnc	$a = 10.13$ $c = 5.50$	arc, Qu, 1200 °C, 2d, 720 h, PXD	BoGYDI, 78	Y 99.83 Fe 99.98 Si 99.99
		$a = 10.503(8)$ $c = 5.335(5)$		Ya, 78	
		$a = 10.43(1)$ $c = 5.47(1)$	arc, Qu, 1200 °C, 2d 800 °C, 2d, PXD $T_c = 2.4$–2.0 K	Br, 80	Y 99.9 Fe 5N Si 7N
$YFe_{0.5}Si_{1.83}$	unknown		arc, Qu, 800 °C 720 h, PXD	BoGYDI, 78	Y 99.83 Fe 99.98 Si 99.99
$Y_2Fe_4Si_9$ [*]	$Y_2Fe_4Si_9$ $P6_3/mmc$	$a = 3.85$ $c = 15.60$	arc, Qu, 800 °C 720 h single crystal data	BoGYDI, 78	Y 99.83 Fe 99.98 Si 99.99
		$a = 3.928(5)$ $c = 15.44(1)$	$\chi(670$ K$) = 0.53 \times 10^{-6}$	GlBYGS, 78	
$Y_3Fe_2Si_7$	$Ho_3Co_2Si_7$ Amm2	$a = 3.868$ $b = 24.760$ $c = 3.915$	arc, Qu 800 °C, 720 h PXD	BoGYDI, 78 Ya, 78 GlBYGS, 78	Y 99.83 Fe 99.98 Si 99.99
$YFe_{4.48}Si_{1.52}$	$ZrFe_4Si_2$ $P4_2/mnm$	$a = 7.117(8)$ $c = 3.784(5)$	arc, Qu, 800 °C 720 h, PXD	Ya, 78	Y 99.83 Fe 99.98 Si 99.99
		$a = 7.20$ $c = 3.79$ at "YFe_4Si_2"	arc, Qu, 1800 °C 720 h, PXD	BoGYDI, 78	

[*] First identified as $Y_2Fe_5Si_8$ by Bodak et al. (1978), but later characterized as $Y_2Fe_4Si_9$ by refinement of X-ray single crystal photographs (Gladyshevskij et al., 1978). Atom parameters obtained were Y in 2c); Fe in 4f) 1/3, 2/3, 0.9034(8); Si in 4f) $z = 0.0596(7)$; Si in 4c) 0, 0, 0.8402(6); 1 Si in 2a) 0, 0, 0.

[○] Earlier identified by Bodak et al. (1978) with composition YFeSi and lattice parameters $a = 3.99$ and $c = 6.80$. The correct composition $YFe_{1.16}Si_{0.86}$ was derived from a refinement of X-ray powder data (Yarovets, 1978); the atom parameters obtained were: Y in 2c) 1/4, 1/4, 0.6673(7); Fe in 2a) 0, 0, 0 and a statistical distribution of 0.84 Si + 0.16 Fe in 2c) 1/4, 1/4, 0.2119(5); $R = 0.124$.

determined from the variation of lattice parameters, but no further details were given: Y_2Fe_{17-x} and Y_2Fe_{17} dissolved up to 13 a/o Si, 7 a/o Fe in YSi; 7 a/o Si in YFe_3 and up to 11 a/o Fe is dissolved in Y_5Si_3.

According to the data by Bodak et al. (1978) seven ternary compounds were observed; the crystal structures of several of them are still unsolved (table 30). Single crystal methods were applied to characterize most of the ternary phases.

Braun et al. (1981) confirmed the $Sc_2Fe_3Si_5$-type structure for $Y_2Fe_3Si_5$. Mössbauer spectra proved the absence of a magnetic moment at the Fe site. Under hydrostatic pressure the superconducting temperature $T_c = 1.7$ K increases until a maximum of 5 K is reached at 18 kbar (Segre and Braun, 1981). The low-temperature heat capacity has been measured by Vining et al. (1983).

Phase equilibria in fig. 54 are mainly based on the work of Bodak et al. (1978) and Gladyshevskij et al. (1978) (see also table 27).

Stadnyk et al. (1979) investigated the electric resistivity of all ternary Y–Fe silicides as a function of temperature (300–1000 K).

References

Bodak, O.I., E.I. Gladyshevskij, V.I. Yarovets, V.N. Davydov and T.V. Il'Chuk, 1978, Izv. Akad. Nauk SSSR, Neorg. Mater. 14(3), 481.
Braun, H.F., 1980, Phys. Lett. 75A(5), 386.
Braun, H.F., C.U. Segre, F. Acker, M. Rosenberg, S. Dey and P. Deppe, 1981, J. Magn. Magn. Mater. 25, 117.
Gladyshevskij, E.I., O.I. Bodak, V.I. Yarovets, Yu.K. Gorelenko and R.V. Skolozdra, 1978, Ukr. Fiz. Zh. 23(11), 77.
Iandelli, A. and A. Palenzona, 1979, in: Crystal Chemistry of Intermetallic Compounds, in: Handbook on the Physics and Chemistry of Rare Earths, vol. 2, eds. K.A. Gschneidner, Jr. and L. Eyring (North-Holland, Amsterdam) p. 1.
Rivlin, V.G. and G.V. Raynor, 1981, Internat. Met. Rev. 3, 133.
Rossi, R., R. Marazza and R. Ferro, 1978, J. Less-Common Metals 58, 203.
Schlatte, G. and W. Pitsch, 1976, Z. Metallkde 67(7) 462, and 1975, Z. Metallkde 66(11), 660.
Schürmann, E. and U. Hensgen, 1980, Archiv f. Eisenhüttenwesen 51(1), 1.
Segre, C.U. and H.F. Braun, 1981, Bull. Am. Phys. Soc. 26, 343.
Skolozdra, R.V., Yu.K. Gorelenko, O.I. Bodak and V.I. Yarovets, 1980, Ukr. Fiz. Zh. 25(10), 1683.
Stadnyk, Yu.V., Yu.K. Gorelenko, R.V. Skolozdra, V.I. Yarovets and O.I. Bodak, 1979, Splavy Redk. Tugoplavk. Met. Osob. Fiz. Svoistvami (Moscow) p. 124.
Vining, C.B., R.N. Shelton, H.F. Braun and M. Pelizzone, 1983, Phys. Rev. B27(5), 2800.
Yarovets, V.I., 1978, Autoreferat Dis. Kand. Khim. (abstract of thesis, Russian) (Nauk, Lvov) 24 p.

Y–Ge–Si

Bodak et al. (1974) determined the phase equilibria of an isothermal section in the system Y–Ge–Si at 600°C by means of X-ray powder analysis of samples annealed at 600°C (no details given).

The binary system Y–Si is based on the work of Skolozdra et al. (1967), already discussed with the system Y–Ni–Si (see there). Y germanides basically agree with a recent determination of the Y–Ge phase diagram by Schmidt et al. (1972): Y_5Ge_3 (Mn_5Si_3-type), Y_5Ge_4 (Sm_5Ge_4-type), $Y_{11}Ge_{10}$ ($Ho_{11}Ge_{10}$-type), YGe (CrB-type), Y_2Ge_3 (AlB_2-derivative type), $YGe_{1.7}$ (Y_3Ge_5-type, $ThSi_2$-defect derivative type, see
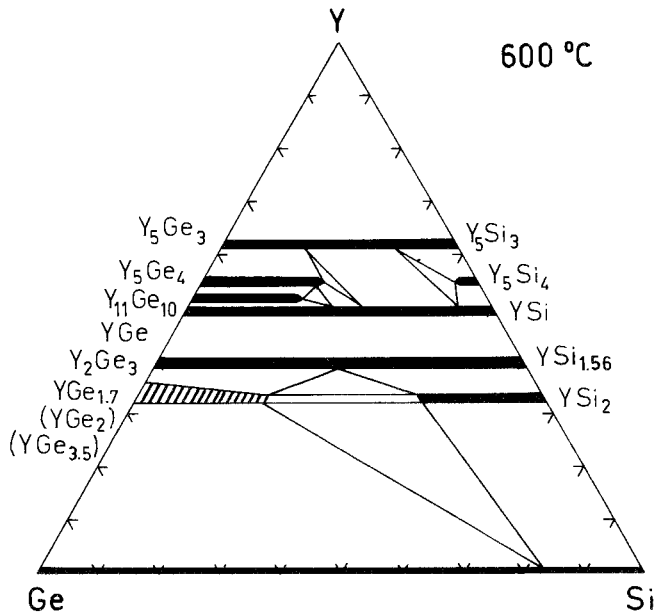
Fig. 55. Y–Ge–Si, isothermal section at 600°C.

Bruskov et al. (1983). According to Schmidt YGe_2 (orthorhombic, $ZrSi_2$-related) and $YGe_{3.5}$ (orthorhombic) are high-temperature phases existing at temperatures $T > 710°C$ (YGe_2) and $T > 760°C$ ($YGe_{3.5}$), respectively. At variance with Bodak et al. (1974) $YGe_{1.7}$ was reported by Schmidt et al. (1972) to be a line compound.

Ternary phase equilibria at 600°C are characterized by the formation of extended solid solutions; no ternary compounds were observed (see fig. 55). Complete solid solutions $Y_5Si_{3-x}Ge_x$ (Mn_5Si_3-type), $YSi_{1-x}Ge_x$ (CrB-type) and $Y_2Ge_{3-x}Si_x$ have also been reported by Muratova and Bodak (1974). The solid solution $Y_2Ge_{3-x}Si_x$ was claimed to exhibit the defect AlB_2-type (Bodak et al., 1974). In this context it is interesting to note, that Schmidt et al. (1972) confirmed the defect AlB_2-type for Y_2Ge_3 from an X-ray study of a single crystal obtained from as-cast alloys. Powder patterns of Y_2Ge_3, however, were said to contain extra lines which were indexed on the basis of an orthorhombically distorted AlB_2-type unit cell; a tentative space group was given as Pccm, $a = a_0\sqrt{3}$, $b = 2c_0$, $c = 2a_0$ (defect-type; dimorphism of Y_2Ge_3).

Despite the fact that both compounds Y_5Ge_4 and Y_5Si_4 crystallize with the Sm_5Ge_4-type, no complete solid solution was observed and a two-phase region $Y_5(Ge, Si)_3 + Y(Ge, Si)$ results from the obviously higher thermodynamic stability of the $Y_5(Ge, Si)_3$- and Y(Ge, Si)-phase solutions with respect to $Y_5(Ge, Si)_4$. At 600°C about 15 a/o Si dissolved in $Y_{11}Ge_{10}$; ~ 20 a/o were found to dissolve in $YGe_{1.7}$, and ~ 20 a/o Ge dissolved in YSi_2 with the $GdSi_2$-type (fig. 55).

References

Bodak, O.I., L.A. Muratova, I.R. Mokra, V.I. Yarovets, A.S. Sobolev and E.I. Gladyshevskij, 1974, Strukt. Faz. Fazov. Prevrash. Diagr. Sostojan. Met. Sist. (Nauka, Moscow, USSR) p. 182.

Bruskov, V.A., O.I. Bodak, V.K. Pecharskij, E.I. Gladyshevskij and L.A. Muratova, 1983, Sov. Phys. Crystallogr. **28**, 151.

Muratova, L.O. and O.I. Bodak, 1974, Tesizy Dokl. Tret. Vses. Konf. Kristallokhim. Intermet. Soedin, 2nd Ed., ed. R.M. Rykhal (Lvov. Gos. Univ., Lvov, USSR) p. 33.

Schmidt, F.A., O.D. McMasters and O.N. Carlson, 1972, J. Less-Common Metals **26**, 53.

Skolozdra, O.E., R.V. Skolozdra and E.I. Gladyshevskij, 1967, Izv. Akad. Nauk SSSR, Neorg. Mater. **3**, 813.

$Y-Ir-Si$

At least three ternary compounds exist in the $Y-Ir-Si$ ternary system.

YIrSi was characterized by means of X-ray powder diffraction by Hovestreydt et al. (1982) with the TiNiSi-type of structure [Pnma, $a = 6.789(4)$, $b = 4.188(2)$, $c = 7.462(6)$]. For sample preparation, see YPdSi; atom parameters as derived for ScPtSi.

$Y_5Ir_4Si_{10}$ crystallizes with the $Sc_5Co_4Si_{10}$-type of structure with the space group P4/mbm and lattice parameters $a = 12.599(8)$ and $c = 4.234(5)$ (Braun and Segre, 1981; X-ray powder analysis). For sample preparation, see $Sc_5Ir_4Si_{10}$. $Y_5Ir_4Si_{10}$ is superconducting below $T_c = 3.0-2.3$ K.

Two polymorphic modifications exist for the compound YIr_2Si_2 (Higashi et al., 1983). Alloys were prepared by arc melting compacted powder mixtures and subsequent annealing at 800°C for 15 d in evacuated silica tubes. The low-temperature form at 800°C was refined from X-ray powder diffraction data to be isostructural with the $ThCr_2Si_2$-type with Si in the 4e sites of I4/mmm and with $z(Si) = 0.375$, $a = 4.032$, $c = 9.87$, $R = 0.15$. The high-temperature form was refined from single crystal counter data. h-YIr_2Si_2 crystallizes with the $CaBe_2Ge_2$-type, P4/nmm, $a = 4.072(3)$, $c = 9.72(1)$; Y in 2c) $z = 0.252(1)$; Ir in 2a); Ir in 2c) $z = 0.626(7)$; Si in 2b) and Si in 2c) $z = 0.867(9)$; $R = 0.069$. h,ℓ-YIr_2Si_2 is superconducting below $T_c = 2.4-2.7$ K. Unit cell dimensions of quenched alloys were $a = 4.089$, $c = 9.72$ (Lejay et al., 1983).

References

Braun, H.F. and C.U. Segre, 1981, Ternary Supeconductors of the $Sc_5Co_4Si_{10}$-type, in Ternary Superconductors, Proc. Intern. Conf. on Ternary Superconductors, Lake Geneva, WI, USA, eds. G.K. Shenoy, B.D. Dunlop and F.Y. Fradin (North-Holland, Amsterdam) pp. 239-246.

Higashi, I., P. Lejay, B. Chevalier, J. Etourneau and P. Hagenmuller, 1984, J. Solid State Chem., to be published.

Hovestreydt, E., N. Engel, K. Klepp, B. Chabot and E. Parthé, 1982, J. Less-Common Metals **86**, 247.

Lejay, P., I. Higashi, B. Chevalier, M. Hirjak, J. Etourneau and P. Hagenmuller, 1983, C.R. Acad. Sci. (Paris), Ser. II **296**, 1583.

$Y-Li-Si$

The crystal structure of Y_2LiSi_2 has been refined by Steinberg and Schuster (1979) on the basis of X-ray single crystal counter data. Y_2LiSi_2 crystallizes with the ordered U_3Si_2-type of structure (P4/mbm, $a = 7.105$, $c = 4.144$, $\rho_{exp} = 3.755$, $\rho_x = 3.785$ kg/dm³). Atom parameters were determined as follows: Y in 4h) 0.181, 0.681, 0.5; Si in 4g) 0.383, 0.883, 0; Li in 2a); $R = 0.045$. Samples were prepared by heating elemental mixtures of nominal composition YLi_2Si in Ta crucibles for 6 h under Ar.

The obtained powdery specimens were ground and reheated for 6 h at 700°C. The excess Li was dissolved in i-C_3H_7OH plus water. Thus a light-grey and shiny crystallized powder of Y_2LiSi_2 was obtained, which proved to be stable against air and water. Dilute acids completely decompose Y_2LiSi_2 into a mixture of Si plus silicic acid. The composition has been checked by chemical analysis [atom absorption (Li), complexometric (Y); classic (Si)].

YLiSi crystallizes with the ZrNiAl-type of structure (ordered Fe_2P-type, $P\bar{6}2m$, $a = 7.023$, $c = 4.212$, $\rho_{exp} = 3.51$, $\rho_x = 3.43$ kg/dm^3). The structure was refined from single crystal X-ray counter data, $R = 0.061$. Atom parameters were determined as follows: Li in 3g) 0.229, 0, 1/2; Y in 3f) 0.575, 0, 0; Si in 1a); Si in 2d). For sample preparation and chemical analysis, see Y_2LiSi_2 (Czybulka et al., 1979).

References

Czybulka, A., G. Steinberg and H.U. Schuster, 1979, Z. Naturforsch. **34B**, 1057.
Steinberg, G. and H.U. Schuster, 1979, Z. Naturforsch. **34B**, 1237.

Y–Mg–Si

Metallurgical interactions were studied in the system Y–Mg–Si by Drits et al. (1975, 1978). Phase equilibria are dominated by the formation of the $Mg_{24}Y_5$-phase.

References

Drits, M.E., E.M. Padezhnova and T.V. Dobatkina, 1975, Redk. Metally Tsvet. Splavakh., pp. 5–11.
Drits, M.E., E.M. Padezhnova and T.V. Dobatkina, 1978, Magnievye Splavy (Mater. Vses. Sovech. Issled Razrab. Primen. Magnievykh Splavov, 1977) (Nauka, Moscow, USSR) p. 74 (as cited by CAS-91-77925s).

Y–Mn–Si

Phase equilibria in the ternary system Y–Mn–Si at 600°C have been established by Knigenko et al. (1977) from alloys prepared by arc melting and subsequent annealing in evacuated silica tubes for 280 h at 600°C (X-ray powder and metallographic analysis). Starting materials were Y 99.9%, Mn 99.56% and Si 99.99%.

The Y manganides observed are in agreement with a recent compilation by Iandelli and Palenzona (1979): YMn_2 ($MgCu_2$-type), Y_6Mn_{23} (Th_6Mn_{23}-type), YMn_{12} ($ThMn_{12}$-type). The Y silicides have been discussed in connection with the system Y–Ni–Si. Some discrepancy exists concerning the binary manganese silicides. Knigenko et al. (1977) confirmed the existence of one of the so-called Nowotny chimney ladder structures with the general formula Mn_nSi_{2n-m}; actually the existence of Mn_4Si_7 ($Mn_{11}Si_{19}$?) was reported by Knigenko et al. (1977). For a most recent review on the Mn_nSi_{2n-m} phases occurring in the narrow range of 63.5–64.5 a/o Si, see the Gmelin Handbook of Inorganic Chemistry, Vol. C8, 1982. Furthermore existence was proven for the compounds MnSi (FeSi-type), Mn_5Si_3 (Mn_5Si_3-type), Mn_3Si (W-type), the so-called N-phase ($Mn_{4.55}Si$), the μ-phase (Mn_6Si) and the R-phase ($Mn_{7.3}Si$). At variance with earlier phase diagram data (see Gmelin, C8, 1982) the D-phase Mn_5Si_2 was not observed. The location of this phase is marked in fig. 56 by a filled circle. Two ternary compounds YMn_2Si_2 and YMnSi
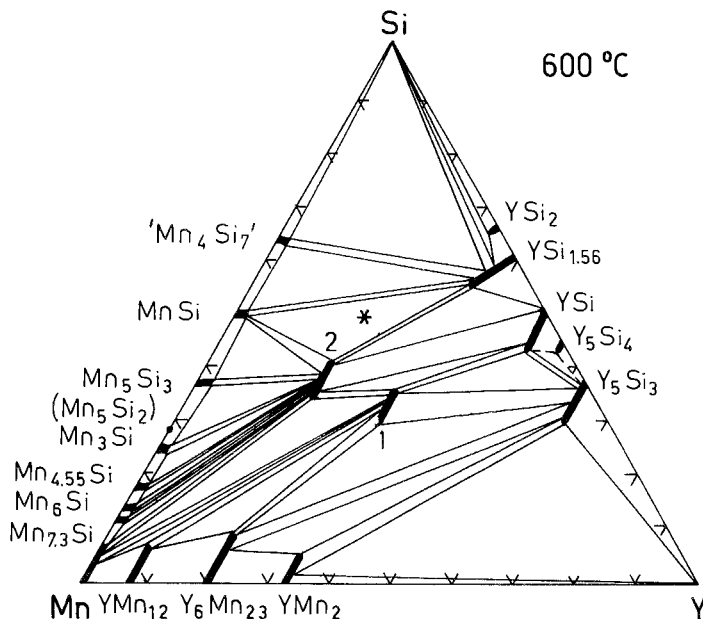
Fig. 56. Y–Mn–Si, isothermal section at 600°C. 1: YMnSi, 2: YMn$_2$Si$_2$. The location of the high-temperature phase (?) Y$_2$Mn$_3$Si$_5$ is marked by an asterisk.

were observed, with small homogeneous regions ($\sim$ 8 a/o) in the direction of Mn/Si exchange. No detailed determination of the homogeneity range by means of metallographic or lattice parameter data has been presented.

Siek and Szytula (1981) studied the crystallographic and magnetic properties of YMn$_2$Si$_2$ (ThCr$_2$Si$_2$-type, I4/mmm) by means of powder X-ray, neutron diffraction and magnetometric measurements. Samples were prepared by melting in an induction furnace, subsequently annealed in evacuated silica tubes at 800°C for 100 h and cooled to room temperature (starting materials were 99.99% pure, Si 99.999%). Complete ordering, i.e. no mixing of Mn, Si atoms, was observed in the 4d and 4e sites of I4/mmm, respectively ($z = 0.372(2)$ at 293 K and $z = 0.370(2)$ at 80 K). Lattice parameters and reliability factors were: $a = 3.939(4)$, $c = 10.501(15)$, $R_n = 0.060$, $R_m = 0.104$ at 80 K, and $a = 3.943(2)$, $c = 10.510(4)$, $R_n = 0.11$, $R_m = 0.025$ at 293 K. YMn$_2$Si$_2$ orders antiferromagnetically at $T_N = 460$ K; the paramagnetic behavior is characterized by $\mu_{eff}^{para} = 3.5$ μ_B mole^{-1} and $\theta_p = 385$ K. Values given by Knigenko et al. (1977) were $a = 3.921(1)$, $c = 10.460(1)$; Y in 2a); Mn in 4d) and Si in 4e) with $z = 0.375$. The existence of YMn$_2$Si$_2$ with the ThCr$_2$Si$_2$-type of structure (I4/mmm, $a = 3.924$, $c = 10.457$, $\rho_x = 5.3$ kg/dm^3) was also reported by Rossi et al. (1978) from X-ray powder analysis. Samples were prepared by melting in an induction furnace under Ar and subsequent annealing at 500°C for 1 week. Starting materials were 99.9% Y, and 99.99% Mn, Si. Etching was performed with dilute nitric acid or a mixture of dilute nitric and hydrofluoric acid. Narasimhan et al. (1976) gave $a = 3.923(5)$, $c = 10.446(5)$ as X-ray powder data from arc-melted alloys

annealed in Ta foil in evacuated silica tubes at 750°C for 15 d. The magnetization was observed to be proportional to the field strength; no saturation was obtained.

$Y_2Mn_3Si_5$ was reported with the $Sc_2Fe_3Si_5$-type of structure, P4/mnc, $a = 10.64(1)$, $c = 5.462(8)$ (Segre, 1981; X-ray powder methods); samples were prepared by arc melting (no annealing). The location of $Y_2Mn_3Si_5$ (high-temperature phase?) has been marked in fig. 56 by an asterisk.

Knigenko et al. (1977) reported YMnSi at 600°C with the TiNiSi-type of structure [Pnma, $a = 6.984(4)$, $b = 4.081(2)$, $c = 8.008(5)$]. Samples were prepared by arc melting under argon, and heat treated for 5 d at 700°C in evacuated silica tubes. At variance Johnson (1974/76) prepared YMnSi at 1000°C (high-temperature modification?) and claimed the PbFCl-type of structure, P4/nmm, $a = 3.984$, $c = 7.106$. Ferromagnetic ordering exists below $T_m = 275$ K. According to Johnson YMnSi can also be obtained at 1000°C (16 h, quench) by solid state reactions from Mn and YSi in sealed silica tubes, lined with Al_2O_3.

References

Iandelli, A. and A. Palenzona, 1979, Crystal Chemistry of Intermetallic Compounds, in: Handbook on the Physics and Chemistry of Rare Earths, vol. 2, eds. K.A. Gschneidner, Jr. and L. Eyring (North-Holland, Amsterdam) p. 1.
Johnson, V., 1974/76, Du Pont de Nemours Co., U.S. Patent 3 963 829.
Knigenko, L.D., I.R. Mokra and O.I. Bodak, 1977, Vestn. Lvov Univ., Ser. Khim. **19**, 68.
Narasimhan, K.S.V.L.V.U.S. Rao and W.E. Wallace, 1976, AIP Conf. Proc. **29**, 594.
Rossi, D., R. Marazza, D. Mazzone and R. Ferro, 1978, J. Less-Common Metals **59**, 79.
Segre, C.U., 1981, Thesis, Univ. of Calif., San Diego, USA.
Siek, S. and A. Szytula, 1981, Solid State Commun. **39**, 863; see also A. Szytula and I. Szott, 1981, Solid State Commun. **40**, 199.

Y–Mo–Si

In a short article Bodak et al. (1974) presented an isothermal section of the system Y–Mo–Si at 800°C (fig. 57).

Binary compounds involved in the phase equilibria at 800°C are in agreement with the literature [$MoSi_2$ ($MoSi_2$-type); Mo_5Si_3 (W_5Si_3-type), Mo_3Si (Cr_3O-type)]; for the Y–Si binary, see Y–Ni–Si. Y and Mo are practically insoluble in each other.

Mutual solid solubilities were found to be about 5 a/o Y in Mo silicides and vice versa. The solubility of Mo in the defect AlB_2-type of $YSi_{1.56}$ was of a special kind, first extending in the direction of $(Mo_xY_{1-x})Si_{1.56}$ up to ~ 7 a/o Mo, then revealing a kink where Si/Mo substitution starts, the Y concentration now remaining constant at 33 a/o Y.

The ternary compound "$YMo_{0.7}Si_{1.3}$" is likely to correspond to the recently reported $Y_2Mo_3Si_4$ with the $U_2Mo_3Si_4$-type of structure; the space group is $P2_1/b$, and the lattice parameters are $a = 6.853(2)$, $b = 6.748(1)$, $c = 6.862(1)$, $\gamma = 108.98°$. From electrical resistivity measurements in the temperature range of $T = 0.05$ K to 300 K and in magnetic fields up to 10 kOe, $Y_2Mo_3Si_4$ was found to be a type II superconductor, $T_c = 1.1$ K and $H_{c2}(0) = 4.8$ kOe (Aliev et al., 1983). $Y_2Mo_3Si_4$ was prepared by arc melting under Ar (high-temperature phase?).
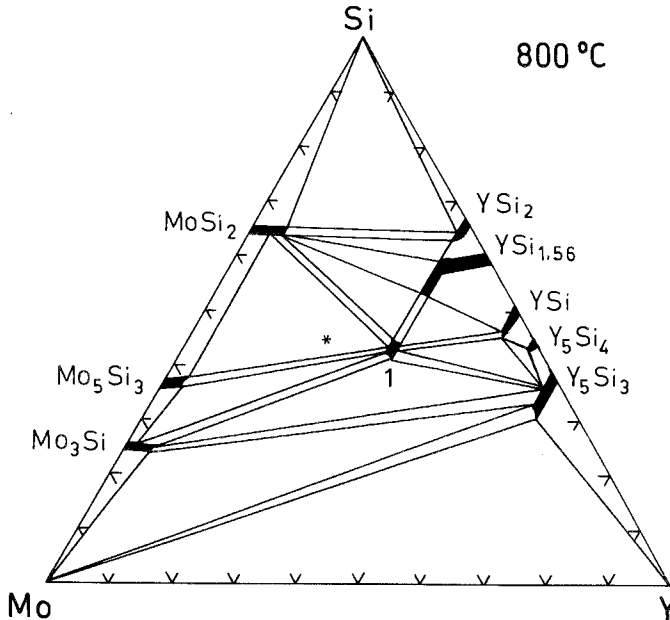
Fig. 57. Y–Mo–Si, isothermal section at 800°C. 1: "YMo$_{0.7}$Si$_{1.3}$" (this compound is likely to be identical with the recently reported Y$_2$Mo$_3$Si$_4$; the composition Y$_2$Mo$_3$Si$_4$ is denoted by an asterisk; see also text).

References

Aliev, F.G., Yu.K. Gorelenko, V.V. Moshchalkov and R.V. Skolozdra, 1983, Sov. J. Low Temp. Phys. 9(2), 101.

Bodak, O.I., L.A. Muratova, N.P. Mokra, V.I. Yarovets, A.S. Sobolev and E.I. Gladyshevskij, 1974, Strukt. Faz. Fazov. Prevrash. Diagr. Sostojan. Met. Sist. (Nauka, Moscow, USSR) p. 182.

Y–Ni–Si

Bodak et al. (1974a) characterized the phase equilibria of the system Y–Ni–Si within two partial isothermal sections at 800°C (region 0–33 a/o Y) and at 600°C (region 33–100 a/o Y), by means of X-ray and metallographic analysis of arc-melted and annealed samples. Starting materials were Si 99.99% and Ni,Y 99.5%. The binary Y–Ni compounds observed at 800°C and 600°C are in agreement with a recent compilation by Iandelli and Palenzona (1979): Y$_3$Ni (Fe$_3$C-type), YNi (FeB-type), YNi$_2$ (MgCu$_2$-type), YNi$_3$ (PuNi$_3$-type), Y$_2$Ni$_7$ (Gd$_2$Co$_7$-type), YNi$_5$ (CaCu$_5$-type) and Y$_2$Ni$_{17}$ (Th$_2$Ni$_{17}$-type). Similarly solid solubilities and compounds of the Ni–Si binary (see also Ce–Ni–Si) agree with the data in the handbooks on binary phase diagrams. Many of the earlier controversial results on the silicon-rich yttrium silicides have been explained by the work of Skolozdra et al. (1967). Thus six binary silicides exist with yttrium: Y$_5$Si$_3$ (Mn$_5$Si$_3$-type), Y$_5$Si$_4$ (Sm$_5$Ge$_4$-type), YSi (CrB-type), YSi$_{1.56}$ (or Y$_2$Si$_3$, defect AlB$_2$-type) and YSi$_2$ (GdSi$_2$-type). Solid solubility of Si in Y–Ni compounds generally was found to be very small and the solubility
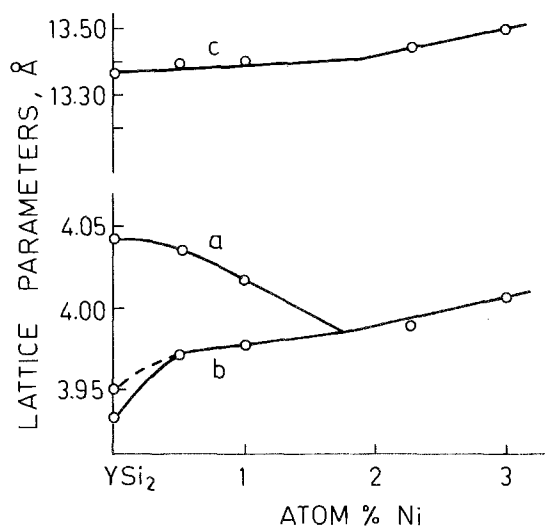
Fig. 58. Y–Ni–Si, section $Y(Si_{2-x}Ni_x)$, lattice parameters versus concentration. After Skolozdra et al. (1967).

of Si in Y–Ni compounds was less than 5 a/o Si (in direction of a Ni/Si exchange), but in a later paper by Yarovets (1978b) a much higher solubility was found at 800°C for Y_2Ni_{17} (15 a/o Si), and YNi_5 (10 a/o Si).

The Y disilicide region of the ternary system was extensively studied by Skolozdra et al. (1967) on the basis of a microstructural and X-ray powder analysis of 27 alloys prepared by arc melting and subsequent annealing in evacuated silica tubes at 600°C, 250 h and finally quenched in cold water, $YSi_{1.6}$ with nominal composition (in a/o) $Y_{38.75}Si_{61.25}$ was homogeneous with the AlB_2-type of structure (P6/mmm, $a = 3.83$, $c = 4.14$). From unit cell dimensions as well as from density measurements it was concluded that up to 11 a/o Ni are dissolved in $YSi_{1.6}$ by gradually filling the Si defects up to the composition $YNi_{0.33}Si_{1.67}$. The maximum solubility of Ni in $YSi_{1.56}$ at 800°C finally was observed at $YNi_{0.75}Si_{1.25}$; between $YNi_{0.33}Si_{1.65}$ and $YNi_{0.75}Si_{1.25}$ the solubility was concluded to be due to Si/Ni substitution; see fig. 58.

$YSi_{1.6}$ is in equilibrium with YSi_2 with the $GdSi_2$-type of structure (Imma, $a = 4.04$, $b = 3.93$, $c = 13.36$) and no polymorphic transformation of YSi_2 to a tetragonal symmetry was observed in the temperature interval from 0–600°C. However, on dissolution of Ni a continuous transformation from the orthorhombic $GdSi_2$-type to the tetragonal α-$ThSi_2$-type of structure was claimed to occur at 1.7 a/o Ni in YNi_xSi_{2-x}, see fig. 58. At 600°C the maximum solubility of Ni in the α-$GdSi_2$-type was $YNi_{0.15}Si_{1.85}$.

Twelve ternary compounds were described in the phase diagram study by Bodak et al. (1974a) (fig. 59a), but in a conference paper by Bodak et al. (1974b) 15 ternary phases have been listed for the same isothermal section at 800°C. No complete correspondence, however, is found between the two sets of compounds (see below and table 31). A more recent version of the Y–Ni–Si system was presented by Yarovets (1978b) containing 14 ternary phases.
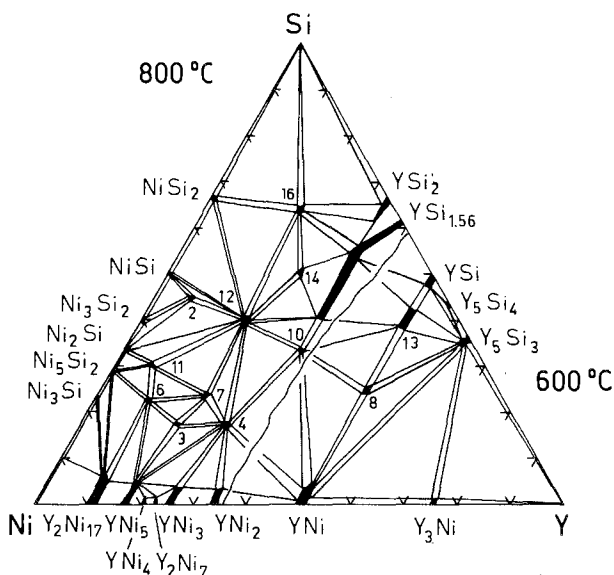
Fig. 59. Y–Ni–Si, partial isothermal sections at 800°C (0–33 a/o Y) and at 600°C (33–100 a/o Y). (a) After Bodak et al. (1974a).
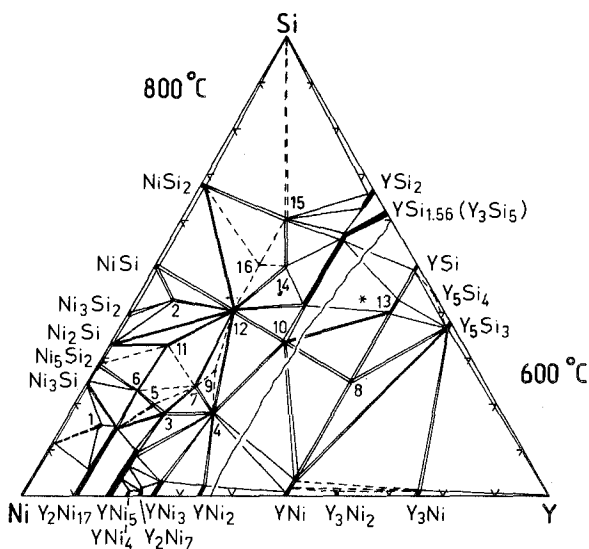
Fig. 59b. Proposed diagram. 1: $YNi_{10}Si_2$ (probably corresponds to the earlier reported YNi_9Si_3), 2: YNi_7Si_6, 3: "$YNi_{3.6}Si$", 4: $Y_3Ni_6Si_2$, 5: $YNi_{4.23}Si_{0.70}$ ("$Y_3Ni_{13}Si_4$"), 6: $YNi_{6.7}Si_{2.3}$ ["$Y(Ni, Si)_9$"], 7: $Y_6Ni_{16}Si_7$, 8: "Y_2NiSi", 9: YNi_2Si", 10: YNiSi, 11: YNi_5Si_3 (correspondence with the earlier reported "YNi_9Si_4"?), 12: YNi_2Si_2, 13: "Y_5NiSi_4", 14: $YNiSi_2$, 15: $YNiSi_3$; 16: $Y_2Ni_3Si_5$; the location of Y_3NiSi_3 is marked by an asrterisk. See also text. The new compound 15 replaces the earlier reported phases "$YNiSi_4$" and "$Y_4Ni_3Si_{11}$"; "YNi_2Si" was not listed among the phase equilibria presented by Yarovets (1978b).

TABLE 31

Formation and structural data of ternary compounds Y–Ni–Si.

Compound	Structure type Space group	Lattice parameters Density	Preparation, Characterization	Refs.	Purity
$YNi_{10}Si_2$ [*]	$YNi_{10}Si_2$ ord. $ThMn_{12}$ I4/mmm	$a = 8.207(7)$ $c = 4.677(3)$	arc(Ar), Qu 800 °C, 720 h, PXD $\mu_{eff}^{para} = 1.2\ \mu_B$, $\theta_p = 150-427$ K	GlBYGS, 77 Ya, 78a	Y 99.9 Ni 99.92 Si 99.9
$Y(Ni,Si)_{13}$ (YNi_7Si_6)	$NaZn_{13}$ Fm3c	$a = 11.05$	arc(Ar), 800 °C, PXD	BoYG, 74 b	
		$a = 11.03$		BoMMYSG, 74 a	
$YNi_{6.72}Si_{6.28}$	$Ce_2Ni_{17}Si_9$? $(NaZn_{13}$-deriv.) I4/mcm ?	$a = 11.014(8)$ $c = 11.115(8)$ [**]	arc(Ar), Qu 800 °C, 720 h PXD	Ya, 78b	Y 99.9 Ni 99.92 Si 99.9
"$YNi_{3.6}Si$" a/o 18–64–18	unknown		arc(Ar) 800 °C, PXD	BoMMYSG, 74a BoYG, 74b	
$Y_3Ni_6Si_2$	$Ce_3Ni_6Si_2$ ord. Ca_3Ag_8 Im3m	$a = 8.78$	arc(Ar) 800 °C, PXD	SkSG, 67 BoYG, 74b BoMMYSG, 74a	
$YNi_{4.23}Si_{0.70}$ a/o 15–65–20 "$Y_3Ni_{13}Si_4$"	$ErNi_{4.23}Si_{0.70}$ ($EuMg_5$ or $Sc_3Ni_{11}Si_4$) $P6_3/mmc$	$a = 8.16(2)$ $c = 8.63(2)$	arc(Ar), Qu 800 °C, 720 h PXD	Ya, 78b BoYG, 74	Y 99.9 Ni 99.92 Si 99.9
$Y(Ni,Si)_9$ a/o 10–67–23	unknown		arc, 800 °C PXD	BoMMYSG, 74a BoYG, 74b	
$Y_6Ni_{16}Si_7$	$Mg_6Cu_{16}Si_7$ Fm3m	$a = 15.22(?)$	arc(Ar) 800 °C, PXD	BoYG, 74b	
Y_2NiSi	unknown		arc(Ar) 600 °C, PXD	BoMMYSG, 74a	
"YNi_2Si" a/o 23–50–27	unknown		arc(Ar) 800 °C, PXD	BoYG, 74b	
YNiSi	TiNiSi Pnma	$a = 6.853$ $b = 4.186$ $c = 7.206$	arc(Ar) 800 °C, PXD	BoYG, 74b BoMMYSG, 74a	
		$a = 6.870(5)$ $b = 4.155(4)$ $c = 7.205(5)$	(YSi, arc)+Ni, arc(Ar), Qu 1000 °C, 1–2 weeks, PXD	HoEKCP, 82	Y 99.9 Ni 99.99 Si 5N
		$a = 6.862$ $b = 4.162$ $c = 7.197$	PXD $\mu_{eff}^{para} = 1.2\ \mu_B$, $\theta_p = -307$ K	Dw, 82 GlBYGS, 77	high purity
$Y_2Ni_3Si_5$ [O]	$U_2Co_3Si_5$ Ibam	$a = 9.5651(4)$ $b = 11.1284(6)$ $c = 5.6453(2)$ $\rho_x = 5.465$	arc(Ar), Qu 1100 °C, 24 h and 1000 °C, 170 h single crystal data	ChP, 84	Y 99.99 Ni 99.99 Si 99.999

TABLE 31 (continued)

Compound	Structure type Space group	Lattice parameters Density	Preparation, Characterization	Refs.	Purity
YNi_5Si_3 [*]	YNi_5Si_3 Pnma	$a = 18.787(5)$ $b = 3.795(2)$ $c = 6.587(3)$ $\rho_E = 6.41$, $\rho_x = 6.57$	arc(Ar), 800 °C single crystal data $R = 0.146$	AkYBYG, 76 BoYG, 74b	Y 99.99 Ni 99.92 Si 99.99
		$a = 18.81(2)$ $b = 3.796(5)$ $c = 6.608(7)$	arc(Ar), Qu 800 °C, 720 h PXD	Ya, 78b	Y 99.9 Ni 99.92 Si 99.9
YNi_2Si_2	$ThCr_2Si_2$ I4/mmm	$a = 3.956(6)$ $c = 9.535(10)$	arc(Ar), Qu 900 °C, 100 h, PXD	RiP, 69	
		$a = 3.95$ $c = 9.53$	arc, 800 °C, PXD	SkSG, 67 BoYG, 74b BoMMYSG, 74a	
Y_3NiSi_3 [*]	Ta_3B_4 Immm	$a = 3.9605(5)$ $b = 4.125(1)$ $c = 17.63(1)$ $\rho_x = 4.72$	arc(Ar), Qu(Ta) 900 °C, 2 weeks single crystal data	KIP, 82	99.99
Y_5NiSi_4 [*] a/o 50–10–40	unknown		arc(Ar), Qu 600 °C, PXD	BoMMYSG, 74a BoYG, 74b	
$YNiSi_2$	$CeNiSi_2$ Cmcm	$a = 3.94$ $b = 16.06$ $c = 3.94$	arc(Ar) 800 °C, PXD	BoMMYSG, 74a	
		$a = 3.985$ $b = 16.478$ $c = 3.980$	arc(Ar), Qu 800 °C, 720 h PXD	Ya, 78b	Y 99.9 Ni 99.92 Si 99.9
		$a = 3.942$ $b = 16.060$ $c = 3.942$	arc(Ar), 800 °C PXD	BoYG, 74b	
$Y_4Ni_3Si_{11}$ [*]	$Y_4Ni_3Si_{11}$ (?) Cmmm	$a = 4.008$ $b = 20.815$ $c = 3.95$	arc(Ar) 800 °C, PXD	BoYG, 74b	
$YNiSi_3$ [*]	$ScNiSi_3$ Amm2	$a = 4.010(1)$ $b = 3.947(1)$ $c = 20.958(3)$ $\rho_E = 4.60$, $\rho_x = 4.81$	arc(Ar), 800 °C, ME single crystal data $\mu_{eff}^{para} = 0.4\,\mu_B$, $\theta_p = 78$ K	Ya, 77 GIBYGS, 77	Y 99.9 Ni 99.8 Si 99.99

[*] See text for discussion.

[**] For a correct setting of a bct-unit cell $a = a_0/\sqrt{2} = 7.788$.

[***] Atom parameters for YNiSi were refined by Yarovets (1978b) from X-ray powder data: $R = 0.136$; Pnma, Y in 4c) 0.0030, 1/4, 0.1881; Ni in 4c) 0.1711, 1/4, 0.5518 and Si in 4c) 0.7691, 1/4, 0.6218; lattice parameters were reported as $a = 6.848(8)$, $b = 4.153(5)$ and $c = 7.197(8)$.

[o] Atom parameters were refined by Chabot and Parthé (1984) from single crystal counter data; $R = 0.074$; Y in 8j) 0.2632(2), 0.3691(2), 0; Ni in 8j) 0.1123(2), 0.1342(3), 0; Ni in 4b) 1/2, 0, 1/4; Si in 8j) 0.3475(7), 0.1074(5), 0; Si in 8g) 0, 0.2663(5), 1/4 and Si in 4a) 0, 0, 1/4.

Akselrud et al. (1976) refined the crystal structure of YNi_5Si_3 on the basis of single crystal X-ray photographs. Single crystals were observed from a composition (in a/o) $Y(11)Ni(56)Si(33)$, by arc melting under argon, followed by a heat treatment at 800°C. The following atom parameters were derived (no R value given; all atoms located in the 4c sites of Pnma, x, $1/4$, z): Y ($x = 0.1439$, $z = 0.8692$), Ni (0.2901, 0.6901), Ni (0.4917, 0.3705), Ni (0.0124, 0.6135), Ni (0.1053, 0.3621), Ni (0.3037, 0.0647), Si (0.4107, 0.0761), Si (0.2425, 0.3886) Si (0.4294, 0.6689). The existence of this compound at 800°C was also mentioned by Bodak et al. (1974b), but no comment was given on an earlier reported phase "YNi_9Si_4" (Bodak et al., 1974a), which was found to be stable at 800°C in the close vicinity of YNi_5Si_3. Thus "YNi_9Si_4" in fact might be better represented by YNi_5Si_3, despite the fact that the earlier assigned unit cell of "YNi_9Si_4" ($a = 3.77$, $b = 7.00$, $c = 16.50$) rather poorly matches the unit cell of YNi_5Si_3.

Earlier results of Bodak et al. (1974a) concerning the formation of "$YNiSi_4$" are likely to be revised with respect to more recent data about the existence of "$Y_4Ni_3Si_{11}$" (Bodak et al., 1974b; structure unsolved) and $YNiSi_3$ (Yarovets, 1977). X-ray powder patterns of the two compounds were claimed to be similar to $YNiSi_2$; very likely the new phases replace the earlier observed "$YNiSi_4$", which in fact has not been mentioned again by Bodak et al. (1974b). The crystal structure of $YNiSi_3$ ($ScNiSi_3$-type, Amm2) has been refined by Yarovets (1977) by means of X-ray single crystal photographs, $R = 0.129$. Atom parameters were determined as follows: Y in 2a) 0, 0, 0.1664(1); Y in 2a) 0, 0, 0.8275(1); Ni in 2b) 1/2, 0, 0.3935(2); Ni in 2b) 0.6141(1); Si in 2b) 0.2855; Si in 2b) 0.7240(5); Si in 2b) 0.0585(4); Si in 2b) 0.9398(7); Si in 2a) 0.5621(2); Si in 2a) 0.4457(3); [Yarovets (1978b) reported $a = 3.993(5)$, $b = 3.916$, $c = 21.143(15)$].

From arc-melted alloys annealed at 900°C for 2 weeks Klepp and Parthé (1982) were able to isolate a single crystal of Y_3NiSi_3 with the Ta_3B_4-type. The crystal structure was refined from single crystal X-ray counter data, $R = 0.088$. Atomic parameters derived were as follows (Immm): Y in 4j) 1/2, 0, 0.18307(9); Si in 4j) 1/2, 0, 0.3599(3); Y in 2a) 0, 0, 0 and a statistical distribution of 0.5 Ni + 0.5 Si in 4i) 0, 0, 0.4349(2). The location of this compound in the phase diagram of fig. 59 has been marked by an asterisk. Possibly this phase is a high-temperature phase ($T > 800°C$) or more likely corresponds to the earlier observed "Y_5NiSi_4" (Bodak et al., 1974a,b).

The crystal structure of $YNi_{10}Si_2$ ($ThMn_{12}$-type) was refined by Yarovets (1978) and atom parameters were derived as follows: Y in 2a) 0, 0, 0; Ni in 8f) 1/4, 1/4, 1/4; Ni in 8j) 0.2847(5), 1/2, 0; Ni + Si in 8i) 0.3706(7), 0, 0. This compound seems to be identical with the ternary phase reported by Bodak et al. (1974b) at the composition (in a/o) $Y(7)Ni(73)Si(20)$.

Stadnyk et al. (1979) investigated the temperature dependence of the electric resistivity (300–100 K) of the ternary compounds $YNi_{6.7}Si_{6.3}$, $Y_3Ni_6Si_2$, Y_2NiSi and "Y_5NiSi_4".

Fig. 59b is an attempt to propose the complicated phase equilibria of the Y–Ni–Si– system at 800°C and 600°C. Fig. 59b is mainly based upon the phase diagram earlier presented by Bodak et al. (1974a), including the more recent data by

Bodak et al. (1974b), Yarovets (1977, 1978b), Klepp and Parthé (1982) and Chabot and Parthé (1984). For a listing of the ternary Y–Ni silicides, see also table 31.

References

Aksel'rud, L.G., V.I. Yarovets, O.I. Bodak, Ya.P. Yarmolyuk and E.I. Gladyshevskij, 1976, Kristallografiya, **21**, 383.

Bodak, O.I., P.A. Muratova, I.P. Mokra, V.I. Yarovets, A.S. Sobolev and E.I. Gladyshevskij, 1974a, Strukt. Faz. Fazov. Prevrash. Diagr. Sosojan. Met. Sist. (Nauka, Moscow, USSR) p. 182.

Bodak, O.I., V.I. Yarovets and E.I. Gladyshevskij, 1974b, Tesizy Dokl. Tret. Vses. Konf. Kristallokhim. Intermet. Soedin, 2nd Ed., ed. R.M. Rykhal (Lvov Gos. Univ., Lvov, USSR) p. 32.

Chabot, B. and E. Parthé, 1984, J. Less-Common Metals **97**, 285.

Dwight, A.E., 1982, private communication.

Gladyshevskij, E.I., O.I. Bodak, V.I. Yarovets, Yu.K. Gorelenko and R.V. Skolozdra, 1977, Fiz. Magnit. Plenok (Irkutsk) **10**, 182.

Hovestreydt, E., N. Engel, K. Klepp, B. Chabot and E. Parthé, 1982, J. Less-Common Metals **86**, 247.

Iandelli, A. and A. Palenzona, 1979, Crystal Chemistry of Intermetallic Compounds, in: Handbook on the Physics and Chemistry of Rare Earths, vol. 2, eds. K.A. Gschneidner, Jr. and L. Eyring (North-Holland, Amsterdam) p. 1.

Klepp, K. and E. Parthé, 1982, Acta Crystallogr. **B38**, 2026.

Rieger, W. and E. Parthé, 1969, Monatsh. Chem. **100**, 444.

Skolozdra, O.E., R.V. Skolozdra and E.I. Gladyshevskij, 1967, Izv. Akad. Nauk SSSR, Neorg Mater. 3(5), 813.

Stadnyk, Yu.V., Yu.K. Gorelenko, R.V. Skolozdra, V.I. Yarovets and O.I. Bodak, 1979, Splavy Redk. Tugoplavk. Met. Osob. Fiz. Svoistvami (Moscow) p. 124.

Yarovets, V.I., 1977, Vestn. Lvov, Univ. Ser. Khim. **19**, 30.

Yarovets, V.I., 1978a, Tesizy Dokl. Tret. Vses. Konf. Kristallokhim. Intermet. Soedin, 2nd Ed., ed. R.M. Rykhal (Lvov Gos. Univ., Lvov, USSR) p. 124.

Yarovets, V.I., 1978b, Autoreferat Dis. Kand. Khim. (abstract of thesis, Russian) (Nauk, Lvov) 24 p.

$Y-Os-Si$

According to Segre (1981) $Y_2Os_3Si_5$ crystallizes with the $Sc_2Fe_3Si_5$-type of structure: $P4/mnc$, $a = 10.68(1)$, $c = 5.658(8)$; X-ray powder analysis of arc-melted samples, annealed at $1150°C$ for 7 d and additionally at $800°C$ for 14 d. The resistivity was measured in the temperature range $1 < T < 300$ K. No superconductivity was observed above $T_n = 1$ K.

From X-ray powder analysis of arc-melted alloys Hiebl et al. (1983) characterized the compound YOs_2Si_2 to be tetragonal with the $ThCr_2Si_2$-type of structure: $I4/mmm$, $a = 4.1354(4)$, $c = 9.6908(27)$. Starting materials were 99.9% pure. Furthermore, the magnetic behavior was investigated in the temperature range $1.5 < T < 1100$ K: YOs_2Si_2 is temperature independent paramagnetic with a characteristic value of $\chi_m(300$ K$) = 0.00012$ cm^3 per mole.

References

Hiebl, K., C. Horvath, P. Rogl and M.J. Sienko, 1983, Solid State Commun. **48**, 211.

Segre, C.U., 1981, Thesis, Univ. of Calif., San Diego, USA.

$Y-Pd-Si$

So for three ternary compounds have been characterized in the system Y–Pd–Si. The crystal structure of YPd_2Si has been refined by Moreau et al. (1982) from

single crystal counter data: ordered Fe_3C-type, Pnma, $a = 7.303(5)$, $b = 6.918(4)$, $c = 5.489(4)$; Y in 4c) 0.0303(9), 1/4, 0.144(2); Pd in 8d) 0.1767(5), 0.0517(5), 0.5928(8), and Si in 4c) 0.362(3), 1/4, 0.853(5); $R = 0.11$. Samples were prepared in an arc melting furnace starting from Y 99.9%, Pd 99.99% and Si 99.999%.

The crystal structure of $Y_3Pd_2Si_3$ has been refined from X-ray single crystal counter data. $Y_3Pd_2Si_3$ is isotypic with the structure type of $Hf_3Ni_2Si_3$: Cmcm, $a = 4.251(3)$, $b = 10.406(8)$, $c = 14.123(7)$. According to the reliability value obtained $R = 0.08$ the atom parameters are as follows: Pd in 8f) 0, 0.7024(7), 0.094(3); Y in 8f) 0, 0.4091(5), 0.1117(4); Y in 4c) 0, 0.1337(7), 1/4; Si in 8f) 0, 0.105(1), 0.037(1); Si in 4c) 0, 0.834(3), 1/4. Samples were prepared by arc melting (Paccard et al., 1982).

YPd_2Si_2 crystallizes with the ordered $ThCr_2Si_2$-type of structure: I4/mmm, $a = 4.122$, $c = 9.92$ (Ballestracci, 1976; powder X-ray analysis). Samples were prepared by melting in an induction furnace under argon.

References

Ballestracci, R., 1976, C.R. Acad. Sci. Paris, Ser. B **282**, 291.
Moreau, J.M., J. Leroy and D. Paccard, 1982, Acta Crystallogr. **B38**, 2446.
Paccard, D., J. Leroy and J.M. Moreau, 1982, Acta Crystallogr. **B38**, 2448.

Y–Pt–Si

YPt_2Si crystallizes with the ordered Fe_3C-type of structure, Pnma, $a = 7.282(2)$, $b = 6.912(2)$, $c = 5.461(1)$ (X-ray powder diffraction data by Moreau et al., 1982). For sample preparation, see YPd_2Si.

YPtSi is isotypic with the structure type of TiNiSi, Pnma, $a = 6.962(1)$, $b = 4.2593(6)$, $c = 7.436(2)$ (Hovestreydt et al., 1982); X-ray powder data). For sample preparation, see ScPtSi.

YPt_2Si_2 was claimed to be primitive tetragonal with lattice parameters $a = 4.156$ and $c = 9.80$ (Ballestracci and Astier, 1978) from X-ray powder diffraction of alloys melted under argon in an induction furnace. More recent X-ray powder data of arc-melted alloys confirm the primitive tetragonal crystal symmetry with an atomic arrangement similar to the $CaBe_2Ge_2$-type (Rogl, 1984): $a = 4.1601(4)$, $c = 9.8123(48)$, $CePt_2Si_2$-type.

References

Ballestracci, R. and G. Astier, 1978, C.R. Acad. Sci. Paris, Ser. B **286**, 109.
Hovestreydt, E., N. Engel, K. Klepp, B. Chabot and E. Parthé, 1982, J. Less-Common Metals **86**, 247.
Moreau, J.M., J. Leroy, D. Paccard, 1982, Acta Crystallogr. **B38**, 2446.
Rogl, P., 1984, Inorg. Chem., to be published.

Y–Re–Si

Phase equilibria have been investigated by Bodak et al. (1978) by means of X-rays analysis of samples which were arc melted and subsequently annealed in evacuated quartz capsules for 400 h at $800°C \pm 10°C$ and quenched in water. Starting materials were Y 99.6%, Re 99.8%, Si 99.99%.

The binary system Re–Si has been modified to include some more recent structural as well as phase diagram data. The composition of the rhenium silicide richest in Re was earlier tentatively claimed to be close to "Re_3Si", "Re_5Si_3" or "Re_7Si_3" (see e.g. Bodak et al., 1978). Pecharskij (1978) investigated the crystal structure of this compound by means of X-ray counter data of single crystals obtained from a slowly cooled melt ($10°C/min$) of composition $Re_{63}Si_{37}$. The structure is of a new and monoclinic type with unit cell parameters as follows: $a = 6.4511(17)$, $b = 5.3938(14)$, $c = 9.6012(20)$ and $\gamma = 94.206(3)°$. All atoms were found in the 4e sites of the space group $P2_1/b$. With respect to the atomic order derived (partial statistical distribution of Re/Si atoms) and with respect to the reliability value obtained $R = 0.139$, the crystallographic data are represented by a more precise formula of "$Re_{13}Si_7$", which is only slightly richer in Re than the earlier accepted "Re_5Si_3".

From a recent X-ray single crystal study of $ReSi_2$, Siegrist and Hulliger (1982) reported a small orthorhombic lattice distortion corresponding to a crystal symmetry Immm. $ReSi_2$ was formerly described with the tetragonal $MoSi_2$-type of structure. In a recent reinvestigation of the phase diagram of Re–Si at high temperatures ($T > 1300°C$) by Jorda et al. (1982) the compound $ReSi_2$ was found to be off-stoichiometric and its actual composition was assigned as $ReSi_{1.8}$. Pecharskij's data concerning the "$Re_{13}Si_7$" compound were confirmed, but ReSi was concluded to be a high-temperature compound decomposing by a eutectoid reaction at 1650(5) K according to $ReSi \rightleftharpoons$ "$Re_{13}Si_7$" $+ ReSi_{1.8}$.

At variance with this new result, Bodak et al. (1978) reported the existence of ReSi at 800°C. It is, however, conceivable that ReSi is retained at low temperatures due to a slow decomposition reaction. In this case the phase equilibria involving ReSi at 800°C as shown by Bodak et al. (1978) in fig. 60 merely represent metastable conditions (dashed lines in fig. 60). For the phase equilibria under stable thermodynamic conditions there will be two-phase equilibria in competition: $Re_{13}Si_7 + Y_2Re_3Si_5$ and $ReSi_2 + YRe_4Si_2$, whereby the latter, because of the higher thermodynamic stability of YRe_4Si_2, is supposed to be more likely.

YRe_2, the only binary Y–Re compound, was confirmed ($MgZn_2$-type); the binary yttrium silicides have been already discussed with the system Y–Ni–Si. Mutual solid solubilities of Y and Re silicides were found to be small: Y_5Si_3 (Mn_5Si_3-type) dissolves up to 7 a/o Re and $YSi_{1.56}$ (AlB_2-type) dissolves up to 3 a/o Re. Re was claimed to replace Y in both cases. A limited (practically no) solid solubility of Re was mentioned for Y_5Si_4 and YSi_2 (α-$ThSi_2$-type!).

Two ternary compounds $Y_2Re_3Si_5$ and YRe_4Si_2 were observed from the 800°C isothermal section in fig. 48.

The crystal structure of $Y_2Re_3Si_5$ was established from X-ray powder photographs (Bodak et al., 1978). $Y_2Re_3Si_5$ is isotypic with the structure type of $Sc_2Fe_3Si_5$ [P4/mnc, $a = 10.88(1)$, $c = 5.533(5)$]. Segre (1981) confirmed the structure type, but reported different lattice parameters from arc-melted alloys [$a = 10.93(1)$, $c = 5.513(8)$]. A small homogeneous range at higher temperatures with a Re/Si exchange is conceivable. $Y_2Re_3Si_5$ is superconducting at $T_c = 1.74$–1.58 K (Segre, 1981).

Bodak et al. (1978) refined the crystal structure of YRe_4Si_2 from single crystal X-ray photographs: YRe_4Si_2 crystallizes with the $ZrFe_4Si_2$-type of structure:
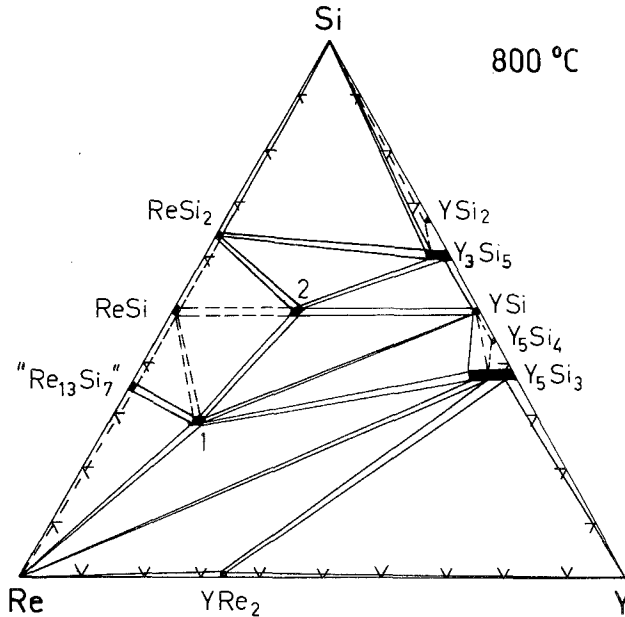
Fig. 60. Y–Re–Si, isothermal section at 800°C; the equilibria involving the compound ReSi are metastable. 1: YRe_4Si_2, 2: $Y_2Re_3Si_5$.

$P4_2/mnm$, $a = 7.321(5)$, $c = 4.113(2)$; the reliability value obtained was $R = 0.125$. Atom parameters were as follows: Y in 2b); Re in 8i) 0.099, 0.349, 0; Si in 4g) 0.211, -0.211, 0.

References
Bodak, O.I., V.K. Pecharskij and E.I. Gladyshevskij, 1978, Izv. Akad. Nauk SSSR, Neorg. Mater. **14**(2), 250.
Jorda, J.L., M. Ishikawa and J. Müller, 1982, J. Less-Common Metals **85**, 27.
Pecharskij, V.K., 1978, Tesizy Dokl. Tret. Vses. Konf. Kristallokhim. Intermet. Soedin, 2nd Ed., ed. R.M. Rykhal (Lvov Gos. Univ., Lvov, USSR) p. 103.
Segre, C.U., 1981, Thesis, Univ. of Calif., San Diego, USA.
Siegrist, T. and F. Hulliger, 1982, paper presented at the 7th Intern. Conf. on Solid Compounds of Transition Elements, Grenoble, France, Collected Abstracts, II A6, and 1983, J. Less-Common Metals **92**, 119.

Y–Rh–Si

Six ternary silicides were observed in the Y–Rh–Si system.

According to Paccard et al. (1982) $Y_3Rh_2Si_3$ crystallizes with the $Hf_3Ni_2Si_3$ type of structure [Cmcm, $a = 4.174(2)$, $b = 10.598(4)$ and $c = 13.726(5)$]. Crystal symmetry has been checked by single crystal Weissenberg photographs. Samples were prepared by arc melting from 99.9 Y, 99.99% Pd and 99.999% Si.

Chevalier et al. (1982a) refined the crystal structure of YRhSi from X-ray powder diffractometer data. YRhSi is isotypic with the structure type of TiNiSi. The

crystallographic data are as follows: Pmna, $a = 6.840(1)$, $b = 4.1847(5)$, $c = 7.399(1)$, $\rho_{exp} = 6.77(6)$, $\rho_x = 6.90$ kg/dm^3; Y in 4c) 0.0141(10), 1/4, 0.1920(10); Rh in 4c) 0.1505(10), 1/4, 0.5642(10); Si in 4c) 0.7872(20), 1/4, 0.6070(20). Samples were prepared in a triarc furnace and then annealed at 800°C for 4 d. Homogeneity was checked by microprobe analysis. YRhSi is not superconducting above $T_n = 4.2$ K. Hovestreydt et al. (1982) confirmed the structure from X-ray powder analysis of arc-melted samples, but reported slightly different unit cell dimensions: $a = 6.860(2)$, $b = 4.207(1)$, $c = 7.423(3)$.

YRh$_2$Si$_2$ is isotypic with the ordered ThCr$_2$Si$_2$-type of structure; the space group is I4/mmm, lattice parameters are $a = 4.031$ and $c = 9.92$ (Ballestracci, 1976; X-ray powder analysis of samples melted in a high-frequency furnace under argon) According to Chevalier et al. (1982b) YRh$_2$Si$_2$ is superconducting below $T_c = 3.11$ K. Felner and Nowik (1983) confirmed the ThCr$_2$Si$_2$-type from X-ray powder data of induction-melted alloys: $a = 4.031(2)$ and $c = 9.92(1)$. Magnetic data [$\theta_p = -8(3)$ K, $\mu_{eff}^{para} = 0.2$ μ_B, $T_m = 5(2)$ K] were interpreted in analogy to LaRh$_2$Si$_2$ as itinerant long-range magnetic order; $T_c = 3.1$ K.

YRh$_3$Si$_2$ is isostructural with the CeCo$_3$B$_2$-type of structure: P6/mmm, $a = 5.504(6)$, $c = 3.542(4)$ (Chevalier et al., 1981; X-ray powder analysis). For sample preparation, see LaRh$_3$Si$_2$. YRh$_3$Si$_2$ is diamagnetic with a characteristic susceptibility value of $\chi_m(300$ K$) = -107 \times 10^{-6}$ emu/mole; $T_n = 50$ mK.

Y$_2$Rh$_3$Si$_5$, crystallizing with the Sc$_2$Co$_3$Si$_5$-type of structure, exhibits a superconducting transition at 2.72(2) K as observed by Chevalier et al. (1982b), by means of resistivity and ac susceptibility measurements. At higher temperatures Y$_2$Rh$_3$Si$_5$ is paramagnetic with a characteristic susceptibility of $\chi_m(300$ K$) = 5.02 \times 10^{-4}$ emu/mole. The crystallographic data given were $a = 9.78(1)$, $b = 11.69(1)$ and $c = 5.672(5)$ (Ibam). For sample preparation, see La$_2$Rh$_3$Si$_5$.

The formation of a compound Y$_2$RhSi$_3$ structurally closely related to the AlB$_2$-type was reported by Chevalier et al. (1982b). Y$_2$RhSi$_3$ is isostructural with Er$_2$RhSi$_3$ [P62c, $a = 8.086(5)$, $c = 7.829(5)$]; samples were arc melted and annealed at 800°C for 4 d. No superconductivity was observed down to $T_n = 1.6$ K (Chevalier et al., 1984).

References

Ballestracci, R., 1976, C.R. Acad. Sci. Paris, Ser. B **282**, 291.
Chevalier, B., A. Cole, P. Lejay and J. Etourneau, 1981, Mater. Res. Bull. **16**, 1967.
Chevalier, B., A. Cole, P. Lejay, M. Vlasse, J. Etourneau and P. Hagenmuller, 1982a, Mater. Res. Bull. **17**, 251.
Chevalier, B., P. Lejay, J. Etourneau, M. Vlasse and P. Hagenmuller, 1982b, Paper presented at the 7th Intern. Conf. on Solid Compounds of Transition Elements, Grenoble, France, Collected Abstracts, II B 16; and 1982, Mater. Res. Bull. **17**, 1211; 1983, Mater. Res. Bull. **18**, 315.
Chevalier, B., P. Lejay, J. Etourneau and P. Hagenmuller, 1984, Solid State Commun. **49**(8), 753.
Felner, I. and I. Nowik, 1983, Solid State Commun. **47**, 831.
Hovestreydt, E., N. Engel, K. Klepp, B. Chabot and E. Parthé, 1982, J. Less-Common Metals **86**, 247.
Paccard, D., J. Lefoy and J.M. Moreau, 1982, Acta Crystallogr. **B38**, 2448.

Y–Ru–Si

According to X-ray powder data by Segre (1981) $Y_2Ru_3Si_5$ crystallizes with the $Sc_2Fe_3Si_5$-type of structure: P4/mnc, $a = 10.68(1)$, $c = 5.623(8)$. For sample preparation, see $Lu_2Os_3Si_5$. Resistivity was measured in the temperature range $1 \leqslant T < 300$ K; no superconductivity was observed above $T_n = 1$ K.

YRu_3Si_2 is isotypic with the crystal structure of $LaRu_3Si_2$, tentative space group P6$_3$/m, $a = 5.543(1)$ and $c = 7.152(2)$ (Vandenberg and Barz, 1980; Barz, 1980). Arc melted mixtures of nominal composition YRu_3Si_2 were two-phase, containing a phase mixture $YRu_3Si_2 + YRu_2Si_2$. Annealing at 1000°C was not successful in increasing the amount of YRu_3Si_2. Alloys richer in Ru contained free Ru indicating the following two-phase equilibria: $Ru + YRu_3Si_2$ and $YRu_2Si_2 + YRu_3Si_2$. The new phase is superconducting with a transition temperature of $T_c = 3.51–3.48$ K.

Hiebl et al. (1983) investigated the structural and magnetic behavior of YRu_2Si_2 crystallizing with the $ThCr_2Si_2$-type of structure: I4/mmm, $a = 4.1557(6)$, $c = 9.5371(34)$ (X-ray powder analysis). For sample preparation, see YOs_2Si_2. From magnetic susceptibility measurements (1.5–1100 K) YRu_2Si_2 was temperature-independent paramagnetic with a characteristic value of χ_m (300 K) $= 0.00020$ cm^3 per mole.

References

Barz, H., 1980, Mater. Res. Bull. **15**, 1489.
Hiebl, K., C. Horvath, P. Rogl and M.J. Sienko, 1983, J. Magn. Magn. Mater. **37**, 287.
Segre, C.U., 1981, Thesis, Univ. of Calif., San Diego, USA.
Vandenberg, J.M. and H. Barz, 1980, Mater. Res. Bull. **15**, 1493.

Yb–Ag–Si

From X-ray powder analysis of a three-phase sample, Rossi et al. (1979) reported $YbAg_2Si_2$ to crystallize with the $ThCr_2Si_2$-type of structure. The crystallographic data were: space group I4/mmm, $a = 4.14$ and $c = 10.89$, $\rho_x = 7.91$ kg/dm^3. For sample preparation, see $CePd_2Si_2$. From the large unit cell dimensions as compared to the homologous members of the series RAg_2Si_2, Yb seems to be divalent.

Reference

Rossi, D., R. Marazza and R. Ferro, 1979, J. Less-Common Metals **66**, P17.

Yb–Al–Si

No ternary phase diagram exists for the system Yb–Al–Si, but the formation of two compounds has been reported: Yb_2Al_2Si and $YbAl_2Si_2$.

Yanson (1975) prepared the compound Yb_2Al_2Si, which from X-ray powder analysis was found to be isostructural with Dy_2Al_2Si—an ordered variant of the U_3Si_2-type of structure (space group P4/mbm). The recorded lattice parameters with $a = 7.145(4)$ and $c = 4.424(3)$ are considerable larger than those of the isostructural R members R_2Al_2Si ($R =$ Ho,Er,Tm) and suggest the presence of Yb^{2+} states.

YbAl$_2$Si$_2$ crystallizes with the La$_2$O$_2$S-type structure: P3m1 (Muravyova et al., 1972; X-ray powder diffraction data). For sample preparation and atom parameters, see Sm–Al–Si. The obtained lattice parameters with $a = 4.14$ and $c = 6.95$ suggest the presence of divalent Yb.

References

Muravyova, A.A., O.S. Zarechnyuk and E.I. Gladyshevskij, 1972, Visn. L'viv. Univ., Ser. Khim. **13**, 14.
Yanson, T.I., 1975, Autoreferat Dis. Kand. Khim. (abstract of thesis, Russian) (Nauk, Lvov) 22 p.

Yb–Au–Si

From an X-ray powder analysis of a nearly single-phase alloy Rossi et al. (1979) observed the compound YbAu$_2$Si$_2$ crystallizing with the ThCr$_2$Si$_2$-type of structure (I4/mmm, $a = 4.287$, $c = 10.050$, $\rho_x = 11.13$ kg/dm^3). For sample preparation, see CePd$_2$Si$_2$.

Reference

Rossi, D., R. Marazza and R. Ferro, 1979, J. Less-Common Metals **66**, P17.

Yb–Co–Si

No ternary phase diagram is available for the Yb–Co–Si system, but the existence of two ternary compounds was reported.

YbCo$_2$Si$_2$ crystallizes with the ordered ThCr$_2$Si$_2$-type of structure: I4/mmm, $a = 3.847$, $c = 9.679$ and $\rho_x = 8.04$ kg/dm^3 (X-ray powder diffraction data by Rossi et al., 1978). For sample preparation and etching conditions, see YCo$_2$Si$_2$. Yarovets (1978) confirmed the structure type from X-ray powder data and measured $a = 3.862$ and $c = 9.671$. Magnetic susceptibilities were measured within the temperature range of 300–1200 K, $\mu_{eff}^{para} = 3.0 \mu_B$, $\theta_p = -55$ K (Yarovets· et al., 1977).

Yb$_3$Co$_2$Si$_7$ crystallizes with the Ho$_3$Co$_2$Si$_7$-type: Amm2, $a = 3.841$, $b = 24.410$ and $c = 3.888$ (X-ray powder data by Yarovets, 1978). For sample preparation, see Ho$_3$Co$_2$Si$_7$. Magnetic susceptibilities have been measured in the temperature range of 348–1182 K, $\mu_{eff}^{para} = 4.13(8) \mu_B$, $\theta_p = -6$ K (Yarovets, 1978).

References

Rossi, D., R. Marazza and R. Ferro, 1978, J. Less-Common Metals **58**, 203.
Yarovets, V.I., Yu.K. Gorelenko and R.V. Skolozdra, 1977, Tesizy Dokl. IX. Ukr. Vses. Konf. Neorg. Khim., Lvov, p. 188.
Yarovets, V.I., 1978, Autoreferat Dis. Kand. Khim. (abstract of thesis, Russian) (Nauk, Lvov) 24 p.

Yb–Cu–Si

Three ternary compounds have been reported in the Yb–Cu–Si system.

Yb$_3$Cu$_4$Si$_4$ has the Gd$_3$Cu$_4$Ge$_4$-type of structure with the space group Immm and lattice parameters as follows: $a = 13.49$, $b = 6.49$ and $c = 4.07$ (X-ray powder diffraction by Hanel and Nowotny, 1970). For sample preparation, see Sc$_3$Cu$_4$Si$_4$.

According to an X-ray powder analysis by Rieger and Parthé (1969) $YbCu_2Si_2$ crystallizes with the $ThCr_2Si_2$-type of structure [I4/mmm, $a = 3.926(6)$, $c = 9.987(10)$]. For sample preparation, see YCu_2Si_2. From X-ray absorption spectroscopy measurements (Hatwar et al., 1980) on an arc-melted $YbCu_2Si_2$ alloy at 77 and 300 K two absorption peaks were observed, corresponding to two different valence states of Yb. The average valency of Yb is nearly temperature independent (Sales and Wohlleben, 1975; Sampathkumaran et al., 1980). Physical properties have been reviewed by Sales and Viswanathan (1976).

Iandelli (1983) reported the existence of a compound YbCuSi with the ordered Ni_2In-type of structure. The crystal data as derived from X-ray powder analysis were: $P6_3/mmc$, $a = 4.130(2)$, $c = 7.150(5)$; Yb in 2a); Cu in 2c) and Si in 2d). From susceptibility measurements (80 to 300 K) Yb was concluded to be tripositive. Samples were prepared in Ta crucibles welded shut under argon, heated in an induction furnace and finally annealed at 740–750°C for 8–12 d. Starting materials were 99.8% Yb, and 99.999% Cu, 99.9999% Si.

References

Hanel, G. and H. Nowotny, 1970, Monatsh. Chem. **101**, 463.
Hatwar, T.K., R.M. Nayak, B.D. Padalia and M.N. Ghatikar, 1980, Solid State Commun. **34**, 617, and 1983, J. Phys. **C16**, 1537.
Iandelli, A., 1983, J. Less-common Metals **90**, 121.
Rieger, W. and E. Parthé, 1969, Monatsh. Chem. **100**, 444.
Sales, B.C. and R. Viswanathan, 1976, J. Low Temp. Phys. **23**(3,4), 449.
Sales, B.C. and D.K. Wohlleben, 1975, Phys. Rev. Lett. **35**, 1240.
Sampathkumaran, E.V., L.C. Gupta and R. Vijayaraghavan, 1980, J. Magn. Magn. Mater. **15–18**, 977; see also 1980, Phys. Rev. Lett. **43**(6), 1189; 1979, J. Phys. **C12**, 4323; 1981, in: Valence Fluctuations in Solids, eds. L.M. Falicov, W. Hanke and M.B. Maple (North-Holland, Amsterdam) p. 241.

Yb–Fe–Si

At least four ternary compounds exist in the Yb–Fe–Si system.

According to X-ray powder diffraction data by Bodak et al. (1970) YbFeSi is tetragonal with the PbFCl-type of structure [P4/nmm, $a = 3.972(3)$, $c = 6.784(5)$]. For sample preparation, see CeFeSi.

$YbFe_2Si_2$ crystallizes with the ordered $ThCr_2Si_2$-type structure: I4/mmm, $a = 3.878$, $c = 9.881$ and $\rho_x = 7.62$ kg/dm^3 (Rossi et al., 1978; X-ray powder diffraction). For sample preparation and etching conditions, see YCo_2Si_2. Yarovets (1978) confirmed the existence of $YbFe_2Si_2$, but no crystallographic data were presented. Magnetic susceptibilities were recorded in the temperature range 293–1151 K, and effective moments were extrapolated as follows: $\mu_{eff} = 4.92$ μ_B, $\theta_p = 129$ K for the region 829–1151 K and $\mu_{eff} = 6.49$ μ_B, $\theta_p = -393$ K for the region 293–829 K. ^{57}Fe and ^{170}Yb Mössbauer data at 300, 4.2 and 1.4 K proved the ordered atomic arrangement with a single nonmagnetic Fe site and confirmed a trivalent state for Yb (Noakes et al., 1983). No magnetic ordering was observed from ac susceptibility measurements as low as 1.4 K.

$Yb_2Fe_4Si_9$ is isostructural with the structure type of $Y_2Fe_4Si_9$ [$P6_3/mmc$, $a = 3.916(5)$, $c = 15.39(1)$, $\rho_{exn} = 5.43$, $\rho_x = 5.6$ kg/dm^3]. Atom parameters were refined

by Gladyshevskij et al. (1978) from X-ray single crystal data: Yb in 2c) $1/3$, $2/3$, $1/4$; Fe in 4f) $1/3$, $2/3$, 0.8917(7); Si in 4f) $z = 0.0444(9)$; Si in 4e) 0, 0, 0.8649(5) and 1 Si atom in 2a) 0, 0, 0, $R = 0.145$. For sample preparation, see $Y_2Fe_4Si_9$. Magnetic susceptibilities were measured within the temperature range of 300–1200 K and indicate a partial trivalency of Yb: $\mu_{eff}^{para} = 3.59$ μ_B mole^{-1} and $\theta_p = -65$ K.

$Yb_2Fe_3Si_5$ crystallizes with the $Sc_2Fe_3Si_5$-type of structure [P4/mnc, $a = 10.36(1)$ and $c = 5.385(8)$]; Braun (1980) by means of X-ray powder diffraction. Arc melted samples were said to contain ~ 20 vol% of impurity phases. No homogeneous sample could be obtained from sintered mixtures of Yb and Fe_3Si_5 at 900°C in an evacuated silica tube. For low temperature heat capacity data, see Vining and Shelton (1983); antiferromagnetic ordering was reported at $T_N = 1.70$ K.

References

Bodak, O.I., E.I. Gladyshevskij and P.I. Kripjakevich, 1970, Zh. Strukt. Khim. **11**(2), 305.

Braun, H.F., 1980, Phys. Lett. **75A**(5), 386; see also Segre, C.U., 1981, Thesis, Univ. of Calif., San Diego, U.S.A.

Gladyshevskij, E.I., O.I. Bodak, V.I. Yarovets, Yu.K. Gorelenko and R.V. Skolozdra, 1978, Ukr. Fiz. Zh. **23**(11), 77.

Rossi, R., R. Marazza and R. Ferro, 1978, J. Less-Common Metals **58**, 203.

Vining C.B. and R.N. Shelton, 1983, Phys. Rev. B. **28**(5), 2732.

Yarovets, V.I., 1978, Autoreferat Dis. Kand. Khim. (abstract of thesis, Russian) (Nauk, Lvov) 24 p.

Yb–Ge–Si   Noakes, D.R., A.M. Umarji and G.K. Shenoy, 1983, J. Magn. Magn. Mater. **39**, 309–316.

Mayer and Fromerman (1968) investigated the phase equilibria within the concentration section $YbGe_{2-x}Si_x$ on the basis of X-ray powder data. Samples were
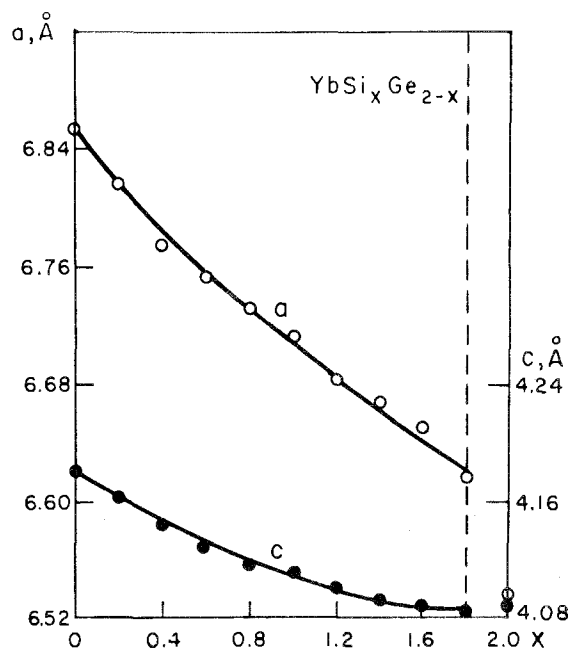
Fig. 61. Yb–Ge–Si, section $YbGe_{2-x}Si_x$, lattice parameters versus concentration. After Mayer and Fromerman (1968).

prepared by direct heating of compacted mixtures of 99.9% purity in a Ta boat under Ar (induction furnace, ~ 1500°C); the melt was cooled and reheated for homogenization.

Practically no Ge is soluble in $YbSi_2$ with the AlB_2-type (P6/mmm), whereas the extended solid solution $YbGe_{2-x}Si_x$ for $x < 1.8$ crystallizes with the Th_3Pt_5-type of structure (P$\bar{6}$2m). Lattice parameters versus x are presented in fig. 61.

Reference
Mayer, I. and Y. Fromerman, 1968, J. Less-Common Metals **15**, 355.

Yb–Mn–Si

Rossi et al. (1978) reported the existence of a compound $YbMn_2Si_2$ with the $ThCr_2Si_2$-type of structure (I4/mmm, $a = 3.877$, $c = 10.391$, $\rho_x = 7.21$ kg/dm³). For

TABLE 32
Formation and structural data of ternary compounds Yb–Ni–Si.

Compound	Structure type Space group	Lattice parameters Density	Preparation, Characterization	Refs.	Purity
$YbNi_{10}Si_2$	$YNi_{10}Si_2$ ord. $ThMn_{12}$ I4/mmm	$a = 8.161$ $c = 4.693$	arc(Ar), Qu 800 °C, 720 h PXD	Ya, 78a	Yb 99.82 Ni 99.98 Si 99.99
$Yb_3Ni_6Si_2$	$Ce_3Ni_6Si_2$ ord. Ca_3Ag_8 Im3m	$a = 8.662(2)$	arc, Qu(Ni) 800 °C, 2 weeks PXD	GlKB, 66	Yb 99.96 Ni 99.99 Si 99.99
$YbNi_5Si_3$	YNi_5Si_3 Pnma	$a = 18.590$ $b = 3.780$ $c = 6.597$	arc(Ar) 800 °C PXD	AkYBYG, 76	Ni 99.92 Si 99.99
		$a = 18.98$ $b = 3.780$ $c = 6.710$	arc(Ar), Qu 800 °C, 720 h PXD	Ya, 78b	Yb 99.82 Ni 99.98 Si 99.99
$YbNi_2Si_2$	$ThCr_2Si_2$ I4/mmm	$a = 3.900(10)$ $c = 9.513(10)$	arc(Ar) PXD	BoGK, 66	Yb 99.9 Ni 99.8 Si 99.9
$YbNiSi_2$ [*]	$CeNiSi_2$ Cmcm	$a = 3.862$ $b = 16.070$ $c = 3.808$	arc(Ar) PXD	BoG, 69	Yb 99.9 Ni 99.8 Si 99.9
$YbNiSi_3$	$YNiSi_3$ Amm2	$a = 3.969$ $b = 3.889$ $c = 21.035$	arc, Qu (10^{-2} Torr Ar) 800 °C, 720 h $\mu_{eff}^{para} = 3.9$, $\theta_p = -117$ K	GoBGY, 77 Ya, 78b	Yb 99.82 Ni 99.98 Si 99.99
$YbNi_{6.72}Si_{6.28}$	$Ce_2Ni_{17}Si_9$? (NaZn$_{13}$-deriv.) I4/mcm ?	$a = 10.972$ $c = 11.127$ [**]	arc(Ar), Qu 800 °C, 720 h PXD	Ya, 78b	Yb 99.82 Ni 99.98 Si 99.99

[*] Could not be obtained in homogeneous form.
[**] For a correct setting of a bct-unit cell, $a = a_0/\sqrt{2} = 7.758$.

sample preparation, see $LaMn_2Si_2$. From unit cell dimensions (X-ray powder analysis) Yb was concluded to be trivalent. In agreement with this, Szytula and Szott (1981) observed a paramagnetic moment $\mu_{eff}^{para} = 4.6$ μ_B indicating trivalency of Yb; antiferromagnetic ordering occurs at $T_N = 513$ K.

References

Rossi, D., R. Marazza, D. Mazzone and R. Ferro, 1978, J. Less-Common Metals **59**, 79.
Szytula, A. and I. Szott, 1981, Solid State Commun. **40**, 199.

Yb–Ni–Si

No ternary phase diagram exists, but seven ternary compounds have been characterized in the Yb–Ni–Si system (see table 32).

References

Aksel'rud, L.G., V.I. Yarovets, O.I. Bodak, Ya.P. Yarmolyuk and E.I. Gladyshevskij, 1976, Sov. Phys. Crystallogr. **21**(2), 210.
Bodak, O.I. and E.I. Gladyshevskij, 1969, Kristallografiya **14**(6), 990.
Bodak, O.I., E.I. Gladyshevskij and P.I. Kripyakevich, 1966, Izv. Akad. Nauk SSSR, Neorg. Mater. **2**(12), 2151.
Gladyshevskij, E.I., P.I. Kripyakevich and O.I. Bodak, 1966, Acta Crystallogr. **A21**, 80, and Z. Anorg. Allg. Chem. **344**, 95.
Gorelenko, Yu.K., O.I. Bodak, E.I. Gladyshevskij and V.I. Yarovets, 1977, Ukr. Fiz. Zh. **22**(6), 1020.
Yarovets, V.I., 1978a, Tesizy Dokl. Tret. Vses. Konf. Kristallokhim. Intermet. Soedin, 2nd Ed., ed. R.M. Rykhal (Lvov Gos. Univ., Lvov, USSR) p. 124.
Yarovets, V.I., 1978b, Autoreferat Dis. Kand. Khim. (abstract of thesis, Russian) (Nauk, Lvov) 24 p.

Yb–Os–Si

From X-ray powder diffraction $YbOs_2Si_2$ was observed to crystallize with the $ThCr_2Si_2$-type of structure and space group I4/mmm. Samples were prepared by sintering powder compacts of prereacted $YbSi_2$ with Os at 1000°C for 1 week. For heat treatment the pellets were wrapped in Ta foil and sealed in evacuated Si tubes. The lattice parameters as derived from X-ray powder photographs were $a = 4.1153(10)$ and $c = 9.6161(99)$. The samples were not single-phase but contained small amounts of secondary phases; magnetic measurements (1.5 to 1100 K) indicated trivalency of Yb (Hiebl et al., 1983).

Reference

Hiebl, K., C. Horvath, P. Rogl and M.J. Sienko, 1983, Solid State Commun. **48**, 211.

Yb–Pd–Si

According to X-ray powder diffraction data by Rossi et al. (1979) $YbPd_2Si_2$ is tetragonal with the $ThCr_2Si_2$-type: I4/mmm, $a = 4.088$, $c = 9.874$ and $\rho_x = 8.89$ kg/dm^3. For sample preparation, see $GdPd_2Si_2$.

Reference
Rossi, D., R. Marazza and R. Ferro, 1979, J. Less-Common Metals **66**, P17.

Yb–Pt–Si

$YbPt_2Si_2$ was reported to be body-centered tetragonal with the $ThCr_2Si_2$-type ($a = 4.097$, $c = 9.962$, $\rho_x = 12.30$ kg/dm^3). Pt and Si atoms were said to be randomly distributed on the 4d and 4e sites of I4/mmm (Rossi et al., 1979; X-ray powder analysis). For sample preparation, see $CePd_2Si_2$. At variance with this more recent powder data by Rogl (1984) reveal a primitive tetragonal lattice with an ordered atomic distribution similar to the $CaBe_2Ge_2$-type: $a = 4.1221(5)$, $c = 9.9091(58)$, $CePt_2Si_2$-type. Samples were arc melted.

References
Rogl, P., 1984, Inorg. Chem., to be published.
Rossi, D., R. Marazza and R. Ferro, 1979, J. Less-Common Metals **66**, 17.

Yb–Rh–Si

By means of an X-ray powder analysis of a heterogeneous sample Rossi et al. (1979) characterized the compound $YbRh_2Si_2$ with the $ThCr_2Si_2$-type of structure (I4/mmm, $a = 4.010$, $c = 9.841$, $\rho_x = 9.12$ kg/dm^3). The alloys were prepared by melting in an induction furnace under argon followed by heat treatment for 1 week at 500°C. Purities of starting materials were Yb 99.9% and Rh, Si 99.99%.

Reference
Rossi, D., R. Marazza and R. Ferro, 1979, J. Less-Common Metals **66**, 17.

Yb–Ru–Si

Barz (1980) reported the existence of a ternary compound $YbRu_3Si_2$ with the $LaRu_3Si_2$-type of structure. No X-ray data have been presented. For sample preparation and melting behavior (phase equilibria), see $LaRu_3Si_2$.

$YbRu_2Si_2$ is isotypic with the crystal structure of $ThCr_2Si_2$. According to X-ray powder data of induction-melted alloys the space group is I4/mmm with lattice parameters $a = 4.139$ and $c = 9.44$ (Ballestracci et al., 1978). Hiebl et al. (1983) confirmed the structure type and measured $a = 4.1361(8)$ and $c = 9.4695(33)$. The alloys were prepared by sintering powder mixtures of prereacted $YbSi_2$ and Ru in quartz tubes. After a short first reaction at 900°C, 24 h the samples were crushed and reground, recompacted, wrapped in Ta foil and subjected to a final heat treatment at 900°C for 120 h. X-ray powder analysis revealed a slightly inhomogeneous product. The reciprocal magnetic susceptibility ($1.5 < T < 1100$ K) indicates trivalency of Yb ($\mu_{\mathrm{eff}}^{\mathrm{para}} = 3.54$ μ_B, $\theta_p = -18$ K).

References
Ballestracci, R. and G. Astier, 1978, Acad. Sci. Paris, Ser. B **286**, 109.
Barz, H., 1980, Mater. Res. Bull. **15**, 1489.
Hiebl, K., C. Horvath, P. Rogl and M.J. Sienko, 1983, J. Magn. Magn. Mater. **37**, 287.

3. Multicomponent systems containing rare earth metals and silicon

Ce–Cu–Mn–Si

Siek and Szytula (1979) studied the magnetic properties along the concentration

section $Ce(Mn_{1-x}Cu_x)_2Si_2$ in the temperature range $100 < T < 600$ K at 11 kOe, and up to 50 kOe using a vibrating sample magnetometer (4.2–300 K). For sample preparation, see Ce–Mn–Ge–Si. A complete solid solution crystallizing with the $ThCr_2Si_2$-type of structure (space group I4/mmm) was observed at 800°C from samples cooled to room temperature. The variation of lattice parameters versus x is shown in fig. 62. Alloys with $x < 0.5$ order antiferromagnetically. The temperature dependence of the magnetization is similar to $LaCo_2Ni_3$ (same interpretation). A metamagnetic transition was observed at 4.2 K and with a critical field of 6.0 kOe.

Reference

Siek, S. and A. Szytula, 1979, J. Physique Coll. C5, 162.

Ce–Fe–Mn–Si

Siek and Szytula (1979) studied the magnetic properties along the concentration section $Ce(Fe_xMn_{1-x})_2Si_2$. For sample preparation and magnetic experimental conditions, see Ce–Mn–Ge–Si. A complete solid solution crystallizing with the $ThCr_2Si_2$-type of structure was reported at 800°C from samples cooled to room temperature. The variation of the lattice parameters versus x is shown in fig. 62. Alloys with $x < 0.5$ order antiferromagnetically; their Néel temperatures linearly decrease with the Fe content. Furthermore, a metamagnetic transition was observed at 4.2 K and with a critical field of 12.5 kOe.
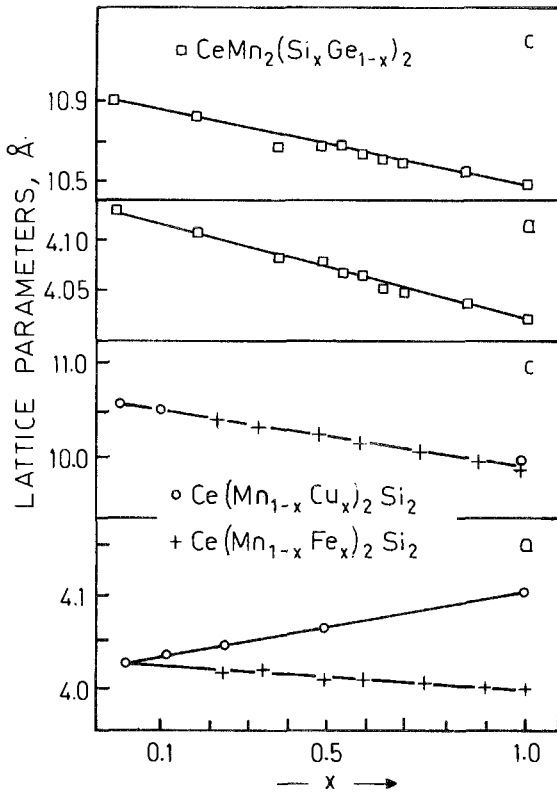
Fig. 62. Variation of lattice parameters versus concentration x along the sections $CeMn_2(Si_xGe_{1-x})_2$, $Ce(Mn_{1-x}Cu_x)_2Si_2$ and $Ce(Mn_{1-x}Fe_x)_2Si_2$. After Siek and Szytula (1979).

Reference
Siek, S. and A. Szytula, 1979, J. Physique Coll. **C5**, 162.

Ce–Ge–Mn–Si

Siek and Szytula (1979) investigated structural and magnetic properties of the
section $CeMn_2(Si_xGe_{1-x})_2$ at 11 kOe and in the temperature range $100 < T < 600$
K. A complete solid solubility was observed by means of X-ray powder analysis of
arc-melted and annealed alloy specimens (800°C, 3 d). Starting materials were
Ce-3N, Mn, Ge-4N, Si-5N.

All samples crystallized with the $ThCr_2Si_2$-type of structure, with Ce in 2a), Mn
in 4d) and a statistical occupation of Si/Ge in the 4e sites of the space group
I4/mmm. Lattice parameters versus x are shown in fig. 62.

The magnetic phase diagram is presented in fig. 63. Alloys are ferromagnetic
($T_m \sim 320$ K) for $x < 0.45$; however, for $0.45 < x \leqslant 0.7$ samples were found to
undergo an antiferromagnetic-to-ferromagnetic transition through a transition state
indicated by the dashed area in fig. 63. For $x \leqslant 0.75$ antiferromagnetic ordering
occurs. The practically linear temperature dependence of the critical field is char-
acteristic for the first-order phase transition. Experiments in strong pulsed magnetic
fields (up to 200 kOe) showed that the antiferromagnetic-to-ferromagnetic transition
—occurring in weak fields at ~ 230 K—can be induced at lower temperatures by
applying a sufficiently strong magnetic field.

Reference
Siek, S. and A. Szytula, 1979, J. Physique Coll. **C5**, 162.

Ce–La–Cu–Si

Aliev et al. (1983) studied the electric and magnetic properties of solid solutions
$Ce_xLa_{1-x}Cu_2Si_2$ for $0 \leqslant x \leqslant 1$ and $0.04 \leqslant T \leqslant 300$ K in magnetic fields up to 40
kOe and under pressures $\leqslant 140$ kbar. A continuous transition was observed from a
Kondo impurity system ($x \leqslant 1$) to a Kondo lattice ($x \sim 1$, $p = 0$, Ce $\approx 3+$).

Reference
Aliev, F.G., N.B. Brandt, V.V. Moshchalkov and S.M. Chudinov, 1983, Solid State Commun. **47**(9), 693.
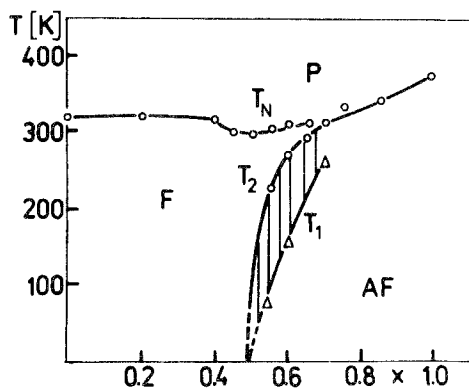
Fig. 63. Ce–Ge–Mn–Si, section
$CeMn_2(Si_xGe_{1-x})_2$, magnetic phase diagram.
After Siek and Szytula (1979).

Ce–Ru–Os–Si

Hiebl et al. (1984) studied the structural and magnetochemical behavior within the concentration section $Ce(Ru_{1-x}Os_x)_2Si_2$. A complete solid solution with the $ThCr_2Si_2$-type of structure and symmetry I4/mmm is found to exist. Lattice parameters from X-ray powder data of as-cast alloys were as listed below, table 33.

Samples were investigated in a cast (arc-melted) as well as in annealed condition, a) 1000°C, 65 h in high vacuum, radiation quenched, b) 500°C, 750 h in evacuated silica tubes. Starting materials were 99.9% pure. Congruent melting behavior was confirmed by metallographic analysis.

Reference
Hiebl, K., C. Horvath, P. Rogl and M.J. Sienko, 1984, Z. Phys. B, in press.

Dy–Ho–Fe–Si

Skolozdra et al. (1980) investigated the temperature dependence of the magnetic susceptibility within the concentration section $Ho_xDy_{1-x}Fe_2Si_2$ and in the temperature range of 80 to 1050 K. Results obtained by X-ray powder diffraction (I4/mmm, $ThCr_2Si_2$-type) and magnetic data are presented in table 34.

Reference
Skolozdra, R.V., Yu.K. Gorelenko, O.I. Bodak and V.I. Yarovets, 1980, Ukr. Fiz. Zh. **25**(10), 1683.

Dy–Lu–Fe–Si

A low-temperature phase diagram (fig. 64) has been investigated by Segre (1981) along the concentration section $(Dy_xLu_{1-x})_2Fe_3Si_5$. A complete solid solution with

TABLE 33

Lattice parameters versus concentration of alloys $Ce(Ru_{1-x}Os_x)_2Si_2$ ($ThCr_2Si_2$-type, as-cast condition).

$Ce(Ru_{1-x}Os_x)_2Si_2$ x_{Os} in mole%	Lattice Parameters	
	a (Å)	c (Å)
$CeRu_2Si_2$	4.1968(8)	9.7972(48)
12.5	4.1936(6)	9.7985(68)
18.75	4.1928(7)	9.8004(32)
25.0	4.1903(7)	9.7998(30)
31.25	4.1910(5)	9.8037(46)
35.0	4.1857(8)	9.8021(29)
43.75	4.1848(5)	9.8043(67)
50.0	4.1824(4)	9.8099(51)
55.0	4.1812(10)	9.8106(92)
57.55	4.1825(4)	9.8126(41)
69.87	4.1772(5)	9.8209(79)
72.5	4.1748(4)	9.8236(23)
75.0	4.1722(5)	9.8248(62)
79.25	4.1722(5)	9.8277(46)
87.5	4.1663(4)	9.8335(47)
93.75	4.1641(4)	9.8423(36)
$CeOs_2Si_2$	4.1617(5)	9.8481(28)

TABLE 34

$Dy_{1-x}Ho_xFe_2Si_2$, $Y_{1-x}Ho_xFe_2Si_2$ and $HoCo_{2-x}Fe_xSi_2$ (all $ThCr_2Si_2$-type): lattice parameters (in Å) and observed effective paramagnetic moment μ_{eff}^{para} per formula unit (in μ_B) as compared to the effective paramagnetic moment per Fe (Co) atom $\mu_{eff}^{para}(Fe,Co)$ derived under the assumption of ideal trivalency of the rare earth component. Based on Skolozdra et al. (1980).

Compound	Lattice parameters		μ_{eff}^{para} (μ_B)	$\mu_{eff}^{para}(Fe,Co)$ (μ_B)	Asymp. Curie temp. θ_p (K)	Ordering temp. T_N (K)
	a (Å)	c (Å)				
$DyFe_2Si_2$	3.905(5)	9.93(1)	12.4	4.5	−95	310
$Dy_{0.74}Ho_{0.26}Fe_2Si_2$	3.905(5)	9.93(1)	12.2	4.3	−95	310
$Dy_{0.25}Ho_{0.75}Fe_2Si_2$	3.905(5)	9.93(1)	−	−	−	−
$Dy_{0.5}Ho_{0.5}Fe_2Si_2$	3.905(5)	9.93(1)	−	−	−	−
$HoFe_2Si_2$	3.900(5)	9.93(1)	11.9	3.8	−100	300
$Y_{0.25}Ho_{0.75}Fe_2Si_2$	3.905(5)	9.93(1)	−	−	−	−
$Y_{0.5}Ho_{0.5}Fe_2Si_2$	3.910(5)	9.93(1)	−	−	−	−
$Y_{0.74}Ho_{0.26}Fe_2Si_2$	3.914(5)	9.93(1)	13.4	3.4	−100	250
YFe_2Si_2	3.914(5)	9.93(1)	−	0.6	100	275
$HoFe_{1.5}Co_{0.5}Si_2$	3.900(5)	9.79(1)	11.7	3.7	−70	280
$HoFe_1Co_1Si_2$	3.900(5)	9.72(1)	11.7	3.6	−70	280
$HoFe_{0.5}Co_{1.5}Si_2$	3.898(5)	9.73(1)	−	−	−	−
$HoCo_2Si_2$	3.878(5)	9.73(1)	11.5	3.2	−47	295

the $Sc_2Fe_3Si_5$-type of structure (P4/mnc) was reported, but no lattice parameter data were given. Samples were prepared by arc melting under Ar, followed by a heat treatment for 7 d at 1150°C and additionally 14 d at 800°C.

Reference
Segre, C.U., 1981, Thesis, Univ. of Calif., San Diego, USA.

Dy–Y–Fe–Si

Segre (1981) investigated the low-temperature phase equilibria in the concentration section $(Dy_xY_{1-x})_2Fe_3Si_5$. A complete solid solution with the $Sc_2Fe_3Si_5$-type of structure (P4/mnc) was reported, but no structural details were presented. The variation of T_c versus x is shown in fig. 65. For sample preparation, see $(Dy_xLu_{1-x})_2Fe_3Si_5$.

Reference
Segre, C.U., 1981, Thesis, Univ. of Calif., San Diego, USA.

Er–Gd–Ni–Si

Raman (1968) investigated combinations of ErSi (CrB-type, branch I, Cmcm) and GdNi (CrB-type, branch II, Cmcm) by means of X-ray powder diffraction methods. No appreciable mutual solid solubility was observed. Powder diffraction patterns were said to be complex. For sample preparation and structural details, see Er–Al–Si.

Reference
Raman, A., 1968, Inorg. Chem. 7(5), 973.
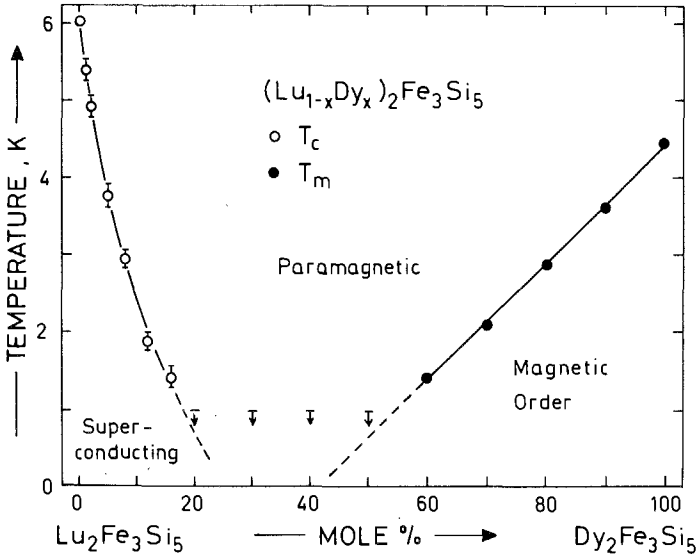
Fig. 64. Dy–Lu–Fe–Si, section $(Lu_{1-x}Dy_x)_2Fe_3Si_5$, low-temperature phase diagram. After Segre (1981).

Er–Ho–Fe–Si

Segre (1981) investigated the effect of competition between two different types of magnetic order in alloys along the concentration section $(Er_{1-x}Ho_x)_2Fe_3Si_5$ crystallizing in space group P4/mnc with the $Sc_2Fe_3Si_5$-type of structure; see fig. 66; no lattice parameters were reported. $Er_2Fe_3Si_5$ and $Ho_2Fe_3Si_5$ both order antiferromag-
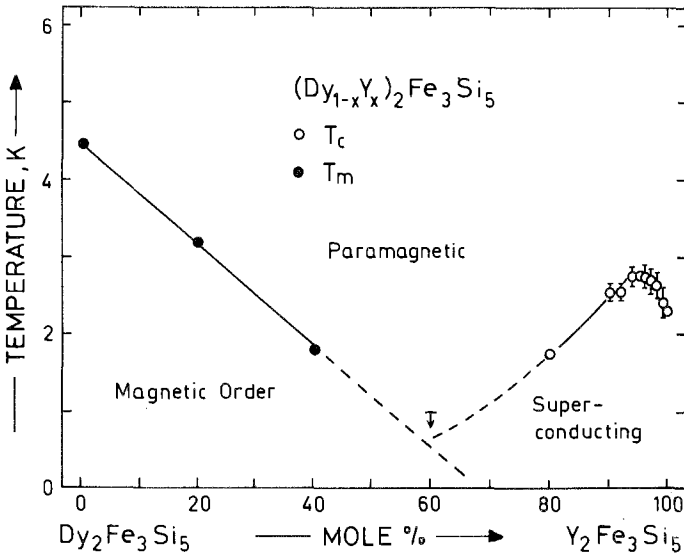
Fig. 65. Dy–Y–Fe–Si, section $(Dy_{1-x}Y_x)_2Fe_3Si_5$, low-temperature phase diagram. After Segre (1981).

netically; the anisotropy of the magnetic susceptibility, however, is different. For sample preparation, see $(Dy_x Lu_{1-x})_2 Fe_3 Si_5$.

Reference
Segre, C.U., 1981, Thesis, Univ. of Calif., San Diego, USA.

Er–Lu–Fe–Si

Segre (1981) determined the low-temperature phase diagram for the section $(Er_x Lu_{1-x})_2 Fe_3 Si_5$ (fig. 67). The crystal structure is isotypic with the $Sc_2 Fe_3 Si_5$-type (P4/mnc); however, no lattice parameters were reported. Preliminary low-temperature ac susceptibility measurements on powdered samples were said to indicate an extension of the paramagnetic-to-antiferromagnetic phase boundary into the superconducting area (dashed line in fig. 67). Thus coexistence of superconductivity and antiferromagnetic order is suggested. For sample preparation, see $(Dy_x Lu_{1-x})_2 Fe_3 Si_5$.

Reference
Segre, C.U., 1981, Thesis, Univ. of Calif., San Diego, USA.

Eu–Au–Pd–Si

Temperature-dependent susceptibility, electrical resistivity and high-field magnetization at 4.2 K have been studied in the concentration section $Eu(Pd_{1-x} Au_x)_2 Si_2$ for $x \leqslant 0.25$ by Gupta et al. (1983) (see fig. 68) and by Segre et al. (1982), by means of ^{151}Eu Mössbauer measurements. In both cases the samples were prepared by arc
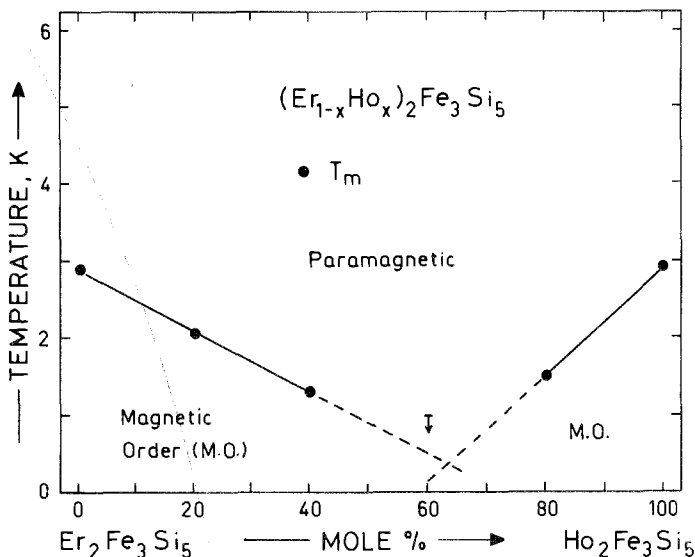
Fig. 66. Er–Ho–Fe–Si, section $(Er_{1-x} Ho_x)_2 Fe_3 Si_5$, low-temperature phase diagram. After Segre (1981).
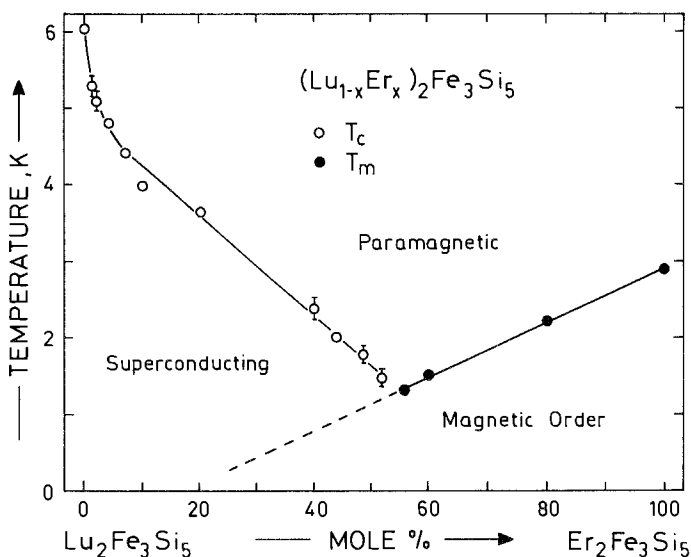
Fig. 67. Er–Lu–Fe–Si, section $(Lu_{1-x}Er_x)_2Fe_2Si_5$, low-temperature phase diagram. After Segre (1981).

melting compacts of 99.99% Eu, 99.95% Pd and 99.999% Si under argon. 2–3 at% of excess Eu was used to compensate for the Eu evaporation losses. All alloys were annealed in vacuum at 800°C for 4–5 d and crystallized with the $ThCr_2Si_2$-type (no crystal data were presented). For $0 \leqslant x \leqslant 0.175$ the system undergoes a valence transition with temperature (nonmagnetic ground state). At higher temperatures a Curie–Weiss-like behavior is characterized by an effective moment close to that of a free Eu^{2+}; the low-temperature Curie tails were attributed to untransformed Eu^{2+} "impurities". For $x > 0.20$ the system exhibits an antiferromagnetic transition. A roughly linear relationship was shown between the inverse zero-temperature suscept-ibility and the valence-transition temperature. This line of first order valence transitions observed for concentrations $0.04 < x < 0.175$ and from an $Eu^{+2.8}$ to an $Eu^{+2.2}$ valency terminates at a critical point $(x \sim 0.04)$; for $x < 0.04$ the valence transition is considered as continuous (see also the Eu–Pd–Si system). Alloys with $x \geqslant 0.175$ reveal a second order magnetic transition to an antiferromagnetic-type spin arrangement: $T_m = 32(1)$ K at $x = 0.2$ and $T_m = 28(1)$ at $x = 0.25$. The regions of mixed valence behavior and of antiferromagnetic order meet at $x \sim 0.175$.

References

Gupta, L.C., V. Murgai, Y. Yeshurun and R.D. Parks, 1983, in: Valence Instabilities, eds. J. Schoenes, J. Sierro, H. Ott and P. Wachter (North-Holland, Amsterdam).

Segre, C.U., M. Croft, J.A. Hodges, V. Murgai, L.C. Gupta and R.D. Parks, 1983, Phys. Rev. Lett. **49**, 1947.

Eu–La–Pd–Si

[151]Eu Mössbauer isomer shifts were measured for $Eu_{1-x}La_xPd_2Si_2$ alloys $(x = 0.3$ and 0.5) in the temperature range of 77 to 300 K, and suggested the presence of both
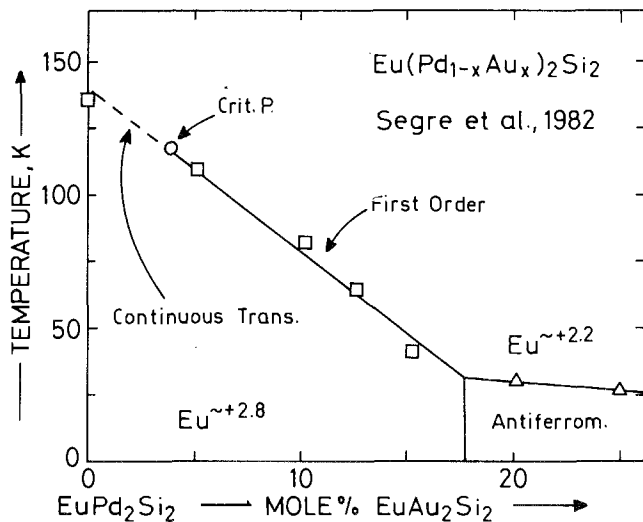
Fig. 68. Eu–Au–Pd–Si, low-temperature phase diagram (after Gupta et al., 1983).

divalent Eu ions and Eu ions with fluctuating valences (Sampathkumaran et al., 1983). Samples at $x = 0.3$ and 0.5 were prepared from $EuPd_2Si_2$ and $LaPd_2Si_2$ master alloys by arc melting and subsequent annealing at 800°C for 15 d. From X-ray powder diffraction analysis a $ThCr_2Si_2$-type (I4/mmm) was reported.

Reference
Sampathkumaran, E.V., R. Nagarayan and R. Vijayaraghavan, 1983, J. Less-Common Metals **94**, 195.

Gd–Lu–Fe–Si

A rapid depression of T_c was observed at the Lu-rich end of the solid solution $(Gd_xLu_{1-x})_2Fe_3Si_5$ with the $Sc_2Fe_3Si_5$-type of structure and space group P4/mnc. No structural data have been presented (Segre, 1981; fig. 69). For sample preparation, see $(Dy_xLu_{1-x})_2Fe_3Si_5$.

Reference
Segre, C.U., 1981, Thesis, Univ. of Calif., San Diego, USA.

Ho–Co–Fe–Si

A complete solid solubility was observed by Skolozdra et al. (1980) for the system $HoCo_{2-x}Fe_xSi_2$ crystallizing with the $ThCr_2Si_2$-type of structure (I4/mmm; X-ray powder data). Magnetic susceptibility data (80–1050 K) were recorded within the temperature range of 80–1050 K and are presented in table 34.

Reference
Skolozdra, R.V., Yu.K. Gorelenko, O.I. Bodak and V.I. Yarovets, 1980, Ukr. Fiz. Zh. **25**(10), 1683.

Ho–Lu–Fe–Si

A low-temperature phase diagram has been established by Segre (1981) for the section $(Ho_xLu_{1-x})_2Fe_3Si_5$ (fig. 70). A continuous solid solution with the
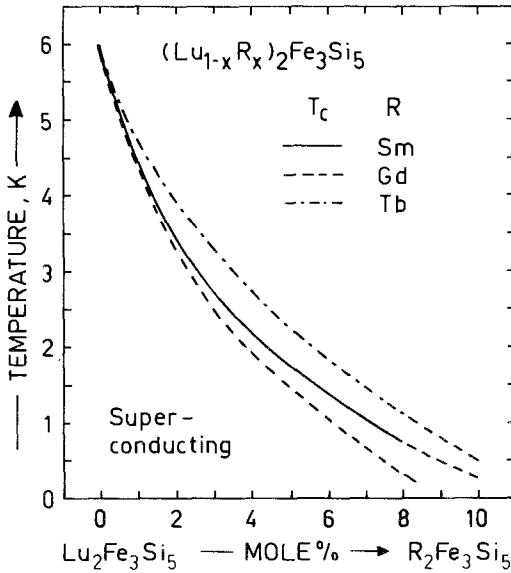
Fig. 69. Partial low-temperature phase diagrams $(x < 0.1)$ for the systems $(Lu_{1-x}R_x)_2Fe_3Si_5$, R = Sm, Gd, Tb.

$Sc_2Fe_3Si_5$-type of structure and space group P4/mnc was reported; however, no lattice parameter data were given. For sample preparation, see $(Dy_xLu_{1-x})_2Fe_3Si_5$.

Reference
Segre, C.U., 1981, Univ. of Calif., San Diego, USA.

Ho–Y–Fe–Si

Skolozdra et al. (1980) investigated the temperature dependence of the magnetic susceptibility (80–1050 K) within the concentration section $Ho_xY_{1-x}Fe_2Si_2$ and in the temperature range of 80 to 1050 K. Results obtained from X-ray powder diffraction ($ThCr_2Si_2$-type, I4/mmm) and magnetic data are presented in table 34.

Reference
Skolozdra, R.V., Yu.K. Gorelenko, O.I. Bodak and V.I. Yarovets, 1980, Ukr. Fiz. Zh. **25**(10), 1683.

La–Y–Mn–Si

Sampathkumaran et al. (1983) and Chaughule et al. (1983) investigated the structural and magnetic properties in the concentration section $La_{1-x}Y_xMn_2Si_2$. A complete solid solubility with the $ThCr_2Si_2$-type of structure was observed from X-ray powder analysis of eight alloys prepared by induction melting on a water-cooled copper boat. Excess manganese was added beforehand in compensation for Mn losses during the melting process. Small amounts of Y_2O_3 were present in the Y samples. Magnetic measurements (77–575 K and in fields up to 10 kOe) indicated a ferromagnetically ordered state in alloys with $x < 0.2$, whereas for $x > 0.2$ antiferro-
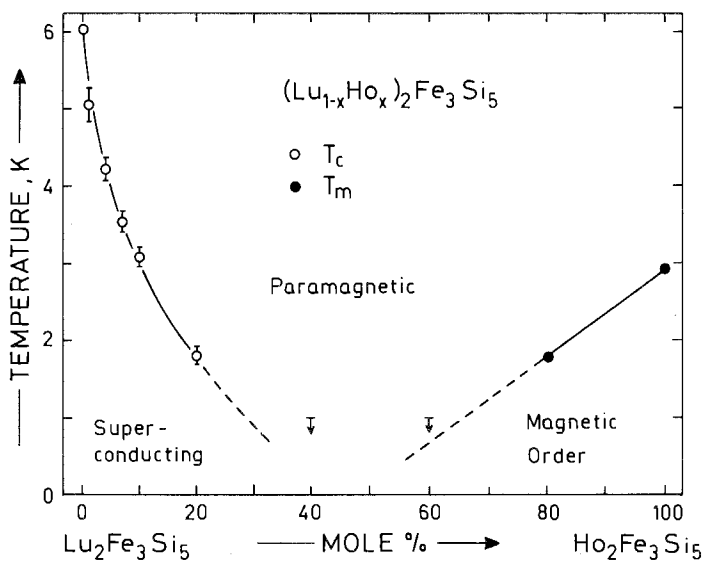
Fig. 70. Ho–Lu–Fe–Si, section $(Lu_{1-x}Ho_x)_2Fe_3Si_5$, low-temperature phase diagram. After Segre (1981).

magnetic ordering was observed (T_N increases with increasing content of the smaller Y atom). Thus for the transition from antiferromagnetism to ferromagnetism a critical Mn–Mn distance was derived to be 2.88 Å in the a-direction, and 5.29 Å in direction of the c-axis (Sampathkumaran et al., 1983). For X-ray and magnetic data of $La_{1-x}Y_xMn_2Si_2$ alloys, see table 35.

The magnetic behavior in the alloys with $x = 0.2$ was complex. From magnetic susceptibility, ^{55}Mn NMR and hysteresis studies on samples ($x \leqslant 0.2$) annealed in vacuum at 800°C for 1 week, Chaughule et al. (1983) reported a mainly single domain state at $x = 0.2$ at room temperatures with a cluster spin-glass-type of ordering at low temperatures, and a gradual change of domain state from mixed domain (multidomain) to single domain particles when x increases from 0 to 0.2.

References

Chaughule, R.S., C. Radhakrishnamurty, E.V. Sampathkumaran, S.K. Malik and R. Vijayaraghavan, 1983, Mater. Res. Bull. **18**, 817.
Sampathkumaran, E.V., R.S. Chaughule, G.V. Gopalakrishnan, S.K. Malik and R. Vijayaraghavan, 1983, J. Less-Common Metals **92**, 35.

Lu–Sc–Fe–Si

Segre (1981) determined the low-temperature phase diagram of the section $(Lu_xSc_{1-x})_2Fe_3Si_5$ ($Sc_2Fe_3Si_5$-type of structure, P4/mnc; fig. 71). No lattice parameter data were reported. Sample preparation as for $(Dy_xLu_{1-x})_2Fe_3Si_5$.

Reference

Segre, C.U., 1981, Thesis, Univ. of Calif., San Diego, USA.

TABLE 35

Crystallographic and magnetic data for $La_{1-x}Y_xMn_8Si_2$ alloys. Based on Sampathkumaran et al. (1983).

x	Lattice parameters		μ_{eff} per formula unit (μ_B)	θ_p (K)	T_m (K)
	a (Å)	c (Å)			
0	4.113	10.620	4.3	310	310 (ferromagnetic)
0.1	4.094	10.607	4.0	310	300 (ferromagnetic)
0.2	4.077	10.582	4.2	310	250 (complex)
0.3	4.049	10.577	4.3	320	328 (antiferromagnetic)
0.4	4.027	10.567	4.3	360	355 (antiferromagnetic)
0.6	3.979	10.520	–	–	430 (antiferromagnetic)
0.8	3.945	10.481	–	–	478 (antiferromagnetic)
1.0	3.925	10.448	–	–	516 (antiferromagnetic)

Lu–Sm–Fe–Si

A rapid depression of the superconducting transition temperature was observed by Segre (1981) at the Lu-rich end of the solid solution $(Sm_xLu_{1-x})_2Fe_3Si_5$ (fig. 69). A $Sc_2Fe_3Si_5$-type of structure with space group P4/mnc was reported, but no further structural details were presented. Sample preparation as for $(Dy_xLu_{1-x})_2Fe_3Si_5$.

Reference
Segre, C.U., 1981, Univ. of Calif., San Diego, USA.

Lu–Tb–Fe–Si

Substitution of Lu by Tb in $(Lu_{1-x}Tb_x)_2Fe_3Si_5$ rapidly decreases the superconducting transition temperatures (Segre, 1981, fig. 69). A $Sc_2Fe_3Si_5$-type of structure was reported for the Lu-rich alloys (P4/mnc); no lattice parameters were given. For sample preparation, see $(Dy_xLu_{1-x})_2Fe_3Si_5$.

Reference
Segre, C.U., 1981, Univ. of Calif., San Diego, USA.

Lu–Tm–Fe–Si

Segre and Braun (1981) investigated the low-temperature phase diagram of the system $(Tm_{1-x}Lu_x)_2Fe_3Si_5$ from ac susceptibility measurements of eleven samples within the composition region $0 < x \leqslant 0.2$. The diamagnetic transition was sharp for samples with $x \leqslant 0.07$, whereas the sample at $x = 0.10$ showed a second sharp transition at 0.95 K indicating a superconducting to magnetically ordered transition, i.e. reentrant superconductivity (fig. 72). Samples were prepared by arc melting under argon. The reguli were then sealed in quartz capsules under a partial pressure of Ar and annealed at 1150°C for 4 d and additionally at 800°C for 8 d. Starting materials were R-3N, Fe-5N and Si-7N.
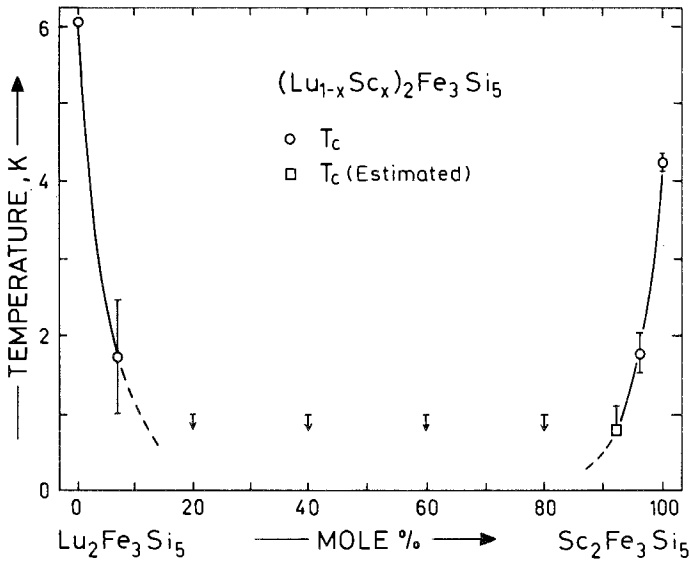
Fig. 71. Lu–Sc–Fe–Si, section $(Lu_{1-x}Sc_x)_2Fe_3Si_5$, low-temperature phase diagram. After Segre (1981).

Reference

Segre, C.U. and H.F. Braun, 1981, Phys. Lett. **85A**(6,7), 372.

Lu–Y–Fe–Si

In a study of the low-temperature phase diagram of the section $(Lu_{1-x}Y_x)_2Fe_3Si_5$, Segre (1981) observed a rapid depression and a strong positive curvature of the
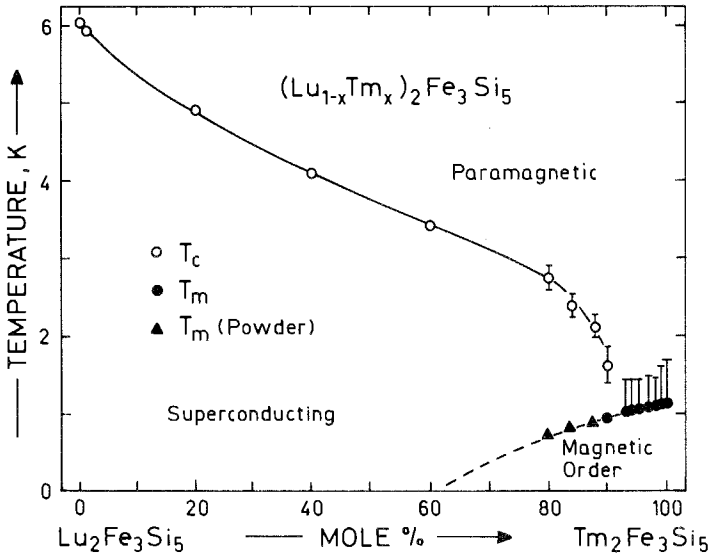
Fig. 72. Lu–Tm–Fe–Si, section $(Lu_{1-x}Tm_x)_2Fe_3Si_5$, low-temperature phase diagram. After Segre (1981).

superconducting phase boundary (fig. 73). $(Lu_{1-x}Y_x)_2Fe_3Si_5$ represents a continuous solid solution with the $Sc_2Fe_3Si_5$-type of structure (P4/mnc); no lattice parameter data were reported. Sample preparation as for $(Dy_xLu_{1-x})_2Fe_3Si_5$.

Reference
Segre, C.U., 1981, Thesis, Univ. of Calif., San Diego, USA.

Nd–Cr–Mn–Si

Obermyer et al. (1979) investigated the phase equilibria and magnetic properties within the concentration section $Nd(Cr_xMn_{1-x})_2Si_2$; see table 36. Samples were prepared by induction melting on a water-cooled copper surface under Ar. Vaporisation of Mn metal was compensated by remelting with excess Mn. Annealing at $\sim 700°C$ (14 d) was performed in vacuum.

From X-ray powder diffraction data the $ThCr_2Si_2$-type of structure (I4/mmm) was observed to be stable in the region $0 \leqslant x \leqslant 0.8$. "$NdCr_2Si_2$" did not crystallize with the $ThCr_2Si_2$-type. Magnetic properties were examined between 4.2 K and 400 K in applied fields up to 20 kOe. The Cr/Mn sublattice appeared to order antiferromagnetically, whereas the Nd sublattice ordered ferromagnetically at temperatures < 100 K. Lattice parameters and magnetic data are listed in table 33. The occurrence of anomalous magnetic behavior in low external fields was suggested to be related to a change in the easy direction of magnetization of the Nd sublattice from the easy c-axis to the basal plane (or cone), when the alloy is cooled below 50 K.

Reference
Obermyer, R., S.G. Sankar and V.U.S. Rao, 1979, J. Appl. Phys. **50**(3), 2312.
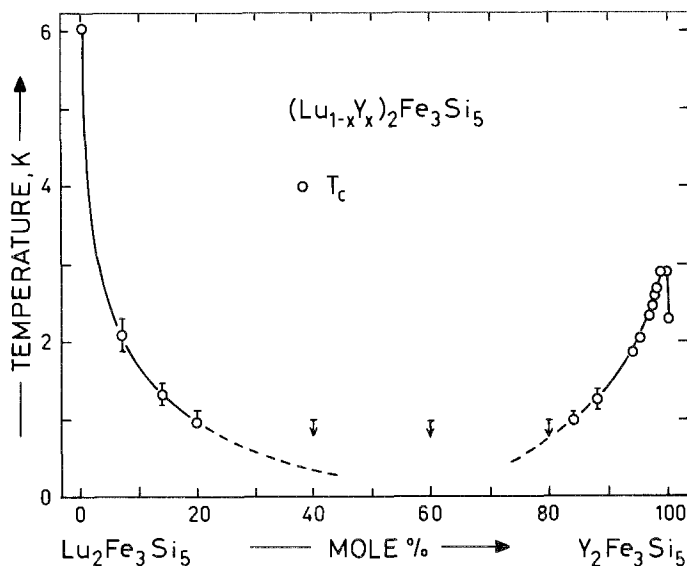
Fig. 73. Lu–Y–Fe–Si, section $(Lu_{1-x}Y_x)_2Fe_3Si_5$, low-temperature phase diagram. After Segre (1981).

TABLE 36

Lattice parameters and magnetic properties of $Nd(Mn_{1-x}Cr_x)_2Si_2$. After Obermyer et al. (1979).

	a (Å)	c (Å)	μ_{sat} (μ_B)	T_N (K)
$NdMn_2Si_2$	4.012	10.549	5.14	380
$NdMn_{1.8}Cr_{0.2}Si_2$	4.023	10.534	5.0	325
$NdMn_{1.6}Cr_{0.4}Si_2$	4.021	10.575	4.08	260
$NdMn_{1.4}Cr_{0.6}Si_2$	4.036	10.595	3.04	200
$NdMn_{1.2}Cr_{0.8}Si_2$	4.031	10.606	2.41	a)
$NdMn_{0.8}Cr_{1.2}Si_2$	4.038	10.658	2.27	b)

[a] Not determined from these experiments.

[b] This composition appears to be paramagnetic in the temperature range investigated.

Sc–Os–Rh–Si

Braun and Segre (1980) investigated superconductivity within the concentration section $Sc_5Os_{3.3}Si_{10}$–$Sc_5Rh_{3.3}Si_{10}$. No appreciable solubility was observed for Os in $Sc_5Rh_{3.3}Si_{10}$, but $Sc_5Os_{3.3}Si_{10}$ dissolves up to ~ 30 a/o Rh. No lattice parameter data were given, but the phase composition and T_c for each compound is shown in table 37. For sample preparation, see $Sc_3Os_2Si_6$.

Reference

Braun, H.F. and C.U. Segre, 1980, Solid State Commun. **35**, 735.

Sc–Y–Fe–Si

Segre (1981) investigated the low-temperature phase diagram of the section $(Y_xSc_{1-x})_2Fe_3Si_5$ (fig. 74) forming a complete solid solution with the $Sc_2Fe_3Si_5$-type (P4/mnc). No lattice parameter data were reported; for sample preparation, see $(Dy_xLu_{1-x})_2Fe_3Si_4$.

Reference

Segre, C.U., 1981, Univ. of Calif., San Diego, USA.

Y–Rh–B–Si

Boron was found to stabilize the $CeCo_3B_2$-type of structure (space group P6/mmm) on substitution of up to 75% Si in YRh_3Si_2 (Chevalier et al., 1981).

TABLE 37

Superconductivity in the $Sc_5(Rh_{1-x}Os_x)_{3.3}Si_{10}$ system. After Braun et al. (1980)

Compound	T_c (K)	Phases present
$Sc_5Rh_{3.3}Si_{10}$	8.4	$Sc_5Rh_4Si_{10} + Sc_4RhSi_{-8}$
$Sc_5(Rh_{0.9}Os_{0.1})_{3.3}Si_{10}$	8.1	$Sc_5Rh_4Si_{10} + Sc_4RhSi_8 + Sc_3Os_2Si_6$
$Sc_5(Rh_{0.7}Os_{0.3})_{3.3}Si_{10}$	7.9	$Sc_5Rh_4Si_{10} + Sc_3Os_2Si_6$
$Sc_5(Rh_{0.5}Os_{0.5})_{3.3}Si_{10}$	7.2	$Sc_5Rh_4Si_{10} + Sc_3Os_2Si_6$
$Sc_5(Rh_{0.3}Os_{0.7})_{3.3}Si_{10}$	a)	$Sc_3Os_2Si_6$
$Sc_5(Rh_{0.1}Os_{0.9})_{3.3}Si_{10}$	a)	$Sc_3Os_2Si_6$

[a] Not superconducting above 1.2 K.
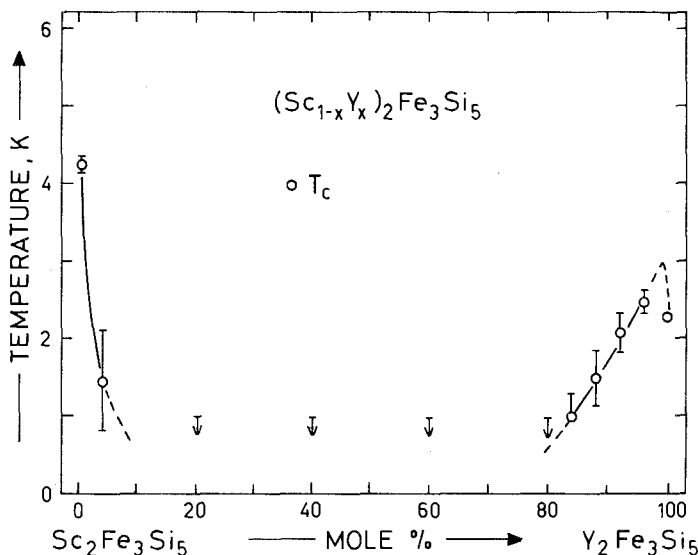
Fig. 74. Sc–Y–Fe–Si, section $(Sc_{1-x}Y_x)_2 Fe_3 Si_5$, low-temperature phase diagram. After Segre (1981).

Samples were prepared by arc melting and subsequent annealing at 950°C for 4 d in evacuated silica tubes. Lattice parameters obtained from X-ray powder data and read from a diagram were as follows: YRh_3Si_2: $[a = 5.504(6), \quad c = 3.542(4)]$; $YRh_3Si_{1.5}B_{0.5}$: $a = 5.45$, $c = 3.45$, YRh_3SiB: $a = 5.42$, $c = 3.34$ and $YRh_3Si_{0.5}B_{1.5}$: $a = 5.38$, $c = 3.22$.

Reference
Chevalier, B., A. Cole, P. Lejay and J. Etourneau, 1981, Mater. Res. Bull. **16**, 1067.

Acknowledgements

TABLE 38

Crystallographic (at RT) and magnetic data of RCu_2Si_2 alloys.[a]

Compound	Lattice parameter		$\Delta(c/a)$ ($\times 10^{-3}$)	$\Delta c/c$ ($\times 10^{-3}$)	μ_{eff} (μ_B)	T_N (K)			Q_s ($\times 10^{-3}$)
	a (Å)	c (Å)				S[b]	M[c]	R[d]	
$LaCu_2Si_2$	4.1521	9.9316	–	–	–	–	–	–	–
$CeCu_2Si_2$	4.100	9.9244	–	–	–	–	–	–	–
$PrCu_2Si_2$	4.0847	9.9311	3	2	2.61	20.8	22.5	–	–4.9
$NdCu_2Si_2$	4.0638	9.9322	2.8	1.9	2.39	–	–	–	–0.4
$SmCu_2Si_2$	4.027	9.9422	4.5	3.0	1.12	9.0	–	–	1.5
$EuCu_2Si_2$	4.0553	9.9175	–	–	–	–	–	–	–
$GdCu_2Si_2$	3.9987	9.9538	0	0	7.93	14.2	12.0	13.5	–0.1
$TbCu_2Si_2$	3.9765	9.9616	4.5	3.0	9.28	12.5	–	11.5	–6.3
$DyCu_2Si_2$	3.9654	9.9616	8.2	5.5	10.58	11.8	10.5	10.9	–9.4
$HoCu_2Si_2$	3.9507	9.972	5.3	3.5	10.42	7.7	7.0	6.8	–3.1
$ErCu_2Si_2$	3.9369	9.9809	5.5	3.7	9.49	–	2.0	4.8	2.5
$TmCu_2Si_2$	3.9247	9.9922	10.3	6.9	7.14	7.0	7.0	6.9	1.2
$YbCu_2Si_2$	3.9232	9.9871	–	–	–	–	–	–	–
$LuCu_2Si_2$	3.9073	9.9955	–	–	–	–	–	–	–

[a] $\Delta(c/a)$ and $\Delta c/c$ are the observed anomalies of the unit cell; Q_s is the value of the saturated magnetostriction of the R ions in $R_x Y_{1-x}Cu_2Si_2$ alloys.
[b] From susceptibility.
[c] From magnetostriction.
[d] From resistivity.

Notes added in proof

R–Cu–Si and R–Y–Cu–Si

Schlabitz et al. (1982) investigated the variation of the lattice parameters versus temperature ($4.2 < T < 300$ K) of alloys RCu_2Si_2 and $Y_{1-x}R_xCu_2Si_2$ with the $ThCr_2Si_2$-type of structure (space group I4/mmm, see table 38). Samples were prepared by induction melting the high-purity elements (4N minimum purity) in a water-cooled copper crucible under argon. After a final heat treatment at 1100 K for 80 h the buttons were powdered in a B_4C-mortar and then further annealed at 700 K for 20 h. Magnetic susceptibilities were obtained from the as-cast specimens. All compounds with a nonzero total angular momentum of the 4f-shell (Pr, Nd, Sm, Tb, Dy, Ho, Er and Tm) reveal an anomalous change in the c/a ratio with a reversal of the sign of the temperature dependency of the c-axis whereby the volume of the unit cell stays constant. The distortion was suggested to arise from the alignment of the quadrupolar moment of the R-charge distribution in the electric field gradient of the noncubic R sites. The low temperature value of the anomaly is nearly the same as that of the saturated magnetostriction of the R ions diluted in YCu_2Si_2. The antiferromagnetic ordering temperatures for the $L \neq 0$ compounds are larger than expected on a spin-only interaction (de Gennes temperature extrapolated from $GdCu_2Si_2$), and the deviation again was found to scale with the observed c/a anomaly.

Reference
Schlabitz, W., J. Baumann, G. Neumann, D. Plümacher and K. Reggentin, 1982, Quadrupole Effects in the Lattice Parameters and Magnetic Ordering Temperatures of RCu_2Si_2, in: Crystalline electric field effects in f-electron magnetism, eds. Guertin, Suski and Zolnierik (Plenum, New York) p. 289.

Er–Fe–Si

Leciejewicz et al. (1984) investigated the type of magnetic order in $ErFe_2Si_2$ from neutron powder diffraction data at 293 K and at 1.8 K; for sample preparation see Er–Mn–Si.

The room temperature neutron diffraction pattern confirmed the atom ordering and crystal symmetry of the $ThCr_2Si_2$-type ($a = 3.882(2)$, $c = 9.876(7)$, z(Si in 4e) $= 0.3753(16)$, $R = 0.087$), whereas a series of superstructure reflections occur in the diffractogram at 1.8 K compatible with a magnetic unit cell: $a = b = a_0 = 3.802(2)$ and $c = 2c_0 = 19.171(15)$. The magnetic structure proposed is collinear antiferromagnetic with ferromagnetic layers of Er-atoms arranged in a sequence $+ - - +$ along the c-axis. The Er-moments $\mu_{Er} = 7.4(3)$ μ_B are perpendicular to the c-axis, $R_n = 0.089$, $R_m = 0.097$.

Reference
Leciejewicz, J., S. Siek and A. Szytula, 1984, J. Magn. Magn. Mater. 40, 265.

Er–Mn–Si

Crystal structure and magnetic order in $ErMn_2Si_2$ has been studied by Leciejewicz et al. (1984) from neutron powder diffraction experiments at 293, 78, 4.2 and

1.8 K. Samples were prepared by induction melting starting from 4N minimum purity elements. The samples were annealed in silica tubes for 100 h at 800 °C and slowly cooled to room temperature. The neutron diffractogram at room temperature was indexed on the basis of a $ThCr_2Si_2$-type of structure with two superlattice reflections (111) and (113) due to an antiferromagnetic collinear arrangement with a $+ - + -$ sequence of ferromagnetic Mn-layers along the c-axis. ($I4/mmm$, $a =$ 3.905(2), $c = 10.420(8)$, z(Si in 4e) = 0.3763(4); the low reliability value $R_n = 0.057$ indicated the absence of atomic disorder on the 4d and the 4e sites.) The magnetic moment of the manganese atoms $\mu_{Mn} = 2.17(9)$ μ_B is aligned parallel to the c-axis; $R_m = 0.064$. Similar values were obtained at 78 K ($a = 3.920(3)$, $c = 10.455(9)$, $z = 0.3748(14)$, $R_n = 0.047$, $\mu_{Mn} = 2.24(8)$, $R_m = 0.049$).
At very low temperatures (4.2 K and 1.8 K) the Er-sublattice was observed to order ferromagnetically with the Er-moment perpendicular to the c-axis; the Curie temperature derived was $T_m = 10(5)$ K. Data obtained at 4.2 K were as follows: $a = 3.911(4)$, $c = 10.437(7)$, $z = 0.3735(22)$, $\mu_{Mn} = 2.30(13)$, $\mu_{Er} = 7.3(2)$, $R_n = 0.064$ and $R_m = 0.086$; at 1.8K: $a = 3.913(4)$, $c = 10.437(7)$, $z = 0.3735(22)$, $\mu_{Mn} = 2.30(13)$, $\mu_{Er} = 8.9(2)$ μ_B, $R_n = 0.065$, $R_m = 0.076$.

Reference
Leciejewicz, J., S. Siek and A. Szytula, 1984, J. Magn. Magn. Mater. 40, 265.

Dy–Sc–Ir–Si

The low-temperature magnetic and superconducting behaviour in the $Sc_{5-x}Dy_xIr_4Si_{10}$ system was established by Braun and Pelizzone (1983) from ac-susceptibility data; samples were prepared by arc melting the high purity (3N-minimum purity) elements and were subsequently annealed in silica tubes for 2 d at 1000 °C. From X-ray powder diffraction analysis complete solid solubility was reported for all values of x with a statistical distribution of Sc and Dy atoms on the rare-earth sites and with a practically linear variation of the unit cell dimensions versus concentration ($Sc_5Co_4Si_{10}$-type). Superconductivity in the Sc-rich region decreases linearly from a $T_c(Sc_5Ir_4Si_{10}) = 8.4$ K to $T_c(Sc(Sc_4Dy_1Ir_4Si_{10}) = 7.2$ K, with a more rapid decrease for higher Dy-contents; and finally superconductivity disappears at $x \sim 1.95$. The magnetic ordering temperatures were found to decrease linearly with decreasing Dy-concentration ($T_N(Dy_5Ir_4Si_{10}) = 5.0$ K, $T_N(Sc_{3.375}Dy_{1.625}Ir_4Si_{10}) = 3.8$ K). For concentrations $x \le 1.875$ superconductivity and antiferromagnetism coexist ($T_N = 3.9$ K, $T_c = 2.6$ K at $x = 0.1875$).

Reference
Braun, H.F. and M. Pelizzone, 1983, Coexistence of superconductivity and antiferromagnetic ordering in $(Sc_{1-x}Dy_x)_5Ir_4Si_{10}$ solid solutions, in: Superconductivity in d- and f-band metals, ed. W. Buckel (KFK-Report, Karlsruhe) p. 245.

Chapter 52

AMORPHOUS ALLOYS

K.H.J. BUSCHOW

Philips Research Laboratories, 5600 JA Eindhoven, The Netherlands

Contents

Symbols

c_M	= Molar fraction of element M		s	= Heating rate
D	= Diffusion coefficient		T_N	= Néel temperature
E_F	= Fermi energy		T_0	= Superconduction transition temperature
H_A	= Anisotropy field		T_s	= Spin freezing temperature
H_c	= Coercive force		T_W	= Writing temperature in magneto-optical recording
H_d	= Demagnetizing field			
H_{eff}	= Effective hyperfine field		u	= Growth velocity
H_{hf}	= Hyperfine field		V_B	= Bias voltage in sputtering
H_m	= Molecular field		V_H	= Hall voltage
I	= Nuclear magnetic moment		V_M	= Molar volume of element M
IS	= Isomer shift		ΔH	= Heat of formation
I_v	= Nucleation frequency		ΔH_{cr}	= Heat of crystallization
J	= Angular moment		ΔH_m	= Heat of mixing
J_{ij}	= Exchange coupling constant between two magnetic species i and j		ΔH_h	= Hole formation enthalpy
			$\Delta l//l$	= Relative thermal expansion
			η	= Viscosity
K	= Knight shift		η_l	= Phase shift
k	= Rate constant		θ	= X-ray diffraction angle
k_F	= Fermi wavevector		θ_F	= Faraday rotation angle
K_u	= Anisotropy constant		θ_p	= Asymptotic Curie temperature
L	= Orbital moment		κ	= Compressibility
M_s	= Spontaneous magnetization		λ	= Wave length
$N(E_F)$	= Density of states at the Fermi level		μ	= Magnetic moment
			μ_B	= Bohr magneton
$P(q)$	= Distribution functions in amorphous alloys of a physical quantity q		$\rho(T)$	= Resistivity
			ρ_H	= Hall resistivity
			$4\pi r^2\rho(r)$	= Radial distribution function
Q	= Wave number		σ	= Magnetization
QS	= Quadrupole splitting		σ_W	= Domain wall energy
R_c	= Critical cooling rate		φ_K	= Kerr rotation angle
R_H	= Hall coefficient		ϕ^*	= Electronegativity (Miedema's scale)
R_o	= Ordinary Hall coefficient			
R_s	= Spontaneous Hall coefficient		χ	= Magnetic susceptibility
r	= Resistivity ratio		M_0	= Volume per atom

1. Introduction

Amorphous alloys can be defined as solids lacking long-range three-dimensional atomic periodicity. In diffraction experiments, which comprise X-ray diffraction, neutron diffraction and electron diffraction, such alloys are characterized by the absence of sharp diffraction peaks. Instead, only a limited number of diffuse halos are observed. There are two fundamentally different general methods of preparation. In the first of these methods, usually referred to as liquid quenching, a molten alloy is cooled rapidly, leaving no time for nucleation and growth of crystallites. The second method is based on vapour quenching. The metal atoms of a gas mixture impinge on the surface of a cold substrate. In this case, too, there is not enough time for the atoms to arrange themselves in an atomically ordered fashion.

The oldest preparation of amorphous alloys goes back to the 1930s and was based on the vapour quenching method (Kramer, 1934, 1937). For completeness, however, it should be mentioned here that the preparation of amorphous alloys may actually be much older. In the first part of the 18th century, amorphous alloys had very probably been prepared by Würtz, using the electrodeless method in which Ni alloy deposits were obtained by decomposition of nickel hypophosphide. Since scientists in that period still lacked X-ray diffraction facilities, a proper characterization of the deposited material by means of X-ray diffraction was not yet possible.

A breakthrough in the preparation of amorphous alloys took place in 1959 when Duwez et al. (1960) succeeded in developing the first technique for so-called splat-quenching. They achieved cooling rates close to 10^6 K s^{-1} by forcing atomized droplets of a liquid alloy to impinge very rapidly onto a cold substrate having a high thermal conductivity. The first amorphous material that was reported to be prepared in this way consisted of a Au–Si alloy close to the eutectic composition (Klement et al., 1960).

For a few years the investigation of amorphous alloys was mainly confined to the systems $Au_{1-x}Si_x$ and $Pd_{1-x}Si_x$. The situation soon changed, however, when it proved possible to prepare liquid-quenched amorphous alloys based on 3d transition metals. The interest in these alloys stemmed primarily from the magnetism side. Gubanov (1960) had predicted that the occurrence of ferromagnetism would extend to amorphous alloys, even though these alloys lacked long-range lattice periodicity. This theoretically predicted retention of ferromagnetism was first confirmed experimentally by Mader and Nowick (1965) on vapour-quenced $Au_{1-x}Co_x$ alloys and later by Tsuei and Duwez (1966) on liquid-quenched ternary alloys based on Pd–Si and ferromagnetic metals. It was also expected that magneto-crystalline anisotropies would be absent in ferromagnetic amorphous alloys (Simpson and Brambley, 1971), giving these materials rather low coercive forces. Many amorphous alloys were found to exist, however, that did have substantial coercive forces. Their origin was discussed later by Chi and Cargill (1976).

The possibility of reaching very low coercivities in amorphous alloys after an annealing treatment (Luborsky et al., 1975; Egami et al., 1975) opened the door to the application of amorphous alloys in systems requiring low magnetic losses. Since then the interest in magnetic amorphous materials has increased by leaps and bounds. The combined MMM–Intermag Conference held in 1982 at Montreal, where about one hundred out of a total of about 600 contributions dealt with the magnetic properties of amorphous alloys, may serve to demonstrate the proliferation in this area.

Although it was already recognized at the beginning of the 1970s that amorphous alloys can have favourable mechanical and strength properties and also can have a comparatively high corrosion resistance, research in this area has not proliferated to anything like the extent of research on the magnetic properties. A possible reason is that there are limited prospects of finding technological applications for amorphous alloys. Apart from the three technological aspects mentioned, there has recently been more interest in the fundamental physics of amorphous alloys. Studies in this field comprise atomic and electronic structure, various kinds of electrical transport

properties including superconductivity, optical and magneto-optical properties, structural relaxations within the amorphous state as well as transformations to the stable crystalline state, and also hydrogen absorption. All these aspects will be discussed in the present review.

This chapter on amorphous alloys is organized as follows: The section following this introduction (section 2) deals with the preparation of amorphous alloys. As already mentioned, amorphous alloys are commonly prepared either by vapour quenching or by liquid quenching. The first method comprises single and multiple source evaporation in high vacuum or ultra high vacuum systems, ion beam sputtering, flash evaporation and plasma spraying. In all these cases the quenching rates are relatively high. Substantially lower quenching rates are involved with liquid quenching. The most common methods that will be discussed are melt spinning, melt extraction, double roller quenching, splat cooling and the so-called piston-and-anvil quenching.

In the third section a review is given of the various models that have been proposed to describe the glass-forming tendency of alloys. This includes a discussion of the possibility to obtain the amorphous state in terms of the avoidance of the so-called nose in the TTT (Time–Temperature–Transformation) diagrams. Included in the discussion is the occurrence of a critical thickness for amorphous ribbons in relation to a sufficiently high cooling rate. It is stressed that the understanding of reaction rates is of paramount importance in the study of amorphous alloy formation. The glass-forming tendency is not to be confused with the stability of amorphous alloys, since both properties need not parallel each other.

Section 4, which deals in detail with the stability of amorphous alloys, shows that these alloys are usually regarded as being stable when one of the following stability criteria is satisfied. The first stability criterium is due to Polk (1970) and describes the stability in terms of high packing density when the alloy comprises components of sufficiently different radii. Even more widely used is the stability criterion of Nagel and Tauc (1975), which is based primarily on a favourable electronic contribution reached in a given concentration range. More sophisticated is the third criterion where a high stability corresponds to a match of the consecutive maxima of the pair distribution function with the consecutive minima of the pair potential function.

All these stability criteria are discussed and their significance is evaluated in terms of the heat of mixing (or heat of formation) and again in terms of the kinetic approach where the resistance against crystallization is governed by a thermally activated rate process with an activation energy ΔE. Several models that have been proposed to estimate ΔE are discussed.

Included in this section is a description of the various transformations taking place in amorphous alloys, such as structural relaxation, glass transition and amorphous-to-crystalline transition. The main techniques employed to study these transitions are described in more detail and further conclusions are given that can be drawn from the results of these studies.

In section 5 the structure or atomic arrangement associated with amorphous alloys is defined in terms of the pair correlation functions and the radial distribution

functions and densities. Several structures for amorphous alloys have been proposed, ranging from a completely random distribution (DRPHS model) to pseudo-micro-crystalline structures. There is a tendency now to abandon models based on a completely random atomic distribution in favour of structures exhibiting some compositional short-range ordering (CSRO). Experimental techniques are described by means of which such conclusions were reached. These include EXAFS, energy dispersive X-ray diffraction, normal X-ray diffraction, neutron diffraction and electron diffraction. Conclusions regarding the presence of CSRO can also be drawn from results of Mössbauer spectroscopy and NMR. Apart from the structure on an atomic level, amorphous alloys can have widely different microstructures associated with their method of preparation (for instance the well-known columnar structure of vapóur-quenched alloys). The discussion in section 5 includes results of electron microscopy.

Section 6 is a survey of the results of magnetic measurements made on various amorphous alloys. The results of magnetic measurements are supplemented by results obtained by means of Mössbauer effect spectroscopy and NMR. The magnetic properties of amorphous alloys and the difference in properties between amorphous and crystalline materials are discussed in terms of various models, describing the manner in which the magnetic properties are influenced by random fluctuations of the exchange integral, by random fluctuations of the number and kind of nearest neighbours and by random fluctuations of the local single-ion anisotropy axes. The presence of CSRO is expected to have a strong effect on the magnetic properties. Also mentioned are models in which the magnetic properties associated with the amorphous state are described in terms of a modified band structure and modified charge transfer effects.

Section 7 is devoted to those magnetic properties that are due to the particular shape in which amorphous materials are frequently obtained. It is discussed how different preparatory conditions may lead to differences in properties. This is true, in particular, with regard to the presence of uniaxial anisotropy in vapour-quenched thin magnetic films. Many investigations described in the literature deal with magneto-optical properties of vapour-deposited amorphous rare-earth–transition-metal alloys. The considerable research efforts made in this area have undoubtedly been triggered by the fact that the use of amorphous rare-earth–3d-metal films in magneto-optical storage and recording devices has become a major issue in the technological application of these alloys. In section 7 we therefore introduce some physical principles of the Kerr and Faraday effects. Experimental results are discussed in the light of current theories, and the significance of these results with respect to technological applications is evaluated.

The atomic disorder associated with the amorphous state leads to completely different transport properties from those encountered in the crystalline state. Experimental results of the electrical resistivity, the Hall effect, magnetoresistance, thermo-electric power and the occurrence of superconductivity are discussed in section 8. The main emphasis is placed on the electrical resistivity. The occurrence of negative temperature coefficients of the resistivity is related to models based on the extended Ziman theory. In the low temperature regime the resistivity often shows a $\ln T$

temperature dependence. This feature is frequently explained in terms of a two-level model, the two levels corresponding to the energies of slightly different atomic arrangements. The general applicability of this model is included in the discussion of section 8.

Miscellaneous properties of amorphous alloys are treated in section 9. These comprise properties that have been investigated in only relatively few cases. Examples of such properties are the specific heat, hydrogen absorption, the concentration dependence of the Mössbauer isomer shift and the few results of ESR on Gd-doped samples.

Some of the favourable properties of the amorphous alloys have led to technical applications which are discussed in section 10. The applications as storage media and magneto-optical recording devices of thin amorphous films mentioned briefly in section 7, comprise both high-density vertical and high-density longitudinal recording. Liquid-quenched ribbons of amorphous alloys can be used as low-loss magnetic cores in distribution transformers. Other applications include magnetic shielding, magnetic switches, modulators for lasers, magnetic power controllers, torque transducers, force transducers and sensitive bistable magnetic sensors. Further possible applications are to be found in magneto-acoustic devices and materials for flash bulbs.

The most outstanding features of amorphous alloys are briefly summarized again and placed in a somewhat broader perspective in the last section of this chapter (section 11). This includes possible limitations of the use of amorphous alloys such as, for instance, surface crystallization and atomic rearrangement processes of much lower activation energies than the crystallization process. All these limitations entail gradual changes of properties that may come into play, involving a time scale that would badly interfere with the time scale to be considered in technological applications. Continued research efforts in these areas seem indicated.

A review is also given of those areas of solid state research where progress has been made mainly due to the possibility of preparing amorphous alloys. Such areas include, for instance, the determination of the strain-free dilute limit of the Mössbauer isomer shift of a given isotope in various host metals. In crystalline alloys this line of research is seriously hampered by the presence of the so-called volume misfit contribution, which is difficult to estimate. Also mentioned is the possibility of using amorphous alloys as starting materials for the preparation of metastable intermetallic compounds.

Although this chapter of the Handbook is concerned primarily with amorphous alloys based on rare earth elements, it seems practical to include in the discussion various aspects that are not exclusively confined to this class of materials. A greater understanding of the principles associated with the amorphous state has been reached by means of models and experimental results pertaining to systems that do not contain rare earth elements. For that reason this chapter is of a somewhat more general nature, though the emphasis is on rare earth based alloys. Readers wishing to make a further study of amorphous alloys are referred to reviews written by Davies (1976), Cargill III (1975), Cahn (1980), Chen (1980), Luborsky (1980), Cargill III (1981a,b) and Mizoguchi (1981).

2. Preparation

It has become customary to designate amorphous solids made by means of liquid quenching as metallic glasses. In this case the high cooling rates are attained by producing a thin layer of the melt on a substrate possessing high thermal conductivity. As the heat transfer between the thin layer of the melt and the substrate largely determines the quenching rate, the thermal conductivity and the thickness of the thin layer itself are also important quantities.

Compared to vapour quenching most of the liquid quenching methods have the advantage that amorphous alloys can be produced in fairly large amounts, the thickness of the solidified melt layer being generally much larger than the thickness of the amorphous metal films obtained by vapour quenching. The latter method has, however, the advantage that the liquid state is completely bypassed. Since the effective quenching rate is comparatively high it is often possible to make amorphous alloys differing widely in composition and concentration, that cannot be prepared by liquid quenching.

Other methods used to obtain amorphous alloys are electro-deposition (Bagley and Turnbull, 1968; Boucher et al. 1976) and electrodeless precipitation (Brenner and Riddell, 1947; Dixmier and Doi, 1963), ion implantation (Andrews et al., 1976; Grant, 1978) and solid state reaction (Schwarz and Johnson, 1983). Since these methods are less widely used than vapour quenching and liquid quenching, they will not be discussed in this section.

2.1. *Liquid quenching*

2.1.1. *Melt spinning*

A technique commonly used to prepare amorphous alloys is melt spinning, developed originally by Bedell (1975). This method produces thin amorphous ribbons with a thickness of 10–40 μm. A melt-spinning apparatus is shown schematically in fig. 1a. The melt is contained in a quartz or alumina vessel (A) which

a   b
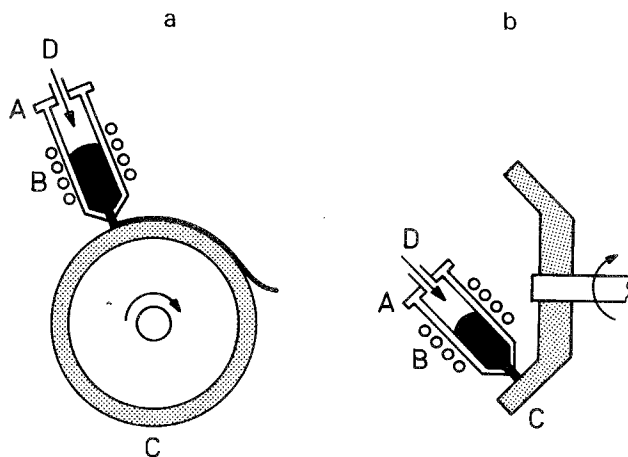
Fig. 1. Schematic representation of the melt spinning method: (a) external melt spinning, (b) internal melt spinning. The alloy is contained in a quartz vessel A and is induction heated by means of the coils B. The molten alloys is ejected by means of an argon pressure (D).

has a narrow orifice at its lower end through which a melt jet can be sprayed onto the outer surface (C) of a rapidly spinning wheel. The starting material usually consists of premelted alloy buttons, although this is not strictly necessary in all cases. The starting materials contained in vessel A are heated by means of induction coils (B). The melt spinning is initiated by increasing the pressure of the inert gas entering through D into the vessel.

A slightly modified version of this method is shown in fig. 1b. Here the melt jet is sprayed onto the inner surface of the spinning wheel. This differs from the set-up in fig. 1a in that, owing to the presence of the centrifugal force, the metal layer is pressed more tightly to the wheel surface, while the mean time of contact with the wheel surface may be longer for a given wheel diameter and revolution frequency. The contact time is important in as much as the high cooling rate is only effective when the melt is in contact with the wheel. After the melt leaves the wheel, cooling proceeds by means of radiation and convection only.

In order to obtain good thermal contact between the wheel surface and the expelled melt the wheel surface is usually required to be rather smooth. This also keeps the solidified ribbon from remaining too long on the wheel surface. When the solidified ribbon is still adhering to the wheel after one complete revolution, multilayered ribbons will be formed. There is then the possibility that the second (and following) layers will be quenched at a much lower rate, resulting in crystalline instead of amorphous materials. The wheel is commonly manufactured of copper owing to the high thermal conductivity of this metal. On a laboratory scale, where only relatively small amounts of amorphous ribbons are required, it has proved helpful to polish the outer surface of the wheel with fine emery cloth (600 grade) before each melt-spinning process.

Other factors that govern the quenching efficacy are the jet diameter and the speed at which the wheel rotates. These two factors together are mainly responsible for the final dimensions of the amorphous ribbons. Fine orifice diameters and high wheel rotation speeds lead to relatively thin ribbons. The width of the ribbons generally increases with increasing wheel rotation speed as a result of a more effective spreading of the melt. In this respect an important influence is also exerted by the jet velocity, which is determined by the ejection pressure of the inert gas.

It can further be shown that the ribbon quality depends on superheating of the melt prior to ejection, the angle of attack of the melt jet and the nature and pressure of the gas inside the chamber in which the melt spinning is performed (Liebermann and Graham, 1976; Ray, 1978; Liebermann, 1978). For rare earth base materials, in particular, it is of importance to perform the melt spinning under conditions that prevent oxidation of the melt. Fine oxide particles temporarily may reduce the diameter of the orifice. This leads to a non-constant jet of molten material which can seriously hamper the total melt-spinning procedure.

The melt-spinning method permits the continuous production of amorphous ribbons on a manufacturing scale at velocities between 10–50 m/s. As such the method has received much attention in cases where the dimensions of the ribbons have to meet specific requirements. Details of the process have been studied by means of high-speed motion pictures (Walter, 1978; Hillmann and Hilzinger, 1978),

which have enabled a careful analysis to be made of the effects of typical parameters of the method. Several investigators (Chen and Miller, 1976; Anthony and Cline, 1978, 1979) have mentioned that a stationary melt puddle is formed between the melt jet and the solidified ribbon. The length and width of this puddle largely determine the dimensions of the ribbons, the height of the puddle being of secondary importance. Model descriptions of the puddle deal mainly with the balance of thermal energy and surface energy and the counteracting of the forces associated with the tangential momentum and the surface tension (Kavesh, 1978; Hillmann and Hilzinger, 1978).

2.1.2. Roller quenching

Roller quenching is a method somewhat less widely used than melt spinning. It is illustrated schematically in fig. 2. Here the melt jet is quenched between two counter-rotating rollers (Chen and Miller, 1970; Babic et al., 1970; Lewis et al., 1977). The dimensions of the amorphous ribbons are determined either by the roller pressure (when the two rollers are in contact) or by the gap between the two rollers. A disadvantage of the method is that extremely fine tolerances are required in the machining of the roller surfaces and the roller axes since otherwise non-uniform dimensions of the ribbon will result. A further disadvantage is the high deterioration rate of the roller surfaces. An advantage is that thermal contact is better than in melt spinning, owing to the presence of a cold substrate on either side of the melt layer. This effect may be offset, however, by the shorter time of contact.

2.1.3. Melt extraction

In this method metal is extracted by the periphery of a rotating disc in contact with the surface of the melt. The melt can be present in the form of a normal melt bath (fig. 3a) or in the form of a small molten pool at the end of a rod of solid alloy continuously fed to the disc (fig. 3b). In both cases the metal solidifies and adheres to the disc until it is eventually thrown off by centrifugal forces (Maringer and Mobley, 1974, 1978). The use of a wiper to remove debris from the disc is essential. The dimensions of the amorphous alloys depend on the shape of the disc edge. A flat
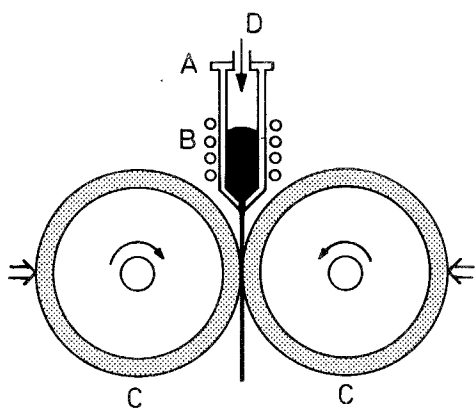
Fig. 2. Schematic representation of roller quenching. The alloy, contained in the quartz vessel A, is heated by means of the induction coils B and ejected from the vessel by means of argon pressure D into the gap between two counter-rotating rollers C.

a   b
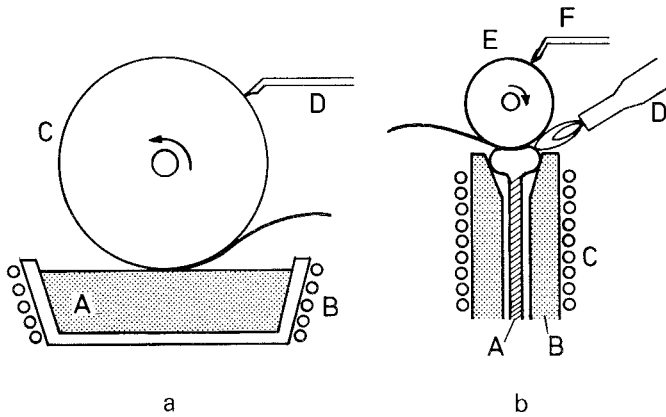
Fig. 3. Schematic representation of melt extraction: (a) crucible melt extraction of an alloy A heated in a crucible by means of induction coils B. The alloy adheres to the wheel C. Remnants of the solidified alloy are removed by means of the wiper D. (b) Laboratory scale melt extraction as proposed by Maringer and Mobley (1978). The alloy A is fed through a crucible B heated by means of coils C. The top of the rod is melted by means of a flame D, the melt being in contact with the rotating wheel E. Remnants of adhering alloy pieces are removed by means of the wiper F.

edge gives rise to ribbon-like material whereas an appropriately profiled edge can produce wires with a nearly round cross-section. Closely related to the method illustrated in fig. 3b is the method of pendant drop melt extraction, where the disc is in contact with a molten pendant drop at the end of a continuously fed rod. As in fig. 3b (when turned upside down) the method requires no crucible, making it particularly useful for dealing with alloys of high melting points. The melt extraction process is rather sensitive to the presence of oxide particles. The cooling rates associated with the melt extraction are substantially lower than in the case of melt spinning and roller quenching.

2.1.4. *Other methods of liquid quenching*

In the piston-and-anvil technique and twin-piston technique a liquid globule is squeezed either between a fixed anvil and a fast-moving piston (Pietrokowsky, 1963; Ohring and Haldipur, 1971; Yamauchi and Nakagawa, 1971; Giessen et al., 1976) or between two fast-moving pistons, respectively (Harbur et al., 1969; Cahn et al., 1976). It will be clear that these methods are suitable for the production of only small quantities of amorphous material. It is frequently used on a laboratory scale since it has the advantage of giving rise to a foil of uniform thickness and relatively large width in all directions, the latter comparing favourably with the small width usually associated with single-nozzle melt spinning. The high kinetic energy associated with the moving piston guarantees good thermal contact with the substrate when the two substrate planes are in good alignment. Some deformation may occur in the quenched samples after solidification, depending on the kinetic energy of the moving parts and the degree of superheating of the initial melt.

In the splat quenching or gun technique a liquid globule is subjected to a shock wave. Extremely fine droplets are produced which impinge with near sonic velocity

on a chilled block substrate having the form of a ski slope. The result is a thin foil of irregular shape and varying thickness (Duwez et al., 1960; Duwez and Willens, 1963; Jones and Suryanarayana, 1973). Splat quenching lends itself to the production of small quantities of amorphous materials and its use is therefore restricted to exclusively scientific purposes. The method has been claimed to give rise to the highest cooling rate, lying between 10^6 K/s and 10^{10} K/s (Predecki et al., 1965; Ruhl, 1967). It therefore enables the vitrification of many more different materials than any of the other techniques mentioned. A disadvantage is the non-uniform thickness of the foil and the inherent variable cooling rate corresponding to different regions of the same foil.

Plasma spraying is a further method that has been used to produce amorphous alloys. The method primarily consists in melting the powder of the alloy to be vitrified in an inert-gas plasma flame and allowing the molten stream of particles to splash down on a chilled block substrate to form the deposit (Moss et al., 1964; Krishnan and Cahn, 1976). A gradual build-up of quenched particles on the substrate can be achieved by using a rapidly rotating substrate which avoids overheating and devitrification of the deposit. It is also possible to use a cross-blast of argon to direct the plasma flame away from the substrate. Amorphous Sm–Co prepared by means of the plasma spray technique has been reported to be partially crystalline (Kumar et al., 1978). In principle the method of plasma spraying lends itself to bulk production of larger quantities of amorphous materials.

In the laser glazing technique a fine laser beam of high power density is rapidly scanned along the surface of an alloy sample. As a result the alloy melts locally on the surface over a relatively small depth, leading to vitrification and subsequent coating (Breinan et al., 1976; Draper et al., 1982). In this way it may be possible to give a piece of metal an amorphous coating, although it would seem that the method is only applicable when the alloy itself is an easy glass former.

2.2. *Vapour quenching*

2.2.1. *Vapour deposition*

Many of the amorphous alloys that cannot be made by liquid quenching can be prepared by vapour quenching. In its simplest form the method uses a crucible in which the alloy is heated up to a temperature sufficiently high to lead to a vapour flux that guarantees a high enough deposition rate. The vapour deposition has to be performed in a protective atmosphere, preferably in high vacuum (HV) or ultra-high vacuum (UHV), in order to prevent the metal vapour from entering into reactions with oxygen and nitrogen. The substrate is usually located sufficiently far from the source to prevent crystallization of the deposited material as a result of radiation heating.

There are only relatively few alloys or intermetallics that evaporate congruently. In most cases the constituent elements differ in vapour pressure so that their relative concentration in the deposited film will be different from that in the original material. Thermomechanical data available for several materials make it possible to predict the compositional changes in these materials and adapt the original con-

centration accordingly. If such thermomechanical information is not available it is necessary to establish the relation between the concentration in the source material and that in the deposited film in an empirical way, which may be a rather cumbersome procedure. Owing to the difference in vapour pressure it is furthermore necessary to take into account that the concentration of the source will change during the deposition process when extended over a long period or when repeated too often with the same ingot. For these reasons the vapour deposition technique involving only a single source has not found widespread application.

Far better results can be expected from multi-source techniques where each of the constituent metals is heated in a separate crucible. The composition of the deposited film will then be determined by the relative vapour pressures and hence by the relative heating rates applied to the various sources. The heating rates of each of the sources has to be controlled independently. Furthermore, in order to keep the ratio of the vapour pressures constant during the entire evaporation process, one has to be able to correct quickly for any deviation from the desired vapour pressure.

For these reasons electron beam evaporation has received considerable interest. An example of electron beam evaporation is shown in fig. 4. A steady flux of electrons is generated by a heated filament. By means of a combination of electric fields and magnetic fields this electron beam is directed into the water-cooled copper crucible containing one of the pure components. Small modulations of the magnetic fields are applied continuously in order to increase the active surface of the impinging electron beam and in order to prevent the beam from burning a hole into the ingot. For a three-component amorphous alloy three of such electron beam
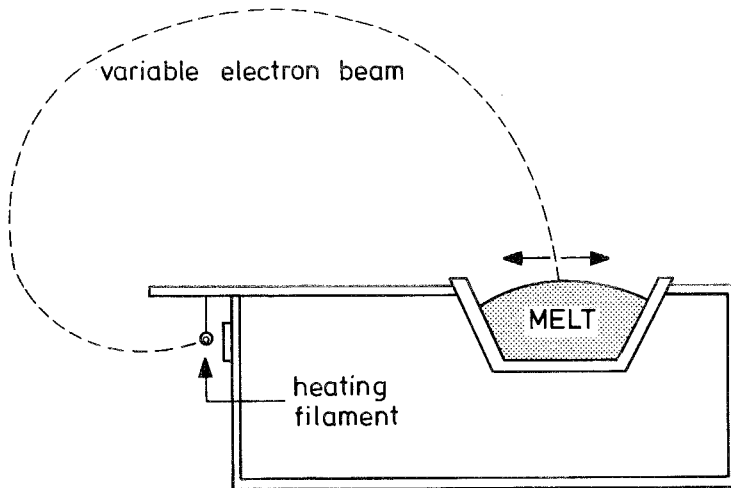
Fig. 4. Schematic representation of an electron beam source used for vapour deposition. Electrons are ejected from a hot filament at the back of the crucible housing. The path of the electron beam is controlled by means of electric and magnetic fields. The beam impinges on the metal to be evaporated, contained in a water-cooled copper crucible. Modulation of the magnetic field is used to increase the effective impingement area of the electron beam.

sources are required, the target being located in a symmetrical way with respect to each of these sources. The vapour flux from each of the sources can be continuously monitored by means of quartz crystal oscillators and controlled via a feedback loop to the electron guns. Electron gun evaporation has the advantage that changes in the desired concentration of the deposited film can be effectuated rather easily.

2.2.2. Flash evaporation

A much more modest equipment is needed in flash evaporation. This method is also suitable for the preparation of amorphous alloys whose constituents have different vapour pressures. It consists of a single heated filament usually made of molybdenum. Powder of the alloy is fed continuously onto this filament, the temperature of which is sufficiently high for evaporation. There are no shifts in composition of the alloy since all the material is evaporated to completion. Equipment for monitoring the vapour flux and the source temperature are not needed. The method is restricted to materials that can be obtained in powdered form, although it also seems possible to feed the hot filament with thin continuous wires. A disadvantage of the method is that the evaporation may not always be complete. Owing to the sudden release of gases when the alloy makes contact with the hot filament fragmentation may occur, the expelled fine particles contaminating the deposited thin films.

2.2.3. Sputtering

Thin film deposition by means of sputtering is a fairly well known method and has been employed for more than a century. An inherent drawback of the method is the tendency of the metal films to become contaminated with the inert gas atoms present as a medium. There is furthermore a multitude of process parameters to be considered. For these reasons the method has not received much attention in the past. Nowadays the ability to prepare amorphous thin films by means of sputtering is employed on a wide scale since it has been shown on different occasions that the films prepared by this method possess properties that compare favourably with those obtained by other methods.

A simplified schematic arrangement for sputtering is shown in fig. 5. The target T and the substrate on the cooled substrate holder S are inside a chamber which, after evacuation, is filled with argon gas of reduced pressure (typically 10^{-2} torr). The target consists of the alloy to be deposited and is connected to a negative high voltage supply V_T (typically -1000 V). Both substrate holder and substrate are facing the target. In many applications the substrate holder is grounded ($V_B = 0$). Frequently it proves fruitful to apply a negative bias voltage (typically $V_B = -100$ V).

After initiation of the glow discharge, positive ions impinge on the target surface and remove mainly neutral target atoms from it by momentum transfer. These atoms condense on the substrate and form the thin amorphous film. However, there may also be a number of other particles that hit the substrate during deposition. Most of these particles originate from the target and comprise secondary electrons and ions as well as gases desorbed during sputtering.
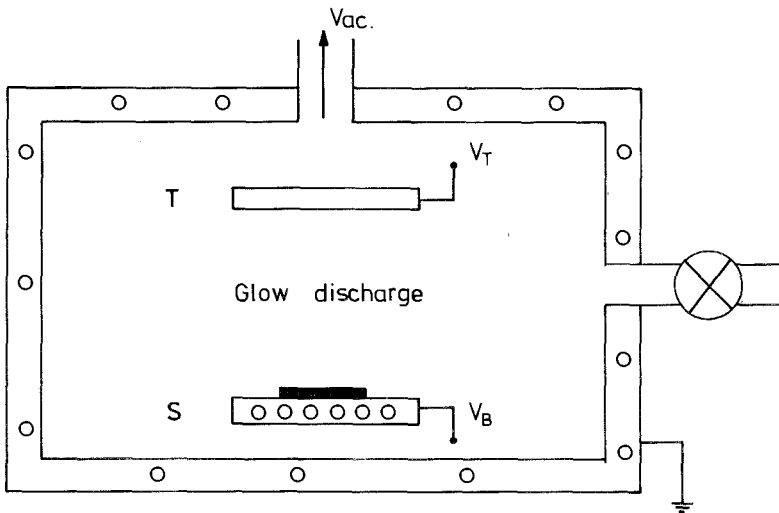
Fig. 5. Schematic representation of sputter deposition. The target T and substrate holder S are inside a cooled chamber that can be evacuated and filled with argon gas under reduced pressure. The target T is connected to a high negative voltage supply V_T. The cooled substrate holder is connected to a voltage supply V_B. The chamber itself is grounded.

The potential of the plasma associated with the glow discharge depends on the argon pressure. It is positive with respect to the chamber potential. When the substrate is not connected to the chamber its potential can be made negative either by means of a reduced argon pressure or by means of an external substrate bias voltage. In these cases one may expect sputtering of surface oxygen and resputtering of the material deposited on the substrate. This leads to structural changes in the sputter-deposited thin film.

One of the advantages of the sputtering method is that it is not necessary to have a target consisting of the alloy of the desired composition. It is equally possible to employ the pure components of the alloy. For instance, in the sputtering of amorphous Gd–Co films the target often consists of a flat Co disc covered with several smaller Gd discs, the effective surface of Co and Gd determining the ultimate composition of the deposited film.

The method as briefly outlined here is usually referred to as planar diode sputtering. Other forms of sputtering are triode sputtering, radio frequency sputtering and magnetron sputtering. For more details on sputtering the reader is referred to textbooks on this subject (Maissel and Glang, 1970; Vossen and Kern, 1978).

3. Formation

3.1. Chemical, structural and electronic factors governing glass formation

Amorphous alloys made by means of vapour quenching have frequently been reported to comprise a fairly large range of concentrations. Difficulties in preparing

amorphous alloys in this way are usually encountered in the two extreme composition ranges in a given binary system, i.e. for concentrations of less than 15% and more than 85% of one of the components. In many cases the inability to prepare amorphous alloys is the result of the crystallization temperature being close to or even lower than room temperature. Since most amorphous alloys are prepared and handled at room temperature the amorphous state then spontaneously transforms into the crystalline state during deposition or shortly after deposition.

The preparation of amorphous alloys by means of liquid quenching entails much narrower concentration ranges (for instance, only 5 at % in the Fe–B system). Many binary systems also exist in which it has even proved impossible to prepare amorphous alloys by this method (for instance Fe–Ge). The concentration ranges in binary systems where it is possible to prepare amorphous alloys by liquid quenching are often called "easy glass-forming" ranges. The term "metallic glass" is widely used for liquid-quenched alloys, indicating a certain analogy with the well-known oxide type of glasses.

The numerous glass-forming binary alloys may be divided into two main categories: metal–metal alloys and metal–metalloid alloys. The former category may again be subdivided into three subgroups comprising alloys of transition metals (3d, 4d, 5d), alloys of simple metals and alloys of transition metals with either rare earths
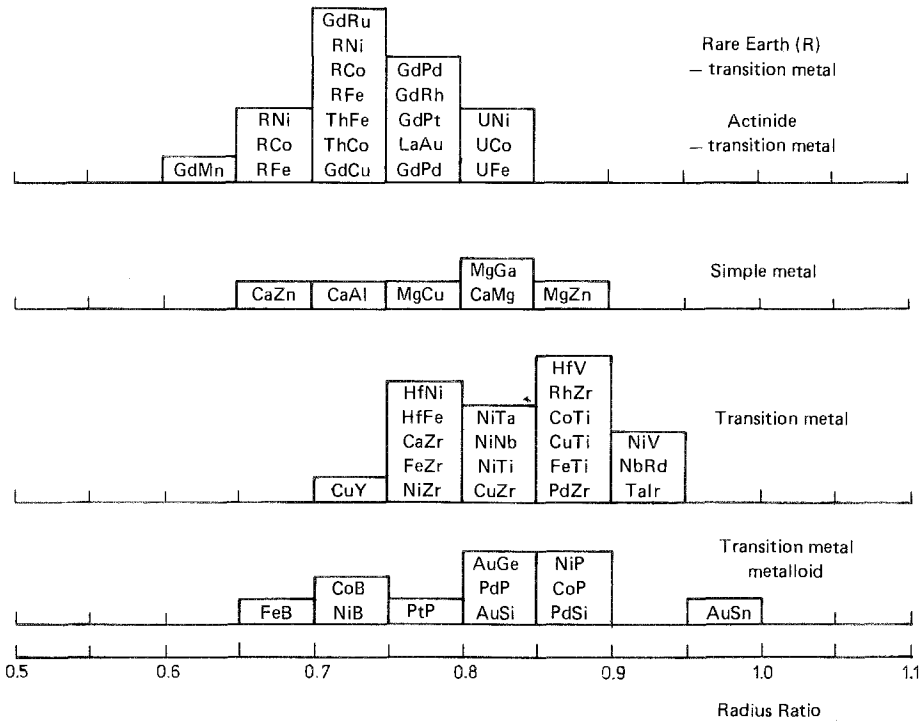
Fig. 6. Representative members of binary metallic glasses arranged according to the radius ratio of the component metals (sorted into intervals of 0.05). The data shown were taken from a paper by Gillot et al. (1983) after supplementing them with some more members and including data of actinide alloys.

or actinides. The distinction between the categories is not a sharp one since the rare earth and actinide metals can also be regarded as transition metals. Representative members of the alloys of the different categories are plotted as a function of the corresponding radius ratio in fig. 6 (Gillot et al., 1983).

Here it should be kept in mind that formation of the metallic glass is restricted to a particular concentration range. As an example we present in fig. 7 the phase diagram of Gd–Co (Buschow and Den Broeder, 1973) together with the region of easy glass formation and the region in which vapour-quenched alloys have been reported to be amorphous. It is seen that the glass-forming region extends primarily to both sides of the deep eutectic occurring near 37% Co. This feature where the glass-forming region is located at concentrations more or less symmetrically around the eutectic composition is quite generally observed. There are a few exceptions such as in the systems Gd–Fe (Buschow, 1979), Al–Ge (Shingu et al., 1976), Ca–Cu and Ca–Mg (Sommer et al., 1982b).

Several attempts have been made to analyse the factors that govern the glass-forming tendency. Masumoto and Maddin (1975) related the glass-forming tendency to the position of the component elements in the periodic table. The glass-forming tendency is enhanced if the constituent elements come from different parts of the periodic table so as to give rise to large differences in valency and atomic size. Wang and Merz (1976) associated the formation of the amorphous phase with a high
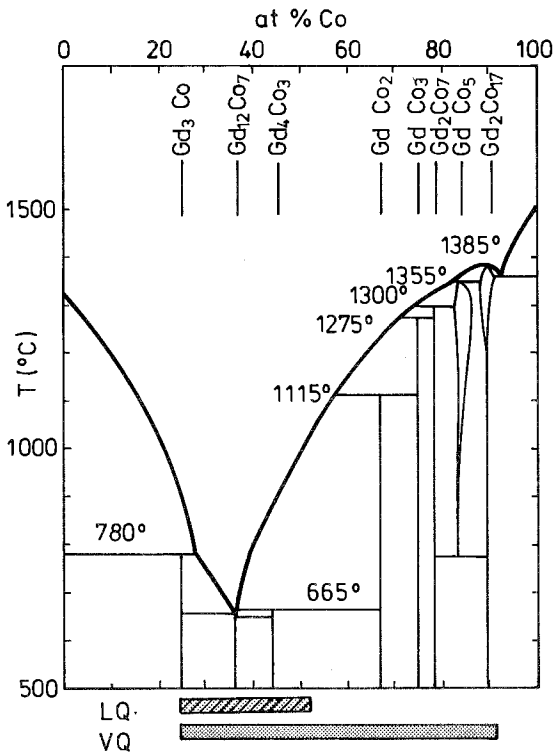
Fig. 7. Phase diagram of the Gd–Co system. Data are from the papers published by Buschow and Den Broeder (1973) and by Parthé and Moreau (1977). Hatched and shaded bars at the bottom indicate the extent of the ranges in which amorphous alloys can be obtained by liquid quenching (LQ) or vapour quenching (VQ).

degree of bonding anisotropy and a high polymorphicity. Polk and Giessen (1978) also concluded that the radius ratio difference is of prime importance for the glass-forming tendency, the requirement being a radius ratio below 0.88. The proliferation in the preparation of metallic glasses differing widely in composition has shown that all the criteria for easy glass formation mentioned above are less generally valid than was initially thought. This can easily be verified by viewing these criteria against the data shown in fig. 6.

In a more recent description of the glass-forming tendency Giessen and Whang (1980) advocate the use of so-called ready-glass-formation plots for obtaining a division between combinations of elements leading to easy glass formation and combinations where this tendency is absent. In such plots the heat of mixing (ΔH_{m}) is plotted versus the corresponding radius ratio (r/R). The former values, if not available from experimental results, can be estimated by means of the model of Miedema et al. (1980). Giessen and Whang suggest that easy glass formation may be expected in binary systems obeying the criteria $r/R < 0.85$ and $\Delta H_{\mathrm{m}} < -42$ kJ/mol (-10 kcal/mol). Their result is quite convincing when applied to Ni alloys. It is less satisfactory, however, when applied to the relatively large group of Fe alloys. It can be derived from the results shown in fig. 8 that virtually none of the Fe alloys plotted satisfies the criteria mentioned above.
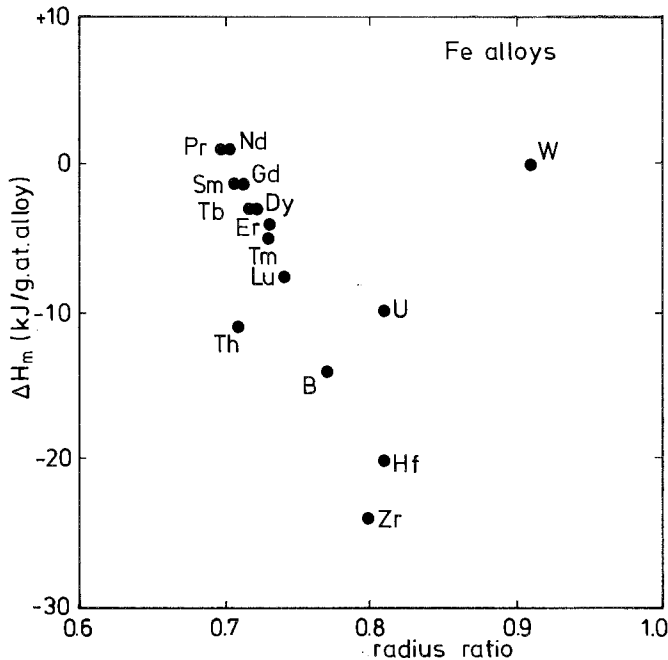
Fig. 8. Heat of mixing (ΔH_{m}) versus radius ratio in Fe base metallic glasses. The R–Fe alloys comprise the approximate composition $R_{0.45}Fe_{0.55}$ when R represents Pr or Nd (Croat, 1981a, b), $R_{0.3}Fe_{0.7}$ when R represents Sm through Lu (Buschow, 1981a), $A_{0.6}Fe_{0.4}$ when A = Zr (Buschow, 1981b) or Hf (Buschow and Beekmans, 1980a), $Th_{0.50}Fe_{0.50}$ (Buschow and Beekmans, 1979a), $U_{0.6}Fe_{0.4}$ (Giessen and Elliot, 1978), $W_{0.5}Fe_{0.5}$ (Wang et al., 1978). The ΔH_{m} values were derived by means of the model of Miedema et al. (1980).

Ramachandrarao (1980) based his model of glass formation on molar volume considerations. He used the method of Varley (1959) to estimate the composition at which the average molar volume will be at a minimum and showed that the glass-forming composition range is determined by the fractional negative deviation of the volume with respect to the ideal volume of mixing. Unfortunately Ramachandrarao did not include in his model the effect of volume contractions due to charge transfer upon alloying. These latter effects may be quite strong in some of the alloy systems considered by this author.

Nagel and Tauc (1976, 1977) approached the description of the glass-forming tendency in quite a different way. These authors note that this tendency will be enhanced near that composition in a binary alloy system where the Fermi vector $2k_F$ equals Q_p, the principal peak position in the structure factor $S(Q)$. At this composition the total energy of the liquid will be relatively low and the eutectic which occurs at this composition will be deep, a situation favourable for glass formation. Owing to the occurrence of a pseudo gap in $S(Q)$ for $2k_F = Q_p$ the corresponding alloys are also considered to possess a relatively high stability against crystallization.

The Nagel and Tauc model has been subjected to serious criticism. Part of this criticism is directed against the application of the nearly free electron model to the alloys considered (Riley et al., 1979) and the possibility of reaching the condition $2k_F = Q_p$ in certain alloy systems (Mizutani and Massalski, 1980). One has also to take into consideration that the eutectic composition is primarily determined by the large difference in the free energies of solid formation of the constituent elements and not so much by a special structural property of the liquid (Allen et al., 1980). So the merit of the Nagel and Tauc model with regard to the formation of glassy alloys is primarily associated with the explanation of the enhanced deepness of the eutectic when $Q_p = 2k_F$ (Beck and Oberle, 1978).

As we will see in the next section, a relative low melting temperature T_m is indeed favourable for glass formation. Since the Nagel and Tauc model has mainly been used to describe the stability of amorphous alloys we will treat this model in more detail in section 4.

3.2. *Kinetic approach to glass formation*

The kinetic approach to glass formation (Turnbull, 1969; Uhlman, 1971; Davies, 1976) has proved to be most successful in relating the glass-forming tendency to other physical quantities. Implicit in this approach is that any liquid alloy is a glass former, provided it is cooled sufficiently rapidly to below a temperature at which crystallization does not occur. In this section we will closely follow the analysis given by Davies (1976). The equations used by Davies are reproduced below (eqs. 1–5). In section 3.2.1 we will use only the final result (eq. 5) of this analysis and describe its implications for the critical cooling rates. Readers who are not interested in the details of the derivation of eq. (5) can jump immediately to section 3.2.1.

The transformation from the liquid alloy to the solid crystal can be described by

means of the kinetic equation due to Johnson and Mehl (1939) and Avrami (1940):

$$X = 1 - \exp(-kt^n), \tag{1a}$$

where X represents the volume fraction that has crystallized in the time t. The quantity k is the rate constant and n is the Armi exponent which indicates the type of the transformation. For a constant nucleation frequency I_v^{hom} one has $n = 4$. Using only the first term in the expansion of eq. (1a) for incipient crystallization (X small) one obtains

$$X \simeq \frac{\pi}{3} I_v^{hom} u^3 t^4, \tag{1b}$$

where both the homogeneous nucleation frequency I_v^{hom} and the growth velocity u of the crystal–liquid interface are assumed to be independent of time.

Since the atomic motion associated with the nucleation is thermally activated one has

$$I_v^{hom} = \frac{N_v^0 D_n}{a_0^2} \exp\left(\frac{-\Delta G^*}{kT}\right), \tag{2a}$$

where N_v^0 is the average number density of atoms per unit volume, a_0 the mean atomic diameter, D_n the diffusion coefficient across the nucleus–liquid interface at a temperature T and ΔG^* the free energy of formation of a critical nucleus. Using the result of Uhlman et al. (1966), i.e. $\Delta G^*/kT \approx 50$ when the undercooling $\Delta T_r = (T_m - T)/T_m$ equals 0.2, eq. (2a) reduces to

$$I_v^{hom} = \frac{N_v^0 D_n}{a_0^2} \exp\left(\frac{-1.024}{T_r^3 \Delta T_r^2}\right), \quad \Delta T_r = (T_m - T)/T_m, \tag{2b}$$

where $T_r = T/T_m$, T_m being the melting temperature.

The growth of the particles is also a thermally activated process requiring atomic motion of the order of an interatomic distance, leading to the relation (Turnbull, 1962):

$$u = \frac{f D_g}{a_0} \left[1 - \exp\left(\frac{-\Delta T_r \Delta H_f^m}{RT}\right)\right] \tag{3}$$

where ΔH_f^m is the molar heat of fusion, f the fraction of sites at the crystal where growth is possible and D_g the diffusion coefficient at the crystal–liquid interface. If one assumes that D_n and D_g are equal and can be described by means of the Stokes–Einstein relation

$$D = kT/3\pi a_0 \eta \tag{4}$$

($\eta =$ bulk liquid viscosity) one arrives at the following relation between the time t_x needed for the formation of a small quantity X of crystalline material, i.e.

$$t_x \sim \frac{9.3}{kT} \eta \left(\frac{X a_0^9}{f^3 N_v^0} \frac{\exp(1.024/T_r^3 \Delta T_r^2)}{[1 - \exp(-\Delta H_f^m \Delta T_r/RT)]^3}\right)^{1/4}. \tag{5}$$

The quantity X is somewhat arbitrary. For barely incipient crystallization one may use the value $X = 10^{-6}$ (Davies, 1976). For a rough interface one may use $f = 1$, while for a smooth interface $f = 0.2 \, \Delta T_r$ is a better approximation.

3.2.1. Critical cooling rates

For a given alloy the insertion of the appropriate parameters ΔH_f^m, T_r, f, a_0, N_r^0 and η in eq. (5) leads to a relation between the time and the temperature of the incipient liquid-to-crystalline transformation. Eq. (5) can therefore be used in constructing the so-called TTT diagrams (time–temperature–transformation). The viscosity is usually taken equal to 10^{13} at the glass temperature T_g, below which the metallic glass is effectively rigid. For values between T_g and T_m the viscosity can be estimated either by extrapolation or by using the Vogel–Fulcher relationship (for more details see Davies, 1976). The TTT diagrams usually have a form like that shown in fig. 9. Crystallization of an alloy will occur after cooling the melt from the melting temperature T_m under conditions that one passes through the shaded area in the diagram. The critical cooling rate for glass formation can therefore be visualized as the cooling rate required to just bypass the nose of this shaded region, leading to the relation

$$R_c = (T_m - T_N)/t_N, \tag{6}$$

where T_N and t_N are the temperature and time corresponding to the nose in the TTT diagram. Davies notes that critical cooling rates, as obtained with eq. (6), may overestimate the required rates, since no account has been taken of the effect of continuous cooling. The construction of continuous cooling curves (CCT) from the isothermal (TTT) curves would have led to R_c values being lowered by a factor of about two.
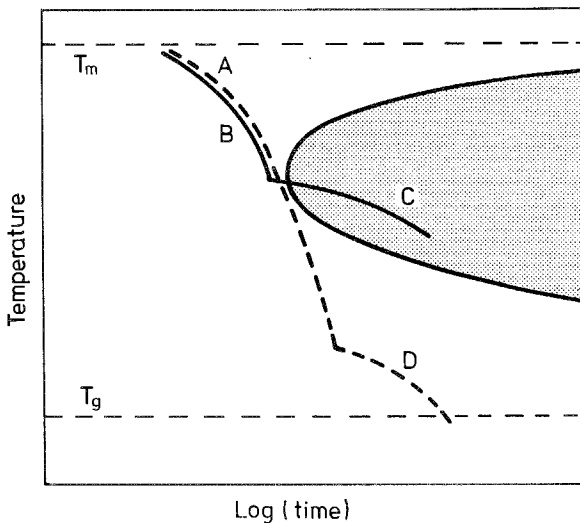
Fig. 9. Schematic representation of a Time–Temperature–Transformation diagram (after Davies, 1978). The full line represents the time–temperature relation for incipient liquid-to-crystalline transformation; T_m is the melting temperature, T_g the glass temperature. A schematic representation of the time–temperature relationship during melt spinning is given by the broken line AD. The relationship during twin roller quenching is given by the full line BC. The deflection of the lines AD and BC into a more horizontal direction corresponds to the time at which the alloy is no longer in contact with the wheels, the contact time in twin roller quenching being shorter than in melt spinning.
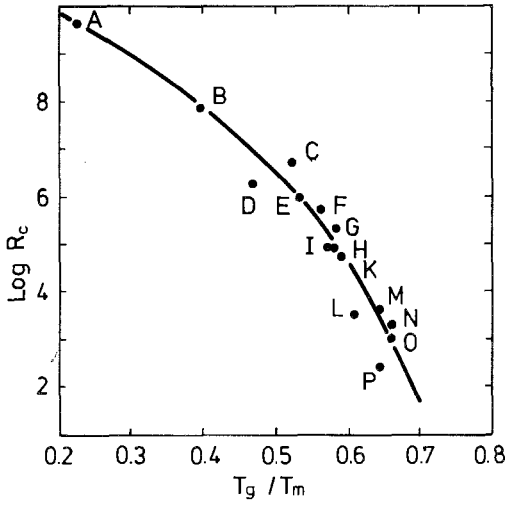
Fig. 10. Calculated values of the critical cooling rate for glass formation (R_c) as a function of the reduced glass temperature ($T_{rg} = T_g/T_m$). The compositions of the melts are: Ni (A), Te (B), $Fe_{0.83}B_{0.17}$ (C), $Au_{0.778}Ge_{0.138}Si_{0.084}$ (D), $Fe_{0.415}N_{0.415}B_{0.17}$ (E), $Co_{0.75}Si_{0.10}B_{0.15}$ (F), $Fe_{0.79}Si_{0.10}B_{0.11}$ (G), $Ni_{0.75}Si_{0.08}B_{0.17}$ (H), $Pt_{0.60}Ni_{0.15}P_{0.25}$ (I), $Fe_{0.80}P_{0.13}C_{0.07}$ (K), $Pd_{0.82}Si_{0.18}$ (L), $Cu_{0.60}Zr_{0.40}$ (M), $Ni_{0.624}Nb_{0.376}$ (N), $Pd_{0.40}Ni_{0.40}P_{0.20}$ (O), $Pd_{0.775}Si_{0.165}Cu_{0.06}$ (P). The data are reproduced from the paper by Lewis et al. (1977).
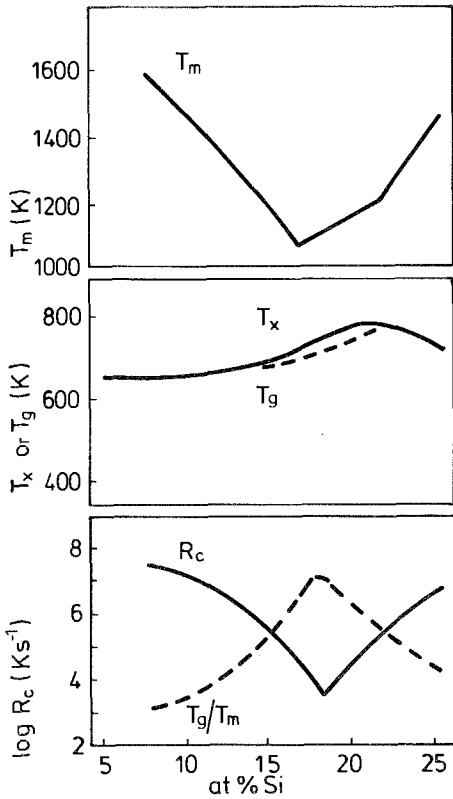
Fig. 11. Composition dependence of the melting temperature T_m (Elliott, 1965), the glass temperature T_g and the crystallization temperature T_x, the ratio T_g/T_m and the critical cooling rate R_c (Lewis and Davies, 1977) in the Pd–Si system.

In a semi-empirical way Davies (1978) showed that the position of the nose (T_N, t_N) is closely related to the ratio T_g/T_m. The implications of this for the critical cooling rate I_c may become clear from the results shown in fig. 10, where R_c is plotted versus the reduced glass temperature $T_{rg} = T_g/T_m$. These results stress the important role played by the melting temperature T_m.

In most practical cases the glass temperature T_g varies only little over the glass forming region. As seen, for instance, in the $Pd_{1-x}Si_x$ system shown in fig. 11, the values of the glass temperature T_g (or the values of the crystallization temperature T_x if T_g cannot be discerned experimentally) do not vary more than 200 K. The values of T_m vary much more drastically in this range so that R_c has a very sharp minimum near the eutectic composition, its value increasing orders of magnitude on either side of this composition. These results form a fair demonstration of what has long been recognized empirically, that the high glass-forming tendency is to be found close to the eutectic compositions in systems giving rise to a deep eutectic.

3.2.2. *Maximum thickness of metallic glasses*

The results obtained in the previous section lend themselves well to estimating the maximum thickness (x_m) of glassy ribbons obtained by means of liquid-quenching techniques (Davies, 1976). In those cases where x_m is relatively large, so that the heat transfer is mainly controlled by the thermal diffusivity D_t and not by the heat transfer coefficient at the interface between the alloy and the thermal sink h_i, the maximum thickness x_m can be related to the nose position in the TTT diagram:

$$x_m = \sqrt{D_t t_N} . \tag{7}$$

For Ni- and Pd-based alloys Davies used the value $D_t \approx 10 \ mm^2 \ s^{-1}$ and predicted the values $x_m = 0.4$ mm, 2.0 mm and 0.5 μm for $Pd_{82}Si_{18}$, $Pd_{77.5}Cu_6Si_{16.5}$ and Ni, respectively. These values are in satisfactory agreement with the maximum thickness observed experimentally.

4. Stability of amorphous alloys

4.1. *Experimental methods for studying crystallization*

The formation enthalpy ΔH_f of amorphous alloys is less negative than that of crystalline materials of similar composition, which means that the former alloys are metastable. As a function of temperature and time the amorphous alloys will therefore transform into the stable crystalline phases. This transformation can conveniently be studied by means of diffraction methods. As will be discussed later on, no sharp diffraction lines occur in the diffraction diagrams of amorphous alloys. The transformation into the crystalline state is generally accompanied by the occurrence of sharp diffraction peaks. In some cases the stable crystalline phases are not reached directly. First one or more metastable crystalline phases may be formed which transform into the stable end products at a later stage of the crystallization process.
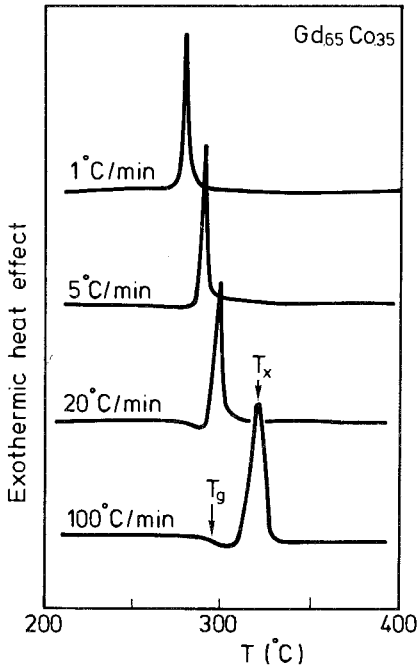
Fig. 12. Results of DSC measurements on amorphous $Gd_{0.65}Co_{0.35}$ made by means of melt spinning. From top to bottom the heating rate is varied from $s = 1°C/min$ to $s = 100°C/min$. In the latter curve the positions of the glass temperature (T_g) and crystallization temperature (T_x) are indicated.

Differential scanning calorimetry (DSC) has been widely used to study the thermally induced transformations in amorphous alloys. In this method the sample in a sample holder (S) is heated simultaneously with a blank sample holder (B) while the heat needed to keep the temperature of S and B the same is recorded continuously. For alloys based on rare earths it is required to perform the DSC measurement in an inert atmosphere. Examples of DSC measurements are shown for $Gd_{65}Co_{35}$ in fig. 12.

The various curves were obtained with different heating rates (s), varying from $s = 1°C/min$ to $s = 100°C/min$. For the curve measured with $s = 100°C/min$ the positions of the glass temperature and crystallization temperature have been indicated by arrows. No heat effects are observed upon cooling of the sample from temperatures above T_x, indicating the irreversible nature of the crystallization process.

The dependence of the crystallization temperature (T_x) on the heating rate (s) can be used to obtain experimental values for the activation energy of crystallization (Luborsky and Liebermann, 1978; Scott, 1978). The method of analysis is based on the results of Kissinger (1957). For a first-order rate process one may write

$$\left(\frac{dx}{dt}\right)_T = k(1-x), \tag{8}$$

where x represents the fraction of amorphous material transformed in time t at temperature T. For a thermally activated process the rate constant k can be

described by means of an equation of the Arrhenius type:

$$k = k_0 \exp(-\Delta E / RT),$$ (9)

where k_0 is the pre-exponential factor and ΔE the activation energy. Taking account of the temperature changing with time one finds

$$\frac{dx}{dT} = \left(\frac{\delta x}{\delta t}\right)_T + \left(\frac{\delta x}{\delta T}\right)_t \frac{dT}{dt},$$ (10)

where the second term on the right-hand side can be shown to be equal to zero. Combining eqs. (8)–(10) one has

$$\frac{dx}{dt} = k_0 (1 - x) \exp(-\Delta E / RT).$$ (11)

The reaction rate at the peak of the exothermic heat effect is a maximum, its time derivative being equal to zero. After setting the time derivative of eq. (11) to zero, inserting $T = T_x$ for the peak maximum and $s = dT/dt$ for the heating rate, one finds

$$k_0 \exp(-\Delta E / RT) = (\Delta E / RT_x^2) s.$$ (12)

It follows from eq. (12) that values of the activation energy ΔE can be obtained from the slope of plots of $\ln(sT_x^{-2})$ versus T_x^{-1}. Later on Boswell (1980) showed that it is more appropriate to derive ΔE values from plots of $\ln(sT_x^{-1})$ versus T_x^{-1}. An example of such a plot is shown in fig. 13 for $Dy_{60}Co_{40}$ (Buschow, 1982a). In practice the ΔE values derived from plots according to Kissinger do not differ much from those derived from plots proposed by Boswell.
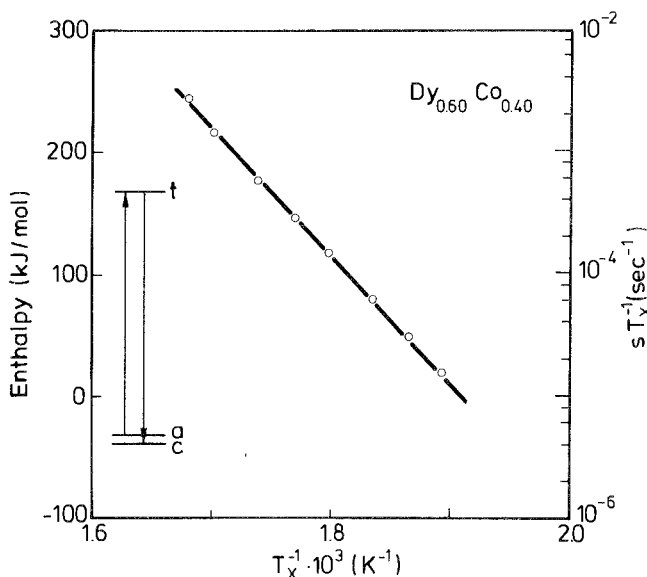
Fig. 13. Kissinger–Boswell plot of the crystallization temperature T_x in amorphous $Dy_{0.60}Co_{0.40}$ studied as a function of the heating rate s (bottom and right-hand scales). The level scheme on the left-hand side indicates the relative energies of the crystalline state (c), the amorphous state (a), and the transitional or activated state (t).
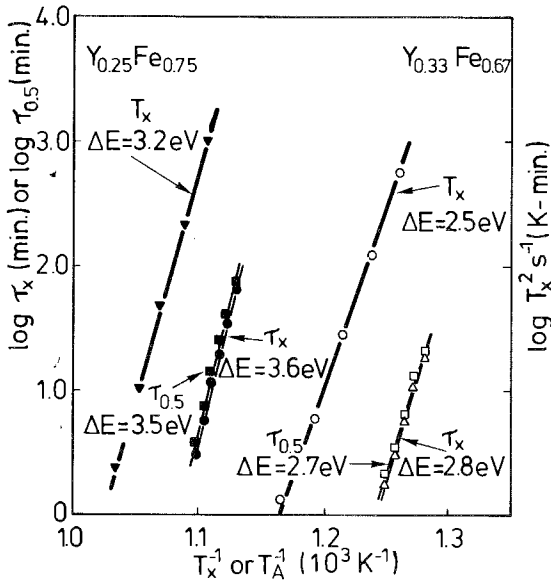
Fig. 14. Transformation rates obtained by Croat (1982a) using DSC measurements on $Y_{0.25}Fe_{0.75}$ (full symbols) and $Y_{0.33}Fe_{0.67}$ (open symbols). The times $\tau_{0.5}$ and τ_x correspond to the elapsed time to 50% conversion and to conversion at T_x, respectively (isothermal annealing plots). T_A is the annealing temperature. Values of $\log \tau_x$ and $\log \tau_{0.5}$ are plotted versus T_x^{-1} and T_A^{-1}, respectively. The crystallization temperatures as defined in fig. 12 (T_x) are used to plot $\log(T_x^2/s)$ versus T_x^{-1}, s being the heating rate (Kissinger plots). The activation energies ΔE derived from the slopes of the plots involving T_x, τ_x or $\tau_{0.5}$ are included in the figure.

An alternative way of determining the activation energy ΔE by means of DSC is isothermal annealing. Integration of eq. (8) leads to the expression:

$$\ln \tau + \text{const.} = \Delta E/kT_A, \tag{13}$$

where τ is the time needed to obtain the transformation of a fraction x at a given annealing temperature T_A. Results obtained by Croat (1982a) on two Y–Fe alloys are reproduced in fig. 14. The straight lines through the data points obtained with $\tau = \tau_{0.5}$ and $\tau = \tau_x$ refer to a conversion of 50% and a conversion corresponding to the peak T_x in the normal DSC plot (see fig. 12), respectively. Included in the figure are plots of $\log(T_x^2/s)$ versus T_x^{-1} (Kissinger method). The values of the activation energies ΔE obtained from the various plots agree within 10% for each of the alloys investigated.

4.2. Models for describing the stability

In the literature several models have been described in which amorphous alloys are considered to be relatively stable if certain requirements are fulfilled. In many of the alloys $A_{1-x}B_x$ that can be obtained in the amorphous state there is a substantial difference in size between the metallic radii of the components ($r_A > r_B$). In addition, the composition of many amorphous alloys made by means of liquid quenching is close to $x = 0.2$. This led Polk (1970) to propose a stability criterion for amorphous alloys in which the size difference in atomic radii and the asymmetry in composition is of prime importance. This stability criterion is based on the possibility of obtaining a higher packing density when the holes available in the dense random packing of the larger A atoms are filled by the smaller B atoms. In recent years it has

been found that many amorphous alloys can be prepared that are relatively rich in the B component, meaning that the Polk criterion and the associated picture of filling up holes has lost much of its predictive power.

A second widely used stability criterion is that of Nagel and Tauc (1975). The Nagel and Tauc model has already been briefly mentioned in connection with glass formation, which is not the same as glass stability since an alloy having a high glass-forming tendency need not be a relatively stable glass. The implications of the Nagel and Tauc model for glass formation and glass stability are therefore different. Nagel and Tauc pointed out that a close analogy exists between the stability of so-called Hume-Rothery electron compounds and the stability of amorphous alloys having a particular valence electron concentration. In Hume-Rothery compounds the crystal structure entails the presence of Brillouin zone planes in reciprocal space, and the interaction of these planes with the electron states near the Fermi surface can lead to a lowering of the density of states and hence to an increased stability.

In amorphous alloys the situation is more complicated. Nagel and Tauc argue that here an analogous interaction may occur between the electron states near E_F and the first pronounced maximum in the structure factor $S(Q)$ associated with the Fourier transform of the atomic radial distribution function. This leads to a pseudo-gap or hybridization gap in the density of states near E_F (such as schematically shown in fig. 15) when the wave vector Q_p of the maximum in the structure factor equals the diameter $2k_F$ of the Fermi sphere. Owing to the lowered kinetic energy of the conduction electrons (fig. 15) amorphous alloys are expected therefore to be stable when $Q_p \approx 2k_F$. In the free electron model (where k_F^3 is proportional to the number of valence electrons) this has as a result that the energetically favourable situation $2k_F \approx Q_p$ can always be reached at a given concentration in an alloy system in which a monovalent metal is combined with a polyvalent metal. Close to this particular concentration one expects to find at the same time a reduced density of states near E_F and an enhanced resistance to crystallization (higher crystallization temperatures).

As already mentioned, several experimental results have recently been reported that are in conflict with the nearly free electron approach associated with the Nagel
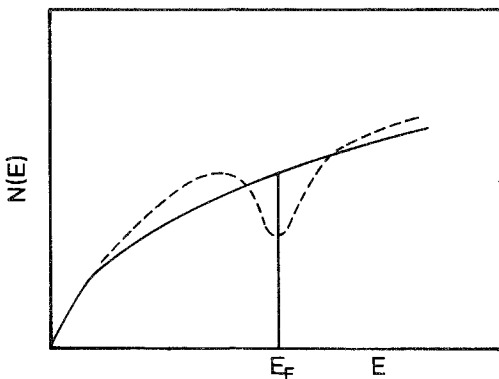
Fig. 15. Pseudo-gap formation in the density of states curve of amorphous alloys (broken line) near E_F when the condition $Q_p = 2k_F$ is met. For more details see text.

and Tauc stability criterion. More fundamental shortcomings of the model for describing the thermal stability of amorphous alloys will be outlined below. Merits of the model in describing physical quantities other than thermal stability will be discussed in section 8.

In both the above-mentioned stability criteria the stability of the amorphous alloys is measured as the energy difference between the crystalline and the amorphous state. Undoubtedly, this energy difference ΔH_{cr} can be regarded as a measure of the driving force for the transformation of amorphous into crystalline material. It will be shown, however, that this energy difference is actually small compared with the activation energy (ΔE) that appears in the rate equations of the transformation reaction of the amorphous alloy into crystalline material discussed in the previous section.

Both the quantities ΔH_{cr} and ΔE are relatively easily accessible to experimental determination. The magnitude of the exothermic heat effect observed when an amorphous alloy is heated in a calorimeter up to its crystallization temperature (T_x) is a direct measure of ΔH_{cr}. It can be derived from the area under the exothermic DSC peak. The activation energy ΔE can be obtained, for instance, from an Arrhenius-type plot when the crystallization temperature T_x is studied as a function of the heating rate (see section 4.1).

Results for amorphous $Dy_{0.60}Co_{0.40}$ were shown in the previous section. The slope of the straight line in fig. 13 leads to $\Delta E = 201.3$ kJ/mol. The heat effect itself has been reported to be equal to $\Delta H_{cr} = 5.67$ kJ/mol (Buschow, 1982a). The relative energies of the crystalline (c), amorphous (a) and transitional or activated state (t) are indicated on the left-hand side of fig. 13. Similar results have been obtained for many other amorphous alloys (Ansara et al., 1982; Eifert et al., 1982; Buschow, 1982b). In all these cases the energy difference $\Delta E = E_t - E_a$ is about two orders of magnitude larger than the energy difference $\Delta H_{cr} = E_a - E_c$ (see inset of fig. 13).

From these results it can be concluded that any favourable $(2k_F = Q_p)$ or unfavourable $(2k_F \neq Q_p)$ influence on E_a, even if it were of the order of ΔH_{cr}, would have little effect on the magnitude of ΔE. This means that the Nagel and Tauc criterion is less suited for describing thermal stability of amorphous alloys, i.e. their resistance against crystallization. As briefly indicated above, it is mainly the transformation kinetics that governs the thermal stability of amorphous alloys. A description of the kinetic approach to thermal stability will be presented in the following section.

4.3. Kinetic approach to stability

In the kinetic approach to thermal stability of amorphous alloys the rate of transformation is assumed to be diffusion-controlled (Uhlman, 1972; Davies, 1976; Takayama, 1976). Atomic motion is expected in all alloys to set in at a temperature T_x where the viscosity η reaches a critical value (about 10^{13} P). In terms of entropy theory of viscous flow as proposed by Adam and Gibbs (1965) this latter quantity can be given by

$$\eta = \eta_0 \exp(\Delta E / S_c T), \tag{14}$$

where η_0 and ΔE are constant. The quantity ΔE is a measure of the potential energy barrier for cooperative atomic transitions. S_c represents the configurational entropy. This quantity decreases exponentially with temperature below the melting point. At temperatures lower than the glass temperature T_g it adopts small values and can be regarded as being approximately temperature independent.

In a first approximation one may assume that the atomic arrangement in all amorphous alloys is similar and corresponds to a statistical distribution of atoms. In that case the values of S_c can be taken to be the same in all alloys. The thermal stability of the glass, when expressed in terms of T_g (or its upper limit T_x), is therefore mainly determined by ΔE. In fact one would derive from eq. (14) that T_g (or T_x) in all alloys is proportional to ΔE, i.e.

$$T_x = \text{const.} \times \Delta E. \tag{15}$$

Eq. (15) would allow the prediction of T_x if it were possible to estimate values of ΔE. Based on the assumption that ΔE is largely determined by the cohesive energy, three different approaches to the estimation of ΔE have been proposed.

In the first approach ΔE is taken to be proportional to a weighted mean of the heat of sublimation or heat of vaporization of A and B in $A_{1-x}B_x$ (Davies, 1976). Although a reasonable correlation is found in a certain class of materials between experimental T_x values and calculated ΔE values, this method does not always lead to the right answer in the prediction of trends. This is shown, for instance, in fig. 16 where T_x is found to increase in going from La to Lu while the heat of vaporization shows the opposite behaviour.

In the second approach ΔE is considered to be largely determined by the heat of formation ΔH_f of the corresponding crystalline phase (Takayama, 1976; Buschow and Beekmans, 1980b; Kübler et al., 1981). This may lead to satisfactory results
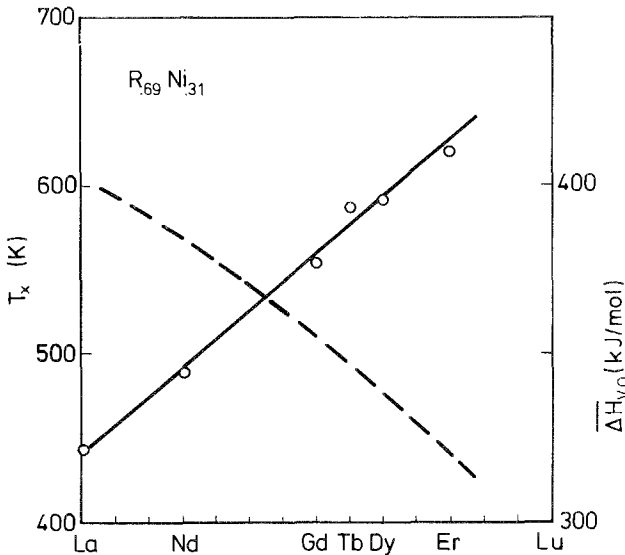
Fig. 16. Crystallization temperature in amorphous $R_{0.7}Ni_{0.3}$ alloys as a function of the R component. The broken line shows the trend expected on the basis of the mean vaporization energy (right-hand scale).
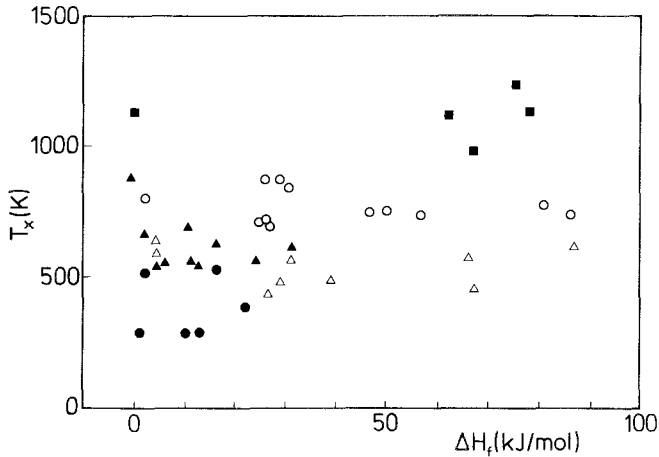
Fig. 17. Plot of experimental T_x values versus calculated ΔH_f values: ▲ actinide-base alloys, △ rare earth base alloys, ■ refractory metal-base alloys, ● Sn-base alloys, ○ alloys based on Ti, Zr or Hf. Details regarding the composition of the various alloys and the calculation of the ΔH_f values are given in table 1.

within a small group of amorphous alloys. A correlation between T_x and ΔH_f is seen (fig. 17) to be absent, however, when the approach is extended to a large number of different amorphous alloys comprising rare earth elements, actinide elements and refractory metals. The alloys that were considered in the plot of fig. 17 are listed in table 1, together with the corresponding T_x values and ΔH_f values.

In the third approach ΔE is taken to be proportional to the formation enthalpy of a hole (ΔH_h), the size of the smaller type of atom in $A_{1-x}B_x$ (Buschow and Beekmans, 1979b; Buschow, 1981c). A plot of T_x versus ΔH_h based on virtually the same materials as considered in fig. 17 is given in fig. 18. An apparent difficulty of this approach is that values of ΔH_h cannot be determined experimentally. On the other hand, these hole enthalpies can be calculated rather easily by using the results of Miedema's semi-empirical approach to describing energy effects in metals (Miedema et al., 1980). To be more specific, the hole enthalpies ΔH_h used in fig. 18 were estimated by means of the amorphous analog of the formula of Miedema (1979) for describing monovacancies in metals and alloys. If $\Delta H_{1v}^{A(B)}$ represents the formation enthalpy of a monovacancy in pure A(B) metal having a molar volume $V_{A(B)}$ the concentration dependence of ΔH_h in the alloy $A_{1-x}B_x$ can be given by

$$\Delta H_h = c\Delta H_{1v}^B + (1-c)(V_B/V_A)^{5/6}\Delta H_{1v}^A, \tag{16}$$

where c is an effective concentration and

$$c = xV_B^{2/3}\left[xV_B^{2/3} + (1-x)V_A^{2/3}\right]^{-1}. \tag{17}$$

Values of the quantities $\Delta H_{1v}^{A(B)}$ listed for most metallic elements in the paper of Miedema (1979), were used to calculate ΔH_h. The results of fig. 18 are quite convincing in showing the existence of the relation between T_x and ΔH_h proposed above. The broken line in fig. 18 corresponds to

$$T_x = c\Delta H_h, \tag{18}$$

TABLE 1

Crystallization temperature (T_x) for several amorphous alloys and formation enthalpies (ΔH) calculated by means of Miedema's model for the corresponding (hypothetical) intermetallic compounds. The ΔH values are given in units of kJ per mol of alloy (Miedema et al., 1980).

Alloy	T_x (K)	ΔH (kJ/mol)	Ref.	Alloy	T_x (K)	ΔH (kJ/mol)	Ref.
$La_{78}Au_{22}$	453	-57	1	$Ti_{77}Co_{23}$	713	-26	1
$La_{69}Ni_{31}$	443	-25	2	$Ti_{76}Co_{24}$	706	-28	1
$Pr_{65}Ni_{35}$	473	-32	3	$Ti_{24}Co_{76}$	848	-34	1
$Pr_{60}Ni_{40}$	483	-34	3	$Ti_{22}Co_{78}$	873	-31	1
$Gd_{69}Co_{31}$	550	-21	4	$Ti_{20}Co_{80}$	863	-28	1
$Gd_{82}Rh_{18}$	563	-32	4	$Zr_{67}Fe_{33}$	700	-28	2
$Gd_{76}Pd_{24}$	569	-67	4	$Zr_{64}Co_{36}$	740	-49	6
$Tb_{60}Fe_{40}$	590	-4	1	$Zr_{64}Ni_{36}$	730	-59	2
$Tb_{50}Fe_{50}$	645	-4	1	$Zr_{70}Rh_{30}$	758	-79	2
$Dy_{69}Pd_{31}$	619	-90	1	$Zr_{66}Rh_{34}$	742	-90	1
$U_{80}Ni_{20}$	613	-16	5	$Zr_{78}Pt_{22}$	768	-85	1
$U_{60}Ni_{40}$	613	-31	5	$Nb_{55}Rh_{45}$	980	-67	1
$U_{80}Co_{20}$	545	-12	5	$Nb_{55}Ir_{45}$	1133	-78	1
$U_{60}Co_{40}$	555	-24	5	$Ta_{55}Rh_{45}$	1118	-62	1
$U_{80}Fe_{20}$	553	-6	5	$Ta_{55}Ir_{45}$	1238	-75	1
$U_{60}Fe_{40}$	560	-11	5	$W_{50}Fe_{50}$	~ 1150	0	8
$U_{65}Mn_{35}$	593	-4	5	$Sn_{73}Ni_{27}$	293	-13	9
$U_{73}Cr_{27}$	658	-2	5	$Sn_{52}Ni_{48}$	378	-22	9
$U_{73}V_{27}$	684	$+1$	5	$Sn_{83}Co_{17}$	290	-10	9
$Th_{60}Mn_{40}$	690	-10	1	$Sn_{45}Co_{55}$	528	-16	9
$Th_{37}Co_{63}$	633	-44	1	$Sn_{75}Fe_{25}$	288	-1	10
$Hf_{57}V_{43}$	808	-3	1				

1. Buschow (1982c)
2. Buschow (1981b)
3. Buschow and Beekmans (1980c)
4. Buschow et al. (1980)
5. Giessens and Elliot (1978)
6. Buschow and Beekmans (1980b)
7. Davis et al. (1978)
8. Wang et al. (1978)
9. Marchal et al. (1980a)
10. Marchal et al. (1980b)

where c is equal to 7.5 when T_x is expressed in K and ΔH_h in kJ/mol. This relation can be used to predict the crystallization temperature of alloys not yet investigated.

The hole model discussed above is different from the hole model proposed by Ramachandrarao et al. (1977) and also used by Hirata (1979). In the latter model the hole formation energy is estimated from experimental data on the changes in specific heat and thermal expansion at the glass transition. Also in this hole model a linear relationship is found between the hole formation energy and the glass transition temperature, although the model lends itself less easily for making predictions.
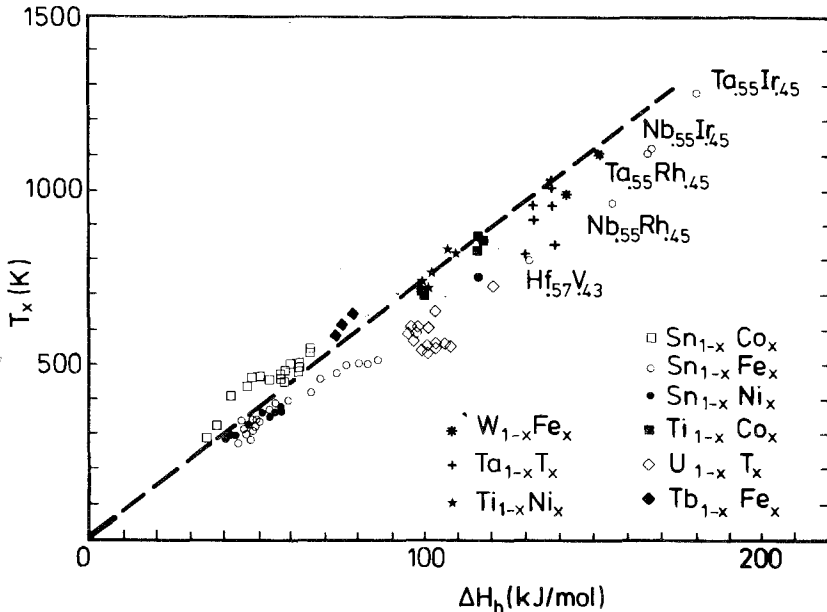
Fig. 18. Plot of experimental T_x values versus calculated ΔH_h values. Details regarding the compositions of the various alloys and the calculation of the corresponding ΔH_h values were described by Buschow (1982c).

4.4. Modes of crystallization

In general, the crystallization mode is fairly simple when the amorphous alloy has a composition which corresponds to that of a stable intermetallic compound in the phase diagram. For instance, a single sharp DSC peak was observed by Buschow and Dirks (1980a) for amorphous $Gd_{0.55}Co_{0.45}$ ($T_x = 590$ K). X-ray diffraction showed this DSC peak to be caused by crystallization of the amorphous alloy into the Gd_4Co_3 phase (see the Gd–Co phase diagram, fig. 7).

Off-stoichiometric compositions generally give rise to more complex crystallization modes. This may be illustrated by means of the results of Tenhover (1981a) shown in fig. 19 for amorphous $Y_{0.66}Fe_{0.34}$. The DSC trace, shown in the middle part of the figure, consists of two distinct exothermal heat effects, occurring at $T = T_1$ and $T = T_2$, respectively. Both heat effects are accompanied by substantial decreases in the electrical resistivity. The results of X-ray diffraction, indicated in the top part of fig. 19, give evidence that the peak at T_1 corresponds to the precipitation of α-Y. As a consequence the matrix left behind (a') must be richer in Fe than the original amorphous alloy. Apart from α-Y, no further diffraction pattern was observed. From this result one may conclude that the phase a' is composed of one (or more) microcrystalline phases or of another amorphous phase. In both cases the Fe content should be higher than corresponding to $x = 0.34$. Tenhover suggests that the matrix a' remaining after crystallization at T_1 is still amorphous and he correlated the
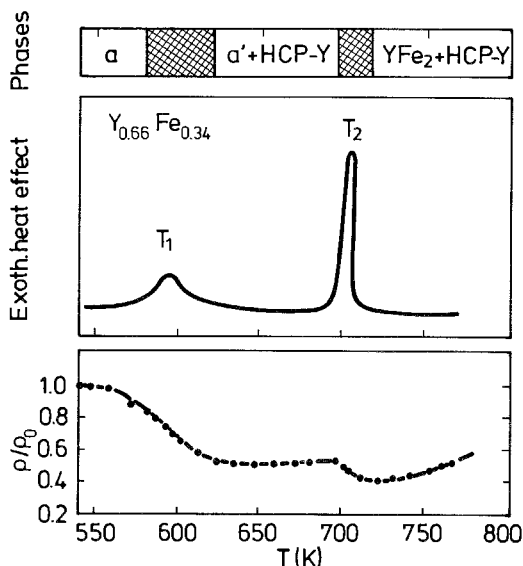
Fig. 19. Results of DSC and high-temperature resistivity ($\rho(T)$) measurements on the metallic glass $Y_{0.66}Fe_{0.34}$. The values of $\rho(T)$ have been normalized by the value of ρ_0 at room temperature ($\rho_0 = 270$ $\mu\Omega$ cm). The designations a and a' refer to completely amorphous material (a) and to the Fe-enriched amorphous phase (a') which remains as HCP-Y is formed. The scanning rates for the DSC and $\rho(T)$ measurements were 10 K min^{-1} and 1 K min^{-1}, respectively (after Tenhover, 1981a).

increase in Fe concentration of this matrix with the increase in isomer shift observed by means of ^{57}Fe Mössbauer spectroscopy. The second exothermic peak ($T = T_2$) was found by X-ray diffraction to correspond to crystallization of the phase YFe_2. The composition $Y_{0.66}Fe_{0.34}$ corresponds to the two-phase region $Y-YFe_2$ in the $Y-Fe$ phase diagram, intermetallic compounds of lower Fe content than YFe_2 being absent. The two peaks at T_1 and T_2 therefore correspond to the two equilibrium phases that take part in the crystallization for this composition.

A more or less similar behaviour was found by Buschow (1981a) for other amorphous rare-earth–iron alloys of about the same composition ($R_{0.69}Fe_{0.31}$). Buschow and Dirks (1980a,b) studied the crystallization of amorphous $Gd_{0.60}Fe_{0.40}$ in more detail by means of transition electron microscopy. They found that the matrix a', remaining after precipitation of α-Gd at T_1, consists of α-Fe in the form of small crystallites, too small to be observable by means of standard X-ray diffraction. In $Tb_{0.70}Fe_{0.30}$ no evidence of formation of α-Fe at $T_1 < T < T_2$ was found, which was interpreted by these authors as meaning that the phase a' remaining after precipitation of α-Tb at T_1 is still amorphous and of higher Fe concentration than the original melt-spun alloy. These findings agree rather closely with those of Tenhover (1981a) on $Y-Fe$ alloys mentioned above.

Amorphous $Y_{1-x}Fe_x$ alloys of considerably higher Fe concentration were investigated by Croat (1982a). In the concentration range $0.4 \leqslant x \leqslant 0.67$ Croat found the relative intensity of the DSC peak at T_1 to decrease with x while the relative intensity of the peak at T_2 increased. Considering the relative amounts of the phases crystallizing and T_1 and T_2 this behaviour is to be expected. Of much more interest, however, is Croat's result that a third peak has appeared in the DSC diagrams, indicating that a further crystallization takes place at temperatures in between T_1
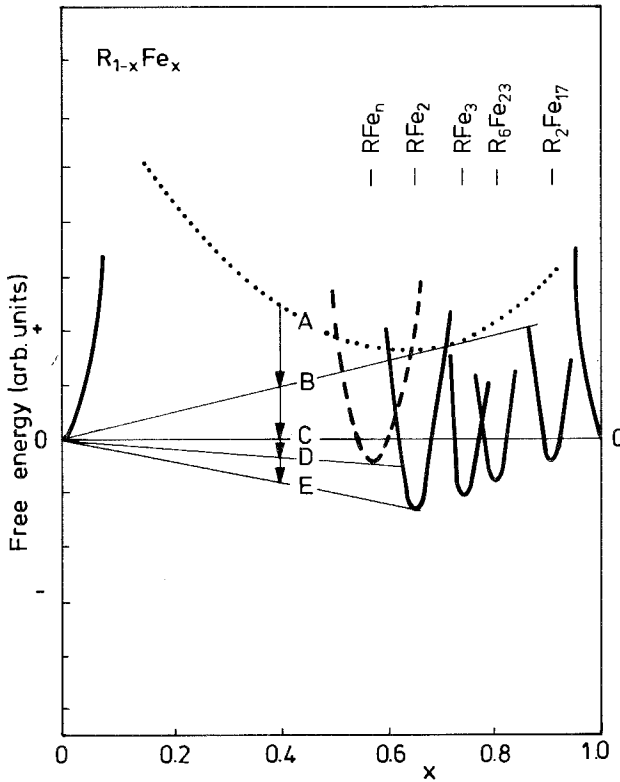
Fig. 20. Schematic representation of the free energy of stable phases (full lines) and metastable phases (broken line) in a fictitious rare-earth–iron system.

and T_2. X-ray diffraction showed that this crystallization involved the formation of a new (metastable) crystalline phase not present in the Y–Fe phase diagram.

An impression of the driving forces associated with the various types of crystallization processes can be obtained by means of fig. 20. For heavy rare earth elements the intermediate phases comprise RFe_2, RFe_3, R_6Fe_{23} and R_2Fe_{17}. For each of these phases the minimum of its free energy function (full lines in fig. 20) is lower than the straight line, being tangent to the two adjacent free energy functions. Apart from these stable phases a gamut of metastable phases may exist for which the corresponding free energy minima are situated above the tangents mentioned. For the sake of clarity only one of such phases has been included in fig. 20 (broken line). Also the amorphous phase can be considered as such a metastable phase (dotted line). It is not known at what concentration the free energy of the amorphous phase will have its minimum. For the present purpose we will assume that this energy minimum is located at the same concentration where the heat of mixing ΔH_m has its minimum. Using the model of Miedema et al. (1980) one can estimate this concentration as being located near $x = 0.65$.

The driving forces for the various transformations possible can be estimated by means of a common tangent construction. For instance, in the case of $x = 0.4$ one has to consider the tangents indicated by the thin straight lines in fig. 20. The largest

driving force for the transformation reaction is obtained when the amorphous alloy $R_{0.6}Fe_{0.4}$ transforms into R metal and the compound RFe_2 ($\Delta G = G_E - G_A$). Increasingly lower values are obtained for the transformation into R and the metastable phase RFe_n ($\Delta G = G_D - G_A$), the parent metals R and Fe ($\Delta G = G_c - G_A$), R and a more R-depleted amorphous alloy ($\Delta G = G_B - G_A$). For the sake of clarity we have left out of consideration transformations involving the other intermetallics contained in fig. 20.

If the driving force were all that mattered, crystallization would involve exclusively the path A → E in fig. 20, which corresponds to the formation of R metal and RFe_2 and gives the largest ΔG value. In practice one has to consider reaction rates and the associated activation energies rather than the ΔG values mentioned above. In fact, one may use the same arguments given in the preceding section to show that the ΔG values are less suited for describing modes of crystallization.

In general, the activation energies corresponding to the various reaction paths will be different. It follows from the experimental results described above that the reaction path A → E is avoided in the initial crystallization of R–Fe alloys. Evidently the associated activation energy is relatively high, which can be interpreted as meaning that the formation of the RFe_2 phase is hampered by difficulties in nucleation and (or) growth. Examples of the initial crystallization involving path A → B are found in the Y–Fe system (Tenhover, 1981a), and in the Tb–Fe system (Buschow and Dirks, 1980a). The transformation proceeding via path A → C as the initial step was reported to occur in the Gd–Fe system (Buschow and Dirks, 1980b). The crystallization mode reported by Croat (1982a) for alloys $Y_{1-x}Fe_x$ in the range $0.4 \leqslant x \leqslant 0.5$ is slightly more complicated since it involves three DSC peaks associated with the crystallization of α-Y, a metastable phase and YFe_2, respectively. It is not improbable that differences in the activation energies associated with the various reaction paths are the results of differences in the microstructure of the corresponding amorphous alloys, i.e. the reaction paths may depend to a certain extent on the preparatory conditions.

Crystallization of the alloy $Y_{0.33}Fe_{0.67}$ was found by Croat (1982a) to take place by means of a single thermal event (crystallization of YFe_2) and was studied by this
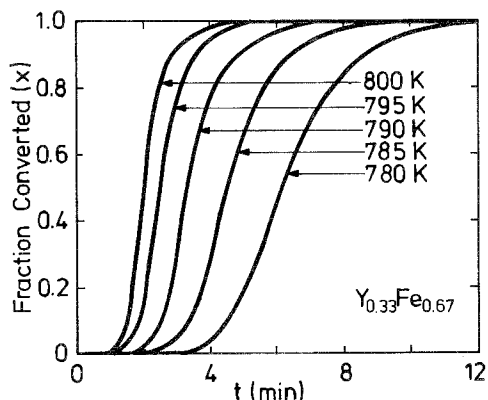
Fig. 21. Time dependence of the fraction of the melt-spun amorphous $Y_{0.33}Fe_{0.67}$ transformed (x) at various annealing temperatures (after Croat, 1982a).
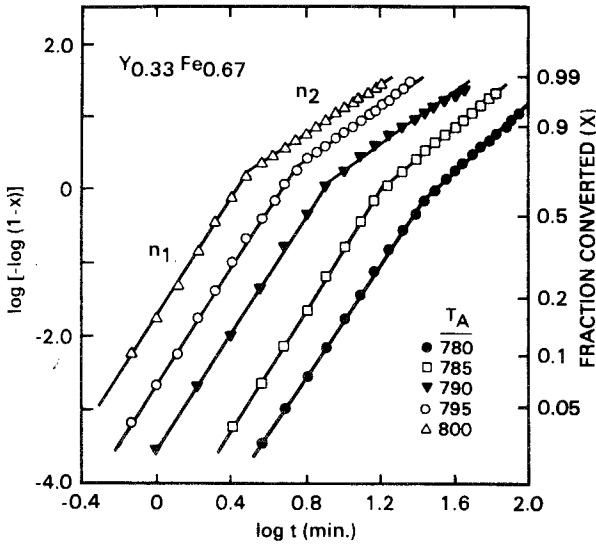
Fig. 22. Avrami plots of melt-spun amorphous $Y_{0.33}Fe_{0.67}$ corresponding to various annealing temperatures.

author in more detail. The fraction X transformed as a function of time is shown for different annealing temperatures in fig. 21. These curves display the characteristic sigmoidal time dependences expected for standard isothermal phase transformation kinetics as described by means of eq. (1a). Rewriting eq. (1a) one finds

$$\log[-\log(1 - X)] = n \log t + \text{const.} \tag{19}$$

Examples of plots made by Croat on the basis of eq. (19) are reproduced in fig. 22. It becomes apparent from these plots that the crystallization transformation consists of two separate stages. The Avrami coefficient of the first stage (n_1) is equal to about 4. This corresponds to a nucleation and growth mechanism involving a three-dimensional interface and a constant nucleation rate. The Avrami coefficient associated with the second step (after about 65% conversion) is much smaller ($n_2 \approx 2$). Criat suggested that this behaviour may be analogous to that observed in recrystallization reactions (Cahn, 1956) and that it may be due to pre-existing nucleation sites which are non-uniformly distributed. At a given stage of the transformation more nucleation sites are consumed than would correspond to the fraction crystallized, leading to a decrease in the rate of nucleation.

5. Structure of amorphous alloys

It will be clear that the considerable atomic disorder present in amorphous solids makes it impossible to give a characterization of the atomic scale structure in the same compact manner as crystalline solids. Either one is faced with innumerable parameters describing the atomic scale structure of an amorphous solid or one has to restrict oneself to a less detailed description of the structure. In practice only the

latter of these two possibilities concerns us, since the information that can be extracted from experiments on amorphous solids, however sophisticated they may be, will only be sufficient for a very rough description of the atomic scale structure.

Most of the information pertaining to the atomic scale structure of amorphous solids has come from diffraction experiments. The first part of this section will therefore be devoted to some general concepts, procedures and experimental results of diffraction studies on amorphous materials. In the second part we will discuss some other experimental means able to shed light on the difficulties associated with structural investigations in amorphous solids.

5.1. Atomic scale structure determined by means of diffraction methods

X-ray electron and neutron diffraction have all been employed in studying the structure of amorphous alloys. Although the concepts and procedures outlined below are made with reference to X-ray diffraction, they can easily be extended to neutron diffraction and electron diffraction.

In fig. 23 we compare the diffraction diagrams of an amorphous alloy with that of a crystalline alloy of about the same composition. In both cases the X-ray intensity is plotted versus the diffraction angle θ. Frequently the X-ray intensity is plotted versus the scattering vector $Q = 4\pi(\sin \theta)/\lambda$, where λ is the wavelength of the radiation applied. It is seen in fig. 23 that the absence of long-range periodicity in the structure of the amorphous alloy (top part) does not lead to sharp diffraction peaks as in the bottom part. Instead there is a strong and rather broadened principal peak followed at higher diffraction angles by several less intense but equally broadened peaks. It is possible to carry out a complete determination of the crystal structure from the X-ray diagram of the crystalline material shown in fig. 23. In fact,
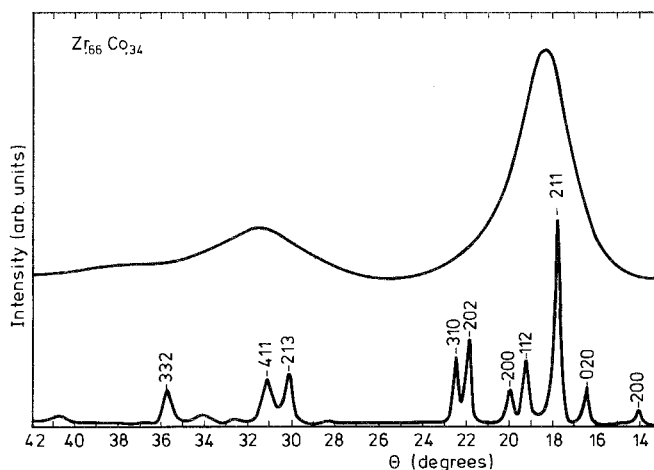
Fig. 23. X-ray diffraction pattern of melt-spun $Zr_{0.66}Co_{0.34}$ before crystallization (upper curve) and after crystallization (bottom curve). The data were taken with CuK_α radiation. The indexing of the bottom curve corresponds to the tetragonal $CuAl_2$ structure.

crystallographers may recognize the X-ray pattern of the well known tetragonal $CuAl_2$ structure, in which the position of each of the atoms is completely specified.

The maximum information that can be obtained from X-ray diagrams of amorphous alloys is much more limited. In the simplest case of an amorphous material, composed of a single atomic species only, it would lead to the knowledge of the so-called radial distribution function (RDF), which provides only spherically averaged information on atomic position correlations. For a given atom at the origin the radial distribution function is defined as

$$RDF(r) = 4\pi r^2 \rho(r), \tag{20}$$

where $\rho(r)$ is the number of atoms located in a spherical shell of radius r and thickness dr.

It is instructive to compare the radial distribution functions of a crystalline material, of an amorphous material and of an ideal gas. As can be inferred from fig. 24a the RDF of a crystalline solid consists of an assembly of delta functions whose weights and r values correspond to the numbers and locations of the neighbour atoms in a given crystal structure. In an amorphous solid the RDF for a given atom would be basically the same if one allowed for the fact that here the interatomic separations tend to cluster around the values in the crystalline solid. The main difficulty in describing RDF's in amorphous solids stems from the fact that each atom has a different RDF. In order to give a description of the total RDF one therefore has to take an average over all the atoms. This leads to an RDF as shown in fig. 24b. Like the situation in an ideal gas (broken line in fig. 24) the RDF is now a continuous function. The first maximum corresponds to the relatively frequently occurring distance associated with the atom-to-atom separation. Note that the RDF's of the amorphous and of the crystalline solid have in common that $RDF(r) = 0$ for r values less than the minimum nearest neighbour distance. The RDF's of the amorphous solid and the ideal gas have in common that at large r values correlations between atom positions have vanished so that the RDF's can be represented by $RDF = 4\pi r^2 \rho_0$, where ρ_0 is the density. The average number of
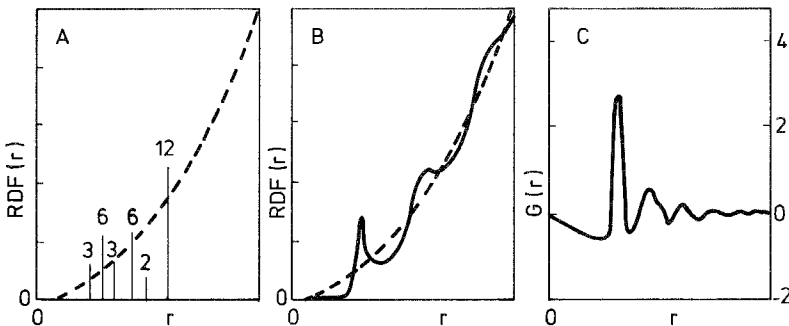
Fig. 24. Schematic representation of radial distribution functions for crystalline (a) and amorphous materials (b). The broken line represents the radial distribution function $4\pi r^2 \rho$ for an ideal gas. The reduced radial distribution function $G(r) = 4\pi r [\rho(r)-\rho_0]$ for an amorphous solid is shown in part c.

atoms located between r_1 and r_2 can be derived from the RDF by means of $\int_{r_1}^{r_2} 4\pi r^2 \rho(r)\,dr$. The area under the first maximum is generally taken as representing the average number of nearest neighbours, or nearest neighbour coordination number.

Very often the reduced radial distribution function $G(r)$ is used instead of the RDF. This quantity is defined as

$$G(r) = 4\pi r\left[\rho(r) - \rho_0\right]. \tag{21}$$

An example of a radial distribution function is shown in fig. 24c. The $G(r)$ function can be obtained from the experimental X-ray diagrams by means of the relation

$$G(r) = 2\pi \int_0^\pi Q[I(Q) - 1]\sin Qr\,dQ. \tag{22}$$

Here $I(Q)$ is the X-ray interference function, representing the wave number dependence of the X-ray intensity after dividing by the squared structure factor $f(Q)^2$ in order to remove the Q-dependence due to intra-atomic interference effects. The function $I(Q)$ has also been corrected for by several other structure-independent quantities such as polarization, absorption and geometrical factors.

Typical X-ray diffraction measurements encompass only a limited range of Q values $Q_1 \leqslant Q \leqslant Q_2$ so that instead of $G(r)$ given by eq. (22) one obtains actually a function represented by

$$G(r) = 2\pi \int_{Q_1}^{Q_2} Q[I(Q) - 1]\sin Qr\,dQ. \tag{23}$$

The consequence of the availability of X-ray data over a limited Q range only is that the experimental $G(r)$ function given by eq. (23) differs from the ideal distribution function owing to so-called termination effects. Termination at too low Q_2 values leads to peak broadening and, more seriously, can give rise to spurious satellite peaks in the low r value region. Termination at too high Q_1 values affects mainly the information pertaining to long wavelength correlations i.e. information on correlations involving distances that are large compared with the nearest neighbour distance.

Considerable interest is shown in amorphous alloys composed of more than one atomic species. It will be clear that in binary alloys $A_{1-x}B_x$ one generally wishes to have information on each of the three partial distribution functions $\rho_{AA}(r)$, $\rho_{BB}(r)$ and $\rho_{AB}(r)$. The first two of these partials describe correlations between similar atoms, the third partial describes correlations between dissimilar atoms ($\rho_{BA} = [(1 - x)/x]\rho_{AB}$). The total correlation function that can be derived from a given X-ray diffraction pattern is composed of three contributions:

$$\rho(r) = \frac{(1-x)f_A^2}{\langle f\rangle^2}\rho_{AA}(r) + \frac{2(1-x)f_A f_B}{\langle f\rangle^2}\rho_{AB}(r) + \frac{x f_B^2}{\langle f\rangle^2}\rho_{BB}(r), \tag{24}$$

where f_A and f_B are the two atomic scattering factors involved. A schematic representation of the various $\rho(r)$ functions in a binary amorphous alloy is given in fig. 25. It is important to realize that a single diffraction pattern obtained on a given
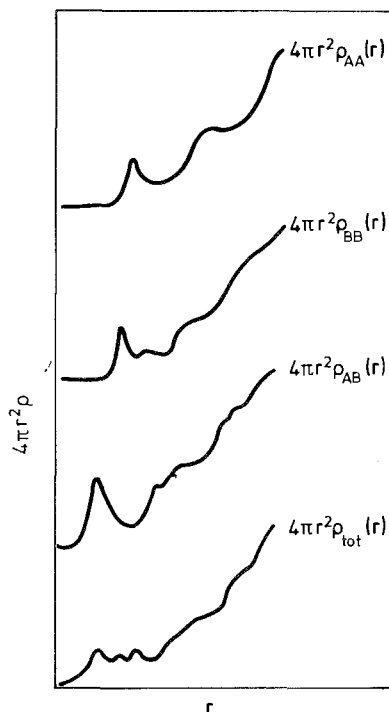
Fig. 25. Schematic representation of partial radial distribution functions and total radial distribution function for an amorphous alloy composed of the elements A and B.

alloy can only result in the determination of $\rho(r)$. At least three different diffraction experiments will be needed in order to determine each of the three partial distribution functions involved.

A common approach to obtaining the three partials for a given binary alloy is to extend the X-ray diffraction (X) to neutron diffraction (N) and electron diffraction (E), provided the three types of atomic scattering factors involved, i.e. $f^X_{A(B)}$, $f^N_{(A(B)}$ and $f^E_{A(B)}$, are sufficiently different to make the solution of the three quantities ρ_{AA}, ρ_{BB}, ρ_{AB} appearing in the three equations (analogous to eq. (24)) for $\rho^X(r)$, $\rho^N(r)$ and $\rho^E(r)$ a meaningful one.

An alternative approach to the problem is the isotopic substitution method. Here one uses the same alloy prepared with different isotopes having different neutron scattering factors (Mizoguchi et al., 1978; Kudo et al., 1978). In the amorphous substitution method several alloys $A_{1-x}B_x$ are used, where x is fixed and B or A is replaced by a component of similar size and chemical affinity but different scattering factor (Chipman et al., 1978; Williams, 1982). In these methods it is tacitly assumed that the atomic distribution functions in the alloy series are the same or, at least, do not differ much.

In cases where the amorphous alloys give rise to ferromagnetic ordering it is also possible to combine X-ray diffraction with neutron diffraction, the latter measurements being performed for two different orientations of the magnetization (Sadoc and Dixmier, 1976). This method will lead to satisfactory results only when all the
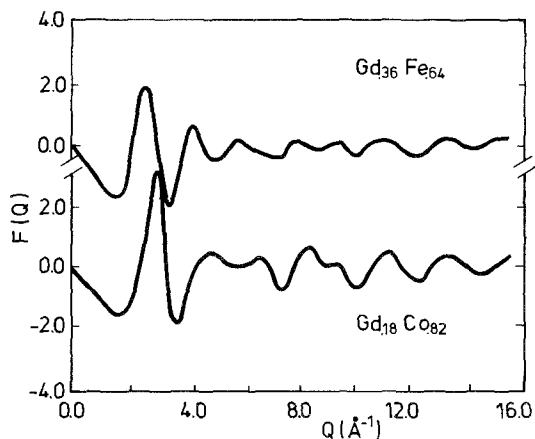
Fig. 26. Reduced interference functions $F(Q)$ reproduced from the data obtained by Cargill III (1975) for the amorphous alloys $Gd_{0.36}Fe_{0.64}$ and $Gd_{0.18}Co_{0.82}$.

atoms of the type responsible for the magnetic order carry the same magnetic moment and when the distribution of local anisotropies is such that all of the moments' directions can follow the direction of the applied field.

Finally we mention the method of Waseda and Tamaki (1976) who used anomalous scattering of X-rays. They applied three different kinds of radiation. The difference in weighting factors of the quantities ρ_{AA}, ρ_{BB} and ρ_{AB} in eq. (24) was brought about by the rather small wavelength-dependent dispersion corrections associated with the two types of scattering factors.

Of all the amorphous alloys investigated so far those between rare earth elements (R) and 3d transition elements (T) occupy a special position, owing to the relatively large difference in metallic radii and the difference in scattering factors. As a consequence, given favourable chosen ranges of concentrations, the three nearest neighbour peaks corresponding to the distribution functions ρ_{RR}, ρ_{RT} and ρ_{TT} will show up as separate peaks in the total distribution function (such as schematically shown in the bottom part of fig. 25). This means that the rather cumbersome combination of different types of scattering experiments is not required when one is chiefly interested in the nearest neighbour contribution of the three partials.

Results obtained by Cargill III (1971, 1975) on amorphous thin films of $Gd_{0.36}Fe_{0.64}$ and $Gd_{0.18}Co_{0.82}$ are reproduced in fig. 26. The corresponding nearest neighbour ranges of the total radial distribution function are shown in fig. 27. The broken lines represent Gaussian components fitted to the experimental curve by means of a least squares method. Using the concentrations and scattering factors appropriate to the alloys $Gd_{0.36}Fe_{0.64}$ and $Gd_{0.18}Co_{0.82}$ the total radial distribution functions are given by means of the relations

$$\rho(r) = 0.91\, \rho_{GdGd}(r) + 0.76\, \rho_{GdFe}(r) + 0.28\, \rho_{FeFe}(r),$$

$$\rho(r) = 0.61\, \rho_{GdGd}(r) + 0.55\, \rho_{GdCo}(r) + 0.54\, \rho_{CoCo}(r).$$

Interpreting the sets of Gaussian components shown in fig. 27 as being due to the
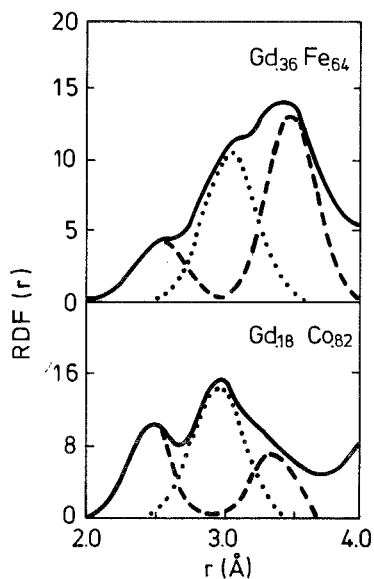
Fig. 27. First maximum in the radial distribution functions of the amorphous alloys $Gd_{0.36}Fe_{0.64}$ and $Gd_{0.18}Co_{0.82}$. The curves and the Gaussian fits were drawn by Cargill III (1975) using his experimental data.

TABLE 2

(Average) distance of j nearest neighbour atoms from i type atoms (r_{ij}) and the corresponding (average) nearest neighbour atoms in amorphous Gd alloys and their crystalline counterparts obtained in diffraction experiments (after Cargill III, 1975). The results listed for the amorphous Y–Ni alloys and crystalline YNi_2 were obtained in EXAFS experiments (after Sadoc et al., 1982). The numbers in brackets under the heading N_{ij} refer to a statistical atomic distribution. These values are given for comparison.

Partials	r_{ij} (Å)	N_{ij}	r_{ij} (Å)	N_{ij}
	a-$Gd_{0.36}Fe_{0.64}$		c-$GdFe_2$	
Gd–Gd	3.47 ± 0.05	6 ± 1	3.20	4
Gd–Fe	3.04 ± 0.05	6.5 ± 0.6	3.06	12
Fe–Fe	2.54 ± 0.05	6.5 ± 0.5	2.61	6
	a-$Gd_{0.18}Co_{0.82}$		c-$GdCo_5$	
Gd–Gd	3.4	3 ± 1		
Gd–Co	2.97 ± 0.005	12 ± 1	2.87	6
			3.18	12
Co–Co	2.47 ± 0.05	7.2 ± 0.7	2.45	4.8
			2.49	2.4
	a-$Y_{0.33}Ni_{0.67}$		c-YNi_2	
Y–Y	3.40	4 (5.3)	3.11	4
Y–Ni	2.71	9	2.98	12
	3.05	3 (10.7)		
Ni–Y	2.71	4.5		6
	3.05	1.5 (4)		
Ni–Ni	2.40	2	2.54	6
	2.55	4 (5.5)		

three types of nearest neighbour pairs, Cargill III (1971, 1975) was able to determine the nearest neighbour coordination numbers and the nearest neighbour distances. The values found by Cargill are given in table 2 where they can be compared with the corresponding values of crystalline materials. Time-of-flight pulsed neutron scattering using accelerator neutron sources was applied by K. Suzuki (1982) to characterize the structure of amorphous alloys. Measurements of the high momentum structure factor are particularly suited to find the short-range atomic structure as well as the precise position of nearest neighbours and their coordination numbers. A high resolution can be obtained by using short wavelength neutrons in the epithermal region generated from accelerator sources. Suzuki showed that the chemical short-range order in amorphous Ti–Cu and Ti–Ni alloys shows a remarkable resemblance with that in the corresponding crystalline phases.

5.2. Atomic scale structure information obtained by miscellaneous methods

Extended X-ray absorption fine structure spectroscopy (EXAFS) is also a useful method for obtaining structural information on amorphous solids. The method consists of measuring the absorption of X-rays in a narrow energy window, located close to the absorption edge of the inner closed shell electrons of the atoms of the constituent elements. These absorption spectra are composed of typical oscillations occurring at the high-energy, high-absorption side of the edge. The oscillations are interpreted as arising from the interference of spherical waves associated with the outgoing photoexcited closed shell electron of the absorbing atom, with spherical waves associated with the back-scattering of the photoelectrons by the neighbouring atoms. The maxima and minima of the absorption spectra oscillations correspond to constructive and destructive interferences, respectively.

In general, the interpretation of EXAFS spectra is considerably facilitated if the measurements are extended to crystalline alloys or intermetallic compounds close in composition to the amorphous alloy under investigation. In cases where nearest neighbour contributions are dominant, the differences in the periodic oscillations, observed between the spectra of the crystalline and the amorphous solid, reflect the differences in nearest neighbour separation to the absorbing atomic species. The amplitude of the oscillations and their rate of decay with increasing wave number depend on the number of nearest neighbour atoms and the width of the nearest neighbour distance distributions. For more details the reader is referred to papers of Stern (1974), Stern et al. (1975, 1978), Eisenberger and Lengeler (1980), Wong (1981), Kobayashi and Takeuchi (1980). Results of Sadoc et al. (1982) on Y–Ni alloys are included in table 2.

Compared with standard diffraction, methods like EXAFS and energy dispersive X-ray diffraction (Egami and Ichikawa, 1978) are more sensitive to details of the local atomic coordination and their changes after annealing. But here too the experimental results reflect mainly the number and radial distances of atoms residing in the first new coordination shells and give no information on their angular distribution. Experimental results obtained by these methods are less suited for distinguishing between structural models for amorphous metals and alloys based

either on dense random packing of hard spheres or on models in which it is of importance to preserve chemical bonding requirements, including specific bond angles.

From this latter point of view the application of experimental techniques able to supply such supplementary information on angular atomic coordinations would be highly desirable. To some extent measurements of the electric quadrupole interaction provide such supplementary information. This interaction involves the quadrupole moment of atomic nuclei and the electric field gradient (EFG) due to the distribution of electric charges around these nuclei. Experimentally this interaction can be observed by nuclear magnetic resonance, by Mössbauer spectroscopy, or by measurements of perturbed angular correlations. Many experimental observations of quadrupole interactions in amorphous solids have been made by means of these techniques. Their relevance to quantitative structural information is, however, still somewhat limited. Nevertheless, several of these studies were able to reveal that the atomic arrangement in the amorphous alloys is far from being a dense random packing of hard spheres.

Panissod et al. (1980) made NMR experiments on amorphous $La_{0.55}Ga_{0.25}$ and on several other amorphous alloys. They showed that in all these cases the local symmetry present in the crystalline counterparts is retained in the amorphous alloys. Friedt et al. (1982) performed [151]Eu, [155]Gd and [197]Au Mössbauer effect measurements on $R_{0.80}Au_{0.20}$ (R = Eu, Gd or Yb) and observed a very narrow distribution of the isomer shift and quadrupole interaction parameters, from which they conclude that there exists a strict compositional and structural short range order of both (R and Au) atomic components of the amorphous alloy. Interesting results were also obtained by Czjzek et al. (1981) who investigated the [155]Gd Mössbauer effect in several amorphous Gd–Ni alloys. They deduced that in general the distribution function $P(V_{zz}, \eta)$ of the electric field gradient V_{zz} and the asymmetry parameter η in amorphous alloys will yield zero probability for $V_{zz} = 0$ and $\eta = 0$. They found it difficult, however, to extract sufficient experimental information from their data as to whether the Gd–Ni alloys have a random atomic arrangement or show compositional short-range ordering.

5.3. Structural models

A substantial amount of effort has been spent on finding model descriptions of the atomic scale structure of amorphous alloys. Such three-dimensional models have attempted to provide concrete though idealized pictures of the arrangements of the atoms that go beyond the information that can usually be obtained from experimental radial distribution functions. The most prominent among them are microcrystalline and cluster models, and models based on the dense random packing of hard spheres (DRPHS).

In the microcrystalline models the amorphous solid is considered as being composed of an assembly of very small, highly ordered regions separated from each other by regions of much lower atomic order. (Valenkov and Porai-Koshits, 1973; Mott and Gurney, 1938). These models come quite close to cluster models in which

one assumes the presence of clusters characterized by a high correlation between the atoms (Frank, 1952; Hoare and Pal, 1975; Farges et al., 1975). The clusters are separated from each other by regions of low correlation between the atomic positions. In general it can be said that these models are not able to reproduce the essential features appearing in the experimental interference functions of the corresponding amorphous solids (Cargill III, 1970).

Models based on DRPHS (Chaudhari et al., 1975; Connell, 1975) have been more successful in reproducing the experimental data. Such models can be generated with a different number of computer algorithms (Adams and Matheson, 1972; Bennet, 1972; Boudreaux, 1977, 1978). Particularly useful results have been obtained after incorporating the tetrahedron perfection concept in the procedure used to generate the atomic structure. This implies that in building up the structure the constituent spheres are added only at those sites where the resulting group of four spheres will form a more or less perfect tetrahedron (Ichikawa, 1975; Cargill and Kirkpatrick, 1976). This means that the three spheres at the periphery of the structural model which define the new site being considered must almost be in hard contact with each other to satisfy the tetrahedron perfection criterion. As a measure of the tetrahedral perfection one may use the ratio $k = r_{ij}^{max}/(R_i + R_j)$, where r_{ij}^{max} is the maximum distance of the three distances r_{12}, r_{13} and r_{23} associated with the hole between the first three spheres of the tetrahedron, while R_i and R_j are the corresponding metallic
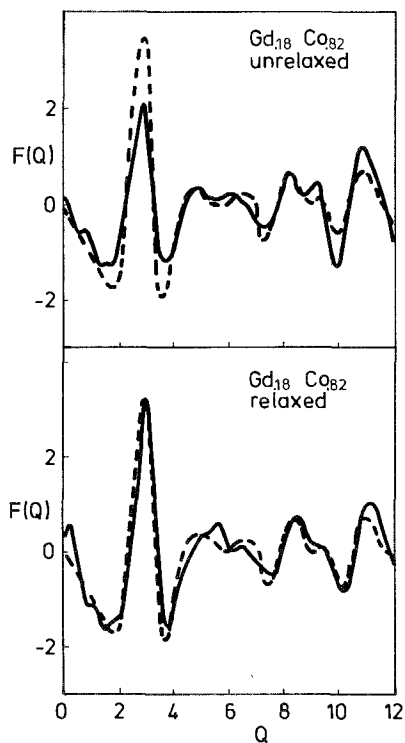
Fig. 28. Model and experimental interference functions for amorphous $Gd_{0.18}Co_{0.82}$ (after Cargill III, 1981b). The dashed line is the experimental result for $F(Q)$. Results are shown for both relaxed and unrelaxed 800 atom models with $k_{max} = 1.1$. Gaussian broadening of the model distribution functions was adjusted to yield approximately the same near neighbour peak widths as those observed experimentally. The model interference functions are also affected by this broadening.

radii. For perfect tetrahedral arrangements one has $k = 1$. If the radii of the constituent atomic species are equal, the inequality $k > 2$ means that such a pocket does not exist.

Cargill and Kirkpatrick (1976) found qualitative agreement to exist between binary DRP distribution and experimental distribution functions for amorphous $Gd_{1-x}Co_x$ alloys when requiring the tetrahedral perfection to be sufficiently high ($k = 1.1$). The model and experimental distribution functions and interference functions $F(Q) = I(Q) - 1$ for amorphous $Gd_{18}Co_{82}$ are compared in fig. 28. No chemical constraints were used in the generation of the structure, the sphere radii being chosen to be consistent with the position of nearest neighbour maxima observed. In these model calculations the high porosity resulting from the high tetrahedron perfection requirement was removed by relaxation, leading to densities about 8% smaller than the experimental values.

Closely related to the DRPHS models described above is the pseudo-crystalline model proposed by Gaskell (1978). In this model small crystalline units of the order of 10 atoms are packed together in a random way. The units are similar in nature to those that exist in intermetallics occurring in the same concentration range, although, owing to the random packing, long-range atomic order is lost.

5.4. Short-range atomic order

Boudreaux and Gregor (1977a,b) have attempted to improve the details of the DRPHS structure of metal–metalloid amorphous alloys by incorporating in their computer algorithm approach the fundamental restriction that no two metalloid atoms could be nearest neighbours. Their computer simulation of the DRPHS structure is closely associated with the Polk model mentioned earlier. First a DRPHS is created on the basis of the larger type of atoms. Atoms of the smaller type are inserted subsequently to fill the holes and simulate the 20 at% metalloid content. The simulated structure obtained by Boudreaux and Gregor after iterative relaxation had a theoretical packing fraction of about 70% which was close to the experimental packing fraction. This structure can be looked upon as one in which compositional short-range ordering (CSRO) exists in the sense that there is a preference for the metalloid atoms to have dissimilar atoms as nearest neighbours.

Apart from the concept of hole filling one may, however, assume the presence of compositional short-range ordering on more general grounds (Buschow and van Engen, 1981a; Buschow and van der Kraan, 1981): Most of the amorphous alloys investigated have a negative heat of mixing (ΔH_m). This means that dissimilar atoms have a tendency to attract each other. The opposite behaviour is expected when ΔH_m is positive, leading to a repulsive interaction between dissimilar atoms. As a rule of thumb one may therefore use the magnitude and sign of the heat of mixing to estimate the degree and the nature of CSRO in amorphous alloys. The sign and the magnitude of ΔH_m can, in general, be determined experimentally (Ansara et al., 1982; Spit et al., 1980; Sommer et al., 1980, 1982).

In cases where such experimental information is not available one may use the semi-empirical values listed for crystalline alloys by Miedema et al. (1980). The

values of ΔH_m in amorphous alloys will be slightly lower than those of crystalline alloys, but for many purposes they are quite suitable, especially when one wishes to predict trends only. In general one expects a higher B–A (or A–B) coordination fraction compared to a statistical atomic distribution in amorphous $A_{1-x}B_x$ alloys for which $\Delta H_m < 0$. This is in agreement with experimental results now available for quite a number of alloys such as R–3d (Cargill III, 1975), $La_{1-x}M_x$ with M = Al, Ga, Au (Williams, 1982; Johnson, 1979) and $Y_{1-x}Ni_x$ (Sadoc et al., 1982).

For liquid-quenched alloys one may assume, as a first approximation, that the CSRO present already in the liquid state will be retained in the amorphous state. Several amorphous alloys are known to give rise to a structural rearrangement upon annealing at temperatures still below the glass temperature, and a similar re-arrangement may occur already during quenching. Sakata et al. (1981) showed by means of neutron diffraction on $Ti_{0.64}Cu_{0.36}$ that chemical short-range order originates in the liquid state and appears to be enhanced on glass formation.

In a more detailed approach to CSRO in amorphous alloys one has to take account of the influence of entropy and to determine in how far the CSRO present is at thermal equilibrium or is frozen-in during quenching. Following a suggestion by Cahn (1982) it is instructive to inspect the results obtained in numerous studies of atomic ordering in crystalline solid solutions such as Cu–Au and Cu–Au alloys. Such alloys also show CSRO associated with the formation of atomically ordered compounds at low temperatures. Even in the compound Cu_3Au, for instance, long-range ordering is never ideal, the Bragg–Williams order parameter S being somewhat less than unity. It is known from studies on the crystalline systems mentioned that the degree of CSRO is a function of temperature. In these crystalline systems these results pertain to equilibrium conditions: CSRO increases as the temperature decreases. In this connection it is interesting to mention the results of Scott (1981) who obtained experimental evidence by means of isothermal calorimetry that CSRO in amorphous $Fe_{0.40}Ni_{0.40}B_{0.20}$ varies reversibly as the temperature is cycled.

Apart from the compositional short-range ordering (CSRO) mentioned above one may also have topological short-range ordering (TSRO). This distinction in the type of SRO was first proposed by Egami (1978). The first type is of chemical origin and is described by the compositional partial RDF, i.e. by the composition of the nearest neighbour atoms. The second type is described by the total RDF and the local stress tensor. It pertains to geometrical packing and can be regarded as increasing when the packing becomes more dense. Egami proposed that reversible changes in SRO are changes in CSRO. These changes are relatively rapid and involve atomic movements over distances of the order of interatomic separations. Irreversible changes in SRO are due to changes in TSRO and involve changes in density and involve long-range diffusion of atoms.

5.5. *Microstructure*

In many respects amorphous alloys can be regarded as having isotropic properties. Texture or preferred orientation of grains as encountered in crystalline melts are
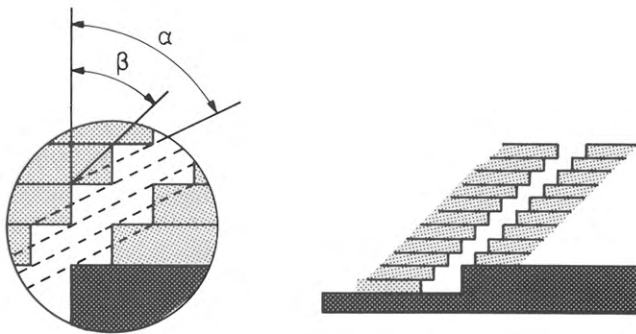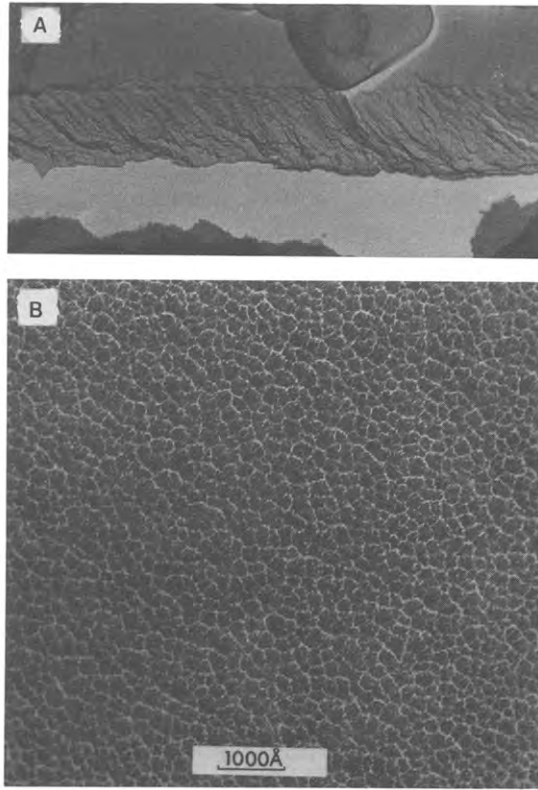
Fig. 29. Column formation: Transmission electron micrograph of a carbon replica of the fractured edge (a) and the top surface (b) of a 1 μm thick vapour-deposited amorphous film of $Gd_{0.22}Co_{0.78}$ (after Leamy and Dirks, 1978). Schematic representation of column formation via serial deposition of monolayers (c). The angles of the deposition direction and the column direction with the normal to the substrate surface are indicated by α and β, respectively (after Leamy and Dirks, 1978).

absent. It was somewhat surprising therefore that amorphous thin Gd–Co films obtained by sputtering showed a strong uniaxial anisotropy (Chaudhari et al., 1973). Initially the pair ordering model (Gambino et al., 1973) was proposed as the origin of K_u. Later on there has been a tendency to explain K_u in terms of a characteristic microstructure of the alloy, associated with the method of vapour deposition. This microstructure, usually referred to as columnar microstructure, is not restricted to Gd–Co alloys but has been observed in crystalline metallic, semiconducting as well as insulating thin films (for a review see Leamy et al., 1980).

A typical example of a columnar microstructure obtained by Leamy and Dirks (1978) on amorphous $Gd_{0.22}Co_{0.78}$ is shown in fig. 29a. Such a microstructure was observed in vapour-deposited as well as in sputtered films. The structure is composed of rods 5–25 nm in diameter. These rods or columns are surrounded by a network of less dense material of 1–2.5 nm thickness. In the example shown in fig. 29a the column axes are perpendicular to the substrate, as can be inferred from the results shown in fig. 29b. This feature is quite generally observed in sputtered films.

On the other hand a perpendicular column orientation is obtained in vapour-deposited films only when the deposition occurs perpendicular to the surface. The column orientation angle β is closely related to the vapour incidence angle α (both angles pertain to the substrate normal). Nieuwenhuizen and Haanstra (1966) found the empirical relationship $2 \tan \beta = \tan \alpha$, known as "tangent-rule" relationship. A schematic representation of the geometrical shadowing effect is shown in fig. 29c. The occurrence of this typical microstructure is not restricted to alloys but has also been observed in amorphous Si and Ge (Nakhadkin and Shaldervan, 1972; Donovan and Heinemann, 1971; Hauser and Staudinger, 1973). Crystalline materials, too, give rise to a columnar microstructure, provided their atomic mobility is relatively low.

The key to understanding the physics of the columnar growth stems from results of computer simulations of the deposition process, first made by Henderson et al. (1974). In their model these authors considered individual hard spheres which were assumed to be deposited in a random way on the growing film. Relaxation following impingement was allowed only to the extent that the added atom be in contact with the hole formed between three spheres at the surface of the film so as to generate a tetrahedron. (This simulation process is close to that described for the generation of amorphous structures in section 5.3.).

By means of this simulation process the characteristic columnar structure was found to be directly related to the geometrical shadowing of the incident atom by the atoms contained in the growing film. It will be clear that the formation of such a columnar microstructure implies a low mobility of the atoms. In films of sufficient thickness the intercolumn period will be largely determined by the atom mobility and, in fact, is to scale with the relaxation distance (Leamy et al., 1980). This implies that such a columnar microstructure will be absent when the deposition is performed at high temperatures or when the deposited material has a relatively high atomic mobility. Annealing after deposition may also lead to the disappearance of this microstructure. The magnetic properties associated with the columnar microstructure will be discussed in more detail in section 6.

6. Magnetic properties of amorphous alloys

The large atomic disorder and the absence of lattice periodicity in amorphous solids will in general lead to magnetic properties that are different from those found in their crystalline counterparts. The reason for this is that some magnetic properties are very structure sensitive. This was recognized long before amorphous magnetic solids were available, since a certain degree of atomic disorder can also be realized in many crystalline systems. A well-known example is the fcc alloy PtCo where the Pt and Co atoms are distributed at random over the available crystallographic positions. Atomic ordering can be attained after annealing at low temperatures, which leads to an fc-tetragonal structure with separate positions for the Co and Pt atoms. Other examples of crystalline materials with atomic disorder are permalloy and the many pseudo-binary compounds like $La(Co_{1-x}Ni_x)_5$, or $Gd_{1-x}Y_xCo_2$.

Nevertheless there is a clear distinction between the types of atomic disorder in crystalline and amorphous alloys. In the former there may be a random distribution of several kinds of atoms over various positions but the positions themselves remain specified, i.e. there is a fixed nearest neighbour distance and a fixed total number of nearest neighbours associated with each site. On the other hand, in amorphous alloys this latter restriction is absent. For these reasons one may characterize the disorder in crystalline alloys as chemical disorder and that in amorphous alloys as a combination of structural disorder and chemical disorder.

In section 6.1 we will discuss the various types of magnetic structures encountered in amorphous solids composed of rare earth and non-magnetic metals. These comprise spin glasses and random uniaxial anisotropy magnets. A phenomenological description of the temperature dependence of the magnetization in amorphous rare-earth–3d-metal alloys will be given in section 6.2, followed by a review of the many experimental results. Section 6.3 will be devoted to the description of the 3d moment variation as a function of alloy composition, while in part 4 it will be explained why the 3d moments in amorphous alloys are expected to be larger than those in crystalline alloys.

Several aspects of the magnetic properties of amorphous alloys composed of rare earths and transition metals have already been discussed by Rhyne (1979) in Volume 2, Chapter 16 of this Handbook. It is difficult to avoid overlap completely, although we shall attempt to focus mainly on supplementary experimental information that has become available in the meantime.

6.1. Magnetic properties of amorphous alloys composed of rare earths and non-magnetic metals

The direction of the magnetic moment of the individual atoms depends on the exchange interaction between these moments and the magnetocrystalline anisotropy which couples the moments to the lattice. In the case of Gd alloys ($L = 0$), the magnetocrystalline anisotropy is usually relatively small so that the magnetic properties can be described by means of the exchange interaction only. Assuming a

Heisenberg interaction between two spins S_i and S_j one has

$$H_{ij} = -J_{ij}S_i \cdot S_j. \tag{25}$$

It is widely accepted that the moment coupling in rare earth alloys proceeds by means of the long-range RKKY mechanism involving a spatial non-uniform conduction electron polarization. The coupling constant J_{ij} of eq. (25) then takes the form (De Gennes, 1962a,b):

$$J_{ij}(r) \propto J_{sf}^2 F(x) \exp\left(-|r_i \sim r_j|/\lambda\right), \tag{26}$$

where $x = 2k_F|r_i - r_j|$ and λ is the electron mean free path. The quantity $F(x)$ is given by

$$F(x) = (x \cos x - \sin x)/x^4. \tag{27}$$

The Fermi wavevector k_F depends on the conduction electron concentration. In the free-electron approximation its value can be estimated by means of the expression

$$k_F^3 = 3\pi Z/V, \tag{28}$$

where Z represents the number of conduction electrons contained in a volume V.

In crystalline solids the various distances $r_i - r_j$ of a given atom i to its nearest and remote neighbours j are fixed by the crystal structure so that the total interaction per moment or the exchange field experienced by a given moment i can be calculated by performing the summation $\Sigma_i F(2k_F|r_i - r_j|) \exp(-|r_i - r_j|/\lambda)$. It has been discussed in more detail in section 5.1 that the neighbour distances $|r_i - r_j|$ in amorphous solids are described in terms of radial distribution functions which are different for the individual atoms, so that one has to take averages. This means that in amorphous
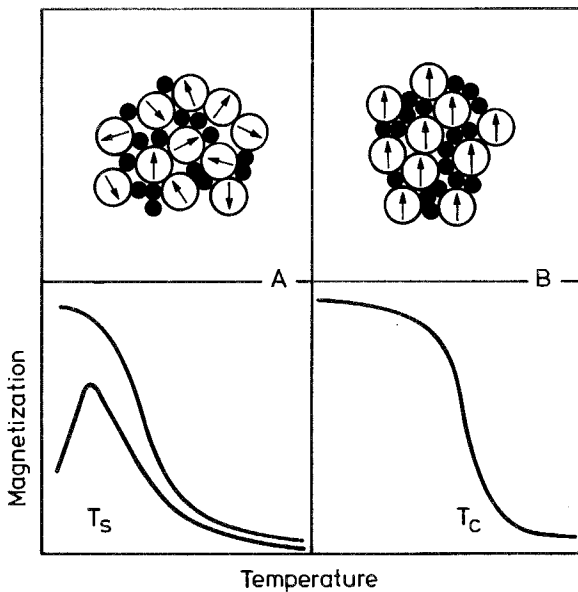
Fig. 30. Schematic representation of the magnetic moment direction in a spin glass (a) or ferromagnet (b) composed of magnetic Gd atoms (open circles) and non magnetic atoms (filled circles). In the bottom part of the figure the corresponding shapes of the temperature dependence of the magnetization are indicated. The cusp-like temperature dependence in the spin glass is only observed in comparatively small applied fields.

alloys one has to consider a distribution of interactions $P(J_{ij})$ and associated with it is a distribution of exchange fields $P(h_{ij})$ experienced by the various moments. These distribution functions are centered around average values J and h which for a given alloy may be negative, zero or positive.

When the distributions are located almost exclusively in the positive regime, the alloy will give rise to a ferromagnetic moment arrangement, as shown in the right-hand part of fig. 30. Although the paramagnetic-to-ferromagnetic transition may be smeared out over a considerable temperature range, the temperature dependence of the magnetization is basically similar to that encountered in ferromagnetic crystalline alloys.

The situation where the distribution functions are centered around zero corresponds to that encountered in spin glasses. Upon cooling, the moments will freeze into random isotropic orientations with no average correlations such as schematically indicated in the left-hand part of fig. 30. The temperature dependence of the magnetization displays a sharp cusp which defines the freezing temperature T_s. It corresponds to the temperature where static spin freezing sets in throughout the whole sample. Not all of the spins may become frozen below T_s, while remnants of short-range clustering may give rise to some superparamagnetic behaviour above T_s. These features can lead to apparently different freezing temperatures and make them dependent on the characteristic time of the measurements. (For more details see Mydosh and Nieuwenhuys, 1980; Fischer, 1977; Edwards and Anderson, 1975, 1976; Sherrington and Kirkpatrick, 1975).

It should be stressed here that in crystalline disordered alloys the spin glass regime is usually restricted to magnetically very dilute systems, whereas the same phenomena are observed in amorphous systems at relatively large concentrations, comprising alloys such as $Gd_{0.37}Al_{0.63}$ (McGuire et al., 1978; Jamet and Malozemoff, 1978), $Gd_{0.33}Al_{0.67}$ (Coey et al., 1977), $Gd_{0.30}Cu_{0.70}$ (McGuire et al., 1978), several amorphous alloys of the type $La_{0.80-x}Gd_xAu_{0.20}$ (Poon and Durand, 1978), but also alloys like $Y_{0.33}Fe_{0.67}$ (Forester et al., 1977) and $Ni_{79}P_{13}B_8$ (Durand, 1977). The freezing temperatures (T_s) of several other Gd-base alloys have been included in table A1 in the Appendix.

The cusp-like temperature dependence of the magnetization is generally observed only in relatively weak applied fields. As indicated in fig. 30 a more ferromagnetic type of $\sigma(T)$ curve is obtained in relatively large ($\gg 0.1$ T) applied fields. When the concentration of the magnetic ions is increased the cusp in the temperature dependence of the magnetization disappears.

A magnetic phase diagram proposed by McGuire et al. (1978) for amorphous $Gd_{1-x}Al_x$ is shown in fig. 31. It can be seen from the figure that the alloys of relatively high Gd content give rise to a freezing temperature (T_s) as well as to a ferromagnetic ordering temperature (T_c). McGuire et al. note that such a possibility indeed exists in the model descriptions given by Sherrington and Kirkpatrick (1975) where one could pass from the ferromagnetic regime into the spin glass regime by decreasing the temperature. They also discuss their results in terms of the model of Vannimenus and Toulouse (1977) where the continuation of an observable spin glass freezing temperature in the ferromagnetic phase is associated with a ferromagnetic
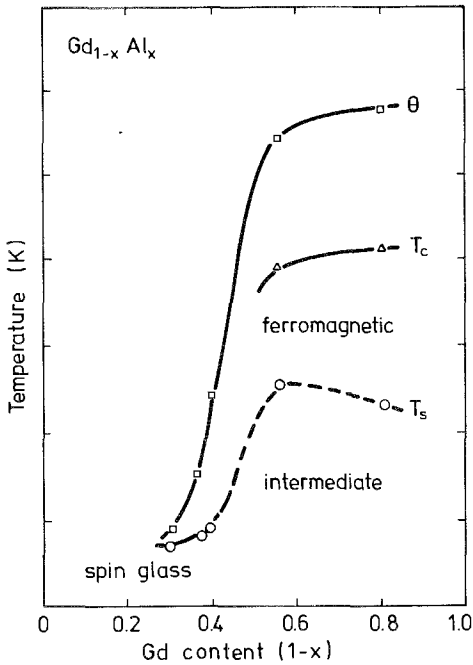
Fig. 31. Magnetic phase diagram of the amorphous $Gd_{1-x}Al_x$ system. The freezing temperatures, ferromagnetic Curie temperatures and asymptotic Curie temperatures are indicated by means of T_s, T_c and θ, respectively (after McGuire et al., 1978).

state with a low coercivity passing into one with a high coercivity and various relaxation phenomena.

The transition from the spin glass regime into the ferromagnetic regime was studied in more detail by Poon and Durand (1978) on the system $La_{0.80-y}Gd_yAu_{0.20}$. The magnetic phase diagram proposed by these authors for this amorphous system is shown in fig. 32. This phase diagram can be divided into four concentration regions. Alloys with Gd concentrations $0.0024 \leqslant y \leqslant 0.01$ were found to behave like canonical spin glass systems where the magnetization $M(H, T)$ and initial susceptibilities $\chi_0(T)$ can be described by means of the universal curves of the scaling prediction such as presented by Souletie and Tournier (1969) and Blandin (1961).

In the range $0.01 \leqslant y \leqslant 0.32$ the classical scaling laws for $M(H, T)$ are no longer obeyed. In this range the reduced remanence $M_r(y, T)/y$ is of dipolar origin and scales with T/y, while the freezing temperature T_s is proportional to y. The alloys corresponding to this concentration region can be characterized as cluster glasses (Ododo and Coles, 1977). Each alloy consists of an assembly of independent clouds composed of several ferromagnetic clusters (consisting of 1–4 individual spins); the clusters inside the cloud are not totally misaligned. A net moment exists which experiences the anisotropy field associated with the anisotropic part of the dipolar interaction. Roughly speaking, the size of the clouds is determined by the balance between the intracloud interaction (mainly of dipolar origin and the intercloud interaction (mainly RKKY). As the Gd concentration increases, the cluster size is no longer determined by the size of the first coordination shell. There is a tendency for
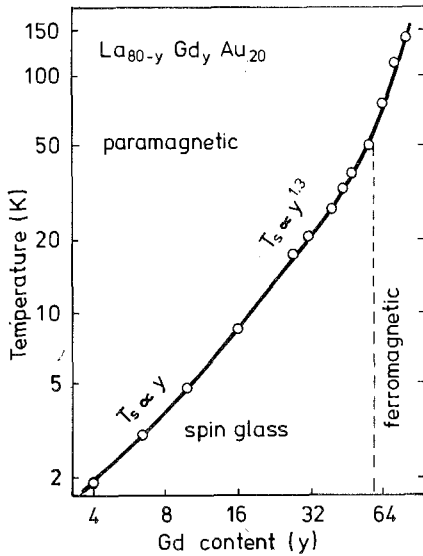
Fig. 32. Magnetic phase diagram pertaining to the amorphous alloy system $La_{0.80-y}Gd_yAu_{0.20}$ proposed by Poon and Durand (1978). The log of the freezing temperatures T_s is plotted versus the log of the Gd concentration.

the Gd atoms to percolate. For this reason the scaling laws mentioned are no longer obeyed.

For $0.32 \leqslant y \leqslant 0.56$ there is still no long range ferromagnetic order, thermomagnetic history effects are present, and T_s varies approximately as $y^{1.3}$. This region could be referred to as micromagnetic (Beck, 1972; Kouvel, 1961). Finally, for $0.56 \leqslant y \leqslant 0.80$ the alloys can be designated as good ferromagnets where the Curie temperatures T_c are well defined by means of Arrott plots and have critical exponents and equations of state corresponding to a second-order phase transition.

The magnetic coupling of the 4f moments in amorphous alloys can proceed indirectly via spin-polarized conduction electrons (RKKY-type, see eqs. (26), (27). It can also proceed via positive intra-atomic 4f–5d exchange, combined with direct positive interatomic 5d–5d exchange (Campbell, 1972). The RKKY-type coupling can lead to both ferromagnetism and antiferromagnetism, whereas the coupling involving the 5d electrons is expected to lead to ferromagnetism. Buschow and Beekmans (1978) suggested that the former type of interaction is of less importance in the amorphous alloys, at least in alloys of relatively large rare earth concentration. They found that Gd-rich amorphous alloys order predominantly ferromagnetically. Variation in valence electron concentration does not seem to have much effect upon ordering type and coupling strength.

Furthermore, the high values of the resistivity in the amorphous alloys imply a considerable reduction in mean free path of the conduction electrons. This may affect the long-range RKKY coupling much more strongly than the coupling involving a direct 5d–5d interaction, and would make the relative importance of the latter type of coupling greater. Indications of a large participation of the 5d electrons in the exchange interactions were also obtained from a correlation between the distance of closest Gd–Gd approach found in these alloys and the Gd–Gd neighbour

distance in crystalline compounds at which the d-electron mediated exchange starts to become of influence. Evidence of a moment coupling in amorphous $R_{0.65}Al_{0.35}$ proceeding via the RKKY mechanism was reported by Giessen et al. (1980). These authors found a negative value for the asymptotic Curie temperature (θ_p) in $Ce_{0.65}Al_{0.35}$, whereas positive values were found in other $R_{0.65}Al_{0.35}$.

Here the discussion of two points is in order. First, it can be shown that in a series of rare-earth-base materials of similar structure and electron concentration the RKKY model predicts $\theta_p = $ constant $\times (g-1)^2 J(J+1)$, where the constant is the same for all members of the series when the R component is varied from La to Lu. When plotted versus the rare earth component R, the θ_p values show a cusp-like behaviour, the maximum being located at R = Gd (see for instance fig. 2 in section 6.2.2). A sign reversal within such a series is inconsistent with the RKKY mechanism. From this point of view the results of Giessen and Hines would not be in favour of the RKKY mechanism but rather against it. Second, the element Ce is known to give rise to the trivalent and tetravalent state in metallic systems. Frequently the Ce atoms in alloys exhibit a so-called intermediate valency, the high-temperature behaviour approaching that of Ce^{3+} ions while at low temperatures a more complex magnetic behaviour is found. A well-known example is $CeAl_2$, which, owing to its unstable valency, has a complex magnetic structure and $\theta_p < 0$ (Barbara et al., 1977; Parks, 1977). In contrast, all the other members of the RAl_2 family are ferromagnets with $\theta_p > 0$ (see for instance Buschow, 1980c). So it may well be that the negative value found by Giessen and Hines in amorphous $Ce_{0.65}Al_{0.35}$ reflects the unstable valency of the Ce ion in this alloy rather than the presumed change in RKKY coupling.

For more details regarding the RKKY coupling mechanism in amorphous alloys the reader is referred to the papers by Madhukar (1974) and Poon (1978).

To describe the magnetic properties of amorphous alloys containing rare earth elements with non-zero orbital moment ($L \neq 0$) the Hamiltonian of eq. (25) is no longer suited. Harris et al. (1973) have proposed a model in which they assume that there is a local uniaxial field of random orientation at each of the rare earth atoms in an amorphous solid. This local uniaxial field of random orientation is closely associated with the presence of an equally random crystalline electric field. The Hamiltonian for this random anisotropy model (RAM) can be written as

$$H_{RAM} = -D\sum_i J_{iz_i}^2 - \tfrac{1}{2}J_{ex}\sum_{ij} J_i J_j - g\mu_B H \sum_i J_{iz}, \tag{29}$$

where J_i represents the rare earth moment at site i. The first term, with a constant second-order anisotropy parameter D, represents the local anisotropy. The directions z_i, corresponding to the components J_{iz_i} of the moments, were assumed to be random vectors. In the simplest treatment, correlations between the z_i vectors for neighbouring sites are absent. The second term is the conventional nearest neighbour Heisenberg interaction with a constant exchange coupling J_{ex}. In the final term is the Zeeman interaction in an external magnetic field H oriented in the unique z-direction.

In the molecular field approximation, the above expression reduces to

$$H_{\mathrm{MFA}} = \sum_i DJ_{iz_i}^2 + NJ_{iz},$$ (30)

where the molecular field constant N is given by

$$N = ZJ_{\mathrm{ex}}\langle J_z \rangle + g\mu_{\mathrm{B}}H,$$ (31)

Z being the R–R coordination number. The angular brackets in eq. (31) represent *both* a thermal average (as in a conventional molecular field approximation) and an average over the disorder associated at each site with the vectors z_i. Since H_{MFA} is a sum over single-site Hamiltonians, it is possible to analyse it in a self-consistent way by finding the crystal field levels at each site in the presence of the molecular field (N). The macroscopic magnetization is then equal to $g\mu_{\mathrm{B}}\langle J_z \rangle$ per atom. Closer analysis of the self-consistent molecular field equations has shown that the most significant effects will occur in the case where the anisotropy and the exchange interaction are at least of comparable magnitude ($D \geqslant ZJ_{\mathrm{ex}}$). Such a situation is seldom encountered in the crystalline state. It is possible in amorphous alloys, owing to the lack of crystal symmetry which allows second-order "crystal field" effects to dominate (Cochrane et al., 1978).

Ferrer et al. (1978) found excellent agreement between the RAM model description and the high-field magnetization curves obtained by various authors on amorphous alloys in which rare earth elements are combined with non-magnetic metals. Values of the parameters D and J_{ex}, obtained by fitting the experimental results obtained by Boucher (1977a,b), Boucher and Barbara (1979) and Ferrer et al. (1978), have been collected in table 3.

Ferrer et al. (1978) invariably found serious deviations of the experimental magnetization curves from model predictions in the low-field region. The deviations originate from the presence of sizable hysteresis loops and magnetic after-effects. These effects were studied in more detail by Boucher and Barbara (1979) on the alloy $Tb_{52}Ag_{48}$. They found that the coercive force depends on the temperature and the observation time according to the following relation:

$$H_c^{-1} = H_0^{-1} + A(T)\ln(\Delta t/t_0).$$ (32)

The quantity A depends on temperature, while H_0 and t_0 are temperature independent. The time lapse between measurement of the initial and final magnetization is

TABLE 3

Anisotropy parameter (D) and exchange coupling constant (J_{ex}) obtained by Ferrer et al. (1978) and Tissier et al. (1980) from fits of the high-field magnetization data. Also included are values of the coercive force H_c and the ratio H_c/J_{ex}^2.

Alloy	D (K)	J_{ex} (K)	D/J_{ex}	H_c (T)	$\mu H_c/J_{\mathrm{ex}}^2$ (K)
$Tb_{52}Ag_{48}$	4.00	0.53	7.55	2.3	0.37
$Dy_{50}Ag_{50}$	3.00	0.14	21.95	0.3	0.035
$Ho_{50}Ag_{50}$	1.50	0.15	10.00	0.8	0.008
$Dy_{41}Cu_{59}$	3	–	–	0.8	–

given by Δt. The quantity H_0 represents the intrinsic coercive force that would have been observed at $T = 0$ for Δt tending to t_0, where t_0 is an intrinsic time of magnetization reversal ($t_0 \approx 6 \times 10^{-5}$ s). Associated with eq. (32) is an activation law of the form

$$t^{-1} = t_0^{-1} \exp(-\Delta E/kT), \tag{33}$$

where the activation energy ΔE can be obtained from the expression

$$\Delta E = kT \ln(\Delta t/t_0) = kT \cdot A(T)(H^{-1} - H_0^{-1}). \tag{34}$$

Boucher and Barbara found that the activation energy ΔE depends on the field strength ($\Delta E \sim 1/H$) as was also observed in crystalline rare earth base inter-metallics (Barbara et al., 1972). It furthermore depends on the measuring time and shows a slight temperature dependence ($\Delta E \sim T^{-1.1}$). Its mean value is about 10^{-21} J. By comparing this value with the value of the energy needed to reverse the magnetization (6×10^{-23} J/atom) Boucher and Barbara obtained an order of magnitude estimate of the volume whose magnetization is reversed as a function of time by activation for given values of T and H. This volume is equal to about 1 to 1.2 nm^3 and contains about 20–25 atoms. The average value of the volumes whose magnetization is reversed at $T \approx 0$ in strong applied fields (1 T) is much larger and comprises 10^3 to 10^4 nm^3. These volumes are much smaller, though, than those corresponding to magnetic domains in the crystalline state.

Tissier et al. (1980) studied the magnetization processes in amorphous $Dy_{0.41}Cu_{0.59}$ and found the following law for the temperature dependence of the coercive force:

$$H_c = H_0 \exp(-\alpha T). \tag{35}$$

The hysteresis loop measured in this alloy at 4.2 K is smoothly varying. In contrast, the loop measured at 100 mK in an adiabatic demagnetization calorimeter is seen in fig. 33 to contain large discrete jumps, reminiscent of Barkhausen jumps.
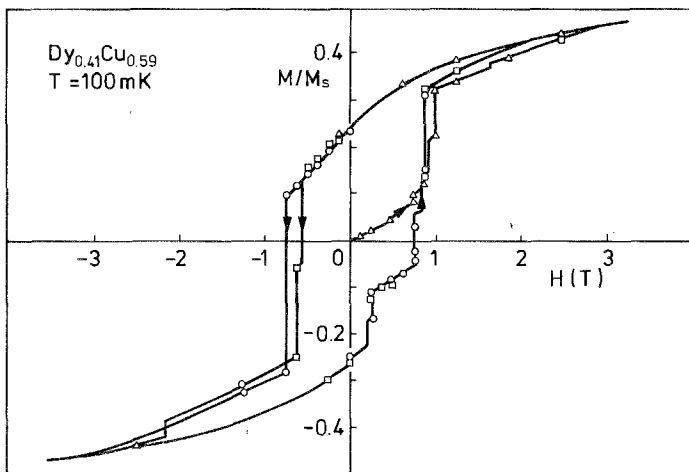
Fig. 33. Hysteresis loop of amorphous $Dy_{0.41}Cu_{0.59}$ measured at 100 mK by Tissier et al. (1980). Different symbols refer to measurements made in different runs.

Tissier et al. estimated that about 10^{18} Dy atoms are involved in each jump, indicating domain sizes between 10^7 and 10^8 μm. From the theoretical side several attempts have been made (Cochrane et al., 1978; Ferrer et al., 1978) to calculate coercive fields as an intrinsic property of the microscopic RAM Hamiltonian (eqs. 29–31, though the results seem less satisfactory than those pertaining to the high-field magnetization curves.

It is interesting to note that in the amorphous alloys discussed above, where large random anisotropy fields far outweigh random exchange fields, the magnetization shows a temperature dependence similar to that observed in Gd-base spin glasses.

For instance, Von Molnar et al. (1980) investigated several amorphous $Dy_{1-x}Cu_x$ alloys and found a cusp-like temperature dependence of the magnetization in samples cooled in zero field and measured in low fields. In a subsequent investigation Von Molnar et al. (1982b) compared the magnetic properties of the amorphous alloys $Dy_{0.52}Cu_{0.48}$, $Gd_{0.52}Ag_{0.48}$ and $Gd_{0.37}Al_{0.63}$. The latter alloy was reported to be a spin glass (Mizoguchi et al., 1977; Barbara et al., 1981). Von Molnar et al. found that the former two alloys behave differently. Their magnetic properties are more adequately described by means of the model proposed for uniaxial anisotropy magnets with small D/J ratios by Aharony and Pytte (1980), although not all aspects of the model are reflected in the experimental data.

O'Shea and Sellmyer (1982) investigated several ternary Gd-rich amorphous alloys, comprising substantial differences in D/J ratio. An increase of this ratio was found to increase the temperature T_h at which a hysteretic transition occurs from the magnetic state to the random ferromagnetic state. At larger D/J values (Tb alloys) the infinite susceptibility state proposed by Aharony and Pytte is suppressed so that there is a direct transition from the paramagnetic to the random ferromagnetic state. O'Shea and Sellmyer also discuss the possibility that at relatively low D/J ratios there is a phase boundary between an infinite-susceptibility state with no magnetic order and an infinite-susceptibility state with ferromagnetic domains.

Bhattacharjee and Coqblin (1983) considered the special case that the crystal field splitting leads to a situation where the lowest levels are two singlets, the corresponding energy splitting varying randomly over the rare earth sites. The authors applied their model to amorphous Pr alloys and found satisfactory agreement with experiment.

6.2. Magnetic properties of amorphous alloys composed of rare earths and 3d metals

6.2.1. Magnetic structures

The magnetic properties of most of the amorphous rare-earth–nickel compounds are similar to those described in the preceding section. The reason is that the Ni atoms do not carry a magnetic moment in these alloys except for the highest Ni concentration (see below). For alloys with a rare earth component having non-zero orbital moment the RAM model mentioned in section 6.1 again predicts the spin structure to be a spatially non-isotropic distribution of moment directions, such as would correspond to a uniform distribution of moment directions over all the points on a hemisphere.
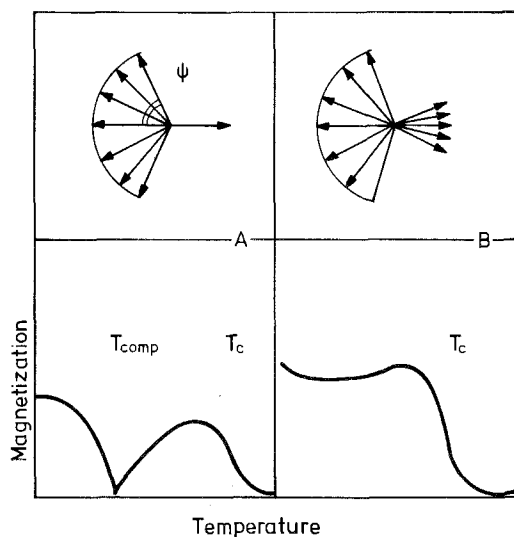
Fig. 34. Schematic representation of the magnetic structure in amorphous Dy–Co alloys (a) and amorphous Dy–Fe alloys (b) of about 25 at% Dy at $T = 0$ K. In the bottom part of the figure the corresponding temperature dependences of the magnetization are given.

In the case of Co and Fe alloys the situation is changed somewhat owing to the presence of a 3d moment when the 3d atom concentration becomes larger than about 30 at%. Typical examples of the spin structures in such alloys are given in fig. 34. Owing to the strong ferromagnetic coupling between the Co spins and the relatively small Co anisotropy fields there will be a parallel alignment of the Co spins. The rare earth spins will tend to be coupled antiparallel to the Co spins. As a consequence the rare earth moment directions will no longer be distributed over a hemisphere but be confined to a cone whose half-angle ψ depends on the relative strength of the R–Co interaction, the strength and distribution width of the R–R exchange interactions and on the local R anisotropy fields. Experimental evidence for the presence of such a spin arrangement was obtained by Coey et al. (1976) by means of ^{161}Dy and ^{57}Fe Mössbauer spectroscopy on amorphous $Dy_{0.23}Co_{0.77}$ doped with ^{57}Fe, where the angle between the applied field and the direction of the γ-rays was varied. From these experiments Coey et al. determined the half-angle ψ to be close to 70°.

The magnetic ordering in all known intermetallic Co compounds (in which the Co atoms are the only magnetic atoms) is ferromagnetic. Closely associated with this fact is a distribution of Co–Co exchange fields in amorphous Co alloys which is restricted to positive values. In contrast, the Fe–Fe exchange is known to be a sensitive function of interatomic separation, changing its sign near 0.3 nm. One expects therefore that in amorphous Fe-base alloys the distribution $P(J)$, mentioned in section 6.1 below eq. (28), will be centered at about $J = 0$ or at small positive values and will comprise a substantial portion of negative values. Such a situation was found to exist, for instance, in amorphous $Y_{0.33}Fe_{0.67}$. Rhyne et al. (1974) showed that long-range magnetic ordering is absent and spin-glass-like properties were reported by Forrester et al. (1977, 1979a,b), Biesterbos et al. (1977), Coey et al.
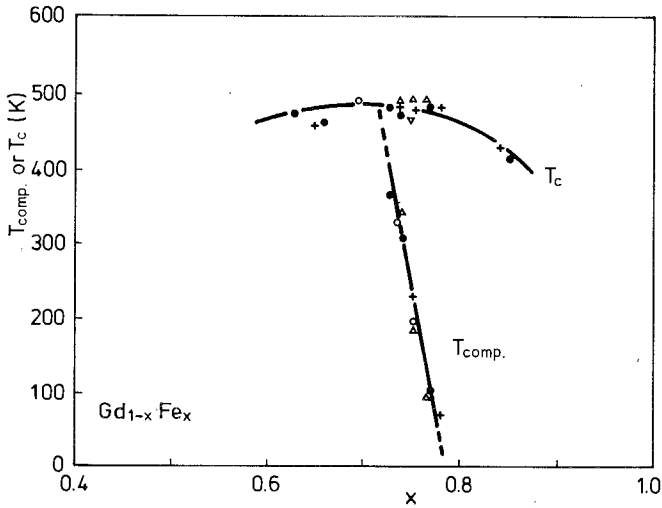
Fig. 35. Concentration dependence of the Curie temperature T_c and compensation temperature T_{comp} in amorphous $Gd_{1-x}Fe_x$ (after Hartmann, 1982). Different symbols correspond to different authors.

(1981), Chappert et al. (1981) and Murani and Rebouillat (1982). The distributions $P(J)$ were found to shift to more positive values when x was increased in amorphous $Y_{1-x}Fe_x$.

Because of the above-mentioned features of the Fe sublattice the magnetic properties of amorphous alloys, in which Fe is combined with a magnetic rare earth metal, are different from those of the corresponding Co alloys. In the former alloys the moment directions are no longer aligned parallel as in fig. 34a but are scattered within a cone (Arrese-Boggiano et al., 1976). The presence of a non-collinear Fe moment arrangement in amorphous $R_{1-x}Fe_x$ has serious consequences with regard to the temperature dependence of thê total magnetization. The antiferromagnetic coupling between rare earth spins and Co spins will, in general, still give rise to a compensation temperature (T_{comp}) in the temperature dependence of the magnetization, such as found in crystalline materials and shown schematically in the bottom part of fig. 34a. In Fe-base amorphous alloys the occurrence of such a compensation temperature is less frequently observed (Rebouillat et al. 1977, Biesterbos 1979). Experimental values of T_{comp} derived from magnetic measurements on amorphous $R_{1-x}Co_x$ and $R_{1-x}Fe_x$ alloys are included in tables A3 and A4 given in the Appendix. For the $Gd_{1-x}Fe_x$ alloys the concentration dependence of T_{comp} and T_c is compared in fig. 35.

6.2.2. Mean field analysis

The dependence of the magnetic properties of amorphous R–3d alloys on temperature and composition is most conveniently described by means of a mean field approach (Hasegawa, 1975; Heiman et al., 1976; Gangulee and Taylor, 1978; Gangulee and Kobliska, 1978; Taylor and Gangulee, 1980; Hansen and Urner-Wille, 1979). For a system consisting of n different components in which x_i is the atomic

fraction of the ith component, the saturation magnetization per unit volume is given by

$$M_s(T) = N\mu_B \sum_{l=1}^{n} x_i g_i \bar{S}_i(T), \tag{36}$$

where N is the total number of atoms per unit volume, μ_B the Bohr magneton, g_i the gyromagnetic ratio of the atoms of type i and $\bar{S}_i(T)$ the effective maximum total angular momentum at temperature T. The temperature dependence of $\bar{S}_i(T)$ can be approximated by means of the Brillouin function

$$\bar{S}_i(T) = S_i B_{S_i}(g_i \mu_B S_i H_i / kT), \tag{37}$$

where the mean field H_i experienced by the total angular momentum S_i is given by

$$H_i(T) = H_{ext} + \sum \omega_{ij} \bar{S}_j(T), \tag{38}$$

where

$$\omega_{ij} = 2 \sum_k J_{ijk} Z_{ijk} / \mu_B g_i.$$

The quantity J_{ijk} is the exchange interaction energy between an atom i and an atom j in the kth neighbour shell. The number of j atoms which are kth nearest neighbours to the ith atom is indicated by Z_{ijk}. If one considers nearest neighbour interactions only, eq. (38) reduces to the simple form

$$\omega_{ij} = 2 J_{ij} Z_{ij} / \mu_B g_i. \tag{39}$$

A typical example of a fit of a curve calculated by means of the mean field approach to experimental data is shown in fig. 36. From such fits values could be
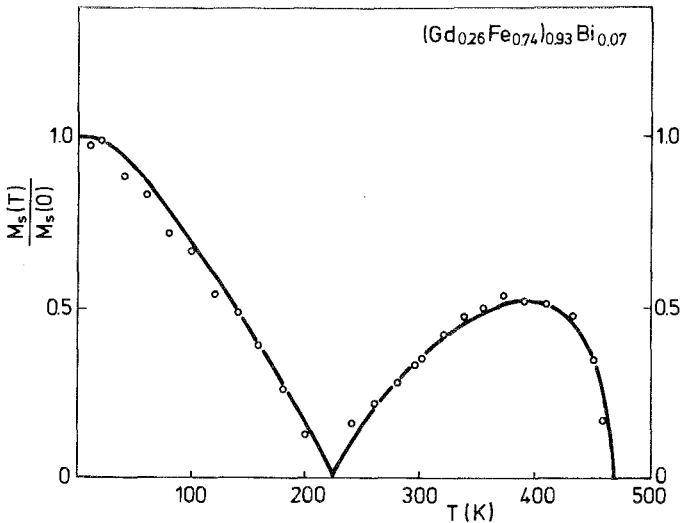
Fig. 36. Temperature dependence of the reduced magnetization $M_s(T)/M_s(0)$ of $(Gd_{0.26}Fe_{0.74})_{0.93}Bi_{0.07}$, calculated by Hansen and Urner-Wille (1979) using the mean field model (full line). The open circles are experimental values.

TABLE 4

Parameters derived by means of mean field analysis of experimental data: S_{3d} represents the 3d spin while the exchange constants J_{11}, J_{12} and J_{22} refer to the R–R, R–3d and 3d–3d interaction, respectively.

Alloy	S_{3d}	J_{ff} (10^{-23} J)	J_{fd} (10^{-23} J)	J_{dd} (10^{-23} J)	Ref.
Gd$_{1-x}$Fe$_x$					
0.5 < x < 1.0	$1.1-(1-x)[2.3-0.47(g-1)J]$	1.6	-28.0	20.5	1
0.5 < x < 1.0		1.6	$2.25-53.0(1-x)$	$20.5+120(1-x)$	1
0.5 < x < 1.0	$0.5\{2.2-\frac{1-x}{x}[3.2-0.7(g-1)J]\}$	1.6	$1.4-46.8(1-x)$	$20.5+115(1-x)$	1
0.70 < x < 0.75	$1.033-0.210(\frac{1-x}{x})^{1.488}$	2	$33.5(\frac{1-x}{x})-34.2$	$48.5+20.1(\frac{1-x}{x})$	2
0.72 < x < 0.75	0.97	–	–	42	3
Nd$_{0.26}$Fe$_{0.74}$	$1.071-0.332(1-x)$	2.0	$+7.0$	60	4
Gd$_{1-x}$Co$_x$					
0.76 < x < 0.90	0.825	2	-23	$510x-280$	5
0.61 < x < 0.89	$0.775-0.848(\frac{1-x}{x})^{1.5}$	2.7	-23.7	200	6
Nd$_{0.24}$Co$_{0.76}$	0.62	2.0	$+9.0$	150	4

1. Heiman et al. (1976)
2. Gangulee and Taylor (1978)
3. Tsunashima et al. (1983)
4. Taylor et al. (1978)
5. Hasegawa (1975)
6. Taylor and Gangulee (1976)

derived for the R–R exchange interaction ($J_{11} = J_{ff}$), the R–3d exchange interaction ($J_{12} = J_{fd}$) and the 3d–3d exchange interaction ($J_{22} = J_{dd}$). A collection of values reported in the literature is given in table 4.

In cases where the concentration ranges investigated were relatively large it proved necessary to treat the parameters S_d, J_{fd}, and J_{dd} as being concentration dependent. The concentration dependences proposed for S_d are based on charge transfer considerations and on variations of the 3d moments due to the polarizing influence of the rare earth spin. Such a variable 3d spin was found by means of ^{57}Fe Mössbauer spectroscopy in various $R_{1-x}Fe_i$ alloys. In fact, the expression used for S_{Fe} by Heiman et al. (1976) reflects the variable ^{57}Fe hyperfine field observed in these amorphous alloys. The values for S_{Fe} and J_{fd} obtained by Hartmann (1982) from fitting the data of various amorphous $Gd_{1-x}Fe_x$ alloys are shown in fig. 37, where they are compared with the concentration dependence proposed by Gangulee and Taylor (1978), which is contained in table 4. As a general conclusion derived from these analyses one may state that the Curie temperature is mainly determined by J_{dd} while the compensation temperature is mainly determined by J_{sf}.

Ternary systems such as $(Gd_{1-x}Co_x)_{1-y}Z_y$, where Z represents Mo or Au (Hasegawa et al., 1975a,b), and $(Gd_{1-x}Fe_x)_{1-y}Z_y$, where Z represents Bi, Pd, or Sn (Hartmann, 1982; Hansen and Urner-Wille, 1979), have also been investigated. In the amorphous Co alloys admixture of Mo as well as Au leads to a reduction in Co moment, which was interpreted as originating from charge transfer effects leading to
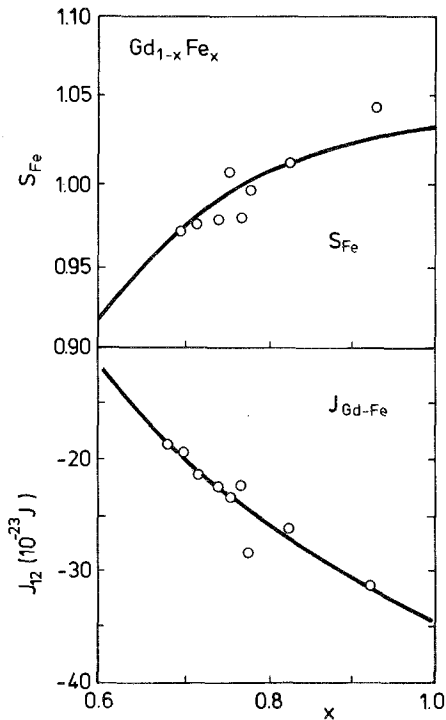
Fig. 37. Concentration dependence of the iron spin S_{Fe} and Gd–Fe exchange constant J_{12} in $Gd_{1-x}Fe_x$, obtained by means of a mean field fit to experimental data (open circles) and calculated by means of the formulae proposed by Gangulee and Taylor given in table 4 (full lines) (after Hartmann, 1982).
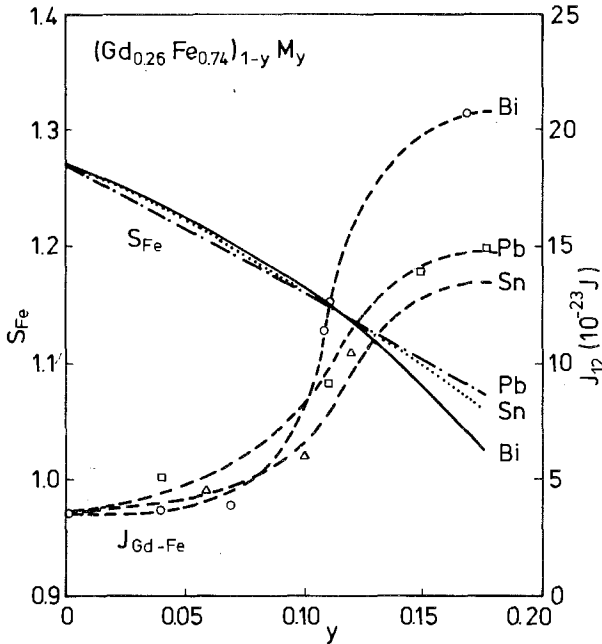
Fig. 38. The Fe–Gd exchange constant J_{12} and the iron spin S_{Fe} in $(Gd_{0.26}Fe_{0.74})_{1-y}M_y$ as a function of M = Bi, Sn or Pb content. The data were deduced from the fitting procedure of the mean field theory to the magnetization data (after Urner-Wille et al., 1980; Hartmann, 1982).

a further filling of the Co 3d band. In contrast, Urner-Wille et al. (1980) found a strong increase of the 3d moment with admixture of Bi, Sn or Pb to amorphous $Gd_{1-x}Fe_x$ alloys. Results of their mean field analyses are shown in fig. 38. It is seen that the strong increase in S_{Fe} is accompanied by a reduction in exchange coupling between the Fe and Gd spins. These effects were interpreted by Urner-Wille et al. as arising from a preference of the Gd atoms for Bi, Sn or Pb atoms as nearest neighbours, leading to larger average Gd–Fe and Fe–Fe distances. This preference of the Gd atoms for Bi, Sn or Pb nearest neighbour atoms was correlated with the heat of solution, which is large and negative for Bi, Sn or Pb in Gd (or Y), while the heat of solution of Bi, Sn or Pb in Fe is positive.

Taylor and Gangulee (1982) investigated B addition to $Gd_{1-x}Fe_x$ and $Gd_{1-x}Co_x$. They concluded from an analysis of their data that the B addition leads to a 3d moment reduction due to 3d band filling by means of charge transfer of more than two electrons per B atom added. Apart from this effect, they report an increase of the Fe moment for higher B concentrations which is ascribed to the promotion of collinearity by the B atoms arising from lower Fe–Fe distances and a lower number of nearest Fe neighbours, which in turn would modify the Fe–Fe exchange energy distribution.

The above results pertain mainly to amorphous alloys rich in 3d metal. Magnetic ordering temperatures for amorphous alloys of lower 3d metal concentrations are included in fig. 39. In the mean field model the magnetic ordering temperatures are given by the expression (Heiman et al., 1976):

$$3kT_c = a_{ff} + a_{dd} + \left[(a_{ff} - a_{dd})^2 + 4a_{fd}a_{df} \right]^{1/2}, \tag{40}$$
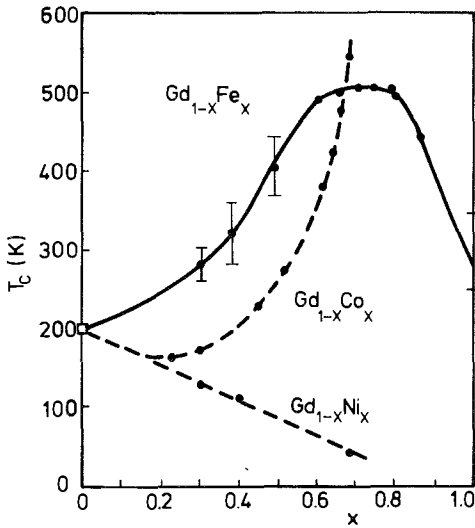
Fig. 39. Concentration dependence of the Curie temperatures in various amorphous Gd-alloys (after Buschow and Van der Kraan, 1981).

where

$$a_{ff} = (1 - x)Z_f J_{ff}(g - 1)^2 J(J + 1),$$ (41)

$$a_{dd} = xZ_d J_{dd}S_d(S_d + 1),$$ (42)

$$a_{fd}a_{df} = x(1 - x)Z_f Z_d J_{fd}^2(g - 1)^2 J(J + 1)S_d(S_d + 1).$$ (43)

Since the Ni moment S_d is essentially zero in the $Gd_{1-x}Ni_x$ alloys, T_c is determined by the term a_{ff} (eq. 41) so that one expects a magnetic ordering temperature increasing with $1 - x$ or decreasing with x, as is indeed the case. In the intermediate concentration range the contribution due to the term a_{fd} predominates (eq. 43). It can be inferred from fig. 39 that this term is larger in the $Gd_{1-x}Fe_x$ alloys than in the $Gd_{1-x}Co_x$ alloys. There are at least three reasons for this. First, the exchange constant J_{fd} is larger for Gd–Fe than for Gd–Co, as can be seen from the results listed in table 4. Second, the value of S_d in eq. (43) is larger for Fe than for Co. And third, the Fe moments are more localized than the Co moments. As a consequence, the critical concentration below which no 3d moment will be present is higher in the Co alloys than in the Fe alloys. This can be inferred, for instance, from the concentration dependence of the ordering temperatures in $Y_{1-x}T_x$ alloys shown in figs. 40 and 41. For these reasons the a_{12} contribution will be higher and will extend to much lower 3d atom concentrations in $Gd_{1-x}Fe_x$ than in $Gd_{1-x}Co_x$.

If the term a_{dd} can be neglected in the small and intermediate 3d atom concentration range one expects T_c (eqs. 40, 41, 43) to be proportional to $(g - 1)^2 J(J + 1)$. Such a behaviour was found in amorphous alloys of the type $R_{0.69}Ni_{0.31}$ (Buschow, 1980a) and $R_{0.69}Co_{0.31}$ (Buschow, 1980b). Results for the latter compounds are shown in fig. 42. The deviations of the data points to above and below the full line for the light and heavy rare earth elements in $R_{0.69}Co_{0.31}$ were interpreted as being
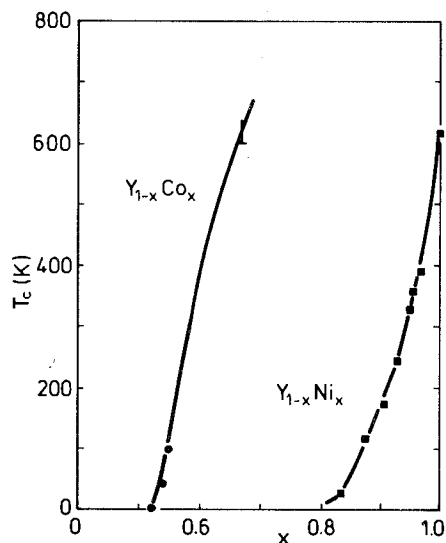
Fig. 40. Magnetic ordering temperatures in amorphous $Y_{1-x}Co_x$ and $Y_{1-x}Ni_x$ alloys. The data of $Y_{1-x}Ni_x$ were taken from the results published by Liénard and Rebouillat (1978).

indications that non-s-type conduction electrons participate in the exchange coupling of the rare earth moments.

Most of the temperature dependences of the magnetization in R–3d amorphous alloys, those of relatively high R content in particular, show a maximum when measured in comparatively low magnetic field. An example of such a $\sigma(T)$ curve is shown for $Dy_{0.60}Co_{0.40}$ in fig. 43. These maxima are not present in field-cooled curves and in $\sigma(T)$ curves measured in strong magnetic fields. The origin of these maxima
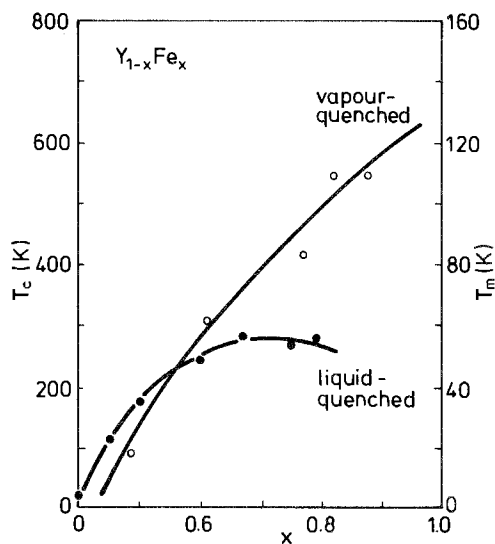
Fig. 41. Magnetic ordering temperatures (T_m) in vapour-quenched amorphous $Y_{1-x}Fe_x$ alloys (taken from the results published by Chappert et al., 1981) and Curie temperatures (T_c) in liquid-quenched amorphous alloys (taken from the results published by Croat, 1982a).
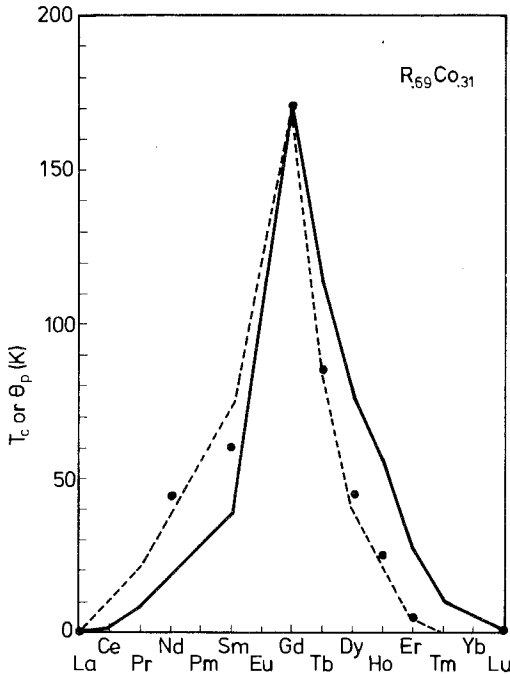
Fig. 42. Curie temperature in a series of amorphous $R_{0.69}Co_{0.31}$ alloys (after Buschow, 1980b). The solid line represents the function $(g-1)^2 J(J+1)$ normalized to the Curie temperature of $Gd_{0.69}Co_{0.31}$. The broken line represents the function $(g-1)^2 J(J+1) - 0.25(g-1)(2-g)J(J+1)$ normalized in the same way.
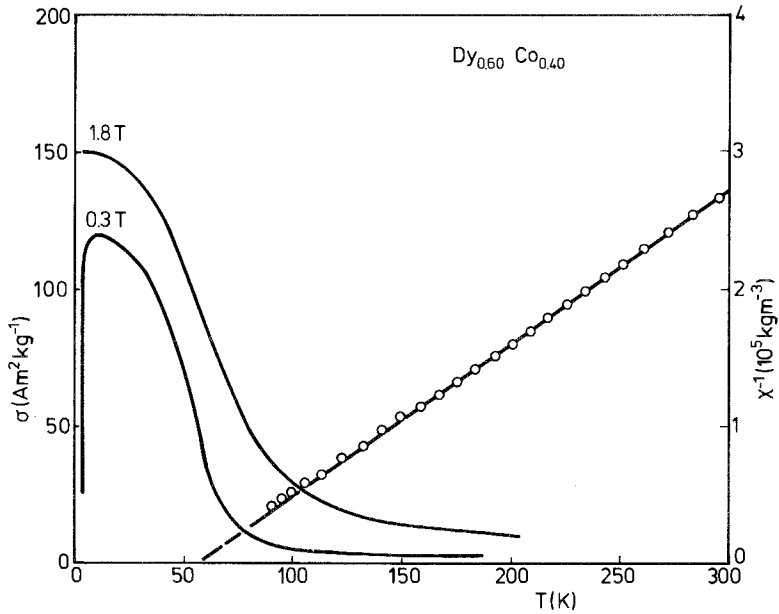
Fig. 43. Temperature dependence of the magnetization $\sigma(T)$ in amorphous $Dy_{0.60}Co_{0.40}$ obtained in a magnetic field of 1.8 T and 0.3 T (left-hand scale). The open circles represent data of the reciprocal susceptibility (right-hand scale).
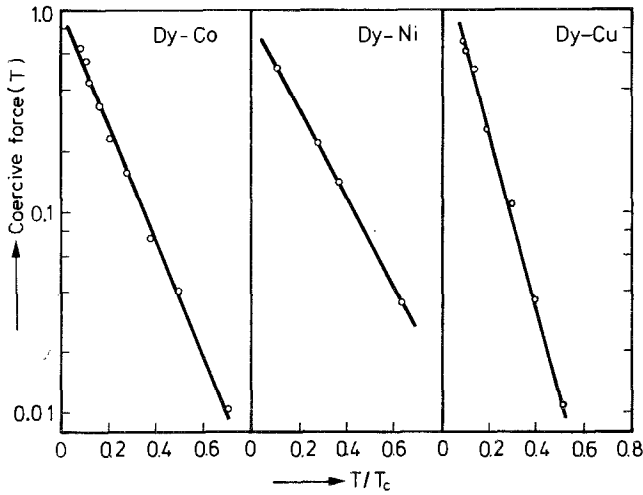
Fig. 44. Plot of $\ln H_c$ versus reduced temperature T/T_c in various amorphous alloys of the composition $Dy_{0.69}M_{0.31}$ (after Gubbens et al., 1981).

is a strongly temperature dependent coercive force. In fact, this temperature dependence is exponential according to the relation $H_c = H_0 \exp(-\alpha T)$. Although it is frequently observed in Co and Fe alloys it does not seem to be tied to the presence of a 3d moment, as can be seen from the results shown in fig. 44 for several alloys of the composition $Dy_{0.69}M_{0.31}$. These features are quite analogous to those obtained by Tissier et al. (1980), and were discussed in section 6.1. For a more detailed discussion of the low-temperature isotherms in amorphous R–3d alloys the reader is referred to the review given by Rhyne (1979) in Vol. 2 of this Handbook and to the papers by Gaunt (1979), Ferrer et al. (1979), and Kronmüller (1980, 1981).

6.3. The magnitude of 3d moments in amorphous alloys

Rare earth ions like, for instance, Gd^{3+} have their 4f electrons buried deep in the interior of the atoms, making these electrons strongly localized, and the same holds for the 4f moment. For this reason the 4f electrons of Gd are not subject to changes when Gd metal is combined with variable amounts of different partner elements. In contrast, the 3d electrons are itinerant and reside in narrow energy bands. As a consequence, alloying 3d metals with other metals gives rise to pronounced changes in the size of the 3d moments. These changes may be due to one or more of the following mechanisms:

(i) Charge transfer from the non-magnetic elements to the 3d metal, leading to less depleted 3d bands.

(ii) Hybridization and mixing effects, leading to sharing of electrons between the 3d atoms and the non-magnetic partner atoms. The changes in band structure will generally lead to a reduction in 3d exchange splitting.

(iii) Environmental effects: In the hypothetical case that the atomic arrangement in a number of alloys is the same (statistical distribution) and that also the combined effects of mechanisms (i) and (ii) are of similar magnitude, it is still possible to
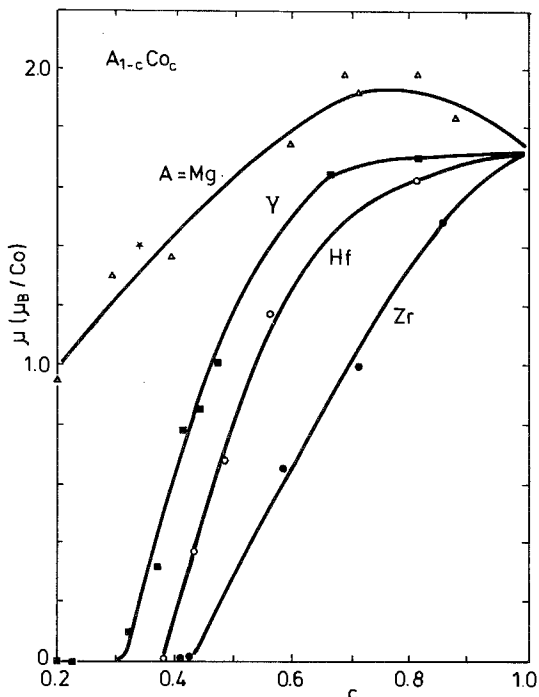
Fig. 45. Dependence of the moment per Co atom in various amorphous $A_{1-c}Co_c$ alloys on the effective concentration c. The value of the Co moment in the amorphous Au–Co alloys obtained by McGuire et al. (1982) has been included as the star slightly above the curve for $A = Mg$.

change the magnitude of the 3d moments by changing the atomic arrangement in the alloys. Clustering of 3d moments is known to entail moment enhancement, whereas anticlustering (i.e. the presence of more non-magnetic neighbour atoms than correspond to the statistical distribution) is expected to bring about moment reduction.

It was mentioned in section 5.4 that deviations from a statistical atomic arrangement may be a common feature in amorphous alloys whenever there is a positive or negative interaction between the atoms of the constituent elements. The type of inherent compositional short-range ordering (CSRO) depends on the sign of the heat of alloying (ΔH). For $\Delta H > 0$ one expects a tendency to clustering but for $\Delta H < 0$ a tendency to anticlustering. If mechanism (iii) predominates one expects therefore a correlation to exist between ΔH and the 3d moment. Such a correlation has indeed been observed in a number of amorphous Co alloys, showing that differences in magnetic properties between various amorphous Co alloys can qualitatively be explained by the presence of CSRO (Buschow and van Engen, 1981b; Buschow 1983b). This may be illustrated by means of the results shown in fig. 45 where the Co moments are plotted versus the effective concentration

$$c_{Co} = xV_{Co}^{2/3}\left[xV_{Co}^{2/3} + (1 - x)V_A^{2/3}\right]^{-1}. \tag{44}$$

These effective concentrations can be regarded as the actual concentrations x and $1 - x$ after weighting these quantities by the corresponding atomic cross-sections (or by atomic volumes $V_{Co}^{2/3}$ and $V_A^{2/3}$). The use of effective concentrations takes account of the fact that, even without CSRO, a given 3d atom will have a larger (or

Moment per Ni atom in various amorphous $A_{1-x}Ni_x$ alloys of equal effective Ni concentration
($c = 0.85$). The values of the heat of solution of A in Ni and the values of the electronegativity difference
$\Delta\phi^* = \phi_{Ni}^* - \phi_A^*$ were derived from the results published by Miedema et al. (1980).

$A_{1-x}Ni_x$	x	μ (μ_B/Ni)	ΔH (kJ/mol)	$\Delta\phi^*$ (V)
A = Zr	0.98	0.14	−239	1.80
Y	0.92	0.26	−160	2.00
Mg	0.91	0.46	−40	1.75

smaller) area of contact with other 3d atoms when the cross-section of the partner element is small (or large). In the absence of CSRO one expects alloys of similar c_{3d} values to have similar areas of contact with other 3d neighbours so that these alloys are expected to give rise to the same average 3d moment. In the presence of CSRO the effective concentration c_{Co} is underestimated when $\Delta H > 0$ but overestimated when $\Delta H < 0$. This means that when comparing different Co alloys having the same effective concentration calculated by means of eq. (44) one would expect a decrease in Co moment as ΔH decreases. The results shown in fig. 44 are quite convincing if one takes account of the fact that ΔH decreases strongly (becomes more negative) in the sequence A = Au, Mg, Y, Hf and Zr.

The number of amorphous Ni alloys for which magnetic data are available in the literature is rather small. The reason for this is that the Ni moment in unalloyed Ni is already rather small so that the concentration range where magnetic amorphous Ni alloys can be expected is rather limited and will only encompass the highest Ni concentrations. For a meaningful comparison only three alloy series are available, consisting of combinations of Ni with Zr, Y or Mg. These alloys behave in a similar way as those shown in fig. 45. Here again the alloys $Zr_{1-x}Ni_x$ with the lowest ΔH value give rise to the lowest μ_{Ni} versus c curve while the alloys $Mg_{1-x}Ni_x$ have the
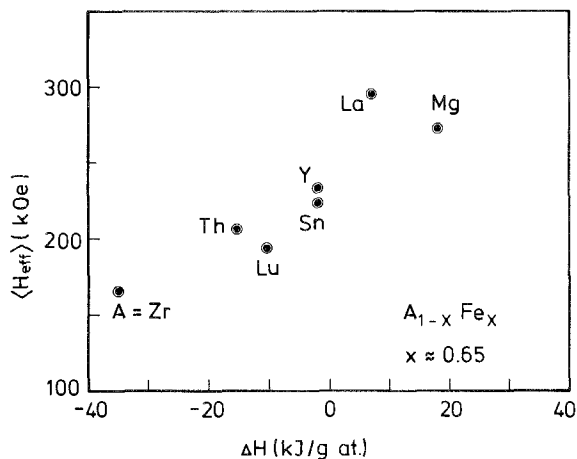
Fig. 46. Average effective hyperfine field in various amorphous alloys $A_{1-x}Fe_x$ of the approximate composition $x = 0.65$, plotted versus the corresponding values of the formation enthalpies (after van der Kraan and Buschow, 1982).

less negative ΔH values and give rise to the highest μ_{Ni} versus c curve. Numerical results for the effective concentration $c = 0.85$ can be compared in table 5. Again one finds a strong correlation between ΔH and μ_{3d} (Buschow, 1983b).

In Fe-base compounds, too, evidence has been found pointing to a correlation between the Fe moment and the heat of formation. Here one has to rely, however, on results of ^{57}Fe Mössbauer effect measurements for estimating the Fe moments since antiferromagnetic interaction may lead to erroneous results when using the results of bulk magnetic measurements (Van der Kraan and Buschow, 1982). An example of an analysis of the average hyperfine fields $\langle H_{eff} \rangle$ observed by ^{57}Fe Mössbauer spectroscopy is shown in fig. 46, where the values of $\langle H_{eff} \rangle$ observed in various amorphous $A_{1-x}Fe_x$ alloys have been plotted versus the corresponding heat of formation ΔH. These results also show that there is a close relationship between the Fe moments (as measured via H_{eff}) and ΔH. Some spread of the data points is present in fig. 46. We note, however, that a (small) part of the total hyperfine field at the Fe nuclei consists of the transferred hyperfine field, which measures the conduction-electron polarization due to the neighbour atoms. This transferred field may vary from one alloy to the other, since the conduction-electron concentration and the moment arrangement are not the same in all these alloys. Keeping this in mind, the observed trend of an increasing $\langle H_{eff} \rangle$ with increasing ΔH is rather convincing in establishing that the degree and the nature of the CSRO play a rather important role in determining the magnetic properties, in Fe-base alloys as well.

It follows from the results sketched above that the inherent CSRO in amorphous alloys carries considerable weight in determining their magnetic properties. This does not mean that the moment reduction according to the mechanism (i) or (ii) mentioned above is inoperative. In fact, the occurrence of CSRO may be looked upon as a means by which the effect of the mechanism (i) or (ii) can become enhanced. It can also be shown from a comparative study on crystalline compounds that environmental effects (iii) are unimportant relative to the effects described under (ii) and possibly (i) in compounds and amorphous alloys in which 3d metals are combined with Ti, Nb, Ta or W. In these amorphous alloys the moment reduction is stronger than in alloys of comparable heat of formation (Buschow, 1983b). This shows that also differences in the moment-reducing power of the A component have to be considered, like in the model of Friedel (1958).

6.4. Comparison with crystalline materials

Numerous investigations have dealt with the description of the magnetism of amorphous alloys compared with that of crystalline materials. It was shown by Brown (1978) and by Bobak (1980) that the random fluctuations in the exchange integral due to the amorphous nature of the alloy lead to an increase in Curie temperature, while Bobak also showed that fluctuations in the number of nearest neighbour atoms have the opposite effect. The atomic disorder was also found to have a strong influence on the temperature dependence of the magnetization. Here it should be mentioned that for a random system even the mean field theory cannot be treated exactly, making it necessary to use different types of approximations
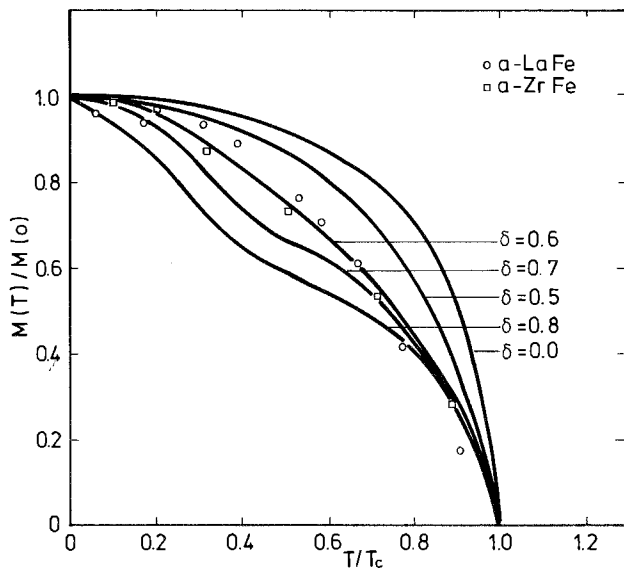
Fig. 47. Normalized magnetization $M(T)/M(0)$ versus reduced temperature T/T_c for various ratios of exchange fluctuations to exchange, i.e. $\delta = \Delta J/J$ (after Heiman and Kazama, 1979). The data for amorphous LaFe and ZrFe yield $\delta \approx 0.6$.

(Handrich, 1969; Slechta, 1975; Jäger, 1977). In general there will be a flattening of the temperature dependence of the reduced magnetization $M(T)/M(0)$. This may be illustrated by means of the results of Heiman and Kazama (1979), who studied the temperature dependence of amorphous $La_{1-x}Fe_x$ and $Zr_{1-x}Fe_x$ alloys ($x \approx 0.7$) and compared their experimental data with model calculations of Handrich (1969). Part of the results of Heiman and Kazama have been reproduced in fig. 47. The calculated curves pertain to different values of the normalized exchange fluctuation $\delta = \Delta J_{dd}/J_{dd}$. Systems with $\delta < 0.8$ are usually regarded as ferromagnets while systems with $\delta > 0.8$ are more like spin glasses. Heiman and Kazama conclude from their analysis that the amorphous Fe alloys investigated ($\delta \approx 0.6$) are not far off from spin glass behaviour.

Apart from the temperature dependence of the magnetization there exists an even more obvious difference in magnetic properties between amorphous and crystalline alloys, namely between the magnitudes of the moments themselves. It was already mentioned in section 6.2.1. that amorphous $Y_{1-x}Fe_x$ alloys are not true ferromagnets but behave more like spin glasses (Coey et al., 1981; Chappert et al., 1981). Owing to the fact that the distribution of exchange interactions encompasses a substantial part of negative (antiferromagnetic) interactions, some Fe sites will experience only weak exchange fields which may show up as a lower atomic moment. A further reduction of the bulk magnetization will occur due to the spin-glass-like structure. The values given for amorphous $Y_{1-x}Fe_x$ in fig. 48 were obtained from extrapolation of data obtained in high magnetic fields. Owing to these experimental difficulties in determining the magnetic moment in amorphous Fe alloys a comparison with magnetic moments observed in the crystalline counterparts may not always be very meaningful. Better estimates of atomic Fe moments may be obtained in some cases on the
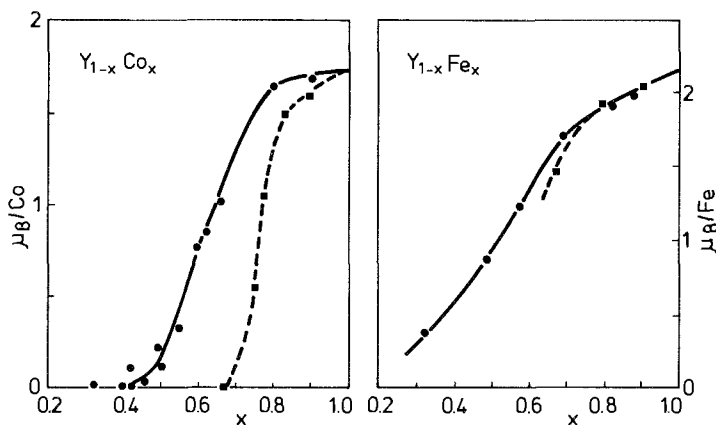
Fig. 48. Concentration dependence of the 3d moments in crystalline and amorphous $Y_{1-x}Co_x$ (left-hand part) and $Y_{1-x}Fe_x$ (right-hand part). The circles and full curves refer to amorphous alloys. The squares and broken curves refer to intermetallics. The data of $Y_{1-x}Fe_x$ were taken from Coey et al. (1981).

basis of results obtained by means of ^{57}Fe Mössbauer spectroscopy. These latter results may suffer, however, from the inaccuracies involved with the conversion of effective hyperfine fields into atomic moments, since it has not yet been established whether the conversion factors are equal in the crystalline and the amorphous state.

A different type of difficulty arises if one wishes to compare the atomic Ni moment in the crystalline and the amorphous state. Owing to the smallness of the Ni moment even in pure Ni metal, alloying with increasing moments of a second metal leads to a relatively rapid decrease of the Ni moment. For instance, in the amorphous $Mg_{1-x}Ni_x$ system ferromagnetism is observed only when $x \geqslant 0.70$ (Buschow, 1982d). A comparison with crystalline alloys is not possible since there are no compounds with Ni concentrations higher than $MgNi_2$ ($MgNi_2$ is Pauli paramagnetic). In the $Y_{1-x}Ni_x$ system the critical concentration is even higher (Liénard and Rebouillat, 1978; see also fig. 40). Furthermore, crystalline Y–Ni compounds give rise to the so-called magnetism resurgence where the Ni atoms carry a magnetic moment only by virtue of the presence of the 4d electrons of the Y atoms (Gignoux et al., 1980).

It follows from the discussion given above that for a comparison of the atomic moments in the amorphous state with those in crystalline materials one is primarily restricted to Co-base materials. Here the experimental situation is quite clear: As shown for $Y_{1-x}Co_x$ in fig. 48 the Co moment in the amorphous alloys is observed to be higher than in crystalline materials.

Such differences in atomic magnetic moments between amorphous and crystalline alloys are less easily described by the models mentioned at the beginning of this section, since in descriptions based on the Heisenberg model no moment difference is expected at $T = 0$. The arguments presented so far to describe the moment differences are based primarily on band effects. Krey (1977) notes that the changes in the 3d band in going from the crystalline to the amorphous state are in the direction of the free atom limit and cause a drastic reduction in the density of states.

As a consequence one would expect the magnetic 3d moment in amorphous alloys to be lower than in crystalline materials. This seems to be in disagreement with experiment (see the compilation of data given by Buschow, 1982d).

A different explanation of the moment difference between amorphous and crystalline alloys was given by Heiman and Kazama (1978a). These authors argue that the charge transfer from the second component to the 3d component is less in amorphous than in crystalline materials. Here, however, one has to take into consideration that it is doubtful whether the reduction in 3d moments upon alloying in crystalline or amorphous alloys is mainly due to charge transfer. In the first place, as will be discussed in more detail in section 9, the occurrence of such charge transfer effects is not found in XPS experiments. In the second place, as will also be discussed in section 9, Mössbauer spectroscopy performed on the 3d atom site as well as on the rare earth site in crystalline and amorphous rare-earth–3d alloys does not reveal significant differences in isomer shift between the two types of alloys.

A relatively straightforward explanation of the difference in moment between amorphous and crystalline alloys can be given on the basis of an extension of the simple model discussed in the previous section for describing differences in magnetic properties between various amorphous alloys. Here one has to realize that the CSRO in amorphous alloys represents a certain degree of deviation from a statistical atomic distribution. In crystalline materials, i.e. in intermetallic compounds, one always has an optimum CSRO in the sense that there is a tendency for each 3d atom to have almost exclusively dissimilar atoms as nearest neighbours. Consequently the saturation moment in intermetallics will be lower than in amorphous alloys. This more complete surrounding of a 3d atom by dissimilar atoms in an intermetallic compound than in a molten alloy or amorphous alloy is reflected in the fact that the heat of compounding is always higher than the heat of mixing. If one wishes one may therefore carry through the correlation mentioned in section 6.3 where a lower 3d moment is expected when ΔH takes more negative values.
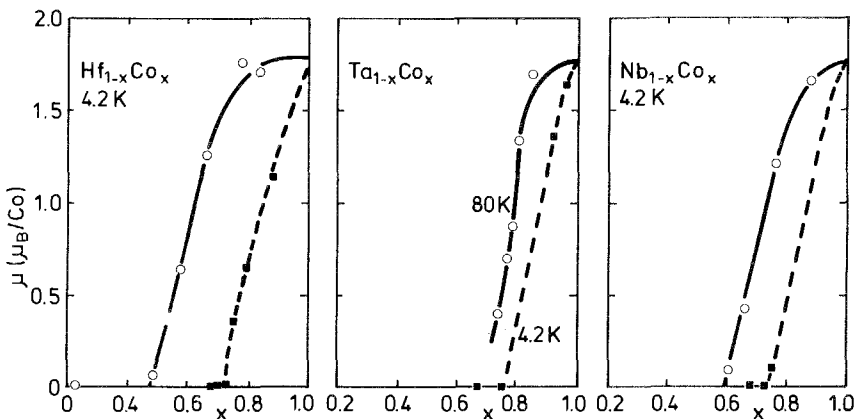
Fig. 49. Comparison of the concentration dependence of the magnetic moment in various amorphous alloys (circles, full curves) and crystalline materials (squares, broken curves). The data on amorphous Ta–Co alloys were obtained from the results of Naoe et al. (1981).

It will be clear that this explanation of the difference between the magnetic moment in crystalline and amorphous materials is not restricted to alloys of 3d metals with rare earth. Its general validity follows for instance from the results shown in fig. 49, where the crystalline curves pertaining to the crystalline states are invariably below those of the amorphous states. Here we wish to stress again that the above explanation of the differences in saturation moment does not mean that band structure effects or charge transfer effects can be completely neglected (Malozemoff et al., 1983). The present analysis only shows that CSRO effects play a rather prominent role in the determination of the magnetic properties.

7. Thin magnetic amorphous films

An extensive treatment of preparation and properties of thin films based on alloys or compounds of rare earth metals was already given by Gasgnier in Chapter 41, Volume 5 of this Handbook (Gasgnier, 1982). In this section the attention will be focussed mainly on the magnetic properties of thin films consisting of amorphous alloys of rare earths and 3d transition metals. Although the discussion will include a large number of results reported in the literature only recently, some overlap with the results described in Gasgnier's chapter is difficult to avoid.

7.1. Uniaxial anisotropy

Amorphous films of rare earths and 3d transition metals have attracted much attention owing to their possible applications as magneto-optic and thermomagnetic recording media with a high information density. A prerequisite for these applications is the presence of a uniaxial anisotropy with the easy magnetization direction perpendicular to the film plane ($K_u > 0$). Sign and magnitude of the anisotropy constant K_u can be determined by means of magnetization measurements in external fields parallel and perpendicular to the film plane, by means of torque measurements and by means of ferromagnetic resonance techniques. Various mechanisms have been proposed for the origin of the positive K_u in these amorphous thin films comprising atomic-scale structure anisotropies, anisotropic phase segregation, columnar microstructures and stress-induced anisotropy. In this section these features will be briefly discussed.

Gambino et al. (1973), by a process of elimination, concluded that short-range atomic ordering is the main source of anisotropy in sputtered amorphous Gd–Co films. They support their conclusion with the results of radiation damage experiments and annealing experiments. A modest damage level proved sufficient to destroy the uniaxial anisotropy when the damage was sustained in zero field. On the other hand, the anisotropy of amorphous Gd–Co films can be adjusted by annealing the films below their crystallization temperature in a saturating perpendicular field. Annealing under the same conditions in zero fields leads to a decrease of the anisotropy. They argue that the annealing temperature is high enough to cause single atomic jumps without giving rise to long-range diffusion necessary for crystallization

to set in. The jump probability is influenced by the magnetization direction so as to favour the formation of atomic short-range order in a given direction.

Gambino et al. also provide a clue as to which type of short-range ordering may cause the anisotropy. On the grounds of studies on hcp cobalt they suggest that the easy magnetization direction may be due to the presence of Co–Co pairs having their pair axis perpendicular to this direction, the magnitude of the anisotropy energy being of the order of 10^{-22} to 10^{-23} J/pair. In order to understand the formation of such Co–Co pairs during vapour deposition one has to consider the following. During the deposition process the adatom impinges on the film surface with considerable kinetic energy, after which it rapidly loses this energy to the substrate and the main body of the film. If the substrate temperature is sufficiently high the adatoms are able to move by means of surface diffusion to favourable sites of relatively low energy, so as to produce eventually a crystalline film. Low substrate temperature and high evaporation rates do not favour such rearrangements of the adatoms and generally lead to amorphous films. In the intermediate case the adatom may still have the opportunity to jump to any of its nearest neighbour surface sites, the jump probability being proportional to the corresponding activation energy. Differences in activation energy for jumps between the initial site and the nearest neighbour surface site may be due to chemical, geometrical and magnetic origins.

Similar arguments may be used to show that pairs of Co atoms (with their axis in the film plane) in excess of a random distribution can be formed during bias sputtering. With this technique an adatom bonded to a similar surface atom is expected to have a higher resputtering probability than an adatom bonded to a dissimilar atom, since Co–Co and Gd–Gd bonds are energetically less favoured than Gd–Co bonds. Consequently the statistical probability of Gd–Co pairs oriented perpendicular to the film plane will be higher than that of Gd–Co pairs oriented parallel to the film plane, while the opposite holds for Co–Co pairs.

Gambino et al. (1973) note that several observations support their model of pair ordering. First, the anisotropy is relatively independent of temperature near room temperature where the magnetic ordering of the Co sublattice is almost complete, in contrast to the Gd sublattice which gradually becomes ordered. This indicates that the anisotropy is to be associated with the Co sublattice. Second, the growth-induced anisotropy increases with increasing resputtering but decreases at high deposition rates and low substrate temperatures. The presence of uniaxial anisotropy was found not to be restricted to Gd–Co amorphous films but was reported to be absent in Gd–Co films when sputtered without bias voltage (Heiman et al., 1975; Lee and Heiman, 1974).

Attempts were made by Wagner et al. (1975) to obtain experimental evidence for the presence of the pair-ordering effect by means of X-ray transmission and reflection techniques. These authors did not find significant differences between the reduced distribution functions $G(T)$ of the biased and unbiased films. They report, though, that the peaks in $G(r)$ at larger values of r ($r > 0.6$ nm) are higher in the biased film than in the unbiased film. This was interpreted by Wagner et al. to indicate that the films in which magnetic anisotropy is present have structural order over larger distances than the unbiased film.

Wang et al. (1979) studied amorphous Gd–Co films by means of electron diffraction and found that the radial distribution functions are significantly different for the perpendicular anisotropic and in-plane anisotropic films. Wang et al. and also Nishihara et al. (1979) conclude from their results that the perpendicular anisotropy is associated with a predominance of Gd–Co pairs. This would agree with the pseudo-dipolar model of Chaudhari and Cronemeyer (1975) where the cross term $M_{Co}M_{Gd}$ predominates in their expression for K_u given by

$$K_u = \sum_{ij} c_{ij} M_i M_j, \tag{45}$$

where M_i and M_j represent the 4f and 3d sublattice magnetizations and where the c_{ij} values depend on the corresponding g values. Cargill and Mizoguchi (1978) calculated the contribution to K_u of classical dipolar interactions, using the relation

$$\Delta K_u \simeq A X_A X_B \left(\frac{M_A}{X_A} + \frac{M_B}{X_B} \right)^2, \tag{46}$$

where the constant A includes the measure p of alignment of dissimilar nearest neighbour pairs, a "packing fraction" and other structural constants. $X_{A,B}$ and $M_{A,B}$ denote the atomic fractions and the sublattice magnetizations, respectively. The latter quantities are related to the atomic moments $m_{A,B}$ via the relations $M_{A,B} = X_{A,B} N m_{A,B}$ (N is Avogadro's number). In their calculations these authors assumed that the magnetization in these alloys was made up of two oppositely directed sublattice magnetizations. With eq. (46), using small positive values for p, the authors were able to explain the anisotropies of $K_u \approx 10^{12}$ J/cm^3 observed in several Co-rich samples.

Algra et al. (1980) studied the anisotropy in various Gd-base amorphous alloys by means of ferromagnetic resonance techniques (FMR). Their samples had a comparatively high Gd concentration and were prepared by melt spinning. Quite surprisingly these samples too showed a large uniaxial anisotropy. Possible effects due to Co–Co pair ordering can be excluded since the high anisotropies were also reported to be present in alloys of the type $Gd_{1-x}Cu_x$. These results suggest that an important role in determining the anisotropy may be played by the Gd atoms and their ordering on an atomic scale. Similar conclusions were reached later on also by Maksymowicz et al. (1983).

Structural inhomogeneities on a microstructural scale rather than on an atomic scale have also been proposed as the origin of the uniaxial anisotropy (Mizoguchi and Cargill, 1979; Herd, 1977, 1978, 1979; Leamy and Dirks, 1979; Yasugi et al., 1981; Kusuda et al., 1982a,b). In section 5.5 it has already been indicated that under certain conditions a columnar microstructure may result from the self-shadowing of the vapour beam during deposition. Leamy and Dirks (1979) investigated amorphous alloys of the type $Gd_{1-x}Co_x$, $Ho_{1-x}Co_x$, $Gd_{1-x}Fe_x$ and $Y_{1-x}Fe_x$ in the range $0.3 < x < 0.9$. They observed an anisotropic microstructure of the columnar type in these alloys when prepared by vapour deposition or sputtering. The structure entails rod-shaped density fluctuations that are parallel and oriented nearer to the film normal than the incident vapour beam. The columnar structure itself was found to

contribute only slightly to the development of the perpendicular magnetic anisotropy. This anisotropy was found to be enhanced, however, by annealing deposition in an oxygen-contaminated atmosphere and by application of a bias voltage during sputtering. This enhancement of the perpendicular anisotropy constant K_u is accompanied by the formation of an inhomogeneous microstructure in the film, which involves oxide decoration of the low-density network of the columnar structure. Evidence in support of this oxide decoration was obtained from the split first diffraction peak observed in electron diffraction patterns. Shen et al. (1981) performed XPS measurements on amorphous Gd–3d films and provided more details of the oxide decoration. They suggest that the first step consists of surface segregation of the Gd atoms to the columnar boundaries. These atoms are subsequently oxidized and help to reduce the oxide of Co formed during annealing in vacuum.

In order to assess the effect of stress on K_u Leamy and Dirks measured the stress σ in several of their samples and found a correlation between K_u and σ as shown in fig. 50. They note, however, that the K_u values in fig. 50 are too large by a factor of about 100 to allow the origin of K_u to be attributed to a simple magnetostrictive effect, and argue that the stress state is rather indicative of the structural state which is directly correlated with K_u. Somewhat different results were obtained by Takagi et al. (1979), who investigated amorphous Gd–Fe and Tb–Fe films and observed that the stress is compressive at low argon pressure and tensile at high argon pressure. These authors measured the anisotropy constant and the stress before and after removal of thin amorphous films from the substrate and they infer from their results that the perpendicular anisotropy originates from the internal stress due to the substrate constraint in thin amorphous Tb–Fe films. A stress-induced anisotropy in Gd–Fe films was also proposed by Togami (1981) and by Labrune et al. (1982).

Itoh et al. (1983) report that the perpendicular magnetic anisotropy in Gd–Fe films, when prepared by means of sputtering under low substrate bias voltage, is mainly stress determined. In alloys where the R component is a non-S state ion the
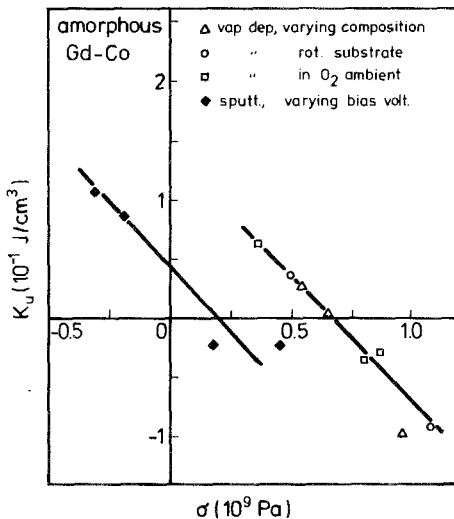
Fig. 50. Dependence of the uniaxial anisotropy constant K_u on stress σ in various amorphous Gd–Co alloys obtained either by vapour deposition (varying composition, rotating substrate or oxygen-containing ambient) or by sputtering 9varying bias voltage). The data are reproduced from the paper published by Leamy and Dirks (1979).

uniaxial anisotropy can also be due to the single-ion anisotropy of R. This was reported by Kobayashi et al. (1983) on amorphous Tb–Fe films that were shown to possess growth-induced anisotropy associated with the anisotropy of the Tb atoms themselves. The effect of preferential resputtering of Tb on K_u in amorphous Tb–Fe films was investigated by Katayama et al. (1983). In amorphous Ho–Co films the presence of a columnar microstructure was held responsible for perpendicular anisotropy (T. Suzuki, 1983).

Herd (1979) and Graczyk (1978) propose that structural inhomogeneities are the source of large positive K_u values and that these inhomogeneities are due to phase separation. The phase separation was assumed by Herd to involve anisotropically shaped Co-rich clusters. They furthermore considered it to be the universal source of K_u in both bias-sputtered films and films obtained by means of electron gun evaporation techniques. Their evidence for this was obtained by means of TEM investigations on samples prepared in different ways.

From small-angle scattering measurements Herd (1979) found that the characteristic period of the microstructure increased from 2.5 nm to 3.5 nm as a function of the bias voltage. In all these cases it was derived from the corresponding electron diffraction diagram that the oxygen content is relatively low, i.e. that large amounts of Gd_2O_3 (which would have led to a split first peak in the electron diffractogram) were absent. Herd notes that the columnar structure and the oxide decoration of the low-density region may aid in producing a large and positive K_u, although they cannot be considered as essential since this structure was found to disappear in the sputtered films with increasing bias voltage prior to the onset of K_u. In this connection Leamy and Dirks (1979) reported that in their samples the columnar microstructure remained visible until complete crystallization occurred.

Support for the presence of regions of higher Co concentrations dispersed uniformly throughout the deposited thin films comes from FMR measurements made by Prasad et al. (1979). These authors found indications that the inhomogeneities mentioned increase with bias voltage.

Esho (1979) found that strong perpendicular magnetic anisotropy can be obtained in thin amorphous Gd–Co films by sputtering in the absence of bias voltage in the presence of N_2 gas contaminations. Esho considers the presence of two sources for the anisotropy, a bias-induced positive anisotropy and a microcrystalline negative anisotropy. The relative contributions of both types are assumed to depend on details of the microstructure, i.e. on details of the method of preparation.

Hoshi et al. (1982) prepared amorphous Gd–Co films by means of ion beam sputtering. Perpendicular magnetization was found in thin films of a Co concentration close to the compensation composition which were deposited without O_2 or N_2 addition, although the value of K_u was found to be smaller than that usually obtained in rf sputtered films. Hoshi et al. (1982) observed that incorporation of nitrogen leads to decreasing values of K_u, which is contrary to the results of Esho mentioned above. Hoshi et al. also report that the incorporation of oxygen leads to an increase in K_u, in agreement with results obtained by Brunsch and Schneider (1978), Tsunashima et al. (1980), Dirks and Leamy (1978), Leamy and Dirks (1979) and by Biesterbos et al. (1979).

Hoshi et al. studied their films by TEM as well. From the corresponding electron diffraction patterns they inferred that phase separation had taken place, involving the formation of a nitride or oxide of part of the Gd. Both the oxygen-contaminated film and the nitrogen-contaminated film had essentially the same microstructure and this microstructure was not composed of columns usually obtained by means of sputtering. From these results the authors conclude that shape anisotropy associated with structural or compositional fluctuations apparently contributes little to the perpendicular anisotropy in Gd–Co films.

Hoshi et al. measured the perpendicular anisotropy constant K_u before and after removal of the film from a rock salt substrate. The values of K_u were found to change only little after removal and furthermore were not much different from the values obtained on films deposited under similar circumstances on glass substrates. From these results the authors conclude that stress-induced anisotropy contributes only little to the perpendicular anisotropy, which agrees with the conclusions of Leamy and Dirks mentioned above.

The effect of a variable transition metal component T in $Gd_{1-x}T_x$ was studied by Chen and Wilson (1978), who found no change in K_u if Co was replaced by Fe in films prepared by means of bias sputtering. These results are contrary to those of Taylor and Gangulee (1977) on vapour-deposited films shown in fig. 51. The possibility of two different mechanisms for the presence of perpendicular anisotropy in Fe- and Co-base sputtered films had already been suggested by Katayama et al. (1977). Apparently stress is of little influence on K_u in the case of Gd–Co films but may have a considerable effect on K_u in the case of Gd–Fe films (Takagi et al., 1979). Hoshi et al. (1982) and also Togami and Kobayashi (1981) emphasize the importance of controlling the O_2 and N_2 content in the argon gas during sputtering. Malmhäll and Chen (1982) found that the nominal concentration changes as a function of film thickness due to changing short-range ordering. This also gives rise to a change in magnetic hardness of the film (Heiman et al., 1974).
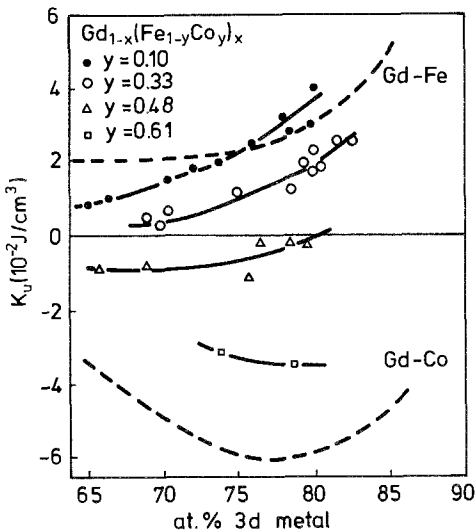
Fig. 51. Concentration dependence of the uniaxial perpendicular anisotropy constant K_u in vapour-deposited films of the type $Gd_{1-x}T_x$, where T is a mixture of Co and Fe. The data were taken from results published by Taylor and Gangulee (1977). The binary alloys are indicated by broken lines.

Survey of amorphous R–3d films in which it has been possible to obtain a perpendicular uniaxial anisotropy (⊥) by evaporation methods (E) or by sputtering (S). Cases where it proved impossible to attain perpendicular anisotropy are labelled by the symbol (≈).

	Gd	Tb	Dy	Ho	Er
Fe E	⊥	⊥		⊥	
S	⊥	⊥	⊥	⊥	⊥
Co E	=	⊥		⊥	
S	⊥		⊥	⊥	≈
Ni E	⊥	≈		⊥	
S	=				

Concluding this section it may be said that the presence of a uniaxial perpendicular anisotropy in amorphous rare-earth–3d films ($R_{1-x}T_x$) depends on a number of different parameters comprising (1) the composition x, (2) the nature of the R component, (3) the nature of the T component, (4) the method of film deposition such as co-evaporation of the components, sputtering with or without bias voltage, (5) argon pressure, (6) heated substrates and post-deposition treatments, (7) contamination with reactive gases like O_2 or N_2 during deposition or (8) during post-deposition treatments, and (9) the presence of a magnetic field during deposition or annealing. A survey of the possible ways and means to obtain a perpendicular anisotropy under special circumstances in various R-base 3d transition metal alloys has been given by Sakurai and Onishi (1983). Their results are reproduced in table 6. A parameter whose influence is less frequently investigated but which nevertheless may be of considerable importance is the deposition rate.

The relatively large number of controversial results mentioned above bears witness to the extreme difficulties that are encountered when performing research in this field, since it is almost impossible to study the effect of a single parameter while keeping the other constant. A typical example concerns the effect of bias voltage (V_B) during sputtering on K_u. A negative substrate potential will lead to sputtering of the surface oxygen and resputtering of the deposited materials. As a consequence a negative bias voltage not only leads to a compositional change but also to a structural change (Yasugi et al., 1981; Kusuda et al., 1982a). Furthermore, not all columnar microstructures behave in the same way since the shape anisotropy can be expressed as (see Kusuda et al., 1982a):

$$K_u = 2\pi M_s^2 \frac{\delta}{a}, \tag{47}$$

where δ is the thickness of the non-magnetic layers between the columns. The column thickness a was found to depend on the Gd concentration and on film thickness. To add two more complications, the quantities a and δ have to be interchanged if the magnetization of the columnar interspace exceeds that of the columns, which makes K_u dependent on the degree of the column boundary oxidations as well. Here we recall that the oxygen content may decrease drastically

with applied bias voltage. There may also be a difference of degree in the change of the surface composition of the target (Chen et al., 1982).

As this example may have shown, variation of a single parameter (V_B) alone produces quite a number of changes which all have some bearing on the magnitude of K_u and these changes need not necessarily carry the same weight in the various experimental set-ups used by the different authors. It is most likely, therefore, that most of the controversial results obtained by different authors originate from the fact that not all of the manifold parameters associated with thin-film preparation are exactly the same.

Apart from uncertainties as to which parameters or combination of parameters may give rise to large and positive K_u values, there is still the more fundamental difficulty of establishing the origin of K_u. Two types of pair ordering (Co–Co or Gd–Co) have been proposed as the origin on an atomic scale, in contrast to the shape anisotropy concept which explains K_u in terms of the microstructures. It should be mentioned here that describing the anisotropy observed experimentally has always been a difficult task. For instance, even in atomically well-ordered materials like the hexagonal compounds YCo_5 and Y_2Co_{17} it is not well understood why the former has $K_u > 0$ (easy c-axis) while the latter has $K_u < 0$ (easy basal plane). The experimental results obtained for crystalline YCo_5 and Y_2Co_{17} (see, for instance, the review published by Buschow, 1980c) open the possibility that K_u in amorphous R–Co alloys may originate from the presence of CSRO, small changes in the degree and/or the topology of the short-range ordering being able to change K_u from positive to negative. It has already been noted in sections 5 and 6 that the presence of CSRO may be expected when ΔH is different from zero, as is certainly the case in the R–Co alloys. Experimental evidence indicating such an origin of K_u was obtained by Gronau et al. (1981) on amorphous $Sm_{1-x}Co_x$ films. As can be seen in fig. 52, the anisotropy constant K_u has a maximum close to the composition corresponding to $SmCo_5$. Interesting results in this respect were also obtained by Nawate et al. (1983).

Summarizing the results of this section, it may be stated that modern process research and fundamental research have been closely intertwined in studies of amorphous materials. Although joint efforts may culminate eventually in a solution being found to the problems associated with the anisotropy, at present the situation is still confusing, but represents at the same time a challenge for many a scientist.
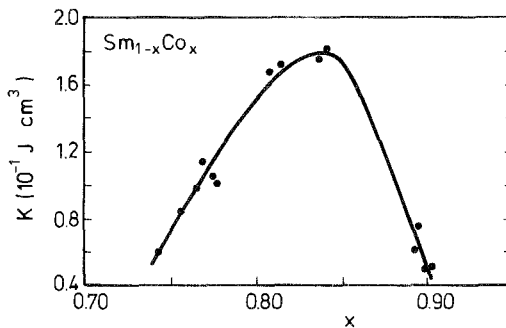
Fig. 52. Concentration dependence of induced anisotropy in amorphous $Sm_{1-x}Co_x$ films (after Gronau et al., 1981).

7.2. Domain stability

Thin films of amorphous alloys of rare earths and 3d metals can be used as erasable magneto-optical recording media of relatively high bit density. In section 6.2 it has been mentioned that the temperature dependence of such $R_{1-x}T_x$ alloys, assuming properly chosen concentrations, gives rise to a compensation temperature T_{comp} where the net magnetization vanishes owing to a cancellation of the R and T sublattice magnetization. An example of a curve representing the temperature dependence of the magnetization was shown in fig. 36. Values of T_{comp} of various alloys are given in tables A3 and A4 in the Appendix (see also fig. 35).

The temperature dependence of the coercivity H_c shows a relatively sharp maximum at T_{comp}. This implies that when T_{comp} is close to room temperature it is very difficult to reverse the magnetization of the magnetic domains. In order to achieve such magnetization reversal applied fields are necessary with a magnitude comparable to H_c. However, if a small spot of the thin film is heated instantaneously by a pulsed laser beam, the local coercive field moves out of the large-H_c region so that magnetization reversal can be achieved by means of applied fields (H_a) considerably below H_c. In this case only the magnetization of the irradiated spot is reversed, i.e. a bit has been written. This procedure is indicated by compensation point writing.

A second procedure involves local heating above the Curie point T_c. The atomic moments which give rise to strong thermal fluctuations in the vicinity of T_c will orient themselves in a direction antiparallel to the main magnetization of the film when the laser beam is switched off and the temperature of the spot decreases. This procedure is known as Curie point writing.

Details of magneto-optical and thermomagnetic recording will be given in section 10. Here we will focus our attention with thermomagnetic writing, such as the stability of domains of reversed magnetization under a variety of circumstances. The description of magnetic domain stability given below does not apply exclusively to thin amorphous R–3d films. Many aspects of the description are very similar to those involved with the bubble-type approach of domain stability on non-rare-earth materials (Bobeck, 1967; Dekker, 1976; Esho et al., 1973; Schuldt and Chen, 1971; Thiele, 1970). The bubble-type approach was adapted by Huth (1974) to amorphous R–3d films into which domains of reversed magnetization were written by means of compensation point writing. In the brief description given below we will follow closely the results obtained by Huth. For a more rigorous treatment the reader is referred to the original paper.

In order to find the equilibrium domain size of a cylindrical domain present in a film of thickness that has a uniformly saturated magnetization M, one has to consider its total energy E_t. This energy is composed of contributions due to the domain well energy per unit area $\sigma_w(R)$, the magnetostatic self-demagnetizing energy $\varepsilon_d(R)$ and the interaction energy between the magnetization and the external field H_a. In the following it will be assumed that the unswitched magnetization is negative whereas the external field (i.e. the "write bias") is positive. The radial coordinate is indicated by r and the wall is located at $r = R$. The force F acting on

the domain wall can be derived from E_t after differentiation of E_t with respect to R:

$$F = 2\pi h\sigma_w(R) + 2\pi Rh[(\partial\sigma_w(R)/\partial R) - (\partial\varepsilon_d(R)/\partial R)] - 4\pi RhH_a|M(R)|.$$
(48)

After averaging over the z-coordinate Huth approximated the demagnetization term by means of the expression

$$\partial\varepsilon_d/\partial R = 4\pi Rh\overline{H}_d(R)|M(R)|,$$
(49)

where $\overline{H}_d$ is an averged demagnetizing field. Positive terms in eq. (48) have the tendency to shrink the reversed domain while negative terms tend to expand it. In bubble materials stable domains are obtained when the various forces contained in eq. (48) exactly cancel, i.e. when $F = 0$. In the rare earth base materials one has to take account of the presence of large coercive forces H_c. As argued by Huth, the domain size is then determined by a force balance between the wall pressure and a quasi-frictional force associated with the coercivity. No wall movement will take place if the wall pressure is lower than this coercivity force. The corresponding stability condition is most conveniently expressed in terms of fields by dividing the forces in eq. (49) by $4\pi Rh|M(R)|$:

$$H_{net} = \left[\frac{\sigma_w(R)}{2R|M(R)|} + \frac{1}{2|M(R)|}\frac{\partial\sigma_w(R)}{\partial R} - \overline{H}_d(R) - H_a\right] \leq H_c(R).$$
(50)

Eq. (50) has to be interpreted as follows: A stable domain is obtained if the absolute magnitude of the sum contained in the left-hand brackets is smaller than the coercive field ($H_{net} < H_c$). A negative sign ($H_{net} < 0$) indicates domain expansion, a positive sign ($H_{net} > 0$) domain compression. In ferromagnetic materials the wall energy depends on the anisotropy constant K_u and the exchange constant J by means of the relation $\sigma_w = 4(K_uA)^{1/2}$, K_u and A each depending on the temperature. In the ferrimagnetic Gd–Gd materials of interest here the compensation temperature (H_c maximum) is considerably lower than the Curie temperature. It may therefore be assumed that the temperature excursion ΔT_0 associated with the local laser beam heating, which is needed to bring about a sufficient drop in H_c, is comparatively small and justifies the assumption $\sigma_w = $ constant. This also implies $\partial\sigma_w/vR = 0$ so that eq. (50) reduces to

$$H_{net}M(R)\equiv\left[\frac{\sigma_w(R)}{R} - \overline{H}_d(R)M(R) - H_aM(R)\right] \leqslant H_c(R)M(R).$$
(51)

Since the temperature dependences of M and H_c have been experimentally determined one has to make assumptions regarding the radial temperature distribution in the heated spot to find the corresponding radial distribution of M and R. If the intensity distribution of the laser beam is Gaussian the temperature distribution in the film can be represented by means of isotherms of ellipsoidal character (Urner-Wille et al., 1980) such as schematically indicated in fig. 53. A Gaussian laser beam profile was also used in the numerical calculations of Huth (1974), presented below.
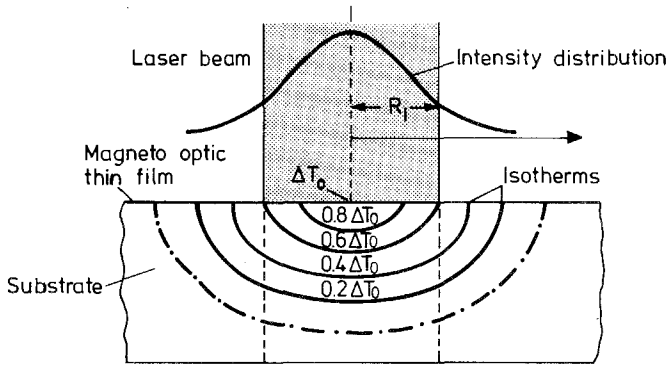
Fig. 53. Isotherms representing the temperature in a thin amorphous film 1 μs after an instantaneous heat pulse induced by a laser beam of Gaussian intensity profile (after Urner-Wille et al., 1980).

The questions one has to ask are: How large is the reversed domain written by the laser beam (R_c) and what happens to the domain size after returning to room temperature and after switching off the bias field H_a? Results of numerical calculations made by Huth (1974) are shown in fig. 54. In these calculations the respective minimum and maximum of $M(T)$ and $H_c(T)$ were taken to be located below room temperature ($T_{comp} = 273$ K). The temperature dependence of these quantities was assumed to be equal to $H_c = 5000/|T - T_{comp}|$ and $4\pi M = 10.6\ |T - T_{comp}|$. Note that $H_c M$ is temperature independent.

In fig. 54a the various terms appearing on the left-hand side in eq. (51) have been represented as a function of the wall radius when the maximum temperature applied during the laser heating is 120°C ($\Delta T_0 = 120$°C) while $H_a = 100$ Oe (8×10^3 A/m). In fig. 54a one recognizes that the highest magnetization corresponds to the highest
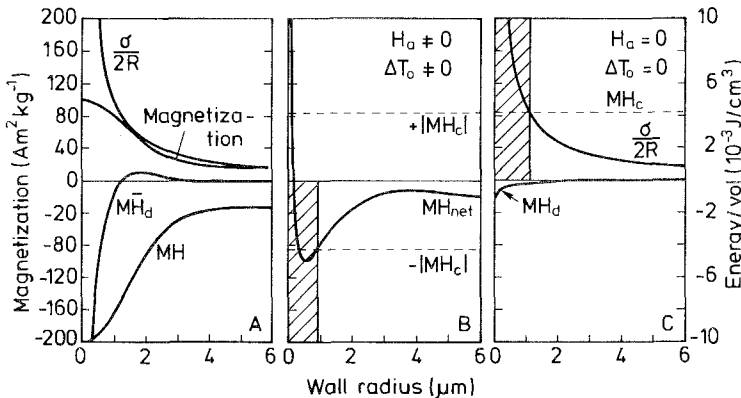
Fig. 54. (a) Dependency on wall radius of the various terms contained in the square brackets of eq. (51). (b) Relative magnitude of the quantities MH_{net} and H_c when plotted as a function of wall radius. The shaded region corresponds to unstable domains when temperature and bias field do not correspond to standard conditions. (c) The same relationships as in b under standard conditions ($H_a = 0, \Delta T_0 = 0$). All these results correspond to those obtained by Huth (1974).

temperature ($R = 0$). In fig. 54b the value of $H_{net} M$ is compared with the right-hand side of eq. (51), i.e. with $H_c M$. These results show that the critical radius is equal to $R_c = 0.96$ μm. Domains of radius R in the range 0.36 μm $< R < R_c$ will expand ($H_{net} < 0$) until $R = R_c$, whereas domains with $R < 0.16$ μm will give rise to domain compression ($H_{net} > 0$). They will collapse and disappear. Domains of a size corresponding to the region 0.16 μm $< R < 0.36$ μm are quasi-stable. Perturbations which bring the radius out of this range do not encounter a restoring force so that the domain will ultimately collapse or expand to $R = R_c$.

The room temperature conditions can be obtained by means of the same procedure using $T_0 = T_{max} = 20°C$ ($\Delta T_0 = 0$). One finds $R'_c = 0.83$ μm. If the bit had been written at $T_{max} = 120°C$ (see above) with $R_c = 0.96$ μm it would still fall into the region of stable domains upon returning to room temperature. If, however, the domains had been written with 0.16 μm $< R < 0.36$ μm (quasi-stable at 120°C) they would collapse. The results in fig. 54c represent the situation where again $T_0 = 20°C$ ($\Delta T_0 = 0$) but where also the bias field H_a has been turned off (standard conditions). In such a case there is a clear dominance of the wall energy since the term MH_a is absent and MH_d is small at room temperature. The critical domain radius is now equal to $R''_c = 1.16$ μm. This means that bits written with $\Delta T_0 = 120°C$ and $H_a = 8 \times 10^3$ A/m would collapse when returning to standard conditions ($\Delta T_0 = 0$, $H_a = 0$). Stable bits may be obtained at temperatures more in excess of T_{comp} than room temperature. In such cases the magnetization is higher so that the corresponding self-magnetostatic energy can counteract the collapsing force of the wall energy and make the domain stable.

Instead of increasing the ambient temperature after writing, one can obtain the same effect by keeping the ambient temperature at $T_0 = 20°C$ while applying slightly lower Gd concentrations, thereby shifting T_{comp} to lower temperatures. It also proves possible to keep T_{comp} close to room temperature and apply only moderate laser powers so as to keep the temperature excursion rather low. Since H_a has a tendency to expand the domains, the bit diameter will decrease with decreasing H_a and the smallest bit diameters (D) are obtained when the write bias is parallel to the demagnetizing field ($H_a < 0$).

Experimental results of Matsushita et al. (1975) are shown in fig. 55 for $Gd_{0.21}Co_{0.79}$, where the smallest stable domains (2.5 μm) were written at 15°C in a slightly negative bias field. Higher values for the negative bias field were reported either to give rise to a collapse of the domains or to make the writing impossible altogether. Similar considerations as applied above to $Gd_{1-x}Co_x$ may also apply to amorphous alloys based on $Gd_{1-x}Fe_x$ (Mimura et al., 1798a; Urner-Wille et al., 1980; Honda et al., 1981).

Apart from the effects on domain stability discussed above, it is also necessary to take account of effects which will become apparent only after a considerable lapse of time. These so-called magnetic after-effects were investigated in amorphous $Tb_{1-x}Fe_x$ films by Ohasi et al. (1980). The origin of this after-effect is the presence of an activation energy which impedes wall motion. Experimentally the after-effect can be observed by first saturating the magnetization in a large external field in one direction and then applying a field in the opposite direction having a fixed
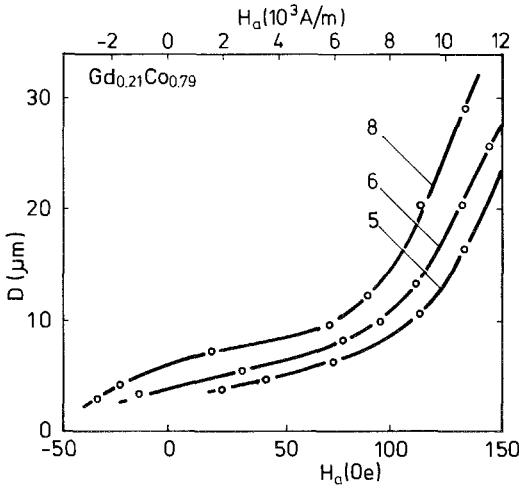
Fig. 55. Domain diameter (D) obtained in films of $Gd_{0.21}Co_{0.79}$ at 15°C in various applied fields H_a. The figures corresponding to the three curves indicate the laser power in mW (after Matsushita et al., 1975).

magnitude (H_a) close to the coercive field. Domain growth can then be studied quantitatively by using a Kerr microscope.

Results of Ohashi et al. (1980) are shown in fig. 56, where the domain growth velocity v is seen to increase exponentially with the value of the applied field H_a (Ohashi et al. note that their set of data might also be interpreted as showing that v decreases exponentially with H_a^{-1}). Ohashi et al. analysed the time (t) dependence of
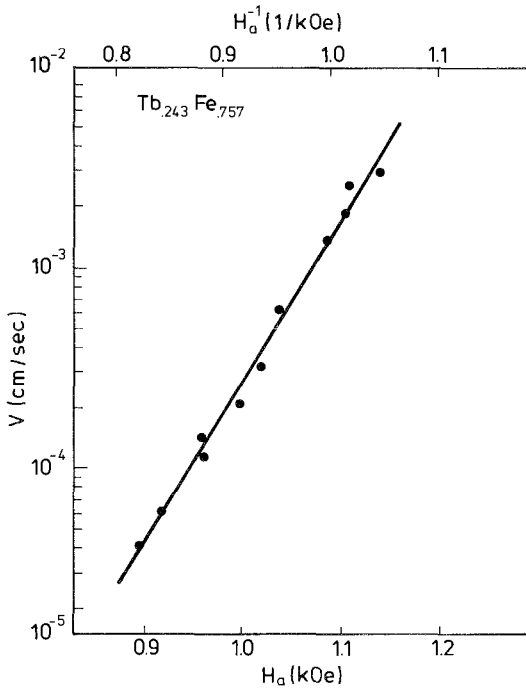
Fig. 56. Dependence of the domain growth velocity (v) on applied field strength (H_a) in amorphous $Tb_{0.243}Fe_{0.757}$ as observed by Ohashi et al. (1980).

the magnetization M in terms of the expression

$$M(t) = M_c + \chi_{irr} S_r \ln t, \tag{52}$$

where χ_{irr} is the irreversible susceptibility derived from $B–H$ curves with a constant field sweeping rate (800 A/m) and S_v is the viscosity coefficient. The viscosity coefficient S_v is inversely proportional to the saturation magnetization M_s at room temperature and decreases with increasing temperature. Ohashi et al. proposed that the slow wall motion observed may be related to the random anisotropy associated with the Tb sublattice. The presence of the after-effect described above may have serious consequences in various magneto-optical and thermo-magnetic applications of thin films, the more so since Tb is frequently used as second rare earth component in R–3d alloys to enhance the coercive force.

Examples of binary amorphous Tb–Fe alloys for magneto-optical applications were presented by Tsunashima et al. (1981), Honda et al. (1983b) and Kobayashi et al. (1981, 1983). The former authors used amorphous double layer films Gd–Fe/Tb–Fe, in which the exchange coupling between those films had led to improved writing characteristics. Amorphous alloys in which Tb is combined with two different 3d metals were investigated by Tsujimoto et al. (1983), while Tsujimoto et al. (1980) studied the magnetic properties of multilayered amorphous films.

7.3. *Magneto-optical properties*

The phenomenon of the rotation of the plane of polarization of linearly polarized light propagating in a magnetized medium is called the Faraday effect. It was discovered as long ago as 1845 in a piece of glass introduced between the poles of a magnet. Closely related to the Faraday effect is the Kerr effect discovered in 1876, where a similar rotation of the plane of polarization takes place when linearly polarized light is reflected from the surface of a magnetized medium. There are three different types of Kerr effect, corresponding to three different configurations between the magnetization direction, the reflecting surface and the plane of incidence. These three configurations are represented schematically in figs. 57a–c. In the polar Kerr effect the direction of the magnetization M is normal to the reflecting surface (a). In the longitudinal Kerr effect the direction is parallel to the reflecting surface and parallel to the plane of incidence (b). In the equatorial or transverse Kerr effect the direction of M is parallel to the reflecting surface and perpendicular to the plane of incidence (c).

The Kerr effect originates from the phase difference between right circularly polarized light (RCP) and left circularly polarized light (LCP) when linearly polarized
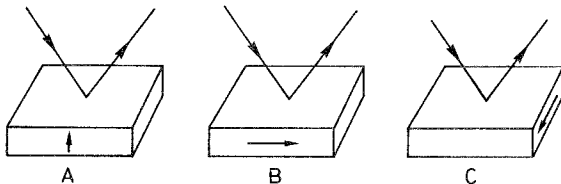
Fig. 57. Three different types of Kerr effect configurations (a) polar, (b) longitudinal, and (c) equatorial. The small arrows indicate the directions of the magnetization.

light propagates in a circularly birefringent medium. If λ is the wavelength of the
light propagating in the positive z direction one has

$$\delta = 2\pi(n_+ - n_-)z/\lambda, \tag{53}$$

where n_+ and n_- are the indices of refraction for RCP and LCP light, respectively.
It is relatively easy to show that a wave which is initially linearly polarized at $z = 0$,
after propagating a distance l through the medium, becomes ellipitically polarized
with the major axis of the ellipse rotated through the angle θ_F ($\theta_F =$ Faraday angle).
The extent of the rotation is given by

$$\theta_F = \mathrm{Re}\left(\frac{\delta}{2}\right) = \mathrm{Re}\,\frac{\pi l}{\lambda}(n_+ - n_-). \tag{54}$$

The corresponding Faraday ellipticity can be obtained by means of the equation

$$\varepsilon_F = -\tanh\,\mathrm{Im}\left[\frac{\pi l}{\lambda}(n_+ - n_-)\right]. \tag{55}$$

In the case of the polar Kerr effect (case a in fig. 57) the amplitude r of the
reflected light is given by

$$r = -\frac{n-1}{n+1}. \tag{56}$$

This can be written in the form $r = |r|e^{i\varphi}$, so that for RCP and LCP components one
obtains

$$\frac{r_+}{r_-} = \left|\frac{r_+}{r_-}\right|\,e^{i(\varphi_+ - \varphi_-)}. \tag{57}$$

This means that the incident linearly polarized light, which can be resolved into two
circular components of equal amplitude, leads to reflected light which is elliptically
polarized because the circular components are no longer of equal amplitude. The
major axis of the ellipse will be rotated through an angle φ_K owing to the phase
difference between the two circularly polarized components. The magnitude of φ_K is
given by

$$2\varphi_K = -(\varphi_+ - \varphi_-) = -\mathrm{Im}\,\frac{2(n_+ - n_-)}{n_+ n_- - 1}. \tag{58}$$

The corresponding Kerr ellipticity is given by

$$2\varepsilon_K = -2\frac{|r_+| - |r_-|}{|r_+| + |r_-|} = -\mathrm{Re}\,\frac{2(n_+ - n_-)}{n_+ n_- - 1}. \tag{59}$$

For a more rigorous treatment of the magneto-optical phenomena the reader is
referred to the review given by Freiser (1968).

In most magneto-optical investigations the quantities φ_K (or θ_F) are studied as a
function of wavelength λ (or energy, $E \propto 1/\lambda$). When combined with measurements
of the wavelength dependence of the reflectivity (R) the off-diagonal elements of the
optical conductivity tensor can be obtained whose imaginary component (absorptive
component) can be directly correlated with the transition matrix elements associated
with the band structure of a given material (Cooper, 1965; Erskine and Stern, 1973).

In ordinary optical absorption there are two components associated with intraband transitions (Drude component) and interband transitions, respectively. A similar situation is encountered in magneto-optical spectroscopy. Of special interest is the interband component which is related to the joint density of states. The intensity of the magneto-optical transitions is proportional to the product of spin–orbit coupling strength and net electron-spin polarization of states excited by the incident light (Erskine and Stern, 1973).

As a consequence the magneto-optical spectra are primarily sensitive to the "magnetic" electrons (d states in ferromagnetic transition metals, and d and f states in rare earth metals). This dependence on the spin–orbit coupling strength strongly discriminates against s, p states even if the corresponding electrons exhibit some spin polarization. It is somewhat unfortunate that most magneto-optical investigations only consider measurements of the wave-number dependence of φ_K while data on reflectivities are usually lacking. It is therefore not possible to make a direct connection with intraband or interband transitions. The discussion of results presented in this section will therefore be mainly of a comparative nature. As will be shown below, the Kerr effect (and Faraday effect) can often be used as a rather convenient method of sampling the local magnetic properties of the thin films.

7.3.1. Fe-base alloys

The temperature dependence of the Faraday rotation θ_F was studied on a number of amorphous $Gd_{1-x}Fe_x$ alloys by Hartmann (1982). Results are reproduced in fig. 58. These results have to be compared with the temperature dependence of the magnetization, shown for a number of such alloys in fig. 59. It follows from the results shown in fig. 59 that $Gd_{1-x}Fe_x$ alloys exhibit a compensation temperature when the Fe concentration lies in the range $0.66 < x < 78$. However, no such features are seen in the θ_F versus T curves of fig. 58.
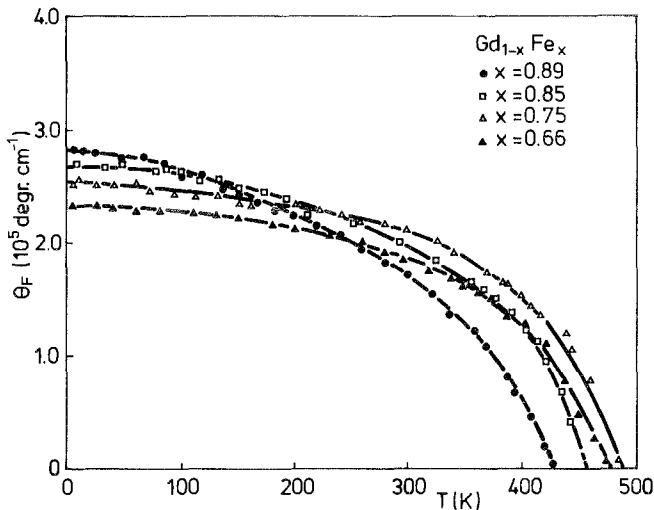
Fig. 58. Temperature dependence of the specific Faraday rotation θ_F in a number of amorphous $Gd_{1-x}Fe_x$ alloys (after Hartmann, 1982).
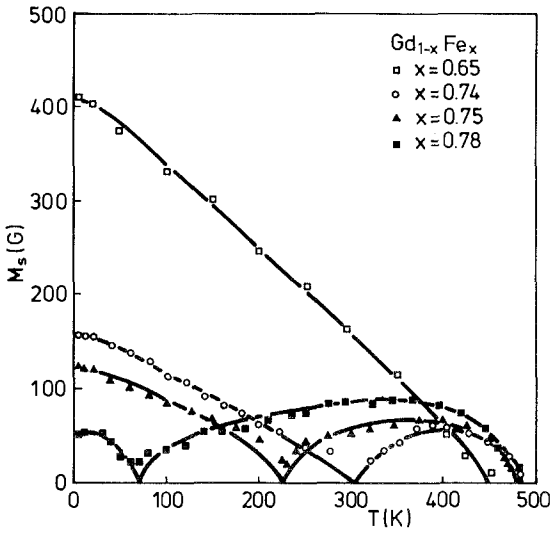
Fig. 59. Temperature dependence of the magnetization for a number of amorphous $Gd_{1-x}Fe_x$ alloys, after Hartmann (1982).

These results make it clear that the magneto-optical effects sample mainly one of the sublattice magnetizations. In agreement with this feature is the observation, by means of φ_K measurements, of normal hysteresis loops at temperatures above T_{comp} but inverted hysteresis loops at temperatures below T_{comp} (Esho, 1976; Imamura and Mimura, 1976). This may be illustrated by means of fig. 60, where the temperature dependence of the magnetization M around $T = T_{comp}$ has been sketched together with the directions of the Gd and Fe sublattice magnetizations. Here it has been assumed that the direction of the total magnetization $M = M_{Fe} - M_{Gd}$ follows the
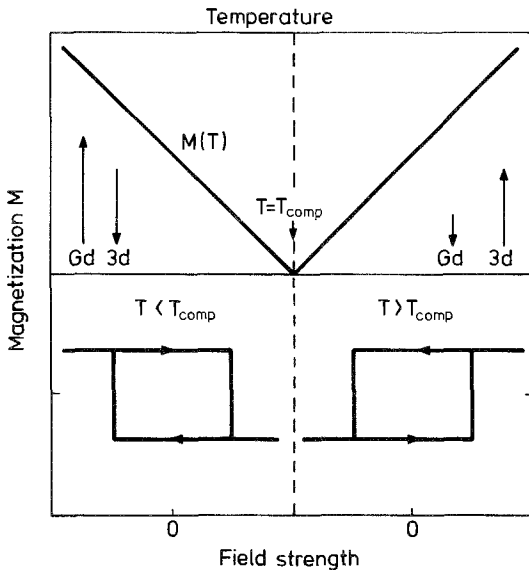
Fig. 60. Temperature dependence of the total magnetization M around T_{comp} and relative directions of the Gd and Fe sublattice magnetization below and above T_{comp} (upper part). The hysteresis loops (measured magneto-optically) expected in the two temperature regions are indicated in the lower part.

direction of the applied field, meaning that both the Fe and the Gd sublattice magnetization reverse their direction when passing from $T > T_{comp}$ to $T < T_{comp}$. If the magneto-optical intensity is mainly due to either the Fe sublattice magnetization or the Gd sublattice magnetization one would expect the hysteresis loop measured via φ_K or θ_F to become inverted at $T = T_{comp}$, as indicated in the lower part of fig. 60.

In the same way it is possible to interpret magnetic and magneto-optical data measured at a fixed temperature by varying the Fe concentration (Imamura and Mimura 1976). It can be seen from the results shown in fig. 61 that the Kerr rotation φ_K does not follow the total magnetization (broken line). Rather it increases with Fe content, suggesting that the magneto-optical active component is the Fe. It is also indicated in the figure that an inversion of the hysteresis loops is observed in the transition from the Fe-dominated range ($x > 0.79$) to the Gd-dominated range ($x < 0.79$).

The wavelength dependence of φ_K of amorphous Gd–Fe alloys was studied by Urner-Wille et al. (1978), Katayama and Hasegawa (1982), and Tsunashima et al. (1983). Magneto-optical spectra of $Tb_{1-x}Fe_x$ alloys were investigated by Connell et al. (1982) and by Hartmann (1982). Results obtained by Tsunashima et al. on $Gd_{0.26}Fe_{0.74}$ and some ternary alloys have been reproduced in fig. 62. In all these cases the Kerr rotation spectra were measured in the range from 1.5 to 4 eV (300–1000 nm) and showed little structure. In this respect the Kerr rotation spectra of these amorphous alloys are similar to the spectrum of Fe metal. The spectrum of Fe metal is characterized by an intensity maximum at about 1 eV which is just outside the range considered in the investigations mentioned above. At higher energies the intensity of φ_K decreases and is more or less constant between 3 and 4 eV.
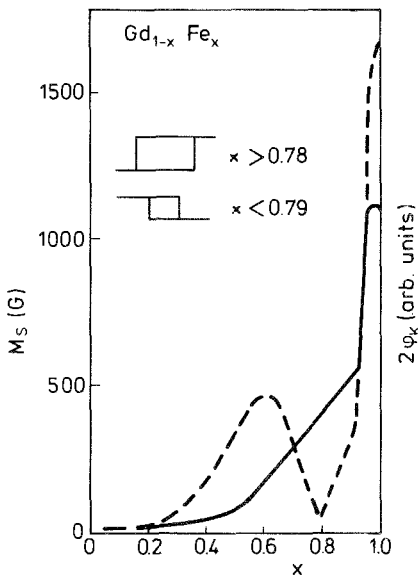
Fig. 61. Compositional dependence of the saturation magnetization M_s and the longitudinal Kerr rotation angle $2\varphi_K$ in GdFe alloys films. The longitudinal Kerr hysteresis loops reverse at the compensation composition $x \approx 0.79$ (after Imamura and Mimura, 1976).
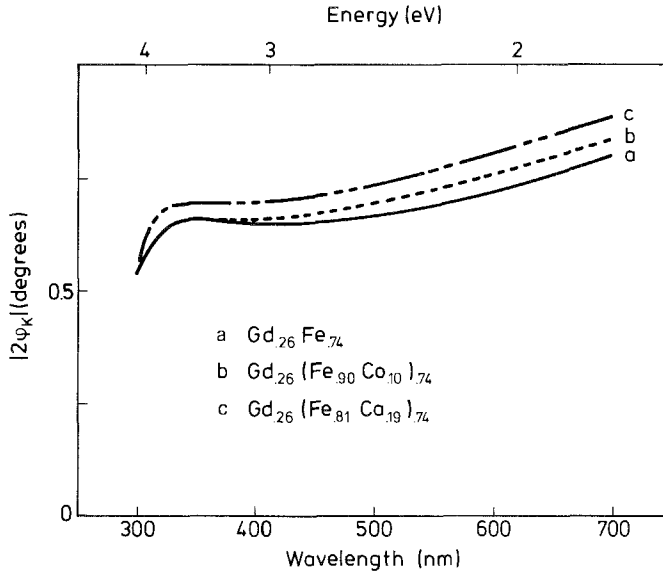
Fig. 62. Kerr rotation spectra of some amorphous Gd–Fe–Co films (after Tsunashima et al., 1983).

Apart from the replacement of Fe by Co in amorphous $Gd_{1-x}Fe_x$ alloys studied by Tsunashima et al. (see fig. 62) there is also a large amount of data pertaining to the effect on $2\varphi_K$ of alloying $R_{1-x}Fe_x$ with third elements like Bi, Sn and Pb (Urner-Wille et al., 1980; Hartmann, 1982). Alloying with these elements proved to have a beneficial influence on the Kerr and Faraday intensities. Results of Urner–Wille et al. are shown in fig. 63. It can be seen from these data that at low temperatures the alloying with 16% Sn of $Gd_{0.26}Fe_{0.74}$ has led to an increase of φ_K by about 50%. Similar enhancement effects on φ_K were also observed after alloying
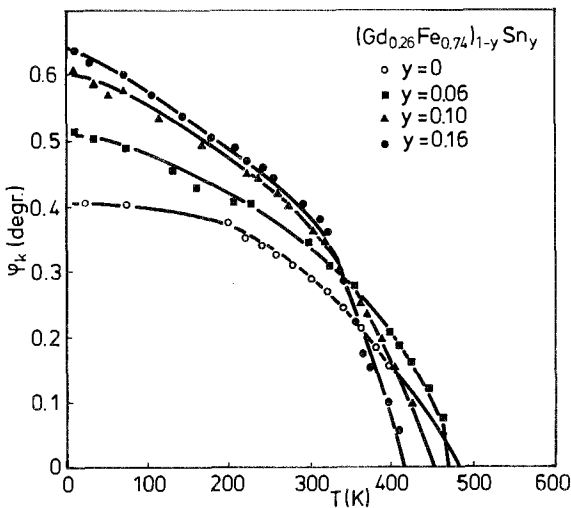
Fig. 63. Temperature dependence of Kerr rotation φ_K at $\lambda = 633$ nm in several amorphous Gd–Fe–Sn alloys (after Urner-Wille et al., 1980).

with Bi and Pb. It is interesting to compare the data shown in fig. 63 with the concentration dependence of S_{Fe} shown for these alloys in fig. 38. For instance, in the case of alloying with 20 at% Sn the Kerr intensity increases by 50% (fig. 63) whereas S_{Fe} increases only by about 20%. This indicates that there is an enhancement effect on the magneto-optical transitions which goes beyond the enhancement expected on the basis of the 3d electron spin polarization.

7.3.2. Co-base alloys

The experimental results obtained on amorphous $Gd_{1-x}Co_x$ films do not differ basically from those reported above for $Gd_{1-x}Fe_x$ films, where the magneto-optical spectra were shown to be primarily due to transitions involving the 3d electrons. The reorientation of the Co moment when passing through the compensation composition for a fixed temperature leads to a reversion of the Kerr hysteresis loop analogous to that described for Fe-base alloys in connection with fig. 60 (Esho, 1976; Argyle et al., 1974; Ogawa et al., 1974; Togami and Kobayashi, 1981). Shen et al. (1983) reported a change in polarity of the air-incident Kerr effect upon annealing in bad vacuum owing to the formation of a surface oxide layer.

An interesting phenomenon was observed by Esho (1976) who investigated the Kerr hysteresis loop on amorphous Gd–Co films on a glass substrate. The hysteresis loops observed on the film side and substrate side are reproduced in fig. 64. Whereas the loop at the film side corresponds to the reverted type of loop discussed above, Esho recorded a rather anomalous type of loop at the substrate side.

This behaviour was explained in terms of a concentration gradient along the film normal, comprising a Gd-rich part and a Co-rich part, such as schematically represented in fig. 65a. Two types of configuration may exist: In type I the total magnetization vectors (thick arrows) reverse in the film where the concentration corresponds to the compensation concentrations, whereas in type II there is no
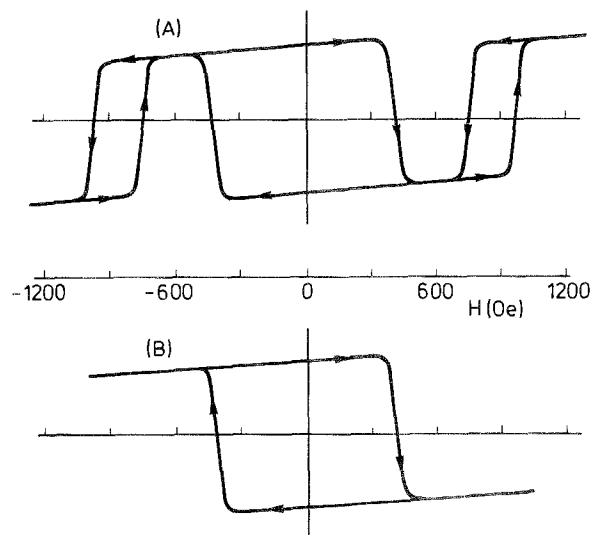
Fig. 64. Room temperature hysteresis loops obtained at the glass–film interface (a) and at the film–air interface (b) of an amorphous Gd–Co film (after Esho, 1976). The quantity corresponding to the vertical axis is the Kerr rotation (in arbitrary units).
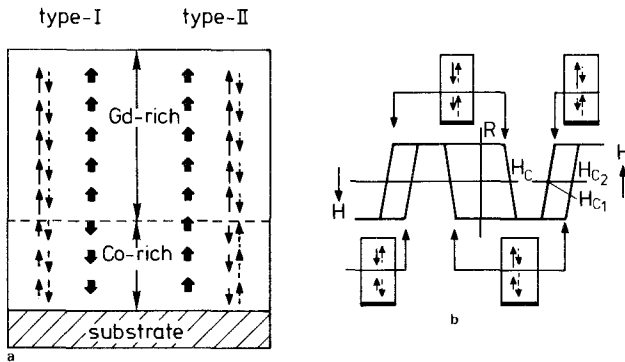
Fig. 65. (a) Spin orientations in an amorphous Gd–Co film having a composition gradient along the film thickness. Solid line and dotted line arrows denote Gd and Co spins, respectively. Thick line arrows indicate the total magnetization vectors. (b) Spin orientations in two layers at each stage of the anomalous hysteresis loop. The solid line and broken line arrows refer to Gd and Co spins, respectively. The Kerr measurements were made through the substrate interface. This side of the layer is indicated by a heavy solid line (after Esho, 1976).

reversal of the total magnetization. With increasing magnetic field strength magnetization reversal in the top layer is assumed to take place (at H_c) independently of the magnetic state of the bottom layer. Esho considered the magnetic energy difference between states I and II as a function of the field strength and found that in low applied fields and in the remanent state $(0 \leqslant H \leqslant H_{c1})$ type I is stable. As illustrated schematically in fig. 65b an increase of the field strength to beyond H_c leads to a magnetization reversal of the top layer. In the case $H_c < H_{c_1}$ the type I configuration is still stable, so that the magnetization reversal in the top layer is followed by a magnetization reversal in the bottom layer. At still higher field strength $H > H_{c_2}$ type II becomes stable, meaning a magnetization reversal in only the bottom layer. The hysteresis of this latter transition gives rise to the side-loops shown in fig. 64 and confined in fig. 65b to the region $H_{c_1} \leqslant H \leqslant H_{c_2}$.

The presence of a concentration gradient in the film or the presence of several layers with different 3d concentrations was also studied later on by Togami (1981) and Chen and Malmhäll (1983). The former authors considered this as a prerequisite for the occurrence of stable domains after laser-induced thermomagnetic writing and returning to standard conditions (see also section 7.2).

Sato and Togami (1983) compared the Kerr rotation and ellipticity spectra of amorphous Gd–Fe and Gd–Co alloys with the dielectric tensor elements of Fe and Co and concluded that the Kerr effect in these materials is mainly due to Fe and Co, respectively.

The wavenumber dependence in $Gd_{1-x}Co_x$ was also studied by Visnovsky et al. (1976) on amorphous $Gd_{0.24}Co_{0.76}$ and by Togami et al. (1982) on amorphous $Gd_{0.27}Co_{0.73}$. These spectra are compared with those obtained by Van Engen et al. (1983) on crystalline Gd–Co intermetallics in fig. 66. In the spectra of Van Engen et al. and Visnovsky et al. the sign convention for the Kerr rotation corresponds to that used by Kahn et al. (1969). No such specification was given by Togami et al., so that
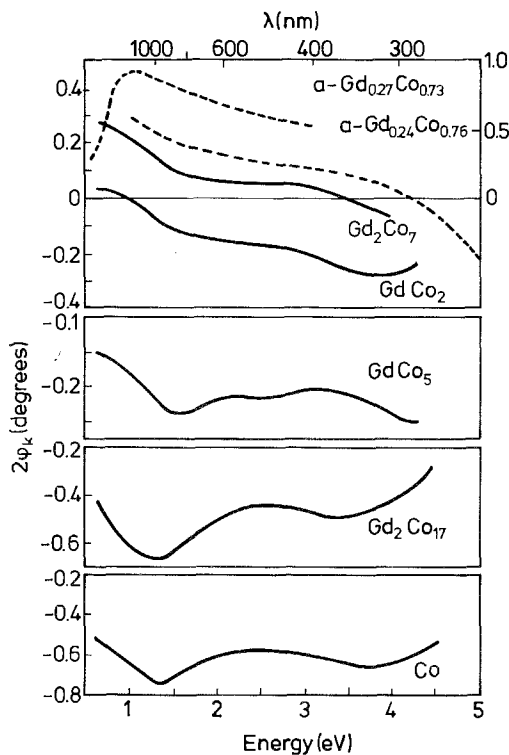
Fig. 66. Comparison of Kerr rotation spectra of several intermetallic Gd–Co compounds (Van Engen et al., 1983) with spectra of amorphous $Gd_{0.24}Co_{0.76}$ (Visnovsky et al., 1976) and amorphous $Gd_{0.27}Co_{0.73}$ (Togami et al., 1982).

it is possible that the spectrum of $Gd_{0.27}Co_{0.73}$ has to be inverted in sign. The two spectra of the amorphous materials bear a faint resemblance to those observed in crystalline Gd_2Co_7. The discrepancy between the results of Togami et al. and those of Visnovsky et al. is difficult to explain and further research in this field seems desirable.

Magneto-optical spectra of ternary alloys of the type $(Gd_{1-x}Tb_x)_{0.29}Co_{0.71}$ were studied by Togami et al. (1983) Crystalline and amorphous materials close in composition to $GdCo_5$ were investigated by Katayama and Hasegawa (1982) who found differences in the φ_K spectra being present mainly at small wavelengths. The effect of oxidation was studied in more detail by Shen et al. (1983).

8. Transport properties

8.1. *Electrical resistivity and magnetoresistance*

The electrical transport properties of amorphous alloys differ considerably from those of crystalline materials. The resistivity of the latter is usually low in the liquid-He temperature range (a few $\mu\Omega$ cm). At higher temperature it tends to increase linearly with temperature, leading to a room temperature value of several
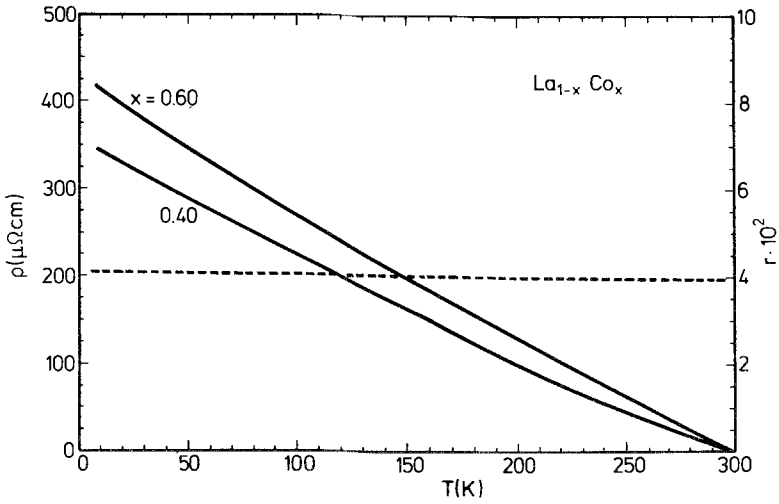
Fig. 67. Temperature dependence of the electrical resistivity in amorphous $La_{0.40}Co_{0.60}$ (dashed line, left-hand scale). The full line (right-hand scale) represents the resistivity ratio $[\rho(T)-\rho(300)]/\rho(300)$ in two amorphous $La_{1-x}Co_x$ alloys (after Buschow and Beekmans, 1980b).

tens of $\mu\Omega$ cm. In amorphous alloys the resistivity is already high in the liquid helium range, while its temperature dependence is extremely low. Typical results are shown for amorphous $La_{1-x}Co_x$ in fig. 67. The temperature dependence of the resistivity (ρ) is usually more clearly revealed in graphs of the resistivity ratio $r = [\rho(T)-\rho(300)]/\rho(300)$ or in graphs of the resistivity coefficient $\alpha = \rho^{-1}\,d\rho/dT$ (both representations are commonly employed in displaying resistivity data of amorphous alloys).

A further often observed feature of the resistivity in amorphous alloy systems is that the concentration dependence of the resistivity gives rise to a maximum, the concentration dependences of α (or r) showing a minimum at the same concentra-
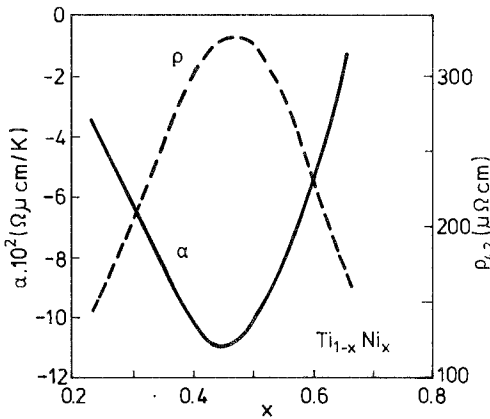
Fig. 68. Concentration dependence of the temperature coefficient (α) of the electrical resistivity in amorphous $Ti_{1-x}Ni_x$ alloys (full line). The concentration dependence of the resistivity at 4.2 K is indicated by a dashed line (after Buschow, 1983c).
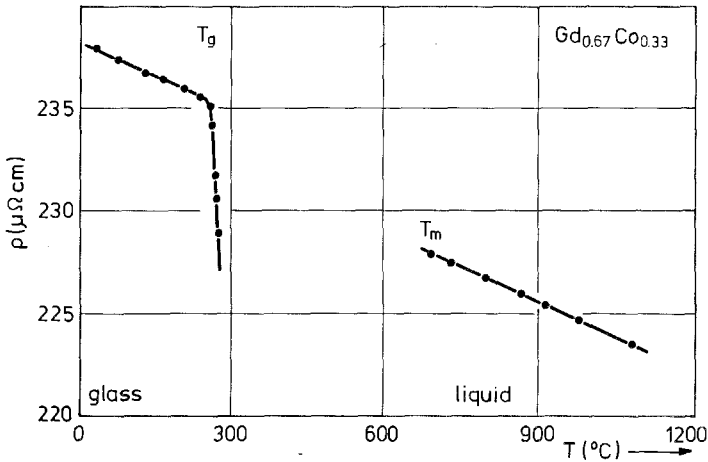
Fig. 69. Comparison of the electrical resistivity in amorphous and liquid $Gd_{0.67}Co_{0.33}$ (after Güntherodt et al., 1979). The glass temperature and melting temperature have been indicated by means of T_g and T_m, respectively.

tion. Such a behaviour was observed, for instance, in amorphous $Ti_{1-x}Ni_x$ alloys, as illustrated in fig. 68. Other examples comprise the systems $Sn_{1-x}Cu_x$ (Korn et al., 1972), $Sn_{1-x}Au_x$ (Blasberg et al., 1979), $Hf_{1-x}Ni_x$ (Buschow and Beekmans, 1979c), and $Sn_{1-x}T_x$ with T = Fe, Co, Ni (Geny et al., 1982).

The fact that the easy glass-forming range is rather limited may be one of the reasons why the $\rho(x)$ maximum and the $\alpha(x)$ minimum is not always observed. For instance, in amorphous $P_{1-x}Ni_x$ $(0.75 \leqslant x \leqslant 0.85)$ one observes only the part in which $\rho(x)$ increases with x while simultaneously $\alpha(x)$ decreases with x (Cote, 1976). Similar phenomena were also observed in $P_{1-x}Ni_x$ alloys in which Ni is partially replaced by other metals (Sinha, 1970). Okuno and Sakurai (1983) investigated amorphous $Gd_{1-x}Co_x$ alloys and found $\alpha(x)$ to increase with x while $\rho(x)$ was found to decrease with x in the range $0.59 \leqslant x \leqslant 0.77$. The resistivity of amorphous $La_{1-x}Ga_x$ alloys was investigated by Shull et al. (1978) in the range $0.16 \leqslant x \leqslant 0.28$. The resistivity showed a maximum for $x = 0.24$, while its temperature coefficient (α) was reported to be positive for $x \leqslant 0.18$ but negative for $x \geqslant 0.20$.

The above described concentration dependences of the resistivity and its temperature coefficient are commonly encountered in liquid alloys. This suggests that there exists a close similarity in resistivity behaviour between amorphous and liquid alloys. This point has convincingly been illustrated by Güntherodt et al. (1978) and Geny et al. (1982). In fig. 69 the high temperature resistivity behaviour of amorphous $Gd_{0.67}Co_{0.33}$ is compared with the corresponding resistivity behaviour of the liquid phase (Güntherodt et al., 1979). These data as well suggest a close correspondence between the resistivity in liquid and amorphous metals. These results indicate that an adequate theoretical model for one of these phases (liquid or amorphous) should directly be extendable to the other phase.

The Ziman–Faber model for liquid metals (Ziman, 1961; Faber and Ziman, 1965) has been widely used to describe the resistivity behaviour of amorphous metals. It is based on the nearly-free-electron approach and the Boltzmann transport equation. When all multiple two-site scattering corrections are neglected, the resistivity for a pure liquid metal can be represented by means of the equation

$$\rho = \frac{12\pi\Omega_0}{\hbar e^2 V_F^2} \int_0^1 S^\rho(Q) |t(Q)|^2 (Q/2k_F)^3 \, d(Q/2k_F), \tag{60}$$

where Q is the scattering vector, k_F is the Fermi wave vector, V_F is the Fermi velocity, Ω_0 is the volume per atom, $S^\rho(Q)$ is the resistivity structure factor and $t(Q)$ is the single site t-matrix. This latter quantity was proposed by Evans et al. (1971) as an appropriate substrate for the pseudopotential matrix element in the original Ziman–Faber expression, when dealing with transition metals. In a muffin-tin approximation it may be expressed in terms of phase shifts η_l for angular momentum quantum number l (Dreirach et al., 1972; Hirata et al., 1977)

$$t(Q) = -\frac{4\pi}{\Omega_0 E_F^{1/2}} \sum_l (2l+1) \sin \eta_l \exp(i\eta_l) P_l(\cos\theta), \tag{61}$$

where θ is the scattering angle.

In the original Ziman–Faber formulation applicable to liquid metals the super-script ρ of $S^\rho(Q)$ did not appear and no distinction was made between the resistivity static structure factor $S^\rho(Q)$ and the X-ray static structure factor $S^x(Q)$. This latter quantity is given by the experimental interference function already introduced in section 5.1. This distinction plays a role only at temperatures below the Debye temperature θ_D (Meisel and Cote, 1978). In binary alloys $A_{1-x}T_x$ the product St^2 in eq. (60) has to be replaced by

$$St^2 = xt_1^2[1 - x - xS_{11}] + (1-x)t_2^2[x + (1-x)S_{22}]$$
$$+ x(1-x)(t_1^*t_2 + t_1t_2^*)[S_{12} - 1], \tag{62}$$

where the subscripts 1 and 2 refer to the components T and A, respectively, and the quantities S_{ij} are the partial structure factors.

Inspection of eq. (60) shows that, as a result of the factor $(Q/2k_F)^3$ in the integral, the major contribution to the resistivity will come from the backscattering region ($Q \approx 2k_F$). In the free electron approximation the concentration dependence of k_F in a given series $A_{1-x}T_x$ can be estimated by means of eq. (28). In general it will increase with the concentration of the polyvalent component. Since most of the alloys are combinations of constituents having different metallic radii the Q_p value for which $S^x(Q)$ reaches a maximum (principal peak in the X-ray interference function) will also vary with concentration. In many binary systems one may therefore have a concentration at which $Q_p \approx 2k_F$. At this particular concentration x_m it is found that $S(Q_p \approx 2k_F)$ in eq. (60) is a maximum (see also fig. 70) and the same holds for the corresponding resistivity ρ. For other concentrations $2k_F$ will move away from the region Q_p where $S(Q)$ is large. Consequently ρ will decrease. This is basically the explanation of a $\rho(x)$ maximum in many amorphous alloy systems.
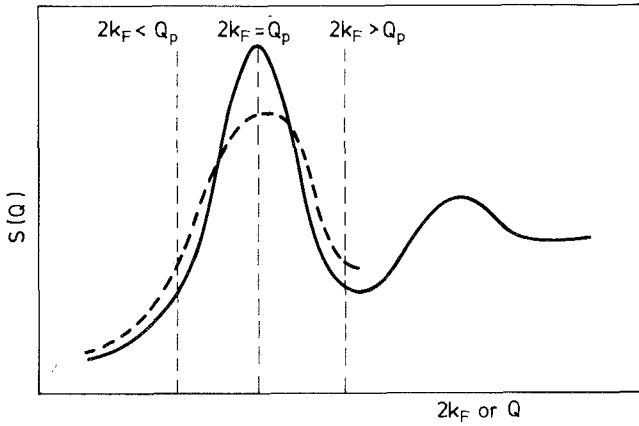
Fig. 70. Wave number depen-
dence of the structure factor
$S(Q)$ for high temperatures
(broken line) and low temper-
atures (full line).

It can also be shown that, if one of the components is a transition metal, the largest contribution to ρ will come from the transition metal d wave phase shift. The maximum resistivity $\rho(x = x_m)$ in alloy series composed of different transition metals can then be compared by means of the simplified form of eq. (60):

$$\rho \propto \sin \eta_l \left[x_m(1 - x_m) + x_m^2 S_{TT}(2k_F = Q_p) \right], \tag{63}$$

where the subscript TT refers to the transition metal component.

The structure factor also plays a dominant role in the determination of the temperature dependence of the resistivity. Theoretically the temperature dependence of ρ can be described by introducing atomic excitation into the structure factor (Cote, 1976; Nagel, 1977; Cote and Meisel, 1977; Esposito et al., 1978), while there is also experimental data for the temperature dependence of $S(Q)$ (Clarke and Nagel, 1978). The effect of temperature on the structure factor can be illustrated by means of fig. 70 where the broken line refers to the lower temperature. The main peak is seen to broaden, owing to increasing disorder with increasing temperature. Keeping in mind that, owing to the factor $(Q/2k_F)^3$ in eq. (60), the values $Q \approx 2k_F$ will be weighed heavily due to back scattering, one expects again that the resistivity will be determined largely by the value of $S(Q)$ for $Q \approx 2k_F$. In the case where $2k_F$ is close to Q_p one finds that $S(Q)$ decreases with increasing temperature, i.e. $\alpha < 0$ or ($r < 0$). If $2k_F$ for a given alloy does not fall into a range close to Q_p, the value for $S(Q)$ is seen in fig. 70 to increase with increasing temperature, hence $\alpha > 0$.

It follows from the discussion given above that when an alloy is of a composition such that $2k_F \approx Q_p$ one has simultaneously a large resistivity and a negative value of α. For compositions outside the range $2k_F \approx Q_p$ the resistivity adopts lower values and α changes from positive to negative. Qualitatively (and for $T < \theta_D$) these results are in good agreement with experimental data. It can also be understood from the above model considerations why related amorphous alloys may give rise to a completely different resistivity behaviour. The behaviour found by Cochrane et al. (1978a, b) in two amorphous Y alloys shown in fig. 71 may be used as an example in this respect.
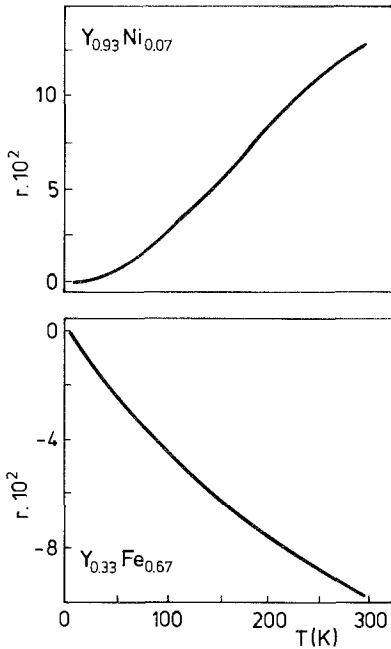
Fig. 71. Resistivity ratio $r = [\rho(T) - \rho(4.2)]/\rho(4.2)$ for two amorphous Y alloys (after Cochrane et al., 1978b).

It will be clear, however, that the model must not be pushed too far, considering the limited validity of the free-electron expression usually adopted for k_F. A more reliable analysis can be made if k_F is derived in a different manner. This was done for instance in the analysis of the resistivity in $Ag_{1-x}Cu_x$ alloys by Mizutani and Yoshida (1982). These authors estimated $2k_F$ from experimental values of the Hall coefficient R_H via the relation

$$2k_F = 1.1139 \times 10^{-3}(-R_H)^{1/3}, \tag{64}$$

where $2k_F$ and R_H are in units of Å^{-1} and $m^3\ A^{-1}\ s^{-1}$. Mizutani and Yoshida found that the $2k_F/Q_p$ ratio indeed closely controls the behaviour of α, although negative values of α continue to exist even when $2k_F/Q_p$ exceeds 1.15.

The particular position taken by alloys for which $2k_F \approx Q_p$ was already mentioned in connection with the Nagel and Tauc criterion discussed in sections 3.1 and 4.2. In the latter section we showed that the Nagel and Tauc criterion is less suited for describing the thermal stability of amorphous alloys. In the former section the possibility was discussed that amorphous alloys for which the criterion $2k_F \approx Q_p$ is satisfied may be amenable to easy glass formation owing to the presence of an enhancement of the deepness of the eutectic.

In the analysis given by Beck and Oberle (1978) one may expect an additional lowering of the electronic energy of the liquid metal when $2k_F \approx Q_p$. As is illustrated in fig. 72, the distances between successive peaks in the pair correlation function $g(R)$ match the distances between the consecutive minima in the pair potential functions $\phi(R)$ when $\lambda_p \approx 2\pi/Q_p$ becomes equal to $\lambda_F \approx 2\pi/2k_F$, i.e. when $2k_F \approx$
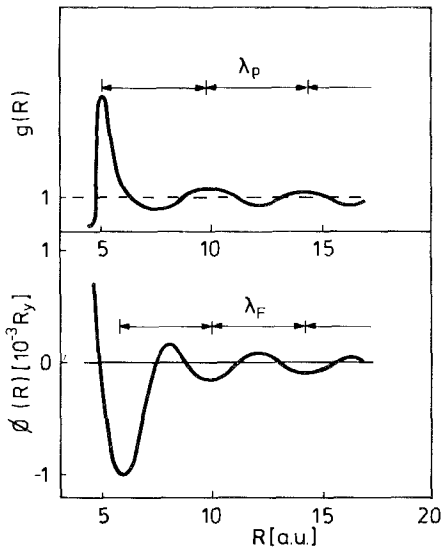
Fig. 72. Comparison of correlation functions $g(R)$ and pair potential functions $\phi(R)$ plotted as a function of distance R (after Beck and Oberle, 1978).

Q_p. (Note that the condition $\lambda_p = \lambda_F$ is necessary for the match of the two functions $g(R)$ and $\phi(R)$ but not sufficient, since it is also requires that $g(R)$ and $\phi(R)$ have to be "in phase".) The more perfect this match of the functions $g(R)$ and $\phi(R)$, the more stable the liquid and the deeper the eutectic.

It follows from the discussion given above that amorphous alloys that are relatively easily prepared by means of liquid quenching tend to have a negative value of α and to have a relatively high resistivity in the middle of the easy glass forming range ($2k_F = Q_p$), while α tends to more positive values and the resistivity decreases somewhat at concentrations near the borders of the easy glass-forming range. This correspondence between easy glass formation and negative α is observed in many amorphous alloys (Beck and Oberle, 1978).

It was stressed by Mueller et al. (1980) that the extended Ziman theory is not the only model that can explain the negative value of α observed in many amorphous alloys. In fact, Mueller et al. showed that the negative temperature dependence in amorphous $La_{0.66}Al_{0.34}$ is better explained in terms of the Kondo mechanism than by the extended Ziman model. We will return to this point later on, after having discussed the resistivity anomalies associated with several types of Kondo mechanisms.

The ordinary Kondo effect originates from spin flip scattering of the conduction electrons on localized magnetic impurities. It was observed, for instance, in various amorphous alloys of the types $Cr_xPd_{1-x}Si_{20}$ (Hasegawa and Tsuei, 1971). It was also observed in La–Gd–Au alloys by Poon et al. (1977), who ascribed it to Kondo scattering on magnetic clusters composed of more than one Gd spin. The resistivity varies logarithmically with temperature and becomes saturated at low temperatures. Owing to the fact that the host resistivity is proportional to T, a total resistivity is found which gives rise to a minimum at a temperature increasing with increasing concentration of the magnetic impurity. Later on Crest and Nagel (1979) modified

this model and applied it to ferromagnetically ordered metallic glasses in which a limited amount of spins still experiences a basically zero effective field.

Cochrane et al. (1975) found that the logarithmic term in several ferromagnetic alloys was field independent. Furthermore, they observed resistivity minima also in non-magnetic amorphous alloys as well. This prompted these authors to abandon explanations based on magnetic atoms and led them to propose a mechanism of structural origin. There is still a close analogy with the ordinary Kondo effect in that, here too, the conduction electrons are scattered from a two-level system. This atomic tunnelling model, originally developed by Cochrane et al. (1975), was generalized by Tsuei (1978) to include conduction electron scattering from any species possessing a localized internal degree of freedom (phonons or magnons), able to generate excitations that are degenerated on the scale of $k_B T$ ($T > \theta_D$). In terms of this structural Kondo approach the temperature dependence of the resistivity can be written as

$$\rho(T) = r_0 + c \ln(kT^2 + \Delta^2),$$ (65)

where Δ is the energy characteristic of the localized internal degree of freedom. In a somewhat different treatment of the scattering problem Kondo (1976) arrived at a result somewhat different from that of Cochrane et al. In his approach the temperature dependence of ρ is given by the relation

$$\rho(T) = c' \ln(T/D)^2,$$ (66)

where c' is of fourth order in the scattering potential.

There are several experimental results on amorphous alloys that corroborate the logarithmic temperature dependence as expressed in eq. (65). These comprise results on amorphous alloys of the type $Co_{1-x}P_x$ (Cochrane et al., 1975), $Ni_{1-x}P$ (Cochrane et al., 1975; Berrada et al., 1978) and also in $Y_{0.07}Ni_{0.93}$ (Cochrane et al., 1978a, b) mentioned earlier in connection with fig. 71. (The shallow resistivity minimum occurs near 11 K and is not visible on the scale of fig. 71.)

It is somewhat unfortunate that all the alloys mentioned above can be suspected to contain small amounts of magnetic atoms, corresponding to the presence of some types of atomic configurations that are particularly favourable in this respect. It is difficult therefore to decide between the ordinary Kondo effect and the Kondo effect of structural origin. Such uncertainty can be excluded in the results obtained by Mueller et al. (1980) on $La_{0.66}Al_{0.34}$. Results of their analysis are shown in fig. 73. Note that in this model, as in the Ziman model, one has a resistivity decreasing with temperature over a wide range. In the Ziman model the temperature dependence is linear in T while in the Kondo model it is logarithmic. This feature can conveniently be used to differentiate between the two models. Evidently in the case of $La_{0.66}Al_{0.34}$ a logarithmic temperature dependence of ρ is indeed the correct description. Similar conclusions were reached for several ternary Tb- and Pr-base metallic glasses by Cornelison and Sellmyer (1983).

The resistivity in amorphous $R_{1-x}Co_x$ alloys has been investigated by several authors (Durand and Poon, 1977; Kästner et al., 1980; Hadjipanayis et al., 1980; Okuno et al., 1981; Honda et al. 1983a). Most of these alloys show a minimum in the
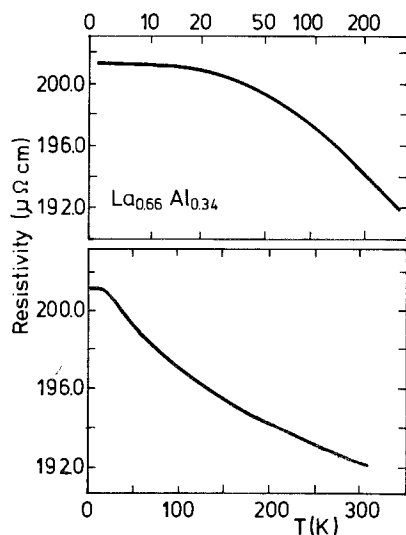
Fig. 73. Temperature dependence of the electrical resis-
tivity in amorphous $La_{0.66}Al_{0.34}$ plotted on a linear T
scale (bottom part) and on a $\ln T$ scale (top part).
Results are due to Mueller et al. (1980).

temperature dependence of $\rho(T)$. Okuno and Sakurai showed that one may dis-
tinguish two separate temperature regions. At relatively low temperatures (4.2–20 K)
the temperature dependence of ρ can be described by means of a log T term, such as
is expressed in eq. (65). Okuno notes that the normalized resistivity in this range
does not vary strongly enough to be associated with the ordinary Kondo effect. At
higher temperatures (above 40 K) the resistivity was analysed in terms of a power
law:

$$\rho = aT^{2/3} - bT + c, \tag{67}$$

where a and b are positive coefficients and c is a positive constant. The first term is
to be associated with electron scattering from magnetic moments, the $T^{2/3}$ depen-
dence arising from the temperature dependence of the magnetization in the magneti-
cally ordered regime. The second term is of non-magnetic origin and comparable to
the lattice contribution in crystalline materials. This contribution can be described in
amorphous alloys by means of the extended Ziman model mentioned above.

For instance, the value of b was found in the analysis given by Okuno and
Sakurai to be equal to -8×10^{-2} in $Gd_{0.40}Co_{0.60}$. This value is virtually the same as
the one that can be derived from the results shown for $La_{0.40}Co_{0.60}$ in fig. 67. A fit to
their data made on the basis of eq. (67) is shown in fig. 74. The interesting point here
is the fact that the resistivity minimum arises as a consequence of the magnetic term
and the Ziman term, the Kondo-like behaviour observed in the low-temperature
regime being of minor importance.

Resistivity minima in the temperature dependence were also found in several
amorphous alloys in which rare earth elements are combined with Ni (Asomoza et
al., 1977a; Fert et al., 1977; Asomoza et al., 1979; Fert and Asomoza, 1979). As an
example, results for the amorphous alloy $Ho_{0.25}Ni_{0.75}$ are shown in fig. 75. Similar
results were obtained for the other alloys of the same series. It can be derived from
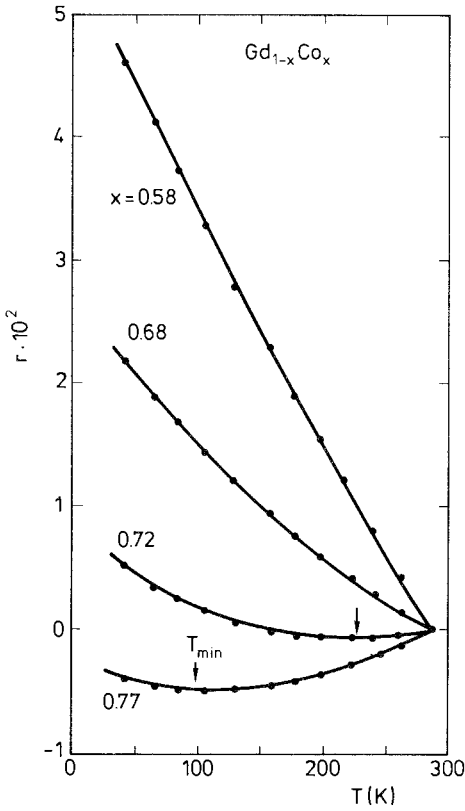
Fig. 74. Power-law temperature dependence of the resistivity ratio $r = [\rho(T) - \rho(288)]/\rho(288)$ in amorphous Gd–Co films of different compositions. The solid lines represent temperature dependencies calculated on the basis of eq. (67) mentioned in the text (after Okuno and Sakurai, 1983).

the data in fig. 75 obtained with non-zero magnetic fields that the minimum is of magnetic origin. The magnetoresistance is positive, close to the ordering temperature ($d\rho/dH$ shows a peak at $T \approx T_c$). These data indicate that there is a positive contribution to ρ due to magnetic ordering.

It is interesting to note, however, that the resistivity increases upon magnetic ordering whereas in crystalline materials it usually decreases. This effect was ascribed by Asomoza et al. and Fert et al. as resulting from coherent exchange scattering. This coherent exchange scattering was originally calculated for crystalline materials by De Gennes and Friedel (1958) and extended to amorphous materials by Fert et al. and Asomoza et al. These authors showed that the coherent exchange scattering makes the following contribution to the resistivity:

$$\rho = (J/J + 1)\rho_M \left\{ C_1 + C_2 \left[S_{11}(2k_F) - 1 \right] \mu_I^2 \right\},$$

$$\rho_M = \frac{m k_F^2 \Gamma^2 J(J+1)}{4\pi e^2 h Z}. \tag{68}$$

The concentration of the magnetic ions is represented by C while Γ is the exchange constant. The quantity μ_I is a parameter of local magnetic ordering and depends on
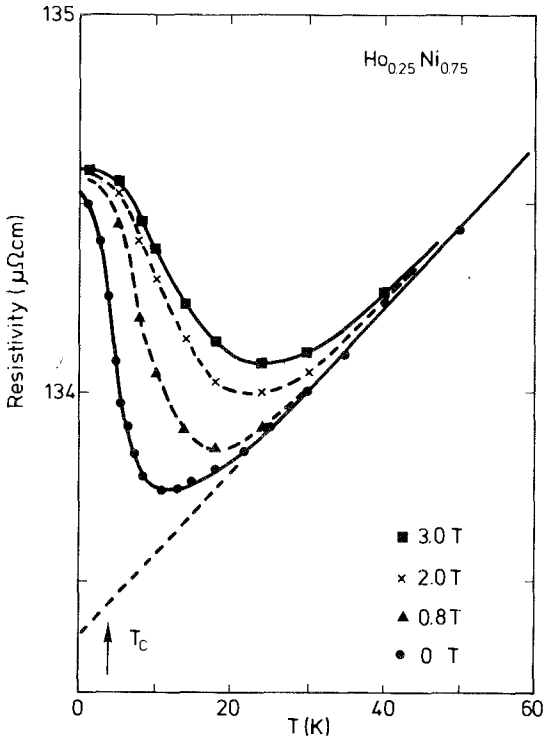
Fig. 75. Resistivity of amorphous $Ho_{0.25}Ni_{0.75}$ against temperature for several values of applied field. The temperature T_c corresponds to magnetic ordering (after Asomoza et al., 1977).

the range of the magnetic interactions. The partial structure factor for the magnetic ions is represented by $S_{11}(Q)$.

It can be derived from eq. (68) that the second term contributes positively upon magnetic ordering ($\mu_l \neq 0$) when there is constructive interference, i.e. $S_{11}(2k_F) > 1$. A negative contribution is expected when the interference is destructive [$S_{11}(2k_F) < 1$]. The former situation is assumed by Asomoza et al. and Fert et al. to explain the low-temperature upturn in their resistivity data.

Eq. (68) can also be used to estimate the magnetoresistance. In the first place, the assumption $S_{11}(2k_F) > 1$ implies a positive magnetoresistance. From the weakness of the magnetoresistance well below T_c Asomoza et al. (1977) obtained indications that μ_l approaches unity, meaning that the distribution of atomic moment directions pertaining to atoms within a few interatomic distances is not of the asperomagnetic type. This result is somewhat surprising in view of the predictions of the RAM model (see section 6). Von Molnar et al. (1981) observed a positive magnetoresistance near T_c in amorphous $Gd_{0.25}Ni_{0.75}$ but the magnetoresistance is slightly negative at 4.2 K. These authors note that this latter fact is not in keeping with the analysis given by Fert et al. (1977) and Asomoza et al. (1979) since it would require that $2k_F$ be substantially different in amorphous $Gd_{0.75}Ni_{0.75}$ from the value found in the other amorphous alloys of the type $R_{0.25}Ni_{0.75}$.

Asomoza et al. note, however, that the situation for Gd (S-state ion) may be quite different from that of the other rare earth components (non-S-state ions). The reason for this is that the inelastic spin-flip scattering can be frozen out in the case of non-S-state ions when kT becomes comparable to the crystal field splitting DJ^2. In Gd alloys the inelastic spin-flip scattering will continue to exist until it is frozen out by the magnetic ordering. This means that the change in resistivity with ordering in amorphous $Gd_{1-x}Ni_x$ alloys is due to two terms of opposite sign, comprising a positive term as in the other $R_{1-x}Ni_x$ alloys and a negative term associated with the freezing of the spin-flip process. Slight differences in composition can bring about relative changes in the strengths of these two contributions. For instance, in one of their $Gd_{1-x}Ni_x$ samples Asomoza et al. observed a negative magnetoresistance in the entire region around T_c. Von Molnar et al. also suggest that for $x > 0.75$ in $Gd_{1-x}Ni_x$ the Ni atoms may acquire a magnetic moment near and below T_c. Since this is a moment induced by the R spin, its occurrence is less likely in the other materials because of the lower value of the expectation value $\langle S \rangle_R$.

A positive magnetoresistance was also found by Felsch et al. (1982) in amorphous $Ce_{0.755}Co_{0.245}$. At low temperature, the zero-field $\rho(T)$ curve exhibits a T^2 dependence up to 0.5 K followed by a linear $\rho(T)$ behaviour up to 5 K. The difference compared with the amorphous rare earth alloys described above is that the positive magnetoresistance observed at low temperatures ($T < 6$ K) is not associated with magnetic ordering. In this respect amorphous $Ce_{0.755}Co_{0.245}$ differs also from other amorphous Ce alloys such as the $Ce_{1-x}Au_x$ alloys investigated by Ernst et al. (1980). These latter alloys give rise to magnetic order at low temperatures and the magnetoresistance is negative, i.e. the resistivity decreases with increasing field strengths, which is in agreement with model considerations (Bhattacharjee and Coqblin, 1978). The different behaviour of $Ce_{0.755}Co_{0.245}$ was attributed by Felsch et al. to the occurrence of a homogeneous intermediate valence state of the Ce ions.

8.2. Hall effect

The Hall resistivity ρ_H can be determined by measuring the voltage V_H in the y direction of a sample of thickness d when a magnetic field H is applied (in the z direction) perpendicular to the direction of the current I (in the x direction):

$$\rho_H = (V_H/I)d. \tag{69}$$

In the ferromagnetic regime the Hall resistivity can be expressed as

$$\rho_H = R_0 H + R_s \cdot 4\pi M_s, \tag{70}$$

where R_0 is the ordinary (or normal) Hall coefficient and R_s the spontaneous (or anomalous or extraordinary) Hall coefficient. In the paramagnetic regime the saturation magnetization has to be replaced by χH, leading to the expression

$$\rho_H = R_0 H + R_s \cdot 4\pi \chi H. \tag{71}$$

The ordinary Hall effect originates form the Lorentz force experienced by the conduction electrons moving in the field H, while the spontaneous Hall effect arises

as a consequence of asymmetric scattering of the conduction electrons by the magnetic atoms (Smith, 1973; Berger, 1973).

If one makes the assumption that R_0 and R_s are temperature independent one may separate these two contributions by plotting ρ_H/H versus $4\pi\chi$ for a number of temperatures. The slope of the resultant straight line gives R_s and from the intercept with the vertical axis one finds the value of R_0. This procedure for analysing ρ_H data was adopted by Gambino et al. (1981) for several amorphous $Gd_{1-x}Au_x$ alloys. The value of R_0 was found to be negative (typically $-1 \times 10^{-12} \ \Omega \ cm/G$) and at least one order of magnitude smaller than the spontaneous Hall coefficient. From the constant behaviour of R_0 over a wide concentration range the authors conclude that the conduction electron concentration does not change much with x. Consequently, they interpreted the linear decrease of T_c with x in $Gd_{1-x}Au_x$ as the result of a constant coordination number, the number of nearest Gd neighbours being simply proportional to $1 - x$.

Gambino et al. also observed a correlation between T_c and the tangent Hall angle ρ_H/ρ or between T_c and R_s. This correlation was interpreted in terms of the side jump mechanism resulting from the conduction electron polarization, i.e. the authors suggest that it is mainly the side jumps which contribute to ρ_H/ρ and R_H. Since the side jump mechanism is proportional to the s conduction electron polarization caused by the localized spins S, the side jump scattering can be expected to be proportional to $s \cdot S$.

The Curie temperature in alloys where the RKKY mechanism is the main source of the localized moment coupling, was taken as a convenient experimental quantity reflecting the strength of this conduction electron polarization. In the RKKY approach the conduction electron polarization produced by a given localized rare earth spin is proportional to $J_{sf}s \cdot S$. A second rare earth spin will orient itself according to the local conduction electron polarization which also involves an interaction of the type $J_{sf}s \cdot S$. For this reason the RKKY expression contains the $J_{sf}s \cdot S$ interaction term squared. it seems therefore that correlating R_s with $T_c^{1/2}$ should be somewhat more satisfactory than correlating R_s with T_c, although the
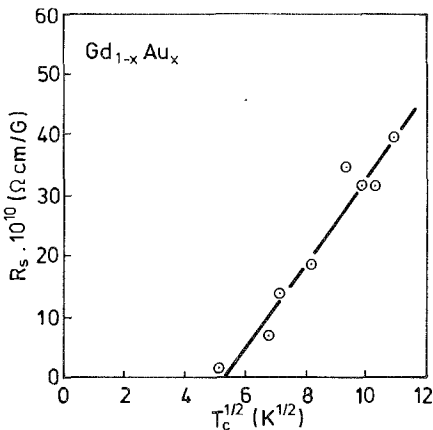
Fig. 76. Correlation between the spontaneous Hall coefficient R_s and the root of the corresponding Curie temperatures T_c in various $Gd_{1-x}Au_x$ alloys based on experimental data of Gambino et al. (1981).

spread in the data does not permit one to determine which of the two correlations is the more appropriate. A plot of R_s vs. $T_c^{1/2}$ made on the basis of the R_s and T_c data of Gambino et al. is shown in fig. 76.

In amorphous alloys the values of R_s are usually expected to be much larger than those of R_0 owing to the fact that in these materials the values of R_s are enhanced as a result of their being proportional to ρ^2 (Smith, 1958; Karplus and Luttinger, 1954). Here it should be recalled that the resistivity in amorphous alloys is much larger than in crystalline materials. McGuire and Gambino (1980) used this result and analysed the Hall data obtained in various amorphous Gd alloys with various non-magnetic metals by neglecting R_0. A correlation between R_s and the Curie temperature was reported to exist in these alloys too.

Hall measurements on amorphous alloys in which Gd is combined with magnetic metals have been reported by several authors. Ogawa et al. (1974) studied the Hall effect in amorphous $Gd_{1-x}Co_x$ alloys. They found that the Hall voltage does not depend on the magnetization but on the atomic fraction of Gd, the contribution of Co being of minor importance. Furthermore they observed that the sign of the Hall voltage was always negative when the direction of the Gd moments was parallel to the magnetic field applied.

When studied as a function of temperature, reversal occurred at the compensation temperature. The results were interpreted on the basis of a localized electron model where each of the two components contributes separately to the Hall effect. Both contributions correspond to a negative value of R_s. The larger contribution of the Gd atoms was ascribed to the spin–orbit splitting in Gd being much larger than in Co. The authors point out that a close analogy exists between the sign reversal of the Hall effect and the Kerr rotation, albeit the former is due to the reversal of the Gd moment direction at T_{comp} whereas the latter is due to the reversal of the Co moment direction at the same temperature. A sign reversal of the Hall voltage in amorphous $Gd_{1-x}T_x$ (T = Fe, Co, Ni) films near T_{comp} was also reported by Okuno et al. (1981) and Tsushima et al. (1982).

Asomoza et al. (1977b), Malmhäll (1983), Mimura et al. (1976b) and Shirakawa et al. (1976) take a view opposite to that of Ogawa et al. (1974) and Tsushima et al. (1982). The latter authors concluded that the Hall voltage is primarily due to the rare earth component in $R_{1-x}M_x$ (M = 3d). For $R_{1-x}Co_x$ Asomoza et al. assume that the Hall voltage is essentially associated with the Co atoms. They base their conclusion on the following experimental results:

(i) In al the amorphous $R_{1-x}Co_x$ alloys studied by them (R = Y, Gd, Dy, Er, Ho; $x \approx 0.75$) the Hall effect has the same sign and nearly the same magnitude when the temperature is higher than T_{comp} and the Co moments point in a direction parallel to the external field applied. The Hall effect is almost the same in all the alloys and there seems to be no difference between alloys where R is magnetic (R = Gd, Er or Ho) and those where R is non-magnetic (R = Y).

(ii) For a given alloy the absolute value of the Hall effect is nearly temperature-independent in the range 4.2–300 K and thus behaves in a similar way as the Co sublattice magnetization. If the Hall effect were associated with the R moment one would have expected its magnitude to have shown the somewhat stronger tempera-

ture dependence of the rare earth sublattice magnetization.

(iii) In amorphous $Gd_{0.25}Co_{0.19}Ni_{0.56}$ the Hall effect is reduced compared to that in $Gd_{0.25}Co_{0.75}$. This reduction would not have been observed if the Gd atoms had been mainly responsible for it.

Lachowicz (1981, 1982) analysed the anomalous Hall effect in several $Gd_{1-x}Co_x$ alloys by means of a kinematic model. He showed that R_s, when defined as

$$R_s^* = \rho_H \left[4\pi (|M_{Gd}| + |M_{Co}|) \right]^{-1},$$

can be expressed by means of the relation $R_1^* = C\rho^n$. From a double logarithmic plot Lachowicz found $n = 1.04 \pm 0.02$, which was taken as an indication that the dominant contribution in $Gd_{1-x}Co_x$ alloys is connected with skew scattering.

Magnetic and transport measurements in amorphous $Gd_{1-x}Ni_x$ alloys were reported by McGuire and Gambino (1978). The Ni atoms have only a small magnetic moment when $x < 0.7$. Nevertheless the Ni atoms were found to contribute substantially to the extraordinary Hall effect. In $Gd_{1-x}Ni_x$ this Hall effect is negative for Gd as well as for Ni when the corresponding moments are parallel to the magnetic field applied. The total extraordinary Hall effect observed is a result of the antiparallel coupling of the Gd and Ni moments. It is positive when $x > 0.6$ and negative for lower x values. Similar results were obtained by Von Molnar et al. (1981) and Asomoza et al. (1979). The situation closely resembles that in amorphous $Gd_{1-x}Co_x$ alloys discussed above. It seems possible that the relatively large contribution of Ni in the former series is a result of the larger spin–orbit splitting in Ni than in Co.

McGuire and Taylor (1979) investigated the magnetic properties and transport properties of amorphous rare earth alloys containing Mn. They studied alloys of the series $Gd_{1-x}Mn_x$, $Y_{1-x}Mn_x$ as well as ternary alloys containing Co in addition to Mn. The interpretation of their results presented some difficulties in view of the fact that the moment formation on the Mn atoms and their coupling with the rare earth moments is less straightforward than in the case of Fe, Co or Ni alloys. In these latter alloys the 3d moment increases with increasing concentration of the 3d component, whereas McGuire and Taylor found that the Mn moment decreases with increasing Mn content. Furthermore the contribution to the anomalous Hall effect had a different sign, R_s being positive for Mn but negative in the case of the other transition metal atoms.

8.3. Superconductivity

The influence of large atomic disorder on the superconducting properties of metals was studied many years ago by Buckel and Hilsch (1954, 1956). The superconducting transition temperatures of noncrystalline films of simple metals were found to be higher than those of the corresponding crystalline materials. The first observation of superconductivity in a metallic glass was made by Johnson et al. (1975) on amorphous La–Au alloys. The interest in superconducting amorphous glasses has been increasing ever since. It is an interest coming partly from the fundamental physics side and partly from the technological side.

The technological interest stems primarily from the fact that melt-spun ribbons have usually much better mechanical properties than crystalline compounds, which are brittle and have a tendency to fracture. These latter properties are highly undesirable in the fabrication of high-field superconducting magnets and devices.

The most obvious physical quantity studied in the amorphous materials mentioned is the superconducting transition temperature T_0 and the corresponding transition width ΔT_0.

In the microscopic theory of Bardeen et al. (1957) the electrons are treated as a nearly free electron gas, individual electrons interacting pairwise via an attractive phonon-mediated potential. The superconducting transition temperature is given by the well-known expression

$$T_0 = 1.14\langle \omega \rangle \exp\left[-1/N(E_F) \cdot V \right],\tag{72}$$

where $\langle \omega \rangle$ is the Debye frequency or a properly averaged phonon frequency. The product $\lambda = N(E_F) \cdot V$ of the density of states $N(E_F)$ and the effective matrix element for the phonon-coupled electron–electron interaction V is often referred to as the electron–phonon coupling constant.

For amorphous alloys this so-called weak-coupling approximation has in general been found to be less well applicable. In the strong coupling limit the coupling constant λ is described in terms of the Eliashberg function $\alpha^2(\omega)F(\omega)$ where $F(\omega)$ is the spectral energy distribution function of the phonon states and $\alpha(\omega)$ the ω-dependent average electron–phonon matrix element. It was shown by McMillan (1968) that λ can be approximated as

$$\lambda_M = \frac{N(E_F)\langle I^2 \rangle}{M\langle \omega^2 \rangle_M},\tag{73}$$

where $\langle I^2 \rangle$ is the squared electronic matrix element averaged over all possible electron–phonon scattering processes. M represents the ionic mass and $\langle \omega^2 \rangle_M$ is the McMillan mean square phonon frequency, which is related to θ_D^2 through a proportionality constant. In the strong coupling limit ($\lambda \approx 1$) the superconducting transition temperature becomes:

$$T_0 = \frac{\langle \omega^2 \rangle^{1/2}}{1.45} \exp\left[-\frac{1.04(1+\lambda_M)}{\lambda_M - \mu^*(1 + 0.62\lambda_M)} \right],\tag{74}$$

where μ^* represents an effective repulsive Coulomb interaction between electrons ($\mu^* \approx 0.1$).

It follows from the equations given above that a comparison of experimentally observed T_0 values with model predictions would require a knowledge of $N(E_F)$. For amorphous thin films in particular, small sample quantities make an accurate determination of $N(E_F)$ by means of specific heat measurements or magnetic measurements rather difficult. It was proposed by Rainer and Bergman (1974) and Bergmann (1976) that $N(E_F)$ can be estimated by measuring the upper critical field gradient dH_{c2}/dT in the superconducting regime and using the relation

$$\left[\frac{dH_{c2}}{dT} \right]_{T_0} = c\rho N^*(E_F) = c\rho(1+\lambda)N(E_F),\tag{75}$$

where c is a constant and ρ the electrical resistivity in the normal state. The quantity $N^*(E_F)$ is commonly referred to as the electron–phonon dressed density of states. When λ data are available from tunnelling experiments one may use eq. (75) to obtain values for $N(E_F)$ and compare these with those calculated in the free electron approximation. Experimental values of T_0, $N(E_F)$, λ and θ_D obtained for various amorphous La-base alloys have been listed in table A5 in the Appendix.

Bulk superconductivity in amorphous $La_{1-x}Au_x$ glasses was studied by Johnson et al. (1975). These authors were able to prepare stable, single-phase amorphous alloys only in the range $0.18 < x < 0.26$. As indicated in the top part of fig. 77 crystalline fcc La with Au in solid solution is formed when $x < 0.14$, while a new cubic crystalline phase was observed in alloys for which $x > 0.30$. Results of resistivity measurements for two alloys of different Au concentration are compared in fig. 78 with liquid quenched La. In the single-phase region the transitions are seen to be rather sharp curves (A and B). For the liquid-quenched La, containing some β-La, the transition is much broader. The onset temperature is close to $T_0 = 6.0$ K, which corresponds to the superconducting transition temperature of β-La. The dependence of T_0 on alloy composition is shown in the lower part of fig. 77 where the single-phase region is recognized by the relatively small widths of the corresponding transitions.

Apart from amorphous alloys composed of La and Au, the authors included in their study amorphous alloys of La with Cu and Ni. The T_0 values were found to be
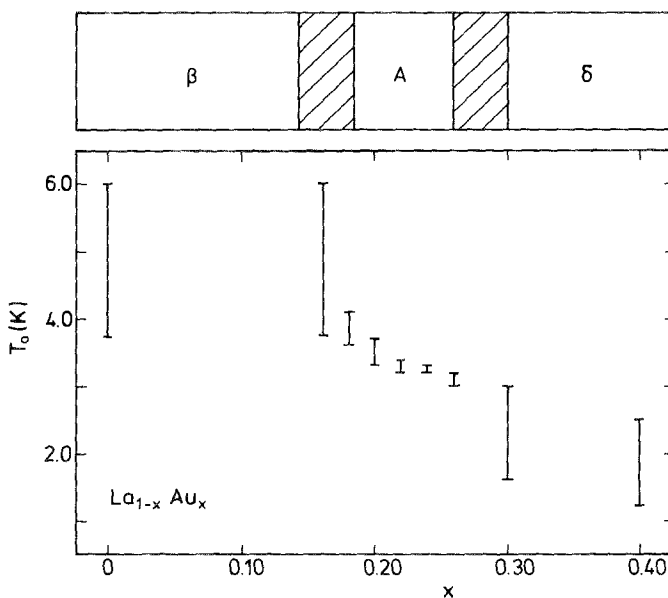
Fig. 77. Superconducting transition temperature in amorphous $La_{1-x}Au_x$ alloys as a function of alloy composition. Vertical bars indicate the width of the transitions (after Johnson et al., 1975). In the top part of the figure the phases present in liquid quenched alloys are indicated as a function of gold concentration. The fcc solid solution is designated as β, the amorphous phase as A, and the cubic crystalline phase as δ. The shaded regions indicate two-phase mixtures.
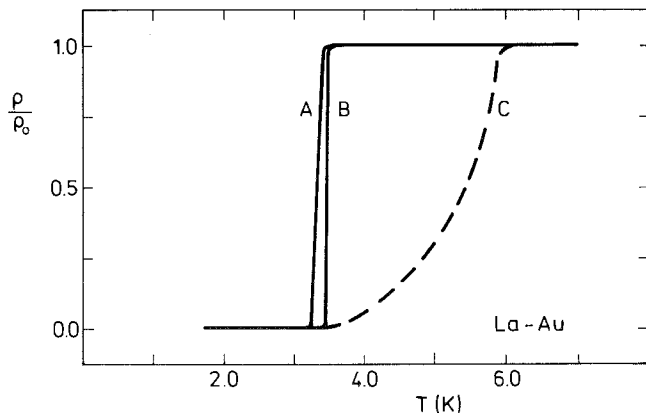
Fig. 78. Temperature dependence of the resistance ratio ρ/ρ_0 for (A) amorphous $Ag_{0.22}La_{0.78}$ obtained using the "gun" technique, (B) amorphous $Au_{0.22}La_{0.78}$ obtained using the "piston-and-anvil" technique, (C) liquid-quenched La containing the β phase obtained using the "gun" technique (after Johnson et al., 1975).

not much different. Taking into consideration that the mean free path in all these alloys is of the order of interatomic distances, Johnson et al. conclude that the pairing of superconducting electrons in these La-base alloys must be of a local nature, indicating that the La–La nearest neighbour bonding plays an important role in determining the superconductive properties.

Shull and Naugle (1977) investigated several liquid-quenched amorphous $La_{1-x}Au_x$ alloys by means of specific heat measurements and the T_0 values reported by them are in good agreement with the data found by Johnson et al. (1975). Considerably different T_0 values were found, however, in amorphous alloys prepared by vapour quenching (Manning and Briscoe, 1978). It was also found that amorphous films made by vapour quenching at 4 K crystallized when kept at room temperature. Stable films were obtained in the range $0.18 \leqslant x \leqslant 0.26$. These results, too, are quite different from those obtained by Johnson et al. (see the top part of fig. 77) and are also in apparent conflict with the crystallization temperature $T_x = 453$ K found for $La_{0.78}Au_{0.22}$ by Buschow (1982c).

Manning and Briscoe offer two possible explanations for the difference in superconducting properties between vapour-quenched and liquid-quenched alloys. The first explanation is based on the assumption that the liquid-quenched alloys are microcrystalline rather than amorphous. The observation of a strongly exothermic heat effect (T_x) observed by Buschow in the differential scanning calorimetry experiments does not corroborate this view. The second explanation is based on the assumption of an atomic arrangement in the vapour-quenched alloy, which is much more uniformly disordered than in the liquid-quenched alloy. The rather low transition widths ΔT_0 seem to be in favour of this explanation, although even lower ΔT_0 values were found in liquid-quenched $La_{1-x}Au_x$ alloys by Johnson and Tsuei (1976).

Since condensation from vapour phase was allowed to take place at 4 K, no atomic rearrangement of the atoms can occur after impingement on the substrate so that the amount of CSRO may be expected to be relatively small. In the liquid-quenched alloy one has at least the degree of CSRO present in the liquid $La_{1-x}Au_x$ alloys and probably even a higher degree owing to the rearrangement still possible

during quenching. Consequently, the configurational entropy S_c is expected to be relatively high in the vapour-quenched and low in the liquid-quenched materials. Since the crystallization temperature scales roughly as $\Delta E/S_c$ (see section 4.3), T_x is expected to have a much lower value in the vapour-quenched materials than in the liquid-quenched alloys. This seems indeed to be the case ($T_x < 300$ K for the vapour-quenched alloys in the range $0.18 \leqslant x \leqslant 0.26$ while $T_x = 453$ K for the liquid-quenched alloy $x = 0.22$). The presence of a higher degree of CSRO in the liquid-quenched alloys is not in conflict with the conclusions of Johnson et al. (1975) mentioned above, that the superconducting properties are localized on the La atoms and depend largely on the La–La separation. In this respect it is interesting to mention the results of Fasol et al. (1978) who studied the superconductive properties of amorphous $La_{0.78}Au_{0.22}$ under high pressure and showed that the normalized pressure dependence of $T_0(P)/T_0(0)$ is almost identical with that found in fcc-La.

Amorphous alloys of the type $La_{1-x}Al_x$ and $La_{1-x}Ge_x$ were studied by Agyeman et al. (1979). Their observations were found to agree with the model prediction (eqs. 73 and 74) that the superconductivity in the amorphous state is largely determined by the product $\eta = N(E_F)\langle I^2 \rangle$, although the concentration dependence of T_0 is mainly determined by variations in $N(E_F)$, the quantity $\langle I^2 \rangle$ being essentially constant. Their results were interpreted as providing further support for the view that superconductivity is largely a localized property associated with the La atoms.

The pressure dependence of superconductivity in amorphous $La_{1-x}Al_x$ alloys was studied by Razavi and Schilling (1982) and by Bindilatti et al. (1981). The pressure derivative of T_0 as well as the values of T_0 themselves were found to decrease linearly with x, the values obtained by extrapolating to $x = 0$ corresponding to $\delta T_0/\delta P$ and T_0 found in fcc-La. The data obtained in $La_{0.78}Au_{0.22}$ by Fasol et al. (1978) also fit into the two concentration dependences, suggesting a rather universal behaviour. Razavi and Schilling found that the value of $\delta T_0/\delta P$ for the $La_{1-x}Al_x$ alloy with $x = 0.165$ is extraordinarily large and does not fit into this picture. The concentration of this alloy is very close to the phase boundary for stable liquid-quenched amorphous alloys, which might provide a hint for explaining the extraordinary $\delta T_0/\delta P$ behaviour.

Amorphous $La_{1-x}Ga_x$ ($0.16 \leqslant x \leqslant 0.28$) alloys were investigated by Shull et al. (1978) and reported to be of the intermediate coupling type with $\lambda = 0.8$. The values of λ were determined by means of eqs. (73) and (74) using values of θ_D and T_0 derived from specific heat data. Shull et al. found an abrupt change of θ_D and $N(E_F)$ for concentrations slightly higher than $x = 0.22$. For these concentrations they also report the appearance of two closely spaced transition temperatures. This was ascribed to a change in the short-range order of the La atoms (see also the results of Johnson and Williams, 1979). The authors associated this with the completion of the filling of Bernal holes in the dense random-packed structure of La by the smaller Ga atoms. These results may, however, also point to a metallurgical phase separation that had occurred during preparation in which the domain dimensions are in the submicrometer range, as proposed for superconducting $La_{0.70}Cu_{0.30}$ by Arce et al. (1982).

Daudin (1981) studied the thermal conductivity of amorphous $La_{0.70}Cu_{0.30}$ below

T_0 and found the classical amorphous behaviour expected on the basis of a two-level model. Poon and Durand (1977) studied the pair-breaking effect of Gd impurities in amorphous $La_{0.80}Au_{0.20}$. The values of T_0 were found to decrease with increasing Gd concentration. This behaviour was satisfactorily described in terms of the model of Abrikosov and Gorkov (1962).

Results of investigations by Favaron et al. (1980) make it clear that the $La_{1-x}Cu_x$ system is less favourable with regard to formation of amorphous alloys. The amorphous state can be obtained free from crystalline material only in a narrow range close to $x = 0.30$. At other concentrations the amorphous phase is contaminated with crystalline material of the fcc structure (β_1) or with the crystalline phases of the composition LaCu (C_1). As indicated in the top part of fig. 79, no amorphous phase is present when $x > 0.40$. The concentration dependence of T_0 and the corresponding transition widths are shown in the main part of fig. 79. Note that there is a similar correspondence between these widths and the microstructural composition of the samples, as was also found for $La_{1-x}Au_x$ (fig. 77).

Apart from the amorphous rare earth base materials mentioned above, numerous other amorphous metals and alloys have been studied. Collver and Hammond (1973) made a systematic study of amorphous transition metal films obtained by vapour deposition on cryogenic substrates. The superconducting properties of these amorphous alloys show clear differences with those of crystalline alloys. The T_0 values of the latter vary continuously with valency and give rise to two sharp peaks for electron-to-atom ratios equal to 4.5 and 6.5, respectively (Matthias, 1957). In contrast, the T_0 values of the amorphous alloys show a more moderate variation with
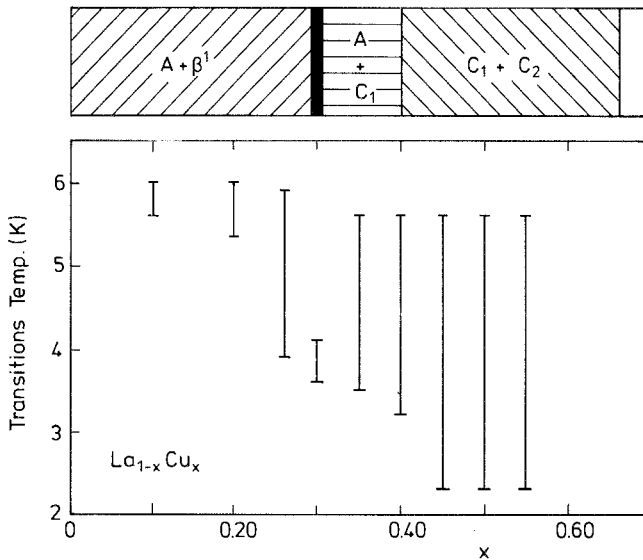
Fig. 79. Superconductive transition temperature as a function of alloy composition. Vertical bars indicate the total transition width corresponding to 100% of the superconductive transition (after Favaron et al., 1980). In the top part of the figure the different phases present in the samples have been indicated (A = amorphous, $\beta' =$ fcc, $C_1 =$ LaCu, $C_2 =$ LaCu$_2$).
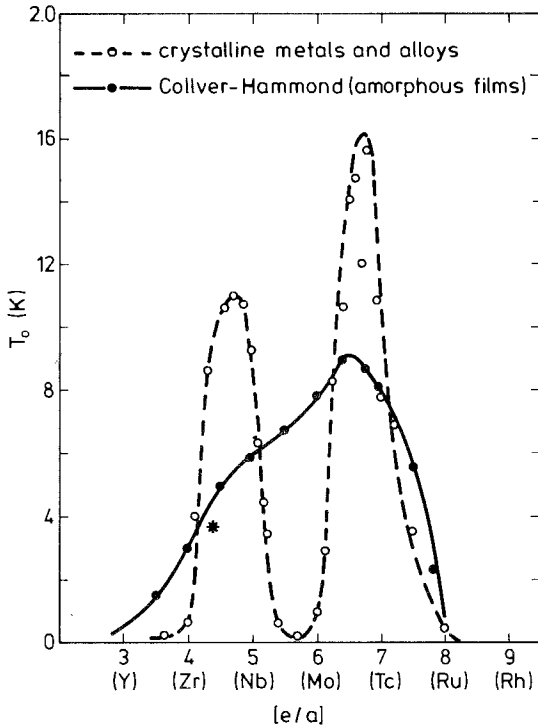
Fig. 80. Superconducting transition temperature of transition metals and alloys of the 4d series in the amorphous and crystalline states, as a function of electron-to-atom ratio. The result obtained on amorphous $La_{0.80}Au_{0.20}$ (*) has been included for comparison (after Johnson, 1978).

e/a. As can be seen in fig. 80, the Collver–Hammond plot for amorphous alloys gives rise to only a single broad peak near $e/a = 6.5$. For comparison the T_0 value for $La_{0.80}Au_{0.20}$ has been indicated by means of an asterisk. For more details regarding the superconducting properties of amorphous alloys of various compositions the reader is referred to reviews written by Johnson (1978, 1979).

9. Miscellaneous properties

9.1. Specific heat

In various disordered and amorphous solids the low-temperature specific heat is approximately linear in temperature. This behaviour was attributed by Anderson et al. (1972) and Phillips (1972) to the existence of a new type of "glassy" excitations, usually associated with the presence of tunnelling levels. The tunnelling model is based on the contention that an amorphous solid can be regarded as being trapped or frozen-in in a region in configurational space that is far removed from that of the crystalline ground state.

This region of configuration space encompasses a relatively high energy and it is reasonable to assume that there must exist other energetically equivalent configurational regions into which the amorphous solid could have been trapped. All these

regions correspond to points of a local minimum on the potential energy surface of the amorphous solid, being separated from each other by large potential barriers.

The existence of numerous energetically equivalent but inaccessible pseudo-ground states for the alloys is in agreement with the observation of a finite zero-point entropy, $S(T = 0) \neq 0$. Not all of these pseudo-ground states will have an energy separation too far to make transitions within an experimental time scale possible. These transitions can then be identified with the tunnelling of single atoms or groups of atoms to new spatial configurations of almost the same energy. The presence of the corresponding constant density of states of low-energy excitation is reflected in the linear T dependence of the specific heat.

In metallic amorphous solids the observation of the linear specific heat term is obscured by the large electronic contribution. It seems possible to detect it, though, in amorphous superconductors when the measurements are extended to temperatures sufficiently below the superconducting transition temperature T_0. Such measurements were reported by Graebner et al. (1977) on amorphous ZrPd. In amorphous rare earth base materials the presence of such low-lying excitations were found in $La_{0.70}Cu_{0.30}$ by Daudin (1981) by means of thermal conductivity studies below T_0.

Amorphous rare earth base alloys in which the rare earth component carries a magnetic moment contain yet another mechanism which can lead to a linear specific heat contribution.

Coey and Von Molnar (1978) studied the specific heat of an amorphous Dy–Cu alloy and found a large linear contribution equal to $\gamma = 155$ mJ/mole K^2 at temperatures well below the spin freezing transition at $T_s = 18$ K. This linear contribution is more than an order of magnitude larger than the conduction electron contribution expected in metal systems with a normal density of states. Coey and Von Molnar explain the large linear contribution in terms of single-ion crystal field excitations of the Dy atoms. They argue that in many amorphous alloys the crystal field interaction becomes dominant, making the crystal field directions virtually uncorrelated with the molecular field directions at each site. If the molecular fields are represented by H_m and if their direction differs from that of the local anisotropy axis by an angle θ, the energy levels at any site may be represented by means of an expression derived from eq. (30):

$$E = -DM_j^2 \pm g\mu_B H_m M_j \cos \theta. \tag{76}$$

If the first term becomes dominant the energy levels for Dy^{3+} ($J = 15/2$) are a set of 8 Kramers doublets, each split by the magnetic perturbation ($\Delta E_i = \pm g\mu_B M_j H_m \cos \theta$). The probability $P(\theta)$ of finding an angle θ between random orientations is $\sin \theta$. But $dE/d\theta$ is also proportional to $\sin \theta$ within the doublet. The density of states for excitations $N(E)$, where $N(E)dE = P(\theta)d\theta$, is therefore a constant. Only the lowest doublet is populated at temperatures that are low compared to the doublet–doublet separation, so that one has $N(E) = 1/g\mu_B H_m J$. The corresponding specific heat is then equal to $C = k^2 T/g\mu_B H_m J$.

Similar low-temperature excitations, associated with spin-flips for those ions which have $\theta \approx \pi/2$, can be expected in many amorphous alloys where the exchange interaction between the rare earth moments is relatively weak and where the rare

earth ions are Kramers ions (odd number of 4f electrons). No such effects are expected for non-Kramers ions because it is no longer required that the levels be n-fold degenerate, where n is even. Accordingly the energy levels will be split by the low symmetry of the crystal field, and the required degeneracy at $\theta = 90°$ is no longer present.

The excitations in systems composed of non-Kramers ions were studied by Fert and Campbell (1978) and Bieri et al. (1982). Here the ground state doublet is split to various degrees, corresponding to a wide distribution of crystal field excitations down to zero energy. This leads to a specific heat contribution at low temperatures which is nearly independent of temperature.

Such effects were observed by Garoche et al. (1980a, b) in amorphous $Pr_{0.21}Ag_{0.79}$. An estimate of the corresponding phonon and electron contributions was obtained from measurements on amorphous $Lu_{0.21}Ag_{0.79}$. The authors also report specific heat data obtained on amorphous $Sm_{0.21}Ag_{0.79}$. In the latter alloy the exchange interactions between the rare earth moments are much stronger, while Sm^{3+} is also a Kramers ion for which the temperature-independent contribution is not expected anyway. The experimental results obtained for the two alloys can be compared in fig. 81. Model calculations for the specific heat in amorphous Pr alloys with ferromagnetic interaction between the Pr moments were made by Borchi and De Gennaro (1981).

Results of magnetic and heat-capacity measurements on amorphous $Gd_{0.33}Al_{0.67}$ were reported by Coey et al. (1977). The temperature dependence of the magnetic susceptibility was found to exhibit a cusp-like shape characteristic of the spin glass freezing temperature. The temperature dependence of the specific heat C showed a
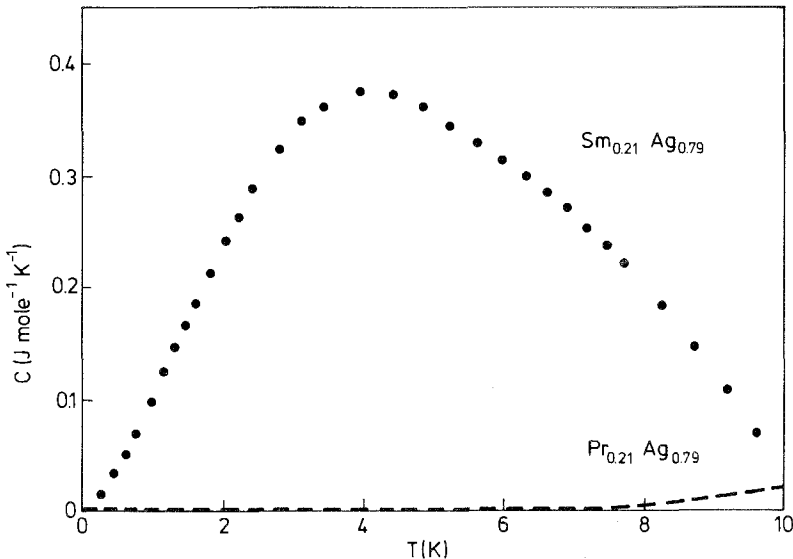
Fig. 81. Molar heat capacity of two amorphous $R_{0.21}Ag_{0.79}$ samples. For the sample $Pr_{0.21}Ag_{0.79}$ shown in the bottom part the lattice and electronic contribution has been subtracted (after Garoche et al., 1980).

broad maximum near this temperature. At low temperatures C varied as $T^{2/3}$, which was interpreted as originating from ferromagnetic spin waves excited in small regions of about 3.5 nm in diameter.

A number of specific heat studies was performed on superconducting La-base amorphous alloys. These comprise measurements on amorphous $La_{1-x}Au_x$ alloys (Shull and Naugle, 1977) and amorphous $La_{1-x}Ga_x$ alloys (Shull et al., 1978). The results of these studies were discussed in section 8.3.

A large linear term [$\gamma = 41$ mJ (mole Ce)$^{-1}$K^{-2}] was furthermore observed by Felsch et al. (1982) in the specific heat of amorphous $Ce_{0.755}Co_{0.245}$. It proved, however, difficult to correlate the specific heat data with the susceptibility in this intermediate valence compound owing to the presence of a specific heat contribution arising from the excitation of magnetic clusters. According to the authors, this latter contribution makes the determination of the linear term somewhat ambiguous. Taken at face value, the large γ value can be considered as evidence for a high density of states associated with the presence of a narrow hybridized 4f density of states near the Fermi energy.

9.2. EPR and FMR

The number of electron paramagnetic resonance (EPR) investigations made on amorphous alloys is rather limited. Bates et al. (1971) investigated amorphous $Gd_{1-x}Ag_x$ alloys prepared by dropping a powdered mixture of Gd and Ag on to a molybdenum filament having a temperature of 2000°C. Condensation of the vapour was allowed to take place on substrates either kept at room temperature or cooled with liquid helium or liquid nitrogen. For various compositions the authors studied the temperature dependence of the linewidth. Curie temperatures were estimated from the position of the minima occurring in the linewidth-versus-temperature plots. Bates et al. found that the concentration dependence of the Curie temperature in $Gd_{1-x}Ag_x$ has a sharp minimum ($T_c = 45$ K) near $x = 0.10$ in alloys deposited on cooled substrates. At lower Gd concentrations it increases strongly again and reaches values of about 350 K at concentrations in the range $0.50 \leq x \leq 0.70$. These results are in strong contrast with the results obtained by Hauser (1975) from magnetic measurements on alloys made by sputtering on cooled substrates. Remarkably enough, the Curie temperatures measured by Bates et al. on samples prepared by using substrates kept at room temperature during vapour deposition, are in better agreement with the susceptibility data of Hauser. As already mentioned, there is a sharp change in the concentration dependence of T_c near $x = 0.10$ in the alloys deposited at low temperatures. From this Bates et al. conclude that a change in the structure of the amorphous alloys takes place close to this concentration.

Amorphous $Gd_{1-x}Al_x$ films prepared by sputtering were investigated by Jamet and Malozemoff (1978). In the paramagnetic regime the alloys of the concentrations $x = 0.19$, 0.44 and 0.63 were found to have a small positive g shift ($\Delta g = 0.006 \pm 0.004$). This is in contrast with the negative value of Δg observed earlier in crystalline Gd–Al compounds (see for instance Davidov et al., 1973). Jamet and Malozemoff analysed their data in terms of the RKKY model and conclude that the

Δg shift observed in the amorphous $Gd_{1-x}Al_x$ alloys is mainly due to the exchange interaction between the 4f electrons and the 5d electrons, the g-shift contribution arising from s electrons being hidden as a result of a thermal bottleneck. Jamet and Malozemoff extracted a value for the spin–lattice relaxation time from their data and found this to be of the same order of magnitude as observed in crystalline systems.

It is well known that Gd can be used as a convenient EPR dope to obtain information on the local density of states (see, for instance, the review given by Taylor, 1975). This method was also applied to a number of amorphous alloys comprising $Pd_{1-x}Si_x$ (Eifert et al., 1983) and various alloys of the type $Zr_{1-x}T_x$, where T represents Cu, Ni, Co, Rh, Pd and Pt (Eifert et al., 1982, 1984). In the former alloys the temperature dependence of the linewidth (Korringa rates) was studied as a function of Si content x. It was derived from these results that the density of states $N(E_F)$ is rather small and that the concentration dependence of $N(E_F)$ is dissimilar from predictions based on the Nagel and Tauc model (Nagel and Tauc, 1975). The estimated magnitude of $N(E_F)$ is in satisfactory agreement with Hall effect measurements and specific heat measurements made by Mizutani and Massalski (1980).

A relatively large density of states was derived from EPR measurements in the Gd-doped $Zr_{1-x}T_x$ alloys. In the Zr-rich alloys $N(E_F)$ was found to be substantially larger than in pure crystalline Zr metal. This was explained in terms of changes in band structure of Zr resulting from alloying with T elements (Kübler et al., 1981). Hybridization of the d states associated with Zr with those associated with the T components leads to a mutual repulsion in energy space between the two sets of d sates. The density of states $N(E_F)$ is then mainly determined by the Zr d electron states. The increase in $N(E_F)$ observed upon alloying is due to the fact that the partial d density of states of Zr moves out of the minimum (Moruzzi et al., 1983). The density of stages derived by means of the Gd-doped samples was found to be in good agreement with specific heat data available for a few of the $Zr_{1-x}T_x$ alloys.

The ferromagnetic resonance technique (FMR) was mainly used to obtain information on the intrinsic anisotropy of ferromagnetic amorphous alloys.

From the FMR data obtained at a variable angle between resonance field and sample surface the uniaxial anisotropy and effective g values can be obtained by solving numerically the following equations:

$$(\omega/\gamma)^2 = \left\{ H \cos(\phi - \theta_0) + 2\left(K_u^{eff}/M \right) \cos^2\theta_0 \right\}$$
$$\times \left\{ H \cos(\phi - \theta_0) + 2\left(K_u^{eff}/M \right) \cos 2\theta_0 \right\}, \qquad (77)$$

$$HM \sin(\phi - \theta_0) = K_u^{eff} \sin 2\theta_0. \qquad (78)$$

Eqs. (77) and (78) describe the resonance for H and M making an angle ϕ and θ_0 with the normal to the plane of the thin film (or the ribbon plane). Eq. (78) defines the equilibrium position of the magnetization M with respect to the applied field H. In these equations ω denotes the resonance frequency. From the gyromagnetic ratio γ the effective g value can be obtained by means of the expression $g_{eff} = 2|\gamma|mc/e$. The effective uniaxial anisotropy constant K_u^{eff} is defined as $K_u^{eff} \sin^2\theta_0 = (K_u - 2\pi M^2) \sin^2\theta_0$. For flat samples the demagnetizing field can usually be taken as

$4\pi M$. This quantity can conveniently be derived from magnetization measurements. Note that eqs. (77) and (78) adopt rather simple forms when the anisotropy is strictly uniaxial in a direction normal to the film plane of the ribbon plane.

The FMR in several amorphous R–3d alloys was investigated by Lubitz et al. (1975). These authors used samples obtained by vapour deposition and found that the FMR spectra were difficult to interpret owing to the presence of inhomogeneities in the sample. In such a situation it may be possible that the FMR probes parts of the sample (having relatively large M and/or K_u) different from those probed by the vibrating sample magnetometer. For the amorphous Gd alloys Lubitz et al. and also Victoria et al. (1978) found that the temperature dependence of the linewidth is in agreement with predictions based on Landau–Lifshitz relaxation rates.

Amorphous $Gd_{1-x}Co_x$ alloys were studied by Nagy et al. (1976) on vapour-deposited samples. They found that the anisotropy field first decreases with decreasing Co concentration but below $x \approx 0.8$ increases again. An easy axis anisotropy normal to the film plane was reported to be present only for the alloy richest in Co ($x = 0.96$). An easy plane anisotropy was found in the other alloys ($0.64 \leqslant x \leqslant 0.93$). Müller et al. (1978) investigated amorphous $Gd_{1-x}Co_x$ alloys by means of FMR in combination with magnetization measurements and torque measurements. These authors, too, found substantial differences between the results of the magnetic measurements and the FMR measurements, particularly in alloys close to the compensation composition. Like Lubitz et al. (1975) they ascribe these differences to inhomogeneities present in the amorphous alloys. Müller et al. report that the anisotropy constant K_u always changed to more negative values upon annealing, regardless of the initial sign of K_u before annealing. They interpreted their results in terms of a favourable type of short range atomic ordering in the as-sputtered films which leads to positive K_u values. It disappears during annealing, leaving only the contribution to K_u which originates from internal stresses.

The effect of post-deposition annealing in various amorphous R–Co alloys was also studied by Krishnan et al. (1978). On amorphous YCo_3 films in particular, the authors observed two resonance modes, corresponding to a surface and a volume mode, respectively. The intensity of the surface mode was found to be reduced after etching with dilute HCl, which made a distinction between the two modes possible. The anisotropy in the surface layer is of the in-plane type while that of the bulk is of the perpendicular type. The occurrence of this latter type was suppressed after annealing, owing to an increase of the thickness of the surface layer. The authors suggest that the diffusion of metal atoms and rare gas atoms along the normal to the film plane creates a sort of columnar structure in which there is a more than average distribution of Co pairs having their axis perpendicular to the film plane. According to the model of Gambino et al. (1973) discussed in section 7.1, this would then lead to an easy plane anisotropy.

Soohoo and Morrish (1979) performed FMR experiments on vapour-deposited $Gd_{1-x}Fe_x$ films ($0.69 \leqslant x \leqslant 0.82$). All these films have positive K_u values–indicating an easy magnetization direction perpendicular to the film plane. A typical set of FMR spectra obtained by Soohoo and Morrish is reproduced in fig. 82. The resonance fields corresponding to the peaks $H_\parallel$ and $H_\perp$ were used in conjunction
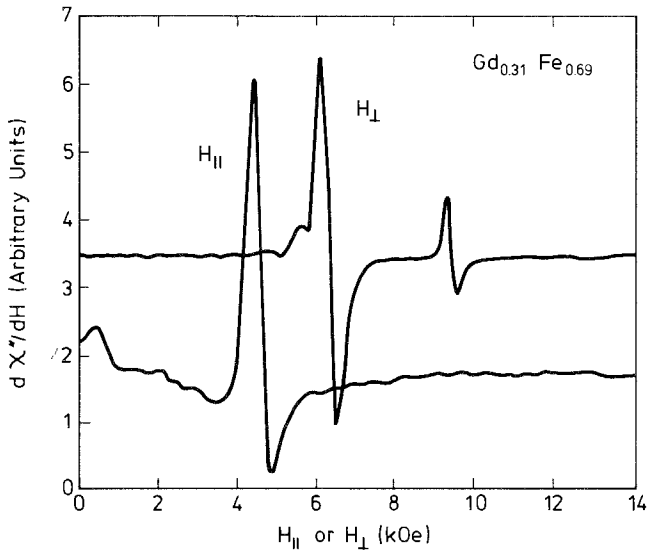
Fig. 82. Differentiated absorption spectra of an amorphous $Gd_{0.309}Fe_{0.691}$ film approximately 500 nm thick with the static field applied parallel and perpendicular to the film plane (after Soohoo and Morrish, 1979).

with equations of a similar type as eqs. (77) and (78) to obtain numerical values for g_{eff} and K_u as a function of concentration. The anisotropy constant K_u was found first to increase with the decreasing Fe concentration x. After passing through a maximum at about $x = 0.71$, K_u decreases again. The values of g_{eff} are in satisfactory agreement with the formula of Wangness (1956) given by:

$$g_{eff} = \frac{g_{Gd}(S - R)}{S - \alpha R},$$ (79)

where $S = (1 - x)/x$, $R = M_{Fe}/M_{Gd}$ and $\alpha = g_{Gd}/g_{Fe}$. For g_{Gd} and g_{Fe} the authors used the values 2 and 2.13, respectively.

Algra et al. (1980) used FMR to investigate the anisotropy in amorphous $Gd_{1-x}Co_x$ and $Gd_{1-x}Cu_x$ alloys obtained by means of melt spinning. They found that the values of K_u were positive and increased strongly with Gd concentration in alloys with $x < 0.6$. The values of K_u scaled approximately with the Gd concentration squared. As there was no significant difference in the behaviour of K_u between the Co and Cu alloys, the authors concluded that the presence of Co–Co pairs is not required for having a large uniaxial anisotropy. Algra et al. were unable to explain their results on the basis of the dipolar model proposed earlier by Mizoguchi and Cargill (1979), noting that the latter model would imply a K_u maximum in the middle concentration range rather than the minimum of K_u observed experimentally.

FMR studies in various Gd-rich $Gd_{1-x}T_x$ alloys with T = Mn, Fe, Co, Ni, Cu, Rh, Pd, Pt or Gd were made by Buschow et al. (1980). For several of these alloys the constant K_u was determined and found to be positive. The broadness of the ferromagnetic-to-paramagnetic transition found in the NMR experiment was explained on the basis of a wide distribution of local magnetizations in these alloys.

The FMR technique can also be used as a convenient means of studying the temperature dependence of the magnetization. In spin wave theory this temperature dependence is given by

$$M(T) = M(0)\left[1 - BT^{2/3} - CT^{5/2} \ldots\right].$$ (80)

Deviations from spin wave theory at low temperatures in various amorphous alloys were found by Bhagat et al. (1980), and explained in terms of a model where proper account is taken of the presence of magnetic clusters. A spin-cluster model was also used by Bhagat and Paul (1975) to explain the FMR data obtained by these authors in several amorphous RFe_2 alloys. Weissenberger et al. (1984) investigated FMR in amorphous Y–Co alloys and did not observe deviations from normal spin wave behaviour below T_c.

9.3. NMR

Nuclear magnetic resonance (NMR) experiments are a useful tool for obtaining information about the electronic properties of amorphous alloys. It is not a general method. Its applicability is restricted to alloys composed of elements having a nucleus with nuclear parameters that allow for an NMR signal in the currently available frequency range of modern NMR equipments.

The great advantage of NMR experiments is the fact that they are able to probe local spin densities. In non-magnetic materials that are metallic in character, there is a shift in resonance frequency (at constant magnetic field H) compared to that in insulators $\Delta\nu$. This shift, usually expressed as the Knight shift K, originates from the hyperfine interaction between the nuclear moment and the conduction electrons. For simple metals the Knight shift can be given as:

$$K = \frac{\Delta H}{H} = \frac{\Delta\nu}{\nu} = \frac{8\pi}{3}\chi_s\langle|\psi(0)|^2\rangle_F = a_s\chi_s,$$ (81)

where χ_s is the Pauli spin susceptibility and $\langle|\psi(0)|^2\rangle_F$ the probability density at the nucleus of the conduction electrons at the Fermi surface. The quantity a_s represents the effective s electron hyperfine coupling parameter. Values of this parameter are known from experiments or from theoretical model calculations. It can be inferred from eq. (81) that measurements of K can serve as a means of determining χ_s. In this way accurate values of the intrinsic χ_s can be obtained that are not biased as a result of the presence of magnetic impurities.

In non-magnetic alloys composed of transition metals the total Knight shift comprises contributions due to d electrons:

$$K = K_s + K_d + K_{orb} = a_s\chi_s + a_d\chi_d + a_{orb}\chi_{orb}.$$ (82)

The same contributions appear in the expression of the bulk susceptibility (corrected for diamagnetism)

$$\chi = \tfrac{2}{3}\chi_s + \chi_d + \chi_{orb}.$$ (83)

A determination of the various contributions can usually be obtained by combining measurements of K with magnetic measurements and by extending the NMR measurements to more than one type of NMR nucleus in the alloy. Such an analysis was made by Eifert et al. (1982) for several $Zr_{1-x}Cu_x$. It was shown by these authors

that combining Zr with Cu or transition metals such as T = Ni, Pt, Pd or Rh leads to a density of states $N(E_F)$ exceeding that of pure crystalline Zr metal. The interesting result of their analysis is that the enhanced density of states is not caused by the d electrons of the T element, but rather by a shift of the Zr d-electron density of states near E_F due to the alloying.

Apart from the nuclear moment (I) several types of nuclei have an electric quadrupole moment (Q). The latter are due to a departure of the nucleus from spherical symmetry. Through the electrostatic interaction of this quadrupole moment with the electric field gradient V due to the surrounding ions, the NMR technique can be used for probing local field gradients. In this way information can be obtained about local symmetry in the alloy. This quadrupolar interaction was studied in detail by Panissod et al. (1980) in a number of amorphous alloys and crystalline materials. These authors conclude that the local symmetries present in the crystalline materials are largely conserved in the corresponding amorphous alloys. These results strongly support the notion of the occurrence of CSRO in amorphous alloys. This point has already been discussed in section 5.2.

In ferromagnetic materials the magnetic field experienced by the nucleus is much larger than in the paramagnetic materials discussed above. This hyperfine field (H_{hf}) can be determined experimentally by sweeping the resonance frequency in zero external field. There are several contributions to H_{hf}. These comprise contributions due to core polarization of the inner s shell by the net d-spin or f-spin density (H_c) and contributions due to conduction electron polarization by the atomic moment associated with the nucleus under consideration (H_s) and a contribution due to conduction electron polarization caused by the atomic moments of the surrounding atoms (H_N). This latter contribution is often referred to as the transferred hyperfine field. Adding up, one therefore has

$$H_{hf} = H_c + H_s + H_N. \tag{84}$$

It will be clear that the distribution of different surroundings present in an amorphous alloy will entail a related distribution in the transferred field H_N. In addition, as was outlined in section 6.3, there will be a distribution in moments for each kind of magnetic atoms. This will lead to a distribution for each of the hyperfine field contributions H_c and H_s. These latter two distributions need not necessarily be congruent since the distribution of H_s values will also be affected by the presence of a distribution in the local conduction-electron densities in the alloy. All these distributions will lead to a rather drastic line broadening of the zero-field NMR line in amorphous alloys compared to that in atomically well-ordered crystalline materials. The results shown in fig. 83 are an example of such a broadened NMR spectrum. This spectrum has been interpreted by Durand (1981) as originating from [59]Co. The corresponding mean Co hyperfine field was found to be positive and to be equal to 7 T (Mizoguchi et al., 1982). This value is higher than that found for [59]Co in crystalline $GdCo_2$ (6.1 T). This is quite remarkable in view of the fact that the Co moment in amorphous Gd_2Co is expected to be much lower than in crystalline $GdCo_2$.

The extreme broadening of the NMR spectrum of amorphous alloys makes it
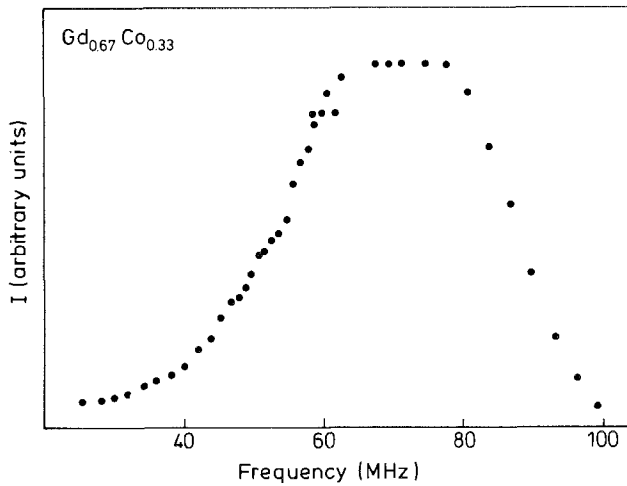
Fig. 83. Spin echo spectrum at 1.3 K of amorphous $Gd_{0.67}Co_{0.33}$ (after Durand et al., 1978).

rather difficult to decompose the total hyperfine field into its three components (H_c, H_s and H_N) using experimental methods such as applied, for instance, by Dormann et al. (1977) on various Gd-base compounds. In spite of these restrictions NMR measurements on amorphous alloys have proved helpful in attempts to unravel the complex nature of magnetism in these materials. Raj et al. (1977, 1978) investigated several Fe- and Co-base alloys and found that the proportionality between the average transition metal hyperfine field and the bulk magnetization was similar to that found in semi-metallic compounds with high transition-metal concentration (Bernas et al., 1967; Vincze et al., 1974). From the fact that this proportionality is retained, Raj et al. conclude that the long-range disorder of the amorphous state does not substantially affect the local properties and the character of the chemical bond. The extent of the distribution of the transferred hyperfine field (H_N) in ferromagnetic amorphous alloys can sometimes conveniently be studied by means of NMR on non-magnetic minority components of the alloys. The ^{11}B NMR proved to be particularly suitable in this respect (Raj et al., 1978; Lerchner et al., 1981). On the ^{11}B nuclei in the amorphous alloy $Fe_{80}B_{18}Ga_2$ the hyperfine field was found to increase continuously with the component concentration of the non-magnetic B (Raj, 1978).

The presence of a substantial line broadening in magnetically ordered alloys due to a distribution in the various components of H_{hf} does not mean that line broadening due to the quadrupolar interaction can be left out of consideration. In fact, examples are known where the quadrupolar broadening exceeds the broadening due to the exchange interaction. This is the case, for instance, in amorphous $Eu_{0.80}Au_{0.20}$ for which the Eu spin echo spectrum is shown in fig. 84. These results indicate that the quadrupolar splitting associated with the ^{153}Eu NMR is about an order of magnitude larger than for instance in crystalline $EuPt_2$, where the total width of the resonance is only about 10 MHz (Kropp et al., 1979).

For a further discussion of the application of NMR to amorphous alloys the reader is referred to the reviews published by Durand (1981) and Kahn and Lüders (1981).
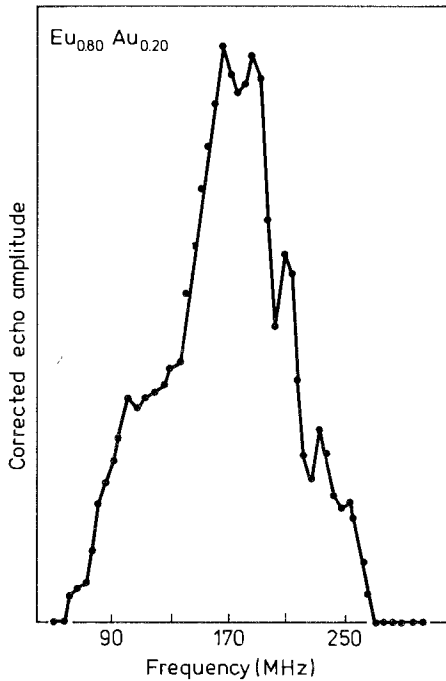
Fig. 84. NMR spin echo spectrum of amorphous $Eu_{0.80}Au_{0.20}$ at 1.4 K (after Durand, 1981).

9.4. Mössbauer spectroscopy

Mössbauer spectroscopy and NMR spectroscopy have in common that they provide information which is basically local in character. Up to now the Mössbauer effect has been more fruitfully applied to amorphous alloys than NMR. There are several reasons for this. In ferromagnetic materials the NMR can give rise to much more accurate values of the hyperfine fields than the Mössbauer effect. Owing to the extremely large line broadening this advantage is lost in amorphous alloys.

Furthermore, most ferromagnetic amorphous alloys are composed of several different elements that all can give rise to an NMR signal. In crystalline materials the different NMR lines are well separated from each other and the lines can be identified by studying the field dependence of the corresponding resonance frequency. In amorphous solids the NMR lines will in general no longer be well separated from each other but may overlap strongly. The determination of the field-induced shift of the resonance frequency, which is commonly employed for identifying a given resonance, is difficult and sometimes even impossible.

These problems with resonance line assignments are not present in Mössbauer spectroscopy. Commonly used Mössbauer isotopes are ^{57}Fe, ^{197}Au, ^{119}Sn, ^{151}Eu, ^{155}Gd, ^{161}Dy and ^{169}Tm. In all these cases (irrespective of whether the alloy contains one or more of these elements) a given Mössbauer spectrum will be composed exclusively of the lines corresponding to the transitions associated with a single type of these Mössbauer isotopes. That is, for each type of isotope a different type of
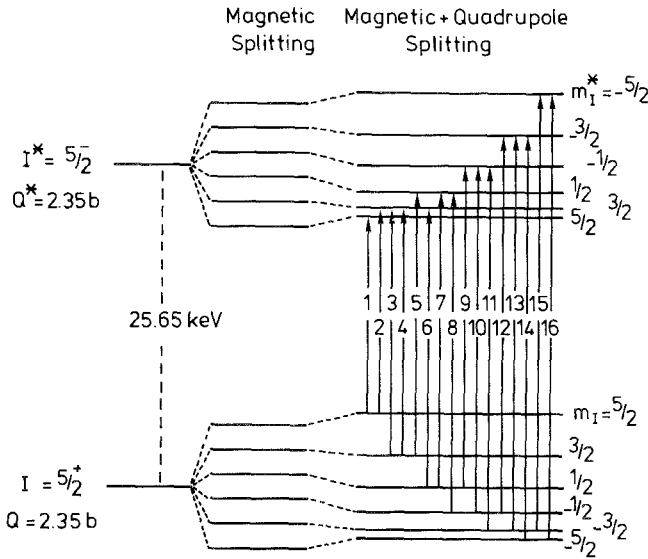
Fig. 85. Hyperfine level scheme for the nuclear $5/2^- \rightarrow 5/2^+$, 25.65 keV gamma transition in ^{161}Dy. The left side illustrates the case of a pure Zeeman interaction. The right side shows the case of a Zeeman interaction plus a collinear quadrupole interaction where the electric field gradient is of rotational symmetry (after Chappert et al., 1982).

spectrometer is required, characterized by a specific Mössbauer source and velocity scale. (For more details see the reviews written by Mössbauer and Clauser (1967), Greenwood and Gibb (1971) and Shenoy and Wagner (1978).)

As an example, we show in fig. 85 the level scheme involved with the 25.65 keV gamma transition in ^{161}Dy. It can be seen from the right-hand part of fig. 85 that the ^{161}Dy Mössbauer spectrum of magnetically ordered materials will in general be composed of 16 lines.

A typical set of simulated spectra was obtained by Chappert et al. (1982) and these spectra have been reproduced in fig. 86. They have a few features that deserve separate mention: Comparison of the spectra shown in figs. 86a and b shows that some of the resonance lines remain unaffected by the presence of a quadrupole interaction. This pertains primarily to the innermost and outermost lines. As a consequence these lines will remain sharp in the presence of various types of distributions in the quadrupolar interactions (figs. 86c and d). Some broadening of these lines will occur, however, in the presence of a distribution in the hyperfine field (fig. 86e). These features led Chappert et al. to argue that in the case of ^{161}Dy Mössbauer spectroscopy it will be possible in general to separate the quadrupolar and magnetic hyperfine distributions even by visual inspection of the spectra.

By comparing the experimental results of amorphous $Dy_{0.5}Ag_{0.5}$ with crystalline DyAg (CsCl type) Chappert et al. arrive at the following conclusions: The magnetic hyperfine field observed in the magnetically ordered regime is virtually the same in both types of materials and corresponds to the Dy^{3+} free-ion value. In the amorphous alloy the lowering in symmetry has resulted in a considerable quadrupolar broadening, at the same time changing the Γ_8 quartet ground state in crystalline DyAg into a well isolated $|\pm 15/2\rangle$ Kramers doublet in amorphous $Dy_{0.5}Ag_{0.5}$. In the magnetically ordered state the $J_z = |15/2\rangle$ state is the electronic ground state in both cases.
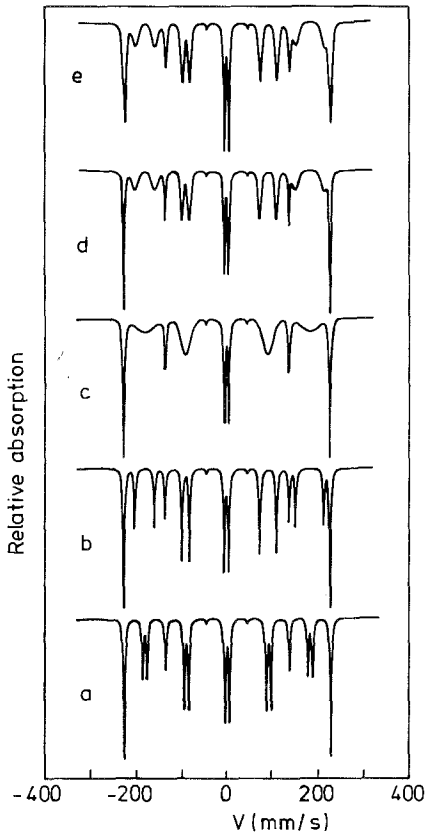
Fig. 86. Simulated ^{161}Dy Mössbauer spectra. (a) Pure Zeeman splitting corresponding to a hyperfine field $B = 582$ T, a full width at half maximum of all resonance lines of $W = 3.5$ mm/s and an isomer shift of IS $= 1.8$ mm/s; (b) same as (a) but with in addition a collinear quadrupole interaction $e^2qQ = 1800$ MHz; (c) same as (b) but with a Gaussian distribution in the quadrupole interaction. Its mean value is $\langle e^2qQ \rangle = 0$ and the half width $(1/e)$ of the distribution corresponds to $\Delta(e^2qQ) = 500$ MHz; (d) the mean value of the Gaussian quadrupole distribution is increased now to $\langle e^2qQ \rangle = 1800$ MHz while the width remained $\Delta(e^2qQ) = 500$ MHz; (e) same as (d) but with Gaussian distribution present also in the magnetic hyperfine field, $\langle B \rangle = 582$ T and $\Delta B = 12$ T (after Chappert et al., 1982).

There is a typical difference in temperature dependence of the hyperfine splitting between the two materials. In crystalline DyAg there is a sharp distinction between the spectra below the magnetic ordering temperature and above it. Below $T_N \approx 60$ K the spectra have an appearance commonly referred to as ferromagnetic relaxation spectra. Above $T_N \approx 60$ K the so-called fast relaxation limit has been reached, leading to a slightly broadened single resonance line without structure. In amorphous $Dy_{0.5}Ag_{0.5}$, however, this collapse of the hyperfine splitting does not occur when passing from the magnetically ordered regime to the paramagnetic regime. The hyperfine field observed in both temperature ranges is the same, from which Chappert et al. conclude that in the paramagnetic regime, too, a fairly pure isolated $|15/2\rangle$ Kramers state must form the ground state. In the absence of exchange interaction such a $|15/2\rangle$ ground state can only exist in the presence of a uniaxial crystalline electric field associated with the local environment of the Dy ions.

The lowering in symmetry is also the reason for the much lower relaxation rate observed in amorphous $Dy_{0.5}Ag_{0.5}$. It stems from the fact that in the isolated $|\pm 15/2\rangle$ state the possibilities of conduction electron relaxation or dipole–dipole relaxation are absent. Enhancement of the relaxation rate can only take place when
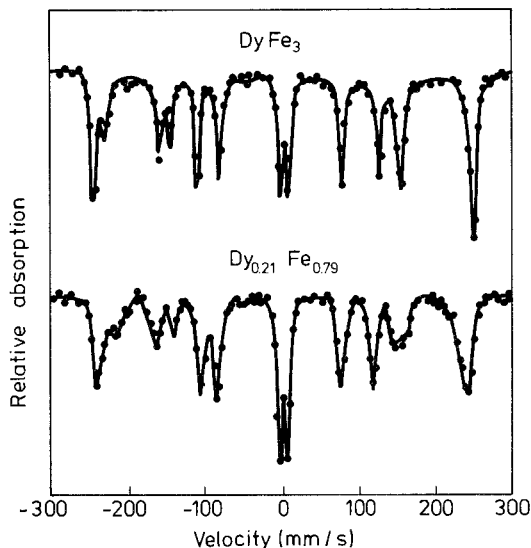
Fig. 87. ^{161}Dy Mössbauer spectra at 4.2 K of amorphous (bottom) and crystalline (top) Dy–Fe alloys. The solid lines represent least squares fits with Lorentzian doublets (after Chappert, 1979).

the temperature becomes high enough for kT to become equal to the energy separation between the $|\pm 15/2\rangle$ ground state doublet and the first excited state.

As already mentioned Chappert et al. observed a large quadrupolar broadening in the spectra of amorphous $Dy_{0.5}Ag_{0.5}$. The distribution of corresponding electrical field gradients (efg) was shown not to be located symmetrically around zero. The asymmetry is a result of the presence of a large 4f gradient fixed in the direction of the hyperfine field. The contribution of the lattice efg to the smeared-out quadrupole interaction corresponds to that expected for an asperomagnetic spin structure.

^{161}Dy Mössbauer spectroscopy has also been used to elucidate the magnetic structure in several amorphous alloys of Dy and 3d metals (Arrese-Boggiano et al., 1976; Chappert, 1979). In these cases, too, several of the Mössbauer lines were found to be broadened if compared to crystalline materials of about the same composition. Results for Dy–Fe alloys are reproduced in fig. 87. Arrese-Boggiano et al. first derived the distribution in magnetic hyperfine fields from the widths of those lines that are not affected by the quadrupole interaction (see fig. 85). The results were used subsequently in the determination of the distribution of the quadrupole interaction from the width of the remaining lines. The magnetic structures proposed by these authors correspond to Dy moments essentially distributed over all directions within a hemisphere (see also section 6.2.1).

The ^{151}Eu, ^{155}Gd and ^{197}Au Mössbauer effect was used by Friedt et al. (1982) to study the magnetic properties of amorphous alloys of Au with Eu and Gd. For the analysis of the ^{151}Eu hyperfine field distribution in amorphous $Eu_{0.80}Au_{0.20}$ the authors decomposed the total hyperfine field according to eq. (84) where

$$H_{hf} = H_c + H_s + H_N.$$

The term H_s, which arises from the polarization of the atoms' own valence electrons, was taken by Friedt et al. to have a constant modulus. The authors argue that this is
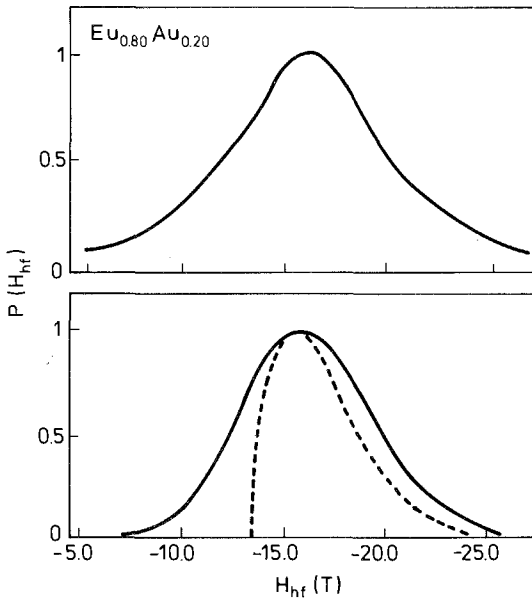
Fig. 88. Distribution of the [151]Eu hyperfine field in amorphous $Eu_{0.80}Au_{0.20}$ at 4.2 K (top part) and distribution of [151]Eu hyperfine field calculated under the assumptions of non-collinear H_s and H_N (broken curve) and of convoluted Gaussian distributions ($\Delta H = 2$ T) on H_N and H_s (full curve). The curves were constructed from the data published by Friedt et al. (1982).

a consequence of the intimate relation between H_s and the isomer shift IS. The constant modulus for H_s then follows from the unique value (i.e. the narrow distribution) found by the authors for IS. Indications that the distribution of the transferred hyperfine fields (H_N) is also a very narrow one were obtained from the observation that there is virtually no distribution of the transferred fields at the Au site (as measured by means of [197]Au Mössbauer spectroscopy). The distribution of H_{hf} actually observed is rather broad. It was explained by Friedt et al. as originating from a distribution in the angle (α) between the direction of H_N on the one hand and $H_c + H_s$ on the other hand. A good fit with the experimental data was obtained by using a Gaussian distribution $P(\alpha)$ having a standard width equal to 25°. The modulus of H_N was estimated from dilution experiments to be equal to $+6.0$ T; for H_c the authors took the usual value of -34.0 T while for H_s they used $+13.0$ T. In addition it proved necessary to include a narrow Gaussian distribution ($\Delta H = 2$ T) for H_s and H_N. Results of the calculated distribution, which is in keeping with experiment, are shown in fig. 88.

Apart from the narrow distribution in IS of [151]Eu in amorphous $Eu_{0.80}Au_{0.20}$ Friedt et al. report on a narrow distribution in the efg as well, as estimated from the quadrupolar splitting. Similar results were also found for [155]Gd and [157]Au, although the quadrupolar splitting in these cases is less sensitive for probing the local efg. From the fact that the isomer shift as well as the quadrupole interaction parameters show such narrow distributions Friedt et al. conclude that the atomic scale structure of amorphous $Eu_{0.80}Au_{0.20}$ must involve strict compositional and structural short-range order associated with both components. These results refute the applicability of random-packing models (DRPHS) to the structure of this amorphous alloy. As discussed in section 5.4, alloys such as $Eu_{0.80}Au_{0.20}$ having a relatively strong heat of

alloying are likely to give rise to a high degree of CSRO. Similar results were also obtained on amorphous alloys of Eu and Mg, Zn and Cd (Maurer et al., 1983).

The ^{57}Fe Mössbauer effect in amorphous $Y_{1-x}Fe_x$ alloys has been studied by quite a number of different authors. Pala et al. (1976) made a detailed study of the magnetic ordering in amorphous $Y_{0.33}Fe_{0.67}$. They suggest that their experimental data can be explained on the basis of a cluster-type model (Rhyne et al., 1972, 1974). Decreasing temperature leads to an increase in the size of the magnetic clusters, as derived from the quadrupolar splitting. Their mean lifetime becomes longer until near $T_c = 55$ K the intra-cluster order becomes static, the magnetic energy becoming competitive to the thermal energy. This results in a hyperfine splitting observable in the transition region. Pala et al. also note that their value of $H_{eff}(T = 0)$ does not follow the general trend of $H_{eff}(T = 0)$ decreasing with rare earth moment in amorphous $R_{0.33}Fe_{0.67}$ alloys. The existence of such a trend was proposed earlier by Heiman et al. (1975). The observed insensitivity of $H_{eff}(T = 0)$ with regard to the R moment was found later on by Heiman and Kazama (1979) too, and was corroborated by the results of a ^{57}Fe Mössbauer effect study on various R-rich amorphous iron alloys made by Buschow and Van der Kraan (1981).

Heiman and Kazama furthermore showed that a correlation exists between H_{eff} and the metallic radii of the rare earth component with which Fe is combined. Buschow and Van der Kraan argued that such a relation is rather unlikely and proposed that the correlation observed by Heiman and Kazama is in fact a correlation between the size of the Fe moment ($\mu_{Fe} \propto H_{eff}$) and the corresponding heat of alloying ΔH. The heat of alloying is a measure of the degree of CSRO. This latter quantity is known to strongly affect the size of the Fe moments. This point has already been discussed in more detail in section 6. Additional evidence of a correlation between H_{eff} and ΔH comes from a study of several other alloy systems. Results were shown in fig. 46.

By using similar arguments it is also possible to explain the difference in H_{eff} between crystalline and amorphous alloys as being due to environmental effects (see also section 6.3). In crystalline compounds there is a tendency for the Fe atoms to have as many dissimilar (Y) neighbours as possible. This is reflected by the fact that in intermetallic compounds the nearest neighbours are always of the dissimilar atom type. The situation is different in amorphous alloys, where the atomic arrangement is more or less statistical, the degree of CSRO being a measure of the deviations from the statistical arrangement. For these reasons one may expect the average number of dissimilar neighbours in amorphous alloys to be lower and the average number of similar neighbours to be higher. As a result, the mean Fe moments in amorphous Fe alloys are expected to be higher for a given nominal concentration. The same holds for $H_{eff}(T = 0)$ and led Arrese-Boggiano et al. (1976) to propose environmental effects as one of the possible reasons for their measured H_{eff} values being lower in amorphous alloys than in their crystalline counterparts. Nishihara et al. (1982a) also observed an H_{eff} value in amorphous $Y_{0.33}Fe_{0.67}$ which was 2.0–2.6 T larger than in crystalline YFe_2. Rather than environmental effects the authors propose a difference in s, p and d electron localization between the amorphous and crystalline state to be responsible for observed difference in H_{eff}.

An environmental model was also used by Chappert et al. (1978, 1981) to explain the concentration dependence of the Fe moments and hyperfine fields in amorphous $Y_{1-x}Fe_x$ alloys. In the alloy of lowest Fe concentrations considered by these authors ($x = 0.32$) the Fe atoms were reported to possess basically zero moment. In the absence of external fields magnetism appears at a concentration of about $x = 0.4$, the fraction of non-magnetic iron atoms corresponding to Fe atoms of seven or more Y neighbour atoms. Magnetism on the Fe atoms appears when the number of Fe neighbours is six or more. The Fe moment is relatively small (a few tenths of a Bohr magneton) for Fe atoms having six Fe neighbours. It increases when the Fe coordination becomes higher and is equal to $2\mu_B$ for Fe atoms having ten or more Fe neighbours. Mössbauer spectra for various Fe concentrations and the corresponding distribution of hyperfine fields can be compared in fig. 89.

In order to explain the temperature dependence of the hyperfine field Chappert et al. (1981) propose a new type of magnetic excitation occurring in amorphous alloys not too far from the condition for the appearance of magnetism. This type of excitation entails thermal single-ion excitations of Fe atoms in environments where they have small moments into a state of slightly higher energy in environments where they are non-magnetic. The Mössbauer spectra measured in an applied field of 5 T were interpreted by Chappert et al. in terms of asperomagnetic model structures, examples of which are shown for various Fe concentrations in fig. 90. Although a complete parallel moment alignment is present in crystalline Fe metal
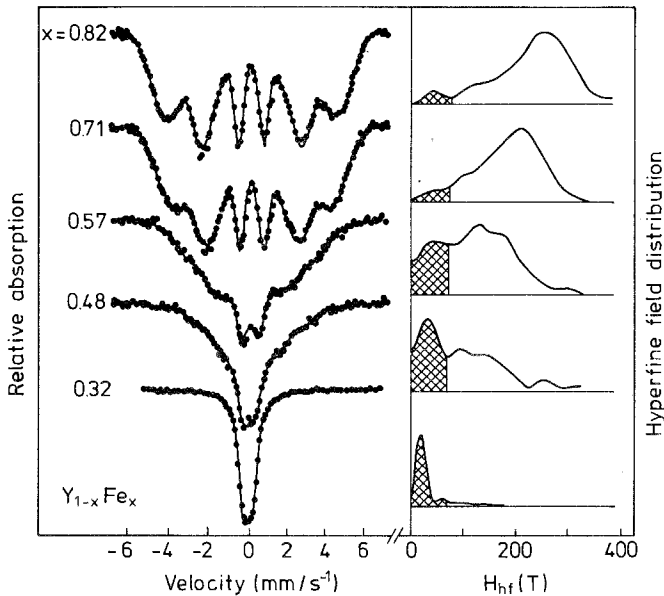
Fig. 89. ^{57}Fe Mössbauer spectra of amorphous $Y_{1-x}Fe_x$ alloys at 1.6 K for various Fe concentrations. The full curves through the data are the fits with the hyperfine field distributions shown on the right. The shaded portions of these distributions correspond to non-magnetic iron atoms (after Chappert et al., 1978).
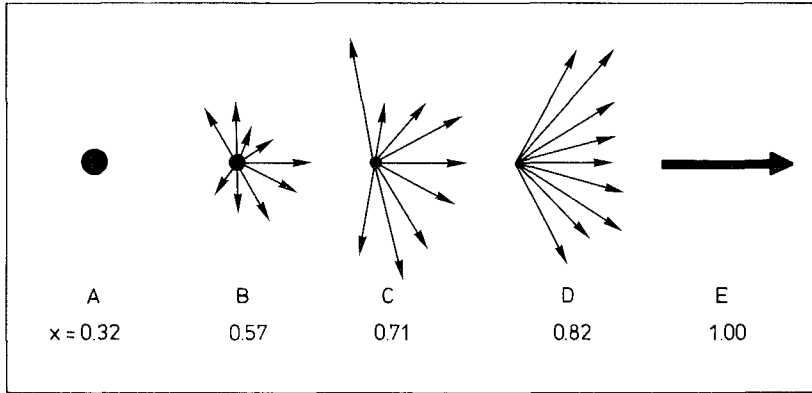
Fig. 90. Schematic representation of magnetic structures of amorphous $Y_{1-x}Fe_x$ alloys (a–d) with $x = 0.32, 0.57, 0.71, 0.82$ and (e) crystalline iron (after Chappert et al., 1981).

(fig. 90e) the authors note that extrapolation of their data on amorphous $Y_{1-x}Fe_x$ to $x = 1$ suggests that pure amorphous iron might not be a collinear ferromagnet.

Tenhover (1981·,a,b) used the ^{57}Fe Mössbauer effect in amorphous $Y_{0.66}(Fe_x(M_{1-x})_{0.34}$ and $Y_{1-x}Fe_x$ alloys to study the concentration dependence of the isomer shift (IS) and quadrupole splitting (QS). Results for $Y_{1-x}Fe_x$ are reproduced in fig. 91. A step-like change in IS and QS can be recognized near
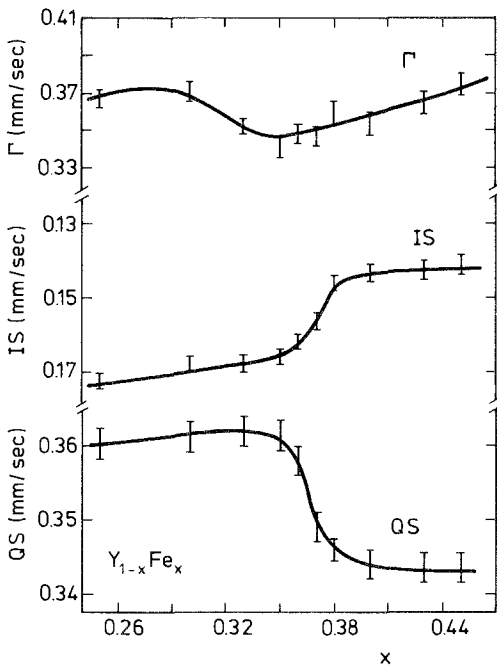
Fig. 91. Concentration dependence of linewidth (Γ), Isomer Shift (IS) and Quadrupole Splitting (QS) for $Y_{1-x}Fe_x$ metallic glasses. The smooth lines have been added to guide the eyes (after Tenhover, 1981b).

$x = 0.36$. This was explained by Tenhover as being the result of an enhancement in CSRO at concentrations where the metallic glass adopts a more or less ideal amorphous structure owing to the tendency to form as many dissimilar neighbour pairs as possible ($\Delta H < 0$).

As an alternative explanation for the step-like change in IS and QS Tenhover discusses the possibility of an intrinsic inhomogeneity of some of the alloys. The amorphous state may comprise two single-phase regions corresponding to a lower and higher Fe content, each of these being characterized by specific IS and QS values. The sudden change observed in these two quantities (fig. 91) might then indicate the presence of a two-phase region, i.e. phase separation occurs at this particular concentration. Tenhover (1981a) also used Mössbauer spectroscopy in conjunction with X-ray diffraction, DSC and resistivity measurements to study the crystallization process in $Y_{0.66}Fe_{0.34}$, which was found to occur in two distinct steps and to involve the formation of hcp Y and the C15 phase YFe_2. Structural relaxation phenomena observed in $Y_{0.33}Fe_{0.67}$ by means of [57]Fe Mössbauer spectroscopy were reported by Nishihara et al. (1982b, c).

Van der Kraan and Buschow (1982, 1983) studied the [57]Fe IS in various amorphous alloys in which Fe was combined with Nb, Zr, Hf, Ti, Y, Th, Mg, Sn, Sb, Ge or B. They analysed the IS data in terms of the model of Miedema and van der Woude (1980), where the strain-free dilute limit $\delta(IS)_{max}$ of the isomer shift is given by the expression

$$\delta(IS)_{max} = P'(\phi_A^* - \phi_{Fe}^*) + Q'(n_{ws}^A - n_{ws}^{Fe})/n_{ws}^{Fe}. \tag{85}$$

For a given class of materials and for the same Mössbauer isotope, the quantities P' and Q' can be regarded as constants. The first term on the right-hand side of eq. (85) implies the existence of a linear relationship between the change in the number of electrons (s and d together) per iron atom and the increase in the s electron density at the Fe nucleus. The extent of the charge transfer relative to pure iron, for a given Fe atom completely surrounded by dissimilar neighbours, is proportional to the difference in electronegativity $\phi_A^* - \phi_{Fe}^*$ between Fe and the A component.

The second term represents the analog of the repulsive term in the heat of formation in Miedema's model (Miedema et al., 1980). The sign of the coefficient Q' follows from the contention that the mismatch in electron density at the Wigner–Seitz atomic cell boundaries (n_{ws}) in transition metal alloys can be removed by means of s–d intra-atomic electron conversion. The s electrons reside predominantly in the outside regions of the atomic cell. Conversion of s-type electrons into d-type electrons will therefore result in a decrease of n_{ws}. It follows then that P' and Q' are of opposite sign.

Results of the analysis made by Van der Kraan and Buschow are shown in fig. 92, where the experimental results are seen to behave as expected on the basis of eq. (85). The values of P' and Q' derived from this plot are equal to -0.75 and $+1.65$, respectively. This means that for a variety of different amorphous alloys one can describe the isomer shift satisfactorily in terms of two contributions $-0.75|\Delta\phi^*| + 1.65|\Delta n_{ws}/n_{ws}^{Fe}|$, associated with charge transfer and intra-atomic s $\leftrightarrow$ d electron conversion, respectively. According to the analysis, in the metal–metal alloys the
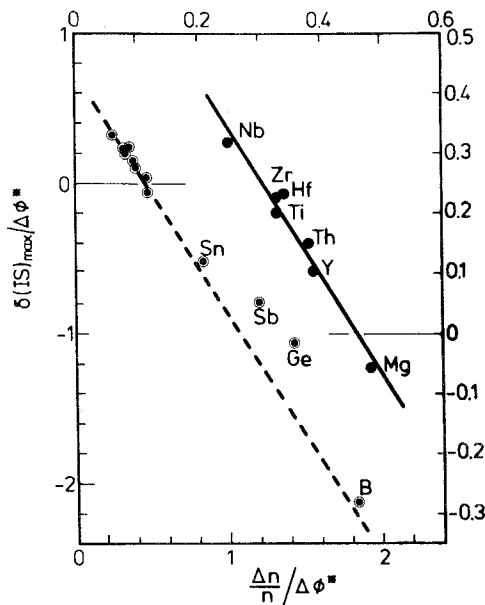
Fig. 92. A plot of $\delta(\mathrm{IS})^{\mathrm{exp}}_{\mathrm{max}}/\Delta\phi^*$ versus $\Delta n_{\mathrm{ws}}/n_{\mathrm{w}}^{\mathrm{Fe}}\Delta\phi^*$. The top and right-hand scales refer to $A_{1-x}\mathrm{Fe}_x$ alloys, where A is a transition metal. The bottom and left-hand scales refer to the lower line, where alloys with A being a metalloid are also included (after Van der Kraan and Buschow, 1983).

charge transfer contribution is dominant, whereas in the metal–metalloid alloys the s–d conversion contribution dominates. This leads to a different sign of the isomer shift in both groups of alloys.

It was mentioned in section 6.3 that one of the explanations of the difference in magnetic behaviour between amorphous and crystalline materials is based on the assumption of a difference in charge transfer between the 3d element and its partner element. For instance, in crystalline $R_{1-x}T_x$ materials charge transfer from the R element to the transition metal is taken to be responsible for the 3d moment reduction owing to band filling. In amorphous alloys this charge transfer effect is assumed to be reduced compared to that in their crystalline counterparts. As a consequence, the 3d moment reduction is also less strong than in crystalline materials. Since the Mössbauer isomer shift is a direct measure of the charge density at a given site, one may test this model by comparing the isomer shift obtained in both classes of materials.

Results are available of Mössbauer spectroscopy pertaining to rare earth nuclei (Gubbens et al., 1981; Chappert et al., 1982; Friedt et al., 1982) as well as to 3d metal nuclei (Buschow et al., 1978; Buschow and van der Kraan, 1979; Chappert et al., 1981; Tenhover, 1981a). Representative results are given in fig. 93. Here the isomer shift is plotted versus the fractional effective area of contact of the Möss-bauer isotope metal atom with atoms of the second component. In the (amorphous) alloys this fractional effective contact area is obtained by weighting the actual concentration x with the atomic cross sections (see eq. 17). In the crystalline materials the fractional areas of contact of a Dy atom with Co neighbours ($f_{\mathrm{Co}}^{\mathrm{Dy}}$) or of an Fe atom with Th neighbours ($f_{\mathrm{Th}}^{\mathrm{Fe}}$) are more difficult to estimate. Here one has to take into account a preference for dissimilar atoms as nearest neighbours.
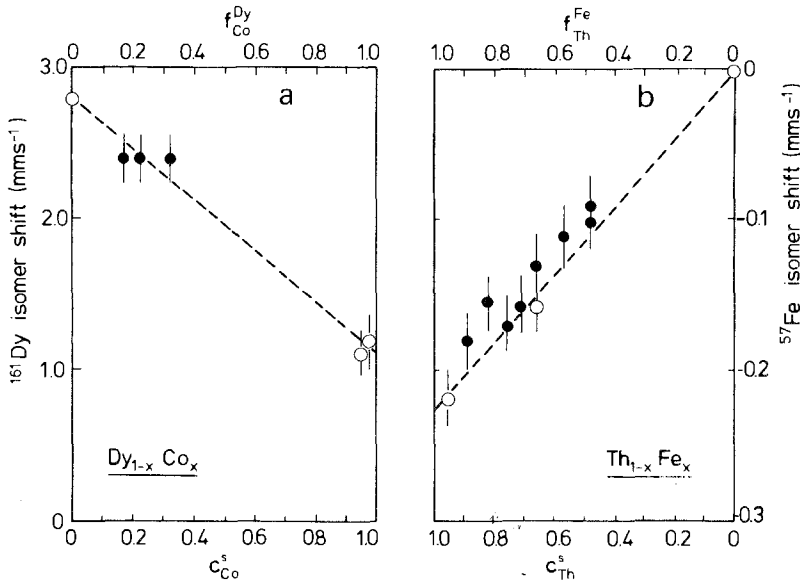
Fig. 93. (a) [161]Dy isomer shift in amorphous and crystalline $Dy_{1-x}Co_x$ vs. the fractional area of contact of Dy atomic cells with Co atomic cells (open circles, top scale: crystalline materials; full circles, bottom scale: melt-spun materials). (b) [57]Fe isomer shift in amorphous and crystalline $Th_{1-x}Fe_x$ vs. the fractional area of contact of Fe atomic cells with Th atomic cells (open circles, top scale: crystalline materials; full circles, bottom scale: melt-spun materials).

In fig. 93a the two open circles close to $f_{Co}^{Dy} = 0.95$ refer to data obtained on the compounds $DyCo_5$ and Dy_2Co_{17} (Gubbens et al., 1981), in which each Dy atom can be regarded as having almost exclusively Co atoms as nearest neighbours. The open circle at $f_{Dy}^{Co} = 0$ represents the isomer shift value in Dy metal (no Co neighbours). By fixing the IS value for the dilute and undilute limit in this way, the broken line in the figure may serve to represent the concentration dependence expected with an increasing number of Co neighbours. It may be seen that the three amorphous alloys investigated do not deviate from the behaviour expected.

A similar behaviour is found for the isomer shift at a 3d atom site (fig. 93b). The broken line connects the IS values in Fe metal with those in Th_7Fe_3 (Viccaro et al., 1979). In these cases, too, the IS values in the amorphous alloys (full circles) do not behave extraordinarily. It seems therefore that in order to understand the differences in magnetic properties between amorphous and crystalline materials, one has to look for a mechanism other than that of a reduced charge transfer. Further experimental evidence refuting charge transfer effects as the main origin for the moment reduction upon alloying will be discussed in the next section, dealing with photoemission experiments.

A more general treatment of Mössbauer effect spectroscopy in amorphous solids is presented in the reviews by Coey (1974) and Litterst and Kalvius (1975). Details regarding the electric field gradient in amorphous solids are treated in the papers by Lines (1982) for [57]Fe and for [155]Gd in the paper by Czjzek et al. (1981).

9.5. Photoemission spectroscopy

The photoemission studies so far reported in the literature comprise crystalline and amorphous alloys of early (T_E) and late (T_L) transition metals with either Zr (Amamou, 1980; Oelhafen et al., 1979, 1980) or Gd (Güntherodt and Shevchik, 1975; Shen et al., 1981). These studies have contributed significantly to the understanding of the electronic structure of amorphous as well as crystalline alloys, especially now that the results of band structure calculations have become available for most of the materials investigated (Kübler et al., 1981; Oelhafen et al. (1982), Moruzzi et al., 1983).

Magnetism of 3d alloys and intermetallics was believed in the past to be mainly governed by charge transfer effects. Even today, vestiges of this belief still surface occasionally in the literature. This charge transfer model involves electron transfer from the less electropositive component to the 3d component. The 3d band becomes less depleted, which causes a reduction in 3d moment. In its most primitive form (tight binding approximation) the d valence electrons of the low-electronegativity component share a common band with the 3d electrons responsible for the magnetic moment. The valence band spectra of several Zr-base alloys obtained by Oelhafen et al. (1979) and band structure calculations made by Kübler et al. (1981) refute this idea since they show quite convincingly that the d bands of the two components do not coalesce into a common d band. The spectra show two well-separated peaks related to the d bands of the two components. Results obtained for amorphous $Gd_{1-x}Fe_x$ alloys by Güntherodt and Shevchik (1975) are reproduced in fig. 94. They
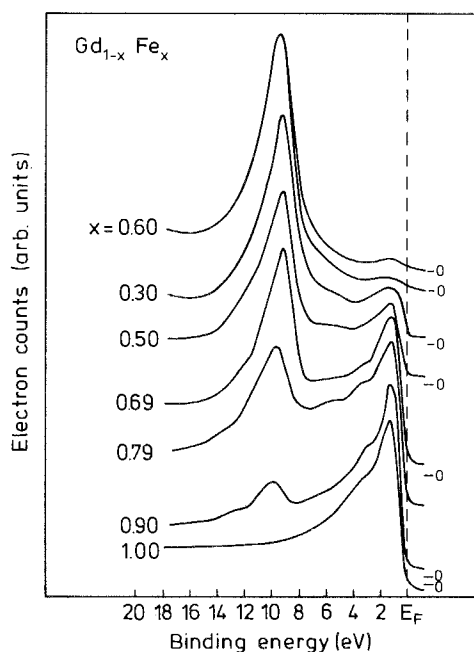
Fig. 94. XPS spectra of amorphous $Gd_{1-x}Fe_x$ alloys (after Güntherodt and Shevchik, 1975).
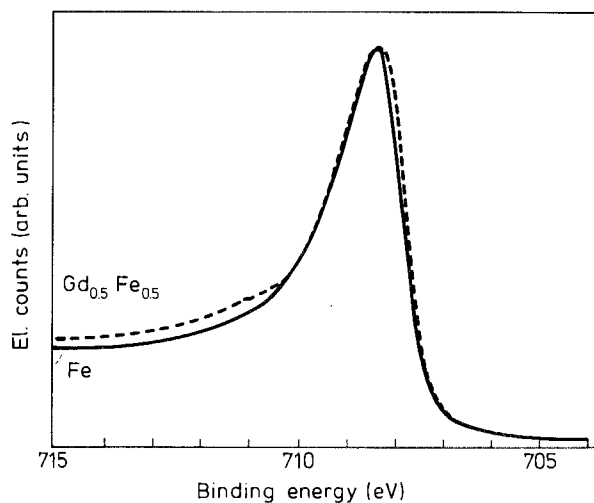
Fig. 95. Photoemission spectrum of amorphous $Gd_{0.5}Fe_{0.5}$ and crystalline Fe showing the position of the iron $2p_{3/2}$ core level (after Güntherodt and Shevchik, 1975).

show that the XPS spectra of these alloys, too, may be described by means of a linear superposition of the pure crystalline metals. Valuable information on the bonding can also be obtained from the core level shifts. In the $Zr_{1-x}T_x$ alloys as well as in the $Gd_{1-x}T_x$ alloys these are relatively small. Results for amorphous $Gd_{0.5}Fe_{0.5}$ are shown in fig. 95. The core level shifts arise from intra-atomic s → d conversion and interatomic charge transfer. The smallness of the core level shifts indicates that charge transfer is indeed relatively small. Similar conclusions were reached by Terzieff and Lee (1979).

Kübler et al. (1981) have estimated that the Fe d electron count in Zr_3Fe is larger by about 0.5 electron than in pure Fe metal, while the total Zr valence electron count has decreased by 0.3 electron. This is less than 10% of the total number of valence electrons. Güntherodt and Shevchik note that the asymmetry of the core level spectra can also be used to obtain information on the local density of states at the Fermi level. Since they did not observe any change in the Fe 2p core level asymmetry upon alloying Fe with Gd over the entire composition range, they conclude that the local Fe density of states at E_F is not significantly changed, i.e. that charge transfer effects are small.

The conclusions arrived at in the photoemission studies described above are in agreement with similar conclusions reached by Azoulay and Ley (1979) for crystalline Gd–Fe compounds. The photoemission results do not reveal major differences in electronic structure between crystalline and amorphous alloys of similar composition, but they make it clear that the reduction in 3d moment in both classes of materials is mainly due to a reduction in 3d band exchange splitting. In conclusion, charge transfer does occur upon alloying but it is too small to account for the changes in 3d moment observed.

XPS studies on amorphous Gd–Co and Gd–Fe films were also made by Shen et al. (1981). In their studies, however, the purpose was quite a different one from that described above, since they used XPS mainly to study the changes occurring in the

amorphous film after vapour deposition. It was discussed extensively in section 7 that the magnetic properties of thin amorphous R–3d films depend on the microstructure of these films. The uniaxial anisotropy, in particular, was found to depend on the presence of a columnar microstructure. Shen et al. deduced from the XPS depth profiles that Gd segregates to the surface of Gd–Co films. To be more specific, the Gd atoms diffuse to the columnar boundaries where they become oxidized. During annealing in vacuum this oxidation is accompanied by a reduction of the oxidized Co atoms. The increased concentration of Co at the columnar boundaries constitutes a high concentration of non-cancelled Co spins which may give rise to a relatively large number of Co pairs in the direction of the film normal and hence enhance the perpendicular anisotropy.

9.6. *Ultrasonic measurements*

It is well known that several rare earth–iron intermetallic compounds have a large magnetostriction (Clark, 1979). In amorphous rare-earth–iron the magnetostriction is lower but still appreciable. One may expect therefore that the relatively large magnetoelastic coupling which is responsible for this magnetostriction will also give rise to a large softening effect on the elastic constants. It is possible to observe these softening effects experimentally by standard ultrasonic measurements in a magnetic field.

Melamud et al. (1979) and Hathaway et al. (1979) performed ultrasonic studies on several amorphous alloys of the composition $R_{0.33}Fe_{0.67}$.

The objective of these authors was to obtain more detailed information on the spin arrangement in these alloys. A second objective was to study a possible correlation between the softening of the elastic constants mentioned above and the large reduction in the integrated Mössbauer intensity below T_c in amorphous $Dy_{0.33}Fe_{0.67}$ reported earlier by Forrester (1976). Hathaway et al. and Melamud et al. observed that in amorphous $Dy_{0.33}Fe_{0.67}$ and $Tb_{0.33}Fe_{0.67}$ the shear waves polarized parallel to the magnetic field propagate more slowly than the shear waves perpendicular to the field. This splitting of the velocities of the two shear waves is a measure of the coupling strength between the magnetic and elastic systems. It was found to increase with decreasing temperature below T_c.

Comparison was also made with model calculations which predict a maximum in the mode splitting for $Dy_{0.33}Fe_{0.67}$ near 135 K. This maximum was not observed experimentally, though, since the authors extended their ultrasonic measurements only down to about 170 K. The authors also note that in amorphous $Dy_{0.33}Fe_{0.67}$ and $Ho_{0.33}Fe_{0.67}$ the mode splitting is smaller than would be expected on the basis of the Stevens factor. With regard to the reduction in [57]Fe Mössbauer fraction observed by Forester, they report that they did not observe the sharp decrease in zero-field bulk modulus at the magnetic transition that would be required if elastic softening accounted for this reduction in Mössbauer fraction.

Quite a different application of ultrasonic measurements to amorphous alloys was made by Doussineau et al. (1978). These authors measured the temperature dependence of the ultrasonic attenuation and described their experimental results in terms of a resonant interaction with two-level systems such as were described in section 8.

9.7. *Hydrogen absorption and magneto-volume effects*

The phenomenon of hydrogen absorption in a large variety of different inter-metallic compounds has already been described extensively in Vol. 6 of this Handbook (Buschow, 1984). The absorption of hydrogen in amorphous alloys has been studied in only a few cases. Hirata and Takayama (1982) studied the changes of the thermal stability of amorphous Pd–Si alloys after hydrogen absorption. A detailed structural investigation pertaining to the location of hydrogen atoms in amorphous metal hydrides was made by Suzuki (1983). The mobility of hydrogen atoms in amorphous hydrides was compared with that in the corresponding crystal-line hydrides by Bowman et al. (1983). Spit et al. (1980) and Aoki et al. (1982) studied hydrogen absorption in amorphous $Zr_{0.36}Ni_{0.64}$. They found that the plateau in the pressure–composition isotherm observed in crystalline $ZrNi_2$ at low tempera-tures is absent in the amorphous alloy. Buschow et al. (1982) note that the observation made by Spit et al. on amorphous alloys of Zr and Ni, which absorb about the same quantity of hydrogen gas as their crystalline counterparts but do not give rise to a plateau pressure, may be quite generally valid. They argue that from the local environment picture one would not expect the occurrence of a plateau pressure since in amorphous materials all interstitial positions are different.

Model descriptions for hydrogen absorption in amorphous alloys have been given by Kirchheim et al. (1982), Kirchheim (1982) and Griessen (1983). Griessen notes that the absence of a plateau pressure in these materials may not always be primarily due to disorder. In his model he describes the hydrogen–hydrogen interaction by means of a mean field approximation and shows that the critical temperature (below which the pressure composition isotherms may exhibit a plateau) is positive if a Stoner-like criterion is satisfied:

$$[-a]n(E_0) \geqslant 1. \tag{86}$$

In this expression the hydrogen–hydrogen interaction strength a is composed of a positive electronic contribution and a negative elastic contribution, while $n(E)$ is the density of *sites* function for hydrogen accommodation. This quantity is taken to be symmetrical with respect to an energy E_0, corresponding to the chemical potential evaluated at the critical point.

Griessen showed that in amorphous Zr–Ni alloys the density of *states* $N(E_F)$ is relatively high so that one expects a relatively low positive electronic contribution to the a parameter in eq. (86). In these alloys the absence of a miscibility gap, i.e. the occurrence of phase separation and the occurrence of a plateau in the isotherms, is mainly due to disorder. In amorphous Pd–Si alloys, on the other hand, $N(E_F)$ is much smaller so that the positive contribution to the a parameter can prevail. In these cases relation (86) with $a > 0$ is not satisfied so that the absence of a plateau pressure may not be mainly due to disorder.

Robbins et al. (1982) investigated the effect of hydrogen absorption on the magnetic properties of amorphous alloys of the type $(R_{0.80}Ga_{0.20})_{1-x}T_x$. The quan-tity of hydrogen absorbed corresponds to hydrogen-to-metal ratios ranging from 0.2 in the alloy with R = Pr and T = Fe up to 1.7 in the alloy with R = Tb and T = Fe.
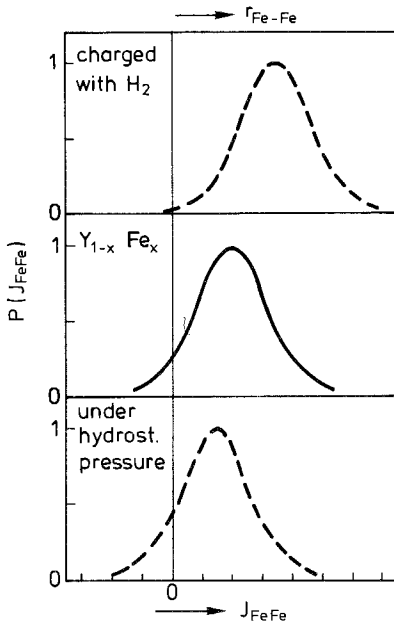
Fig. 96. Schematic representation of the distribution of magnetic Fe–Fe interactions (J_{FeFe}) in amorphous $Y_{1-x}Fe_x$ alloys before hydrogen absorption (full line, middle part) after hydrogen absorption (broken line, top part) and after applying external pressure (broken line, bottom part).

The changes in magnetic properties observed were thought to arise primarily from phase separation into H-rich and H-deficient regions.

Coey et al. (1982) studied the changes in magnetic properties of Fe-rich amorphous $Y_{1-x}Fe_x$ after charging them electrolytically with hydrogen. They report that the alloys lose their asperomagnetic nature after charging and become strong ferromagnets with Curie temperatures in excess of 400 K. These ordering temperatures compare favourably with the freezing temperatures near or below 100 K before charging. In addition to the increase in ordering temperature, a slight increase in saturation magnetization was also found.

Coey et al. explained the changes in ordering temperature in terms of a hydrogen-induced modification of the distribution of Fe–Fe exchange interactions. This may be illustrated by means of fig. 96. In the uncharged material the distribution of Fe–Fe interactions (J_{FeFe}) comprises a certain fraction of antiferromagnetic interactions, owing to the strong distance dependence of J_{FeFe} and the presence of rather small Fe–Fe distances in the amorphous alloy. This feature was discussed extensively in the papers by Coey et al. (1981) and Chappert et al. (1981). The presence of the antiferromagnetic coupling leads to asperomagnetic structures, examples of which were shown in fig. 90 (section 9.4). The introduction of hydrogen leads to an expansion of the lattice which then also results in a shift of the mean Fe–Fe separation. As seen in fig. 96, this may lead to a disappearance of that part of the distribution where J_{FeFe} is negative. The results of Coey et al. (1982) and also those of Fujimori et al. (1982) show that amorphous Fe alloys are similar to crystalline Fe-base materials, in that the main effect on the coupling originates from a modified Fe–Fe distance and not so much from a change in the electronic structure.

Many rare earth 3d intermetallics lose the sharp diffraction lines in their X-ray diffraction patterns after hydrogen absorption (see, for instance, Buschow, 1984). This suggests that these materials might become amorphous after charging, opening the possibility of preparing amorphous alloys in large quantities by a charging–decharging treatment. Buschow and Beekmans (1979d) showed, however, that the attainment of the amorphous state via the hydrogenated state is less likely. They based their arguments on the fact that the rate-controlling step in both the decomposition of a metastable hydride (which causes the disappearance of the X-ray diffraction peaks) and the crystallization of an amorphous alloy is the diffusion of metal atoms. If conditions are present that make diffusion of metal atoms possible, no reason exists why the metastable amorphous state, if formed, should be preserved. Buschow and Beekmans suggest that it is more likely that the disappearance of diffraction peaks stems from phase separation, in which the precipitating phases have not yet had the opportunity to grow to particles of a size sufficiently large to give rise to sharp X-ray reflections.

The pressure dependence of the magnetic ordering temperature and magnetization was studied in various amorphous R–3d alloys by Biesterbos et al. (1975). These authors found that the pressure effects in some of these amorphous alloys are quite pronounced and often surpass those measured in their crystalline counterparts. Some experimental results obtained by Biesterbos et al. are reproduced in fig. 97. The behaviour of the amorphous alloy $Y_{0.13}Fe_{0.87}$ in particular is worth noticing. As can be inferred from fig. 97, the decrease of T_c is more than 70% at 23 kbar (2.3 GPa), which is rather uncommon. Furthermore the reduction in magnetization may become quite considerable. In amorphous $Y_{0.16}Fe_{0.85}$ Biesterbos et al. found $(1/M)dM/dP = 4 \times 10^{-2}$ kbar^{-1}, while in crystalline Y_2Fe_{17} no moment change was detected within experimental error.
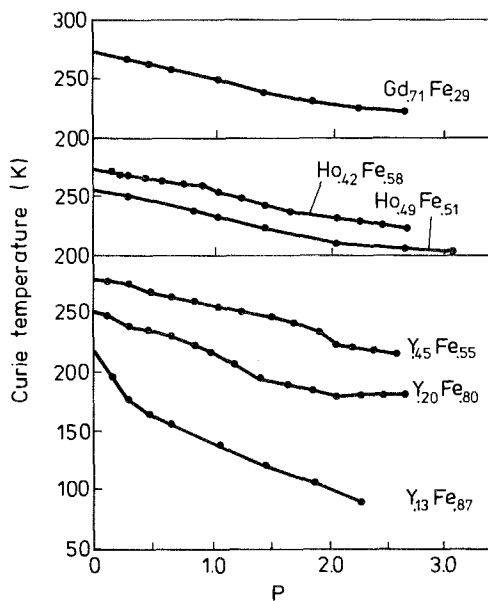
Fig. 97. Pressure dependence of the Curie temperature in several amorphous rare-earth–3d alloys (after Biesterbos et al., 1975).

It is interesting to view these data against the results described by Coey et al. (1982) when charging amorphous $Y_{1-x}Fe_x$ alloys with hydrogen. Increasing pressure means decreasing volume and hence leads to a reduction in the Fe–Fe distances. This is just the opposite of the effect obtained by charging with hydrogen, where the associated volume expansion brings about an increase in Fe–Fe separation. As a consequence one expects the distribution of moment couplings (see fig. 96) and the ordering temperatures to be affected in opposite ways when charging and when applying pressure, respectively. This is indeed observed experimentally. If one were to apply the same reasoning to the magnetic moment changes one would predict from the positive value of dM/dP that the moment would decrease after hydrogen absorption. Here one has to take into consideration, however, that changes in electronic properties due to the hydrogen absorption are also present and may have a considerable effect on the moment size, although their effect on the moment coupling is relatively unimportant.

The comparatively large pressure effects observed in amorphous Fe-rich alloys do not seem to be restricted to rare earth base alloys. The pressure dependence of the Curie temperature was studied by Kamråd et al. (1981) in several Fe-rich alloys where Fe was combined with Zr, B, P and Ge. In amorphous $Zr_{0.1}Fe_{0.9}$ the relative reduction in T_c per unit of pressure applied, reached virtually the same value as in amorphous $Y_{0.13}Fe_{0.87}$ mentioned above. One is tempted therefore to explain the large pressure effect in the amorphous Fe alloys mainly in the spirit of fig. 96 rather than on the basis of the Wohlfarth relation:

$$\frac{dT_c}{dP} = \tfrac{5}{3}\kappa T_c - \tfrac{5}{6}\kappa B T_c^{-1} \approx -\alpha T_c^{-1}, \tag{87}$$

(κ = compressibility, B = constant depending on the band structure) used currently to describe pressure effects (Biesterbos et al., 1975; Kaneko et al., 1981; Shirakawa et al., 1981a; Kamråd et al., 1981). Experimental evidence of the fact that amorphous Zr–Fe alloys, like amorphous Y–Fe alloys, are not true ferromagnets but must rather be classified as asperomagnets, has been amply provided by the experimental results of Hiroyoshi and Fukamichi (1981). In this connection it is interesting to note that amorphous Fe-rich boron alloys, which are considered to have only a slight asperomagnetic character compared to the Y- and Zr-base alloys, do not give rise to such extraordinarily large dT_c/dP values (Kamråd et al., 1980). There are also various Co-base amorphous alloys, being true ferromagnets with a J_{dd} distribution situated entirely in the positive regime, that show normal values of dT_c/dP (Biesterbos et al., 1975; Shirakawa et al., 1981b).

The Fe-rich portions of several amorphous alloy systems form part of the rather seldom encountered family of materials where the concentration dependence of the magnetic moment (μ) increases while the concentration dependence of the magnetic ordering temperature (T_c) decreases. Systems showing such opposite tendencies of μ and T_c often have a further peculiar feature associated with them, namely an anomalous thermal expansion also known as invar anomaly (Masumoto, 1931, 1934). In amorphous $B_{1-x}Fe_x$ alloys such invar-type anomalies were observed by Fukamichi et al. (1977). Similar results were obtained in amorphous $Z_{1-x}Fe_x$ alloys
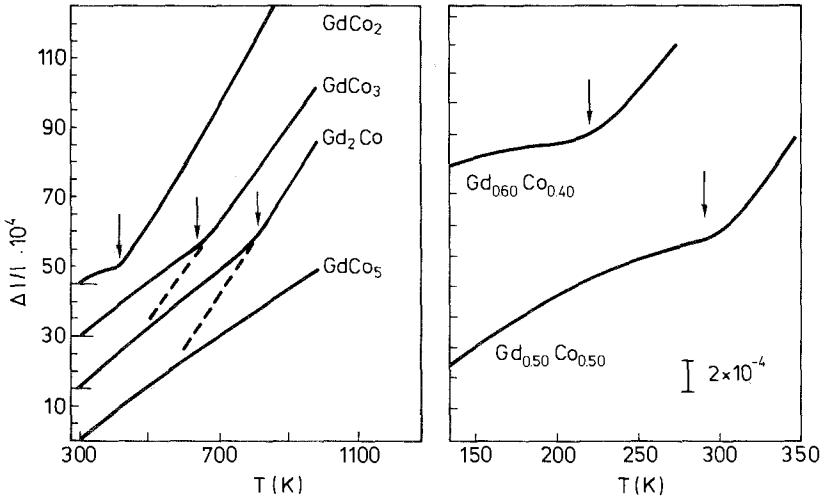
Fig. 98. Comparison of invar type anomalies in the thermal expansion ($\Delta l/l$) of crystalline Gd–Co materials (left-hand part) and amorphous $Gd_{1-x}Co_x$ alloys (right-hand part). The data of the amorphous alloys were obtained by Fukamichi et al. (1979).

and related ternary alloys by Shirakawa et al. (1980).

The occurrence of invar-type anomalies does not appear, however, to be exclusively tied to systems showing the feature of decreasing T_c with increasing μ. Such anomalies were also observed in crystalline (Buschow et al., 1974) and amorphous (Fukamichi et al., 1979a) Co alloys where T_c as well as μ_{Co} increase with Co content. Results for these materials are compared in fig. 98, where the Curie temperatures have been indicated by arrows. Arguments were presented (Brouha et al., 1974) that the observation of invar anomalies is intimately connected with the observation of negative values of the corresponding pressure derivative dT_c/dP. This correlation can be verified to hold for the amorphous alloys based on Fe mentioned above ($Y_{1-x}Fe_x$, $Zr_{1-x}Fe_x$, $B_{1-x}Fe_x$) as well as for the amorphous and crystalline $Gd_{1-x}Co_x$ alloys shown in fig. 98.

10. Technological applications

The main technological applications of amorphous alloys comprise thin films for magneto-optical recording, transformer materials, recording heads, corrosion-resistant coatings and flashbulb materials. Before discussing the various applications in more detail, it seems desirable to give a brief survey of several properties of amorphous alloys that make them preferable in these applications to standard crystalline materials. The advantages of amorphous alloys are the following:

(i) A much wider choice of alloy composition. Here one has to consider that in most applications a single-phase material is desired. A restricted compositional freedom in this respect is present only in those binary systems where the parent

metals give rise to regions of solid solubility. In binary systems where none of the two parent metals is soluble in the partner element one is restricted to the few compositions corresponding to intermetallic compounds, if they exist. A wide choice of alloy compositions is very often required in order to be able to achieve a reasonable tailoring of various properties associated with a given application. As will be shown below, this compositional freedom is essential for the success of magneto-optical applications of several amorphous rare-earth–3d-transition-metal alloys.

(ii) Absence of grain boundaries. In some applications the degree of homogeneity required is so high that even the presence of grain boundaries can give rise to difficulties. The possibility of being able to prepare metal systems in which such grain boundaries are absent is therefore highly welcome. Furthermore the presence of lattice imperfections associated with grain boundaries is frequently considered as the origin of severe corrosion and wear. The absence of grain boundaries therefore implies that amorphous alloys generally show a relatively large corrosion resistance and wear resistance. The absence of grain boundaries is furthermore of influence in regard to the mechanical properties of amorphous alloys. In so far as the grain boundaries can be considered as providing pinning sites for Bloch walls in ferromagnetic materials, the absence of grain boundaries leads to materials with low coercive forces, i.e. low magnetic losses.

(iii) A high atomic disorder. It was outlined already in section 8 of this chapter that the high atomic disorder in amorphous alloys gives rise to a large electrical resistivity and associated with it is a low thermal conductivity. It will be shown below that the low thermal conductivity is useful, in particular for magneto-optical applications where a high bit density is required.

10.1. *Magneto-optical applications of thin amorphous films*

With regard to high density storage, erasable magnetic discs, on which writing and reading can be done by means of laser beams, are in many ways superior to systems based on purely magnetic or on purely optical techniques. For the magneto-optically active component of such discs amorphous alloys of 3d metals and rare earth metals have proved to be most suitable. The application of thin amorphous Gd–Co films for this purpose was initially developed by IBM researchers. Later on
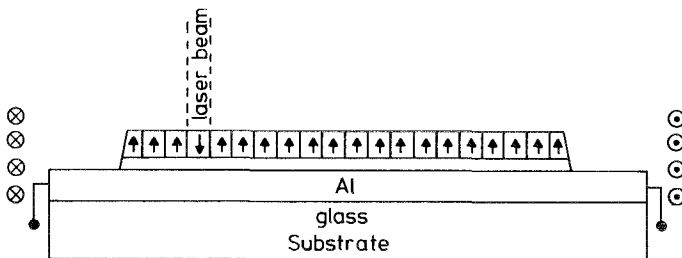
Fig. 99. Schematic representation of a disc suitable for magneto-optical recording, where the magneto-optically active constituent on top of the disc consists of amorphous R–3d alloys.

it received somewhat less attention since small written bits were found to possess insufficient stability. This difficulty has now been solved by employing either Gd–Fe alloys (Hartmann, 1982; Heitmann et al., 1980) or multilayer Gd–Co films (Togami, 1981).

The writing procedure is illustrated schematically in fig. 99. The thin Al film on top of the glass substrate is needed only when the amorphous thin film consists of Gd–Co prepared by means of sputtering. In that case a suitable microstructure with a sufficiently high uniaxial anisotropy can, in general, only be obtained by applying a negative bias voltage to the substrate (see section 7.1). This is done through the thin Al layer. Other metals instead of Al can also be used, particularly where the metal film has a different function, namely to act as a reflector (Connell and Allen, 1982; Mansuripur et al., 1982; Tanaka and Imamura, 1983) to improve the reading characteristics.

A further improvement is a quarter-wave intermediate layer of a dielectric material on top of the reflector, which may also act as a thermal buffer layer. The top layer in fig. 99 consists of the magneto-optical active amorphous alloy. Owing to its uniaxial anisotropy the magnetization direction is perpendicular to the film plane everywhere and can be represented by means of the array of arrows shown. For an external field of a strength H_e lower than the coercive field at room temperature $H_c(T = 298$ K) no magnetization reversal will take place. Local heating to a temperature T_w (writing temperature) can be achieved by means of a laser beam. Owing to the decreasing coercive field with increasing temperature one then can bring about the situation where $H_e > H_c(T = T_w)$ so that magnetization reversal within the irradiated spot can take place. After removal of the laser beam the coercive force adopts again the higher room temperature value so that the reversed domain magnetization persists even in the presence of the external field H_c. When viewed under a Kerr microscope the reversed domain looks like a black spot in a white matrix. Digital information can be stored in this way by using a pulsed laser beam. A typical digital information pattern written in this way is shown in fig. 100. A typical experimental set-up for reading the stored information is shown in fig. 101.

The physics of the reading and writing process will be discussed in the light of the magnetic properties of the amorphous Gd–3d alloys as outlined in section 6. For convenience the temperature dependence of the magnetization in amorphous Gd–Fe alloys is again shown schematically in fig. 102. Also included is the temperature dependence of the coercive force. The requirements which the properties of the material have to meet for magneto-optical thin-film application will be discussed by using Gd–Fe base alloys as an example. For Gd–Co base alloys (and other R–3d alloys) the situation is not much different. The various requirements regarding the material properties are summarized on the left of table 7. The magneto-optical and related quantities affected by these properties are summarized on the right of the table.

One of the basic requirements for high-density magneto-optical recording is the presence of a uniaxial anisotropy sufficiently strong to be able to compete with the shape anisotropy of the thin film. This leads to the condition $K_u > 2\pi M^2$, which must be satisfied at temperatures near room temperature. This requirement is met
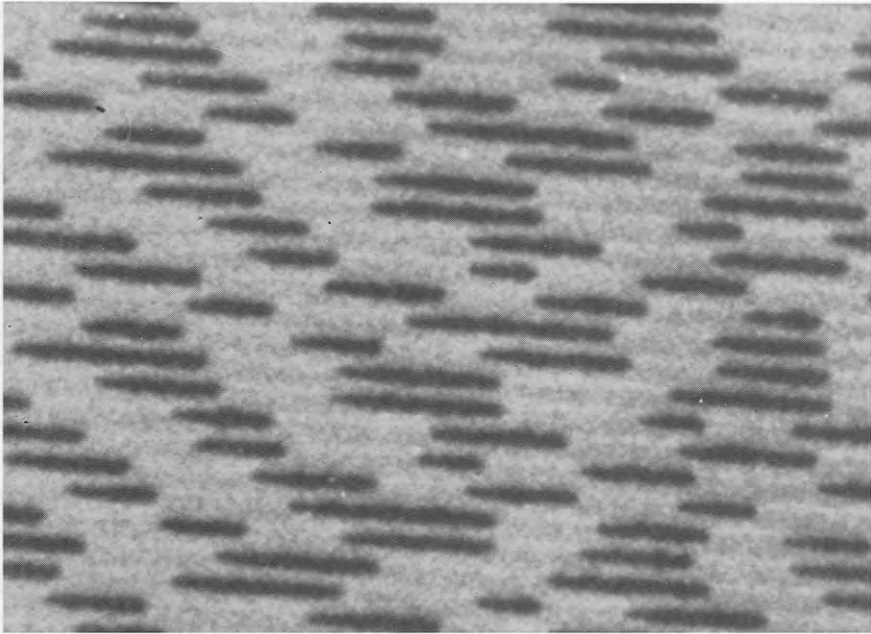
Fig. 100. Typical domain pattern (viewed by means of a Kerr microscope) of a Gd–Fe base magneto-optical disc in which digital information has been written by means of a laser beam (after Schouwhamer-Immink and Braat, 1983).

more easily the lower the value of the magnetization M near room temperature. As can be inferred from the schematic representation shown in fig. 102, one is therefore restricted to that concentration region in $Gd_{1-x}Fe_x$ where the compensation temperature T_{comp} is close to room temperature ($x \approx 0.75$, see fig. 60 in section 7.3).
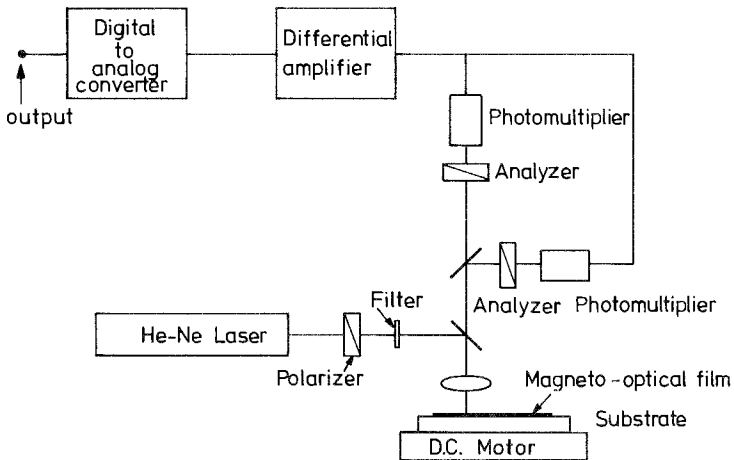
Fig. 101. Schematical representation of an experimental set-up for magneto-optical and thermomagnetic recording experiments (after Mimura et al., 1978b).
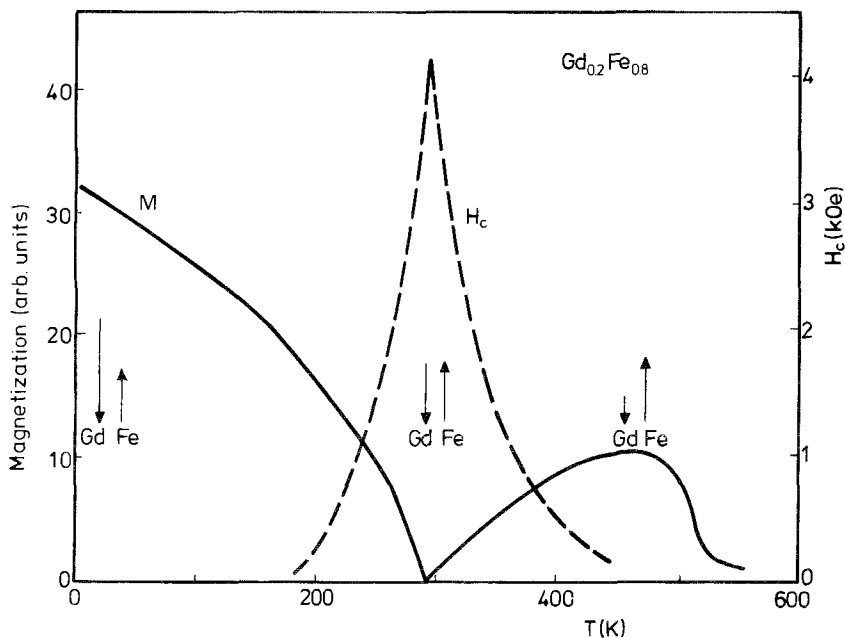
Fig. 102. Schematic representation of the temperature dependence of the magnetization (σ) and coercive force (H_c) in amorphous alloys of the approximate composition $Gd_{0.2}Fe_{0.8}$. The relative magnitude and orientation of the Gd- and Fe-sublattice magnetizations is indicated by arrows.

TABLE 7

Survey of the requirements regarding the physical properties of amorphous R–3d thin films used for magneto-optical and thermomagnetic recording. The requirements for the physical parameters are listed on the left of the table. The effect of these requirements is listed on the right. For a definition of the various symbols, see main text.

$K_u > 2\pi M_s^2$	$M_s \perp$ film plane
$T_{comp} \lesssim 293$ K	domain size small
($dH_c/dT < 0$ when $T > 293$ K)	bit density high
H_c large	stable written domains when $H_{ext} = 0$
high film homogeneity	sharp T_{comp} cusp-type $H_c(T)$
large φ_K large R	$S/N \propto R\varphi_K^2$
$T_{cr} \gg T_{wr}$	no crystallization during writing
high corrosion resistance	no deterioration
low σ_{th}	low laser power for writing high bit density

An even more restricted location of T_{comp} is required when considering the domain stability after writing. If the compensation temperature is above room temperature the reversed domain may collapse after writing and removal of the laser beam, since upon cooling down to room temperature it will encounter the situation where the magnetization increases while H_c decreases. Furthermore, as already explained in more detail in section 7.2, a high bit density requires small domains. For this reason it is favourable to have $H_c(T)$ increasing with decreasing temperature. All these requirements correspond to a situation where T_{comp} is lying close to, but below, room temperature. To find the concentration appropriate to such a situation one may use the results shown in fig. 36 of section 6.2.1.

A somewhat more gradual shift of T_{comp} into the desired direction can also be reached by alloying of a third component (Chaudhari et al., 1974; Urner-Wille et al., 1980, 1981) such as shown for Sn, Pb or Bi additives in fig. 103. This has the additional advantage that it increases the film homogeneity (Hartmann, 1982). The reason for the increased homogeneity is probably the relatively large fractional increase in the absolute value of the heat of alloying when adding Bi, Sn or Pb. Since the value of ΔH_m for $Gd_{1-x}Fe_x$ is negative but relatively low, a further decrease of ΔH_m to more negative values will enhance the tendency to anticlustering (see section 5.4). A similar reasoning was used by Hartmann (1982) to explain the changes in magnetic properties upon adding Bi, Sn or Pb. It will be clear that local deviations in composition associated with a less perfect homogeneity can lead to an increase of the error rate in writing. Furthermore the region where the magnetization becomes zero (T_{comp}) will become smeared out, and as a consequence the $H_c(T)$ curve would be less sharp and will lose its cusp-type shape.
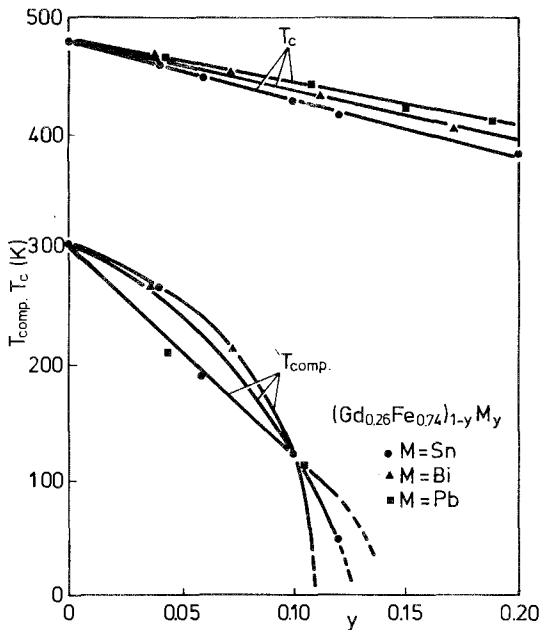
Fig. 103. Dependence of the Curie temperature (T_c) and compensation temperature (T_{comp}) on the amount of Sn, Bi or Pb added (after Hartmann, 1982).

It was mentioned earlier that magnetization reversal in a tiny region during heating by laser irradiation was achieved by means of a small external field (H_e). As can be inferred from the discussion in section 7.2, the application of such an external field has the disadvantage that the diameters of the written domain will remain relatively large, implying a lower bit density. Better results can be obtained without an external field. For an appropriate magnetization and demagnetizing field at the writing temperature T_w the magnetization reversal of the irradiated spot can proceed by means of this demagnetization field only. This effect has been illustrated by means of fig. 55 in section 7.2, where the smallest domain diameters are found in the region where the field is small or negative. In the cases that the writing is performed without external field it also proves advantageous to alloy with Bi, Pb or Sn to obtain a more optimal shape of the $H_c(T)$ curve in regard to the ultimate diameter of the stable bit at room temperature. Further benefits from the Bi, Sn or Pb additives are an increase in the Kerr rotation angle φ_K (see fig. 63 of section 7.3). This increase in φ_K is accompanied, however, by a decrease in the reflectivity. Nevertheless, since the signal-to-noise ratio varies as $S/N = R\varphi_K^2$ the overall effect is favourable. Here it is perhaps worth recalling that optimizing the magneto-optical properties by means of additives such as mentioned above would have been impossible in the case of crystalline materials, where the additives undoubtedly would have led to the occurrence of a multiphase microstructure.

A further materials requirement is that the crystallization temperature T_x be much higher than the writing temperature T_w. Repeated heating of the material to temperatures close to T_x may still not lead to crystallization but may entail changes in magnetic properties which eventually will impair the reading and writing characteristics. Additives such as Bi, Pb and Sn give rise to a lowering of the crystallization temperature. The T_x values of the three-component alloys remain, however, sufficiently high to satisfy the condition $T_w < T_x$. It is of some interest to note that the heating rates involved with the laser irradiation are considerably higher than those applied in most DSC experiments described in section 4.1. This, in fact, means that the effective T_x values to be considered here are substantially higher than those considered in section 4.

The discussion of the material properties of magneto-optically active amorphous thin films will be terminated by mentioning two more favourable features associated with the amorphous state which have been most helpful in leading to a successful application. The first of these is the absence of grain boundaries and the resulting corrosion resistance. Even without any further covering of the thin film with a protective layer, magnetic properties have been reported to remain preserved even after several years of exposure to normal atmospheric conditions (Togami, 1982). The high metallic luster of the thin film is also preserved, a fact which is not encountered with crystalline rare earth alloy buttons of similar composition. Finally the low thermal conductivity has as a consequence that the heat associated with the laser irradiation remains located in an area not differing much in cross section from the diameter of the laser beam. This implies that the written bits can be kept small, too.

A different application of thin amorphous R–3d films was proposed by Matsushita

et al. (1977). These authors showed that amorphous $Tb_{1-x}Fe_x$ thin films can be used for thermomagnetic contact printing. In this application information is transferred thermomagnetically to the Tb–Fe film by placing the latter on the magnetic medium (tape or disc) containing the information. The Tb–Fe film is then heated up ($T > T_c$) through the glass substrate by an electronic flash (heat pulse width 1 ms). During cooling down from a temperature above T_c the magnetization of the Tb–Fe films is reoriented by the normal components of the stray field of the magnetic medium. The transferred information can be observed via the Kerr effect.

The possibility of using thin R–3d films, for high density magnetic recording was suggested by Tanaka et al. (1982) and Jeannost and Desserre (1983).

10.2. *Applications of metallic glasses*

After it had proved possible to make metallic glasses commercially available on a sufficiently large scale, the first applications considered in the early seventies were mainly based on the mechanical and strength properties of these alloys. The applications considered encompassed tire cords, flywheel components, acoustic delay lines, razor blades and corrosion-resistant superstrong biomedical implants. Almost a decade later the interest in such applications had gradually faded away, the applications considered now being based on the favourable magnetic properties of metallic glasses (see for instance Gilman, 1975; Luborsky, 1978; Warlimont, 1980; Davis et al., 1981). The METGLAS alloy 2604 produced on a commercial basis by Allied Chemical Corporation is a well-known example of such an amorphous alloy. Like many other similar alloys consisting mainly of 3d metals with B or Si as the minority component it has a saturation induction as high as 1.6 T while the magnetic losses for 60 Hz amount to only one third of the losses in grain-oriented silicon steel.

Rising energy prices, and the simultaneous decrease in the production costs of the glassy ribbons together with the capability of manufacturing alloy ribbons as wide as 100 mm have made these alloys good candidates for core material in distribution transformers (Smith, 1982). In such applications one has to consider that the shapes of the B–H loops of metallic glasses are amenable to alterations obtainable by means of annealing treatments performed below their crystallization temperature in the presence of a magnetic field. The induced anisotropy achieved in this way can lead to an easy magnetization direction parallel to the ribbon direction, favouring a square hysteresis loop. It is also possible to have the easy magnetization direction make some angle with the ribbon direction, favouring a rounded or even sheared hysteresis loop (Chen et al., 1975).

In general, it can be said that most of the liquid-quenched alloys contain residual stresses due to the quenching or contain stresses as a result of the winding of cores from the ribbons (Luborsky et al., 1975; Luborsky, 1977). A certain type of annealing treatment will therefore be necessary to obtain optimum properties. For instance, an annealing treatment close to the Curie temperature in a longitudinal dc field leads to square loops. Owing to the absence of grain boundaries and the low demagnetization factor in the ribbon direction the domain pattern consists of wide stripe domains. This pattern can be changed drastically by annealing in an oxidizing

atmosphere, owing to the stress produced by the oxide surface layer. Careful annealing not too far below T_x can also induce partial crystallization and give rise to the precipitation of barely detectable crystallites of α-Fe. The effect of such heat treatments is the generation of rounded loops, higher initial permeabilities and lower losses in high frequency applications (for more details see Pfeifer and Behuke, 1977; Nathasingh and Smith, 1980; Datta et al., 1982; Hasegawa et al., 1982).

Relatively large amounts of amorphous ribbons are furthermore involved in the manufacturing of flexible woven magnetic shields (Mendelsohn et al., 1976; Sellers, 1977; Shiau et al., 1978; Borek, 1982). The dimensions of the woven materials can be made up to 100 cm wide and as long as needed. The strength and flexibility of the narrow ribbons lend themselves also to the manufacture of braided and spirally wrapped shields (Smith, 1982).

Applications in which relatively small amounts of glassy ribbons are involved comprise magnetically tuneable acoustic delay lines. In these applications the giant ΔE effects exhibited in some glasses is of prime importance (Arai and Tsuya, 1978; Fukamichi et al., 1979b). Amorphous ribbons combining a low magnetostriction and thermal expansion with a high saturation induction and a high abrasion resistance are applied in tape heads (Shiiki et al., 1981; Hayakawa et al., 1982). The fact that in several glassy alloys the magnetomechanical coupling coefficient reaches values as high as 0.96 may indicate why such alloys are good starting materials in various types of transducers and sensors. (Modzelewski et al., 1981; Mohri and Sudoh, 1981). Investigations are furthermore being undertaken to determine in how far amorphous alloys can be used in pulsed power applications such as nonlinear pulse compressors (Birx et al., 1982), saturation inductors in high power magnetic switches (Birx et al., 1981; Van Devender and Reber, 1981; Stocton et al., 1982; Nunnally, 1981) and non-saturating inductors in linear induction accelerators (Birx et al., 1982; Schwartzschild, 1982).

Metallic glasses in which metals like rare earths or Zr are combined with Cu were reported to be good materials for flash bulbs (Van den Nieuwenhuizen and Buschow, 1982). The heating of the ribbon to above their melting point during burning is so rapid that crystallization and phase separation is suppressed. Soon after ignition in a cold oxidizing atmosphere the alloy gives rise to the phenomenon of explosive combustion. This leads to an extremely high fragmentation. Associated with this phenomenon is a very high lumen output in a relatively narrow time interval.

It is well known that crystalline rare-earth–cobalt phases lend themselves fairly well to permanent magnet applications. Materials related to $SmCo_5$ are currently reported to offer energy products higher than 340 kJ m^{-3}. The manufacturing costs are still appreciable, and have prevented large scale applications. This has led to a search for less expensive materials based on the less expensive Fe rather than on Co. All these attempts have failed thus far since the crystalline phases studied do not have the required type of magnetocrystalline anisotropy and coercive forces are generally low.

Croat (1982a, b) and to some extent Clark (1973) reported that much better results can be reached when starting from melt-spun rare-earth–iron alloys. Large coercive forces can be attained which develop either directly during the quenching
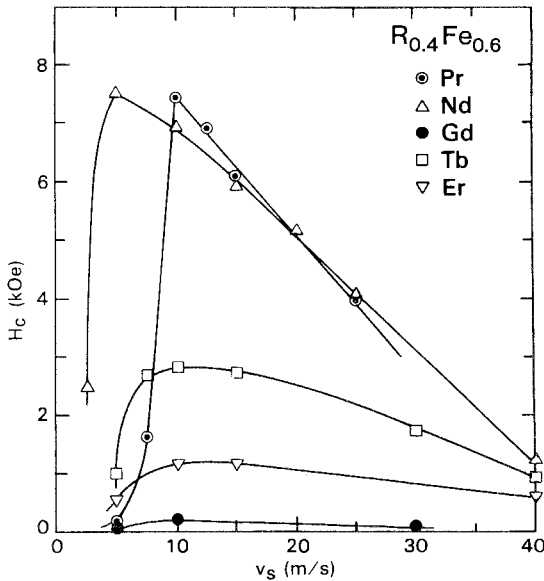
Fig. 104. Room temperature coercive field (H_c) in melt-spun $R_{0.4}Fe_{0.6}$ alloys (R = Pr, Nd, Gd, Tb and Er) as a function of substrate velocity v_s during the melt-spinning (after Croat, 1982b).

process or during crystallization. The origin of these coercive forces is ascribed to the formation of a metastable or non-equilibrium phase in conjunction with a finely divided microstructure, approaching the single domain optimum when the quenching rate is properly chosen. Results obtained by Croat (1982b) are shown in fig. 104 for the alloys $R_{0.4}Fe_{0.6}$.

Of particular interest are alloys based on Fe and the light rare earth metals (La, Ce, Pr, Nd) since these latter are most abundant and less expensive. For instance in melt-spun $Nd_{0.4}Fe_{0.6}$ the room temperature coercive forces can become as high as 7.5 kOe (see fig. 105) and in $Sm_{0.4}Fe_{0.6}$ even as high as 24 kOe (Croat, 1982b). Crystalline Nd–Fe alloys of the same composition consist of a mixture of Nd and Nd_2Fe_{17}. For comparison, it is noted that the coercive force reaches only rather negligible values (about 0.1 kOe) in the crystalline alloys.

Interesting in this respect are furthermore results of annealing treatments made on the rapidly quenched alloys. It can be seen from Croat's results reproduced in fig. 105 that the annealing leads to a steady small decrease of H_c in the alloy having already the alleged single domain optimum in the microstructure. Alloys that have suffered a slightly too large quenching (15 m/s and 25 m/s) can still acquire a more favourable microstructure upon annealing, while the alloy (2.5 m/s) that was quenched too slowly does not show this feature. X-ray diffraction performed on the samples after annealing at various temperatures (T_A) indicated that the drop of H_c for $T_A > 725$ K results from the decomposition of the magnetic phase into a mixture of Nd and a yet unidentified phase. Formation of Nd_2Fe_{17} (the only stable intermetallic compound in the Nd–Fe system) was not reported to occur until $T_a > 900$ K.

Croat furthermore notes that the heavy rare-earth–iron systems are less likely to give good results. In the corresponding binary systems several stable intermetallic
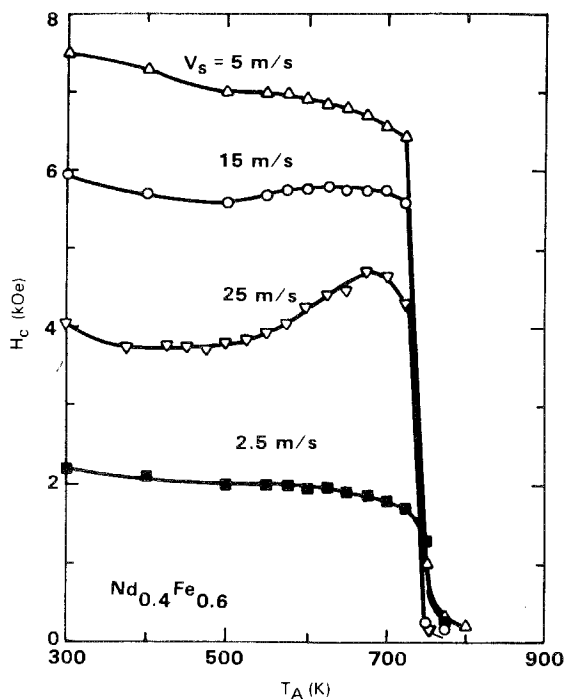
Fig. 105. Room temperature coercive field H_c of several melt-spun $Nd_{0.4}Fe_{0.6}$ alloys versus anneal temperature T_A (after Croat, 1982b).

compounds (RFe_2, RFe_3, R_6Fe_{23}) are known to exist (see, for instance, the survey of R–Fe phases shown in fig. 4 of the review by Buschow (1984)). The presence of these phases is assumed to have an unfavourable influence on the formation of the metastable phase mentioned. Inspection of the results shown in fig. 104 shows that the H_c values obtained for the Gd compound are quite low. Since Gd is the only ion in this series that does not have an orbital moment, one may conclude from these results that the large H_c values originate from the single-ion anisotropy associated with the rare earth component (Croat, 1982b).

A further application of amorphous alloys was reported by Chraplyvy et al. (1982). These authors obtained an amorphous thin film of $Pr_{0.25}Co_{0.75}$ by DC sputtering techniques. In contrast to crystalline $PrCo_3$, the magnetic properties of the amorphous $Pr_{0.25}Co_{0.75}$ alloy were found to be magnetically soft. Selective tempering of tiny regions of the amorphous film was shown to induce substantial magnetic hardness owing to crystallization. As a possible application the authors suggest a read-only memory for a microprocessor for use in a rugged automotive, under-hood environment.

11. Summary and outlook

In this chapter we have attempted to give a cross section of the various research efforts made in the field of amorphous alloys. The main topics of this review are
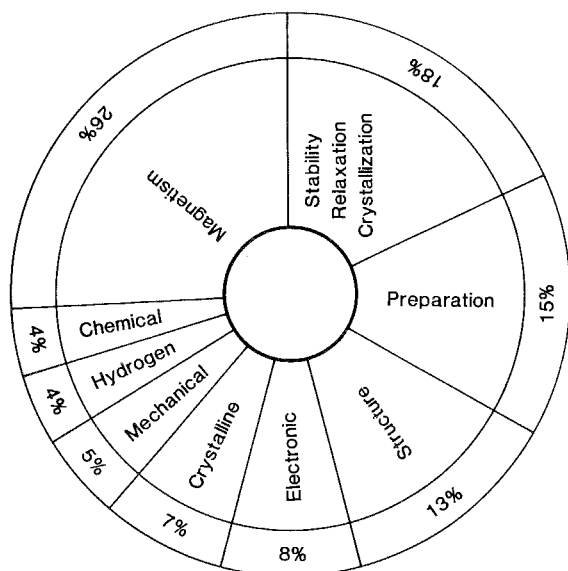
Fig. 106. Distribution of topics in research on rapidly quenched metals (from Masumoto, 1982).

preparation, formation and stability, atomic structure and magnetism. Substantial attention has also been paid to the electronic structure of amorphous alloys and to technological applications of these materials. A brief account has furthermore been given of hydrogen absorption in amorphous alloys. Without losing sight of the research on amorphous alloys not composed of rare earth elements, attention has been focussed mainly on the rare earth base materials. It is interesting to compare the relative research efforts in the various fields on these latter alloys with those on amorphous alloys in general. If one considers the more than 400 contributions presented at the Fourth International Conference on Rapidly Quenched Metals (held in 1981, Sendai, Japan) as representative, one arrives at the distribution shown in fig. 106. If one compares this distribution with that obtained after perusal of the various sections of the present chapter, one may state that the research on amorphous rare earth base alloys does not occupy a special position.

It is plausible that in the field of preparation the work on amorphous alloys carries a relatively large weight when compared, for instance, with the work on intermetallic compounds or crystalline alloys. Progress in this field will lead directly to the discovery of new amorphous alloys, to the improvement of the physical properties of already existing amorphous alloys and will increase the feasibility of large scale production in cases where technological applications are involved. With the exception of several methods of preparation employed in liquid quenching, there is a general lack of accurate experimental values describing the cooling rates associated with the different types of quenching. A knowledge of these values would be extremely helpful not only for evaluating the relative merits of the different quenching techniques but also by contributing to a better understanding of the differences in properties of the corresponding amorphous alloys. If progress from this side is accompanied by progress in research on the structure of amorphous

metals, one would eventually be able to establish a reliable correlation between quenching rate and structure on the atomic scale.

It was mentioned in section 3 that quite a number of models exist for describing the glass-forming tendency. None of these models is perfect or complete, and one might wonder whether continued research in this area will eventually lead to a more unified model for glass formation in which all the aspects of the different models are properly accounted for. An important point requiring further investigation in the near future is the occurrence of short-range ordering in the molten alloy as opposed to the amorphous alloy. Here it is desirable to compare not only the degree of the short-range ordering but also the concentrations at which it occurs in the liquid and the amorphous state. Promising results in this direction have already been obtained with amorphous $Ti_{1-x}Cu_x$ glasses (Sakata et al., 1981, 1982). An extension of similar studies to alloy systems differing widely in nature would be highly welcome.

It is also important to establish in how far the concentrations at which intermediate compounds occur in the stable crystalline state differ from the concentrations of maximum short-range ordering in the liquid amorphous state. If chemical short-range ordering is present in the liquid state or in the amorphous state but occurs at compositions differing from those of the stable crystalline state, one may expect a chemically hindered nucleation of the crystalline phase. This will have a significant influence on the glass-forming tendency or on the thermal stability of the alloy, as the case may be. These aspects of glass formation and stability are currently being investigated by Sommer et al. (1982a) on alloy systems based on alkaline earth metals. It seems promising to include rare earth base materials into similar studies in view of the larger freedom of choice of the heat of alloying.

Numerous investigations performed mainly by means of calorimetry but also by measurements of the resistivity or other physical properties, have shown that the temperature dependence and the time dependence of the crystallization involve an exponential law, the activation energy being typically of the order of several eV for amorphous alloys stable up to several hundreds of degrees centigrade. Apart from the crystallization process the amorphous alloys may also be subject to a process of structural relaxation. This transformation involves markedly lower activation energies than the amorphous-to-crystalline transformation and may encompass reversible as well as irreversible changes (Balanzat et al., 1980; Chambron and Chamberod, 1980; Cost and Stanley, 1982; Taub and Spaepen, 1980; Kelten and Spaepen, 1982). Investigations in this field are in full progress.

A clear picture of the possible occurrence of structural relaxation processes is of considerable importance where technological applications are concerned. The irreversible processes in particular may give rise to a gradual change of properties that may come into play on a time scale that interferes badly with the time scale envisioned in technological applications. The same holds for the effect of surface crystallization, studied in some detail by Fiedler (1982) and Gonser et al. (1983), on amorphous Fe-base alloys. All these transformations, which reflect the metastable character of the amorphous alloy in one way or the other, constitute an interesting and not yet fully investigated field of research.

There is still a long way to go before it will be possible to describe the magnetic

properties of amorphous alloys from first principles. The reason for this does not lie in the amorphous state itself. Even in atomically well-ordered intermetallics the description of 3d electron magnetism is still an object of current experimental and theoretical studies. Substantial understanding of the 3d moment formation in some types of crystalline materials has been obtained from band structure calculations (Williams et al., 1983). No such calculations yet exist to explain why, for instance, compounds like $ScFe_2$, YFe_2 and $ZrFe_2$ are strongly ferromagnetic while $NbFe_2$ and $TaFe_2$ are non-magnetic. It seems therefore that progress in understanding the 3d electron magnetism in amorphous alloys can only be expected after it has proved possible to solve the problems associated with the electronic structure in crystalline materials.

It has been shown in this chapter that some progress has already been made in describing the differences in magnetism between amorphous and crystalline alloys. The absence of lattice periodicity does not seem to be all that important. Instead of fixed values for quantities like the number of neighbours, the exchange constants etc., one has to take the distributions of these quantities. Using these latter distributions it seems possible in most cases to relate the magnetic properties of amorphous alloys in one way or the other to those of their crystalline counterparts. Even more sophistication in the description of the mentioned differences between the crystalline and amorphous state is expected to occur within a reasonable lapse of time. It therefore seems likely that the difference between the crystalline state and the amorphous state will not be the rate-determining step in the understanding of amorphous magnetism.

It will have become clear after perusal of the many papers that have appeared on amorphous solids that the knowledge of solid state physics has been greatly enriched by this research, not only in the field of magnetism but also in numerous other fields such as mentioned in sections 8 and 9. In some cases solid state physics has profited from the amorphous state in a rather indirect way. We will conclude this chapter by illustrating this point with two examples.

It has repeatedly been mentioned that the amorphous state is metastable. Upon crystallization the stable crystalline phases can be reached directly or via a metastable crystalline phase. This offers the opportunity of obtaining metastable phases that would otherwise have remained undetected. Investigations in this rich area have already begun (Tenhover et al., 1982; Cadieu et al., 1982; Croat, 1982b; Tanaka et al., 1982; Wang et al., 1982) and the results obtained thus far are encouraging.

The second example relates to the interpretation of the Mössbauer isomer shift. When the atoms of a given Mössbauer isotope are incorporated as solute atoms into different metallic hosts one generally observes a change of the isomer shift relative to the parent metal. At concentrations where the solute atoms are surrounded exclusively by host atoms (dilute limit) this isomer shift change enables important conclusions to be drawn regarding the charge transfer accompanying the alloying. In the case of [57]Fe Mössbauer spectroscopy the dilute limit was measured for numerous host metals by doping the latter with small amounts of [57]Fe (Shenoy and Wagner, 1978). In general, the Fe atoms will occupy crystallographic positions in these alloys belonging to the host lattice, which may entail a significant volume mismatch. In

order to obtain the strain-free dilute limit for the isomer shift, a volume correction has to be applied to the experimental IS values. The corrections involved are made on the basis of model calculations (Ingalls, 1974; Watson and Bennett, 1977). In several cases they are several times larger than the measured value of the IS change itself. These difficulties are no longer present when amorphous alloys are used in which the Fe atoms are free to choose their own volume. The method of obtaining the strain-free dilute limit of the isomer shift by means of amorphous alloys has already been successfully applied to ^{57}Fe Mössbauer spectroscopy (see section 9.4) and its application to the other Mössbauer isotopes seems promising.

Appendix

In tables A1 to A4 data on magnetic properties of amorphous alloys based on rare earth metals are listed together with the crystallization temperatures of these alloys (T_x). The magnetic ordering temperatures comprise Curie temperatures (T_c) or spin glass freezing temperatures (T_s). The magnetic moments μ and μ' pertain to the R sublattice magnetization and 3d sublattice magnetization, respectively. They were derived from results of measurements made at low temperatures $(T \ll T_c)$ in high magnetic fields. The values of the paramagnetic Curie temperature (θ_p) and the effective moment (μ_{eff}) pertain to the paramagnetic state. For all alloys listed the method of preparation has been indicated by means of the symbols vq. (vapour quenched), lq (liquid quenched) or el (electrolytical).

In table A5 the superconducting transition temperatures (T_0) of several amorphous alloys are listed together with information on the density of states at the Fermi level $N(E_F)$. These latter values are expressed in stages eV^{-1} atom^{-1} spin^{-1}. Included are also values for the electron–phonon coupling constant (λ) and the Debye temperature (θ_D). The method used in the preparation of the alloys is indicated by the symbols lq (liquid quenched) or vq (vapour quenched).

TABLE A1

Amorphous $R_{1-x}M_x$ alloys with non-magnetic M component

Alloy	T_x (K)	T_c, T_s (K)	θ_p (K)	μ (μ_B/R)	μ_{eff} (μ_B/R)	$4\pi M_s$ (kG)	Method	Ref.
$Pr_{0.40}Cu_{0.60}$		< 4.2	8			2.3	vq	1
$Nd_{0.44}Cu_{0.56}$		< 4.2				3.0	vq	1
$Gd_{1-x}Cu_x$								
$x = 0.04$			250		7.9		vq	2
0.07		193	193		7.9		vq	2
0.10			115		7.9		vq	2
0.12			65		7.9		vq	2
0.13			40		7.9		vq	2
0.24	473	142		6.4			lq	5
0.34	473	148	152	6.7	8.9		lq	5
0.27			129				vq	3
0.30	470	144		6.6			lq	4,5
0.39		140	152				vq	3
0.40		100					vq	6
0.50		74					vq	6
0.58		77	85			14.8	vq	1
0.60		37					vq	6
0.75		21	40				vq	3
0.79		6	29				vq	3
$Tb_{0.50}Cu_{0.50}$		23	39			7.8	vq	1
$Dy_{1-x}Cu_x$								
$x = 0.20$		33					vq	7
0.28		27					vq	7
0.30	540	42	46			10.9	lq	8
0.42		26					vq	7
0.44		26					vq	7
0.52		20					vq	7
0.55		16	20			12.8	vq	1
0.59		18					vq	7
0.60		15					vq	7
0.62		9					vq	7
0.80		6					vq	7
$Ho_{0.44}Cu_{0.56}$		8	8			11.8	vq	1
$Er_{0.51}Cu_{0.49}$		< 4.2	11			8.4	vq	1
$Tm_{0.61}Cu_{0.39}$			−3			10.2	vq	1
$Pr_{1-x}Ag_x$								
$x = 0.79$			−10		3.39		vq	9
0.50			−40		3.42		vq	9
$Nd_{1-x}Ag_x$								
$x = 0.79$			0.0		3.68		vq	9
0.50			−37.5		4.11		vq	9
$Eu_{1-x}Ag_x$								
$x = 0.19$	480	70	85	3.8	7.52		lq	10
0.25	423	37	42	7.39	8.41		lq	10

TABLE A1 (continued)

Alloy	T_x (K)	T_c, T_s (K)	θ_p (K)	μ (μ_B/R)	μ_{eff} (μ_B/R)	$4\pi M_s$ (kG)	Method	Ref.
$Eu_{1-x}Ag_x$								
$x = 0.74$	518		~ 0		7.96		lq	10
0.82	659		~ 0		8.27		lq	10
$Gd_{1-x}Ag_x$								
$x = 0.13$		40			7.6		vq	11
0.30		149		7.0			lq	4
		160					vq	12
0.33		157					vq	12
0.46		122	130	6.7	8.36		el	13,14
0.49		110					vq	12
0.52		101					vq	12
0.55		101					vq	12
0.76		~ 0					vq	12
0.79		15					vq	12
$Tb_{0.50}Ag_{0.50}$		64	76	5.0	9.8		vq	14
$Dy_{0.50}Ag_{0.50}$		18	20	4.8	10.08		vq	14
$Ho_{0.50}Ag_{0.50}$		11	12	5.7	9.74		vq	14
$Er_{0.50}Ag_{0.50}$		6	8	4.9	9.48		vq	14
$Ce_{0.80}Au_{0.20}$		1.7	-0.3	>1	2.10		lq	15
$Pr_{0.47}Au_{0.53}$		< 4.2	7			1.6	vq	1
$Nd_{0.38}Au_{0.62}$		10	15			2.0	vq	1
$Sm_{0.43}Au_{0.57}$			4			0.6	vq	1
$Eu_{0.80}Au_{0.20}$		85, 90					lq	16,17
$Eu_{0.20}Au_{0.80}$		< 4.2	10			3.8	vq	1
$Gd_{1-x}Au_x$								
$x = 0.20$		149	165	7.0	9.37		lq	18
0.28		118	125			20	vq	19
0.31		89	97			16.8	vq	19
0.37		107	117			18.6	vq	19
0.46		99	109			17.6	vq	1,19,20
0.55		66	61			14.5	vq	19
0.62		52				13.5	vq	19
0.67		47				13.0	vq	19
0.74		26				8.8	vq	19
0.85		0	-6			3.2	vq	19
$Tb_{1-x}Au_x$								
$x = 0.48$		32	38		9.83		el	21
0.53		> 4.2	31			9.4	vq	1
$Dy_{0.46}Au_{0.54}$		15	18			10.2	vq	1
$Ho_{0.44}Au_{0.56}$		11	24			13.5	vq	1
$Er_{0.58}Au_{0.42}$		9.5	10			9.9	vq	1
$Tm_{0.61}Au_{0.39}$			-3			10.2	vq	1
$Gd_{0.85}Ru_{0.15}$	573	78	80	6.1	8.5		lq	5
$Gd_{0.70}Ru_{0.30}$	728	77	79	7.1	8.8		lq	5
$Gd_{0.60}Ru_{0.40}$	765	57	56	6.0	8.1		lq	5
$Gd_{0.82}Rh_{0.18}$	563	111		5.6			lq	5
$Gd_{0.76}Pd_{0.24}$	569		145	5.7			lq	5
$Dy_{0.69}Pd_{0.31}$		49	43		11.0		lq	8

TABLE A1 (continued)

Alloy	T_x (K)	T_c, T_s (K)	θ_p (K)	μ (μ_B/R)	μ_{eff} (μ_B/R)	$4\pi M_s$ (kG)	Method	Ref.
$Gd_{0.83}Pt_{0.17}$	628	150	156	6.5	7.7		lq	5
$Eu_{0.70}Mg_{0.30}$		131 , 52		6.85			lq	25
$Gd_{0.73}Mg_{0.27}$		130	133			15.8	vq	20
$Ce_{0.65}Al_{0.35}$			-40		2.31		lq	22
$Pr_{0.65}Al_{0.35}$		6.2	8		3.47		lq	22
$Eu_{0.78}Al_{0.22}$		47					lq	25
$Eu_{0.70}Al_{0.30}$		42					lq	25
$Eu_{0.60}Al_{0.40}$		41					lq	25
$Gd_{1-x}Al_x$								
x = 0.19		83	110				vq	3,
			116				vq	23
0.22	591	144			5.3		lq	4
0.44		79	104				vq	3,
			110				vq	23
0.60		18	49				vq	3
0.63		17	30				vq	3,23
0.70		14	18				vq	3
$Dy_{0.65}Al_{0.35}$		30.3	40.5		11.0		lq	22
$Gd_{0.58}Si_{0.42}$		87	111			12.9	vq	20
$Gd_{0.56}Ti_{0.44}$		88	116			17.2	vq	20
$Gd_{0.54}V_{0.46}$		105	144			14.7	vq	20
$Gd_{0.50}Cr_{0.50}$		75	102			15.0	vq	20
$Gd_{1-x}Mn_x$								
x = 0.40	520	230		5.3			lq	5
0.52		210				15.0	vq	24
0.65		145				10.8	vq	24
0.68		115				8.0	vq	24
0.72		5				6.5	vq	24
$Dy_{0.65}Mn_{0.35}$	118						lq	8
$Y_{0.19}Mn_{0.81}$	Pauli paramagnetic						vq	24
$Gd_{0.79}Ga_{0.21}$	558	129	150	6.2	8.1	–	lq	4
$Gd_{0.75}Ga_{0.15}$		148		5.8			lq	5
$Eu_{0.70}Zn_{0.30}$		133		6.85			lq	25
$Eu_{0.75}Cd_{0.25}$		134		6.8			lq	25
$Gd_{0.55}Ge_{0.45}$		71	101			17.8	vq	20
$Gd_{0.56}Nb_{0.44}$		48	90			10.5	vq	20

1. McGuire and Gambino (1979)
2. Popplewell and Charles (1978)
3. McGuire et al. (1978)
4. Buschow (1978)
5. Buschow et al. (1980)
6. Heiman and Kazama (1978b)
7. Von Molnar et al. (1980)
8. Buschow (1983a)
9. Pappa and Boucher (1980)
10. Buschow and Van den Hoogenhof (1979)
11. Popplewell et al. (1978)
12. Hauser (1975)
13. Boucher (1976)
14. Boucher (1977a)
15. Ernst et al. (1980)
16. Berrada et al. (1979)
17. Friedt et al. (1982)
18. Poon and Durand (1977)
19. Gambino et al.(1981)
20. McGuire and Gambino (1980)
21. Boucher (1977b)
22. Giessen and Hines (1980)
23. Jamet and Malozemoff (1978)
24. McGuire and Gambino (1979)
25. Maurer and Friedt (1983)

TABLE A2

Amorphous $R_{1-x}Ni_x$ alloys.

Alloy	T_x (K)	T_c, T_s (K)	θ_p (K)	μ (μ_B/R)	μ_{eff} (μ_B/R)	Method	Refs.
$Pr_{0.69}Ni_{0.31}$	449		2	1.0	3.6	lq	1
$Nd_{0.69}Ni_{0.31}$	489	18	15	1.3	3.5	lq	1
$Gd_{1-x}Ni_x$							
$x = 0.31$	553	130	138	7.0	9.0	lq	1
0.33		125		7.1		lq	4
0.40	538	108, 118	122	8.0	8.4	vq, lq	4,5,6
0.46		88				vq	5
0.59		65				vq	5
0.64		55				vq	5
0.67		38		8.7		vq	7
0.70		43		7.0		vq	2
0.72		37		6.72		vq	2
0.74		38		6.61		vq	2
0.75		38	37	6.0	7.7	vq	3
0.76		40				vq	5
0.78		43	44	5.98	7	vq	2
0.80		45				vq	5
0.82		45				vq	5
0.84		60				vq	5
$Tb_{0.69}Ni_{0.31}$	587	55	65	5.0	8.9	lq	1
$Dy_{0.69}Ni_{0.31}$	591	40	35	4.5	10.6	lq	1
$Dy_{0.21}Ni_{0.79}$		10, 47	12	5.15	9.7	vq	2,8
$Ho_{1-x}Ni_x$							
$x = 0.67$		15		4.0		vq	7
0.77		4	4	5.5	10.3	vq	2
0.83		400				vq	7
0.89		> 400				vq	7
$Er_{1-x}Ni_x$							
$x = 0.31$	← 6 20		5	4.4	9.8	lq	1
0.75		2	2	4.05	8.74	vq	2
$Y_{1-x}Ni_x$							
$x = 0.31$	608	$\chi = 25 \times 10^{-8}$ m^{3}kg^{-1}				lq	1
0.75		20		0.03 *		vq	9
0.83		27		0.03 *, 0.04 *		vq	5,9
0.87		118		0.12 *		vq	9
0.905		175		0.20 *		vq	9
0.930		242		0.26 *		vq	9
0.950		327		0.36 *		vq	9
0.956		356		0.38 *		vq	9
0.970		390		0.41 *		vq	9

* in μ_B/Ni

1. Buschow (1980a)
2. Asomoza et al. (1979)
3. Von Molnar et al. (1981)
4. Durand and Poon (1977)
5. McGuire and Gambino (1978)
6. Buschow et al. (1980)
7. Lee and Heiman (1974)
8. Rebouillat et al. (1977)
9. Lienard and Rebouillat (1978)

TABLE A3
Amorphous $R_{1-x}Co_x$ alloys

Alloy	T_x (K)	T_c, T_s (K)	T_{comp} (K)	μ (μ_B/R)	μ' (μ_B/Co)	Method	Refs.
$La_{1-x}Co_x$							
$x = 0.32$	421	Pauli paramagnetic				lq	1,2
0.37					0	vq	3
0.48					0.1	vq	3
0.60					0.6	vq	3
0.71					1.1	vq	3
0.83					1.4	vq	3
$Nd_{1-x}Co_x$							
$x = 0.31$	460	45		2.4		lq, vq	2,3,4
0.34		38		1.9		lq	4
0.35		31.7		1.9		lq	4
0.50		176				vq	5
0.70		523				vq	5
0.76		682		2.59	1.38	vq	5
$Sm_{1-x}Co_x$							
$x = 0.31$	516	60				lq	1,2
0.35		57.8				lq	6
0.43		137				lq	7
$Gd_{1-x}Co_x$							
$x = 0.26$		190				lq	8
0.27		170				lq	8
0.31	550	170		6.6		lq, vq	2,3
0.33		172		7.1		lq	9
0.35		170 –218				lq	4,6,8
0.37		190				vq	10
0.40		193				lq	8
0.43		230				lq	7
0.45		230				lq	8
0.50		277				lq	8
0.55		330				lq	8
0.58		347				vq	11
0.60		383				vq	11
0.61		310				vq	10
0.64		428				vq	11
0.65		488				vq	11
0.67		550	510		4.2	vq	10,12
0.73			571			vq	14
0.75		750	40		2.8	vq	12
0.76			380 , 546			vq	11
0.78		> 500	300 , 320		4.2	vq	12,13
0.79			295 , 423			vq	10,11,13
0.82			180 , 296			vq	10,11
0.83		> 500	80 , 325	0		vq	11,12
0.89		> 500				vq	10
0.94							

TABLE A3 (continued)
Amorphous $R_{1-x}Co_x$ alloys

Alloy	T_x (K)	T_c, T_s (K)	T_{comp} (K)	μ (μ_B/R)	μ' (μ_B/Co)	Method	Refs.
$Tb_{1-x}CO_x$							
x = 0.25	528	82		4.5		lq	1,2
0.31	570	90		5.3		lq	1,2
0.35		90.4		6.2		lq	6
0.40	573	113		5.1		lq	1,2
0.43		137				lq	7
0.50		165		5.4		lq	1
0.60	528	210		2.5		lq	1
0.67		> 600	500	4.3		vq	12
0.70			473			vq	11
0.74			350			vq	11
0.75		> 600	250	2.5		vq	12
0.77			293			vq	11
0.83		> 600		2.4		vq	12
$Dy_{1-x}Co_x$							
x = 0.31		48		5.1		lq	1
0.35		43		5.8		lq	6
0.40		61		5.4		lq	15
0.43		69				lq	7
0.50		110		5.0		lq	15
0.77		930	228 , 230	2.36		vq	14,16
$Ho_{1-x}Co_x$							
x = 0.31	608			5.9		lq	1,2
0.53		291				vq	11
0.55		375				vq	12
0.57		360				vq	11
0.58		545				vq	11
0.60		600	325 , 373			vq	11,12
0.67		> 600	270	4.8		vq	12
0.68			321				
0.70			298			vq	11
0.75		> 600	150	4.3		vq	12
0.76		900	190	3.38		vq	16
0.87		> 600		0.2		vq	12
$Er_{1-x}Co_x$							
x = 0.31	633			4.3		lq	1,2
0.35		10.3–12		4.9–5.1		lq	4,6
0.57		23				lq	7
0.77		940	94		2.13	vq	16
$Y_{1-x}Co_x$							
x = 0.30	615	$\chi = 27 \times 10^{-8}$ m^{3}kg^{-1}				lq	1
0.35					0	vq	3
0.40	642	$\chi = 3.1 \times 10^{-8}$ m^{3}kg^{-1}				lq	1
0.42					0.1	vq	17
0.43		450			0.2	vq	12

TABLE A3 (continued)

Alloy	T_x (K)	T_c, T_s (K)	T_{comp} (K)	μ (μ_B/R)	μ' (μ_B/Co)	Method	Refs.
$Y_{1-x}Co_x$							
$x = 0.50$					0.14–0.6	lq, vq	12,18
0.54		42			0.28	lq	19
0.55		72			0.30	lq	18,19
0.58					0.77	vq	17
0.62					0.85	vq	17
0.67		> 600			1.0, 1.6	vq	12,17
0.70					1.0	vq	3
0.75		> 600			0.8–0.9	vq	12,18,20
0.80					1.3–1.65	vq	3–17
0.83		> 600			1.5	vq	12
0.90					1.71	vq	17

1. Buschow (1980b)
2. Buschow and Beekmans (1980b)
3. Heiman and Kazama (1978a)
4. Gerber et al. (1978)
5. Taylor et al. (1978)
6. Berrada et al. (1982)
7. Apostolov et al. (1982)
8. Algra et al. (1980)
9. Durand et al. (1978)
10. Tao et al. (1974)
11. Biesterbos (1979)
12. Lee and Heiman (1974)
13. Taylor and Gangulee (1976)
14. Rebouillat et al. (1977)
15. Gubbens et al. (1981)
16. Jouve et al. (1978)
17. Buschow et al. (1977)
18. Buschow (1982d)
19. Buschow (1983a)
20. Suran et al. (1977)

Amorphous $R_{1-x}Fe_x$ alloys.

Alloy	T_x (K)	T_c, T_s (K)	T_{comp} (K)	μ (μ_B/FU)	μ' (μ_B/Fe)	Method	Refs.
$La_{1-x}Fe_x$							
$x = 0.67$		275		0.91	1.36	vq	1
0.69		275, 330		0.94	1.36	vq	2
0.76		300, 330		1.16	1.53	vq	1,2
0.82		310				vq	2
$Ce_{1-x}Fe_x$							
$x = 0.80$		190			0.8	vq	3
0.82		190			1.1	vq	3
0.90					1.0	vq	3
$Pr_{1-x}Fe_x$							
$x = 0.45$		456				lq	4
0.50		468				lq	4
0.55		456				lq	4
0.60		475				lq	4
0.68		455				lq	4
0.75		385				lq	4
0.80		308				lq	4
0.90		277				lq	4
$Nd_{1-x}Fe_x$							
$x = 0.30$		205				vq	6
0.40		475				lq	5
0.45		470				lq	5
0.46		280				vq	6
0.50		485				lq	5
0.55		495				lq	5
0.60		485				lq	5
0.63		255				vq	6
0.66		475				lq	5
0.67		305, 380			1.3	vq	1,6,7
0.74		400				vq	6
0.75		425				lq	5
0.80		390				lq	5
0.83		370				vq	6
$Sm_{1-x}Fe_x$							
$x = 0.40$	618	> 300		0.4		lq, vq	8,9,19
$Gd_{1-x}Fe_x$							
$x = 0.32$		290		3.9		lq	8,19
0.40	~ 410	310		3.4		lq	8,19,20
0.43		350				vq	1
0.50		400		2.5		lq	8,19
0.60		493				vq	1,17
0.66		498				vq	17
0.67		490	450–500			vq	1,11,21
0.70		503	400			vq	17,11
0.74		503	438			vq	17

TABLE A4 (continued)

Alloy	T_x (K)	T_c, T_s (K)	T_{comp} (K)	μ (μ_B/FU)	μ' (μ_B/Fe)	Method	Refs.
$Gd_{1-x}Fe_x$					.		.
$x = 0.75$		460	130, 150			vq	1,11
0.77			60			vq	11
0.78		503				vq	17
0.79		420, 483	~100			vq	1,17
0.80		430, 493				vq	11,17
$Tb_{1-x}Fe_x$							
$x = 0.30$		240		4.1		lq	8
0.40	590	220		4.1		lq	8,19
0.57		423				vq	17
0.61		420				vq	17
0.65		428				vq	17
0.67		383, 390		> 1.3		vq	1,15
0.69		428				vq	17
0.74		423				vq	16,17
0.75		404, 423				vq	14,17
0.72		423				vq	17
0.80		420				vq	17
0.83		380				vq	14
0.85		483				vq	17
0.88		365				vq	17
0.98		245				vq	14
$Dy_{1-x}Fe_x$							
$x = 0.31$	603	135		3.5		lq	8,19
0.40		135		2.9		lq	8
0.60		334				vq	17
0.64		331				vq	17
0.71		333				vq	17
0.74		333				vq	16
0.78		333				vq	17
0.80		333				vq	17
0.84		325				vq	17
$Ho_{1-x}Fe_x$							
$x = 0.31$	608	77		4.1		lq	8,19
0.60		250	180			vq	1
0.67		195, 260	120	1.8		vq	1,10
0.79		300				vq	1
$Er_{1-x}Fe_x$							
$x = 0.25$	633	20				lq	22
0.31	631	36		3.0		lq	8,19
0.32	631	35				lq	20
0.37		40		3.0		lq	8
0.40	628	6				lq	19
$Tm_{1-x}Fe_x$							
$x = 0.31$	648					lq	8,19

TABLE A4 (continued)

Alloy	T_x (K)	T_c, T_s (K)	T_{comp} (K)	μ (μ_B/FU)	μ' (μ_B/Fe)	Method	Refs.
$Yb_{1-x}Fe_x$							
$x = 0.60$				0.62		vq	3
0.70				0.69		vq	3
0.75				0.67		vq	3
0.80				0.73		vq	3
0.85				0.83		vq	3
$Lu_{1-x}Fe_x$							
$x = 0.31$	683	Pauli paramagnetic				lq	19
0.40	698	Pauli paramagnetic				lq	8,19
0.62		55			0.7	vq	18
0.67		119				vq	1
0.75		220				vq	23
0.79		230				vq	23
$Y_{1-x}Fe_x$							
$x = 0.32$					0.36	vq	12
0.40	638 , 650	15			0.70	lq	13,19
0.45	688	115			0.95	lq	13
0.48		18			0.86	vq	12
0.50	741 , 760				1.07	vq, lq	1,13,19
0.57		40			1.22	vq	12
0.60	805	245			1.37	lq	13
0.67	860	275, 400			1.46	lq, vq	1,13
0.68		70			1.69	vq	12
0.70		73			1.15	vq	18
0.75	960	98, 260			1.20	vq, lq	1,13,18
					1.60		
0.79	948	278			1.77	lq	13
0.80		108			1.89	vq	12
0.83		128			1.15	vq	18

1. Heiman and Lee (1976)
2. Kazama et al. (1980)
3. Buschow and van Engen (1980)
4. Croat (1981a)
5. Croat (1981b)
6. Taylor et al. (1978)
7. Alperin et al. (1979)
8. Buschow and Van der Kraan (1981)
9. Croat and Herbst (1982)
10. Pickart et al. (1974)
11. Heiman et al. (1975)
12. Coey et al. (1981)
13. Croat (1982a)
14. Alperin et al. (1975)
15. Rhyne et al. (1974)
16. Mimura et al. (1976a)
17. Biesterbos (1979)
18. Heiman and Kazama (1979)
19. Buschow (1981a)
20. Buschow (1979)
21. Vittoria et al. (1978)
22. Buschow (1983a).
23. Heiman et al. (1976)

TABLE A5

Superconducting transition temperatures (T_0), Debye temperatures (θ_D), density of states $N(E_F)$ and electron–phonon coupling parameters λ of several amorphous alloys.

Alloy	T_0 (K)	$N(E_F)$ (eV^{-1} atom^{-1} spin^{-1})	λ	θ_D (K)	Method	Ref.
La$_{1-x}$Al$_x$						
$x = 0.00$	~ 6.0					1
0.16	4.75				lq	2
0.20	3.33–4.75	0.75	0.81	112	lq	2–4,12
0.22	4.30	0.70	0.79	113	lq	4
0.25	3.80–3.98	0.64	0.76	116	lq	2,4
0.27	3.82	0.63	0.74	117	lq	4
0.30	3.15				lq	2
0.32	3.23	0.62	0.68	121	lq	4
La$_{1-x}$Ga$_x$						
$x = 0.16$	3.94	1.25	0.85	109.6	lq	5
0.18				109.6	lq	5
0.20	3.84	1.29	0.84	108.6	lq	5
0.22	3.64	1.17	0.82	115.3	lq	5
0.24	3.52–3.68	1.44	0.81	111.6	lq	5
0.26	3.22–3.39	1.15	0.77	118.7	lq	5
0.28	3.09	0.87	0.75	117.8	lq	5
La$_{1-x}$Ge$_x$						
$x = 0.20$	4.75				lq	4
0.22	5.12				lq	4
La$_{1-x}$Au$_x$						
$x = 0.00$	4.3				vq	6
0.05	4.27				vq	6
0.10	4.21				vq	6
0.16	3.51				vq	6
0.16	4.9				lq	7
La$_{1-x}$Au$_x$						
$x = 0.18$	3.8				lq	7
0.19	3.30				vq	6
0.20	3.28				vq	6
0.20	3.5–3.71	1.50	0.88	96	lq	8–10,13
0.22	3.3–3.93				lq	7,10
0.24	2.98				vq	6
0.24	3.28	1.33	0.82	99	lq	7,8
0.26	3.1				lq	7
0.29	1.90				vq	6
0.30	2.3				lq	7
0.32	1.6				vq	6
La$_{1-x}$Cu$_x$						
$x = 0.10$	5.8				lq	15
0.20	5.7				lq	15
0.26	4.9				lq	15
0.30	3.5–3.85				lq	7,11,14,15
0.35	4.5				lq	15
0.40	4.4				lq	15

Alloy	T_0 (K)	$N(E_F)$ (eV^{-1} atom^{-1} spin^{-1})	λ	θ_D (K)	Method	Ref.
$La_{1-x}Ni_x$						
$x = 0.22$	3.0				lq	7

1. Balster and Wittig (1975)
2. Razavi and Schilling (1982)
3. Zolotukhin et al. (1980)
4. Agyeman et al. (1979)
5. Shull et al. (1978)
6. Manning and Briscoe (1978)
7. Johnson et al. (1975)
8. Shull and Naugle (1977)

9. Logan (1975)
10. Johnson and Tsuei (1976)
11. Arce et al. (1982)
12. Bindilatti et al. (1981)
13. Poon and Durand (1977)
14. Daudin (1981)
15. Favaron et al. (1980)

References

Abrikosov, A.A.A. and L.P. Gorkov, 1962, Sov. Phys. JETP **15**, 752.

Adam, G. and J.H. Gibbs, 1965, J. Chem. Phys. **43**, 139.

Adams, D.J. and A.J. Matheson, 1972, J. Chem. Phys. **56**, 1989.

Agyeman, K., R. Müller and C.C. Tsuei, 1979, Phys. Rev. B **19**, 193–198.

Aharony, A. and E. Pytte, 1980, Phys. Rev. Lett. **45**, 1583–1586.

Algra, H.A., K.H.J. Buschow and R.A. Henskens, 1980, J. Physique **41**, C8-646–649.

Allen, J.W., A.C. Wright and G.A.N. Connell, 1980, J. Non-Cryst. Solids **42**, 509–524.

Alperin, H.A., J.R. Cullen and A.E. Clark, 1975, AIP Conf. Proc. **29**, 186–187.

Alperin, H.A., W.R. Gillmor, S.J. Pickart and J.J. Rhyne, 1979, J. Appl. Phys. **50**, 1958–1960.

Amamou, A., 1980, Solid State Commun. **33**, 1029–1034.

Anderson, P.W., B.I. Halperin and C.M. Varma, 1972, Phil. Mag. **25**, 1.

Andrews, R., W.A. Grant, P.J. Grundy and J.S. Williams, 1976, Nature **262**, 380–381.

Ansara, I., A. Pasturel and K.H.J. Buschow, 1982, Phys. Stat. Sol. (a) **69**, 447–453.

Anthony, T.R. and H.E. Cline, 1978, J. Appl. Phys. **49**, 829;

Anthony, T.R. and H.E. Cline, 1979, J. Appl. Phys. **50**, 239.

Aoki, K., A. Horata and T. Masumoto, 1982, in: Rapidly Quenched Metals IV, eds. T. Masumoto and K. Suzuki (Japan Inst. of Metals, Sendai, Japan) pp. 1649–1653.

Apostolov, A., H. Hristov, T. Mydlarz, M. Mihov and V. Skumriev, 1982, in: Crystalline Electric Field Effects in f-Electron Magnetism, eds. R.P. Guertin, W. Suski and Z. Zolnierek (Plenum, New York) pp. 493–499.

Arai, K.I., N. Tsuya, 1978, J. Appl. Phys. **49**, 1718.

Arce, R., F. de la Cruz and H.J. Fink, 1982, Solid State Commun. **42**, 575–577.

Argyle, B.E., R.J. Gambino and K.Y. Ahn, 1974, AIP Conf. Proc. **24**, 564–565.

Arrese-Boggiano, R., J. Chappert and J.M.D. Coey, 1976, J. Physique **37**, C6-771–775.

Asomoza, R., A. Fert, I.A. Campbell and R. Meyer, 1977a, J. Phys. F **7**, L327–332.

Asomoza, R., I.A. Campbell and R. Meyer, 1977b, J. Appl. Phys. **48**, 3229–3231.

Asomoza, R., I.A. Campbell, A. Fert, A. Liénard and J.P. Rebouillat, 1979, J. Phys. F **9**, 349–371.

Avrami, M., 1940, J. Chem. Phys. **8**, 212.

Azoulay, J. and L. Ley, 1979, Solid State Commun. **31**, 131–141.

Babic, E., E. Girt, R. Krsnik and B. Leontic, 1970, J. Phys. E **3**, 1014.

Bagley, B.G. and D. Turnbull, 1968, J. Appl. Phys. **39**, 5681.

Balanzat, F., C. Mairy and J. Hillairet, 1980, J. Physique **41**, C8-871–874.

Balster, H. and J. Wittig, 1975, J. Low Temp. Phys. **21**, 1377.

Barbara, B., G. Fillon, D. Gignoux and R. Lemaire, 1972, Solid State Commun. **10**, 1149.

Barbara, B., J.X. Boucherle, J.L. Buevoz, M.F. Rossignol and J. Schweizer, 1977, Solid State Commun. **24**, 481–485.

Barbara, B., A.P. Malozemoff and Y. Imry, 1981, Physica B + C **108**, 1289.

Bardeen, J., L. Cooper and J. Schrieffer, 1957, Phys. Rev. **108**, 1175.

Bates, P.A., J. Popplewell and S.W. Charles, 1971, J. Physique **32**, C1-567–568.

Beck, H. and R. Oberle, 1978, in: Rapidly Quenched Metals III, ed. B Cantor (Chameleon, London).

Beck, P.A., 1972, J. Less-Common Metals **28**, 193.

Bedell, J.R., 1975, U.S. Patent No. 3, 862, 658 (Jan. 28, 1975).

Bennett, C.H., 1972, J. Appl. Phys. **43**, 2727.

Berger, L., 1973, Phys. Rev. B **8**, 2351.

Bergmann, G., 1976, Phys. Rep. **27**, 161.

Bernas, H., I.A. Campbell and R. Fruchart, 1967, J. Phys. Chem. Solids **28**, 17.

Berrada, A., M.F. Lapierre, B. Loegel, P. Panissod and C. Robert, 1978, J. Phys. F **8**, 845.

Berrada, A., J. Durand, N. Hasshain and B. Loegel, 1979, J. Appl. Phys. **50**, 7621–33.

Berrada, A., J. Durand, T. Mizoguchi, J.I. Budnick, B. Loegel, J.C. Ousset, S. Askenazy and H.J. Güntherodt, 1982, in: Rapidly Quenching Metals IV, eds. T. Masumoto and K. Suzuki (Japan Inst. of Metals, Sendai) pp. 829–834.

Bhagat, S.M. and D.K. Paul, 1975, AIP Conf. Proc. **29**, 176–177.

Bhagat, S.M., M.L. Spano, H.S. Chen and K.V. Rao, 1980, Solid State Commun. **33**, 303–307.

Bhattacharjee, A.K. and B. Coqblin, 1978, J. Phys. F. **8**, L221–224.

Bhattacharjee, A.K. and B. Coqblin, 1983, J. Magn. Magn. Mater. **31–34**, 1575–1576.

Bieri, J.B., J. Sanchez, A. Fert, D. Bertrand and A.R. Fert, 1982, J. Appl. Phys. **53**, 2347–2349.

Biesterbos, J.W.M., 1979, J. Physique **40**, C5-274–279.

Biesterbos, J.W.M., M. Brouha and A.G. Dirks, 1975, AIP Conf. Proc. **29**, 184–187.

Biesterbos, J.W.M., M. Brouha and A.G. Dirks, 1977, Physica **86–88B**, 770–772.

Biesterbos, J.W.M., A.G. Dirks, M.A.J.P. Farla and P.J. Grundy, 1979, Thin Solid Films **58**, 259–263.

Bindilatti, V., F.P. Missell and M. Tenhover, 1981, Physica B + C **107**, 391.

Birx, D.L., E.J. Lauer, L.L. Reginato, D. Rogers Jr., M.W. Smith and T. Zimmerman, 1981, Proc. 3rd IEEE Int. Pulsed Conf., Albuquerque, NM, p. 262.

Birx, D.L., E.G. Cook, L.L. Reginatto, J.A. Smith and M.E. Smith, 1982, IEEE Conf. Record 15th Power Modulator Symp., Baltimore, MD.

Blandin, A., 1961, Thesis, Université de Paris (unpublished).

Blasberg, E., D. Korn, H. Pfeifle, 1979, J. Phys. F **9**, 1821.

Bobak, A., 1980, Phys. Stat. Sol. (b) **97**, K99–K101.

Bobeck, A.H., 1967, Bell System Tech. J. **46**, 1901.

Borchi, E. and S. de Gennaro, 1981, J. Magn. Magn. Mater. 25, 279–283.

Borek, L., 1982, Elektronik **4/26.2**, 43.

Boswell, F.G., 1980, J. Thermal Anal. **18**, 353.

Boucher, B., 1972, J. Non-Cryst. Solids **7**, 277.

Boucher, B., 1976, J. Physique Lett. **37**, L345–347.

Boucher, B., 1977a, IEEE Trans. Magn. **MAG-13**, 1601–1602.

Boucher, B., 1977b, Phys. Stat. Sol. (a) **42**, K165–169.

Boucher, B. and B. Barbara, 1979, J. Phys. F **9**, 151–159.

Boucher, B., D. Luzet and C. Sella, 1976, Compt. Red. 2e Colloq. Int. de Pulverisation Cathodique, Nice.

Boudreaux, D.S., 1977, in: Amorphous Magnetism II, eds. R.A. Levy and R. Hasegawa (Plenum, New York) p. 463.

Boudreaux, D.S., 1978, Phys. Rev. B **18**, 4039.

Boudreaux, D.S. and J.M. Gregor, 1977, J. Appl. Phys. **48**, 152; **48**, 5057.

Bowman, R.C., Jr., A. Attalla, A.J. Maeland and W.J. Johnson, 1983, Solid State Commun. **47**, 779–782.

Breinan, E.M., B.H. Kear and C.M. Banas, 1976, Physics Today (Nov. 1976) 44.

Brenner, A. and G. Riddell, 1947, J. Res. Natl. Bur. Stand. **39**, 385.

Brouha, M., K.H.J. Buschow and A.R. Miedema, 1974, IEEE Trans. Magn. **MAG-10**, 182–185.

Brown, H.A., 1978, Phys. Stat. Sol. (b) **90**, K165.

Brunsch, A. and J. Schneider, 1978, IEEE Trans. Magn. **MAG-14**, 731–734.

Buckel, W. and R. Hilsch, 1954, Z. Phys. **138**, 109.

Buckel, W. and R. Hilsch, 1956, Z. Phys. **146**, 27.

Buschow, K.H.J., 1978, in: Rapidly Quenched Metals III, ed. B. Cantor (Chameleon, London) pp. 133–136.

Buschow, K.H.J., 1979, J. Less-Common Met. **66**, 89–97.

Buschow, K.H.J., 1980a, J. Magn. Magn. Mater. **21**, 97–100.

Buschow, K.H.J., 1980b, J. Appl. Phys. **51**, 2795–2798.

Buschow, K.H.J., 1980c, in: Ferromagnetic Materials, Vol. 1, ed. E.P. Wohlfarth (North-Holland, Amsterdam).

Buschow, K.H.J., 1981a, J. Less-Common Metals **79**, 9–18.

Buschow, K.H.J., 1981b, J. Less-Common Metals **79**, 243–253.

Buschow, K.H.J., 1981c, J. Appl. Phys. **52**, 3319–3323.

Buschow, K.H.J., 1982a, J. Magn. Magn. Mater. **29**, 91–99.

Buschow, K.H.J., 1982b, Phys. Scr. **T1**, 125–129.

Buschow, K.H.J., 1982c, Solid State Commun. **43**, 171–174.

Buschow, K.H.J., 1982d, J. Appl. Phys. **53**, 7713–7716.

Buschow, K.H.J., 1983a, unpublished results.

Buschow, K.H.J., 1983b, J. Appl. Phys. **54**, 2578–2781.

Buschow, K.H.J., 1983c, J. Phys. F **13**, 563–571.

Buschow, K.H.J., 1984, in: Handbook on the Physics and Chemistry of Rare Earths, Vol. 6, eds. K.A. Gschneidner and L. Eyring (North-Holland, Amsterdam).

Buschow, K.H.J. and N.M. Beekmans, 1978, in: Rapidly Quenched Metals III, vol. 2, ed. B. Cantor (Chameleon, London) pp. 133–136.

Buschow, K.H.J. and N.M. Beekmans, 1979a, Phys. Stat. Sol. (a) **56**, 505–511.

Buschow, K.H.J. and N.M. Beekmans, 1979b, Phys. Rev. (b) **19**, 3843–3849.

Buschow, K.H.J. and N.M. Beekmans, 1979c, J. Appl. Phys. **50**, 6348–6352.

Buschow, K.H.J. and N.M. Beekmans, 1979d, Phys. Stat. Sol. (a) **60**, 193–200.

Buschow, K.H.J. and N.M. Beekmans, 1980a, J. Less-Common Metals 72, 141–145.

Buschow, K.H.J. and N.M. Beekmans, 1980b, Phys. Stat. Sol. (a) **60**, 193–200.

Buschow, K.H.J. and N.M. Beekmans, 1980c, Solid State Commun. **35**, 233.

Buschow, K.H.J. and F.J.A. Den Broeder, 1973, J. Less-Common Metals 33, 191–201.

Buschow, K.H.J. and A.G. Dirks, 1980a, J. Electrochem. Soc. 127, 2430–2432.

Buschow, K.H.J. and A.G. Dirks, 1980b, J. Phys. D 13, 251–258.

Buschow, K.H.J. and W.W. Van den Hoogenhof, 1979, J. Magn. Magn. Mater. 12, 123–126.

Buschow, K.H.J. and A.M. Van der Kraan, 1979, Phys Stat. Sol. (a) 53, 665–669.

Buschow, K.H.J. and A.M. Van der Kraan, 1981, J. Magn. Magn. Mater. 22, 220–226.

Buschow, K.H.J. and P.G. Van Engen, 1980, J. Physique 41, C8-650–653.

Buschow, K.H.J. and P.G. Van Engen, 1981a, J. Appl. Phys. 52, 3557–3561.

Buschow, K.H.J. and P.G. Van Engen, 1981b, Mater. Res. Bull. 16, 1177.

Buschow, K.H.J., A.R. Miedema and M. Brouha, 1974, J. Less-Common Metals 38, 9–13.

Buschow, K.H.J., M. Brouha, J.W.M. Biesterbos and A.G. Dirks, 1977, Physica 91B, 261–270.

Buschow, K.H.J., A.M. Van Diepen, N.M. Beekmans and J.W.M. Biesterbos, 1978, Solid State Commun. 28, 181–185.

Buschow, K.H.J., H.A. Algra and R.A. Henskens, 1980, J. Appl. Phys. 51, 561.

Buschow, K.H.J., P.C.P. Bouten and A.R. Miedema, 1982, Rep. Prog. Phys. 45, 937–1039.

Cadieu, F.J., T.D. Cheung, S.H. Aly, L. Wickramasekara and A.G. Pirich, 1982, J. Appl. Phys. 53, 8338–8340.

Cahn, J.W., 1956, Acta Metall. 4, 449.

Cahn, R.W., 1980, Contemp. Phys. 21, 43–86.

Cahn, R.W., 1982, Proc. Fifth Int. Conf. Physics Non-Cryst. Solids, Montpellier (Les Editions de Physique).

Cahn, R.W., K.D. Krishnanand, M. Laridjani, M. Greenholz and R. Hill, 1976, Mater. Sci. Eng. 23, 83.

Campbell, I.A., 1972, J. Phys. F 2, L47–50.

Cargill III, G.S., 1970, J. Appl. Phys. 41, 12.

Cargill III, G.S., 1971, J. Appl. Cryst. 4, 227.

Cargill III, G.S., 1975, Solid State Phys. 30, 227–320.

Cargill III, G.S., 1981a, in: Diffraction Studies on Non-Crystalline Substances, eds. I. Hargittai and W.J. Orville-Thomas (Elsevier, Amsterdam) pp. 731–780.

Cargill III, G.S., 1981b, in: Diffraction Studies on Non-Crystalline Substances, eds. I. Hargittai and W.J. Orville-Thomas (Elsevier, Amsterdam) pp. 781–808.

Cargill III, G.S. and S. Kirkpatrick, 1976, AIP Conf. Proc. 31, 339.

Cargill, G.S. and T. Mizoguchi, 1978, J. Appl. Phys. 49, 1753–1755.

Chambron, W. and A. Chamberod, 1980, J. Physique 41, C8-710–713.

Chappert, J., 1979, J. Physique 40, C2-107–114.

Chappert, J., R. Arrese-Boggiano and J.M.D. Coey, 1978, J. Magn. Magn. Mater. 7, 175–177.

Chappert, J., J.M.D. Coey, A. Liénard and J.P. Rebouillat, 1981, J. Phys. F 11, 2727–2744.

Chappert, J., L. Asch, M. Bogé, G.M. Kalvius and B. Boucher, 1982, J. Magn. Magn. Mater. 28, 124–136.

Chaudhari, P. and D.C. Cronemeyer, 1975, AIP Conf. Proc. 29, 113–114.

Chaudhari, P., J.J. Cuomo and R.J. Gambino, 1973, IBM J. Res. Dev. 17, 66.

Chaudhari, P., J.J. Cuomo, R.J. Gambino, S. Kirkpatrick and L.J. Tao, 1974, AIP Conf. Proc. 24, 562–563.

Chaudhari, P., J.F. Graczyk, D. Henderson and D. Steinhardt, 1975, Phil. Mag. 31, 727–737.

Chen, C.T. and W.L. Wilson, 1978, J. Appl. Phys. 49, 1756–1758.

Chen, H.S., 1980, Rep. Prog. Phys. 43, 353–432.

Chen, H.S. and C.E. Miller, 1970, Rev. Sci. Instrum. 41, 1237.

Chen, H.S. and C.E. Miller, 1976, Mater. Res. Bull. 11, 49.

Chen, H.S., S.D. Ferris, E.M. Gyorgy, H.J. Leamy and R.C. Sherwood, 1975, Appl. Phys. Lett. 26, 405.

Chen, T. and R. Malmhäll, 1983, J. Magn. Magn. Mater. 35, 269–271.

Chen, T., R. Malmhäll and G.B. Charlan, 1982, J. Appl. Phys. 53, 2356–2358.

Chi, G.C. and G.S. Gargill, 1976, Mater. Sci. Eng. 23, 155.

Chipman, D.R., L.D. Jennings and B.C. Giessen, 1978, Bull. Am. Phys. Soc. 23, 467.

Chraplyvy, R., J.F. Herbst and J.J. Croat, 1982, US Patent No. 4,347,086 (1982).

Clark, A.E., 1973, Appl. Phys. Lett. 23, 642.

Clark, A.E., 1979, in: Handbook on the Physics and Chemistry of Rare Earths, Vol. 2, eds. K.A. Gschneidner and L. Eyring (North-Holland, Amsterdam) pp. 231–258.

Clarke, R. and S.R. Nagel, 1978, Solid State Commun. 27, 215–217.

Cochrane, R.W., R. Harris, J.O. Ström-Olsen and M.J. Zuckermann, 1975, Phys. Rev. Lett. 35, 676.

Cochrane, R.W., R. Harris and M.J. Zuckermann, 1978a, Phys. Rep. 48, 1.

Cochrane, R.W., J. Ström-Olsén, G. Williams, A. Liénard and J.P. Rebouillat, 1978b, J. Appl. Phys. 49, 1677–1679.

Coey, J.M.D., 1974, J. Physique 35, C6-89–105.

Coey, J.M.D. and S. Von Molnar, 1978, J. Physique Lett. 39, L327–330.

Coey, J.M.D., J. Chappert, J.P. Rebouillat and T.S. Wang, 1976, Phys. Rev. Lett. 36, 1061.

Coey, J.M.D., S. Von Molnar and R.J. Gambino, 1977, Solid State Commun. 24, 167–170.

Coey, J.M.D., D. Givord, A. Liénard and J.P. Rebouillat, 1981, J. Phys. F 11, 2707–2725.

Coey, J.M.D., D. Ryan, D. Gignoux, A. Liénard and J.P. Rebouillat, 1982, J. Appl. Phys. 53, 7804–7806.

Collver, M.M. and R.H. Hammond, 1973, Phys. Rev. Lett. 30, 92.

Connell, G.A.N., 1975, Solid-State Commun. 16, 109–112.

Connell, G.A.N. and R. Allen, 1982, in: Rapidly Quenched Metals IV, eds. T. Masumoto and K. Suziki (Japan Inst. of Metals, Sendai).

Connell, G.A.N., R. Allen and Mansuripur, 1982, J. Appl. Phys. 53, 7759–7661.

Connell, G.A.N., R. Allen and M. Mansuripur, 1983, J. Magn. Magn. Mater. 35, 337–339.

Cooper, B.R., 1965, Phys. Rev. A 139, 1504.

Cornelison, S.G. and D.J. Sellmyer, 1983, J. Appl. Phys. **53**, 7722–7724.

Cost, J.R. and J.T. Stanley, 1982, in: Rapidly Quenched Metals IV, eds. T. Masumoto and K. Suzuki (Japan Inst. of Metals, Sendai) pp. 491–494.

Cote, P.J., 1976, Solid State Commun. **18**, 1311.

Cote, P.J. and V. Meisel, 1977, Phys. Rev. Lett. **39**, 102–105.

Crest, J.S. and S.R. Nagel, 1979, Phys Rev. B **19**, 3571.

Croat, J.J., 1981a, J. Appl. Phys. **52**, 2509–2511.

Croat, J.J., 1981b, J. Magn. Magn. Mater. **24**, 125–131.

Croat, J.J., 1982a, J. Appl. Phys. **53**, 6932–6941.

Croat, J.J., 1982b, IEEE Trans. Magn. **MAG-18**, 1442–1447.

Croat, J.J. and J.F. Herbst, 1982, J. Appl. Phys. **53**, 2404–2406.

Datta, A., N.J. De Cristofaro and L.A. Davis, 1982, in: Rapidly Quenched Metals IV, eds. T. Masumoto and K. Suzuki (Japan Institute of Metals, Sendai) p. 1007.

Czjzek, G., J. Fink, F. Götz, H. Schmidt, J.M.D. Coey, J.-P. Rebouillat and A. Lienard, 1981, Phys. Rev. B **23**, 2513–2519.

Daudin, B., 1981, Solid State Commun. **37**, 149–152.

Davidov, D., A. Chelkowski, C. Rettori, R. Orbach and M.B. Maple, 1973, Phys. Rev. **7**, 1029–1038.

Davies, H.A., 1976, Phys. Chem. Glasses **17**, 159.

Davies, H.A., 1978, in: Rapidly Quenched Metals III, Vol. 1, ed. B. Cantor (Chameleon, London) pp. 1–21.

Davis, L.A., N.J. De Cristofaro and C.H. Smith, 1981, in: Proc. Conf. on Metallic Glasses: Science and Technology, eds. C. Hargitai, I. Bakonyi and T. Kemeny (Central Research Inst. for Physics, Budapest) p. 1.

Davis, S., M. Fischer, B.C. Giessen and D.E. Polk, 1978, in: Rapidly Quenched Metals, Vol. 2, ed. B. Cantor (Chameleon, London) p. 425.

De Gennes, P.G., 1962a, J. Phys. Radium **23**, 510–520.

De Gennes, P.G., 1962b, J. Phys. Radium **23**, 630–641.

De Gennes, P.G. and J. Friedel, 1958, J. Phys. Chem. Solids **4**, 71.

Dekker, P., 1976, IEEE Trans. Magn. **MAG-12**, 311–327.

Dirks, A.G. and H.J. Leamy, 1978, J. Appl. Phys. **49**, 1735–1743.

Dixmier, J. and K. Doi, 1963, C.R. Acad. Sci. Paris **257**, 2451.

Donovan, T.M. and K. Heinemann, 1971, Phys. Rev. Lett. **27**, 1794.

Dormann, E., M. Huck and K.H.J. Buschow, 1977, J. Magn. Magn. Mater. **4**, 47–54.

Doussineau, P., P. Legros, A. Levelut and A. Robin, 1978, J. Physique Lett. **39**, L265–269.

Draper, C.W., F.J.A. Den Broeder, D.C. Jacobson, E.N. Kaufmann, M.L. McDonnald and J.M. Vandenberg, 1982, in: Laser and Electron Beam Interactions with Solids, eds. B.R. Appleton and G.K. Celler (Elsevier, Amsterdam).

Dreirach, O., R. Evans, H.J. Güntherodt and H.U. Künzi, 1972, J. Phys. F **2**, 709.

Durand, J., 1977, in: Proc. 2nd Int. Symp. on Amorphous Magnetism, Troy, NY, eds. R.A. Levy and R. Hasegawa (Plenum, New York).

Durand, J., 1981, Atomic Energy Review, Suppl. No. 1, 143–172.

Durand, J. and S.J. Poon, 1977, IEEE Trans. Magn. `MAG-13`, 1556–1558.

Durand, J., K. Raj, S.J. Poon and J.I. Budnick, 1978, IEEE Trans. Mag. **MAG-14**, 722–725.

Duwez, P. and R.H. Willens, 1963, Trans. Met. Soc. AIME **227**, 362.

Duwez, P., R.H. Willens and W. Klement, 1960, J. Appl. Phys. **31**, 1136.

Edwards, S.F. and P.W. Anderson, 1975, J. Phys F **5**, 965–974.

Edwards, S.F. and P.W. Anderson, 1976, J. Phys. F **6**, 1927–1937.

Egami, T., 1978, Mater. Res. Bull. **13**, 575.

Egami, T. and T. Ichikawa, 1978, Mater. Sci. Eng. **32**, 293–295.

Egami, T., P.J. Flanders and C.D. Graham, Jr., 1975, AIP Conf. Proc. **24**, 697.

Eifert, H.J., B. Elschner and K.H.J. Buschow, 1982, Phys. Rev. B **25**, 7441–7448.

Eifert, H.J., B. Elschner and K.H.J. Buschow, 1983, Phys. Stat. Sol. (b) **115**, 455–462.

Eifert H.J., B. Elschner and K.H.J. Buschow, 1984, Phys. Rev. B **29**, 2905–2910.

Eisenberger, P. and B. Lengeler, 1980, Phys. Rev. B **22**, 3551–3562.

Elliott, R.P., 1965, Constitution of Binary Alloys, First Suppl. (McGraw-Hill, New York).

Ernst, U., W. Felsch and K. Samwer, 1980, J. Magn. Magn. Mater. **15–18**, 1375–1376.

Erskine, J.L. and E.A. Stern, 1973, Phys. Rev. Lett. **30**, 1329–1332.

Esho, S., 1976, Jpn. J. Appl. Phys. **15**, Suppl. 93–98.

Esho, S., 1979, J. Appl. Phys. **50**, 1006–1009.

Esho, S., Noguchi, Y. Ono and M. Nagao, 1973, Proc. Topical Meeting on Optical Storage of Digital Data, Aspen, Col. 1973.

Esposito, E., H. Ehrenreich and C.D. Gelatt, 1978, Phys. Rev. B **18**, 3913.

Evans, R., D.A. Greenwood and P. Lloyd, 1971, Phys. Lett. A **35**, 57.

Faber, T.E. and J.M. Ziman, 1965, Phil. Mag. **11**, 153.

Farges, J., M.F. De Ferraday, B. Raoult and G. Torchet, 1975, J. Physique **36**, C2.

Fasol, G., J.S. Schilling, C.C. Tsuei and F. Zimmer, 1978, J. Phys. F **8**, L257–260.

Favaron, J., M.E. de la Cruz, P. Esquinazi and F. de la Cruz, 1980, Phys. Rev. B **21**, 2804–2808.

Felsch, W., S.G. Kushniv, K. Sammer, H. Schröder, R. van den Berg and H. von Löhneysen, 1982, Z. Phys. B **48**, 99–107.

Ferrer, R., R. Harris, S.H. Sung and M.J. Zuckermann, 1978, in: Rapidly Quenched Metals III, ed. B. Cantor (Chameleon, London) pp. 137–144.

Ferrer, R., R. Harris, S.H. Sung and M.J. Zuckermann, 1979, J. Physique **40**, C5-221–224.

Fert, A. and R. Asomoza, 1979, J. Appl. Phys. **50**, 1886–1891.

Fert, A. and I.A. Campbell, 1978, J. Phys. F **8**, L57–60.

Fert, A., R. Asomoza, I. Campbell and H. Jouve, 1977, C.R. Acad. Sci. Paris **285**, B-113–119.

Fiedler, H.C., 1982, IEEE Trans. Magn. **MAG-18**, 1388–1390.

Fischer, K.H., 1977, Physica **86–88B**, 813.

Forrester, D.W., 1976, AIP Conf. Proc. **31**, 384.

Forrester, D.W., W.P. Pala and R. Segnan, 1977, in: Amorphous Magnetism II, eds. R.A. Levy and R. Hasegawa (Plenum, New York) pp. 135–143.

Forrester, D.W., N.C. Koon, J.H Schelleng and J.J. Rhyne, 1979a, Solid State Commun. **30**, 177.

Forrester, D.W., N.C. Koon, J.H. Schelleng and J.J. Rhyne, 1979b, J. Appl. Phys. **50**, 7336.

Frank, F.C., 1952, Proc. R. Soc. London Ser. A **215**, 43–46.

Freiser, M.J., 1968, IEEE Trans. Magn. **MAG-1**, 152–161.

Friedel, J., 1958, Nuov. Cim. Suppl. Vol. VII, Ser. X, 287–298.

Friedt, J.M., M. Maurer, J.P. Sanchez and J. Durand, 1982, J. Phys. F **12**, 821–836.

Fujimori, H., K. Nakanishi, K. Shirakawa, T. Masumoto, T. Kaneko and N.S. Kazama, 1982, in: Rapidly Quenched Metals IV, eds. T. Masumoto and K. Suzuki (Japan Inst. of Metals, Sendai) pp. 1629–1632.

Fukamichi, K., M. Kikuchi, S. Arakawa and T. Masumoto, 1977, Solid State Commun. **23**, 955–958.

Fukamichi, K., M. Kikuchi, T. Masumoto and M. Matsuura, 1979a, Phys. Lett. **73A**, 436–438.

Fukamichi, K., T. Masumoto and M. Kikuchi, 1979b, IEEE Trans. Magn. **MAG-15**, 1404–1409.

Gambino, R.J., P. Chaudhari and J.J. Cuomo, 1973, AIP Conf. Proc. **18**, 578–592.

Gambino, R.J., T.R. McGuire and K. Fukamichi, 1981, J. Appl. Phys. **52**, 2190–2192.

Gangulee, A. and R.J. Kobliska, 1978, J. Appl. Phys. **49**, 4896–4901.

Gangulee, A. and R.C. Taylor, 1978, J. Appl. Phys. **49**, 1762–1764.

Garoche, P., A. Fert, J.J. Veyssié and B. Boucher, 1980a, J. Magn. Magn. Mater. **15–18**, 1397–1398.

Garoche, P., J.J. Veyssié and J. Durand, 1980b, J. Physique Lett. **41**, 357–359.

Gasgnier, M., 1982, in: Handbook on the Physics and Chemistry of Rare Earths, Vol. 5, eds. K.A. Gschneidner and L. Eyring (North-Holland, Amsterdam) ch. 41.

Gaskell, P.H., 1978, Nature **276**, 484.

Gaunt, P., 1979, Phys. Rev. B **19**, 521–524.

Geny, J.F., G. Marchal, Ph. Mangin, Chr. Janot and M. Piecuch, 1982, Phys Rev. B **25**, 7449–7466.

Gerber, J.A., D.J. Miller, D.J. Sellmyer, 1978, J. Appl. Phys. **49**, 1696–1699.

Giessen, B.C. and R.O. Elliot, 1978, in: Rapidly Quenched Metals, Vol. 1, ed. B. Cantor (Chameleon, London) pp. 406–410.

Giessen, B.C. and S. Whang, 1980, J. Physique **41**, C8-95–102.

Giessen, B.C., M. Madhava, D.E. Polk and J. Vander Sande, 1976, Mater. Sci. Eng. **23**, 145.

Giessen, B.C., W.A. Hines and L.T. Kabacoff, 1980, IEEE Trans. Magn. **MAG-16**, 1203–1206.

Gignoux, D., R. Lemaire, P. Molho and F. Tasset, 1980, J. Magn. Magn. Mater. **21**, 307.

Gillot, L., P.N. Guile, N. Cowlam and K.H.J. Buschow, 1983, Proc. 2nd Intern. Conf. on the Structure of Non-Crystalline Materials, Cambridge (July 1982).

Gilman, J.J., 1975, Physics Today **28**(5), 46.

Gonser, U., M. Ackermann and H.-G. Wagner, 1983, J. Magn. Magn. Mater. **31–34**, 1605–1607.

Graczyk, J.F., 1978, J. Appl. Phys. **49**, 1738.

Graebner, J.E., B. Golding, R.J. Schutz, F.S.L. Hsu and H.S. Chen, 1977, Phys. Rev. Lett. **39**, 1480.

Grant, W.A., 1978, J. Vac. Sci. Technol. **15**, 1644–1648.

Greenwood, N.N. and T.C. Gibb, 1971, Mössbauer Spectroscopy (Chapman and Hall, London).

Griessen, R., 1983, Phys. Rev. B **27**, 7575–7582.

Gronau, M., H. Goeke and S. Methfessel, 1981, in: Rapidly Quenched Metals IV, eds. T. Masumoto and K. Suzuki (Japan Institute of Metals, Sendai).

Gubanov, A.I., 1960, Sov. Phys.–Solid State **2**, 468.

Gubbens, P.C.M., A.M. van der Kraan and K.H.J. Buschow, 1981, Phys. Stat. Sol. (a) **64**, 657–563.

Güntherodt, G. and N.J. Shevchik, 1975, AIP Conf. Proc. **29**, 174–175.

Güntherodt, H.J., M. Müller, R. Oberle, C. Hauser, H.U. Künzi, M. Liard and R. Müller, 1978, Inst. Phys. Conf. Ser. **39**, 436.

Güntherodt, H.J., H. Beck, P. Oelhafen, K.P. Ackermann, M. Liard, M. Müller, H.U. Künzi, H. Rudin and K. Agyeman, 1979, in: Electrons in Disordered Metals and at Metallic Surfaces, eds. P. Pharisean and B.L. Gyorffy (Plenum, New York).

Hadjipanayis, G., S.G. Cornelison, J.A. Gerber and D.J. Sellmyer, 1980, J. Magn. Magn. Mater. **21**, 101–107.

Handrich, K., 1969, Phys. Stat. Sol. **32**, K55.

Hansen, P. and M. Urner-Wille, 1979, J. Appl. Phys. **50**, 7471–7476.

Harbur, D.R., J.W. Anderson and W.J. Maraman, 1969, Trans. Met. Soc. AIME **245**, 1055.

Harris, R., M. Plischke and M.J. Zuckermann, 1973, Phys. Rev. Lett. **31**, 160–165.

Hartmann, M., 1982, Thesis, University Osnabrück, Germany (unpublished).

Hasegawa, R., 1975, J. Appl. Phys. **46**, 5263–5267.

Hasegawa, R. and C.C. Tsuei, 1971, Phys. Rev. B **2**, 1631.

Hasegawa, R., R.J. Gambino and R. Ruf, 1975a, Appl. Phys. Lett. **27**, 512–513.

Hasegawa, R., B.E. Argyle and L.J. Tao, 1975b, AIP Conf. Proc. **24**, 110.

Hasegawa, R., G.E. Fish and V.R.V. Ramanan, 1982, in: Rapidly Quenched Metals IV, eds. T. Masumoto and K. Suzuki (Japan Inst. of Metals, Sendai) pp. 929–934.

Hathaway, K., M. Melamud, J. Cullen and G. Blessing, 1979, J. Appl. Phys. 50, 1636–1638.

Hauser, J.J., 1975, Phys. Rev. B 12, 5160.

Hauser, J.J. and A. Staudinger, 1973, Phys. Rev. B 8, 607.

Hayakawa, M., K. Hotai, K. Aso, S. Dedaira, Y. Ochiai and Y. Makino, 1982, in: Rapidly Quenched Metals IV, eds. T. Masumoto and K. Suzuki (Japan Inst. of Metals, Sendai) p. 949.

Heiman, N. and N. Kazama, 1978a, Phys. Rev. B 17, 2215–2220.

Heiman, N. and N. Kazama, 1978b, J. Appl. Phys. 49, 1686–1688.

Heiman, N. and N. Kazama, 1979, Phys. Rev. B 19, 1623–1632.

Heiman, N. and K. Lee, 1976, AIP Conf. Proc. 34, 319–321.

Heiman, N., A. Onton, D.F. Kyser, K. Lee and C.R. Guarnieri, 1974, AIP Conf. Proc. 24, 573–575.

Heiman, N., K. Lee and I. Potter, 1975, AIP Conf. Proc. 29, 130–135.

Heiman, N., K. Lee, I. Potter and S. Kirkpatrick, 1976, J. Appl. Phys. 47, 2634–2638.

Heitmann, H., I. Sander, M. Urner-Wille and K. Witter, 1980, J. Magn. Magn. Mater. 21, 233–238.

Henderson, D., M.H. Brodsky and P. Chaudhari, 1974, Appl. Phys Lett. 25, 641.

Herd, S.R., 1977, Phys. Stat. Sol. 44, 363.

Herd, S.R., 1978, J. Appl. Phys. 49, 1747.

Herd, S.R., 1979, J. Appl. Phys 50, 1645–1647.

Hillmann, H. and H.R. Hilzinger, 1978, in: Rapidly Quenched Metals III, ed. B. Cantor (Chameleon, London) pp. 22–29.

Hirata, T., 1979, Scr. Metall. 13, 555–559.

Hirata, T. and S. Takayama, 1982, J. Mater. Sci. Lett. 1, 516–519.

Hirata, K., Y. Waseda, A. Jain and J. Srivastava, 1977, J. Phys. F 7, 419.

Hiroyoshi, H. and K. Fukamichi, 1981, Phys. Lett. 85A, 242–244.

Hoare, M.R. and P. Pal, 1975, Adv. Phys. 24, 645–678.

Honda, S., K. Ueda and T. Kusuda, 1981, J. Appl. Phys. 52, 2295–2297.

Honda, S., M. Ohkoshi and T. Kusuda, 1983a, J. Magn. Magn. Mater. 35, 238–240.

Honda, S., J. Hirokane, M. Ohkoshi and T. Kusuda, 1983b, J. Magn. Magn. Mater. 35, 208–210.

Hoshi, Y., M. Naoe and S. Yamanaka, 1982, J. Appl. Phys. 53, 2344–2346.

Huth, B., 1974, IBM J. Res. Dev. 18, 100–109.

Ichikawa, T., 1975, Phys. Stat. Sol. (a) 29, 293.

Imamura, N. and Y. Mimura, 1976, J. Phys. Soc. Jpn. 41, 1067–1068.

Ingalls, R., 1974, Solid State Commun. 14, 11–16.

Itoh, A., H. Uekusa, Y. Tarusawa, F. Inoue and K. Kawanishi, 1983, J. Mag. Magn. Mater. 35, 241–242.

Jäger, E., 1977, Phys. Stat. Sol. (b) 80, K81–83.

Jamet, J.P. and A.P. Malozemoff, 1978, Phys. Rev. B 18, 75–91.

Jeanniot D. and J. Desserre, 1983, J. Appl. Phys. 54, 2820–2823.

Johnson, W.A. and R.F. Mehl, 1939, Trans. Am. Inst. Min. Metall. Pet. Eng. 135, 416.

Johnson, W.L., 1978, in: Rapidly Quenched Metals III, Vol. 2, ed. B. Cantor (Chameleon, Oxford) pp. 1–16.

Johnson, W.L., 1979, J. Appl. Phys. 50, 1557–1563.

Johnson, W.L. and C.C. Tsuei, 1976, Phys. Rev. B 13, 4827–4833.

Johnson, W.L. and A.R. Williams, 1979, Phys. Rev. 20, 1640–1655.

Johnson, W.L., S.J. Poon and P. Duwez, 1975, Phys. Rev. B 11, 150–154.

Jones, H. and C. Suryanarayana, 1973, J. Mater. Sci. 8, 705.

Jouve, H., J.P. Rebouillat and R. Meyer, 1978, AIP Conf. Proc. 29, 97–98.

Kahn, F.J., P.S. Pershan and J.P. Remeika, 1969, Phys. Rev. 186, 891–899.

Kahn, H.R. and K. Lüders, 1981, Phys. Stat. Sol. (b) 108, 9–18.

Kamrád, J., Z. Arnold, J. Schneider and S. Krupicka, 1980, J. Magn. Magn. Mater. 15–18, 1409.

Kamrád, J., J. Schneider and Z. Arnold, 1981, Phys. Stat. Sol. (a) 67, K85–88.

Kaneko, T., K. Shirakawa, S. Ohnuma, M. Nose, H. Fujimori and T. Masumoto, 1981, J. Appl. Phys. 52, 1826–1829.

Karplus, R. and J.M. Luttinger, 1954, Phys. Rev. 94, 1154.

Kästner, J., H.J. Schink and E.F. Wassermann, 1980, Solid State Commun. 33, 527–530.

Katayama, T. and K. Hasegawa, 1982, in: Rapidly Quenched Metals IV, eds. T. Masumoto and K. Suzuki (Japan Inst. of Metals, Sendai) pp. 915–918.

Katayama, T., M. Hirano, Y. Koizumi, K. Kawanishi and T. Tsushima, 1977, IEEE Trans. Magn. MAG-13, 1603.

Katayama, T., M. Miyazaki, Y. Nishihara and T. Shibata, 1983, J. Magn. Magn. Mater. 35, 235–237.

Kavesh, S., 1978, in: Metallic Glasses, eds. H.J. Leamy and J.J. Gilman (Am. Soc. Metals, Metals Park, OH).

Kazama, N.S., H. Fujimori and H. Watanabe, 1980, J. Magn. Magn. Mater. 15–18, 1523–1424.

Kelten, K.F. and F. Spaepen, 1982, in: Rapidly Quenched Metals IV, eds. T. Masumoto and K. Suzuki (Japan Inst. of Metals, Sendai) pp. 527–530.

Kirchheim, R., 1982, Acta Metall. 30, 1069–1078.

Kirchheim, R., F. Sommer and G. Schluckebier, 1982, Acta Metall. 30, 1059–1068.

Kissinger, H.E., 1957, Anal. Chem. 29, 1702–1712.

Kobayashi, H., T. Ono, A. Tsushima and T. Suzuki, 1983, Appl. Phys. Lett.

Kobayashi, K., Y. Togami, and T. Terenishi, T., 1980, Jpn. J. Appl. Phys. 19, L581–584.

Kobayashi, S. and S. Takeuchi, 1980, J. Phys. C 13, L969–974.

Kobayashi, T., H. Tsjui, S. Tsunashima and S. Uchiyama, 1981, Jpn. J. Appl. Phys. 20, 2089–2095.

Klement, W., R.H. Willens and P. Duwez, 1960, Nature 187, 869.

Kondo, J., 1976, Physica B**84**, 207.

Korn, D., W. Muner and G. Zibold, 1972, Phys. Lett. **47A**, 117–120.

Kouvel, J.S., 1961, J. Phys. Chem. Solids **21**, 57.

Kramer, J., 1934, Ann. Phys. **19**, 37.

Kramer, J., 1937, Ann. Phys. **106**, 675.

Krey, U., 1977, J. Magn. Magn. Mater. **6**, 27.

Krishnan, R., G. Suran, J. Sztern, H. Jouve and R. Meyer, 1978, J. Appl. Phys. **49**, 4592–4594.

Krishnanand, K.D. and R.W. Cahn, 1976, Proc. 2nd Int. Conf. Rapidly Quenched Metals, eds. N.J. Grant and B.C. Giessen (MIT Press, Cambridge, MA) pp. 67–75.

Kronmüller, 1980, J. Physique **41**, C8-618–625.

Kronmüller, 1981, J. Appl. Phys. **52**, 1859–1864.

Kropp, H., W. Zipf, E. Dormann and K.H.J. Buschow, 1979, J. Magn. Magn. Mater. **13**, 224–230.

Kübler, J., K.H. Benneman, R. Lapka, F. Rösel, P. Oelhafen and H.J. Güntherodt, 1981, Phys. Rev. B **23**, 5176–5184.

Kudo, T., T. Mizoguchi, N. Watanabe, N. Nimura, M. Misawa and K. Suzuki, 1978, J. Phys. Soc. Jpn. Lett. **45**, 1773–1774.

Kumar, K., D. Das and E. Wettstein, 1978, J. Appl. Phys. **49**, 2052–2054.

Kusuda, T., S. Honda and M. Ohkoshi, 1982a, J. Appl. Phys. **53**, 2338–2340.

Kusuda, T., S. Honda and M. Ohkoshi, 1982b, in: Rapidly Quenched Metals IV, eds. T. Masumoto and K. Suzuki (Japan Inst. of Metals, Sendai) pp. 877–880.

Labrune, M., S. Hamzaoui and I.B. Puchalska, 1982, J. Magn. Magn. Mater. **27**, 323–336.

Lachowicz, H.K., 1981, Phys. Stat. Sol. (a) **67**, K131–135.

Lachowicz, H.K., 1982, in: Rapidly Quenched Metals IV, eds. T. Masumoto and K. Suzuki (Japan Inst. of Metals, Sendai) pp. 867–872.

Leamy, H.J. and A.G. Dirks, 1978, J. Appl. Phys. **49**, 3430–3448.

Leamy, H.J. and A.G. Dirks, 1979, J. Appl. Phys. **50**, 2871–2881.

Leamy, H.J., G.H. Gilmer and A.G. Dirks, 1980, in: Current Topics in Materials Science, Vol. 6, ed. E. Kaldis (North-Holland, Amsterdam) pp. 311–342.

Lee, K. and N. Heiman, 1974, AIP Conf. Proc. **24**, 108–110.

Lerchner, H., K. Erdmann, D. Welz, M. Rosenberg and F.E. Luborsky, 1981, IEEE Trans. Magn. **MAG-17**, 2609.

Lewis, B.G. and H.A. Davies, 1977, in: The Structure of Non-Crystalline Materials, ed. P.H. Gaskell (Taylor and Francis, London) p. 89.

Lewis, B.G., I.W. Donald and H.A. Davies, 1977, Proc. Int. Conf. on Solidification and Casting, Sheffield.

Liebermann, H.H., 1978, in: Rapidly Quenched Metals IV, Vol. 1, ed. B. Cantor (Chameleon, London) p. 34.

Liebermann, H.H. and C.D. Graham, 1976, IEEE Trans. Magn. **MAG-12**, 921.

Lienard, A. and J.P. Rebouillat, 1978, J. Appl. Phys. **49**, 1680–1682.

Lines, M.E., 1982, J. Phys. Chem. Solids **43**, 723–730.

Litterst, F.J. and G.M. Kalvius, 1975, Proc. Int. Conf. Mössbauer Spectroscopy, Vol. 2, Cracow, pp. 189–192.

Logan, J., 1975, Scr. Metall. **9**, 379–382.

Lubitz, P., J. Schelleng and C. Vittoria, 1975, AIP Conf. Proc. **29**, 178–179.

Luborsky, F.E., 1977, in: Amorphous Magnetism II, eds. R.A. Levy and R. Hasegawa (Plenum, New York) p. 345.

Luborsky, F.E., 1978, IEEE Trans. Magn. **MAG-14**, 1008.

Luborsky, F.E. and H.H. Liebermann, 1978, Appl. Phys. Lett. **33**, 233.

Luborsky, F.E., 1980, in: Ferromagnetic Materials, vol. 1, ed. E.P. Wohlfarth (North-Holland, Amsterdam) pp. 451–530.

Luborsky, F.E., Becker, J.J. and R.O. McCary, 1975, IEEE Trans. Magn. **MAG-11**, 1644.

Mader, S. and A.S. Nowick, 1965, Appl. Phys. Lett. **7**, 57.

Madhukar, A., 1974, J. Physique **35**, C4-295–298.

Maksymowicz, L.J., L. Dargel, M. Lubecka and M. Pyka, 1983, J. Magn. Magn. Mater. **35**, 281–282.

Maisel, L.I. and R. Glang, 1970, Handbook of Thin Film Technology (McGraw Hill, New York).

Malmhäll, R., 1983, J. Appl. Phys. **54**, 5128–5131.

Malmhäll, R. and T. Chen, 1982, J. Appl. Phys. **53**, 7843–7845.

Malozemoff A.P., A.R. Williams, K. Terakura, V.L. Moruzzi and K. Fukamichi, 1983, J. Magn. Magn. Mater. **35**, 192–199.

Manning, J.S. and C.V. Briscoe, 1978, Phys. Rev. B **18**, 1177–1183.

Mansuripur, M., G.A.N. Connell and D. Treves, 1982, IEEE Trans. Magn. **MAG-18**, 1241–1243.

Marchal, G., J.F. Geny, Ph. Mangin and Chr. Janot, 1980a, J. Physique **41**, C8-477.

Marchal, G., D. Tierlinck, Ph. Mangin, Chr. Janot and J. Hübsch, 1980b, J. Physique **41**, C8-662.

Maringer, R.E. and C.E. Mobley, 1974, J. Vac. Sci. Techn. **11**, 1067.

Maringer, R.E. and C.E. Mobley, 1978, in: Rapidly Quenched Metals III, Vol. 1, ed. B. Cantor (Chameleon, London) p. 49–56.

Masumoto, H., 1931, Sci. Rep. Tohoku Univ. **20**, 101.

Masumoto, H., 1934, Sci. Rep. Tohoku Univ. **23**, 256.

Masumoto, T., 1982, in: Rapidly Quenched Metals IV, eds. T. Masumoto and K. Suzuki (Japan Inst. of Metals, Sendai) pp. 5–10.

Masumoto, T. and R. Maddin, 1975, Mater. Sci. Eng. **29**, 1–24.

Matsushita, S., K. Sunago and Y. Sakurai, 1975, IEEE Trans. Magn. **MAG-11** 1109–1111.

Matsushita, S., Y. Yamada, K. Sunago and Y. Sakurai, 1977, IEEE Trans. Magn. **MAG-13**, 1382–1384.

Matthias, B.T., 1957, Progress in Low Temperature Physics, Vol. 2 (North-Holland, Amsterdam) p. 138.

Maurer, M. and J.M. Friedt, 1983, J. Phys. F **13**, 2175–2188.

Maurer, M., J.M. Friedt and G. Krill, 1983, J. Phys. F **13**, 2389–2405.

McGuire, T.R. and R.J. Gambino, 1978, IEEE Trans. Magn. **MAG-14**, 838–840.

McGuire, T.R. and R.J. Gambino, 1979, J. Appl. Phys. **50**, 763–766.

McGuire, T.R. and R.J. Gambino, 1980, J. Magn. Magn. Mater. **15–18**, 1401–1403.

McGuire, T.R. and R.C. Taylor, 1979, J. Appl. Phys. **50**, 1605–1607.

McGuire, T.R., T. Mizoguchi, R.J. Gambino and S. Kirkpatrick, 1978, J. Appl. Phys. **43**, 1689–1690.

McGuire, T.R., J.A. Aboaf, E. Klokholm, 1982, J. Appl. Phys. **52**, 2205 (1981); **53**, 8219–8221 (1982).

McMillan, W.L., 1968, Phys. Rev. **167**, 331.

Meisel, V. and P.J. Cote, 1978, Phys. Rev. B **17**, 4652–4658.

Melamud, M., K. Hathaway and J. Cullen, 1979, Phys. Lett. **73A**, 58–62.

Mendelsohn, L.I., E.A. Nesbitt and G.R. Bretts, 1976, IEEE Trans. Magn. **MAG-12**, 924.

Miedema, A.R., 1979, Z. Metallkde **70**, 345–352.

Miedema, A.R. and F. Van der Woude, 1980, Physica B **100**, 145.

Miedema, A.R., P.F. De Châtel and F.R. de Boer, 1980, Physica B **100**, 1–28.

Mimura, Y., N. Imamura and T. Kobayashi, 1976a, IEEE Trans. Magn. **MAG-12**, 779–781.

Mimura, Y., N. Imamura and Y. Kushiro, 1976b, J. Appl. Phys. **47**, 3371.

Mimura, Y., N. Imamura and T. Kobayashi, 1978a, Jpn. J. Appl. Phys. **17**, 1365–1369.

Mimura, Y., N. Imamura and T. Kobayashi, 1978b, Jpn. J. Appl. Phys. **17**, 2007–2012.

Mizoguchi, T., 1981, in: Diffraction Studies on Non-Crystalline Substances, eds. I. Hargittai and W.J. Orville-Thomas (Elsevier, Amsterdam) pp. 811–867.

Mizoguchi, T. and G.S. Gargill, 1979, J. Appl. Phys. **50**, 3570–3582.

Mizoguchi, T., T.R. McGuire, S. Kirkpatrick and R.J. Gambino, 1977, Phys. Rev. Lett. **38**, 89–94.

Mizoguchi, T., T. Kudo, T. Irisawa, N. Watanabe, N. Niimura, M. Misawa and K. Suzuki, 1978, in: Rapidly Quenched Metals III, vol. 2, ed. B. Cantor (Metals Society, London) p. 384.

Mizoguchi, T., J.I. Budnick, P. Panissod, J. Durand and H.J. Güntherodt, 1982, in: Rapidly Quenched Metals IV, eds. T. Masumoto and K. Suzuki (Japan Inst. of Metals, Sendai) pp. 1149–1152.

Mizutani, U. and T.B. Massalski, 1980, Phys Rev. B **21**, 3180.

Mizutani, U. and T. Yoshida, 1982, J. Phys. F **12**, 2331–2348.

Modzelewski, C., H.T. Savage, L.T. Kabacoff and A.E. Clark, 1981, IEEE Trans. Magn. **MAG-17**, 2837.

Mohri, K. and E. Sudoh, 1981, IEEE Trans. Magn. **MAG-17**, 1317.

Moruzzi, V.L. P. Oelhafen, R. Williams, R. Lapka, H.J. Güntherodt and J. Kübler, 1983, Phys. Rev. B **27**, 2049–2055.

Moss, M., D.L. Smith and R.A. Lefever, 1964, Appl. Phys. Lett. **5**, 120–121.

Mössbauer, R.L. and M.J. Clauser, 1967, in: Hyperfine Interactions, eds. A.J. Freeman and R.B. Frankel (Academic Press, New York) pp. 497–552.

Mott, N.F. and R.W. Gurney, 1938, Rep. Prog. Phys **5**, 46–63.

Mueller, R., K. Agyeman and C.C. Tsuei, 1980, Phys. Rev. B **22**, 2665–2669.

Müller, H.R., W. Keiling, R. Kosicik, P. Rosemann and Z. Frait, 1978, Phys. Stat. Sol. (a) **50**, 537–542.

Murani, A.P. and J.P. Rebouillat, 1982, J. Phys. F **12**, 1427–1437.

Mydosh, J.A. and G.J. Nieuwenhuys, 1980, in: Ferromagnetic Materials, Vol. 1, ed. F.P. Wohlfarth (North-Holland, Amsterdam) pp. 73–182.

Nagel, S.R., 1977, Phys. Rev. B **16**, 1649.

Nagel, R.S. and J. Tauc, 1975, Phys. Rev. Lett. **35**, 380.

Nagel, R.S. and J. Tauc, 1976, in: Rapidly Quenched Metals, Vol. 1, eds. N.J. Grant and B.C. Giessen (MIT Press, Cambridge, MA) pp. 337–342.

Nagel, R.S. and J. Tauc, 1977, Solid State Commun. **21**, 129–132.

Nagy, I., T. Tarnoczi and Z. Frait, 1976, Magn. Lett. **1**, 7–9.

Nakhadkin, N.G. and A.I. Shaldervan, 1972, Thin Solid Films **10**, 109.

Naoe, M., M. Kodaira, Y. Hoshi and S. Yamanaka, 1981, IEEE Trans. Magn. **MAG-17**, 3062.

Nathasingh, D. and C.H. Smith, 1980, Powercon 7, San Diego, CA, p. B2-1.

Nawate, M., M. Ohkoshi, S. Honda and T. Kusuda, 1983, Jpn. J. Appl. Phys. **22**, L447–L449.

Nieuwenhuizen, J.M. and H.B. Haanstra, 1966, Philips Tech. Rev. **27**, 87.

Nishihara, Y., T. Katayama, Y. Yamaguchi, S. Ogawa and T. Tsushima, 1979, Jpn. J. Appl. Phys. **18**, 1281–1288.

Nishihara, Y., T. Katayama and S. Ogawa, 1982a, J. Phys. Soc. Jpn. **51**, 2487–2492.

Nishihara, Y., T. Katayama and S. Ogawa, 1982b, J. Appl. Phys. **53**, 2285–2287.

Nishihara, Y., T. Katayama, S. Ogawa and T. Tsushima, 1982c, in: Rapidly Quenched Metals IV, eds. T. Masumoto and K. Suzuki (Japan Inst. of Metals, Sendai) pp. 1183–1186.

Nunnally, W.C., 1981, Proc. 3rd IEEE Int. Pulsed Power Conf. Albuquerque, NM, p. 210.

Ododo, J.C. and B.R. Coles, 1977, J. Phys. F 7, 2393–2399.

Oelhafen, P., E. Hauser, H.J. Güntherodt and K.H Bennemann, 1979, Phys. Rev. Lett. 1134–1137.

Oelhafen, P., V.L. Moruzzi, A.R. Williams, D.S. Yee, J.J. Cuomo, U. Gubler, G. Indlekofer and H.J. Güntherodt, 1982, Solid State Commun. **44**, 1551–1555.

Oelhafen, P., E. Hauser and H.J. Güntherodt, 1980, Solid State Commun. **35**, 1017–1019.

Ogawa, A., T. Katayama, M. Hirano and T. Tsushima, 1974, AIP Conf. Proc. **24**, 575–576.

Ohashi, K., H. Tsuji, S. Tsunashima and S. Uchiyama, 1980, Jpn. J. Appl. Phys. 1333–1338.

Ohring, M. and A. Haldipur, 1971, Rev. Sci. Instrum. **42**, 530–531.

O'Shea, M.J., and D.J. Sellmyer, 1982, J. Appl. Phys. **53**, 7722–7724.

Okuno, H. and Y. Sakurai, 1983, J. Appl. Phys. **53**, 8245–8247.

Okuno, H., S. Matsushita and Y. Sakurai, 1981, IEEE Trans. Magn. **MAG-17**, 2831–2833.

Pala, W.P., D.W. Forrester and R. Segnan, 1976, AIP Conf. Proc. **34**, 323–333.

Panissod, P., D. Aliaga Guerra, A. Amamou, J. Durand, W.L. Johnson, W.L. Carter and S.J. Poon, 1980, Phys. Rev. Lett. **44**, 1465–1468.

Pappa, C. and B. Boucher, 1980, J. Magn. Magn. Mater. **15–18**, 97–98.

Parks, R.D., 1977, Valence Instabilities and Related Narrow Band Phenomena (Plenum, New York).

Parthé, E. and J.M. Moreau, 1977, J. Less-Common Metals **53**, 1–24.

Pfeifer, F., W. Behnke, 1977, J. Magn. Magn. Mater. **6**, 80.

Phillips, W.A., 1972, J. Low Temp. Phys. **7**, 351.

Pickart, S.J., J.J. Rhyne and H.A. Alperin, 1974, AIP Conf. Proc. **24**, 117–118.

Pietrokowsky, P., 1963, Rev. Sci. Instrum. **34**, 445–446.

Polk, D.E., 1970, Scr. Metall. **4**, 117.

Polk, D.E. and B.C. Giessen, 1978, in: Metallic Glasses, eds. H.J. Leamy and J.J. Gilman (Am. Soc. Metals, Metals Park, OH) p. 1.

Poon, S.J., 1978, Phys. Lett. **68A**, 403–405.

Poon, S.J. and J. Durand, 1977, in: Amorphous Magnetism II, eds. R.A. Levy and R. Hasegawa (Plenum, New York) p. 245–256.

Poon, S.J. and J. Durand, 1978, Phys. Rev. B **18**, 6253–6264.

Poon, S.J., J. Durand and M. Yung, 1977, Solid State Commun. **22**, 475–479.

Popplewell, J. and S.W. Charles, 1978, J. Magn. Magn. Mater. **7**, 195–197.

Popplewell, J., D.D. Jenkins and S.W. Charles, 1978, J. Non-Cryst. Solids **27**, 319–329.

Prasad, S., R. Krishnan, G. Suran and J. Sztern, 1979, J. Appl. Phys. **50**, 1623–1625.

Predecki, P., A.W. Mullendore and N.J. Grant, 1965, Trans. Met. Soc. AIME **233**, 1581–1586.

Rainer, D. and G. Bergmann, 1974, J. Low Temp. Phys. **14**, 501.

Raj, K., J. Durand, J.I. Budnick, C.C. Tsuei and S. Skalski, 1977, Solid State Commun. **24**, 189–192.

Raj, K., J. Durand, J.I. Budnick and S. Skalski, 1978, J. Appl. Phys. **49**, 1671–1676.

Ramachandrarao, P., 1980, Z. Metallk. **71**, 172–177.

Ramachandrarao, P., B. Cantor and R.W. Cahn, 1977, J. Mater. Sci. **12**, 2488–2502.

Ray, R., 1978, U.S. Patent No. 4,067,732 (Jan. 10, 1978).

Razavi, F.S. and J.S. Schilling, 1982, Z. Phys. B **48**, 123–126.

Rebouillat, J.P., A. Lienard, J.M.D. Coey, R. Arrese-Boggiano and J. Chappert, 1977, Physica **86–88B**, 773–774.

Rhyne, J.J., 1979, in: Handbook on the Physics and Chemistry of Rare Earths, Vol. 2, eds. K.A. Gschneidner and L. Eyring (North-Holland, Amsterdam) Ch. 16.

Rhyne, J.J., S.J. Pickart and A. Alperin, 1972, Phys. Rev. Lett. **29**, 1562.

Rhyne, J.J., J.H. Schelleng and N.C. Koon, 1974, Phys. Rev. B **10**, 4672.

Riley, J.D., L. Ley, J. Azoulay and K. Terakura, 1979, Phys. Rev. B **20**, 776.

Robbins, C.G., Z.D. Chen, J.G. Zhao, M.J. O'Shea and D.J. Sellmyer, 1982, J. Appl. Phys. **52**, 7798–7800.

Ruhl, R.C., 1967, Mater. Sci. Eng. **1**, 313–320.

Sadoc, J.F. and J. Dixmier, 1976, Mater. Sci. Eng. **23**, 187–192.

Sadoc, A., D. Raoux, P. Lagarde and A. Fontaine, 1982, J. Non-Cryst. Solids **50**, 331–349.

Sakata, M., N. Cowlam and H.A. Davies, 1981, J. Phys. F. **11**, L157.

Sakata, M., N. Cowlam and H.A. Davies, 1982, in: Rapidly Quenched Metals IV, eds. T. Masumoto and K. Suzuki (Japan Inst. of Metals, Sendai) pp. 327–330.

Sakurai, Y., and K. Onishi, 1983, J. Magn. Magn. Mater. **35**, 183–191.

Sato, K. and Y. Togami, 1983, J. Magn. Magn. Mater. **35**, 181–182.

Schouhamer-Immink, K.A. and J.J.M. Braat, 1983, Proc. 73rd AES Convention, Eindhoven (March 1983).

Schuldt, S. and D. Chen, 1971, J. Appl. Phys. **42**, 1970.

Schwartzschild, B.M., 1982, Physics Today **35**(2), 20.

Schwarz, R.B. and W.L. Johnson, 1983, Phys. Rev. Lett. **51**, 415–419.

Scott, M., 1978, in: Rapidly Quenched Metals III, Vol. 1 (Chameleon, London) pp. 198–210.

Scott, M.G., 1981, Scr. Metall. **15**, 1073.

Sellers, G.J., 1977, Proc. IEEE Int. Symp. on Electromagnetic Compatibility, p. 129.

Shen, D.F., T. Numata, Y. Sakurai and K. Sato, 1983, J. Magn. Magn. Mater. **35**, 202–204.

Shen, D.H., Y. Mizokawa, H. Iwasaki, D.F. Shen, T. Numata and S. Nakamura, 1981, Jpn. J. Appl. Phys. **20**, L757–760.

Shenoy, G.K. and F.E. Wagner, 1978, Mössbauer Isomer Shifts (North-Holland, Amsterdam).

Sherrington, D. and S. Kirkpatrick, 1975, Phys. Rev. Lett. **35**, 1792–1795.

Shiau, Y., J. Bridges and G.J. Sellers, 1978, Proc. IEEE Int. Symp. on Electromagnetic Compatibility, p. 155.

Shiiki, K., S. Otomo and M. Kudo, 1981, J. Appl. Phys. **52**, 2483.

Shingu, P.H., K. Shimomura, K. Kobayashi and R. Ozaki, 1976, in: Rapidly Quenched Metals I, eds. N.J. Grant and B.C. Giessen (MIT Press, Cambridge, MA) p. 45–50.

Shirakawa, T., Y. Nakajima, K. Okamoto, S. Matsushita and Y. Sakurai, 1976, AIP Conf. Proc. **34**, 349.

Shirakawa, K., S. Ohnuma, M. Nose and T. Masumoto, 1980, IEEE Trans. Magn. **MAG-16**, 910–912.

Shirakawa, K., T. Kaneko, M. Nose, S. Ohnuma, T. Fujimori and T. Masumoto, 1981a, J. Appl. Phys. **52**, 1829–1831.

Shirakawa, K., S. Ohnuma, T. Kaneko, T. Masumoto and J. Kanehira, 1981b, J. Appl. Phys. **52**, 2264–2265.

Shull, W.H. and D.G. Naugle, 1977, Phys. Rev. Lett. **39**, 1580–1583.

Shull, W.H., D.G. Naugle, S.J. Poon and W.L. Johnson, 1978, Phys. Rev. B **18**, 3263–3270.

Simpson, A.W. and D.R. Brambley, 1971, Phys. Stat. Sol. (b) **43**, 291.

Sinha, A.K., 1970, Phys. Rev. B**1**, 4541.

Slechta, J., 1975, Phys. Stat. Sol. (b) **67**, 595.

Smit, J., 1958, Physica **24**, 39.

Smit, J., 1973, Phys. Rev. B **8**, 2349–2350.

Smith, C.H., 1982, IEEE Trans. Magn. **MAG-18**, 1376–1383.

Sommer, F., G. Bucher and B. Predel, 1980, J. Physique **41**, C8-563–567.

Sommer, F., M. Fripan and B. Predel, 1982a, in: Rapidly Quenched Metals IV, eds. T. Masumoto and K. Suzuki (Japan Inst. of Metals, Sendai) pp. 209–212.

Sommer, F., W. Vogelbein and B. Predel, 1982b, J. Non-Cryst. Solids **51**, 333–343.

Soohoo, R.F. and A.H. Morrish, 1979, J. Appl. Phys. **50**, 1639–1641.

Souletie, J. and R. Tournier, 1969, J. Low Temp. Phys. **1**, 95.

Spit, F.H.M., J.W. Drijver, W.C. Turkenburg and S. Radelaar, 1980, J. Physique **41**, C8-890–893.

Stern, E.A., 1974, Phys. Rev. B **10**, 3027.

Stern, E.A., D.E. Sayers and F.W. Lytle, 1975, Phys. Rev. B **11**, 4836.

Stern, E.A., S. Rinaldi, E. Callen, S. Heald and B. Bunker, 1978, J. Magn. Magn. Mater. **7**, 188–189.

Stobiecki, F., H. Hoffmann and W. Pamler, 1980, IEEE Trans. Magn. **MAG-16**, 1206–1208.

Stocton, M., E.L. Neau and J.P. VanDevender, 1982, J. Appl. Phys. **53**, 2765.

Suran, G., R. Krishnan, H. Jouve and R. Meyer, 1977, IEEE Trans. Magn. **MAG-13**, 1532–1533.

Suzuki, T., 1983, J. Magn. Magn. Mater. **35**, 232–234.

Suzuki, K., 1982, in: Rapidly Quenched Metals IV, eds. T. Masumoto and K. Suzuki (Japan Inst. of Metals, Sendai) pp. 309–314.

Suzuki, K., 1983, J. Less-Common Metals **89**, 183–195.

Takagi, H., S. Tsunashima, S. Uchiyama and T. Fujii, 1979, J. Appl. Phys. **50**, 1642–1644.

Takayama, S., 1976, J. Mater. Sci. **11**, 164.

Tanaka, F. and N. Imamura, 1983, J. Magn. Magn. Mater. **35**, 173–175.

Tanaka, T., M. Yoshida, S. Takahashi and A. Tasaki, 1982, Jpn. J. Appl. Phys. **21**, L619–620.

Tao, L.J., R.J. Gambino, S. Kirkpatrick, J.J. Cuomo and H. Lilienthal, 1974, AIP Conf. Proc. **18**, 641–645.

Taub, A.I. and F. Spaepen, 1980, Acta Metall. **28**, 1781.

Taylor, R.C. and A. Gangulee, 1976, J. Appl. Phys. **47**, 4666–4668.

Taylor, R.C. and A. Gangulee, 1977, J. Appl. Phys. **48**, 358–361.

Taylor, R.C. and A. Gangulee, 1980, Phys. Rev. (B) **22**, 1320–1326.

Taylor, R.C. and A. Gangulee, 1982, J. Appl. Phys. **53**, 2341–2343.

Taylor, R.C., T.R. McGuire, J.M.D. Coey and A. Gangulee, 1978, J. Appl. Phys., **49**, 2885–2893.

Taylor, R.H., 1975, Adv. Phys. **24**, 681–758.

Tenhover, M., 1981a, J. Phys. F **11**, 2697–2706.

Tenhover, M., 1981b, J. Phys. Chem. Solids **42**, 329–332.

Tenhover, M., B.M. Clemens and P. Duwez, 1982, J. Phys. F **12**, L167–171.

Terzieff, P. and K. Lee, 1979, J. Appl. Phys. **50**, 3565–3569.

Thiele, A.A., 1970, J. Appl. Phys. **41**, 1139–1145.

Tissier, B., R. Ruder and J.M.D. Coey, 1980, J. Magn. Magn. Mater. **15–18**, 1393–1396.

Togami, Y., 1981, U.S. Patent No. 4,293,621.

Togami, Y., 1982, IEEE Trans. Magn. **MAG-18**, 1233–1237.

Togami, Y. and K. Kobayashi, 1981, Jpn. J. Appl. Phys. **20**, 1457–1465.

Togami, Y., K. Kobayashi and I. Yanagida, 1980, Jpn. J. Appl. Phys. **19**, 1663–1665.

Togami, Y., K. Kobayashi, M. Kajiura, K. Sato and T. Teranishi, 1982, J. Appl. Phys. **53**, 2335–2337.

Togami, Y., T. Tamaki, K. Sato and A. Yoshihara, 1983, J. Magn. Magn. Mater. 131–34, 1497–1498.

Tsuei, C.C., 1978, Solid State Commun. 27, 691.

Tsuei, C.C. and P. Duwez, 1966, J. Appl. Phys. 37, 435.

Tsujimoto, H., D.F. Shen, S. Matsushita and Y. Sakurai, 1980, IEEE Trans. Magn. **MAG-16**, 1209–1211.

Tsujimoto, H., M. Shouji, A. Saito, S. Matsushita and Y. Sakurai, 1983, J. Magn. Magn. Mater. **35**, 199–201.

Tsunashima, S., T. Shinoda, H. Miijatake and S. Uchiyama, 1980, J. Appl. Phys. **51**, 5901–5905.

Tsunashima, S., H. Tsuji, T. Kobayashi and S. Uchiyama, 1981, IEEE Trans. Magn. **MAG-17**, 2840–2842.

Tsunashima, S., S. Masui, T. Kobayashi and S. Uchiyama, 1983, J. Appl. Phys. **53**, 8175–8178.

Tsushima, T., K. Kawanishi, A. Ito, H. Uekusa and K. Tarusawa, 1982, in: Rapidly Quenched Metals IV, eds. T. Masumoto and K. Suzuki (Japan Inst. of Metals, Sendai) pp. 873–876.

Turnbull, D., 1962, J. Phys. Chem. **64**, 609.

Turnbull, D., 1969, Contemp. Phys. 10, 473–488.

Uhlman, D.R., 1972, J. Non-Cryst. Solids 7, 337.

Uhlman, D.R., J.F. Hays and D. Turnbull, 1966, Phys. Chem. Glasses 7, 159.

Uhlman, D.R., 1971, J. Non-Cryst. Solids 7, 337–348.

Urner-Wille, M., T.S. Te Velde and P.G. Van Engen, 1978, Phys. Stat. Sol. (a) **50**, K29.

Urner-Wille, M., P. Hansen and K. Witter, 1980, IEEE Trans. Magn. **MAG-16**, 1188.

Urner-Wille, M., R. Kobs and K. Witter, 1981, Trans. Magn. **MAG-17**, 2621–2623.

Valenkov, N. and E. Porai-Koshits, 1973, Z. Kristallogr. **95**, 195.

Van der Kraan, A.M. and K.H.J. Buschow, 1982, Phys. Rev. B **25**, 3311–3319.

Van der Kraan, A.M. and K.H.J. Buschow, 1983, Phys. Rev. B **27**, 2693–2697.

Van Devender, J.P. and R.A. Reber, 1981, Proc. 3rd IEEE Int. Pulsed Power Conf., Albuquerque, NM, p. 256.

Van Engen, P.G., K.H.J. Buschow and R. Jongebreur, 1983, unpublished results.

Vannimenus, J. and G. Toulouse, 1977, J. Phys. C **10**, L2537–2541.

Varley, J.H., 1959, The Physical Chemistry of Metallic Solutions and Intermetallic Compounds (Her Majesty's Stationary Office, London).

Viccaro, P.J., G.K. Shenoy, B.D. Dunlap, D.G. Westlake, S.K. Malik and W.E. Wallace, 1979, J. Physique **40**, C2-157.

Vincze, I., M.C. Cadeville, R. Jesser and L. Takacs, 1974, J. Physique **35**, C6-533.

Visnovsky, S., B. Knappe, V. Prosser and H.R. Müller, 1976, Phys. State. Sol. (a) **38**, K53–56.

Vittoria, C., P. Lubitz and V. Ritz, 1978, J. Appl. Phys. **49**, 4908–4917.

Von Molnar, S., C.N. Guy, R.J. Gambino and T.R. McGuire, 1980, J. Magn. Magn. Mater. **15–18**, 1391–1392.

Von Molnar, S., R.J. Gambino and J.M.D. Coey, 1981, J. Appl. Phys. **52**, 2123–2125.

Von Molnar, S., B. Barbara, T.R. McGuire and R.J. Gambino, 1982a, J. Appl. Phys. **53**, 2350–2352.

Von Molnar, S., T.R. McGuire, R.J. Gambino and B. Barbara, 1982b, J. Appl. Phys. **53**, 7666–7671.

Vossen, J.L. and W. Kern, 1978, Thin Film Processes (Academic, New York).

Wagner, C.N.J., N. Heiman, T.C. Huang, A. Onton and W. Parrish, 1975, AIP Conf. Proc. **29**, 188–189.

Walter, J.L., 1978, in: Rapidly Quenched Metals III, Vol. 1, ed. B. Cantor (Chameleon, London) p. 30.

Wang, R., and M.D. Merz, 1976, Nature **35**, 260.

Wang, R., M.D. Merz, J.M. Brimhall and S.D. Dahlgren, 1978, in: Rapidly Quenched Metals, Vol. 1, ed. B. Cantor (Chameleon, London) p. 420.

Wang, W.K., H. Iwasaki, C. Suryanarayana, T. Masumoto, K. Fukamichi, Y. Syono and T. Goto, 1982, in: Rapidly Quenched Metals IV, eds. T. Masumoto and K. Suzuki (Japan Inst. of Metals, Sendai) pp. 663–666.

Wang, Y.J., F.H. Li, Zh.Q. Wang and J.J. Gao, 1979, J. Physique **40**, C5-239–242.

Wangness, R.K., 1956, Am. J. Phys. **24**, 60.

Warlimont, H., 1980, Phys. in Technol. **11**, 28.

Waseda, Y. and S. Tamaki, 1976, Z. Phys. B **23**, 315–319.

Watson, R.E., and L.H. Bennett, 1977, Phys. Rev. B **15**, 5136–5142.

Weissenberger, V., B. Elschner and K.H.J. Buschow, 1984, J. Magn. Magn. Mater.

Williams, A., 1982, Solid State Commun. **44**, 983–986.

Williams, A.R., V.L. Moruzzi, C.D. Gelatt and J. Kübler, 1983, J. Magn. Magn. Mater. **31–34**, 88–95.

Wong, J., 1981, in: Glassy Metals, eds. H.J. Güntherodt and H. Beck (Springer, Berlin) pp. 45–77.

Yamauchi, K. and Y. Nakagawa, 1971, Jpn. J. Appl. Phys. **10**, 1730.

Yasugi, S., S. Honda, M. Ohkoshi and T. Kusuda, 1981, J. Appl. Phys. **52**, 2298–2300.

Ziman, J.M., 1961, Phil. Mag. **6**, 1013.

Zolotukhin, I.V., I.N. Panteleyev and V.Ye., Miloshenko, 1980, Phys. Met. Metall. **50**, 165–167.

Van den Nieuwenhuizen, H.C.M. and K.H.J. Buschow, 1982, High Temp. Sci. **15**, 301.

Chapter 53

ORGANOMETALLIC COMPOUNDS OF THE RARE EARTHS

Herbert SCHUMANN and Wolfgang GENTHE
Institut für Anorganische und Analytische Chemie, Technische Universität Berlin, D-1000 Berlin 12, Fed. Rep. Germany

Contents

Symbols and abbreviations

Bu	$= C_4H_9$	dec.	= decomposition point
C_5Me_5	$= (CH_3)_5C_5$	J	= coupling constant
COT	$= C_8H_8$	m	= multiplet signal
Cp	$= C_5H_5$	m.p.	= melting point
DME	= dimethoxyethane	qu	= quartet signal
Et	$= C_2H_5$	s	= singlet signal
Ind	= indenyl	subl.	= sublimation point
Me	$= CH_3$	t	= triplet signal
MeCp	$= CH_3C_5H_4$	$\varnothing$	= center of a ring
Ph	$= C_6H_5$	β	= CH ring deformation vibration
py	= pyridine	γ	= CH ring deformation vibration
THF	= tetrahydrofuran	δ	= chemical shift
tmed	= tetramethylethylenediamine	ν	= infrared stretching vibration
TMS	$= Si(CH_3)_4$	η	= bonds to the metal
d	= doublet signal	ω	= ring deformation frequency
		ΔG	= activation energy

1. Introduction and history

A malodorous spontaneously inflammable liquid, which is formed from the pyrolysis of arsenous oxide with potassium acetate, was described as Cadet's Fuming Liquid in 1760 (Cadet de Gassicourt, 1760), marking the starting point of Organometallic Chemistry. It was not until 100 years later that Cahours and Rieche (1854) established the correct formula for this first compound having a covalent σ-bond between carbon and a metalloid, arsenic. The first genuine organometallic compound containing a metal–carbon σ-bond, ethyl zinc iodide, was prepared by Frankland (1849). This publication ignited the fascinating evolution of organometallic chemistry between 1850 and 1950. However, the only compounds that were characterized during this period were those that contained σ-bonds between carbon and certain metal atoms, specifically metals which contained completely empty or completely filled d-orbitals, main group elements or elements of the zinc group. The first example of a completely characterized organo–transition-metal complex was $C_6H_5Ti(OC_3H_7)_3 \cdot LiOC_3H_7 \cdot LiBr \cdot (C_2H_5)_2O$ prepared by Herman and Nelson (1952), although Zeise's Salt, $K[Pt(C_2H_4)Cl_3]$ was noted in the 19th century (Zeise, 1827).

In contrast to the σ-bonded organometallic compounds of the main group elements, all organometallic compounds of the transition metals containing metal-to-carbon σ-bonds are mostly thermal, air and moisture sensitive substances. This feature can be explained by the high reactivity of these compounds due to the incompletely filled d-orbitals. Whereas the main group metals form stable metal-to-carbon σ-bonds if the element has eight electrons available for bonding, the transition metals need eighteen electrons. This situation becomes even more complicated, when one goes from the transition metals to the lanthanides, which involve 4f-orbitals in their outer valence shells, creating sixteen outer orbitals that have to be occupied by thirty two electrons. Therefore problems in preparing organometallic compounds of the lanthanides are to be anticipated. Grosse (1925) postulated the nonexistence of alkyl or aryl derivatives of the lanthanides.

In this article the term organometallic compound includes alkyl and aryl derivatives of the rare earths—the transition metals of group III, scandium, yttrium, lanthanum and the lanthanides cerium to lutetium with covalent metal-to-carbon σ-bonds, as well as the so-called π-complexes with more than monohapto metal-to-carbon bonds, for example cyclopentadienyl and olefin complexes, metal acetylides, but not carbonyls, cyanides and isocyanide complexes. Derivatives of scandium, yttrium and lanthanum are included and discussed together with the compounds of the lanthanides, because of many similarities in the synthesis and the chemistry of these organometallic derivatives of the rare earths.

The common oxidation state of the rare earth elements is $+3$. Therefore organometallic compounds of the type RL_3 (R = rare earth metal, L = ligand) will be diamagnetic for R = Sc, Y, La and Lu, but paramagnetic for the other lanthanides. The redox properties of some of the lanthanides, reflecting the electronic situation with an unfilled, half-filled, or completely filled f shell make the existence of organometallic compounds with the lanthanides in the oxidation state $+2$ and $+4$ possible, namely EuL_2, YbL_2, and CeL_4.

The rare earths are rather electropositive elements and are hard acids following the Pearson concept (Pearson, 1973). This causes, in combination with the contracted nature of the 4f-orbitals of the lanthanides, poor overlap with ligand orbitals and therefore high ionic character in the metal-to-carbon bonds. Large ionic radii especially of the lanthanide ions give rise to organometallic compounds in which the metals have higher coordination numbers than normally found with transition metals. Because of the lanthanide contraction, lanthanum has the largest ionic radius of 1.061 Å for La^{3+}, lutetium has the smallest of the 0.848 Å for Lu^{3+} (see table 1; Templeton and Dauben, 1954).

The first indications of the existence of an organometallic compound of the rare earths was the work of Rice and Rice (1935). Using the Paneth technique, free radicals were reacted with a variety of metals, including lanthanum. But no mention was made of the isolation or identification of any of these alkyl lanthanum species. Three years later, Plets (1938) described the first organometallic compounds of the rare earths. Triethyl scandium and triethyl yttrium etherates were prepared from $ScCl_3$ and YCl_3 by their reaction with ethyl magnesium bromide. However this work is questionable, since it could not be repeated by other scientists (Jones, 1942; Gilman and Jones, 1945; Afanasev and Tsyganova, 1948). In connection with the Manhattan Project Gilman and Jones (1945) described the next attempts to prepare organometallic compounds of the lanthanides. They found biphenyl was produced either from the reactions of $LaCl_3$ with LiC_6H_5 in ether, or from lanthanum with diphenyl mercury at 135°C in a sealed tube for 100 days.

The discovery of ferrocene and of the other sandwich complexes initiated a new field of organometallic chemistry, the chemistry of the π-complexes. Wilkinson and Birmingham (1954) prepared the first organometallic π-complexes of the rare earths, the tricyclopentadienyl complexes of Sc, Y, La, Ce, Pr, Nd, Sm and Gd. It was not until 14 years later with the synthesis of triphenyl scandium (Hart and Saran, 1968) that the first σ-bonded aryl–rare-earth compound was made.

Organometallic chemistry of the rare earths has become an area of vigorous activity in the last decade. This area of organometallic chemistry, which was ignored

TABLE 1
Crystal radii of the rare earth ions R^{3+} in Å.

Sc^{3+}	0.68 [a]	Gd^{3+}	0.938 [b]
Y^{3+}	0.88 [a]	Tb^{3+}	0.923 [b]
La^{3+}	1.061 [b]	Dy^{3+}	0.908 [b]
Ce^{3+}	1.034 [b]	Ho^{3+}	0.894 [b]
Pr^{3+}	1.013 [b]	Er^{3+}	0.881 [b]
Nd^{3+}	0.995 [b]	Tm^{3+}	0.869 [b]
Pm^{3+}	0.979 [c]	Yb^{3+}	0.858 [b]
Sm^{3+}	0.964 [b]	Lu^{3+}	0.848
Eu^{3+}	0.950 [b]		

[a] Zachariasen (1954).
[b] Templeton and Dauben (1954).
[c] Estimated.

for a long time, is very promising from the theoretical viewpoint as well as from their use as reagents or catalysts in synthetic chemistry. A number of review articles covering this area of chemistry appeared in recent years (Gysling and Tsutsui, 1970; Hayes and Thomas, 1971; Kanellakopulos and Bagnall, 1972; Tsutsui et al., 1976; S.A. Cotton, 1977; Marks, 1978a; Schumann, 1979a, b; Marks and Ernst, 1982). Since 1964 there is an annual survey available, covering the literature in the field of organometallic chemistry of the rare earths and of the actinides (Seyferth and King, 1965, 1966, 1967; Calderazzo, 1968, 1969, 1970, 1972, 1973, 1974; Marks, 1974, 1975, 1976, 1977, 1978b, 1979, 1980, 1982). An excellent article containing all the knowledge on organometallic compounds of the rare earths with a literature closing date of the end of 1981 but with many references from recent publications including conference reports appeared in the Gmelin Handbook of Inorganic Chemistry (Forsberg and Moeller, 1983).

2. Organometallic compounds of the rare earths in the oxidation state +3

2.1. Organometallic compounds of the rare earths containing only π-ligands

2.1.1. Cyclopentadienyl complexes Cp_3R, Cp_2RX, $CpRX_2$

The tris(cyclopentadienyl) complexes of the rare earths were the first compounds discovered and the most intensively investigated class of organometallic compounds of these elements. They were reported for the first time in 1954 by Wilkinson and Birmingham, and generally prepared by reaction of anhydrous rare earth trichlorides with sodium cyclopentadienide in tetrahydrofuran at room temperature and isolated by sublimation of the crude products in vacuum at about 220°C (Wilkinson and Birmingham, 1954; Krasnova et al., 1971):

$$RCl_3 + 3\,NaC_5H_5 \xrightarrow{\text{THF}} (C_5H_5)_3R \cdot THF + 3\,NaCl, \tag{1}$$

$$(C_5H_5)_3R \cdot THF \xrightarrow[10^{-3}\,\text{torr}]{220°C} (C_5H_5)_3R + THF. \tag{2}$$
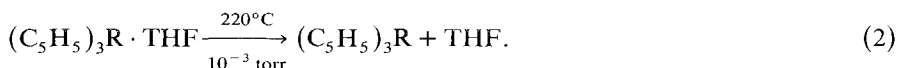
To prepare the radioactive $(C_5H_5)_3Pm$ another method was developed, using molten $Mg(C_5H_5)_2$ or molten $Be(C_5H_5)_2$ as solvents and cyclopentadienide precursor, to avoid the problems of α-radiolysis of the solvent (Kopunec et al., 1969; Lauberau and Burns, 1970). The high vapor pressure of these starting materials allows easy removal of them from the reaction mixture. The same method, using rare earth trifluorides and triiodides was also used for the synthesis of the tricyclopentadienides of scandium, cerium, samarium and neodymium (Reid and Wailes, 1966; Atwood and Smith, 1973a), and the promethium compound has also been prepared by neutron bombardment of the neodymium complex (Baumgärtner et al., 1967).

$$2\,PmCl_3 + 3\,Mg(C_5H_5)_2 \rightarrow 2\,(C_5H_5)_3Pm + 3\,MgCl_2, \tag{3}$$

$$^{150}Nd(C_5H_5)_3 \xrightarrow{(n,\,\gamma)} {}^{151}Nd(C_5H_5)_3 \xrightarrow{\beta^-} {}^{151}Pm(C_5H_5)_3. \tag{4}$$
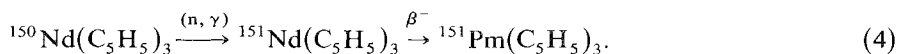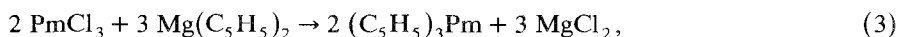
Another method available for the synthesis of such derivatives is the reaction of the rare earth trichlorides with KC_5H_5 or TlC_5H_5 in benzene (E.O. Fischer and H. Fischer, 1965b; Manzer, 1976a). This method allows the synthesis of tris(cyclopentadienyl) europium, which could not be prepared by the reaction in tetrahydrofurane, because of the decomposition of $(C_5H_5)_3Eu \cdot THF$ during sublimation:

$$RCl_3 + 3 \, KC_5H_5 \xrightarrow{\text{benzene}} (C_5H_5)_3R + 3 \, KCl. \tag{5}$$
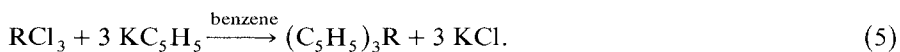
The synthesis of $(C_5H_5)_3Eu$ has also been described by Tsutsui et al. (1966) by the reaction of $CpEuCl_2 \cdot (THF)_3$ and NaCp followed by careful removal of THF.

The tris(cyclopentadienyl) compounds of the rare earths have high thermal stability and a definite melting point. They are sensitive to moisture and air, and hydrolyze forming the rare earth hydroxides and cyclopentadiene. The reactions with alcohols are similar giving rare earth alkoxides (Maginn et al., 1963). The magnetic moments, which are nearly identical with the R^{3+} ions in aqueous solution, as well as the reaction of the complexes with $FeCl_2$, yielding ferrocene, speak for a high degree of ionic character in the rare-earth-to-cyclopentadienyl bond (Birmingham and Wilkinson, 1956).

The rare earth tricyclopentadienyls are insoluble in aliphatic hydrocarbons, and only sparingly soluble in aromatic hydrocarbons. They dissolve in polar solvents like tetrahydrofuran with complexation. Similarly, numerous bases like ethers, amines, isonitriles, phosphines and other compounds react with Cp_3R, yielding stable 1:1 complexes.

The solubility of the compounds Cp_3R in tetrahydrofuran was studied between 15 and 60°C by Borisov et al. (1975). From the temperature dependence of the solubility the heat of dissolution was determined to be about 5 kcal/mole for all of the tris(cyclopentadienyl) compounds of the rare earths.

The vapor pressure and the temperature of the triple point of the tricyclopentadienyls of the rare earth elements Y, La, Ce, Pr, Nd, Sm, Gd, Tb, Dy, Ho, Er, Tm, Yb and Lu have been measured in the temperature range of 195 to 390°C and the heats of sublimation were calculated from the temperature variation of the vapor pressure (Borisov et al., 1973; Duncan and Thomas, 1964; Haug, 1971; Devyatykh et al., 1972, 1973a). The volatility increases with increasing atomic number, the sublimation temperature decreases. The enthalpy of combustion and formation as well as the mean dissociation energies of the cyclopentadienyl–metal bonds have been measured for the $(C_5H_5)_3R$ compounds of Sc, Y, La, Pr, Tm and Yb, showing a decrease of the bond energy with increasing atomic number (Devyatykh et al., 1974b). The colors and some physical properties of the rare earth tricyclopentadienides are given in table 2.

Tricyclopentadienyl rare earth compounds form stable 1:1 adducts with many bases. THF adducts have been described for yttrium, lanthanum and nearly all lanthanides (Manastyrskyj and Dubeck, 1964; Calderazzo et al., 1966; E.O. Fischer and H. Fischer, 1966; R.D. Fischer and H. Fischer, 1967; Pappalardo, 1969; Raymond and Eigenbrodt, 1980; Rogers et al., 1981; Deacon et al., 1982). Tetrahydrofuran can be removed in high vacuum from all the complexes except for

TABLE 2

Physical properties of rare earth tricyclopentadienides.

Compound	Color	Melting point (°C)	μ_{eff} (B.M.)	Refs.
$(C_5H_5)_3Sc$	straw	240	diamag.	1
$(C_5H_5)_3Y$	pale yellow	295	diamag.	1
$(C_5H_5)_3La$	colorless	395	diamag.	1
$(C_5H_5)_3Ce$	orange	435	2.46	2
			2.30	6
$(C_5H_5)_3Pr$	pale green	415	3.61	2
$(C_5H_5)_3Nd$	reddish blue	380	3.62	2
$(C_5H_5)_3Pm$	yellow-orange			3
$(C_5H_5)_3Sm$	orange	365	1.54	2
$(C_5H_5)_3Eu$	brown			4
$(C_5H_5)_3Gd$	pale yellow	350	7.98	2
$(C_5H_5)_3Tb$	colorless	316	8.9	5
$(C_5H_5)_3Dy$	yellow	302	10.0	2
$(C_5H_5)_3Ho$	yellow	295	10.2	5
$(C_5H_5)_3Er$	pink	285	9.44	2
$(C_5H_5)_3Tm$	green-yellow	278	7.1	5
$(C_5H_5)_3Yb$	dark green	273	4.00	2
$(C_5H_5)_3Lu$	colorless	264	diamag.	5

1. Wilkinson and Birmingham (1954).
2. Birmingham and Wilkinson (1956).
3. Lauberau and Burns (1970).
4. Tsutsui et al. (1966).
5. E.O. Fischer and H. Fischer (1965b).
6. Deacon et al. (1983c).

$(C_5H_5)_3Eu \cdot THF$. The THF complexes exhibit a bathochromic shift in their color because of the coordination of the oxygen to the rare earth metal. Tetrahydrofurane adducts with 2 and 3 THF coordinated to the tricyclopentadienyl lanthanide complex are also known (Suleimanov et al., 1982c).

Tricyclopentadienyl rare earth cyclohexyl isonitrile complexes have been prepared by addition of cyclohexyl isonitrile to the corresponding tris(cyclopentadienyl) rare earth compounds in benzene. They show definite melting points and are sublimable in vacuum at about 150 to 160°C (E.O. Fischer and H. Fischer, 1965a, 1966; Von Ammon and Kanellakopulos, 1972):

$$(C_5H_5)_3R + C_6H_{11}NC \rightarrow (C_5H_5)_3R-CNC_6H_{11}, \tag{6}$$
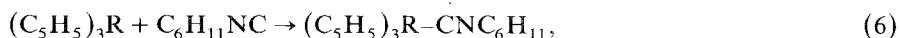
R = Y, La, Ce, Pr, Nd, Sm, Eu, Gd, Tb, Dy, Ho, Er, Tm, Yb, Lu.

Tricyclopentadienyl ytterbium reacts with liquid ammonia with formation of a stable 1:1 complex, which can be sublimed, but which decomposes above 200°C with formation of dicyclopentadienyl ytterbium amide and cyclopentadiene (E.O. Fischer and H. Fischer, 1966). The corresponding 1:1 adducts of NH_3 could also be isolated for $(C_5H_5)_3Pr$ and $(C_5H_5)_3Sm$ (Birmingham and Wilkinson, 1956), as well

as 1:1 complexes of several rare earth tricyclopentadienyls with pyridine (R.D. Fischer and H. Fischer, 1965), methylpyrrolidone (Von Ammon et al., 1969), nicotine (Von Ammon et al., 1969), hydrazine (Hayes and Thomas, 1969b), and pyrazine (Baker and Raymond, 1977).

Triphenylphosphine forms a stable adduct with tricyclopentadienyl ytterbium (E.O. Fischer and H. Fischer, 1966), and also tributylphosphine gives an analogous 1:1 complex with the same lanthanide complex (R.D. Fischer and Bielang, 1980b); however, attempts to prepare such complexes of tricyclopentadienyl ytterbium with PPh_2H, $PPhH_2$, $P(C_6H_{11})_3$, $P(C_6H_{11})_2H$, $P(C_6H_{11})H_2$, PMe_2Ph, $P(t-Bu)_2Cl$, as well as with some isonitriles like CH_3NC, C_6H_4NC, $4\text{-}MeC_6H_4NC$, and $4\text{-}ClC_6H_4NC$ yielded only solutions of these adducts in pentane or toluene, which decomposed during the evaporation of the solvents (Bielang and Fischer, 1978).

Tricyclopentadienyl ytterbium reacts with tricyclopentadienyl uranium fluoride in benzene with formation of an adduct with a fluorine bridge between ytterbium and uranium. Tricyclopentadienyl thulium does not give an analogous complex with Cp_3UF. These reactions are unique to the uranium–fluorine bond for Cp_3UCl fails to give an adduct with Cp_3Yb (Kanellakopulos et al., 1970).

The Lewis acidity of tricyclopentadienyl rare earth compounds was investigated by reactions with some transition-metal carbonyl and nitrosyl complexes. Infrared spectra showed coordination only between $CrCp(NO)_2Cl$ and Cp_3Er or Cp_3Yb, and in the case of $(MeCp)_3Sm$ only with a large excess of the base. Spectral changes in the infrared and ^1H NMR spectra of $MnCp(CO)_3$, $MCp(CO)_2NO$ with M = Cr, Mo, W, $Co_2(CO)_8$ and $[NiCp(CO)]_2$ in the presence of some tricyclopentadienyl rare earth complexes indicate coordination at both the CO and the NO ligands, with stronger Lewis basicity for NO and the bridging CO groups in comparison with the terminal CO groups. However, Cp_2YbCl and $(MeCp)_2YbCl$ gave no coordination with the nitrosyl or with the carbonyl complexes already described (Crease and Legzdins, 1972, 1973b). The interaction of Cp_3Sm with a number of anions $[Mn(CO)_{5-n}L_n]^-$ also causes a shift of the νCO upon coordination. Infrared and ^1H NMR measurements indicate that the oxygen atom functions as the Lewis base in complexes with $[Mn(CO)_{5-n}L_n]Br$, while the manganese atom was the site of basicity in anions of the type $[Mn(CO)_{5-n}\{P(OPh)_3\}_n]^-$ (Onaka and Furuchi, 1979). IR spectra of the reaction mixtures of Cp_3Sm and $CrCp(CO)_2NO$, $(FeCpNO)_2$, $[CrCp(NO)_2]_2$, $[Mn(MeCp)]_3(NO)_4$ and $[(MeCp)Mn(CO)NO]_2$ displayed bands diagnostic of Cp_3Sm coordinated to terminal, two-metal bridging, and three-metal bridging NO (Onaka, 1980).

Rare earth tricyclopentadienides like Cp_3Yb react with a number of protic acids like β-diketones, β-ketoimines, alkynes, indene and fluorine with formation of unstable complexes and in some cases of definite products (see sections 2.3 and 2.7.1) (R.D. Fischer and Bielang, 1980b).

The isolated complexes of tricyclopentadienyl rare earth compounds are shown in table 3.

Dicyclopentadienyl rare earth chlorides can be prepared by treating the rare earth trichlorides with two equivalents of cyclopentadienyl sodium or with its respective tricyclopentadienyl derivative in tetrahydrofuran (Maginn et al., 1963; Schumann

TABLE 3

Complexes of tricyclopentadienyl rare earth compounds.

Complex	Color	Other data	Refs.
$Cp_3Y \cdot (THF)$	white	subl. $160-180°C/10^{-3}$	1
$Cp_3La \cdot (THF)$	white	subl. $260°C/10^{-3}$	1
$Cp_3Pr \cdot (THF)$			2
$Cp_3Nd \cdot (THF)$			3
$Cp_3Sm \cdot (THF)$			3
$Cp_3Eu \cdot (THF)$	brown		4
$Cp_3Gd \cdot (THF)$			5
$Cp_3Tb \cdot (THF)$	dark green		6
		luminescence spectra	18
$Cp_3Ho \cdot (THF)$			6
$Cp_3Er \cdot (THF)$			2
$Cp_3Tm \cdot (THF)$			7
$Cp_3Yb \cdot (THF)$	green	m.p. $223-226°C$	8
		UV	19
$Cp_3Pr \cdot (NH_3)$			9
$Cp_3Sm \cdot (NH_3)$			9
$Cp_3Yb \cdot (NH_3)$	green	m.p. $345-351°C$	8
$Cp_3Yb \cdot (C_5H_5N)$			10
$Cp_3Yb_2 \cdot (N_2H_4)$			11
$Cp_3Nd \cdot (MeNC_4H_8)$			12
$(Cp_3Yb)_2 \cdot (C_4H_4N_2)$	green-brown	μ_{eff} 3.48 B.M.	13
$Cp_3Pr \cdot [(-)\text{-nicotine}]$			12
$Cp_3Nd \cdot [(-)\text{-nicotine}]$			12
$Cp_3Tm \cdot [(-)\text{-nicotine}]$			12
$Cp_3Yb \cdot PBu_3$			14
$Cp_3Yb \cdot P(t\text{-}Bu)_2Cl$			15
$Cp_3Yb \cdot P(C_6H_{11})_3$			15
$Cp_3Yb \cdot PH(C_6H_{11})_2$			15
$Cp_3Yb \cdot PH_2(C_6H_{11})$			15
$Cp_3Yb \cdot PPh_3$	black	m.p. $185°C$	6
$Cp_3Yb \cdot PHPh_2$			15
$Cp_3Yb \cdot PH_2Ph$	green		15
$Cp_3Yb \cdot PMe_2Ph$			15
$Cp_3YbCNMe$			15
$Cp_3YbCNPh$			15
$Cp_3YbCNC_6H_4-4-Cl$			15
$Cp_3YCNC_6H_{11}$		m.p. $163°C$	16
$Cp_3LaCNC_6H_{11}$		m.p. $110°C$	16
$Cp_3CeCNC_6H_{11}$		m.p. $134°C$	16
$Cp_3PrCNC_6H_{11}$	green		16
$Cp_3NdCNC_6H_{11}$	violet	m.p. $147°C$, μ_{eff} 3.4 B.M.	6,16
$Cp_3SmCNC_6H_{11}$		m.p. $148°C$	16
$Cp_3EuCNC_6H_{11}$		m.p. $150°C$	16
$Cp_3GdCNC_6H_{11}$		m.p. $200°C$	16
$Cp_3TbCNC_6H_{11}$	colorless	m.p. $162°C$, μ_{eff} 10.1 B.M.	6,16
$Cp_3DyCNC_6H_{11}$		m.p. $163°$	16
$Cp_3HoCNC_6H_{11}$	yellow	m.p. $165°C$, μ_{eff} 10.6 B.M.	6,16
$Cp_3ErCNC_6H_{11}$		m.p. $168°C$	16
$Cp_3TmCNC_6H_{11}$		m.p. $162°C$	16

TABLE 3 (continued)

Complex	Color	Other data	Refs.
$Cp_3YbCNC_6H_{11}$	green	m.p. 167°C, μ_{eff} 4.4 B.M.	6,16
$Cp_3LuCNC_6H_{11}$		m.p. 170°C	16
$Cp_3YbFUCp_3$			17
$Cp_3Sm \cdot (THF)_2$		dec. 360°C	20
$Cp_3Eu \cdot (THF)_2$		dec. 270°C	20
$Cp_3Yb \cdot (THF)_2$		dec. 270°C	20
$Cp_3La \cdot (THF)_3$		dec. 370°C	20
$Cp_3Tm \cdot (THF)_3$		dec. 265°C	20
$Cp_3Yb \cdot NEt_3$		UV	19
$Cp_3Yb \cdot$ pyrrole		UV	19
$Cp_3Yb \cdot PEt_3$		UV	19
$Cp_3Yb \cdot \overline{SCH_2CH_2CH_2CH_2}$			19

1. Rogers et al. (1981).
2. R.D. Fischer and H. Fischer (1967).
3. Deacon et al. (1982).
4. Manastyrskyj and Dubeck (1964).
5. Rogers et al. (1980).
6. E.O. Fischer and H. Fischer (1966).
7. Pappalardo (1969).
8. Calderazzo et al. (1966).
9. Birmingham and Wilkinson (1956).
10. R.D. Fischer and H. Fischer (1965).
11. Hayes and Thomas (1969b).
12. Von Ammon et al. (1969).
13. Baker and Raymond (1977).
14. R.D. Fischer and Bielang (1980b).
15. Bielang and Fischer (1978).
16. Von Ammon and Kanellakopulos (1972).
17. Kanellakopulos et al. (1970)
18. Brittain et al. (1983).
19. Schlesener and Ellis (1983).
20. Suleimanov et al. (1982c).

and Jarosch, 1976; Holton et al., 1979b):

$$RCl_3 + 2 NaCp \xrightarrow{THF} Cp_2RCl + 2 NaCl, \tag{7}$$

R = Y, Sm, Gd, Tb, Dy, Ho, Er, Tm, Yb, Lu,

$$RCl_3 + 2 Cp_3R \xrightarrow{THF} 3 Cp_2RCl, \tag{8}$$

R = Sm, Gd, Dy, Ho, Er, Yb.
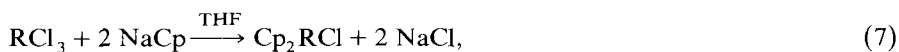
The scandium derivative has been prepared from $ScCl_3$ and magnesium cyclopentadienide (Coutts and Wailes, 1970), the samarium and ytterbium compounds could be made from the respective tricyclopentadienides by reaction with ammoniumchloride in benzene (Dornberger et al., 1978), and some dicyclopentadienyl rare earth chlorides can be prepared from the tricyclopentadienyl complexes by the reaction with HCl (Maginn et al., 1963):

$$ScCl_3 + Mg(C_5H_5)_2 \xrightarrow{THF} (C_5H_5)_2ScCl + MgCl_2, \tag{9}$$

$$(C_5H_5)_3R + NH_4Cl \xrightarrow{benzene} (C_5H_5)_2RCl + C_5H_6 + NH_3, \tag{10}$$

$$(C_5H_5)_3R + HCl \rightarrow (C_5H_5)_2RCl + C_5H_6. \tag{11}$$
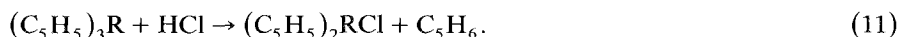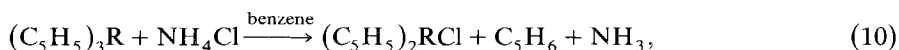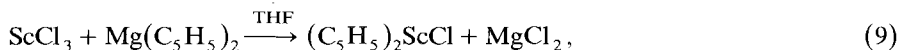
It has not been possible to prepare dicyclopentadienyl lanthanide chlorides of the lighter lanthanides. It is thought that the lighter lanthanides, which have larger ionic

radii, produce coordinately unsaturated complexes, which have not been isolated. Whereas the dicyclopentadienyl rare earth chlorides are dimers in the solid state and in benzene solution, the tetrahydrofuran adducts are monomers, as demonstrated with the Sc, Gd, Yb and Lu derivatives (Manzer, 1976a; Gomez-Beltran et al., 1975; Schumann and Genthe, 1981).

Solvent-free cyclopentadienyl rare earth dichlorides have not been prepared. Only the cyclopentadienyl lanthanide dichlorides coordinated by three tetrahydrofuran molecules of the heavier lanthanides could be isolated and some of their properties were investigated (Manastyrskyj et al., 1963; Ely and Tsutsui, 1975). The corresponding yttrium complex was mentioned in a paper by Jamerson et al. (1974), but no characterization of the compound was given. The preparation of the cyclopentadienyl rare earth dichloride complexes with 2 coordinated tetrahydrofuran ligands of Eu, with 3 THF ligands of La and TM and with 4 THF ligands of La, Sm, Eu, Tm, and Yb was also described in the meantime (Suleimanov et al., 1982c, d).

$$RCl_3 + NaC_5H_5 \xrightarrow{\text{THF}} C_5H_5RCl_2 \cdot (THF)_3 + NaCl, \tag{12}$$

$$R = Sm, Eu, Gd, Dy, Ho, Er, Yb, Lu,$$

$$(C_5H_5)_3Er + 2\,ErCl_3 \xrightarrow{\text{THF}} 3\,C_5H_5ErCl_2 \cdot (THF)_3, \tag{13}$$

$$(C_5H_5)_2YbCl + HCl \xrightarrow{\text{THF}} C_5H_5YbCl_2 \cdot (THF)_3 + C_5H_6. \tag{14}$$
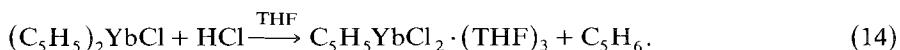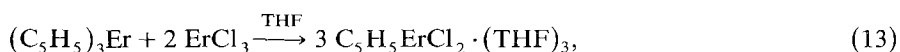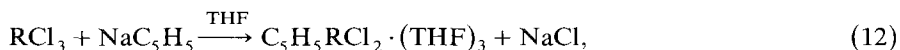
Iodine cleaves one erbium–cyclopentadienyl bond in tricyclopentadienyl erbium with formation of pink dicyclopentadienyl erbium iodide (Maginn et al., 1963), and the tricyclopentadienyl complexes of neodymium and ytterbium are cleaved by hydrogen cyanide with formation of the corresponding dicyclopentadienyl lanthanide cyanide (Kanellakopulos et al., 1974). The colors and some physical data of the cyclopentadienyl rare earth halides and cyanides are given in table 4.

The dimeric dicyclopentadienyl methyl yttrium complex reacts readily with methyl aluminum dichloride with loss of the methyl group and formation of a stable di-μ-chloro-bridged dicyclopentadienyl yttrium dimethyl aluminum complex (Holton et al., 1979c), and dicyclopentadienyl yttrium chloride reacts with aluminum hydride in ether with formation of a white crystalline 2 : 1 : 1 complex, of which the X-ray structure was determined (Lobkovskii et al., 1982):

$$(Cp_2YMe)_2 + (MeAlCl_2)_2 \rightarrow 2\,Cp_2Y{\begin{array}{c} Cl \\ < \quad > \\ Cl \end{array}}AlMe_2 + 2\,MeCl, \tag{15}$$

$$(Cp_2YCl)_2 + AlH_3 \xrightarrow{\text{ether}} (Cp_2YCl)_2 \cdot AlH_3 \cdot Et_2O. \tag{16}$$
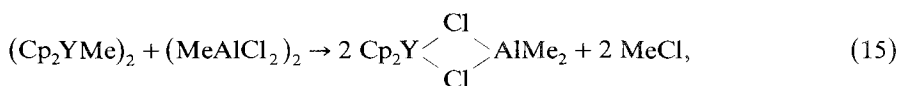
X-ray structures have been investigated of many cyclopentadienyl derivatives of the rare earths. Among the tricyclopentadienyl compounds, the structures of the Sc and the Sm derivative have been solved. The structure of Cp_3Sc, which is orthorhombic with space group $Pbc2_1$, is shown in fig. 1 (Atwood and Smith, 1973a). It shows four molecules in the unit cell with an infinite chain arrangement of the Cp_3Sc

TABLE 4

Physical properties of cyclopentadienyl rare earth halides.

Compound	Color	Other data		Refs.
Cp_2ScCl	green-yellow	m.p.	313–315°C	1
Cp_2YCl	colorless	subl.	250°C/10^{-3}	2
Cp_2SmCl	yellow	m.p.	200°C (dec.),	3
		μ_{eff}	1.62 B.M.	3
Cp_2GdCl	colorless	m.p.	140°C (dec.),	3
		μ_{eff}	8.86 B.M.	3
Cp_2TbCl		IR		14
Cp_2DyCl	yellow	m.p.	343–346°C,	3
		μ_{eff}	10.6 B.M.	3
Cp_2HoCl	yellow-orange	m.p.	340–343°C,	3
		μ_{eff}	10.3 B.M., IR	3,14
Cp_2ErCl	pink	m.p.	200°C (dec.),	3
		μ_{eff}	9.79 B.M.	3
		IR		14
Cp_2TmCl	green-yellow	subl.	200°C/10^{-4}	2
Cp_2YbCl	orange-red	m.p.	240°C (dec.),	3
		μ_{eff}	4.81 B.M.	3
		IR		14
Cp_2LuCl	white	m.p.	318–320°C	3
$Cp_2ScCl \cdot (THF)$	white	m.p.	303–307°C,	5
$Cp_2GdCl \cdot (THF)$		μ_{eff}	8.18 B.M.	6
$Cp_2YbCl \cdot (THF)$				6
$Cp_2LuCl \cdot (THF)$				7
$Cp_2Y(\mu\text{-}Cl)_2AlMe_2$				8
$(Cp_2YCl)_2 \cdot AlH_3 \cdot Et_2O$	white			9
$CpGdCl_2$				10
$CpYCl_2 \cdot (THF)_3$				11
$CpSmCl_2 \cdot (THF)_3$	beige	m.p.	50°C (dec.)	12
		dec.	50°C	16
$CpEuCl_2 \cdot (THF)_3$	purple	m.p.	50°C (dec.),	12
		μ_{eff}	4.24 B.M.	12
$CpGdCl_2 \cdot (THF)_3$	lavender	m.p.	82–86°C (dec.)	12
$CpDyCl_2 \cdot (THF)_3$	colorless	m.p.	85–90°C (dec.),	12
		μ_{eff}	11.81 B.M.	12
$CpHoCl_2 \cdot (THF)_3$	yellow	m.p.	84–92°C	12
$CpErCl_2 \cdot (THF)_3$	pink	m.p.	91–94°C,	12
		μ_{eff}	9.68 B.M.	12
$CpYbCl_2 \cdot (THF)_3$	orange	m.p.	78–81°C,	12
		μ_{eff}	7.52 B.M.	12
		dec.	70–72°C	16
$CpLuCl_2 \cdot (THF)_3$	colorless	m.p.	76–78°C	12
Cp_2ErI	pink	subl.	150–250°C/10^{-5}	3
Cp_2NdCN	blue			13
Cp_2YbCN	yellow			13
$[Cp_2YCl \cdot AlH_3 \cdot NEt_3]_2$	colorless			15
$CpLaCl_2 \cdot (THF)_3$		dec.	65°C	16
$CpLaCl_2 \cdot (THF)_4$				17
$CpSmCl_2 \cdot (THF)_4$				17
$CpEuCl_2 \cdot (THF)_2$		dec.	60°C	16

TABLE 4 (continued)

Compound	Color	Other data		Refs.
$CpEuCl_2 \cdot (THF)_4$				17
$CpTmCl_2 \cdot (THF)_3$		dec.	58–64°C	16
$CpTmCl_2 \cdot (THF)_4$		dec.	76–80°C	17
$CpYbCl_2 \cdot (THF)_4$				17

1. Coutts and Wailes (1970).
2. Holton et al. (1979b).
3. Maginn et al. (1963).
4. Schumann and Jarosch (1976).
5. Manzer (1976).
6. Gomez-Beltran et al. (1975).
7. Schumann and Genthe (1981).
8. Holton et al. (1979c).
9. Lobkovskii et al. (1982).

10. Dubois et al. (1977).
11. Jamerson et al. (1974).
12. Manastyrskyj et al. (1963).
13. Kanellakopulos et al. (1974).
14. Changtao Qian et al. (1983).
15. Lobkovskii et al. (1983).
16. Suleimanov et al. (1982c).
17. Suleimanov et al. (1982d).

units, in which each scandium is bound to two η^5-cyclopentadienyl ligands with an average scandium–carbon bond length of 2.49 Å and two bridging η^1-cyclopenta-dienyl ligands with an average Sc–C bond length of 2.57 Å. For the η^1-cyclopenta-dienyl groups, the angles of the Sc–C bonds with the plane of the rings are 61° and 73°.

For tricyclopentadienyl samarium Wong et al. (1969) describe an orthorhombic space group Pbcm with eight formula units per unit cell (fig. 2). However, this structure has been disputed by Atwood and Smith (1973a). But also this structure shows two symmetrically independent and structurally different groups of chains with samarium atoms surrounded by two η^5-bound cyclopentadienyl ligands and two η^1-bound cyclopentadienyls showing similar bonding distances. In addition to these two structures, the unit cell dimensions of the tricyclopentadienyl derivatives of Pr, Pm, Sm, Gd, Tb and Tm have been determined and compared with each other by
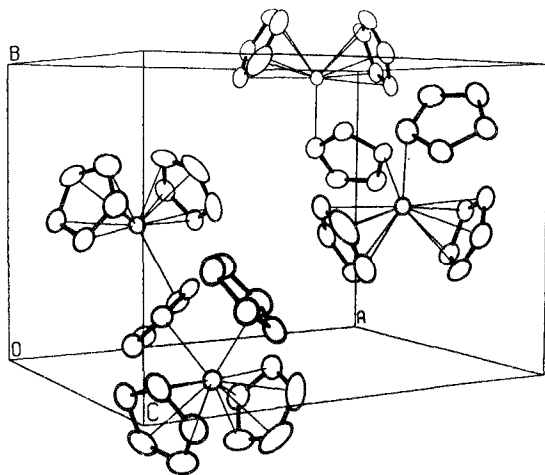
Fig. 1. Structure and unit cell packing of $Sc(C_5H_5)_3$ (after Atwood and Smith, 1973a).
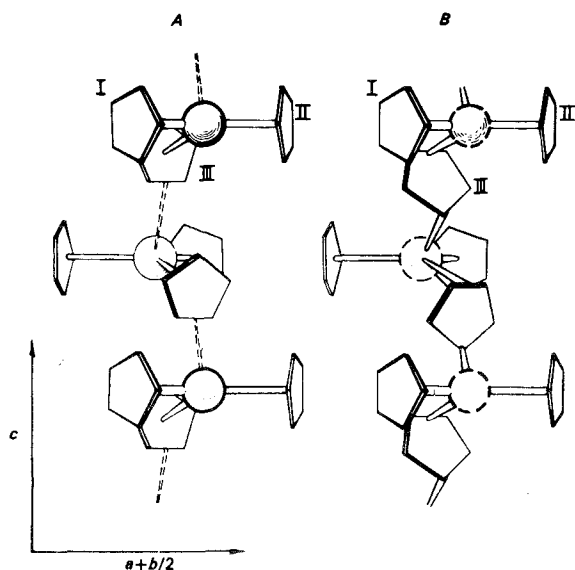
Fig. 2. The molecular structure of $Sm(C_5H_5)_3$ (after Wong et al., 1969).

Lauberau and Burns (1970) (table 5). They show that the tricyclopentadienyls of Pr, Pm, Sm, Gd and Tb are isomorphous, but tricyclopentadienyl thulium is not . Its single crystal diffraction study showed systematic absence for the space group Pnma or Pna2₁.

The single crystal X-ray analysis of sublimated tricyclopentadienyl praseodymium (Hinrichs et al., 1983) shows a singular polymeric chain structure with three η^3-coordinated cyclopentadienyl rings and one η^2-coordinated ring for every Pr atom. The formal coordination number of Pr is 11, which is in contrast to tricyclopentadienyl scandium, where Sc has a coordination number of only 8. As expected the bonding distances of the bridging C_5H_5 ring become larger with respect to the other C_5H_5 groups.

TABLE 5

Unit cell dimensions of rare earth tricyclopentadienyls.

Compound	Radius M^{+3} (Å)	a (Å)	b (Å)	c (Å)
$(C_5H_5)_3Sc$	0.68	12.881(5)	8.954(4)	9.925(4) [a]
$(C_5H_5)_3Pr$	1.013	14.20	17.62	9.79 [b]
$(C_5H_5)_3Pm$	0.979	14.12	17.60	9.76 [b]
$(C_5H_5)_3Sm$	0.964	14.23(2)	17.40(1)	9.73(2) [c]
		14.15	17.52	9.77 [b]
$(C_5H_5)_3Gd$	0.938	14.09	17.52	9.65 [b]
$(C_5H_5)_3Tb$	0.923	14.20	17.28	9.65 [b]
$(C_5H_5)_3Tm$	0.869	19.98	13.82	8.59 [b]

[a] Atwood and Smith (1973a).
[b] Lauberau and Burns (1970).
[c] Wong et al. (1969).
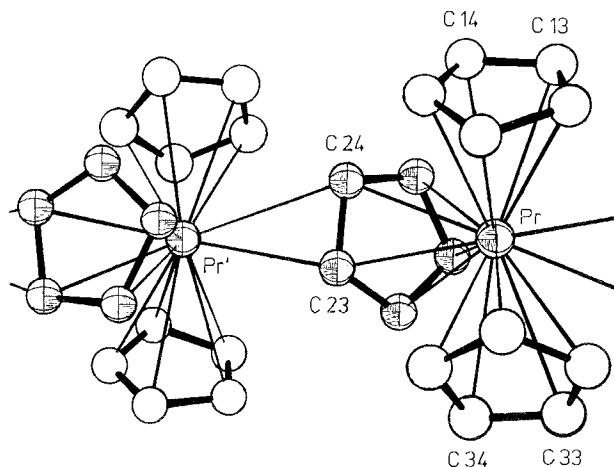
Fig. 2a. Molecular structure of $(C_5H_5)_3Pr$ (after Hinrichs et al., 1983).

The structures of the adducts of tricyclopentadienyl rare earth complexes with tetrahydrofuran and cyclohexylisonitrile show monomeric units with three η^5-bound cyclopentadienyl ligands (figs. 3 and 4). The unit cell parameters of the three isomorphous tetrahydrofuran complexes of tricyclopentadienyl yttrium, lanthanum and gadolinium (Rogers et al., 1980, 1981) together with their main bonding distances and bonding angles are given in table 6 as well as the unit cell parameters and some bonding distances of tricyclopentadienyl praseodymium cyclohexyl iso-nitrile (Burns and Baldwin, 1976).

The centrosymmetric complex of two cyclopentadienyl ytterbium molecules with one pyrazine ligand crystallizes in the space group C2/c with the unit cell dimensions: $a = 14.006(5)$ Å, $b = 8.299(3)$ Å, $c = 24.637(9)$ Å, and $\beta = 102.83(1)°$ with four molecules in the unit cell (fig. 5.) (Baker and Raymond, 1977). The coordination

TABLE 5a

Unit cell parameters, bond lengths and angles of tricyclopentadienyl praseodymium.

space group	P2
a (Å)	8.314(8)
b (Å)	9.714(5)
c (Å)	8.372(5)
β (deg)	116.06(6)
Z	2

bond lengths (Å)		bond angles	(deg)
Pr–$\varnothing 1$	2.526	$\varnothing 1$–Pr–$\varnothing 2$	111.63
Pr–$\varnothing 2$	2.602	$\varnothing 1$–Pr–$\varnothing 3$	119.17
Pr–$\varnothing 3$	2.488	$\varnothing 2$–Pr–$\varnothing 3$	116.79
Pr–C24	2.966(11)	Pr–C24–Pr′	141.74
Pr–C23	2.892(12)	Pr–C23–Pr′	161.96
Pr′–C24	3.130(12)		
Pr′–C23	2.940(12)		
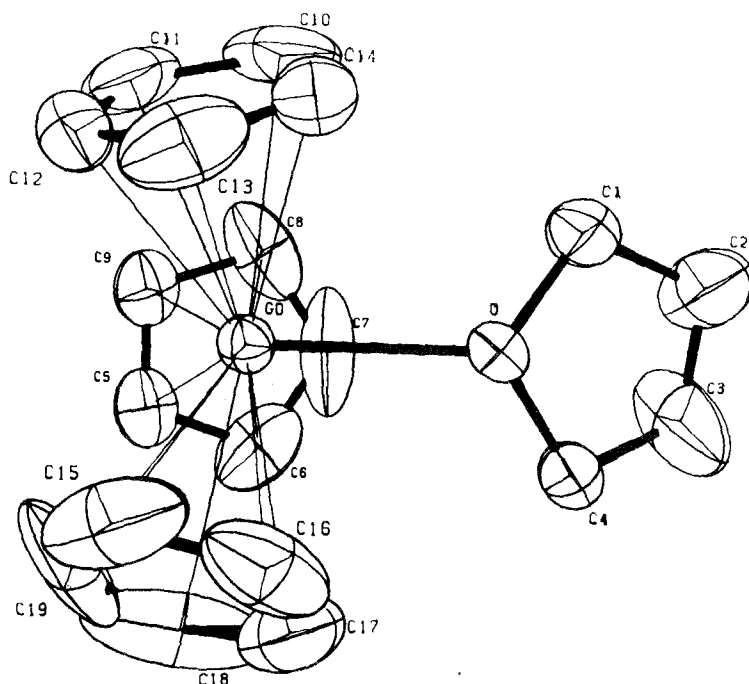
Fig. 3. Molecular structure of $(C_5H_5)_3Gd \cdot THF$ (after Rogers et al., 1980).

around the ytterbium atoms is nearly C_{3v} with angles of the centers of the cyclopentadienyl rings to ytterbium to the nitrogens of pyrazine of 118° and 98.5° average. Pertinent bond distances are: Yb–C = 2.684(11) Å, and Yb–N = 2.61(1) Å. Metal–metal interactions could not be detected by magnetic investigations.
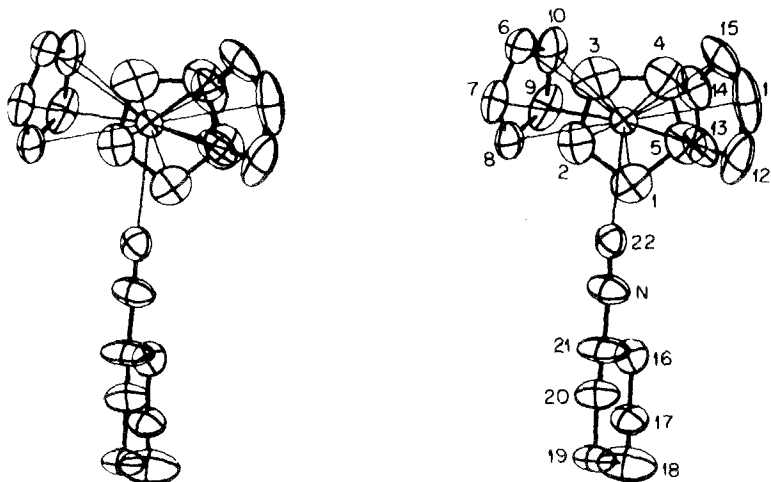
Fig. 4. Stereoscopic view of the structure of $(C_5H_5)_3Pr \cdot CNC_6H_{11}$ (after Burns and Baldwin, 1976).

TABLE 6

Unit cell parameters, bond lengths and angles of tricyclopentadienyl rare earth complexes.

	$Cp_3Y \cdot (THF)$	$Cp_3La \cdot (THF)$	$Cp_3Gd \cdot (THF)$	$Cp_3PrCNC_6H_{11}$
space group	$P2_1/n$	$P2_1/n$	$P2_1/n$	$P2_1/n$
a (Å)	8.170(3)	8.371(4)	8.220(4)	8.298(3)
b (Å)	24.595(5)	24.636(5)	24.650(9)	21.66(1)
c (Å)	8.260(3)	8.454(3)	8.317(4)	11.943(4)
β (deg)	101.32(3)	101.84(3)	101.39(3)	104.98(3)
bond lengths (Å)				
$R-\varnothing 1$	2.438	2.575	2.47	2.78 [1]
$R-\varnothing 2$	2.453	2.575	2.49	2.79 [1]
$R-\varnothing 3$	2.454	2.576	2.49	2.77 [1]
$R-O$	2.451(4)	2.57(1)	2.494(7)	
$Pr-C22$				2.65(1)
bond angles (deg)				
$\varnothing 1-R-\varnothing 2$	119.2	120	118.6	
$\varnothing 2-R-\varnothing 3$	115.4	116	117.0	
$\varnothing 1-R-O$	96.4	96.2	96.3	
$\varnothing 2-R-O$	100.8	102.2	101.0	
$Pr-C22-N$				171.1(1.1)

[1] Average distance $Pr-C_{ring\ 1}$, $Pr-C_{ring\ 2}$, $Pr-C_{ring\ 3}$.

The yellow green crystals of the dimeric dicyclopentadienyl scandium chloride show six dimeric molecules in the unit cell of the monoclinic space group $P2_1/c$ with $a = 13.54(1)$ Å, $b = 16.00(1)$ Å, $c = 13.40(1)$ Å, and $\beta = 93.97(5)°$. Four chlorine-bridged dimers lie in general positions, the other two on a center of symmetry. There are two crystallographically different molecules in the cell which do not differ
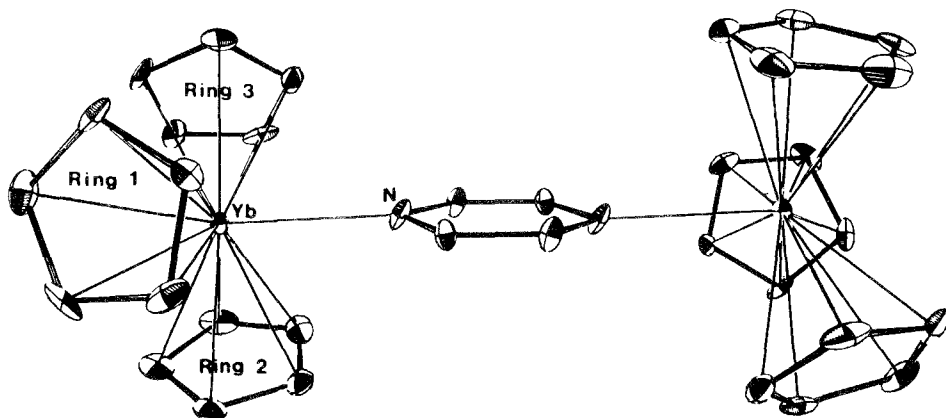
Fig. 5. Structure of $(C_5H_5)_3Yb \cdot NC_4H_4N \cdot Yb(C_5H_5)_3$ (after Baker and Raymond, 1977).
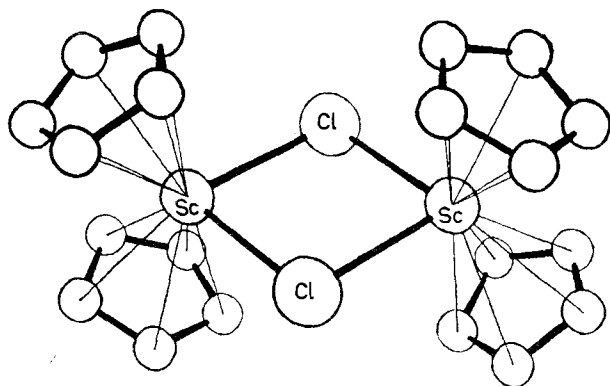
Fig. 6. Molecular structure of $[(C_5H_5)_2ScCl]_2$ (after Atwood and Smith, 1973b).

significantly in any respect. The cyclopentadienyl rings form a η^5-bond with Sc–C bond lengths between 2.39 and 2.49 Å. The scandium–chloride bond lengths average 2.575 Å with a Cl–Sc–Cl angle averaging 81.5° (fig. 6) (Smith and Atwood, 1972; Atwood and Smith, 1973b).

The crystal structure of cyclopentadienyl erbium dichloride tris(tetrahydrofuranate) (fig. 7) shows formally eight-coordinated erbium, but is more accurately described as an octahedral erbium atom with an η^5-cyclopentadienyl ring (average Er–C distance $= 2.667$ Å) occupying a single polyhedral vertex; the THF ligands have a meridional disposition (Er–O distances are 2.350, 2.365 and 2.452 Å), and the chloride ligands occupy trans sites of the octahedron with Er–Cl bond lengths of 2.613 and 2.620 Å. The main bond angles are: Cl–Er–Cl: 154.85(4)°,
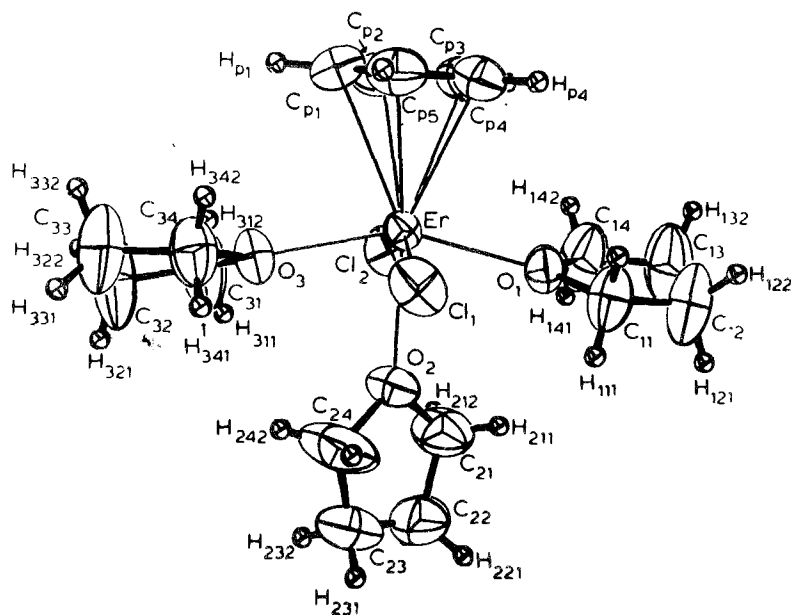
Fig. 7. The molecular structure of $C_5H_5ErCl_2 \cdot (THF)_3$ (after Day et al., 1982).

∅ Cp–Er–O(cis): 102.5(2)°, ∅ Cp–Er–O(trans): 179.3(1)°. The major distortion in this structure is a displacement of 0.54 Å of the Er atom out of the equatorial plane toward the cyclopentadienyl ligand. The unit cell dimensions for the monoclinic compound (space group P2$_1$/n) are: a = 7.822(2) Å, b = 17.096(4) Å, c = 15.162(3) Å, and β = 95.80(2)° (Day et al., 1982).

The 2 : 1 : 1 complex of dicyclopentadienyl yttrium chloride, aluminum hydride and ether forms rhombic crystals of space group Pcab with the unit cell dimensions a = 13.521(5) Å, b = 12.877(5) Å, c = 30.73(1) Å (Lobkovskii et al., 1982). The structure shows a polymeric chain made up of dimeric dicyclopentadienyl yttrium chloride fragments and aluminum hydride monoetherate units linked with each other through Y–H–Al bridges with a Y–H distance of 2.35 Å, Al–H bond distance of 1.5 Å and secondary Al–Cl bonds of 3.007 Å (fig. 8). Two dicyclopentadienyl yttrium sandwiches are linked with each other by two chlorine bridges with two different Y–Cl bond lengths of 2.705(5) and 2.802(3) Å at one yttrium and 2.756(5) and 2.711(4) Å at the other. The nearly rhombic yttrium chlorine ring is slightly nonplanar with a dihedral angle of 10.5° about the Cl–Cl axis.

In addition the structure of [(C$_5$H$_5$)$_2$YCl · AlH$_3$ · NEt$_3$]$_2$ has been determined (Lobkovskii et al., 1983). The complex crystallizes in the monoclinic space group P2$_1$/a with a = 12.325(5) Å, b = 18.780(7) Å, c = 8.848(2) Å, β = 69.89(2)° and Z = 2. The molecule is a (C$_5$H$_5$)$_2$YCl dimer bonded to the AlH$_3$ · NEt$_3$ groups via hydrogen bridges to yttrium as well as weaker Al–Cl bonds. The Cl, Y, Al and H atoms all lie in the same plane. The Y–H-bridge distance is 2.1(1) Å and the Al–Cl distance is 3.00(1) Å. The Al–H-bridge distance is significantly longer than the distances of Al to the nonbridging hydrogen atoms.

The structural investigations carried out with cyclopentadienyl derivatives of the
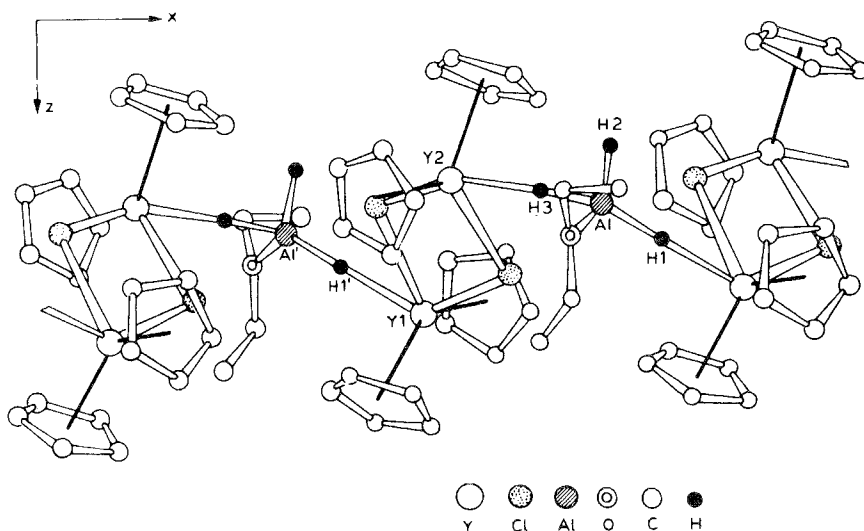
Fig. 8. The structure of the polymer chain in [(C$_5$H$_5$)$_2$YCl]$_2$·AlH$_3$·O(C$_2$H$_5$)$_2$ (after Lobkovskii et al., 1982).

rare earths allow some conclusions to be drawn concerning the bonding situation in these molecules. Ionic compounds differ from covalent ones by their irregular geometries, which are dependent on number, charge, and size of the ligands as well as the bond distances, which can be calculated from the ionic radii. Raymond and Eigenbrodt (1980) conclude from these definitions that an ionic model is a more appropriate description of the bonding situation in cyclopentadienyl compounds of the rare earths.

The optical absorption spectra for many tricyclopentadienyl and dicyclopentadienyl rare earth complexes have been reported. An excellent review with a detailed discussion of the work in this area done until 1970 is given by Hayes and Thomas (1971). An interpretation of the energy level structure of these complexes derived from the optical spectra is given by Carnall (1979).

The spectra have been measured either in coordinating solvents such as tetrahydrofuran or methyltetrahydrofuran or from a sublimed polycrystalline film or glassy melt. Because of some uncertainties in the molecular structure in these different states of aggregation, the interpretation of the spectra was not easy. The positions of the different J levels, which are influenced mainly by interelectron repulsion and spin–orbit coupling, show a smaller nephelauxetic effect for the tricyclopentadienyl compounds in comparison with the transition metals, which show a larger decrease of those parameters, but a larger nephelauxetic effect than for the corresponding rare earth chlorides. The crystal field splitting is less important because of the contracted nature of the 4f-orbitals. The absorption spectrum of $(C_5H_5)_3Nd$ at liquid-helium temperature in 2-methyltetrahydrofuran gives transitions from levels at about 70, 310, 570 and 670 cm^{-1} over the ground state. Two hypersensitive lines at 16828 and 16986 cm^{-1} cause the intense blue color of this compound (Pappalardo, 1965). The absorption spectrum of the erbium derivative at room temperature, liquid-nitrogen and liquid-helium temperature shows hypersensitive line groups at about 19000 and 26000 cm^{-1} and large splittings of the $J = 3/2$ levels (Pappalardo, 1968). The absorption spectra of $(C_5H_5)_3Tm$ have been studied by Pappalardo (1969) and R.D. Fischer and H. Fischer (1967). The spectra show an unusually large ligand field splitting of the $4f^n$-multiplet terms. An estimate of the Racah parameter E^3 indicates a remarkably large nephelauxetic effect for the 4f-electrons. Above 20000 cm^{-1}, medium intense, rather broad bands appear for electron transitions from non-bonding ligand orbitals into the appropriate 4f-orbitals. Several hypersensitive line groups were observed too. Investigations with tricyclopentadienyl ytterbium and some of its derivatives by R.D. Fischer and H. Fischer (1965), Calderazzo et al. (1966) and Pappalardo and Jorgensen (1967) show an unperturbed $4f^{13}$ electron configuration. The green color of these compounds is caused by a weak band with a very pronounced fine structure at low temperatures, which is probably due to an electron transfer from a linear combination of cyclopentadienyl orbitals having particularly low ionization energy because of strong ligand–ligand repulsion. The tricyclopentadienyl derivatives of lanthanum and gadolinium show an intense yellow or green fluorescence under excitation of 3660 Å radiation (Pappalardo and Losi, 1965). Extensive studies of the absorption spectra of adducts of $(C_5H_5)_3Yb$ with a number of organic phosphines and isonitriles by Bielang and Fischer (1978)

demonstrate that the shifting of the long-wave charge-transfer band as well as the changes of the $^2F_{5/2}$ term appear to a lesser degree governed by the basicity of the ligands then by essentially steric influences. Schmieder et al. (1970) have shown that a method to obtain good optical spectra of rare earth derivatives is by scattered transmission of the polycrystalline compounds compressed with teflon powder in the case of $(C_5H_5)_3Nd$ and $(C_5H_5)_3Yb$. Jorgensen et al. (1965) discuss the nephelauxetic effect of $(C_5H_5)_3Pr$ in comparison with that of other rare earth compounds in a study about reflection spectra.

Significant changes in the ligand-to-metal charge-transfer transitions and the f–f transitions in the electronic spectra of $(C_5H_5)_3Yb$ are observed, when bases like pyrrolidine, triethylphosphine, tetrahydrofuran, or tetrahydrothiophene are added to the complex in benzene solution (Schlesener and Ellis, 1983). The photolumines-cence of $(C_5H_5)_3Tb$ and $(CH_3C_5H_4)_3Tb$ in tetrahydrofuran solutions have been studied at different temperatures (Brittain et al., 1983).

The X-ray photoelectron spectrum of $(C_5H_5)_2ScCl$ gives core level binding energies of 400.9 eV for $Sc(^2p_{3/2})$, 405.8 eV for $Sc(^2p_{1/2})$, 284.3 eV for $C(1s)$, 199.0 eV for $Cl(^2p_{3/2})$, and 200.3 eV for $Cl(^2p_{1/2})$ (Westerhof and De Liefde Meijer, 1978). Dubois et al. (1977) obtained information by comparison of the intensity of the $Gd(^3d_{5/2})$ photopeak within the series $(C_5H_5)_3Gd$, $(C_5H_5)_2GdCl$, $C_5H_5GdCl_2$ to the intensity of its "electron shake-up" satellite peaks in the direction of some covalency due to 4f participation in bonding. He-I and He-II photoelectron spectra of $(C_5H_5)_2YCl$ and $(C_5H_5)_2GdCl$ show no ionization of the f-electrons (Green et al., 1981). The spectra are very similar. They have a band at 8.62 eV for the yttrium derivative and at 8.59 eV for the gadolinium compound for the ionization of the e_1 orbital of the cyclopentadienyl ligand and a broad band between 11 and 14 eV due to higher cyclopentadienyl ionizations.

The vibrational spectra of the tricyclopentadienyl derivatives of the rare earths are typical for transition metal cyclopentadienides. Fritz (1959) assigns the infrared bands in the range of 3100 cm^{-1} to the ν(C–H), between 1410 and 1440 cm^{-1} to ν(C–C) and ω(C–C), between 1100 and 1150 cm^{-1} to ν_{as} and ν_s(C–C) in the ring, at 1000 cm^{-1} to a β(C–H) and in the range between 770 and 830 cm^{-1} to a γ(C–H). The γ(C–H) out-of-plane deformation band around 800 cm^{-1} in the spectra of the tricyclopentadienides of Tb, Ho, Tm and Lu points towards centric covalent σ-bonding between the cyclopentadienyl rings and the metals (E.O. Fischer and H. Fischer, 1965b). The Raman spectra of $(C_5H_5)_3R$, with R = La, Pr, Nd, Sm, Gd, Dy and Tm, show up to seven bands between 180 and 280 cm^{-1} which are assigned to rare-earth–cyclopentadienyl ring vibrations ν(R–Cp) (Aleksanyan et al., 1974). In a second investigation of the Raman spectra of $(C_5H_5)_3R$ (R = Y, Pr, Gd, Tb, Ho, Er and Lu) Aleksanyan et al. (1977) show at room temperature, at the temperature of liquid nitrogen and in the molten state, that the spectra of the cyclopentadienyl ring vibrations are typical for η^5-coordinated ligands and that the intensities of the bands reflect considerable ionic character of the rare earth metal to cyclopentadienyl ring bonds. The ν(R–Cp) are not assigned specifically, but they are located in the region between 200 and 250 cm^{-1}. Reflection spectra of solid $(C_5H_5)_3Sc$, $(C_5H_5)_3Nd$ and a large number of other metal cyclopentadienyl compounds have been studied by

Reid et al. (1964). They assign a sharp overtone of a ν(C–H) between 6100 and 6200 cm^{-1} in the near infrared spectrum as characteristic of an η^5-bonded cyclopentadienyl ring.

The infrared spectra of tricyclopentadienyl rare earth cyclohexyl isonitrile complexes show considerable shifting of the ν(C≡N) of 73 to 78 cm^{-1} versus the free cyclohexyl isonitrile ligand to higher wave numbers. This demonstrates a σ-donor carbon to rare earth metal bond (E.O. Fischer and H. Fischer, 1966; Von Ammon and Kanellakopulos, 1972).

Infrared investigations have also been done by Tsutsui et al. (1966) for $(C_5H_5)_3$Sm, by Pappalardo (1969) for $(C_5H_5)_3$Tm, by Calderazzo et al. (1966), Kanellakopulos et al. (1970) and Baker and Raymond (1977) for $(C_5H_5)_3$Yb and some of its complexes, by Ely and Tsutsui (1975) for $(C_5H_5)_2$ErCl, by Maginn et al. (1963) for $(C_5H_5)_2$RCl, and by Kanellakopulos et al. (1974) for $(C_5H_5)_2$NdCN and $(C_5H_5)_2$YbCN. By recording the IR spectra of $(C_5H_5)_3$Er, $(C_5H_5)_3$Yb, $(C_5H_5)_2$ErC$_4$H$_5$CH$_3$, and $(C_5H_5)_2$YbC$_5$H$_4$CH$_3$ and some dicyclopentadienyl rare earth chlorides (Changtao Qian et al., 1983) showed that there is a characteristic absorption for η^5-bonded C$_5$H$_5$ in the 250 cm^{-1} region of the spectrum.

A number of ^{1}H NMR spectroscopic investigations have been done and excellent reviews including an extensive overview of the theoretical background have been written by Hayes and Thomas (1971) and by R.D. Fischer (1973, 1979). With the exception of the compounds of scandium, yttrium, lanthanum and lutetium, all the other organometallic compounds of the rare earths with oxidation state R^{3+} are paramagnetic because of the unpaired f-electrons, resulting in broadened and shifted ^{1}H NMR signals. These isotropic shifts are caused by contact interactions of the unpaired f-electron spin density with the ligand nuclei and by magnetic anisotropy. The contact contribution to the proton NMR spectra of the compounds of the trivalent rare earths is very small because of the very contracted nature of their f-orbitals; therefore the paramagnetic shifts are mostly pseudo-contact shifts.

Table 7 gives the chemical shifts, the paramagnetic ^{1}H NMR shifts and the line width of some lanthanide tricyclopentadienyls. The extreme line broadening caused by very long relaxation times of Gd^{3+} and Er^{3+} are the reason, that no resonances are detected for the gadolinium and the erbium derivatives (Von Ammon et al., 1969; R.D. Fischer, 1973).

Extensive studies have been done with the cyclohexyl isonitrile adducts of the tricyclopentadienyl compounds of the rare earths. Von Ammon et al. (1971) found all 13 possible signals for two slowly inverting conformers of the praseodymium complex at $-70°$C. At room temperature rapid inversion of the cyclohexyl ring gives rise to 7 discrete cyclohexyl proton lines. The ΔG value was found to be 282 ± 15 cal/mole for the ring inversion. The proton NMR spectrum of Cp$_3$EuCNC$_6$H$_{11}$ shows an anomalous temperature dependence of the ^{1}H contact shift which is connected with the strong second-order paramagnetism of the europium ion (Von Ammon et al., 1973). The spectrum shows a signal without any line width changes between -90 and $+90°$C, but with a decreasing isotropic shift with decreasing temperature. This observation is not consistent with the Curie–Weiss law. The paramagnetic shift in the ^{13}C NMR spectrum is positive in contrast to the

^{1}H NMR chemical shifts (δ), paramagnetic ^{1}H NMR shifts ($\Delta\nu^{iso}$) and half width of the NMR signals of $(C_5H_5)_3R$ at room temperature.

Compound	δC_5H_5 [a] (ppm)	$\Delta\nu^{iso}(Cp)/\nu$ (ppm)	$\Delta\nu^{iso}(\delta H)/\nu$ (ppm)	half width [a] (ppm)
$(C_5H_5)_3Ce$		-2.07 [b]	$+4.19$ [b]	20
$(C_5H_5)_3Pr$	-7.73	-9.13 [b]	$+6.23$ [b]	4.3
$(C_5H_5)_3Nd$	$+3.22$	$+3.20$ [b]	$+2.90$ [b]	27
$(C_5H_5)_3Sm$		-6.69 [b]	$+1.14$ to $+2.53$	22
$(C_5H_5)_3Eu$		-10.46 [b]	$-11.04;$ -11.60 [b]	30
$(C_5H_5)_3Tb$		-159 [b]	$+28.8;$ $+32.4$ [b]	770
$(C_5H_5)_3Dy$		-215 [b]	$+56.6;$ $+58.8$ [b]	480
$(C_5H_5)_3Ho$	-134	-137 [b]	$+36.9$ [b]	130
$(C_5H_5)_3Tm$	$+69$	$+55.1$ [c]	-16.4 [c]	160
$(C_5H_5)_3Yb$	$+54$	$+51.1$ [c]	-12.9 [c]	280

[a] In tetrahydrofurane–d_8.

[b] $C_6H_{11}NC$ adduct in toluene–d_8.

[c] PBu_3 adduct in toluene–d_8.

negative shift in the proton spectrum. A comparison of the wavenumbers of the $\nu(CN)$ from the infrared spectra and the ^{1}H NMR spectra of all known tricyclopentadienyl rare earth cyclohexyl isonitrile complexes implicate partial covalent character in the rare-earth–carbon bond to the isonitrile ligand. An analysis of the paramagnetic shifts of the cyclohexyl protons in the low temperature NMR spectra of the cerium, praseodymium, neodymium and europium complexes indicates a weak bending of the isonitrile group (Von Ammon and Kanellakopulos, 1972).

The diamagnetic $(C_5H_5)_2ScCl$ shows a chemical shift for the cyclopentadienyl protons of $\delta = 6.16$ ppm in tetrahydrofuran solution (Coutts and Wailes, 1970); the signal for the tetrahydrofuran complex in benzene solution appears at $\delta = 6.25$ ppm (Manzer, 1976a). The chemical shift for tricyclopentadienyl lutetium is $\delta = 5.83$ ppm in tetrahydrofuran and $\delta = 5.90$ ppm in benzene solution (E.O. Fischer and H. Fischer, 1965b).

The mass spectra of all known tricyclopentadienyl complexes of the rare earths with exception of promethium and europium have been studied (Müller, 1969; Thomas and Hayes, 1970; Borisov and Chuganova, 1976; Devyatykh et al., 1970, 1973b, 1974a; Gaivoronskii and Larin, 1973; Gaivoronskii et al., 1978). The major fragmentation of the molecular ions is loss of one of the cyclopentadienyl rings. Further fragmentation of the $(C_5H_5)_2R^+$ ion involves loss of C_2H_2 and C_3H_3 groups from the metal bound C_5H_5 rings. In some cases metastable transformations are observed. The base peak is the $(C_5H_5)_2R^+$ ion, except in the cases of the samarium and ytterbium derivatives, which give the $C_5H_5R^+$ ion as the base peak because of the high stability of compounds with oxidation state R^{+2}. This is in accordance with the dissociation energy of the tricyclopentadienyl compounds of the

rare earths, calculated from the appearance potentials, which decrease with increasing atomic number of the metals. The dissociation energy for the removal of the second cyclopentadienyl ring is in the same range as that for the first ligand for $(C_5H_5)_3Yb$, whereas in the other cases much more energy is necessary for the removal of the second ligand.

Dimeric dicyclopentadienyl ytterbium chloride monomerizes at the ion source temperature of 250°C, but at 180°C removal of cyclopentadienyl ligands is found with formation of $Yb_2Cl_2^+$ ions (Müller, 1969).

2.1.2. Complexes $Cp_3'R$, $Cp_2'RX$ and $Cp'RX_2$ with substituted cyclopentadienyl ligands

Compounds with bonds between a rare earth metal and substituted cyclopentadienyl rings were synthesized immediately after the unsubstituted derivatives. Reynolds and Wilkinson (1959) prepared the reddish blue tris(methylcyclopentadienyl) neodymium by the reaction of neodymium trichloride with sodium methylcyclopentadienide in tetrahydrofuran. The corresponding colorless lanthanum derivative was made by Strohmeier et al. (1961), who found that this complex is a 1:1 electrolyte by conductivity measurements in dimethoxyethane, tetrahydrofuran and diethyl ether (Strohmeier et al., 1962). Green-yellow $(CH_3C_5H_4)_3Tm$ was prepared by the same method. This complex melts at 160°C without decomposition. In the absorption spectrum of this compound several hypersensitive line groupings could be observed between 4000 and 25000 cm^{-1} (Pappalardo, 1969). The tris(methylcyclopentadienyl) derivatives of samarium, gadolinium, holmium and erbium have been mentioned together with infrared and NMR investigations of a number of adducts between Lewis bases such as $[FeCp(CO)_2]_2$, $Co_2(CO)_8$, $[NiCp-(CO)_2FeCp(CO)]$, $[NiCp(CO)]_2$, $[Mn(MeCp)(CO)_3]$, $[CrCp(NO)_2]Cl$, $[CrCp(CO)_2(NO)]$, and $[WCp(CO)_2(NO)]$, and the rare earth complex as a Lewis acid. Spectral changes indicate that the rare earths can act as Lewis acids towards bases such as bridging and terminal carbonyl ligands, terminal nitrosyl ligands, appropriate transition metals and some carbon–carbon triple bonds. The yellow adduct of $(CH_3C_5H_4)_3Sm$ with $Co(CO)_4$ as well as the red complex $(MeCp)_3SmFeCp(CO)_2$ could be isolated and characterized (Crease and Legzdins, 1972, 1973b).

He-I and He-II photoelectron spectra of $(MeCp)_3Pr$ and $(MeCp)_3Dy$ show the first bands between 7 and 8.5 eV, which are assigned to ionization from the cyclopentadienyl e_1 orbitals. Ionizations for the 5f-electrons are not identified (Green et al., 1981).

The crystal structure of tris(methylcyclopentadienyl) neodymium (fig. 9) shows a tetramer (Burns et al., 1974). The crystals are monoclinic with space group $P2_1/c$ and unit cell dimensions of $a = 14.257(7)$ Å, $b = 26.85(1)$ Å, $c = 9.286(3)$ Å, $\beta = 120°17(5)'$ and eight molecules in the cell. Each neodymium atom is bonded to three η^5-bound cyclopentadienyl ligands with average bond distances of the neodymium–carbon bond of 2.79(1) Å and one η^1-bond to an η^5-ligand of another $(MeCp)_3Nd$ unit with bonding distances of 2.990(7) and 2.978(7) Å. This additional bonding interaction is assigned to a mainly ionic nature in the bonds between neodymium and the methylcyclopentadienyl ligands.
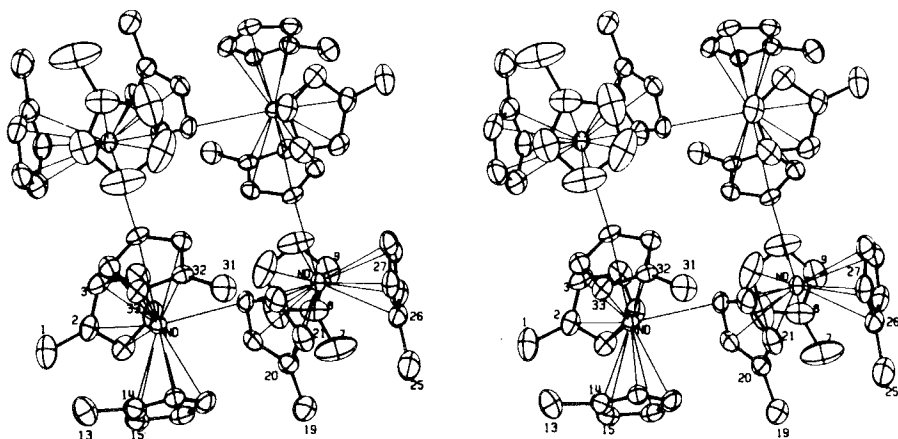
Fig. 9. Stereoscopic view of the structure of tetrameric $(CH_3C_5H_4)_3Nd$ (after Burns et al., 1974).

As mentioned before, Changtao Qian et al. (1983) prepared the mixed cyclopentadienyl complexes $(C_5H_5)_2R(C_5H_4CH_3)$ with R = Er, Yb.

The cyclohexyl isonitrile complexes of the tris(methylcyclopentadienyl) cerium, praseodymium, and neodymium compounds have been mentioned in a discussion of the NMR spectra of these and the corresponding tricyclopentadienyl rare earth complexes, which showed that the ΔG values of the fluxionality of the cyclohexyl ligands decreased in contrast to those of the unsubstituted cyclopentadienyl derivatives (R.D. Fischer, 1979).

The bis(methylcyclopentadienyl) rare earth chlorides of gadolinium, erbium and ytterbium have been prepared according to eq. (17) as colorless, pink or red crystals. They are monomeric in tetrahydrofuran, but dimeric in benzene solution (Maginn et al., 1963). The corresponding dysprosium and holmium compounds were prepared by Crease and Legzdins (1973b), the yttrium and lutetium derivatives by W.J. Evans et al. (1982a) and characterized by NMR spectroscopy.

$$RCl_3 + 2\,NaC_5H_4CH_3 \xrightarrow{\text{THF}} (CH_3C_5H_4)_2RCl + 2\,NaCl, \qquad (17)$$
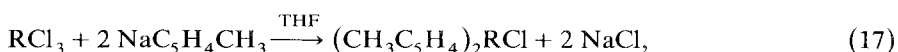
R = Y, Gd, Dy, Ho, Er, Yb, Lu.

Solid bis(methylcyclopentadienyl) ytterbium chloride is a dimer, as shown by a single crystal X-ray structural determination by Baker et al. (1975) (fig. 10). The orange plates have space group C2/c with $a = 20.377(6)$ Å, $b = 9.185(2)$ Å, $c = 13.253(4)$ Å, $\beta = 108.97(2)°$, and $Z = 4$, each dimer having a crystallographic inversion center with an ytterbium–ytterbium distance of 3.979(1) Å. The coordination around the ytterbium atoms is a distorted tetrahedron with planar methylcyclopentadienyl rings in each case, showing equal mean ytterbium–carbon bond distances of 2.585(7) Å, and an approximately square bridging Yb_2Cl_2 unit with an average Yb–Cl distance of 2.64 Å and an Yb–Cl–Yb angle of 97.95(5)°.

Tris(iso-propylcyclopentadienyl) lanthanum, praseodymium, and neodymium
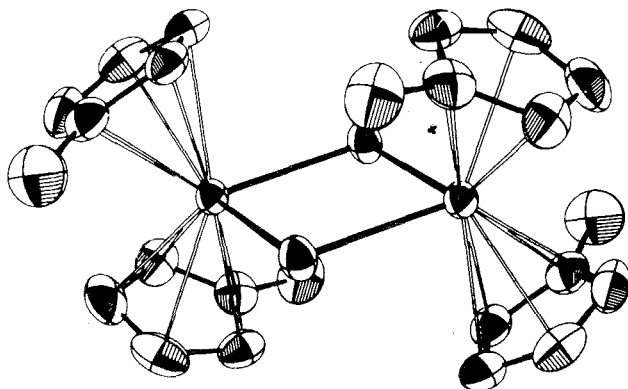
Fig. 10. The molecular structure of $[(CH_3C_5H_4)_2YbCl]_2$ (after Baker et al., 1975).

have been synthesized by the reaction of the corresponding rare earth trichlorides with sodium iso-propylcyclopentadienide in tetrahydrofuran. The vapor pressure of the compounds increase with increasing atomic number of the rare earth, but is lower than that of the corresponding tris(cyclopentadienyl) rare earth complexes (Devyatykh et al., 1980). Mass spectrometric studies of the same compounds by Gaivoronskii et al. (1978) show that the introduction of the iso-propyl group into the cyclopentadienyl ring leads to a higher complexity of the fragmentation of the molecular ion under the influence of electron collision.

Ring-bridged bis(cyclopentadienyl) rare earth complexes have been synthesized according to eq. (18) by reacting the disodium salt of 1,3-dicyclopentadienyl propane with $LaCl_3$ or $CeCl_3$ in tetrahydrofuran (John and Tsutsui, 1980, 1981). The derivatives of Pr, Nd, Gd, Dy, Ho, Er, Yb, and Lu have been made in the same way and isolated as $1:1$ complexes with tetrahydrofuran. These complexes react with nitrogen bases, like α,α'-bipyridine with exchange of the THF ligand (Changtao Qian et al., 1981).

$$RCl_3 + NaC_5H_4(CH_2)_3C_5H_4Na \xrightarrow{\text{THF}} (CH_2)_3 \qquad RCl + 2\,NaCl. \qquad (18)$$
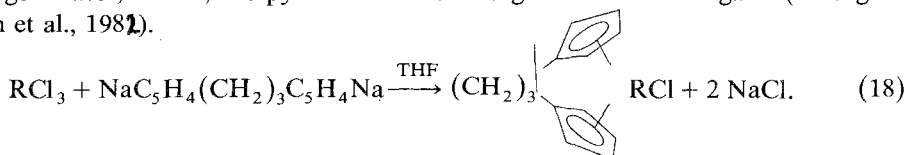
The NMR spectrum of the lanthanum derivative shows two singlets for the two cyclopentadienyl ligands at $\delta = 7.57$ and 7.74 ppm in tetrahydrofuran and a multiplet for the six CH_2 protons at 4.24 ppm. Further characterization of the compounds was done by infrared and mass spectroscopy as well as magnetic susceptibility investigations. The X-ray photoelectron spectrum of the lanthanum compound gives binding energies of the La 3d-electrons of 833.0 eV, and of the Cl $2p_{1/2}$- and $2p_{3/2}$-electrons of 198.8 and 197.6 eV, respectively.

A very important ligand in transition-metal chemistry as well as in the organometallic chemistry of the f-elements is the pentamethylcyclopentadienyl anion. The isolation of unsubstituted bis(cyclopentadienyl) metal chlorides of the early lanthanides like cerium, praseodymium, or neodymium has not been possible (see

section 2.1.1), but lithium pentamethylcyclopentadienide reacts in tetrahydrofuran with neodymium trichloride with formation of blue bis(pentamethylcyclopen-tadienyl) neodymium chloride coordinated with one lithium chloride and two tetrahydrofurans (Wayda and W.J. Evans, 1980):

$$NdCl_3 + 2\ LiC_5Me_5 \xrightarrow{THF} \qquad\qquad + LiCl. \qquad (19)$$
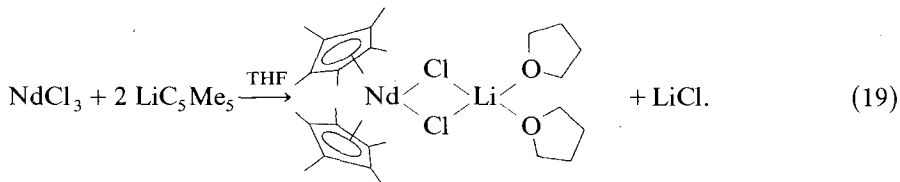
Watson (1980), Watson et al. (1981) and Tilley and Andersen (1981b) prepared bis(pentamethylcyclopentadienyl) ytterbium, lutetium, neodymium and samarium chlorides and iodides. Some physical data of these compounds together with those of the other complexes with substituted cyclopentadienyl ligands are given in table 8. The following synthetic methods have been used: ytterbium metal is oxidized by C_5Me_5I in the presence of LiI in ether to give, via C_5Me_5YbI, the complexes shown in eq. (20). In the absence of LiI, only dimeric pentamethylcyclopentadiene was isolated.

$$Yb + C_5Me_5I + LiI$$

$$\xrightarrow{Et_2O} Li[YbI_3(C_5Me_5)] \cdot (Et_2O)_{0-2} + \qquad\qquad . \qquad (20)$$
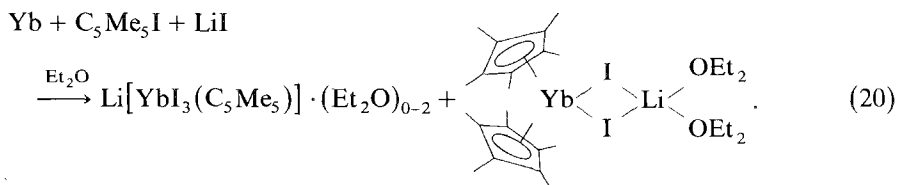
Corresponding chlorides are formed by substitution reactions from $YbCl_3$ and LiC_5Me_5 in tetrahydrofuran. $LuCl_3$ preferably forms $(C_5Me_5)_2Lu(\mu\text{-}Cl)_2Li$. The isolation of the monocyclopentadienyl complex $C_5Me_5Lu(\mu\text{-}Cl)_3Li$ is also possible in some cases. The oxidation of the dimethoxyethane complex of bis(pentamethyl-cyclopentadienyl) ytterbium (II) with $[FeCp_2]PF_6$ gives $(C_5Me_5)_2YbPF_6 \cdot DME$ as purple crystals, and the oxidation of the same ytterbium(II) complex with CH_2Cl_2 yields $(C_5Me_5)_2YbCl$. Attempts to prepare a $(C_5Me_5)_2Yb^+$ cation failed. Ether-free $(C_5Me_5)_2Yb(\mu\text{-}Cl)_2Li$ reacts with Al_2Cl_6 in pentane only with formation of a blue complex with $AlCl_3$, which loses this Lewis acid upon reaction with tetrahydrofuran forming the THF complex:

$$Yb \overset{Cl}{\underset{Cl}{<>}} Li + AlCl_3 \rightarrow \qquad Yb \overset{Cl}{\underset{Cl}{<>}} AlCl_2 + LiCl, \qquad (21)$$
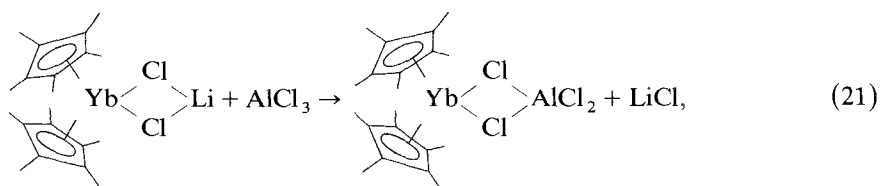
TABLE 8
Complexes of the rare earths with substituted cyclopentadienyl ligands.

Compound	Color	Other data		Refs.
(MeCp)$_3$La	colorless	m.p.	155–156°C	1
(MeCp)$_3$Pr				2
(MeCp)$_3$Nd	blue	m.p.	165°C	3
(MeCp)$_3$Sm	orange			4
(MeCp)$_3$Gd				4
(MeCp)$_3$Dy				4
(MeCp)$_3$Ho				4
(MeCp)$_3$Er				4
(MeCp)$_3$Tm	green	m.p.	160°C	5
(MeCp)$_3$CeCNC$_6$H$_{11}$				6
(MeCp)$_3$PrCNC$_6$H$_{11}$				6
(MeCp)$_3$NdCNC$_6$H$_{11}$				6
(MeCp)$_3$Sm·Co(CO)$_4$	yellow			4
(MeCp)$_3$Sm·FeCp(CO)$_2$	red	dec.	120°C	4
(MeCp)$_2$YCl				7
(MeCp)$_2$DyCl				4
(MeCp)$_2$HoCl				4
(MeCp)$_2$ErCl	pink	m.p.	119–122°C	8
		IR		25
(MeCp)$_2$YbCl	red	m.p.	115–120°C	8
(MeCp)$_2$LuCl				9
(i-C$_3$H$_7$C$_5$H$_4$)$_3$La				10
		MS		27
(i-C$_3$H$_7$C$_5$H$_4$)$_3$Pr				10
		MS		27
(i-C$_3$H$_7$C$_5$H$_4$)$_3$Nd				10
		MS		27
[C$_5$H$_4$(CH$_2$)$_3$C$_5$H$_4$]LaCl	pale yellow			11
[C$_5$H$_4$(CH$_2$)$_3$C$_5$H$_4$]CeCl	brown			11
[C$_5$H$_4$(CH$_2$)$_3$C$_5$H$_4$]PrCl·THF				12
[C$_5$H$_4$(CH$_2$)$_3$C$_5$H$_4$]NdCl·THF				12
[C$_5$H$_4$(CH$_2$)$_3$C$_5$H$_4$]GdCl·THF				12
[C$_5$H$_4$(CH$_2$)$_3$C$_5$H$_4$]DyCl·THF				12
[C$_5$H$_4$(CH$_2$)$_3$C$_5$H$_4$]HoCl·THF				12
[C$_5$H$_4$(CH$_2$)$_3$C$_5$H$_4$]ErCl·THF				12
[C$_5$H$_4$(CH$_2$)$_3$C$_5$H$_4$]YbCl·THF				12
[C$_5$H$_4$(CH$_2$)$_3$C$_5$H$_4$]LuCl·THF				12
(C$_5$Me$_5$)$_2$NdCl·THF	green	m.p.	220–223°C	13
(C$_5$Me$_5$)$_2$Nd(μ-Cl)$_2$Li·(Et$_2$O)$_2$	blue	dec.	114°C	13
(C$_5$Me$_5$)$_2$Nd(μ-Cl)$_2$Li·(THF)$_2$	blue			14
(C$_5$Me$_5$)$_2$Nd(μ-Cl)$_2$Li·(tmed)$_2$	blue	m.p. > 300°C		13
(C$_5$Me$_5$)$_2$Nd(μ-Cl)$_2$Na·(Et$_2$O)$_2$	blue	m.p. > 300°C		13
(C$_5$Me$_5$)$_2$Sm(μ-Cl)$_2$Li·(THF)$_2$				15
(C$_5$Me$_5$)$_2$Sm(μ-Cl)$_2$Li·(tmed)	yellow	dec.	200°C	13
(C$_5$Me$_5$)$_2$Sm(μ-Cl)$_2$Na·(Et$_2$O)$_2$	orange	m.p. > 300°C		13
(C$_5$Me$_5$)$_2$Sm(μ-Cl)$_2$Na·(tmed)	yellow	m.p. > 300°C		13
(C$_5$Me$_5$)$_2$Yb(μ-F)$_2$PF$_4$·(DME)	purple			16
(C$_5$Me$_5$)$_2$YbCl·THF	purple/violet	m.p.	221–230°C	13,17

TABLE 8 (continued)

Compound	Color	Other data		Refs.
$(C_5Me_5)_2YbCl \cdot py$	purple	m.p.	270–272°C	13
$(C_5Me_5)_2Yb(\mu\text{-}Cl)_2AlCl_2$	blue	m.p.	175°C	17
$(C_5Me_5)_2Yb(\mu\text{-}Cl)_2Li$	green			17
$(C_5Me_5)_2Yb(\mu\text{-}Cl)_2Li \cdot (Et_2O)_2$	purple/violet	dec.	130°C	13,16
$(C_5Me_5)_2Yb(\mu\text{-}Cl)_2Li \cdot (tmed)$	violet	dec.	255°C	13
$(C_5Me_5)_2Yb(\mu\text{-}Cl)_2Na \cdot (Et_2O)_2$	violet	dec.	280°C	13
$(C_5Me_5)_2Yb(\mu\text{-}Cl)_2Na \cdot (tmed)$	violet	dec.	120°C	13
$(C_5Me_5)_2Yb(\mu\text{-}I)_2Li \cdot (Et_2O)_2$	purple			16,17
$(C_5Me_5)_2Lu(\mu\text{-}Cl)_2AlCl_2$	white			17
$(C_5Me_5)_2Lu(\mu\text{-}Cl)_2Li \cdot (Et_2O)_2$	white			17
$C_5Me_5Nd(\mu\text{-}Cl)_3Na \cdot (Et_2O)_2$	blue	dec.	125°C	13
$C_5Me_5Yb(\mu\text{-}Cl)_3Li \cdot (Et_2O)_2$				16
$C_5Me_5Yb(\mu\text{-}Cl)_3Li \cdot THF$	blue			17
$C_5Me_5Yb(\mu\text{-}I)_3Li \cdot (Et_2O)_2$	green			16,17
$C_5Me_5Lu(\mu\text{-}Cl)_3Li \cdot (Et_2O)$	white			17
$(C_5Me_4Et)_2Y(\mu\text{-}Cl)_2Li$				18
$(Me_3SiC_5H_4)_2YCl$				18
$(Me_3SiC_5H_4)_2Y(\mu\text{-}Cl)_2Li \cdot (tmed)$	colorless			18
$(Me_3SiC_5H_4)_2Y(\mu\text{-}Cl)_2Li \cdot (THF)_2$	colorless			18
$(Me_3SiC_5H_4)_2YbCl$	red	m.p.	183–185°C	19
$(Me_3SiC_5H_4)_2YbI$	redbrown	m.p.	187–190°C	19
$(MePh_2SiC_5H_4)_2Yb(\mu\text{-}Cl)_2Li \cdot (Et_2O)_2$	orange			17
$(MePh_2SiC_5H_4)_2Lu(\mu\text{-}Cl)_2Li$	white			17
$[(Me_3Si)_2C_5H_3]_2ScCl$				20
$[(Me_3Si)_2C_5H_3]_2Sc(\mu\text{-}Cl)_2Li \cdot (THF)_2$				20
$[(Me_3Si)_2C_5H_3]_2YCl$				20
$[(Me_3Si)_2C_5H_3]_2Y(\mu\text{-}Cl)_2Li \cdot DME$				21
$[(Me_3Si)_2C_5H_3]_2Y(\mu\text{-}Cl)_2Li \cdot (tmed)$				21
$[(Me_3Si)_2C_5H_3]_2Y(\mu\text{-}Cl)_2Li \cdot (THF)_2$				20
$[N(PPh_3)_2][Y\{(Me_3Si)_2C_5H_3\}_2Cl_2]$				22
$[(Me_3Si)_2C_5H_3]_2LaCl$				20
$[(Me_3Si)_2C_5H_3]_2La(\mu\text{-}Cl)_2Li \cdot (tmed)$				21
$[(Me_3Si)_2C_5H_3]_2La(\mu\text{-}Cl)_2Li \cdot (THF)_2$				20
$[Li(THF)_4][La\{(Me_3Si)_2C_5H_3\}_2Cl_2]$				22
$[(Me_3Si)_2C_5H_3]_2CeCl$				20
$[(Me_3Si)_2C_5H_3]_2Ce(\mu\text{-}Cl)_2Li \cdot (THF)_2$				20
$[(Me_3Si)_2C_5H_3]_2PrCl$				20
$[(Me_3Si)_2C_5H_3]_2Pr(\mu\text{-}Cl)_2Li \cdot (THF)_2$				20
$[PPh_4][Pr\{(Me_3Si)_2C_5H_3\}_2Cl_2]$				22
$[(Me_3Si)_2C_5H_3]_2NdCl$				20
$[(Me_3Si)_2C_5H_3]_2Nd(\mu\text{-}Cl)_2Li \cdot DME$				21
$[(Me_3Si)_2C_5H_3]_2Nd(\mu\text{-}Cl)_2Li \cdot (THF)_2$				20
$[PPh_2CH_2Ph][Nd\{(Me_3Si)_2C_5H_3\}_2Cl_2]$				22
$[AsPh_4][Nd\{(Me_3Si)_2C_5H_3\}_2Cl_2]$				22
$[(Me_3Si)_2C_5H_3]_2SmCl$				20
$[(Me_3Si)_2C_5H_3]_2EuCl$				20
$[(Me_3Si)_2C_5H_3]_2GdCl$				20
$[(Me_3Si)_2C_5H_3]_2TbCl$				20

TABLE 8 (continued)

Compound	Color	Other data	Refs.
$[(Me_3Si)_2C_5H_3]_2DyCl$			20
$[PPh_2CH_2Ph][Dy\{(Me_3Si)_2C_5H_3\}_2Cl_2]$			22
$[(Me_3Si)_2C_5H_3]_2HoCl$			20
$[(Me_3Si)_2C_5H_3]_2ErCl$			20
$[(Me_3Si)_2C_5H_3]_2TmCl$			20
$[PPh_4][Tm\{(Me_3Si)_2C_5H_3\}_2Cl_2]$			22
$[(Me_3Si)_2C_5H_3]_2YbCl$			20
$[(Me_3Si)_2C_5H_3]_2Yb(\mu\text{-}Cl)_2Li\cdot(THF)_2$			20
$[(Me_3Si)_2C_5H_3]_2LuCl$			20
$(CH_2=CHMeCH_2CHMe=CH_2)_3Nd$	green		23
$(MeCp)_3Tb\cdot(THF)$		luminescence spectra	24
$(MeCp)_2GdCl$	colorless	m.p. 188–197°C IR	8 25
$(MeCp)_2SmCl\cdot(THF)$	orange	NMR, IR	26
$(i\text{-}C_3H_7C_5H_4)_3Sm$		MS	27
$(i\text{-}C_3H_7C_5H_4)_3Yb$		MS	27
$Cp_2ErC_5H_4CH_3$	pink	m.p. 115–118°C IR	25
$Cp_2YbC_5H_4CH_3$	green	m.p. 135–137°C IR	25
$(C_5Me_5)_2La(\mu\text{-}Cl)_2K\cdot(DME)_2$	colorless		28
$(C_5Me_5)_2PrCl$	green		28
$(C_5Me_5)_2Pr(\mu\text{-}Cl)_2Na\cdot(Et_2O)_2$	green		28
$(C_5Me_5)_2Pr(\mu\text{-}Cl)_2Na\cdot(DME)$	green	NMR	28
$(C_5Me_5)_2YbCl\cdot(Me_2PCH_2PMe_2)$	purple	m.p. 208°C, $\mu_{eff} = 4.4$, IR	29
$(C_5Me_5)_2Lu(\mu\text{-}Cl)_2Na\cdot(Et_2O)_2$	colorless		28
$C_5Me_5PrCl_2\cdot Et_2O$	light green		28
$C_5Me_5Pr(\mu\text{-}Cl)_3Na\cdot Et_2O$	green	NMR	28
$C_5Me_5Yb(\mu\text{-}Cl)_3K\cdot(Et_2O)$	blue		28

1. Strohmeier et al. (1961).
2. Green et al. (1981).
3. Reynolds and Wilkinson (1959).
4. Crease and Legzdins (1973b).
5. Pappalardo (1969).
6. R.D. Fischer (1979).
7. Ballard et al. (1978).
8. Maginn et al. (1963).
9. W.J. Evans et al. (1982a).
10. Devyatykh et al. (1980).
11. John and Tsutsui (1981).
12. Qian Changtao et al. (1982).
13. Tilley and Andersen (1981b).
14. Wayda and Evans (1980).
15. W.J. Evans et al. (1981a).

16. Watson (1980).
17. Watson et al. (1981).
18. Atwood and Smith (1973a).
19. Lappert et al. (1980).
20. Lappert et al. (1981a).
21. Lappert et al. (1981b).
22. Lappert et al. (1983a).
23. Ernst and Cymbaluk (1982).
24. Brittain et al. (1983).
25. Changtao Qian et al. (1983).
26. W.J. Evans et al. (1983c).
27. Chernyaev et al. (1982).
28. Schumann and Albrecht (1984).
29. Tilley et al. (1983).
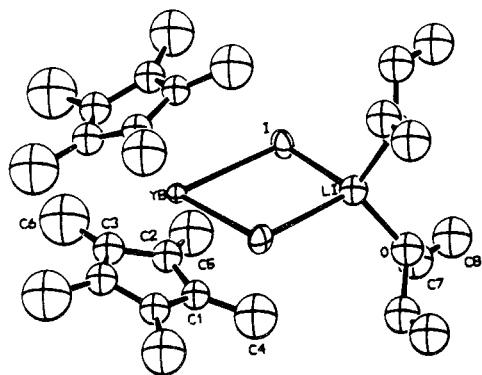
Fig. 11. The molecular structure of $(C_5Me_5)_2$-$Yb(\mu\text{-}I)_2Li\cdot(Et_2O)_2$ (after Watson et al., 1981).

$$\underset{\text{Yb}}{\overset{\text{Cl}}{\diagdown}}\underset{\text{Cl}}{\overset{}{\diagup}}AlCl_2 \xrightarrow{\text{THF}} \underset{\text{Yb}}{\overset{\text{Cl}}{\diagdown}}\underset{\text{O}}{\overset{}{\diagup}} + AlCl_3. \qquad (22)$$
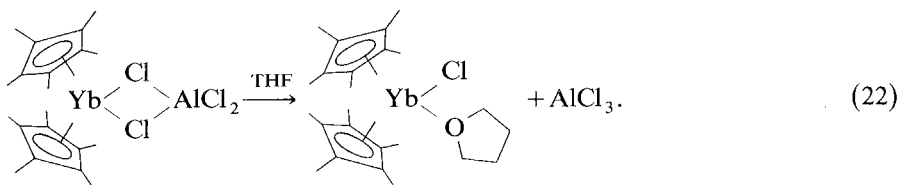
X-ray structural studies have been undertaken for the following complexes: $(C_5Me_5)_2Yb(\mu\text{-}Cl)_2Li\cdot(Et_2O)_2$, $(C_5Me_5)_2Yb(\mu\text{-}I)_2Li\cdot(Et_2O)_2$, and $(C_5Me_5)_2Yb(\mu\text{-}Cl)_2AlCl_2$, as well as for the complex $(MePh_2SiC_5H_4)_2Yb(\mu\text{-}Cl)_2Li\cdot(Et_2O)_2$, (Watson et al., 1981). All four compounds contain planar $Yb(\mu\text{-}X)_2M$ units with X = Cl, I and M = Al, Li and with pseudotetrahedral coordination spheres around the ytterbium as well as the lithium or the aluminum (figs. 11 to 14). Some crystallographic data, bonding distances and bonding angles are given in table 9.

Another peralkylated cyclopentadienyl derivative, the complex $(C_5Me_4Et)_2Y(\mu\text{-}Cl)_2Li$, is mentioned by Atwood et al. (1978).

$(C_5Me_5)_2Yb(Me_2PCH_2PMe_2)$ reacts with $YbCl_3$ in toluene to give a complex which cyrstallizes in the monoclinic space group $P2_1/c$ with $a = 16.358(6)$ Å,
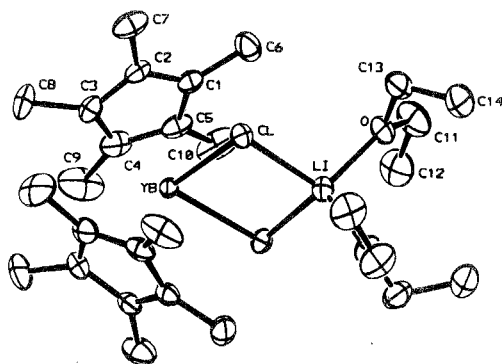
Fig. 12. The molecular structure of $(C_5$-$Me_5)_2Yb(\mu\text{-}Cl)_2Li\cdot(Et_2O)_2$ (after Watson et al., 1981).
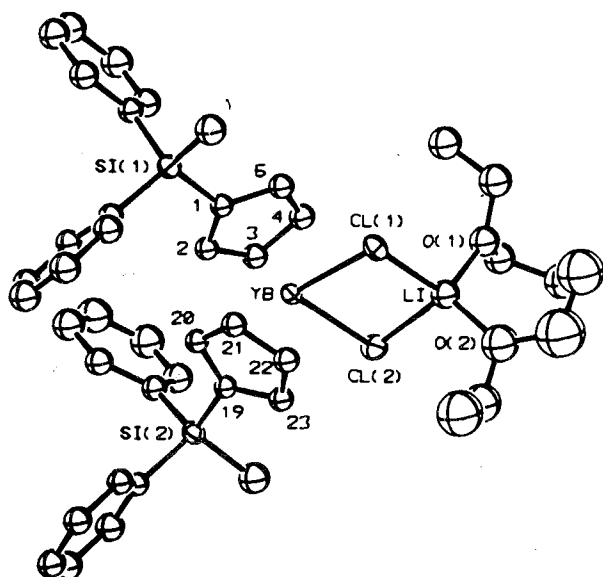
Fig. 13. The molecular structure of $(MePh_2SiC_5H_4)_2Yb(\mu\text{-}Cl)_2Li \cdot (Et_2O)_2$ (after Watson et al., 1981).

$b = 8.595(4)$ Å, $c = 20.712(7)$ Å, $\beta = 104.75(4)°$ and $Z = 4$. The Yb atom is nearly tetrahedral surrounded by the ligands and only one of the P atoms is bonded to the Yb atom. The Yb–Cl bond length is 2.532(3) Å and the Yb–P1 bond distance is 2.941(3) Å. Because the complex is paramagnetic ($\mu_{eff} = 4.4$ B.M. at 30°C in benzene), the ^{31}P NMR could not be obtained and the monodentate character of the phosphine ligand in solution could not be shown (Tilley et al., 1983).

Another bulky substituted cyclopentadienyl ligand was introduced in the organometallic chemistry of the rare earths by Lappert et al. (1981a, b), the
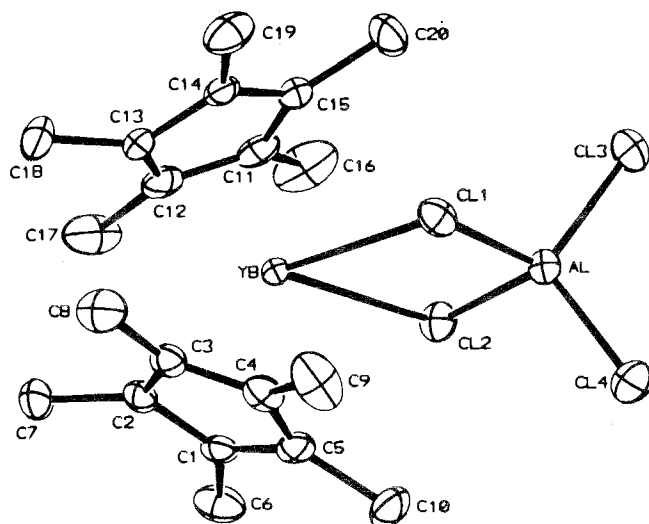
Fig. 14. The molecular structure of $(C_5Me_5)_2Yb(\mu\text{-}Cl)_2AlCl_2$ (after Watson et al., 1981).

H. SCHUMANN and W. GENTHE

TABLE 9

Crystallographic data, bonding distances and angles in pentamethylcyclopentadienyl ytterbium complexes.

	$(C_5Me_5)_2YbI_2Li(Et_2O)_2$	$(C_5Me_5)_2YbCl_2Li(Et_2O)_2$	$(C_5H_4X)_2YbCl_2Li(Et_2O)_2$ [a]	$(C_5Me_5)_2YbCl_2AlCl_2$
crystal system	tetragonal	monoclinic	triclinic	monoclinic
space group	$P\bar{4}2_1m$	$C2/c$	$P\bar{1}$	$P2_1/n$
a (Å)	11.257(2)	16.170(2)	14.053(2)	18.184(3)
b (Å)		13.774(2)	15.495(3)	12.923(2)
c (Å)	13.068(13)	13.998(2)	10.423(3)	10.364(2)
α (deg)			98.85(3)	
β (deg)		90.19(1)	101.03(1)	
γ (deg)			88.33(1)	
Z	2	4	2	4
distances (Å)				
	Yb–Li 3.027 (1)	Yb–Cl1 2.596 (1)	Yb–Cl 2.593 (1)	Yb–Cl1 2.760 (1)
		Yb–Cl2 2.594 (1)		Yb–Cl2 2.752 (1)
	Yb··Li 4.119 (12)	Yb··Li 3.478 (6)	Yb··Li 3.506 (6)	Yb··Al 3.65
	Li–I 2.812 (15)	Li–Cl1 2.390 (6)	Li–Cl 2.390 (4)	Al–Cl1 2.187 (1)
		Li–Cl2 2.412 (6)		Al–Cl2 2.185 (1)
	Li–O 1.904 (15)	Li–O1 1.924 (7)	Li–O 1.957 (4)	Al–Cl3 2.094 (1)
		Li–O2 1.935 (7)		Al–Cl4 2.097 (1)
angles (deg)				
	I–Yb–I 86.10 (2)	Cl–Yb–Cl 85.95 (2)	Cl–Yb–Cl 87.14 (3)	Cl–Yb–Cl 73.36 (3)
		Yb–Cl–Li 89.3 (1)	Yb–Cl–Li 88.3 (2)	Yb–Cl–Al 94.33 (4)
	I–Li–I 94.6 (6)	Cl–Li–Cl 95.4 (2)	Cl–Li–Cl 96.3 (2)	Cl–Al–Cl 97.71 (5)
		Cl–Li–O 111.33 (6)	Cl–Li–O 112.4 (3)	Cl–Al–Cl 111.88 (6)

[a] $X = SiMePh_2$.

bis(trimethylsilyl)cyclopentadienyl anion. This ligand increases the solubility in aprotic media and it allows the isolation of dicyclopentadienyl derivatives of the early lanthanides. Reaction of a rare earth trichloride with bis(trimethylsilyl)cyclopentadienyl lithium in tetrahydrofuran yields complexes of the type $[(Me_3Si)_2C_5H_3]_2R(\mu\text{-}Cl)_2Li \cdot (THF)_2$ which decomposes above 140°C with formation of the solvent-free derivatives. The latter are also isolated after sublimation of the reaction product from RCl_3 and $(Me_3Si)_2C_5H_3Li$ at 250 to 280°C/10^{-3} torr for the whole series of the rare earths from scandium to lutetium as crystalline solids.

$$RCl_3 + 2\,LiCp' \quad \xrightarrow[0-20°C]{THF} \quad Cp'_2R \begin{smallmatrix} Cl \\ < > \\ Cl \end{smallmatrix} Li \cdot (THF)_2, \tag{23}$$

$$R = Sc, Y, La, Ce, Pr, Nd, Yb$$

$$\xrightarrow[60-80°C]{THF} \quad Cp'_2Eu \begin{smallmatrix} Cl \\ < > \\ Cl \end{smallmatrix} EuCp'_2, \tag{24}$$

$$\xrightarrow[\substack{subl.\ at \\ 250-280°C/10^{-3}}]{THF} \quad Cp'_2R \begin{smallmatrix} Cl \\ < > \\ Cl \end{smallmatrix} RCp'_2, \tag{25}$$

$$R = Sc, Y, La, Ce, Pr, Nd, Sm,$$
$$Gd, Tb, Dy, Ho, Er, Tm, Yb, Lu$$
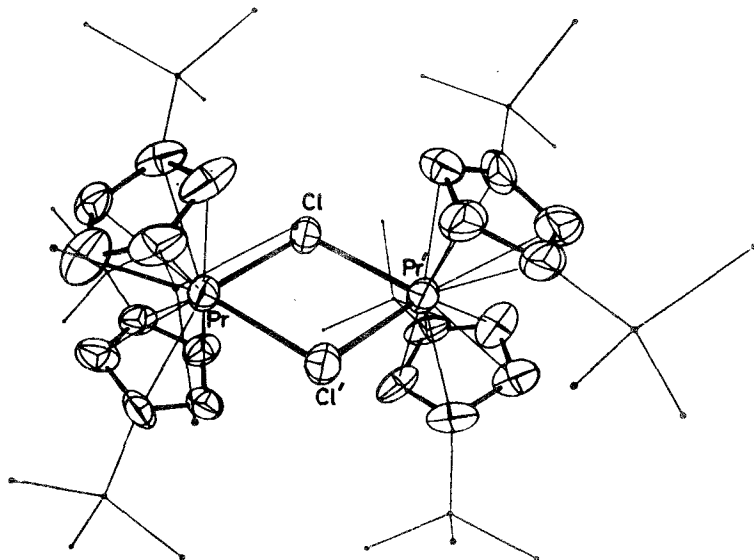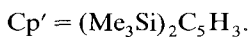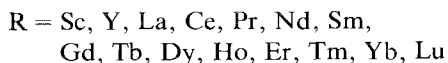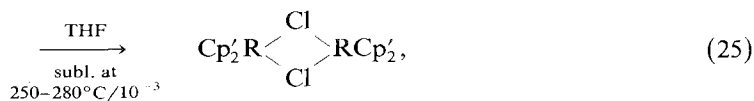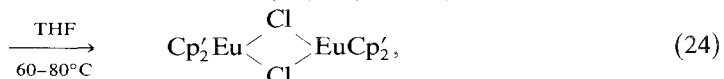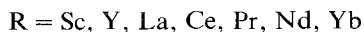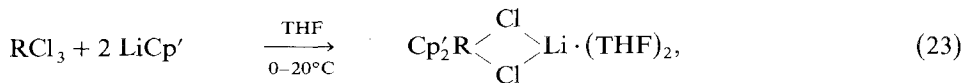
$$Cp' = (Me_3Si)_2C_5H_3.$$

Fig. 15. Molecular structure of $\{[(Me_3Si)_2C_5H_3]_2PrCl\}_2$ (after Lappert et al., 1981a).

TABLE 10

Crystallographic data, bonding distances and angles in bis(trimethylsilyl)cyclopentadienyl rare earth complexes; Cp$'$ = (Me$_3$Si)$_2$C$_5$H$_3$.

	[Cp$_2'$ScCl]$_2$	[Cp$_2'$PrCl]$_2$	[Cp$_2'$YbCl]$_2$	Cp$_2'$NdCl$_2$Li·(THF)$_2$
crystal system	triclinic	triclinic	triclinic	orthorhombic
space group	P1̄	P1̄	P1̄	Pbca
a (Å)		10.630(5)		13.008(6)
b (Å)		11.817(5)		20.280(7)
c (Å)		13.293(5)		31.964(9)
α (deg)		109.30(4)		
β (deg)		99.42(4)		
γ (deg)		86.66(4)		
Z		1 (dimer)		8
distances (Å)	Sc–Cl 2.58 Sc–C 2.51	Pr–Cl 2.81 Pr–C 2.76 Pr···Pr 4.372(1)	Yb–Cl 2.65 Yb–C 2.62	Nd–Cl 2.744 Li–Cl 2.405 Nd…Li 3.63(3)
angles (deg)	Cl–Sc–Cl 79 Sc–Cl–Sc 101 Cp$'$–Sc–Cp$'$ 131	Cl–Pr–Cl 78 Pr–Cl–Pr 102 Cp$'$–Pr–Cp$'$ 130	Cl–Yb–Cl 80 Yb–Cl–Yb 100 Cp$'$–Yb–Cp$'$ 130	Cl–Nd–Cl 82.1 Cl–Li–Cl 97.2(9)

Fig. 16. Molecular structure of $[(Me_3Si)_2C_5H_3]_2Nd(\mu-Cl)_2Li\cdot(THF)_2$ (after Lappert et al., 1981b).

The X-ray structure of $\{[(Me_3Si)_2C_5H_3]_2PrCl\}_2$ (fig. 15), as well as the corresponding isostructural scandium and ytterbium derivatives show distorted tetrahedrally coordinated rare earth metals. Some detailed data are given in table 10, including the data for the complex $[(Me_3Si)_2C_5H_3]_2Nd(\mu-Cl)_2Li\cdot(THF)_2$ (fig. 16). This bis[(trimethylsilyl)cyclopentadienyl] tetrahydrofuran complexes of yttrium, lanthanum and neodymium chloride react with tetramethylethylenediamine as well as with dimethoxyethane with exchange of the coordinated tetrahydrofurane, yielding new complexes with the chelating tmed and DME ligands coordinating the lithium atoms (Lappert et al., 1981b).

The dimers $[\{(Me_3Si)_2C_5H_3\}_2RCl]_2$ react with chlorides of large cations MCl with formation of stable complexes $[M][(\{Me_3Si)_2C_5H_3\}_2RCl_2]$ which decompose on melting at about 165 to 175°C (Lappert et al., 1983a):

$$2\,MCl + \left[\{(Me_3Si)_2C_5H_3\}_2RCl\right]_2 \rightarrow 2[M]\left[\{(Me_3Si)_2C_5H_3\}_2RCl_2\right], \qquad (26)$$

$M = N(PPh_3)_2$, R = Y;
$M = PPh_4$, R = Pr, Tm;
$M = AsPH_4$, R = Nd;
$M = PPh_3(CH_2Ph)$, R = Nd, Dy.
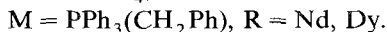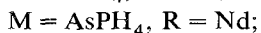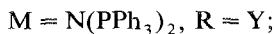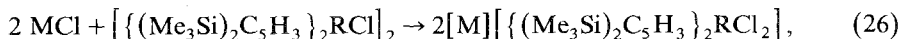
The molecular structure of $[AsPh_4][\{(Me_3Si)_2C_5H_3\}_2NdCl_2]$ consists of discrete triclinic monomers, space group $P\bar{1}$ [$a = 12.334(4)$ Å, $b = 13.924(4)$ Å, $c = 15.844(5)$ Å, $\alpha = 91.60(3)°$, $\beta = 97.96(3)°$, $\gamma = 104.35(3)°$, $Z = 2$], in which the anion (fig. 17) shows the following bond lengths and angles: Nd–Cl(1) 1.669(3) Å, Nd–Cl(2) 2.667(3) Å, Nd–C (aver.) 2.78 Å, Cl(1)–Nd–Cl(2) 99.3(1)°, $\varnothing$Cp(1)–Nd–$\varnothing$Cp(2) 126.3°.
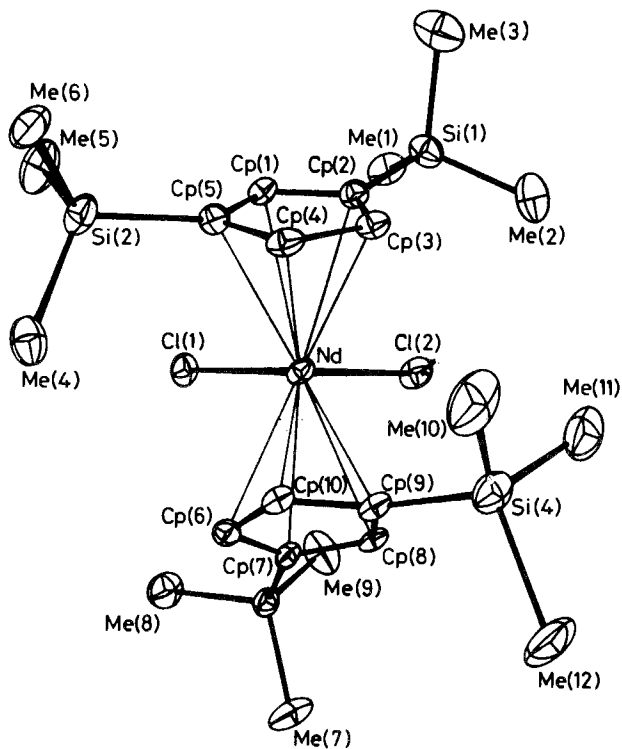
Fig. 17. Molecular structure of the anion of [AsPh$_4$][(Me$_3$Si)$_2$-C$_5$H$_3$]$_2$NdCl$_2$ (after Lappert et al., 1983).
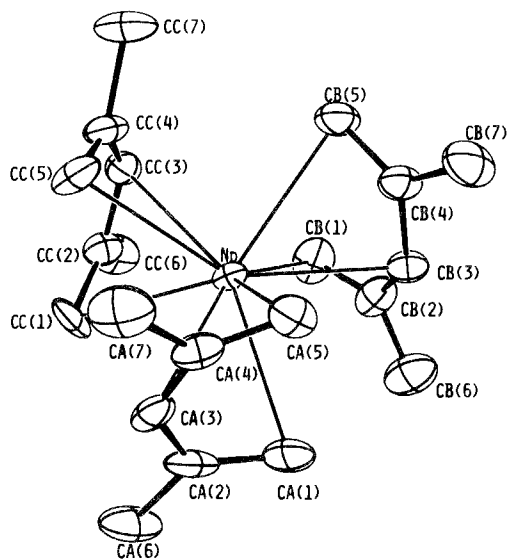
Fig. 18. Molecular structure of Nd[C$_5$H$_3$-(CH$_3$)$_2$]$_3$ (after Ernst and Cymbaluk, 1982).

TABLE 11

Crystallographic data and important bond distances and angles in $Nd[C_5H_3(CH_3)_2]_3$.

space group		$C_i^1-P\bar{1}$	
a (Å)		12.793(7)	
b (Å)		13.012(4)	
c (Å)		8.419(5)	
α (deg)		91.42 (4)	
β (deg)		107.29 (4)	
γ (deg)		118.90 (4)	
Z		2	
distances	(Å)	angles	(deg)
Nd–C A(1)	2.800(22)	$\varnothing$ A–Nd–$\varnothing$ B	119.9(3)
Nd–C A(2)	2.859(15)	$\varnothing$ A–Nd–$\varnothing$ C	119.8(4)
Nd–C A(3)	2.766(15)	$\varnothing$ B–Nd–$\varnothing$ C	120.4(3)
Nd–C A(4)	2.836(17)		
Nd–C A(5)	2.748		

Some analogous complexes with the cyclopentadienyl ligand substituted only by one organosilyl group have also been described. Atwood et al. (1978) report the colorless compounds $(Me_3SiC_5H_4)_2Y(\mu\text{-}Cl)_2Li \cdot (THF)_2$ and $(Me_3SiC_5H_4)_2Y(\mu\text{-}Cl)_2Li \cdot$ (tmed), and the crystalline dimer $[(Me_3SiC_5H_4)_2YCl]_2$, which was obtained after sublimation of the tetrahydrofuran complex above 250°C. Lappert et al. (1980) prepared the red-brown dimers $[(Me_3SiC_5H_4)_2YbCl]_2$ and $[(Me_3SiC_5H_4)_2YbI]_2$, and Watson et al. (1981) isolated the compounds $Cp_2'Lu(\mu\text{-}Cl)_2Li$ and $Cp_2'Yb(\mu\text{-}Cl)_2Li \cdot (Et_2O)_2$ (see table 9 and fig. 13).

An "open" cyclopentadienyl complex of a rare earth was described recently by Ernst and Cymbaluk (1982). Neodymium trichloride reacts with 2,4-dimethylpentadienyl potassium in tetrahydrofuran with formation of bright green, highly ionic tris(2,4-dimethylpentadienyl) neodymium. The ^1H NMR spectrum shows four peaks at $\delta = 20.6$, 8.5, -1.7, and -29.8 ppm, which are not easily assigned. The X-ray structural analysis (fig. 18, table 11) shows nearly planar 2,4-dimethylpentadienyl ligands, with the carbon atoms in the 2- and 4-positions bent out of the plane in a direction away from the neodymium atom. An unsymmetric charge distribution is postulated in this ligand, having the biggest charge at carbon 3. Two different C–C bond distances are observed, averaging 1.373(12) and 1.421(12) Å, which supports this resonance hybrid model.

All known compounds of this section 2.1.2 are shown in table 8.

2.1.3. *Organometallic compounds of the rare earths with indenyl, cyclooctatetraenyl and other π-ligands*

Tris(indenyl) complexes of some rare earths were prepared by Tsutsui and Gysling (1968, 1969) by the reaction of the metal trichlorides with the sodium salt of indene. They are isolated as tetrahydrofuran adducts. The solvent-free tris(indenyl) samarium has been made by the interaction of samarium trichloride with bis(inde-

nyl) magnesium in benzene (Atwood et al., 1973):

$$RCl_3 + 3\,NaC_9H_7 \xrightarrow{THF} (C_9H_7)_3R \cdot (THF) + 3\,NaCl, \tag{27}$$

R = La, Sm, Gd, Tb, Dy, Yb,

$$2\,SmCl_3 + 3\,Mg(C_9H_7)_2 \xrightarrow{benzene} 2\,(C_9H_7)_3Sm + 3\,MgCl_2. \tag{28}$$
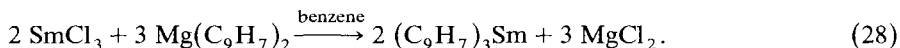
The compounds are sensitive to moisture and air. The coordinated tetrahydrofur-ane can be removed by heating in vacuo to 70°C, and it can be replaced by dioxane and other Lewis bases. The magnetic properties correspond to that of the corre-sponding cyclopentadienyl complexes (table 12). The proton NMR spectrum of $(C_9H_7)_3La$ in THF-d_8 resembles that of the ionic sodium indenide with two low field double doublets at $\delta = 7.36$ and 6.76 ppm, of relative intensity 2, due to the protons of the benzene ring. A singlet at $\delta = 5.48$ ppm with a slight shoulder on the low field side with intensity 2 and a triplet with intensity 1 at $\delta = 3.19$ ppm may be interpreted as an A_2X pattern for the five-membered ring. In contrast, the spectrum of the samarium derivative is indicative of an η^1-indenyl ligand with an ABX pattern of the five-membered ring protons at $\delta = 6.67$, 6.25, and 3.18 ppm in addition to a multiplet for the four benzene ring protons at $\delta = 6.98$ ppm.

The X-ray structure of the solvent-free $(C_9H_7)_3Sm$ (fig. 19), done by Atwood et al. in 1973, shows the samarium atom surrounded by the three five-membered rings of the indenyl ligands in an approximately trigonal planar arrangement of the ring centers around the metal. The crystal data and some bonding distances and angles are given in table 13.

TABLE 12
Indenyl complexes of the rare earths.

Compound	Color	Other data	Refs.
$(C_9H_7)_3Sm$	red		1
$(C_9H_7)_3La \cdot (THF)$	pale tan		2
$(C_9H_7)_3Sm \cdot (THF)$	deep red	m.p. 185–200°C, μ_{eff} 1.55 B.M.	2
$(C_9H_7)_3Gd \cdot (THF)$	pale green	μ_{eff} 7.89 B.M.	2
$(C_9H_7)_3Tb \cdot (THF)$	pale yellow	μ_{eff} 9.43 B.M.	2
$(C_9H_7)_3Dy \cdot (THF)$	pale tan	μ_{eff} 9.95 B.M.	2
$(C_9H_7)_3Yb \cdot (THF)$	dark green	μ_{eff} 4.10 B.M.	2
$(C_9H_7)_3Ce \cdot (py)$	yellow		3
$(C_9Me_7)_3Nd \cdot (THF)_5$			4
$(C_9Me_7)_3Er \cdot (THF)_3$			4
$(C_9Me_7)_2NdCl \cdot (THF)$			4
$(C_9Me_7)_2ErCl$			4
$(C_9Me_7)LaCl_2 \cdot (THF)$			4
$(C_9Me_7)NdCl_2$			4
$(C_9Me_7)ErCl_2 \cdot (THF)_{0.5}$			4

1. Atwood et al. (1973).
2. Tsutsui and Gysling (1969).
3. Zazzetta and Greco (1979).
4. Tsutsui et al. (1982).
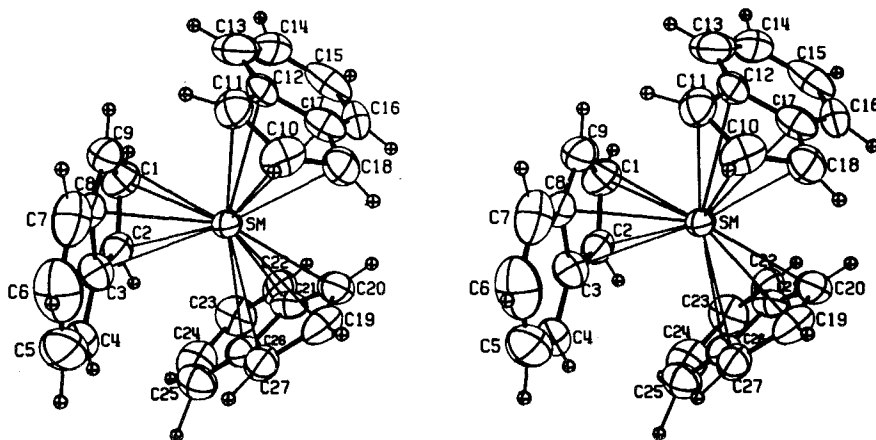
Fig. 19. Stereoscopic view of the structure of $(C_9H_7)_3Sm$ (after Atwood et al., 1973).

The structure of tris(indenyl) cerium pyridinate (fig. 20, table 12), which is prepared by the reduction of $Ce(O-i-C_3H_7)_4 \cdot (py)$ by triethyl aluminum (Zazzetta and Greco, 1979), confirms this π-complexation for the indenyl derivatives. The π-bonded five-membered portions of the indenyl ligands and the σ-bonded nitrogen atom of the pyridine ring are arranged tetrahedrally around the cerium atom.

Heptamethylindenyl complexes of lanthanum, neodymium and erbium were synthesized by the reaction of the appropriate rare earth trichloride with potassium heptamethylindenide in tetrahydrofuran by Tsutsui et al. in 1982. Corresponding to the ratio of the starting materials, the tris(heptamethylindenyl) derivatives of

TABLE 13

Crystallographic data and important bond distances and angles in $(C_9H_7)_3Sm$ and $(C_9H_7)_3Ce \cdot (py)$.

	$(C_9H_7)_3Sm$		$(C_9H_7)_3Ce \cdot (py)$	
crystal system	orthorhombic		orthorhombic	
space group	Pbca		Pbca	
a (Å)	15.568(3)		13.106(3)	
b (Å)	31.348(8)		26.364(4)	
c (Å)	8.265(2)		13.832(2)	
Z	8		8	
distances (Å)				
	Sm–C (aver.)	2.75	Ce–C (aver.)	2.858
	Sm–∅A	2.45	Ce–N	2.684
	Sm–∅B	2.44		
	Sm–∅C	2.48		
angles (deg)				
	∅A–Sm–∅B	120	∅A–Ce–∅B	116.9
	∅A–Sm–∅C	121	∅A–Ce–N	104.3
	∅B–Sm–∅C	116	∅B–Ce–N	103.9
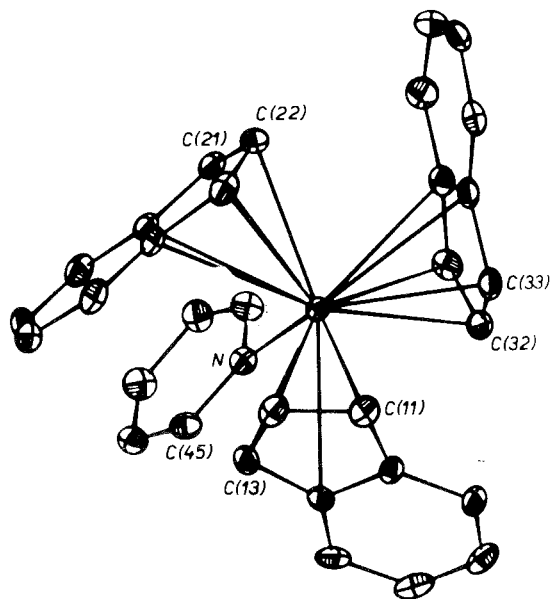
Fig. 20. Molecular structure of $(C_9H_7)_3$-Ce·(py) (after Zazzetta and Greco, 1979).

neodymium and erbium, the bis(heptamethylindenyl) chlorides of neodymium and erbium, and the heptamethylindenyl dichlorides of lanthanum, neodymium and erbium can be isolated, coordinated with different amounts of tetrahydrofuran:

$$RCl_3 + n \, K \underset{}{\overset{\text{THF}}{\longrightarrow}} [\quad]_n RCl_{3-n} + n \, KCl. \qquad (29)$$
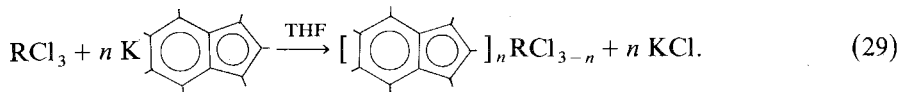
^{13}C NMR spectra, UV and infrared spectra confirm the proposed structure of these compounds with η^5 ligation.

Trifluorenyl cerium is described as a bright yellow solid by Kalsotra et al. (1972a). The compound, which was prepared from cerium trichloride, fluorene and sodium in tetrahydrofuran is immiscible with water, stable in dry and inert atmosphere and it melts with decomposition at 98°C:

$$CeCl_3 + 3 \, NaC_{13}H_9 \overset{\text{THF}}{\longrightarrow} (C_{13}H_9)_3Ce + 3 \, NaCl. \qquad (30)$$
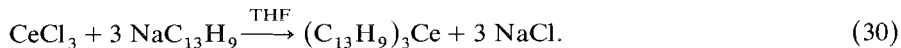
The fluorenyl complexes $(C_{13}H_9)_2R(Cl)_2Li(THF)_2$ of La, Sm, and Ho are mentioned by Rybakova et al. (1981).

Cyclooctatetraenyl derivatives of the rare earths were synthesized shortly after the characterization of uranocene first for europium and ytterbium in the oxidation state R^{+2} by Hayes and Thomas (1969a). But one year later, Mares et al. (1970) prepared complexes of the type $K[R(C_8H_8)_2]$, where $R = Ce$, Pr, Nd, Sm, and Tb. The corresponding yttrium, lanthanum and gadolinium derivatives are described by Hodgson et al. (1973); and the scandium compound was made by Westerhof and De Liefde Meijer in 1976:

TABLE 14
Cyclooctatetraenyl complexes of the rare earths in the oxidation state R^{3+}.

Compound	Color	Other data		Refs.
$K[Sc(C_8H_8)_2]$	yellow-brown			1
$K[Y(C_8H_8)_2]$	yellow			2
$K[La(C_8H_8)_2]$	green			2
$K[Ce(C_8H_8)_2]$	pale green	dec.	160°C,	3
		μ_{eff}	1.88 B.M.	
$K[Pr(C_8H_8)_2]$	yellow-gold	dec.	160°C,	3
		μ_{eff}	2.84 B.M.	
$K[Nd(C_8H_8)_2]$	pale green	dec.	160°C,	3
		μ_{eff}	2.98 B.M.	
$K[Sm(C_8H_8)_2]$	brown	dec.	160°C,	3
		μ_{eff}	9.86 B.M.	
$K[Gd(C_8H_8)_2]$	yellow	μ_{eff}	9.86 B.M.	2
$K[Tb(C_8H_8)_2]$	yellow-brown	dec.	160°C,	3
		μ_{eff}	9.86 B.M.	
$[K(diglyme)][Ce(C_8H_8)_2]$				4
$[K(monoglyme)][Ce(C_8H_8)_2]$	green			5
$C_8H_8ScCl \cdot (THF)$	yellow			1
$C_8H_8YCl \cdot (THF)_2$				6
$C_8H_8CeCl \cdot (THF)_2$	yellow-green	μ_{eff}	1.79 B.M.	7
$C_8H_8PrCl \cdot (THF)_2$	pale green	μ_{eff}	3.39 B.M.	7
$C_8H_8NdCl \cdot (THF)_2$	bright green	μ_{eff}	3.37 B.M.	7
$C_8H_8SmCl \cdot (THF)_2$	purple	μ_{eff}	1.36 B.M.	7
$[La(C_8H_8)(THF)_2][La(C_8H_8)_2]$	gold			8
$[Ce(C_8H_8)(THF)_2][Ce(C_8H_8)_2]$	gold	μ_{eff}	1.86 B.M.	8
$[Nd(C_8H_8)(THF)_2][Nd(C_8H_8)_2]$	green	μ_{eff}	3.20 B.M.	8
$[Er(C_8H_8)(THF)_2][Er(C_8H_8)_2]$	reddish brown	μ_{eff}	9.31 B.M.	8
$Ce_2(C_8H_8)_3$	green			5
$C_5H_5ScC_8H_8$		subl.	120°C/0.1	1
$C_5H_5YC_8H_8$				6
$C_5H_5NdC_8H_8$				6
$C_5H_5HoC_8H_8$				6
$C_5H_5YC_8H_8 \cdot (THF)$				6
$C_5H_5NdC_8H_8 \cdot (THF)$				6
$C_5H_5SmC_8H_8 \cdot (THF)$				6
$C_5H_5HoC_8H_8 \cdot (THF)$				6
$C_5H_5ErC_8H_8 \cdot (THF)$				6
$C_5H_5YC_8H_8 \cdot (py)$				6
$C_5H_5HoC_8H_8 \cdot NH_3$				6
$C_5H_5HoC_8H_8 \cdot C_6H_{11}NC$				6
$C_8H_8LaCl \cdot (THF)_2$	yellow	IR, NMR		9
$C_8H_8ErCl \cdot (THF)$	pink			9
$C_8H_8LuCl \cdot (THF)$	white	NMR		9

1. Westerhof and De Liefde Meijer (1976).
2. Hodgson et al. (1973).
3. Mares et al. (1970).
4. Hodgson and Raymond (1972a).
5. Greco et al. (1976).
6. Jamerson et al. (1974).
7. Mares et al. (1971).
8. De Kock et al. (1978).
9. Wayda (1983).

$$2 \text{ K}_2\text{C}_8\text{H}_8 + \text{RCl}_3 \xrightarrow{\text{THF}} \text{K}\big[\text{R}(\text{C}_8\text{H}_8)_2\big] + 3 \text{ KCl}, \tag{31}$$

R = Y, La, Ce, Pr, Nd, Sm, Gd, Tb,

$$\text{C}_8\text{H}_8\text{ScCl} \cdot (\text{THF}) + \text{K}_2\text{C}_8\text{H}_8 \xrightarrow{\text{THF}} \text{K}\big[\text{Sc}(\text{C}_8\text{H}_8)_2\big] + \text{KCl}. \tag{32}$$
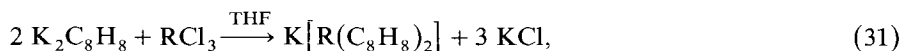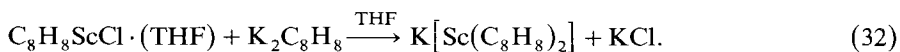
$\text{K}[\text{Pr}(\text{C}_8\text{H}_8)_2]$ is proposed to be an intermediate in the conversion of cis,cis-1,5-cyclooctadiene to the cyclooctatetraenyl dianion by potassium in the presence of PrCl_3 (W.J. Evans et al., 1978b). All known cyclooctatetraenyl compounds of the rare earths are shown in table 14.

The complexes are sensitive to moisture and air, but stable up to about 160°C. Controlled oxidation of these complexes by air yields cyclooctatriene, and the reaction with UCl_4 forms uranocene in high yields. Infrared, Raman (Aleksanyan et al., 1981), visible and ultraviolet spectra as well as semiempirical LCAO calculations (Clark and Warren, 1976) and the chemical behavior are consistent with a high degree of ionic character in these compounds.

The cerium complexes with the potassium cation coordinated by monoglyme (Greco et al., 1976) and diglyme (Hodgson and Raymond, 1972a) have also been described, the X-ray structure of the latter is shown in fig. 21 with the crystallographic data and structural parameters in table 15. It shows a discrete $[\text{Ce}(\text{C}_8\text{H}_8)_2]^-$ anion with planar C_8H_8 rings having equal aromatic C–C bond distances of 1.39 Å in an approximately staggered conformation. The potassium atom in the cation is
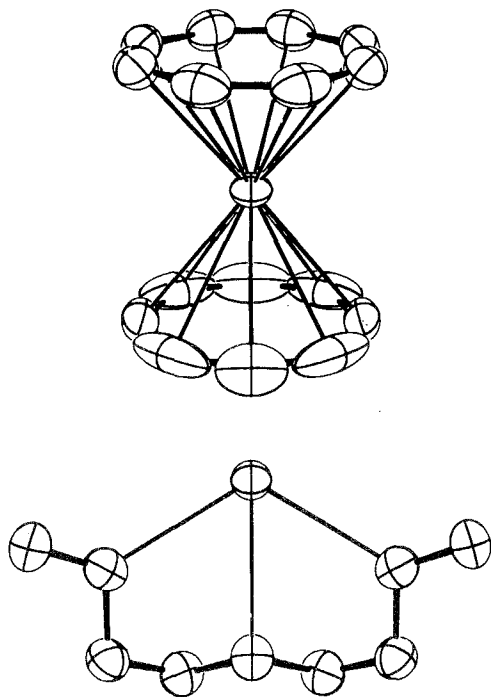
Fig. 21. Molecular structure of [K(diglyme)]-$[\text{Ce}(\text{C}_8\text{H}_8)_2]$ (after Hodgson and Raymond, 1972a).

TABLE 15

Crystallographic data, bonding distances and angles in rare earth cyclooctatetraene complexes.

	$[K(diglyme)][Ce(C_8H_8)_2]$		$C_8H_8CeCl\cdot(THF)_2$		$[Nd(C_8H_8)(THF)_2][Nd(C_8H_8)_2]$	
crystal system	orthorhombic		monoclinic		monoclinic	
space group	Pnma		$P2_1/c$		$P2_1/c$	
a (Å)	16.897(4)		11.869(6)		16.664(3)	
b (Å)	14.014(5)		12.621(5)		12.778(3)	
c (Å)	9.358(2)		13.497(7)		14.347(4)	
β (deg)			122.91(3)		108.90(2)	
Z	4		2 (4 monomers)		4	
distances (Å)						
	C—C (aver)	1.388(28)	Ce—Ce	4.642(3)	Nd1—C (aver. COT1)	2.68(1)
	Ce—C (aver.)	2.742(8)	Cl—Cl'	3.461(3)	Nd1—C (aver. COT2)	2.79(1)
	K—C (aver.)	3.160(32)	Ce—Cl	2.855(2)	Nd2—C (aver. COT3)	2.68(1)
	K—O1	2.792(5)	Ce—Cl'	2.935(2)	Nd2—C14	2.69(2)
	K—O2	2.741(4)	Ce—C (aver.)	2.710(2)	Nd2—C13	2.89(2)
			Ce—O (aver.)	2.583(2)	Nd2—C15	3.02(2)
					Nd2—O (aver.)	2.58
angles (deg)						
	C_l–Ce–C_{i+1} (aver.)	30.2(10)	Cl—Ce—Cl'	73.41(5)	O1—Nd2—O2	73.4(5)
	C_i–Ce–C_{i+4} (aver.)	81.7(9)	O1—Ce—O2	69.01(13)		
			O1—Ce—Cl	104.07(10)		
			O2—Ce—Cl	76.47(9)		

Fig. 22. Stereoscopic view of the molecular structure of dimeric $C_8H_8CeCl \cdot (THF)_2$ (after Hodgson and Raymond, 1972b).

coordinated by the diglyme on one side and by one of the cyclooctatetraenyl rings on the other side.

The reaction of the rare earth trichlorides with dipotassium cyclooctatetraenyl in a 1 : 1 ratio produces dimeric cyclooctatetraenyl complexes $[C_8H_8RCl \cdot (THF)_2]_2$ for Ce, Pr, Nd, and Sm (Mares et al., 1971; Hodgson et al., 1973) and the complex $C_8H_8ScCl \cdot (THF)$ (Westerhof and De Liefde Meijer, 1976):

$$RCl_3 + K_2C_8H_8 \xrightarrow{\ THF\ } \tfrac{1}{2} \left[C_8H_8RCl \cdot (THF)_2 \right]_2 + 2\,KCl, \tag{33}$$
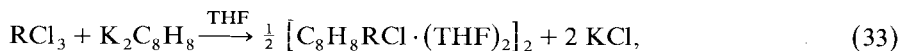
R = Ce, Pr, Nd, Sm.

The complexes lose tetrahydrofuran upon heating to 60°C in vacuo. The X-ray structural analysis of the cerium complex (fig. 22, table 15), done by Hodgson and Raymond (1972b), shows the two cerium atoms bridged asymmetrically by the two chlorine atoms. The planar cyclooctatetraenyl rings are symmetrically bonded to the cerium atoms. Two tetrahydrofuran oxygen atoms and the two chlorine atoms form a plane parallel to and below the cyclooctatetraene rings to complete the inner coordination geometry.

Cocondensation of La, Ce, Nd, or Er metal atoms with cyclooctatetraene at $-196°C$ yielded dinuclear complexes of the formula $[C_8H_8R(THF)_2][R(C_8H_8)_2]$ after extraction with tetrahydrofuran (De Kock et al., 1978). The structure of the neodymium complex (fig. 23, table 15) shows two cyclooctatetraene rings in the anion, which are neither equidistant from the neodymium atom, nor parallel. The neodymium atom in the cation is asymmetrically located with respect to the central cyclooctatetraene ring with neodymium–carbon distances between 2.68 and 4.63 Å (Ely et al., 1976; De Kock et al., 1978).

A tripledecker sandwich structure is possible for the green microcrystalline compound $Ce_2(C_8H_8)_3$, which is formed in the reduction of $Ce(O\text{-}i\text{-}C_3H_7)_4$ by triethyl aluminum in the presence of cyclooctatetraene (Greco et al., 1976). The
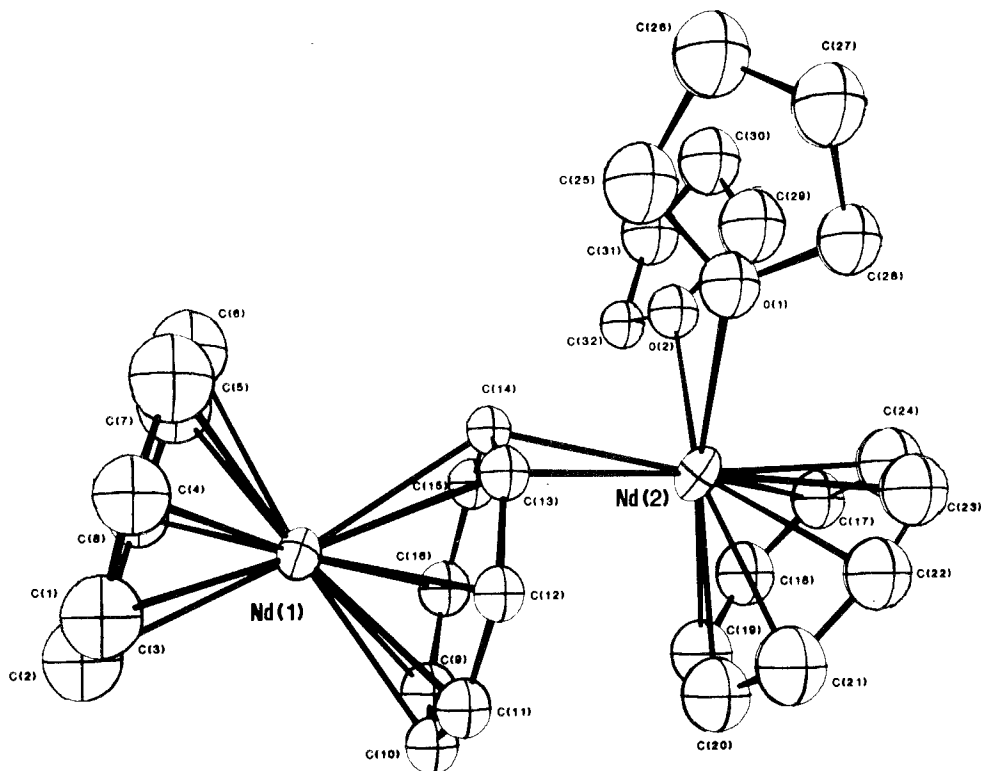
Fig. 23. Molecular structure of $[Nd(C_8H_8)(THF)_2][Nd(C_8H_8)_2]$. (after De Kock et al., 1978).

compound is highly sensitive to oxygen, water and alcohols. The infrared spectra suggest the presence of two different types of cyclooctatetraene rings. Heating of $Ce_2(C_8H_8)_3$ with excess C_8H_8 and a trace of triethyl aluminum yields $Ce(C_8H_8)_2$.

$$2 Ce(O\text{-}i\text{-}C_3H_7)_2 \cdot (i\text{-}C_3H_7OH) + 10 AlEt_3 + 3 C_8H_8$$

$$\rightarrow Ce_2(C_8H_8)_3 + 10 Et_2AlO\text{-}i\text{-}C_3H_7 + 2 C_2H_6 + 8 C_2H_5^- \qquad (34)$$
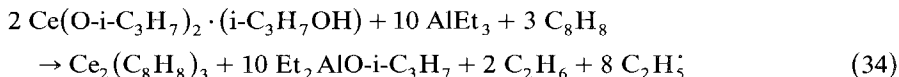
Mixed sandwich complexes of the rare earths containing cyclopentadienyl and cyclooctatetraenyl ligands were prepared either by the reaction of cyclopentadienyl rare earth dichlorides with dipotassium cyclooctatetraenide or form cyclooctatetraenyl rare earth chlorides and sodium cyclopentadienide in tetrahydrofuran (Jamerson et al., 1974):

$$C_5H_5RCl_2 \cdot (THF)_3 + K_2C_8H_8 \xrightarrow{THF} C_5H_5RC_8H_8 \cdot (THF) + 2 KCl,$$

$$R = Y, Sm, Ho, Er, \qquad (35)$$

$$[C_8H_8RCl \cdot (THF)_2]_2 + 2 NaC_5H_5 \xrightarrow{THF} 2 C_5H_5RC_8H_8 \cdot (THF) + 2 NaCl,$$

$$R = Y, Nd. \qquad (36)$$
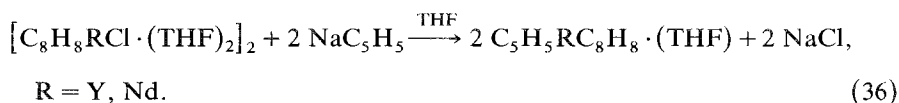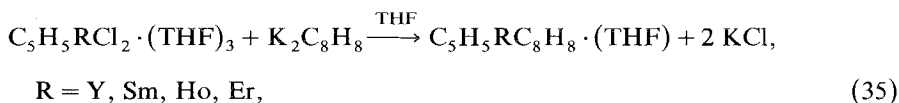
The air-sensitive compounds are isolated as THF adducts. Tetrahydrofuran can be liberated by vacuum drying, but also complexes with other Lewis bases can be made, like $C_5H_5YC_8H_8 \cdot (Py)$, $C_5H_5HoC_8H_8 \cdot (NH_3)$ and $C_5H_5HoC_8H_8 \cdot (C_6H_{11}NC)$. The infrared spectra show extra vibrational bands, which may indicate bridging interactions in the structure of the solid molecules. The mass spectra show the parent ion as well as $RC_5H_5^+$ and $RC_8H_8^+$ with equal intensity. Another fragmentation shows elimination of C_2H_2 from the cyclooctatetraene ring yielding the ion $C_6H_6RC_5H_5^+$.

The corresponding scandium derivative was made solvent free according to eq. (37) and isolated as a yellowish white rather air-sensitive powder, which is characterized by NMR, infrared, and mass spectra (Westerhof and De Liefde Meijer, 1976). The X-ray electron spectrum of $C_5H_5ScC_8H_8$ shows the charges on the cyclopentadienyl ligand not significantly differing from that in the analogous titanium compound, whereas the cyclooctatetraenyl ligand is more negatively charged in the scandium than in the titanium compound (Westerhof and De Liefde Meijer, 1978).

$$C_8H_8ScCl \cdot (THF) + NaC_5H_5 \xrightarrow{\text{THF}} C_5H_5ScC_8H_8 + NaCl. \qquad (37)$$
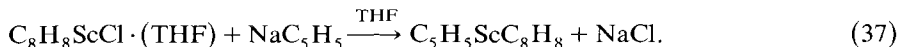
2.2. Cyclopentadienyl rare earth alkyl and aryl complexes

The first dicyclopentadienyl rare earth alkyl and aryl derivatives were described in 1975 (Tsutsui and Ely, 1975a; N.M. Ely and Tsutsui, 1975). The methyl and phenyl derivatives of dicyclopentadienyl gadolinium, erbium and ytterbium have been prepared and the UV, IR spectra, as well as the magnetic moments were given (table 16). No structural information is available. The compounds should be monomeric without coordinating solvents like $(C_5H_5)_2GdCH_3$ (Dubois et al., 1977). The coordination of the nitrogen atom in $(C_5H_5)_2ScC_6H_4-2-CH_2N(CH_3)_2$, which forms a chelated 5-membered ring, makes such a formulation more acceptable (Manzer, 1978). Some ^1H NMR data are given in table 17.

The structural problems were solved by Holton et al. (1976a, b) via the synthesis and the demonstration of the reactive behavior of some bimetallic complexes of the rare earths. The reaction of dicyclopentadienyl rare earth chlorides with lithium tetramethyl aluminate or lithium tetraethyl aluminate in toluene at $0°C$ gives in high yields the crystalline complexes shown in eq. (38) (Holton et al., 1979b, c):

$$(Cp_2RCl)_2 + 2 LiAlL_4 \xrightarrow[0°C]{\text{toluene}} 2 Cp_2R\Big\langle \begin{matrix} L \\ L \end{matrix} \Big\rangle AlL_2 + 2 LiCl, \qquad (38)$$
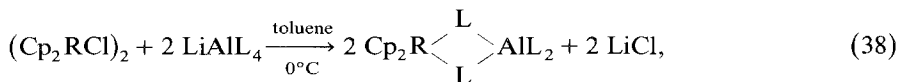
$R = Sc, Y, Gd, Dy, Ho, Er, Tm, Yb, L = Me;$
$R = Sc, Y, Ho, L = Et.$

The isolated compounds (table 16) are soluble in aromatic hydrocarbons and CH_2Cl_2, but insoluble in saturated hydrocarbons. The complexes of the early lanthanides samarium and gadolinium were insoluble in toluene, and for this reason,

TABLE 16

Cyclopentadienyl alkyl and aryl complexes.

Compound	Color	m.p. (°C)	μ_{eff} (B.M.)	Refs.
$(C_5H_5)_2ScC_6H_4$-2-$CH_2N(CH_3)_2$	white	150		1
$(C_5H_5)_2Sc(\mu\text{-}CH_3)_2Al(CH_3)_2$	pale yellow	108–110		2
$(C_5H_5)_2Sc(\mu\text{-}C_2H_5)_2Al(C_2H_5)_2$	pale yellow			2
$(C_5H_5)_2ScCH_3\cdot THF$	cream			3
$(C_5H_5)_2ScCH_3\cdot py$	cream			3
$(C_5H_5)_2Y(\mu\text{-}CH_3)_2Al(CH_3)_2$	colorless	143		2
$(C_5H_5)_2Y(\mu\text{-}C_2H_5)_2Al(C_2H_5)_2$	colorless			2
$[(C_5H_5)_2YCH_3]_2$	colorless	> 158 dec.		3
$(CH_3C_5H_4)_2Y(\mu\text{-}CH_3)_2Al(CH_3)_2$				4
$(Me_3SiC_5H_4)_2Y(\mu\text{-}CH_3)_2Al(CH_3)_2$				4
$[(CH_3C_5H_4)_2YCH_3]_2$				4
$[(CH_3C_5H_4)_2YC_4H_9]_2$				4
$[(CH_3C_5H_4)_2YC_8H_{17}]_2$				4
$[(C_5Me_4Et)_2YCH_3]_2$				4
$[(Me_3SiC_5H_4)_2YCH_3]_2$				4
$[(CH_3C_5H_4)YC_5H_3CH_3]_2$				4
$(C_5H_5)_2YC(CH_3)_3\cdot THF$	light yellow			5
$(CH_3C_5H_4)_2YC(CH_3)_3\cdot THF$	yellow			5
$(C_5H_5)_2SmCH_2SiMe_3$	colorless	< 50 dec.		7
$(C_5H_5)_2SmC(CH_3)_3\cdot N(C_2H_5)_3$	orange			6
$(C_5H_5)_2SmC_4H_9\cdot N(C_2H_5)_3$	orange			6
$(C_5H_5)_2SmC(CH_3)_3\cdot THF$	orange			6
$(C_5H_5)_2SmC_4H_9\cdot THF$	orange			6
$(C_5H_5)_2GdCH_3$	lavender		7.69	8
$(C_5H_5)_2GdC_6H_5$	white	> 170 dec.		9
$(C_5H_5)_2Gd(\mu\text{-}CH_3)_2Al(CH_3)_2$				2
$(C_5H_5)_2Dy(\mu\text{-}CH_3)_2Al(CH_3)_2$	pale yellow	145–146		2
$[(C_5H_5)_2DyCH_3]_2$	pale yellow	> 145 dec.	9.9	3

TABLE 16 (continued)

Compound	Color	m.p. (°C)	μ_{eff} (B.M.)	Refs.
$(C_5H_5)_2Ho(\mu\text{-}CH_3)_2Al(CH_3)_2$	straw	142–143		2
$(C_5H_5)_2Ho(\mu\text{-}C_2H_5)_2Al(C_2H_5)_2$	straw			2
$[(C_5H_5)_2HoCH_3]_2$	straw	> 160 dec.	10.0	3
$(CH_3C_5H_4)_2Ho(\mu\text{-}CH_3)_2Al(CH_3)_2$				4
$(C_5H_5)_2ErCH_3$	pink		9.41	9
$(C_5H_5)_2ErC_6H_5$	pink	128–130	9.53	9
$(C_5H_5)_2Er(\mu\text{-}CH_3)_2Al(CH_3)_2$	pink	133–135		2
$[(C_5H_5)_2ErCH_3]_2$	pink	> 159 dec.	9.50	3
$(CH_3C_5H_4)_2Er(\mu\text{-}CH_3)_2Al(CH_3)_2$				4
$[(CH_3C_5H_4)_2ErCH_3]_2$				4
$[Me_3SiC_5H_4)_2ErCH_3]_2$				4
$[Me_3SiC_5H_4)_2ErC_4H_9]_2$				4
$(C_5H_5)_2ErC(CH_3)_3 \cdot THF$	light brown	> 40 dec.		7
$(C_5H_5)_2ErCH_2SiMe_3 \cdot THF$	light brown	> 50 dec.		7
$(CH_3C_5H_4)_2ErC(CH_3)_3 \cdot THF$	pink			5
$(C_5H_5)_2Tm(\mu\text{-}CH_3)_2Al(CH_3)_2$	pale green	130 dec.		2
$[(C_5H_5)_2TmCH_3]_2$	pale green	> 160 dec.	7.5	3
$(C_5H_5)_2TmC(CH_3)_3 \cdot THF$	pale green			6
$(C_5H_5)_2TmC_4H_9 \cdot THF$	pale green			6
$(C_5H_5)_2YbCH_3$	orange	194–198	4.14	9
$(C_5H_5)_2YbC_6H_5$	orange		3.86	9
$(C_5H_5)_2Yb(\mu\text{-}CH_3)_2Al(CH_3)_2$	orange–red	133–135		2
$[(C_5H_5)_2YbCH_3]_2$	orange–red	> 165 dec.	4.0	3
$(CH_3C_5H_4)_2Yb(\mu\text{-}CH_3)_2Al(CH_3)_2$				4
$[(CH_3C_5H_4)_2YbCH_3]_2$				4
$(C_5H_5)_2YbC(CH_3)_3 \cdot THF$	orange	40–50 dec.		7
$(C_5H_5)_2YbCH_2SiMe_3 \cdot THF$	red brown	40–50 dec.		7
$(C_5H_5)_2YbC_4H_9 \cdot THF$	orange			6
$(C_5Me_5)_2YbCH_3 \cdot O(C_2H_5)_2$				10
$(C_5Me_5)_2YbCH_3 \cdot THF$	orange			11
$(C_5Me_5)_2Yb(\mu\text{-}CH_3)_2Li$				10

Compound	Color	m.p.		Ref.
$(C_5Me_5)_2Yb(\mu\text{-}CH_3)_2Li\cdot(THF)_3$	yellow			10
$(C_5Me_5)_2Yb(\mu\text{-}CH_3)_2Al(CH_3)_2$				10
$(C_5Me_5)_2Yb(\mu\text{-}CH_3)_2Li\cdot[O(C_2H_5)_2]_2$				11
$(C_5Me_5)_2Yb(\mu\text{-}CH_3)(\mu\text{-}Cl)Li\cdot[O(C_2H_5)_2]_2$	brown			11
$(C_5H_5)_2LuC(C_6H_5)_3$	red yellow			7
$(C_5H_5)_2LuCH_3\cdot THF$	colorless	<20 dec.		7
$(C_5H_5)_2LuC_2H_5\cdot THF$	colorless	<20 dec.		7
$(C_5H_5)_2LuCH(CH_3)_2\cdot THF$	colorless	<20 dec.		7
$(C_5H_5)_2LuC_4H_9\cdot THF$	colorless	<20 dec.		7
$(C_5H_5)_2LuC(CH_3)_3\cdot THF$	colorless	70–80 dec.		12
$(C_5H_5)_2LuCH_2SiMe_3\cdot THF$	colorless	100–110 dec.		7
$(C_5H_5)_2LuCH_2C(CH_3)_3\cdot THF$	colorless	90–100 dec.		7
$(CH_3C_5H_4)_2LuC(CH_3)_3\cdot THF$	white			5
$(C_5H_5)_2LuCH_2C_6H_5\cdot THF$	colorless	100–110 dec.		7
$(C_5H_5)_2LuC_6H_4\text{-}4\text{-}CH_3\cdot THF$	colorless	110–120 dec.		7
$(C_5Me_5)_2LuCH_3$				13
$(C_5Me_5)_2LuCH_2CH(CH_3)_2$				10
$(C_5Me_5)_2LuCH_2CH(CH_3)C_3H_7$				13
$(C_5Me_5)_2LuCH_2CH(CH_3)CH_2CH(CH_3)_2$				13
$(C_5Me_5)_2LuCH_3\cdot O(C_2H_5)_2$				10
$(C_5Me_5)_2LuCH_3\cdot N(C_2H_5)_3$				13
$(C_5Me_5)_2LuCH_3\cdot py$				10
$(C_5Me_5)_2Lu(\mu\text{-}CH_3)_2Li$				10
$(C_5Me_5)_2Lu(\mu\text{-}CH_3)_2Li\cdot(THF)_3$				10
$(C_5Me_5)_2Lu(\mu\text{-}CH_3)_2Al(CH_3)_2$				10
$(C_5Me_5)_2La(\mu\text{-}CH_3)_2Li\cdot(DME)_2$	colorless	144 dec.		14
$(C_5H_5)_2GdC_6H_4\text{-}4\text{-}CH_3$	pale yellow	115 dec.		15
$(C_5H_5)_2GdC_6H_4\text{-}4\text{-}CH_3\cdot THF$	orange yellow	94 dec.		15
$(C_5H_5)_2ErC_6H_4\text{-}4\text{-}CH_3$	pink	92 dec.	9.28	15
$(C_5H_5)_2ErC_6H_4\text{-}4\text{-}CH_3\cdot THF$	pink	76–78 dec.		15
$(C_5H_5)_2ErC_6H_4\text{-}4\text{-}Cl$	pink	78–80		15
$(C_5H_5)_2ErC_6H_4\text{-}4\text{-}Cl\cdot THF$	orange red	104–106 dec.	11.09	15
$(C_5H_5)_2Er(\mu\text{-}CH_3)_2Li\cdot(THF)_2$	pink	108–112		16
$(C_5H_5)_2Er(\mu\text{-}CH_3)_2Li\cdot(tmed)$	pink			16

TABLE 16 (continued)
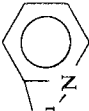
Compound	Color	m.p. (°C)	μ_{eff} (B.M.)	Refs.
$(CH_3C_5H_4)_2ErC_6H_4\text{-}4\text{-}CH_3$	pink	150 dec.	9.23	15
$(CH_3C_5H_4)_2ErC_6H_4\text{-}4\text{-}CH_3 \cdot THF$	orange red	130–134		15
$(C_5H_5)_2YbC_6H_4\text{-}4\text{-}CH_3$	orange red	100 dec.	3.96	15
$(C_5H_5)_2YbC_6H_4\text{-}4\text{-}CH_3 \cdot THF$	orange red	85–90		15
$(C_5H_5)_2Lu(\mu\text{-}CH_3)_2Li \cdot (THF)_2$	colorless	108–110 dec.	16	16
$(C_5H_5)_2Lu(\mu\text{-}CH_3)_2Li \cdot (tmed)$	colorless	118–122 dec.		17
$(C_5Me_5)_2LuCH_2SiMe_3$				17
$(C_5Me_5)_2LuC_6H_5$				17
$(C_5Me_5)_2Lu\text{—}\langle\text{pyridyl-}N\rangle$				17
$(C_5Me_5)_2Lu\text{—}\langle C_6H_4\rangle\text{—}Lu(C_5Me_5)_2$	colorless			17
$(C_5Me_5)_2Lu(\mu\text{-}CH_3)_2Li \cdot (tmed)_2$	colorless			16
$(C_5Me_5)_2Lu(\mu\text{-}CH_2SiMe_3)_2Li \cdot (DME)_{3.5}$	colorless			16
$C_5Me_5Lu(\mu\text{-}CH_3)_3Li \cdot (tmed)$	colorless			16
$C_5Me_5Lu(\mu\text{-}CH_2SiMe_3)_3Li \cdot (DME)_{4.5}$	colorless			16

1. Manzer (1978).
2. Holton et al. (1979b).
3. Holton et al. (1979c).
4. Ballard et al. (1978).
5. W.J. Evans et al. (1982a).
6. Schumann and Jeske (1983).
7. Schumann et al. (1982).
8. Dubois et al. (1977).
9. Ely and Tsutsui (1975).
10. Watson (1982).
11. Watson (1980).
12. W.J. Evans et al. (1978a).
13. Watson and Roe (1982).
14. Schumann and Albrecht (1984).
15. Changtao Qian et al. (1983).
16. Schumann et al. (1984b).
17. Watson (1983).

TABLE 17

^{1}H NMR spectral data for dicyclopentadienyl rare earth alkyl compounds (δ in ppm, J in Hz).

Compound	NMR data
$Cp_2ScCH_3 \cdot THF$ [1]	δCp 6.14s, δCH_3 0.03s, δTHF 3.25m, 1.2m
$Cp_2ScCH_3 \cdot py$ [1]	δCp 5.85s, δCH_3 −0.6s, δpy 8.2, 7.35, 7.25
$Cp_2Sc(\mu\text{-}CH_3)_2Al(CH_3)_2$ [2]	δCp 6.12s, δCH_3 −0.29s, $\delta AlCH_3$ −0.84s
$Cp_2Sc(\mu\text{-}C_2H_5)_2Al(C_2H_5)_2$ [2]	δCp 6.19s, δCH_2 −0.58q, δCH_3 1.48t, δAlC_2H_5 −0.01q, 1.15t
$Cp_2ScC_6H_4CH_2N(CH_3)_2$ [3]	δCp 5.95s, δCH_2 3.23s, δNCH_3 1.67s
$(Cp_2YCH_3)_2$ [2]	δCp 6.21s, δCH_3 −0.811, $^2J(HY)$ 3.6
$Cp_2Y(\mu\text{-}CH_3)_2Al(CH_3)_2$ [2]	δCp 6.18s, δCH_3 −0.32d, $^3J(HY)$ 5, $\delta AlCH_3$ −0.98s
$Cp_2Y(\mu\text{-}C_2H_5)_2Al(C_2H_5)_2$ [2]	δCp 6.20s, δCH_2 −0.36m, $^2J(HY)$ 4, δCH_3 1.30t, δAlC_2H_5 −0.19q, 1.01t
$Cp_2YC(CH_3)_3 \cdot THF$ [4]	δCp 6.07s, δCH_3 1.25s, δTHF 3.12m, 0.94m in C_6D_6
$Cp_2YbC(CH_3)_3 \cdot THF$ [5]	δCp −30.30, δCH_3 0.33, δTHF 1.39, 0.97 in C_6D_6
$Cp_2YbCH_2SiMe_3 \cdot THF$ [5]	δCp −29.92, δCH_2 0.16, δCH_3 −0.11, δTHF 1.44, 1.02 in C_6D_6
$Cp_2LuCH_3 \cdot THF$ [5]	δCp 6.27s, δCH_3 −0.62s, δTHF 3.57m, 1.53m in C_6D_6
$Cp_2LuC_2H_5 \cdot THF$ [5]	δCp 6.17s, δCH_2 0.16q, δCH_3 1.77t, δTHF 3.41m, 1.41m in toluene–d_8
$Cp_2LuCH(CH_3)_2 \cdot THF$ [5]	δCp 6.03s, δCH 0.22sp, δCH_3 1.65t, δTHF 3.80m, 1.41m in C_6D_6
$Cp_2LuC_4H_9 \cdot THF$ [5]	δCp 6.15s, δC_4H_9 0.15m, 1.27m, δTHF 3.45m, 1.45m in C_6D_6
$Cp_2LuC(CH_3)_3 \cdot THF$ [5]	δCp 6.16s, δCH_3 1.39s, δTHF 3.32m, 1.13m in C_6D_6
$Cp_2LuCH_2C(CH_3)_3 \cdot THF$ [5]	δCp 6.25s, δCH_2 0.27s, δCH_3 1.51s, δTHF 3.21m, 1.17m in C_6D_6
$Cp_2LuCH_2SiMe_3 \cdot THF$ [5]	δCp 6.17s, δCH_2 −0.63s, δCH_3 0.55s, δTHF 3.16m, 1.15m in C_6D_6
$Cp_2LuCH_2C_6H_5 \cdot THF$ [5]	δCp 6.17s, δCH_2 1.97s, δC_6H_5 7.45m, 7.37m, 7.17m, δTHF 3.27m, 1.24m in C_6D_6
$Cp_2LuC_6H_4\text{-}4\text{-}CH_3 \cdot THF$ [5]	δCp 6.25s, δC_6H_4 7.93d, 7.39d, 2.78s, δTHF 3.21m, 1.10m in C_6D_6
$(CH_3C_5H_4)_2LuC(CH_3)_3 \cdot THF$ [4]	$\delta MeCp$ 5.98, 5.93, 5.78, δCH_3Cp 2.11, δCH_3C 1.34s, δTHF 3.18m, 0.96m
$(C_5Me_5)_2LuCH_3 \cdot (C_2H_5)_2O$ [6]	δCH_3Cp 2.18s, δCH_3Lu −0.49s, δC_2H_5 3.48q, 1.11t, in toluene–d_8
$(C_5Me_5)_2LuCH_2CH(CH_3)_2$	δCH_3Cp 2.11s, δCH_2 0.53d, $J(HH)$ 8.2, δCH 2.42sp of t, $J(HH)$ 6.59 and 8.8. δCH_3CH 1.17d, $J(HH)$ 6.59 in toluene–d_8 [6]
$Cp_2Lu(\mu\text{-}CH_3)_2Li \cdot (THF)_2$ [8]	δCH_3Cp 1.97s, δCH_2 0.17d, $J(HH)$ 8.28, δCH_3 0.82d, $J(HH)$ 6.59 in C_6D_{12} [7]
$Cp_2Lu(\mu\text{-}CH_3)_2Li \cdot (tmed)$ [8]	δCp 6.31s, δCH_3 −0.77s, δTHF 3.52t, 1.39t in C_6D_6
$(C_5Me_5)_2LuCH_3$ [7]	δCp 6.26s, δCH_3 −0.89s, $\delta tmed$ 1.84s, 1.57s in C_6D_6
$(C_5Me_5)_2LuCH_2SiMe_3$ [9]	δCH_3Cp 1.98s, δCH_3 −0.96 in C_6D_{12}
$(C_5Me_5)_2LuC_6H_5$ [9]	δCH_3Cp 1.98s, δCH_2 −0.39s, δCH_3 −0.03s in C_6D_{12}
$(C_5Me_5)_2LuC_5H_4N$ [9]	δCH_3Cp 1.84s, $\delta o\text{-}C_6H_5$ 6.84d ($J(HH)$ 6.45), $\delta m\text{-}C_6H_5$ 7.14t, $J(HH)$ 7.6 in C_6D_{12}
$(C_5Me_5)_2LuC_6H_4Lu(C_5Me_5)_2$ [9]	δCH_3Cp 1.75s, δC_5H_4N 6.89ddd, 7.32ld, 7.73dt, 8.23dt, $J(HH)$ 7.36, 5.12, 1.4 in C_6D_{12}
$(C_5Me_5)_2Lu(\mu\text{-}CH_3)_2Li \cdot (tmed)_2$ [10]	δCH_3Cp 1.85s, δC_6H_4 6.60s in C_6D_{12}
$(C_5Me_5)_2Lu(\mu\text{-}CH_2SiMe_3)_2Li \cdot (DME)_{3,5}$ [10]	δCH_3Cp 1.93s, δCH_3 −1.77s, $\delta tmed$ 2.44s, 2.28s in THF–d_8
	δCH_3Cp 1.88s, δCH_2 −1.86s, δCH_3 −0.11s, δDME 3.42s, 3.26s in THF–d_8

[1] Holton et al. (1979c).
[2] Holton et al. (1979b).
[3] Manzer (1978).
[4] W.J. Evans et al. (1982a).
[5] Schumann et al. (1982).
[6] Watson (1982).
[7] Watson and Roe (1982).
[8] Schumann et al. (1984b).
[9] Watson (1983a).
[10] Schumann and Albrecht (1984).
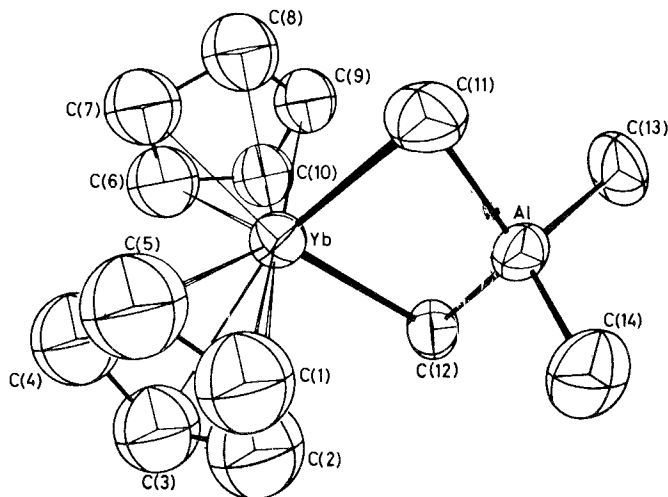
Fig. 24. Molecular structure of $Cp_2Yb(\mu\text{-}CH_3)_2Al(CH_3)_2$ (after Holton et al., 1979b).

are thought to be more ionic. The yellow samarium complex was not isolated free of lithium chloride. Attempts to prepare analogous complexes with $In(CH_3)_3$ were without success, as in the case of the preparation of chlorine containing compounds like $(C_5H_5)_2Y(\mu\text{-}Cl)(\mu\text{-}CH_3)Al(CH_3)_2$ or $(C_5H_5)_2Y(\mu\text{-}CH_3)_2Al(CH_3)Cl$.

Single crystal X-ray structural analysis has been carried out for the compounds $(C_5H_5)_2R(\mu\text{-}CH_3)_2Al(CH_3)_2$ for R = Y (Scollary, 1978; Holton et al., 1976b) and Yb (Holton et al., 1979b) (fig. 24). The crystallographic data and some important bonding distances and bond angles are given in table 18. The compounds have an approximately tetrahedral environment around both rare earths and the aluminum atom with a $R(\mu\text{-}CH_3)_2Al$ unit as in the dimeric trimethyl aluminum. The yttrium compounds are fluxional at 40°C, but at −40°C the bridging and the terminal methyl as well as the ethyl groups give distinct NMR signals (tables 17, 19). Coalescence of these signals in $(C_5H_5)_2Y(\mu\text{-}CH_3)_2Al(CH_3)_2$ takes place at 40°C. $\Delta G^{\ddagger}$ was calculated to be 15.9 kcal/mol at 392 K. Both scandium complexes are nonfluxional at room temperature, but their NMR signals collapse to a singlet for the methyl derivative above 100°C. The infrared spectra of the series are nearly identical. They show bands for the bridging methyl groups at 1235 and 1250 cm^{-1}.

The reaction of di-μ-alkyl-bis(cyclopentadienyl) rare earth dialkylaluminum complexes with equimolar amounts of pyridine in toluene at room temperature gives dimeric dicyclopentadienyl rare earth methyl complexes, which are isolated in about 80% yield as air-sensitive crystalline solids. They are stable for short periods up to 150°C, soluble in CH_2Cl_2, hot toluene or benzene, partly soluble in cold toluene or benzene, but insoluble in saturated hydrocarbons (Holton et al., 1976a and 1979c). The similar reaction of the corresponding scandium derivative with pyridine or tetrahydrofuran does not give the bridging dimer, but a monomer with coordinated pyridine or tetrahydrofuran:
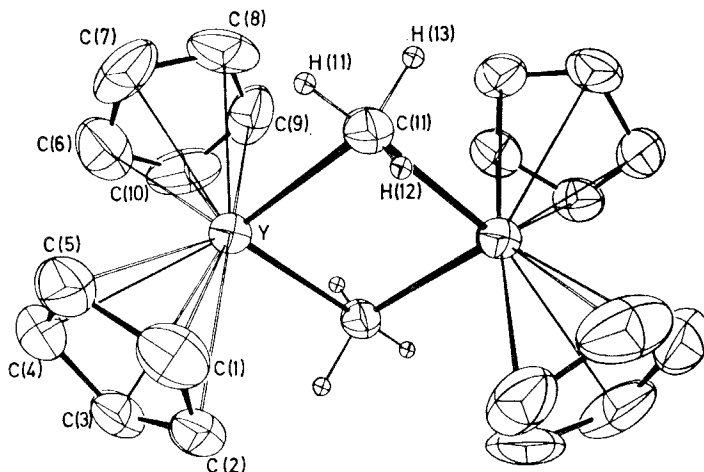
Fig. 25. Molecular structure of $[(C_5H_5)_2YCH_3]_2$ (after Holton et al., 1979c).

$$2\,Cp_2R\!\!<\!\!\begin{array}{c}CH_3\\[4pt]CH_3\end{array}\!\!>\!\!Al(CH_3)_2 + 2\,py$$

$$\xrightarrow[\;25°C\;]{\text{toluene}} 2\,(CH_3)_3Al\cdot py + Cp_2R\!\!<\!\!\begin{array}{c}CH_3\\[4pt]CH_3\end{array}\!\!>\!\!RCp_2, \tag{39}$$

R = Y, Dy, Ho, Er, Tm, Yb,

$$2\,Cp_2Sc\!\!<\!\!\begin{array}{c}CH_3\\[4pt]CH_3\end{array}\!\!>\!\!Al(CH_3)_2 + 2\,L \xrightarrow[\;25°C\;]{\text{toluene}} 2\,Cp_2Sc\!\!<\!\!\begin{array}{c}CH_3\\[4pt]L\end{array} + Al_2(CH_3)_6, \tag{40}$$
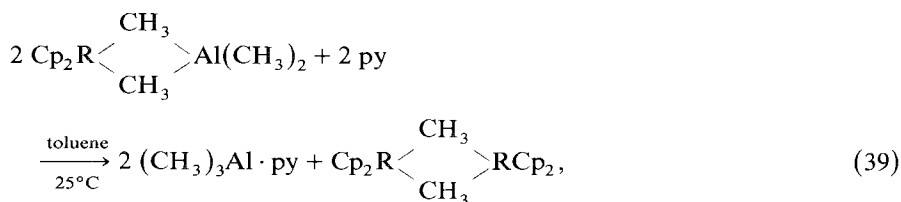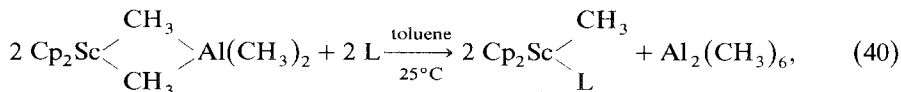
L = py, THF.

The isolated compounds (table 16) show identical infrared spectra with a characteristic band at 1195 cm^{-1} for a methyl group attached to a rare earth metal. The single crystal X-ray analysis of the yttrium (table 18, fig. 25) and of the ytterbium derivative (table 18) show both compounds to be isostructural with an approximately tetrahedral metal environment and a $R(\mu\text{-}CH_3)_2R$ unit like the trimethyl aluminum dimer. The ^1H and ^{13}C NMR spectra of the diamagnetic yttrium complex were invariant between $-40°C$ and $+40°C$ with a triplet for the bridging methyl protons due to the coupling with the two equivalent yttrium atoms (tables 17, 19).

The yttrium complex reacts with Lewis bases, like amines, tetrahydrofurane or phosphine oxides, but less readily with soft donors like phosphines, as monitored by NMR spectra. The triplet at -0.81 ppm collapses to a doublet at lower field, but no isolation of an adduct was possible, pointing out a weaker Lewis acidity for Y^{+3} in comparison to Sc^{+3}. Alkyl- or alkylchloroaluminum compounds react with dimeric dicyclopentadienyl methyl yttrium to give di-μ-alkyl- or di-μ-chloro-bridged compounds as shown in eqs. (41) and (42). The chloro- and methyl-bridged complex (eq. 43) decomposes with formation of trimethyl aluminum and dicyclopentadienyl

yttrium chloride:

$$(Cp_2YCH_3)_2 + (CH_3AlCl_2)_2 \rightarrow 2\ Cp_2Y\!\!<^{Cl}_{Cl}\!\!>\!Al(CH_3)_2, \tag{41}$$

$$(Cp_2YCH_3)_2 + \left[Al(CH_3)_3\right]_2 \rightarrow 2\ Cp_2Y\!\!<^{CH_3}_{CH_3}\!\!>\!Al(CH_3)_2, \tag{42}$$

$$(Cp_2YCH_3)_2 + \left[(CH_3)_2AlCl\right]_2 \rightarrow 2\ Cp_2Y\!\!<^{CH_3}_{Cl}\!\!>\!Al(CH_3)_2 \rightarrow \tag{43}$$

$$(Cp_2YCl)_2 + \left[Al(CH_3)_3\right]_2.$$
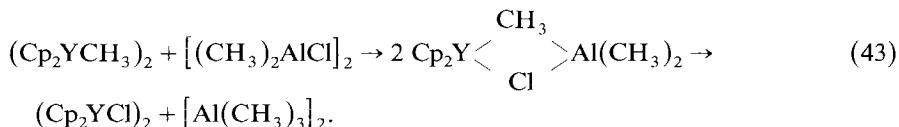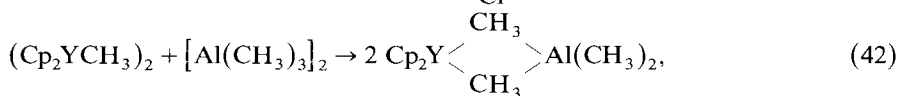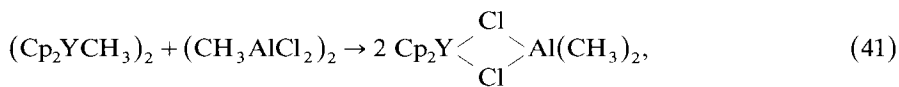
Dicyclopentadienyl erbium methyl and dicyclopentadienyl ytterbium methyl react with alkynes like $HC\equiv CC(CH_3)_3$ with formation of dimeric alkynide-bridged complexes of the type $[Cp_2RC\equiv CC(CH_3)_3]_2$ (Atwood et al., 1981).

Some other alkyl-bridged complexes of the types $Cp_2R(\mu\text{-}L)_2AlL_2$ and $Cp_2R(\mu\text{-}L)_2RCp_2$ with methylcyclopentadienyl, trimethylsilylcyclopentadienyl, and tetramethylethylcyclopentadienyl ligands bonding to the rare earth metal, containing CH_3, C_4H_9, and C_8H_{17} as bridging ligands L as well as $MeCpY(\mu\text{-}C_5H_3CH_3)_2YCpMe$, have been prepared in connection with an investigation of homogenous ethylene polymerization catalysts of the rare earth metals yttrium, holmium, erbium and ytterbium (Ballard et al., 1978).

Dicyclopentadienyl lutetium chloride reacts with organolithium compounds in tetrahydrofurane at $-78°C$, to give monomeric alkyldicyclopentadienyl lutetium derivatives $(C_5H_5)_2LuL \cdot (THF)$ (Schumann et al., 1981a, 1982). But only when L is a more or less bulky alkyl or aryl group are the compounds isolable at room temperature. Compounds with $L = CH_3$, C_2H_5, $i\text{-}C_3H_7$ or C_4H_9 are detected by NMR. The other derivatives (W.J. Evans et al., 1981e, 1982a; Schumann et al., 1981a, 1982), as well as some yttrium and erbium (W.J. Evans et al., 1982a; Schumann et al., 1982), samarium, thulium and ytterbium derivatives (Schumann and Jeske, 1983); Schumann et al., 1982), and bis(methylcyclopentadienyl) derivatives of yttrium, erbium and lutetium (W.J. Evans et al., 1982a) were obtained as crystalline powders or crystals after extraction with benzene or toluene and subsequent crystallization from pentane-ether. They are soluble in benzene, toluene, and tetrahydrofurane, but insoluble in saturated hydrocarbons.

$$Cp_2RCl + Li\text{-}L \xrightarrow[-78°C]{THF} Cp_2R\text{-}L \cdot (THF) + LiCl, \tag{44}$$

$$R = Y, \quad L = C(CH_3)_3,$$

$$R = Sm, \quad L = C_4H_9, C(CH_3)_3,$$

$$R = Er, \quad L = C(CH_3)_3, CH_2SiMe_3,$$

$$R = Tm, \quad L = C_4H_9, C(CH_3)_3,$$

$$R = Yb, \quad L = C_4H_9, C(CH_3)_3, CH_2SiMe_3,$$

$$R = Lu, \quad L = CH_3, C_2H_5, CH(CH_3)_2, C_4H_9, C(CH_3)_3, CH_2C(CH_3)_3,$$
$$CH_2SiMe_3, CH_2C_6H_5, C_6H_4\text{-}4\text{-}CH_3,$$
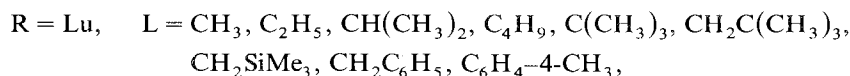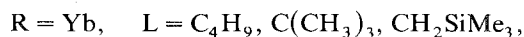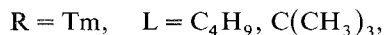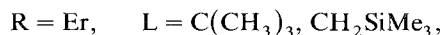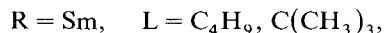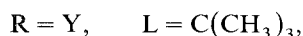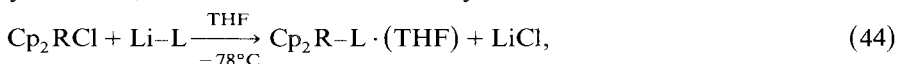
TABLE 18

Crystallographic data, bond distances and angles in dicyclopentadienyl rare earths methyl compounds.

	Cp$_2$Y(μ-CH$_3$)$_2$Al(CH$_3$)$_2$	Cp$_2$Yb(μ-CH$_3$)$_2$Al(CH$_3$)$_2$	Cp$_2$Y(μ-CH$_3$)$_2$YCp$_2$	Cp$_2$Yb(μ-CH$_3$)$_2$YbCp$_2$
crystal system	orthorhombic	orthorhombic	monoclinic	monoclinic
space group	Pna2$_1$	Pna2$_1$	P2$_1$/n	P2$_1$/n
a (Å)	17.969(6)	17.866(5)	10.715(4)	10.656(5)
b (Å)	7.988(4)	7.973(3)	7.607(4)	7.535(4)
c (Å)	10.870(4)	10.871(3)	13.388(5)	13.216(4)
β (deg)			112.84(4)	112.62(4)
Z	4	4	2	2
distances (Å)	Y–C(Cp) 2.62	Yb–C(Cp) 2.61(3)	Y–C(Cp) 2.655(18)	Yb–C(Cp) 2.613(13)
	Y–C1(Me) 2.57(2)	Yb–C11 2.609(23)	Y–C11 2.553(10)	Yb–C11 2.536(17)
	Y–C2(Me) 2.60(2)	Yb–C12 2.562(18)	Y–C11' 2.537(9)	Yb–C11' 2.486(17)
	Al–C1 2.08(2)	Al–C11 2.165(22)		
	Al–C2 2.11(2)	Al–C12 2.096(18)		
	Y–Al 3.056(6)	Yb–Al 3.014(6)		
angles (deg)	Y–C1–Al 81.5(7)	Yb–C11–Al 77.7(7)	Y–C11–Y' 87.7(3)	Yb–C11–Yb' 86.6(5)
	Y–C2–Al 80.1(7)	Yb–C12–Al 80.0(6)	C11–Y–C11' 92.3(3)	C11–Yb–C11' 93.4(5)
	C1–Y–C2 84.5(6)	C11–Al–C12 87.1(6)	Cp1–Y–Cp2 128.9	Cp1–Yb–Cp2 128.2
	C1–Al–C2 112 (1)	C11–Al–C12 113.3(8)	Cp1–Y–C11 106.1	Cp1–Yb–C11 105.9
		Cp1–Yb–C11 107.8	Cp1–Y–C11' 110.2	Cp1–Yb–C11' 110.0
		Cp2–Yb–C11 104.5		

TABLE 19

^{13}C NMR spectral data for dicyclopentadienyl rare earth alkyl compounds (δ in ppm, J in Hz).

Compound	Data
$Cp_2Sc(\mu\text{-}CH_3)_2Al(CH_3)_2$ [1]	δCp 113.2, δCH$_3$ 20.7, δAlCH$_3$ −6.3
$Cp_2Sc(\mu\text{-}C_2H_5)_2Al(C_2H_5)_2$ [1]	δCp 112.1, δCH$_2$ 34.9, δCH$_3$ 15.5, δAlC$_2$H$_5$ 1.5, 10.4
$Cp_2Y(\mu\text{-}CH_3)_2Al(CH_3)_2$ [1]	δCp 112.2, δCH$_3$ 7.86, ^1J(CY) 12.2, δAlCH$_3$ −7.9
$Cp_2Y(\mu\text{-}C_2H_5)_2Al(C_2H_5)_2$ [1]	δCp 111.7, δCH$_2$ 20.75, ^1J(CY) 12.2, δCH$_3$ 13.0, δAlC$_2$H$_5$ −0.34, 10.4
$(Cp_2YCH_3)_2$ [2]	δCp 111.3, δCH$_3$ 23.0, ^1J(CY) 25.0
$[(MeCp)_2YC_4H_9]_2$ [3]	δCp 109.7, 112.9, 120.2, δCH$_2$Y 38.7, ^1J(CY) 22.8, δCH$_3$Cp 15.9
$[(MeCp)_2YC_8H_{17}]_2$ [3]	δCH$_2$Y 39.3, ^1J(CY) 23.0
$[(MeCp)Y(C_5H_3CH_3)]_2$ [3]	δCp 112.3, 116.6, 121.9, δCH$_3$Cp 15.1
$Cp_2LuCH(CH_3)_2 \cdot (THF)$ [4]	δCp 109.6, δCH 36.4, δCH$_3$ 25.4, δTHF 69.7, 25.9
$Cp_2LuC(CH_3)_3 \cdot (THF)$ [4]	δCp 111.3, δC 38.6, δCH$_3$ 36.8, δTHF 73.8, 25.9
$Cp_2LuCH_2C(CH_3)_3 \cdot (THF)$ [4]	δCp 110.8, δCH$_2$ 37.7, δC 62.6, δCH$_3$ 38.3, δTHF 72.9, 25.9
$Cp_2LuCH_2SiMe_3 \cdot (THF)$ [4]	δCp 110.8, δCH$_2$ 28.3, δCH$_3$ 5.9, δTHF 72.6, 26.0
$Cp_2LuCH_2C_6H_5 \cdot (THF)$ [4]	δCp 111.4, δCH$_2$ 48.6, δC$_6$H$_5$ 128.9, 125.7, 118.4, δTHF 73.4, 26.0
$Cp_2LuC_6H_4\text{-}4\text{-}CH_3 \cdot (THF)$ [4]	δCp 111.8, δC$_6$H$_4$ 184.2, 142.2, 129.7, 134.3, δCH$_3$ 22.6, δTHF 73.1, 25.9
$(C_5Me_5)_2LuCH_2CH(CH_3)_2$ [5]	δCp 118.3, δCH$_3$Cp 10.9, δCH$_2$ 49.3, δCH 29.2, δCH$_3$CH 29.4
$Cp_2Lu(\mu\text{-}CH_3)_2Li \cdot (THF)_2$ [6]	δCp 108.53, δCH$_3$ 15.21, δTHF 68.22, 25.38 in C$_6$D$_6$
$Cp_2Lu(\mu\text{-}CH_3)_2Li \cdot (tmed)$ [6]	δCp 108.49, δCH$_3$ 15.77, δtmed 45.94, 56.53 in C$_6$D$_6$
$(C_5Me_5)_2LuCH_2SiMe_3$ [7]	δCp 118.54, δCH$_3$Cp 11.5, δCH$_2$ 22.96, δCH$_3$ 4.8 in C$_6$D$_6$
$(C_5Me_5)_2LuC_6H_5$ [7]	δCp 118.81, δCH$_3$Cp 10.73, δC$_6$H$_5$ 125.01, 126.94, 135.98, 198.54 in C$_6$D$_{12}$
$(C_5Me_5)_2LuC_5H_4N$ [7]	δCp 115.88, δCH$_3$Cp 10.45, δC$_5$H$_4$N 120.82, 133.43, 133.81, 145.3, 234.26 in C$_6$D$_{12}$
$(C_5Me_5)_2LuC_6H_4Lu(C_5Me_5)_2$ [7]	δCp 117.7, δCH$_3$Cp 10.57, δC$_6$H$_4$ 134.87, 194.78 in C$_6$D$_{12}$
$(C_5Me_5)_2Lu(\mu\text{-}CH_3)_2Li \cdot (tmed)_2$ [8]	δCp 111.2, δCH$_3$Cp 12.1, δCH$_3$ 22.2, δtmed 58.8, 46.0 in THF-d$_8$
$(C_5Me_5)_2Lu(\mu\text{-}CH_3)_2Li \cdot (DME)_{3.5}$ [8]	δCp 112.39, δCH$_3$Cp 12.76, δCH$_3$ 25.87, δCH$_3$ 6.27, δDME 72.55, 58.79 in THF-d$_8$

[1] Holton et al. (1979b).
[2] Holton et al. (1979c).
[3] Ballard et al. (1978).
[4] Schumann et al. (1982).
[5] Watson and Roe (1982).
[6] Schumann et al. (1984).
[7] Watson (1983a).
[8] Schumann and Albrecht (1984).
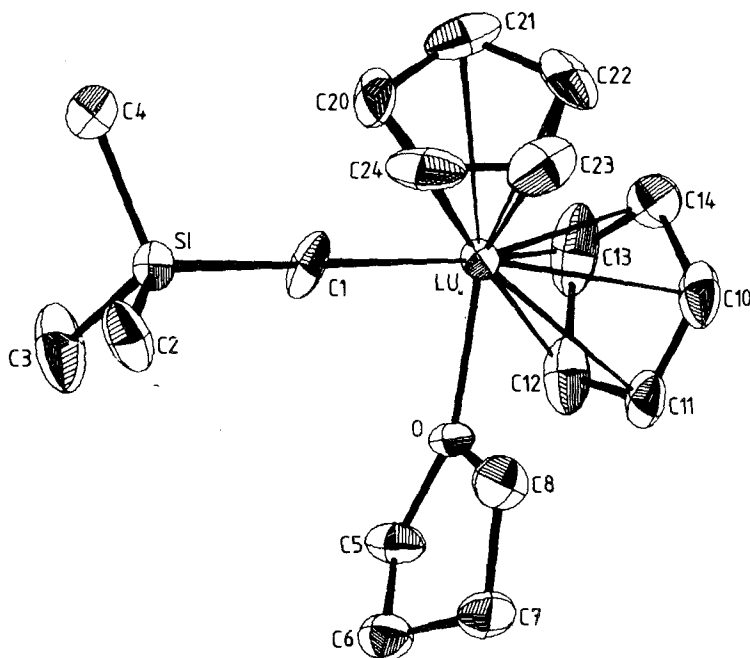
Fig. 26. Molecular structure of $(C_5H_5)_2LuCH_2Si(CH_3)_3\cdot(THF)$ (after Schumann et al., 1982).

$$(MeCp)_2RCl + LiC(CH_3)_3 \xrightarrow[-78^\circ C]{THF} (MeCp)_2RC(CH_3)_3 \cdot THF + LiCl, \quad (45)$$
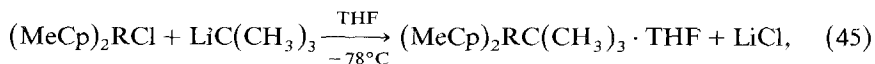
$R = Y, Er, Lu.$

The ^{1}H and ^{13}C NMR spectra are consistent with the presence of monomeric complexes with η^5-cyclopentadienyl rings and terminal alkyl ligands as well as a coordinated tetrahydrofuran ligand (tables 17, 19). Single crystal X-ray structural investigations have been done from three lutetium derivatives: $(C_5H_5)_2LuC(CH_3)_3\cdot$ (THF) (W.J. Evans et al., 1981e), $(C_5H_5)_2LuCH_2SiMe_3\cdot(THF)$ (fig. 26) and $(C_5H_5)_2LuC_6H_4\text{-}4\text{-}CH_3\cdot(THF)$ (fig. 27) (Schumann et al., 1982). The crystallographic data, together with some important bond distances and angles are given in table 20. The structures show the lutetium atom in a distorted tetrahedral array of the centers of two cyclopentadienyl ligands, the oxygen atom of tetrahydrofuran, and the σ-bonded carbon atom. The structure of the tolyl derivative shows a crystallographic mirror plane containing the oxygen atom and C21 of the tetrahydrofuran ligand. That implies two possibilities for the arrangement of the THF ring, which are statistically distributed over the crystal. The surprisingly large bond angle of 130.7° at C1 in the Me_3SiCH_2 derivative is determined by the spatial requirement of the trimethylsilyl group bound to the same carbon atom and the cyclopentadienyl and tetrahydrofuran ligands around lutetium.

Changtao Qian et al. (1983) also described the biscyclopentadienyl-p-tolyl complexes of Gd, Er, and Yb as well as the p-chlorophenyl complex of Er. The infrared

TABLE 20

Crystallographic data, bond distances and angles in dicyclopentadienyl lutetium alkyl and aryl compounds.

	$Cp_2LuC(CH_3)_3 \cdot THF$		$Cp_2LuCH_2SiMe_3 \cdot THF$		$Cp_2LuC_6H_4-4-CH_3 \cdot THF$	
crystal system	orthorhombic		orthorhombic		orthorhombic	
space group	Pnma		$P2_12_12_1$		Pnma	
a (Å)	16.066(7)		17.381(8)		15.814(36)	
b (Å)	12.790(5)		12.268(3)		12.511(11)	
c (Å)	8.699(4)		9.170(3)		9.467(18)	
Z	4		4		4	
distances (Å)						
	Lu–C(σ)	2.47(2)	Lu–C1	2.376(17)	Lu–C14	2.345(39)
	Lu–C(Cp) (aver.)	2.63(1)	Lu–C(Cp) (aver.)	2.605(7)	Lu–C(Cp) (aver.)	2.594(6)
	Lu–O	2.31(2)	Lu–O	2.288(10)	Lu–O	2.265(28)
angles (deg)						
	Cp1–Lu–Cp2	125.6	Cp1–Lu–Cp2	130.2	Cp1–Lu–Cp2	128.8
	Cp1–Lu–C(σ)	110	Cp1–Lu–C1	105.4	Cp1–Lu–C14	108.5
	Cp1–Lu–O	106	Cp1–Lu–O	105.7	Cp1–Lu–O	107.2
	C(σ)–Lu–O	94.1	C1–Lu–O	95.8(9)	C14–Lu–O	89.6(12)
			Lu–C1–Si	130.7(8)	Lu–C14–C11	169.2(31)

Fig. 27. PLUTO drawing of the molecular structure of $(C_5H_5)_2LuC_6H_4-4-CH_3\cdot(THF)$ (after Schumann et al., 1982).

spectra of these compounds are discussed.

The X-ray structure of the methylbridged complex $[(C_5H_5)_2Er(\mu\text{-}CH_3)_2Li\cdot$ (tmed)] has been determined by Schumann et al. (1984b) (table 20a, fig. 27a). The complex was prepared in a one-pot-reaction of $ErCl_3$ with stochiometric amounts of C_5H_5Na and $LiCH_3$ in tetrahydrofuran at $-78°C$ in the presence of tmed, followed by recrystallization from diethylether. In a similar manner the analogous lutetium complex could be obtained. When the reaction is carried out in the presence of dimethoxyethane instead of tmed then only a complex with two molecules of tetrahydrofuran coordinated to the lithium atom is obtained.

TABLE 20a

Crystallographic data, bond distances and angles in $(C_5H_5)_2Er(\mu\text{-}CH_3)_2Li\cdot(tmed)$.

space group	$P4_32_12$ [b]
a	8.359(1) Å
c	28.78(3) Å
Z	4
distances (Å)	
$Er-\varnothing Cp$	2.340(21)
$Er-C6$	2.456(19)
$Li-C6$	2.263(30)
$Er\cdots Li$	3.017(25)
angles (deg.)	
$\varnothing Cp-Er-\varnothing Cp'$	131.1(8)
$C6-Er-C6'$	95.0(6)
$C6-Li-C6'$	106 (1)
$Li-C6-Er$	79.3(8)
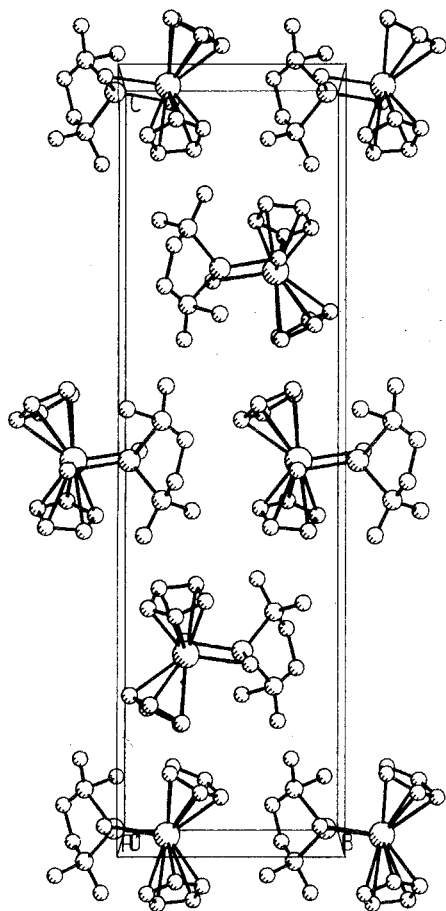
Fig. 27a. PLUTO drawing of the unit cell for $Cp_2Er(\mu\text{-}CH_3)_2Li\cdot(tmed)$, view down the x axis.

Pentamethylcyclopentadienyl derivatives of ytterbium have been prepared by Watson (1980). The complex $[(C_5Me_5)_2Yb(\mu\text{-}Cl)_2Li]\cdot(Et_2O)_2$ reacts with methyl lithium in tetrahydrofuran below $-20°C$ with formation of orange $(C_5Me_5)_2YbCH_3$ $\cdot(THF)$. In ether, $[(C_5Me_5)_2Yb(\mu\text{-}Cl)(\mu\text{-}CH_3)Li]\cdot(Et_2O)_2$ was formed as a brown complex exclusively and with two equivalents of methyl lithium the yellow compound $[(C_5Me_5)_2Yb(\mu\text{-}CH_3)_2Li]\cdot(Et_2O)_2$ could be isolated. Some other ytterbium and lutetium derivatives with pentamethylcyclopentadienyl ligands and methyl as well as isobutyl, isohexyl and isoheptyl ligands bond to the lanthanides have been isolated (table 16) and their structures studied by NMR investigations (tables 17, 19). The lanthanide–carbon bonds insert olefins, producing longer alkyl chains (Watson, 1982), and the bis(pentamethylcyclopentadienyl) lutetium isobutyl complex shows a β-alkyl elimination during its thermal decomposition forming a bis(pentamethylcyclopentadienyl) lutetium hydride and isobutene (Watson and Roe, 1982).

$(C_5Me_5)_2LuX$ complexes, where $X = H, CH_3$, are able to cleave activated sp^2

C–H bonds in inter- and intramolecular reactions. They are even able to cleave sp^3 C–H bonds of tetramethylsilane (Watson, 1983a). All products of eqs. (45a and b) are characterised by NMR, IR and elementary analyses. Watson (1983b) also showed with ^{13}C-labeled CH_4 in C_6D_{12} at 70°C that the methyl group of $(C_5Me_5)_2LuCH_3$ exchanges.

$$(C_5Me_5)_2LuCH_3 \xrightarrow[-CH_4]{\text{pentane, } H_2} (C_5Me_5)_2LuH,$$

$$(C_5Me_5)_2LuH \xrightarrow[-C_6D_5H \text{ (or HD)}]{C_6D_6 \text{ (or } D_2)} (C_5Me_5)_2LuD,$$

$$\xrightarrow[-C_2H_6]{Et_2O} (C_5Me_5)_2LuOC_2H_5, \qquad (45a)$$

$$\xrightarrow[-H_2]{C_6H_6} (C_5Me_5)_2LuC_6H_5$$

$$\xrightarrow[-H_2]{(C_5Me_5)_2LuH} (C_5Me_5)_2Lu-C_6H_4-Lu(C_5Me_5)_2,$$

$$\begin{array}{c} (C_5Me_5)_2LuL \\ L = CH_3, H \end{array} \xrightarrow[-CH_4 \text{ or } H_2]{+ \text{pyridine}} (C_5Me_5)_2Lu\underset{N}{\overset{}{\diagdown}} ,$$

$$\xrightarrow[-CH_4 \text{ or } H_2]{+ Si(CH_3)_4} (C_5Me_5)_2LuCH_2SiMe_3, \qquad (45b)$$

$$\xrightarrow[-CH_4 \text{ or } H_2]{+ CH_2=PPh_3} (C_5Me_5)_2Lu\qquad PPh_2 .$$
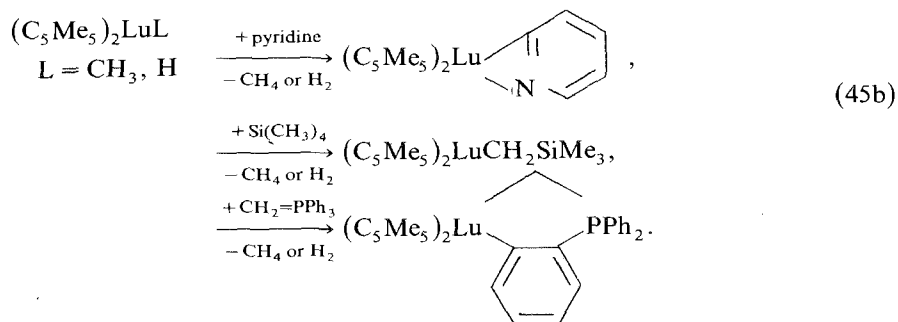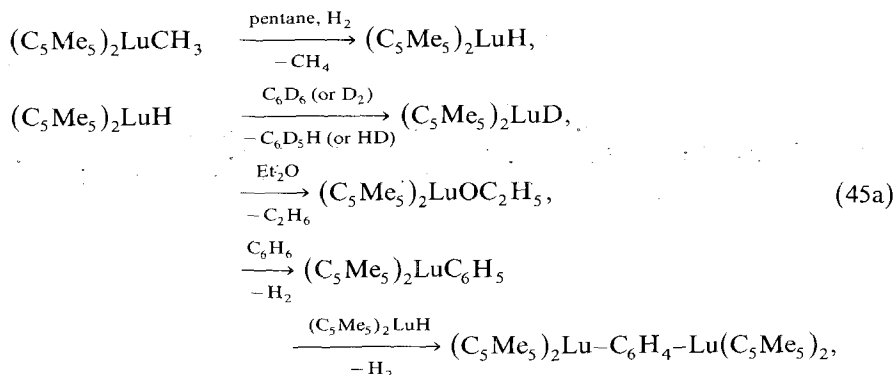
Recently Wayda (1983) prepared $(C_8H_8)LuCH_2SiMe_3 \cdot (THF)_2$ and $(C_8H_8)Lu-C_6H_4-2-CH_2NMe_2 \cdot (THF)$ whereas attempts to prepare the analogous compounds of the earlier lanthanides La and Sm failed.

2.3. Organometallic compounds of the rare earths with allyl and alkynyl ligands

The first allyl derivative of a rare earth was the complex dicyclopentadienyl allyl scandium, prepared by Coutts and Wailes (1970) from dicyclopentadienyl scandium chloride and allyl magnesium chloride in benzene–tetrahydrofuran. The orange compound shows an NMR spectrum with a singlet for the cyclopentadienyl protons at 5.90 ppm, and a quintet at 7.29 and a doublet at 3.05 ppm for the fluxional allyl group. The fluxional allyl group is also implicated by the IR band at 1475 cm^{-1} for a delocalized $C \doteq C$ stretching vibration.

The corresponding samarium, holmium and erbium complexes have been made in the same way by Tsutsui and Ely (1975b), which show also an IR band at 1533 cm^{-1} for the delocalized allyl stretching vibration. But the complete structure of these compound is not clear. Additional bands in the optical spectra of the tetrahydro-

furan solutions at 513 nm ($\varepsilon = 97.3$) for the Sm compound, at 425 nm ($\varepsilon = 29.4$) for the Ho derivative and at 373 nm ($\varepsilon = 132.4$) for $Cp_2ErCH_2CH=CH_2$ are a hint for the coordination of a tetrahydrofuran in solution.

$$Cp_2RCl + C_3H_5MgX \rightarrow Cp_2RCH_2CH=CH_2 + MgClX, \qquad (46)$$
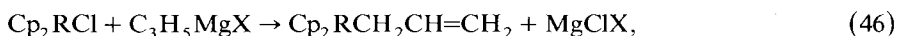
$$R = Sc, X = Cl; R = Sm, Ho, Er, X = Br.$$

In connection with investigations on the catalytic activity of organometallic compounds of the rare earths, anionic homoleptic allyl derivatives of Ce, Nd, Sm, Gd and Dy have been prepared according to eq. (47). Allyl lithium was generated in situ from $Sn(C_3H_5)_4$ and another lithium alkyl LiL. The compounds, isolated as their dioxane complexes after precipitation from ethereal solution by addition of dioxane, are described as containing fluxional allyl groups from their infrared and ^1H NMR spectra (Mazzei, 1979):

$$RCl_3 + 4 LiL + Sn(C_3H_5)_4 \xrightarrow{THF} Li[R(C_3H_5)_4] + SnL_4 + 3 LiCl,$$
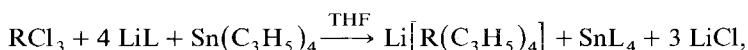
$$R = Ce, Nd, Sm, Gd, Dy. \qquad (47)$$

A bis(Pentamethylcyclopentadienyl) lutetium allyl and $(C_5Me_5)_2LuCH_2$-$CMe=CH_2$ are found to be among the final products of the decomposition of $(C_5Me_5)_2LuCH_2CHMe_2$ as shown by Watson and Roe (1982). The ^{13}C NMR spectrum of the allyl complex shows δCH_2 at 68 and δCH at 163 ppm, proving a fluxional σ-allyl structure.

The first alkynyl derivatives have been prepared together with the corresponding allyl complexes. Coutts and Wailes (1970) described the dicyclopentadienyl scandium phenylacetylide as a non-sublimable dimer, which decomposes above 245°C. The gadolinium, holmium, erbium, and ytterbium derivatives and even a monocyclopentadienyl holmium bis(phenylacetylide) have been made according to eqs. (49, 50) (Tsutsui and Ely, 1974; N.M. Ely and Tsutsui, 1975). All of these compounds show a strong $\nu(C\equiv C)$ around 2045 cm^{-1}. The optical spectra are discussed in terms of a covalent σ-bond between the rare earth and the acetylenic carbon. Dubois et al. (1977) examined the X-ray photoelectron spectrum of $Cp_2GdC\equiv CPh$ in connection with investigations on other gadolinium compounds and found no support for the hypothesis that σ-bonded organolanthanides are more covalent than their π-bonded analogues.

$$2\ Cp_2ScCl + 2\ NaC\equiv CPh \xrightarrow{benzene} (Cp_2ScC\equiv CPh)_2 + 2\ NaCl. \qquad (48)$$

$$Cp_2RCl + LiC\equiv CPh \xrightarrow{THF} Cp_2RC\equiv CPh + LiCl, \qquad (49)$$

$$R = Gd, Ho, Er, Yb.$$

$$CpHoCl_2 \cdot (THF)_3 + 2\ LiC\equiv CPh \xrightarrow[-78°C]{THF} CpHo(C\equiv CPh)_2 + 2\ LiCl. \qquad (50)$$
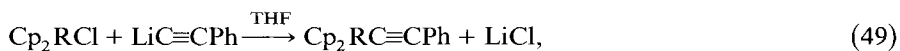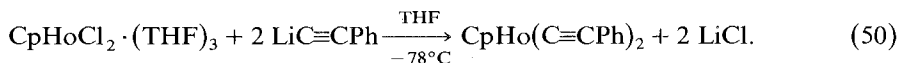
Tricyclopentadienyl ytterbium and tricyclopentadienyl neodymium react with various terminal alkynes by liberating cyclopentadiene although C_5H_6 is a stronger protic acid. While the formation of dimeric dicyclopentadienyl ytterbium derivatives

involving C≡CL bridges is preferred, neodymium avoids the formation of corresponding complexes (R.D. Fischer and Bielang, 1980a):

$$Cp_3Yb + HC\equiv CL \rightarrow \frac{1}{x} (Cp_2YbC\equiv CL)_x + C_5H_6, \tag{51}$$

$$L = C_4H_9,\ C_6H_{13},\ c\text{-}C_6H_{11},\ C_6H_5,\ C_5H_4FeC_5H_5.$$
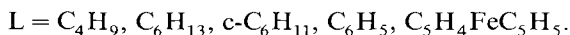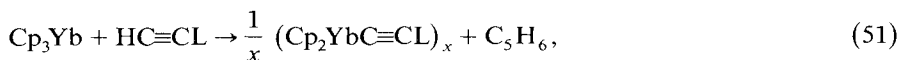
The reaction rate increases with increasing alkyne concentration. Only one cyclopentadienyl can be replaced from ytterbium. Side reactions, like addition to the Yb–C bond or to an η^1-bonded cyclopentadienyl, produced by rearrangements, can be elicited because cyclopentadiene is the only reaction product in addition to $Cp_2YbC\equiv CL$. The $\nu(C\equiv C)$ in the infrared spectrum is found 55 cm^{-1} lower than in the free acetylene. The complexes are oligomers. Cryoscopic molecular weight determinations show an association of 2.5 for the derivative with L = Bu, and of 3.0 for $L = C_6H_{13}$. The ^1H NMR spectrum of $Cp_2YbC\equiv CC_6H_{13}$ shows the expected seven peaks with the intensities $2:2:2:2:2:3:10$ in toluene-d_8. The chemical shift for all protons is linearly dependent with $1/T$. Addition of pyridine to a toluene solution of $Cp_2YbC\equiv CBu$ shifts the signal of the cyclopentadienyl protons from -57.6 to -31.5 ppm, which is caused by the fission of the alkyne bridges.

The pink erbium derivative $(Cp_2ErC\equiv CCMe_3)_2$ and the bright orange complex $[(MeCp)_2YbC\equiv CCMe_3]_2$ have been synthesized by the halide-free reaction of $(Cp_2ErMe)_2$ or $[(MeCp)_2YbMe]_2$ with $HC\equiv CCMe_3$ in tetrahydrofuran in high yields (W.J. Evans and Wayda, 1980). The X-ray structural analysis of the erbium
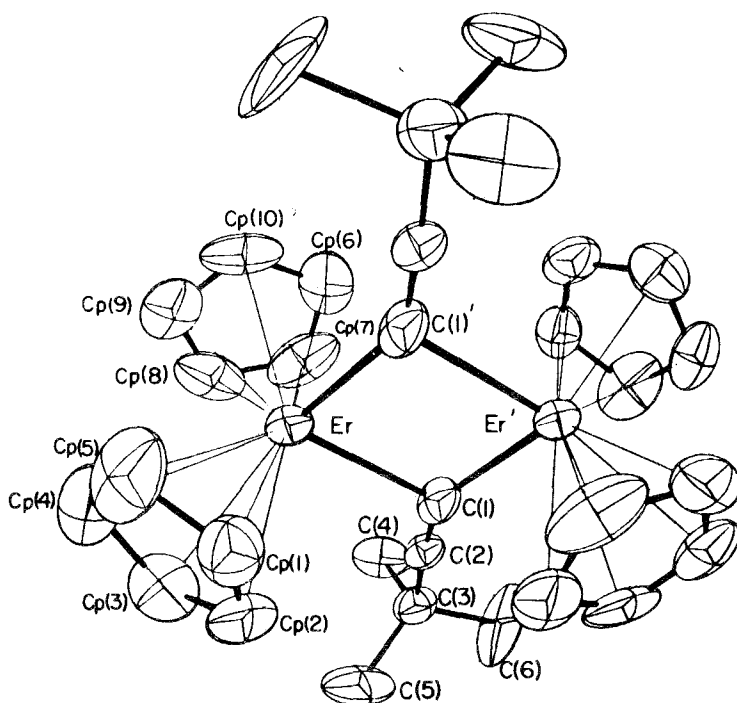
Fig. 28. Molecular structure of $[Cp_2ErC\equiv C\text{-}t\text{-}Bu]_2$ (after Atwood et al., 1981).

TABLE 21

Crystallographic data, bond distances and angles in $(Cp_2ErC\equiv CCMe_3)_2$.

crystal system	triclinic
space group	$P\bar{1}$
a (Å)	3.602(3)
b (Å)	8.767(3)
c (Å)	10.216(5)
α (deg)	77.86(3)
β (deg)	84.50(3)
γ (deg)	76.61(3)
Z	1 (dimer)
distances (Å)	
Er–Er′	3.657(2)
Er–Cl	2.42(2)
Er–Cl′	2.47(2)
Er–∅ Cp1	2.325
Er–∅ Cp2	2.245
angles (deg)	
Cl–Er–Cl′	83.4(7)
Er–Cl–Er′	96.6(7)
∅ Cp1–Er–∅ Cp2	130.2

derivative, done by Atwood et al. (1981) (fig. 28) proves the dimeric formulation. Two dicyclopentadienyl erbium units are connected by two asymmetric alkynide bridges. The complex is also dimeric in tetrahydrofuran solution. The crystallographic data and some important bond distances and bond angles are given in table 21. An analogous samarium compound $[(CH_3C_5H_4)_2SmC\equiv CC(CH_3)_3]_2$ has a more symmetric alkynyl-bridge (W.J. Evans et al., 1983c) as determined by its molecular structure. The $\nu(C\equiv C)$ absorption in the infrared spectrum of this compound is found at 2035 cm^{-1}, while the alkynyl stretching frequency for the erbium and ytterbium analogs is at 2050 cm^{-1}. The complex appears to be monomeric in tetrahydrofurane and it reacts with $(C_6H_5)_2PH$ in toluene to yield the complex $(CH_3C_5H_4)_2SmP(C_6H_5)_2$.

Two ring-bridged dicyclopentadienyl rare earth phenylacetylides have been synthesized according to eq. (52) by John and Tsutsui (1980, 1981). The lanthanum complex shows two singlets in the proton NMR spectrum at $\delta = 7.57$ and 7.74 ppm with equal intensity, which are assigned to the cyclopentadienyl protons, and broad peaks at 4.24 and 4.54 ppm for the methylene protons. The phenyl proton signal appears at $\delta = 8.92$ ppm. The cerium complex shows a singlet at $\delta = 9.16$ ppm for Ph and a multiplet between 7.29 and 7.59 ppm for the cyclopentadienyl protons.

$$(H_2C)_3 \overset{\displaystyle \text{RCl} + NaC\equiv CPh} {} \xrightarrow[0°C]{THF} (H_2C)_3 \text{RC}\equiv CPh + NaCl, \qquad (52)$$

R = La, Ce.
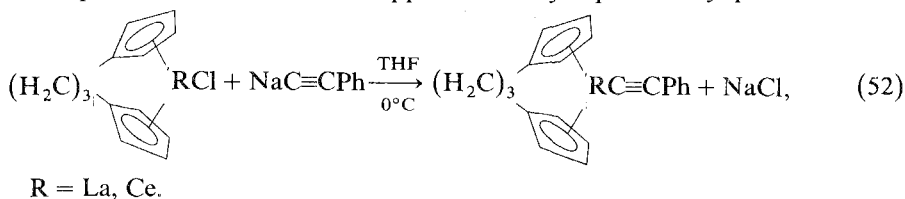
Finally some homoleptic alkyne complexes of scandium and some rare earths are known. Tris(phenylethynyl) scandium is formed as a dark brown product after treatment of phenylethyne with butyl lithium at $-78°C$ in hexane, followed by the addition of scandium trichloride at room temperature. The compound is inflammable in air (Hart and Saran, 1968; Hart et al., 1970). The reaction of the anionic

TABLE 22

Allyl and alkynyl derivatives of the rare earths.

Compound	color	other data	Ref.
$Cp_2ScCH_2CH=CH_2$	orange	m.p. 151° (dec.)	1
$Cp_2SmCH_2CH=CH_2$	yellow		2
$Cp_2HoCH_2CH=CH_2$	orange		2
$Cp_2ErCH_2CH=CH_2$	pink		2
$(C_5Me_5)_2LuCH_2CH=CH_2$			3
$(C_5Me_5)_2LuCH_2CMe=CH_2$			3
$Li[Ce(CH_2CH=CH_2)_4]\cdot(dioxane)$			4
$Li[Nd(CH_2CH=CH_2)_4]\cdot(dioxane)$			4
$Li[Sm(CH_2CH=CH_2)_4]\cdot(dioxane)$			4
$Li[Gd(CH_2CH=CH_2)_4]\cdot(dioxane)$			4
$Li[Dy(CH_2CH=CH_2)_4]\cdot(dioxane)$			4
$Cp_2ScC≡CPh$	yellow	m.p. 254°C (dec.)	1
$Cp_2GdC≡CPh$	yellow	m.p. 279–282°C (dec.)	5
		μ_{eff} 7.89 B.M.	5
$Cp_2HoC≡CPh$	sand	μ_{eff} 10.08 B.M.	5
$Cp_2ErC≡CPh$	pink	μ_{eff} 9.64 B.M.	5
$Cp_2YbC≡CPh$	orange	dec. 180°C	6
		μ_{eff} 4.31 B.M.	5
$(Cp_2ErC≡CCMe_3)_2$	pink		7
$Cp_2YbC≡CBu$	orange-red	dec. 150°C	6
$Cp_2YbC≡CC_6H_{11}$	orange-red	dec. 150°C	6
$Cp_2YbC≡CC_6H_{13}$	yellow	dec. 180°C	6
$Cp_2YbC≡CC_5H_4FeC_5H_5$	orange	dec. 130°C	6
$[(MeCp)_2YbC≡CCMe_3]_2$	orange		7
$[C_5H_4(CH_2)_3C_5H_4]_2LaC≡CPh$	tan	dec. 150–200°C	8
$[C_5H_4(CH_2)_3C_5H_4]_2CeC≡CPh$	brown	dec. 150°C	8
$CpHo(C≡CPh)_2$	sand	dec. 190–340°C	5
		μ_{eff} 10.48 B.M.	5
$Sc(C≡CPh)_3$	dark brown		9
$Li[Sm(C≡CCMe_3)_4]\cdot(THF)$	off-white	μ_{eff} 1.66 B.M.	10
$Li[Er(C≡CCMe_3)_4]\cdot(THF)$	pink	μ_{eff} 9.79 B.M.	10
$Li[Lu(C≡CCMe_3)_4]\cdot(THF)$	white		10
$[(CH_3C_5H_4)_2SmC≡CC(CH_3)_3]_2$	yellow	^1H, ^{13}C NMR, X-ray	11
		μ_{eff} 1.9 B.M., UV	
$(C_5Me_5)_2SmC(Ph)=C(Ph)Sm(C_5Me_5)_2$	black	IR, NMR	11

[1] Coutts and Wailes (1970).
[2] Tsutsui and Ely (1975b).
[3] Watson and Roe (1982).
[4] Mazzei (1979).
[5] N.M. Ely and Tsutsui (1975).
[6] R.D. Fischer and Bielang (1980a).
[7] Atwood et al. (1981).
[8] John and Tsutsui (1981).
[9] Hart et al. (1970).
[10] W.J. Evans and Wayda (1980).
[11] W.J. Evans et al. (1983c).

tert-butyl complexes $Li[R(t-Bu)_4] \cdot (THF)_4$ with an 8-fold molar excess of tert-butylacetylene in tetrahydrofuran at room temperature proceeds according to eq. (53) with formation of the corresponding homoleptic rare earth alkynides (W.J. Evans and Wayda, 1980). The ^{13}C NMR spectrum of the samarium derivative shows the γ and δ carbons at 27.7 and 32.4 ppm. The α and β carbons are not observed.

$$Li[R(t\text{-}Bu)_4] \cdot (THF)_4 + 4\ HC\equiv CCMe_3$$

$$\xrightarrow{\text{THF}} 4\ C_4H_{10} + Li[R(C\equiv CCMe_3)_4] \cdot (THF), \tag{53}$$
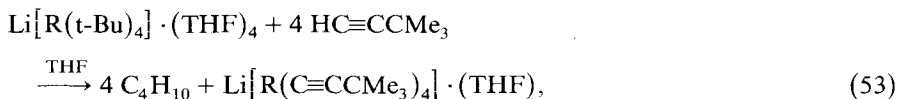
$$R = Sm,\ Er,\ Lu.$$

The reaction of $(C_5Me_5)_2Sm \cdot (THF)_2$ in pentane at $-78°C$ with an excess of diphenylacetylene yields the olefine $(C_5Me_5)_2Sm(C_6H_5)C=C(C_6H_5)Sm(C_5Me_5)_2$ which probably has a trans configuration (W.J. Evans et al., 1983c), since hydrolysis generates only trans-stilbene. An intense charge-transfer-like absorption starting at 1050 nm is responsible for the black color of the compound. With tetrahydrofuran the reaction can be readily reversed.

The colors, melting points or decomposition points and the magnetic moments of the known allyl and alkynyl derivatives of the rare earths are given in table 22.

2.4. Homoleptic alkyl and aryl derivatives of the rare earths

The simplest organometallic derivatives of the rare earths in the oxidation state R^{3+} are compounds of the general formula RL_3. The coordinative unsaturated nature of these compounds causes high reactivity of nucleophilic reagents at the metal center. Therefore a lot of early attempts to prepare such simple homoleptic organometallic compounds of this metals have been unsuccesful. For a long time only indirect evidence for the existence of such derivatives could be found (F.A. Cotton, 1955). The solution to this problem and the synthesis of homoleptic organometallic compounds of the rare earths was possible only a couple of years ago. A review on homoleptic organometallic compounds of the rare earths appeared recently (Schumann, 1983).

2.4.1. Neutral homoleptic derivatives

Scandium trichloride and yttrium trichloride react with methyl lithium as well as with phenyl lithium yielding air-sensitive products. But only the phenyl derivatives could be isolated and definitely characterized (Hart and Saran, 1968; Hart et al., 1970):

$$RCl_3 + 3\ LiC_6H_5 \xrightarrow{\text{THF}} R(C_6H_5)_3 + 3\ LiCl, \tag{54}$$

$$R = Sc,\ Y.$$

Their reactions with carbon dioxide, benzophenone, and $HgCl_2$, as well as their infrared spectra and their elemental analyses prove the given formula. Both compounds are pyrophoric. They are insoluble in benzene, but soluble in tetrahydro-

furan. In vacuo or under nitrogen, they are stable up to 215°C. The reaction of phenyl lithium with $LaCl_3$ or with the trichlorides of some lanthanides did not give analogous derivatives. In the case of lanthanum and praseodymium compounds of the type $Li[R(C_6H_5)_4]$ have been formed; the other lanthanides have not until recently given reproducible results.

A considerable stabilization of homoleptic organometallic compounds of the rare earths can be achieved by the use of bulky alkyl groups, such as neopentyl, $CH_2Si(CH_3)_3$, or $CH[Si(CH_3)_3]_2$. The compounds $R[CH_2C(CH_3)_3]_3$ and $R[CH_2Si(CH_3)_3]_3$, with R = Sc and Y, have been isolated from the reaction of the appropriate organolithium reagent with $ScCl_3$ or YCl_3. The compounds were obtained as analytically pure but air-sensitive, colorless crystals from pentane, containing two THF molecules coordinated to the metal. The NMR data are consistent with a trigonal bipyramidal structure, the THF ligands occupying the axial sites. The coordinated tetrahydrofuran could not be removed in vacuo (Lappert and Pearce, 1973). Whereas the compounds $Y[CH(SiMe_3)_2]_3$ and $Sc[CH(SiMe_2C_6H_4-2-OMe)_2]_3$ could be obtained solvent free (Lappert and Pearce, 1973; Barker and Lappert, 1974).

The latter compound is the first example for another possibility to stabilize three-coordinated organometallic compounds of the rare earths. Alkyl ligands or aryl ligands containing built-in chelating groups, like N,N-dimethylamino-o-benzyl or N,N-dimethylaminomethylphenyl could be used to prepare solvent-free derivatives of Sc, Y, La, Nd and Er (Manzer, 1977a, b, 1978). The benzyl scandium complex $Sc(CH_2C_6H_4-2-NMe_2)_3$ was prepared from anhydrous $ScCl_3$ and three equivalents of $LiCH_2C_6H_4-2-NMe_2$ in tetrahydrofuran and isolated as an extremely air-sensitive, pale yellow crystalline solid. The NMR spectrum proves the formulation of the structure with an octahedral arrangement formed by three covalent Sc–C σ-bonds and three N–Sc bonds (table 23). The yttrium, lanthanum and erbium derivatives could be prepared in the same manner, as well as compounds $R(C_6H_4-2-CH_2NMe_2)_3$,

TABLE 23

NMR data of homoleptic alkyl derivatives of Sc, Y and Lu.

Compound	δ in ppm, J in Hz	Ref.
$Sc(CH_2SiMe_3)_3\cdot(THF)_2$	δCH_2 −0.27, δ Me 1.33	1
$Sc(CH_2CMe_3)_3\cdot(THF)_2$	δCH_2 0.62, δ Me 1.37	1
$Sc(CH_2C_6H_4-2-NMe_2)_3$	δCH_2 −1.64, δ Me −2.27	2
$Sc[CH(SiMe_3)_2]_3\cdot(THF)_2$	δCH −0.16, δ Me 0.69	3
$Sc(CH_2SiMe_2C_6H_4-2-OMe)_3$	δCH_2 0.08, δ Me 0.55	1
$Y(CH_2SiMe_3)_3\cdot(THF)_2$	δCH_2 −0.35d, ^2J(YH) 2.5, δ Me 0.35	1
$Y[CH(SiMe_3)_2]_3$	δCH −0.53d, ^2J(YH) 2.5, δ Me 0.40	1
$Y(CH_2CMe_3)_3\cdot(THF)_2$	δCH_2 −0.07d, ^2J(YH) 2.5, δ Me 1.32	1
$Y[CH(SiMe_3)_2]_3\cdot(THF)_2$	δCH −0.43d, ^2J(YH) 2.5, δ Me 0.64	3
$Lu(CH_2SiMe_3)_3\cdot(THF)_2$	δCH_2 −0.91, δ Me 0.28	4
	^{13}C NMR: δCH_2 41.80, δ Me 4.79	4

1. Lappert and Pearce (1973).
2. Manzer (1978).
3. Barker and Lappert (1974).
4. Schumann and Müller (1979).
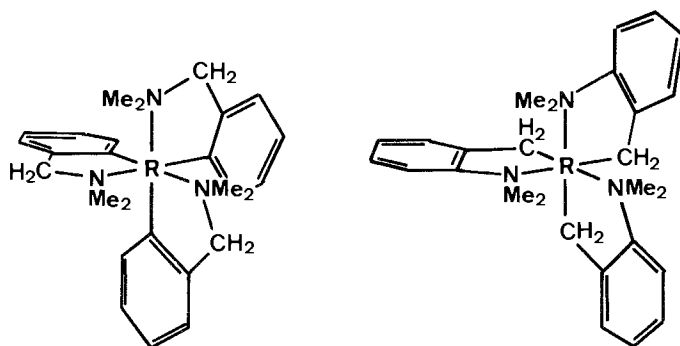
Fig. 29. Configuration of rare earth organometallics containing built-in chelating groups.

with R = Sc, Y, Nd, Er, from the appropriate trichlorides and LiC_6H_4-2-CH_2NMe_2 in refluxing tetrahydrofuran as white or pink insoluble compounds, which are pyrophoric (fig. 29).

When 2-dimethylamino-5-methylbenzyl lithium, or 5-tert-butyl-2-dimethyl-aminomethylphenyl lithium are reacted with $ScCl_3$, scandium tris(2-dimethylamino-5-methylbenzyl) or scandium tris(5-tert-butyl-2-dimethylaminomethylphenyl) are formed in the same way.

Several lanthanide trichlorides react with trimethylsilylmethyl lithium, yielding complexes, in which two or three tetrahydrofuran ligands are bound to the organo-lanthanide (Atwood et al., 1978; Schumann and Müller, 1978a, 1979). $ErCl_3$ and $TmCl_3$ give pink or white air-sensitive complexes $RL_3 \cdot (THF)_3$, which crystallize from pentane at low temperature. Above -35 to $-25°C$ one THF is lost irreversibly, precipitating the dissolvated complexes on recrystallization (Schumann and Müller, 1979). $YbCl_3$ and $LuCl_3$ form the corresponding complexes $RL_3 \cdot (THF)_2$ (Atwood et al., 1978; Schumann and Müller, 1979). The NMR data of the lutetium compound are consistent with a trigonal bipyramidal structure with the THF ligands occupying axial sites (Schumann and Müller, 1979) (table 23).

Maintaining a pentane solution of $R(CH_2SiMe_3)_3 \cdot (THF)_2$, with R = Er, Lu, at room temperature for several days results in the loss of THF and tetramethylsilane and precipitate an extremely pyrophoric material. Quantitative experiments showed one $Si(CH_3)_4$ is lost from one molecule of the complex, forming polymeric complexes of the formula $[R(CH_2SiMe_3)(CHSiMe_3)]_n$ with a decomposition point between 380 and 390°C (Schumann and Müller, 1979):

$$RCl_3 + 3\ LiCH_2SiMe_3 \xrightarrow{\text{THF}} R(CH_2SiMe_3)_3 \cdot (THF)_3 + 3\ LiCl, \qquad (55)$$

R = Er, Tm,

$$R(CH_2SiMe_3)_3 \cdot (THF)_3 \xrightarrow{-25°C} R(CH_2SiMe_3)_3 \cdot (THF)_2 + THF, \qquad (56)$$

R = Er, Tm, Yb, Lu,

$$R(CH_2SiMe_3)_3 \cdot (THF)_2$$

$$\xrightarrow{40°C} \left[R(CH_2SiMe_3)(CHSiMe_3) \right] + Si(CH_3)_4 + 2\ THF. \tag{57}$$
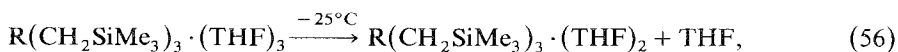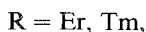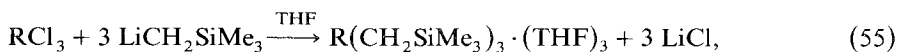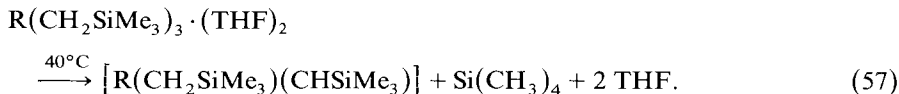
R = Er, Lu.

A similar decomposition is reported for some related derivatives of yttrium and neodymium (Guzman et al., 1979; Dolgoplosk et al., 1980; Vollershtein et al., 1980). YCl_3 and $NdCl_3$ react with $LiCH_2SiMe_3$, $LiCH_2Ph$, and $LiCH_2CMe_2Ph$ to give unusual organometallic compound. The first step is probably the formation of unstable compounds RL_3 which decompose immediately in the reaction medium, yielding carbene type complexes. These are discussed later (see section 5).

$$RCl_3 + 3\ LiCH_2Ph \rightarrow R(CH_2Ph)_3 + 3\ LiCl, \tag{58}$$

$$R(CH_2Ph)_3 \rightarrow \left[R(CH_2Ph)(ChPh) \right] + C_6H_5CH_3, \tag{59}$$
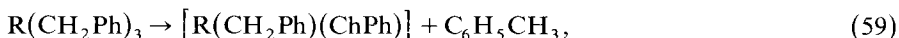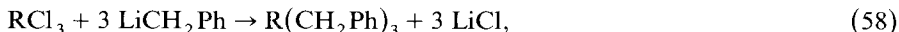
R = Y, Nd.

Carboranyl derivatives of lanthanum, thulium and ytterbium are formed when the C-mercuro derivatives of methyl- and phenylcarboranes react with the rare earth metals in tetrahydrofuran at 20°C (Suleimanov et al., 1982a), or from the lithium derivatives of methyl- and phenylcarboranes with the rare earth trichlorides in benzene–ether at 20°C (Bregadze et al., 1983) as complexes with THF. A carboranyl derivative with a thulium–boron bond is also described. The reaction (eq. 62) may proceed via the formation of B–Tm–C derivatives, followed by disproportionation.

$$3\ Hg(\underset{B_{10}H_{10}}{C\text{------}C\ L})_2 + 2\ R \xrightarrow[20°C]{THF} 2(LC\underset{B_{10}H_{10}}{\text------}C)_3 R \cdot (THF)_n + 3\ Hg, \tag{60}$$

R = La, Tm, L = Me, Ph, n = 1 or 3,

$$RCl_3 + 3\ Li\ \underset{B_{10}H_{10}}{C\text{------}C\ L} \xrightarrow{THF/benzene} (L\ C\underset{B_{10}H_{10}}{\text------}C)_3 R \cdot (THF)_n + 3\ LiCl, \tag{61}$$

R = La, Tm, Yb, L = Me, Ph, n = 1, 2.
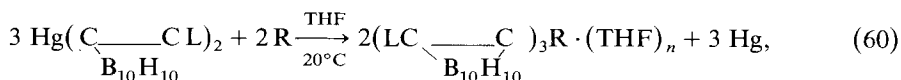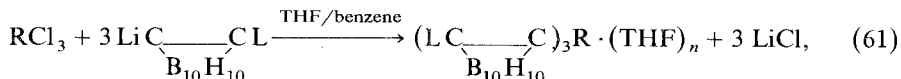
$$C_2B_{10}H_{11}HgMe + Tm \xrightarrow[20°C]{THF} (C_2B_{10}H_{11})_3Tm \cdot (THF) + Hg. \tag{62}$$
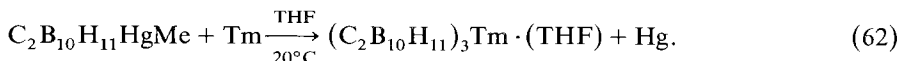
All known homoleptic rare earth organyls are tabulated in table 24.

2.4.2. Anionic homoleptic derivatives

The first homoleptic organometallic compounds of the lanthanides have been prepared by Hart et al. (1970). The reaction of phenyl lithium with $LaCl_3$ or $PrCl_3$ yields products, inflammable in air, which contain lithium. From analysis and infrared spectra, the formulation of $Li[R(C_6H_5)_4]$ was suggested:

$$RCl_3 + 4\ LiC_6H_5 \xrightarrow{THF} Li\left[R(C_6H_5)_4 \right] + 3\ LiCl, \tag{63}$$
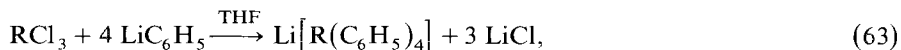
R = La, Pr.

Both compounds are soluble in benzene when first obtained from the original tetrahydrofuran solution but, after complete drying in vacuo, they are insoluble in

TABLE 24

Homoleptic alkyl and aryl derivatives of rare earths.

Compound	color	other data	Ref.
$ScPh_3$	yellow	m.p. $140°C$ (dec.)	1
$Sc(CH_2SiMe_3)_3 \cdot (THF)_2$	colorless	m.p. $62–63°C$	2
$Sc(CH_2CMe_3)_3 \cdot (THF)_2$	colorless	m.p. $66–68°C$	2
$Sc(C_6H_4\text{-}2\text{-}CH_2NMe_2)_3$	white	m.p. $180–182°C$	3
$Sc(CH_2C_6H_4\text{-}2\text{-}NMe_2)_3$	yellow	m.p. $115–118°C$	3
$Sc[CH(SiMe_3)_2]_3 \cdot (THF)_2$	white		4
$Sc(CH_2SiMe_2C_6H_4\text{-}2\text{-}OMe)_3$	colorless	m.p. $115–120°C$ (dec.)	2
$Sc(CH_2C_6H_3\text{-}2\text{-}NEt_2\text{-}6\text{-}Me)_3$			5
YPh_3	brown	$210°C$ (dec.)	1
$Y(CH_2SiMe_3)_3 \cdot (THF)_2$	colorless	m.p. $48–50°C$	2
$Y(CH_2Ph)_3$			6
$Y(CH_2SiMe_3)_3$	white		4
$Y(CH_2CMe_3)_3 \cdot (THF)_2$	colorless	m.p. $78–79°C$	2
$Y(C_6H_4\text{-}2\text{-}CH_2NMe_2)_3$			5
$Y(CH_2C_6H_4\text{-}2\text{-}NMe_2)_3$			5
$Y[CH(SiMe_3)_2]_3 \cdot (THF)_2$	white		4
$Y(CH_2CMe_2Ph)_3$			6
$La(CH_2C_6H_4\text{-}2\text{-}NMe_2)_3$			5
$La(CB_{10}H_{10}CPh)_3 \cdot (THF)$		dec. $260°C$	7
$Nd(CH_2SiMe_3)_3$			8
$Nd(C_6H_4\text{-}2\text{-}CH_2NMe_2)_3$			5
$Nd(CH_2CMe_2Ph)_3$			6
$Tb(CH_2SiMe_3)_3 \cdot (THF)_2$	colorless	m.p. $50–54°C$ μ_{eff} 9.12 B.M.	9
$Er(CH_2SiMe_3)_3 \cdot (THF)_2$	pink	m.p. $49–51°C$ μ_{eff} 8.82 B.M.	9
$Er(CH_2SiMe_3)_3 \cdot (THF)_3$	pink	m.p. $-25°C$	10
$Er(C_6H_4\text{-}2\text{-}CH_2NMe_2)_3$	pink		5
$Er(CH_2C_6H_4\text{-}2\text{-}NMe_2)_3$	orange	m.p. $161–163°C$	5
$Tm(B_{10}H_9C_2H_2)_2 \cdot (THF)$		dec. $265°C$	7
$Tm(CH_2SiMe_3)_3 \cdot (THF)_2$	green	m.p. $49–52°C$	11
$Tm(CB_{10}H_{10}CMe)_3 \cdot (THF)_3$		dec. $280°C$	7
$Tm(CH_2SiMe_3)_3 \cdot (THF)_3$	green	dec. $-35°C$	12
$Tm(CB_{10}H_{10}CPh)_3 \cdot (THF)_3$		dec. $275°C$	7
$Yb(CH_2SiMe_3)_3 \cdot (THF)_2$	red	m.p. $53–54°C$ μ_{eff} 4.64 B.M.	9
$Yb(CB_{10}H_{10}CMe)_3 \cdot (THF)$		dec. $280°C$	13
$Lu(CH_2SiMe_3)_3 \cdot (THF)_2$	white	m.p. $49–52°C$	12

1. Hart et al. (1970).
2. Lappert and Pearce (1973).
3. Manzer (1978).
4. Barker and Lappert (1974).
5. Manzer (1977b).
6. Guzman et al. (1979).
7. Suleimanov et al. (1982a).
8. Vollershtein et al. (1980).
9. Atwood et al. (1978).
10. Schumann and Müller (1978a).
11. Schumann and Müller (1978c).

12. Schumann and Müller (1979).
13. Bregadze et al. (1983).
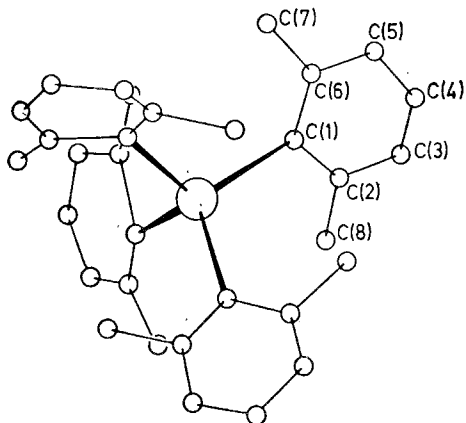
Fig. 30. Molecular structure of the anion in $[Li(THF)_4][Lu(C_6H_3Me_2)_4]$ (after S.A. Cotton et al., 1972).

aromatic hydrocarbons. Therefore the original product is probably a THF complex, which polymerizes upon removal of tetrahydrofurane.

The first definitive compound of this class, tetrakis(tetrahydrofurane) lithium tetrakis(2,6-dimethylphenyl) lutetiate has been prepared by the action of 2,6-dimethylphenyl lithium with anhydrous lutetium trichloride in tetrahydrofurane at $-78°C$, following by repeated concentration, filtration, and redissolution in tetrahydrofurane. This procedure ultimately gave, on addition of benzene, colorless needles. X-ray diffraction shows the lutetium atom to be bound to four η^1-aryl groups in an approximately tetrahedral array; the four Lu–C distances are 2.425 Å, 2.439 Å, 2.442 Å and 2.501 Å. The four Lu–C1–C4 angles deviate somewhat from 180° (see fig. 30), taking values from 175.6° to 167.7°; the six C–Lu–C angles around lutetium are 99.4°, 101.2°, 111.0°, 112.4°, 115.5° and 118.2°. The analogous ytterbium compound has been similarly prepared and is isostructural. It smoulders instantly on exposure to air while the lutetium compound appears less readily affected (S.A. Cotton et al., 1972).

The first peralkylated complexes of the lanthanides containing only methyl ligands could be synthesized using tetramethylethylenediamine as a stabilizing base (Schumann and Müller, 1978b). Dropwise addition of an ethereal solution of methyl lithium to a suspension of the rare earth trichloride in diethylether with a stoichiometric amount of tmed affords good yields of the reaction products, as analytically pure, in some cases colored crystals which were free of excess methyl lithium after recrystallization (Schumann et al., 1981b, Schumann and Bruncks, 1982; Schumann and Lauke, 1982; Schumann et al., 1984a; Schumann and Ziep, 1984):

$$RCl_3 + 6\ LiCH_3 + 3\ tmed \xrightarrow{Et_2O} [Li(tmed)]_3[R(CH_3)_6] + 3\ LiCl,$$

$$tmed = (CH_3)_2NCH_2CH_2N(CH_3)_2, \tag{64}$$

R = Sc, Y, La, Ce, Pr, Nd, Sm, Gd, Tb, Dy, Ho, Er, Tm, Yb, Lu.
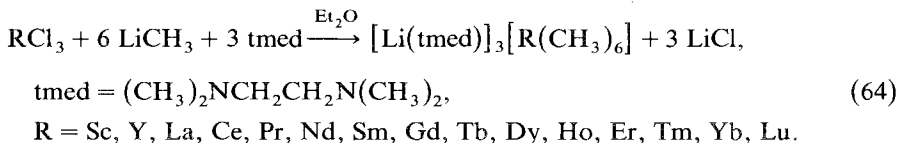
The compounds are extremely sensitive to air and moisture; however, the heavier ones with R = Tb to Lu exhibit surprising thermal stability and decompose only

slowly at their melting points around 140°C. Hydrolysis and alcoholysis liberate 6 moles of methane per mole of organolanthanide. The NMR spectrum of the diamagnetic lutetium compound shows a singlet for the methyl groups bound to lutetium at $\delta = 1.18$ ppm in addition to the peaks of tmed.

The single crystal X-ray structural analysis of the Er and Ho derivatives show the lanthanides surrounded by the six CH_3 groups in a slightly distorted octahedral arrangement. Fig. 31 shows the molecular structure of the holmium derivative (Schumann et al., 1981b, 1984a). All Ho–C bonds are of equal length, and the methyl groups are bridged pairwise by lithium atoms, resulting in a slight widening of the corresponding CH_3–Ho–CH_3 angles to 89.2°. The lithium atoms are each located at the centers of tetrahedra made up of two methyl groups and two nitrogen atoms of a tmed ligand. Thus, an octahedron results that is coupled via three corners, which are not linked with each other, to three tetrahedra.

The bond angles at holmium and erbium as well as the lanthanide–carbon bond lengths in this electron deficient organolanthanide compounds (table 25) are comparable with those in other electron-deficient compounds with other metal atoms (Schumann and Bruncks, 1982; Schumann et al., 1984a).

By substituting the base tmed, the R–CH_3 distances do not change as Schumann et al. (1984c) showed by an X-ray structure of $[Li(DME)]_3[Lu(CH_3)_6]$, whereas the Li–C and Li–O distances are shorter than in the mentioned complexes. $[Li(DME)]_3[Lu(CH_3)_6]$ crystallizes in the monoclinic space group Cc with $a = 13.90(2)$, $b = 10.83(2)$, $c = 18.39(4)$ Å, $\beta = 94.08(13)°$ and $Z = 4$.

Slow addition of a freshly prepared solution of tert-butyl lithium to a suspension of anhydrous $SmCl_3$, $ErCl_3$, $YbCl_3$ or $LuCl_3$ in tetrahydrofuran at $-55°C$ yields (after stirring and warming up to room temperature), in 50 to 75% yield, the
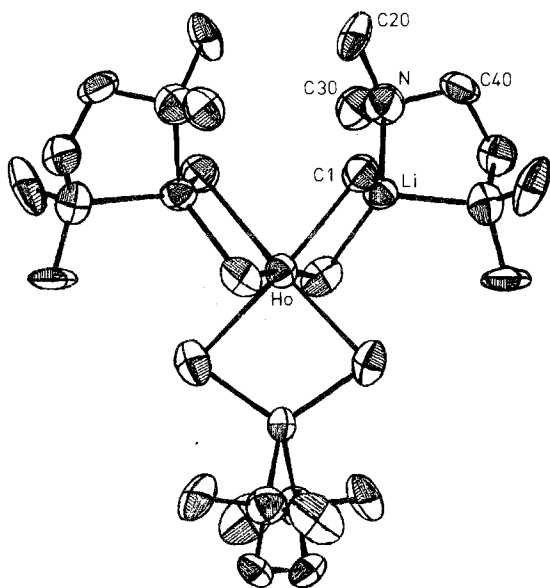
Fig. 31. Molecular structure of $[Li(tmed)]_3[Ho(CH_3)_6]$ (after Schumann et al., 1984a).

TABLE 25
Crystallographic data, bonding distances and angles in $[Li(tmed)]_3[RMe_6]$, R = Er, Ho.

	$[Li(tmed)]_3[ErMe_6]$		$[Li(tmed)]_3[HoMe_6]$	
crystal system	rhombohedral		rhombohedral	
space group	R3c		R3c	
a (Å)	10.309(2)		12.807(20)	
α (deg)	79.39(10)		79.84(13)	
Z	2		2	
distances (Å)				
	Er–C	2.57(2)	Ho–C	2.563(18)
	Li–C	2.22(4)	Li–C	2.208(18)
	Li–N	2.21(4)	Li–N	2.129(16)
angles (deg)				
	C–Er–C	93 (1)	C1–Ho–C2	92.4(8)
			C1–Ho–C3	91.2(8)
			C1–Ho–C4	175.1(8)
			C1–Ho–C5	91.2(8)
			C1–Ho–C6	85.5(8)
	Er–C–Li	77 (2)	Ho–C1–Li	76.3
	C–Li–C	114 (2)	C1–Li–C	114.5(9)
	N–Li–N	86 (2)	N–Li–N	84.8(10)
	C–Li–N	111 (2)	C–Li–N	115.0(5)

air-sensitive complexes $Li[R(t-Bu)_4]$, which contain four molecules of tetrahydrofurane for Sm, Er and Lu, but only three for Yb (Wayda and Evans, 1978; W.J. Evans et al., 1979a):

$$RCl_3 + 4\ Li–t–Bu \xrightarrow[-55°C]{THF} Li[R(t-Bu)_4] \cdot (THF)_x + 3\ LiCl, \tag{65}$$
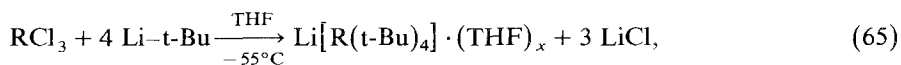
$$R = Er,\ Sm,\ Lu,\ x = 4,$$
$$R = Yb,\ x = 3.$$

Variable-temperature magnetic susceptibility measurements confirm the structure of the complexes as well as the proton NMR spectrum of the samarium compound, which shows a sharp singlet for the 36 tert-butyl protons at $\delta = -0.79$ ppm.

These compounds are rarely stable due to β-hydride elimination during the decomposition reactions. But the thermal decomposition of the samarium derivative in tetrahydrofuran at 40°C yields 2-methylpropane as the main product and ethylene as the other organic product. The absence of equivalent quantities of 2-methylpropene and 2-methylpropane in this decomposition is remarkable and suggests that β-hydride elimination is not the most facile decomposition pathway.

The trichlorides of terbium, erbium or lutetium as well as the erbium and the lutetium tert-butoxides react in pentane in the presence of ether or tmed with formation of complexes of the same type with diethylether or tmed as stabilizing

ligands (Schumann and Müller, 1978c; Schumann et al., 1984a):

$$RCl_3 + 4Li\text{-}t\text{-}Bu \xrightarrow[-78°C]{\text{pentane/Et}_2O} \left[Li(Et_2O)_4\right]\left[R(t\text{-}Bu)_4\right] + 3\ LiCl, \qquad (67)$$

R = Tb, Er, Lu,

$$R(O\text{-}t\text{-}Bu)_3 + 4\ Li\text{-}t\text{-}Bu \xrightarrow[-78°C]{\text{pentane/tmed}} \left[Li(tmed)_2\right]\left[R(t\text{-}Bu)_4\right] + 3\ LiO\text{-}t\text{-}Bu,$$
$$\qquad (67a)$$
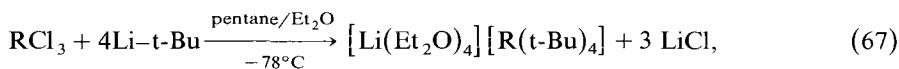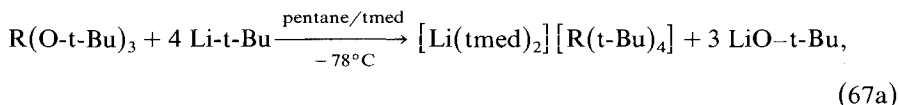
R = Er, Lu.

Complexes Li[R(t-Bu)$_4$] are starting materials for the synthesis of homoleptic lanthanide acetylide compounds. They react with an excess of 3,3-dimethylbut-1-yne in tetrahydrofuran at room temperature with complete replacement of the tert-butyl ligands and formation of 2-methylpropane in addition to the new lanthanide acetylides (W.J. Evans and Wayda, 1980) (see eq. 53).

"Ate"-complexes [LiL$_2$][R(CH$_2$SiMe$_3$)$_4$], with L = tmed, and [LiL$_4$]-[R(CH$_2$SiMe$_3$)$_4$], with L = THF and Et$_2$O, can be prepared by the action of the neutral homoleptic rare earth complex R(CH$_2$SiMe$_3$)$_3 \cdot$(THF)$_2$ with LiCH$_2$SiMe$_3$ either in tetrahydrofuran or in tmed, or from the rare earth trichlorides with an excess of LiCH$_2$SiMe$_3$ (Atwood et al., 1978; Schumann and Müller, 1979; Schumann, 1979a):

$$R(CH_2SiMe_3)_3 \cdot (THF)_2 + 2\ LiCH_2SiMe_3 \xrightarrow{\text{THF}} \left[LiL_4\right]\left[R(CH_2SiMe_3)_4\right], \quad (68)$$

R = Y, L = THF,
R = Y, Er, Yb, L$_2$ = tmed,

$$LuCl_3 + 4\ LiCH_2SiMe_3 \xrightarrow[-LiCl]{\text{Et}_2O} \left[Li(Et_2O)_4\right]\left[Lu(CH_2SiMe_3)_4\right], \qquad (69)$$

$$\left[Li(Et_2O)_4\right]\left[Lu(CH_2SiMe_3)_4\right] + 2\ tmed$$
$$\rightarrow \left[Li(tmed)_2\right]\left[Lu(CH_2SiMe_3)_4\right] + 4\ Et_2O \qquad (70)$$
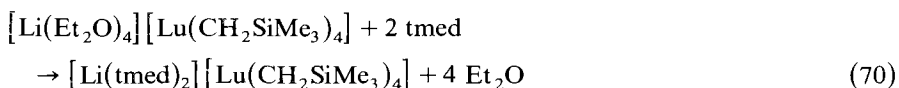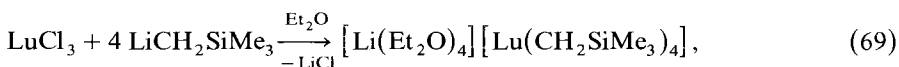
The colorless, yellow or pink yttrium, ytterbium or erbium compounds are insoluble in nonpolar solvents but readily soluble in tetrahydrofuran and ether. With halogenated solvents like CH$_2$Cl$_2$, vigorous reaction occurs. The yttrium tetrahydrofuran complex shows an infrared spectrum with bands for the coordinated THF shifted to higher frequencies. The ^{1}H and ^{13}C NMR spectra in ether at room temperature are consistent with the given formula, although coupling between yttrium and ^{1}H or ^{13}C was not observed. The CH$_2$ signal in the ^{13}C NMR spectrum appears as a weak doublet at $-80°$C, suggesting a rapid dissociation–recombination equilibrium at room temperature:

$$\left[Li(THF)_4\right]\left[Y(CH_2SiMe_3)_4\right]$$
$$\rightleftharpoons Y(CH_2SiMe_3)_3 \cdot (THF)_2 + LiCH_2SiMe_3 \cdot (THF)_x. \qquad (71)$$
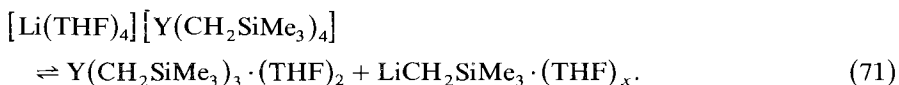
The ether-stabilized lutetium complex shows a different decomposition pathway (Schumann and Müller, 1979). In benzene the compound shows broadening for the

CH_2 resonance in the proton NMR spectrum, which indicates a relatively slow dissociation with respect to the NMR time scale. In a subsequent reaction the complex loses tetramethylsilane by an α-elimination route over a period of one week. At $-10°C$, a white-green compound could be isolated:

$$\left[Li(Et_2O)_4\right]\left[Lu(CH_2SiMe_3)_4\right]$$

$$\rightarrow Si(CH_3)_4 + 4\ Et_2O + Li\left[Lu(CH_2SiMe_3)_2(CHSiMe_3)\right]. \tag{72}$$
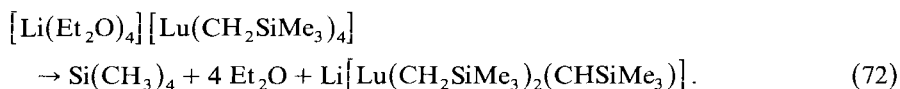
Addition of a base like tmed, THF or DME, leads to stabilized, but benzene-insoluble compounds. The NMR spectrum of $[Li(tmed)][Lu(CH_2SiMe_3)_2(CHSiMe_3)]$ in THF-d_8 shows only some of the expected signals. At $\delta = 0.02$ and -0.05 ppm two peaks appear for the trimethylsilyl groups, the signal at -0.05 having a half width of 5 Hz. The CH_2 resonance at -1.06 ppm is also broadened to 5 Hz; the CH signal cannot be located with certainty due to its low intensity. Cooling to $-35°C$ leads to two sharp signals for the trimethylsilyl protons with an approximate integrated ratio of $2:1$, suggesting a definite kinetically rather stable compound.

Furter loss of one $Si(CH_3)_4$ occurs for the complex $Li[Lu(CH_2SiMe_3)_2(CHSiMe_3)]$ as revealed by NMR. At room temperature the spectrum grows a broad unresolved signal centered around 0.40 ppm. After 3 weeks the reaction is complete and the tetramethylsilane concentration remains constant.

Careful investigations in the rare earth trichloride trimethylsilylmethyl lithium system revealed the simultaneous formation of neutral and ionic species, even with an excess of RCl_3. The ionic derivatives decompose by the outlined α-elimination mechanism, finally resulting in an extremely pyrophoric compound with the unusual stoichiometry $Li:R = 1:2$. All analytical figures are best rationalized by the following formulation: $\{[Li(THF)_2][R_2(CH_2SiMe_3)_2(CHSiMe_3)(CSiMe_3)]\}_n$ (Schumann and Müller, 1978c; Schumann, 1979a).

$ErCl_3$ and $YbCl_3$ react with $LiCH(SiMe_3)_2$ containing the even bulkier ligand bis(trimethylsilyl) methyl with formation of moderately soluble complexes with both rare-earth–carbon and rare-earth–chlorine bonds (Atwood et al., 1978):

$$RCl_3 + 3\ LiCH(SiMe_3)_2 \xrightarrow{\text{THF}} \left[Li(THF)_4\right]\left[R\{CH(SiMe_3)_2\}_3Cl\right] + 2\ LiCl, \tag{73}$$
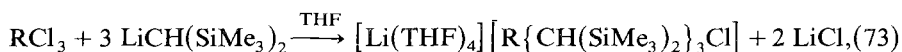
$$R = Er, Yb.$$

The erbium compound decomposes upon heating in hexane with formation of a pink solution, which contains the lithium salt of the homoleptic anion $[Er\{CH(SiMe_3)_2\}_4]^-$. This complex could not be prepared independently via chloride–silyl exchange from $[Li(THF)_4][Er\{CH(SiMe_3)_2\}_3Cl]$ and excess $LiCH(SiMe_3)_2$.

A single crystal X-ray structural analysis of the ytterbium complex (Atwood et al., 1978) shows a tetrahedral arrangement around ytterbium (fig. 32). The bond lengths Yb–C (2.372, 2.373, 2.391 Å) and Yb–Cl (2.486 Å) are shorter than in previous know organometallics of the lanthanides. The bond angles around ytterbium give a distorted tetrahedron (table 26).

All known anionic homoleptic rare earth derivatives are shown in table 27; some NMR data in table 28.
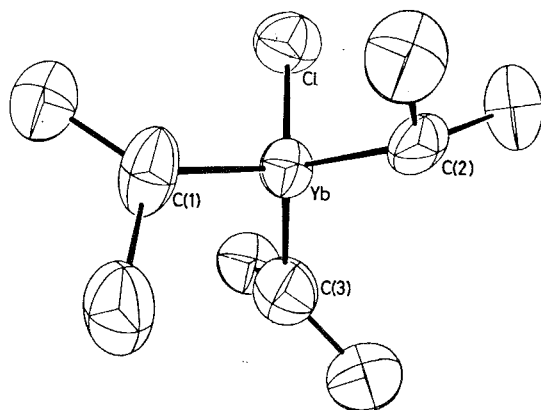
Fig. 32. The structure of the anion
$\{Yb[CH(SiMe_3)_2]_3\}^-$ (after Atwood et
al., 1978).

TABLE 26

Crystallographic data and important bond distances and bond angles of
$[Li(THF)_4][Yb\{CH(SiMe_3)_2\}_3Cl]$.

crystal system	orthorhombic
space group	$P2_12_12_1$
a (Å)	12.751(5)
b (Å)	19.280(7)
c (Å)	23.210(8)
Z	4
bond distances (Å)	
Yb–C(1)	2.373(24)
Yb–C(2)	2.372(16)
Yb–C(3)	2.391(20)
Yb–Cl	2.486(6)
bond angles (deg)	
C(1)–Yb–C(2)	115.9(7)
C(2)–Yb–C(3)	107.6(8)
C(1)–Yb–C(3)	107.1(6)
C(2)–Yb–Cl	110.3(5)
C(1)–Yb–Cl	104.0(5)
C(1)–Yb–Cl	112.0(6)

2.5. *Organometallic compounds of the rare earths with ylidic ligands*

The addition of trimethylmethylenephosphorane to a suspension of rare earth
trichlorides in pentane or hexane results in the formation of pyrophoric phos-
phonium salts in quantitative yields. While no dehydrochlorination of these salts was

TABLE 27

Anionic homoleptic alkyl and aryl derivatives of rare earths.

Compound	Color	Other data	Refs.
$[Li(tmed)]_3[ScMe_6]$	colorless	m.p. 94–98°C	4
$[Li(tmed)]_3[YMe_6]$	white	m.p. 128–130°C	1
$[Li(THF)_4][Y(CH_2SiMe_3)_4]$	colorless	m.p. 85–90°C	2
$[Li(tmed)_2][Y(CH_2SiMe_3)_4]$	colorless	m.p. 123–124°C	2
$[Li(tmed)]_3[LaMe_6]$	white	m.p. 79–82°C	1
$Li[LaPh_4]$	brown	dec. 200°C	3
$[Li(tmed)]_3[CeMe_6]$	yellow	dec. 86–89°C	4
$[Li(tmed)]_3[PrMe_6]$	green	dec. 59–62°C	1,5
$Li[PrPh_4]$	brown	dec. > 200°C	3
$[Li(tmed)]_3[NdMe_6]$	blue	dec. 78–83°C	1,5
$[Li(tmed)]_3[SmMe_6]$	yellow	dec. 85–88°C	1,5
$Li[Sm(t-Bu)_4]\cdot(THF)_4$	dark gold	μ_{eff} 2.1 B.M.	6
$[Li(tmed)]_3[GdMe_6]$	yellow green	dec. 110–112°C	1
$[Li(DME)]_3[GdMe_6]$	colorless	dec. 83–85°C	4
$[Li(tmed)]_3[TbMe_6]$	white	m.p. 114–115°C	1
$[Li(Et_2O)_4][Tb(t-Bu)_4]$	white		7
$[Li(tmed)_2][Tb(t-Bu)_4]$	colorless	dec. 50°C	1
$[Li(tmed)]_3[DyMe_6]$	white	m.p. 106–108°C	1
$[Li(DME)]_3[DyMe_6]$	colorless	dec. 68–69°C	4
$[Li(tmed)]_3[HoMe_6]$	white	m.p. 122–126°C	1
$[Li(tmed)]_3[ErMe_6]$	pink	m.p. 138–139°C	1,8
$[Li(DME)]_3[ErMe_6]$	pink	dec. 82–84°C	9
$Li[Er(t-Bu)_4]\cdot(THF)_4$	pink	μ_{eff} 9.7 B.M.	6
$[Li(Et_2O)_4][Er(t-Bu)_4]$	pink	dec. 40°C	1
$[Li(tmed)_2][Er(t-Bu)_4]$	pink		7
$[Li(tmed)_2][Er(CH_2SiMe_3)_4]$	pink	m.p. 122–124°C	2
$[Li(THF)_4][Er\{CH(SiMe_3)_2\}_3Cl]$	pink	dec. 122–123°C	2
$[Li(tmed)]_3[TmMe_6]$	white	m.p. 109–114°C	1
$[Li(tmed)]_3[YbMe_6]$	white	m.p. 141–142°C	1
$Li[Yb(t-Bu)_4]\cdot(THF)_3$	white	μ_{eff} 4.6 B.M.	6
$[Li(tmed)_2][Yb(CH_2SiMe_3)_4]$	yellow	m.p. 136–138°C	2
$[Li(THF)_4][Yb\{CH(SiMe_3)_2\}_3Cl]$	red	dec. 123–124°C	2
$[Li(tmed)]_3[LuMe_6]$	white	m.p. 141–142°C	1,8
$[Li(DME)]_3[LuMe_6]$	colorless	dec. 84–88°C	9
$Li[Lu(t-Bu)_4]\cdot(THF)_4$			10
$[Li(Et_2O)_4][Lu(t-Bu)_4]$	white		7
$[Li(tmed)_2][Lu(t-Bu)_4]$	white	dec. 95°C	7
$[Li(Et_2O)_4][Lu(CH_2SiMe_3)_4]$	white		11
$[Li(tmed)_2][Lu(CH_2SiMe_3)_4]$	white	m.p. 138–142°C	11
$[Li(THF)_4][Lu(C_6H_3-2,6-Me_2)_4]$	white		12
$[Li_2(teed)(Et_2O)_2]_2[LuMe_5]_2$	colorless	NMR	13

[1] Schumann et al. (1984a).
[2] Atwood et al. (1978).
[3] Hart et al. (1970).
[4] Schumann and Ziep (1984).
[5] Schumann et al. (1981b).
[6] Wayda and Evans (1978).
[7] Schumann and Müller (1978c).
[8] Schumann and Müller (1978b).
[9] Schumann et al. (1984b).
[10] W.J. Evans et al. (1979a).
[11] Schumann and Müller (1979).
[12] S.A. Cotton et al. (1972).
[13] Schumann et al. (1984c).

TABLE 28

NMR data of homoleptic alkyl derivatives of the rare earths.

Compound	δ in ppm, J in Hz	Ref.
[Li(tmed)]$_3$[YMe$_6$]	δCH_3Y -0.52, δCH_3N 2.26, δCH_2N 2.1, $\delta^{13}CY$ 5.9.	1
[Li(tmed)]$_3$[LaMe$_6$]	δCH_3La -0.33, δCH_3N 2.24, δCH_2N 1.95, $\delta^{13}CLa$ 17.8	1
[Li(tmed)]$_3$[PrMe$_6$]	δCH_3Pr -5.9, δCH_3N 5.4, δCH_2N 5.1	1
[Li(tmed)]$_3$[NdMe$_6$]	δCH_3Nd -6.2, δCH_3N 3.7, δCH_2 3.5	1
[Li(tmed)]$_3$[SmMe$_6$]	δCH_3Sm -2.8, δCH_3N 2.9, δCH_2N 2.6	1
[Li(tmed)]$_3$[TbMe$_6$]	δCH_3Tb -103, δCH_3N 5.2, δCH_2N 2.5	1
[Li(tmed)]$_3$[DyMe$_6$]	δCH_3Dy -74	1
[Li(tmed)]$_3$[HoMe$_6$]	δCH_3Ho -60 δ(tmed) 10 to -3	1
[Li(tmed)]$_3$[TmMe$_6$]	δCH_3Tm -92, δ(tmed) 20 to -40	1
[Li(tmed)]$_3$[LuMe$_6$]	δCH_3Lu -1.16, δCH_3N 2.23, δCH_2N 2.3, $\delta^{13}CLu$ 4.5	1
[Li(THF)$_4$][Y(CH$_2$SiMe$_3$)$_4$]	δMe_3Si -0.09, δCH_2 -0.82, δTHF 3.76, 2.15, $\delta^{13}CH_3Si$ 3.74, $\delta^{13}CH_2$ 34.6, J(YC) 28, $\delta^{13}C$(THF) 68.0, 34.6	2
Li[Sm(t-Bu)$_4$]·(THF)$_4$	$\delta^{13}C$ -0.79	3
[Li(tmed)$_2$][Lu(t-Bu)$_4$]	δCH_3C 0.97, δCH_3N 2.13, δCH_2N 2.27	4
[Li(Et$_2$O)$_4$][Lu(CH$_2$SiMe$_3$)$_4$]	δMe_3Si 0.42, δCH_2 -0.64, δEt_2O 0.87, 3.14	5
[Li(tmed)$_2$][Lu(CH$_2$SiMe$_3$)$_4$]	δMe_3Si -0.02, δCH_2 -1.03, δCH_3N 2.32, δCH_2N 2.46, $\delta^{13}CH_3Si$ 5.12, $\delta^{13}CH_2$ 46.44, $\delta^{13}CH_3N$ 45.93, $\delta^{13}CH_2N$ 57.50	5
[Li(tmed)]$_3$[CeMe$_6$]	δCH_3Ce -6.4, δCH_3N 3.8, δCH_2N 3.6	6
[Li(DME)]$_3$[LuMe$_6$]	δCH_3Lu -0.273, δCH_3O 3.292, δCH_2O 3.079, $\delta^{13}CH_3$ 4.5, $\delta^{13}CH_3O$ 58.9, $\delta^{13}CH_2O$ 71.1, δ^7Li 0.682	7
[Li$_2$(teed)(Et$_2$O)$_2$]$_2$[LuMe$_5$]$_2$	δ 0.068 and -0.307, $\delta CH_3\underline{CH_2}O$ 1.008, $\delta \underline{CH_3}CH_2O$ 3.38, $\delta CH_3\underline{CH_2}N$ 2.57, $\delta \underline{CH_3}CH_2N$ 1.19, $\delta N\underline{CH_2CH_2}N$ 2.31	7

1. Schumann et al. (1984a).
2. Atwood et al. (1978).
3. Wayda and Evans (1978).
4. Schumann and Müller (1978c).
5. Schumann and Müller (1979).
6. Schumann and Ziep (1984).
7. Schumann et al. (1984c).

observed, as evidenced by the reaction of them with an excess of the ylide with formation of tetramethyl phosphonium chloride, the compounds react with butyl lithium in ether–hexane, with the formation of lithium chloride, butane, and a new class of uncharged homoleptic rare earth alkyls (Schumann and Hohmann, 1976):

$$RCl_3 + 3\ Me_3P{=}CH_2 \rightarrow R(CH_2PMe_3Cl)_3, \tag{74}$$

$$R(CH_2PMe_3Cl)_3 + 3\ LiBu \rightarrow R(\underset{CH_2}{\overset{CH_2}{<\quad >}}PMe_2)_3 + 3\ LiCl + 3\ C_4H_{10}, \tag{75}$$
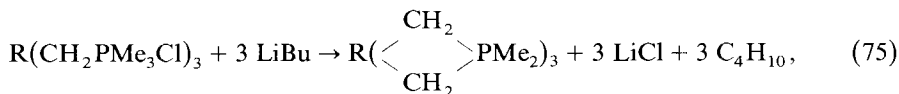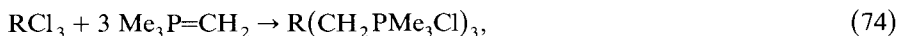
R = La, Pr, Nd, Sm, Gd, Ho, Er, Lu.

These highly air-sensitive complexes apparently owe their high stability to the incorporation of chelating phosphorus ylide ligands. The neutral complexes show dynamic behavior in solution producing dimeric, trimeric and polymeric species in addition to the monomers. This could be demonstrated with the di-tert-butyl phosphonium derivative of lutetium (Schumann and Reier, 1982a):

$$LuCl_3 + 3\ Li(CH_2)_2P(t\text{-}Bu)_2 \rightarrow Lu[\underset{CH_2}{\overset{CH_2}{<\quad >}}P(t\text{-}Bu)_2]_3 + 3\ LiCl. \tag{76}$$
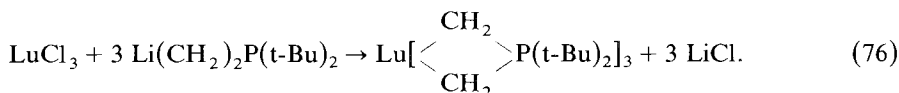
The complex can be isolated free of coordinating solvents. The colorless crystals decompose above 136°C. The NMR spectra indicate dynamic behavior of the compound in solution. The complicated ^1H NMR spectrum at room temperature is reduced to two doublets at $-26°C$, which are assigned to an octahedral compound with six η^1-Lu–C bonds. This spectrum as well as the ^{13}C and ^{31}P NMR spectra, which contain many signals of low intensity in addition to the main signal, argue for a dynamic oligomerization in solution as indicated in fig. 33.

This dynamic behavior is not observed when using blocking ligands like η^5-cyclopentadienyl. Dicyclopentadienyl lutetium di-tert-butylphosphonium bis(methylid), prepared from dicyclopentadienyl lutetium chloride and lithium di-tert-butylphosphonium bis(methylid) in tetrahydrofuran is a monomeric compound in solution, which crystallizes from toluene free of solvent (Schumann and Reier, 1982a):

$$Cp_2LuCl + Li(CH_2)_2P(t\text{-}Bu)_2 \xrightarrow{THF} Cp_2Lu\underset{CH_2}{\overset{CH_2}{<\quad >}}P(t\text{-}Bu)_2 + LiCl. \tag{77}$$
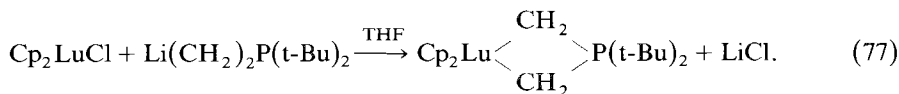
The NMR data (decoupled) confirm the proposed structure:

^1H NMR: δCp 6.1 ppm (s), δCH_2 -0.3 (d), $^2J(HP) = 12$ Hz, δCH_3 1.02 (d), $^3J(HP) = 13.8$;

^{31}P NMR: δ 57 ppm (relative to 85% H_3PO_4);

^{13}C NMR: δCP 110.2 ppm (s), δCH_2 3.8 (d), $^1J(CP) = 17.6$ Hz, δCP 33.8 (d), $^1J(CP) = 30.6$, δCH_3 28.9 (s).

An analogous scandium derivative was prepared from dicyclopentadienyl scandium chloride and $Li(CH_2)_2PPh_2$ in ether. It was characterized by proton NMR: δCp 6.0 ppm and δCH_2 0.86 ppm as a doublet with $^2J(HP) = 11$ Hz (Manzer, 1976).
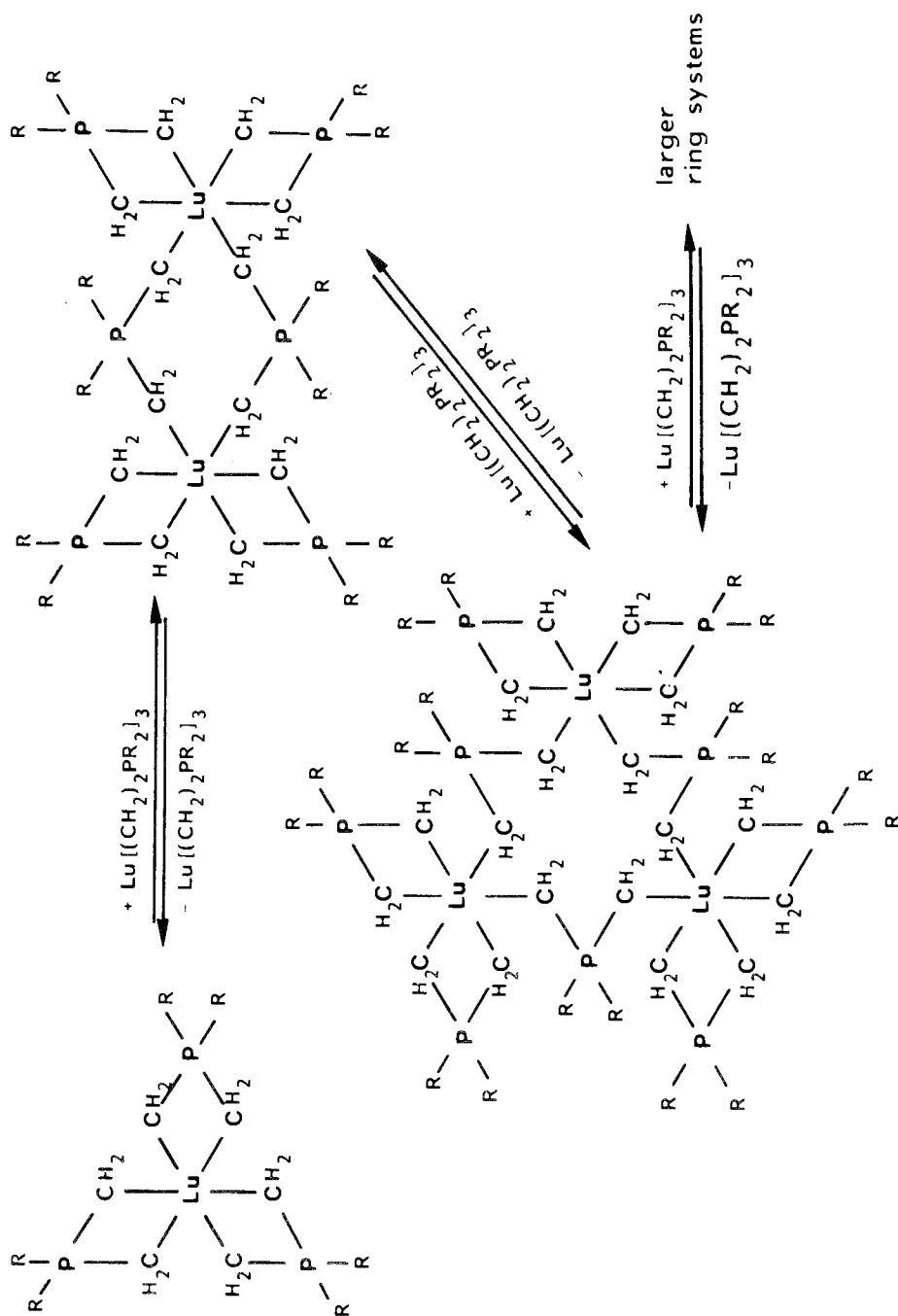
Fig. 33. Oligomerization equilibria in the system $[Lu\{(CH_2)_2P(t\text{-}Bu_2)\}_3]_n$ with $n = 1, 2, 3, \ldots$ (after Schumann and Reier, 1982a).

Tricyclopentadienyl lutetium reacts with triphenylmethylenephosphorane in tetra-hydrofuran with formation of a $1:1$ complex, which precipitates from the solvent in colorless crystals, decomposing above $108°C$ (Schumann and Reier, 1984b). Di-cyclopentadienyl lutetium chloride forms in the same way in toluene an $1:1$ complex with triphenylmethylenephosphorane, which is zwitterionic containing a η^1-Lu–C bond (Schumann and Reier, 1981):

$$Cp_2LuCl + Ph_3P\text{=}CH_2 \rightarrow Cp_2\overline{Lu}\underset{CH_2\overset{+}{P}Ph_3}{\overset{Cl}{\big<}} \tag{78}$$
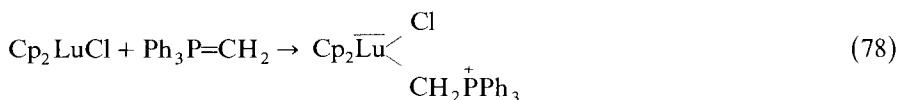
The colorless compound, which decomposes at $172°C$ without melting shows an NMR spectrum at room temperature with one sharp signal for the cyclopentadienyl protons at 6.1 ppm, and the expected doublet for CH_2 at 0.92 with a large coupling constant $^2J(HP)$ of 17.5 Hz in comparison to the 7.5 Hz for the starting ylide. The formation of the Lu–C bond causes a decrease of electron density at the ylide carbon, shown by the low field shift in the ^{13}C NMR spectrum to $\delta = -4.2$ from $\delta = 7.5$ of the starting ylide and by the drastically reduced coupling constant $^1J(CP)$ of 28.8 Hz in comparison to 99.6 Hz in the ylide and 83.7 Hz for tetraphenylphos-phonium chloride. The non-decoupled ^{13}C NMR spectrum confirms two protons at the ylide carbon, showing a coupling constant of $^1J(CH)$ of 118 Hz.

$(C_5H_5)_2Lu(Cl)CH_2P(C_6H_5)_3$ hydrolyzes with formation of cyclopentadiene, lutetium hydroxide and triphenylmethylphosphonium chloride. It reacts with methyl lithium in toluene at $-78°C$ with formation of the methylated derivative, which shows an additional NMR signal at $\delta = -0.4$ ppm for $LuCH_3$. It decomposes at room temperature with evolution of CH_4 via a carbon–hydrogen activation at the δ position of the initial adduct and formation of a five-membered metallacycle (Schumann and Reier, 1984a, b). The corresponding pentamethylcyclopentadienyl derivative shows the same behavior (Watson, 1983):

$$Cp_2\overline{Lu}\underset{CH_2\overset{+}{P}(C_6H_5)_3}{\overset{Cl}{\big<}} + CH_3Li \xrightarrow[-LiCl]{} Cp_2Lu\underset{CH_2P(C_6H_5)_3}{\overset{CH_3}{\big<}} \tag{79}$$
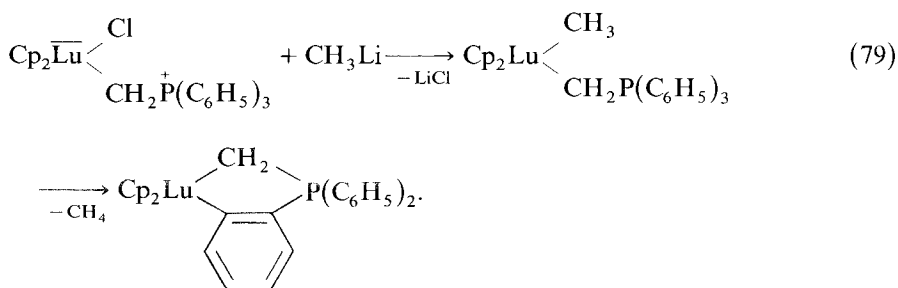
The same metallacycle 1,1-diphenyl-3,3-dicyclopentadienyl-1-phospha-3-luteto-in-dane is also isolated as a product of the reaction of tert-butyl lithium with triphenylmethylenephosphorane and dicyclopentadienyl lutetium chloride in tetra-hydrofuran at $-78°C$ and as the product of the NaH reduction of $(C_5H_5)_2Lu(Cl)CH_2P(C_6H_5)_3$ in toluene at $-15°C$ (Schumann and Reier, 1984a, b):

$$Cp_2LuCl(THF) + Ph_3P\text{=}CH_2 + \text{t-BuLi} \rightarrow Cp_2Lu \tag{80}$$

$$Cp_2\overline{Lu}\!\!\begin{array}{c}Cl\\ \\CH_2\overset{+}{P}Ph_3\end{array}\ + NaH \rightarrow Cp_2Lu\!\!\begin{array}{c}H\\ \\CH_2PPh_3\end{array}\ + NaCl \qquad (81)$$

$$\Big\downarrow -H_2$$

$$Cp_2Lu\!\!\begin{array}{c}{}^{CH_2}\\ \diagup\!\!\!\diagdown\\ \end{array}\!\!P(C_6H_5)_2.$$
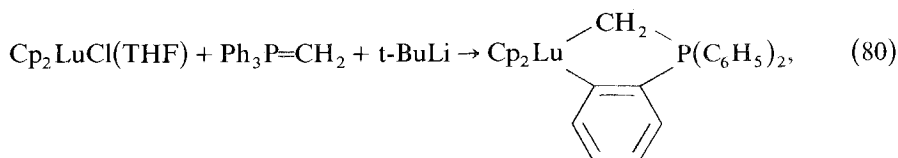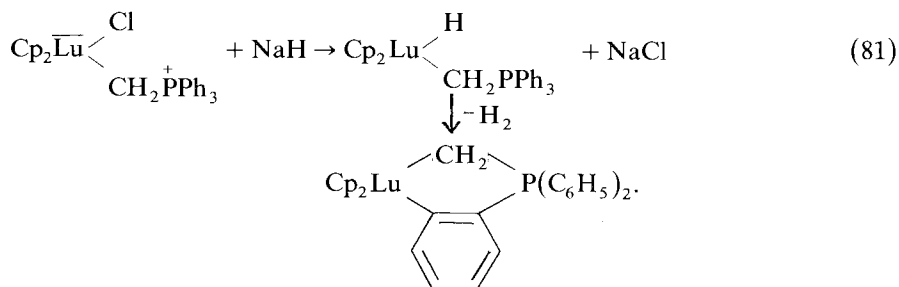
Organometallic compounds of the rare earths such as dicyclopentadienyl rare earth chlorides or dicyclopentadienyl(alkyl) derivatives are stabilized by coordinating donor solvents like tetrahydrofuran, increasing the coordination number of the rare earth metal. These donor solvents can be replaced by ylides, as shown with the formation of the zwitterionic complex $Cp_2Lu(Cl)CH_2PPh_3$ (Schumann and Reier, 1981). Dicyclopentadienyl(tert-butyl) lutetium tetrahydrofuranate also reacts at room temperature in toluene with triphenylmethylenephosphorane yielding a colorless solid, which decomposes above 122°C with formation of isobutane. The same exchange reaction is found between $Cp_2LuCH_2SiMe_3(THF)$ and $Ph_3P{=}CH_2$ in toluene at $-78°C$, and $Cp_2Lu(t\text{-}Bu)(THF)$ and $Me_3P{=}CHSiMe_3$ react in toluene at $-15°C$ also with exchange of tetrahydrofuran against the ylide (Schuman et al., 1983):

$$Cp_2Lu\!\!\begin{array}{c}L\\ \\OC_4H_8\end{array}\ + CH_2{=}PPh_3 \rightarrow Cp_2Lu\!\!\begin{array}{c}L\\ \\CH_2PPh_3\end{array}\ + C_4H_8O, \qquad (82)$$

$$L = CH_2SiMe_3,\ t\text{-}Bu.$$
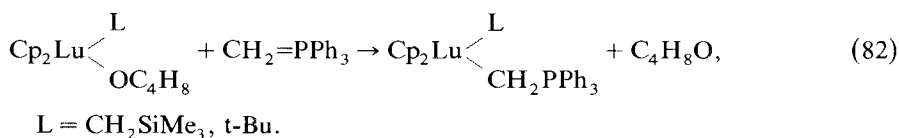
Ylide derivatives of lutetium with high thermal stability are obtained using pentamethylcyclopentadienyl lutetium halides as starting materials (Schumann et al., 1984d):

$$(C_5Me_5)_2Lu\!\!\begin{array}{c}Cl\\ \diagup\diagdown\\ Cl\end{array}\!\!Na(Et_2O)_2 + Li\!\!\begin{array}{c}CH_2\\ \diagup\diagdown\\ CH_2\end{array}\!\!P(CH_3)_2$$

$$\rightarrow (C_5Me_5)_2Lu\!\!\begin{array}{c}CH_2\\ \diagup\diagdown\\ CH_2\end{array}\!\!P(CH_3)_2 + LiCl + NaCl, \qquad (83)$$

$$C_5Me_5Na(THF) + LuCl_3 + 2\,Li\!\!\begin{array}{c}CH_2\\ \diagup\diagdown\\ CH_2\end{array}\!\!P(CH_3)_2$$

$$\rightarrow C_5Me_5Lu\!\!\left[\begin{array}{c}CH_2\\ \diagup\diagdown\\ CH_2\end{array}\!\!P(CH_3)_2\right]_2 + 2\,LiCl + NaCl. \qquad (83a)$$
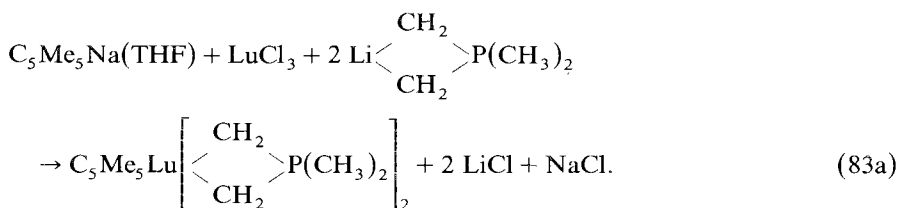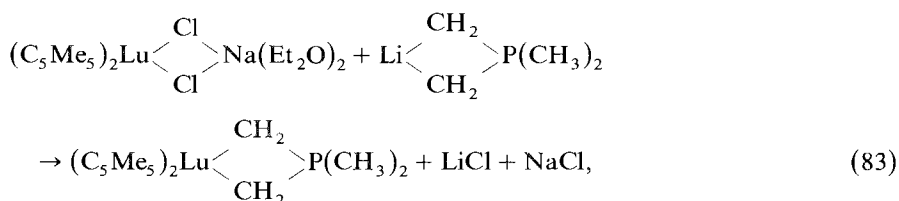
$(C_5Me_5)_2Lu(\mu\text{-}CH_2)_2P(CH_3)_2$ crystallizes in the space group $P2_1$ with $a = 9.406(14)$, $b = 15.932(26)$, $c = 8.253(11)$ Å, $\beta = 106.90°$ (fig. 33a). Some important
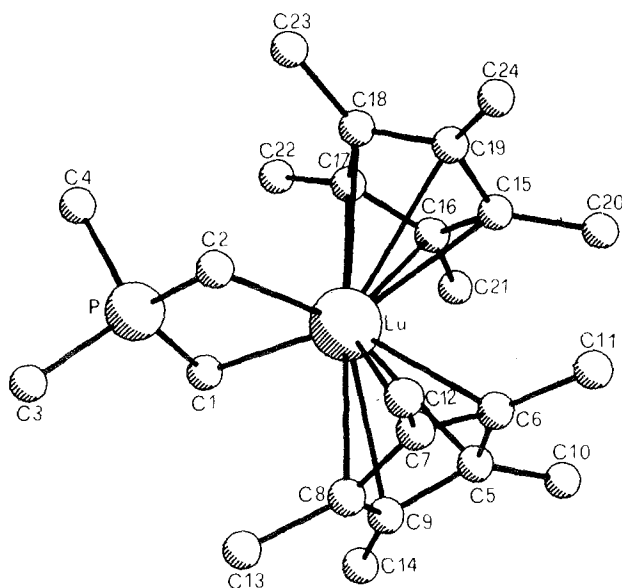
Fig. 33a. Molecular structure of $(C_5Me_5)_2Lu(\mu\text{-}CH_2)_2P(CH_3)_2$ (after Schumann et al., 1984d).

TABLE 28a

Important bond distances and angles in $(C_5Me_5)_2Lu(\mu\text{-}CH_2)_2P(CH_3)_2$.

bond distances	(Å)
Lu–C1	2.360(1)
Lu–C1′	2.340(1)
Lu–C(Cp) (av.)	2.650(1)
P–C1	1.780(3)
P–C1′	1.780(3)
P–C2	1.810(3)
P–C2′	1.840(3)
bond angles	(deg.)
∅ Cp1–Lu–∅ Cp2	140.0(10)
C1–Lu–C1′	120.0(10)
C1–P–C2	110.0(10)
C2–P–C2′	110.0(10)
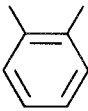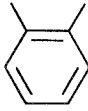
bond distances and angles are shown in table 28a. (Schumann et al., 1984d).

All known ylide derivatives of the rare earths are shown in table 29.

2.6. Organometallic compounds of the rare earths with hydride ligands

Organo rare earth hydrides were prepared first independently by three groups in the early 1980s by the hydrogenolysis of dicyclopentadienyl yttrium, erbium and

TABLE 29

Ylidic derivatives of rare earths.

Compound	Color	Other data	Refs.
$Cp_2Sc(\mu\text{-}CH_2)_2PPh_2$	pale yellow		1
$La[(\mu\text{-}CH_2)_2PMe_2]_3$	white	dec. 195–205°C	2
$La(CH_2PMe_3Cl)_3$	white	dec. 155°C	2
$Pr[(\mu\text{-}CH_2)_2PMe_2]_3$	green	dec. 188–195°C	2
$Pr(CH_2PMe_3Cl)_3$	green	dec. 140°C	2
$Nd[(\mu\text{-}CH_2)_2PMe_2]_3$	blue	dec. 160–180°C	2
$Nd(CH_2PMe_3Cl)_3$	blue	dec. 160°C	2
$Sm[(\mu\text{-}CH_2)_2PMe_2]_3$	white	dec. 179–180°C	2
$Sm(CH_2PMe_3Cl)_3$	white	dec. 181°C	2
$Gd[(\mu\text{-}CH_2)_2PMe_2]_3$	white	dec. 180°C	2
$Gd(CH_2PMe_3Cl)_3$	white	dec. 155°C	2
$Ho[(\mu\text{-}CH_2)_2PMe_2]_3$	white	dec. 190–200°C	2
$Ho(CH_2PMe_3Cl)_3$	white	dec. 180°C	2
$Er[(\mu\text{-}CH_2)_2PMe_2]_3$	pink	dec. 195–205°C	2
$Er(CH_2PMe_3Cl)_3$	pink	dec. 160°C	2
$Lu[(\mu\text{-}CH_2)_2PMe_2]_3$	white	dec. 210°C	2,6
$Lu(CH_2PMe_3Cl)_3$	white	dec. 140°C	2
$Cp_2Lu(\mu\text{-}CH_2)_2P(t\text{-}Bu)_2$	white	dec. 156°C	3
$Cp_2Lu(t\text{-}Bu)CH(SiMe_3)PMe_3$	white	m.p. 132°C, IR, NMR	4
$Cp_2Lu(Cl)CH_2PPh_3$	white	dec. 172°C	5
$Cp_2Lu(Me)CH_2PPh_3$	white	dec. 40°C	7
$Lu[(\mu\text{-}CH_2)_2P(t\text{-}Bu)_2]_3$	white	dec. 136°C	3
$Cp_2Lu(t\text{-}Bu)CH_2PPh_3$	white	dec. 122°C, IR, NMR	4
$Cp_2Lu(CH_2SiMe_3)CH_2PMe_3$	white	m.p. 103°C, IR, NMR	4
$Cp_3LuCH_2PPh_3$	colorless	dec. 108°C, IR, NMR	7
$Cp_2LuCH_2PPh_2$ 	colorless	m.p. 126°C	7
$(C_5Me_5)_2Lu(\mu\text{-}CH_2)_2PMe_2$	colorless	m.p. 208°C, IR, NMR	6
$C_5Me_5Lu[(\mu\text{-}CH_2)_2PMe_2]_2$	colorless	dec. 152°C, IR, NMR	6
$(C_5Me_5)_2LuCH_2PPh_2$ 		NMR	8

1. Manzer (1976a).
2. Schumann and Hohmann (1976).
3. Schumann and Reier (1982a).
4. Schumann et al. (1983).
5. Schumann and Reier (1981).
6. Schumann et al. (1984d).
7. Schumann and Reier (1984b).
8. Watson (1983a).

lutetium alkyl derivatives at atmospheric or high pressure (Schumann and Genthe, 1981; W.J. Evans et al., 1982a; Marks and Ernst, 1982):

$$Cp_2LuL \cdot (THF) + H_2 \xrightarrow[50\ atm.]{THF} \frac{1}{n}\left[Cp_2LuH \cdot (THF)\right]_n + LH, \tag{84}$$

$$L = t\text{-Bu, } CH_2C(CH_3)_3,\ CH_2SiMe_3,\ CH_2C_6H_5,$$

$$2\ Cp_2R\text{-}t\text{-Bu} \cdot (THF) + 2\ H_2 \xrightarrow{toluene} \left[Cp_2RH \cdot (THF)\right]_2 + 2\ (CH_3)_3CH, \tag{85}$$

$$R = Y,\ Er,\ Lu,$$
$$2\ (MeCp)_2R\text{-}t\text{-Bu} \cdot (THF) + 2\ H_2$$

$$\xrightarrow{toluene} \left[(MeCp)_2RH \cdot (THF)\right]_2 + 2\ (CH_3)_3CH, \tag{86}$$

$$R = Y,\ Er,\ Lu,$$

$$\left[(MeCp)_2ErCH_2SiMe_3\right]_2 + 2\ H_2 \xrightarrow{toluene} \left[(MeCp)_2ErH\right]_2 + 2\ SiMe_4. \tag{87}$$
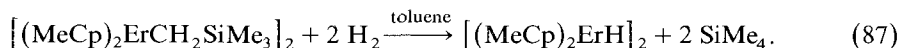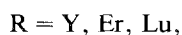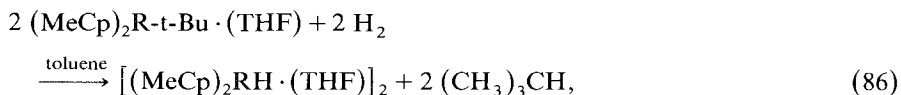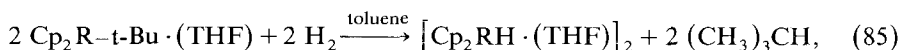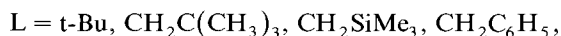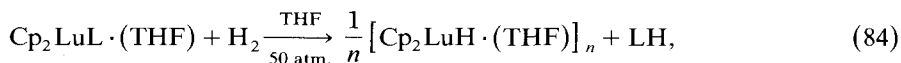
^{1}H and ^{13}C NMR spectra as well as the IR spectra of the lutetium derivatives with H (eq. 84) have been interpreted for a hydrogen-bridged, oligomeric structure

TABLE 30

Crystallographic data and important bond distances and bond angles of $[(MeCp)_2YH \cdot (THF)]_2$ and $[(MeCp)_2ErH \cdot (THF)]_2$.

	$[(MeCp)_2YH \cdot (THF)]_2$		$[(MeCp)_2ErH \cdot (THF)]_2$
crystal system	monoclinic		orthorhombic
space group	$P2_1/c$		Pnnm
a (Å)	8.731(3)		10.111(5)
b (Å)	19.772(6)		12.152(5)
c (Å)	9.054(3)		12.711(5)
β (deg)	98.71(3)		
Z	2 (dimer)		2 (dimer)
bond distances (Å)			
	Y–Y′	3.664(1)	Er–Er′ 3.616(5)
	Y–⌀Cp1	2.397	
	Y–⌀Cp2	2.414	
	Y–O	2.460(8)	
	Y–H1	2.17(8)	
	Y–H2	2.19(8)	
bond angles (deg)			
	Y–H1–Y′	114 (3)	
	H1–Y–H1′	66 (3)	
	O–Y–H1	137 (2)	
	H1–Y–⌀Cp1	112	
	H1′–Y–⌀Cp1	101	
	H1–Y–⌀Cp2	120	
	H1′–Y–⌀Cp2	100	

(Schumann and Genthe, 1981). W.J. Evans et al. (1982a) established a dimeric nature for their products by X-ray crystallography of [(MeCp)$_2$YH · (THF)]$_2$ and the analogous Er complex (table 30, fig. 34), as well as Marks and Ernst (1982) for the solvent-free erbium hydride, by cryoscopic molecular weight determination in benzene. [Cp$_2$LuH · (THF)]$_2$ shows a ν(LuH) in the infrared spectrum at 1350 cm^{-1} (ν(LuD) = 975 cm^{-1} for the D-derivative) and NMR signals at δ = 3.61 and 1.77 ppm for THF, 5.90 ppm for Cp and 4.69 ppm for the hydrogen bridge. [Cp$_2$YH · (THF)]$_2$ shows δH at 2.02 ppm with ^1J(YH) = 27 Hz (W.J. Evans et al., 1982a). [(MeCp)$_2$ErH]$_2$ exhibited ν(ErH) at 1520 and 1180 cm^{-1} which shifted to 1173 and 840 cm^{-1} on deuteration (Marks and Ernst, 1982). A colorless lutetium hydride formed in the reaction of dicyclopentadienyl lutetium chloride with sodium hydride in tetrahydrofuran has the composition [Na(THF)$_6$][(Cp$_3$Lu)$_2$H · (THF)$_2$], as proved by X-ray structural analysis (Schumann et al., 1984e).

The lutetium derivative [Cp$_2$LuH · (THF)]$_n$ does not react with olefins, but with Me$_3$SiCl with formation of Me$_3$SiH (Schumann and Genthe, 1981). The complexes [(C$_5$H$_4$L)$_2$YH · (THF)]$_2$, with L = H, Me, react with t-butyl isonitrile to form a formimidoyl dimer of the composition [(C$_5$H$_4$L)$_2$Y(HC=NCMe$_3$)]$_2$ (W.J. Evans et al., 1983a).

The enediyl complex (C$_5$Me$_5$)$_2$SmC(Ph)=C(Ph)Sm(C$_5$Me$_5$)$_2$, which is formed by the reaction of bis(pentamethylcyclopentadienyl) bis(tetrahydrofurano) samarium
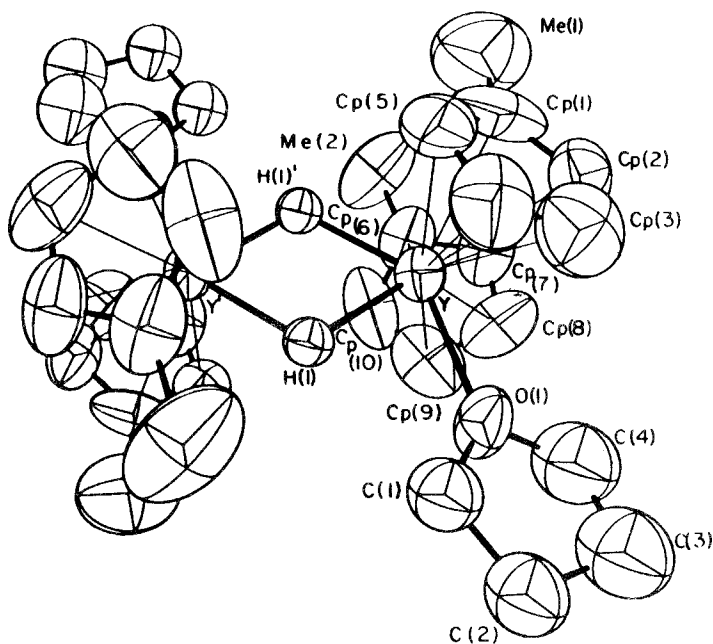
Fig. 34. Molecular structure of [(MeCp)$_2$YH·(THF)]$_2$ (after W.J. Evans et al., 1982a).
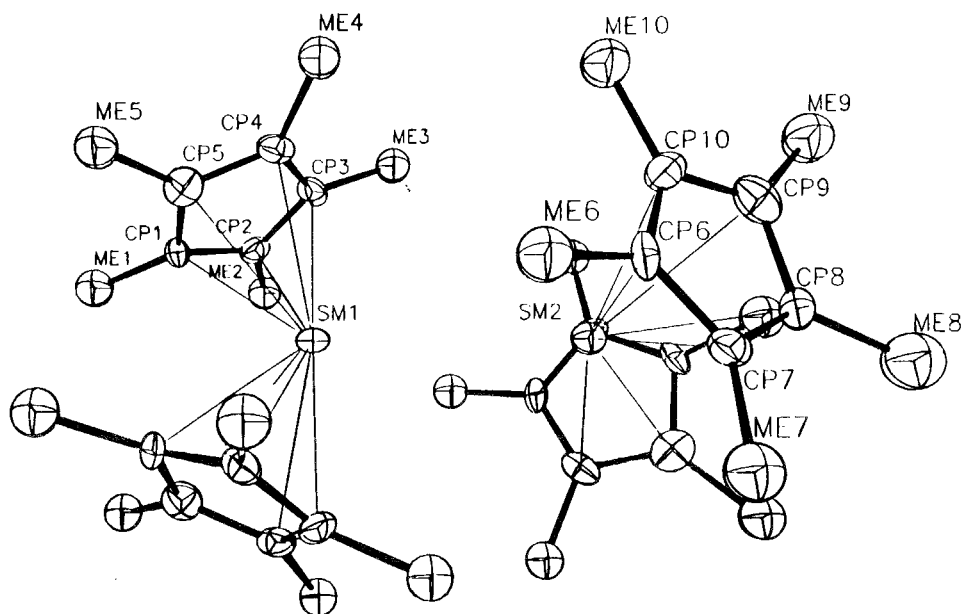
Fig. 35. Molecular structure of $[(C_5Me_5)_2SmH]_2$ (after W.J. Evans et al., 1983b).

and diphenylacetylene, reacts with hydrogen in hexane solution to give a solvent-free, orange hydride $[(C_5Me_5)_2SmH]_2$. The thermal stability of this compound is limited to one to two days in solution and five to seven days in the solid state. The ^1H NMR spectrum shows a broad signal at $\delta = 15.61$ ppm for the hydride and a singlet at -0.80 ppm for the methyl groups. The infrared spectrum shows the $\nu(SmH)$ at 1140 cm^{-1} and the $\nu(SmD)$ for the analogous deuterium derivative, formed from the hydride by reaction with D_2, at 820 cm^{-1}. The X-ray diffraction (fig. 35, table 31) shows that in contrast to the former described hydrides $[(MeCp)_2RH \cdot (THF)]_2$, with $R = Y$, Er, one of the $(C_5Me_5)_2Sm$ units is rotated with respect to the other with a dihedral angle of 87° (W.J. Evans et al., 1983b).

A highly reactive pentamethylcyclopentadienyl lutetium derivative was prepared by the reaction of bis(pentamethylcyclopentadienyl) methyl lutetium with hydrogen at 20°C in hexane (Watson, 1982; Watson and Roe, 1982). The ^1H NMR spectrum at $-95°C$ ($\delta LuH = 9.27$ ppm) confirms an asymmetric structure of a dimer containing a bridging and a terminal hydrogen, which shows a rapid monomer–dimer equilibrium with ΔG^0 at 25°C for the dissociation to be less than 2 kcal/mol.

$$\left[(C_5Me_5)_2LuCH_3\right]_2 + 2\ H_2 \xrightarrow[20°C]{\text{hexane}} \left[(C_5Me_5)_2LuH\right]_2 + 2\ CH_4. \qquad (88)$$
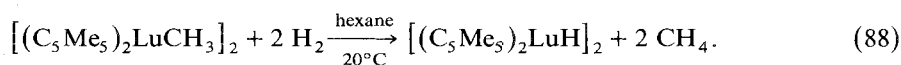
$(C_5Me_5)_2LuH$ cleaves activated carbon–hydrogen bonds even in compounds like $Si(CH_3)_4$ (Watson, 1983a). This hydride as well as the corresponding deuterated

TABLE 31

Crystallographic data and important bond distances and bond angles of $[(C_5Me_5)_2SmH]_2$.

crystal system	monoclinic
space group	C2/c
a (Å)	16.532(6)
b (Å)	14.260(4)
c (Å)	16.948(4)
β (deg)	104.26(4)
Z	4 (dimer)
bond distances (Å)	
Sm–Sm	3.905(3)
Sm1–∅Cp1	2.478
Sm2–∅Cp2	2.470
bond angles (deg)	
∅Cp1–Sm1–∅Cp2	130.381
∅Cp2-Sm2–∅Cp2	134.469

derivative show an analogous reactive behavior like $(C_5Me_5)_2LuCH_3$ (see in section 2.2.). The $\nu(Lu–H)$ in the IR spectrum of $(C_5Me_5)_2LuH$ is found at 1345 cm^{-1} and the $\nu(Lu–D)$ in the deuterium derivative at 975 cm^{-1} (Watson, 1983a).

A new class of polymetallic organolanthanide polyhydride complexes was found by W.J. Evans et al. (1982b). Dicyclopentadienyl-tert-butyl erbium tetrahydrofuranate decomposes in toluene in the presence of lithium chloride within ten hours at room temperature with formation of 2-methylpropane, 2-methylpropene and a pink compound, which shows a broad absorption in the infrared spectrum between 1250 and 1200 cm^{-1} for the $\nu(ErH)$. A single crystal X-ray structural determination of a pink prismatic crystal shows cation–anion pairs with three dicyclopentadienyl
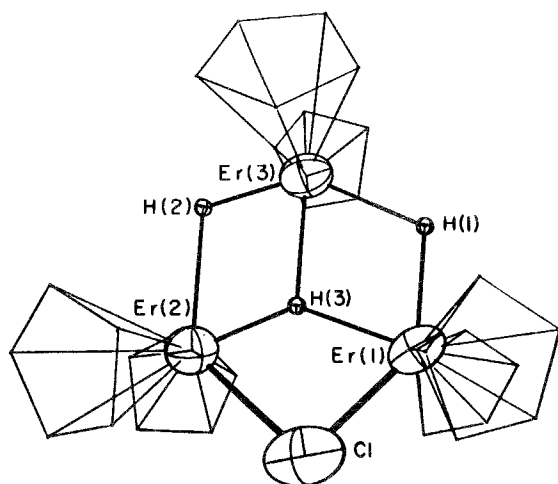
Fig. 36. Molecular structure of the anion $[Cp_2ErH]_3Cl^-$ (after W.J. Evans et al., 1982b).

TABLE 32
Crystallographic data and important bond distances and bond angles of $[Li(THF)_4][(Cp_2ErH)_3Cl]$.

crystal system		monoclinic	
space group		$P2_1/c$	
a (Å)		10.324(5)	
b (Å)		28.132(9)	
c (Å)		16.773(6)	
β (deg)		101.00(4)	
Z		4	
bond distances	(Å)	bond angles	(deg)
Er1–Er2	3.926(2)	Cl–Er1–H3	64
Er1–Er3	3.692(1)	H1–Er–H3	75
Er2–Er3	3.684(1)	Er1–H1–Er3	100
Er1–Cl	2.64(1)	H1–Er3–H3	74
Er2–Cl	2.735(9)	H2–Er3–H3	71
Er1–H1	2.48	Er2–H2–Er3	108
Er3–H1	2.33	H2–Er2–H3	76
Er3–H2	1.99	Cl–Er2–H3	64
Er2–H2	2.54	Er2–Cl–Er1	93.9(3)
Er1–H3	2.18	Er1–H3–Er2	139
Er2–H3	2.02	Er1–H3–Er3	108
Er3-H3	2.39	Er2-H3-Er3	113

erbium units, three hydrogens and one chlorine arranged in the anions, providing a formal coordination number of nine for each erbium atom (fig. 36, table 32).

Another complex of this type, $[Li(THF)_3][Cp_2LuH)_3H]$ is formed when the reaction product of Cp_2LuCl and $LiC(CH_3)_3$ in ether is allowed to warm up to room temperature and additional stirring is continued for several hours. The 270 MHz NMR spectrum of the white crystalline powder isolated from THF shows signals at $\delta = 3.61$ and 1.77 ppm for THF, one singlet at $\delta = 5.38$ ppm for all Cp protons and a quartet at $\delta = 1.83$ ppm ($J = 7.8$ Hz) for the hydrogens (W.J. Evans et al., 1982b).

Acetylide hydride complexes of samarium, erbium and ytterbium have been made by the cocondensation reactions of Sm, Er, and Yb metal vapor with 1-hexyne at 77K. Polymeric compounds containing $[(BuC\equiv C)_2SmH]$, $[(BuC\equiv C)_2ErH]$ and $[(BuC\equiv C)_3Yb_2H]$ units are isolated and shown to be active catalysts for hydrogenation reactions (W.J. Evans et al., 1981c).

Interaction of the dicyclopentadienyl rare earth chlorides of Sm, Er, Yb, and Lu and sodium borohydride in tetrahydrofuran yields the borohydride complexes, which are isolated as complexes with one tetrahydrofuran (Marks and Grynkewich, 1976; Schumann et al., 1982):

$$Cp_2RCl \cdot (THF) + NaBH_4 \xrightarrow{THF} Cp_2RBH_4 \cdot (THF) + NaCl, \qquad (89)$$

$R = Sm, Er, Yb, Lu.$

The vibrational spectra of the samarium borohydride and borodeuteride complex suggested a tridentate borohydride or borodeuteride bridge. For the smaller Er and

Yb atoms, bidentate bridges are proposed (Marks and Grynkevich, 1976). The lutetium complex shows a $1:1:1:1$ quartet in the ^{1}H NMR spectrum at $\delta = 1.07$ ppm for BH_4 with $J(BH) = 84$ Hz (Schumann et al., 1982). The compound loses the coordinated THF reversibly upon heating in vacuo or toluene.

Complexes of the type $[(Me_3Si)_2C_5H_3]_2RBH_4 \cdot (THF)$, with R = La, Pr, Nd, and Sm, have been prepared with the tetrahydridoborate as a tridentate ligand, and with R = Y and Yb as well as a tetrahydrofuran-free Sc complex with the BH_4 group as a non-fluxional bidentate ligand. The monoclinic scandium complex (P2/c, $a = 11.245(3)$ Å, $b = 13.114(3)$ Å, $c = 10.588(3)$ Å, $\beta = 103.31(2)°$, Z = 2; fig. 37) confirms the structure showing a scandium–hydrogen bond length of 2.03(4) Å (Lappert et al., 1983b).
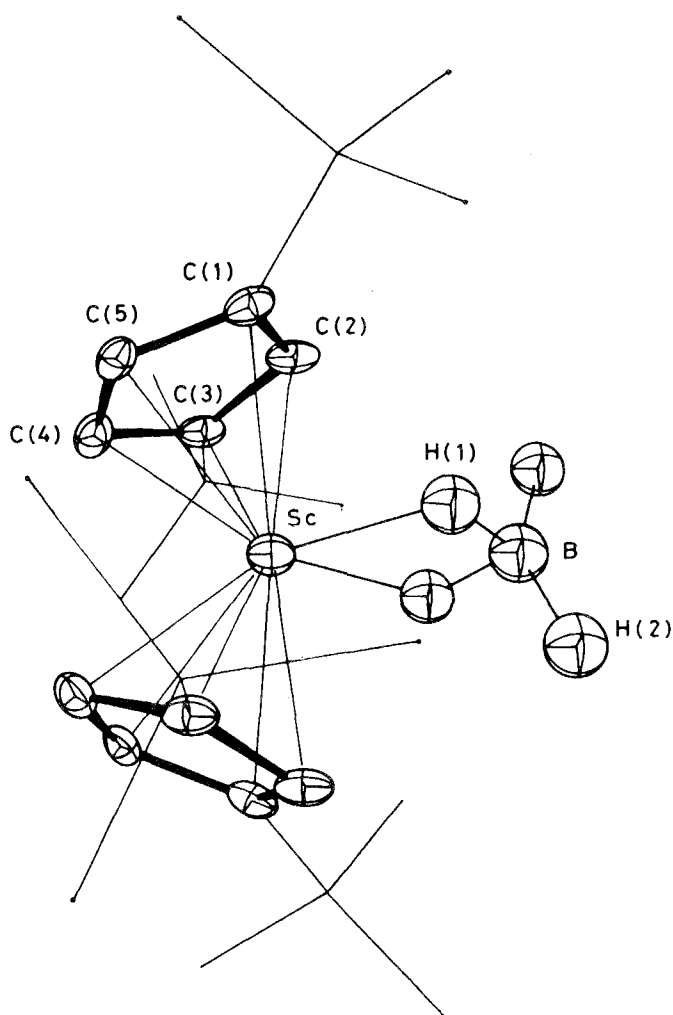
Fig. 37. Molecular structure of $[(Me_3Si)_2C_5H_3]_2Sc(\mu-H)_2BH_2$ (after Lappert et al., 1983b).

TABLE 33

Organometallic compounds of the rare earths with hydride ligands.

Compound	color	other data	Refs.
$[Cp_2YH \cdot (THF)]_2$	white		1
$[Cp_2ErH \cdot (THF)]_2$	pink		1
$[Cp_2LuH \cdot (THF)]_2$	colorless		1
$[Cp_2LuH \cdot (THF)]_n$	colorless		2
$[(MeCp)_2YH \cdot (THF)]_2$	colorless		1
$[(MeCp)_2ErH]_2$			3
$[(MeCp)_2ErH \cdot (THF)]_2$	pink		1
$[(MeCp)_2LuH \cdot (THF)]_2$	colorless		1
$[(C_5Me_5)_2SmH]_2$	orange	μ_{eff} 1.4 B.M.	4
$(C_5Me_5)_2LuH$	colorless	IR, NMR	5,11
$(C_5Me_5)_2LuD$		IR, NMR	11
$Cp_2SmBH_4 \cdot (THF)$	yellow		6
Cp_2ErBH_4	pink		6
$Cp_2ErBH_4 \cdot (THF)$	peach		6
Cp_2YbBH_4	orange		6
$Cp_2YbBH_4 \cdot (THF)$	orange		6
$Cp_2LuBH_4 \cdot (THF)$	colorless		7
$[(Me_3Si)_2C_5H_3]_2ScBH_4$	white	m.p. 82–84°C	8
$[(Me_3Si)_2C_5H_3]_2YBH_4 \cdot (THF)$	white	m.p. 130–132°C	8
$[(Me_3Si)_2C_5H_3]_2LaBH_4 \cdot (THF)$	white	m.p. 93–95°C	8
$[(Me_3Si)_2C_5H_3]_2PrBH_4 \cdot (THF)$	green	m.p. 105–107°C	8
$[(Me_3Si)_2C_5H_3]_2NdBH_4 \cdot (THF)$	blue-violet	m.p. 113–115°C	8
$[(Me_3Si)_2C_5H_3]_2SmBH_4 \cdot (THF)$	yellow	m.p. 115–117°C	8
$[(Me_3Si)_2C_5H_3]_2YbBH_4 \cdot (THF)$	maroon	m.p. 125–128°C	8
$[Li(THF)_4][(Cp_2ErH)_3Cl]$	pink		9
$[Li(THF)_3][(Cp_2LuH)_3H]$	colorless		9
$[Na(THF)_6][(Cp_3Lu)_2H \cdot (THF)_2]$	colorless	X-ray	12
$[(BuC{\equiv}C)_2SmH]_n$			10
$[(BuC{\equiv}C)_2ErH]_n$			10
$[(BuC{\equiv}C)_3Yb_2H]_n$	purple		10

1. W.J. Evans et al. (1982a).
2. Schumann and Genthe (1981).
3. Marks and Ernst (1982).
4. W.J. Evans et al. (1983b).
5. Watson and Roe (1982).
6. Marks and Grynkewich (1976).
7. Schumann et al. (1982).
8. Lappert et al. (1983b).
9. W.J. Evans et al. (1982b).
10. W.J. Evans et al. (1981c).
11. Watson (1983a).
12. Schumann et al. (1984e).

Some data of the known organometallic compounds of the rare earths with hydride ligands are given in table 33.

2.7. Miscellaneous compounds with bonds between a rare earth and an element other than carbon

2.7.1. Compounds with rare earth to main group element bonds

Cyclopentadienyl rare earth halides, indenyl rare earth halides and cyclooctatetraenyl rare earth halides are the starting materials for the synthesis of compounds with bonds between the rare earth metals and other elements of the periodic table. They are described as key substances in sections 2.1.1, 2.1.2, 2.1.3.

Dichloro(triphenylmethyl) (2,2,2-cryptate)lanthanum(III), a deep red crystalline solid, was prepared by Campari and Hart (1982) and characterized by its infrared and electronic spectrum:

$$LaCl_3 \cdot N(CH_2CH_2OCH_2CH_2OCH_2CH_2)_3N + LiCPh_3$$

$$\xrightarrow{\text{THF}} (Ph_3C)LaCl_2 \cdot N(CH_2CH_2OCH_2CH_2OCH_2CH_2)_3N + LiCl. \tag{90}$$
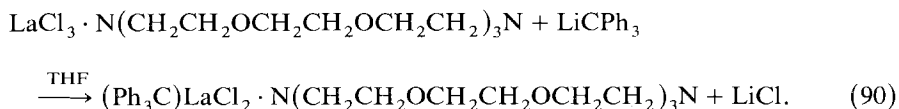
The following carboranyl derivatives of La, Tm, and Yb have been prepared by interaction of the lithium derivatives of carboranes with the appropriate rare earth trichlorides in tetrahydrofuran benzene–ether in 1983 by Bregadze et al.:

$MeCB_{10}H_{10}CLaCl_2$, m.p. 133–135°C,
$MeCB_{10}H_{10}CTmCl_2 \cdot (THF)_4$, m.p. 86–88°C,
$(PhCB_{10}H_{10}C)_2TmCl \cdot (THF)_5$, m.p. 78–80°C,
$Li[(PhCB_{10}H_{10}C)_2TmCl_2] \cdot (THF)_5$, m.p. 106–108°C,
$Li[(MeCB_{10}H_{10}C)_2YbCl_2] \cdot (THF)_2$, m.p. 113–115°C.
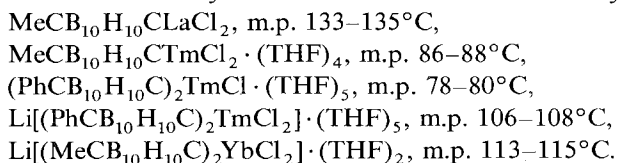
Dicyclopentadienyl rare earth chlorides react with a variety of compounds containing other anions than Cl. Maginn et al. (1963) prepared some methoxides and one phenoxide, Schumann et al. (1982) isolated the dicyclopentadienyl samarium tert-butoxide, and Watson (1982) found bis(pentamethylcyclopentadienyl) lutetium ethoxide as one of the reaction products of the ethanolysis of bis(pentamethylcyclopentadienyl) methyl lutetium. These compounds are much more stable against oxidation. No X-ray structural determination of these complexes has been done.

$$Cp_2RCl + NaOL \xrightarrow{\text{THF}} Cp_2ROL + NaCl, \tag{91}$$

R = Dy, Er, Yb, L = Me,

R = Yb, L = Ph,

R = Lu, L = t-Bu.
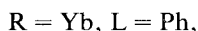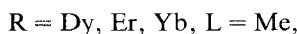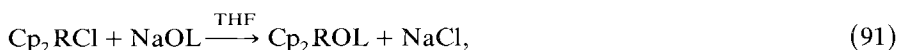
The corresponding reactions of dicyclopentadienyl and di(methylcyclopentadienyl) rare earth chlorides with sodium formiate, sodium acetate, sodium valerate and sodium benzoate yield the carboxylates (Maginn et al., 1963; Coutts and Wailes, 1970; R.D. Fischer and Bielang, 1980a, b). Molecular-weight determinations in boiling benzene indicate these complexes as dimers with μ-carboxylate bridges in this solvent:

$$Cp_2RCL + NaO_2Cl \xrightarrow{\text{THF}} Cp_2RO_2CL + NaCl, \tag{92}$$

R = Er, Yb, L = H,

R = Sc, Er, Yb, L = Me,

R = Yb, L = Bu, Ph,

$$2 \, (MeCp)_2RCl + 2 \, NaO_2CCH_3$$

$$\xrightarrow{\text{THF}} (MeCp)_2 R \overset{\displaystyle CH_3}{\underset{\displaystyle CH_3}{\underset{O \quad O}{\overset{O \quad O}{\diamond}}}} R(MeCp)_2 + 2 \, NaCl, \tag{93}$$

$$R = Gd, Er.$$
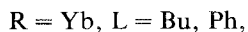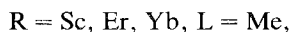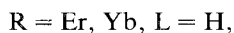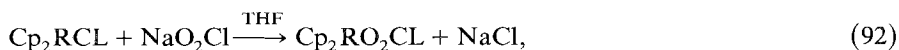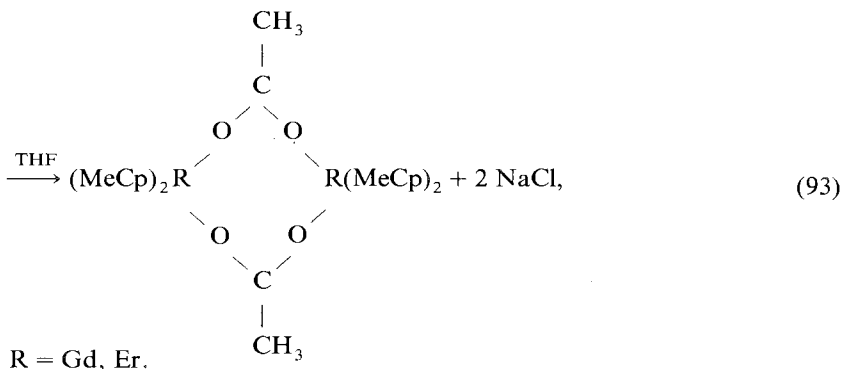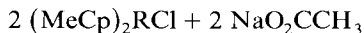
Dicyclopentadienyl scandium chloride reacts with sodium acetylacetonate in benzene with formation of pale yellow $Cp_2ScOC(Me)CHC(O)Me$, which is mono-meric in boiling benzene and sublimes at $110°C/10^{-3}$ torr (Coutts and Wailes, 1970). The ^1H NMR spectrum shows peaks for the Cp groups at $\delta = 5.94$ ppm, δCH at 5.06 and δCH_3 at 1.51 ppm. Tricyclopentadienyl ytterbium reacts with acetylace-tone, 2,2,6,6-tetramethyl-3,5-heptadione and 4-anilino-3-pentene-2-one at room tem-perature in toluene or pentane with liberation of one cyclopentadiene and formation of the dicyclopentadienyl ytterbium derivatives. $CpYb(Cl)OC(Me)CHC(Me)NPh$ was made analogously from Cp_2YbCl; and $Cp_2YbOC(Me)CHC(Me)NPh$ reacts with an excess of the aminoketone with formation of $CpYb[OC(Me)CHC(Me)NPh]_2$ (Bielang and Fischer, 1979):

$$Cp_3Yb + HOCL \rightarrow Cp_2YbOCL + CpH, \tag{94}$$

$$HOCL = MeC(O)CH_2C(O)Me, \, t\text{-}BuC(O)CH_2C(O)\text{-}t\text{-}Bu,$$

$$MeC(O)CH_2C(Me)NPh.$$
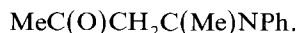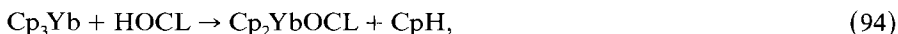
Dicyclopentadienyl tert-butyl lutetium tetrahydrofuranate reacts with carbon monoxide at room temperature in toluene with formation of a pale yellow insertion product, which is air and moisture sensitive and characterized by infrared and NMR spectra [$\nu(CO)$ at 1490 cm^{-1}, δCH_3 at 0.90 ppm (^1H) and 25.25 ppm (^{13}C)] as a η^2-acyl complex (W.J Evans et al., 1981d):

$$Cp_2LuCMe_3 \cdot (THF) + CO \rightarrow Cp_2Lu\underset{\displaystyle O}{\overset{\displaystyle \|}{-}}C\,\text{-}CMe_3 \leftrightarrow Cp_2Lu\text{-}C\text{-}CMe_3. \tag{95}$$
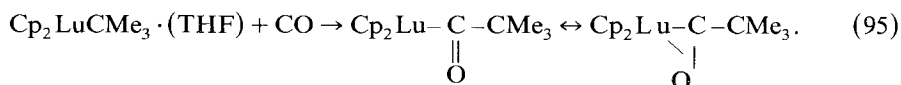
This acyl complex reacts with an excess of CO to produce a deep red solution, from which a purple compound can be isolated. This has been shown to contain two lutetium atoms bridged by the enedione diolate ligand 4,5-dihydroxy-2,2,7,7-tetra-methyloct-4-ene-3,6-dionato (2), which forms a 6-membered metallocyclic ring with each lutetium atom. Investigations with ^{13}CO labelled analogs give evidence for ketene–carbene intermediates during the formation of the final complex, which shows δCH_3 at 1.24 ppm (^1H) and 26.89 ppm (^{13}C):
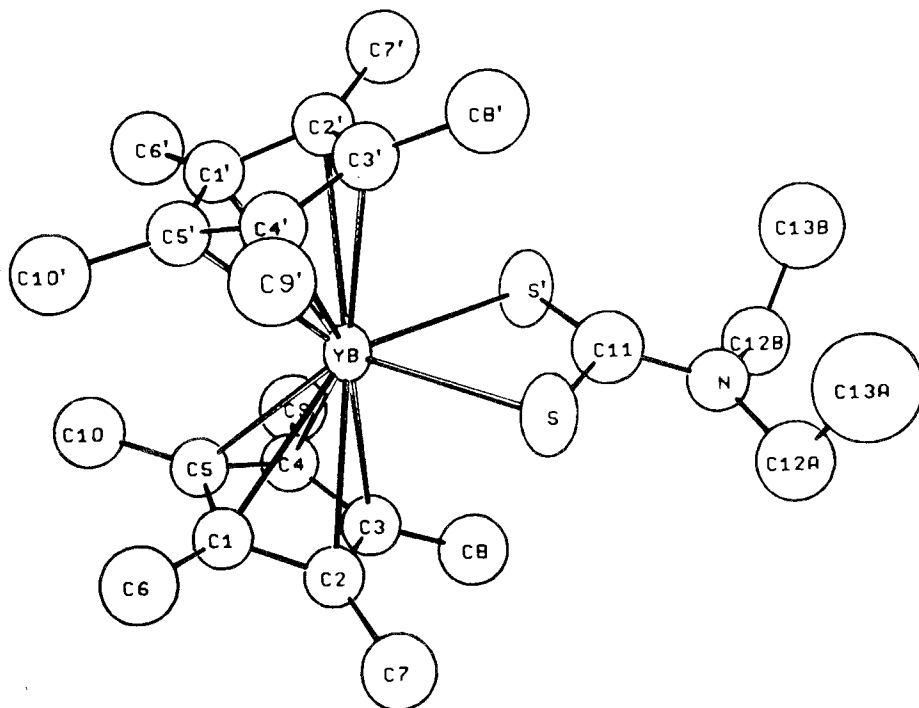
Fig. 37a. Molecular structure of $(C_5Me_5)_2YbS_2CNEt_2$ (after Tilley et al., 1982c).

$$2\,Cp_2LuCMe_3 \cdot (THF) + 4\,CO \rightarrow Cp_2Lu \overset{\displaystyle O=C=C}{\underset{\displaystyle O-C=O}{\diagdown}} \overset{\displaystyle CMe_3}{\underset{\displaystyle CMe_3}{\diagup}} LuCp_2$$

(96)

$$Cp_2Lu \overset{O}{\underset{O=C}{\diagdown}} \overset{CMe_3}{\underset{CMe_3}{\diagup}} LuCp_2 \leftarrow Cp_2Lu \overset{O}{\underset{O=C-C}{\diagdown}} \overset{CMe_3}{\underset{CMe_3}{\diagup}} LuCp_2.$$
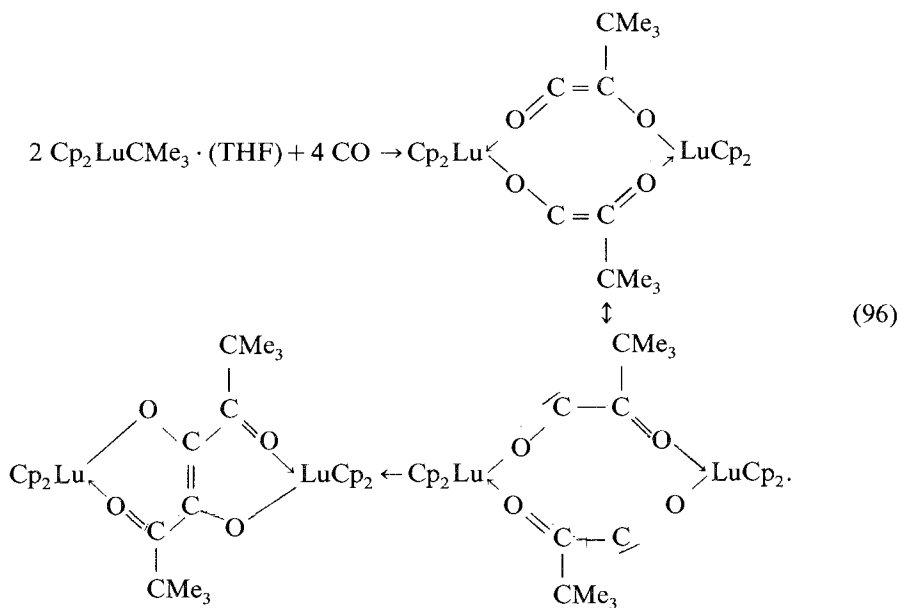
Bis(pentamethylcyclopentadienyl)carboxylato and -dithiocarbamato derivatives of neodymium and ytterbium have been prepared by Tilley et al. (1982c). The mono-clinic crystals of the purple $(C_5Me_5)_2YbS_2CNEt_2$ (space group $C2/c$, $a = 12.268(4)$ Å, $b = 15.536(6)$ Å, $c = 14.269(5)$ Å, $\beta = 105.23(3)°$; $Z = 4$) show average Yb–C distances of 2.63(3) Å and an Yb–S distance of 2.70(1) Å (fig. 37a).
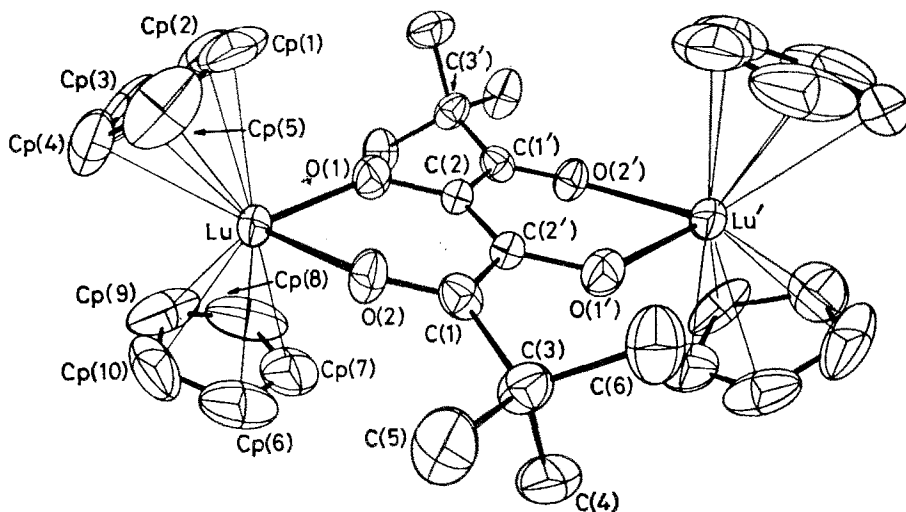
Fig. 38. Molecular structure of $[Cp_2LuOCCMe_3CO]_2$ (after W.J. Evans et al., 1981d).

The results of an X-ray structural analysis are given in fig. 38 and table 34.

The reduction of cerium tetra-isopropylate with triethyl aluminum in toluene in he presence of cyclooctatetraene at about 100°C yields cyclooctatetraenyl cerium

TABLE 34

Crystallographic data and important bond distances and bond angles of $[(C_5H_5)_2LuOCC(CH_3)_3CO]_2$.

crystal system	triclinic
space group	$P\bar{1}$
a (Å)	8.284(4)
b (Å)	9.522(4)
C (Å)	10.738(5)
α (deg)	68.01(4)
β (deg)	75.17(4)
γ (deg)	80.78(4)
Z	1 (dimer)
bond distances (Å)	
Lu–O1	2.09
Lu–O2	2.219
O1–C2	1.33
C2–C2'	1.40
C1–C2'	1.48
C1–O2	1.24
Lu–∅Cp	2.60
bond angles (deg)	
Lu–O2–C1	135
O2–C1–C2'	122
C1–C2'–C2	122

di-μ-isopropoxydiethyl aluminum as a yellow crystalline solid containing some toluene which can not be removed in vacuo at room temperature. The compound forms a 1:1 complex with acetonitrile, when dissolved in this solvent at room temperature and cooled to $-30°C$ (Greco et al., 1977):

$$Ce(O\text{-}i\text{-}C_3H_7)_4 \cdot L + 4 \, AlEt_3 + C_8H_8 \xrightarrow{\text{toluene}} C_8H_8Ce(\mu\text{-}O\text{-}i\text{-}C_3H_7)_2AlEt_2, \quad (97)$$

$$L = i\text{-}C_3H_7OH, \, C_5H_5N.$$
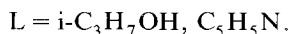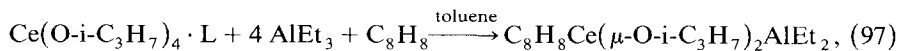
The known organometallic compounds with bonds between the rare earth metals and oxygen are shown in table 35.

The first compound containing a rare-earth-to-nitrogen bond, dicyclopentadienyl erbium amide, is formed when sodium amide is added to a solution of dicyclo-

TABLE 35

Organometallic compounds of the rare earths containing rare earth to oxygen bonds.

Compound	color	other data	Refs.
Cp_2DyOCH_3	yellow	dec. $> 235°C$	1
Cp_2ErOCH_3	pink	m.p. $236–240°C$	1
Cp_2YbOCH_3	orange	m.p. $290–305°C$	1
$Cp_2YbOC_6H_5$	red	m.p. $382–386°C$	1
$Cp_2SmOC(CH_3)_3$	colorless	dec. $> 50°C$	2
$(C_5Me_5)_2LuOC_2H_5$		NMR	3,10
Cp_2ErO_2CH	pink	dec. $> 270°C$	1
Cp_2YbO_2CH	orange		1
$Cp_2ScO_2CCH_3$	yellow	m.p. $282°C$ (dec.)	4
$Cp_2ErO_2CCH_3$	pink	m.p. $331–335°C$	1
$Cp_2YbO_2CCH_3$	orange	m.p. $325–329°C$	1
$Cp_2YbO_2CC_4H_9$	yellow		5
$Cp_2YbO_2CC_6H_5$	orange	m.p. $350–375°C$	1
$(MeCp)_2GdO_2CCH_3$	white	m.p. $207–209°C$	1
$(MeCp)_2ErO_2CCH_3$	pink	m.p. $199–201°C$	1
$Cp_2ScOC(Me)CHC(O)Me$	pale yellow	m.p. $75°C$	4
$Cp_2YbOC(Me)CHC(O)Me$	orange	dec. $115°C$	6
$Cp_2YbOC(t\text{-}Bu)CHC(O)\text{-}t\text{-}Bu$		m.p. $> 80°C$ (dec.)	6
$Cp_2YbOC(Me)CHC(Me)NPh$	yellow	m.p. $104°C$	6
$CpYb[OC(Me)CHC(Me)NPh]_2$	yellow	m.p. $84°C$	6
$CpYb(Cl)OC(Me)CHC(Me)NPh$	red-brown	dec. $92°C$	6
$Cp_2LuOCC(CH_3)_3$	pale yellow		7
$[Cp_2LuOC(CMe_3)CO]_2$	deep purple		7
$(COT)Ce(\mu\text{-}O\text{-}i\text{-}C_3H_7)_2AlEt_2$	yellow	dec. $170–180°C$	8
$(COT)Ce(\mu\text{-}O\text{-}i\text{-}C_3H_7)_2AlEt_2 \cdot MeCN$	yellow		8
$(C_5Me_5)_2YbO_2CCMe_3$	red	m.p. $154–155°C$, μ_{eff} 3.29 B.M.	9
$(C_5Me_5)_2YbO_2CCF_3$	violet	m.p. $262–263°C$	9

1. Maginn et al. (1963).
2. Schumann et al. (1982).
3. Watson (1982).
4. Coutts and Wailes (1970).
5. R.D. Fischer and Bielang (1980a).
6. Bielang and Fischer (1979).
7. W.J. Evans et al. (1981d).
8. Greco et al. (1977).
9. Tilley et al. (1982c).
10. Watson (1983a).

pentadienyl erbium chloride in tetrahydrofuran, and the reaction is allowed to stirr at room temperature for 54 hours (Maginn et al., 1963). The corresponding ytterbium compound results, when tricyclopentadienyl ytterbium amine complex is heated to 250°C (E.O. Fischer and H. Fischer, 1966):

$$Cp_2ErCl + NaNH_2 \xrightarrow{\text{THF}} Cp_2ErNH_2 + NaCl, \tag{98}$$

$$Cp_3Yb \cdot (NH_3) \xrightarrow{250°C} Cp_2YbNH_2 + C_5H_6. \tag{99}$$
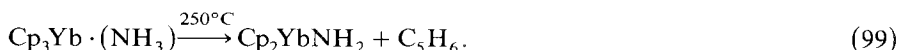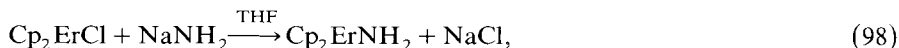
Some bis(trimethylsilyl) amido derivatives of neodymium and ytterbium are described as compounds stable up to 300°C by Tilley and Andersen (1981b). They result from the reaction of sodium bis(trimethylsilyl)amide with $[Li(Et_2O)_2][(C_5Me_5)_2NdCl_2]$, $[Na(Et_2O)_2][(C_5Me_5)NdCl_3]$, or $(C_5Me_5)_2YbCl \cdot C_5H_5N$ in toluene or diethylether.

The complexes $[Cp_2YH \cdot (THF)]_2$ and $[(MeCp)_2YH \cdot (THF)]_2$ react with t-butyl isonitrile to form a formimidoyl dimer $[Cp_2Y(HC=NCMe_3)]_2$ or $[(MeCp)_2Y(HC=NCMe_3)]_2$ (W.J. Evans et al., 1983a). The ^1H NMR spectrum of the cyclopentadienyl compound shows resonances at $\delta = 5.93$ ppm (Cp), 0.98 ppm ($HC=NCMe_3$) and a triplet at $\delta = 9.25$ ppm ($J = 1.5$ Hz) for the formimidoyl proton. The ^{13}C NMR spectrum has signals at $\delta = 108.6$ (Cp), 29.4 ($HC=NC\underline{Me}_3$), 60.6 ($HC=N\underline{C}Me_3$) and a doublet of doublets at $\delta = 217.0$ ppm ($^1J(YC) = 35$ Hz, $^1J(YC)' = 5$ Hz) for the formimidoyl carbon. By exchange of the formimidoyl proton with deuterium the $\nu(CH)$ in the infrared spectrum shifts from 2765 to 2020 cm^{-1} as well as the $\nu(C=N)$ from 1540 to 1528 cm^{-1}. The spectra of the methylcyclopenta-
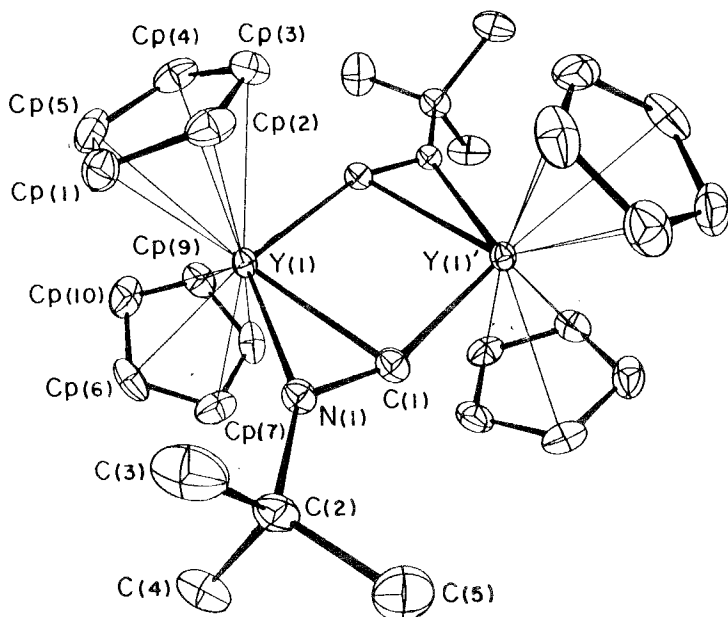
Fig. 39. Molecular structure of $[Cp_2Y(HC=NCMe_3)]_2$ (after W.J. Evans et al., 1983a).

Crystallographic data and important bond distances and bond angles of $[Cp_2Y(HC{=}NCMe_3)]_2$.

crystal system	triclinic
space group	$P\bar{1}$
a (Å)	8.496(5)
b (Å)	8.549(5)
c (Å)	10.459(6)
α (deg)	77.13(4)
β (deg)	86.58(4)
γ (deg)	73.56(4)
Z	1 (dimer)
bond distances (Å)	
Y1–Y1'	3.607(1)
Y1–$\varnothing$Cp1	2.399
Y1–C1	2.545(5)
Y1–N1	2.325(4)
C1–N1	1.275(6)
bond angles (deg)	
$\varnothing$Cp1–Y1–$\varnothing$Cp2	127.2
C1–Y1–N1	29.9(1)
C1–N1–C2	124.3(4)
C1–Y1–C1'	90.1(2)

dienyl analog are similar. The X-ray diffraction of this complex (fig. 39, table 36) is the first example of a crystallographically characterized dihapto coordination of a multiply bonded organic moiety within bonding distance of a rare earth element.

Lithium di-tert-butyl phosphide and lithium tert-butyl phenylphosphide react with some dicyclopentadienyl lanthanide chlorides with elimination of lithium chloride and formation of the corresponding dicyclopentadienyl (organophosphide) lanthanide derivatives. Molecular-weight determinations indicate an oligomeric structure in solution (Schumann and Jarosch, 1976; Schumann and Frisch, 1981):

$$Cp_2RCl \cdot (THF) + LiP(t\text{-}Bu)_2 \xrightarrow{THF} Cp_2RP(t\text{-}Bu)_2 + LiCl, \qquad (100)$$

R = Tb, Ho, Er, Tm, Yb, Lu

$$Cp_2RCl \cdot (THF) + LiPPh(t\text{-}Bu) \xrightarrow{THF} Cp_2RPPh(t\text{-}Bu) + LiCl, \qquad (101)$$

R = Tb, Ho, Er, Yb, Lu.
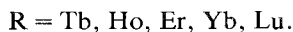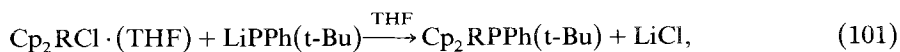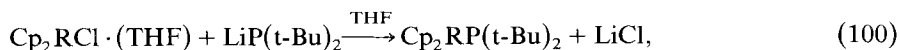
Investigations by Bielang and R.D. Fischer (1978) demonstrate that the reactions of dicyclopentadienyl ytterbium chloride with lithium di(cyclohexyl)phosphide, lithium cyclohexylphosphide and lithium phenylphosphide are rather complicated. The decomposition behavior of these very sensitive substances is complex. It was possible to isolate $Cp_2YbP(C_6H_{11})_2$, but $Cp_2YbPHPh$ and $Cp_2YbPHC_6H_{11}$ decompose with formation of polymeric species $[CpYbPPh]_n$ and $[CpYbPC_6H_{11}]_n$.

Organometallic compounds of the rare earths containing bonds between the rare earths and main group elements other than carbon or oxygen.

Compound	color	other data	Refs.
Cp_2ErNH_2	pink	m.p. 330–334°C	1
Cp_2YbNH_2	yellow	subl. 230°C	2
$(C_5Me_5)_2NdN(SiMe_3)_2$	blue	m.p. > 300°C	3
$(C_5Me_5)_2YbN(SiMe_3)_2$	purple	m.p. 294–295°C	3
$(C_5Me_5)Nd[N(SiMe_3)_2]_2$	blue	m.p. 234–236°C	3
$Cp_2TbP(t-Bu)_2$	white	dec. 159°C	4
$Cp_2HoP(t-Bu)_2$	yellow	dec. 158°C	4
$Cp_2ErP(t-Bu)_2$	pink	dec. 145°C	4
$Cp_2TmP(t-Bu)_2$	yellow	dec. 148°C	4
$Cp_2YbP(t-Bu)_2$	white	dec. 155°C	4
$Cp_2LuP(t-Bu)_2$	white	dec. 128°C	4
$Cp_2TbP(t-Bu)Ph$	yellow	dec. 126°C	4
$Cp_2HoP(t-Bu)Ph$	yellow	dec. 129–135°C	4
$Cp_2ErP(t-Bu)Ph$	pink	dec. 118°C	4
$Cp_2YbP(t-Bu)Ph$	yellow	dec. 132°C	4
$Cp_2LuP(t-Bu)Ph$	white	dec. 137°C	4
$Cp_2YbP(C_6H_{11})_2$	orange		5
$[CpYbPC_6H_{11}]_n$	orange		5
$[CpYbPPh]_n$	orange		5
$[Li(DME)_2][Cp_2Sm(SiMe_3)_2]$	yellow	X-ray	9
$Cp_2ErGePh_3$	pink	m.p. 98–100°C, μ_{eff} 9.7 B.M.	6
$Cp_2ErSnPh_3$	pink	m.p. 200–205°C, μ_{eff} 7.2 B.M.	6
$Cp_2YbSnPh_3\cdot(THF)_2$	yellow	m.p. 185–190°C	6
$(C_5Me_5)_2NdS_2CNEt_2$	green	m.p. 229–231°C, μ_{eff} 2.75 B.M.	7
$(C_5Me_5)_2YbS_2CNEt_2$	purple	m.p. 226–227°C, μ_{eff} 3.39 B.M.	7
$(CH_3C_5H_4)_2SmP(C_6H_5)_2$	orange	$\mu_{eff} = 1.8$ B.M.,NMR	8

1. Maginn et al. (1963).
2. E.O. Fischer and H. Fischer (1966).
3. Tilley and Andersen (1981b).
4. Schumann and Frisch (1981).
5. Bielang and Fischer (1978).
6. Schumann and Cygon (1978).
7. Tilley et al. (1982c).
8. W.J. Evans et al. (1983c).
9. Schumann et al. (1984f).

The first compounds containing bonds between dicyclopentadienyl rare earth moieties and elements of group IV have been prepared by Schumann and Cygon (1978). Dicyclopentadienyl erbium chloride and dicyclopentadienyl ytterbium chloride react with lithium triphenylgermane or triphenylstannane with formation of dicyclopentadienyl erbium triphenylgermane and -stannane and dicyclopentadienyl ytterbium triphenylstannane, the latter containing two tetrahydrofuran molecules coordinated to ytterbium:

$$Cp_2RCl + LiMPh_3 \xrightarrow{THF} Cp_2R-MPh_3 - LiCl, \qquad (102)$$

$$R = Er, M = Ge, Sn; R = Yb, M = Sn.$$

The X-ray structure analysis of $[Li(DME)_2][Cp_2Sm(SiMe_3)_2]$ shows that the product of the reaction between Cp_2SmCl and $LiSiMe_3$ in DME, even when used in a molar ratio 1:1, is an ionic complex with two Sm–Si bonds (Schumann et al., 1984f).

The known organometallic compounds with bonds between the rare earth metals and main group elements other than carbon or oxygen are shown in table 37.

2.7.2. Compounds with rare earth to transition metal bonds

Organometallic compounds of the rare earth elements with covalent bonds between the rare earth metal of an organoscandium, organoyttrium, organolanthanum or organolanthanide group and a transition metal are not proved by an X-ray structural analysis. It could be shown (Crease and Legzdins, 1973a) that a lanthanide metal interacts with metal carbonyl or metal nitrosyl complexes, but there may be lanthanide–transition-metal bonds or lanthanide–isocarbonyl or lanthanide–isonitrosyl interactions. The reactions of tris(cyclopentadienyl) derivatives of some lanthanide metals with $Co_2(CO)_8$, $Mn(MeCp)(CO)_3$, $[FeCp(CO)_2]_2$, $CrCp(CO)_2Cl$, and $MCp(CO)_2(NO)$, with M = Cr, Mo, W, yields compounds containing either isocarbonyl or isonitrosyl linkages to the lanthanide metals. For the established compounds of this class, see section 2.1.2. (Crease and Legzdins, 1973a, b).

The reaction of some dicyclopentadienyl lanthanide chlorides and some bis(methylcyclopentadienyl) lanthanide chlorides with $Na[WCp(CO)_3]$ results in some complexes, stable up to 220°C, which are soluble in tetrahydrofuran and dimethylsulfoxide. Other anionic metal carbonyl or metal nitrosyl compounds gave no satisfying results, mainly because of side reactions. Infrared spectra indicate polymeric structures containing isocarbonyl bridges (Crease and Legzdins, 1973b):

$$Cp_2RCl + Na[WCp(CO)_3] \xrightarrow{\text{THF}} Cp_2R[WCp(CO)_3] + NaCl, \qquad (103)$$

$$R = Dy, Er, Yb,$$

$$(MeCp)_2RCl + Na[WCp(CO)_3] \xrightarrow{\text{THF}} (MeCp)_2R[WCp(CO)_3] + NaCl, \quad (104)$$
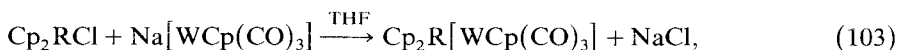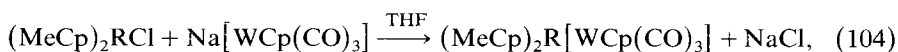
$$R = Dy, Ho.$$

An upfield shift of 0.36 ppm for the signal of the cyclopentadienyl protons and one of 2.3 ppm for the signal of the hydride protons in the ^1H NMR spectrum of Cp_2WH_2 after adding $(MeCp)_3Nd$ to a benzene solution of the tungsten hydride is interpreted as due to a neodymium tungsten bond (Crease and Legzdins, 1973b). The observation of three terminal $\nu(CO)$ bands in the infrared spectrum of the complex between Cp_3Sm and some anions $[Mn(CO)_3L]^-$ (see section 2.1.1.) together with a shift of these frequencies to higher wave numbers supports a samarium–manganese bond in the complex $Cp_3Sm[Mn(CO)_3P(OPh)_3]$ (Onaka and Furuchi, 1979).

Three other pentamethylcyclopentadienyl ytterbium derivatives containing transition metals in the same molecule have been prepared by Tilley and Andersen (1981a, 1982). $(C_5Me_5)_2Yb \cdot (Et_2O)$ splits the cobalt–cobalt bond in $Co_2(CO)_8$ with forma-
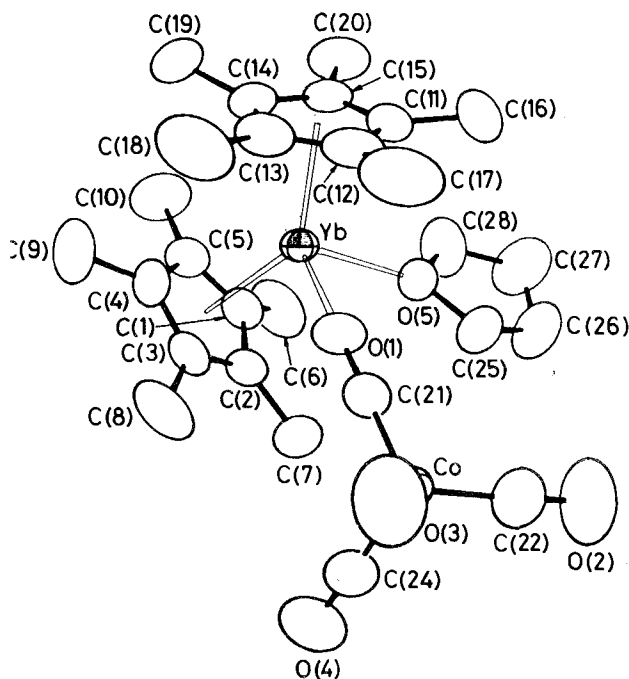
Fig. 40. Molecular structure of $(C_5Me_5)_2YbCo(CO)_4 \cdot (THF)$ (after Tilley and Andersen, 1981a).

TABLE 38

Crystallographic data, bond distances and angles in pentamethyl cyclopentadienyl ytterbium transition metal compounds.

	$(C_5Me_5)_2YbCo(CO)_4 \cdot (THF)$		$[(C_5Me_5)_2Yb]_2[Fe_3(CO)_{11}]$	
crystal system	triclinic		triclinic	
space group	P$\bar{1}$		P$\bar{1}$	
a (Å)	10.1626(11)		14.525(2)	
b (Å)	10.9795(8)		18.058(2)	
c (Å)	13.7124(12)		18.324(2)	
α (deg)	89.041(7)		72.151(11)	
β (deg)	85.478(8)		84.050(11)	
γ (deg)	71.774(7)		72.151(11)	
Z	2		3	
distances (Å)				
	Yb–$\varnothing$Cp	2.302	Yb–$\varnothing$Cp	2.289
	Yb–C(Cp)	2.596(2)	Yb–C(Cp)	2.573(13)
	Yb–O5	2.335(2)	Yb–O (aver.)	2.243(5)
	Yb–O1	2.258(2)	C1–O1	1.161(9)
	O1–C21	1.188(5)	Fe1–Fe2	2.524(1)
	C–O (aver.)	1.14(2)	Fe1–C1	1.698(8)
angles (deg)				
	$\varnothing$Cp–Yb–$\varnothing$Cp	139.4(7)	$\varnothing$Cp–Yb–$\varnothing$Cp	141.6
	O5–Yb–O1	83.3(7)	Fe2–Fe1–Fe3	161.8
	C–Co–C	108.9(4)		
	C–Co–C(μCO)	110.0(6)		
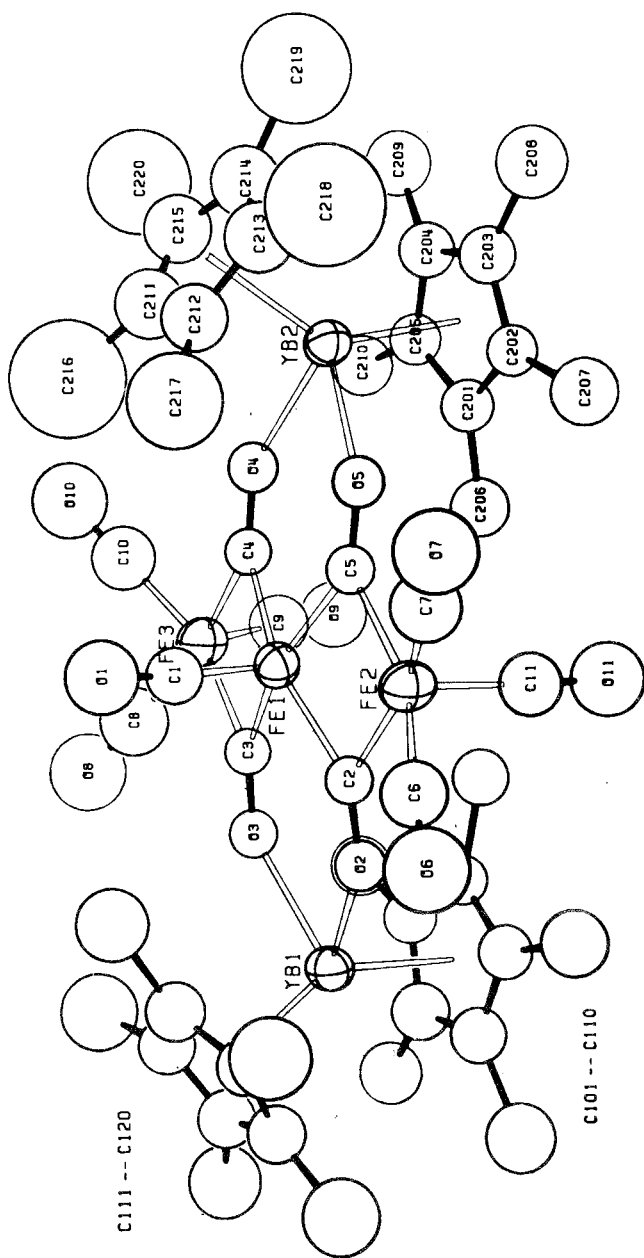
Fig. 41. Molecular structure of $[(C_5Me_5)_2Yb]_2[Fe_3(CO)_{11}]$ (after Tilley and Andersen, 1982).

TABLE 39
Organometallic compounds containing rare earths and transition metals.

Compound	color	other data	Refs.
$Cp_2ErMoCp(CO)_3$			1
$Cp_2DyWCp(CO)_3$			1
$Cp_2ErWCp(CO)_3$			1
$Cp_2YbWCp(CO)_3$	golden	dec. $> 220°C$	1
$(MeCp)_2DyWCp(CO)_3$			1
$(MeCp)_2HoWCp(CO)_3$			1
$(C_5Me_5)_2YbCo(CO)_4 \cdot (THF)$	blue	μ_{eff} 4.1 B.M.	2
$[(C_5Me_5)_2Yb]_2[Fe_3(CO)_{11}]$	violet	m.p. 307–310°C, μ_{eff} 3.91 B.M.	3
$[(C_5Me_5)_2Yb(THF)]_2Fe(CO)_4$			3

1. Crease and Legzdins (1973b).
2. Tilley (1981a).
3. Tilley and Andersen (1982).

tion of a blue precipitate, that yields blue prisms of $(C_5Me_5)_2YbCo(CO)_4 \cdot (THF)$ from a $3:1:1$ mixture of diethylether tetrahydrofuran pentane at $-10°C$ (Tilley and Andersen, 1981a). The X-ray structural analysis (fig. 40, table 38) shows the complex surrounded by the two pentamethylcyclopentadienyl rings, the tetrahydro-furan oxygen and the oxygen atom of one CO group, which is bridging between ytterbium and the cobalt atom.

$(C_5Me_5)_2Yb \cdot (Et_2O)$ reacts with $Fe_2(CO)_9$ or $Fe_3(CO)_{12}$ in toluene yielding a dark red solution from which violet prisms of $[(C_5Me_5)_2Yb]_2[Fe_3(CO)_{11}]$ were isolated. The infrared spectrum shows $\nu(CO)$ bands at 1667 and 1604 cm^{-1}, indicating η^2-,η^1-triply bridging carbonyl ligands (fig. 41, table 38) (Tilley and Andersen, 1982). This cluster molecule did not react with hydrogen or carbon monoxide at 18 atm during a 24 hour period. Pentacarbonyl iron reacts with $(C_5Me_5)_2Yb \cdot (Et_2O)$ with formation of another complex of this type for which the following structure is formulated:

$$(THF)(C_5Me_5)_2YbOCFe(CO)_2COYb(C_5Me_5)_2(THF)$$
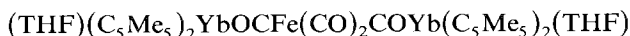
(Tilley and Andersen, 1982).
Also rare earth metal–cobalt bonds are proposed for products from reactions of rare earth trichlorides and cobalt carbonyl derivatives (Suleimanov et al., 1982e).

The rare-earth–transition-metal organometallic compounds are tabulated in table 39.

3. Organometallic compounds of the rare earths in the oxidation state $+2$

The first described organometallic compound of a rare earth element in the oxidation state $+2$ was dicyclopentadienyl europium, prepared by E.O. Fischer and H. Fischer (1964) by reacting europium with cyclopentadiene in liquid ammonia. Ytterbium metal reacts in the same way (E.O. Fischer and H. Fischer, 1965b). By

sublimation in vacuo at 400 to 420°C, ammonia-free complexes are obtained.

$$R + 3\,C_5H_6 \xrightarrow{\text{liq. NH}_3} Cp_2R + C_5H_8, \tag{105}$$
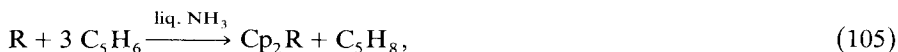
R = Eu, Yb.

Infrared spectra show a γ(CH) vibration for the europium derivative at 739 cm^{-1} and for Cp$_2$Yb at 750 cm^{-1} (E.O. Fischer and H. Fischer, 1965b); this is interpreted as indicative of ionic nature for these compounds. ^{151}Eu Mössbauer spectra of Cp$_2$Eu gave an isomeric shift of -1.32 cm s^{-1} relative to EuF$_3$, demonstrating that this compound is nearly equal in covalency to EuCl$_2$ (Brix et al., 1964; Hüfner et al., 1965).

Dicyclopentadienyl ytterbium is also available by other methods (Calderazzo et al., 1966), and the Sm, Eu and Yb derivatives result from the interaction of dicyclopentadienyl mercury with the activated lanthanides in tetrahydrofuran (Suleimanov et al., 1982b):

$$Cp_2YbCl + Na \xrightarrow{\text{THF}} Cp_2Yb + NaCl, \tag{106}$$

$$3\,Cp_2YbCl + Yb \xrightarrow{\text{THF}} 3\,Cp_2Yb + YbCl_3, \tag{107}$$

$$Cp_3Yb \cdot (THF) + Na \xrightarrow{\text{THF}} Cp_2Yb + NaCp, \tag{108}$$

$$Cp_2Hg + m\,R \xrightarrow{\text{THF}} (m-1)\,R/Hg + Cp_2R \cdot (THF)_n, \tag{109}$$
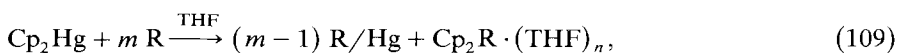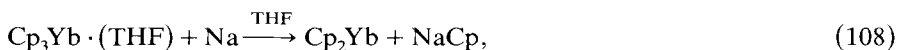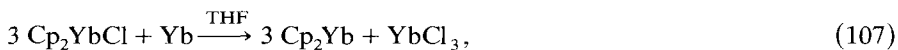
R = Sm, Eu, Yb.

All three reactions in eqs. (106)–(108) result in deep red solutions, which yield a yellow solid of Cp$_2$Yb $\cdot$ (THF) after precipitation with hexane. The tetrahydrofuran is separated in vacuo yielding a green product, which sublimes at 360°C/10^{-3} torr. The emerald green product was identified as the solvent-free Cp$_2$Yb. A brick red sublimate obtained during the sublimation of these reactions is some Yb^{3+} complex as revealed by its spectrum in the 10000 cm^{-1} region (Calderazzo et al., 1966). Hayes and Thomas (1969b) isolated three fractions during the sublimation of the reaction product of ytterbium with cyclopentadiene in liquid ammonia. The third compound sublimating at 360°C was identified as red Cp$_2$Yb on the basis of mass spectra and an NMR signal at $\delta = 5.4$ ppm for the cyclopentadienyl protons. The appearance potential for the Cp$_2$Yb$^+$ ion in the mass spectrum was found to be 7.62 ± 0.09 eV (Thomas and Hayes, 1970).

The tetrahydrofuran complex of dicyclopentadienyl samarium is made by reduction of tricyclopentadienyl samarium with KC$_{10}$H$_8$ in naphthalene in the presence of tetrahydrofuran and was isolated as a purple pyrophoric product (Watt and Gillow, 1969). Ytterbium also reacts with thallous cyclopentadienide in dimethoxyethane in the presence of a little metallic mercury with formation of Cp$_2$Yb $\cdot$ DME (Deacon et al., 1982a).

This complex crystallizes in the space group Cc with $a = 9.25(2)$, $b = 23.49(5)$, $c = 8.23(2)$ Å, $\beta = 123.59(4)°$, and $Z = 4$. The ytterbium atom is nearly tetrahedrally

surrounded by the two cyclopentadienyl ring centers and the oxygen atoms of the DME molecule. The angle $\varnothing\,Cp1-Yb-\varnothing\,Cp2$ is 131° and the bond distances $Yb-\varnothing\,Cp$ are 2.41 and 2.46 Å. The $Yb-O$ distances of 2.50(3) Å and 2.45(3) Å are normal for this type of compounds (Deacon et al., 1983a).

$(MeCp)_2Yb \cdot (THF)$ is prepared by the reaction of methyl cyclopentadiene with YbC_6H_{10}, by reduction of $[(MeCp)_2YbMe]_2$ with hydrogen and by photolysis and thermolysis of $[(MeCp)_2YbMe]_2$. The yellow complex has a solid-state structure consisting of chains of repeating units $(\mu\text{-}MeCp)(MeCp)YbOC_4H_8$ related by a two-fold screw axis and connected by one bridging methylcyclopentadienyl group per ytterbium (fig. 42, table 40) (Zinnen et al., 1980). Reduction of $[(Me_3SiC_5H_4)_2YbCl]_2$ by sodium amalgam in tetrahydrofuran yields the purple, diamagnetic complex $(Me_3SiC_5H_4)_2Yb \cdot (THF)_2$, which loses the coordinated tetrahydrofuran upon warming to 30°C at 10^{-3} torr followed by sublimation at $300°C/10^{-3}$ torr, forming green crystals. Tetramethylethylenediamine replaces THF yielding blue $(Me_3SiC_5H_4)_2Yb \cdot (tmed)$. The X-ray analysis of the THF complex
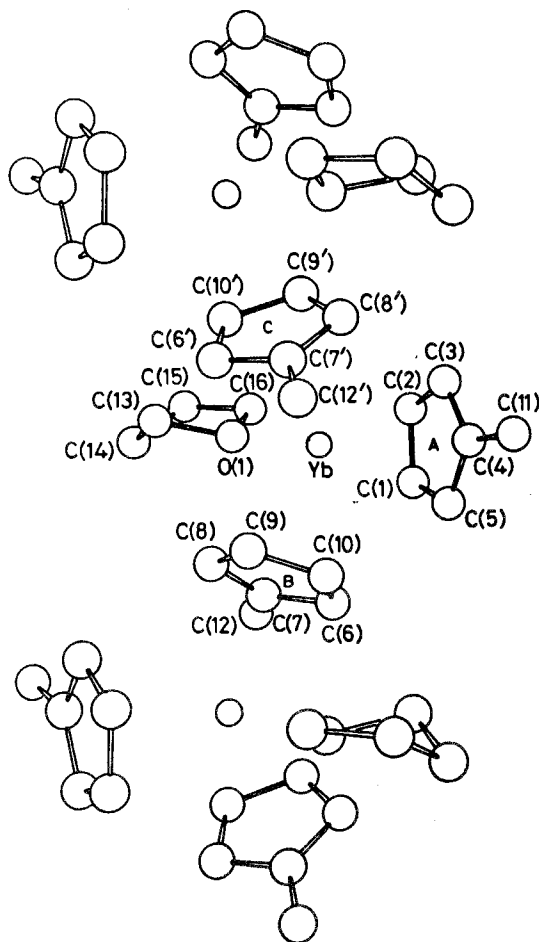
Fig. 42. ORTEP plot of the structure of $(MeCp)_2Yb \cdot (THF)$ (after Zinnen et al., 1980).

TABLE 40

Crystallographic data, bond distances and angles in $(MeCp)_2Yb \cdot (THF)_2$ and $(Me_3SiC_5H_4)_2Yb \cdot (THF)_2$.

	$(MeCp)_2Yb \cdot (THF)_2$		$(Me_3SiC_5H_4)_2Yb \cdot (THF)_2$	
crystal system	monoclinic		monoclinic	
space group	$P2_1$		$P2_1/n$	
a (Å)	9.055(1)		13.439(7)	
b (Å)	8.834(1)		10.322(7)	
c (Å)	9.809(2)		21.340(9)	
β (deg)	106.79(1)		105.57(3)	
Z	2		4	
distances (Å)				
	Yb–C(A) (av.)	2.76	Yb–C (av.)	2.75
	Yb–C(B) (av.)	2.91	Yb–O (av.)	2.41
	Yb–C(C) (av.)	2.87		
	Yb–O1	2.53(2)		
angles (deg)				
	$\varnothing$CpA–Yb–$\varnothing$CpB	114.6	$\varnothing$Cp1–Yb–$\varnothing$Cp2	133
	$\varnothing$CpB–Yb–$\varnothing$CpC	118.0	$\varnothing$Cp1–Yb–O1	107
	$\varnothing$CpA–Yb–$\varnothing$CpC	116.8	$\varnothing$Cp1–Yb–O2	109
			$\varnothing$Cp2–Yb–O1	107
			$\varnothing$Cp2–Yb–O2	106
			O1–Yb–O2	85
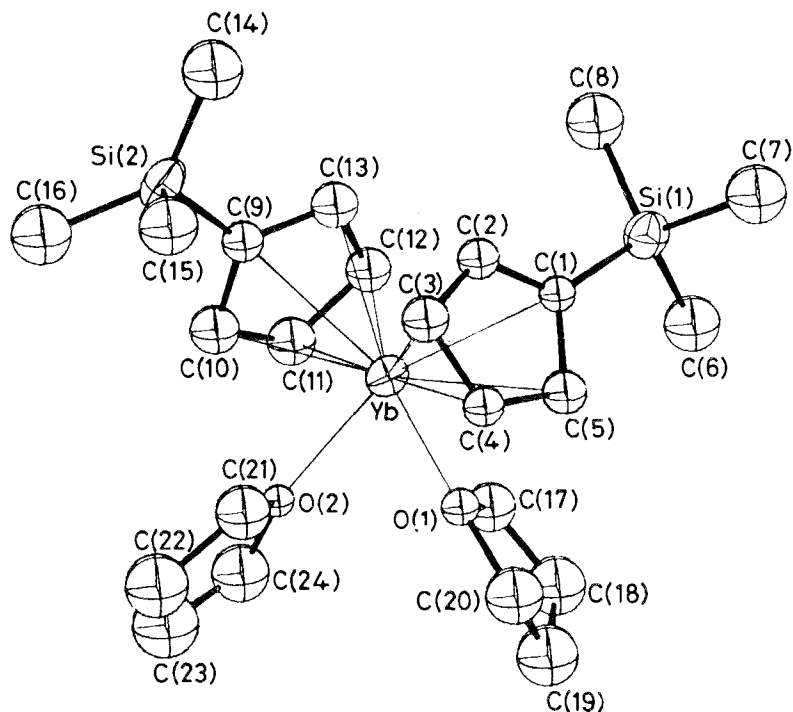
Fig. 43. Molecular structure of $(Me_3SiC_5H_4)_2Yb \cdot (THF)_2$ (after Lappert et al., 1980).

(fig. 43, table 40) shows a roughly tetrahedral disposition of valencies around the central ytterbium (Lappert et al., 1980).

Pentamethylcyclopentadienyl complexes of Sm(II), Eu(II) and Yb(II) have been prepared and characterized after 1980. Red bis(pentamethylcyclopentadienyl) europium(II) complexes with one coordinated THF or one THF and one Et_2O are isolated from the reactions of europium trichloride and sodium pentamethylcyclopentadienide in refluxing tetrahydrofuran and crystallization from toluene or ether (Tilley et al., 1980). Red diamagnetic bis(pentamethylcyclopentadienyl) ytterbium(II) coordinated with THF or Et_2O are formed in the analogous reaction, but using $YbCl_2$ as the starting material.

$$YbCl_2 + 2 \, C_5Me_5Na \xrightarrow{\text{THF}} (C_5Me_5)_2Yb \cdot L + 2 \, NaCl, \tag{110}$$
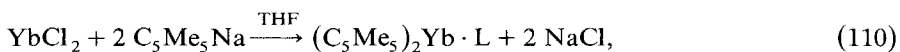
$$L = THF, \, Et_2O.$$

When the THF complex is recrystallized from toluene, a hemitoluene complex $(C_5Me_5)_2Yb \cdot (THF) \cdot (C_6H_5CH_3)_{1/2}$ precipitates, which X-ray structural determination (fig. 44, table 41) shows the ytterbium atom coordinated to two pentamethylcyclopentadienyl rings and the oxygen atom of the THF. The molecule has C_2 symmetry about the Yb–O bond; the pentamethylcyclopentadienyl rings are staggered with respect to each other. The toluene molecule is not coordinated to the ytterbium. It is on a center of symmetry in a disordered configuration.

$(C_5Me_5)_2Yb$ coordinated with two molecules of diethylether or tetrahydrofuran
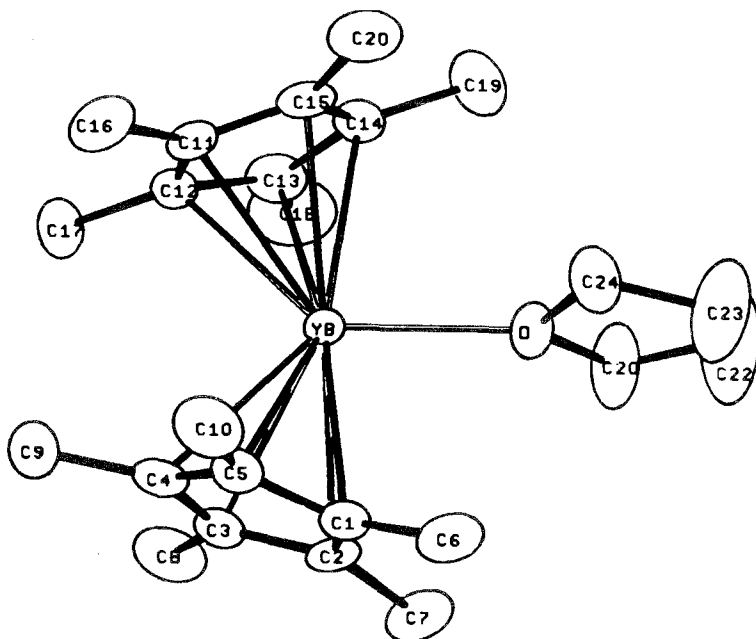
Fig. 44. Molecular structure of $(C_5Me_5)_2Yb \cdot (THF)$ (after Tilley et al., 1980).

TABLE 41

Crystallographic data, bond distances and angles in $(C_5Me_5)_2Yb\cdot(THF)\cdot(PhMe)_{1/2}$, $(C_5Me_5)_2Sm\cdot(THF)_2$ and $(C_5Me_5)_2Yb\cdot(py)_2$.

	$(C_5Me_5)_2Yb\cdot(THF)\cdot(PhMe)_{1/2}$		$(C_5Me_5)_2Sm\cdot(THF)_2$		$(C_5Me_5)_2Yb\cdot(py)_2$	
crystal system	monoclinic		triclinic		monoclinic	
space group	$P2_1/n$		$P\bar{1}$		$P2_1/c$	
a (Å)	11.358(8)		15.155(6)		16.092(6)	
b (Å)	21.756(19)		16.141(6)		9.883(4)	
c (Å)	10.691(7)		16.179(6)		17.872(7)	
α (deg)			55.92(3)			
β (deg)	101.84(5)		65.13(3)		98.46(3)	
γ (deg)			62.18(3)			
Z	4		4		4	
distances (Å)						
	Yb–C (aver.)	2.66	Sm–C (aver.)	2.86(3)	Yb–C (aver.)	2.74
	Yb–ØCp (aver.)	2.37	Sm–O (aver.)	2.63(1)	Yb–ØCp (aver.)	2.46
	Yb–O	2.41			Yb–N (aver.)	2.56
angles (deg)						
	ØCp1–Yb–ØCp2	143.5(3)			ØCp1–Yb–ØCp2	136.3(3)
	ØCp1–Yb–O	107.7(3)			N1–Yb–N2	82.5(2)
	ØCp2–Yb–O	108.8(3)			N1–Yb–ØCp1	103.6(2)
					N1–Yb–ØCp2	111.5(3)
					N2–Yb–ØCp1	107.7(3)
					N2–Yb–ØCp2	102.0(3)

or with one DME was also synthesized from ytterbium dibromide and potassium pentamethylcyclopentadienide by Watson (1980). The red complex $(C_5Me_5)_2Yb \cdot (THF)_2$ loses one THF when heated up to 90°C forming the orange complex $(C_5Me_5)_2Yb \cdot (THF)$.

A bis(pentamethylcyclopentadienyl) samarium(II) complex containing two tetrahydrofuranes was made by W.J. Evans et al. (1981a) by vaporization of samarium metal into a mixture of pentamethylcyclopentadiene in hexane at $-120°C$. From the reaction mixture a purple crystalline compound could be isolated and characterized by an X-ray structural analysis (fig. 45, table 41), as well as by ^1H and ^{13}C NMR spectra.

The reaction of $(C_5Me_5)_2Sm \cdot (THF)_2$ with diphenylacetylene yields, after removal of the solvent, a black, glassy material, which is identified as the enediyl compound $(C_5Me_5)_2Sm(Ph)C=C(Ph)Sm(C_5Me_5)_2$. This complex generates pure trans-stilbene upon hydrolysis (W.J. Evans et al., 1983b).

Addition of 1,2-bis(dimethylphosphino)ethane to the complexes $(C_5Me_5)_2R \cdot Et_2O$, R = Eu, Yb, yields insoluble and probably polymeric compounds, which dissolve in tetrahydrofuran to give $(C_5Me_5)_2R \cdot (THF)$. In contrast the reaction of $(C_5Me_5)_2R \cdot Et_2O$ with bis(dimethylphosphino)methane gives soluble complexes,
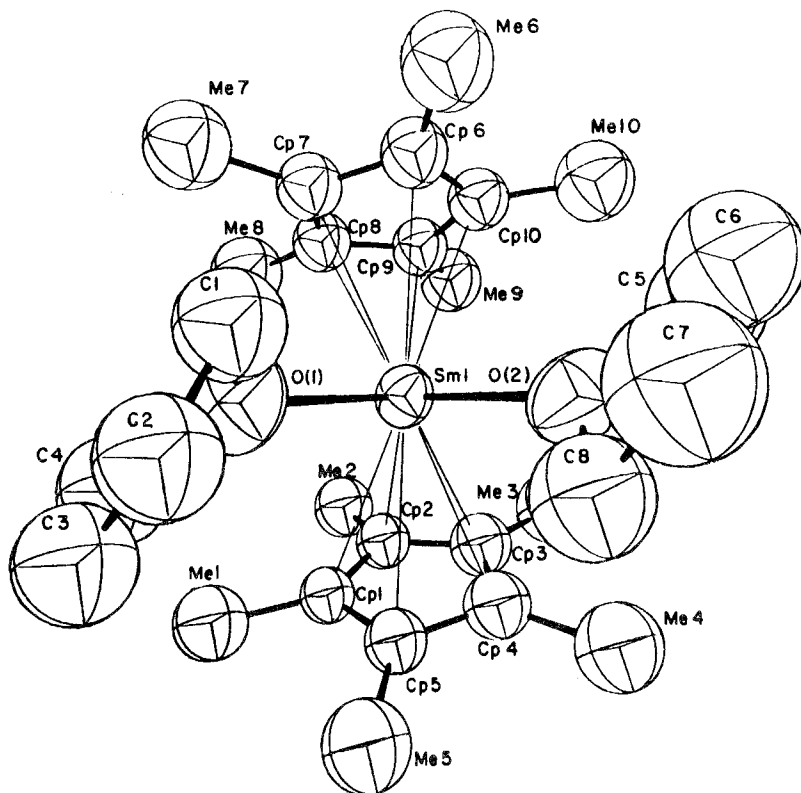
Fig. 45. Molecular structure of $(C_5Me_5)_2Sm \cdot (THF)_2$ (after W.J. Evans et al., 1981a).
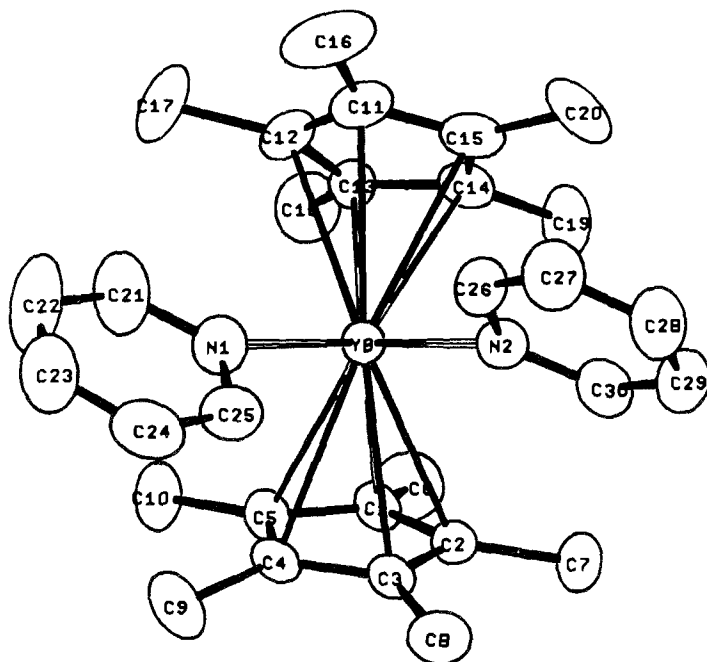
Fig. 46. Molecular structure of $(C_5Me_5)_2Yb \cdot (py)_2$ (after Tilley et al., 1982a).

with only one signal in the ^{31}P NMR spectrum, which is shifted significantly down field with respect to the free phosphine (Tilley et al., 1983).

Dark green prisms of $(C_5Me_5)_2Yb \cdot (py)_2$ crystallize when $(C_5Me_5)_2Yb \cdot (Et_2O)_2$ is reacted with an excess of pyridine in toluene. The X-ray structural analysis shows also a distorted tetrahedral arrangement with approximately C_2 symmetry with two cyclopentadienyl rings and two nitrogen atoms of the two pyridine molecules coordinated to the ytterbium atom (fig. 46, table 41) (Tilley et al., 1982a).

Cyclooctatetraenyl europium and cyclooctatetraenyl ytterbium were isolated as orange or pink solid compounds, after europium or ytterbium, dissolved in liquid ammonia reacted with cyclooctatetraene (Hayes and Thomas, 1969a; De Kock et al., 1978):

$$R + C_8H_8 \xrightarrow{\text{liq. } NH_3} RC_8H_8, \tag{111}$$

$$R = Eu, Yb.$$

The cyclooctatetraene ligand is also able to stabilize cerium in the oxidation state Ce^{+2}. According to eq. (112), dicyclooctatetraene cerium(IV) is reduced by potassium in monoglyme forming an olive green solution, which precipitates as a microcrystalline green complex (Greco et al., 1976):

$$Ce(C_8H_8)_2 + 2\,K \xrightarrow[30°C]{\text{monoglyme}} [K(\text{monoglyme})]_2[Ce(C_8H_8)_2]. \tag{112}$$
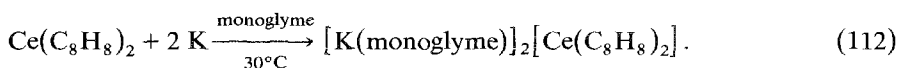
Grignard type compounds of some lanthanide metals in the oxidation state $+2$ have been investigated by D.F. Evans et al. (1970, 1971). Europium, samarium and ytterbium react in tetrahydrofuran with alkyl and aryl iodides between -20 and $+30°C$ forming colored solutions containing mixtures of compounds, which give some Grignard-type reactions. Characterization of the compounds was done only by magnetic susceptibility measurements and some titrimetric analyses.

$$R + LI \xrightarrow{\text{THF}} L-R-I, \tag{113}$$

R = Eu, Sm, Yb,

L = Me, Ph, $4\text{-MeC}_6\text{H}_4$, $2,6\text{-Me}_2\text{C}_6\text{H}_3$, $2,4,6\text{-Me}_3\text{C}_6\text{H}_2$.

A solution of C_6H_5Yb, prepared by the reaction of ytterbium metal and C_6H_5I in tetrahydrofuran reacts with ketones, aldehydes, and nitriles just as Grignard reagents would. However, with esters the complex reacts to produce ketones as the main product (Fukagawa et al., 1981). With benzoyl chloride the ketone is obtained selectively in modest yields which is in contrast to the Grignard reaction (Fukagawa et al., 1982).

Europium and ytterbium metal react with propyne in liquid ammonia at $-78°C$ with evolution of hydrogen. But only europium(II) propynide could be isolated and characterized (Murphy and Toogood, 1971).

$$Eu + 2 CH_3C{\equiv}CH \xrightarrow{\text{liq. NH}_3} Eu(C{\equiv}CCH_3)_2 + H_2. \tag{114}$$
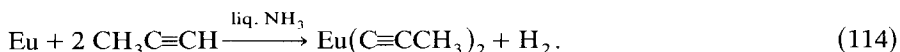
Bis(phenylethynyl) ytterbium is available by the reaction of ytterbium metal with bis(phenylethynyl) mercury in tetrahydrofuran, or from the ligand exchange reaction between bis(pentafluorophenyl) ytterbium and phenylacetylene in the same solvent (Deacon and Koplick, 1978):

$$Yb + Hg(C{\equiv}CPh)_2 \xrightarrow{\text{THF}} Yb(C{\equiv}CPh)_2 + Hg, \tag{115}$$

$$Yb(C_6F_5)_2 + 2 HC{\equiv}CPh \xrightarrow{\text{THF}} Yb(C{\equiv}CPh)_2 + 2 C_6HF_5. \tag{116}$$
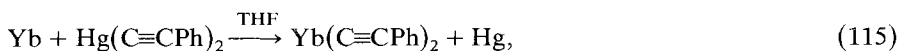
The air-sensitive compound was isolated without any coordinating ligands in addition to the alkyne, but an associated structure is supposed. It reacts with aldehydes LCHO and ketones L_2CO followed by hydrolysis with formation of alcohols $(PhC{\equiv}C)LCHOH$ or $(PhC{\equiv}C)L_2COH$, but, with benzophenone, reduction to benzopinacol is also found (Deacon and Tuong, 1981).

Similar to eq. (115) the complex $(\text{t-BuC}{\equiv}C)_2R$, R = Eu or Yb, can be prepared (Deacon et al., 1982b). The hydrolysis of these complexes yields the acetylene as well as a significant amount of alkene and alkane.

Bis(pentafluorophenyl) ytterbium is prepared similarly by transmetallation from ytterbium metal and bis(pentafluorophenyl) mercury (Deacon and Vince, 1976; Deacon et al., 1977, 1979). The complex $(C_6F_5)_2Yb \cdot (THF)_4$ is characterized by infrared, ultraviolet, ^1H and ^{19}F NMR spectra. Evidence is presented for green $(C_6F_5)_2Eu$ (Deacon et al., 1979), and less stable derivatives $(C_6HF_4)_2Yb$ with the

Compound	Color	Other data		Refs.
$Cp_2Sm \cdot (THF)$	purple	μ_{eff}	3.6 B.M.	1
Cp_2Eu	yellow	μ_{eff}	7.63 B.M.	2
Cp_2Yb	red	subl. 400–420°C		2
	green			3
$Cp_2Yb \cdot (DME)$				4
		molecular structure		20
$(MeCp)_2Yb \cdot (THF)$	yellow			5
$(Me_3SiC_5H_4)_2Yb$	green	m.p. 308–310°C		6
$(Me_3SiC_5H_4)_2Yb \cdot (THF)_2$	purple	m.p. 120°C		6
$(Me_3SiC_5H_4)_2Yb \cdot (tmed)$	blue	m.p. 115°C		6
$(C_5Me_5)_2Sm \cdot (THF)_2$	purple	μ_{eff}	3.6 B.M.	7
$(C_5Me_5)_2Eu \cdot (THF)$	red	m.p. 178–181°C		8
$(C_5Me_5)_2Eu \cdot (THF) \cdot (Et_2O)$	red	m.p. 181–182°C,		8
		μ_{eff}	7.99 B.M.	
$(C_5Me_5)_2Yb \cdot (THF)$	red	m.p. 206–209°C		8
$(C_5Me_5)_2Yb \cdot (THF) \cdot (C_6H_5CH_3)_{1/2}$	brown-red	m.p. 204–206°C		8
$(C_5Me_5)_2Yb \cdot (THF)_2$	red	dec. 90°C		9
$(C_5Me_5)_2Yb \cdot (Et_2O)$	green	dec. 145°C		8
$(C_5Me_5)_2Yb \cdot (Et_2O)_2$				9
$(C_5Me_5)_2Yb \cdot (DME)$				9
$(C_5Me_5)_2Yb \cdot (py)_2$	green	m.p. 208–210°C		10
C_8H_8Eu	orange			11
C_8H_8Yb	pink			11
$[K(DME)]_2[Ce(C_8H_8)_2]$	olive green			12
C_6H_5EuI				13
CH_3YbI				13
C_2H_5YbI				13
C_6H_5YbI				13
		reactivity		22,23
$4-CH_3C_6H_4YbI$				13
$2,6-(CH_3)_2C_6H_3YbI$				13
$2,4,6-(CH_3)_3C_6H_2YbI$				13
$(CH_3C{\equiv}C)_2Eu$	yellow-brown			14
$(C_6H_5C{\equiv}C)_2Yb$	purple			15
		dec. 200°C, NMR, UV		24
$(C_6F_5)_2Eu$	green			16
$(C_6F_5)_2Yb$				16
		reactivity		25
$(C_6F_5)_2Yb \cdot (THF)_4$	orange	dec. 78°C		17
$(C_6HF_4)_2Yb$		reactivity		25
$(C_6F_4H-2)_2Yb$				16
$(C_6F_4H-4)_2Yb$				16
$(C_6F_4H-4)_2Yb \cdot (THF)_4$	orange			17
$(CH_3CB_{10}H_{10}C)_2Yb \cdot (THF)_2$		dec. 287°C		18
$(C_6H_5CB_{10}H_{10}C)_2Yb \cdot (THF)_2$		dec. 262°C		18
$(C_2H_2B_{10}H_9)_2Yb \cdot (THF)$		dec. 290°C		18
$Cp_2Sm \cdot (THF)_2$		dec. 390–410°C		19
$Cp_2Eu \cdot (THF)_2$		dec. 400–420°C		19
$Cp_2Yb \cdot (THF)_2$		dec. 400–410°C		19
$(C_5Me_5)_2Eu \cdot (Me_2PCH_2PMe_2)$	red	m.p. 251–253°C, IR		21
$(C_5Me_5)_2Eu \cdot (Me_2PCH_2CH_2PMe_2)$	red	m.p. 288–292°C, IR		21

TABLE 42 (continued)

Compound	Color	Other data	Refs.
$(C_5Me_5)_2Yb \cdot (Me_2PCH_2PMe_2)$	green	m.p. 250–253°C, IR, NMR	21
$(C_5Me_5)_2Yb \cdot (Me_2PCH_2CH_2PMe_2)$	green	m.p. 283–285°C	21
$(t\text{-}C_4H_9C \equiv C)_2Eu$			24
$(C_6H_5C \equiv C)_2Eu \cdot (THF)_{0.25}$	brown-orange	dec. 245–248°C, UV, IR, NMR	24
$(t\text{-}C_4H_9C \equiv C)_2Yb$			24
$C_6H_5CB_{10}H_{10}CSmI$			26
$C_6H_5CB_{10}H_{10}CEuI$			26
$C_6H_5CB_{10}H_{10}CYbI$			26

1. Watt and Gillow (1969).
2. E.O. Fischer and H. Fischer (1965b).
3. Calderazzo et al. (1966).
4. Deacon et al. (1982).
5. Zinnen et al. (1980).
6. Lappert et al. (1980).
7. W.J. Evans et al. (1981a).
8. Tilley et al. (1980).
9. Watson (1980).
10. Tilley et al. (1982a).
11. Hayes and Thomas (1969a).
12. Greco et al. (1976).
13. D.F. Evans et al. (1971).

14. Murphy and Toogood (1971).
15. Deacon and Koplick (1978).
16. Deacon et al. (1979).
17. Deacon et al. (1977).
18. Suleimanov et al. (1982a).
19. Suleimanov et al. (1982c).
20. Deacon et al. (1983a).
21. Tilley et al. (1983).
22. Fukagawa et al. (1981).
23. Fukagawa et al. (1982).
24. Deacon et al. (1982b).
25. Deacon et al. (1983b).
26. Suleimanov et al. (1983).

hydrogen in 2- or 4-position are mentioned (Deacon et al., 1977, 1979). An analogous samarium complex could not be isolated in a pure state.

Treatment of trans-$Rh(CO)Cl(PPh_3)_2$, $NiCl_2(bipy)$, $NiCl_2(PPh_3)_2$ and $PtCl_2(bipy)$ with $(C_6F_5)_2Yb$ or $(C_6HF_4)_2Yb$ in tetrahydrofuran gives the corresponding polyfluorophenyl organometallics in similar yields with respect to other polyfluorophenyl reagents. Carbonation of $(C_6F_5)_2Yb$ in tetrahydrofuran and acidic quench yields pentafluorobenzoic acid and 2,3,4,5-tetrafluorobenzoic acid, where the hydrogen is derived from tetrahydrofuran (Deacon et al., 1983b).

C- and B-ytterbium carboranes have been prepared according to eqs. (117) and (118) from ytterbium metal and C- and B-mercurocarboranes in tetrahydrofuran at room temperature (Suleimanov et al., 1982a):

$$Yb + (o\text{-}LCB_{10}H_{10}C)_2Hg \xrightarrow{\text{THF}} (o\text{-}LCB_{10}H_{10}C)_2Yb \cdot (THF) + Hg, \qquad (117)$$

$$L = Me, Ph,$$

$$m\ Yb + (o\text{-}C_2H_2B_{10}H_9)_2Hg \xrightarrow{\text{THF}} (o\text{-}C_2H_2B_{10}H_9)_2Yb \cdot (THF) + Hg/Yb,$$

$$(118)$$

$$m = 5, 6.$$
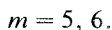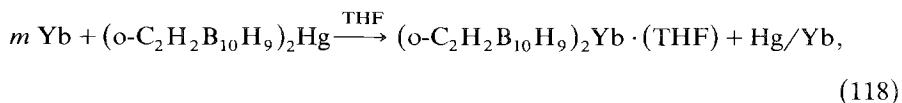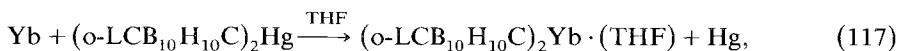
A Grignard-like intermediate $C_6H_5C\text{-}B_{10}H_{10}\text{-}C\text{-}R\text{-}I$, has been postulated in the

reactions of $C_6H_5C-B_{10}H_{10}-C-Li$ with RI_2 (R = Sm, Eu, Yb) and C_6H_5- $C-B_{10}H_{10}-C-I$ with R (R = Eu, Yb), followed by quenching the reaction mixtures with $(CH_3)_3SiCl$ and $CH_3C(O)Cl$ (Suleimanov et al., 1983).

The known organometallic compounds of the rare earths in the oxidation state R^{+2} are shown in table 42.

4. Organometallic compounds of the rare earths in the oxidation state +4

The best element of the rare earths for the oxidation state +4 should be cerium, because of the electron configuration of the rare gas xenon for the ion Ce^{4+}. It is also known from inorganic chemistry, that within the rare earths the lanthanide oxidation state +4 is only stable for Ce^{4+} in aqueous solution, showing a very strong oxidation strength. The literature of organometallic chemistry contains a few papers dealing with the preparation of some derivatives of Ce^{4+}, which are described to have an astonishingly high stability.

Tetracyclopentadienyl cerium and tetraindenyl cerium have been prepared as red-orange or yellow solids by interaction of cerium hexachloride dipyridinium complex with sodium cyclopentadienide or sodium indenide, respectively. Both compounds are described as stable against dilute acids and alkalis (Kalsotra et al., 1971a).

$$(C_5H_6N)_2CeCl_6 + 4\,NaL \rightarrow CeL_4 + NaCl + 2\,py \cdot HCl, \qquad (119)$$

$$L = Cp, Ind, C_{13}H_9.$$

Deacon et al. (1983a) showed that the reaction of sodium cyclopentadienide with dipyridinium hexachlorocerate(IV) in tetrahydrofuran yields only tris(cyclopentadienyl) cerium (III) and not tetrakis(cyclopentadienyl) cerium(IV).

The tetrafluorenyl derivative, which is yellow-brown and is stable in dry and inert atmosphere, is prepared in the same manner (Kalsotra et al., 1972c). An attempt to repeat this synthesis has been reported to be unsuccessful, perhaps due to the low thermal stability (Greco et al., 1976).

The di(cyclooctatetraenyl) cerium complex was prepared by the reaction of cerium tetra-iso-propoxide with triethyl aluminum in cyclooctatetraene at 140°C (Greco et al., 1976):

$$Ce(OCHMe_2)_4 \cdot Me_2CHOH + 5\,AlEt_3$$

$$\xrightarrow{\text{excess COT}} Ce(C_8H_8)_2 + 5\,Et_2AlOCHMe_2 + C_2H_6 + 4\,Et^{\cdot}. \qquad (120)$$
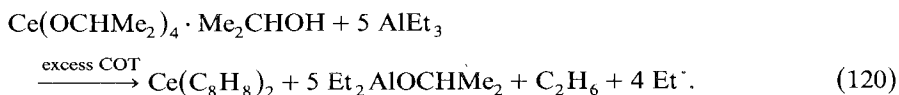
The black crystalline compound is pyrophoric, but stable to water. The ^1H NMR spectrum consists of a sharp singlet at $\delta = 5.6$ ppm. The X-ray studies indicate a sandwich type structure as in uranocene. The compound is reduced by potassium to the anion $Ce(COT)_2^{2-}$ in essentially quantitative yield, and with an excess of potassium in monoglyme to the Ce^{2+} derivative $[K(monoglyme)]_2[Ce(COT)_2]$.

The preparations of tricyclopentadienyl cerium chloride, bisindenyl cerium dichloride, and dicycloheptatrienyl cerium dichloride are described by the reaction of

the cerium hexachloride dipyridinium complex with either sodium cyclopentadienide, sodium indenide, or cycloheptatriene in tetrahydrofuran or benzene, or by redistribution between dipyridinium cerium hexachloride and tetracyclopentadienyl cerium or tetraindenyl cerium (Kalsotra et al., 1971b, d):

$$(C_5H_6N)_2CeCl_6 + 3\ NaCp \rightarrow Cp_3CeCl + 3\ NaCl + 2\ py \cdot HCl, \tag{121}$$

$$(C_5H_6N)_2CeCl_6 + 2\ NaInd \rightarrow Ind_2CeCl_2 + 2\ NaCl + 2\ py \cdot HCl, \tag{122}$$

$$(C_5H_6N)_2CeCl_6 + 2\ C_7H_8 \rightarrow (C_7H_7)_2CeCl_2 + 2\ py \cdot HCl + 2\ HCl, \tag{123}$$

$$(C_5H_6N)_2CeCl_6 + 3\ Cp_4Ce \rightarrow 4\ Cp_3CeCl + 2\ py \cdot HCl, \tag{124}$$

$$(C_5H_6N)_2CeCl_6 + Ind_4Ce \rightarrow 2\ Ind_2CeCl_2 + 2\ py \cdot HCl. \tag{125}$$
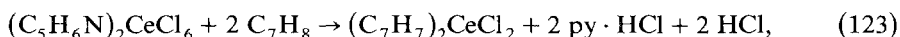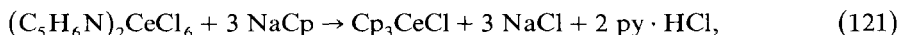
The brown compounds are described to be stable in water. They should act as starting materials for numerous synthesis yielding tricyclopentadienyl cerium and bisindenyl cerium derivatives of the types Cp_3CeL and Ind_2CeL_2 with bonds between the organocerium(IV) moieties and the pseudohalides CN^-, NCO^-, NCS^-, and N_3^- (Kalsotra et al., 1972c), nitro-nitrito, and nitrato groups (Mehra and Vij, 1978), alkoxides (Kapur et al., 1973c), phenols (Kapur et al., 1972), carboxylates (Kalsotra et al., 1971c), and thiols (Kapur et al., 1973a):

$$Cp_3CeCl + ML \xrightarrow{\text{THF}} Cp_3CeL + MCl, \tag{126}$$

$$Ind_2CeCl_2 + 2\ ML \xrightarrow{\text{THF}} Ind_2CeL_2 + 2\ MCl, \tag{127}$$

$$M = Na,\ L = N_3,\ NO_2,\ ONO_2,\ O_2CH,\ O_2CCH_3,\ O_2CC_2H_5,$$
$$O_2CC_3H_7,\ O_2CPh,\ SCH_3,\ SC_2H_5,\ SC_3H_7,\ SCHMe_2,$$
$$SC_4H_9,\ S\text{-i-}C_4H_9,\ S\text{-i-}C_5H_{11},$$
$$M = K,\ L = CN,\ NCO,\ NCS,$$
$$M = Ag,\ L = ONO,$$

$$Cp_3CeCl + LOH + NEt_3 \xrightarrow{\text{benzene}} Cp_3CeOL + Et_3N \cdot HCl, \tag{128}$$

$$L = CH_3,\ C_2H_5,\ C_3H_7,\ i\text{-}C_3H_7,\ C_4H_9,\ i\text{-}C_4H_9,\ i\text{-}C_5H_{11},$$

$$Cp_3CeCl + LOH \xrightarrow{\text{THF}} Cp_3CeOL + HCl, \tag{129}$$

$$Ind_2CeCl_2 + 2\ LOH \xrightarrow{\text{THF}} Ind_2Ce(OL)_2 + 2\ HCl, \tag{130}$$

L = phenol, resorcinol, pyrogallol, phloroglucinol, α-naphthol, β-naphthol.

Even tetrahydroborate derivatives (Kapur et al., 1973b), hydride and amide derivatives (Kapur et al., 1974), as well as some alkyl and aryl derivatives were synthesized. Their infrared spectra have been tabulated (Kalsotra et al., 1973). For all Ce^{4+} derivatives, further confirmation is necessary.

$$Cp_3CeCl + NaL \xrightarrow{\text{THF}} Cp_3CeL + NaCl, \tag{131}$$

$$\text{Ind}_2\text{CeCl}_2 + 2\,\text{NaL} \xrightarrow{\text{THF}} \text{Ind}_2\text{CeL}_2 + 2\,\text{NaCl}, \tag{132}$$

$$\text{L} = \text{H, BH}_4,\ \text{NH}_2,$$

$$\text{Cp}_3\text{CeCl} + \text{ML} \xrightarrow{\text{solvent}} \text{Cp}_3\text{CeL} + \text{MCl}, \tag{133}$$

$$\text{Ind}_2\text{CeCl}_2 + 2\,\text{ML} \xrightarrow{\text{solvent}} \text{Ind}_2\text{CeL}_2 + 2\,\text{MCl}, \tag{134}$$

$$\text{M} = \text{Mg-halide, L} = \text{CH}_3,\ \text{C}_2\text{H}_5,\ \text{Ph, CH}_2\text{Ph, solvent} = \text{THF}$$

$$\text{M} = \text{Li, L} = \text{CH}_3,\ \text{C}_2\text{H}_5,\ \text{Ph, CH}_2\text{Ph, solvent} = \text{Et}_2\text{O}.$$
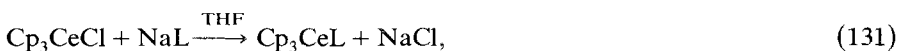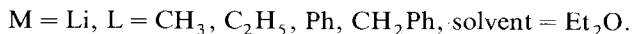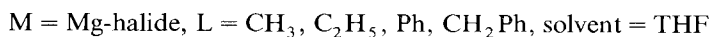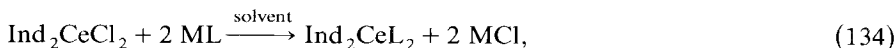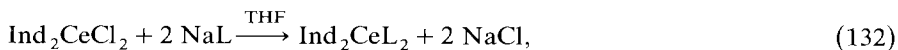
5. Other organometallic compounds of the rare earths

This section describes recent advances on the synthesis of rare earth organometallic compounds in the $+1$ and 0 oxidation state as well as some compounds which do not significantly belong to one of the earlier described sections.

Complexes between some lanthanides in a low oxidation state and olefins were isolated by W.J. Evans et al. (1978a, 1981b). Cocondensation of lanthanum, neodymium, samarium or erbium metal with butadiene or 2,3-dimethylbutadiene at $-196°\text{C}$ in a metal vaporization reactor produces a brown solid, which can be extracted by toluene and tetrahydrofuran yielding soluble brown products with the empirical formulas $\text{R}(\text{C}_4\text{H}_6)_3$ for $\text{R} = \text{Nd, Sm, Er, and R}[(\text{CH}_3)_2\text{C}_4\text{H}_4]_2$ for $\text{R} = \text{La, Er}$. For these complexes the following three formulas have been suggested:
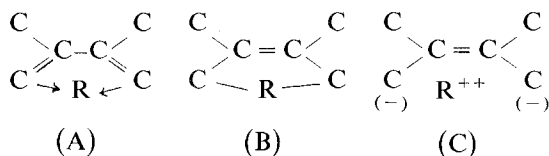
of which formula B is the most widely accepted. These complexes are extremely sensitive to both moisture and air. They polymerize immediately on exposure to air. Hydrolytic decomposition produces 2-butenes, 1-butenes and octadienes. The magnetic susceptibility of the complexes differs from those known for lanthanide(III) compounds. $\text{La}[(\text{CH}_3)_2\text{C}_4\text{H}_4]_2$ is the first known paramagnetic organolanthanum compound (W.J. Evans et al., 1978a).

Samarium, erbium and ytterbium metal vapor also react with ethene, propene, and 1,2-propadiene at $-196°\text{C}$. The colored matrices, orange to black, contain up to 80% of the appropriate metal as shown by the infrared absorptions of the coordinated olefinic double bond. The reaction product of erbium metal and propene was characterized by elemental analysis as $\text{Er}(\text{CH}_2{=}\text{CHCH}_3)_3$. The predominant volatile products after hydrolysis of the complexes are CH_4, C_2H_6, $\text{C}_3\text{H}_6/\text{C}_3\text{H}_8$ and $\text{C}_4\text{H}_8/\text{C}_4\text{H}_{10}$ for the ethene complexes, $\text{C}_3\text{H}_6/\text{C}_3\text{H}_8$, $\text{H}_2\text{C}{=}\text{C}{=}\text{CH}_2$, and $\text{CH}_3\text{C}{\equiv}\text{CH}$ for the 1,2-propadiene complexes, and $\text{C}_3\text{H}_6/\text{C}_3\text{H}_8$, and $\text{CH}_3\text{C}{\equiv}\text{CH}$ for the propene complexes. Since ethene is only a minor reaction product in the hydrolysis of

its complexes with the rare earths, a simple π-complex structure is not predicted for these complexes. The structure of them is not completely understood (W.J. Evans et al., 1981b).

The cocondensation of samarium, erbium, and ytterbium with 3-hexyne at $-196°C$ forms brown solids, which upon warming up to room temperature and extraction with toluene or tetrahydrofuran give isolable complexes. Complete elemental analyses of these complexes together with molecular weight determinations in benzene indicate the empirical formulas SmC_6H_{10}, $Er_2C_{18}H_{30}$, and YbC_6H_{10}. Although a structural characterization has not been performed (W.J. Evans et al., 1979a, b), the complexes are active hydrogenating catalysts (W.J. Evans et al., 1979b). The ytterbium hexyne complex can be used as starting material for new derivatives of ytterbium(III) (Zinnen et al., 1980).

Neutral and anionic alkylidene complexes of erbium, thulium, ytterbium and lutetium have been found and investigated by Schumann and Müller (1978c, 1979). The homoleptic species $R(CH_2SiMe_3)_3 \cdot (THF)_2$ of the lanthanides Er, Tm, Yb and Lu decompose slowly even at room temperature over several days, generating tetrahydrofuran and tetramethylsilane. The remaining complexes contain CH_2SiMe_3 and $CHSiMe_3$ groups bound to the lanthanide metals. They decompose above $380°C$, indicating a polymeric nature of the compounds, consisting of bridging units like $[Me_3SiCH_2R(\mu\text{-}CHSiMe_3)_2RCH_2SiMe_3]$, but the complete structure has not been solved.

Similar structural units containing both carbene and carbyne ligands are proposed to be present in the decomposition products of anionic lutetium alkyl complexes, which have been investigated by Schumann and Müller (1978c, 1979):

$$[Li(Et_2O)_4][Lu(CH_2SiMe_3)_4]$$
$$\rightarrow Li[Lu(CH_2SiMe_3)_2CHSiMe_3] + SiMe_4 + 4\,Et_2O, \tag{135}$$

$$Li[Lu(CH_2SiMe_3)_2CHSiMe_3] + tmed$$
$$\rightarrow [Li(tmed)][Lu(CH_2SiMe_3)CHSiMe_3], \tag{136}$$

$$LuCl_3 + 3\,LiCH_2SiMe_3$$
$$\xrightarrow{\text{THF}} Lu(CH_2SiMe_3)_3 \cdot (THF)_3 + LiCl + SiMe_4$$
$$+ [Li(THF)_2][Lu_2(CH_2SiMe_3)_2(CHSiMe_3)(CSiMe_3)]. \tag{137}$$
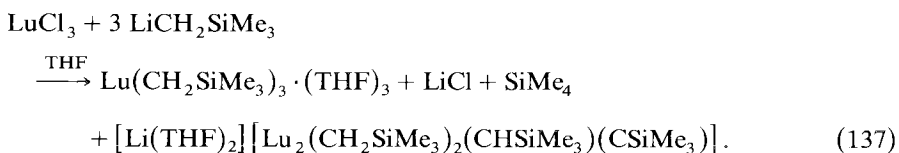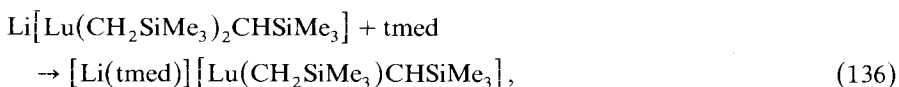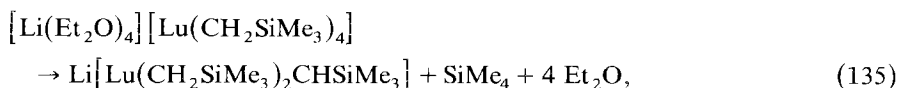
Similar organometallic compounds of the rare earths yttrium and neodymium have been described by Russian scientists (Guzman et al., 1979; Vollershtein et al., 1980; Dolgoplosk et al., 1980). YCl_3 and $NdCl_3$ react with organolithium compounds, with the formation of complexes which are stable in hydrocarbon solutions. In analogy to the previously mentioned work of Schumann and Müller (1979), the formation and immediate decomposition of a homoleptic neodymium(III) derivative is discussed in the reaction of $NdCl_3$ with $LiCH_2SiMe_3$ (Vollershtein et al., 1980):

$$NdCl_3 + 3\,LiCH_2SiMe_3 \rightarrow Nd(CH_2SiMe_3)_3 + 3\,LiCl, \tag{138}$$

$$2\,Nd(CH_2SiMe_3)_3 \rightarrow (Me_3SiC{=}Nd)_2CHSiMe_3 + 3\,SiMe_4. \tag{139}$$

Benzyl lithium reacts with YCl_3 and $NdCl_3$ in diethylether with evolution of toluene. The following reaction mechanism has been postulated (Guzman et al., 1979; Dolgoplosk et al., 1980):

$$RCl_3 + 3 \, LiCH_2Ph \rightarrow R(CH_2Ph)_3 + 3 \, LiCl, \tag{140}$$

$$R(CH_2Ph)_3 \rightarrow PhCH_2-R=CHPh + C_6H_5CH_3, \tag{141a}$$
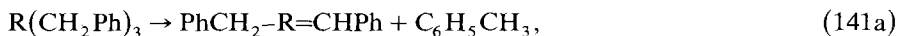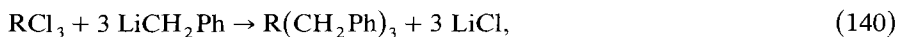
$PhCH_2-R=CHPh \rightarrow$ polymers with the following units:

$$\text{Ph-C}\underset{R}{\overset{R}{\diagdown}}\text{C-Ph,} \quad -R=C-, \quad PhC\equiv R, \tag{141b}$$
$$\underset{Ph}{|}$$
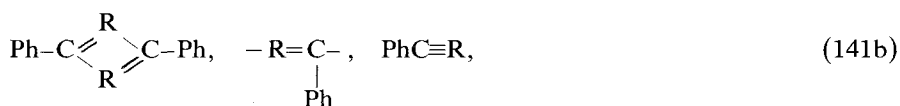
R = Y, Nd.

The neophyl derivative of yttrium is formed by the same mechanism. The fact that 2 moles of tert-butyl benzene are evolved per yttrium in this reaction indicates the possible formation of a compound containing an yttrium–carbon triple bond (Guzman et al., 1979; Dolgoplosk et al., 1980):

$$YCl_3 + 3 \, PhCMe_2CH_2Li \rightarrow Y\equiv CCMe_2Ph + 2 \, C_6H_5CMe_3 + 3 \, LiCl. \tag{142}$$
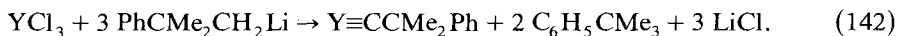
A vinyl derivative of scandium without having a stabilizing cyclopentadienyl ligand was proposed by Cardin and Norton (1979) according to eq. (143). The
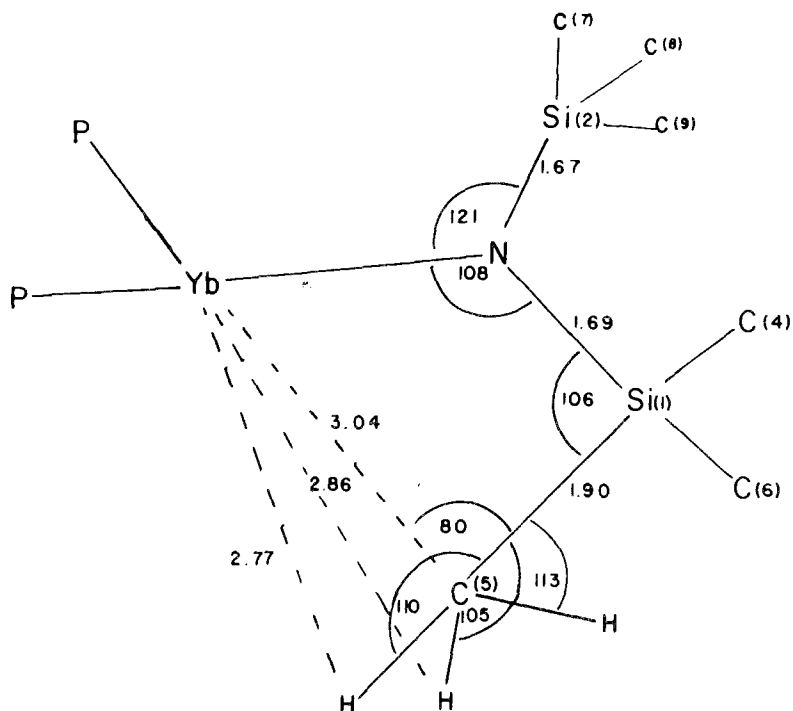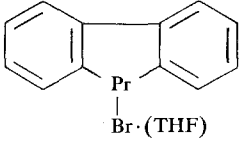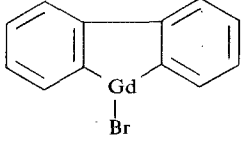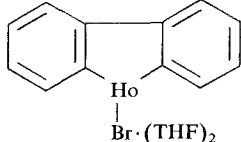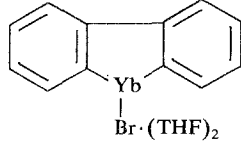
Fig. 47. Line drawing showing the Yb–C interaction in $Yb[N(SiMe_3)_2]_2[Me_2PCH_2CH_2PMe_2]$ (after Tilley et al., 1982b).

TABLE 43
Other organometallic compounds of the rare earths

Compounds	color	other data	Ref.
$Er(CH_2=CHCH_3)_3$	orange	μ_{eff} 8.1 B.M.	1
$Nd(CH_2=CHCH=CH_2)_3$	brown	dec. 175°C, μ_{eff} 3.7 B.M.	2
$Sm(CH_2=CHCH=CH_2)_3$	brown	dec. 130°C, μ_{eff} 2.1 B.M.	2
$Er(CH_2=CHCH=CH_2)_3$	brown	dec. 100°C, μ_{eff} 9.1 B.M.	2
$La(CH_2=CMeCMe=CH_2)_2$	brown	dec. 80°, μ_{eff} 1.6 B.M.	2
$Nd(CH_2=CMeCMe=CH_2)_2$	brown	dec. 190°C	2
$Er(CH_2=CMeCMe=CH_2)_2$	brown	μ_{eff} 9.4 B.M.	2
$Sm(CH_3CH_2C\equiv CCH_2CH_3)$			3
$Er_2(CH_3CH_2C\equiv CCH_2CH_3)_3$	brown		3
$Yb(CH_3CH_2C\equiv CCH_2CH_3)$			3
$[Er(CH_2SiMe_3)(CHSiMe_3)]_n$	pink	m.p. 385°C	4
$Li[Lu(CH_2SiMe_3)_2CHSiMe_3]$	white		4
$[Li(tmed)][Lu(CH_2SiMe_3)_2CHSiMe_3]$		m.p. 113–115°C	4
$Y\equiv CC(CH_3)_2C_6H_5$			5
$(Me_3SiCH=Nd)_2CHSiMe_3$			6
$Me_2C=CPhScCl_2\cdot(THF)_3$			7
$Yb[N(SiMe_3)_2]_2(Me_2PCH_2)_2$	purple	m.p. 195–197°C	8
$(C_6H_5)_3CPrCl_2$			9
$(C_6H_5)_3CNdCl_2$			9
$[(C_6H_5)_3C]_3Nd_2Cl_3$			9
$(C_6H_5)_3CGdCl_2$			9
$(C_6H_5)_3CHoCl_2$			9

[fluorenyl] Pr | Br·(THF) | | | 10

[fluorenyl] Gd | Br | | | 10

[fluorenyl] Ho | Br·(THF)$_2$ | | | 10

[fluorenyl] Yb | Br·(THF)$_2$ | brown | dec. 100°C | 10

1. W.J. Evans et al. (1981b).
2. W.J. Evans et al. (1978a).
3. W.J. Evans et al. (1979b).
4. Schumann and Müller (1979).
5. Guzman et al. (1979).
6. Vollershtein et al. (1980).
7. Cardin and Norton (1979).
8. Tilley et al. (1982b).
9. Dolgoplosk et al. (1983).
10. Syutkina et al. (1983).

complex, which is extremely sensitive to water and other protic reagents shows the olefinic methyl protons at $\delta = 1.768$ ppm.

$$ScCl_3 + Me_3SnCPh=CMe_2 \xrightarrow{\text{THF}} Me_2C=CPhScCl_2 \cdot (THF)_3 + Me_3SnCl. \quad (143)$$
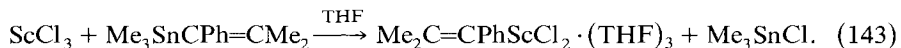
Finally it should be stated that an ytterbium–carbon bond is claimed to exist in a phosphine complex of an ytterbium–nitrogen compound via an ytterbium–γ-carbon interaction (Tilley et al., 1982b). The X-ray diffraction study of the complex $Yb[N(SiMe_3)_2]_2[Me_2PCH_2CH_2PMe_2]$ shows an Yb–C bond distance of 3.04 Å (fig. 47). This distance is less than the sum of the Van der Waals radius of a methyl group (2.0 Å), and the divalent metallic radius of ytterbium (1.7 Å), but longer than the $Yb(III)-C_{methyl}$ distance of 2.57 Å in a bridged compound like $(Cp_2YbMe)_2$ (Holton et al., 1979a, b).

The reaction of triphenylmethyl chloride, benzyl chloride and phenyl bromide with several metallic rare earth elements like Nd, Pr, Gd and Ho in tetrahydrofuran at room temperature has been described but no pure products could be isolated (Dolgoplosk et al., 1983, Markevich et al., 1983, Yakovlev et al., 1983). The structure of the proposed compounds is unclear. In the reaction of 2,2'-dilithium biphenyl with several rare earth tribromides (R = Pr, Sm, Gd, Ho, Yb) the proposed products are metallacycles (Syutkina et al., 1983).

Allyl iodide reacts in situ with cerium amalgam to generate allyl cerium iodide, which in turn reacts with ketones to give homoallylic alcohols to good yields (Imamoto et al., 1981).

Organometallic compounds of the rare earths which do not belong to one of the former chapters are listed in table 43.

6. Catalytic application of organometallic compounds of the rare earths

The efficiency of a catalytic system based on an organometallic coordination compound depends on the number of metal-atom orbitals that can be involved in bonding. Therefore derivatives of the reare earths, especially the lanthanides with their partially filled d- and f-orbitals, should provide interesting new opportunities for catalyzing a great variety of organic reactions.

A large number of lanthanide oxides, halides, alkoxides and similar compounds show activity as cracking catalysts as well as in oligomerizations, polymerizations and other organic syntheses. Organometallic compounds of the lanthanides are quite likely to be the active species when aluminum alkyls, lithium alkyls or other organometallic compounds are simultaneously present in such reactions. Reviews of these organolanthanide catalysts formed in situ are given by Mazzei (1979) and Marks and Ernst (1982). Imamoto et al. (1982) generated organocerium compounds via the transmetallation reaction of butyl lithium with CeI_3. These catalysts react with ketones at $-65°C$ to form tertiary alcohols in high yields. More extensive research in the near future may inform us about the real nature of the organo-lanthanide intermediates in such catalytic processes.

The first oligomerization process catalyzed by an isolated organometallic compound of a lanthanide metal was described in 1970 by Gysling and Tsutsui with the trimerization of diphenylacetylene and other derivatives by tricyclopentadienyl samarium. The yttrium aluminum complex $Cp_2Y(\mu\text{-}CH_3)_2AlMe_2$ (Ballard and Pearce, 1975) and some alkyl-bridged complexes of yttrium and erbium, $(Cp_2RL)_2$, $[(MeCp)_2RL]_2$ and $[(Me_3SiC_5H_4)_2RL]_2$ with $L = CH_3$, C_4H_9, are active homogeneous ethylene polymerization catalysts (Ballard et al., 1978). $Ce(C_8H_8)_2$, $Ce_2(C_8H_8)_3$ and $(C_8H_8)Ce(\mu\text{-}OCHMe_2)_2AlEt_2$ are active in Ziegler–Natta catalysts for the ethylene polymerization (Mazzei, 1979). Butadiene can be polymerized to a predominantly 1,4-trans product in yields up to 94% by a system containing $Li[R(CH=CHCH_3)_4] \cdot (dioxane)/ AlBr_3$ or tmed or THF with $R = $ Ce, Nd, Sm, Gd, Dy (Mazzei, 1979). The reaction of $(C_5Me_5)_2LuCH_3$ with propene, which results in insertion of the olefin into the lutetium–carbon bond, was studied as an experimental model for the coordination catalysis of olefin polymerization by Watson (1982) and Watson and Roe (1982). The kinetics of this insertion reaction, as well as that of the decomposition of the lutetium isobutyl complex formed, are the basis of a general mechanism for the polymerization of ethylene catalyzed by bis(pentamethylcyclopentadienyl) lutetium methyl and for the β-alkyl transfer reaction which is a part of the insertion–deinsertion equilibria.

The cocondensation products of lanthanum or erbium metal atoms and 3-hexyne are effective hydrogenation catalysts. 3-Hexyne is hydrogenated to 3-hexene, with a 97% yield of cis product, and a turnover frequency of 0.02 to 0.04 hexyne molecules per metal atom per minute for the erbium compound. 3-Hexene is also hydrogenated (W.J. Evans et al., 1978b, 1979a, b). Alkynide hydrides of samarium, erbium and ytterbium, prepared from metal vapor and neutral unsaturated hydrocarbons, are also able to hydrogenate 3-hexyne to give more than a 96% yield of cis-3-hexene at room temperature and atmospheric pressure (W.J. Evans et al., 1981b, c). Also bis(methylcyclopentadienyl) ytterbium tetrahydrofuranate (Zinnen et al., 1980) and pentamethylcyclopentadienyl samarium hydride derivatives can be used to initiate the catalytic hydrogenation of alkynes like diphenylacetylene or 3-hexyne (W.J. Evans et al., 1983b).

Finally it should be noted that organolanthanides like dicyclopentadienyl(tert-butyl) lutetium tetrahydrofuranate activate carbon monoxide to form a new complex with an endiolate ligand (see section 2.7.1.), a reaction which should become quite important in synthetic organic chemistry (W.J. Evans et al., 1981d). A review dealing with his own work in this area appeared recently (W.J. Evans, 1983).

References

Afanasev, B.N. and P.A. Tsyganova, 1948, Zh. Obshch. Khim. **18**, 306.

Aleksanyan, V.T., G.K. Borisov, G.G. Devyatykh, B.F. Gächter, J.A. Koningstein and B.E. Schneider, 1974, J. Raman Spectrosc. **2**, 345.

Aleksanyan, V.T., G.K. Borisov, I.A. Garbuzova and G.G. Devyatykh, 1977, J. Organometal. Chem. **131**, 251.

Aleksanyan, V.T., I.A. Garbusova, T.M. Chernyshova, Z.V. Todres, M.R. Leonov and N.I. Gramateeva, 1981, J. Organometal. Chem. **217**, 169.

Atwood, J.L. and K.D. Smith, 1973a, J. Amer. Chem. Soc. **95**, 1488.

Atwood, J.L. and K.D. Smith, 1973b, J. Chem. Soc., Dalton Trans. 2487.

Atwood, J.L., J.H. Burns and P.G. Laubereau, 1973, J. Amer. Chem. Soc. **95**, 1830.

Atwood, J.L., W.E. Hunter, R.D. Rogers, J. Holton, J. McMeeking, R. Pearce and M.F. Lappert, 1978, Chem. Commun. 140.

Atwood, J.L., W.E. Hunter, A.L. Wayda and W.J. Evans, 1981, Inorg. Chem. **20**, 4115.

Baker, E.C. and K.N. Raymond, 1977, Inorg. Chem. **16**, 2710.

Baker, E.C., L.D. Brown and K.N. Raymond, 1975, Inorg. Chem. **14**, 1376.

Ballard, D.G.H. and R. Pearce, 1975, Chem. Commun. 621.

Ballard, D.G.H., A. Courties, J. Holton, J. McMeeking and R. Pearce, 1978, Chem. Commun. 994.

Barker, G.K. and M.F. Lappert, 1974, J. Organometal. Chem. **76**, C45.

Baumgärtner, F., E.O. Fischer and P. Lauberau, 1967, Radiochim. Acta **7**, 188.

Bielang, G. and R.D. Fischer, 1978, J. Organometal. Chem. **161**, 335.

Bielang, G. and R.D. Fischer, 1979, Inorg. Chim. Acta **36**, L389.

Birmingham, J.M. and G. Wilkinson, 1956, J. Amer. Chem. Soc. **78**, 42.

Borisov, G.K. and S.G. Chuganova, 1976, Gidridy Galidy Metalloorgan. Soedin, Osoboi Chistoty 110.

Borisov, G.K., S.G. Krasnova and G.G. Devyatykh, 1973, Zh. Neorgan. Khim. **18**, 663; Russ. J. Inorg. Chem. **18**, 346.

Borisov, G.K., S.G. Chuganova and G.G. Devyatykh, 1975, Zh. Neorgan. Khim. **20**, 2850; Russ. J. Inorg. Chem. **20**, 1579.

Bregadze, V.I., N.A. Kovalchuk, N.N. Godovikov, G.Z. Suleimanov and I.P. Beletskaya, 1983, J. Organometal. Chem. **241**, C13.

Brittain, H.G., J.H. Meadows and W.J. Evans, 1983, Organometal. **2**, 1661.

Brix, P., S. Hüfner, P. Kienle and D. Quitmann, 1964, Phys. Lett. **13**, 140.

Burns, J.H. and W.H. Baldwin, 1976, J. Organometal. Chem. **120**, 361.

Burns, J.H., W.H. Baldwin and F.H. Fink, 1974, Inorg. Chem. **13**, 1916.

Cadet de Gassicourt, L.D., 1760, Memoires de Mathematique et de Physique, Vol. 3, p. 623.

Cahours, A. and A. Rieche, 1854, Justus Liebigs Ann. Chem. **92**, 361.

Calderazzo, F., 1968, Organometal. Chem. Rev. B **4**, 10.

Calderazzo, F., 1969, Organometal. Chem. Rev. B **5**, 545.

Calderazzo, F., 1970, Organometal. Chem. Rev. B **6**, 997.

Calderazzo, F., 1972, Organometal. Chem. Rev. B **9**, 131.

Calderazzo, F., 1973, J. Organometal. Chem. **53**, 173.

Calderazzo, F., 1974, J. Organometal. Chem. **79**, 175.

Calderazzo, F., R., Pappalardo and S. Losi, 1966, J. Inorg. Nucl. Chem. **28**, 987.

Campari, G. and F.A. Hart, 1982, Inorg. Chim. Acta **65**, L217.

Cardin, D.J. and R.J. Norton, 1979, Chem. Commun. 513.

Carnall, W.T., 1979, Optical spectroscopy of f-element compounds, in: Organometallics of the f-elements, eds. T.J. Marks and R.D. Fischer (Reidel, Dordrecht) pp. 281–307.

Changtao Qian, Changqing Ye, Hanzhang Lu, Yuqin Li, Jialie Zhou, Yuanwen Ge and M. Tsutsui, 1982, Abstracts of Papers, 2nd China–Japan–USA Symp. Organometallic and Inorganic Chemistry, Shanghai, p. 83.

Changtao Qian, Changqing Ye, Hanzhang Lu, Yuqin Li, Jialie Zhou and M. Tsutsui, 1983, J. Organometal. Chem. **247**, 161.

Chernyaev, N.P., Yu.B. Zverev, E.M. Gavrishchuk, I.V. Runovskaya, S.G. Chesnokova and V.F. Kutsepin, 1982, Zh. Neorg. Khim. **27**, 2231; Russ. J. Inorg. Chem. **27**, 1259.

Clark, D.W. and K.D. Warren, 1976, J. Organometal. Chem. **122**, C28.

Cotton, F.A., 1955, Chem. Rev. **55**, 551.

Cotton, S.A., 1977, J. Organometal. Chem. Libr. **3**, 189.

Cotton, S.A., F.A. Hart, M.B. Hursthouse and A.J. Welch, 1972, Chem. Commun. 1225.

Coutts, R.S.P. and P.C. Wailes, 1970, J. Organometal. Chem. **25**, 117.

Crease, A.E. and P. Legzdins, 1972, Chem. Commun. 268.

Crease, A.E. and P. Legzdins, 1973a, Chem. Commun. 775.

Crease, A.E. and P. Legzdins, 1973b, J. Chem. Soc., Dalton Trans. 1501.

Day, C.S., V.W. Day, R.D. Ernst and S.H. Vollmer, 1982, Organometal. **1**, 998.

Deacon, G.B. and A.J. Koplick, 1978, J. Organometal. Chem. **146**, C43.

Deacon, G.B. and T.D. Tuong, 1981, J. Organometal. Chem. **205**, C4.

Deacon, G.B. and D.G. Vince, 1976, J. Organometal. Chem. **112**, C1.

Deacon, G.B., W.D. Raverty and D.G. Vince, 1977, J. Organometal. Chem. **135**, 103.

Deacon, G.B., A.J. Koplick, W.D. Raverty and D.G. Vince, 1979, J. Organometal. Chem. **182**, 121.

Deacon, G.B., A.J. Koplick and T.D. Tuong, 1982a, Polyhedron **1**, 423.

Deacon, G.B., A.J. Koplick and T.D. Tuong, 1982b, Aust. J. Chem. **35**, 941.

Deacon, G.B., P.I. Mackinnon, T.W. Hambley and J.C. Taylor, 1983a, J. Organometal. Chem. **259**, 91.

Deacon, G.B., P.I. Mackinnon and T.D. Tuong, 1983b, Aust. J. Chem. **36**, 43.

Deacon, G.B., T.D. Tuong and D.G. Vince, 1983c, Polyhedron **2**, 969.

De Kock, C.W., S.R. Ely, T.E. Hopkins and M.A. Brault, 1978, Inorg. Chem. **17**, 625.

Devyatykh, G.G., S.G. Krasnova, G.K. Borisov, N.V. Larin and P.E. Gaivoronskii, 1970, Dokl. Akad. Nauk SSSR **193**, 1069; Proc. Acad. Sci. USSR **193**, 580.

Devyatykh, G.G., G.K. Borisov and S.G. Krasnova, 1972, Dokl. Akad. Nauk SSSR **203**, 110; Proc. Acad. Sci. USSR **203**, 204.

Devyatykh, G.G., G.K. Borisov, L.F. Zyuzina and S.G. Krasnova, 1973a, Dokl. Akad. Nauk SSSR **212**, 127; Proc. Acad. Sci. USSR **212**, 703.

Devyatykh, G.G., N.V. Larin, P.E. Gaivoronskii, G.K. Borisov, S.G. Krasnova and L.F. Zyuzina, 1973b, Dokl. Akad. Nauk SSSR **208**, 1094; Proc. Acad. Sci. USSR **208**, 111.

Devyatykh, G.G., P.E. Gaivoronskii, N.V. Larin, G.K. Borisov, S.G. Krasnova and L.F. Zyuzina, 1974a, Zh. Neorgan. Khim. **19**, 912; Russ. J. Inorg. Chem. **19**, 496.

Devyatykh, G.G., I.B. Rabinovich, V.I. Telnoi, G.K. Borisov and L.F. Zyuzina, 1974b, Dokl. Akad. Nauk SSSR **217**, 609; Proc. Acad. Sci. USSR **217**, 673.

Devyatykh, G.G., N.P. Chernyaev, Yu.B. Zverev, E.M. Gavrishchuk, I.V. Runovskaya, E.F. Krupnova and S.G. Chesnikova, 1980, Zh. Neorgan. Khim. **25**, 2109; Russ. J. Inorg. Chem. **25**, 1168.

Dolgoplosk, B.A., E.I. Tinyakova, I.Sh. Guzman, E.L. Vollershtein, N.N. Chigir, G.N. Bondarenko, O.K. Sharaev and V.A. Yakovlev, 1980, J. Organometal. Chem. **201**, 249.

Dolgoplosk, B.A., E.I. Tinyakova, I.N. Merkevich, T.V. Soboleva, G.M. Chernenko, O.K. Sharaev and V.A. Yakovlev, 1983, J. Organometal. Chem. **255**, 71.

Domberger, E., R. Klenze and B. Kanellakopulos, 1978, Inorg. Nucl. Chem. Lett. **14**, 319.

Dubois, R., J.C. Carver and M. Tsutsui, 1977, J. Coord. Chem. **7**, 31.

Duncan, J.F. and F.G. Thomas, 1964, J. Chem. Soc. 360.

Ely, N.M. and M. Tsutsui, 1975, Inorg. Chem. **14**, 2680.

Ely, S.R., T.E. Hopkins and C.W. de Kock, 1976, J. Amer. Chem. Soc. **98**, 1624.

Ernst, R.D. and T.H. Cymbaluk, 1982, Organometal. **1**, 708.

Evans, D.F., G.V. Fazakerley and R.F. Phillips, 1970, Chem. Commun. 244.

Evans, D.F., G.V. Fazakerley and R.F.Phillips, 1971, J. Chem. Soc. A 1931.

Evans, W.J., 1983, J. Organometal Chem. **250**, 217.

Evans, W.J. and A.L. Wayda, 1980, J. Organometal Chem. **202**, C6.

Evans, W.J., S.C. Engerer and A.C. Neville, 1978a, J. Amer. Chem. Soc. **100**, 331.

Evans, W.J., A.L. Wayda, Chia-Wun Chang and W.M. Cwirla, 1978b, J. Amer. Chem. Soc. **100**, 333.

Evans, W.J., S.C. Engerer, P.A. Piliero and A.L. Wayda, 1979a, Fundam. Res. Homog. Catal. **3**, 941.

Evans, W.J., S.C. Engerer, P.A. Piliero and A.L. Wayda, 1979b, Chem. Commun. 1007.

Evans, W.J., I. Bloom, W.E. Hunter and J.L. Atwood, 1981a, J. Amer. Chem. Soc. **103**, 6507.

Evans, W.J., K.M. Coleson and S.C. Engerer, 1981b, Inorg. Chem. **20**, 4320.

Evans, W.J., S.C. Engerer and K.M. Coleson, 1981c, J. Amer. Chem. Soc. **103**, 6672.

Evans, W.J., A.L. Wayda, W.E. Hunter and J.L. Atwood, 1981d, Chem. Commun. 706.

Evans, W.L., A.L. Wayda, W.E. Hunter and J.L. Atwood, 1981e, Chem. Commun. 292.

Evans, W.J., J.H. Meadwos, A.L. Wayda, W.E. Hunter and J.L. Atwood, 1982a, J. Amer. Chem. Soc. **104**, 2008.

Evans, W.J., J.H. Meadows, A.L. Wayda, W.E. Hunter and J.L. Atwood, 1982b, J. Amer. Chem. Soc. **104**, 2015.

Evans, W.J., J.H. Meadows, W.E. Hunter and J.L. Atwood, 1983a, Organometal. **2**, 1252.

Evans, W.J., I. Bloom, W.E. Hunter and J.L. Atwood, 1983b, J. Amer. Chem. Soc. **105**, 1401.

Evans, W.J., I. Bloom, W.E. Hunter and J.L. Atwood, 1983c, Organometal. **2**, 709.

Fischer, E.O. and H. Fischer, 1964, Angew. Chem. **76**, 52; Angew. Chem. Int. Engl. Ed. **3**, 132.

Fischer, E.O. and H. Fischer, 1965a, Angew. Chem. **77**, 261; Angew. Chem. Int. Engl. Ed. **4**, 246.

Fischer, E.O. and H. Fischer, 1965b, J. Organometal. Chem. **3**, 181.

Fischer, E.O. and H. Fischer, 1966, J. Organometal. Chem. **6**, 141.

Fischer, R.D., 1973, Lanthanide and Actinide Complexes, in: NMR of paramagnetic molecules, eds. G.N. Lamar, W.D.W. Horrocks and R.H. Holm (Academic Press, New York) Ch. 13.

Fischer, R.D., 1979, NMR-Spectroscopy of Organometallic Compounds of the f-Elements: Practical Applications, in:Organometallics of the f-elements, eds. T.J. Marks and R.D. Fischer (Reidel, Dordrecht) pp. 337–377.

Fischer, R.D. and G. Bielang, 1980a, J. Organometal. Chem. **191**, 61.

Fischer, R.D. and G. Bielang, 1980b, ACS Symposium Series No. **131**, 59.

Fischer, R.D. and H. Fischer, 1965, J. Organometal. Chem. **4**, 412.

Fischer, R.D. and H. Fischer, 1967, J. Organometal. Chem. **8**, 155.

Forsberg, J.H. and T. Moeller, 1983, Gmelin Handbook of Inorganic Chemistry, 8th ed., Sc, Y, La–Lu, Rare Earths Elements, part 6D (Springer, Berlin, Heidelberg, New York, Tokyo) pp. 137–287.

Frankland, E., 1849, J. Chem. Soc. **2**, 263.

Fritz, H.P., 1959, Chem. Ber. **92**, 780.

Fukagawa, T., Y. Fujiwara, K. Yokoo and H. Taniguchi, 1981, Chem. Lett. 1771.

Fukagawa, T., Y. Fujiwara and H. Taniguchi, 1982, Chem. Lett. 601.

Gaivoronskii, P.E. and N.V. Larin, 1973, Tr. Khim., Khim. Tekhnol. 68.

Gaivoronskii, P.E., E.M. Gavrishchuk, N.P. Chernyaev and Yu.B. Zverev, 1978, Zh. Neorgan. Khim. **23**, 3139; Russ. J. Inorg. Chem. **23**, 1742.

Gilman, H. and R.G. Jones, 1945, J. Org. Chem. **10**, 505.

Gomez-Beltran, F., L.A. Oro and F. Ibanez, 1975, J. Inorg. Nucl. Chem. **37**, 1541.

Greco, A., S. Cesca and G. Bertolino, 1976, J. Organometal. Chem. **113**, 321.

Greco, A., B. Bertolino and S. Cesca, 1977, Inorg. Chim. Acta **21**, 245.

Green, J.C., M.R. Kelly, J.A. Long, B. Kanellakopulos and P.I.W. Yarrow, 1981, J. Organometal. Chem. **212**, 329.

Grosse, A. von, 1925, Z. Anorg. Allg. Chem. **152**, 133.

Guzman, I.Sh., N.N. Chigir, O.K. Sharaev, G.N. Bondarenko, E.I. Tinyakova and B.A. Dolgoplosk, 1979, Dokl. Akad. Nauk SSSR **249**, 860; Proc. Acad. Sci. USSR **249**, 519.

Gysling, H. and M. Tsutsui, 1970, Adv. Organometal. Chem. **9**, 361.

Hart, F.A. and M.S. Saran, 1968, Chem. Commun. 1614.

Hart, F.A., A.G. Massey and M.S. Saran, 1970, J. Organometal. Chem. **21**, 147.

Haug, H.O., 1971, J. Organometal. Chem. **30**, 53.

Hayes, R.G. and J.L. Thomas, 1969a, J. Amer. Chem. Soc. **91**, 6876.

Hayes, R.G. and J.L. Thomas, 1969b, Inorg. Chem. **8**, 2521.

Hayes, R.G. and J.L. Thomas, 1971, Organometal. Chem. Rev. A **7**, 1.

Herman, D.F. and W.K. Nelson, 1952, J. Amer. Chem. Soc. **74**, 2693.

Hinrichs, W., D. Melzer, M. Rehwoldt, W. Jahn and R.D. Fischer, 1983, J. Organometal. Chem. **251**, 299.

Hodgson, K.O. and K.N. Raymond, 1972a, Inorg. Chem. **11**, 3030.

Hodgson, K.O. and K.N. Raymond, 1972b, Inorg. Chem. **11**, 171.

Hodgson, K.O., F. Mares, D.F. Starks and A. Streitwieser, Jr., 1973, J. Amer. Chem. Soc. **95**, 8650.

Holton, J., M.F. Lappert, D.G.H. Ballard, R. Pearce, J.L. Atwood and W.E. Hunter, 1976a, Chem. Commun. 480.

Holton, J., M.F. Lappert, G.R. Scollary, D.G.H. Ballard, R. Pearce, J.L. Atwood and W.E. Hunter, 1976b, Chem. Commun. 425.

Holton, J., M.F. Lappert, D.G.H. Ballard, R. Pearce, J.L. Atwood and W.E. Hunter, 1979a, Kinetically stable Lanthanide Metal Alkyls and Bridging Methyls, in: Organometallics of the f-elements, eds. T.J. Marks and R.D. Fischer (Reidel, Dordrecht) pp. 179–220.

Holton, J., M.F. Lappert, D.G.H. Ballard, R. Pearce, J.L. Atwood and W.E. Hunter, 1979b, J. Chem. Soc., Dalton Trans. 45.

Holton, J., M.F. Lappert, D.G.H. Ballard, R. Pearce, J.L. Atwood and W.E. Hunter, 1979c, J. Chem. Soc., Dalton Trans. 54.

Hüfner, S., P. Kienle, D. Quitmann and P. Brix, 1965, Z. Phys. **187**, 67.

Imamoto, T., Y. Hatanaka, Y. Tawarayama and M. Yokoyama, 1981, Tetrahedron Lett. **22**, 4987.

Imamoto, T., T. Kusumoto and M. Yokoyama, 1982, Chem. Commun. 1042.

Jamerson, J.D., A.P. Masino and J. Takats, 1974, J. Organometal. Chem. **65**, C33.

John, J. and M. Tsutsui, 1980, J. Coord. Chem. **10**, 177.

John, J.N. and M. Tsutsui, 1981, Inorg. Chem. **20**, 1602.

Jones, R.G., 1942, Iowa State Coll. J. Sci. **17**, 88.

Jorgensen, C.K., R. Pappalardo and J. Flahaut, 1965, J. Chim. Phys. **62**, 444.

Kalsotra, B.L., S.P. Anand, R.K. Multani and B.D. Jain, 1971a, J. Organometal. Chem. **28**, 87.

Kalsotra, B.L., R.K. Multani and B.D. Jain, 1971b, Israel J. Chem. **9**, 569.

Kalsotra, B.L., R.K. Multani and B.D. Jain, 1971c, J. Chin. Chem. Soc. (Taipei) **18**, 189.

Kalsotra, B.L., R.K. Multani and B.D. Jain, 1971d, J. Organometal. Chem. **31**, 67.

Kalsotra, B.L., R.K. Multani and B.D. Jain, 1972a, Curr. Sci. **41**, 155.

Kalsotra, B.L., R.K. Multani and B.D. Jain, 1972b, J. Inorg. Nucl. Chem. **34**, 2265.

Kalsotra, B.L., R.K. Multani and B.D. Jain, 1972c, J. Inorg. Nucl. Chem. **34**, 2679.

Kalsotra, B.L., R.K. Multani and B.D. Jain, 1973, J. Inorg. Nucl. Chem. **35**, 311.

Kanellakopulos, B., E. Dornberger, R. von Ammon and R.D. Fischer, 1970, Angew. Chem. **82**, 956; Angew. Chem. Int. Engl. Ed. **9**, 957.

Kanellakopulos, B. and K.W. Bagnall, 1972, M.T.P. Int. Rev. Sci., Inorg. Chem. Ser. One, **7**, 299.

Kanellakopulos, B., E. Dornberger and H. Billich, 1974, J. Organometal. Chem. **76**, C42.

Kapur, S., B.L. Kalsotra and R.K. Multani, 1972, J. Chin. Chem. Soc. (Taipei) **19**, 197.

Kapur, S., B.L. Kalsotra and R.K. Multani, 1973a, J. Inorg. Nucl. Chem. **35**, 3966.

Kapur, S., B.L. Kalsotra, R.K. Multani and B.D. Jain, 1973b, J. Inorg. Nucl. Chem. **35**, 1689.

Kapur, S., R.K. Multani and B.L. Kalsotra, 1973c, J. Chin. Chem. Soc. (Taipei) **20**, 171.

Kapur, S., B.L. Kalsotra and B.K. Multani, 1974, J. Inorg. Nucl. Chem. **36**, 932.

Kopunec, R., F. Macasek, V. Mikulaj and P. Drienovska, 1969, Radiochim. Radioanal. Lett. **1**, 117.

Krasnova, S.G., G.K. Borisov and G.G. Devyatykh, 1971, Zh. Neorgan. Khim. **16**, 1733; Russ. J. Inorg. Chem. **16**, 918.

Lappert, M.F. and R. Pearce, 1973, Chem. Commun. 126.

Lappert, M.F., P.I.W. Yarrow, J.L. Atwood and R. Shakir, 1980, Chem. Commun. 987.

Lappert, M.F., A. Singh, J.L. Atwood and W.E. Hunter, 1981a, Chem. Commun. 1190.

Lappert, M.F., A. Singh, J.L. Atwood and W.E. Hunter, 1981b, Chem. Commun. 1191.

Lappert, M.F., A. Singh, J.L. Atwood, W.E. Hunter and H.M. Zhang, 1983a, Chem. Commun. 69.

Lappert, M.F., A. Singh, J.L. Atwood and W.E. Hunter, 1983b, Chem. Commun. 206.

Lauberau, P.G. and J.H. Burns, 1970, Inorg. Chem. **9**, 1091.

Lobkovskii, E.B., G.L. Soloveichik, A.B. Erofeev, B.M. Bulychev and V.K. Belskii, 1982, J. Organometal. Chem. **235**, 151.

Lobkovskii, E.B., G.L. Soloveichik, B.M. Bulychev, A.B. Erofeev, A.I. Gusev and N.I. Kirilova, 1983, J. Organometal. Chem. **254**, 167.

Maginn, R.E., S. Manastyrskyj and M. Dubeck, 1963, J. Amer. Chem. Soc. **85**, 672.

Manastyrskyj, S. and M. Dubeck, 1964, Inorg. Chem. **3**, 1647.

Manastyrskyj, S., R.E. Maginn and M. Dubeck, 1963, Inorg. Chem. **2**, 904.

Manzer, L.E., 1976a, J. Organometal. Chem. **110**, 291.

Manzer, L.E., 1976b, Inorg. Chem. **15**, 2567.

Manzer, L.E., 1977a, J. Organometal. Chem. **135**, C6.

Manzer, L.E., E.I. du Pont de Nemours Co., 1977b, U.S. Patent 4057565.

Manzer, L.E., 1978, J. Amer. Chem. Soc. **100**, 8068.

Mares, F., K. Hodgson and A. Streitwieser, Jr. 1970, J. Organometal. Chem. **24**, C68.

Mares, F., K.O. Hodgson and A. Streitwieser, Jr., 1971, J. Organometal. Chem. **28**, C24.

Markevich, I.N., O.K. Sharaev, E.I. Tinyakova and B.A. Dolgoplosk, 1983, Dokl. Akad. Nauk SSSR **268**, 892; Proc. Acad. Sci. USSR **268**, 43.

Marks, T.J., 1974, J. Organometal. Chem. **79**, 181.

Marks, T.J., 1975, J. Organometal. Chem. **95**, 301.

Marks, T.J., 1976, J. Organometal. Chem. **119**, 229.

Marks, T.J., 1977, J. Organometal. Chem. **138**, 157.

Marks, T.J., 1978a, Progr. Inorg. Chem. Radiochem. **24**, 51.

Marks, T.J., 1978b, J. Organometal. Chem. **158**, 325.

Marks, T.J., 1979, J. Organometal. Chem. **180**, 153.

Marks, T.J., 1980, J. Organometal. Chem. **203**, 415.

Marks, T.J., 1982, J. organometal. Chem. **227**, 317.

Marks, T.J. and R.D. Ernst, 1982, Sandium, yttrium and the lanthanides and actinides, in: Comprehensive organometallic chemistry, Vol. 3, eds. G. Wilkinson, F.G.A. Stone and E.W. Abel (Pergamon, Oxford) pp. 173–270.

Marks, T.J. and G.W. Grynkewich, 1976, Inorg. Chem. **15**, 1302.

Mazzei, A., 1979, Catalysis and other applications of f-element organometallics, in: Organometallics of the f-elements, eds. T.J. Marks and R.D. Fischer (Reidel, Dordrecht) pp. 379–393.

Mehra, S. and P.K. Vij, 1978, T'ai-wan K'o Hsueh **32**, 56.

Müller, J., 1969, Chem. Ber. **102**, 152.

Murphy, E. and G.E. Toogood, 1971, Inorg. Nucl. Chem. Lett. **7**, 755.

Onaka, S., 1980, Inorg. Chem. **19**, 2132.

Onaka, S. and N. Furuchi, 1979, J. Organometal. Chem. **173**, 77.

Pappalardo, R., 1965, Helv. Chim. Acta **38**, 178.

Pappalardo, R., 1968, J. Chem. Phys. **49**, 1545.

Pappalardo, R., 1969, J. Mol. Spectrosc. **29**, 13.

Pappalardo, R. and C.K. Jorgensen, 1967, J. Chem. Phys. **46**, 632.

Pappalardo, R. and S. Losi, 1965, J. Inorg. Nucl. Chem. **27**, 733.

Pearson, R.G., 1973, Hard and Soft Acids and Bases (Dowden, Hutchinson, and Ross, Stroudsburg, PA).

Plets, V.M., 1938, Compt. Rend. Acad. Sci. USSR **20**, 27.

Raymond, K.N. and C.W. Eigenbrodt, 1980, Acc. Chem. Res. **13**, 276.

Reid, A.F. and P.D. Wailes, 1966, Inorg. Chem. **5**, 1213.

Reid, A.F., D.E. Scaife and P.C. Wailes, 1964, Spectrochim. Acta **20**, 1257.

Reynolds, L.T. and G. Wilkinson, 1959, J. Inorg. Nucl. Chem. **9**, 86.

Rice, F.O. and K.K. Rice, 1935, The aliphatic free radicals (John Hopkins Press, Baltimore) p. 58.

Rogers, R.D., R. vann Bynum and J.L. Atwood, 1980, J. Organometal. Chem. **192**, 65.

Rogers, R.D., J.L. Atwood, A. Emad, D.J. Sikora and M.D. Rausch, 1981, J. Organometal. Chem. **216**, 383.

Rybakova, L.F., A.B. Sigalov, O.P. Syutkina, E.N. Egorova and I.P. Beletskaya, 1981, Izv. Akad. Nauk SSSR 2415; Bull. Acad. Sci. USSR 1995.

Schlesener, C.J. and A.B. Ellis, 1983, Organometal. **2**, 529.

Schmieder, H., E. Dornberger and B. Kanellakopulos, 1970, Appl. Spectrosc. **24**, 499.

Schumann, H., 1979a, Organometallic compounds with lanthanide–carbon sigma bonds, one of the last problems in organometallic chemistry, in: Organometallics of the f-elements, eds. T.J. Marks and R.D. Fischer (Reidel, Dordrecht) pp. 81–112.

Schumann, H., 1979b, Nachr. Chem. Tech. Lab. **27**, 393.

Schumann, H., 1983, Comments Inorg. Chem. **2**, 247.

Schumann, H. and I. Albrecht, 1984, unpublished results.

Schumann, H. and N. Bruncks, 1982, unpublished results.

Schumann, H. and M. Cygon, 1978, J. Organometal. Chem. **144**, C43.

Schumann, H. and G.M. Frisch, 1981, Z. Naturf. **36b**, 1244.

Schumann, H. and W. Genthe, 1981, J. Organometal. Chem. **213**, C7.

Schumann, H. and S. Hohmann, 1976, Chemiker-Zeitung **100**, 336.

Schumann, H. and H. Jarosch, 1976, Z. Anorg. Allgem. Chem. **426**, 127.

Schumann, H. and G. Jeske, 1983, unpublished results.

Schumann, H. and H. Lauke, 1982, unpublished results.

Schumann, H. and J. Müller, 1978a, J. Organometal. Chem. **146**, C5.

Schumann, H. and J. Müller, 1978b, Angew. Chem. **90**, 307; Angew. Chem. Int. Engl. Ed. **17**, 276.

Schumann, H. and J. Müller, 1978c, unpublished results.

Schumann, H. and J. Müller, 1979, J. Organometal. Chem. **169**, C1.

Schumann, H. and F.W. Reier, 1981, J. Organometal. Chem. **209**, C10.

Schumann, H. and F.W. Reier, 1982a, J. Organometal. Chem. **235**, 287.

Schumann, H. and F.W. Reier, 1982b, unpublished results.

Schumann, H. and F.W. Reier, 1984a, Inorg. Chim. Acta **95**, 43.

Schumann, H. and F.W. Reier, 1984b, J. Organometal. Chem., in press.

Schumann, H. and K.D. Ziep, 1984, unpublished results.

Schumann, H., W. Genthe and N. Bruncks, 1981a, Angew. Chem. **93**, 126; Angew. Chem. Int. Engl. Ed. **20**, 121.

Schumann, H., J. Pickardt and N. Bruncks, 1981b, Angew. Chem. **93**, 127; Angew. Chem. Int. Engl. Ed. **20**, 120.

Schumann, H., W. Genthe, N. Bruncks and J. Pickardt, 1982, Organometal. **1**, 1194.

Schumann, H., F.W. Reier and M. Dettlaff, 1983, J. Organometal. Chem. **255**, 305.

Schumann, H., J. Müller, N. Bruncks, H. Lauke, J. Pickardt, H. Schwarz and K. Eckardt, 1984a, Organometal. **3**, 69.

Schumann, H., H. Lauke, E. Hahn, H.J. Heeg and D. van der Helm, 1984b, Organometal. **3**, in press.

Schumann, H., H. Lauke, E. Hahn and J. Pickardt, 1984c, J. Organometal. Chem. **263**, 29.

Schumann, H., I. Albrecht, F.W. Reier and E. Hahn, 1984d, Angew. Chem., in press.

Schumann, H., W. Genthe and E. Hahn, 1984e, unpublished results.

Schumann, H., S. Nickel and E. Hahn, 1984f, unpublished results.

Scollary, G.R., 1978, Aust. J. Chem. **31**, 411.

Seyferth, D. and R.B. King, 1965, Ann. Survey Organometal. Chem. **1**, 165.

Seyferth, D. and R.B. King, 1966, Ann. Survey Organometal. Chem. **2**, 203.

Seyferth, D. and R.B. King, 1967, Ann. Survey Organometal. Chem. **3**, 281.

Smith, K.D. and J.L. Atwood, 1972, Chem. Commun. 593.

Strohmeier, W., H. Landsfeld, F. Gernet and W. Langhäuser, 1961, Z. Anorg. Allgem. Chem. **307**, 120.

Strohmeier, W., H. Landsfeld and F. Gernet, 1962, Z. Elektrochem. **66**, 823.

Suleimanov, G.Z., V.I. Bregadze, N.A. Kovalchuk and I.P. Beletskaya, 1982a, J. Organometal. Chem. **235**, C17.

Suleimanov, G.Z., L.F. Rybakova, Ya.A. Nuriev, T.Kh. Kurbanov and I.P. Beletskaya, 1982b, J. Organometal. Chem. **235**, C19.

Suleimanov, G.Z., T.Kh. Kurbanov, Ya.A. Nuriev, L.F. Rybakova and I.P. Beletskaya, 1982c, Dokl. Akad. Nauk SSSR **265**, 896; Proc. Acad. Sci. USSR **265**, 254.

Suleimanov, G.Z., Ya.A. Nuriev, O.P. Syutkina, T.Kh. Kurbanov and I.P. Beletskaya, 1982d, Izv. Akad. Nauk SSSR 1671; Bull. Acad. Sci. USSR 1490.

Suleimanov, G.Z., L.F. Rybakova, A.B. Sigalov, Ya.A. Nuriev, N.S. Kochetkova and I.P. Beletskaya, 1982e, Zh. Org. Khim. **18**, 2482; J. Org. Chem. USSR **18**, 2191.

Suleimanov, G.Z., V.I. Bregadze, N.A. Kovalchuk, K.S. Khalilov and I.P. Beletskaya, 1983, J. Organometal. Chem. **255**, C5.

Syutkina, O.P., L.F., Rybakova, E.N. Egorova, A.B. Sigalov and I.P. Beletskaya, 1983, Izv. Akad. Nauk SSSR 648; Bull. Acad. Sci. USSR 586.

Templeton, D.H. and C.H. Dauben, 1954, J. Amer. Chem. Soc. **76**, 5237.

Thomas, J.L. and R.G. Hayes, 1970, J. Organometal. Chem. **23**, 487.

Tilley, T.D. and R.A. Andersen, 1981a, Chem. Commun. 985.

Tilley, T.D. and R.A. Andersen, 1981b, Inorg. Chem. **20**, 3267.

Tilley, T.D. and R.A. Andersen, 1982, J. Amer. Chem. Soc. **104**, 1772.

Tilley, T.D., R.A. Andersen, B. Spencer, H. Ruben, A. Zalkin and D.H. Templeton, 1980, Inorg. Chem. **19**, 2999.

Tilley, T.D., R.A. Andersen, B. Spencer and A. Zalkin, 1982a, Inorg. Chem. **21**, 2647.

Tilley, T.D., R.A. Andersen and A. Zalkin, 1982b, J. Amer. Chem. Soc. **104**, 3725.

Tilley, T.D., R.A. Andersen, A. Zalkin and D.H. Templeton, 1982c, Inorg. Chem. **21**, 2644.

Tilley, T.D., R.A. Andersen and A. Zalkin, 1983, Inorg. Chem. **22**, 856.

Tsutsui, M. and N. Ely, 1974, J. Amer. Chem. Soc. **96**, 4042.

Tsutsui, M. and N.M. Ely, 1975a, J. Amer. Chem. Soc. **97**, 1280.

Tsutsui, M. and N. Ely, 1975b, J. Amer. Chem. Soc. **97**, 3551.

Tsutsui, M. and H.J. Gysling, 1968, J. Amer. Chem. Soc. **90**, 6880.

Tsutsui, M. and H.J. Gysling, 1969, J. Amer. Chem. Soc. **91**, 3175.

Tsutsui, M., T. Takino and D. Lorenz, 1966, Z. Naturf. **21b**, 1.

Tsutsui, M., N. Ely and R. Dubois, 1976, Acc. Chem. Res. **9**, 217.

Tsutsui, M., Li-Ban Chen, D.E. Bergbreiter and T. Ken Miyamoto, 1982, J. Amer. Chem. Soc. **104**, 855.

Vollershtein, E.L., V.A. Yakovlev, E.I. Tinyakova and B.A. Dolgoplosk, 1980, Dokl. Akad. Nauk SSSR **250**, 365; Proc. Acad. Sci. USSR **250**, 19.

Von Ammon, R., B. Kanellakopulos, R.D. Fischer and P. Lauberau, 1969, Inorg. Nucl. Chem. Lett. **5**, 315.

Von Ammon, R., R.D. Fischer and B. Kanellakopulos, 1971, Chem. Ber. **104**, 1072.

Von Ammon, R. and B. Kanellakopulos, 1972, Ber. Bunsenges. Phys. Chem. **76**, 995.

Von Ammon, R., B. Kanellakopulos, R.D. Fischer and V. Formacek, 1973, Z. Naturf. **28b**, 200.

Watson, P.L., 1980, Chem. Commun. 652.

Watson, P.L., 1982, J. Amer. Chem. Soc. **104**, 337.

Watson, P.L., 1983a, J. Chem. Soc., Chem. Commun. 276.

Watson, P.L., 1983b, J. Amer. Chem. Soc. **105**, 6491.

Watson, P.L. and D.C. Roe, 1982, J. Amer. Chem. Soc. **104**, 6471.

Watson, P.L., J.F. Whitney and R.L. Harlow, 1981, Inorg. Chem. **20**, 3271.

Watt, G.W. and E.W. Gillow, 1969, J. Amer. Chem. Soc. **91**, 775.

Wayda, A.L., 1983, Organometal. **2**, 565.

Wayda, A.L. and W.J. Evans, 1978, J. Amer. Chem. Soc. **100**, 7119.

Wayda, A.L. and W.J. Evans, 1980, Inorg. Chem. **19**, 2190.

Westerhof, A. and H.J. de Liefde Meijer, 1976, J. Organometal. Chem. **116**, 319.

Westerhof, A. and H.J. de Liefde Meijer, 1978, J. Organometal Chem. **144**, 61.

Wilkinson, G. and J.M. Birmingham, 1954, J. Amer. Chem. Soc. **76**, 6210.

Wong, C., T. Lee and Y. Lee, 1969, Acta Cryst. B **25**, 2580.

Yakovlev, V.A., E.L. Vollershtein, L.S. Cherezova, E.I. Tinyakova and B.A. Dolgop-losk, 1983, Dokl. Akad. Nauk SSSR **268**, 1422; Proc. Acad. Sci. USSR **268**, 74.

Zachariasen, W.H., 1954, in: The actinide elements, eds. G.T. Seaborg and J.J. Katz (Mc Graw-Hill, New York) p. 775.

Zazzetta, A. and A. Greco, 1979, Acta Cryst. B **35**, 457.

Zeise, W.C., 1827, Pogg. Ann. **9**, 623.

Zinnen, H.A., J.J. Pluth and W.J. Evans, 1980, Chem. Commun. 810.

SUBJECT INDEX

573